NASA Conference Publication 3254

The 1993 NASA Aerospace Battery Workshop

Proceedings of a workshop held at
Space and Rocket Center
Huntsville, Alabama
November 16–18, 1993

NASA

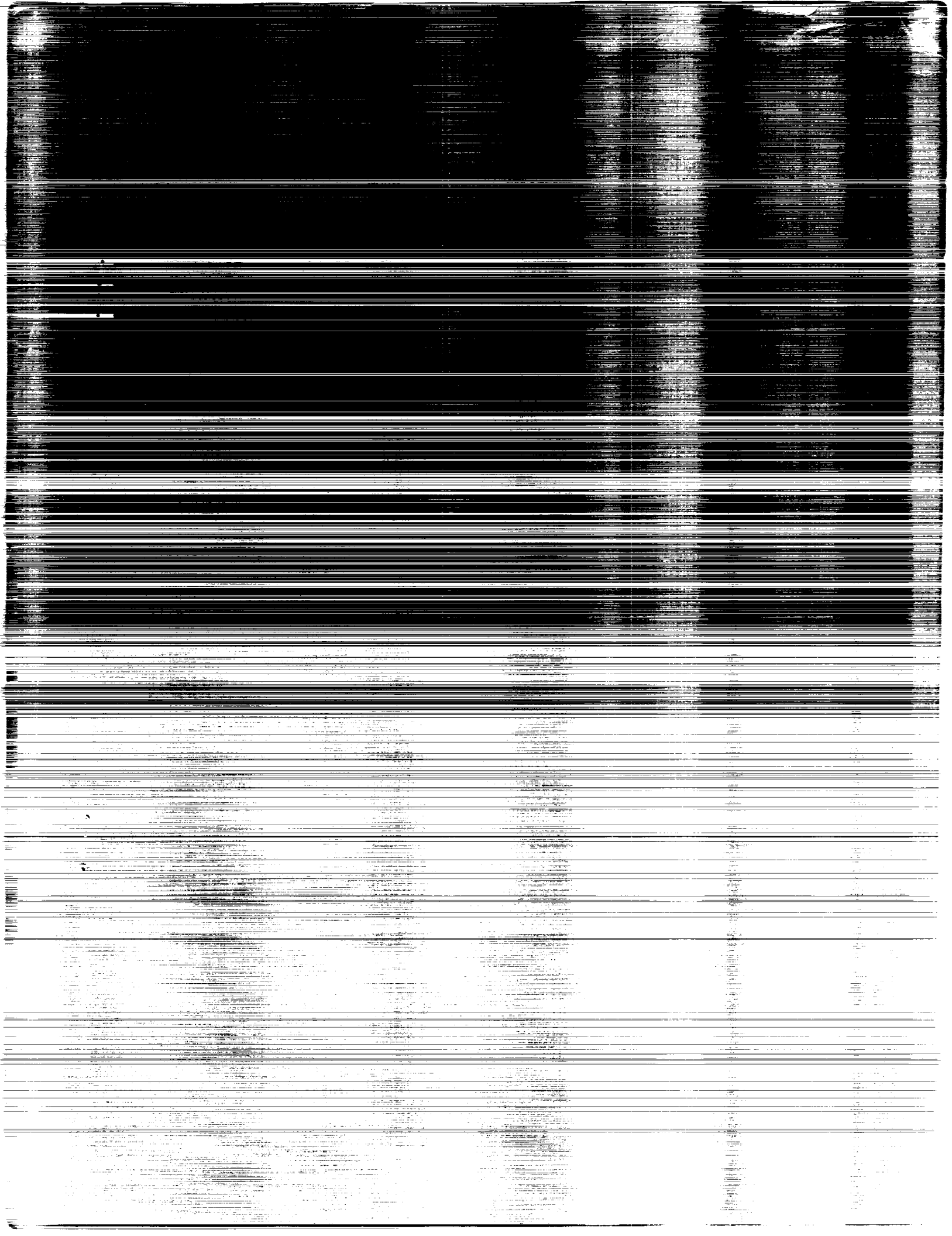

NASA Conference Publication 3254

The 1993 NASA Aerospace Battery Workshop

Jeffrey C. Brewer, *Compiler*
NASA George C. Marshall Space Flight Center
Marshall Space Flight Center, Alabama

Proceedings of a workshop sponsored by
the NASA Aerospace Flight Battery Systems
Program, hosted by the George C. Marshall
Space Flight Center, and held at the
U.S. Space and Rocket Center
Huntsville, Alabama
November 16–18, 1993

NASA
National Aeronautics and
Space Administration
Office of Management
Scientific and Technical
Information Program
1994

Preface

This document contains the proceedings of the 26th annual NASA Aerospace Battery Workshop, hosted by the Marshall Space Flight Center on November 16-18, 1993. The workshop was attended by scientists and engineers from various agencies of the U.S. Government, aerospace contractors, and battery manufacturers, as well as international participation in like kind from a number of countries around the world.

The subjects covered included nickel-cadmium, nickel-hydrogen, nickel-metal hydride, and lithium based technologies, as well as advanced technologies including various bipolar designs.

Introduction

The NASA Aerospace Battery Workshop is an annual event hosted by the Marshall Space Flight Center. The workshop is sponsored by the NASA Aerospace Flight Battery Systems Program which is managed out of NASA Lewis Research Center and receives support in the form of overall objectives, guidelines, and funding from Code Q, NASA Headquarters.

The 1993 Workshop was held on three consecutive days and was divided into five sessions. The first day consisted of a General Topic Session and the Nickel-Hydrogen Technologies Session. The second day began with the Nickel-Cadmium Technologies Session and concluded with a Special Topic (charge control) Session. The third and final day was devoted to the Advanced Technologies Session.

On a personal note, I would like to take this opportunity to thank all of the many people that contributed to the organization and production of this workshop:

The NASA Aerospace Flight Battery Systems Program, for their financial support as well as their input during the initial planning stages of the workshop.

Bob Bechtel and **Eric Lowery**, NASA Marshall Space Flight Center; **Pat O'Donnell**, NASA Lewis Research Center; **Eric Darcy**, NASA Johnson Space Center; and **Joe Stockel**, Office of Research & Development, for serving as Session Organizers, which involved soliciting presentations, organizing the session agenda, and orchestrating the session during the workshop;

U.S. Space and Rocket Center, for doing an outstanding job in providing an ideal setting for this workshop and for the hospitality that was shown to all who attended;

Marshall Space Flight Center employees, for their help in stuffing envelopes, registering attendees, handling the audience microphones, and flipping transparancies during the workshop.

Finally, I want to thank all of you that attended and/or prepared and delivered presentations for this workshop. You were the key to the success of this workshop.

Jeff Brewer
NASA Marshall Space Flight Center

Table of Contents

Preface iii

Introduction v

General Session 1

Summary of NASA Aerospace Flight Battery Systems Program Activities
Michelle Manzo and Patricia O'Donnell, NASA Lewis Research Center 3

NSWC Crane Aerospace Cell Test History Database
Harry Brown and Bruce Moore, Naval Surface Warfare Center -- Crane Division ... 83

Advanced Energy Storage for Space Applications: A Follow-Up
Gerald Halpert and Subbarao Surampudi, Jet Propulsion Laboratory 91

Experimental Evaluation of Battery Cells for Space-Based Radar Application
Craig A. Maskell, Defence Research Establishment Ottawa; and John R. Metcalfe, CAL Corporation 111

Battery Study for the Mars Environmental Survey (MESUR) Pathfinder
S. Dawson, B. Otzinger, D. Perrone, S. Di Stefano, and G. Halpert, Jet Propulsion Laboratory 119

Screen Test for Cadmium and Nickel Plates
Angie H. Phan and Albert H. Zimmerman, The Aerospace Corporation 133

Analysis for Nickel (III) and (IV) in Positive Plates from Nickel-Cadmium Cells
Harlan L. Lewis, Naval Surface Warfare Center -- Crane Division 141

Nickel-Hydrogen Technologies Session 147

Space Station Freedom Ni-H_2 Cell Testing Program
Bruce Moore, Naval Surface Warfare Center -- Crane Division; and Dave Frate, NASA Lewis Research Center 149

Ni-H_2 Cell Characterization for INTELSAT Programs
Andrew Dunnet, INTELSAT; and Martin Earl, COMSAT Laboratories 241

SAFT Nickel-Hydrogen Cell Cycling Status
Yannick Borthomieu and Didier Duquesne, SAFT Advanced Batteries 261

Calculation of the Thermoneutral Potential of Ni-Cd and Ni-H_2 Cells
Albert H. Zimmerman, The Aerospace Corporation 289

Performance Model of a Recirculating Stack Nickel-Hydrogen Cell
Albert H. Zimmerman, The Aerospace Corporation 295

Thermal Modeling of Ni-H_2 Batteries
Agnes Ponthus, SAFT; and Alain Alexandre, TSR 329

Nickel-Hydrogen Cell Reversal Characteristics
Chuck Lurie, TRW Space and Electronics Group 361

Cycle Life vs. Depth of Discharge Update on Modeling Studies
Lawrence H. Thaller, The Aerospace Corporation 377

Air Force Standards for Nickel-Hydrogen Battery
Warren Hwang and Martin Milden, The Aerospace Corporation 397

Charging Efficiency of Ni-H_2 Cells During Transfer Orbit of Telstar 4 Satellites
W.C. Fang, D.W. Maurer, B. Vyas, and M. Thomas, AT&T Bell Labs 405

Nickel-Cadmium Technologies Session 423

Orbital Management and Design Considerations for Ni-Cd Satellite Power Systems
Benjamin J. Tausch II, Martin Marietta Astronautics 425

TOPEX/POSEIDON Battery Performance During the First Year of Operation
Frank Deligiannis, Sal Di Stefano, Eric Lopez, and Rob Sherwood, Jet Propulsion Laboratory 439

Nickel-Cadmium Battery Operations On-Orbit: Trials, Tribulations, and Success on the Upper Atmosphere Research Satellite
Gopalakrishna M. Rao, NASA Goddard Space Flight Center; and Scott D. Miller, Martin Marietta Services Inc. 459

Performance Test Results of ETS-VI Ni-Cd Cells
K. Nakatani and Y. Yano, Sanyo Electric Co., Ltd.; S. Kuwajima and H. Kusawake, National Space Development Agency of Japan 491

Air Force Ni-Cd Cell Qualification Program
S. Hall and H. Brown, Naval Surface Warfare Center -- Crane Division; G. Collins and W. Hwang, The Aerospace Corporation 513

Discriminating Performance Parameters for 50 Amp-Hour and 60 Amp-Hour Nickel-Cadmium Plates and Battery Cells
Mark R. Toft, McDonnell Douglas Aerospace 545

Charge Control Session 577

INTELSAT Battery Charge Philosophy
Andrew Dunnet, INTELSAT 579

Pressure-Based Charge Control on Ni-H_2 Cells
Dean Maurer, AT&T / Bell Labs 581

Battery Charge Control: Which Approach is Best?
Chuck Lurie, TRW Space and Electronics Group 585

Some Observations on Battery Charge Control
George Methlie 589

Construction of Temperature Compensated Constant Voltage (VT) Curves for Super Ni-Cd™ Cells
David A. Baer, David F. Pickett, and James M. Pearce, Hughes Industrial Electronics Company; Gopalakrishna Rao, NASA Goddard Space Flight Center 599

A Pressure Based Charge Control System for the DSPSE Ni-H_2 CPV Battery
C. Garner, W. Barnes, and G. Hickman, Naval Research Laboratories 607

Use of Calorimetry for End of Charge Determination
Chris J. Johnson, Boeing Defense & Space Group 627

Advanced Technologies Session 641

Advanced Nickel-Hydrogen Spacecraft Battery Development
D.K. Coates, C.L. Fox, D.J. Standlee, and B.K. Grindstaff, Eagle-Picher Industries, Inc. 643

Development of Nickel-Metal Hydride Cell: An Update
S. Kuwajima and H. Kusawake, National Space Development Agency of Japan; K. Nakatani and Y. Yano, Sanyo Electric Co., Ltd. 653

Ni-MH Storage Test and Cycle Life Test
R. Dan Dell, Glenn C. Klein, and David F. Schmidt, Gates Aerospace Batteries ... 687

Determination of Thermal Properties of Commercial Ni-MH Cells
Eric Darcy, NASA Johnson Space Center 701

High Rate Lithium/Thionyl Chloride Bipolar Battery Development
P.G. Russell and F. Goebel, Yardney Technical Products, Inc. 717

Bipolar Lead-Acid Batteries for Electrical Actuation Applications
Douglas C. Pierce and Dr. William O. Gentry, Johnson Controls Battery Group, Inc.; David Hall, NASA Marshall Space Flight Center 753

Bi-Polar Ag-Zn Battery
L. John Giltner, Eagle-Picher Industries, Inc. 773

Advanced Silver-Zinc Battery Development for the SRB and ET Range Safety Subsystems
Zoe Adamedes, BST Systems 775

List of Attendees 833

General Session

Session Organizer: *Bob Bechtel*
NASA Marshall Space Flight Center

AEROSPACE TECHNOLOGY DIRECTORATE

POWER TECHNOLOGY DIVISION

Lewis Research Center

SUMMARY OF NASA AEROSPACE FLIGHT BATTERY SYSTEMS PROGRAM ACTIVITIES

MICHELLE MANZO
PATRICIA O'DONNELL
NASA LEWIS RESEARCH CENTER
CLEVELAND, OHIO 44135

1993 NASA AEROSPACE BATTERY WORKSHOP
MARSHALL SPACE FLIGHT CENTER
HUNTSVILLE, ALABAMA

NOVEMBER 16-18, 1993

NASA AEROSPACE FLIGHT BATTERY SYSTEMS PROGRAM OBJECTIVES

The NASA Aerospace Flight Battery Systems Program represents a unified NASA wide effort with the overall objective of providing NASA with the policy and posture which will increase the safety, performance, and reliability of space power systems. The specific objectives of the program are listed on the facing page.

In late 1991, the NASA Administrator formed a Battery Review Board to investigate recent problems experienced with flight programs. The recommendations of the Battery Review Board were presented at the 1992 NASA Battery Workshop. Those recommendations impacted the NASA Aerospace Flight Battery Systems Program in a variety of ways. In the past year several tasks under the NASA Aerospace Flight Battery Systems Program have been redirected as a result of the Battery Reveiw Board investigation. While the major objectives of the program remain unchanged, the approach has been modified to reflect the current recommendations.

AEROSPACE TECHNOLOGY DIRECTORATE

POWER TECHNOLOGY DIVISION

Lewis Research Center

PROGRAM OBJECTIVES

ENHANCE CELL/BATTERY SAFETY AND RELIABILITY

MAINTAIN CURRENT BATTERY TECHNOLOGY

INCREASE FUNDAMENTAL UNDERSTANDING OF PRIMARY AND SECONDARY CELLS

PROVIDE A MEANS TO BRING FORTH ADVANCED TECHNOLOGY FOR FLIGHT USE

ASSIST FLIGHT PROGRAMS IN MINIMIZING BATTERY TECHNOLOGY RELATED FLIGHT RISKS

ENSURE THAT SAFE, RELIABLE BATTERIES ARE AVAILABLE FOR NASA'S FUTURE MISSIONS

NASA AEROSPACE FLIGHT BATTERY SYSTEMS PROGRAM

NASA AEROSPACE FLIGHT BATTERY SYSTEMS PROGRAM - APPROACH

The approach to achieving the program objectives involves:

1) increasing the fundamental understanding of primary and secondary cells;

2) providing for improved cell/battery manufacturing process control, specifically in the area of secondary nickel-cadmium and nickel-hydrogen batteries;

3) opening and maintaining communication lines within NASA and the aerospace community;

4) providing for qualification of new technologies as they become available; and

5) implementing checks and balances for the verification of various cell technologies.

AEROSPACE TECHNOLOGY DIRECTORATE

POWER TECHNOLOGY DIVISION

Lewis Research Center

APPROACH

ESTABLISH SPECIFICATIONS, DESIGN AND OPERATIONAL GUIDELINES FOR PRIMARY AND SECONDARY CELLS AND BATTERIES

PROVIDE IMPROVED PROCESS CONTROL

OPEN AND MAINTAIN COMMUNICATION LINES WITHIN NASA AND THE AEROSPACE COMMUNITY

PROVIDE FOR QUALIFICATION OF NEW TECHNOLOGIES

IMPLEMENT INDEPENDENT CHECKS AND BALANCES FOR CELL VERIFICATIONS

NASA AEROSPACE FLIGHT BATTERY SYSTEMS PROGRAM ORGANIZATION

This program is designed to enhance the safety, reliability, and performance of NASA's aerospace primary and secondary batteries as well as battery power systems. The NASA Aerospace Flight Battery Systems Program is organized under four major tasks: Program Management, Battery Systems Technology, Secondary Battery Technology, and Primary Battery Technology. The NASA Lewis Research Center (LeRC) has the overall responsibility for management of the program. Dr. Patricia O'Donnell of the Lewis Research Center is the program manager. The overall objectives, guidelines and funding are provided by NASA Headquarters through Code Q, the Office of Safety and Mission Quality. Mr. Shahid Habib is the Headquarters, Code Q program manager.

AEROSPACE TECHNOLOGY DIRECTORATE

POWER TECHNOLOGY DIVISION

Lewis Research Center

PROGRAM ORGANIZATION

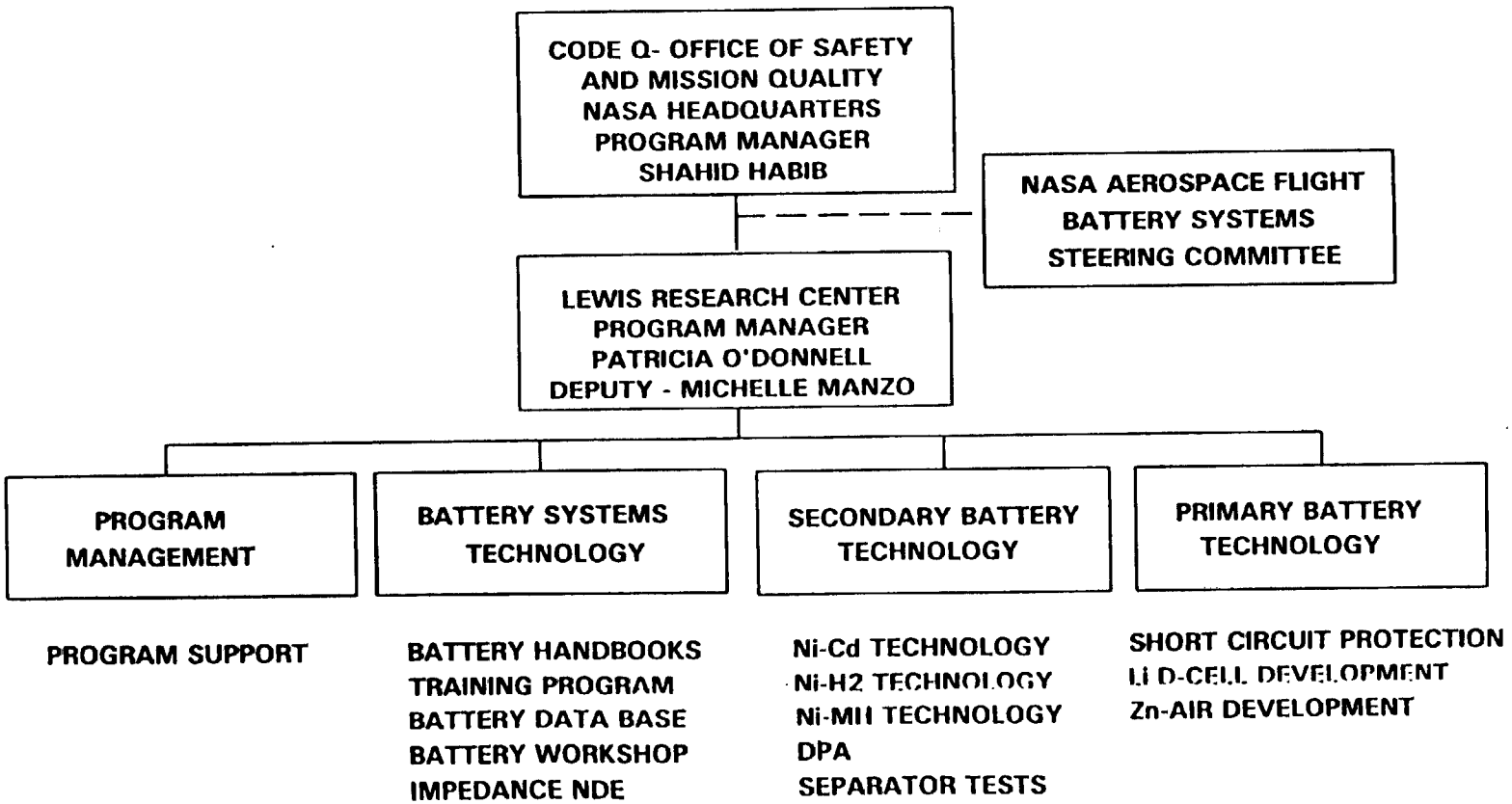

NASA AEROSPACE FLIGHT BATTERY SYSTEMS PROGRAM

NASA AEROSPACE FLIGHT BATTERY SYSTEMS PROGRAM ORGANIZATION

The majority of the NASA centers are involved in the execution of specific tasks within the program. The Lewis Research Center Program Manager has full responsibility for technical management, cost and scheduling of the program. The NASA Lewis Research Center Program Manager also provides continuing coordination with all the NASA centers, Jet Propulsion Laboratory (JPL), NASA Headquarters and the NASA Aerospace Flight Battery Systems Steering Committee.

The NASA Aerospace Flight Battery Systems Steering Committee provides advice on battery issues. The Committee is chaired by the Office of Safety and Mission Quality, membership is comprised of one representative from each of the NASA centers and one representative from Aerospace Corporation, representing the Air Force.

AEROSPACE TECHNOLOGY DIRECTORATE

POWER TECHNOLOGY DIVISION

Lewis Research Center

PROGRAM ORGANIZATION

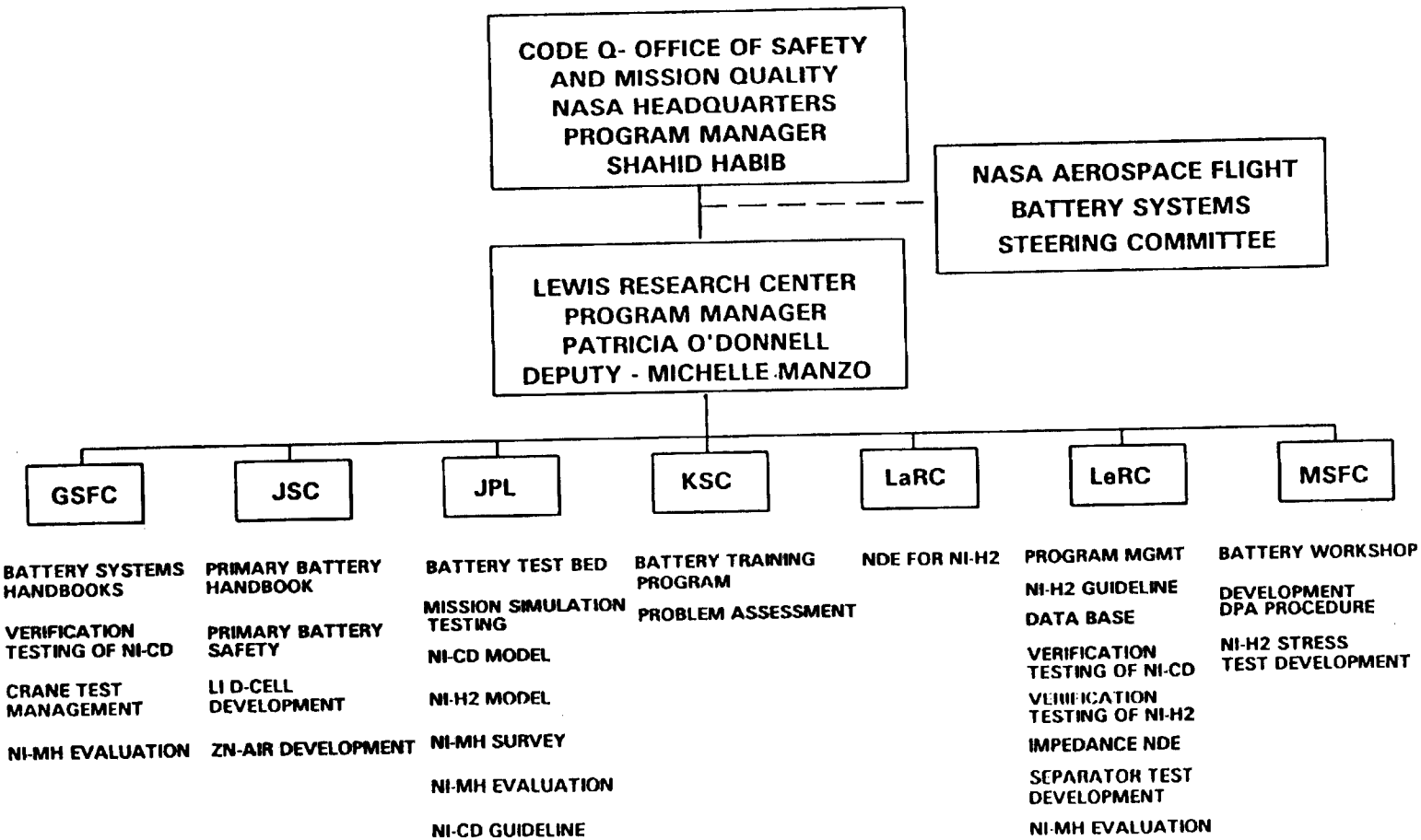

NASA AEROSPACE FLIGHT BATTERY SYSTEMS PROGRAM

BATTERY SYSTEMS TECHNOLOGY

The Battery Systems Technology Task addresses the overall systems aspects associated with the integration of cells into batteries and batteries into power systems. The objective is to improve the reliability of energy storage, space power system design, integration, and checkout.

AEROSPACE TECHNOLOGY DIRECTORATE

POWER TECHNOLOGY DIVISION

Lewis Research Center

BATTERY SYSTEMS TECHNOLOGY TASK OBJECTIVE

TO IMPROVE RELIABILITY OF ENERGY STORAGE SPACE POWER SYSTEM DESIGN, INTEGRATION, AND CHECKOUT

SYSTEMS ASPECTS - INTEGRATION OF CELLS INTO BATTERIES AND BATTERIES INTO POWER SYSTEMS

AEROSPACE TECHNOLOGY DIRECTORATE

POWER TECHNOLOGY DIVISION

Lewis Research Center

BATTERY SYSTEMS TECHNOLOGY TASK

NASA BATTERY HANDBOOKS

BATTERY TRAINING PROGRAM

BATTERY DATA BASE

NASA BATTERY WORKSHOP

IMPEDANCE NDE

RUSSIAN BATTERY TECHNOLOGY ASSESSMENT

NASA AEROSPACE FLIGHT BATTERY SYSTEMS PROGRAM

AEROSPACE TECHNOLOGY DIRECTORATE

POWER TECHNOLOGY DIVISION

Lewis Research Center

NASA BATTERY HANDBOOKS

OBJECTIVE: DEFINE GOOD CONSISTENT PRACTICES FOR THE DESIGN, INTEGRATION AND CHECKOUT, AND TESTING OF PRIMARY AND SECONDARY BATTERY SYSTEMS. PROVIDE GUIDELINES AND REQUIREMENTS TO ENSURE MISSION SUCCESS

NASA HANDBOOK FOR NICKEL-HYDROGEN BATTERIES

HANDBOOK FOR HANDLING AND STORAGE OF NICKEL-CADMIUM BATTERIES

REVISION OF NHB8073.1 - "NASA SPECIFICATIONS FOR MANUFACTURING AND PERFORMANCE REQUIREMENTS OF NASA STANDARD AEROSPACE NICKEL-CADMIUM CELLS" TO A GUIDELINES DOCUMENT

PREPARATION OF A GUIDELINES DOCUMENT FOR NICKEL-HYDROGEN CELLS

PRIMARY BATTERY DESIGN AND SAFETY HANDBOOK

BATTERY SYSTEMS TECHNOLOGY TASK

NICKEL-HYDROGEN BATTERY HANDBOOK

The Goddard Space Flight Center (GSFC), contracted with Mr. Jim Dunlop for the development of a NASA Handbook for Nickel-Hydrogen Batteries. The handbook has been completed and was published in September of this year. The *NASA Handbook for Nickel-Hydrogen Batteries* addresses the following subjects: 1) Nickel-Hydrogen Cell Design, 2) Aerospace Applications of Nickel-Hydrogen Batteries, 3) Nickel-Hydrogen Battery Design, 4) Advanced Battery Design Concepts, 5) Performance of Nickel-Hydrogen Batteries 6) Battery Procurement, 7) Standard Test Procedures for NASA, 8) Storage and Handling, and 9) Safety.

AEROSPACE TECHNOLOGY DIRECTORATE

POWER TECHNOLOGY DIVISION

Lewis Research Center

NASA BATTERY HANDBOOKS

NASA HANDBOOK FOR NICKEL-HYDROGEN BATTERIES - GSFC

PUBLISHED - SEPTEMBER 1993, JIM DUNLOP - AUTHOR

NICKEL-HYDROGEN CELL DESIGN
AEROSPACE APPLICATIONS OF NICKEL-HYDROGEN BATTERIES
NICKEL-HYDROGEN BATTERY DESIGN
ADVANCED BATTERY DESIGN CONCEPTS
PERFORMANCE OF NICKEL-HYDROGEN BATTERIES
STORAGE AND HANDLING
STANDARD TEST PROCEDURES FOR NASA
BATTERY PROCUREMENT
SAFETY

BATTERY SYSTEMS TECHNOLOGY TASK

NICKEL-CADMIUM BATTERY HANDBOOK

As a part of the Handbook Development Task of the Battery Program, GSFC is also preparing a *Handbook for the Handling and Storage of Aerospace Nickel-Cadmium Batteries*. This handbook is not intended to duplicate the information covered in NASA reference Publication 1052,*Sealed-Cell Nickel-Cadmium Battery Applications Manual*. The purpose of this handbook is to update the handling procedures and practices for working with nickel-cadmium batteries. The Handbook covers changes in guidelines resulting from improvements in design, manufacturing, and testing of nickel-cadmium cells and batteries. The heritage of many GSFC flight Ni-Cd battery developments over the past three decades is covered in the handbook. This handbook specifically covers the following 1) Background, 2) Nickel-Cadmium Cell Primer, 3) The Environment and Nickel-Cadmium Batteries, 4) Battery Handling and Storage Guidelines and 5) Nickel-Cadmium Cell Design and Evolution (from 1960-1989).

AEROSPACE TECHNOLOGY DIRECTORATE

POWER TECHNOLOGY DIVISION

Lewis Research Center

NASA BATTERY HANDBOOKS

HANDBOOK FOR HANDLING AND STORAGE OF AEROSPACE NICKEL-CADMIUM BATTERIES - LESSONS LEARNED - GSFC

TO BE PUBLISHED BY END OF 1993 - FLOYD FORD - AUTHOR

UPDATE HANDLING PROCEDURES AND PRACTICES FOR NICKEL-CADMIUM BATTERIES

- BACKGROUND
- NICKEL-CADMIUM CELL PRIMER
- THE ENVIRONMENT AND NICKEL-CADMIUM BATTERIES
- BATTERY HANDLING AND STORAGE GUIDELINES
- NICKEL-CADMIUM CELL DESIGN AND EVOLUTION - A HISTORICAL PERSPECTIVE

BATTERY SYSTEMS TECHNOLOGY TASK

NICKEL-CADMIUM/NICKEL-HYDROGEN GUIDELINES DOCUMENTS

As a result of recommendations made by the Battery Review Board, NASA has dropped the standard Ni-Cd cell designation. The defining document for the specification of NASA standard Ni-Cd cells, NHB 8073.1, NASA Specification for Manufacturing and Performance Requirements of NASA Standard Aerospace Nickel-Cadmium Cells is being revised into a guidelines type document. JPL is responsible for the Ni-Cd guidelines document. A similar guidelines type document for Nickel-hydrogen batteries is also being prepared under the direction of the Lewis Research Center.

AEROSPACE TECHNOLOGY DIRECTORATE

POWER TECHNOLOGY DIVISION

Lewis Research Center

NASA BATTERY HANDBOOKS

NICKEL-CADMIUM GUIDELINES DOCUMENT - JPL

DOCUMENT TO SERVE AS GUIDELINE AND CHECKLIST FOR THE PROCUREMENT OF Ni-Cd CELLS FOR FLIGHT PROJECTS

ENCOMPASS STANDARD AND ADVANCED Ni-Cd CELL TECHNOLOGIES

RATIONALE FOR TECHNICAL SPECIFICATIONS

REPRESENTATIVE VALUES AND RANGES FOR CRITICAL DESIGN PARAMETERS

NICKEL-HYDROGEN GUIDELINES DOCUMENT - LeRC

FOLLOW OUTLINE OF Ni-Cd GUIDELINES DOCUMENT

BATTERY SYSTEMS TECHNOLOGY TASK

PRIMARY BATTERY DESIGN AND SAFETY HANDBOOK

A Primary Battery Design and Safety Handbook has been prepared and is expected to be published in the near future. It is intended that the handbook provide National Space Transportation System users with the necessary guidelines, standard testing procedures and requirements to ensure mission success.

AEROSPACE TECHNOLOGY DIRECTORATE

POWER TECHNOLOGY DIVISION

Lewis Research Center

NASA BATTERY HANDBOOKS

PRIMARY BATTERY DESIGN AND SAFETY HANDBOOK - JSC

HANDBOOK TO PROVIDE NATIONAL SPACE TRANSPORTATION SYSTEM USERS WITH THE NECESSARY GUIDELINES AND STANDARD TESTING PROCEDURES TO ENSURE MISSION SUCCESS

PUBLICATION EXPECTED BY END OF THE CALENDAR YEAR

BATTERY SYSTEMS TECHNOLOGY TASK

NASA BATTERY TRAINING PROGRAM

The handbooks are intended to serve as the basis for a training plan, at the engineer and technician levels, that will ensure that personnel involved with the test and operations of batteries and their related power systems are fully qualified to implement safe and proper operational procedures including storage practices. The Kennedy Space Center (KSC) has responsibility for this task. A subcommittee consisting of engineers who have direct flight battery expertise has been formed at KSC. The subcommittee is in the process of assessing battery training requirements first at KSC then within the agency. Safety and handling procedures used by individual projects are being assembled. Presently, safety and handling procedures have been mission specific. This task will attempt to develop an integrated plan to be used agency wide.

AEROSPACE TECHNOLOGY DIRECTORATE

POWER TECHNOLOGY DIVISION

Lewis Research Center

NASA BATTERY TRAINING PROGRAM - KSC

OBJECTIVE: DEFINE TRAINING NEEDS AND TRAINING PLAN FOR QUALIFICATION OF PERSONS INVOLVED WITH TEST AND OPERATION OF BATTERIES

TRAINING NEEDS UNDER INVESTIGATION

DEFINE REQUIREMENTS - ASSESSMENT OF TRAINING NEEDS AT KSC FOLLOWED BY AGENCY-WIDE ASSESSMENT OF TRAINING NEEDS

EVALUATION OF VARIOUS TRAINING PROGRAMS IS UNDERWAY

BATTERY SYSTEMS TECHNOLOGY TASK

BATTERY DATA BASE

The Battery Data Base subtask addresses a NASA Battery System Data Base Environment to serve the NASA battery community for the dissemination of technical notes, policy documentation and test data. Efforts are underway to develop a battery specific data base that would provide access to operational cycle test data in addition to a problem reporting system. The Lewis Research Center has the responsibility for the implementation this subtask.

The majority of the NASA cell test data base resides at the Naval Weapons Support Center, Crane, IN. The Crane data has bee organized and structured into a battery test data base. As part of this subtask, Crane has updated NASA pack history files dating back to 1975, provided pack record structure information, and converted data tapes to a useable format for all NASA tests dating back to 1981. On-line access of the data has been established.

The Battery Review Board recommended expansion of data base to include flight data as well as ground test data. A survey has been initiated by JPL to scope the effort, evaluate the availability of flight data outside of the agency, and to define the resources required to establish such a data base.

AEROSPACE TECHNOLOGY DIRECTORATE

POWER TECHNOLOGY DIVISION

Lewis Research Center

BATTERY DATA BASE - LeRC

OBJECTIVE: DEVELOP DATA BASE FOR THE DISSEMINATION OF TECHNICAL NOTES, POLICY DOCUMENTATION AND TEST DATA

ENDORSED BY BATTERY REVIEW BOARD

DATA BASE IS FUNCTIONAL - OPERATION HAS BEEN DEMONSTRATED

OPERATIONAL CYCLE TEST DATA - 75% OF POST 1990 DATA FROM CRANE TESTING HAS BEEN ENTERED INTO THE DATA BASE

BATTERY PROGRAM FUNDS SUPPORT MARTIN MARIETTA TESTING - DATA AVAILABLE FOR DATA BASE

EVALUATE EXPANSION OF DATA BASE ACTIVITIES TO INCLUDE INDUSTRY GROUND TEST DATA AND FLIGHT DATA - JPL SURVEY

BATTERY SYSTEMS TECHNOLOGY TASK

NASA BATTERY WORKSHOP

The NASA Battery Workshop comes under the sponsorship of the NASA Aerospace Battery Systems Program. Previously held at NASA Goddard, the Marshall Space Flight Center has hosted yearly Workshops since December 1990. The workshop serves as a forum for open communication of battery related activities between industry and government.

AEROSPACE TECHNOLOGY DIRECTORATE

POWER TECHNOLOGY DIVISION

Lewis Research Center

NASA BATTERY WORKSHOP - MSFC

OBJECTIVE: PROVIDE FORUM FOR OPEN COMMUNICATION OF BATTERY RELATED ACTIVITIES

WORKSHOP ADDRESSES TECHNOLOGY STATUS OF ESTABLISHED AND EMERGING TECHNOLOGIES

SESSION ON FOCUSED TOPICS ADDRESSES CURRENT ISSUE RELATING TO AEROSPACE BATTERIES - 1993 TOPIC CHARGE CONTROL FOR Ni-Cd AND Ni-H_2 BATTERIES

BATTERY SYSTEMS TECHNOLOGY TASK

IMPEDANCE/NDE

The use of impedance spectroscopy as an interpretive tool for predicting cell performance, life, and quality is being investigated. The Lewis Research Center is responsible for this effort. To date Ni-Cd, Ni-H_2, and Li-SO_2 cells have been evaluated. Cells of the same chemistry exhibit characteristic impedance spectra that relate to manufacturer. It remains to be seen if these characteristics correlate with life and performance.

AEROSPACE TECHNOLOGY DIRECTORATE

POWER TECHNOLOGY DIVISION

Lewis Research Center

IMPEDANCE NDE - LeRC

OBJECTIVE: INVESTIGATE THE USE OF IMPEDANCE SPECTROSCOPY AS AN INTERPRETIVE TOOL FOR DETERMINING CELL PERFORMANCE AND PREDICTING LIFE

VARIOUS CHEMISTRIES ARE UNDER INVESTIGATION

- SUPER Ni-Cd CELLS
- Ni-MH CELLS
- IPV & BIPOLAR Ni-H_2 CELLS

BATTERY SYSTEMS TECHNOLOGY TASK

SECONDARY BATTERY TECHNOLOGY

The Secondary Battery Technology Task was established to improve the performance, quality, safety, and reliability of secondary battery systems. This task presently focuses on the nickel-cadmium and nickel-hydrogen systems which encompass the majority of NASA's present and planned secondary battery applications. Recommendations of the Battery Review Board are presently being implemented under this task area.

Presently, nickel-cadmium batteries provide the storage capability for the majority of NASA's missions. As a result, the future of nickel-cadmium manufacturing and the availability of nickel-cadmium cells are of major concern to the agency. NASA is in the process of evaluating nickel-cadmium cells from a variety of sources in an effort to ensure a supply of qualified cells for future NASA missions.

Ni-H_2 cell verification activities have also been expanded based on the recommendations of the Battery Review Board. The need for a program addressing nickel-metal-hydride development has been assessed, preliminary evaluation of the technology has been initiated.

AEROSPACE TECHNOLOGY DIRECTORATE

POWER TECHNOLOGY DIVISION

Lewis Research Center

SECONDARY BATTERY TECHNOLOGY TASK

OBJECTIVE: IMPROVE PERFORMANCE, QUALITY, SAFETY AND RELIABILITY OF SECONDARY BATTERY SYSTEMS

FOCUS ON Ni-Cd AND Ni-H_2 SYSTEMS - EXPAND TO INCLUDE Ni-MH

IMPLEMENT RECOMMENDATIONS OF BATTERY REVIEW BOARD

- RESOLVE PROBLEMS WITH EXISTING Ni-Cd TECHNOLOGY
- ABANDON NASA STANDARD CELL CONCEPT - IDENTIFY ALTERNATE SOURCES OF Ni-Cd CELLS
- FORMULATE POLICY REGARDING Ni-MH TECHNOLOGY
- EVALUATE Ni-H_2 CELL DESIGN FEATURES

NASA AEROSPACE FLIGHT BATTERY SYSTEMS PROGRAM

AEROSPACE TECHNOLOGY DIRECTORATE

POWER TECHNOLOGY DIVISION

Lewis Research Center

SECONDARY BATTERY TECHNOLOGY TASK

NICKEL- CADMIUM BATTERY TECHNOLOGY

NICKEL-HYDROGEN BATTERY TECHNOLOGY

NICKEL-METAL HYDRIDE BATTERY TECHNOLOGY

DEVELOPMENT OF DPA PROCEDURES

DEVELOPMENT OF SEPARATOR TEST PROCEDURES

NASA AEROSPACE FLIGHT BATTERY SYSTEMS PROGRAM

VERIFICATION OF SECONDARY CELLS

In order to support flight programs and address NASA's future needs with respect to nickel-cadmium cells, the NASA Aerospace Flight Battery Systems Program has a subtask that involves the evaluation of current technology Ni-Cd cells from a variety of sources, including Gates Aerospace Batteries, Hughes, SAFT, Sanyo, and Acme.

AEROSPACE TECHNOLOGY DIRECTORATE

POWER TECHNOLOGY DIVISION

Lewis Research Center

NICKEL-CADMIUM BATTERY TECHNOLOGY VERIFICATION OF SECONDARY CELLS

OBJECTIVE: PROVIDE INDEPENDENT VERIFICATION OF MANUFACTURING FLIGHT CELLS BY PROCURING AND TESTING REPRESENTATIVE CELLS FROM VARIOUS MANUFACTURERS

GATES Ni-Cd CELLS - INTERACTIVE CONTRACT

ADVANCED Ni-Cd VERIFICATION
- SUPER Ni-Cd & MAGNUM Ni-Cd

FOREIGN SOURCE EVALUATION
- SAFT CELLS
- SANYO CELLS

ALTERNATE SOURCE - ACME Ni-Cd CELLS

MISSION SPECIFIC SUPPORT - MO/TOPEX

SECONDARY BATTERY TECHNOLOGY TASK

NICKEL-CADMIUM CELL TEST STATUS

The testing of state-of the art Ni-Cd cells has been ongoing for several years. The status of the current tests on cells from Hughes, Gates and SAFT is summarized on the facing chart.

AEROSPACE TECHNOLOGY DIRECTORATE

POWER TECHNOLOGY DIVISION

Lewis Research Center

NICKEL-CADMIUM CELL TEST STATUS

VENDOR	DESCRIPTION	CAP (AH)	# CELLS ORIG	# CELLS LEFT	CONDITIONS DOD (%)	CONDITIONS TEMP (oC)	STATUS CYCLES	FAILURES
HUGHES	ADVANCED NI-Cd - Z/PS	20	5	5	40	20	20400	
HUGHES	ADVANCED NI-Cd - Z/PS	20	5	5	40	20	20300	
HUGHES	ADVANCED NI-Cd - PP/PBI	20	5	5	40	20	19700	
HUGHES	ADVANCED NI-Cd - Z/PBI	20	8	8	40	20	18600	
HUGHES	ADVANCED NI-Cd - Z/PS	20	8	8	25	30	18700	
HUGHES	ADVANCED NI-Cd - Z/PS	20	8	6	40	30	17700	RECONDITIONED @ 16K
HUGHES	SUPER NI-Cd - Z/PBI +ADD	20	8	8	40	20	18000	
SAFT		24	5	5	40	0	24400	
SAFT	VOS B	20	5	5	40	20	20900	STOPPED TESTING
SAFT	VOS A	24	5	5	40	20	24600	
SAFT		40	5	5	40	20	2400	
HUGHES	MO SUPER NI-CD CELLS	37	5	5	40	20	8200	
GATES	MO FLIGHT CELLS	42	5	5	40	20	10800	
GATES	TOPEX FLIGHT CELLS	50	4	4	40	20	6100	

10/93

NASA AEROSPACE FLIGHT BATTERY SYSTEMS PROGRAM

GATES INTERACTIVE CELL CONTRACT

Modifications to the present Gates cells are also being investigated as a part of nickel-cadmium cell verification activities. An interactive contract with Gates, under the management of the Lewis Research Center, allows for variations in the porosity, nickel attack level, and the loading level of the positive electrodes as well as the incorporation of alternate separators, and varied electrolyte levels. Modified cells will be constructed and tested to evaluate the effectiveness of the component changes. The composite Task Force Group on Near Term Nickel-Cadmium Cell Design has made recommendations regarding the selected parameters and levels to be evaluated. Plans are to initially evaluate the effects of nickel attack level, positive plate loading and negative plate loading in a statistically designed experiment. Cell construction has been delayed in order to accommodate recommended design changes to the negative electrode to address current problems associated with GRO and UARS satellites.

AEROSPACE TECHNOLOGY DIRECTORATE

POWER TECHNOLOGY DIVISION

Lewis Research Center

NICKEL-CADMIUM BATTERY TECHNOLOGY VERIFICATION OF SECONDARY CELLS

GATES INTERACTIVE CELL CONTRACT - LeRC

CONTRACT TO PURCHASE CELLS WITH MODIFICATIONS TO PLATES AND SEPARATORS - VERIFY DESIGN MODIFICATIONS TO SOLVE PRESENT PROBLEMS

WORKING WITH COMPOSITE TASK FORCE GROUP ON NEAR TERM CELL DESIGN

STATISTICALLY DESIGNED EXPERIMENT EVALUATING NICKEL ATTACK, POSITIVE LOADING AND NEGATIVE LOADING HAS BEEN FORMULATED

CELL DESIGN PARAMETERS HAVE BEEN MODIFIED TO REFLECT RECOMMENDATIONS OF "BATTERY TECHNOLOGY STEERING GROUP"

SECONDARY BATTERY TECHNOLOGY TASK

EXPANSION OF MANUFACTURER VERIFICATION TESTING

In addition to the on-going testing on cells from Gates, Hughes and SAFT, cells from Sanyo, Acme, Eagle Picher and additional cells from SAFT have been ordered to expand cell verification activities per the recommendation of the Battery Review Board. The expansion of the cell verification activities is outlined here.

AEROSPACE TECHNOLOGY DIRECTORATE

POWER TECHNOLOGY DIVISION

Lewis Research Center

NICKEL-CADMIUM BATTERY TECHNOLOGY VERIFICATION OF SECONDARY CELLS

EXPANSION OF CELL VERIFICATION ACTIVITIES

FOREIGN CELL EVALUATION - LeRC

SANYO CELLS	25, 35 AH CELLS ON TEST ATP COMPLETED
SAFT CELLS	21, 50 AH CELLS ON ORDER

ADVANCED Ni-Cd EVALUATION - LeRC, GSFC

SUPER Ni-Cd CELLS	25, 21 AH CELLS ON ORDER 10, 50 AH CELLS TO BE TESTED
MAGNUM Ni-Cd CELLS	25, 21 AH CELLS ON ORDER

ALTERNATE SOURCE CELL EVALUATION - LeRC

ACME CELLS	12 EA 18 & 55AH CELLS NYLON & PP SEPARATORS

SECONDARY BATTERY TECHNOLOGY TASK

VERIFICATION TEST PLAN

Cells are being procured in groups of 20-25 and being evaluated according to the plan outlined here. The verification test plan is summarized on the following two charts.

AEROSPACE TECHNOLOGY DIRECTORATE

POWER TECHNOLOGY DIVISION

Lewis Research Center

NICKEL-CADMIUM CELL VERIFICATION

PROPOSED VERIFICATION TEST PLAN

REPEAT PORTIONS OF MANUFACTURERS INSPECTION/ACCEPTANCE TESTS

RUN NASA STANDARD ACCEPTANCE TEST PROCEDURE FOR INFORMATION ONLY

PERFORM LIFE CYCLE TESTING

FOR 20 CELLS FROM SAME LOT (MINIMUM):

1 PACK	PERFORM V/T CHARACTERIZATION FOLLOWED BY ACCELERATED GEO
3 PACKS	LEO REGIME @ VARIOUS TEMPERATURES

FOR 25 CELLS FROM SAME LOT (MINIMUM):

1 PACK	PERFORM V/T CHARACTERIZATION
1 PACK	ACCELERATED GEO
3 PACKS	LEO REGIME @ VARIOUS TEMPERATURES

SECONDARY BATTERY TECHNOLOGY TASK

AEROSPACE TECHNOLOGY DIRECTORATE

POWER TECHNOLOGY DIVISION

Lewis Research Center

NICKEL-CADMIUM CELL VERIFICATION

PROPOSED LIFE CYCLE TEST REGIMES FOR Ni-Cd CELL EVALUATION
PACKS OF 5 CELLS EACH

TEST/ PACK	DESCRIPTION	DOD (%)	TEMP (°C)	DETAILS OF REGIME
1	V/T CHARACTERIZATION - SHOCK/VIBRATION			V/T CHARACTERIZATION - PROCEDURE TBD
2	STANDARD STRESS TEST	40	20	CHARGE - 1 HR, 0.8C TO V/T LIMIT, TAPER DISCHARGE - 0.8C FOR 30 MINUTES - TO 40% DOD
3	HIGH TEMPERATURE STRESS TEST	40	30	CHARGE - 0.8C TO V/T LIMIT, TAPER DISCHARGE - 0.8C FOR 30 MINUTES - TO 40% DOD
4	LOW TEMPERATURE STRESS TEST	40	0	CHARGE - 0.8C TO V/T LIMIT, TAPER DISCHARGE - 0.8C FOR 30 MINUTES - TO 40% DOD
5	ACCELERATED GEO	80	10	2 WEEK SUN PERIODS/RECONDITIONING TBD

PLAN REQUIRES MINIMUM OF 25 CELLS - IF ONLY 20 CELLS ARE AVAILABLE - THE SAME PACK WILL BE USED FOR TESTS 1 AND 5.

SECONDARY BATTERY TECHNOLOGY TASK

MISSION RELATED CELL VERIFICATION

Stress testing of packs of cells representing the flight lots and mission simulation testing of cells for Mars Observer and Topex are other ongoing cell verification activities.

AEROSPACE TECHNOLOGY DIRECTORATE

POWER TECHNOLOGY DIVISION

Lewis Research Center

NICKEL-CADMIUM BATTERY TECHNOLOGY VERIFICATION OF SECONDARY CELLS

MISSION RELATED CELL VERIFICATION

MARS OBSERVER - JPL

42 AH NASA STANDARD GATES CELLS SUPER Ni-Cd CELLS STRESS TEST, MISSION SIMULATION TEST

TOPEX - JPL

50 AH NASA STANDARD CELLS - STRESS TEST & MISSION SIMULATION TEST

BATTERY TEST BED - JPL

MISSION SUPPORT - GRO, UARS ETC.

MANAGE DIVERGENT CELLS/BATTERIES - FACILITY SIMULATE MPS POWER SYSTEM

APPLIED NICKEL-CADMIUM TECHNOLOGY TASK

The Jet Propulsion Laboratory is responsible for the Applied Nickel-Cadmium Technology subtask. This subtask involves the development of an electrochemical model of the nickel-cadmium system that involves physical, chemical, and electrochemical studies at the component and cell levels. The model will be used to develop an accelerated test which can be used to determine the quality and reliability of flight lot cells without extensive life testing and to predict the performance of a battery from a set of spacecraft operating conditions. Phase I of the model, which involves using a table lookup approach for determining cell performance, has been implemented and made available for distribution through COSMIC. Phase II of the model involves the replacement of the table lookup approach used in Phase I with a one dimensional electrochemical model, developed under a contract with Texas A&M. The model, simulating the charge and discharge has been developed. The model predictions match actual test data through much of the cycle life. The third and final phase of the model involves the expansion to a two dimensional model and the incorporation of factors to predict performance degradation. The modeled is scheduled for completion this fiscal year.

AEROSPACE TECHNOLOGY DIRECTORATE

POWER TECHNOLOGY DIVISION

Lewis Research Center

NICKEL-CADMIUM BATTERY TECHNOLOGY
APPLIED NICKEL-CADMIUM TECHNOLOGY - JPL

OBJECTIVE: DEVELOPMENT OF PERFORMANCE MODEL FOR PREDICTION OF BATTERY PERFORMANCE UNDER SPECIFIED SPACECRAFT OPERATIONAL CONDITIONS

PHASE I LOOKUP TABLE FOR PREDICTING PERFORMANCE / VOLTAGE AND EFFICIENCY VS TEMPERATURE AND STATE-OF-CHARGE

PHASE II DEVELOPMENT OF ONE DIMENSIONAL ELECTROCHEMICAL MODEL TO REPLACE LOOKUP TABLES

PHASE III EXPAND PHASE II - INCORPORATE DEGRADATION INTO PERFORMANCE MODEL

AEROSPACE TECHNOLOGY DIRECTORATE

POWER TECHNOLOGY DIVISION

Lewis Research Center

NICKEL-CADMIUM BATTERY TECHNOLOGY
APPLIED NICKEL-CADMIUM TECHNOLOGY - JPL

Ni-Cd MODEL STATUS

FINAL STAGES OF DEVELOPMENT - OPTIMIZATION

COMPARE PREDICTIONS WITH ACTUAL PERFORMANCE DATA

MODIFICATIONS TO TREATMENT OF POSITIVE ACTIVE MATERIAL

SCHEDULED FOR COMPLETION THIS FISCAL YEAR

SECONDARY BATTERY TECHNOLOGY TASK

NICKEL-HYDROGEN TECHNOLOGY

The major goal of the Nickel-Hydrogen Technology subtask is to evaluate design features for incorporation into nickel-hydrogen cells for NASA missions. Steps are underway to evaluate the critical aspects of nickel-hydrogen technology in order to prevent a situation similar to that presently being experienced with nickel-cadmium cells and to ensure the consistent production of quality cells. The Lewis Research Center has responsibility for the Nickel-Hydrogen Technology subtask. Currently, the effects of the NASA advanced design features and the effects of 26% vs 31% KOH, cell design variations including stacking arrangements and impregnation processes are being evaluated in flight cells being tested at Crane.

AEROSPACE TECHNOLOGY DIRECTORATE

POWER TECHNOLOGY DIVISION

Lewis Research Center

NICKEL-HYDROGEN BATTERY TECHNOLOGY
CELL COMPONENT AND DESIGN EVALUATION - LeRC

OBJECTIVE: PROVIDE INDEPENDENT VERIFICATION OF DESIGN AND COMPONENT VARIATIONS TO MANUFACTURING FLIGHT CELLS BY PROCURING AND TESTING REPRESENTATIVE CELLS FROM VARIOUS MANUFACTURES

VERIFICATION OF 26% KOH
- CELLS FROM HUGHES, EP, GATES, YARDNEY

EVALUATION OF DESIGN FEATURES
- CATALYZED WALL WICK
- CELL STACKING

EVALUATION OF CELL COMPONENTS
- NICKEL ELECTRODE IMPREGNATION PROCESS
- SEPARATOR

SECONDARY BATTERY TECHNOLOGY TASK

NICKEL-HYDROGEN CELL TEST STATUS

The testing of various design features for Ni-H_2 cells has been ongoing for several years. The status of the current tests on cells is summarized on the facing chart.

AEROSPACE TECHNOLOGY DIRECTORATE

POWER TECHNOLOGY DIVISION

Lewis Research Center

NICKEL-HYDROGEN CELL TEST STATUS

VENDOR	DESCRIPTION	CAP (AH)	# CELLS ORIG	# CELLS LEFT	CONDITIONS DOD (%)	CONDITIONS TEMP (oC)	STATUS CYCLES	FAILURES
HUGHES	26% KOH - AF STANDARD	50	3	0	80	10	-	15314,19500,23700
HUGHES	31% KOH - AF STANDARD	50	3	0	80	10	-	3729,4165,11355
EPI	NASA ADV DESIGN w/CAT WW	125	3	3	60	10	25400	
EPI	NASA ADV DESIGN w/o CAT WW	125	3	0	60	10	-	9588,13900,20575
GATES	26% KOH	65	5	5	60	10	8585	
GATES	31% KOH	65	5	5	60	10	8585	
EPI	26% KOH - AQUEOUS	65	3	3	60	10	8490	
EPI	31% KOH - AQUEOUS	65	3	3	60	10	8490	
EPI	26% KOH - ALCOHOLIC	65	3	3	60	10	8490	
EPI	31% KOH - ALCOHOLIC	65	3	3	60	10	8490	
EPI	BTB DESIGN w/CAT WW	65	3	3	60	10	6315	
EPI	RECIRCULATION	65	3	3	60	10	6315	
YTP	26% KOH	56	3	3	60	10	5700	
YTP	31% KOH	56	3	3	60	10	5700	
EPI	PE FILM/PE PAPER	50	3	0	60	10	0	LOW CAPACITY - NO LEO
EPI	PE FILM/PP FELT	50	3	0	60	10	0	LOW CAPACITY - NO LEO
EPI	ASBESTOS	50	3	0	60	10	-	2309,2309,2756
EPI	PE FILM/ZIRCAR	50	3	0	60	10	-	All @ ~6700

11/4/93

NASA AEROSPACE FLIGHT BATTERY SYSTEMS PROGRAM

CPV BATTERY EVALUATION

Based on a recommendation made by the Battery Review Board, cell verification activities have been expanded to include CPV nickel-cadmium batteries. Batteries from Eagle Picher and Johnson Controls have been ordered.

AEROSPACE TECHNOLOGY DIRECTORATE

POWER TECHNOLOGY DIVISION

Lewis Research Center

NICKEL-HYDROGEN BATTERY TECHNOLOGY
CPV BATTERY EVALUATION - LeRC

OBJECTIVE: EVALUATE POTENTIAL OF EMERGING CPV TECHNOLOGY TO MEET NASA'S FUTURE NEEDS

JOHNSON CONTROLS

28 VOLT, 50 AH BATTERY - DELIVERY JULY '94

EAGLE PICHER

2 CELL, 10AH CPV BATTERIES - ON ORDER
DELIVERY 9/94

NICKEL-HYDROGEN MODEL

JPL is responsible for developing a computer model for nickel-hydrogen batteries that parallels the work done on the nickel-cadmium model. The electrochemical model that will serve as the core for the cell model is being developed for the Office of Research and Development at the University of South Carolina.

AEROSPACE TECHNOLOGY DIRECTORATE

POWER TECHNOLOGY DIVISION

Lewis Research Center

NICKEL-HYDROGEN BATTERY TECHNOLOGY
NICKEL-HYDROGEN MODEL - JPL

OBJECTIVE - DEVELOP A COMPUTER MODEL CAPABLE OF PREDICTION ORBITAL PERFORMANCE OF A NICKEL-HYDROGEN BATTERY USING A CELL LEVEL ELECTROCHEMICAL MODEL BASED ON FUNDAMENTAL PHENOMENA

ELECTROCHEMICAL MODEL BEING DEVELOPED AT UNIVERSITY OF SOUTH CAROLINA - JOE STOCKEL SUPPORT

DEVELOPMENT WILL PARALLEL THAT OF THE Ni-Cd MODEL

DEVELOPMENT OF A STRESS TEST FOR NICKEL- HYDROGEN CELLS

The Marshall Space Flight Center is responsible for the task defining the conditions for a nickel-hydrogen stress test similar to the 40%DOD, 20 °C test currently used for Ni-Cd cells. Available data is being analyzed and conditions for defining the stress test are being established.

AEROSPACE TECHNOLOGY DIRECTORATE

POWER TECHNOLOGY DIVISION

Lewis Research Center

NICKEL-HYDROGEN BATTERY TECHNOLOGY DEVELOPMENT OF $Ni-H_2$ STRESS TEST - MSFC

OBJECTIVE: DEFINE AND VERIFY A STRESS TEST FOR NICKEL-HYDROGEN, COMPARABLE TO THE 40% DOD, 20°C TEST FOR NICKEL-CADMIUM CELLS

AVAILABLE LIFE TEST DATA EVALUATED

STRESS PARAMETERS HAVE BEEN IDENTIFIED

MATRIX HAS BEEN PROPOSED

SECONDARY BATTERY TECHNOLOGY TASK

ESTABLISHMENT OF STANDARD DPA PROCEDURES

The Marshall Space Flight Center has the responsibility for developing and establishing guidelines for NASA for the performance of destructive physical analyses for Ni-Cd and Ni-H_2 chemistries. Current DPA procedures used in the industry are being evaluated in an effort to identify a standard procedure for the agency. Drafts of the guidelines documents have been prepared.

AEROSPACE TECHNOLOGY DIRECTORATE

POWER TECHNOLOGY DIVISION

Lewis Research Center

DEVELOPMENT OF DPA TEST PROCEDURES - MSFC

OBJECTIVE: DEFINE GENERAL GUIDELINES TO BE FOLLOWED BY FACILITIES PERFORMING DPA PROCEDURES ON NICKEL-CADMIUM AND NICKEL-HYDROGEN CELLS

AVAILABLE PROCEDURES HAVE BEEN EVALUATED

DRAFT GUIDELINES DOCUMENTS HAVE BEEN PREPARED

SECONDARY BATTERY TECHNOLOGY TASK

SEPARATOR TEST PROCEDURES TASK

The Lewis Research Center is involved in defining improved tests that will more closely evaluate separator characteristics as related to the actual cell environment. Detailed procedures are being developed. Publication of a document containing the recommended test procedures is expected by the end of the fiscal year.

AEROSPACE TECHNOLOGY DIRECTORATE

POWER TECHNOLOGY DIVISION

Lewis Research Center

DEVELOPMENT OF SEPARATOR TEST PROCEDURES - LeRC

OBJECTIVE: DESIGN AND DEVELOPMENT OF UNIFORM RELIABLE TEST PROCEDURES FOR EVALUATING CANDIDATE SEPARATOR MATERIALS FOR Ni-Cd, Ni-H_2 & Ni-MH CELLS

RECOMMENDATIONS REGARDING TEST PROCEDURES - DETAILED PROCEDURES BEING DEVELOPED

ACCEPTANCE CRITERIA

PUBLICATION BY END OF FISCAL YEAR

SECONDARY BATTERY TECHNOLOGY TASK

NICKEL-METAL HYDRIDE TECHNOLOGY

The Battery Program funded a task at JPL to assess the status of nickel-metal hydride technology for aerospace applications. The survey has been completed and the present approach is to perform preliminary evaluations of aerospace cells from any available sources.

AEROSPACE TECHNOLOGY DIRECTORATE

POWER TECHNOLOGY DIVISION

Lewis Research Center

NICKEL-METAL HYDRIDE TECHNOLOGY

NICKEL-METAL HYDRIDE TECHNOLOGY ASSESSMENT - JPL

DETERMINE STATUS OF Ni-MH TECHNOLOGY AND ASSESS POTENTIAL FOR USE IN NASA LEO, GEO AND PLANETARY MISSIONS

NICKEL-METAL HYDRIDE TECHNOLOGY EVALUATION - GSFC, JPL, LeRC

COORDINATED EFFORT - PROCUREMENT AND TESTING OF AEROSPACE DESIGN CELLS

SECONDARY BATTERY TECHNOLOGY TASK

PRIMARY BATTERY TECHNOLOGY

The objective of the Primary Battery Technology Task is to improve the performance, reliability and safety of primary battery systems. The major thrust of this effort is to reduce the number of different cell chemistries now used by identifying and qualifying high performance NASA Standard Primary Cells. The Johnson Space Center has primary responsibility for work performed in the primary battery area.

AEROSPACE TECHNOLOGY DIRECTORATE

POWER TECHNOLOGY DIVISION

Lewis Research Center

PRIMARY BATTERY TECHNOLOGY TASK

OBJECTIVE: IMPROVE PERFORMANCE, QUALITY, SAFETY AND RELIABILITY OF PRIMARY BATTERY SYSTEMS

REDUCE NUMBER OF CHEMISTRIES USED IN PRIMARY CELL APPLICATIONS

NASA AEROSPACE FLIGHT BATTERY SYSTEMS PROGRAM

AEROSPACE TECHNOLOGY DIRECTORATE

POWER TECHNOLOGY DIVISION

Lewis Research Center

PRIMARY BATTERY TECHNOLOGY TASK

SHORT CIRCUIT PROTECTION

LITHIUM D- CELL DEVELOPMENT

DEVELOPMENT OF ZN-AIR CELL

NASA AEROSPACE FLIGHT BATTERY SYSTEMS PROGRAM

SHORT CIRCUIT PROTECTION

JSC contracted with Yardney Technical Products to investigate the development of internal/external short circuit protection for lithium cells. The objective of this subtask was to develop a positive control for both internal and external short circuits in lithium cells. The control is activated by temperature, shutting the cells down from the heat generated by shorts. The protective coating developed under this contract was so thick (~25 mils) that the capacity was reduced by 50% and the rate capability was also substantially reduced. Alternate concepts are under evaluation.

AEROSPACE TECHNOLOGY DIRECTORATE

POWER TECHNOLOGY DIVISION

Lewis Research Center

NASA PRIMARY BATTERY - JSC

DEVELOPMENT OF INTERNAL/EXTERNAL SHORT CIRCUIT PROTECTION FOR LITHIUM CELLS

POSITIVE CONTROL (COMPOSITE THERMAL SWITCH) INCORPORATED INTO CATHODE FOR INTERNAL/EXTERNAL SHORT CIRCUIT PROTECTION

FILM DEVELOPED - TOO THICK, RESULTING IN LOSS OF CAPACITY AND RATE CAPABILITY

ALTERNATE CONCEPTS ARE UNDER INVESTIGATION

PRIMARY BATTERY TECHNOLOGY TASK

LITHIUM D-CELL DEVELOPMENT

Lithium D-Cell development encompasses the development of an optimized lithium D-cell, or a family of D-cells, that can serve as a building block for the for the varied applications now flying and those to be flown in the near future. The goal is to develop cells capable of meeting relatively high rate requirements while being as tolerant as possible to electrical and thermal abuse. The candidates evaluated include the JSC Li-BCX, the JPL high rate $LiSOCl_2$, and the Wilson Greatbatch, Ltd. Li-CSC. The WGL cell was recommended, however there are concerns with its short and abuse tolerance. Present efforts involve qualification of separate cells for high and low rate applications. con

AEROSPACE TECHNOLOGY DIRECTORATE

POWER TECHNOLOGY DIVISION

Lewis Research Center

NASA PRIMARY BATTERY - JSC

$LiSOCl_2$ D CELL DEVELOPMENT

EVALUATION OF JPL HIGH RATE $LiSOCl_2$ D, JSC LiBCX AND WILSON GREATBATCH LiCSC TO IDENTIFY OPTIMUM CELL CONFIGURATION - COMPLETED

WGL CELL RECOMMENDED - CONCERNS WITH SHORT AND ABUSE TOLERANCE

PROPOSED FOLLOW-ON ENGINEERING AND QUAL OF LOW TO MODERATE RATE CELL

PRIMARY BATTERY TECHNOLOGY TASK

ZINC-AIR DEVELOPMENT

The NASA Aerospace Flight Battery Systems Program also supports the development of a pair of Zn-O_2 cells. A high capacity cell of 200 AH at rates of 25-100 hours is under investigation. A low capacity, high rate cell has been successfully developed.

AEROSPACE TECHNOLOGY DIRECTORATE

POWER TECHNOLOGY DIVISION

Lewis Research Center

NASA PRIMARY BATTERY - JSC

DEVELOPMENT OF $Zn-O_2$ CELL

DEVELOPMENT OF LARGE CAPACITY LOW RATE AND LOW CAPACITY, HIGH RATE CELL/BATTERY DESIGNS FOR SHUTTLE ORBITER APPLICATIONS

HIGH CAPACITY CELL UNDER EVALUATION
- 200 AH, 25-100 HR RATES

LOW CAPACITY, HIGH RATE CELL SUCCESSFULLY DEVELOPED
- 20 AH, 3 AMP RATE -160 WH/#

EMPIRICAL PERFORMANCE MODEL AND THEORETICAL MATH MODEL HAVE BEEN DELIVERED

ALTERNATE WCCS BATTERY - 6 VOLTS, 13 AH DEVELOPED - UNDERGOING QUAL TESTING AT JSC

PRIMARY BATTERY TECHNOLOGY TASK

SUMMARY REMARKS

The NASA Aerospace Flight Battery Systems Program provides for a balanced cell, battery and systems program which includes primary and secondary battery activities in support of NASA's flight programs. It has provided for increased communication within the agency and with the battery industry as well. The program addresses flight battery and related flight power system activities which are essential for ensuring safe and reliable performance. Based on recommendations made by the Battery Review Board following an investigation of the aerospace battery industry as it pertains to NASA, the program has undergone considerable redirection over the past year.

AEROSPACE TECHNOLOGY DIRECTORATE

POWER TECHNOLOGY DIVISION

Lewis Research Center

SUMMARY REMARKS

PROGRAM HAS UNDERGONE REDIRECTION BASED ON BATTERY REVIEW BOARD RECOMMENDATIONS

EMPHASIS IS ON SECONDARY BATTERY SYSTEMS - VERIFICATION OF TECHNOLOGIES FOR FLIGHT APPLICATIONS

BATTERY PROGRAM HAS RESULTED IN INCREASED COMMUNICATION AND COOPERATION AMONG NASA CENTERS AND WITHIN THE AEROSPACE BATTERY COMMUNITY

THE PROGRAM ADDRESSES FLIGHT BATTERY ISSUES RELATING TO NASA'S FLIGHT PROGRAMS

NSWC Crane
Aerospace Cell Test History Database

Presented At:
The 1993 NASA Aerospace Battery Workshop
Marshall Space Flight Center
16-18 November 1993

Prepared By:

Harry Brown
Bruce Moore
Aerospace Power Systems Branch
Naval Surface Warefare Center, Crane Division

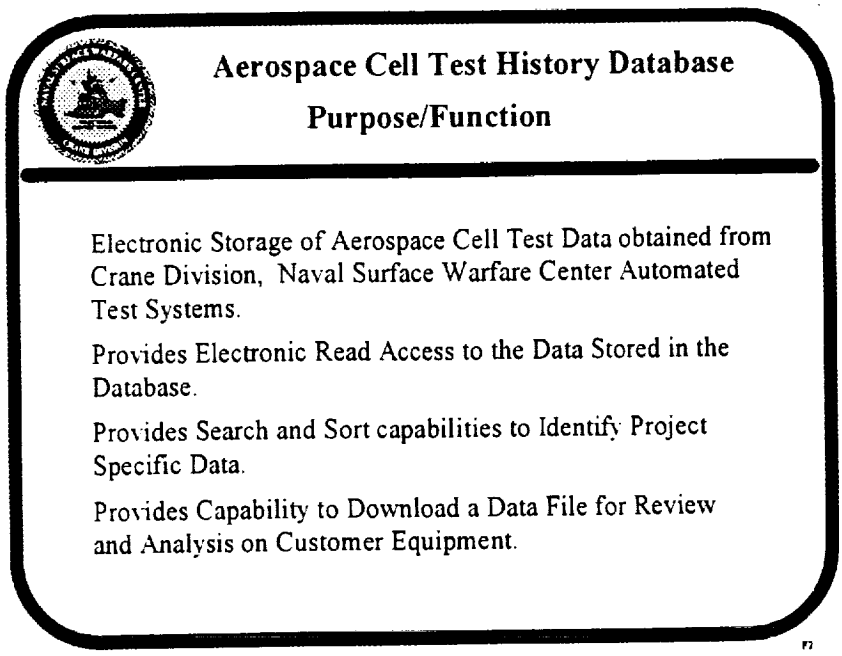

The Aerospace Cell Test History Database was developed to provide project engineers and scientists ready access to the data obtained from testing of aerospace cell designs at Naval Surface Warfare Center, Crane Division.

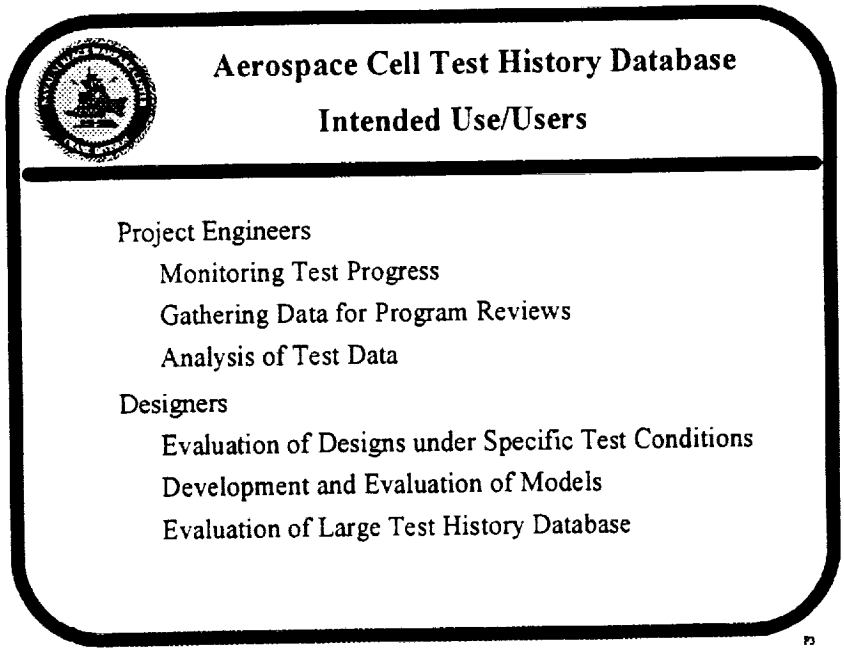

The database is intended for use by all Aerospace engineers and scientists involved in the design of power systems for satellites. Specifically, the database will provide a tool for project engineers to review the progress of their test at Crane and to have ready access to data for evaluation. Additionally, the database will provide a history of test results that designers can draw upon to answer questions about cell performance under certain test conditions and aid in selection of a cell for a satellite battery.

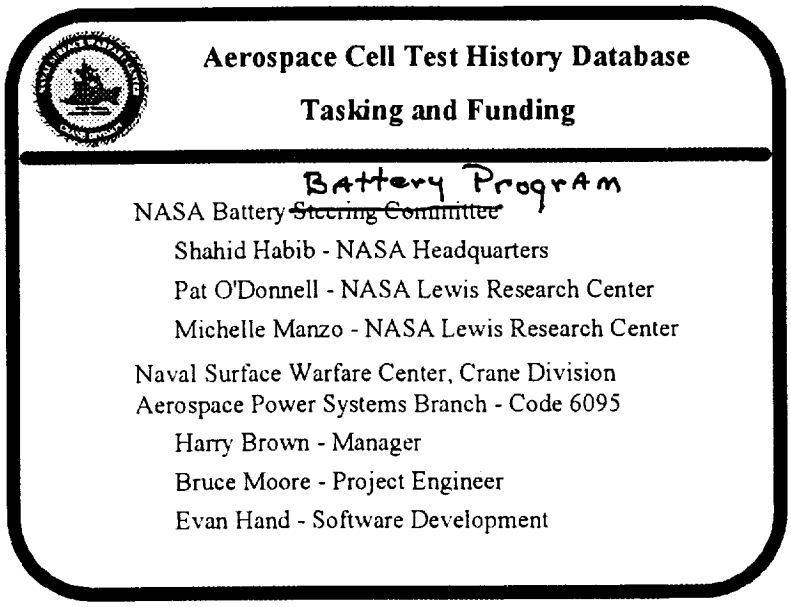

The tasking and funding for the establishment of this database is provided by the NASA Battery ~~Steering Committee~~ Program with program direction by NASA Lewis Research Center. The hardware and software design and implementation is being done by personnel in the Aerospace Power Systems Branch at Crane.

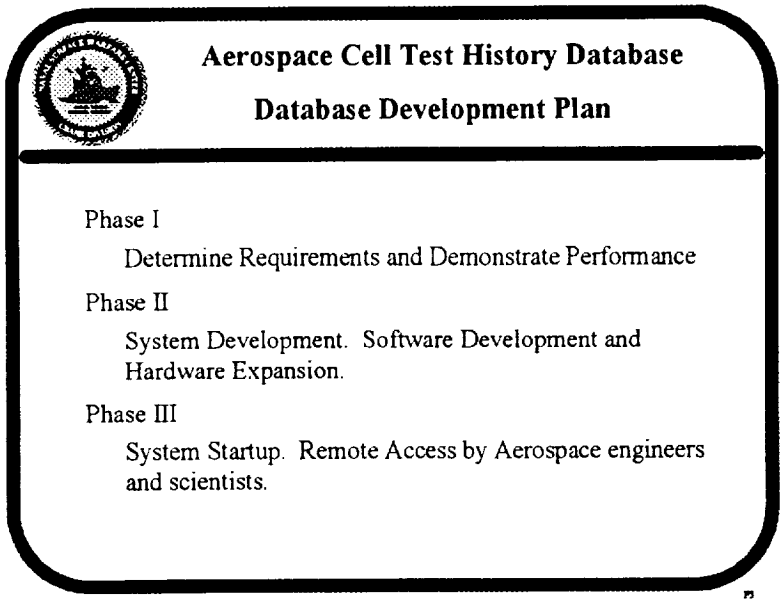

The database was developed in 3 Phases. The requirements and demonstration phase was completed in September 1992. Phase II began in FY 93 and for the most part is complete. The initial version of the software is installed, the hardware is in place, and automated transfer of data from the test systems to the database has begun. Transfer of Historical data is in process. Trial access by Crane personnel and selected NASA engineers is being permitted with system startup later this FISCAL year.

Aerospace Cell Test History Database

Database Considerations

- Hardware Based on Standard PC Computers
  - High Availability of Repair Parts
  - Existing PC Knowledge Base
  - Good Upgrade Path
- Software Developed with Off the Shelf Products
  - Database Software - DBase IV
  - Network - Novell Netware 3.11
  - Access Server - Novell Onlan/PC
- Ease Of Access
  - Accessable by Standard Modem Conections

F6

From the Phase I requirements the database considerations were developed.

Aerospace Cell Test History Database

Database Configuration

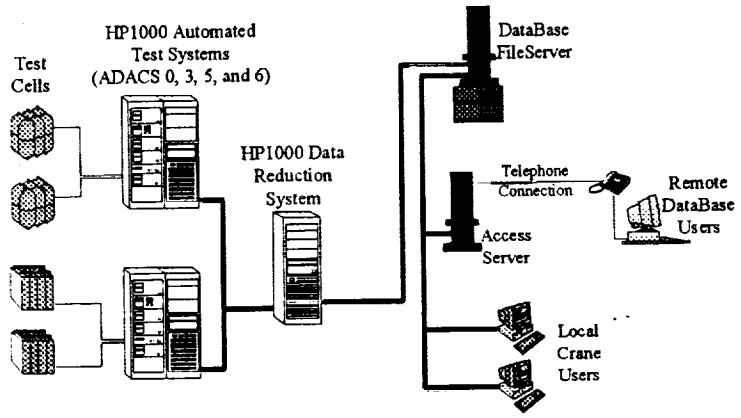

The data is stored on a File Server having 12 gigabytes of hard disk (DATABASE FILE SERVER). The FILE SERVER receives the data from the tests systems over a network connection (BATTERY TEST SYSTEMS). The network also provide access via the Branch local network. Remote access is obtained from a user PC through a modem to an ACCESS SERVER. The planned capability is to have six telephone lines accessing the system.

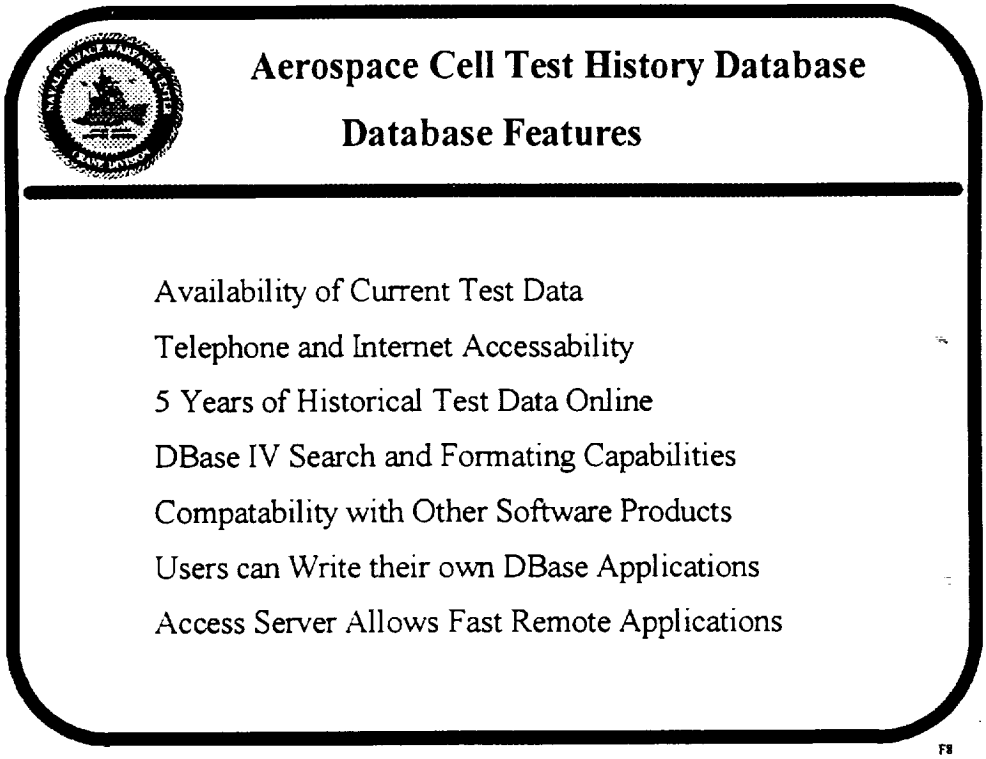

Some of the Features built into the database are:

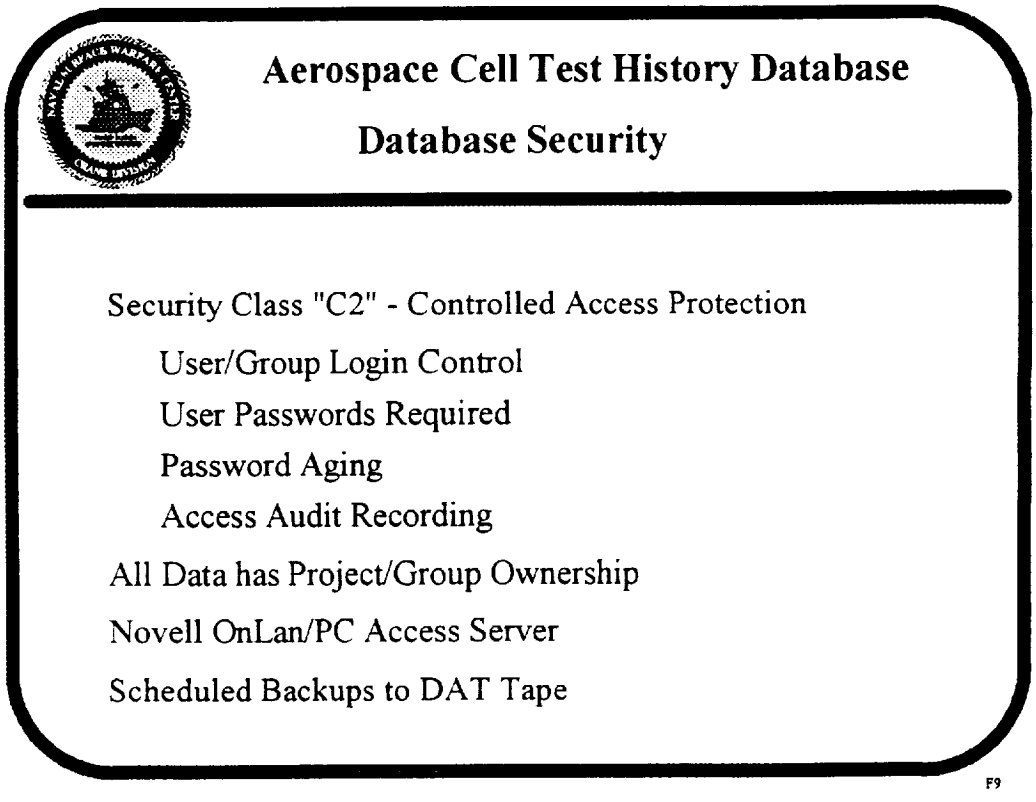

Security of the system is provided.

DEMONSTRATION - In the next few viewgraphs, I will show some the screens that you will see when using the system.

THESE VIEWGRAPHS WERE NOT INCLUDED IN THE PROCEEDINGS

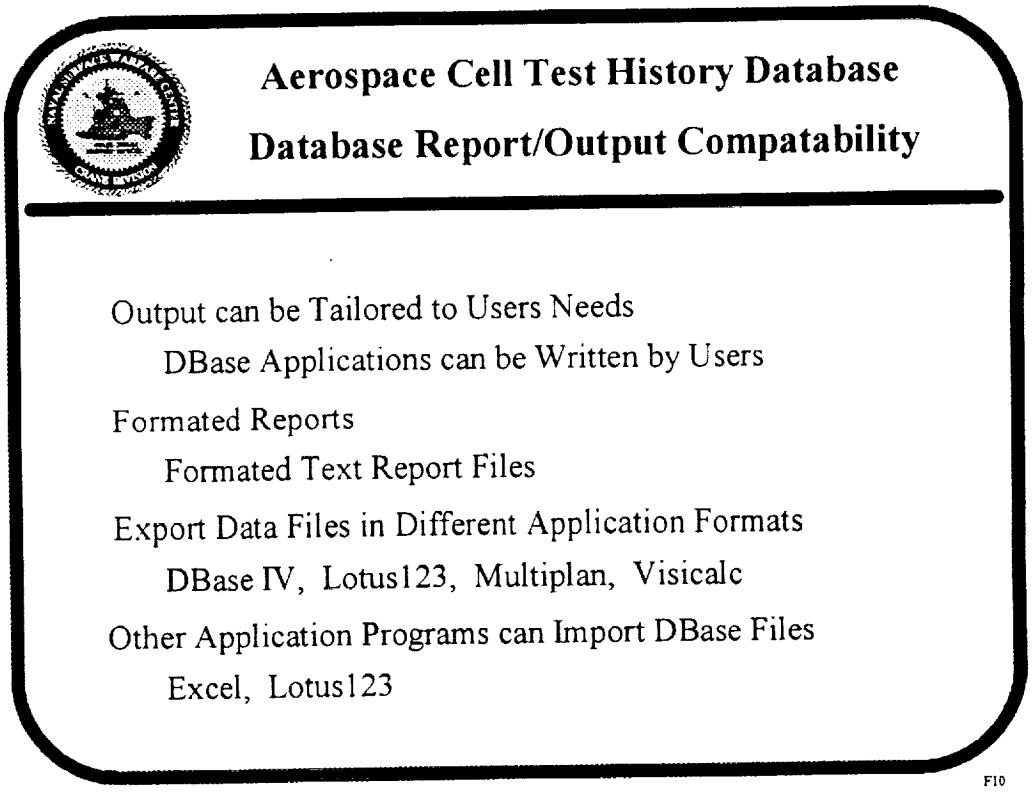

The output you obtain from the database can be used in many ways. Some of the more common that we anticipate are:

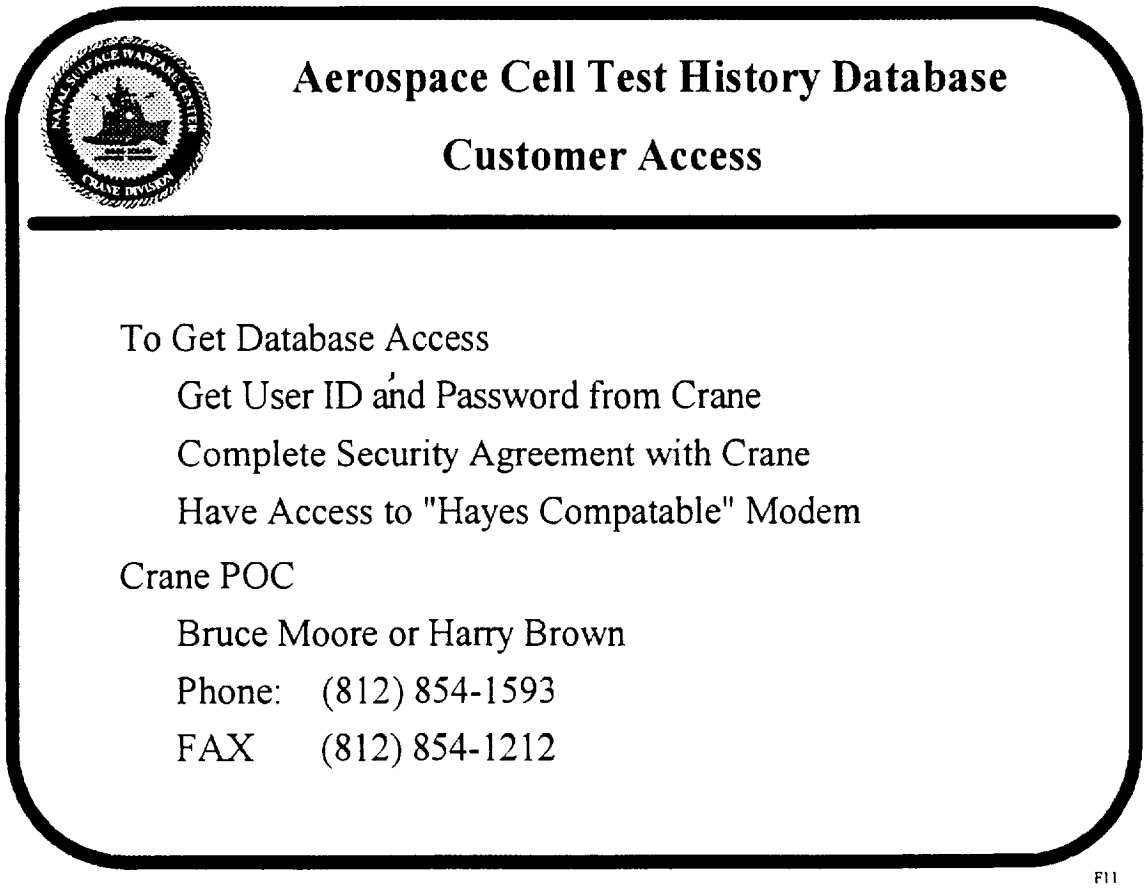

To gain access to the database you must agree to abide by the government regulation on electronic data transfer, agree to protect the data and to not publish or divulge any data, results or analysis without the consent of the program manger or owner of the project. If these conditions are acceptable, you may request access from (SEE Viewgraph) You also must get specific access approval from the project manager or owner of the data.

ADVANCED ENERGY STORAGE FOR SPACE APPLICATIONS A FOLLOW - UP

JPL

GERALD HALPERT
SUBBARAO SURAMPUDI

1993 NASA BATTERY WORKSHOP
NASA/MARSHALL SPACE FLIGHT CENTER
HUNTSVILLE, ALABAMA
NOVEMBER 16, 1993

AGENDA / OVERVIEW

- FUTURE SPACE MISSIONS
- OVERVIEW AND PERFORMANCE CHARACTERISTICS OF ADVANCED BATTERY TECHNOLOGIES
  - PRIMARY BATTERIES
  - RECHARGEABLE BATTERIES
- JPL EXPERIENCE WITH ADVANCED BATTERIES

CATEGORIES OF SPACE MISSIONS USING BATTERIES

- **PRIMARY CELL APPLICATIONS**

  LAUNCH VEHICLES
  PROBES AND PENETRATORS
  SHUTTLE EXPERIMENTS
  PLANETARY STATIONS

- **RECHARGEABLE CELL APPLICATIONS**

  LOW EARTH MISSIONS
  GEOSYNCHRONOUS ORBIT MISSIONS
  ROVERS
  PLANETARY STATIONS

BATTERY CHALLENGES

- REDUCED WEIGHT
- REDUCED VOLUME
- INCREASED OPERATIONAL LIFE
- INCREASED SPECIFIC POWER AND POWER DENSITY
- INCREASE ACTIVE STORAGE AND CHARGE RETENTION
- EXTEND OPERATION TO EXTREME ENVIRONMENTS

C-2

PROPERTIES OF SOA AND ADVANCED PRIMARY BATTERIES

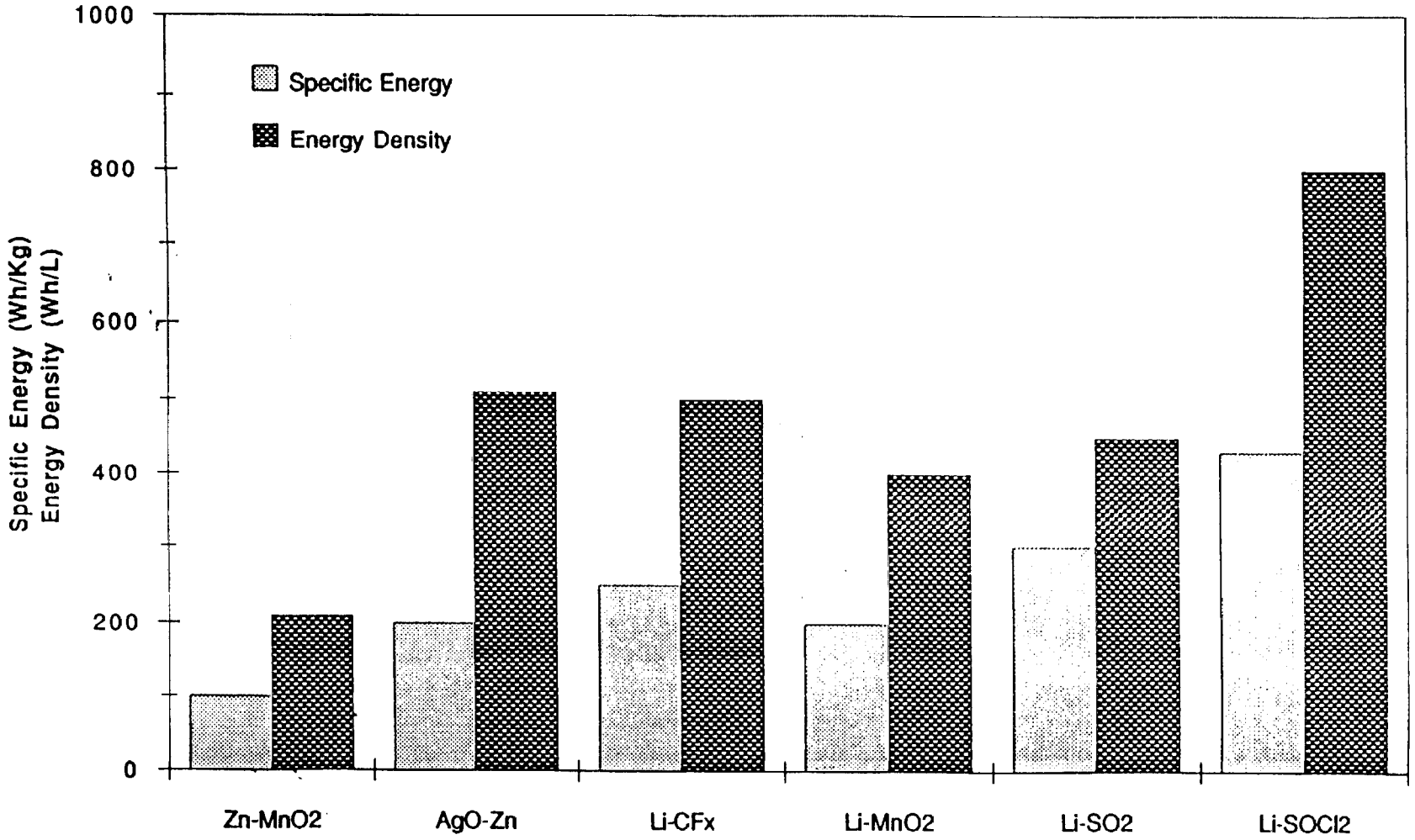

LITHIUM PRIMARY CELL APPLICATIONS

- CREW EQUIPMENT, TOOLS, EXPERIMENTS
  - EXTRAVEHICULAR MOBILITY LIGHT (1 Li - BCX)
  - EXTRAVEHICULAR MOBILITY TV (8 Li - BCX)
  - ACCELEROMETER RECORDING UNIT (2, 3 C Li - BCX)
  - CASSETTE DATA TAPE RECORDER (2 Li - BCX)
  - MINIOSCILLOSCOPE ((4 D Li - BCX)
  - ULTRASONIC LIMB PLETHYSMOGGRAPH (2 Li - BCX)
  - PRC - 112 MILITARY RADIO (3 C Li - BCX)
  - CAMCORDER, CAMERA, PRIMARY POWER, PAYLOADS (Li - X)
    WHERE X = $SOCl_2$, SO_2, CFx, MnO_2, I, Ag_2CrO_4

- RANGE SAFETY (4, 28V Li - CFx)

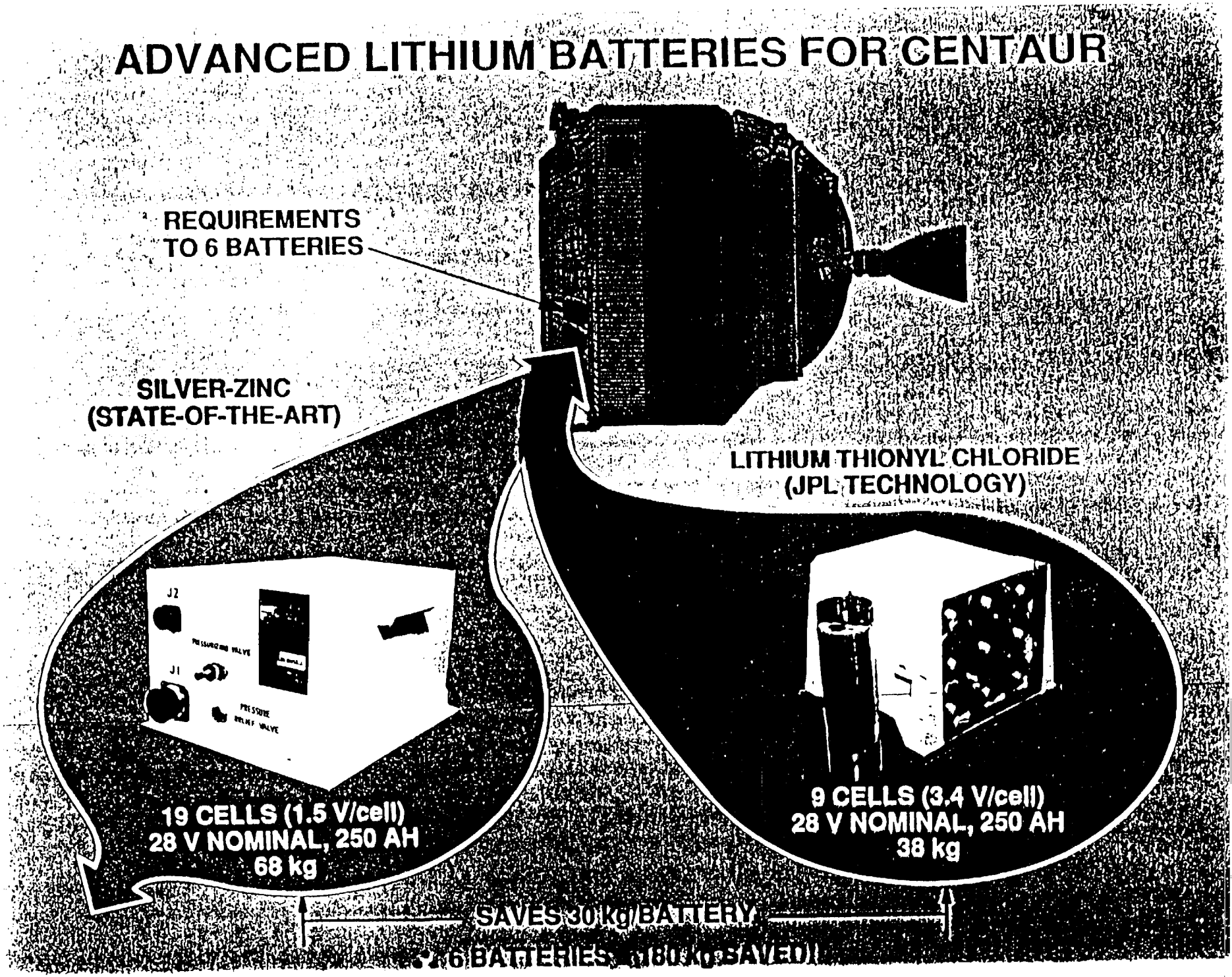
ADVANCED LITHIUM BATTERIES FOR CENTAUR
REQUIREMENTS
TO 6 BATTERIES
SILVER-ZINC
(STATE-OF-THE-ART)
LITHIUM THIONYL CHLORIDE
(JPL TECHNOLOGY)
J2
J1
19 CELLS (1.5 V/cell)
28 V NOMINAL, 250 AH
68 kg
9 CELLS (3.4 V/cell)
28 V NOMINAL, 250 AH
38 kg
SAVES 30 kg/BATTERY
x 6 BATTERIES = 180 kg SAVED!

ADVANCED RECHARGEABLE BATTERY APPLICATIONS

LEO	GEO	PLANETARY
Ni- MH ?	Ni-MH	Ni - MH
Na - S	Na - S	Li - ION
Na - $NiCl_2$	Na - $NiCl_2$	Li - TiS_2
	Li - ION	Li - POLYMER
	Li - TiS_2	
	Li - POLYMER	

SPECIFIC ENERGY OF RECHARGEABLE CELLS AND BATTERIES

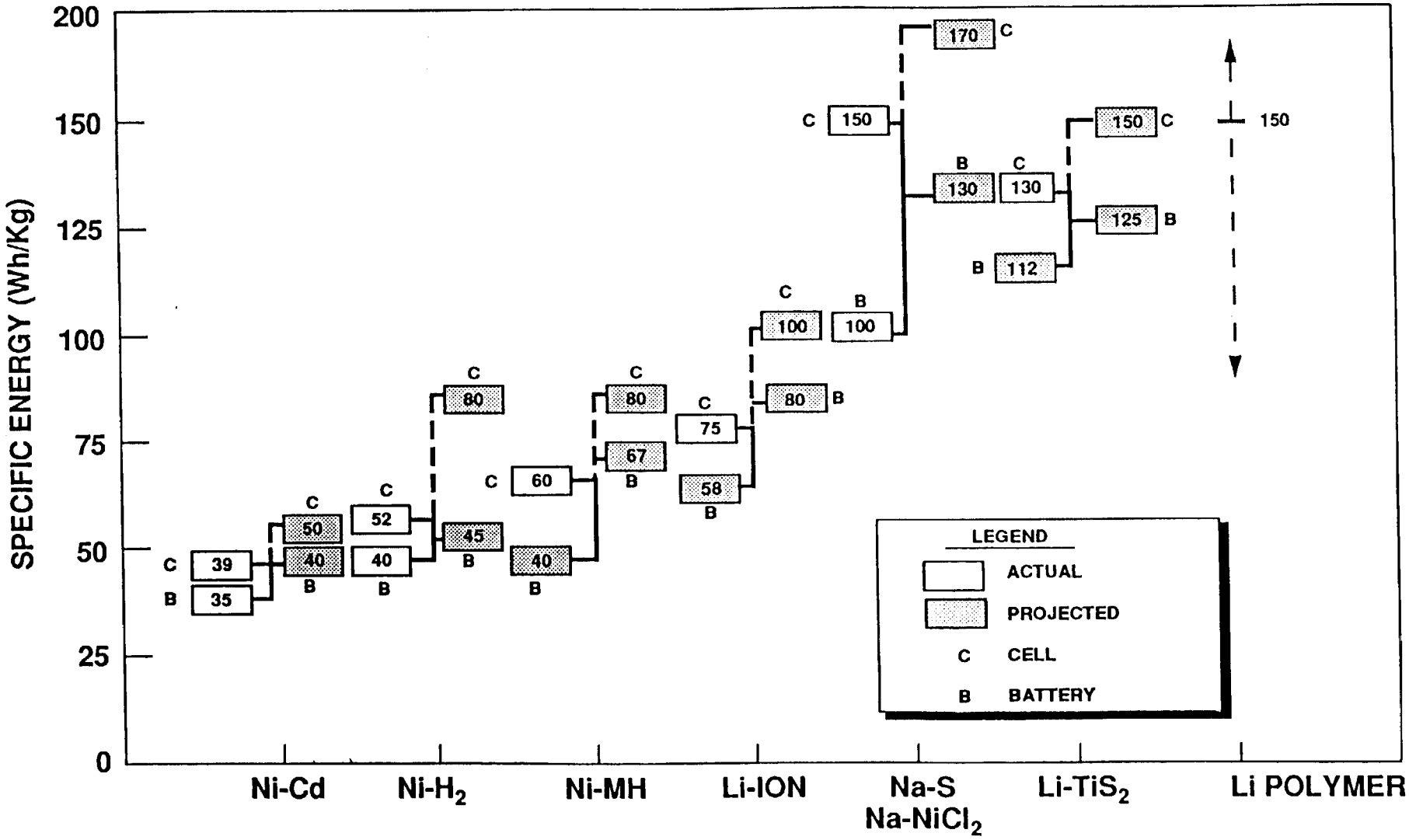

ENERGY DENSITY OF RECHARGEABLE CELLS AND BATTERIES

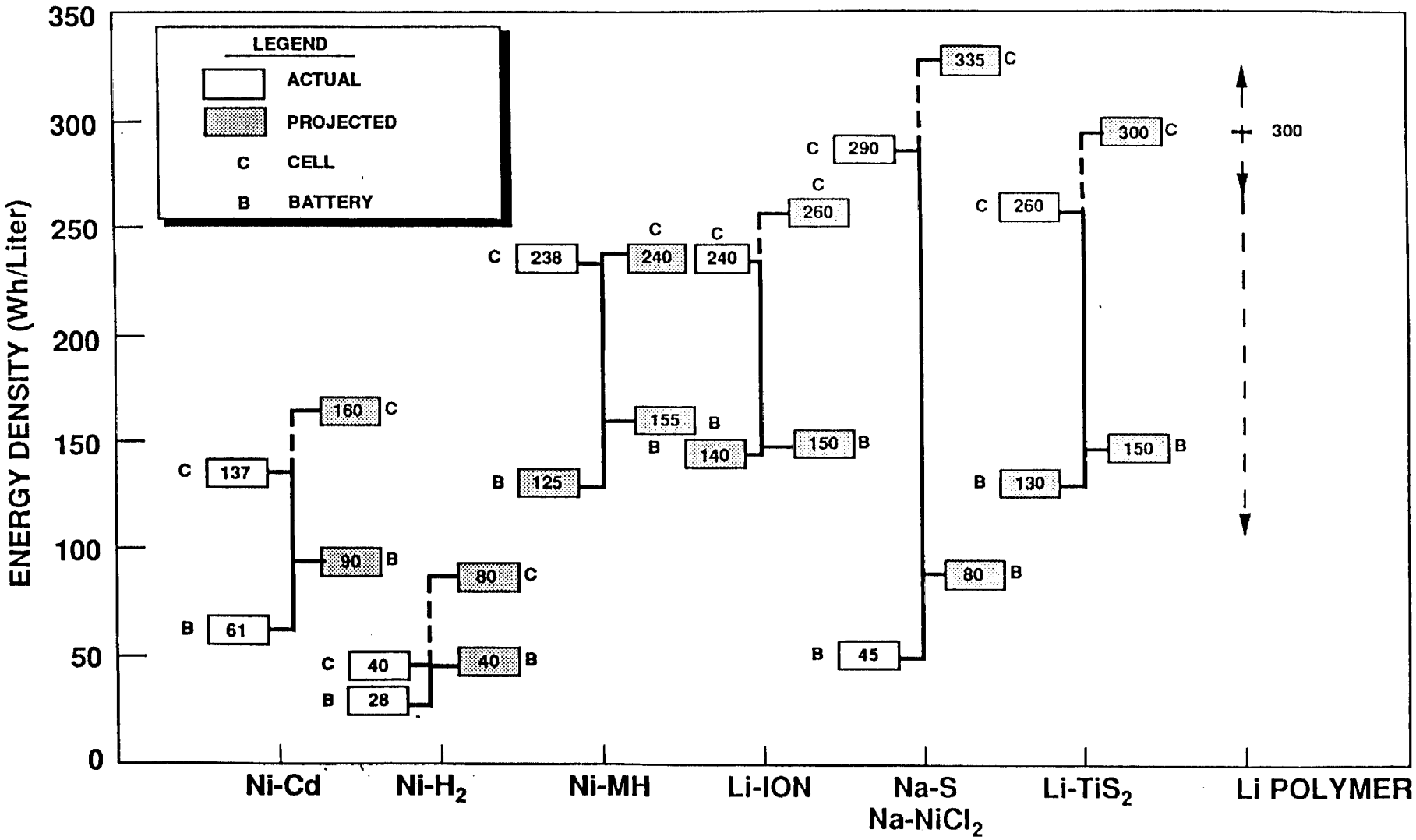

PRESENT LIMITATIONS OF ADVANCED BATTERY TECHNOLOGIES

- SMALL - MEDIUM CAPACITY CELLS ARE AVAILABLE
- TO DATE ADVANCED BATTERIES ARE HANDMADE OR BATCH PROCESSED
- CYCLE LIFE GENERALLY LIMITED TO 1000 CYCLES
- ADVANCES IN CHARGE CONTROL NEEDED TO BALANCE CELLS IN BATTERY
- SAFETY AND ABUSE AFFECTS NOT WELL KNOWN

STATUS OF Li-TiS_2 CELL TECHNOLOGY

Schematic Diagram of a Li-TiS_2 Cell

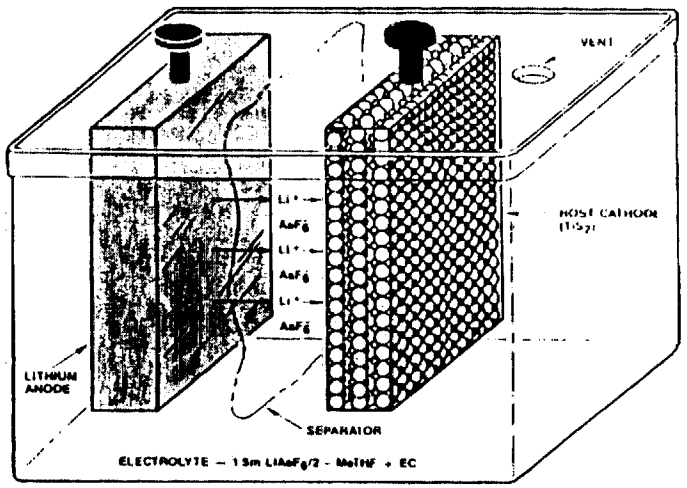

Specific Power vs Specific Energy

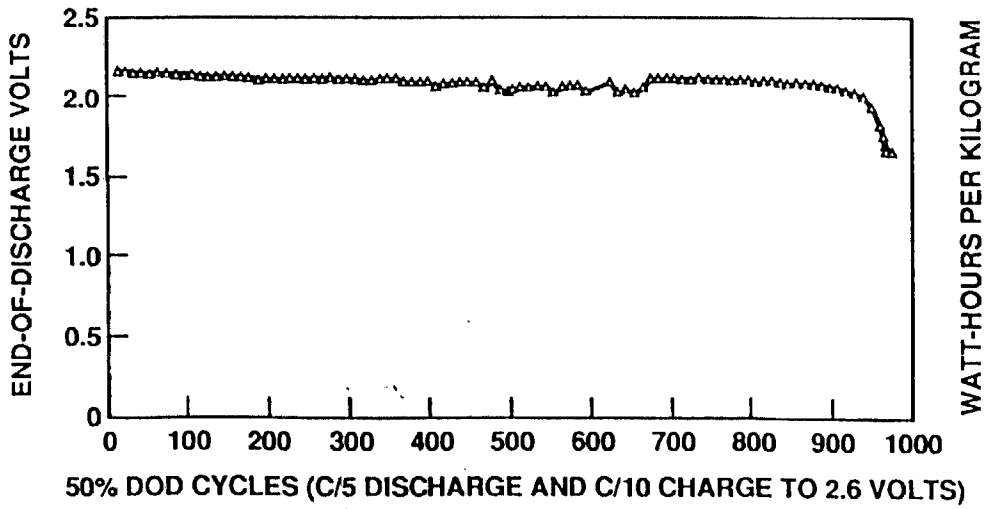

Cycle Life Performance

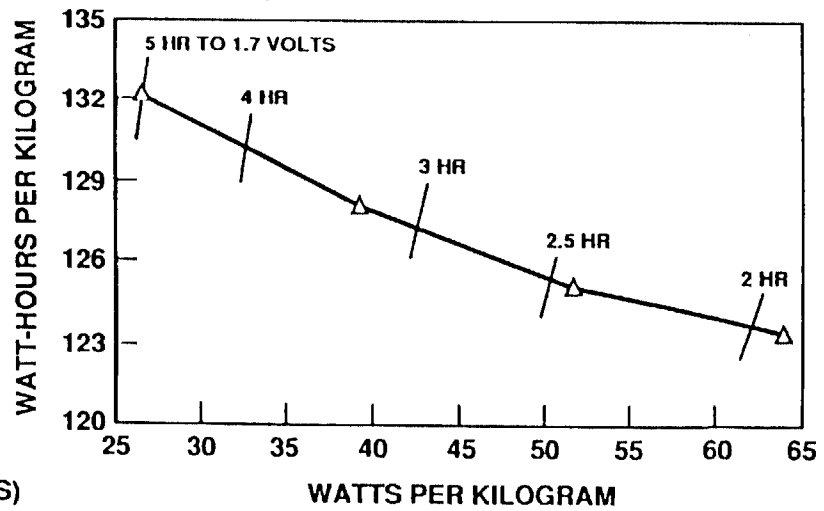

STATUS OF Li ION CELL TECHNOLOGY

CARBON MATERIALS UNDER STUDY

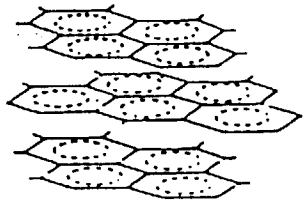

GRAPHITE

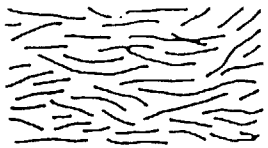

PETROLEUM COKE

PITCH-BASED CARBON FIBER

REVERSIBLE Li CAPACITY OF SELECTED CARBONS

• PITCH COKE:	0.070 Li PER CARBON
• PETROLEUM COKE:	0.057 - 0.077 Li PER CARBON
• CARBON FIBER:	0.097 Li PER CARBON
• GRAPHITE:	0.124 Li PER CARBON

* PAN FIBER HAS VERY SLOW RATE CAPABILITY

INTERCALATION & DE-INTERCALATION OF Li IN GRAPHITE

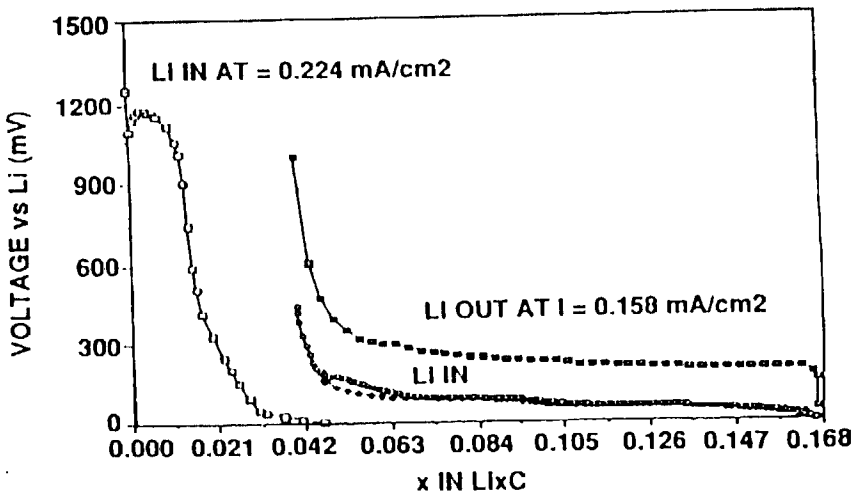

STATUS OF Li-TiS_2 CELL TECHNOLOGY

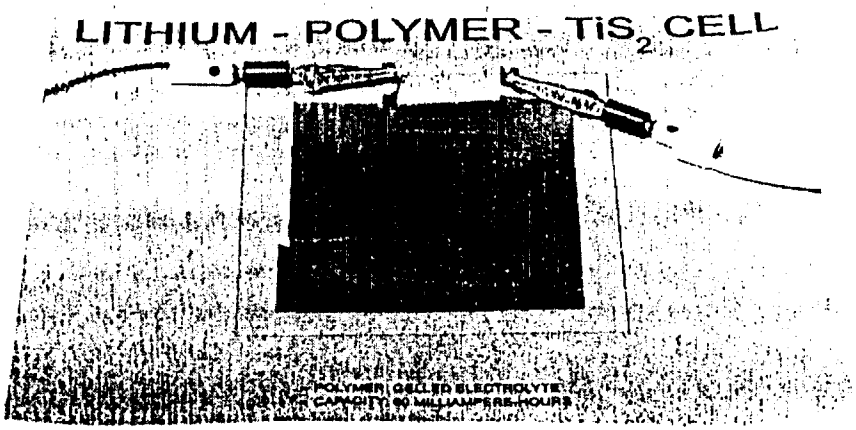

PROPERTIES OF JPL Li/POLYMER ELECTROLYTES

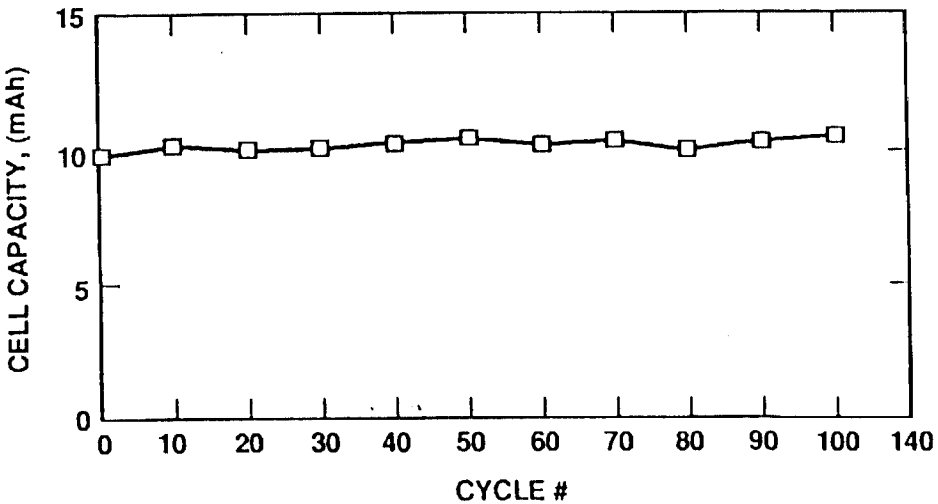

CYCLE LIFE OF Li-TiS_2 CELL

ELECTROLYTE	CONDUCTIVITY (S/CM) RT 90°C	LI TRANSPORT #	ELECTROCHE WINDOW (V)	Li CYCLING EFFICIENCY (%)
PEO/12-CR4/LIBF$_4$	10^{-8} 8X10^{-4}	0.2-0.4	1.4-4.6	88-93%
PEO/LII/Al_2O_3	--- 8X10^{-5}	0.8-1.0	1.4-3.7	88-93%
ENVIBAR/EC-DEC/LIAsF$_6$	2X10^{-3} - - - -	0.2-0.4	1.4-4.3	87-93%

STATUS OF THE Ni-MH CELL TECHNOLOGY

MH MATERIALS UNDER STUDY

- $LaNi_5$ (5978)
- $LA_{0.3}Ce_{0.51}Pr_{0.07}Nd_{0.13}Ni_{3.56}Co_{0.76}Mn_{0.4}Al_{0.3}$ (6025)
- $La_{0.25}Ce_{0.55}Pr_{0.07}Nd_{0.13}Ni_{3.68}Co_{0.75}Mn_{0.4}Al_{0.34}$ (6062)
- $La_{0.64}Ce_{0.25}Pr_{0.04}Nd_{0.08}Ni_{3.51}Co_{0.77}Mn_{0.4}Al_{0.31}$ (6039)
- $La_{0.49}Ce_{0.20}Pr_{0.09}Nd_{0.22}Ni_{3.05}Co_{1.50}Al_{0.53}$ (6077)
- $MmNi_{3.5}Co_{0.8}Mn_{0.4}Al_{0.3}$ (IBA MH NO 5)
- JPL/CALTECH/JPL MATERIAL

PERFORMANCE OF 250 mAh Ni-MH CELLS DURING CYCLING

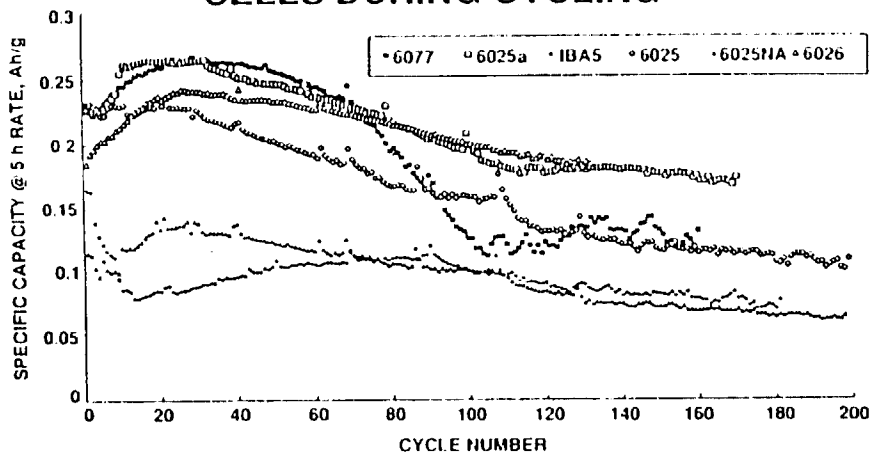

VARIATION OF CAPACITY WITH Mn COMPOSITION AND CYCLING

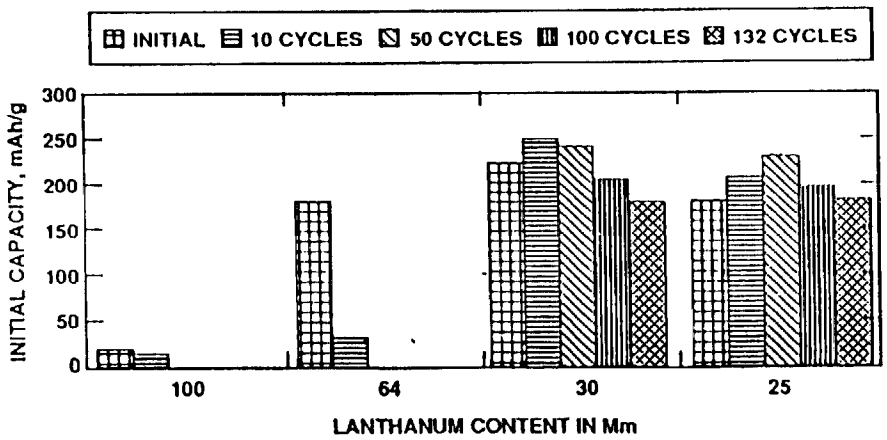

SPECIFIC CAPACITIES OF MH ALLOYS

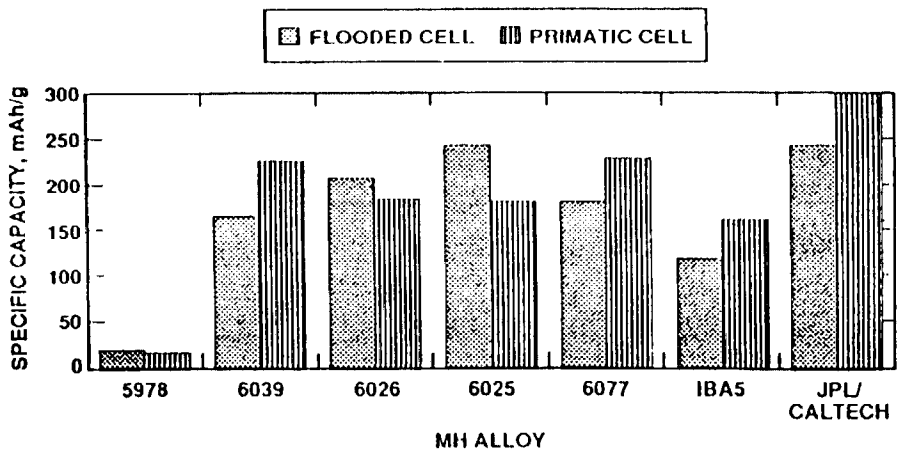

STATUS OF Na -$NiCl_2$ CELL TECHNOLOGY

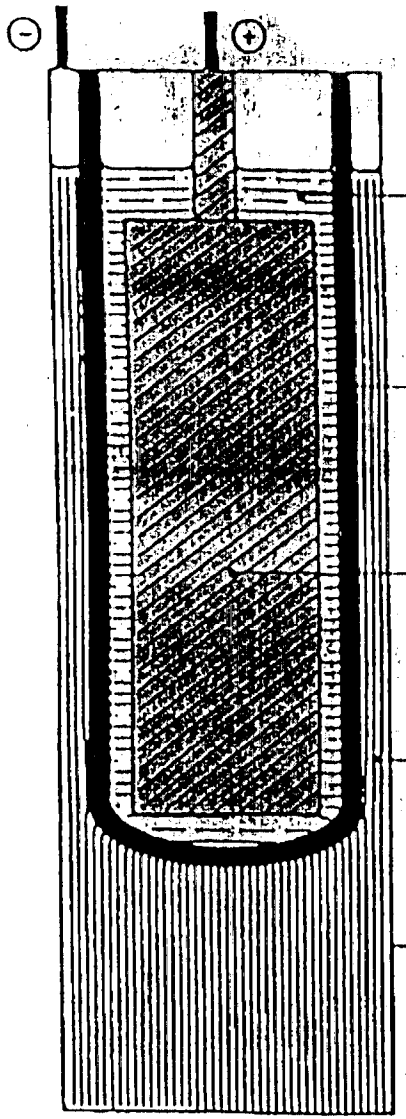

$NaAlCl_4$ FUSED SALT ELECTROLYTE

BETA ALUMINA CERAMIC TUBE ACTING AS Na^+ ION SOLID ELECTROLYTE AND SEPARATOR

POROUS M / MCl_2 CATHODE

LIQUID SODIUM

CELL CASE

CYCLE LIFE OF 2 Ah Na -NiCl2 CELLS WITH DIFFERENT ADDITIVES

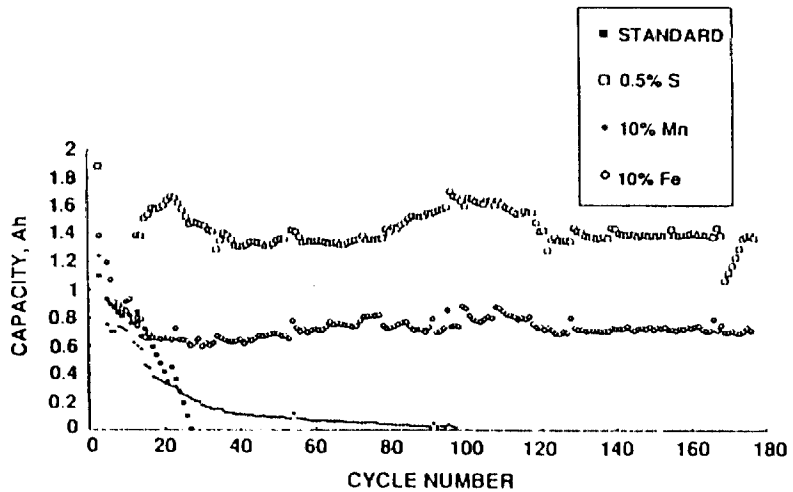

PROJECTED PERFORMANCE ENEVELOPE STATE OF ART AND ADVANCED CELLS

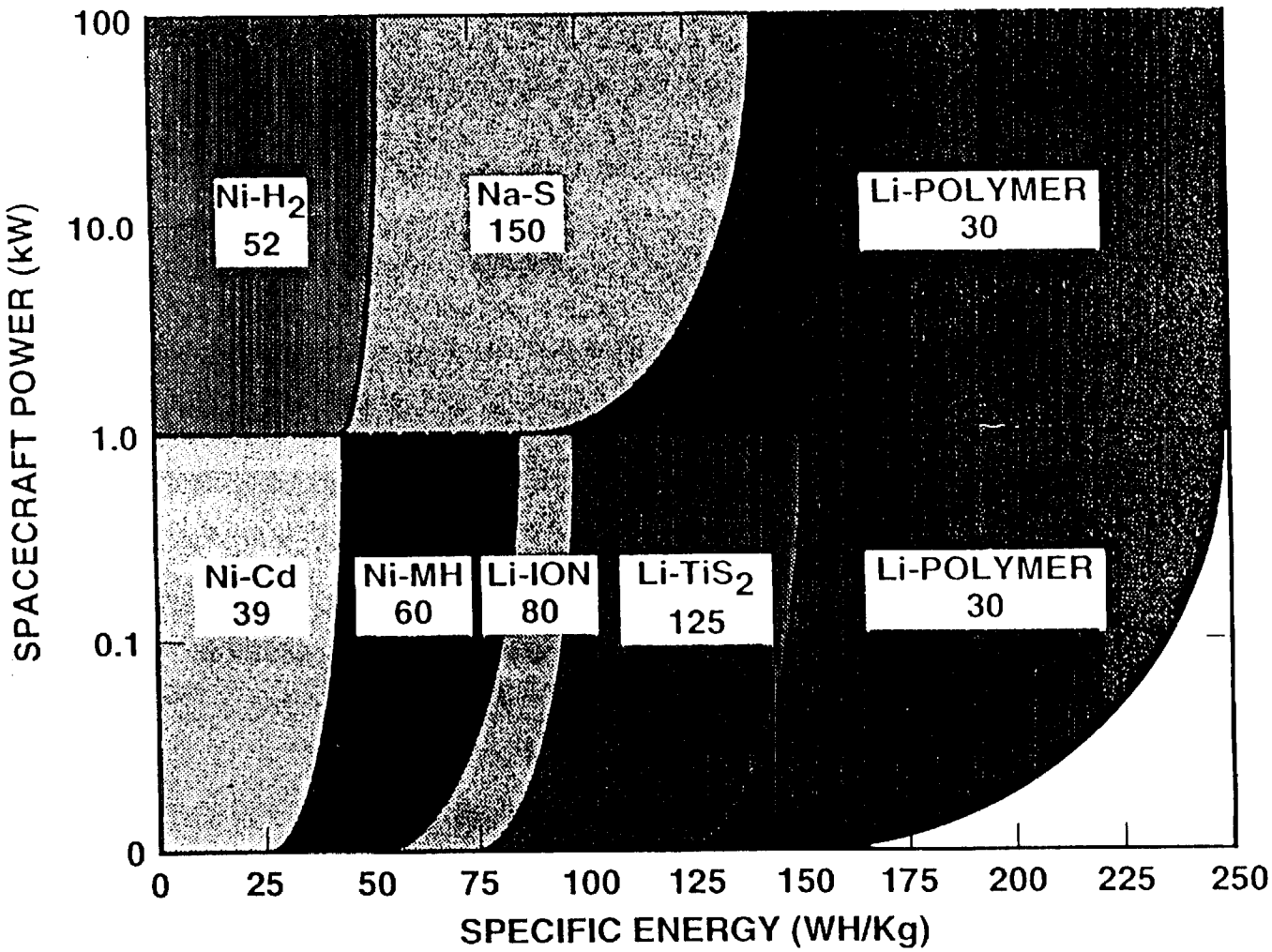

SUMMARY

- FUTURE SPACE MISSIONS REQUIRE LIGHTER WEIGHT, SMALLER VOLUME, HIGHER ENERGY BATTERIES ("SMALLER, CHEAPER ,BETTER")

- SEVERAL ADVANCED BATTERY SYSTEMS ARE UNDER DEVELOPMENT

- SEVERAL, PRIMARY LITHIUM BATTERY SYSTEMS ARE IN USE

- SELECTION OF THE NEW RECHARGEABLE SYSTEMS REQUIRES ADDED CYCLE LIFE AND BATTERY PERFORMANCE DEMONSTRATION

ACKNOWLEDGEMENT

- THE AUTHORS ARE APPRECIATIVE OF THE SUPPORT OF NASA HEADQUARTERS CODE C AND CODE Q FOR THIS EFFORT

- THE BATTERY SYSTEM COMPARATIVE DATA WAS DERIVED FROM REPORTS IN:
  - THE 1991-3 NASA BATTERY WORKSHOP PROCEEDINGS
  - THE 1991 AND 1993 SPACE ELECTROCHEMICAL RESEARCH AND TECHNOLOGY PROCEEDINGS

EXPERIMENTAL EVALUATION OF BATTERY CELLS FOR SPACE-BASED RADAR APPLICATION

Craig A. Maskell

Defence Research Establishment Ottawa
Department of National Defence
3701 Carling Avenue
Ottawa, Ontario, K1A 0K2
Canada

John R. Metcalfe

Engineering and Quality Group
CAL Corporation
1050 Morrison Drive
Ottawa, Ontario, K2H 8K7
Canada

Abstract

A test program was conducted to characterize five space-quality nickel-hydrogen (NiH_2) battery cells. A subset of those tests was also done on five commercial nickel-cadmium (NiCd) cells, for correlation to the characteristics of an Energy Storage Unit Simulator. The test program implemented the recommendations of a 1991 study, as reported to IECEC-92. The findings of the tests are summarized, and expected impacts on the performance of the electrical power system (EPS) of a large space-based radar (SBR) surveillance satellite are derived. The main characteristics examined and compared were terminal voltage (average and transient) and capacity through discharge, equivalent series resistance, derived inductance and capacitance, charge return efficiency and inter-pulse charge effectiveness.

Introduction

Space-based radar needs a pulsed waveform and high power to detect targets, at long ranges against earth clutter. Many of the potential mission and radar profiles impose stringent requirements on the satellite's EPS. In many proposed concepts, for example, the radar coverage does not allow a sun-synchronous orbit, so the solar array must be augmented by a large battery. In addition, studies have shown that it is most efficient to supply most of the energy used by the radar from a battery — even during sunlit operation. Such SBR EPS concepts generally have battery charge/discharge pulse periods of 5-50 ms at duty cycles of 50% [1][2].

This SBR EPS concept configures up to 12 identical but independent sections, called power module strings, each to draw power from its own section of the solar array, contain its own battery and conditioning equipment, and feed a portion of the radar antenna. The batteries feed all loads during eclipse and provide about 70% of the radar power during sunlight. The solar array provides power to charge the battery between transmit bursts and when the radar is off. A module string battery is connected directly to the unregulated main transmission bus, with a nominal voltage of 120 V dc.

The discharge rate will be as high as 3C during radar transmit bursts. There may be up to a 0.8C charge rate available between those bursts. Assurance of good transient regulation of the bus is a major concern. Under such conditions, regulation is greatly influenced by the effective series resistance (ESR) and ac impedance characteristics of a 100-cell battery.

Terminal voltage (both average and transient) and capacity during discharge are important considerations. ESR, ac impedance characteristics, and charge return efficiency are parameters in predicting such performance factors.

NiH_2 battery cells are prime candidates for a first-generation SBR. In particular, NiH_2 cells have been demonstrated to have long cycle life at favorable depths-of-discharge. However, a study published in early 1992 revealed that their characteristics under the envisaged pulsed-loading were virtually unknown [1]. Until then, test programs generally looked at the performance, electrical characteristics, or life-cycle prediction under dc conditions. During the last year or so, however, some pulsed-mode tests have been done [3][4]. At least one cell manufacturer (Eagle-Picher Industries, Inc.) has also done some similar testing. Our test program extends this fledgling information base, with the parameters of the SBR EPS configuration in mind [1]. The results confirm that some of the critical performance variables of the cell, and consequently the battery, are markedly affected by this type of operation.

Our experimental evaluation had the following objectives:

- Determine various electrical characteristics of NiH_2 cells under representative pulsed-loading.
- Quantify the NiH_2 cell type's charge return efficiency and cell effective capacity.
- Detect anomalies or signs of NiH_2 cell degradation, but without cycle life testing.
- Compare the characteristics of the NiH_2 cells to commercial-type NiCd cells of similar capacity, to facilitate correlations with the Energy Storage Unit of a ground-based demonstration system.
- Predict EPS performance impacts of findings.

Table 1 — Description of the two types of battery cells tested under the evaluation program.

Cell Type	NiH_2	NiCd
Manufacturer	Eagle-Picher Industries, Inc.	SAFT Batteries Ltd.
Model No.	RNH 50-47 CAL	SHP 520
No. of Sample Cells	5	5
Rating (nameplate), Ah	50	52
Other features	• spaceflight quality • individual pressure vessel • 8.9 cm (3.5 inch) diameter; 1.5 kg • electrolyte concentration 27% KOH • positive (nickel) pre-charge • "rabbit-ear" terminal configuration	• commercial professional quality • electrolyte-flooded, vented • 8.5 x 8.5 x 27.0 x 26.4 cm • 3.6 kg • electrolyte: 20% KOH • single-ended terminal config.

Laboratory Set-Up

The test activities were carried out at CAL Corporation, Ottawa, Ontario. The NiH_2 and the NiCd cells (two series-connected strings tested consecutively) are described in Table 1. The installation centered on the facility's temperature control chamber — into which the test items on their fixture were placed. The facility included appropriate power connections, lighting, exhaust ducts and ventilation louvers. Provisions for safety and hazard control included a chamber hydrogen monitor and nitrogen purge equipment.

During all characterization cycles, the cell case temperatures were kept within ±2°C of the respective values specified for the NiH_2 and NiCd cells. For both cell types, auxiliary fans were placed to assist temperature regulation during high rate discharges.

To prevent unintentional electrical contact, the cases of the NiH_2 cells were conformally coated prior to installation in their heat-conductive mounting saddles.

Figure 1 shows the functional elements of the test system. The inter-pulse charging in some test cycles was accomplished by applying a constant current bias from the charger supply. The pulse generator drive level to the electronic load was set for the desired net cell current during the discharge pulses. This direct interconnection of the charger supply to the load and the test cell string resulted in some rounding of current transition edges due to regulating feedback loop, and output filter capacitance, of the charger supply. To get a response more representative of the intended application, at least for the load-off transition, a high-power schottky diode was installed in series with the supply's output.

Fig. 1 — Overview of the main functional elements of the battery cell test system.

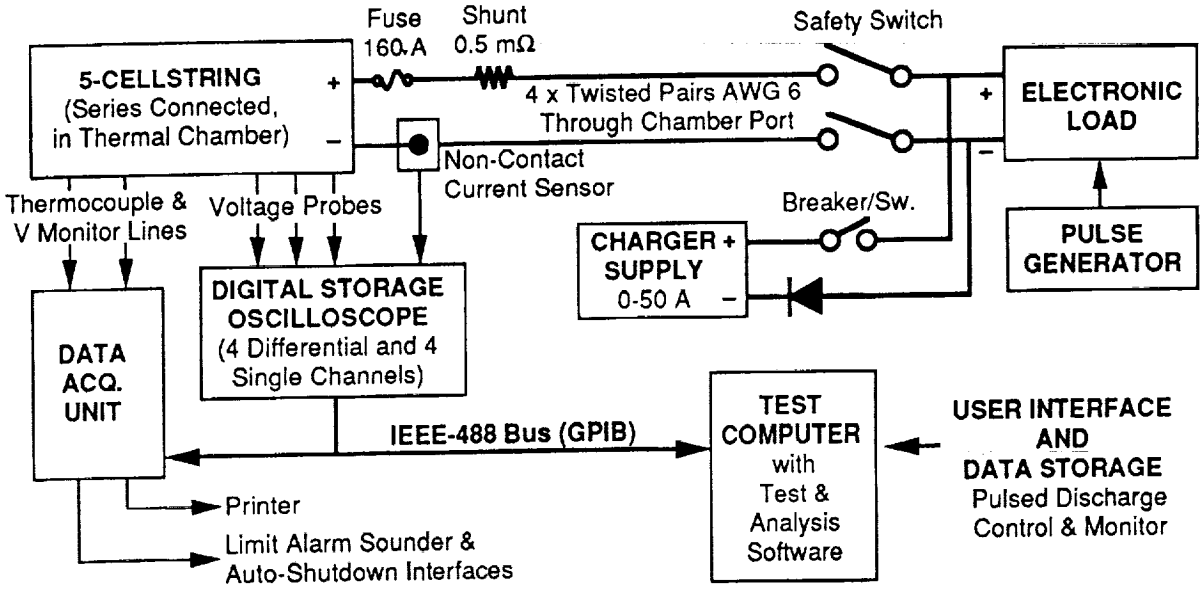

Test Procedures and Analysis Methods

The NiH_2 cell characteristics were influenced by the following test parameters:

- Discharge Rate - pulsed (1-3C rates) & dc (1C and 2.5C rates) conditions
- Charge Rate - dc conditions only (at 0.5C and 0.8C rates, with step-down)
- Pulse Length (5, 20 & 40 ms "half-cycle")
- Current Rise/Fall Time (0.2-1.5 ms)
- Inter-Pulse Charge Rate (0.3-1.0C rates)

The NiCd cells were subjected to a limited subset of the parameters. The nominal test temperatures were restricted to 0°C for the NiH_2 cells and 10°C for the NiCd cells. Other cell types, and pulsed-mode life testing, were not explored. To further limit the number of test steps, the effects of changing only one variable at a time were tested, for a fixed set of the other variables.

A step-down in the charge rate was implemented during recharge of the cells. This was found necessary to limit cell voltage to a "safe maximum", and to provide an assessment point for consistency of cycle-to-cycle voltage versus state-of-charge (SoC).

SEQUENCE OF TESTS — Testing was done in 1992/93 in the following phases:

a. Initialization cycles of the NiH_2 cells; for re-activation and for comparison of reference capacity with that measured in acceptance testing.

b. Non-pulsed ("dc") characterization cycles of the NiH_2 cells; with combinations of 0.5C or 0.8C initial charge rates and 1C or 2.5C discharge rates through 1.0 V per cell.

c. Pulsed-discharge characterizations of NiH_2 cells; one load pulse amplitude, for three values of half-cycle time (load pulse width), versus two values of recharge rate, with and without inter-pulse charging.

d. Pulsed-discharge characterizations of the NiH_2 cells; one value of half-cycle time, for three values of load pulse amplitude, versus two values of recharge rate, with and without inter-pulse charging.

e. Pulsed-discharge characterizations of the NiH_2 cells; one value of half-cycle time and one of load pulse amplitude, versus four values of load current transition time, with and without inter-pulse charging.

f. Pulsed-discharge characterizations of the NiH_2 cells; one value of half-cycle time and one of load pulse amplitude, versus two values of inter-pulse charge rate.

g. Pulsed-mode and non-pulsed-mode capacity checks of the NiH_2 cells.

h. Activation cycles of the NiCd cells ; low-rate, non-pulsed.

i. Non-pulsed ("dc") characterization cycles of the NiCd cells; with 0.5C initial charge rate and 2.5C discharge rate through 1.0 V per cell.

j. Pulsed discharge characterization cycles of NiCd cells; with the "standard parameter set" of charge rate, load pulse width, amplitude and current transition time, with and without inter-pulse charging.

k. Non-pulsed-mode capacity check of NiCd cells.

Fig. 2 — Depiction of typical pulsed-discharge record "snapshot".

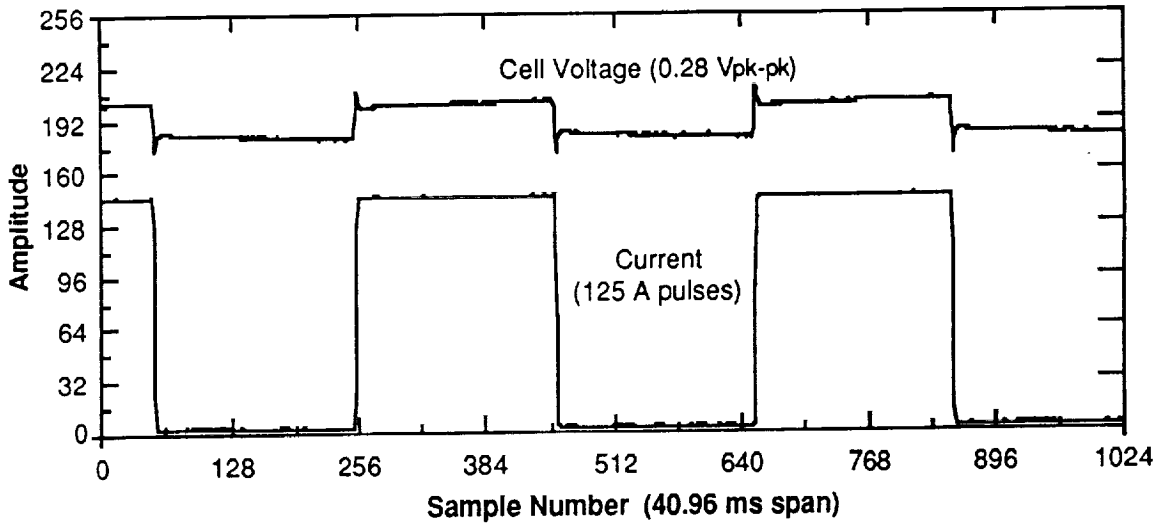

DATA ACQUISITION & STORAGE — During pulsed-discharges, periodic wave-form "snapshots" from the digital storage oscilloscope were stored as ASCII files on the hard disk of the Test Computer, as shown in the example in Fig. 2. After each day of testing the files were copied onto floppy disks. These snapshots were formatted for easy loading into spreadsheet and graphing programs. Generally, two columns containing from 1024 to 5001 amplitude values of current and voltage, respectively, were stored.

Each data file has a header containing the record number and, the date, time, cell string current, cell voltages and cell temperatures, as transferred from the data acquisition unit just prior to capturing the oscilloscope trace. Eight different record types were stored, in sequence, for most discharges. The voltages of all five cells, and the cell string, were recorded individually with several combinations of resolution of sample time and amplitude.

Non-pulsed data, such as from dc charging, was hardcopy-printed at regular intervals.

DATA RESOLUTION EFFECTS — The accuracy of the results was limited by test equipment effects such as the electronic load's current regulation behaviour, and the ability to reduce measurement data during analysis. We improved our analysis tools to improve the typical quantizing resolution from 7 mV / 100 µs to 3.5 mV / 10 µs. In determining plateau currents and voltages, and in estimating cell resistances, averaging and/or iterating techniques further reduced granularity and improved accuracy.

ANALYSIS METHODS — Two main methods were employed. The Observed Results Method is suited for tabulation of larger quantities of calculated voltages, currents and times, and the resulting first-order approximations of effective series resistance (ESR) and effective series inductance (ESL). The Equivalent Model Method is an iterative process which concentrates on a smaller number of snapshot records to produce more accurate values of the various impedance characteristics, including an estimate of the capacitive component.

The two analysis methods are complementary. For example, correction factors obtained from a few runs of the Equivalent Model Method can be applied to many values tabulated from the Observed Results Method. All calculations were done on recent versions of well-known spreadsheet programs.

EQUIVALENT MODEL ANALYSIS METHOD — This method could be the subject of a separate paper. (This is a cursory description only.) The technique is intended to determine the values applicable to an equivalent circuit model of the cell under scrutiny.

We first postulated that the model would consist of a voltage generator (electromotive force - emf), a resistive element (ESR), and an inductive element (ESL), all connected in series. During the course of the analysis the necessity of including a further element became clear. A capacitive element (EPC) was thus added in parallel with the series combination of emf and ESR, shown in Fig. 3.

Fig. 3 — Final equivalent circuit model of a cell. The model does not include a possible second-order capacitance in parallel with the circuit, being barely detectable within the resolution of the data taken.

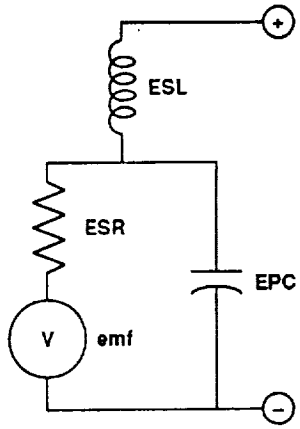

The values of ESR, ESL, EPC and emf can only be considered as constants for the particular set of conditions at the time the record was taken. By determining values for these variables at various spot-points of a pulsed discharge, it is possible to relate their variations to SoC, and consequently to interpolate the dynamic performance over the whole discharge range.

The Equivalent Model Method evaluates the elements one at a time and subtracts the effects of that element from the original voltage vs. time data. Typically, the value of the current multiplied by the ESR is first subtracted to produce a new record showing only emf and reactive-component voltage effects. This reveals more clearly the effects of ESL and enables its value to be estimated. Similarly, the effect of inductance is then removed, enabling an estimation of EPC.

After making any corrections necessary to time-synchronize the current and voltage data columns, the data values are converted to engineering units and plotted one against the other. The best straight line for the resistive component is visually estimated. The variations from that line are the reactive components of the cell.

The ESR estimate is multiplied by the current of each sample point and the result subtracted from the sample voltage. This yields the constant (emf) component and the sum of the reactive components.

Fig. 4 — Example "eye" diagram for calculation of inductance.

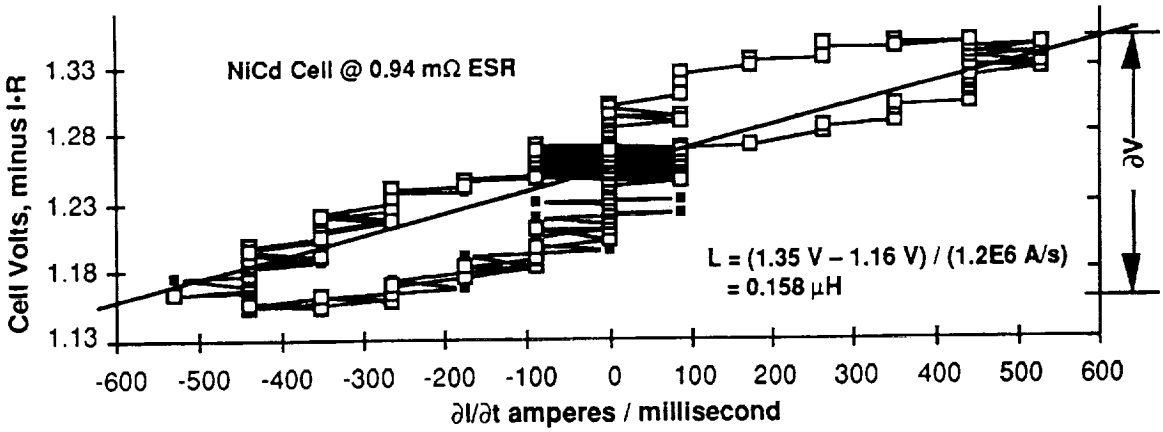

The value of the inductance is then estimated from a plot of the $\partial I/\partial t$ value vs. the I*R product for each data sample (Fig. 4). The slope of the best straight line over the $\partial I/\partial t$ range then gives a ∂V value for use in computing inductance.

The time constant of the parallel RC circuit, resulting from the voltage generated across the ESR by the load current turning on and off, is then estimated. This involves a limited amount of averaging to filter the high frequency "noise" caused by the quantization levels of the digital storage oscilloscope. The decay is plotted. Dividing the time constant by the cell's ESR provides an estimate of the effective capacitance.

Cross-checking and result-refinement methods were also incorporated in the analysis. For example, the chart used to estimate the capacitance provided a sensitive tool for improving the resistance estimate. We could more accurately define the points where reactive effects have dissipated on the load-on and load-off pulsed-voltage profiles of the cell.

OBSERVED RESULTS ANALYSIS METHOD — This method assumes no equivalent circuit model for a cell, other than a series resistor for the ESR estimation and a series inductor for the inductance estimation. The "capacitive effect", as determined by the equivalent model method, is ignored for the ESR and L calculations here.

The Observed Results Method provides tables and plots to find overall voltage performance versus SoC (e.g., Fig. 5). It also provides rapid estimates of reactive components which can be correlated with the results of the equivalent model method.

The voltage plateaus (load-on and load-off) are defined here as the segments, in time, following observed recovery from the inductive spike and until just prior to the start of the next transition. The average voltage for each selected plateau period was computed. The ESR of the cell (for that part of the discharge) is the ratio of the difference between two successive average plateau voltages to the difference between two corresponding average current plateaus (converted to A). The ESR by this method is an "apparent ESR" because it still contains some of the complex components of plateau impedance (Fig.7).

Voltage recovery from an inductive spike is arbitrarily defined as the point where the data values representing the cell voltage do not vary more than ±1 bit in amplitude over three samples (usually just two or three samples into the period of settled current on the record). The converse definition applies to define the end of a voltage plateau before a transition.

Results and Discussion

The analyses of pulse plateau voltage and cell resistance showed that the capacitive time constant of the cell decreases the apparent ESR of the cell for the shortest test load-pulse width (5 ms). Better ripple-voltage performance thus results from shorter pulses.

No performance degradation or malfunction of any kind was detected in the NiH_2 cells. This was confirmed by examining cell round-trip efficiency, discharge capacity and mid-discharge voltage tabulated over the course of the testing.

Following are observed trends, from the overall results, in values of equivalent circuit elements versus state-of-charge:

- emf decreases with decreasing SoC, sharply from full charge, for both NiH_2 & NiCd cells.
- ESR increases at lower SoCs, for both the NiH_2 and NiCd cells tested.
- Inductance appears to *increase* slightly at lower SoCs — NiH_2 cells.
- Inductance appears to *decrease* slightly at lower SoCs — NiCd cells.
- EPC decreases gradually with decreasing SoC, for both the NiH_2 & NiCd cells tested (Fig.6).

Fig. 5 — NiH_2 discharge voltage profile, pulsed-mode standard vs. dc-mode standard conditions — one of several plotted from test results of different load current levels. SoC is referenced to 1 V EODV defining 100% discharge.

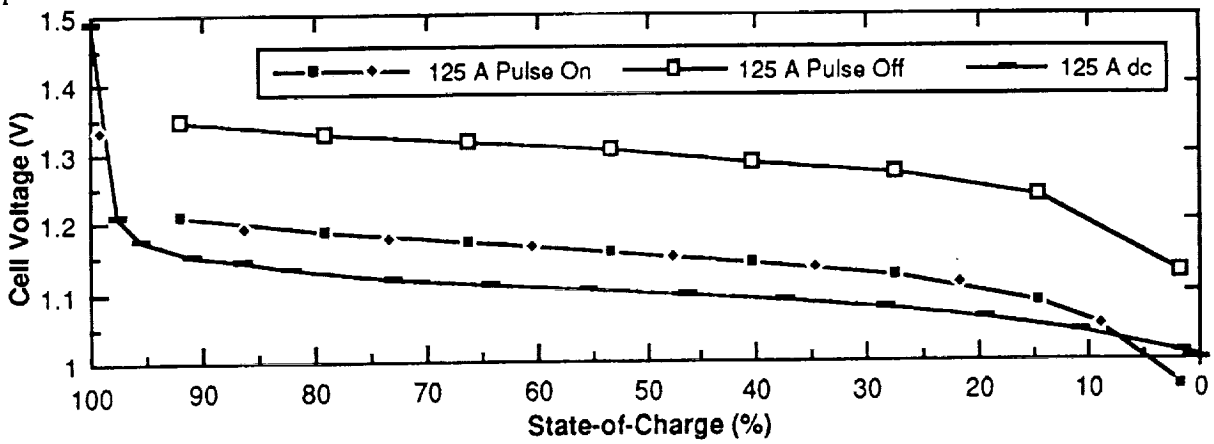

Fig. 6 — NiH_2 and NiCd cell capacitance vs. SoC results of Equivalent Model Method; standard test condition. SoC is referenced to 1 V EODV defining 100% discharge. Typical cell characteristics are listed in Table 3.

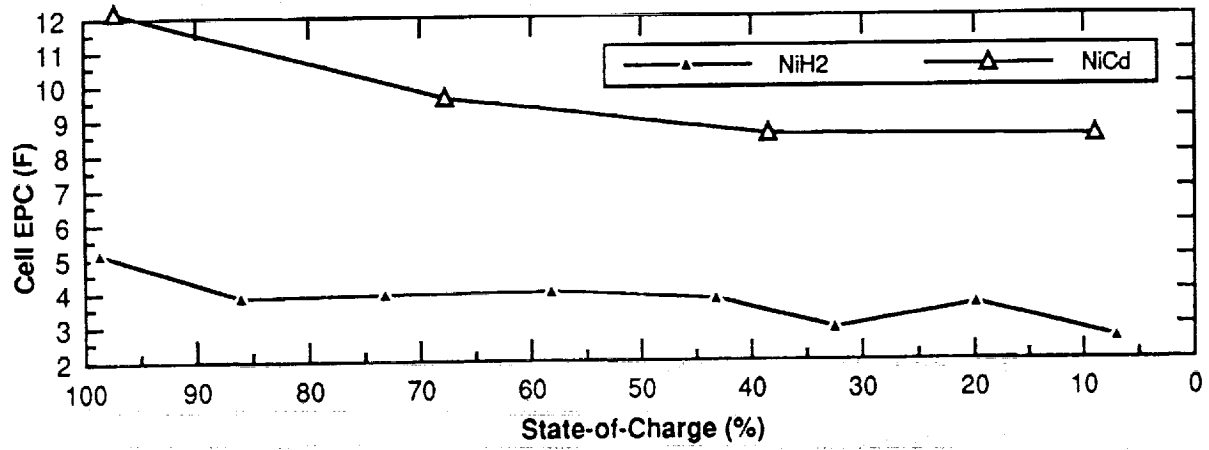

PERFORMANCE PREDICTIONS FOR FLIGHT NiH_2 BATTERY — The performance of an SBR battery may be predicted coarsely by extrapolating the transient characteristics of the five-cell test string. For example, under the "standard parameter regime" (2.5C rate pulses; 400 μs transitions), the typical 1.73 V peak-to-peak spike voltage envelope of the string extrapolates to 6.92 V for a 20-cell pack. With an allowance of 10% for inter-pack connections, this spike envelope would increase to 38 V for the five-pack (100-cell) battery envisaged for SBR. Computer P-Spice modelling indicates that, should this be a problem, putting a moderate-size RC filter across the main bus interface of the Energy Storage Unit will sufficiently dampen spike amplitudes in the SBR EPS configuration [5].

Regulating the ripple between the two voltage plateaus then becomes the EPS performance trait influenced most directly by the cells' ESR and time-constant characteristics. A typical 0.75 V plateau-to-plateau ripple of the five-cell string under "standard parameters" (125 A load pulse, 20 ms half-cycle) can thus be similarly extrapolated to 16.7 V for the full-battery estimate.

Table 2 — Performance extrapolated to a 100-cell NiH_2 battery (five series-connected packs of 20 cells). The source values used for these estimates are for approximately 80% SoC and, except for emf and plateau voltage, were considered typical for the 60-100% SoC range.

emf (V)	Plateau Avg. Load-Off (V)	Plateau Avg. Load-On (V)	Line Regulation (Ripple; V)	ESR (mΩ)	ESL (μH)	EPC (F)
133.8	132.5	115.8	16.7	151	15	0.04

Table 3 — The principal correlations between the NiH_2 and NiCd cell characteristics.

Variable	NiH_2 Cell	NiCd Cell	Notes
Voltage	1.47 V	1.38 V	Electromotive Force; 98% SoC with 125 A pulse amplitude
Voltage	1.32 V	1.27 V	Electromotive Force; 60% SoC with 125 A pulse amplitude
Capacity (dc 1)	55.8 Ah	32.3 Ah (24°C)*	Discharge to 1.0 V; avg. 50 A rate; non-pulsed
Capacity (dc 2)	46.8 Ah	21.0 Ah *	Discharge to 1.0 V; avg. 125 A rate; non-pulsed
Capacity (Pulse)	56.2 Ah	24.8 Ah *	Discharge to 1.0 V; avg. 125 A pulses (62.5 A avg.)
Round-Trip Efficiency	~92% (1C dc rate) ~80% (2.5C dc rate) ~89% (1C pulses) ~90% (2.5C pulses) ~89.5% (3C pulses)	inconclusive for NiCds (52.5-58% range in tests due to extended charges)	Typ. Round-Trip Capacity Efficiency; charge removed in discharge divided by previous charge I/P of same cycle. NiH_2 R-T.C. efficiencies slightly less (typ. 1%) w. inter-pulse charging & slightly more w. 0.8C rate charging.
Inter-Pulse Charge Eff.	~95%	~99% (inconclusive)	% of charge I/P seen as useful capacity at load (vs. std. disch.)
Static Resistance	1.52 mΩ	1.38 mΩ	R from $\partial V/\partial I$ for const. 125 A vs. 50 A disch. rates; 80% SoC
ESR	1.25 mΩ	0.87 mΩ	Equivalent Series Resistance (Avg. from 60-100% SoC)
ESL	~0.15 μH	~0.2 μH	Equivalent Series Inductance (Avg. from 60-100% SoC)
EPC	~4 F	~11 F	Equivalent Parallel Capacitance (Avg. from 60-100% SoC)

* Nameplate capacity defined by *low-rate* discharge in commercial cells.

Fig. 7 — Comparison of the NiH_2 and NiCd ESR results from the two analysis methods — the Equivalent Model Method (E.M.M.) and the Observed Results Method (O.R.M.). The static resistance of the NiH_2 cell (measured by comparing voltages at different dc discharge currents) is about 25% greater than its ESR (based on pulsed waveform voltage and current analysis). For the NiCd cell model tested, the static resistance is about 50% greater than the ESR.

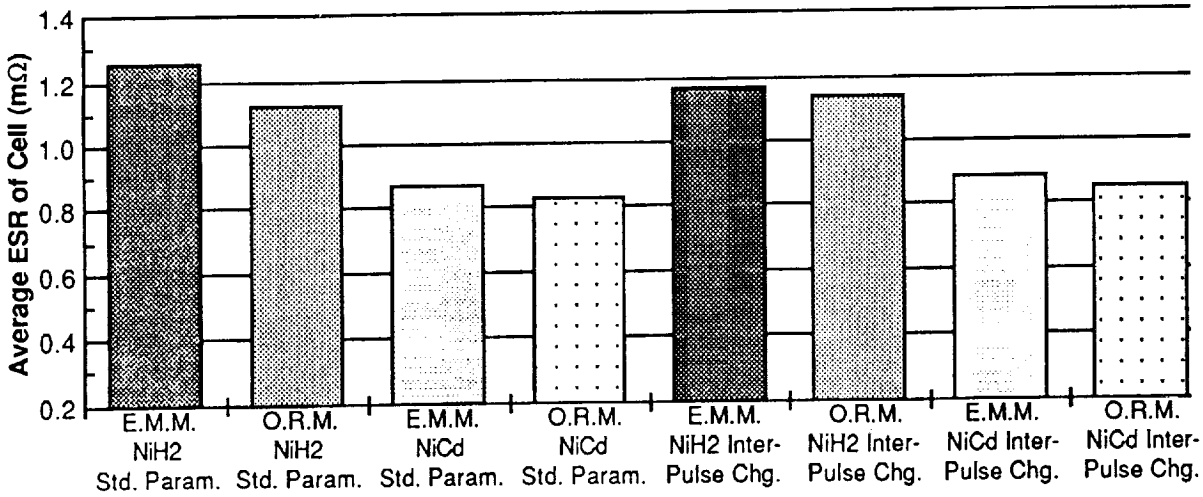

By the same reckoning, an improvement to about 15 V of ripple can be predicted from the 5 ms half-cycle-time results.

Some of characteristics in Table 2 are also dependent on other battery variables. For example, the 151 mΩ ESR estimate may be reduced, perhaps by more than 10%, by use of ultra-low-resistance cell and cell-pack interconnection techniques.

Recommendations

The NiH_2 cells tested are well-suited to this type of pulsed-load application. However, they are slightly higher in equivalent series resistance than desired. For such a high-current application, this might be improved by having larger connection terminals to lower the contact and feed-through resistances. This possibility should be investigated, but any modification should not change the basic cell design, nor significantly impact specific energy. Another possible way to decrease cell resistance is to consider cells of higher capacity ratings, e.g., having more electrodes, but of the same basic design.

In the near term, cells of the design variant tested here are virtually ideal for an SBR-type application. However, common pressure vessel technology is maturing rapidly. For example, two-cell modules have been accumulating impressive life-cycle numbers. In the longer term, such mass and energy saving modules should be considered for the SBR application, and pulsed-modes characterization testing should be done.

The test program has unveiled questions regarding cell and battery performance and its impact on performance of the SBR EPS. For example, the effects of pulsed-discharge and inter-pulse charge conditions on cycle life of a cell are not known: Does inter-pulse charge accelerate capacity degradation because each pulse cycle resembles a very low-depth charge/discharge cycle? A long-term cycle life test would answer that question.

Conclusions

NiH_2 cells of the type tested should provide good performance in the envisaged SBR EPS. No operational anomalies were observed and performance variables such as discharge capacity were consistent. Use of the 27% KOH electrolyte concentration and of the nickel pre-charge process did not adversely affect suitability of the cycle voltage profile nor of any other traits examined.

The goal of an operational pulsed-mode battery resistance of less than 150 mΩ, with acceptable amplitudes of bus voltage swing, is achievable with the NiH_2 cells tested. For the Energy Storage Unit Demonstrator, also containing 100 cells — but of the commercial NiCd model, an operational resistance of about 80 mΩ has been achieved due to lower cell ESR and low interconnection resistances.

An apparently capacitive time constant, which can improve bus voltage regulation at faster radar burst repetition rates, has been identified and quantified. Voltage ripple between the load-on and load-off plateaus of a NiH_2 cell is less for a half-cycle time briefer than the "capacitive" time constant (i.e., the characterized 5 ms period vs. 20 ms and 40 ms periods).

The transient voltage spikes are greater at higher pulsed current rates and with faster current pulse transition times, due largely to the ESL of the cells. For all of the pulsed parameter combinations tested, these spikes will be readily manageable by capacitive filtering on the main power bus.

The fact that pulsed-mode ESR is substantially lower than static cell resistance indicates that a large improvement in cell efficiency can be expected in the pulsed mode of operation over the normal dc mode. The operation should be restricted to the higher states-of-charge, as is usual.

Charging between radar transmit bursts is reasonably efficient under the tested parameters. Charge and discharge round-trip efficiency is reduced at high inter-pulse charge current rates.

Charge and discharge round-trip efficiencies were found to be much less affected by the amplitude of the discharge current in pulsed mode than in dc mode.

The impedance characteristics of the NiCd test cells have been shown to be similar to those of the NiH_2 cells. This commercial type of NiCd should thus be satisfactory for use in the energy storage demonstration unit.

The data provides an abundance of information on the cells' dynamic electrical characteristics.

Acknowledgements

The test program was sponsored by the Space-Based Radar R&D Project, Department of National Defence, Ottawa. Test engineering consulting was provided by M.H. Moody of CAL Corporation, who also developed the equivalent model techniques for computation of impedance characteristics.

References

1. Maskell, C.A.; Metcalfe, J.R. *Proc. 27th IECEC*, 1992, pp 1.153-1.157.
2. Maskell, C.A. *Proc. 26th IECEC*, 1991, pp 1.340-1.345
3. Capulli, J.; Myers R.; Murray, I.; Lurie, C.; Johnson, E.W.; Griebel, R. *Proc. 27th IECEC*, 1992, pp 1.511-1.519.
4. Hafen, D. *Proc. 27th IECEC*, 1992, pp 2.99-2.104.
5. Tanju, M.C. Proc. *European Space Power Conference*, 1993, pp 1.87-1.92.

1993 NASA AEROSPACE BATTERY WORKSHOP

BATTERY STUDY FOR THE MARS ENVIRONMENTAL SURVEY (MESUR) PATHFINDER

JPL

S. DAWSON, B. OTZINGER, D. PERRONE, S. Di STEFANO, G. HALPERT

NOVEMBER 16-18, 1993
U.S. SPACE AND ROCKET CENTER
HUNTSVILLE, AL

MESUR PATHFINDER - BATTERY WORKSHOP
BATTERY STUDY OVERVIEW

- MESUR PATHFINDER INTRODUCTION
- POWER SUBSYSTEM CONCEPT
- BATTERY TECHNOLOGY SELECTION
- MISSION BATTERY PERFORMANCE
- CELL/BATTERY BASELINE DESIGN
- CHARGE METHODOLOGY
- PROPOSED TESTING

MESUR PATHFINDER - BATTERY WORKSHOP
LANDER Ag/Zn BATTERY
MESUR POWER SYSTEM BLOCK DIAGRAM

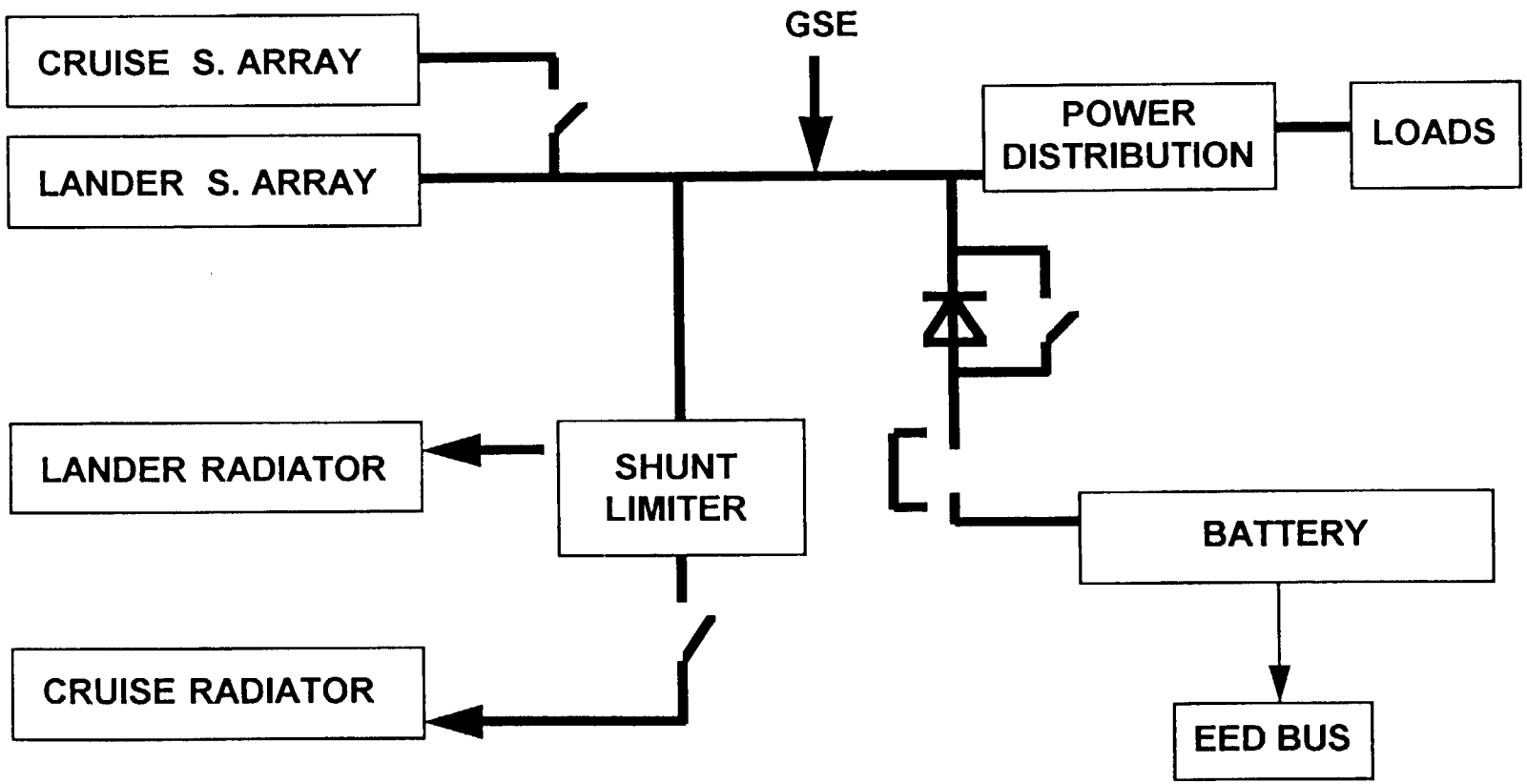

MESUR PATHFINDER - BATTERY WORKSHOP
LANDER Ag/Zn BATTERY
Ag/Zn INTRODUCTION

- BATTERY MISSION PROFILE

  PROVIDE AND STORE ELECTRICAL POWER FOR THE MESUR LANDER DURING LAUNCH, CRUISE, ENTRY - DESCENT - LANDING, AND MARS SURFACE OPERATION.

- TECHNOLOGY SELECTION

  PERFORMANCE

SPECIFIC ENERGY DENSITY (0^0 C)	~75 Wh/Kg
VOLUMETRIC ENERGY DENSITY	~158 Wh/L
RATE CAPABILITY	~C RATE
CYCLE LIFE	~50 CYCLES

  FLIGHT HERITAGE (GENERIC)

  SURVEYOR, MARINER, PIONEER, TITAN, VIKING

  CELL AND BATTERY DESIGN GENERIC

MESUR PATHFINDER - BATTERY WORKSHOP
LANDER Ag/Zn BATTERY
Ag/Zn HERITAGE

BATTERY PROGRAM	MAR 4557-X MESUR	CELL US ARMY	SAR -4265 APOLLO	MAR - 4333 LOCKHEED / SAT.	LARGE PROBE PIONEER/VENUS	UNKNOWN CLASSIFIED
FLIGHT EXPERIENCE	YES	N/A	YES	YES	YES	YES
NUMBER OF CELLS	18	one	20	16	19	one
WEIGHT (Kg)	13.3		12.9	52.7	13.4	
SIZE (cm)	22.5x21x18.1		29.9x17.4x14.6	50.8x34.3x20.3	33.3x19.3x14.4	
CAPACITY (A-H)	40	43	40	300	40	30
VOLTAGE (NOMINAL)	27	1.5	30	24	28.5	1.5
RATE (AMPERES)	1	10 TO 60	25-35	9 TO 12	10 to 50	5 TO 20
CYCLE LIFE (actual)	30	100 (200)	6 (20)	3200 (6700)	1 (25)	50 (100)
DEPTH-OF-DISCH. (%)	80 (max)	62.5	80 (max)	1 to 4	90	100
WET LIFE (MONTHS)	15	12	12	9	12	12
GROUND (MONTHS)	2	12	11	2	7	7
FLIGHT (MONTHS)	8	N/A	1	7	5	5
CELL PART No.	SZLR 40-3	BB-465/U	1560-7	2599-3	SZLR40	SZHR30
CELL WEIGHT (Kg)	0.577	0.581	0.51	2.951	0.51	0.49
CELL Vol. (cm^3)	278	373	271	1066	271	260
ELECTRO. CONC. (%)	40	42	40	40	45	45
NEG. to POS. RATIO	1.53	1.67	1.9	1.04	1.46	1.6
SEPARATION SYSTEM						
POS. ABSORBER *	1 WEBRIL	1 DYNEL	1 PELLON	1 PELLON	1 PELLON	1 WEBRIL
MEMBRANE	5 CELLOPHANE	5 CELLOPHANE	4 CELLOPHANE	5 CELLOPHANE	6 CELLOPHANE	6 CELLOPHANE
MEMBRANE			1 PVA	1 PVA		
NEG. ABSORBER *	1 VISKON	1 DYNEL	1 VISKON	1 VISKON	1 VISKON	1 VISKON

MESUR PATHFINDER - BATTERY WORKSHOP
LANDER Ag/Zn BATTERY
BATTERY OVERVIEW

- PERFORMANCE DRIVEN DESIGN
  - OPERATIONAL PARAMETERS WILL BE DETERMINED BY CELL AND BATTERY PERFORMANCE
- DERIVED PERFORMANCE TARGETS
  - BATTERY VOLTAGE 22-36 VOLTS
  - LOAD 1 - 4 AMPERES
  - TWO MONTHS ACTIVE STORAGE 20^{0}C (SHIP AND LAUNCH)
  - SEVEN MONTH CRUISE
  - 30 CYCLES MARS SURFACE 20 Ah AT 10 TO -20^{0}C
  - CAPACITY
    - 40 AH AT RT AND BOL
    - 20 Ah AT 0^{0}C
  - VOLUME: 8.3 X 7.37 X 7.12 INCHES (ESTIMATE)
  - MASS: LESS THAN 14 KG

MESUR PATHFINDER - BATTERY WORKSHOP
LANDER Ag/Zn BATTERY
CELL DESIGN

- CELL BASELINE DESIGN

ELECTRODE	POSITIVE	NEGATIVE
MATERIAL	SINTERED Ag	Zn OXIDE BLEND
NUMBER	4	5
SURFACE AREA	124.5	
CAPACITY		
THEORETICAL	66.5 AH	101.4 AH
INITIAL EXPECTED	54.5 Ah	
SEPARATOR SYSTEM	5/6 LAYERS - CELLOPHANE	
ELECTROLYTE	40 % KOH, 85 ml	
DIMENSION	6.61 X 3.54 X 0.725 INCHES	
WEIGHT	445 grams DRY (APPX)	

MESUR PATHFINDER - BATTERY WORKSHOP
LANDER Ag/Zn BATTERY
BATTERY DESIGN

- **BATTERY BASELINE DESIGN**
  - BASED ON CURRENT 20 CELL, 3 CONNECTORS, Ti HOSING
  - 18 CELL CELL BATTERY
  - THREE CONNECTOR. MAIN POWER, INSTRUMENTATION, HEATER POWER
  - DIMENSIONS 8.30 X (8.87) X 7.12 INCHES
  - FOOTPRINT TBD (HOLE PATTERN) FLANGE 0.75 INCH
  - HEATER SET POINT APPX 80 F, POWER TBD, THERMOSTATS TBD
  - WEIGHT (ACTIVE BATTERY) ESTIMATES

18 CELLS	22.86	TOTAL = 29.25 lbs
HOUSING	3.22	13.28 KG
COMPOSITE	1.07	EXPECT WEIGHT GROWTH
CONNECTORS	0.28	
WIRING	0.40	
HEATER	0.03	
MISC	1.39	

MESUR PATHFINDER - BATTERY WORKSHOP
LANDER Ag/Zn BATTERY
DESIGN/PERFORMANCE ISSUES

- **DESIGN**
  - DESIGN BASED ON EXISTING TECHNOLOGY
  - CELL 5 OR 6 LAYERS OF SEPARATOR
  - 18 CELL BATTERY (CONCEPT BASED ON 20 CELL BATTERY)
- **OPERATIONAL**
  - CHARGE
    - ENERGY BALANCE IS CRITICAL
    - 20 Ah CHARGE IN 6 HOURS
    - CHARGE/DISCHARGE TEMPERATURE LIMITS (PREFER 20°C)
    - CHARGE METHODOLOGY (CP OR TAPER)
  - DISCHARGE
    - TEMPERATURE LIMIT FOR CAPACITY (NOMINAL 20Ah)
  - CRUISE
    - TEMPERATURE 0C PREFERRED WILL TEST AT 20°C
    - OCV OR 1.86 VOLT FLOAT

MESUR PATHFINDER - BATTERY WORKSHOP
LANDER Ag/Zn BATTERY
PROPOSED CHARGE METHODOLOGY

BATTERY CHARGE VOLTAGE/CURRENT

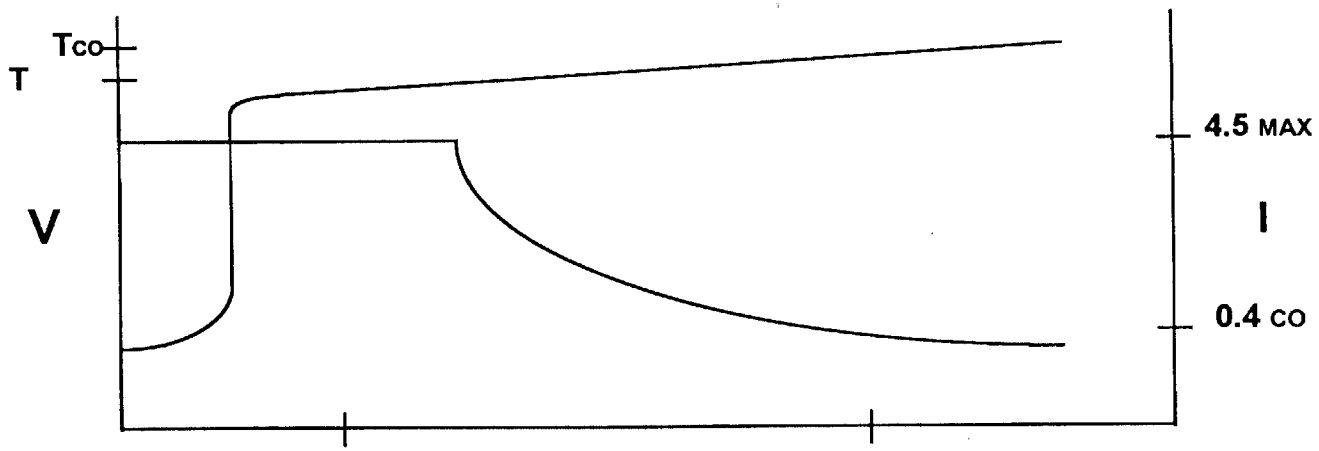

TAPER

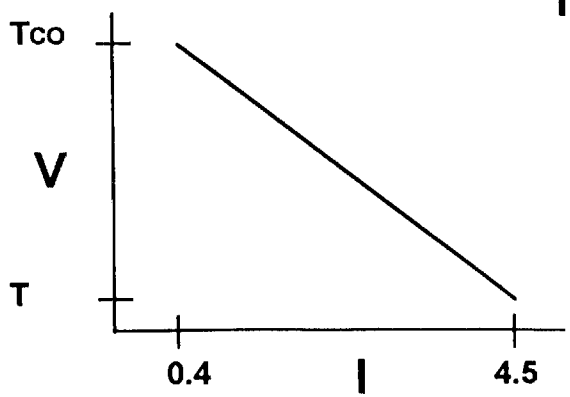

MESUR PATHFINDER - BATTERY WORKSHOP
LANDER Ag/Zn BATTERY
CELL CHARACTERIZATION TESTING

- **CHARGE DEFINITION**
  - CONSTANT POTENTIAL
    - V = 1.91 TO 1.94, I = 4.5 MAX TO 0.4, TEMP., 23 TO 10C
  - VIRTUAL RESISTANCE
    - V_{VO} = 1.91 TO 1.94, VT_{OS} = 1.91, TEMP. = -10 TO 10C
- **CHARGE/STAND CYCLE LIFE**
  - 8 MONTH STAND, 0 AND 25C, OCV AND 1.86V FLOAT
- **DISCHARGE CHARACTERISTIC**
  - TEMP. -40, -20, -10, 0, 10C, RATES 1.5, 4.35, 12.5, 1.5 AMPS
- **SYSTEM PERFORMANCE**
  - FLIGHT - PRELAUNCH, CRUISE/TCM, EDL, MARS SURFACE OPERATION
- **CYCLE LIFE INITIAL**
  - CHARGE/DISCHARGE CYCLE AT 0C TO 1.22V, TAPER TBD

MESUR PATHFINDER - BATTERY WORKSHOP
LANDER Ag/Zn BATTERY
DESIGN OPTIONS DETERMINED BY TESTING

- **HARDWARE**
  - 18 OR 17 CELL BATTERY
  - 5 OR 6 LAYERS OF SEPARATOR
- **OPERATION**
  - CHARGE
    - LIMITED CHARGE MAY LEAD TO NEGATIVE ENERGY BALANCE
    - DURATION OF CHARGE PERIOD AND CHARGE ACCEPTANCE
    - CHARGE TEMPERATURE COMPENSATION REQUIRED
    - CHARGE METHODOLOGY
  - CRUISE
    - TEMPERATURE, OCV OR 1.86 VOLT FLOAT

MESUR PATHFINDER - BATTERY WORKSHOP

SUMMARY

- SELECTION OF Ag/Zn BATTERY BASED ON DERIVED MISSION REQUIREMENTS.

- CELL AND BATTERY DESIGNS ARE CONSISTENT WITH FLIGHT REQUIREMENTS.

- CELL TESTING WILL PROVIDE DATA ON
  - CHARGE/DISCHARGE TEMPERATURE COMPENSATION
  - CYCLE LIFE
  - CHARGE METHODOLOGY
  - CRUISE REQUIREMENTS

Screen Test for Cadmium and Nickel Plates

Angie H. Phan and Albert H. Zimmerman
The Aerospace Corporation
El Segundo, California 90245

Abstract

A new procedure is described here which was recently developed to quantify loading uniformity of nickel and cadmium plates and to screen finished electrodes prior to cell assembly. The technique utilizes the initial solubility rates of the active material in a standard chemical deloading solution at fixed conditions. The method can provide a reproducible indication of plate loading uniformity in situations where high surface loading limits the free flow of deloading solution into the internal porosity of the sinter plate. A preliminary study indicates that "good" cell performance is associated with higher deloading rates.

I. Introduction:

The performance of nickel cadmium (Ni-Cd) and nickel hydrogen (Ni-H_2) battery cells has been found to be critically dependent on the variability in active material loading of the nickel and cadmium electrodes used in them. Several recent ground test problems and orbital battery anomalies have been attributed to such inappropriate loading of active material, which is often caused by process instability, or a lack of manufacturing process control. At the present time, no effective procedure is available to quantify the loading uniformity at the microscope level, or to screen the finished electrodes prior to cell assembly. The new technique described here shows correlation between plate performance and deloading rates of cadmium and nickel plates. This report communicates the preliminary results obtained from the new method.

II. Experimental:

Experiments were performed to develop a procedure for characterization of loading uniformity of cadmium and nickel plates. Two small samples (approximately 1.85 cm x 1.85 cm) of finished plates were chosen for analysis from each plate, with one sample being within the middle of the electrode and away from the edges of the electrodes, and the other sample being near one edge. The edges of the samples were coated with viscous epoxy to prevent the leaching

of the active material from the cut edges of the samples. The epoxy-edged samples were allowed to cure at room temperature for approximately 24 hours. The weights with epoxy and dimensions of samples were obtained. During the epoxy coating process, small spots on the samples were occasionally smeared with wet epoxy and therefore, an area correction factor was measured to determine the actual surface areas of samples. A standardized chemical extraction solution was prepared by dissolving 154g of reagent grade ammonium acetate in 1.3 liter (ℓ) of concentrated ammonium hydroxide (reagent grade) and then diluting to 2.0ℓ with deionized water. Active material in the sample electrodes was allowed to leach out by complexing with the ammonia solution, held at 50°C ± 2°C, for a period of 5 minutes, after which the samples were thoroughly rinsed until the rinse solution was near to a neutral pH condition. After drying at room temperature for about 12 hours or more, the samples were then weighed, and the weight losses were recorded to determine the standard deloading rate at 50°C. Care must be taken to maintain uniform solution temperature (50°C ± 2°C) during the deloading. A sample holder was used to keep the specimen in a vertical position. Pure nickel is suggested as an ideal sample holder material due to its inert nature in the basic ammonia solution.

III. Results and Discussion:

Method Development:

Cadmium electrodes were obtained from "bad" and "good" cells, and subjected to the previous described procedure to determine the appropriate extraction conditions which could provide useful data representative of surface loading characteristics. "Bad" electrodes, as defined here, exhibited anomalously rapid cadmium migration in cells, causing premature short circuits in some cases. It is expected that any surface loading which blocks movement of the deloading solution into the interior of the porous plate should reduce the deloading rate. Figure 1 indicates the kinetic data obtained from two different cell lots, L6A, and L2A which are known to be "good" and "bad", respectively. The preliminary data indicates that the initial solubility rate of active material in the standard extraction solution for fixed conditions provides reproducible measurements of surface loading uniformity of cadmium plates. The five minutes extraction time was selected as the standard time interval to measure the initial deloading rate of cadmium in ammonia solution, because this interval gave roughly 10-20% deloading.

Results:

Figure 2 shows preliminary data, which indicate that "good" cell performance is typically associated with higher deloading rates, ranging from 6-10 mg/(min.cm^2). This implies that the interior structure of the electrode is more open to chemical deloading and thus there is lesser degree of blockage within the porous structure of the electrodes. Samples from lot 2A, 2B, 3, and 4 are identified with "bad" electrodes, which are usually characterized by lower deloading rates, i.e. 0.3-3 mg/(min.cm^2).

Figure 3 shows the variation in deloading rates for electrode samples from different spirals within one production post. These differences could be attributed to the variation of the spiral locations in the impregnation tank, resulting in higher or lower surface active material loading. These results clearly show that variability can be significant not only from lot to lot but also within a single post of production.

The screen test has also been applicable to the nickel electrode, for which excessive amounts of surface loading of active material has often resulted in poor electrode utilization and accelerated swelling over cycle life. As shown in Figure 4, the deloading rates of nickel plate samples were found to be proportional to the fractional utilization which is defined as the ratio of the C/2 plate capacity to 0.0 V (vs. Hg/HgO) over the total capacity stored in the electrode. It is believed that with an appropriate data base, an expression of electrode utilization as a function of various parameters (EQ. 1) could be obtained and used to screen finished plates prior to cell assembly, thus preventing costly problems from "bad" plates in spacecraft batteries or in ground tests.

$$\text{Utilization} = k_1L + k_2P + k_3W + k_4Co + k_5D + k_6 \qquad \text{(EQ. 1)}$$

Where

L : Loading level

P: Sinter porosity

W: Wt. of sinter

Co: Percentage of cobalt in active material

D: deloading rate, related to surface loading uniformity

k_1, k_2, k_3, k_4, k_5, k_6 are constants

L, P, W, and Co could be found by chemical analysis of electrodes, and D may be determined from the deloading experiment.

IV. Summary and Recommendations:

Currently, we are in the process of perfecting the technique and obtaining more data to evaluate method reliability and effectiveness under various conditions. Communication with battery manufacturers will be considered to obtain representative electrodes that are known to be either "good" or "bad" to build up a large data base in an attempt to predict electrode utilization as a function of multiple variables which affect plate performance. In the near future this technique, the methods of interpretation, and our results will be forwarded to spacecraft battery manufacturers to allow and encourage them to utilize this new capability.

Acknowledgment

This work is supported by The Aerospace Sponsored Research Program and by NASA Lewis Research Center. The support from these organizations is gratefully acknowledged.

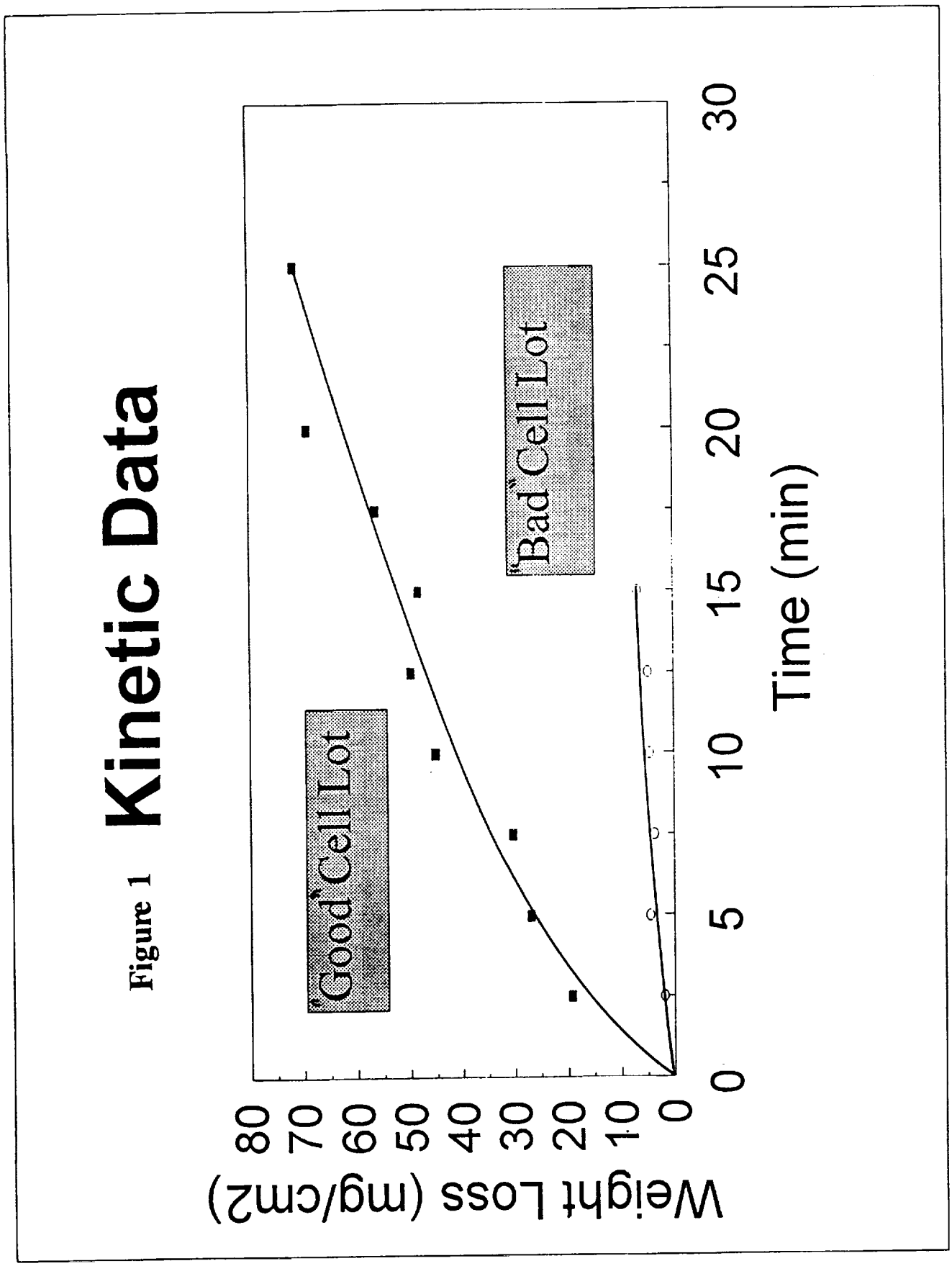
Figure 1 Kinetic Data
Weight Loss (mg/cm2)
0
10
20
30
40
50
60
70
80
Time (min)
0
5
10
15
20
25
30
"Good" Cell Lot
"Bad" Cell Lot

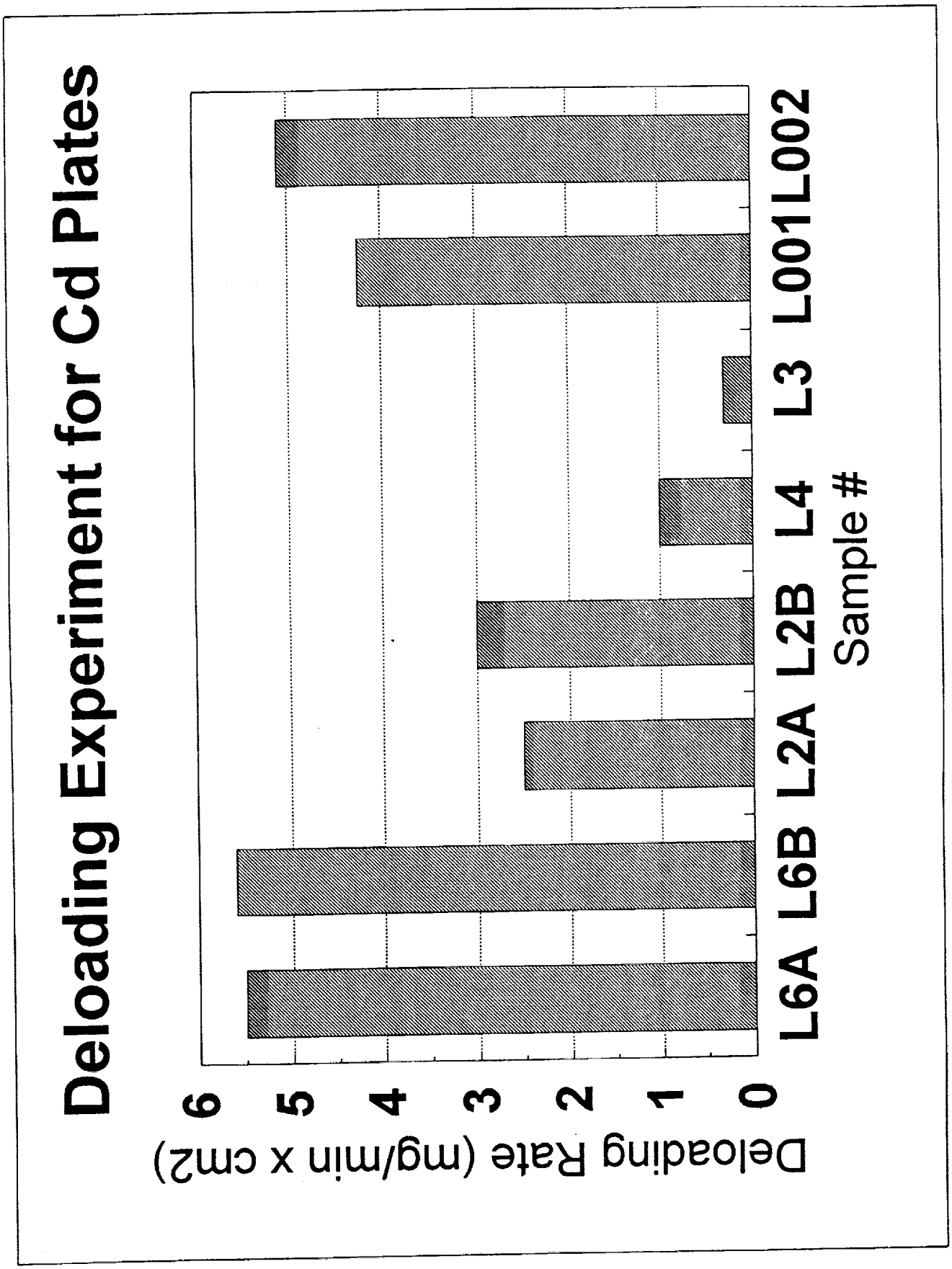
Deloading Experiment for Cd Plates
Deloading Rate (mg/min x cm2)
0
1
2
3
4
5
6
L6A L6B L2A L2B L4 L3 L001L002
Sample #

Figure 2

Figure 3

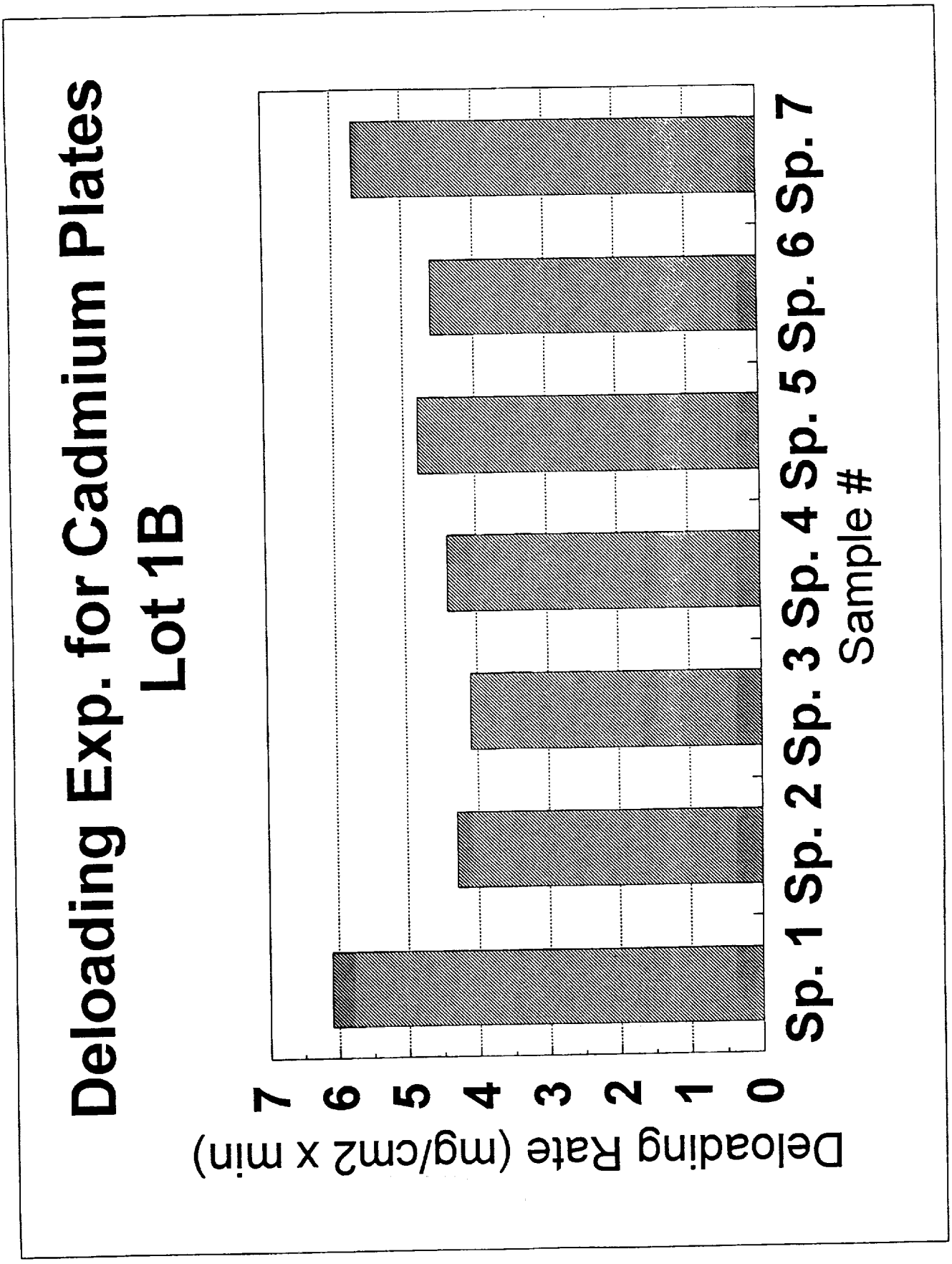
Deloading Exp. for Cadmium Plates
Lot 1B
Deloading Rate (mg/cm2 x min)
0
1
2
3
4
5
6
7
Sp. 1 Sp. 2 Sp. 3 Sp. 4 Sp. 5 Sp. 6 Sp. 7
Sample #

Figure 4

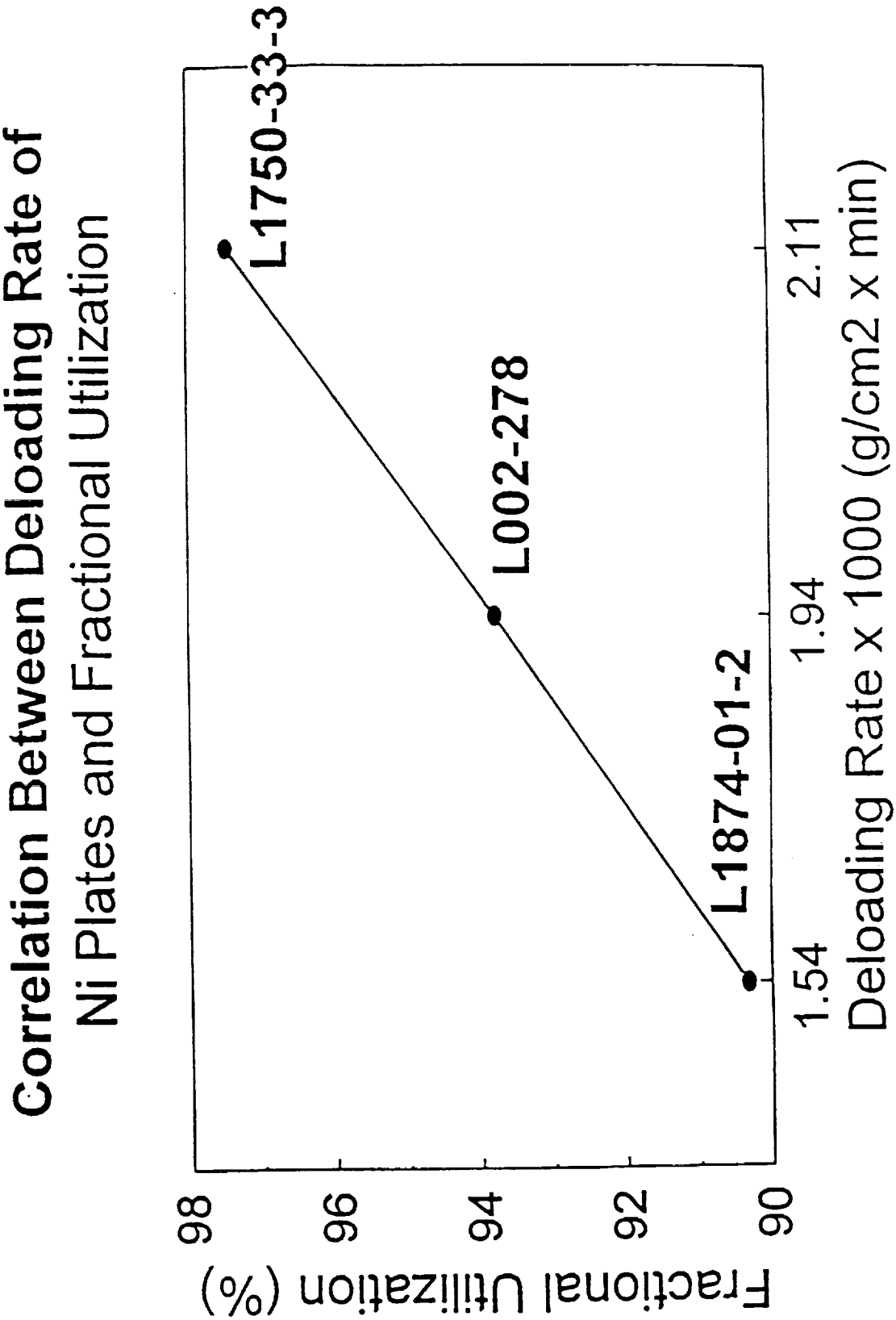
Correlation Between Deloading Rate of
Ni Plates and Fractional Utilization
L1750-33-3
L002-278
L1874-01-2
98
96
94
92
90
Fractional Utilization (%)
1.54
1.94
2.11
Deloading Rate x 1000 (g/cm2 x min)

ANALYSIS FOR NICKEL (III AND IV) IN POSITIVE PLATES FROM NICKEL-CADMIUM CELLS

INTRODUCTION

The NASA-Goddard procedure for destructive physical analysis (DPA) of nickel-cadmium cells contains a method for analysis of residual charged nickel as NiOOH in the positive plates at complete cell discharge, also known as nickel precharge. In the method, the Ni(III) is treated with an excess of an Fe(II) reducing agent and then back titrated with permanganate. The Ni(III) content is the difference between Fe(II) equivalents and permanganate equivalents.

Problems have arisen in analysis at NAVSURFWARCENDIV, Crane because for many types of cells, particularly AA-size and some "space-qualified" cells, zero or negative Ni(III) contents are recorded for which the manufacturer claims 3-5% precharge.

Our approach to this problem has been to reexamine the procedure for the source of error, and correct it or develop an alternative method.

EXPERIMENTAL

In this work, results will be presented from analysis of two brands of AA-size cells, 12Ah and 20Ah space qualified cells, and a 30Ah cell from an aircraft battery.

The role of the iron reducing agent was investigated by using the standard reagent, ferrous ammonium sulfate (FAS), ferrous sulfate (FeS), and prepared FAS (FeS + ammonium sulfate (AS)). Also, the possibility of using a substitute reducing agent was investigated with stannous chloride (TDC, tin dichloride).

RESULTS AND DISCUSSION

Table 1 illustrates the problems encountered with the five plate sample materials when FAS is

TABLE 1
Residual NiOOH Content For Five Plate Sample Materials

30Ah Aircraft Battery Cell		G-AA Cell (3 Cells)	
1. 5.75%	2. 5.52%	1. -1.48%	2. -1.70%
3. 4.83%	4. 5.48%	3. -1.20%	4. -1.10%
5. 5.93%	6. 5.18%	5. -1.51%	6. -0.85%

20Ah Space Cell		S-AA Cell (3 Cells)	
1. -0.09%	2. -1.23%	1. -3.76%	2. -2.97%
3. -0.51%	4. -0.31%	3. -1.26%	4. -1.70%
5. -1.30%	6. -0.47%	5. -2.38%	6. -1.67%

12Ah Space Cell	
3. 3.17%	4. 3.26%
1. 3.72%	2. 3.32%

the reductant. A search for an alternative reagent for the reduction step resulted in the selection of TDC. In Table 2 are given the analytical results for FAS and TDC in side-by-side analyses.

TABLE 2
Comparison Of Residual NiOOH Results
For FAS And TDC

Sample Description	%NiOOH
1. 0.1394g GAA Ni + 0.4002g FAS	0.55
2. 0.1392g GAA Ni + 0.4007g FAS	0.64
3. 0.1400g GAA Ni + 0.1106g TDC	2.30
4. 0.1396g GAA Ni + 0.1112g TDC	1.97
5. 0.1390g SAA Ni + 0.3995g FAS	-1.57
6. 0.1398g SAA Ni + 0.4000g FAS	-1.48
7. 0.1400g SAA Ni + 0.1108g TDC	1.41
8. 0.1403g SAA Ni + 0.1107g TDC	1.35
9. 0.1408g 20Ah SC + 0.3987g FAS	-1.02
10. 0.1405g 20Ah SC + 0.3994g FAS	-1.24
11. 0.1388g 20Ah SC + 0.1096g TDC	3.43
12. 0.1412g 20Ah SC + 0.1089g TDC	3.18
13. 0.1420g 12Ah SC + 0.4013g FAS	2.69
14. 0.1403g 12Ah SC + 0.3995g FAS	3.09
15. 0.1393g 12Ah SC + 0.1112g TDC	8.32
16. 0.1414g 12Ah SC + 0.1103g TDC	8.01
17. 0.1389g 30Ah AB + 0.4000g FAS	5.21
18. 0.1399g 30Ah AB + 0.4006g FAS	4.61
19. 0.1412g 30Ah AB + 0.1120g TDC	7.61
20. 0.1400g 30Ah AB + 0.1110g TDC	8.17

The TDC data are uniformly positive, and in the ranges expected for the respective cells.

In the procedure, a magnetic stirbar is used, and at the conclusion of the reduction period, it is removed to prevent the metal particulates which cling to the bar from interfering in the permanganate back titration. The data in Table 3 illustrate the consequences, shown for FAS and TDC, of leaving one of the metal particulates, iron, in the samples during permanganate titration. With FAS, the amount of titrant required increases steadily with increasing iron content, while the TDC titration is practically unaffected by the particulate iron. Normally, the particulates are removed before the titration step, but a different interaction definitely occurs with the sample particulates during the titration step when FAS is the reductant compared to when TDC is used. Similar results are obtained for particulate nickel and cobalt.

TABLE 3
Effect Of Metallic Iron On Expected Titers

Sample Description	Act. MnO_4^-	Theo. MnO_4^-
FAS		
1. 0.4500g	11.55ml	11.48ml
2. 0.4478g	11.40ml	11.43ml
3. 0.4483g + 0.0094g Fe*	11.45ml	11.44ml
4. 0.4496g + 0.0103g Fe*	11.50ml	11.47ml
5. 0.4505g + 0.0109g Fe@	16.00ml	11.48ml
6. 0.4507g + 0.0204g Fe@	20.70ml	11.50ml
7. 0.4500g + 0.0300g Fe@	25.10ml	11.48ml
TDC		
1. 0.1286g	10.90ml	10.92ml
2. 0.1327g	11.30ml	11.27ml
3. 0.1298g + 0.0104g Fe*	11.00ml	11.02ml
4. 0.1297g + 0.0096g Fe*	11.00ml	11.01ml
5. 0.1296g + 0.0103g Fe@	11.00ml	11.00ml
6. 0.1322g + 0.0123g Fe@	11.30ml	11.23ml

* stirbar removed prior to titration
@ stirbar left in during titration

In an attempt to obtain more information about the interaction of reducing agents with the metal particulates prior to the back titration in the analysis, a series of analyses were performed with AB plate materials, with the following reductant combinations: FAS, FeS, FeS + AS, and TDC. In the cases where AB plate material was used, in half the samples with each reductant the stirbar with particulates was removed prior to acidification with H_2SO_4 and titration, while in the other half, the stirbar was left in during the MnO_4^- titration. In Table 4a the results for the Ni(III) titrations are given, while in Table 4b the analyses for the residues are presented. In the residues, only iron and nickel were found present to any extent, and trace amounts of cadmium and cobalt were also noted. Therefore, only the Fe and Ni are reported in Table 4b.

TABLE 4a
AB Nickel Plate Material Analysis With
Several Reducing Agents

Sample Description		Vol MnO_4^-	% NiOOH
wt Ni	wt FeS		
1. 0.1401	+ 0.3010	10.82*	7.08
2. 0.1402	+ 0.3002	10.80*	7.00
3. 0.1411	+ 0.3012	10.85*	6.89
4. 0.1409	+ 0.2998	27.25@	----
5. 0.1407	+ 0.3008	26.75@	----
6. 0.1301	+ 0.3000	28.75@	----

TABLE 4a (cont.)

Sample Description	Vol MnO_4^-	% NiOOH
wt Ni wt FeS Wt AS		
7. 0.1399 + 0.3006 + 0.1206	10.85*	6.79
8. 0.1412 + 0.2995 + 0.1202	10.80*	6.77
9. 0.1408 + 0.3006 + 0.1203	10.80*	7.08
10. 0.1407 + 0.2995 + 0.1200	27.15@	----
11. 0.1409 + 0.3008 + 0.1999	28.10@	----
12. 0.1402 + 0.3004 + 0.1202	28.65@	----
wt Ni wt FAS		
13. 0.1396 + 0.4208	9.80*	6.08
14. 0.1399 + 0.4198	9.90*	5.23
15. 0.1400 + 0.4208	9.85*	5.66
16. 0.1403 + 0.4204	23.95@	----
17. 0.1403 + 0.4196	27.85@	----
18. 0.1405 + 0.4208	27.65@	----
wt Ni wt TDC		
19. 0.1392 + 0.1270	9.55*	8.60
20. 0.1396 + 0.1282	9.60*	8.92
21. 0.1411 + 0.1277	9.70*	7.89
22. 0.1398 + 0.1292	9.80@	8.15
23. 0.1405 + 0.1277	9.80@	7.28
24. 0.1390 + 0.1278	9.70@	8.07

TABLE 4b
Residue Analysis (wt $x10^{-2}$)

Sample	g Res	g Fe	g Ni	Equiv MnO_4
1.	----	0.0146	6.33	21.67
2.	----	0.0161	6.03	20.68
3.	----	0.0169	6.32	21.65
4.	----	0.0087	1.13	3.90
5.	----	0.0103	0.0953	3.31
6.	----	0.0059	0.120	4.09
7.	----	0.0160	6.62	22.67
8.	----	0.0144	6.61	22.63
9.	----	0.0167	6.41	21.96
10.	1.62	0.0100	1.29	4.46
11.	1.62	0.0117	0.82	2.86
12.	1.75	0.0086	0.78	2.71

TABLE 4b (cont.)
Residue Analysis (wt $x10^{-2}$)

Sample	g Res	g Fe	g Ni	Equiv MnO_4^-
13.	7.03	0.0144	5.92	20.27
14.	6.24	0.0183	5.88	20.15
15.	7.27	0.0182	5.78	19.81
16.	2.24	0.0097	1.74	5.98
17.	1.09	0.0082	0.48	1.68
18.	1.30	0.0087	0.69	2.40
19.	7.78	0.0004	5.77	19.69
20.	7.70	0.0006	5.72	19.52
21.	6.43	0.0002	5.28	18.00
22.	7.22	0.0003	5.29	18.04
23.	7.08	0.0006	5.43	18.53
24.	7.20	0.0007	5.31	18.12

The data in Table 4a show that the Fe(II)-based reductants give a consistently lower ß-NiOOH content for the discharged positive plate material than TDC. The average of the sum of sets 1-3, 7-9, and 13-15 is 30% lower than the average of the set 19-21, and the FAS data alone are 50% lower, on average. Thus, there is a clear difference between Fe(II) and Sn(II) reduction. Also, the presence or absence of ammonium ion is not a significant factor in the observations. Finally, it appears that leaving the particulate-clad stirbar in the TDC solutions during MnO_4^- titrations may yield a slightly lower ß-NiOOH content, so that it is advisable to remove it prior to titration.

The data in Table 4b show that the principle component of the particulate matter is, not surprisingly, nickel. However, it also appears that there is considerably more residual iron in the Fe(II)-based solutions than in the TDC solutions, by a factor of 35-40X. If Fe(II) is being reduced to Fe(0) in samples 1-18, what is the reductant? If Fe(0) is being oxidized in samples 19-21 (before MnO_4^- titration), only Ni(III) could be the oxidant, but then less Sn(II) would be oxidized by Ni(III), so the eventual titer with MnO_4^- would be too large, leading to a low value for ß-NiOOH. Thus, these results for AB plate material indicate that an interaction occurs with the sample when an Fe(II)-based reductant is used which not only yields artificially low Ni(III) values, but also leads to an unusual level of metallic iron in the particulates which are removed with the stirbar.

CONCLUSIONS

The inquiry into the role of an iron (II) based reducing agent, in the form of ferrous ammonium sulfate or other ferrous-type reductants, shows that this cationic species leads to artificially low results in an analysis for nickel precharge in positive plates from nickel/cadmium cells. The substitution of a tin (II) species in the compound stannous chloride gives more acceptable values, in terms of what might be expected from manufacturing requirements.

A great many questions remain to be resolved about this analysis, for the nature of the

interaction between Fe(0, II, and III) and permanganate which leads to the low Ni(III) analyses, and which facilitates solution of metallic iron, cobalt, and nickel, needs to be understood. Also, it is puzzling how the NiOOH retains its stability during the reduction step in dilute acetic acid. Some answers may be provided if known Ni(III) or Ni(IV) content materials could be used as standards. It is hoped that this work can be extended in order to answer these questions. In the meanwhile, use of stannous chloride as the reducing agent in the determination of nickel precharge appears to be a recommended alternative to the standard procedure.

Nickel-Hydrogen Technologies Session

Session Organizer: *Eric Lowery*
NASA Marshall Space Flight Center

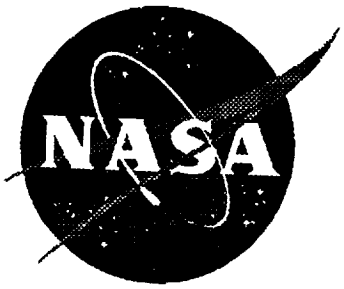

Space Station Freedom NiH_2 Cell Testing Program

Presented At:
The 1993 NASA Aerospace Battery Workshop
Marshall Space Flight Center
16-18 November 1993

Prepared By:

Bruce Moore
Aerospace Power Systems Branch
Naval Surface Warefare Center, Crane Division

Dave Frate
Solar Power Module Division
NASA Lewis Research Center

Table Of Contents

	Page
Summary	2
Introduction	3
Test Plan	3
Test Equipment	6
Test Results	7
Preliminary Findings	11
Appendix A. Life Cycle Trend Plots	A1

1. SUMMARY

a. Testing for the Space Station Freedom Nickel Hydrogen Cell Test Program began in 1990 at Crave Division, Naval Surface Warfare Center. The program has included receipt inspection, random vibration, acceptance, characterization, and life cycle testing of Ni-H_2 cells in accordance with the NASA LeRC Interagency Order C-31001-J.

b. A total of 400 Ni-H_2 cells have been received at NAVSURFWARCENDIV Crane from three separate manufacturers; Yardney Technical Products (Yardney), Eagle Picher Industries (Eagle Picher), and Gates Energy Products (Gates). Of those, 308 cells distributed among 39 packs have undergone life cycle testing under a test regime simulating low earth orbit conditions. As of 30 September 1993, there are 252 cells assembled into 32 packs still on life cycle test.

c. Since the beginning of the program, failed cells have been detected in all phases of testing. The failures include the following; seven 65 AmpHr and 81 AmpHr Yardney cells were found to be leaking KOH on receipt, one 81 AmpHr Eagle Picher cell failed the acceptance test, one 65 AmpHr Gates cell failed during the characterization test, and six 65 AmpHr Gates cells failed the random vibration test. Of the 39 life cycle packs, testing on seven packs, 56 cells, has been suspended because of low end of discharge voltages. All of the failed life cycle packs were cycled at 60% depth of discharge.

2. INTRODUCTION

a. Initial funding for the Space Station Freedom Nickel Hydrogen Cell Test Program was received at Crane Division, Nav Surface Warfare Center (NAVSURFWARCENDIV) in March 1987 under NASA LeRC Interagency Order C-31001-J. The first cells were received in April 1990. Cell testing began in May 1990 with t first LEO life cycle testing starting in July 1990. The last scheduled life cycle pack was started in February 1993.

b. The purpose of the cell test program is to develop a statistically significant Ni-H_2 database on representative cell from U.S manufacturers and to establish facilities which can perform special testing in support of Space Station Freedom. T major test objective is to evaluate cell life at 35% and 60% Depth of Discharge (DOD) and -5°C and 10°C. The goal of the li cycle testing is to reach 20,000 cycles at 60% DOD and 33,000 cycles at 35% DOD.

3. TEST PLAN

a. The cells were from three different manufacturers; Yardney Technical Products, Eagle Picher Industries and Gates Energy Products. Different designs from each manufacturer were used in the tests including variations in plate arrangement, separator type, use of catalyzed walls, KOH concentration and t nickel plate manufacturing process, Table I.

b. The cell test program included receipt inspection, random vibration, acceptance, characterization, and LEO life cycle testing. Receipt inspection consisted of a visual inspection plus measuring physical and electrical characteristic such as dimensions, weight, internal impedance, insulation resistance between the cell wall and the mounting flange, and a phenolphthalein leak test. Following the receipt inspection, al of the cells were cycled under various temperatures to determine if they met the capacity and voltage performance requirements in the acceptance test. Based on the data from the acceptance test, the cells were assigned to life cycle test packs or storage groups. Before the life cycle packs were assembled and started, 20% of the cells from each pack were subjected to random vibration testing. An equal number of cells went through characterization testing where they were cycled under various charge/discharge rates and temperatures to provide fundamental efficiency and operation characteristics. The cells were then assembled into LEO life cycle packs of 4 to 10 cells or the storage groups based on the test matrix shown in Table II.

c. A standard LEO life cycle test consisted of dividing each group or lot of cells into four separate packs. Of the four packs, two were tested at a DOD of 35% at 10°C and -5°C. The

		Yardney			Eagle Picher			Gates		
		65 AmpHr Standard	65 AmpHr Advanced	81 AmpHr Advanced	65 AmpHr Standard	65 AmpHr Advanced	81 AmpHr Advanced	65 AmpHr Standard	65 AmpHr Standard	81 AmpHr Advanced
Stack Arrangement	Recirculating	X						X	X	X
	Back-To-Back		X	X	X	X	X			
Stack Type	Dual	X	X	X	X	X	X			
	Single							X	X	X
Separator Material	Zircar	X	X	X	X^2	X	X	X^2	X^2	X^2
	Asbestos	X	X	X		X	X			
	Serrated		X	X					X^3	
KOH Concentration	26%		X	X					X^3	X
	31%	X			X	X	X	X		
Wall Recombination	Yes		X	X		X	X			
	No	X			X			X	X	X
Ni Electrode	Slurry	X	X	X^1	X	X	X			
	Dry Sinter							X	X	X

(1) Ni Electrode is thinner than the 65 AmpHr advanced design.

(2) Separator is two layers of Zircar.

(3) Half of the cells are 26% KOH and half are 31% KOH.

Table I. Ni-H_2 Cell Design Matrix

remaining two packs were tested to a DOD of 60% at 10°C and -5°C. The charge/discharge regime varied from group to group. Most packs used a test regime that discharged the specified DOD in .6 hours. The discharge was followed by a high rate charge for .6 to .667 hours (36 to 40 minutes) that put 95% of the discharged Amp-Hours back into the pack. Following the high rate charge, a low rate charge for .233 or .3 hours brought the pack to a constant recharge rate that varied from 101% to 107%. Table III shows a summary for a typical test regime used with the 81 AmpHr Gates cells.

d. Some of the packs used variances to the standard charge/discharge regime. They included varying the state of charge (SOC) at the beginning of the test, the use of a taper charge, a single step charge, and a trickle charge at the end of the charge step. For the Gates 65 AmpHr cells, 3600G through 3604G and Eagle Picher 3600X through 3605X, different SOC were used. SOC tests are set by starting the LEO cycle tests with the cells at a specific SOC. Currently, these packs are being run at 90%, 94% and 100% SOC.

		Yardney			Eagle Picher			Gates			
		65 AmpHr Standard	65 AmpHr Advanced	81 AmpHr Advanced	65 AmpHr Standard	65 AmpHr Advanced	81 AmpHr Advanced	65 AmpHr Standard	65 AmpHr Standard	81 AmpHr Advanced	
35% DOD LEO Test	-5°C	10 5635W	5 5735W	10 3835Y	0	5 5735E	10 3835E	10 3635G	0	10 3835G	
	10°C	10 5631W	5 5731W	10 (2) 3831Y	24 (4) 360xX	5 3731E	10 3831E	10 3631G	12 (9) 360xG	10 3831G	
60% DOD LEO Test	-5°C	10 (1) 5665W	5 (1) 5765W	0	0	5 (1) 3765E	10 3865E	0	0	10 3865G	
	10°C	10 (1) 5661W	5 (1) 5761W	20 (3) 386xY	24 (5) 360xX	5 3761E	10 3861E	20 (7) 366xG	8 (10) 360xG	10 3861G	
Storage		10	0	17	2	0	17 (6)	10 (8)	0	17	
Shipped to GSFC for Additional Testing		0	0	3	0	0	3	0	0	3	
On Test at Crane Under Another Project		0	0	0	0	0	0	0	10	0	

(1) These packs have failed and have been discontinued.
(2) One cell was removed from the pack of 10 when it failed.
(3) Split between two 10 cell packs, 3861Y and 3865Y.
(4) Split between three 8 cell packs, 3600X, 3601X, and 3602X.
(5) Split between three 8 cell packs, 3603X, 3604X, and 3605X.
(6) One of these 17 cells failed during characterization testing.
(7) Split between two 10 cell packs, 3661G and 3665G.
(8) Seven of this group of 10 cells have failed. One failure occured during acceptance tesing. The remaining 6 cells failed during vibration testing.
(9) Split between three 4 cell packs, 3600G, 3602G and 3603G.
(10) Split between two 4 cell packs, 3601G and 3604G.

TABLE II. Ni-H_2 Cell Test Matrix

e. In addition to using varying SOC, the Eagle Picher 65 AmpHr cells in packs 3600X through 3605X are using single step, and taper charges. The six packs are all running at 10°C. Three packs are operating at 35% DOD and three at 60% DOD. In each DOD group, the packs were started at 100%, 94%, or 90% SOC. The 100% SOC tests use a taper charge at the end of the high rate charge. When the tests were first started, the charge regime

	Discharge Regime	Charge Regime		Temp °C
3831G	35%DOD in .6Hr	Hi Rate for .600Hr	Lo Rate for .300Hr	10
3835G	35%DOD in .6Hr	Hi Rate for .600Hr	Lo Rate for .300Hr	-5
3861G	60%DOD in .6Hr	Hi Rate for .667Hr	Lo Rate for .233Hr	10
3865G	60%DOD in .6Hr	Hi Rate for .667Hr	Lo Rate for .233Hr	-5

All tests are 10 cells per pack

TABLE III. Gates 81 AmpHr Test Regime Summary

included a 2 Amp trickle charge at the end of the charge. This reflected the trickle charge that was part of the charge profile for Space Station Freedom (SSF). When the trickle charge was dropped from the SSF charge profile, the test profile for the six Eagle Picher packs was also modified to reflect the difference. A summary of the 65 AmpHr Eagle Picher charge/discharge profiles are shown in Table IV.

	Cycle Range	Discharge Regime	Charge Regime			State of Charge
3600X	1-2727	35%DOD in .6Hr	Hi Rate	Taper	2 Amp Trickle	100%
	2738-8694	35%DOD in .6Hr	Hi Rate	Taper		
3601X	1-2749	35%DOD in .6Hr	Hi Rate		2 Amp Trickle	94%
	2758-8746	35%DOD in .6Hr	Hi Rate			
3602X	1-2736	35%DOD in .6Hr	Hi Rate		2 Amp Trickle	90%
	2748-8575	35%DOD in .6Hr	Hi Rate			
3603X	1-2752	60%DOD in .6Hr	Hi Rate	Taper	2 Amp Trickle	100%
	2758-8297	60%DOD in .6Hr	Hi Rate	Taper		
3604X	1-2724	60%DOD in .6Hr	Hi Rate		2 Amp Trickle	94%
	2730-8249	60%DOD in .6Hr	Hi Rate			
3605X	1-2668	60%DOD in .6Hr	Hi Rate		2 Amp Trickle	90%
	2678-8122	60%DOD in .6Hr	Hi Rate			

All tests are 8 cells per pack at 10°C

TABLE IV. Eagle Picher 65 AmpHr Test Regime Summary

4. *TEST EQUIPMENT*

a. All of the cyclic testing has been done on one of two automated test systems that have been developed and built at NAVSURFWARCENDIV Crane. Each system is built around a Hewlett Packard HP1000 mini computer. The computers use Hewlett Packard HP3497 Data Acquisition/Control units and HP3456 Digital Voltmeters to monitor and control process functions. All of the equipment is maintained and calibrated to the NAVWPNSUPPCEN Instruction 4355.17K, covering the implementation of the Naval Sea System Command Calibration Program.

b. Each test system is capable of simultaneously controlling and monitoring a variety of test scenarios on up to 40 separate packs. Each pack's charge/discharge current, cell voltage, cycle time, and operational limits are monitored by the test software on a two minute interval. To assure prompt action during test upsets and interruptions, the test labs are staffed 24 hours a day, 7 days a week.

c. A recent upgrade to the test system capabilities has been to add a centralized database of all of the test data at Crane. Access is available through phone in connections to all

NASA customers at this time. Data base users have access to any data that is part of their project. Security is provided by a user/password entry during login. All of the automated test systems that are operated by the Aerospace Power Systems Branch are interfaced to the database via network connections. A diagram of the test systems, database, and remote access interconnection are shown in Figure 1.

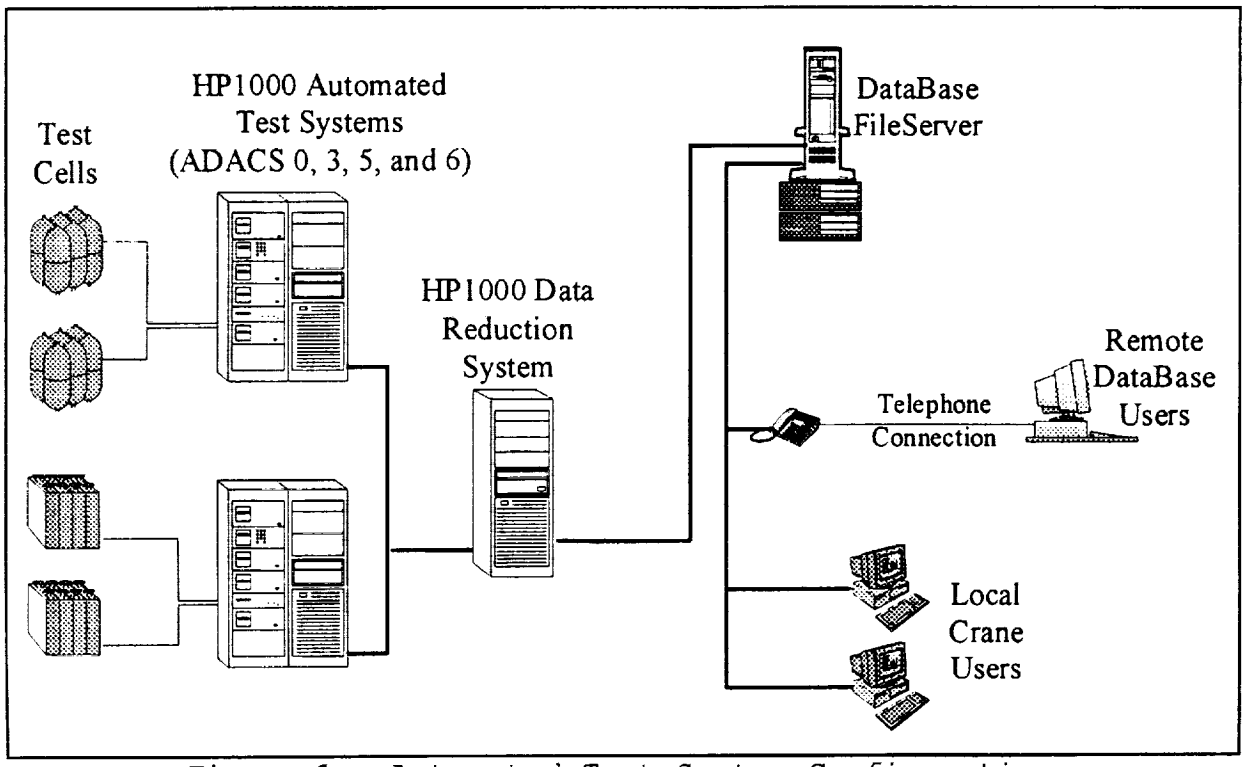

Figure 1. Automated Test System Configuration

5. *TEST RESULTS*

a. Seven cells showed signs of KOH leakage around one or both terminals during the initial receipt inspection. Leaks were discovered in two 65 AmpHr Yardney cells and five 81 AmpHr Yardney cells. All of the leaking cells were returned to Yardney for repair. When they were received back at NAVSURFWARCENDIV, no KOH leakage was detected. The two 65 AmpHr cells were put in a storage group. The 81 AmpHr cells were placed into LEO life cycle packs, 3831Y and 3865Y. Of the three that were put in pack 3831Y, one was removed at cycle 3199 because of low EOD voltages. At cycle 6440, all of the cells in the pack were rechecked for leaks. The failed cell in 3831Y showed signs of KOH at both terminals. The remaining cells did not appear to have any leaks.

b. One 65 AmpHr Gates cell failed acceptance testing when it showed little to no capacity in the first cycle. The cell was shipped to Gates where a Destructive Physical Analysis (DPA) was

performed. The cause of failure was determined to be a twisted cell stack from the assembly process.

c. An 81 AmpHr Eagle Picher cell failed during characterization with a gradual loss of capacity after 15 deep cycles to .5 volts. The cell was DPA'd at Crane. The cause of failure was determined to be shorting of the positive plates to the case.

d. Six of the eight 65 AmpHr Gates cells that were subjected to vibration testing failed. One of the cells showed signs of leaking immediately after the vibration test. A subsequent capacity check of the cells showed little capacity, 1 to 5 AmpHr, on four cells and a reduced capacity on one more cell. The four cells with little capacity showed signs of leaking after the capacity test. The final cell showed signs of leaks prior to beginning life cycle testing 5 months later. The two cells that passed the vibration test are currently life cycle packs 3661G and 3635G. Their EOD voltages compared to the pack average voltage are 1.158V/1.162V and 1.224V/1.226V respectively.

e. During the program, a total of 39 packs, 308 cells, have been cycled under a LEO test regime. Currently there are 32 packs, 252 cells still under test. Figures 2, 3, and 4 represent the cycling history and current status of the LEO packs for each of the three manufacturers. For the SSF test program.

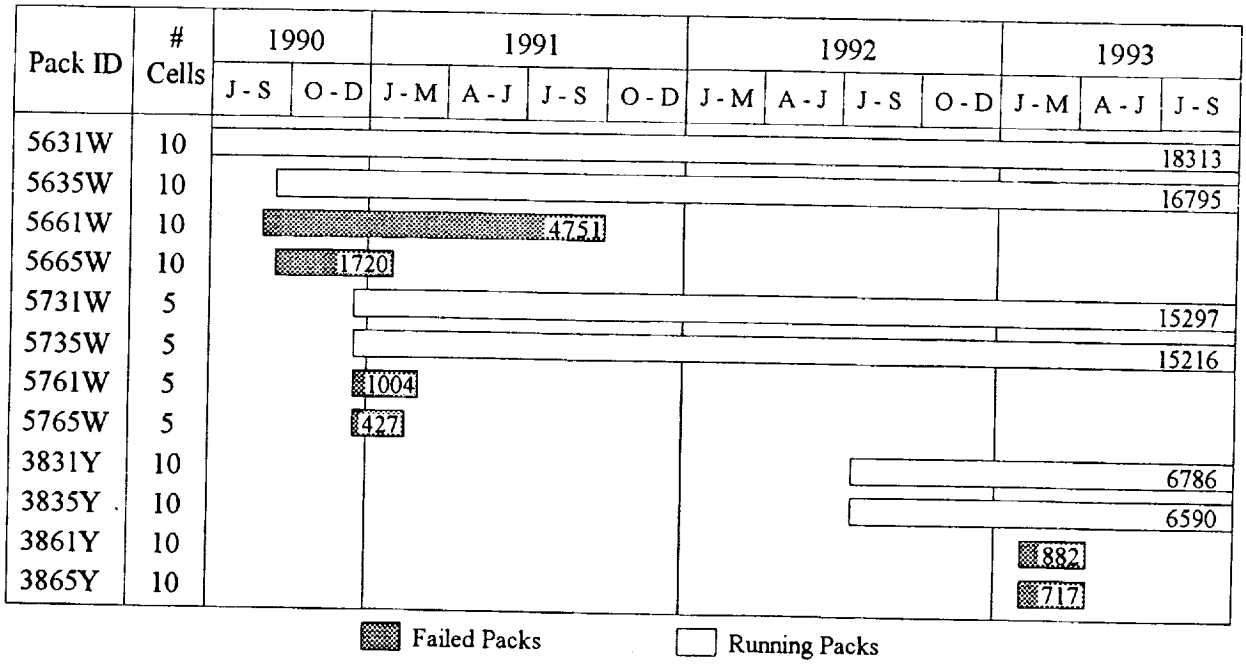

Figure 2. Yardney Life Cycle Test Summary

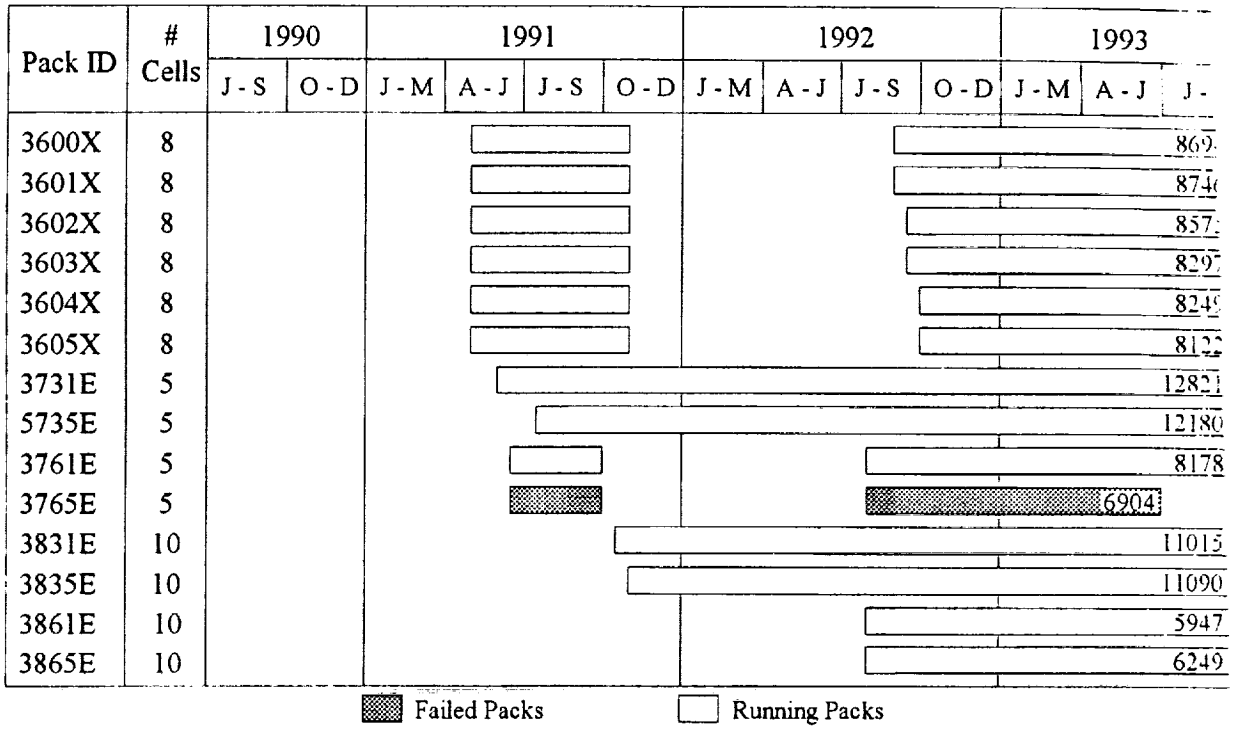

Figure 3. Eagle Picher Life Cycle Test Summary

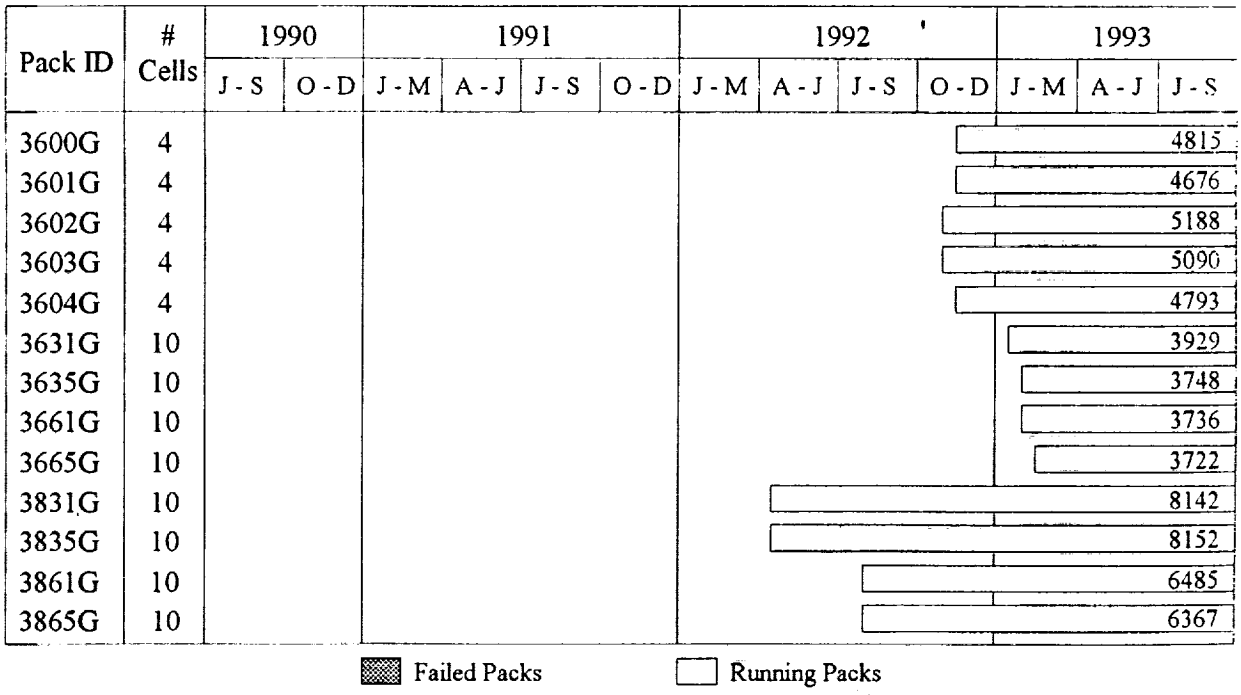

Figure 4. Gates Life Cycle Test Summary

life cycle failure occurs when the majority of the cells in a pack fall below EOD voltage of 1.0V.

f. Four Yardney 65 AmpHr packs that started LEO testing early in the program, failed after 427 to 4751 cycles. Post LEO capacity tests showed a variance of 58% to 83% of the original capacities, Table V. All of the cells were cycling at 60% DOD.

g. Two packs that were started at 60% DOD, 3861Y and 3865Y, dropped below the 1.0V EOD limit after 882 cycles and 717 cycles respectively. Post LEO capacity testing showed little capacity loss, Table V. The post life cycle capacity of 3861Y was measured to be 73 AmpHrs, a 2.6% loss from the 75 AmpHrs measured before life cycle testing began. Similarly, the post life cycle capacity of 3865Y was measured to be 67 AmpHr, a 6.9% capacity loss. Both packs have been considered as failed and testing has been discontinued.

h. A more recent failure is the -5°C, 60% DOD 65 AmpHr Eagle Picher pack, 3765E. It failed at 6904 cycles. Post LEO capacity was measured at 43% of the original value, Table V. The 10°C, 60% DOD pack, 3761E, that is from the same lot as 3765E, is near failure. One cell dropped below an EOD voltage of 1.0V at 6171 cycles. At 7927 cycles the same cell was removed from the pack when the cell EOD voltage dropped to 0.0V. At 8178 cycles, the average EOD voltage of the remaining 4 cells in the pack is 1.038V.

Pack Capacities to 1.0V				
PACK	Number of Cycles	Pre L.C. Capacity (AmpHr)	Post L.C. Capacity (AmpHr)	Discharge Rate
5661W	4751	67	39	C
5665W	1720	72	52	C
5761W	1004	60	50	C
5765W	427	66	50	C
3861Y	882	75	73	C/2
3865Y	717	72	67	C/2
3765E	6904	79	34	C

TABLE V. Pre and Post Life Cycle Failure Capacities

i. In addition to the cells already mentioned, there are some packs that have EOD voltages that are approaching levels of concern. The 81 AmpHr, 60% DOD Eagle Picher pack, 3865E is running with an EOD voltage of .995 at 6249 cycles. Four of ten cells have fallen below the 1.0V EOD value. Two 60% DOD 81 AmpHr Gates packs have cells that are approaching 1.0V at EOD. 3861G has one cell that has dropped to .940V while the pack average is still 1.085V. 3865G has three cells below 1.0V with a pack average of 1.095V.

6. *PRELIMINARY FINDINGS*

a. Even though the majority of the life cycle testing is still ongoing, some early conclusions can be made. The testing has provided a method to test the feasibility of a state of charge test. Of the six 65 AmpHr Eagle Picher packs, 3600X - 3605X, four are being operated at less than 100% SOC. So far the lower SOC has not resulted in large voltage dispersions.

b. Cells with the double layer Zircar separators have performed better than the asbestos or asbestos-Zircar combination in 60% DOD tests. Of the 39 life cycle packs tested during the program, 19 were at 60% DOD. So far, seven of the 19 packs have failed. All of the failed packs have had the asbestos-Zircar separator combination and had a completed cycle range from 717 to 6904. There are still three packs with the asbestos-Zircar separators running with a completed cycle range of 5947 to 8178. Of those, two are expected to fail within the next 1000 cycles. The remaining nine packs have a double layer Zircar separator with a completed cycle range from 3722 to 8297. None of them are in any immediate danger of failing.

c. Identical cells run at higher pressures at -5°C vs 10°C when cycled at 35% DOD. Cells run at 60% DOD also run at higher pressures than cells run at 35% DOD. The Eagle Picher 81 AmpHr packs 3831E, 3835E, 3861E, and 3865E are an example of the pressure differences. The 35% DOD packs 3831E (10°C) and 3835E (-5°C) have EOD/EOC pressures of 410/640 psi and 550/770 psi respectively. The 60% DOD packs, 3861E (10°C) and 3865E (-5°C) have EOD/EOC pressures of 430/840 and 420/790 psi.

d. At 60% DOD, cells perform better at 10°C than at -5°C. In all life cycle failures so far, packs running at -5°C completed fewer cycles than identical packs that ran at 10°C. The colder temperature and higher current result in undesirable voltage performance. The performance at 60% DOD has fallen short of anticipated life cycle expectancy.

Appendix A

Life Cycle Trend Plots

NSWC Crane Pack ID 3600X 8 cells

Voltage/Pressure/Recharge EOC/EOD Trend Plot 04/28/91 - 09/28/93

Eagle Picher 65 AmpHr 35% DOD 10 Deg C Taper Chg

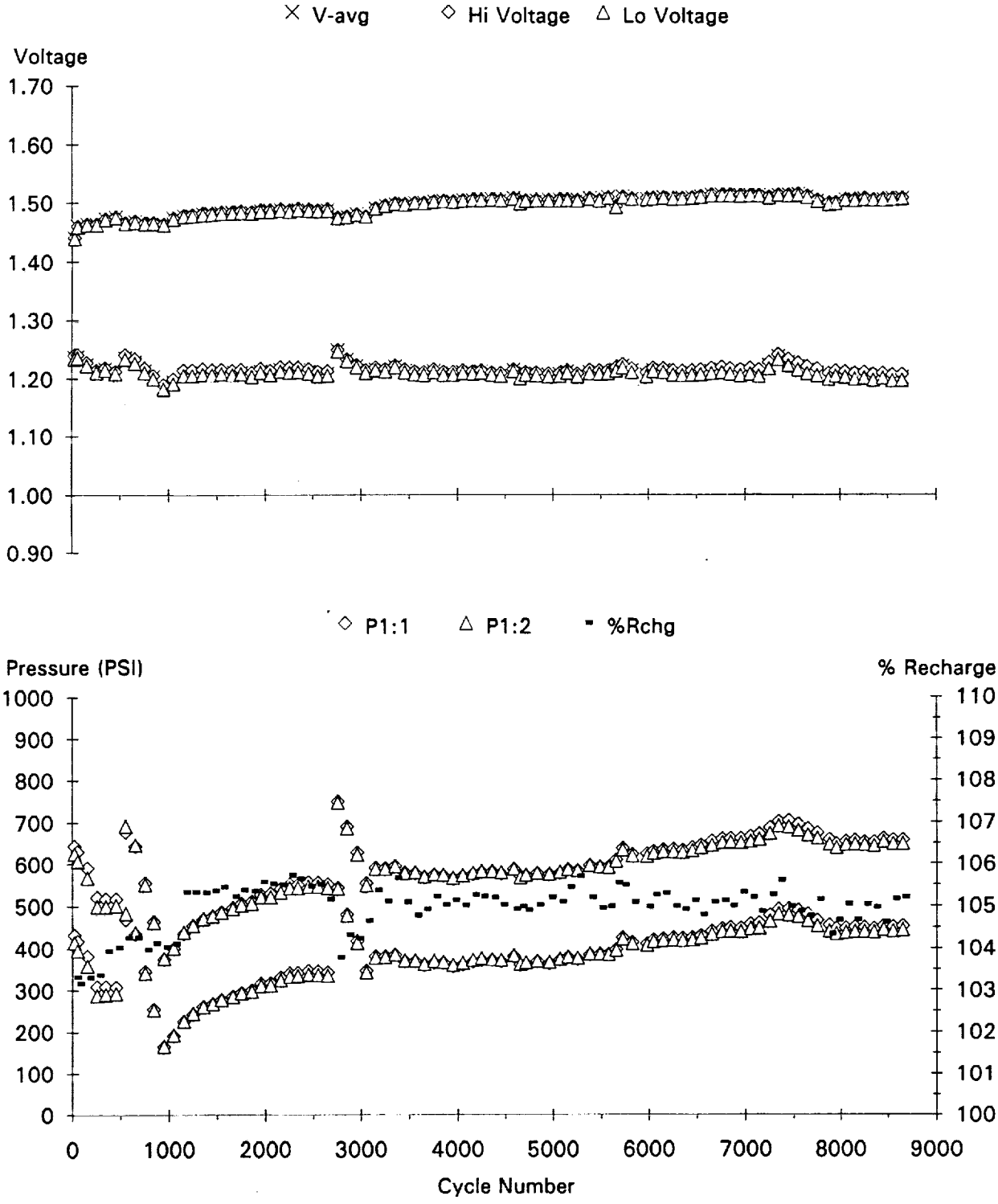

Note. Cycles 1-2727 display the total Recharge rate, including the .73% from the 2.0A trickle charge at the end of the charge cycle. The target recharge rate does not include the 2.0A trickle charge.

Cycle 1. Started Life Cycle Test.
-37.92A for .6Hr ; 31.42A for .6Hr ; 30.575 to 8.703A Taper for .233 Hr ; 2.0A for .083Hr
Rchg = 103.0%

Cycle 492. Power Supply failure during discharge caused pack to be overcharged.

Cycle 1287. Raised Rchg from 103.0% to 104%.
-37.92A for .6Hr ; 31.42A for .6Hr ; 30.645 to 10.584A Taper for .233Hr ; 2.0A for .083Hr

Cycle 2727. 11/01/91. Halted test for evaluation. Cells were left in a discharged state.

Cycles 2728 - 2737. These cycles were used for capacity testing.

Cycle 2738. Pack restarted under a new test regime.
-37.92A for .6Hr ; 29.76A for .633Hr ; 29.03 to 7.045A Taper for .266Hr ;
Rchg = 104.0%

Cycle 3154. Raised Rchg from 104.0% to 105.0%.
-37.92A for .6Hr ; 29.76A for .6Hr ; 29.084 to 8.698A Taper for .266Hr

NSWC Crane **Pack ID 3601X** **8 cells**

Voltage/Pressure/Recharge EOC/EOD Trend Plot 04/25/91 - 09/25/93

Eagle Picher 65 AmpHr 35% DOD 10 Deg C 94% SOC

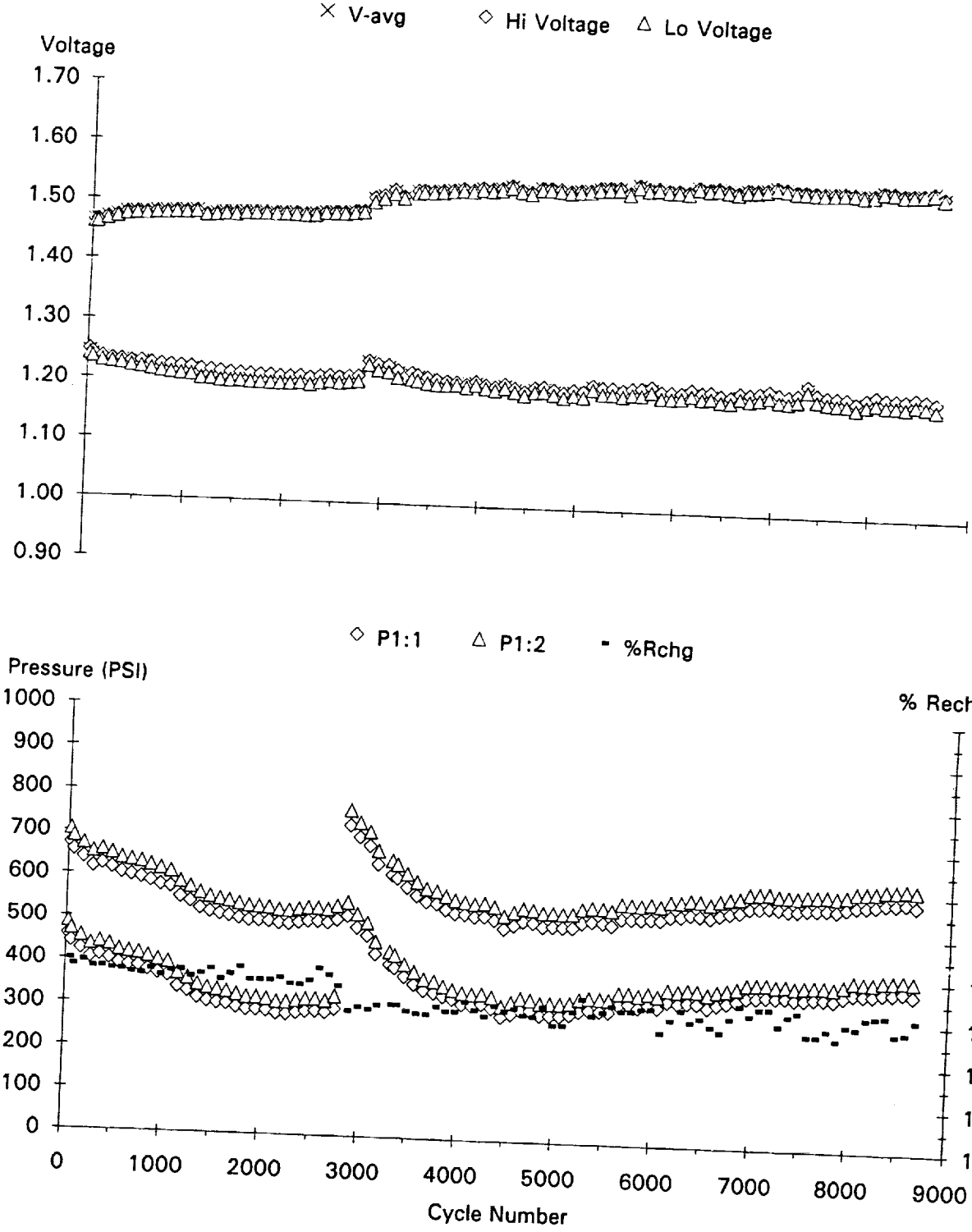

Note. Cycles 1-2749 display the total Recharge rate, including the .73% from the 2.0A trickle charge at the end of the charge cycle. The target recharge rate does not include the 2.0A trickle charge.

Cycle 1. Started Life Cycle Test.

-37.92A for .6Hr ; 26.52A for .883Hr ; 2.0 A for .083 Hr ; Rchg = 103.0%

Cycle 2749. 11/25/91. Halted test for evaluation. Cells were left in a discharged state.

Cycles 2750 - 2757. These cycles were used for capacity testing.

Cycle 2758. Pack restarted under a new test regime.

-37.92A for .6Hr ; 26.04A for .9Hr ; 103.0% Rchg

NSWC Crane **Pack ID 3602X** **8 cells**

Voltage/Pressure/Recharge EOC/EOD Trend Plot 04/25/91 - 09/29/93

Eagle Picher 65 AmpHr 35% DOD 10 Deg C 90% SOC

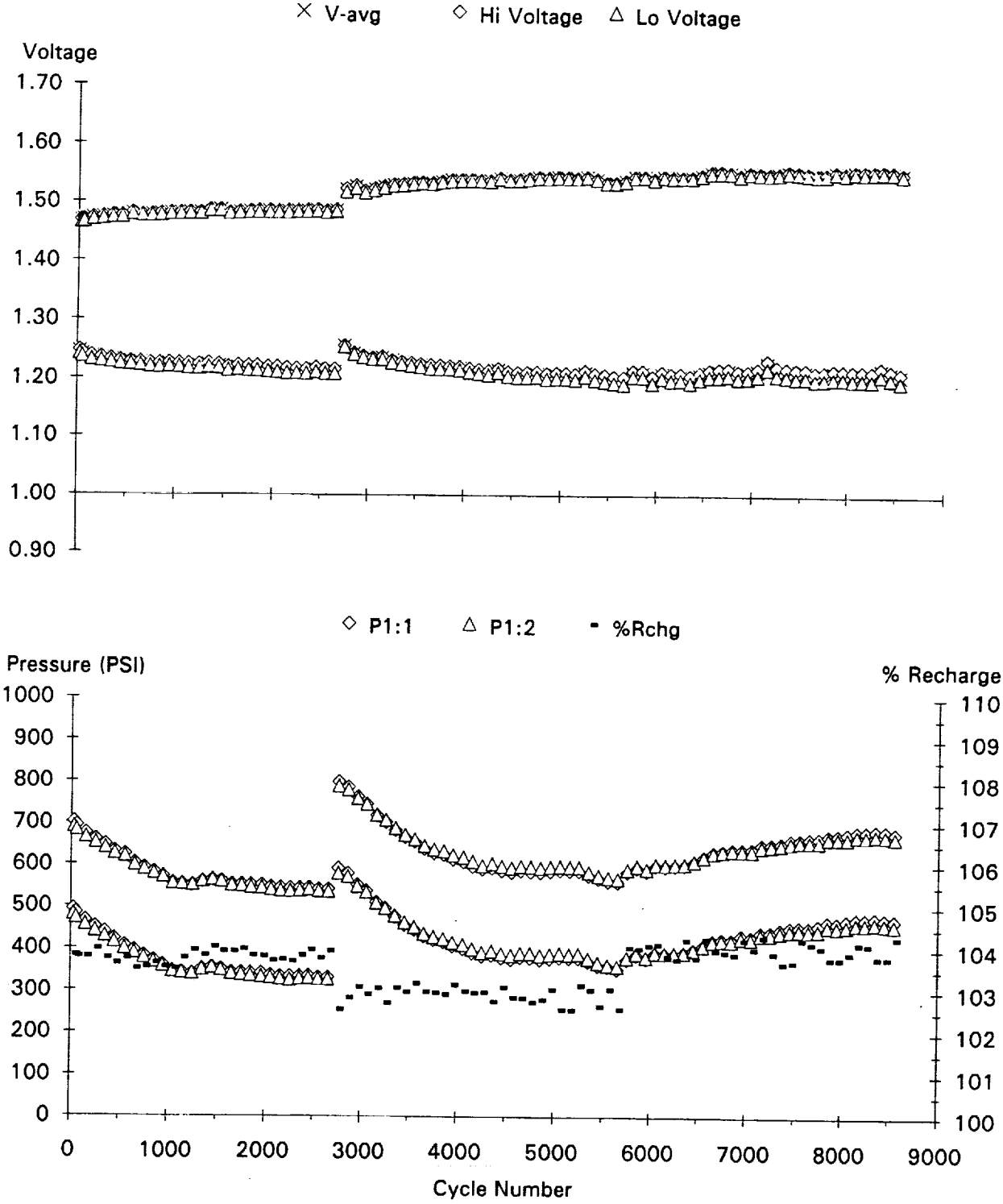

Note. Cycles 1-2736 display the total Recharge rate, including the .73% from the 2.0A trickle charge at the end of the charge cycle. The target recharge rate does not include the 2.0A trickle charge.

Cycle 1. Started Life Cycle Test.

-37.92A for .6Hr ; 26.52A for .883Hr ; 2.0A for .083Hr ; Rchg = 103.0%

Cycle 2736. 10/24/91. Halted test for evaluation. Cells were left in a discharged state.

Cycles 2737 - 2747. These cycles were used for capacity testing.

Cycle 2748. Pack restarted under a new test regime.

-37.92A for .6Hr ; 26.04A for .9Hr ; Rchg = 103.0% Rchg

Cycle 5698 Raised Rchg from 103.0% to 104.0%.

-37.92A for .6Hr ; 26.28A for .9Hr

NSWC Crane **Pack ID 3603X** **8 cells**

Voltage/Pressure/Recharge EOC/EOD Trend Plot 05/03/91 - 09/27/93

Eagle Picher 65 AmpHr 60% DOD 10 Deg C Taper Chg

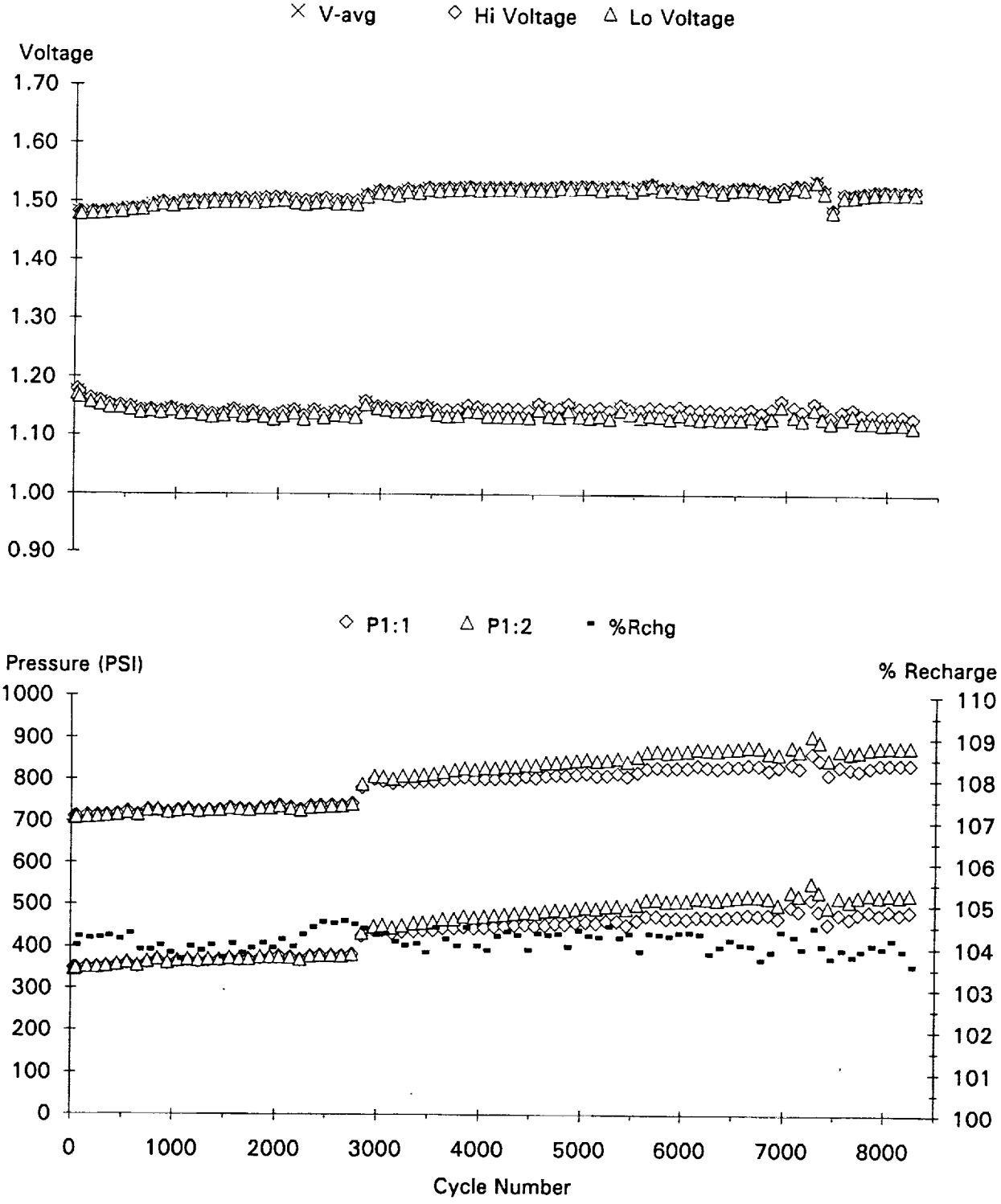

Note. Cycles 1-2752 display the total Recharge rate, including the 1.0% from the 2.0A trickle charge at the end of the charge cycle. The target recharge rate does not include the 2.0A trickle charge.

Cycle 1. Started Life Cycle Test.

-65.0A for .6Hr ; 54.0A for .65Hr ; 45.435 to 14.129A Taper for .183Hr ; 2.5A for .2Hr ; Rchg = 104.0%

Cycle 630. Corrected Taper Charge.

-65.0A for .6Hr ; 54.0A for .65Hr ; 45.435 to 14.129A Taper for .183Hr ; 2.0A for .2Hr ; Rchg = 104.0%

Cycle 2752. 11/01/91. Halted test for evaluation. Cells were left in a discharged state.

Cycles 2753 - 2757. These cycles were used for capacity testing.

Cycle 2758. Pack restarted under a new test regime.

-65.0A for .6Hr ; 50.14A for .7Hr ; 48.237 to 6.363A Taper for .2Hr ; Rchg = 104.0%

NSWC Crane **Pack ID 3604X** **8 cells**

Voltage/Pressure/Recharge EOC/EOD Trend Plot 04/25/91 - 10/01/93

Eagle Picher 65 AmpHr 60% DOD 10 Deg C 94% SOC

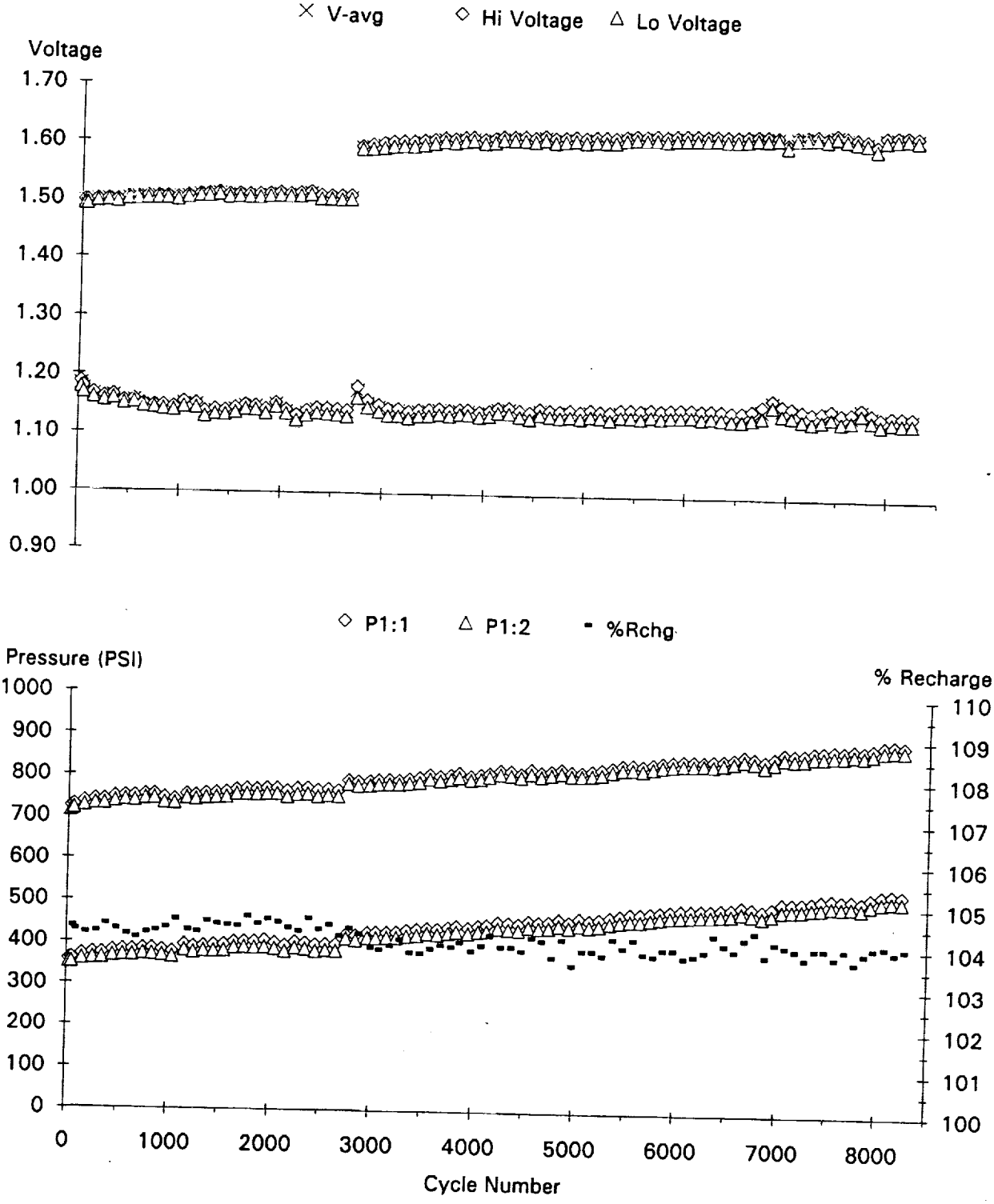

Note. Cycles 1-2754 display the total Recharge rate, including the .425% from the 2.0A trickle charge at the end of the charge cycle. The target recharge rate does not include the 2.0A trickle charge.

Cycle 1. Started Life Cycle Test.
-65.0A for .6Hr ; 45.93A for .883Hr ; 2.0A for .083Hr ; Rchg = 104.0%

Cycle 2724. 11/08/91. Halted test for evaluation. Cells were left in a discharged state.

Cycles 2725 - 2729. These cycles were used for capacity testing.

Cycle 2730. 09/30/92. Pack restarted under a new test regime.
-65.0A for .6Hr ; 45.07A for .9Hr ; Rchg = 104.0%

NSWC Crane **Pack ID 3605X** **8 cells**

Voltage/Pressure/Recharge EOC/EOD Trend Plot 04/26/91 - 09/26/93

Eagle Picher 65 AmpHr 60% DOD 10 Deg C 90% SOC

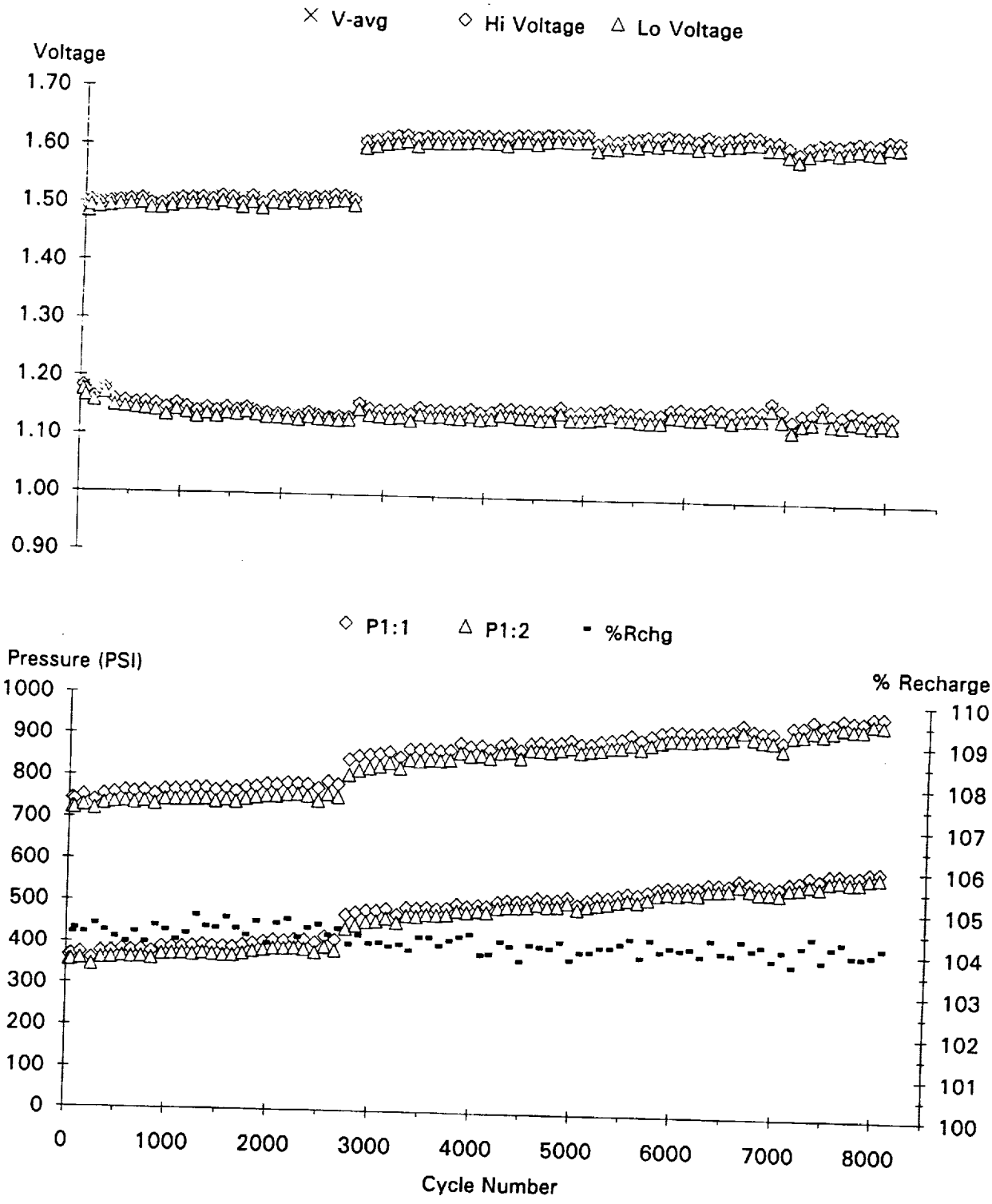

Note. Cycles 1-2668 display the total Recharge rate, including the .425% from the 2.0A trickle charge at the end of the charge cycle. The target recharge rate does not include the 2.0A trickle charge.

Cycle 1. Started Life Cycle Test.
-65.0A for .6Hr ; 45.93A for .883Hr ; 2.0A for .033Hr ; Rchg = 104.0%

Cycle 2668. 11/08/91. Halted test for evaluation. Cells were left in a discharged state.

Cycles 2669 - 2677. These cycles were used for capacity testing.

Cycle 2678. 09/24/92. Pack restarted under a new test regime.
-65.0A for .6Hr ; 45.07A for .9Hr ; Rchg = 104.0%

NSWC Crane **Pack ID 3731E** **5 cells**

Voltage/Pressure/Recharge EOC/EOD Trend Plot 06/22/91 - 09/26/93

Eagle Picher 65 AmpHr 35% DOD 10 Deg C

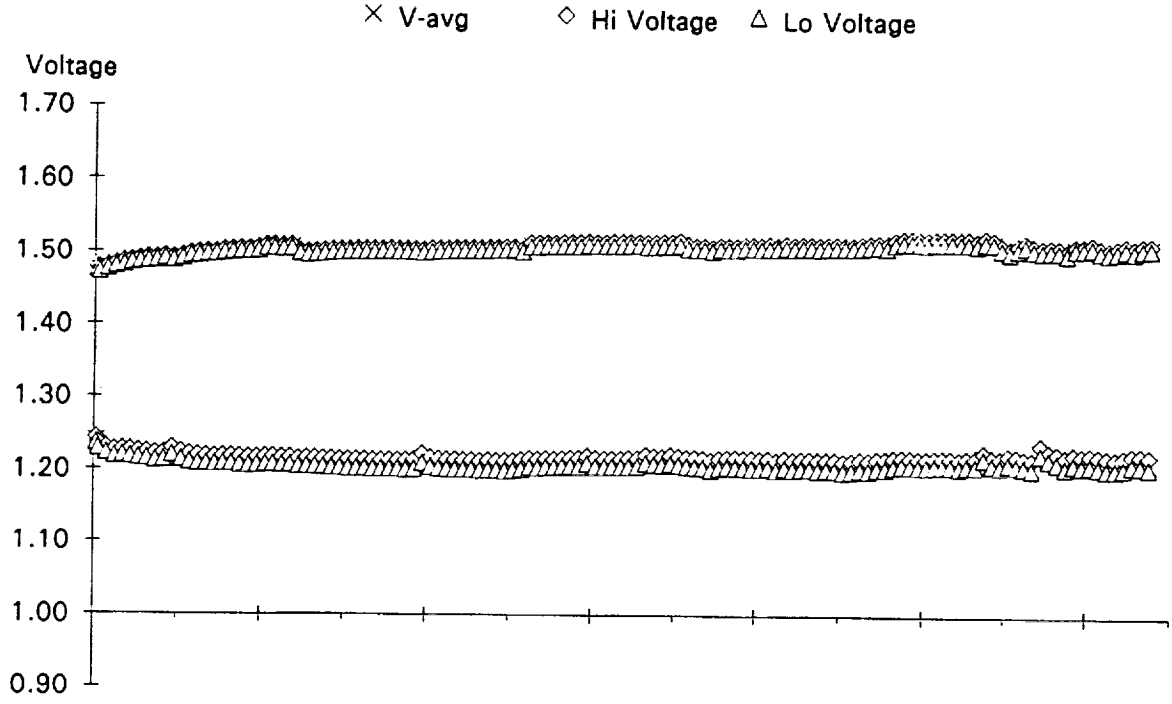

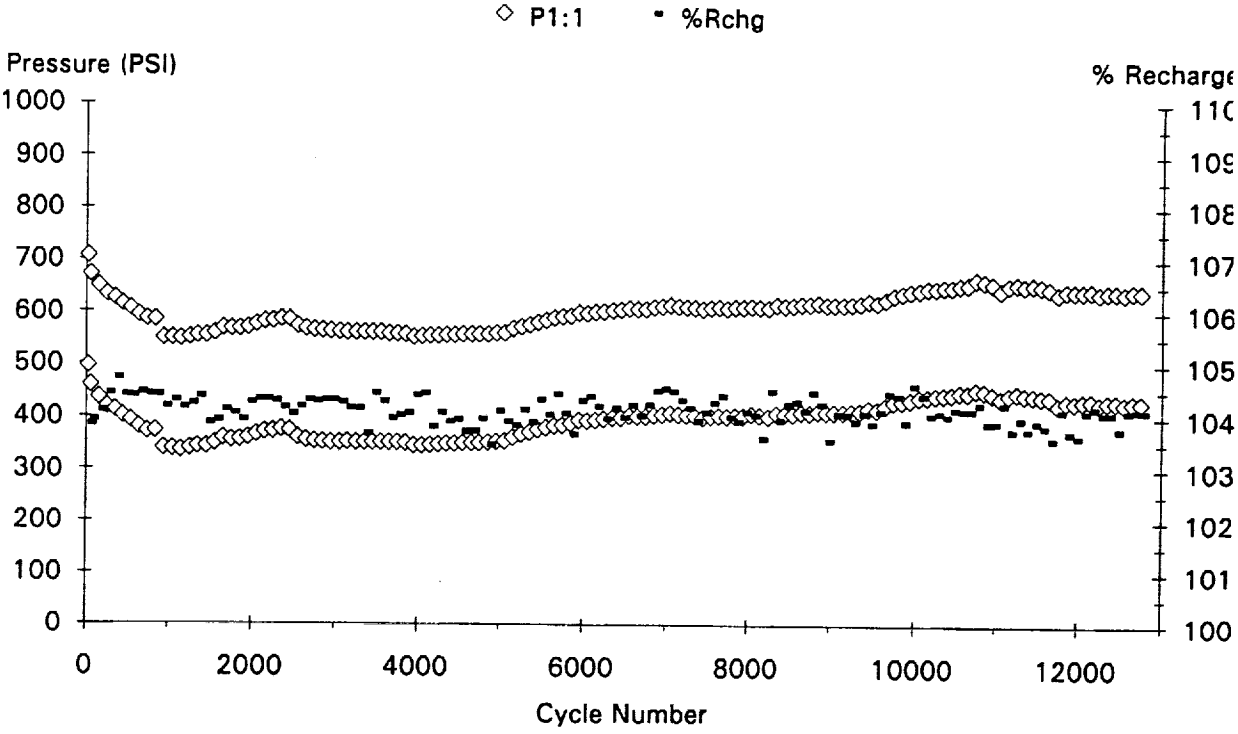

Cycle 1. Started Life Cycle Test.
-37.9A for .6Hr ; 36.0A for .6Hr ; 6.82A for .3Hr ; Rchg = 104.0%

NSWC Crane **Pack ID 5735E** **5 cells**

Voltage/Pressure/Recharge EOC/EOD Trend Plot 07/16/91 - 09/29/93

Eagle Picher 65 AmpHr 35% DOD -5 Deg C

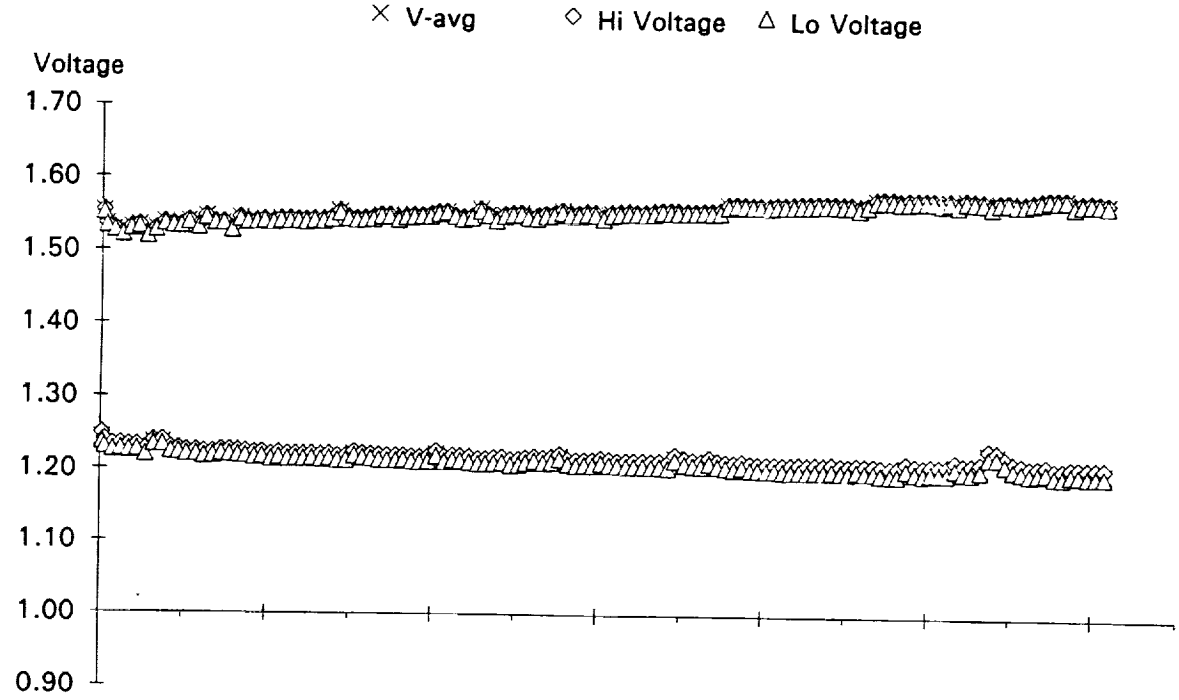

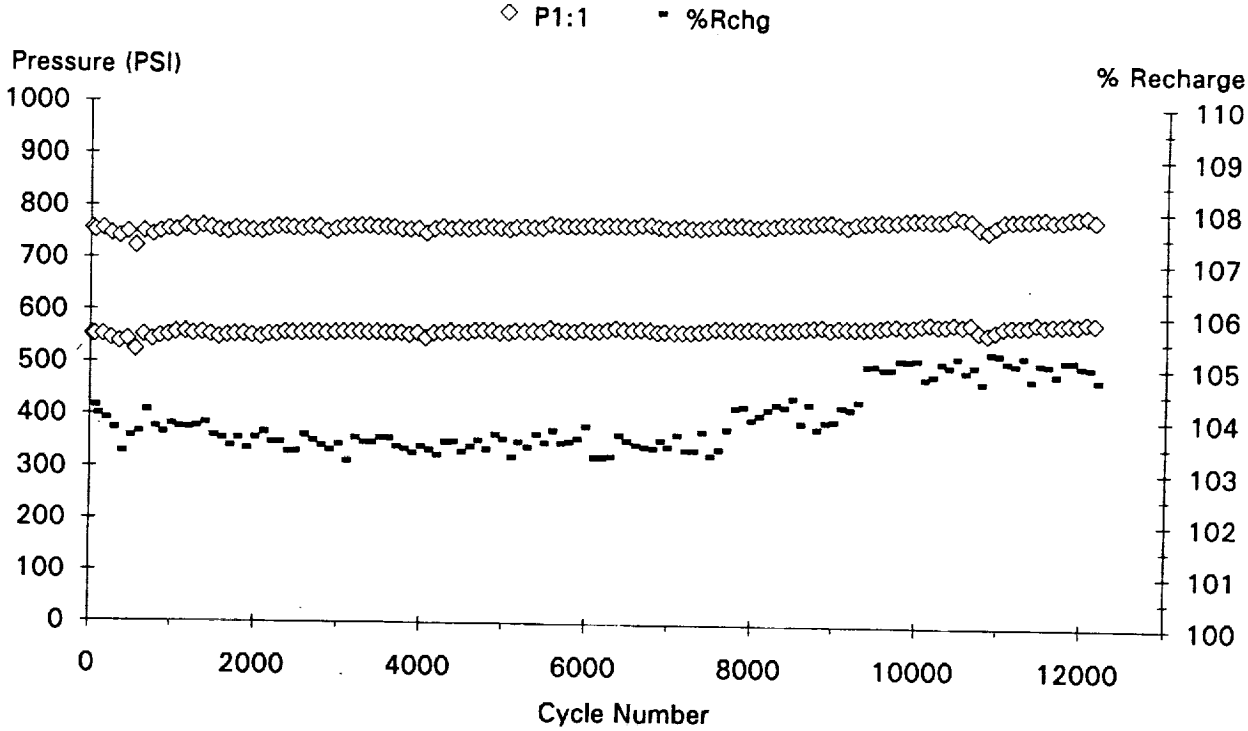

Cycle 1. Started Life Cycle Test.
-37.9A for .6Hr ; 36.0A for .6Hr ; 6.49A for .3Hr ; Rchg = 103.5%
Cycle 7491. Raised Rchg from 103.5% to 104%.
-37.9A for .6Hr ; 36.0A for .6Hr ; 6.87A for .3Hr
Cycle 9347. Raised Rchg from 104% to 105%.
-37.9A for .6Hr ; 36.0A for .6Hr ; 7.63A for .3Hr

NSWC Crane **Pack ID 3761E** **5 cells**

Voltage/Pressure/Recharge EOC/EOD Trend Plot 06/22/91 - 09/29/93

Eagle Picher 65 AmpHr 60% DOD 10 Deg C

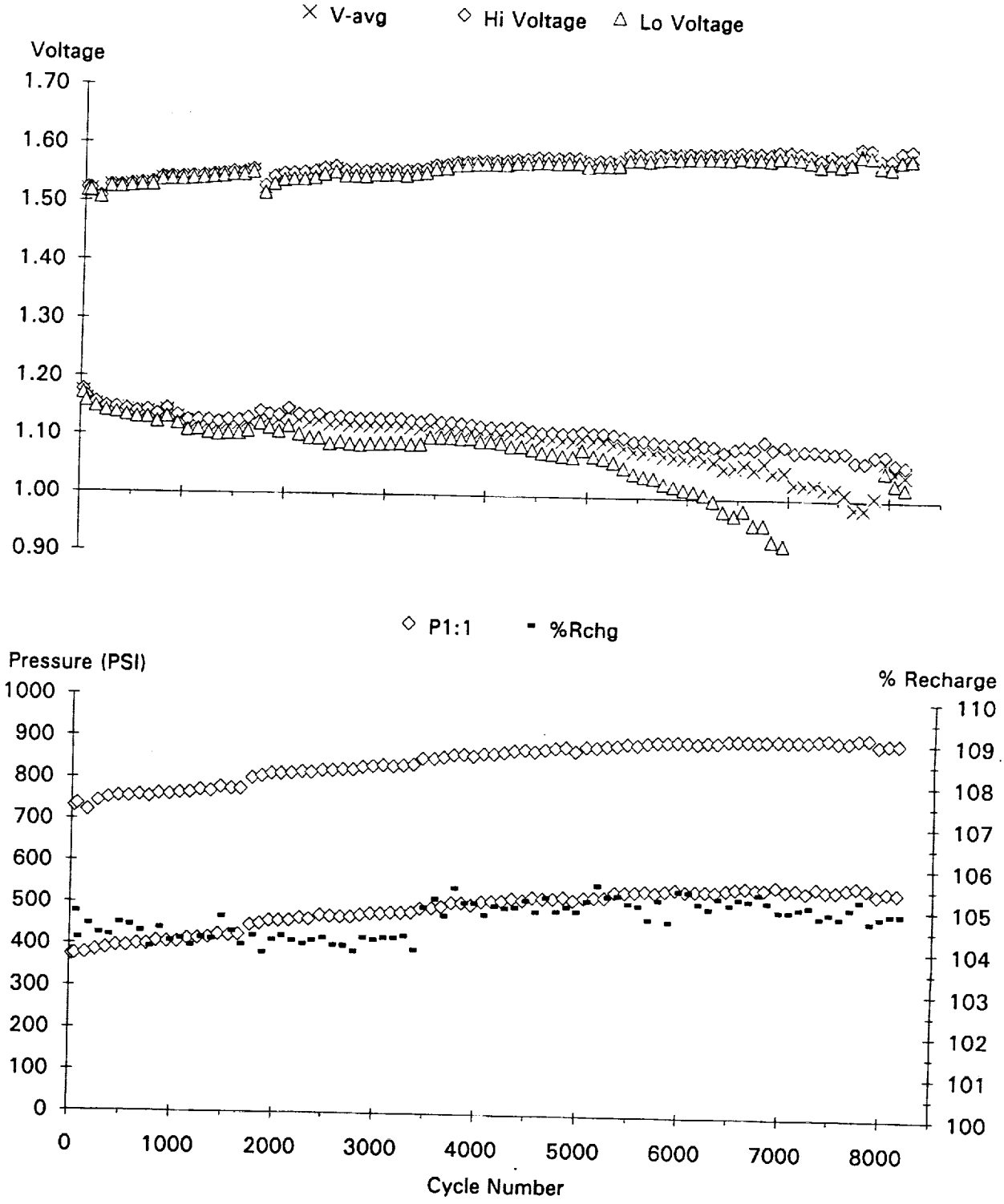

Cycle 1. Started Life Cycle Test.
-65.0A for .6Hr ; 61.75A for .6Hr ; 11.7A for .3Hr ; Rchg = 104.0%
Cycle 1649. Pack removed from testing. 10/07/91.
Cycle 1660. Pack restarted L.C. testing. 07/27/92.
-65.0A for .6Hr ; 61.75A for .6Hr ; 11.7A for .3Hr ; Rchg = 104.0%
Cycle 1784. Test regime modified to;
-65.0A for .6Hr ; 55.57A for .667Hr ; 15.06A for .233Hr ; Rchg = 104.0%
Cycle 3392. Raised Rchg from 104.0% to 105.0%
-65.0A for .6Hr ; 55.57A for .667Hr ; 16.74A for .233Hr ; Rchg = 105.0%
Cycle 6171. Cell #4 (SN22) hit 1.0V at EOD. Pack average voltage was 1.063V.
Cycle 7582. Pack average EOD voltage fell below 1.0V. EOD voltage of cell #4 was .7325V. The EOD voltage of the remaining 4 cells ranged from 1.036V to 1.068V.
Cycle 7927. Cell #4 removed from pack. EOD voltage dropped to 0V. Capacity testing was run on this cell under the Pack ID of 3761X.

NSWC Crane **Pack ID 3765E** **5 cells**

Voltage/Pressure/Recharge EOC/EOD Trend Plot 06/22/91 - 07/10/93

Eagle Picher 65 AmpHr 60% DOD -5 Deg C Test Ended at Cycle 6904

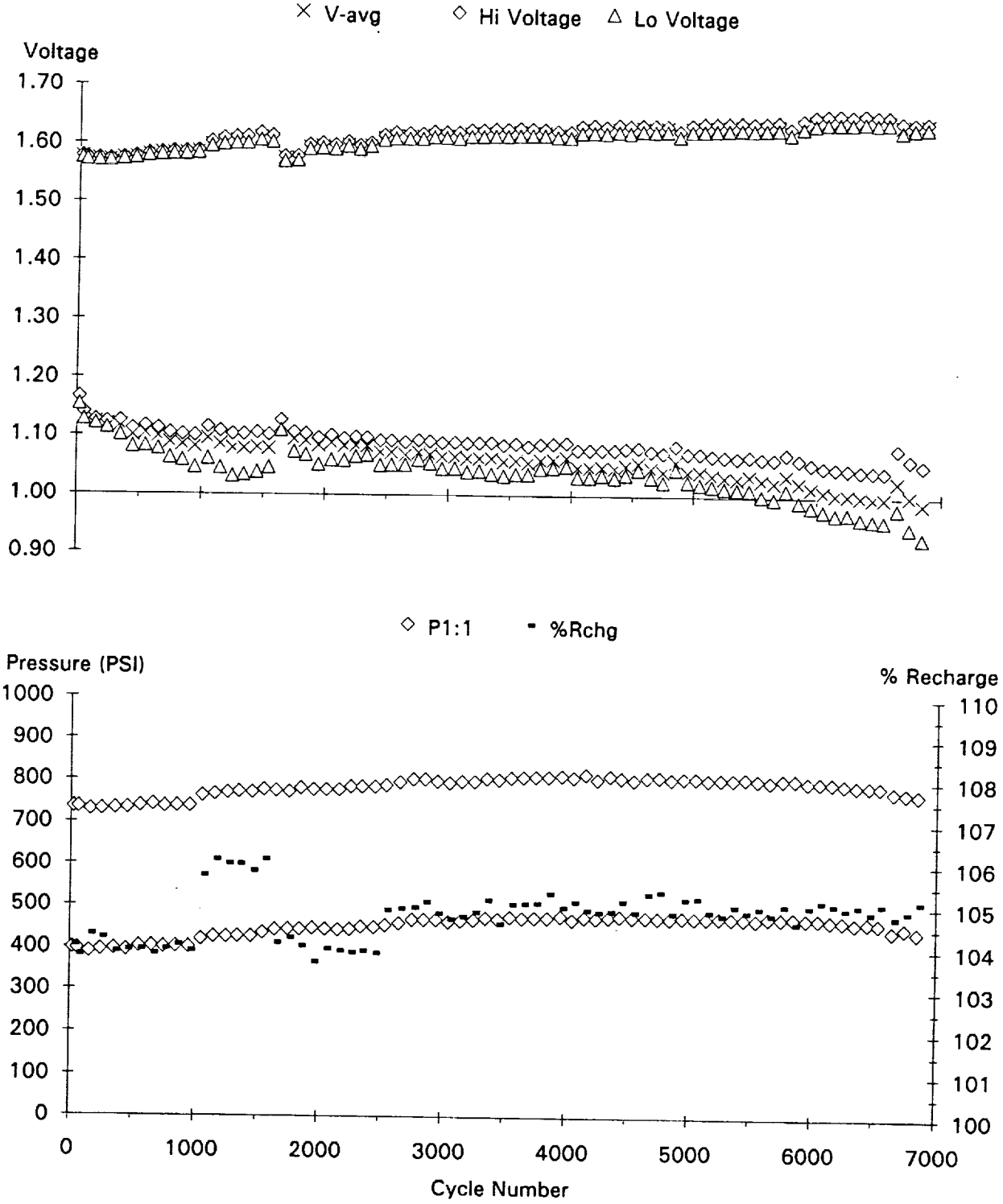

Cycle 1. Started Life Cycle Test.
-65.0A for .6Hr ; 61.75A for .6Hr ; 11.7A for .3Hr ; Rchg = 104.0%
Cycle 1091. Raised Rchg from 104.0% to 106.0%.
-65.0A for .6Hr ; 61.75A for .6Hr ; 14.3A for .3Hr ; Rchg = 106.0%
Cycle 1604. Pack removed from testing. 10/07/91.
Cycle 1615. Pack restarted L.C. testing. 07/27/92.
-65.0A for .6Hr ; 61.75A for .6Hr ; 11.7A for .3Hr ; Rchg = 104.0%
Cycle 1723. Test regime modified to;
-65.0A for .6Hr ; 55.57A for .667Hr ; 15.06A for .233Hr ; Rchg = 104.0%
Cycle 2536. Raised Rchg from 104.0% to 105.0%
-65.0A for .6Hr ; 55.57A for .667Hr ; 16.74A for .233Hr ; Rchg = 105.0%
Cycle 6904. Pack removed from Life Cycle testing. End of discharge voltages fell below 1.0V.
Cycles 6910 - 6929. Cycles used to run capacity tests on cell number 4.
Cycles 6930 - 6948. Cycles used to run capacity tests on cell number 5.

NSWC Crane Pack ID 3831E 10 cells

Voltage/Pressure/Recharge EOC/EOD Trend Plot 10/08/91 - 09/26/93

Eagle Picher 81 AmpHr 35% DOD 10 Deg C

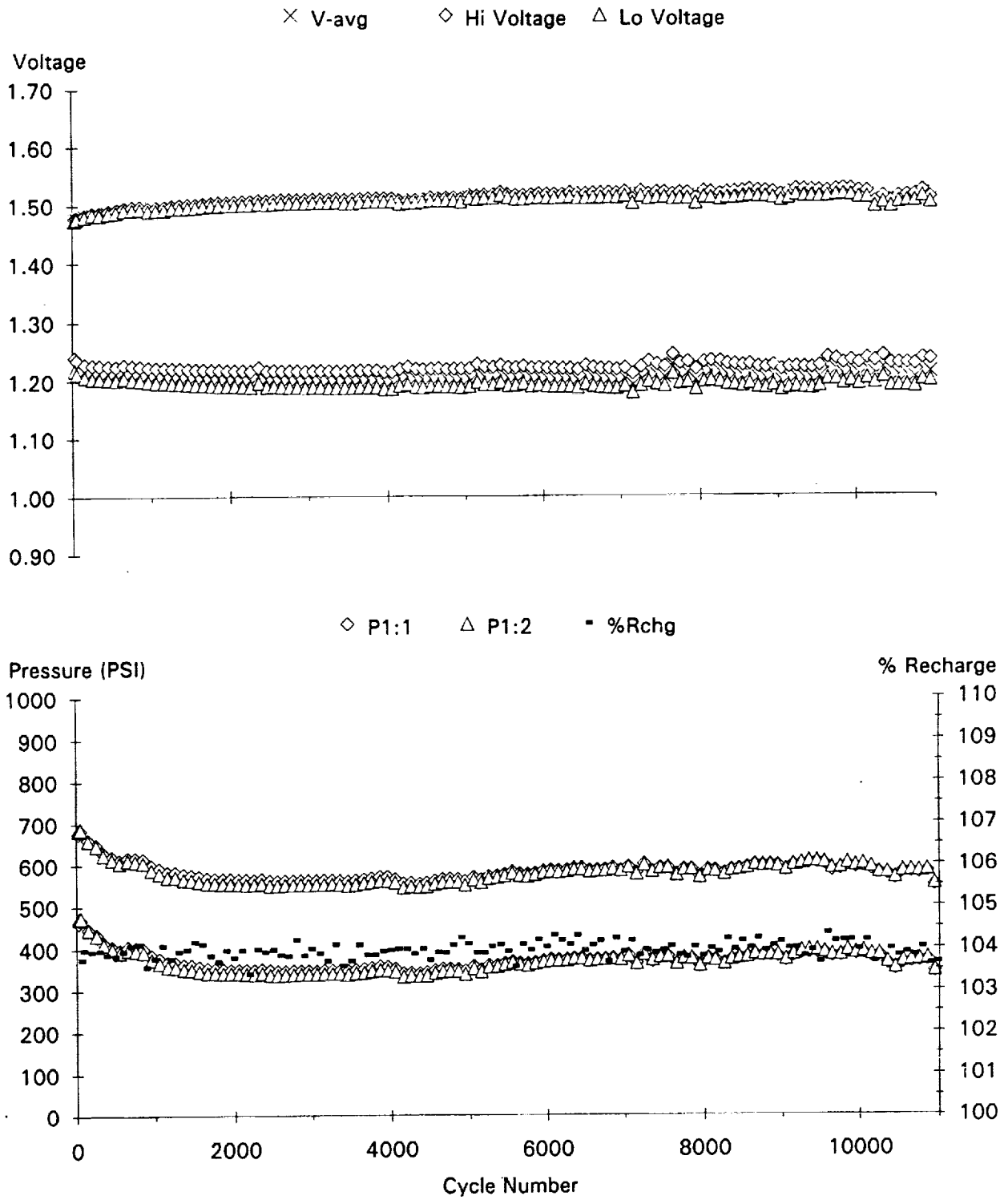

Cycle 1. Started Life Cycle Test.
-47.25A for .6Hr ; 44.89A for .6Hr ; 8.9A for .3Hr ; Rchg = 104.0%

NSWC Crane **Pack ID 3861E** **10 cells**

Voltage/Pressure/Recharge EOC/EOD Trend Plot 08/07/92 - 10/01/93

Eagle Picher 81 AmpHr 60% DOD 10 Deg C

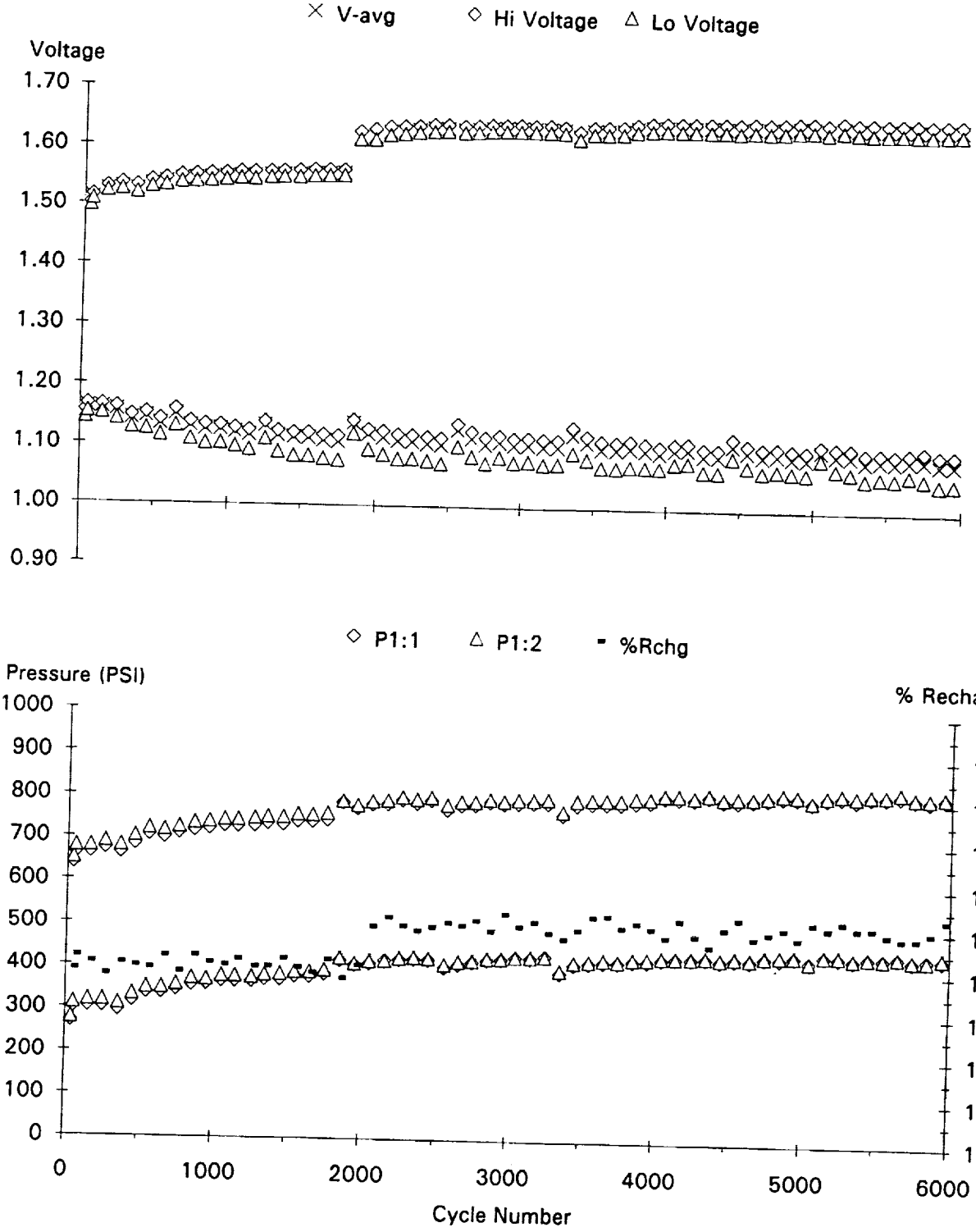

Cycle 1. Started Life Cycle Test.
-81.0A for .6Hr ; 69.25A for .667Hr ; 18.77A for .233Hr ; Rchg = 104.0%
Cycles 1818 - 1825. packs were cycled for capacity tests.
Cycle 1837. Test Regime changed to:
-81.0A for .6Hr ; 56.16A for .9Hr ; Rchg = 104.0%
Cycle 2034. Raised Rchg from 104.0% to 105.0%.
-81.0A for .6Hr ; 56.7A for .9Hr

NSWC Crane **Pack ID 3865E** **10 cells**

Voltage/Pressure/Recharge EOC/EOD Trend Plot 08/07/92 - 10/01/93

Eagle Picher 81 AmpHr 60% DOD -5 Deg C Test Ended at Cycle 6538

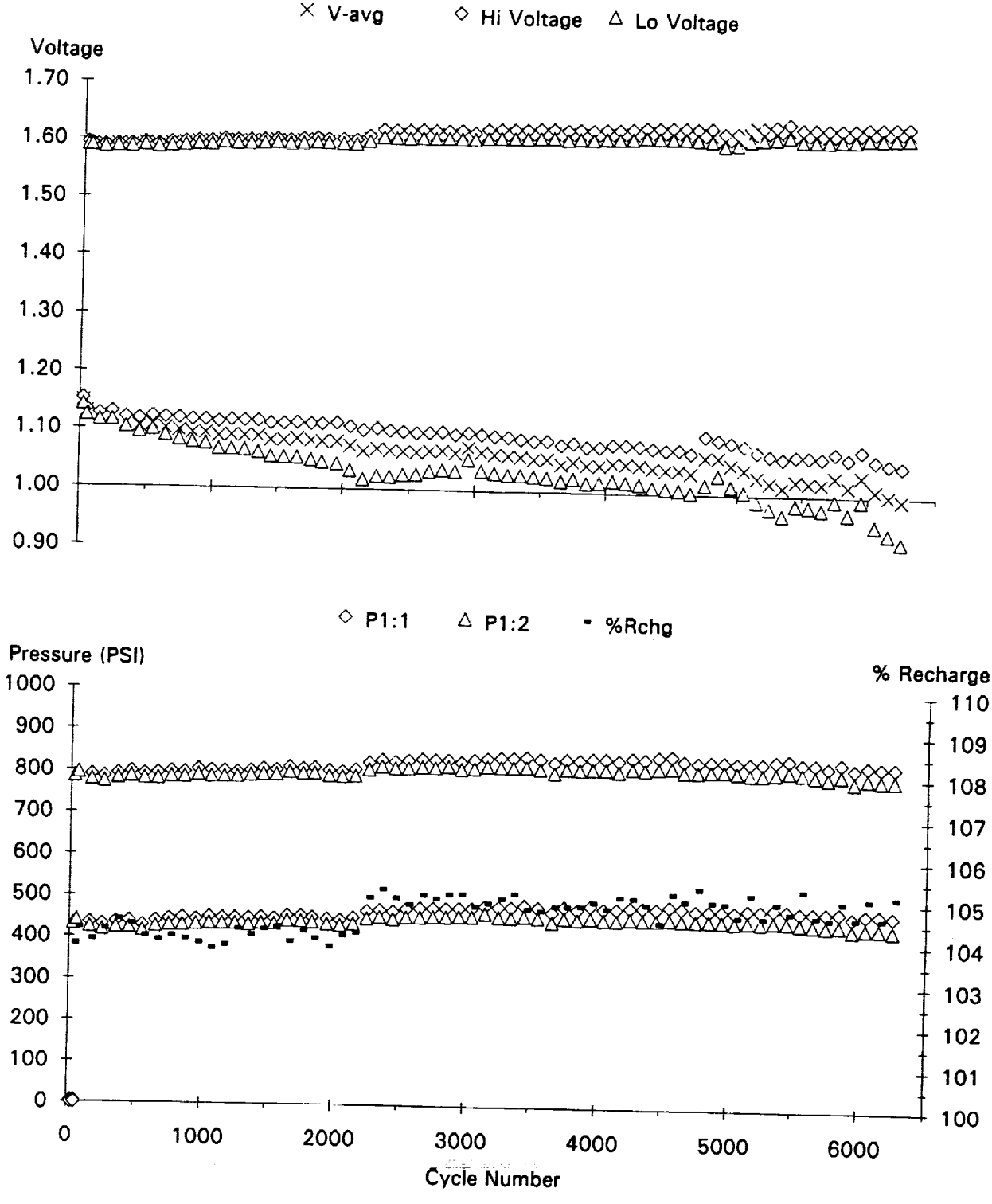

Cycle 1. Started Life Cycle Test.
-81.0A for .6Hr ; 69.25A for .667Hr ; 18.77A for .233Hr ; Rchg = 104.0%
Cycle 2250. Raised Rchg from 104.0% to 105.0%.
-81.0A for .6Hr ; 69.25A for .667Hr ; 20.86A for .233Hr ; Rchg = 105.0%
Cycle 5091. Cells #4 and #6 (SN36 and SN39) hit 1.0V at EOD. Pack average votage was 1.036V.
Cycle 6188. Average pack EOD voltage fell below 1.0V. Five of the four cells have voltages of less than 1.0V.

NSWC Crane **Pack ID 3600G** **4 cells**

Voltage/Pressure/Recharge EOC/EOD Trend Plot 11/21/92 - 09/27/93

Gates 65 AmpHr 35% DOD 10 Deg C Taper Chg

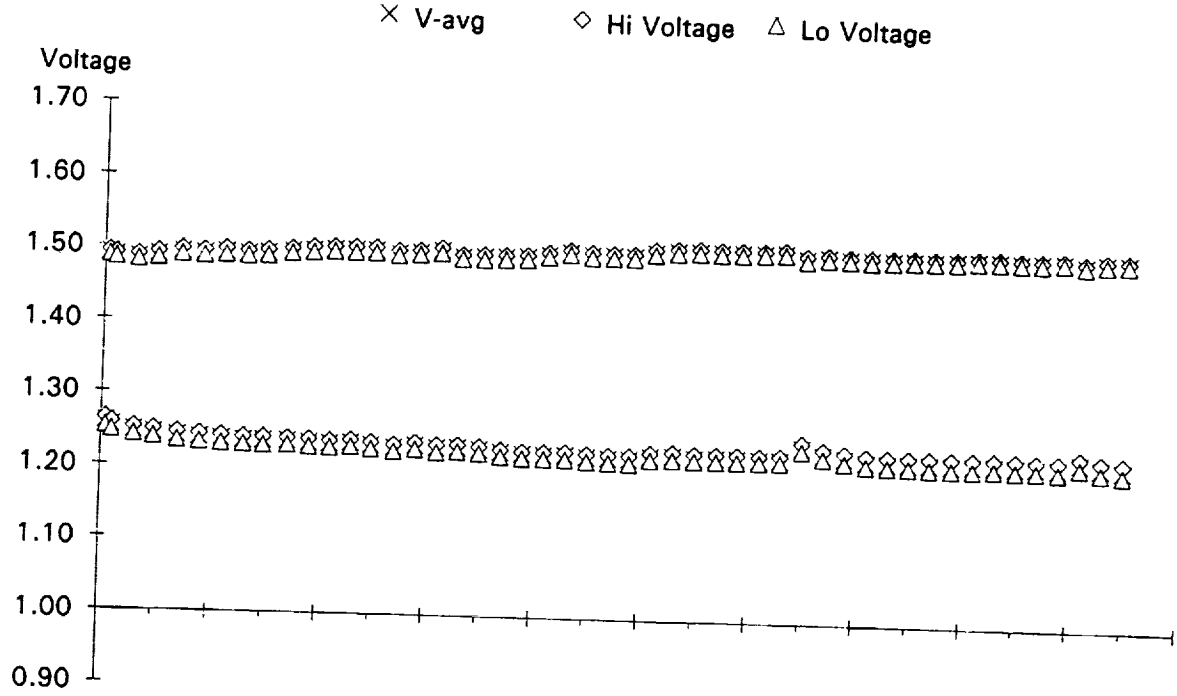

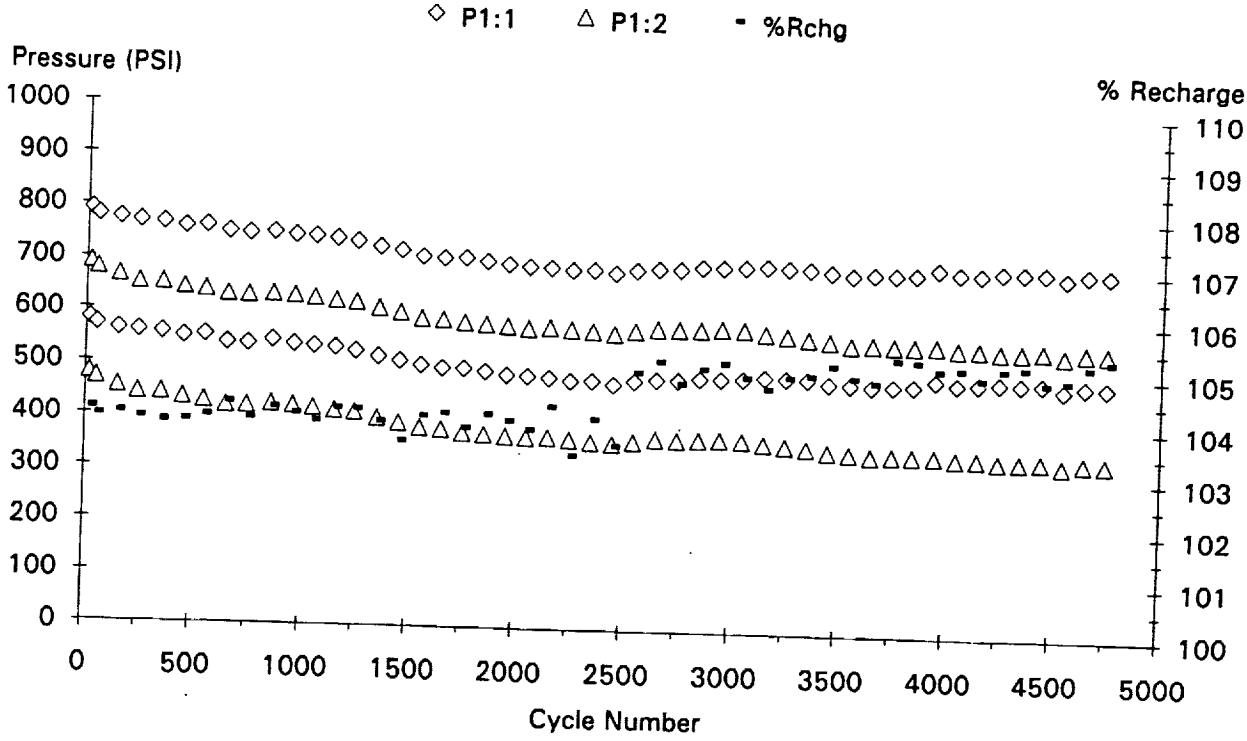

Cycle 1. Started Life Cycle Test.
-37.92A for .6Hr ; 26.76A for .633Hr ; 29.03 to 7.045A Taper for .266Hr ;
Rchg = 104.0%
Cycle 2468. Raised Rchg from 104.0% to 105.0%.
-37.92A for .6Hr ; 26.76A for .633Hr ; 29.084 to 8.698A Taper for .266Hr

NSWC Crane **Pack ID 3601G** **4 cells**

Voltage/Pressure/Recharge EOC/EOD Trend Plot 11/25/92 - 09/29/93

Gates 65 AmpHr 60% DOD 10 Deg C Taper Chg

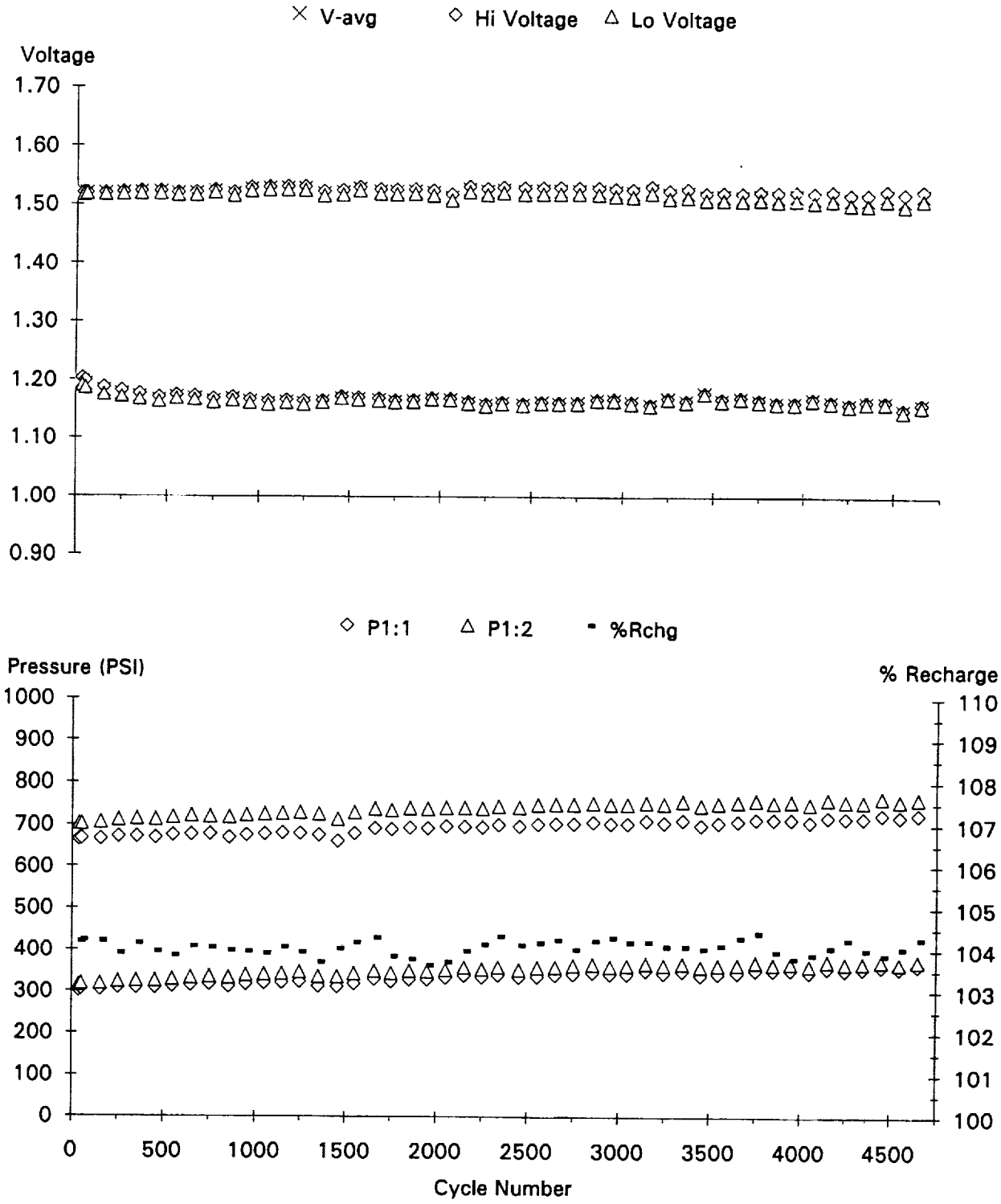

Cycle 1. Started Life Cycle Test.
-65.0A for .6Hr ; 50.14A for .7Hr ; 48.237 to 6.363A Taper for .2Hr ; Rchg = 104.0%

NSWC Crane **Pack ID 3602G** **4 cells**

Voltage/Pressure/Recharge EOC/EOD Trend Plot 10/28/92 - 09/28/93

Gates 65 AmpHr 35% DOD 10 Deg C

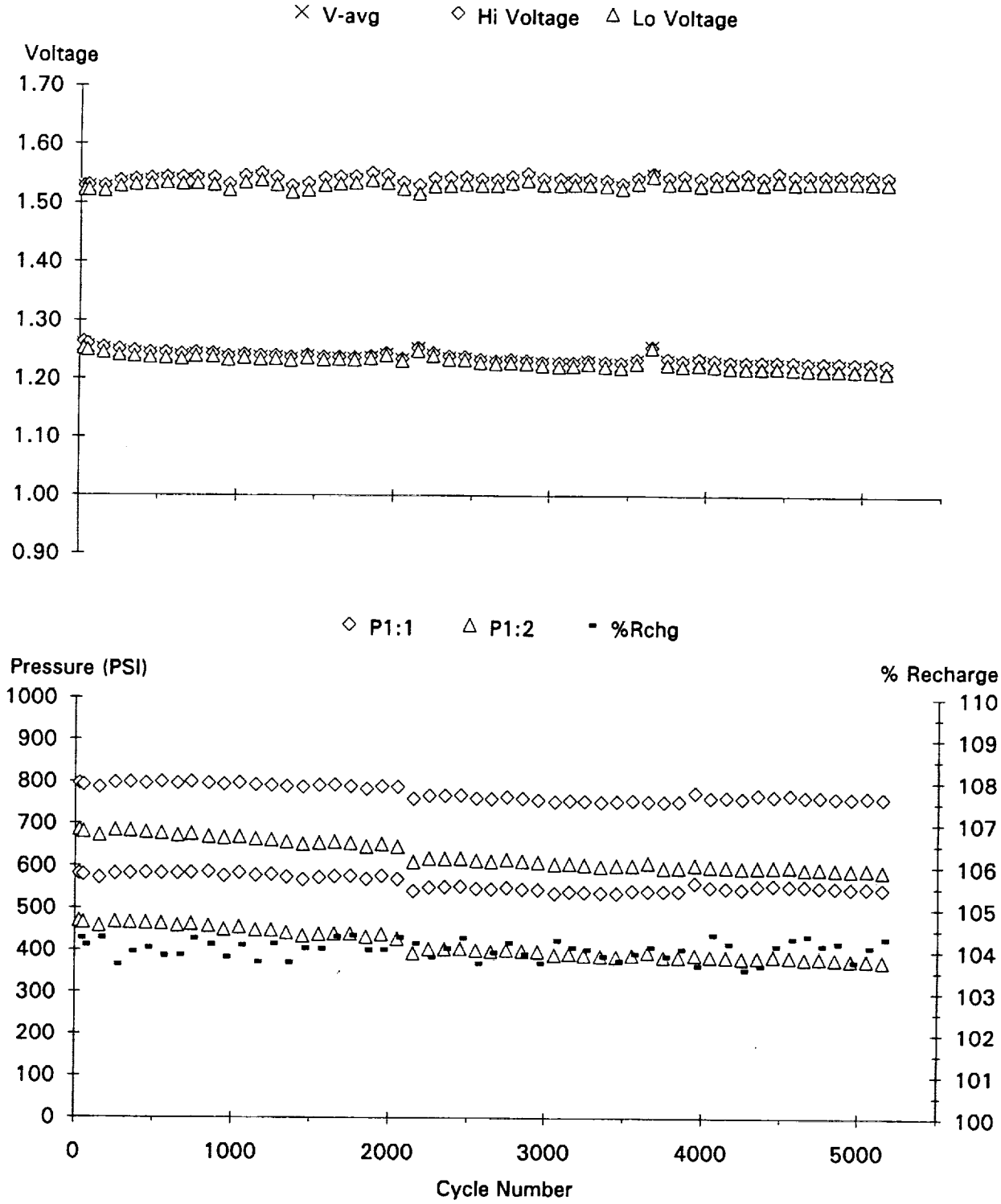

Cycle 1. Started Life Cycle Test.
-37.92A for .6Hr ; 26.29A for .9Hr ; Rchg = 104.0%

NSWC Crane **Pack ID 3603G** **4 cells**

Voltage/Pressure/Recharge EOC/EOD Trend Plot 10/28/92 - 09/28/93

Gates 65 AmpHr 35% DOD 10 Deg C 94% SOC

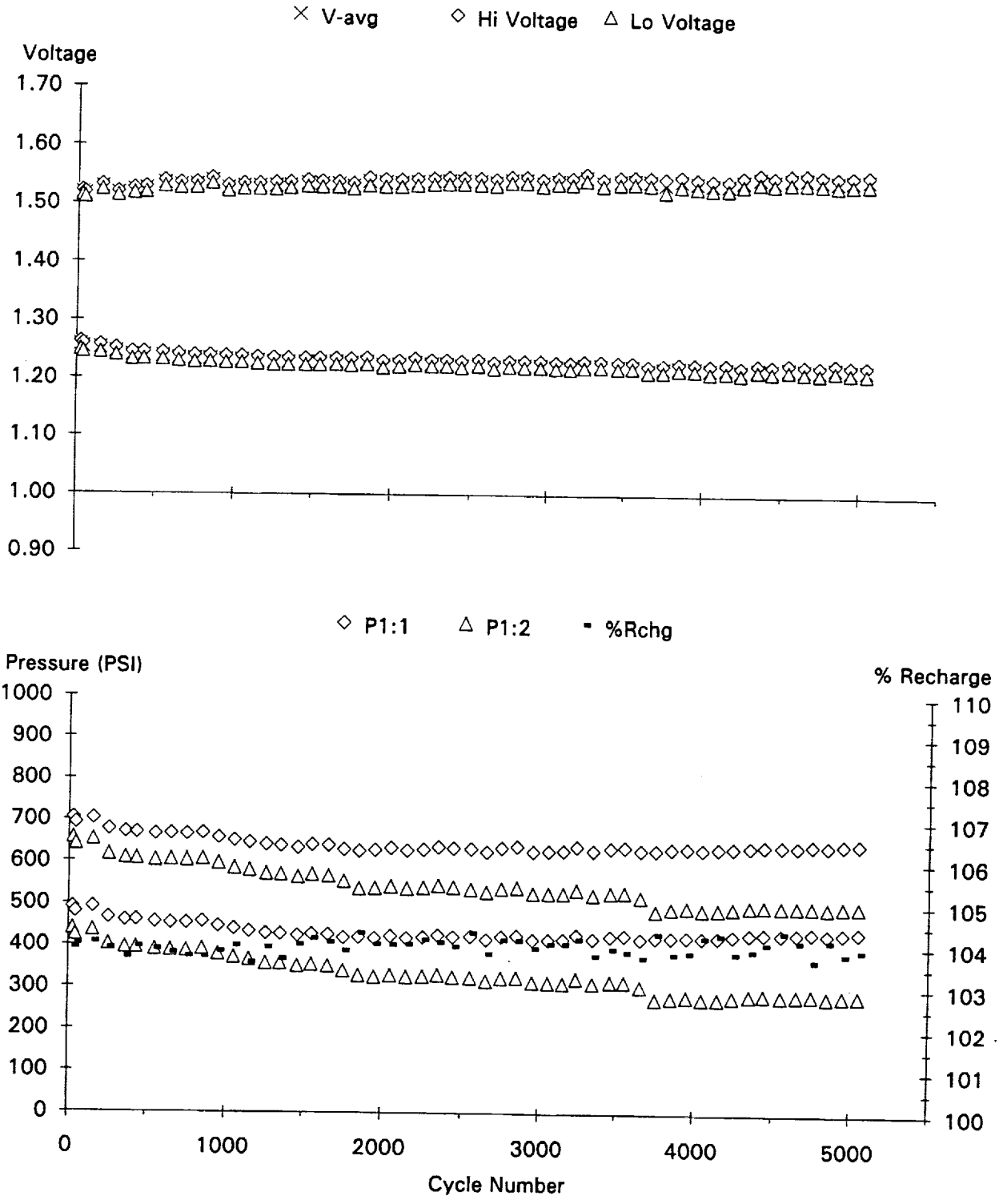

Cycle 1. Started Life Cycle Test.
-37.92A for .6Hr ; 26.29A for .9Hr ; Rchg = 104%

NSWC Crane **Pack ID 3604G** **4 cells**

Voltage/Pressure/Recharge EOC/EOD Trend Plot 11/21/92 - 09/28/93

Gates 65 AmpHr 60% DOD 10 Deg C 94% SOC

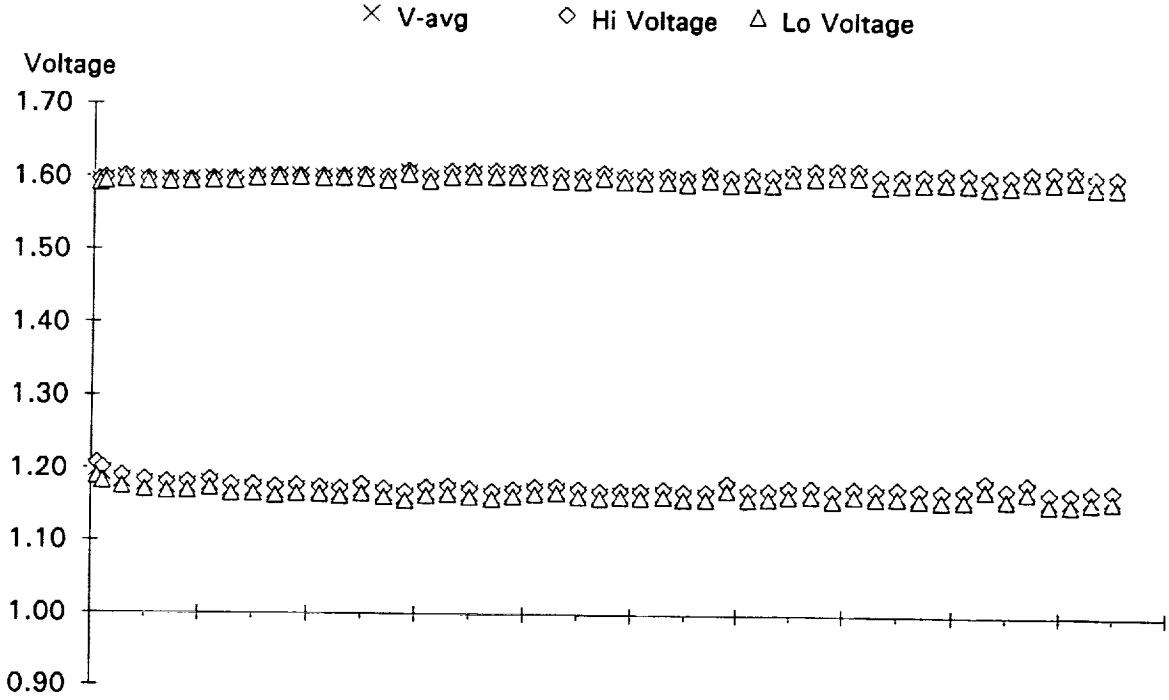

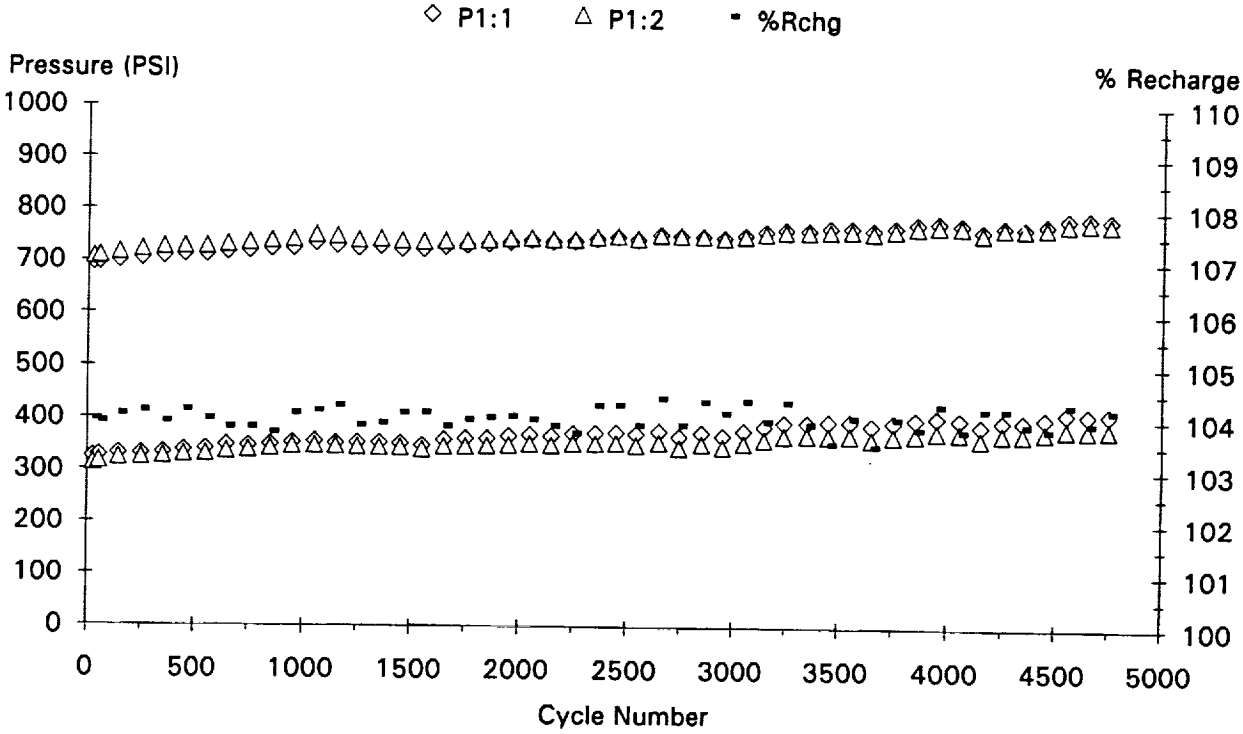

Cycle 1. Started Life Cycle Test.
-65.0A for .6Hr ; 45.07A for .9Hr ; Rchg = 104.0%

NSWC Crane **Pack ID 3631G** **10 cells**

Voltage/Pressure/Recharge EOC/EOD Trend Plot 01/18/93 - 09/26/93

Gates 65 AmpHr 35% DOD 10 Deg C

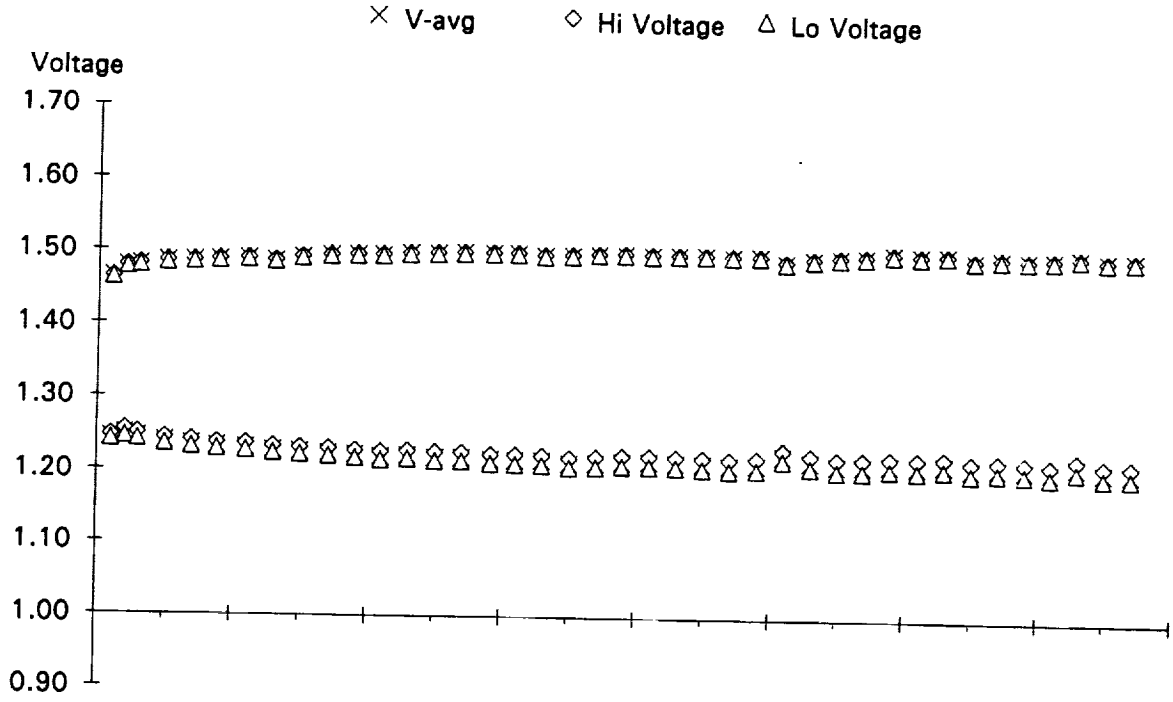

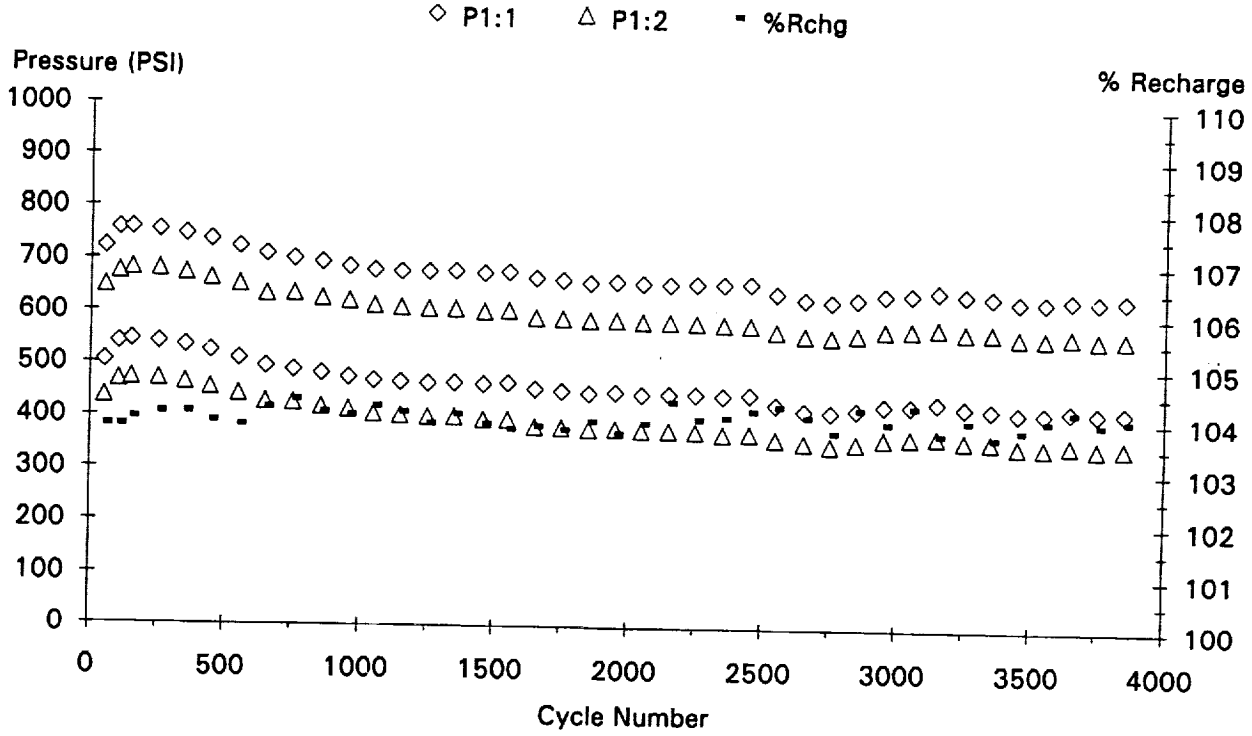

Cycle 10. Started Life Cycle Test.
-37.92A for .6Hr ; 36.02A for .6Hr ; 6.883A for .3Hr ; Rchg = 104.0%

NSWC Crane **Pack ID 3635G** **10 cells**

Voltage/Pressure/Recharge EOC/EOD Trend Plot 01/30/93 - 10/01/93

Gates 65 AmpHr 35% DOD -5 Deg C

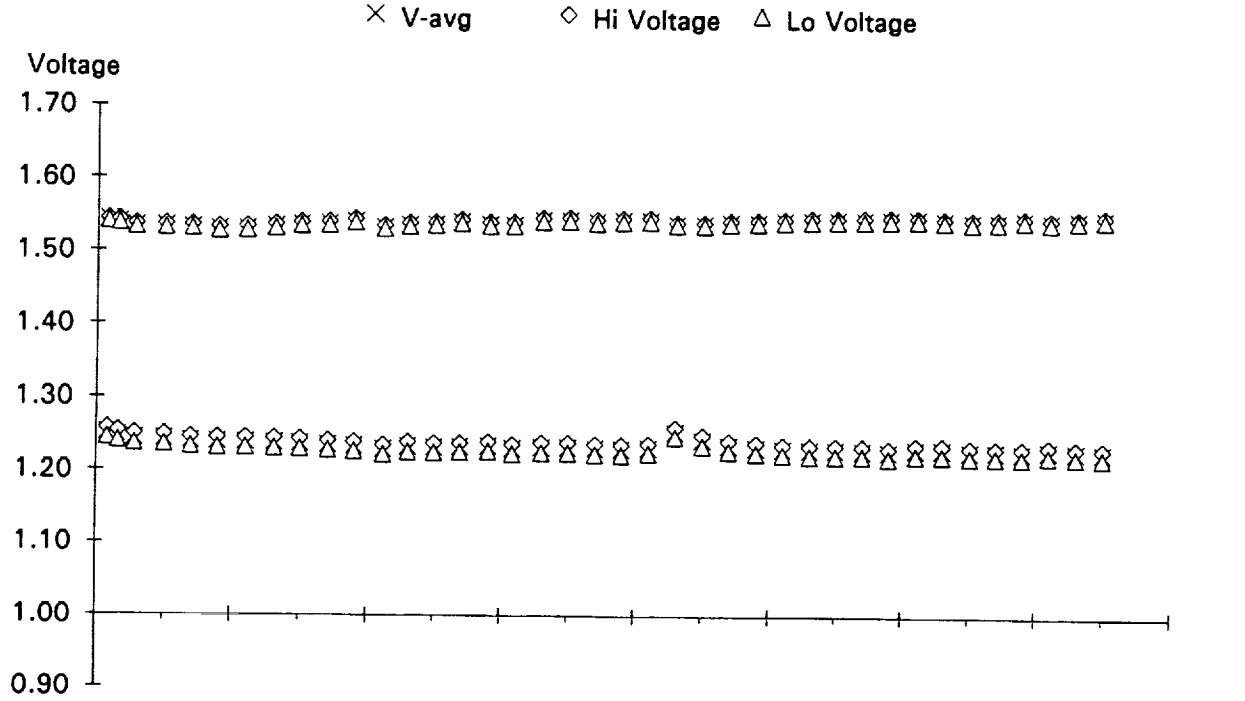

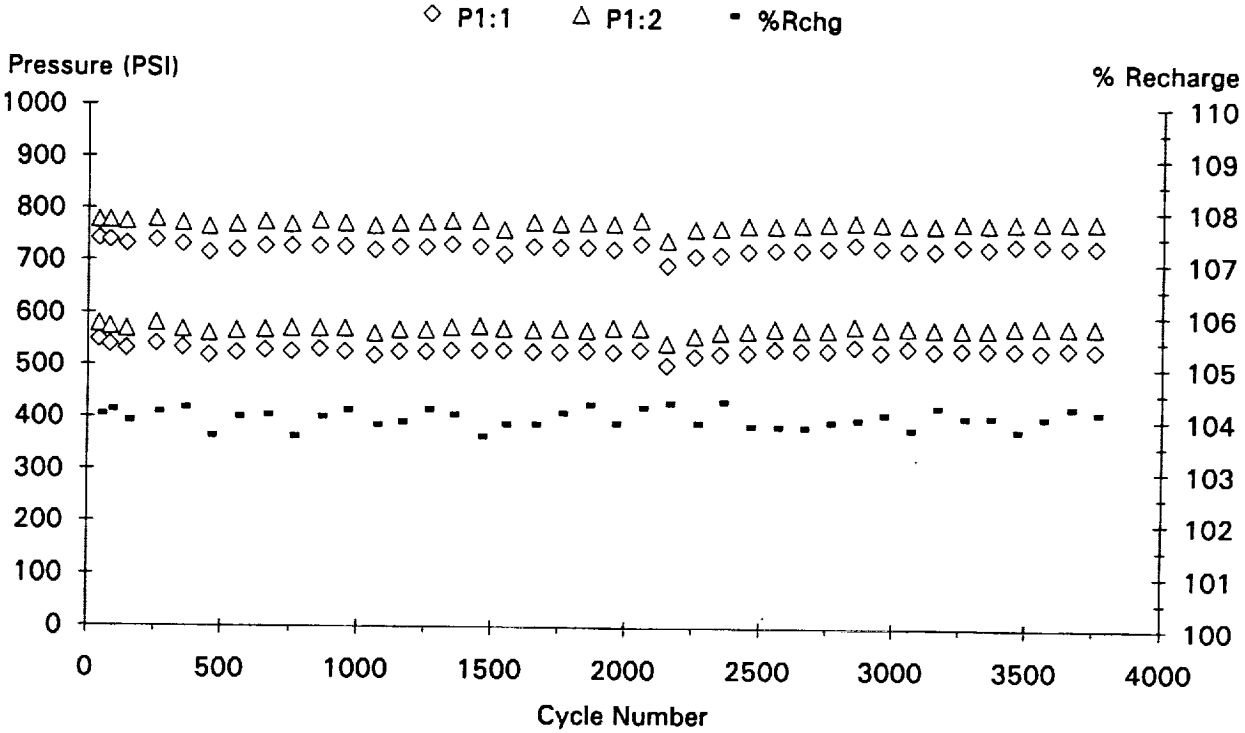

Cycle 11. Started Life Cycle Test.
-37.92A for .6Hr ; 36.02A for .6Hr ; 6.883A for .3Hr ; Rchg = 104.0%

NSWC Crane **Pack ID 3661G** **10 cells**

Voltage/Pressure/Recharge EOC/EOD Trend Plot 01/30/93 - 09/25/93

Gates 65 AmpHr 60% DOD 10 Deg C

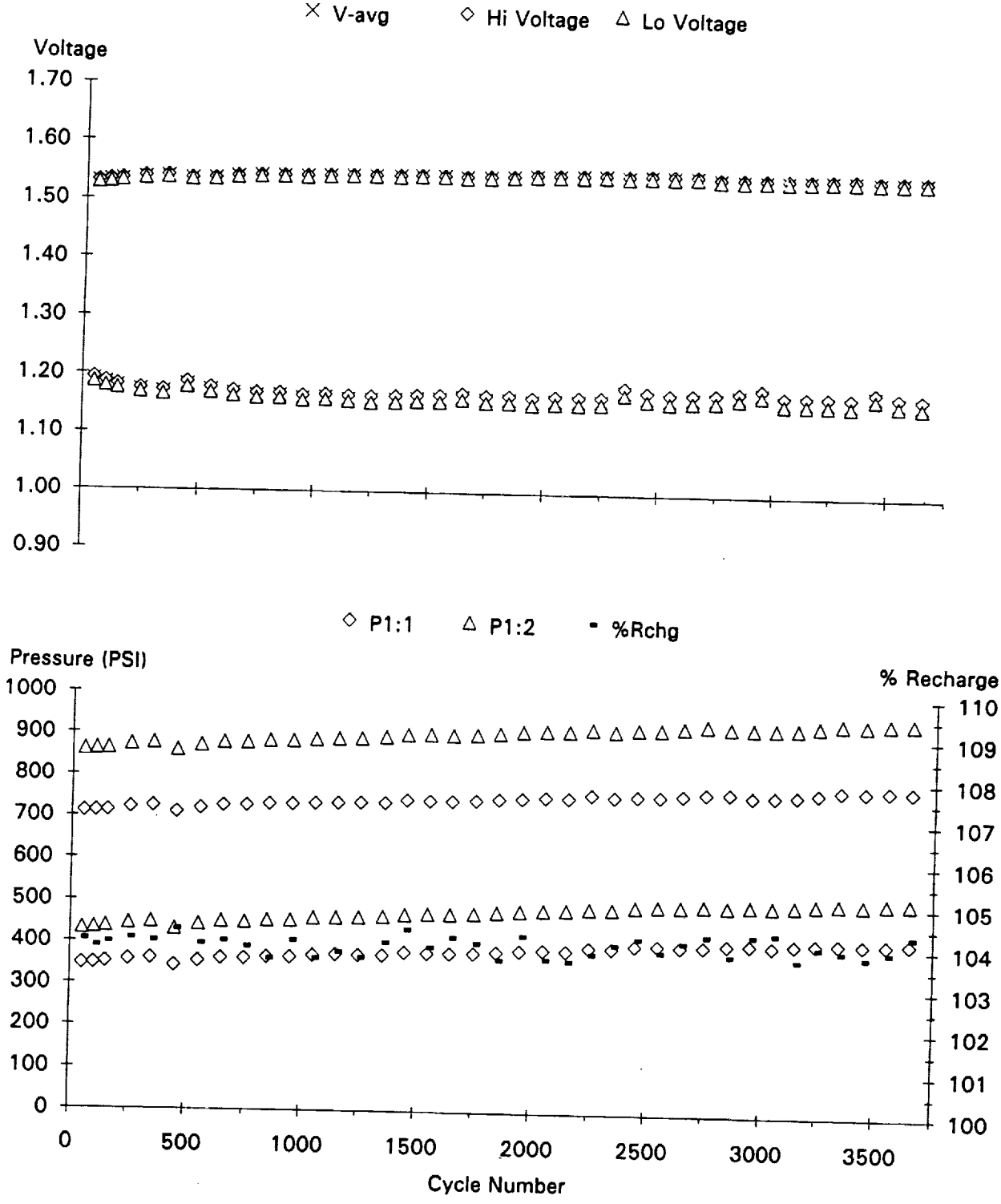

Cycle 13. Started Life Cycle Test.
-65.0A for .6Hr ; 55.57A for .67Hr ; 15.06A for .23Hr ; Rchg = 104.0%

NSWC Crane **Pack ID 3665G** **10 cells**

Voltage/Pressure/Recharge EOC/EOD Trend Plot 01/31/93 - 09/26/93

Gates 65 AmpHr 60% DOD 10 Deg C

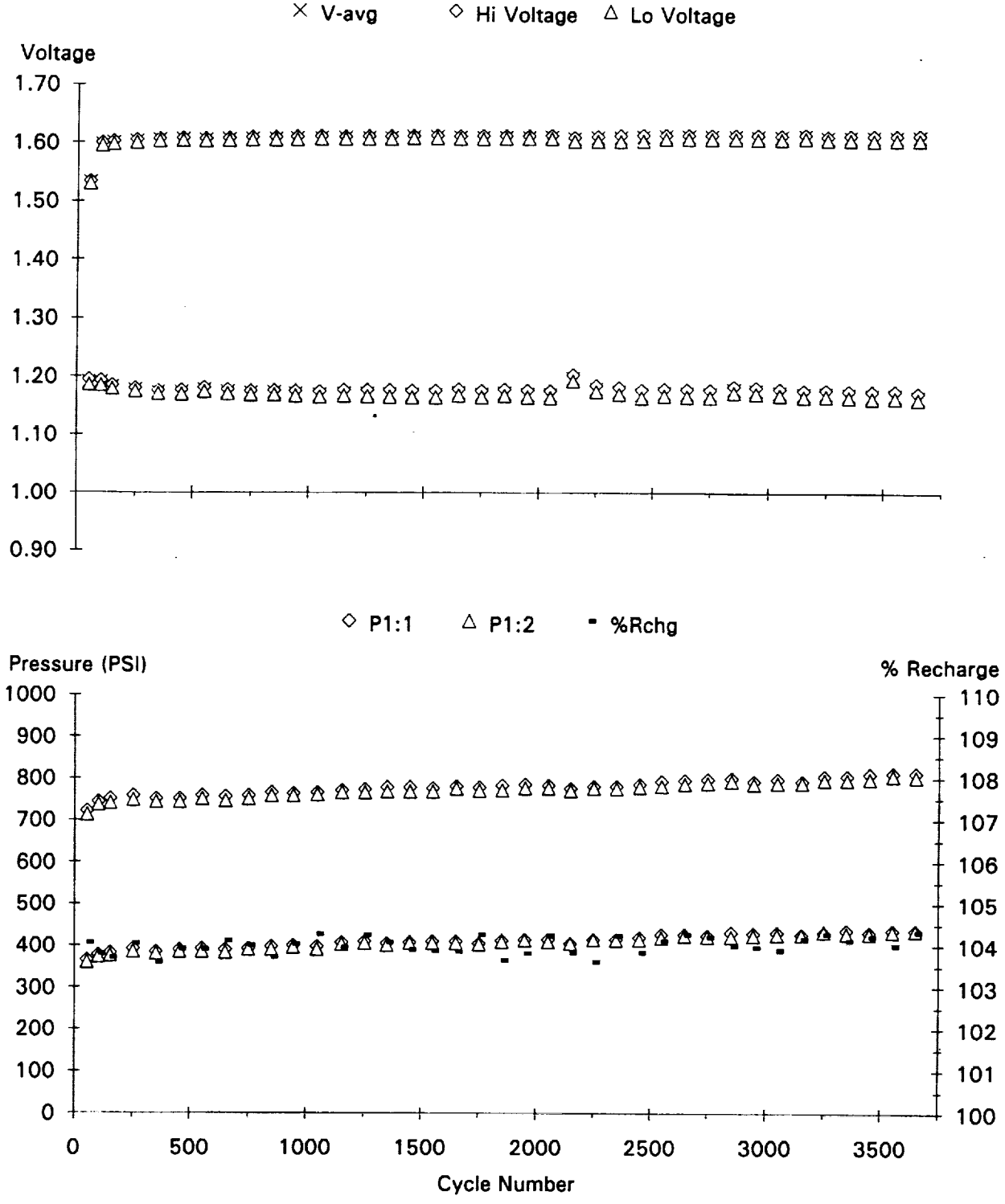

Cycle 14. Started Life Cycle Test.
-65.0A for .6Hr ; 55.57A for .67Hr ; 15.06 A for .23Hr ; Rchg = 104.0%
Cycle 78. Restarted L.C. with a different regime.
-65.0A for .6Hr ; 45.07A for .9Hr ; Rchg = 104.0%

NSWC Crane **Pack ID 3831G** **10 cells**

Voltage/Pressure/Recharge EOC/EOD Trend Plot 04/19/92 - 10/01/93

Gates 81 AmpHr 35% DOD 10 Deg C

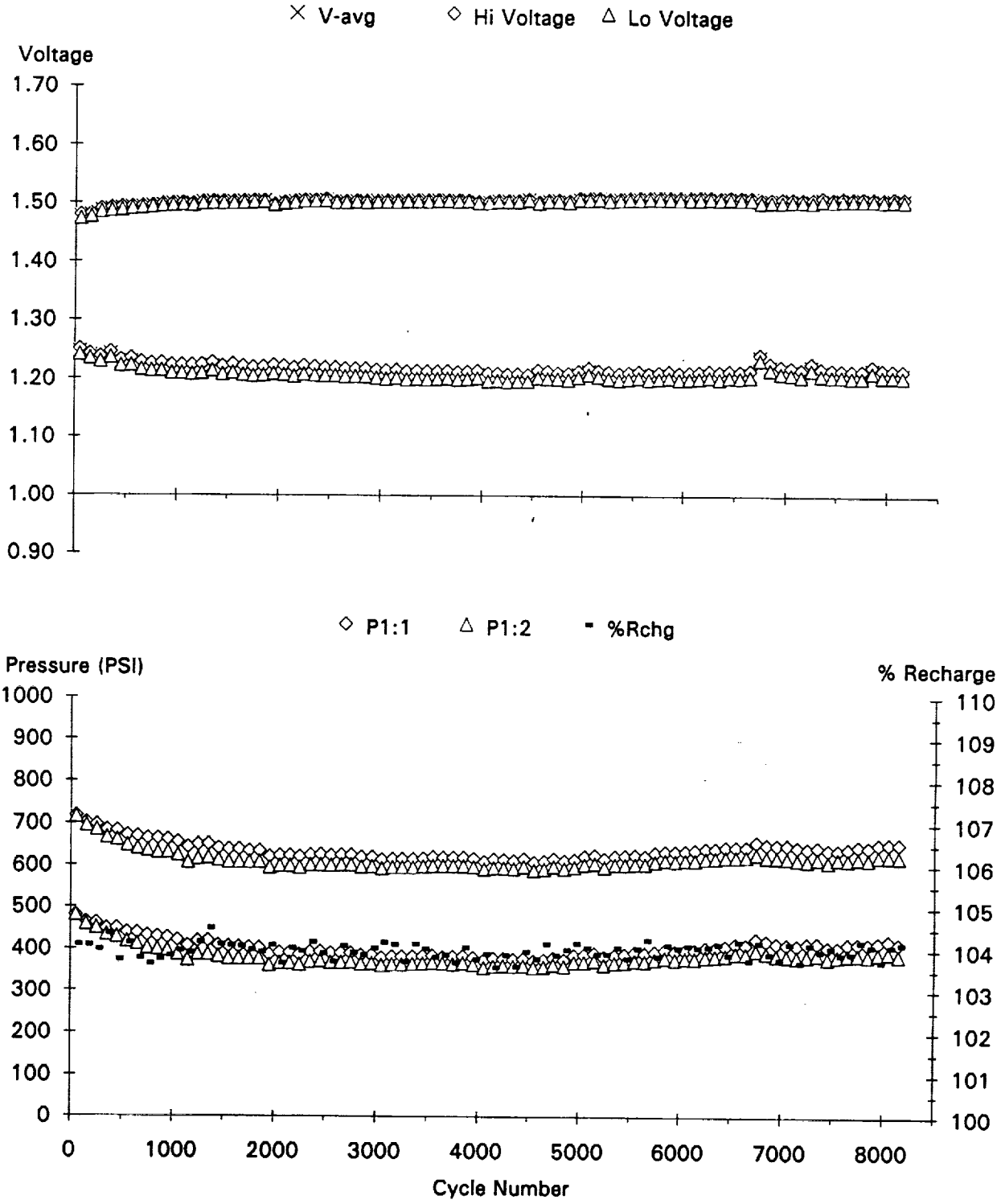

Cycle 1. Started Life Cycle Test.
-47.25A for .6Hr ; 44.88A for .6Hr ; 8.5A for .3Hr ; Rchg = 104.0%

NSWC Crane **Pack ID 3835G** **10 cells**

Voltage/Pressure/Recharge EOC/EOD Trend Plot 04/19/92 - 10/01/93

Gates 81 AmpHr 35% DOD -5 Deg C

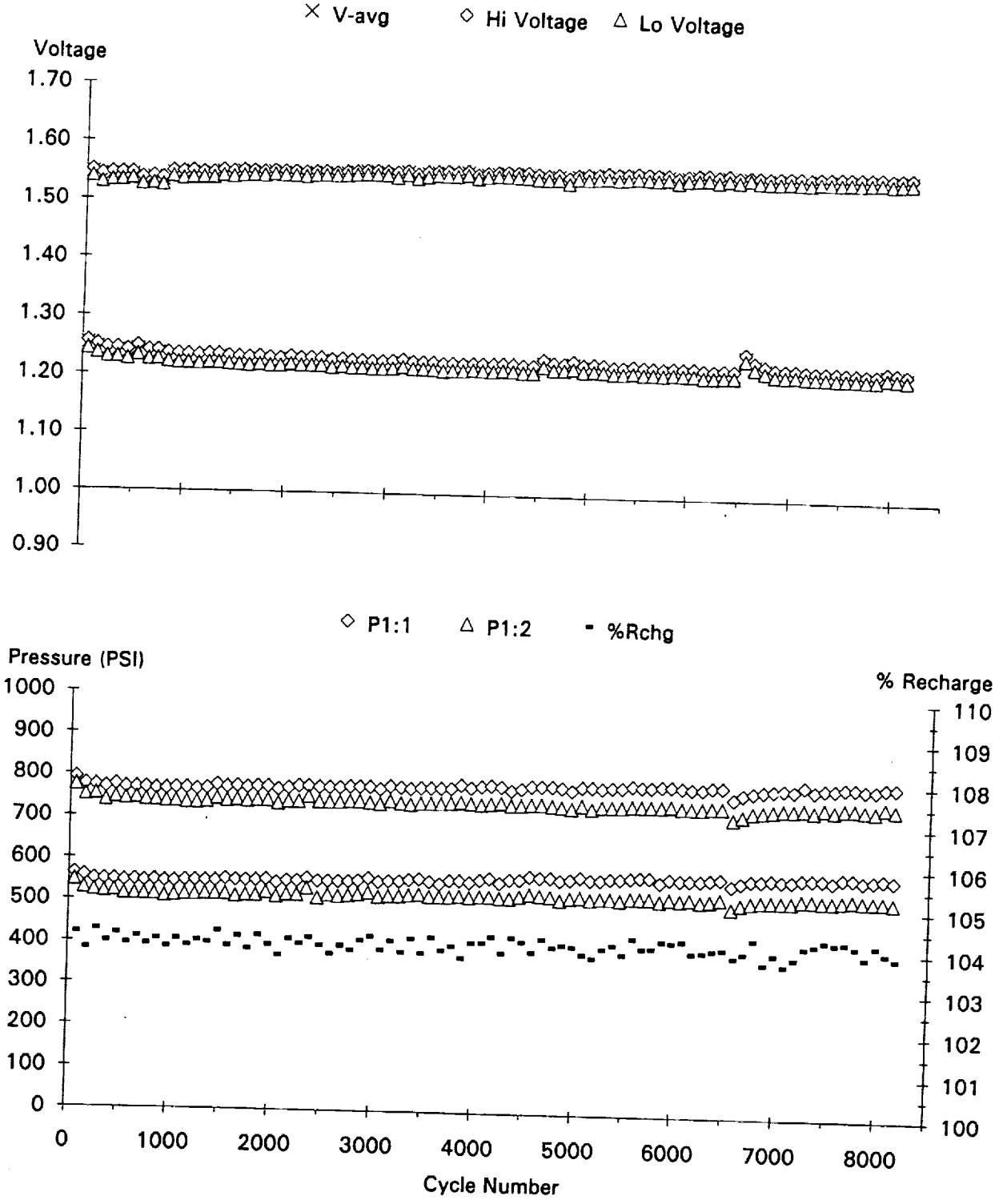

Cycle 1. Started Life Cycle Test.
-47.25A for .6Hr ; 44.88A for .6Hr ; 8.5A for .3Hr ; Rchg = 104.0%

NSWC Crane Pack ID 3861G 10 cells

Voltage/Pressure/Recharge EOC/EOD Trend Plot 08/04/92 - 09/28/93

Gates 81 AmpHr 60% DOD 10 Deg C

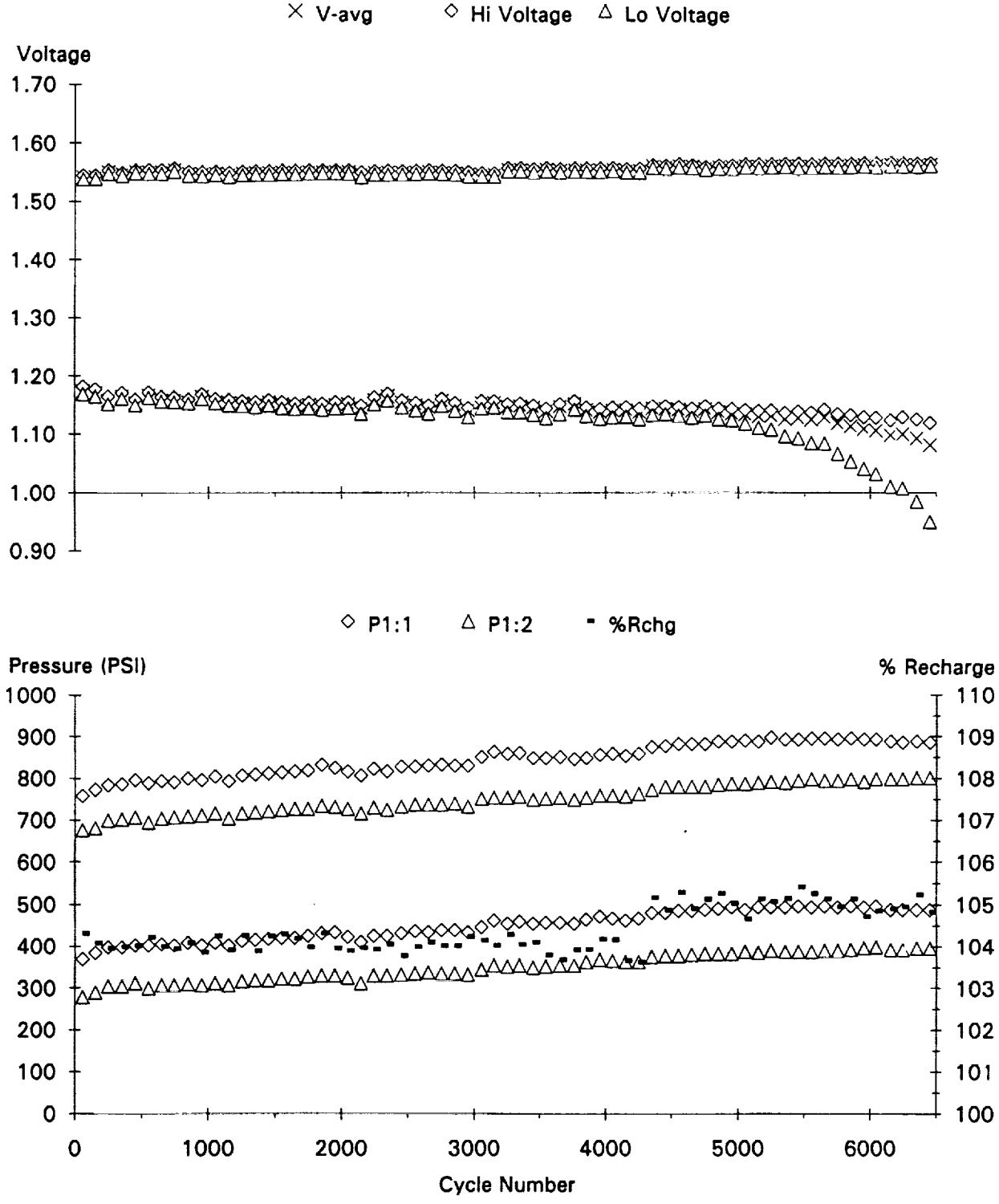

Cycle 1. Started Life Cycle Test.
-81.0A for .6Hr ; 69.25A for .667Hr ; 18.77A for .233Hr ; Rchg = 104.0%
Cycle 4276. Raised Rchg fro 104.0% to 105.0%.
-81.0A for .6Hr ; 69.25A for .667Hr ; 20.86A for .233Hr

NSWC Crane Pack ID 3865G 10 cells

Voltage/Pressure/Recharge EOC/EOD Trend Plot 08/05/92 - 09/30/93

Gates 81 AmpHr 60% DOD -5 Deg C

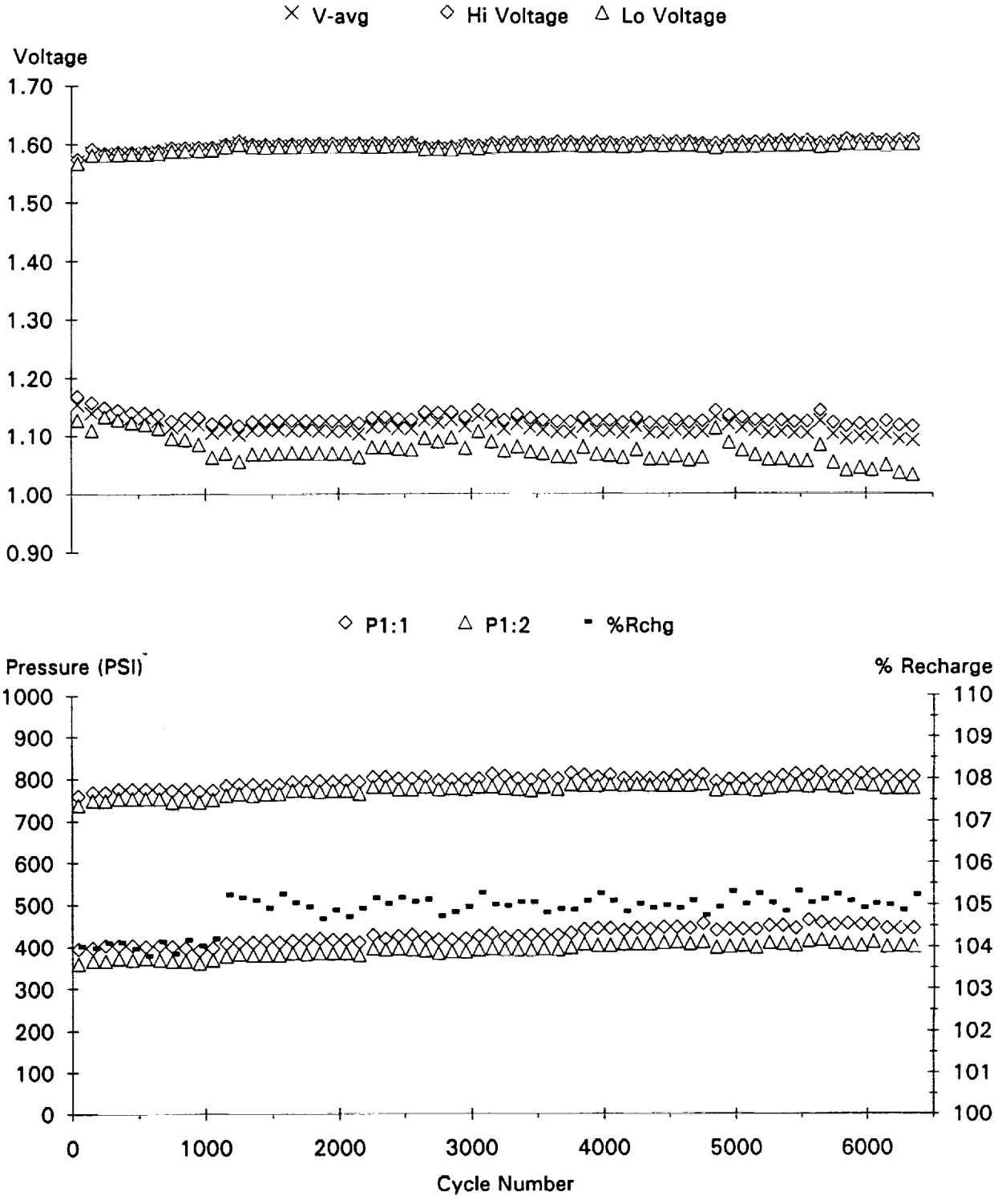

Cycle 1. Started Life Cycle Test.
-81.0A for .6Hr ; 69.25A for .667Hr ; 18.77A for .233Hr ; Rchg = 104.0%
Cycle 1096. Raised Rchg from 104.0% to 105.0%.
-81.0A for .6Hr ; 69.25A for .667Hr ; 20.86A for .233Hr

NSWC Crane Pack ID 3831Y 10 cells

Voltage/Pressure/Recharge EOC/EOD Trend Plot 07/16/92 - 09/28/93

Yardney 81 AmpHr 35% DOD 10 Deg C

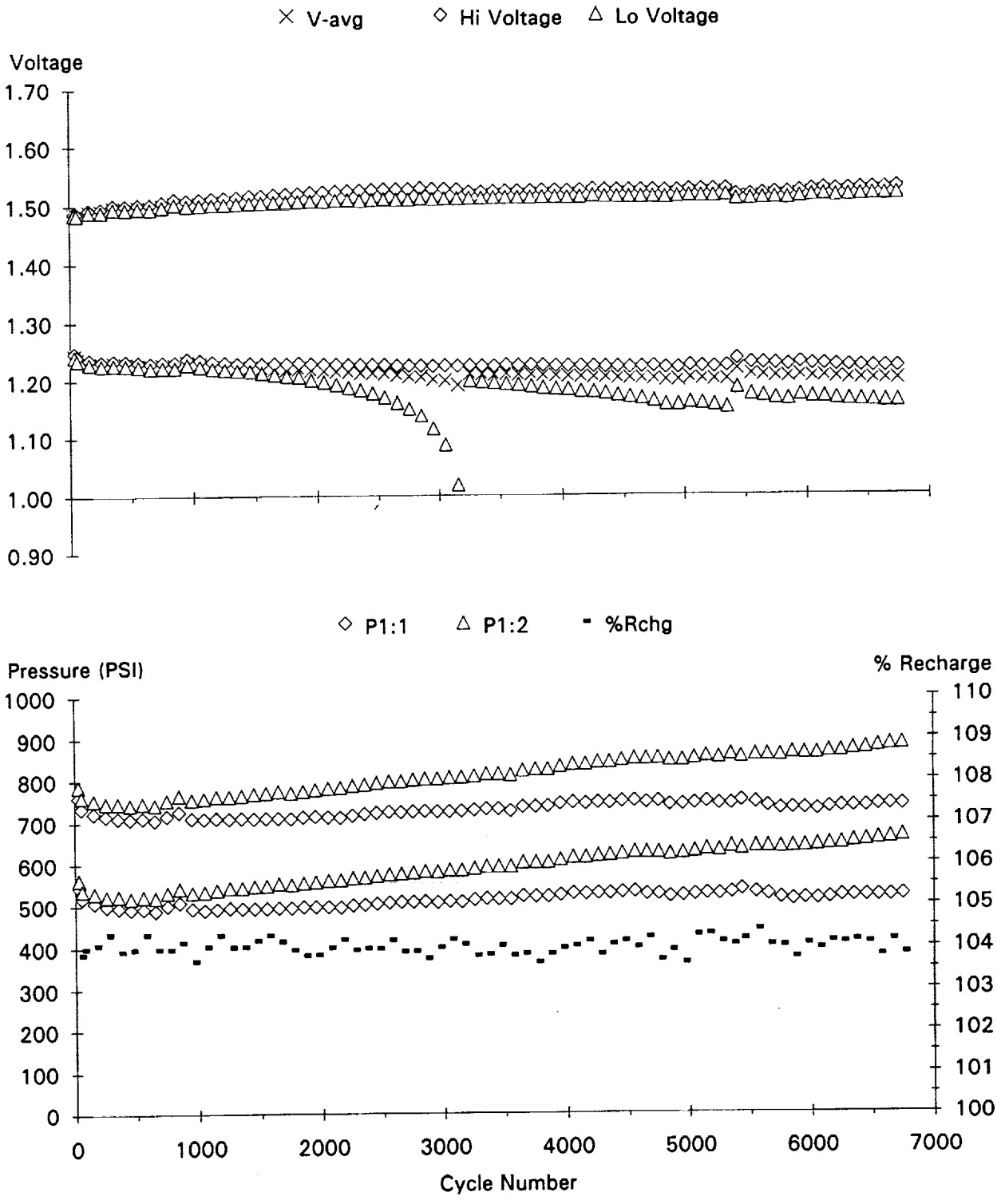

Cycle 20. Started Life Cycle Test.
-47.25A for .6Hr ; 44.88A for .6Hr ; 8.50A for .3Hr ; Rchg = 104.0%
Cycle 3199. Removed cell #2 (SN08) from pack because of low EOD voltage.

NSWC Crane **Pack ID 3835Y** **10 cells**

Voltage/Pressure/Recharge EOC/EOD Trend Plot 07/17/92 - 09/28/93

Yardney 81 AmpHr 35% DOD -5 Deg C

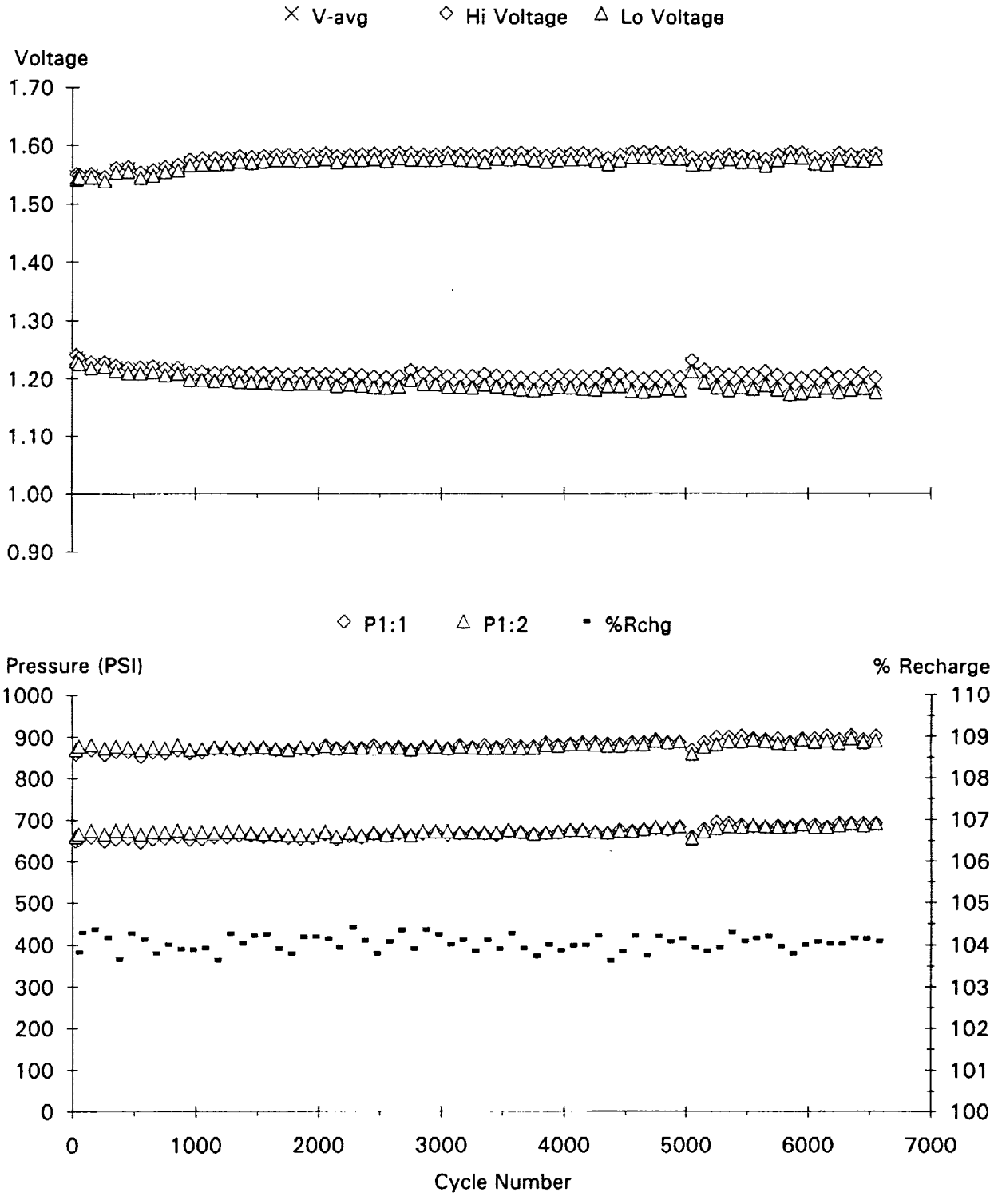

Cycle 23. Started Life Cycle Test.
-47.25A for .6Hr ; 44.88A for .6Hr ; 8.50A for .3Hr ; Rchg = 104.0%

NSWC Crane **Pack ID 3861Y** **10 cells**

Voltage/Pressure/Recharge EOC/EOD Trend Plot 02/08/93 - 04/06/93

Yardney 81 AmpHr 60% DOD 10 Deg C

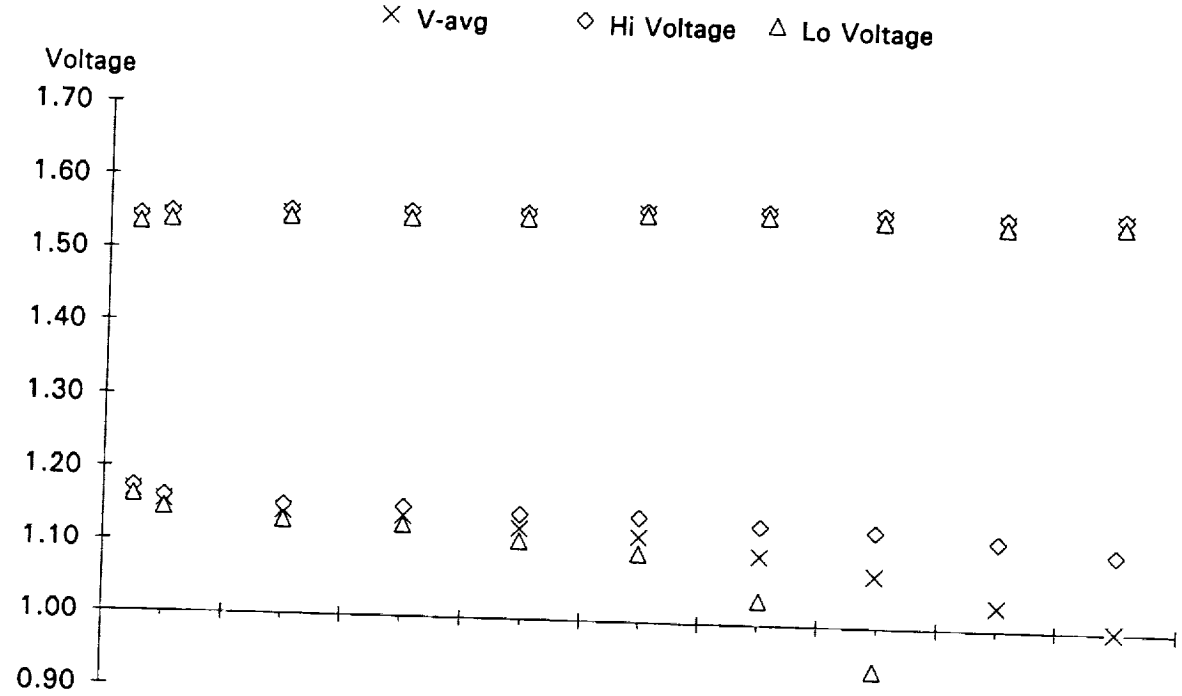

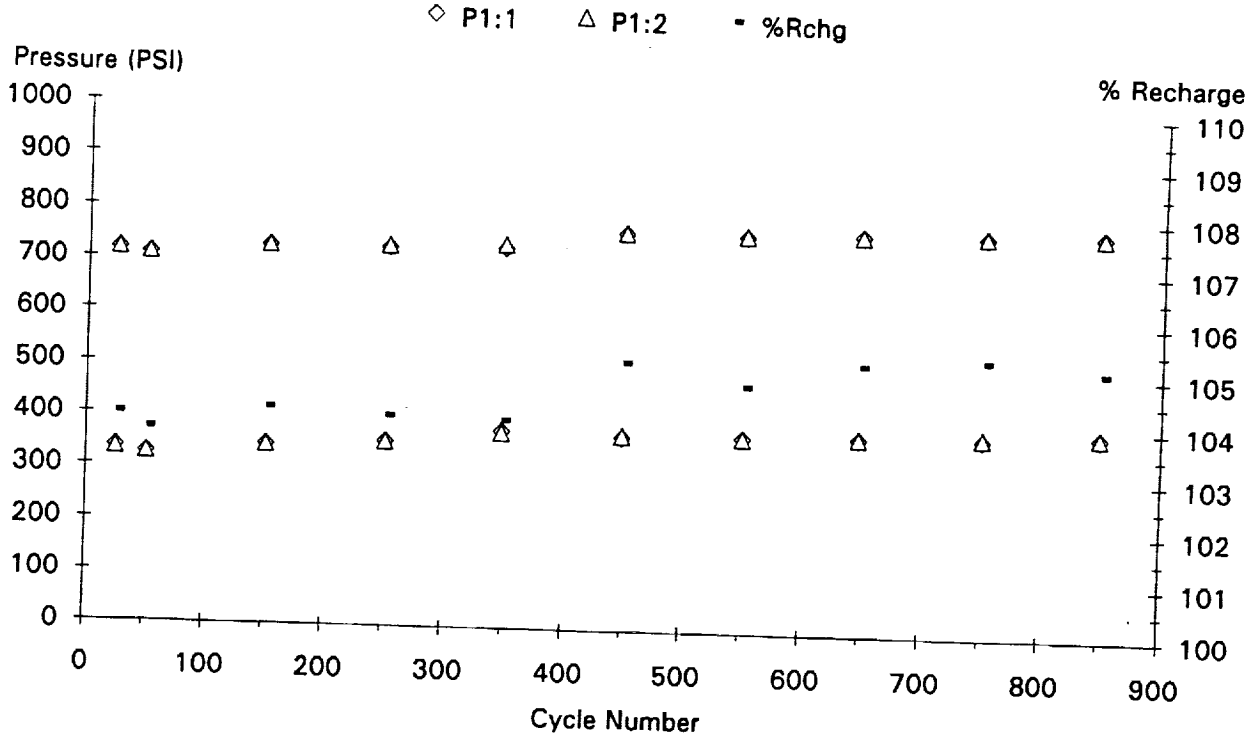

Cycle 19. Started Life Cycle Test.
-81.0A for .6Hr ; 69.25A for .667Hr ; 18.77A for .233Hr ; Rchg = 104.0%
Cycle 429. Raised Rchg from 104.0% to 105.0%.
-81.0A for .6Hr ; 69.25A for .667Hr ; 20.86A for .233Hr
Cycle 504. Restarted L.C. Test regime modified as follows;
-81.0A for .6Hr ; 56.7A for .9Hr Tchg = 105.0%
Cycle 583. Cell #6 (SN09) fell below 1.0V EOD. Pack Average was 1.085V EOD.
Cycles 713 - 717. Halted life cycle test for capacity cycles.
Cycle 858. Pack average EOD voltage fell below 1.0V. Low cell was #6 at .766V.
Cycle 881. 4/8/93. Life Cycle test halted. Low cell at EOD was #6 at .757V. Pack average voltage at EOD was .986.

NSWC Crane **Pack ID 3865Y** **10 cells**

Voltage/Pressure/Recharge EOC/EOD Trend Plot 02/05/93 - 03/26/93

Yardney 81 AmpHr 60% DOD -5 Deg C

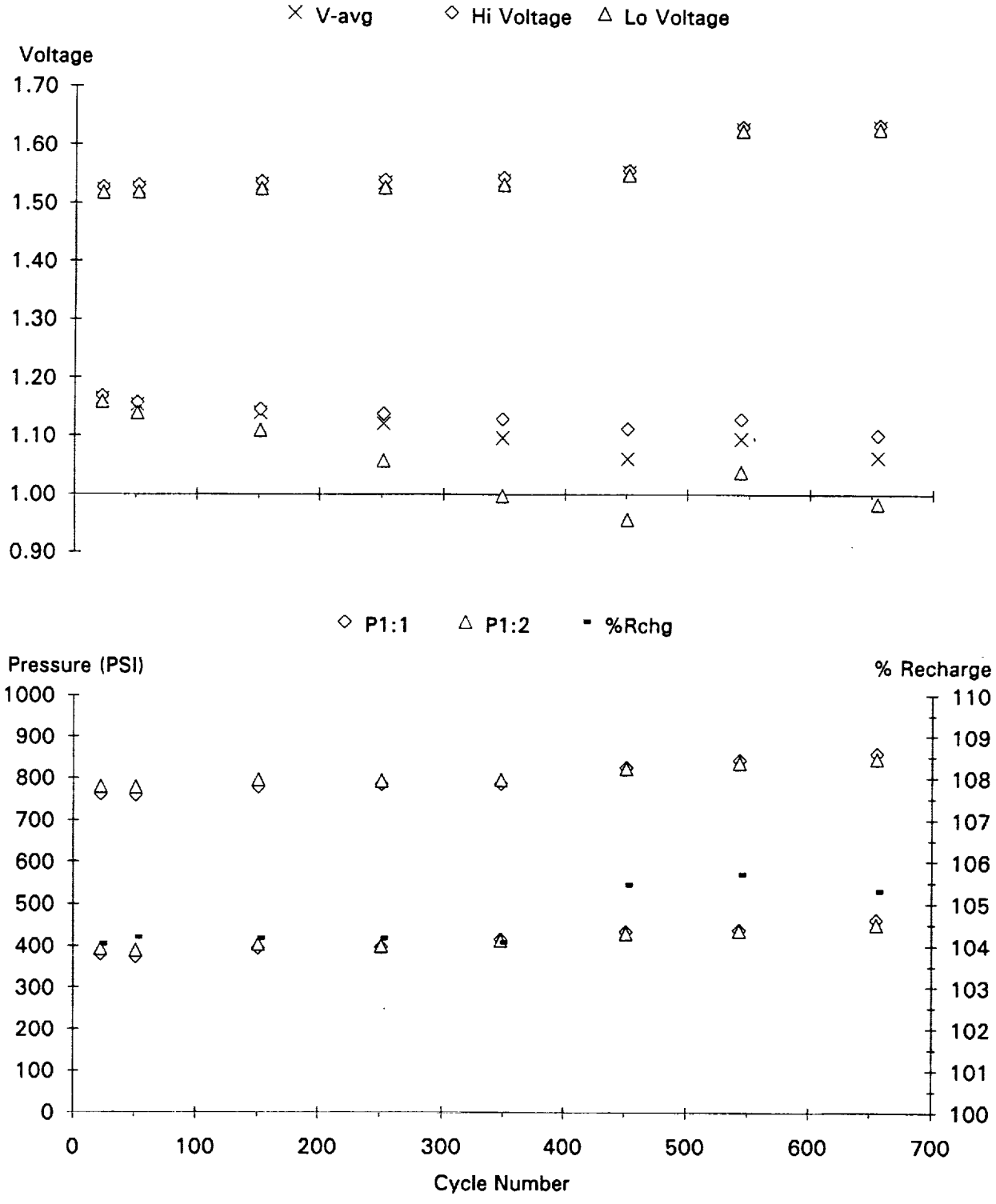

Cycle 15. Started Life Cycle Test.
-81.0A for .6Hr ; 62.49A for .7Hr ; 60.118-7.923A Taper for .2Hr ; Rchg = 104.0%
Cycle 323. Cell #1 (SN10) fell below EOD voltage of 1.0V. Pack average EOD voltage was 1.079V.
Cycle 406. Raised Rchg from 104.0% to 105.0%.
-81.0A for .6Hr ; 62.49A for .7Hr ; 60.320-12.580A Taper for .2Hr
Cycles 502 - 503. Halted life cycle test for capacity cycles.
Cycle 709. 3/29/93. Life Cycle test halted. Low cell at EOD was #2 SN15) at .902V. Pack average voltage at EOD was 1.041.

NSWC Crane **Pack ID 5631W** **10 cells**

Voltage/Pressure/Recharge EOC/EOD Trend Plot 07/01/90 - 09/26/93

Yardney 65 AmpHr 35% DOD 10 Deg C

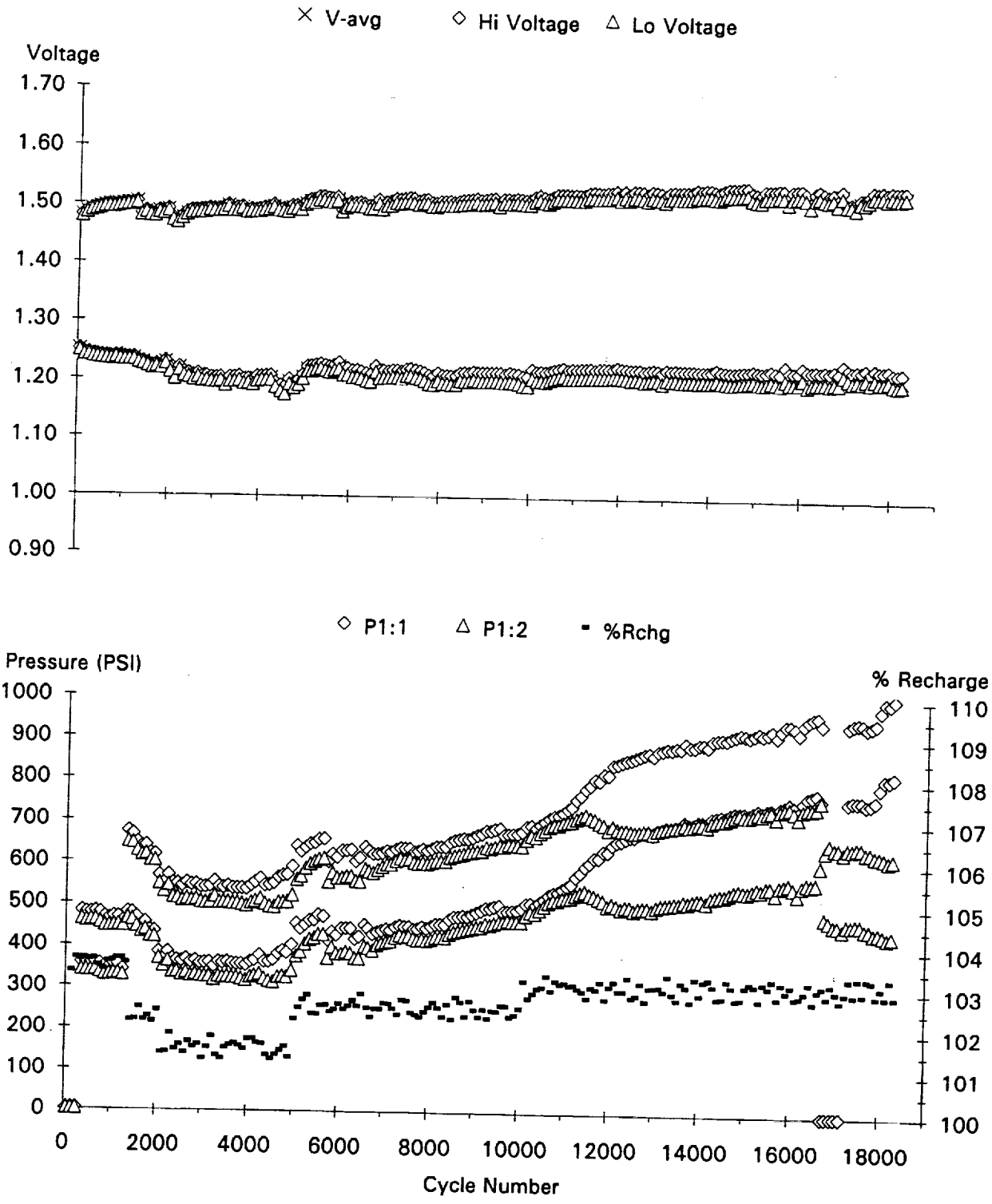

Cycle 1. Started Life Cycle Test.
-37.9A for .6Hr ; 36.0A for .6Hr ; 6.49A for .3Hr ; Rchg = 103.5%
Cycle 1368. Lowered Rchg from 103.5% to 101.5%.
-37.9A for .6Hr ; 36.0A for .6Hr ; 4.97A for .3Hr
Cycle 4864. Raised Rchg from 101.5% to 102.5%.
-37.9A for .6Hr ; 36.0A for .6Hr ; 5.73A for .3Hr
Cycle 10144. Raised Rchg from 102.5% to 103.0%.
-37.9A for .6Hr ; 36.0A for .6Hr ; 6.11A for .3Hr
Cycle 16707 - 17180. P1:1 pressure indication not working.

NSWC Crane Pack ID 5635W 10 cells

Voltage/Pressure/Recharge EOC/EOD Trend Plot 09/22/90 - 09/28/93

Yardney 65 AmpHr 35% DOD -5 Deg C

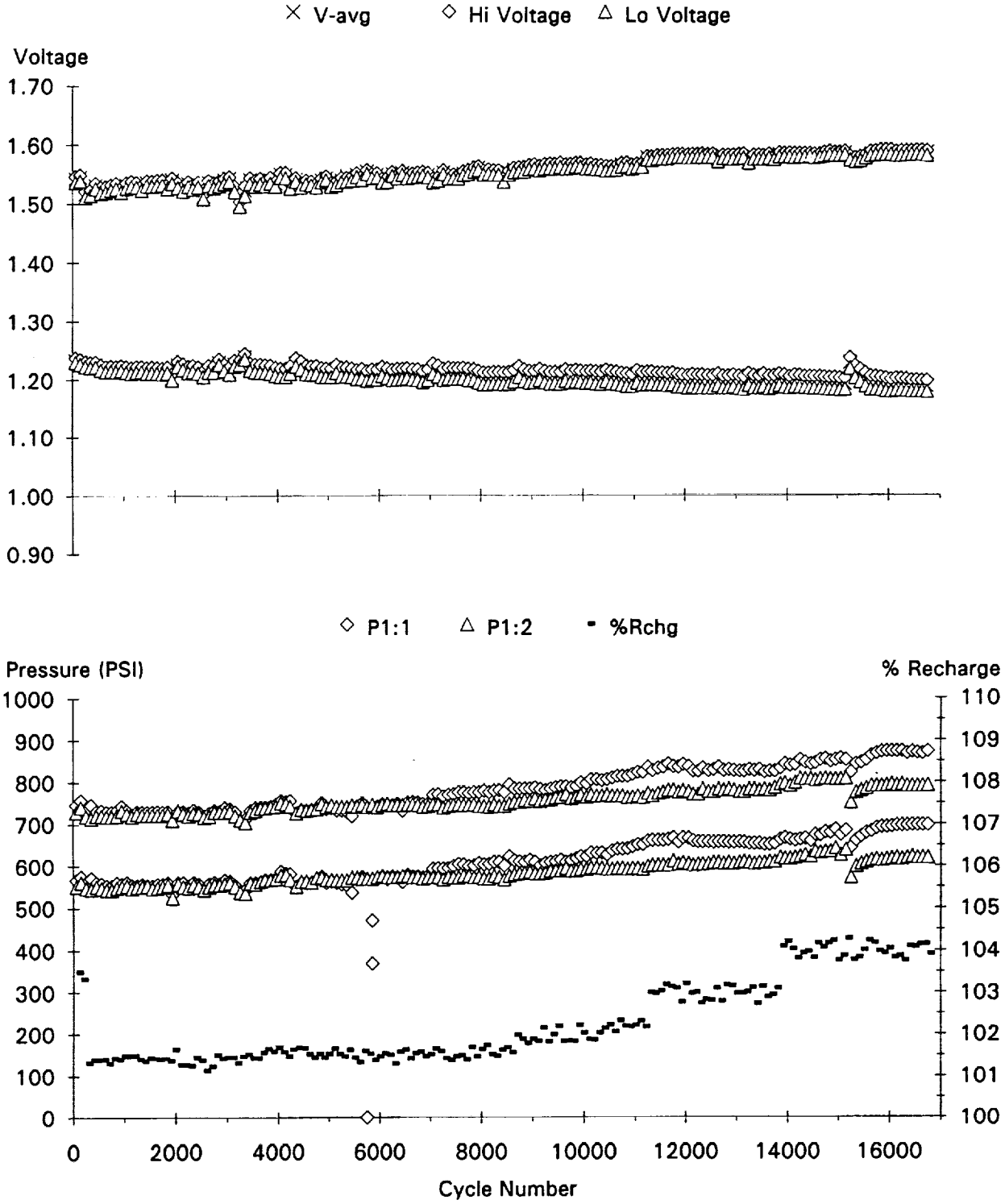

Cycle 1. Started Life Cycle Test.
-37.9A for .6Hr ; 36.0A for .6Hr ; 4.97A for .3Hr ; Rchg = 101.5%
Cycle 5654. Strain Gauge on Pressre P1:1 failed. Changed to monitor a different cell on cycle 5885.
Cycle 8630. Raised Rchg from 101.5% to 102.0%.
-37.9A for .6Hr ; 36.0A for .6Hr ; 5.35A for .3Hr
Cycle 11243. Raised Rchg from 102.0% to 103.0%.
-37.9A for .6Hr ; 36.0A for .6Hr ; 6.11A for .3Hr
Cycle 13748. Raised Rchg from 103.0% to 104.0%.
-37.9A for .6Hr ; 36.0A for .6Hr ; 6.87A for .3Hr

NSWC Crane **Pack ID 5661W** **10 cells**

Voltage/Pressure/Recharge EOC/EOD Trend Plot 09/10/90 - 07/22/91

Yardney 65 AmpHr 60% DOD 10 Deg C Test Ended at Cycle 4751

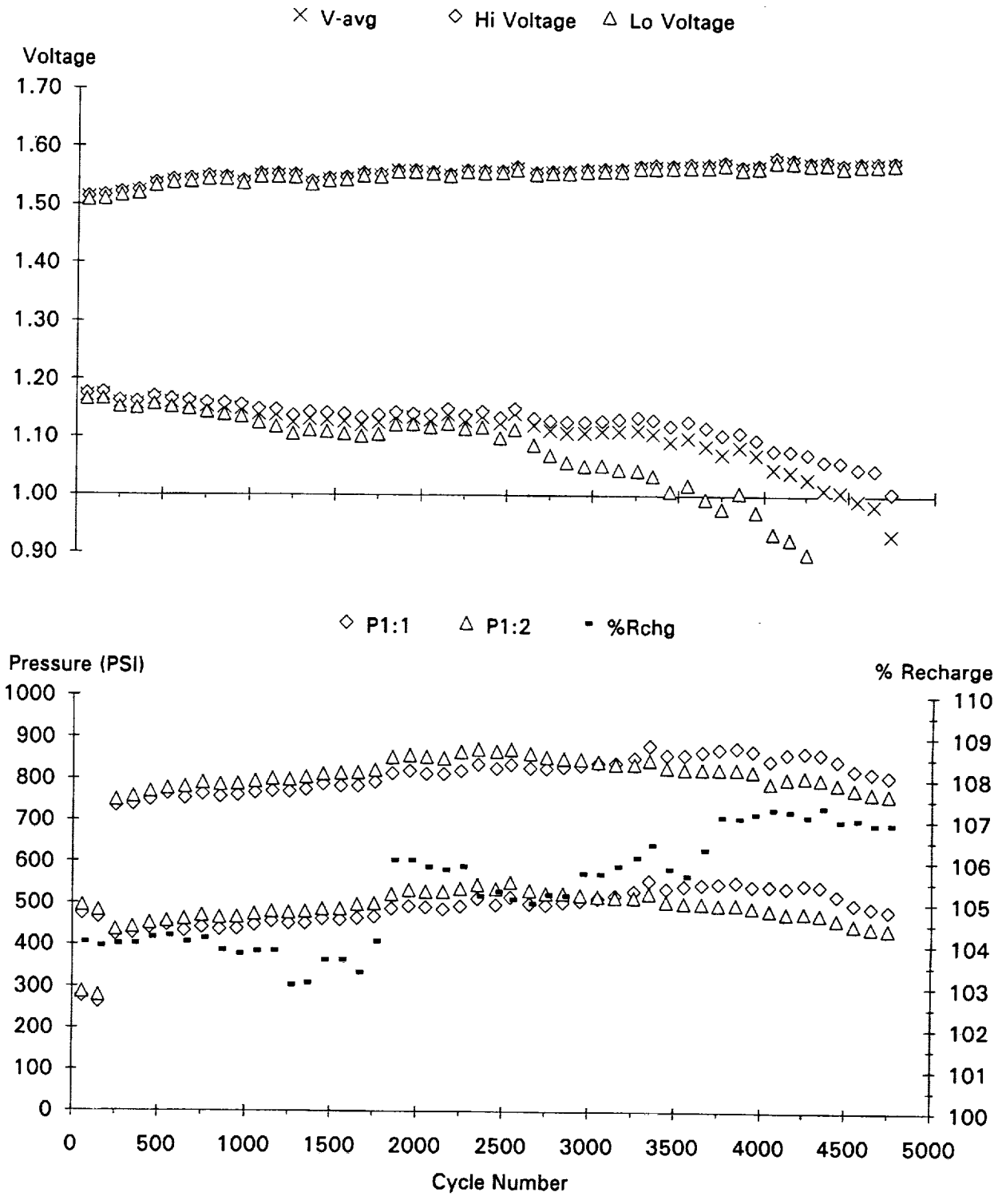

Cycle 1. Started Life Cycle Test.
-65.0A for .6Hr ; 61.75A for .6Hr ; 11.7A for .3Hr ; Rchg = 104.0%
Cycle 1828. Raised Rchg from 104.0% to 106.0%.
-65.0A for .6Hr ; 61.75A for .6Hr ; 14.3A for .3Hr
Cycle 3716. Raised Rchg from 106.0% to 107.0%.
-65.0A for .6Hr ; 61.75A for .6Hr ; 15.6A for .3Hr
Cycle 4751. Pack failed. EOD Pack Average Voltage below 1.0V.

NSWC Crane **Pack ID 5665W** **10 cells**

Voltage/Pressure/Recharge EOC/EOD Trend Plot 09/14/90 - 01/25/91

Yardney 65 AmpHr 60% DOD -5 Deg C Test Ended at Cycle 1720

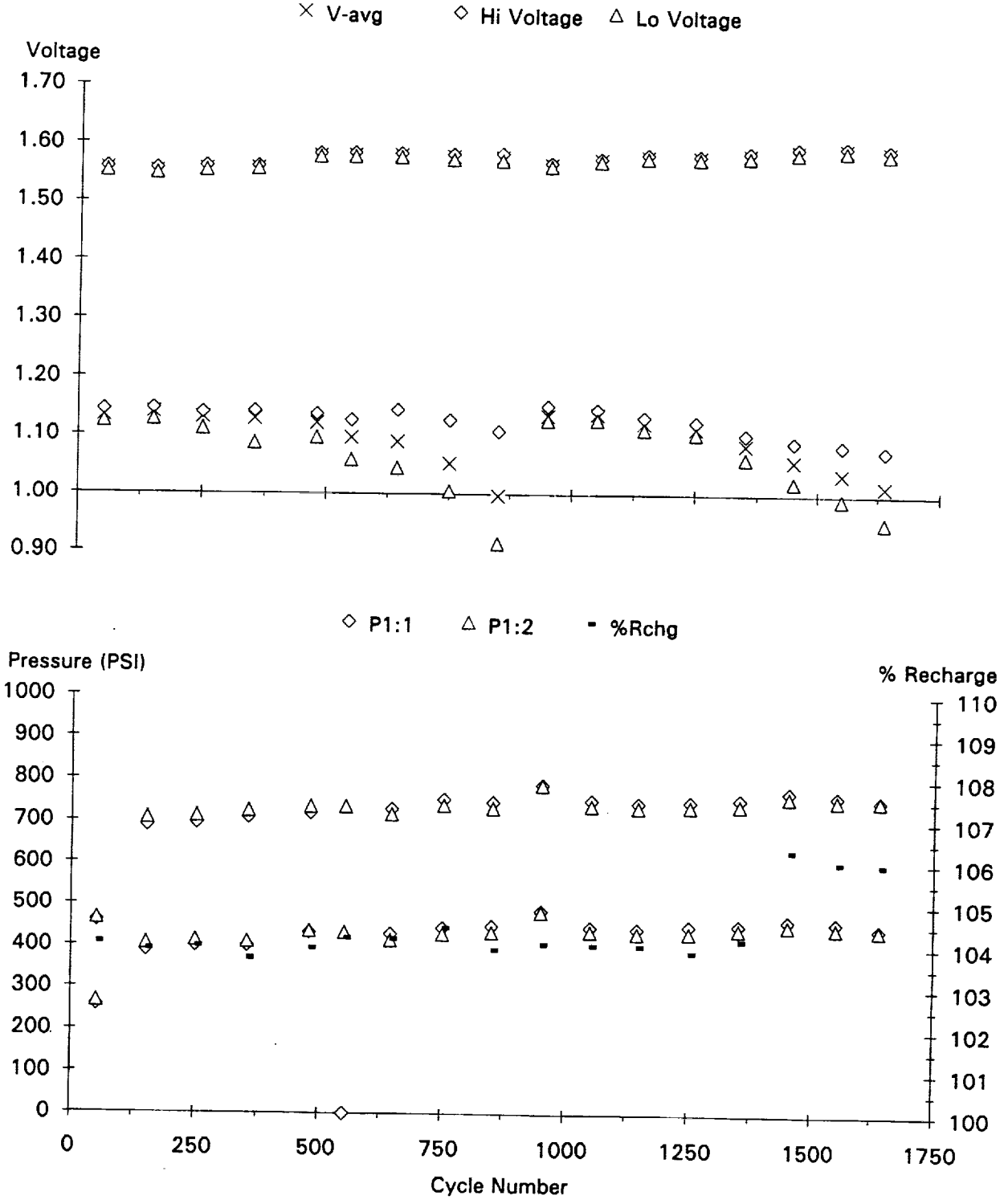

Cycle 1. Started Life Cycle Test.
-65.0A for .6Hr ; 61.75A for .6Hr ; 11.7A for .3Hr ; Rchg = 104.0%
Cycle 1400. Raised Rchg from 104.0% to 106.0%.
-65.0A for .6Hr ; 61.75A for .6Hr ; 14.3A for .3Hr

NSWC Crane Pack ID 5731W 5 cells

Voltage/Pressure/Recharge EOC/EOD Trend Plot 12/14/90 - 09/22/93

Yardney 65 AmpHr 35% DOD 10 Deg C

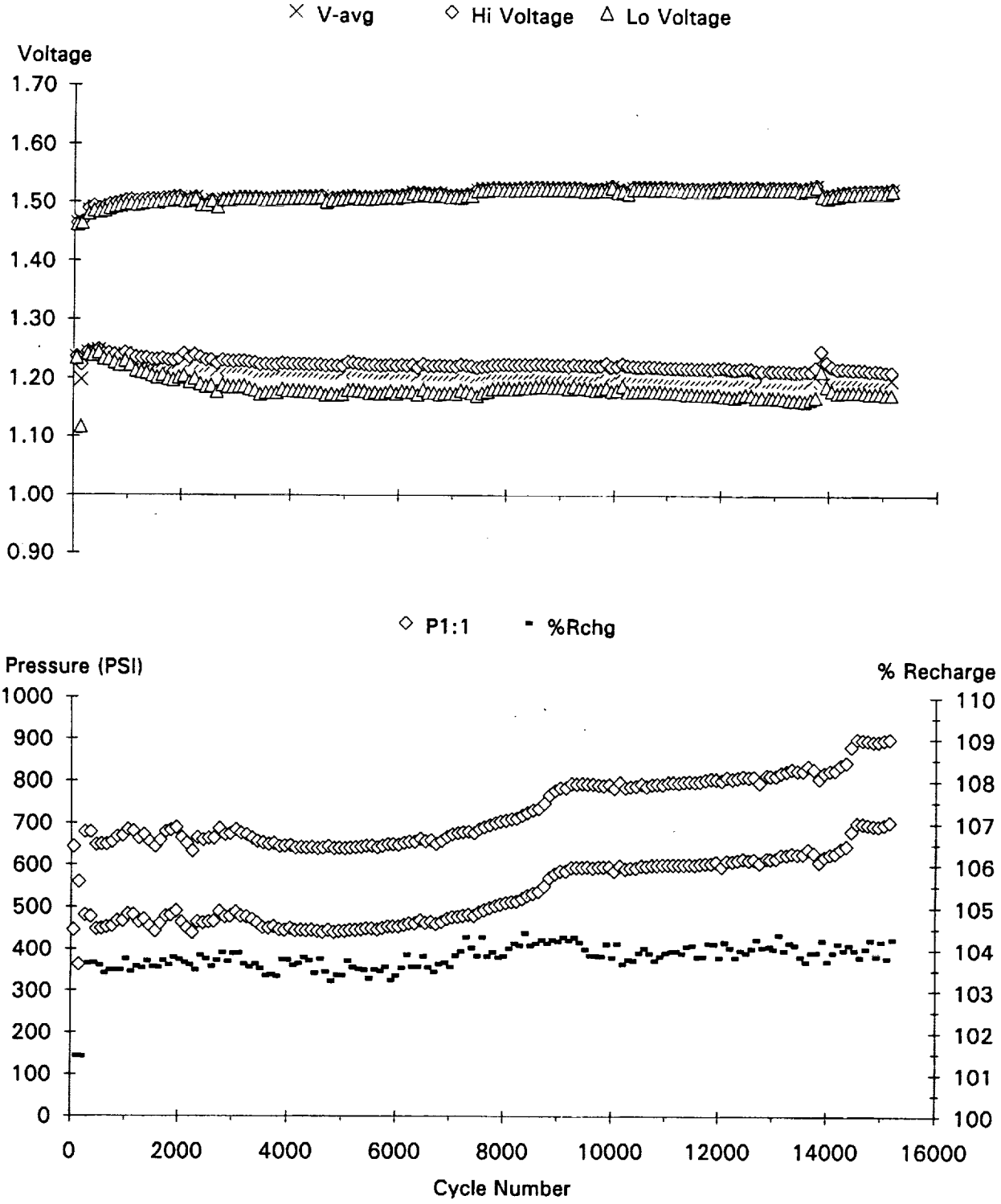

Cycle 1. Started Life Cycle Test.
-37.9A for .6Hr ; 36.0A for .6Hr ; 6.49A for .3Hr ; Rchg = 103.5%
Cycle 7065. Raised Rchg from 103.5% to 104.0%.
-37.9A for .6Hr ; 36.0A for .6Hr ; 6.87A for .3Hr

NSWC Crane Pack ID 5735W 5 cells

Voltage/Pressure/Recharge EOC/EOD Trend Plot 12/14/90 - 10/03/93

Yardney 65 AmpHr 35% DOD -5 Deg C

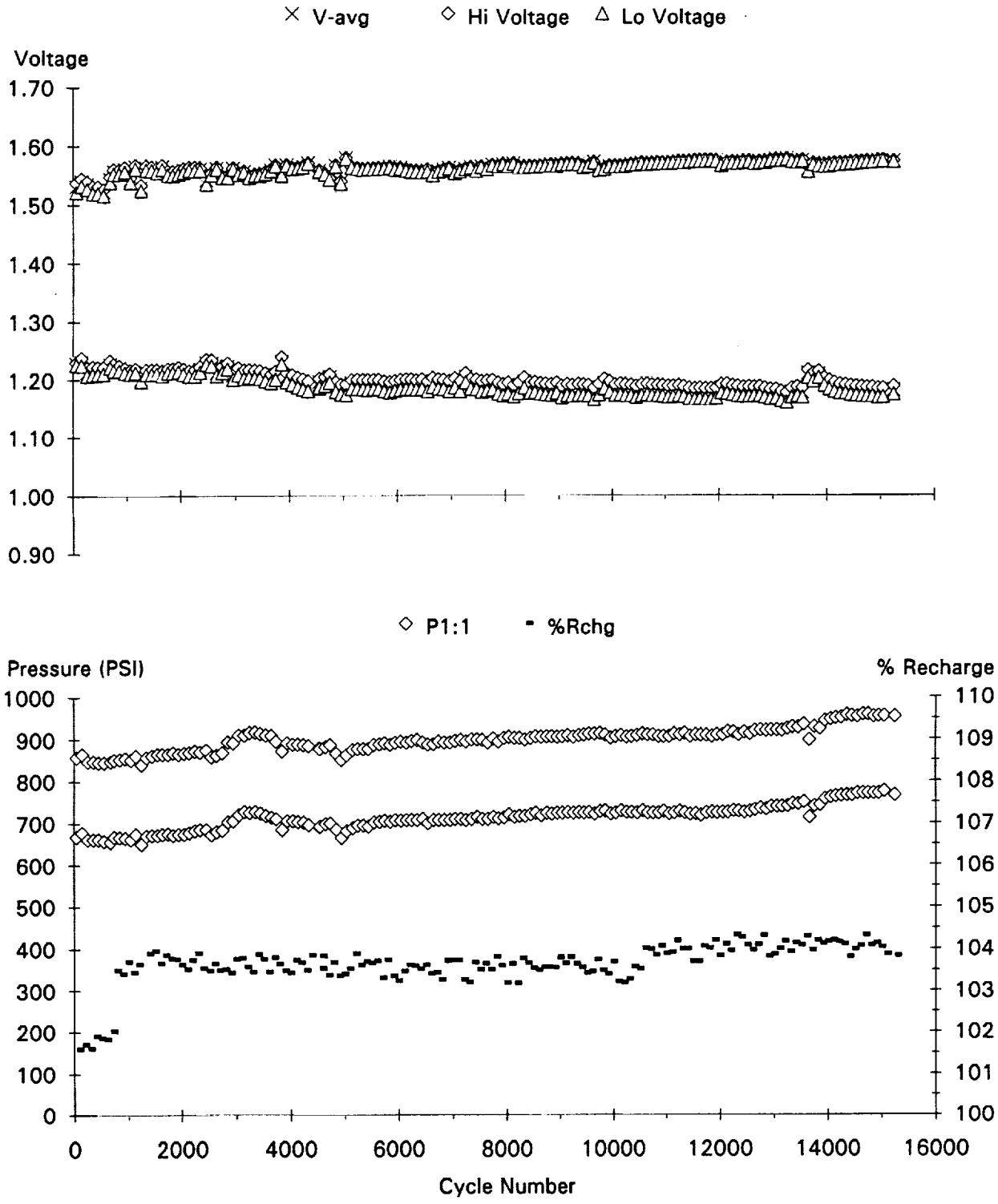

Cycle 1. Started Life Cycle Test.
-37.9A for .6Hr ; 36.0A for .6Hr ; 6.49A for .3Hr ; Rchg = 103.5%
Cycle 10492. Raised Rchg from 103.5% to 104.0%.
-37.9A for .6Hr ; 36.0A for .6Hr ; 6.87 A for .3 Hr

NSWC Crane **Pack ID 5761W** **5 cells**

Voltage/Pressure/Recharge EOC/EOD Trend Plot 12/13/90 - 03/06/91

Yardney 65 AmpHr 60% DOD 10 Deg C Test Ended at Cycle 1067

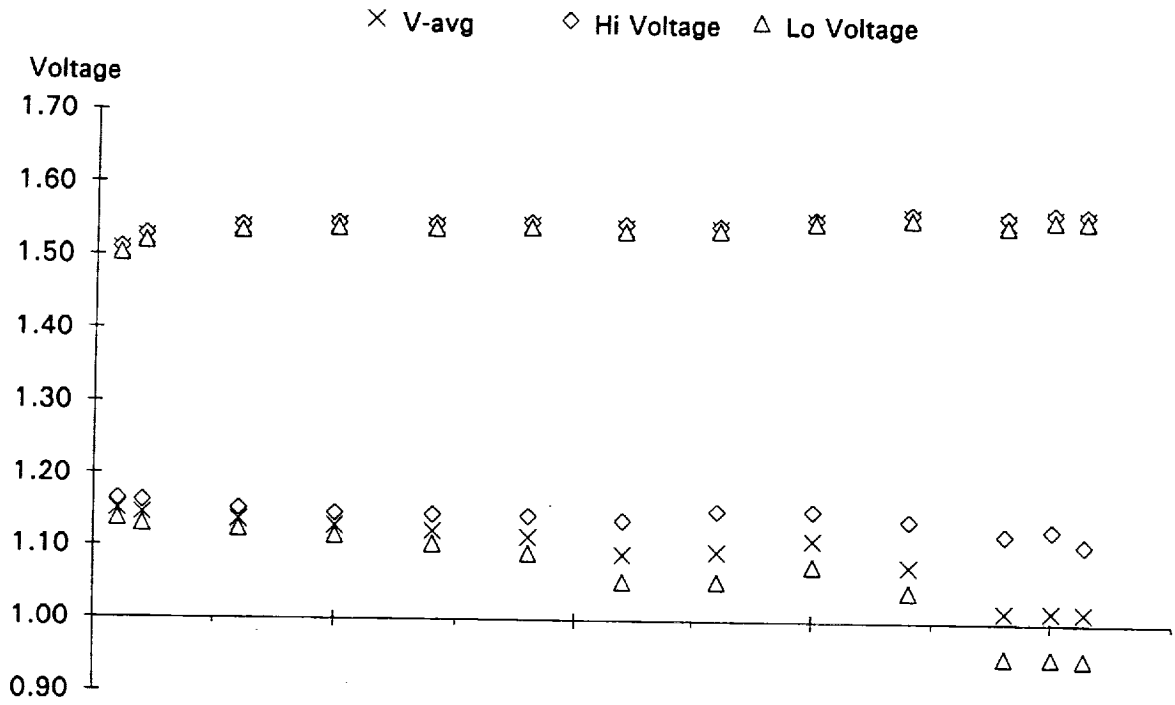

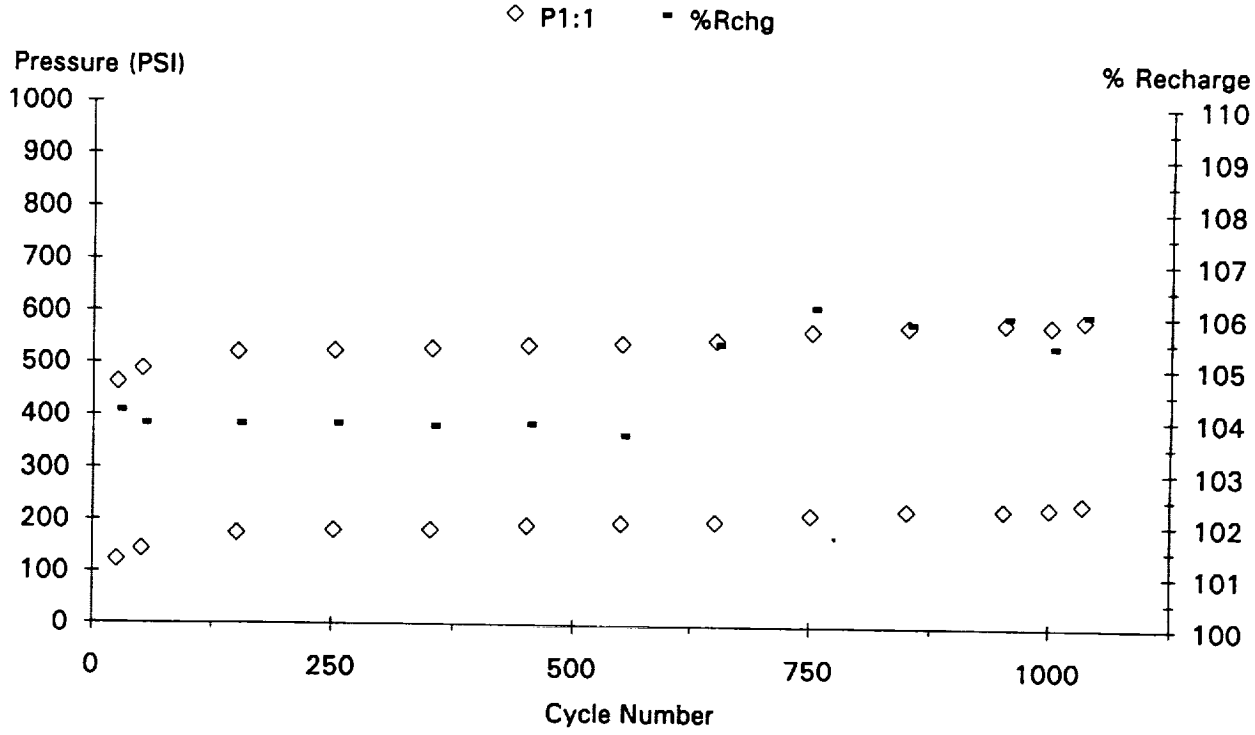

Cycle 1. Started Life Cycle Test.
-65.0A for .6Hr ; 61.75A for .6Hr ; 11.7A for .3Hr ; Rchg = 104.0%
Cycle 650. Raised Rchg from 1.04.0% to 1.06%.
-65.0A for .6Hr ; 61.75A for .6Hr ; 14.3A for .3Hr
Cycle 1004. Pack failed. EOD Pack Average Voltage below 1.0V.
Cycle 1046. Last LEO Cycle.
Cycle 1047-1067. Special testing run on pack to determine post LEO characteristics.

NSWC Crane **Pack ID 5765W** **5 cells**

Voltage/Pressure/Recharge EOC/EOD Trend Plot 12/14/90 - 02/02/91

Yardney 65 AmpHr 60% DOD -5 Deg C Test Ended at Cycle 427

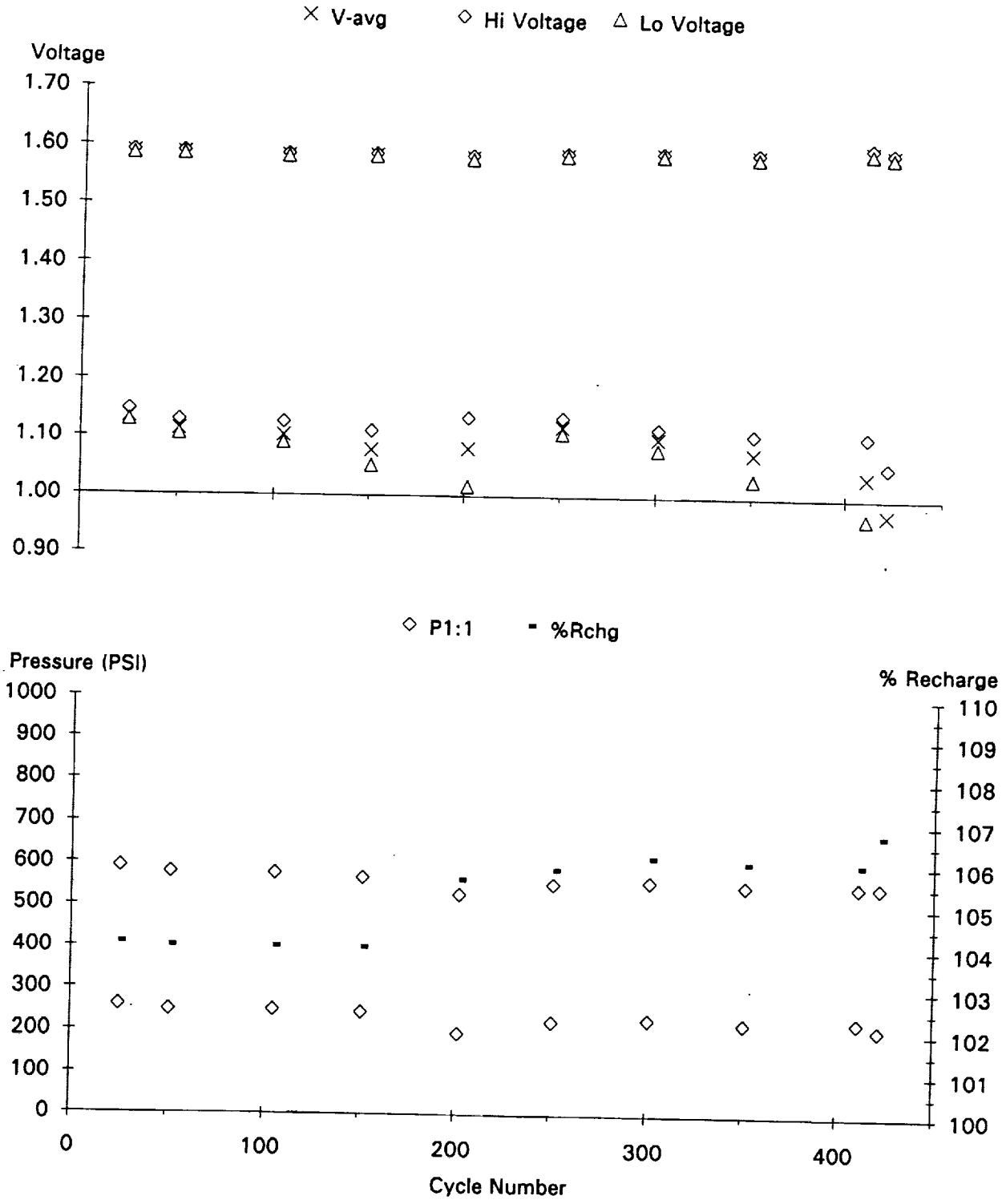

Cycle 1. Started Life Cycle Test.
-65.0A for .6Hr ; 61.75A for .6Hr ; 11.7A for .3Hr ; Rchg = 104.0%
Cycle 194. Raised Rchg from 1.04.0% to 1.06%.
-65.0A for .6Hr ; 61.75A for .6Hr ; 14.3A for .3Hr
Cycle 427. Pack failed. EOD Pack Average Voltage below 1.0V. Last LEO Cycle,
Cycle 428-448. Special testing run on pack to determine post LEO characteristics.

Ni-H_2 Cell Characterization for INTELSAT Programs

Andrew Dunnet
INTELSAT
Washington, D.C. 20008-3098

Martin Earl
COMSAT Laboratories
Clarksburg, MD. 20871-9475

ABSTRACT

Various Ni/H_2 cell designs manufactured for INTELSAT Programs during the past decade have been characterized electrically as a function of temperature. The resulting data for these INTELSAT V, VI, VII and VIIA cells are assembled in a manner which allows ready comparison of performance. Also included is a detailed description of each design.

INTRODUCTION

As part of a coordinated program to extend the operational lives of its spacecraft, INTELSAT characterizes the performance of each type of battery cell flown.

INTELSAT is operating batteries using 30 Ah cells made by Eagle-Picher, Industries, 48 Ah cells from Hughes Aircraft Company, and 85 Ah cells made by Gates Aerospace Batteries. In the near future we will be operating 120 Ah Gates cells also.

Life testing, performance characterization, and associated analytical work is done at COMSAT Corporation Laboratory, Clarksburg, Md.

This paper reports on the results of the performance characterization, with temperature, of the four types of Ni/H_2 cells in or about to be in operation with the INTELSAT fleet of geostationary communications satellites.

BACKGROUND

One reason why INTELSAT is successful in achieving long life for its operational fleet of spacecraft is the care taken in the operation of the spacecraft batteries. In support of the orbital operation, batteries of each type flown are placed into real time life test. These tests, performed at COMSAT Laboratories, simulate the operation in orbit as closely as possible. A test is normally started three seasons before the first use of the batteries in orbit. Individual cells are operated in the same test with the battery and are periodically removed from the test for destructive physical analysis (DPA). These tests are not intended to validate the design of the batteries; rather they are to address problems on the ground before they are encountered in orbit. Solutions can be devised and tested to ensure continued operation in orbit.

In addition to the life testing, COMSAT also performed a series of parametric performance tests, at the cell level, to characterize the response of the batteries under a variety of thermal and charge conditions.

Since 1983 INTELSAT spacecraft have all had Ni/H_2 batteries. These batteries have used cells from the three main Ni/H_2 cell manufacturers in the USA. Sixteen batteries using 30 Ah Eagle-Picher Industries (EPI) cells are in operation on the later INTELSAT V spacecraft, ten batteries using 44 Ah Hughes Aircraft Company cells are in operation on the INTELSAT VI spacecraft, and two batteries using 85 Ah Gates Aerospace Batteries have recently been launched on the first INTELSAT VII. This is the first of at least six similar spacecraft which will be joined by three INTELSAT VIIA spacecraft equipped with batteries using 120 Ah Gates cells. These are the four types of cell reported upon.

Details of the cells are given in Table 1. Figures 1 to 4 show cross-sectional drawings of each cell. While Table 2 gives details of each battery, INTELSAT has always flown two batteries per spacecraft. Figures 5 to 7 are pictures of each type of battery. As yet no pictures are available of an INTELSAT VIIA battery.

PARAMETRIC TESTING

In each of the four cases, a minimum of four cells of each type were subjected to charge/discharge cycles at 10°C intervals from +30 to -20°C except for the I-5 cells which, because of their design, operate successfully down to -30°C. In addition, self discharge performance data was generated at 10, 20, and 30°C for durations of 144 hours. The testing sequence is presented in Table 3. Pressure, temperature, cell voltage, charge, and discharge current are carefully monitored.

Figure 8 displays a typical series of charge/discharge voltage and temperature profiles. From this type of data, cell end-of-charge voltage, mid-discharge voltage and capacity are determined as a function of cell temperature. This is a modification to the data which was previously presented using chamber set point temperature for the abscissa [1]. Two cells of each group were instrumented with strain-gauges. A typical series of charge/discharge pressure profiles are displayed in Figure 9. When this data is normalized to 0°C using the gas law and cell temperature data, the resulting profiles indicate the degree to which the gauges are temperature compensated. The charging pressure profiles can be used to generate plots of instantaneous charge efficiency by taking their derivative with respect to time. Finally, pressure profiles for 144 hours of self-discharge were determined at 10, 20, and 30°C. These pressure profiles were converted to capacity remaining profiles by considering the pressure range for capacity measurements. The results for each case are displayed in Figures 10 to 13. Plotted are capacity, end-of-charge voltage and mid-discharge voltage as a function of cell temperature; charge efficiency versus charge in and percent capacity remaining as a function of open-circuit time at temperature.

The self-discharge data can be further developed assuming first order kinetics and Arrhenius behavior [2]. The resulting self-discharge characteristics and Arrhenius plots are displayed in Figure 14. The activation energy associated with the rate constant for each case is included in Table 4.

[1] J. D. Dunlop, et. al., "NASA Handbook for Nickel-Hydrogen Batteries," NASA Reference Publication 1314, 1993, Chapter 5.

[2] J. F. Stockel, "Self-Discharge Performance and Effects of Electrolyte Concentration on Capacity of Nickel-Hydrogen (Ni/H_2) Cells," 20th Intersociety Energy Conversion Engineering Conference, Miami Beach, Florida, August 1985, Vol. 1, pp. 1.171-1.174.

TABLE 1. SUMMARY OF INTELSAT NI-H_2 CELL DESIGNS

	IV	IVI	IVII	IVII-A
Manufacturer	EPI	HAC/EPI	GAB	GAB
Cell Dimensions (cm)				
Diameter	8.9	8.7	8.7	11.8
Total Length	21.2	28.0	29.3	20.2
Cell Mass (g)	890	1460	1840	2640
Capacity @ 10°C to 1.0V (Ah)	34	56	90	122
Stack Design				
Component Shape	Truncated Disk	Pineapple Slice	Pineapple Slice	Pineapple Slice
Configuration	Single	Single	Single	Single
Arrangement	Back to Back	Recirculating	Back to Back	Back to Back
Terminal Design	Ziegler/Axial	Teflon/Axial	Ceramic/Axial	Ceramic/Rabbit Ear
Positive Electrode				
Plaque Type	Wet Slurry	Dry Powder	Dry Powder	Dry Powder
Impregnation Type	Aqueous EC	Alcohol EC	Aqueous EC	Aqueous EC
$Ni(OH)_2$ Loading (g/cc)	1.42	1.29	1.49	1.52
$Co(OH)_2$ Loading (g/cc)	0.12	0.16	0.13	0.12
Plate Thickness (mm)	0.775	0.880	0.920	0.920
No. of Plates	24	40	48	38
Mass Fraction (%)	37.3	34.4	37.3	35.2
Separator Type	Asbestos	2 Layer Zircar	2 Layer Zircar	2 Layer Zircar
Thickness (mm)	0.25	0.60	0.60	0.60
Mass Fraction	2.0	5.9	6.1	5.3
Electrolyte				
Discharged State (w/o)	38	31	31	31
Mass Fraction (%)	10.7	15.9	15.0	13.7
Negative Electrode				
No. of Plates	34	41	48	38
Thickness (mm)	0.137	0.148	0.116	0.116
Pt Loading (g/cm^2)	8.10	7.52	3.20	2.80
Mass Fraction (%)	4.2	4.4	4.2	4.0

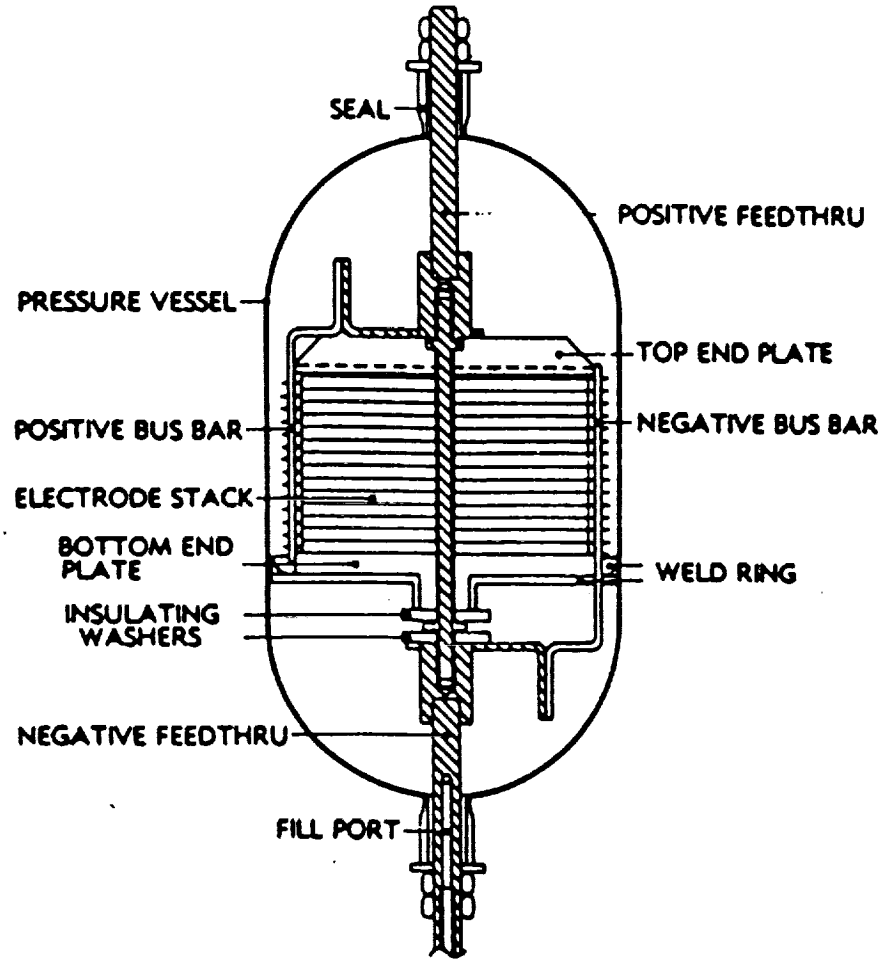

Figure 1. Cross-sectional view of an INTELSAT V NiH2 Cell

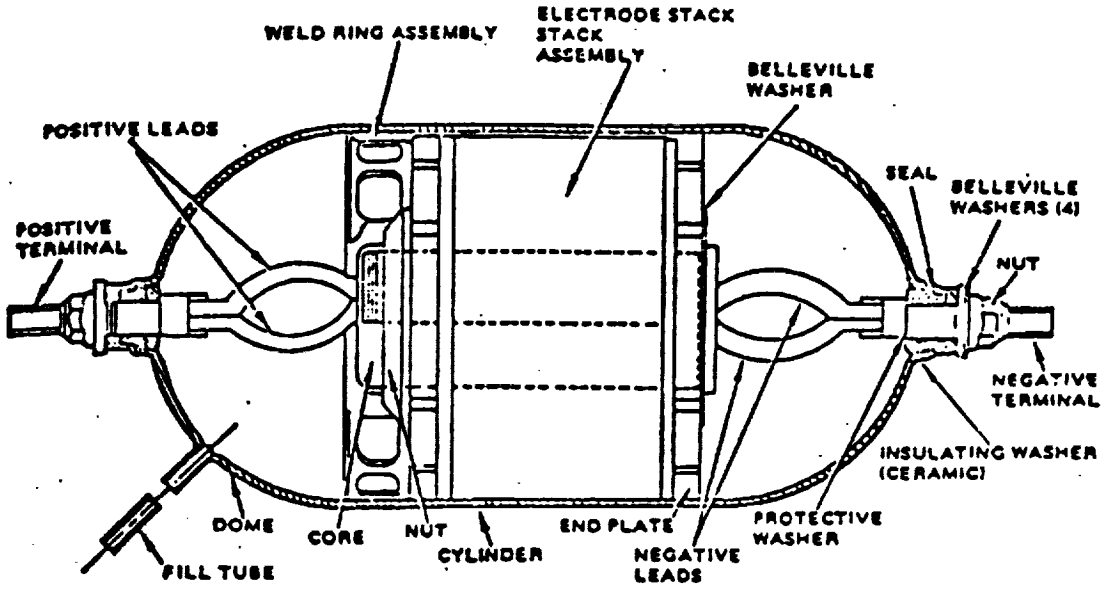

Figure 2. Cross-sectional view of an INTELSAT VI NiH2 Cell

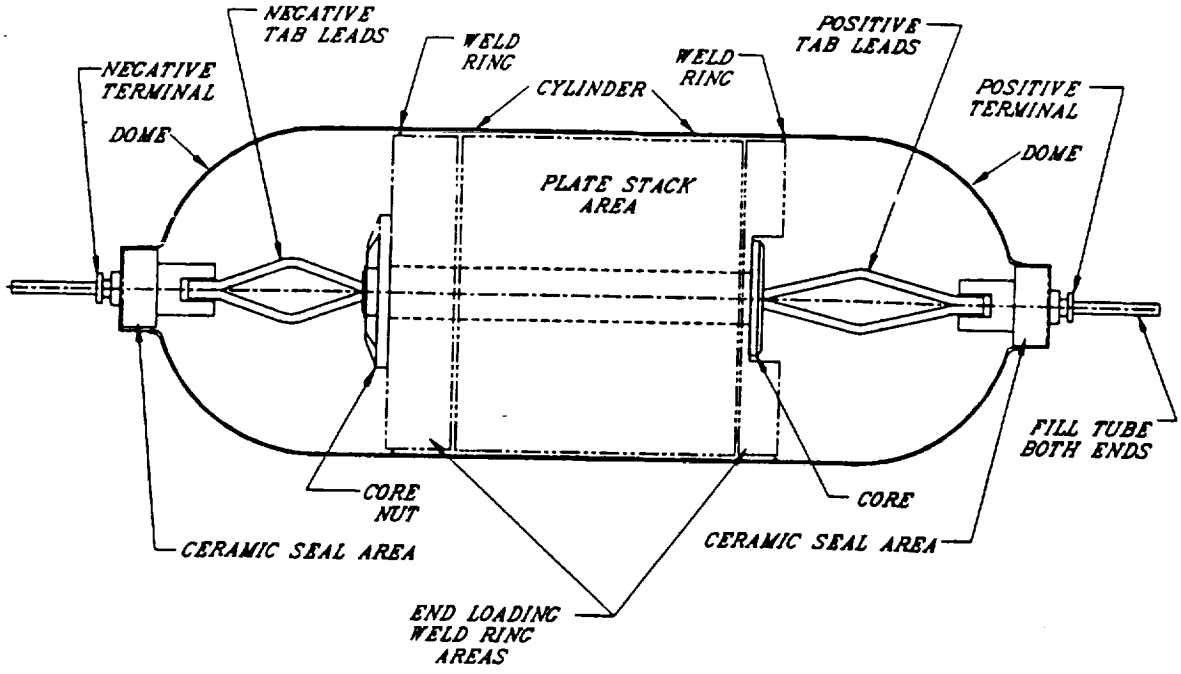

Figure 3. Cross-sectional view of an INTELSAT VII NiH2 Cell

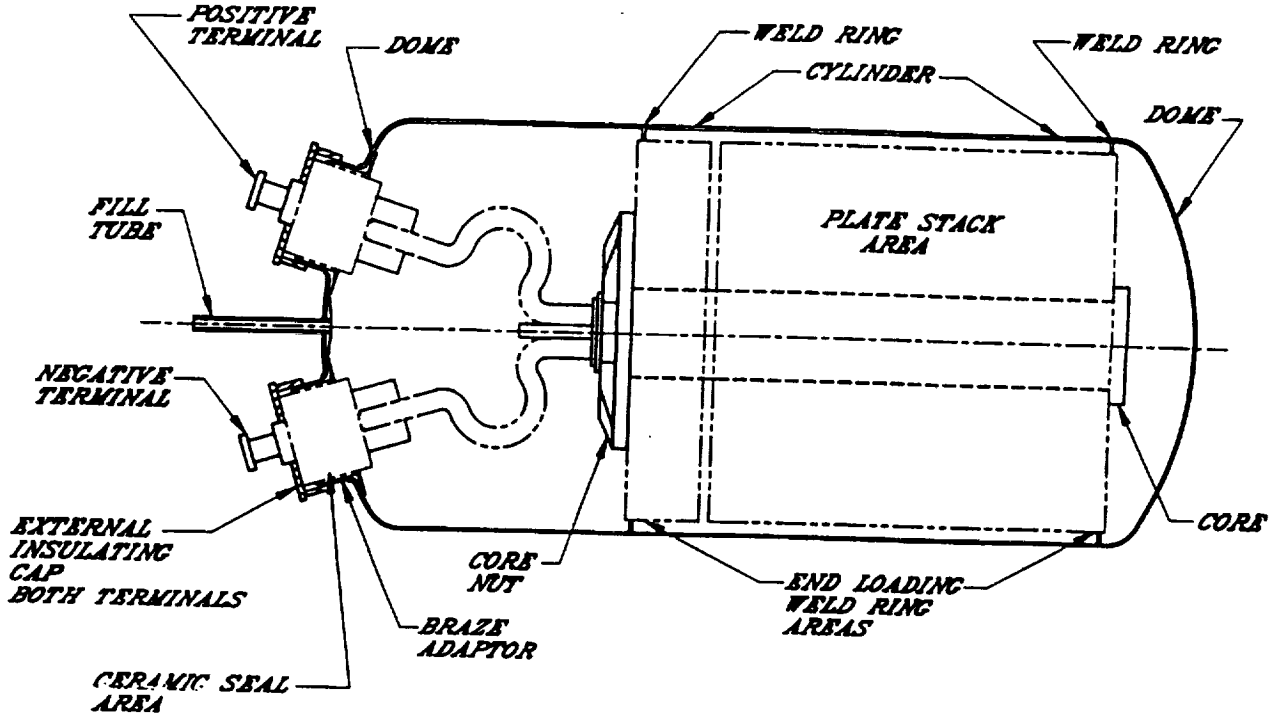

Figure 4. Cross-sectional view of an INTELSAT VIIA NiH2 Cell

Gates Energy Products

Gates Aerospace Batteries

TABLE 2. SUMMARY OF INTELSAT BATTERY DESIGNS

	I-V	I-VI	I-VII	I-VII-A
Manufacturer	Ford Aerospace	HAC	SS/Loral	SS/Loral
No. Batteries/SC	2	2	2	2
No. Packs/Battery	1	2	2	2
No. Cells/Battery	27	32	27	27
Battery Dimenions (cm)		2 Quadrants	Pack 1 Pack 2	Pack 1 Pack 2
Length	51.8		51.0 51.0	50.8 50.8
Width	52.1		51.0 37.8	52.8 39.5
Height	22.2	28	30.4 30.4	23.5 23.5
Radius		80		
Battery Mass (Kg)	30.12	63.9	66.8	81.45
Rated Capacity (Ah)	30	44	85.5	120
Reconditioning (Ω)				
Load A	50	43.2	23.5	16.2
Load B		86.4		
Diode Bypass	✓	✓	✓	✓

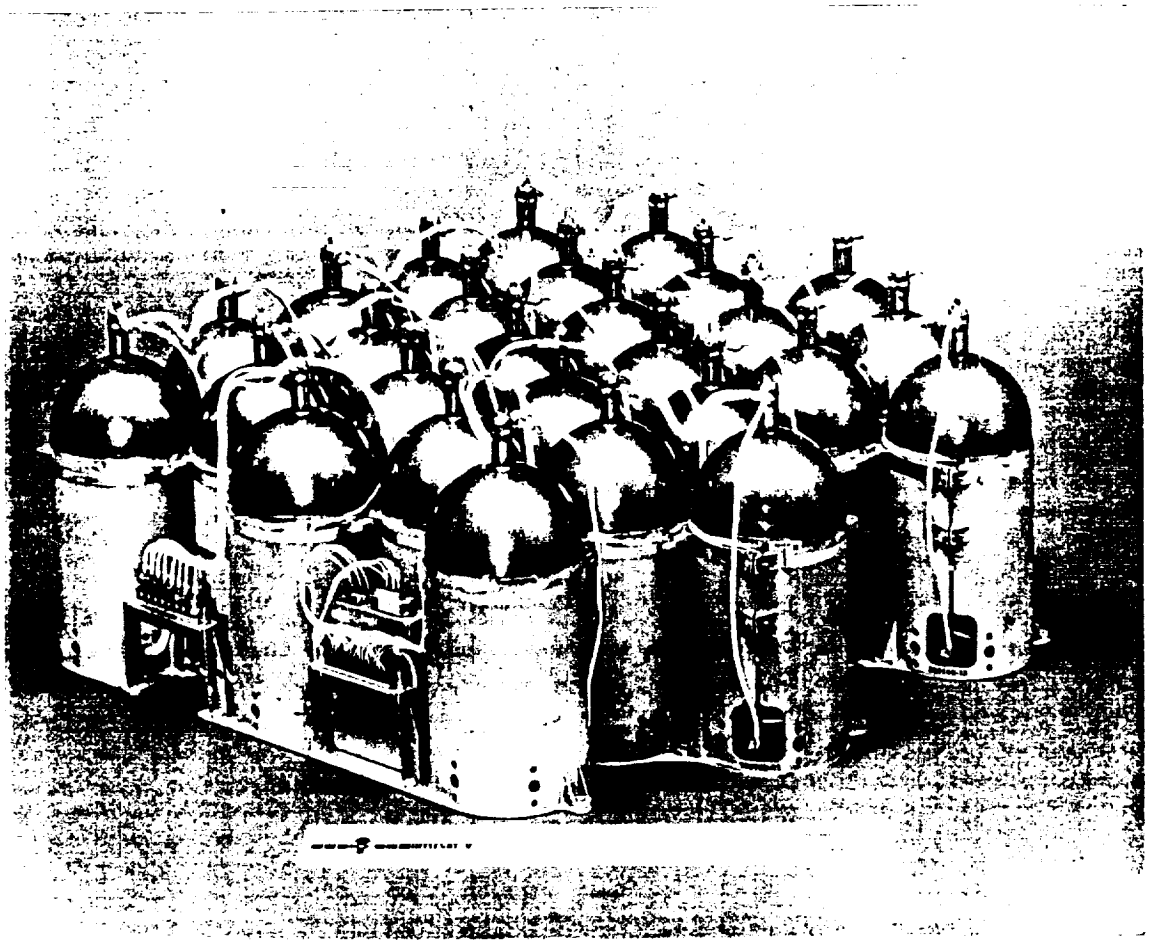

Figure 5. INTELSAT V NiH2 Battery

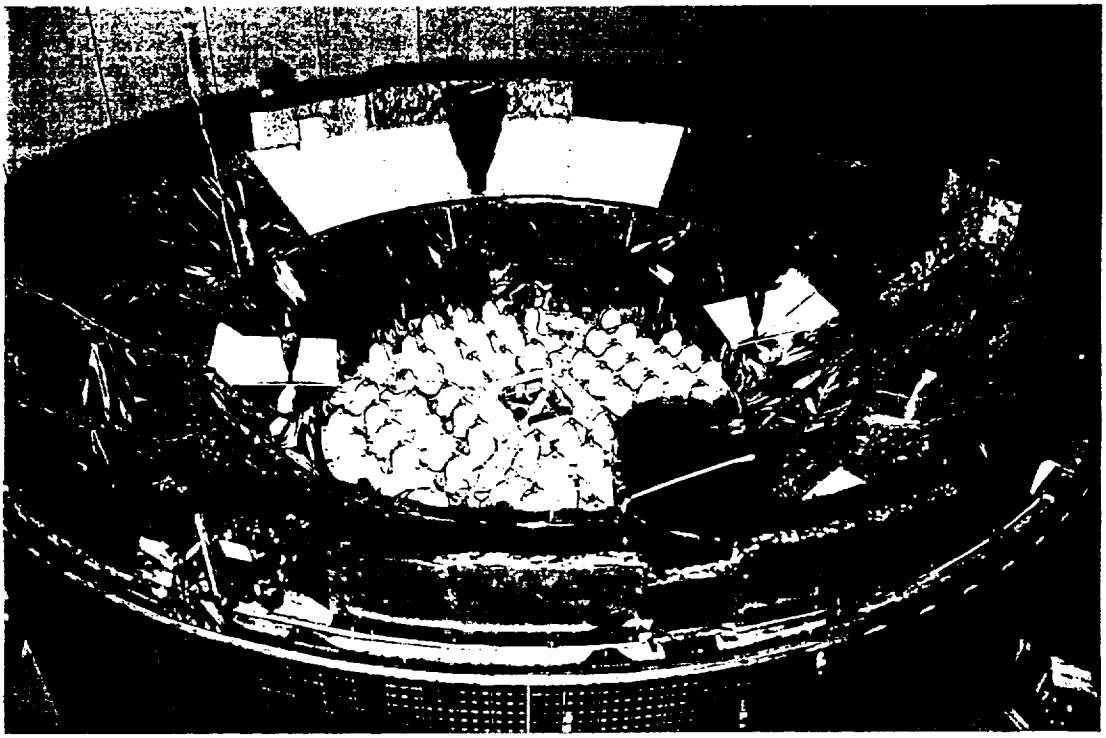

Figure 6. Two INTELSAT VI NiH2 Batteries on the Flt. 1 S/C

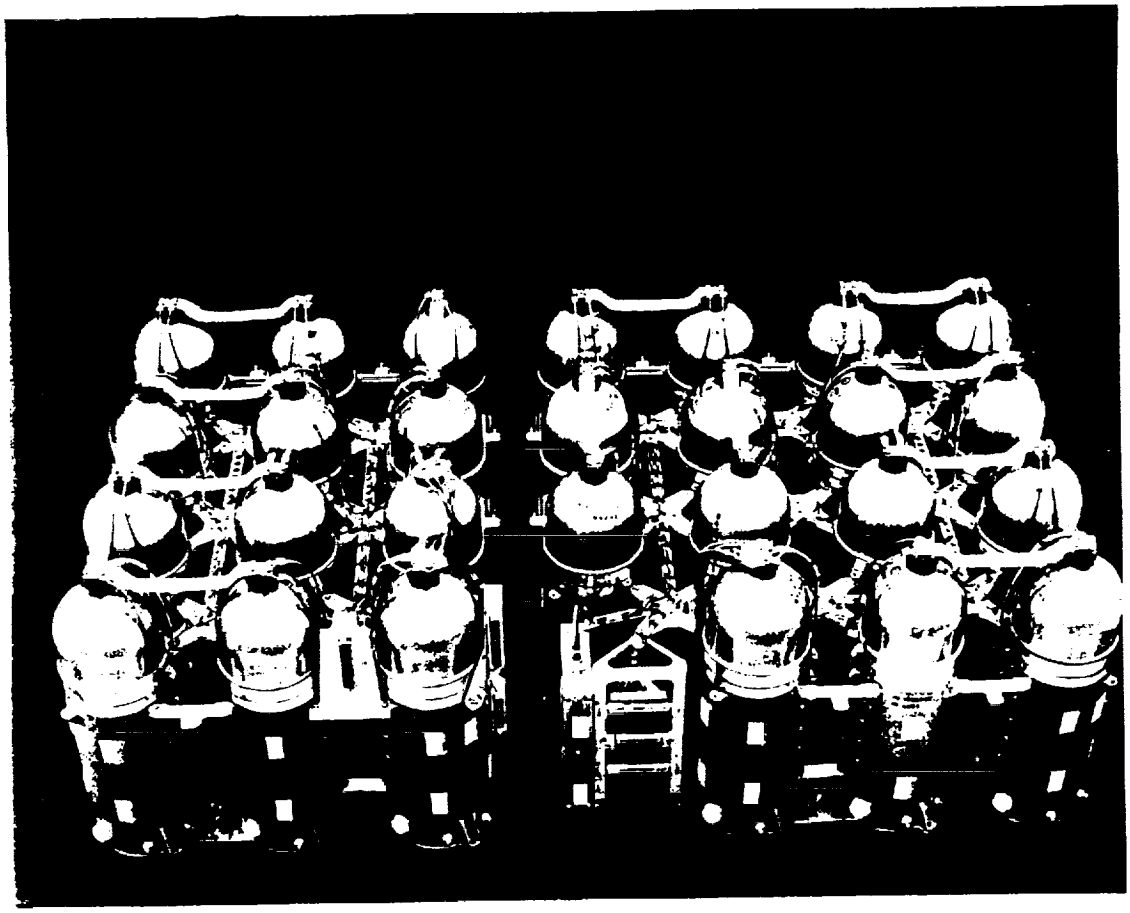

Figure 7. INTELSAT VII NiH2 Battery

TABLE 3 - INTELSAT CHARACTERIZATION TEST REGIME

Sequences	Temp.	Measurements	Charge/Discharge	I-V	I-VI	I-VII	I-VIIA	Remarks
1	10° C	Reconditioning	C/20 , C/2	x	x	x	x	
2	10° C	Capacity	C/10 , C/2	x	x	x	x	
3	10° C	Capacity	C/10 , C/2	x	x	x		
4	0° C	Capacity	C/10 , C/2	x	x	x	x	
5	0° C	Capacity	C/10 , C/2	x	x	x	x	
6	-10° C	Capacity	C/10 , C/2	x	x	x	x	
7	-10° C	Capacity	C/10 , C/2	x	x	x	x	
8	-20° C	Capacity	C/10 , C/2	x	x	x	x	
9	-20° C	Capacity	C/10 , C/2	x	x	x	x	
10	-30° C	Capacity	C/10 , C/2	x			x	
11	-30° C	Capacity	C/10 , C/2	x			x	
12	10° C	Capacity	C/10 , C/2	x	x	x	x	
13	10° C	Capacity	C/10 , C/2	x	x	x	x	
14	20° C	Capacity	C/10 , C/2	x	x	x	x	
15	20° C	Capacity	C/10 , C/2	x	x	x	x	
16	30° C	Capacity	C/10 , C/2	x	x		x	
17	30° C	Capacity	C/10 , C/2	x	x		x	
18	10° C	Capacity	C/10 , C/2	x	x	x	x	
19	10° C	Charge Stand	C/10 , C/2	x	x	x	x	1
20	20° C	Charge Stand	C/10 , C/2	x	x	x	x	2
21	30° C	Charge Stand	C/10 , C/2	x	x	x	x	3
				C=30Ah	C=48Ah	C=86Ah	C=120Ah	
			CELLS #	L4-04	L003*	L1-001*	L1-002*	
				L4-84	L012*	L1-022*	L1-004*	
				L4-90 *	L013	L2-023	L1-016	
				L4-107*	L014	L2-060	L1-018	
							L1-022	
							L1-032	

(1) Charge for 16 hours @ 10°C, Open circuit for 144 hours @ 10°C, Discharge to 0.1V @ 10°C
(2) Charge for 16 hours @ 10°C, Open circuit for 144 hours @ 20°C, Discharge to 0.1V @ 20°C
(3) Charge for 16 hours @ 10°C, Open circuit for 144 hours @ 30°C, Discharge to 0.1V @ 30°C

* Cells with Strain Gauge

		(TO 0.1V)	(TO 0.1V)	(TO 0.1V)	(TO 1.0V)	(TO 1.0V)	(TO 1.0V)
———	0°C	1.241	138.60	171.13	1.242	137.10	170.05
—·—·—	-10°C	1.230	149.30	182.60	1.232	147.00	180.81
—··—··—	-20°C	1.211	154.15	185.25	1.214	149.32	181.27
—·—·—	10°C	1.248	123.22	151.96	1.249	120.33	149.81
— — —	20°C	1.261	109.34	135.54	1.262	106.51	133.46
— — —	30°C	1.263	87.40	108.13	1.265	84.30	105.85

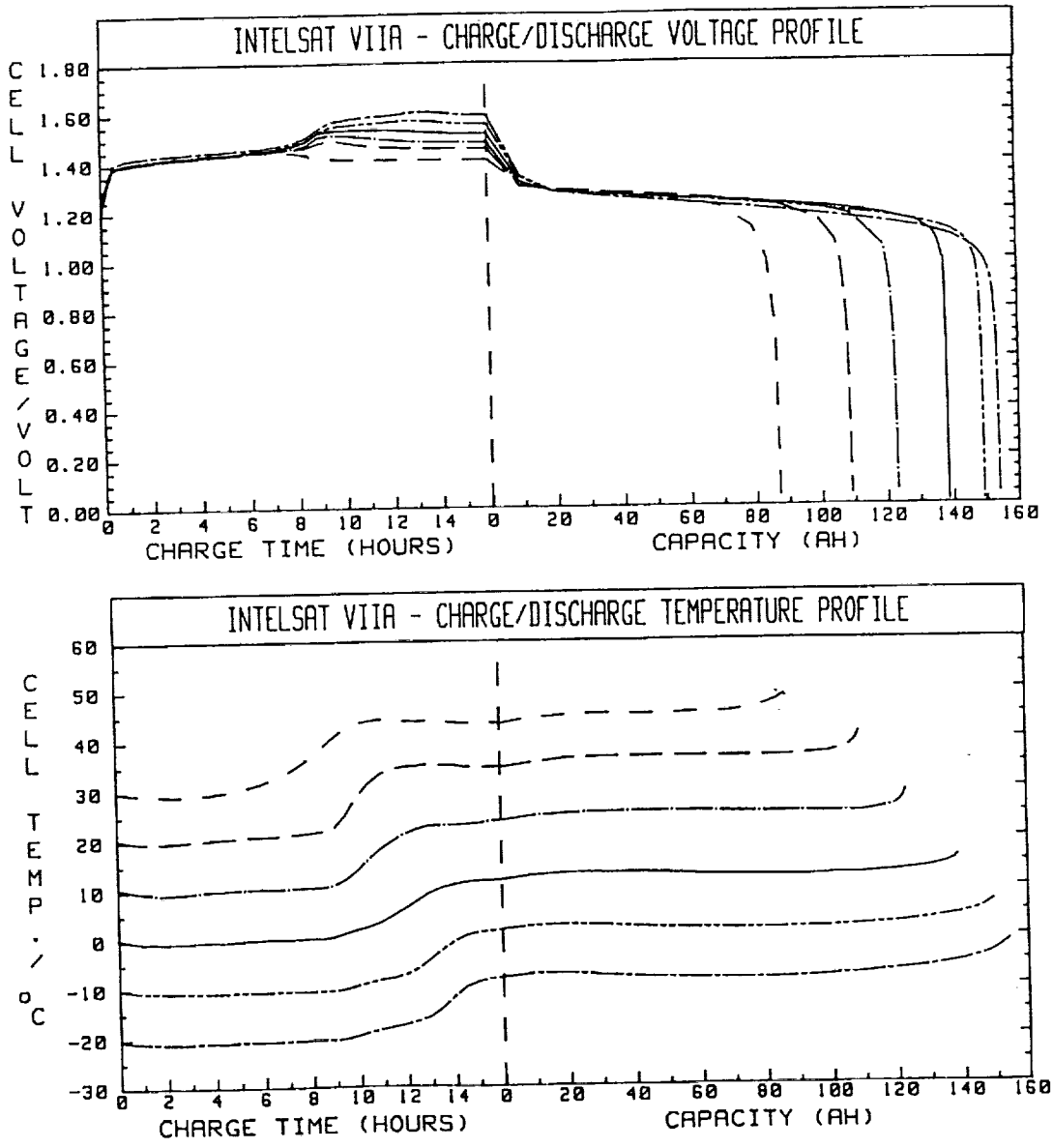

FIGURE 8

	Temp.	CHARGE Slope	CHARGE Intercept	DISCHARGE Slope	DISCHARGE Intercept
———	0°C	64.05	18	-5.716	815
—·—·—	-10°C	61.2	20	-5.48	841
—··—··—	-20°C	58.77	19	-5.251	833
————	10°C	66.79	31	-6.161	794
— — —	20°C	68.95	27	-6.438	734
— — —	30°C	69.93	26	-6.656	608

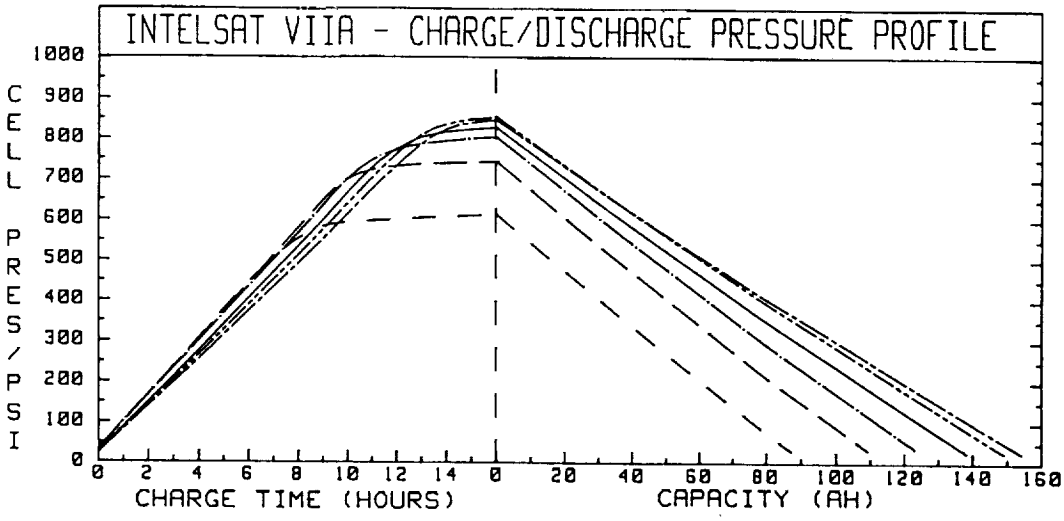

	Temp.	CHARGE Slope	CHARGE Intercept	DISCHARGE Slope	DISCHARGE Intercept
———	0°C	63.53	19	-5.467	779
—·—·—	-10°C	63.28	21	-5.443	835
—··—··—	-20°C	63.04	21	-5.415	858
————	10°C	63.91	31	-5.65	727
— — —	20°C	63.84	26	-5.698	649
— — —	30°C	63.29	26	-5.734	523

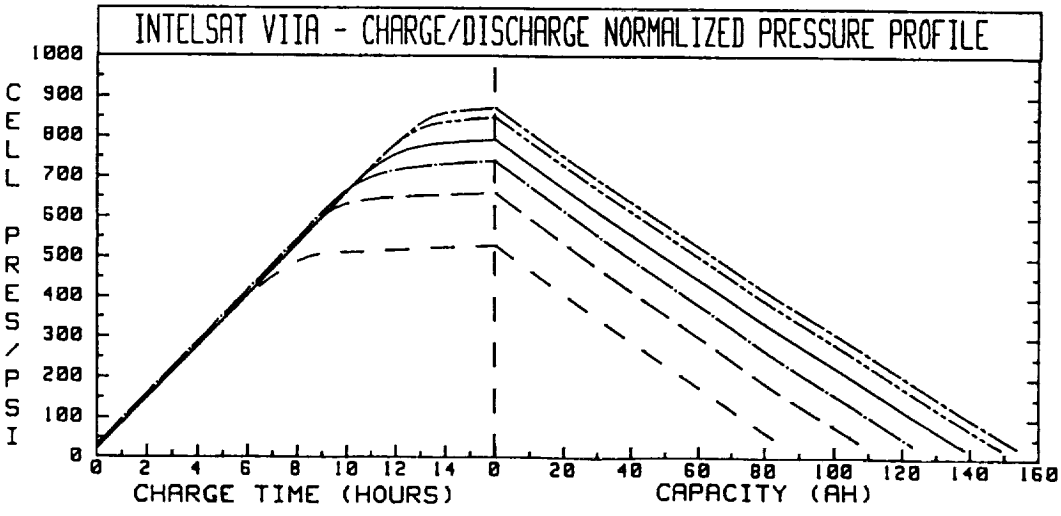

FIGURE 9

COMSAT LABORATORIES

INTELSAT

INTELSAT V

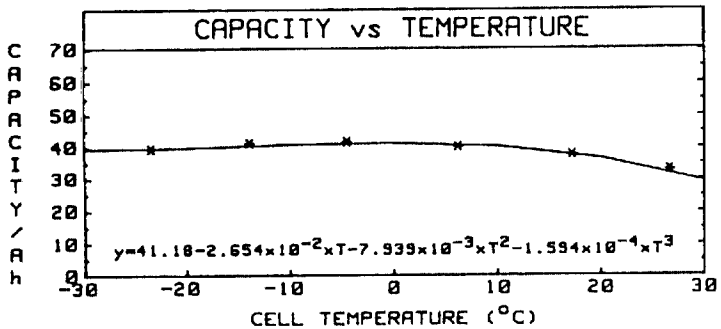

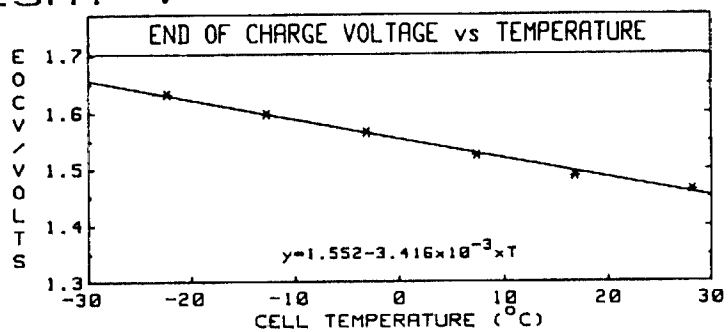

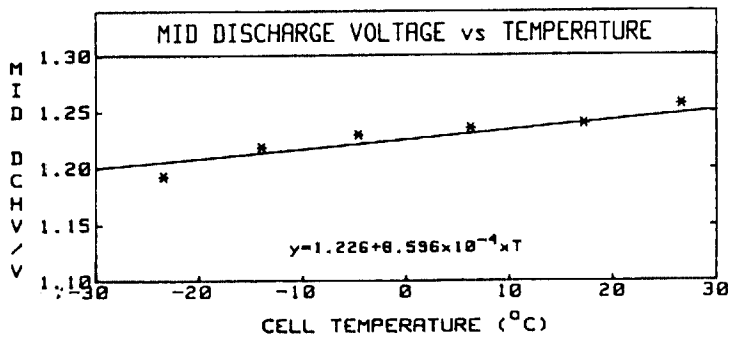

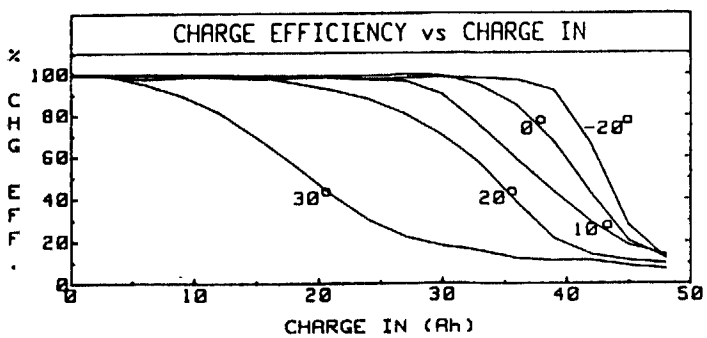

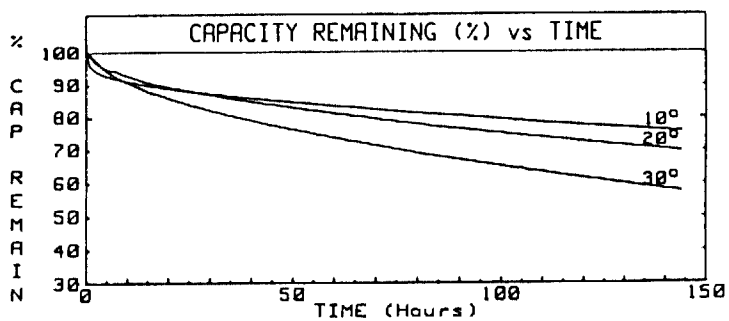

FIGURE 10

COMSAT LABORATORIES

INTELSAT

INTELSAT VI

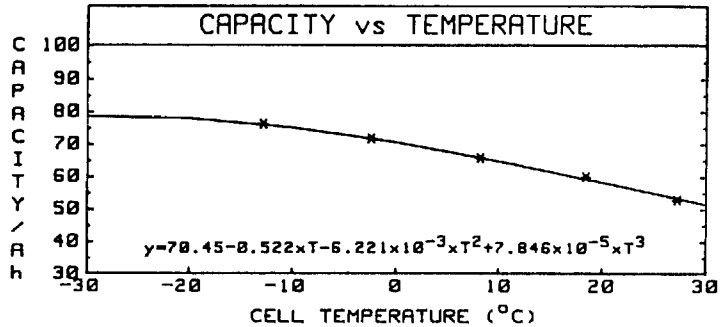

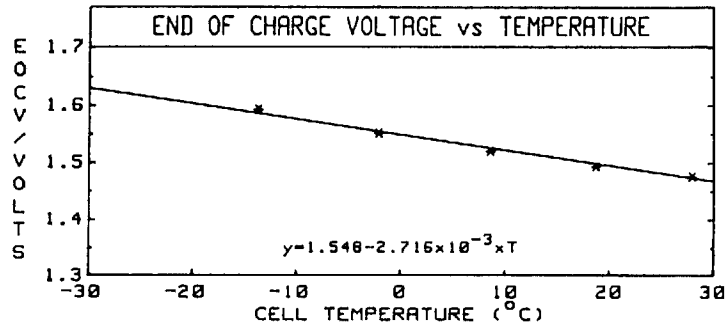

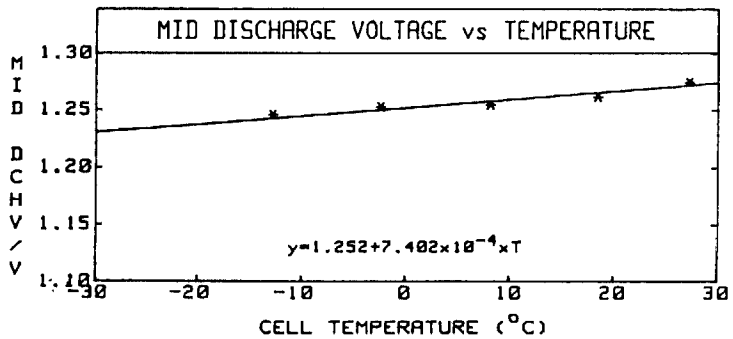

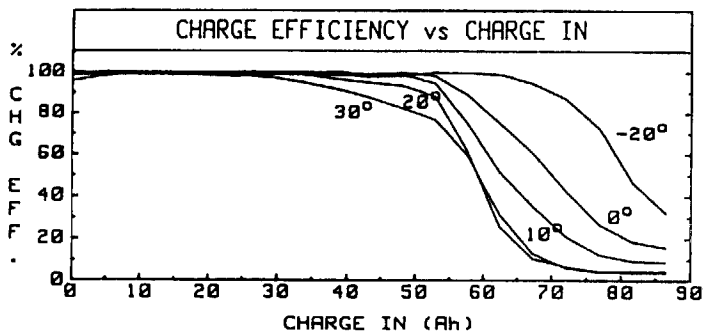

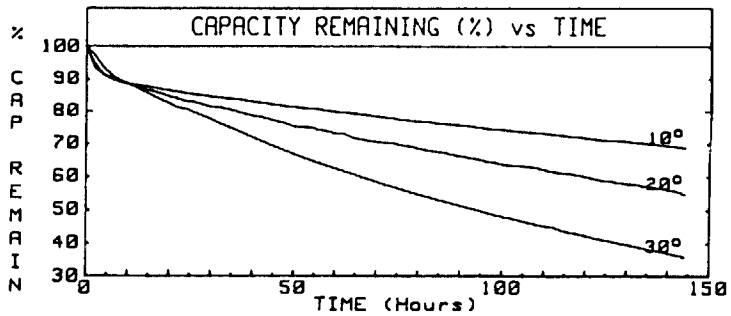

FIGURE 11

COMSAT LABORATORIES

INTELSAT

INTELSAT VII

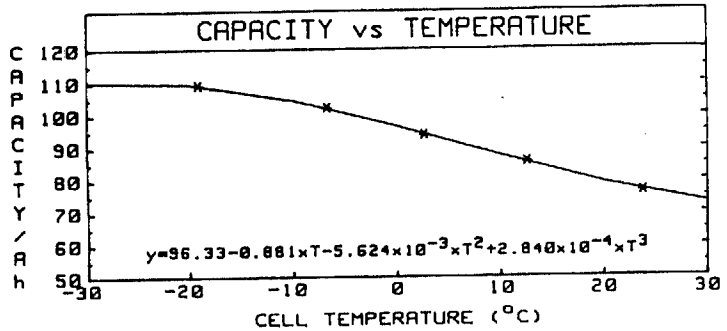

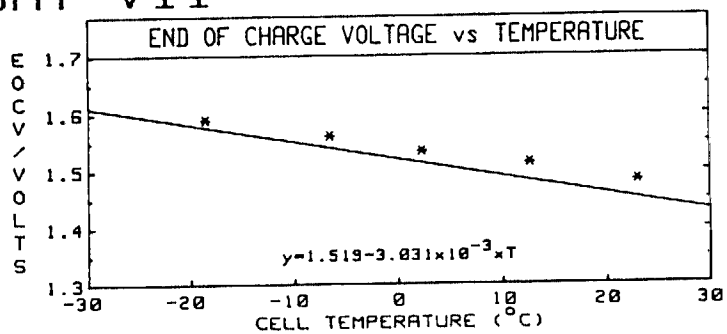

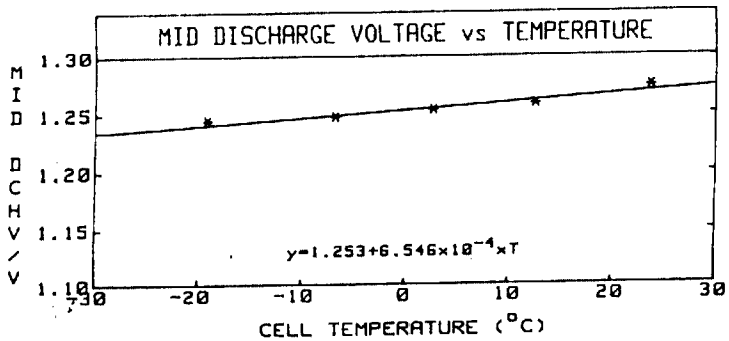

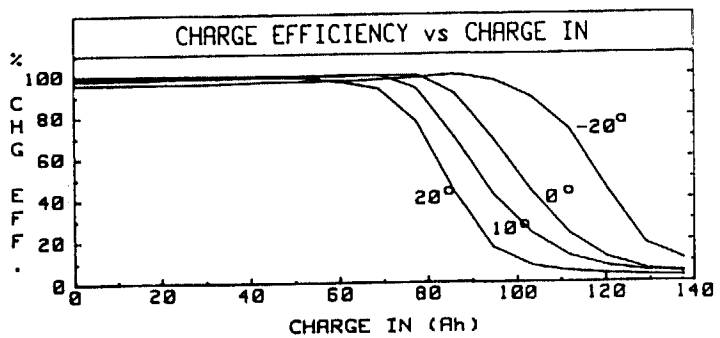

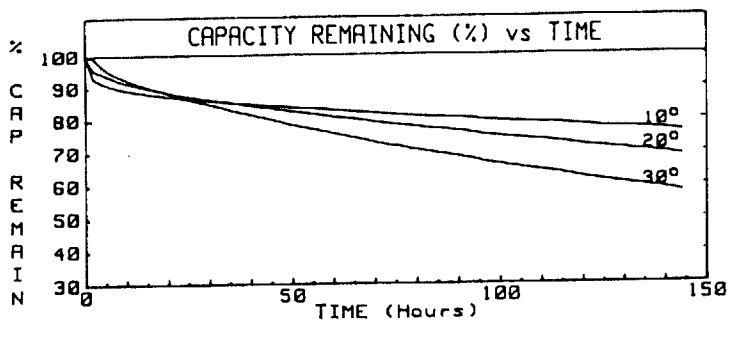

FIGURE 12

COMSAT LABORATORIES

INTELSAT

INTELSAT VIIA

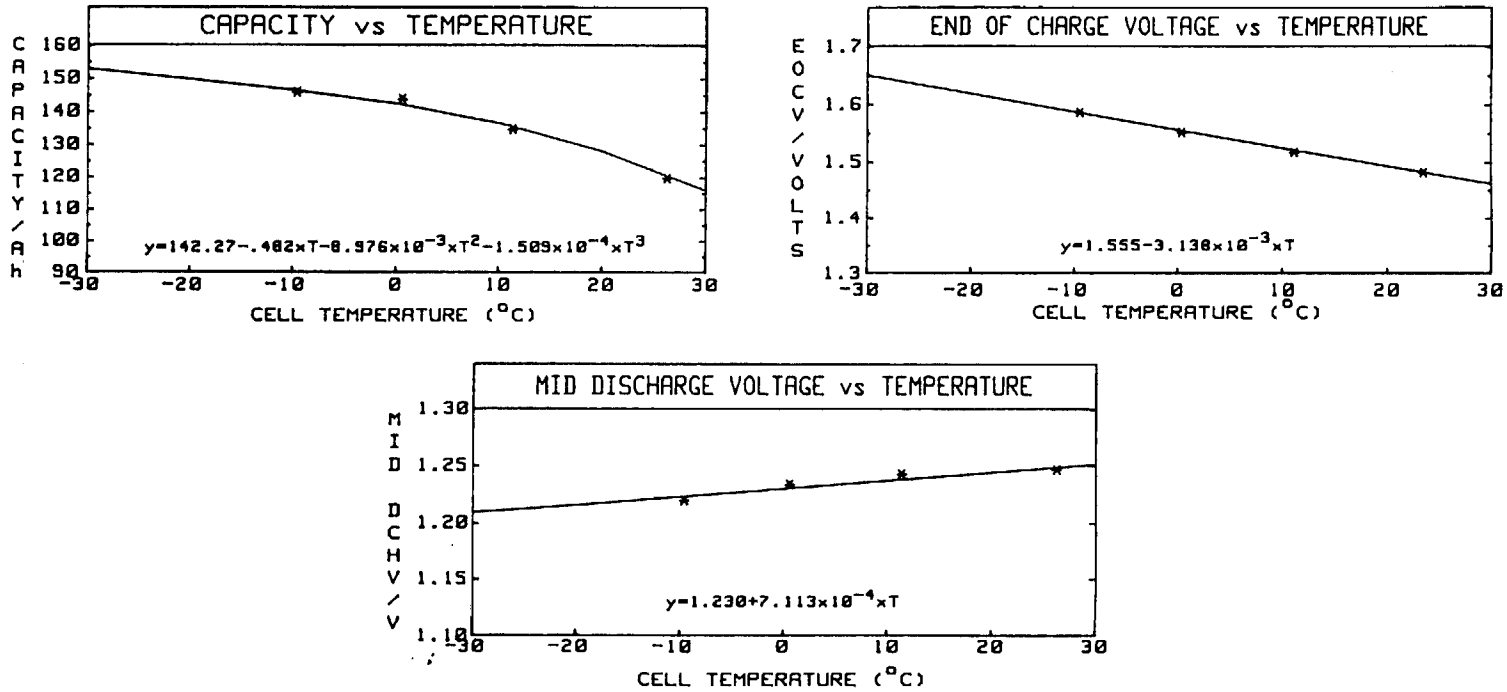

FIGURE 13

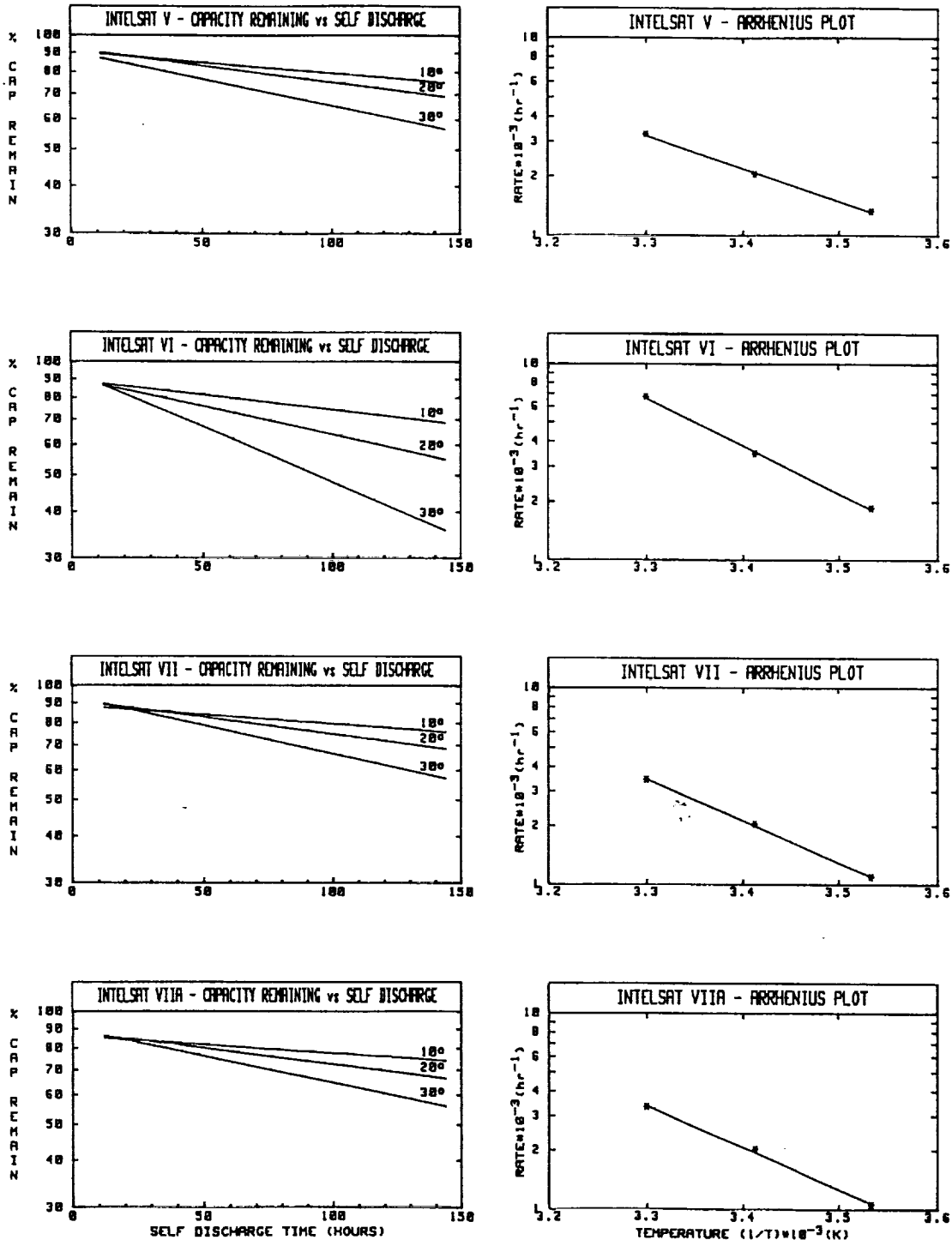
INTELSAT V - CAPACITY REMAINING vs SELF DISCHARGE
% CAP REMAIN
10°
20°
30°
INTELSAT V - ARRHENIUS PLOT
RATE*10^-3 (hr^-1)
INTELSAT VI - CAPACITY REMAINING vs SELF DISCHARGE
% CAP REMAIN
10°
20°
30°
INTELSAT VI - ARRHENIUS PLOT
RATE*10^-3 (hr^-1)
INTELSAT VII - CAPACITY REMAINING vs SELF DISCHARGE
% CAP REMAIN
10°
20°
30°
INTELSAT VII - ARRHENIUS PLOT
RATE*10^-3 (hr^-1)
INTELSAT VIIA - CAPACITY REMAINING vs SELF DISCHARGE
% CAP REMAIN
10°
20°
30°
SELF DISCHARGE TIME (HOURS)
INTELSAT VIIA - ARRHENIUS PLOT
RATE*10^-3 (hr^-1)
TEMPERATURE (1/T)*10^-3 (K)

FIGURE 14

TABLE 4. SELF-DISCHARGE ANALYSIS

	Intercept				Slope			Rate x 10^{-3}		
	10°C	20°C	30°C	Ave.	10°C	20°C	30°C	10°C	20°C	30°C
INTELSAT V	90.51	92.05	90.16	90.91	-.00132	-.00203	-.00324	1.32	2.03	3.24
INTELSAT VI	89.11	90.09	93.64	90.95	-.00184	-.00346	-.00671	1.84	3.46	6.71
INTELSAT VII	88.52	91.44	93.36	91.11	-.00109	-.00203	-.00343	1.09	2.03	3.43
INTELSAT VIIA	85.93	88.36	89.78	88.02	-.00105	-.00201	-.00331	1.05	2.01	3.31

THE SELF-DISCHARGE CHARACTERISTICS (Self-Discharge Time, t>10 hours)

	10°C	20°C	30°C
INTELSAT V	ln(PR)=ln(90.51)-.00132xt	ln(PR)=ln(92.05)-.00203xt	ln(PR)=ln(90.16)-.00324xt
INTELSAT VI	ln(PR)=ln(89.11)-.00184xt	ln(PR)=ln(90.09)-.00346xt	ln(PR)=ln(93.64)-.00671xt
INTELSAT VII	ln(PR)=ln(88.52)-.00109xt	ln(PR)=ln(91.44)-.00203xt	ln(PR)=ln(93.36)-.00343xt
INTELSAT VIIA	ln(PR)=ln(85.93)-.00105xt	ln(PR)=ln(88.36)-.00201xt	ln(PR)=ln(89.78)-.00331xt

THE EQUATIONS THAT BEST FIT THE ARRHENIUS PLOT

INTELSAT V	$\ln(\text{Rate}) = \ln(11.100 * 10^{2}) - 3864.3/\text{Temperature(K)}$
INTELSAT VI	$\ln(\text{Rate}) = \ln(57.462 * 10^{4}) - 5538.4/\text{Temperature(K)}$
INTELSAT VII	$\ln(\text{Rate}) = \ln(38.126 * 10^{3}) - 4912.9/\text{Temperature(K)}$
INTELSAT VIIA	$\ln(\text{Rate}) = \ln(36.958 * 10^{3}) - 4911.5/\text{Temperature(K)}$

PERCENT CAPACITY REMAINING FOR ANY OPEN-CIRCUIT TIME AND AT ANY TEMPERATURE

INTELSAT V	$PR = 90.91/e^{yt}$ (where $y = 11.100 \times 10^{2}/e^{3864.3/\text{Temp.(K)}}$, time>10 hrs)
INTELSAT VI	$PR = 90.95/e^{yt}$ (where $y = 57.462 \times 10^{4}/e^{5538.4/\text{Temp.(K)}}$, time>10 hrs)
INTELSAT VII	$PR = 91.11/e^{yt}$ (where $y = 38.126 \times 10^{3}/e^{4912.9/\text{Temp.(K)}}$, time>10 hrs)
INTELSAT VIIA	$PR = 88.02/e^{yt}$ (where $y = 36.958 \times 10^{3}/e^{4911.5/\text{Temp.(K)}}$, time>10 hrs)

ACTIVATION ENERGY (kcal/mole)

INTELSAT V	INTELSAT VI	INTELSAT VII	INTELSAT VIIA
7.729	11.077	9.826	9.823

SAFT
ADVANCED BATTERIES

SAFT NICKEL HYDROGEN CELL CYCLING STATUS

Yannick BORTHOMIEU and Didier DUQUESNE

SAFT ADVANCED BATTERIES
POITIERS FRANCE

1993 NASA AEROSPACE BATTERY WORKSHOP
US SPACE AND ROCKET CENTER
HUNTSVILLE AL
NOVEMBER 16–18, 1993

SAFT
ADVANCED BATTERIES

SAFT NICKEL HYDROGEN CELL CYCLING STATUS

TABLE OF CONTENTS

1– SAFT NiH2 CELL DEVELOPMENT

2– SAFT CELLS DESIGN

2–1 POSITIVE ELECTRODE
2–2 NEGATIVE ELECTRODE
2–3 STACK CONFIGURATION

3– CYCLING STATUS

3–1 LEO CYCLING
3–2 GEO CYCLING

4– DPA RESULTS

5– CONCLUSION

SAFT
ADVANCED BATTERIES

SAFT NICKEL HYDROGEN CELL CYCLING STATUS

1– SAFT NIH2 CELL DEVELOPMENT

1972–1984

Development of NiH2 at SAFT (mass advantage over NiCd) : HRN cell design.

1985–1988

Common CNES–ESA–SAFT–AEROSPATIALE development of VHS BL cell.
Study on reproducibility of electrochemical impregnation and mechanical design.

1989

Qualification of the VHS50BL
Common CNES–ESA–SAFT–AEROSPATIALE development of VHS CM cell : GEO applications.
Focus on pressure vessel fracture mechanical analysis.

1990

Beginning of the battery 27 VHS CM development

SAFT
ADVANCED BATTERIES

SAFT NICKEL HYDROGEN CELL CYCLING STATUS

1– SAFT NIH2 CELL DEVELOPMENT (Cont'd)

1992

VHS CM range 35–107 Ah : ESA qualified for GEO applications
VHS BL cells reach 33 simulated GEO eclipse seasons
Battery 23 VHS 60 CM selected for ARTEMIS program
Commmon ESA–CNES–SAFT development of VHS DM (LEO applications) for COLOMBUS/MTFF program

1993

Qualification of the VHS CM battery
Battery 27 VHS 50 CM selected for ARABSAT II program
HRN 42 cells reach 6.5 years simulated LEO operation

SAFT
ADVANCED BATTERIES

SAFT NICKEL HYDROGEN CELL CYCLING STATUS

2– CELLS DESIGN

The NiH2 SAFT system is an electrochemical (single or dual) stack (IPV). The stack is mounted in an hydroformed inconel 718 vessel operating at high pressure (up to 75 bars, 1090 psi with a safety factor of 2.5), equipped with "rabit ears" ceramic brazed electrical feedthroughs.

Two container diameters used :

- 81 mm (3.2') for HRN and VHS BL designs
- 89 mm (3.5') for VHS CM and VHS DM designs

ENERGY DENSITY (Wh/Kg):

- BETWEEN 50 TO 60 Wh/Kg FOR THE VHS CM CELL (GEO DESIGN)
- BETWEEN 45 TO 55 Wh/Kg FOR THE VHS DM CELL (LEO DESIGN)

SAFT
ADVANCED BATTERIES

SAFT NICKEL HYDROGEN CELL CYCLING STATUS

2– CELLS DESIGN (Cont'd)

2–1 POSITIVE ELECTRODE

– *Sintered material on steel perforated grid*
– *Active material deposited by electrochemical process*

	HRN	VHS BL/DM	VHS CM
Sinter manufacturing	Wet slurry	Wet slurry	Wet slurry
Sintered material thickness (mm)	0.82	0.82	0.87
Perforated grid thickness (mm)	0.10	0.10	0.08
Total sinter material thickness (mm)	0.92	0.92	0.95
Porosity (%)	86	86	86
Impregnation	ECI	ECI	ECI
Loading (g/cm3 of void)	1.65	1.7	1.7
Average electrode thickness (mm)	0.98	1.00	1.06
Capacity Ah/electrode	1.00	1.22/1.52	1.79

SAFT
ADVANCED BATTERIES

SAFT NICKEL HYDROGEN CELL CYCLING STATUS

2– CELLS DESIGN (Cont'd)

2–2 NEGATIVE ELECTRODE

- *Active charcoal with platinum on expanded nickel collector*
- *Goretex hydrophobic layer with polypropylen grid*

	HRN	VHS BL/DM	VHS CM
Active material thickness (mm)	0.35	0.35/0.30	0.22
Electrode thickness (mm)	0.39	0.39/0.35	0.27
Pt concentration (%)	5	5	5
Binding material	PTFE	PTFE	PTFE
Expanded grid (collector)	1.45 /12/10	1.45 /12/10	2.5/12/10
Hydrophobic layer material	Teflon SAFT	Teflon SAFT/GORE	Teflon GORE
Support	None	None/Polypropylen grid	Polypropylen grid
Polarization (mV) at 70 mA/cm2	100	100/70	60

SAFT
ADVANCED BATTERIES

SAFT NICKEL HYDROGEN CELL CYCLING STATUS

2– CELLS DESIGN (Cont'd)

2–3 STACK CONFIGURATION

- *Back to back configuration*
- *Positive expansion accomodation*
- *Central tie rod*
- *Optimised oxygen recirculating*

	HRN	VHS BL/DM	VHS CM
Number of electrodes	24 to 42	24 to 42/20 to 60	20 to 60
Stack assembly	Single/Single or dual	Single/Single or dual	Single or dual
Separator	Non Woven polyamid felt	Non Woven polyamid felt	Non Woven polyamid felt
Gaz screen	Woven nylon	Woven nylon	Woven nylon
Electrolyte	KOH 31%	KOH 31% or 26 %	KOH 31%
Stack expansion system	None	Belleville/Spring	Spring
Interelectrode spacing (mm)	0.26	0.26	0.26

SAFT
ADVANCED BATTERIES

SAFT NICKEL HYDROGEN CELL CYCLING STATUS

3- CYCLING STATUS

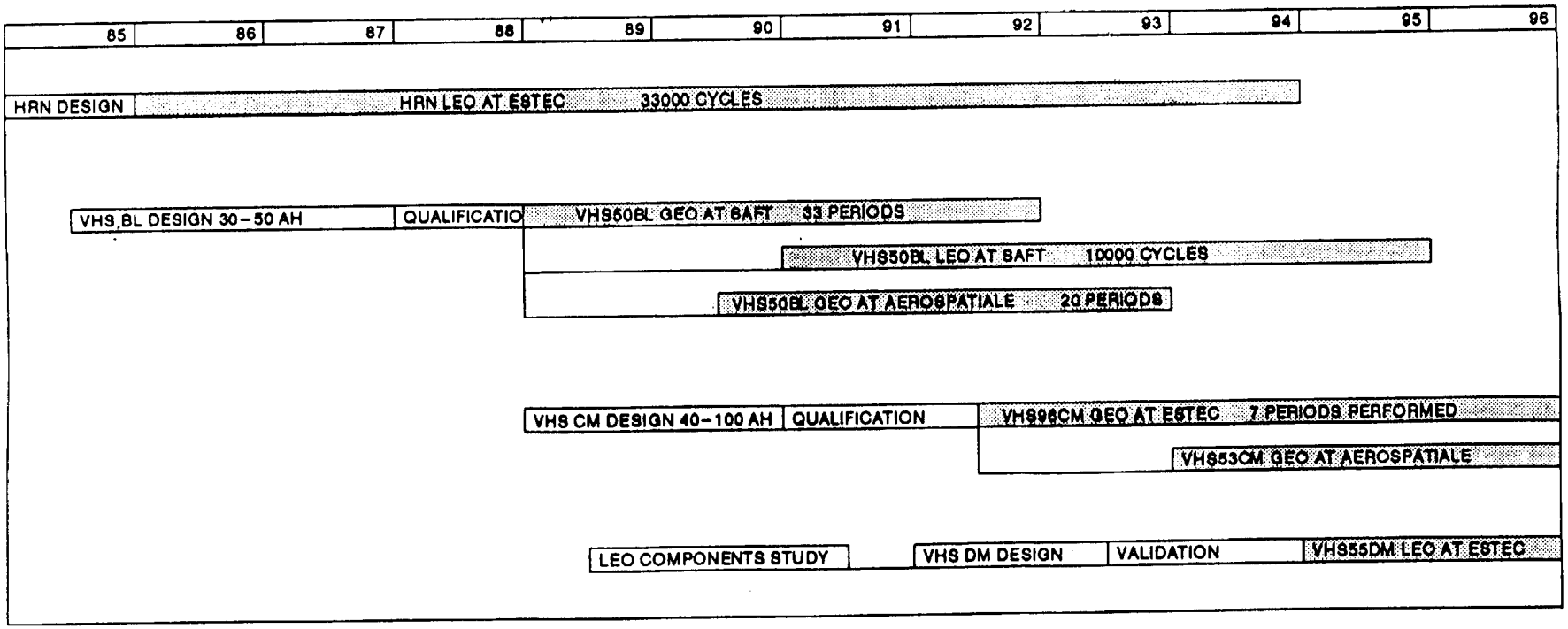

SAFT
ADVANCED BATTERIES

SAFT NICKEL HYDROGEN CELL CYCLING STATUS

3–1 LEO CYCLING

3 LOW EARTH ORBIT CYCLING RUNNING :

- HRN42 CYCLING BEGUN IN 1985 : 33,000 CYCLES PERFORMED (T=10°C, DOD=40 %)
  Test the suitability of HRN design (electrochemistry) for LEO missions
  Compare taper versus cut–off charge management
  Test in horizontal position

- VHS50BL CYCLING : 10,000 CYCLES PERFORMED (T=10°C, DOD= 40 %)
  Compare cycle life of different cells (DBAG and SAFT) under Colombus/MTFF conditions
  Compare 26 % versus 31 % KOH
  Investigate reduction of charge power at EOC
  Test in horizontal position

- VHS50BL CYCLING : 10,000 CYCLES PERFORMED (T=10°C, DOD= 40 %)
  Verify the cycle life VHS BL versus HRN
  Test in vertical position, in sleeves

SAFT
ADVANCED BATTERIES

SAFT NICKEL HYDROGEN CELL CYCLING STATUS

3–1 LEO CYCLING (Cont'd)

	ESA					CNES
CELL TYPE	HRN 42 S2	HRN 42 S2	VHS 50 BL	VHS 50 BL	VHS 50 BL	VHS 50 BL
SAFT TEST REFERENCE	504	503	511	512	513	509
BATTERY REFERENCE	35	33	1	2	5	
DOD (%)	40*	40*	31	40	40	40
TEMPERATURE (°C)	10	10	10	10	10	10
DISCHARGE (A)	26.88	26.88	cst power	34.29	34.29	34.29
CHARGE (A)	17.35	21	cst power	22.69	22.69	30
VOLTAGE LIMIT (V)	1.67	1.54	1.54	1.585	1.59	1.56
RECHARGE RATIO	1.04	1.04	1.04	1.04	1.04	1.04
CYCLES	33954	35264	11800	11800	11800	10000
END OF DISCHARGE VOLTAGE (V)	1.04	1.19	1.167	1.2	1.16	1.05
* BASED ON 42 Ah	1 CELL REMOVED FOR DPA After 15694 Cycles	1 FAILED CELL After 31629 Cycles		26% KOH 1 CELL REMOVED at beginning of life after 5500 cycles		2 FAILED CELLS at beginning of life

SAFT
ADVANCED BATTERIES

SAFT NICKEL HYDROGEN CELL CYCLING STATUS

3–1 LEO CYCLING (Cont'd)

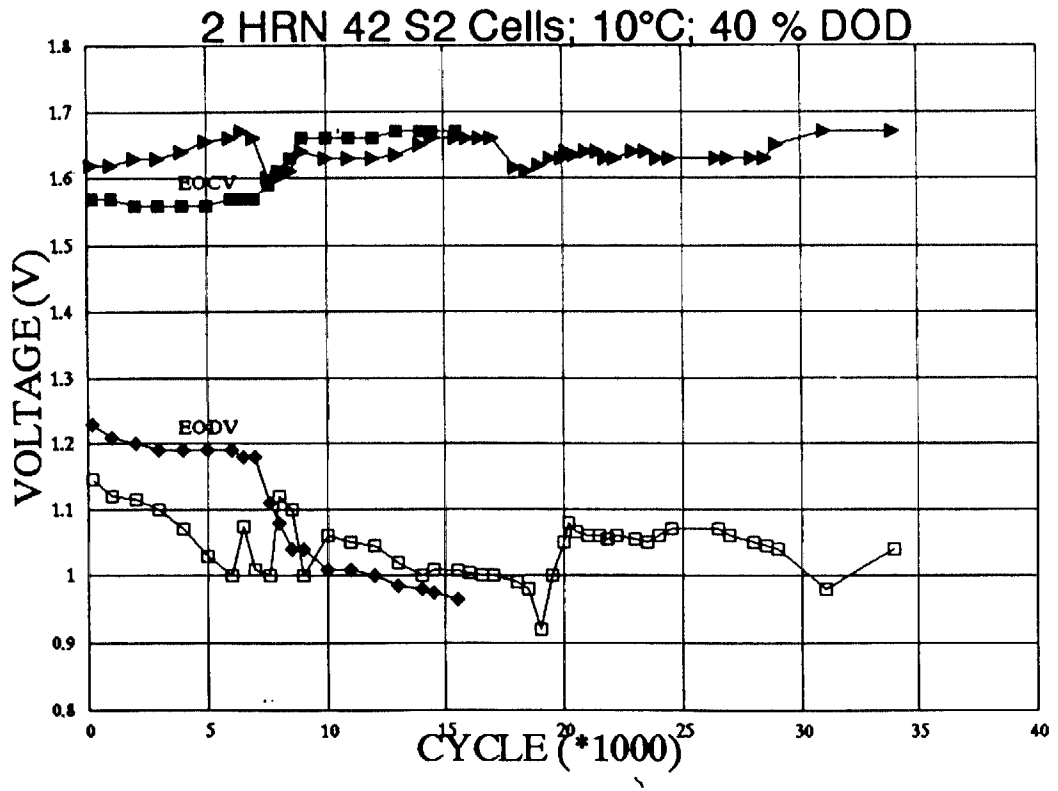

SAFT TEST N°504

DISCHARGE:
37.5 mn
at 26.88 Amps

CHARGE:
60 mn at 17.35A
Non tapering

No reconditioning

As per june 93

1 cell removed
for DPA
(CYCLE 15694)
Cycling still
running

SAFT
ADVANCED BATTERIES

SAFT NICKEL HYDROGEN CELL CYCLING STATUS

3–1 LEO CYCLING (Cont'd)

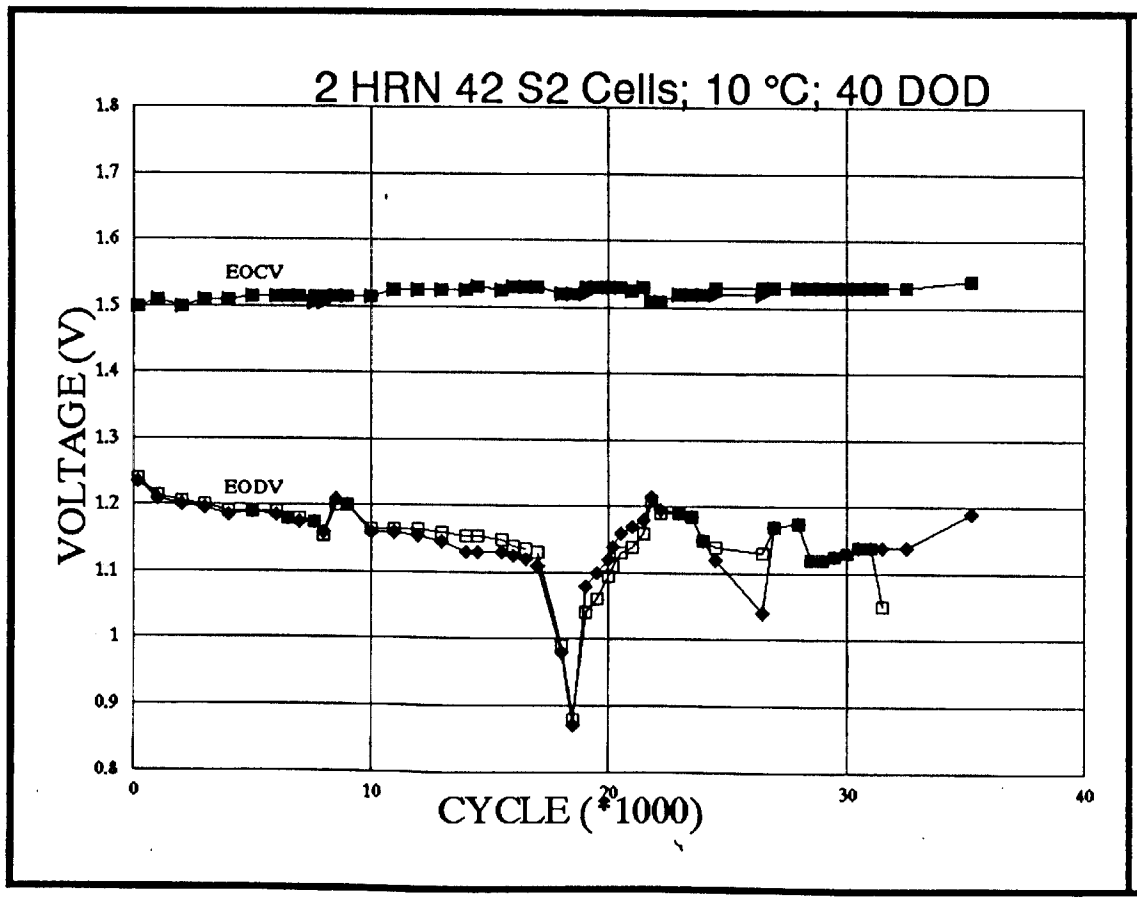

SAFT TEST N°503

DISCHARGE:
37.5 mn
at 26.88 Amps

CHARGE:
21 A max
Voltage tapering

No reconditioning

As per june 93

1 failed cell removed (cycle 31629)
Cycling still running

SAFT
ADVANCED BATTERIES

SAFT NICKEL HYDROGEN CELL CYCLING STATUS

3–1 LEO CYCLING (cont'd)

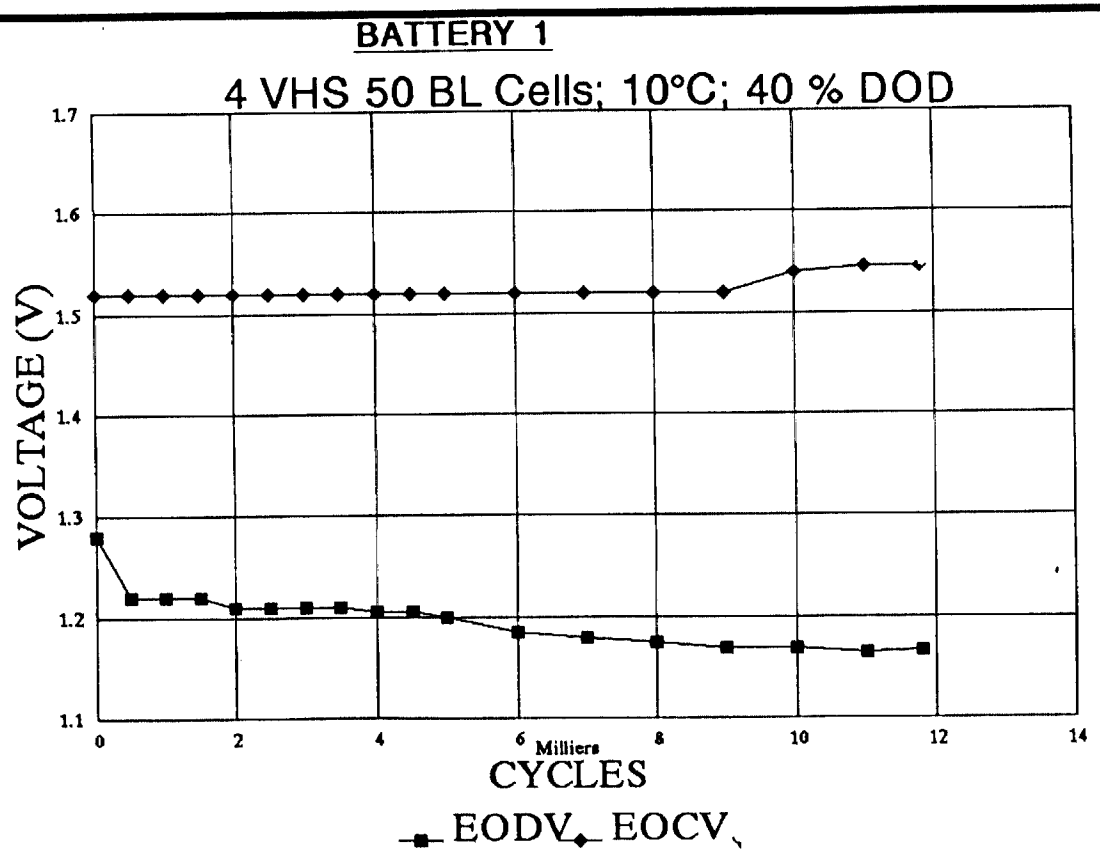

SAFT TEST N°511

COLUMBUS Program

Discharge:
58 mn at 130 W

Charge:
54 mn at 130 W
26 mn at 70 W

As per June 1993

No Cell removed
Cycling still running

SAFT
ADVANCED BATTERIES

SAFT NICKEL HYDROGEN CELL CYCLING STATUS

3–1 LEO CYCLING (cont'd)

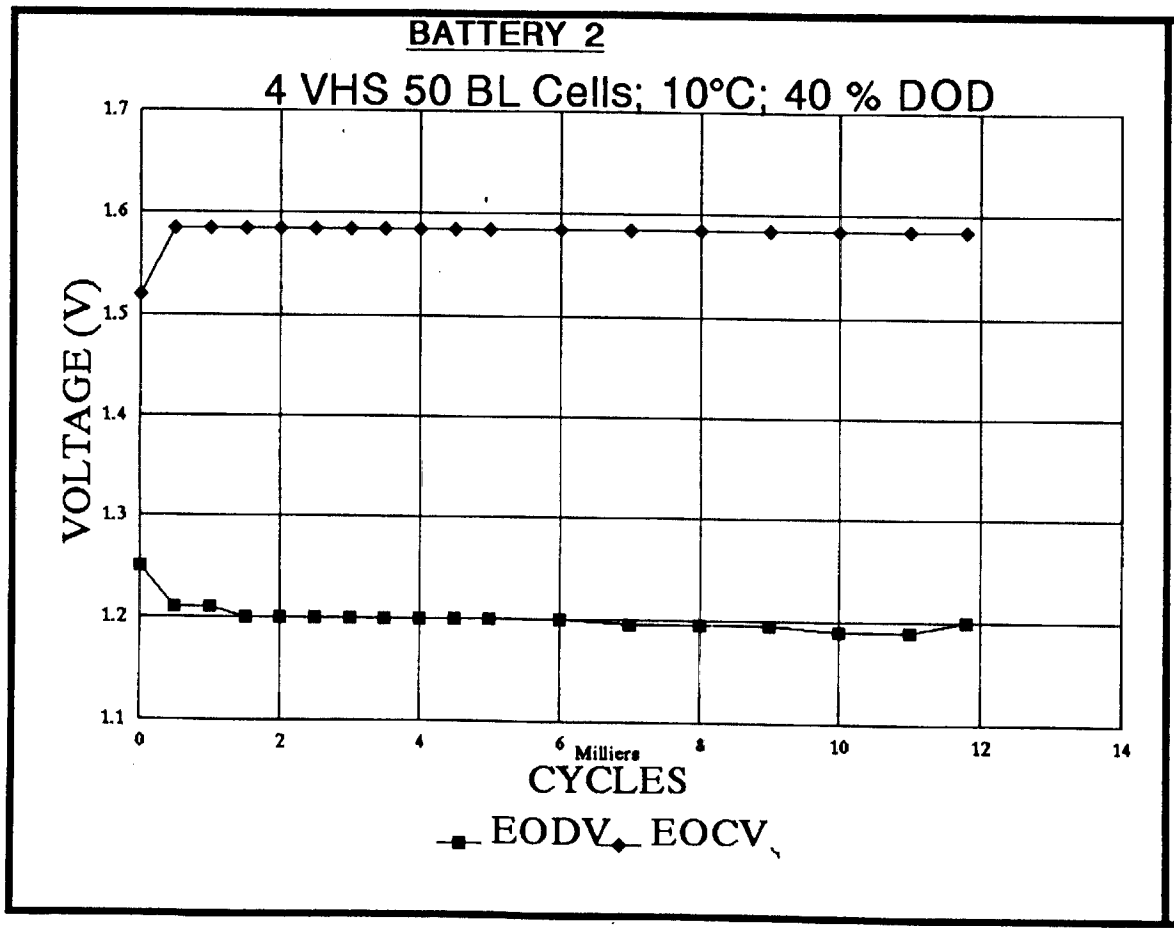

SAFT TEST N°512

COLUMBUS Program

Discharge: 34.29 A

Charge: 22.69 A

As per June 1993

1 Cell removed at beginning of life

Cycling still running

SAFT

SAFT NICKEL HYDROGEN CELL CYCLING STATUS

3-1 LEO CYCLING (cont'd)

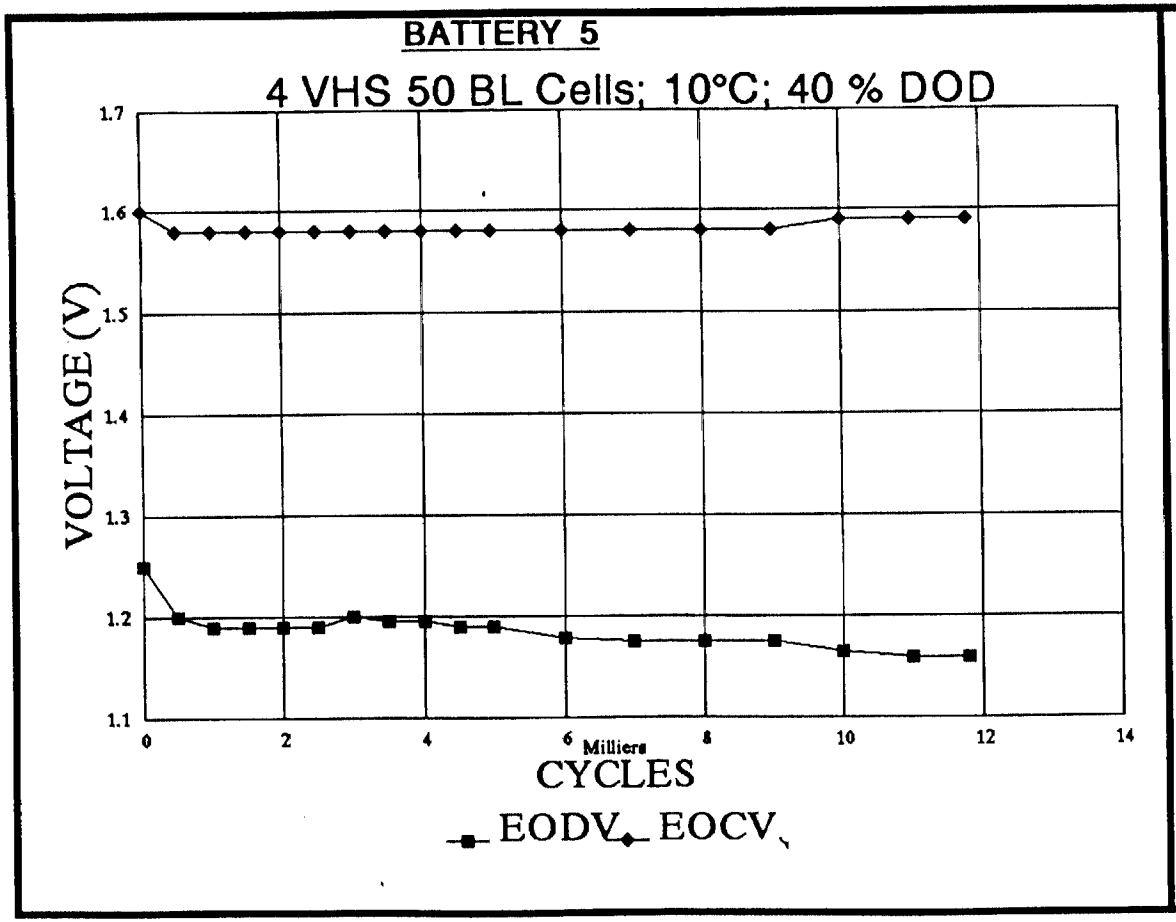

SAFT TEST N°513

COLUMBUS Program

Discharge: 34.29 A

Charge: 22.69 A

As per June 1993

No Cell removed

Cycling still running

SAFT

SAFT NICKEL HYDROGEN CELL CYCLING STATUS

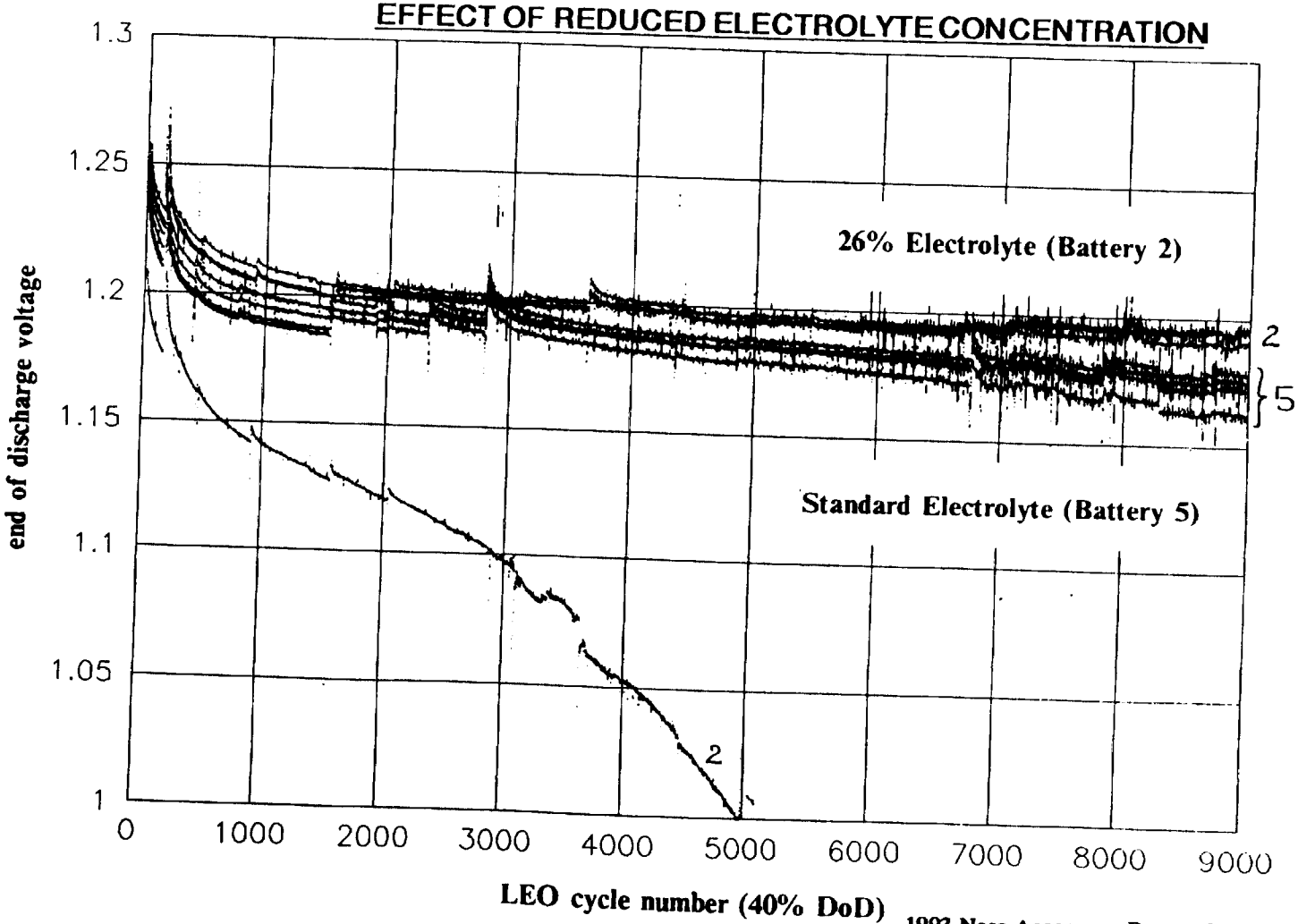

SAFT

SAFT NICKEL HYDROGEN CELL CYCLING STATUS

3–1 LEO CYCLING (Cont'd)

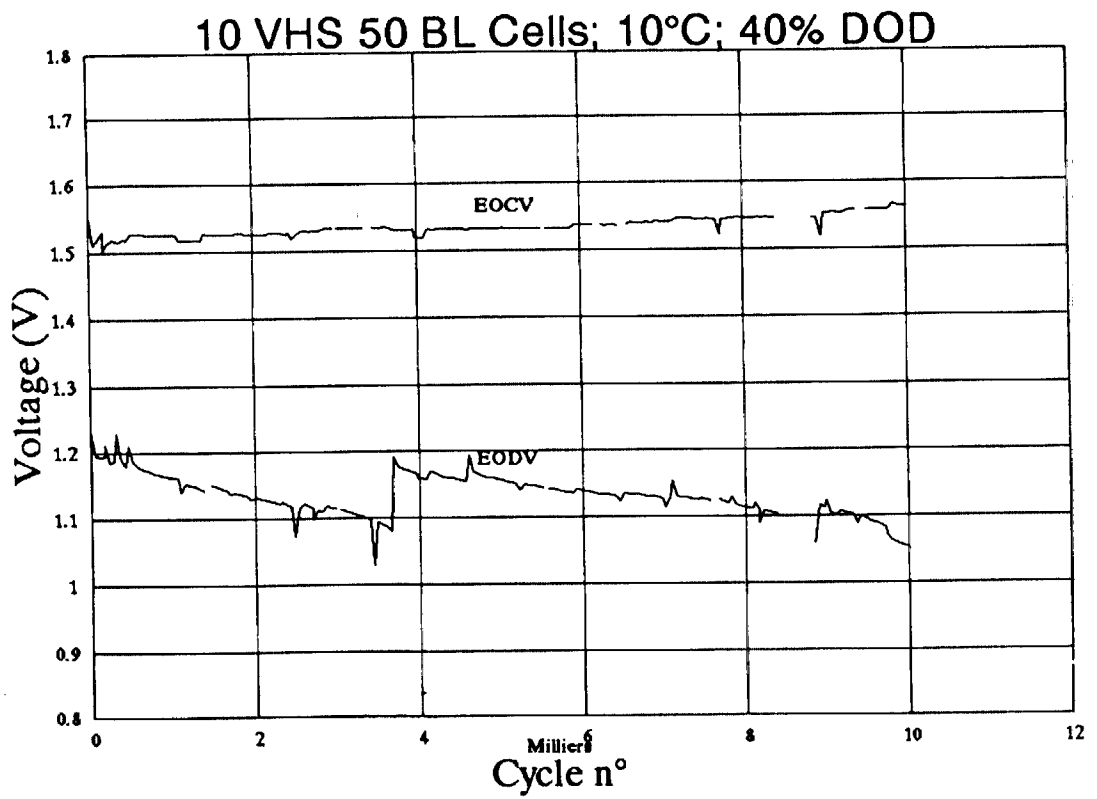

SAFT TEST N°509

DISCHARGE:
35 mn at 34.3 A

Charge:
55 mn at 30 A
Voltage Tapering

As per April 1993

2 cells removed
(cycles 448, 3691)

Cycling still running

Test performed at SAFT

SAFT
ADVANCED BATTERIES

SAFT NICKEL HYDROGEN CELL CYCLING STATUS

3–2 GEO CYCLING

3 GEOSTATIONNARY EARTH ORBIT CYCLING :

– VHS50BL CYCLING : 33 PERIODS DEMONSTRATED
Test the suitability of VHS BL for GEO applications
Test completed
Accelerated shadow period

– VHS50BL CYCLING : 20 PERIODS PERFORMED
Demonstrate the GEO life cycle with a constant DOD profile (70 %)
Reconditionning after each season

– VHS96CM CYCLING : 7 PERIODS PERFORMED
Compare GEO cycle life of VHS BL and VHS CM
Test in semi accelerated conditions at 80 %
Reconditionning before each season

SAFT
ADVANCED BATTERIES

SAFT NICKEL HYDROGEN CELL CYCLING STATUS

3–2 GEO CYCLING (Cont'd)

	ESA	CNES	AEROSPATIALE SPACEBUS
CELL TYPE	VHS 96 CM	VHS 50 BL	VHS 50 BL
SAFT TEST REFERENCE	514	507	510
DOD MAX (%)	80	70	70
TEMPERATURE (°C)	10	10	10
DISCHARGE (A)	64	29.2	29
CHARGE (A)	9.6	3.7	3.7
VOLTAGE LIMIT (V)	1.53	1.5	1.49
RECHARGE RATIO	1.18	1.15	1.15
SHADOW NUMBER	7	33	20
END OF DISCHARGE VOLTAGE (V)	1.09	1.16	1.09
	RECONDITIONING BEFORE EACH SHADOW PERIOD	1 FAILED CELL AT PERIOD 28 TEST COMPLETED	RECONDITIONING AFTER EACH SHADOW PERIOD

SAFT
ADVANCED BATTERIES

SAFT NICKEL HYDROGEN CELL CYCLING STATUS

3-2 GEO CYCLING (Cont'd)

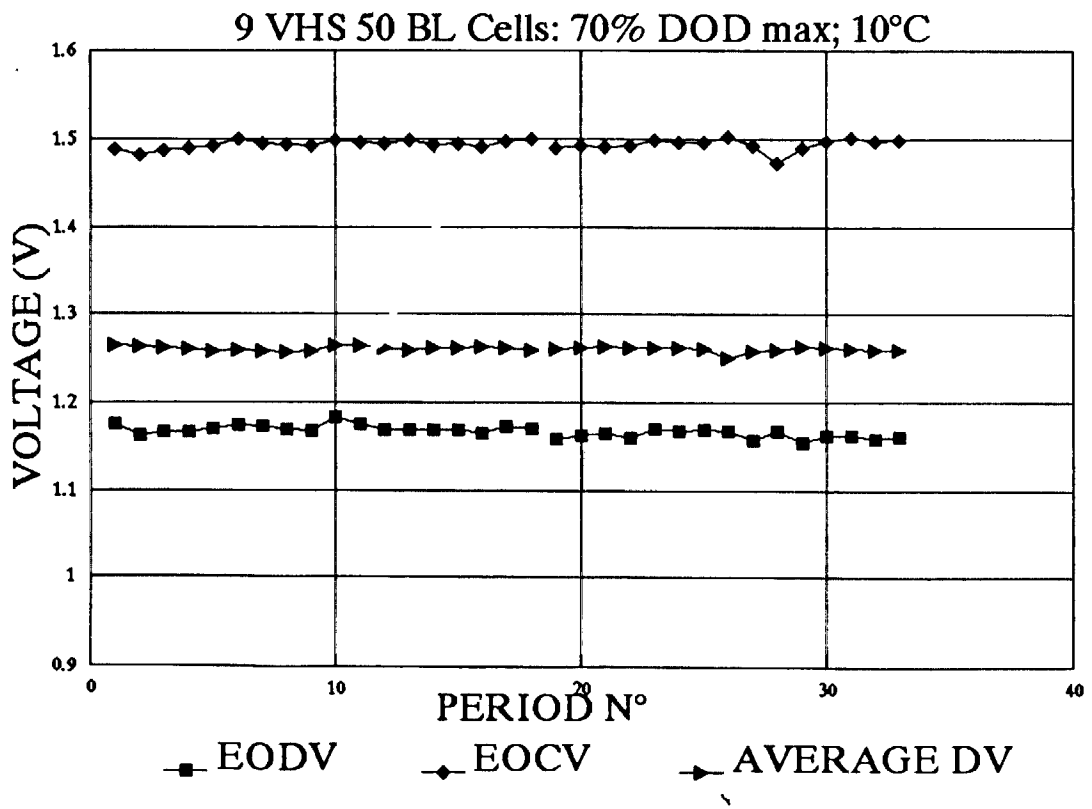

SAFT test N°507

Real DOD profile

Discharge: 29.2 A
Charge: 3.7 A

Accelerated shadow period

1 Cell removed after shadow period 28

Test completed

End of life characterization:
Int. resistance: +6%
Capacity: −10%

SAFT
ADVANCED BATTERIES

SAFT NICKEL HYDROGEN CELL CYCLING STATUS

3-2 GEO CYCLING (Cont'd)

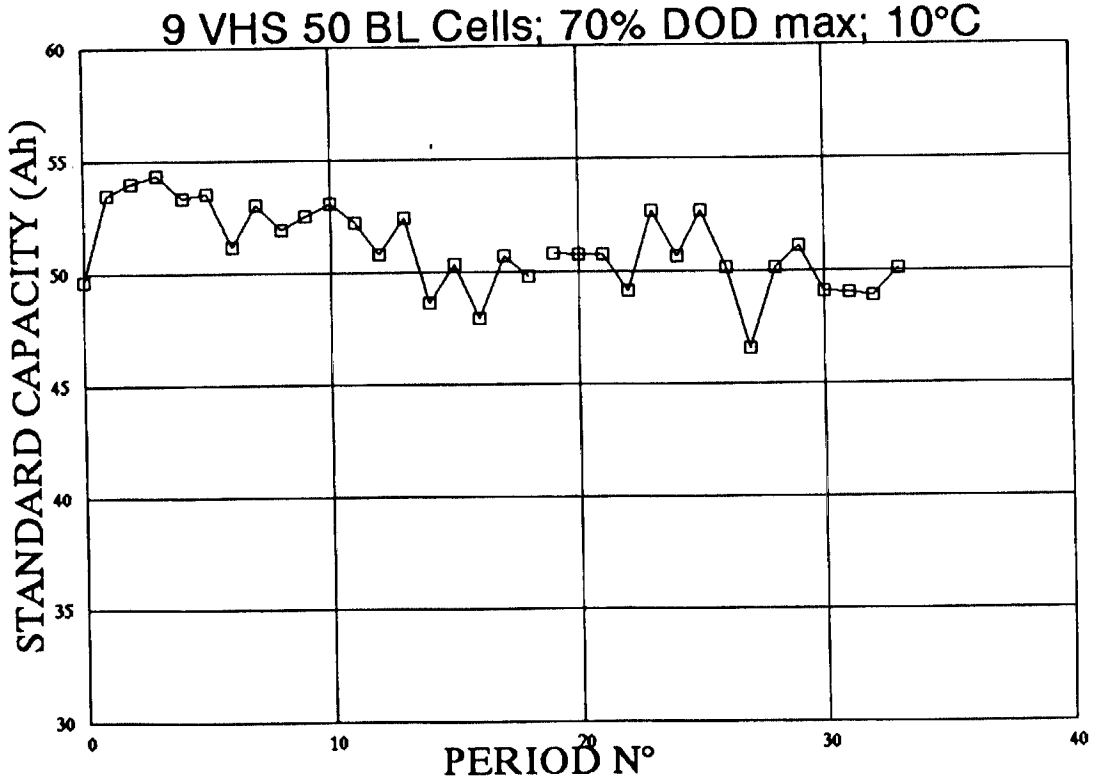

SAFT test N°507

Capacity check between each shadow period

Charge:
7 H 42 mn at 10 A

Discharge:
25 A first Cell to 1 V
10 A first Cell to 0.5V

SAFT
ADVANCED BATTERIES

SAFT NICKEL HYDROGEN CELL CYCLING STATUS

3–2 GEO CYCLING (Cont'd)

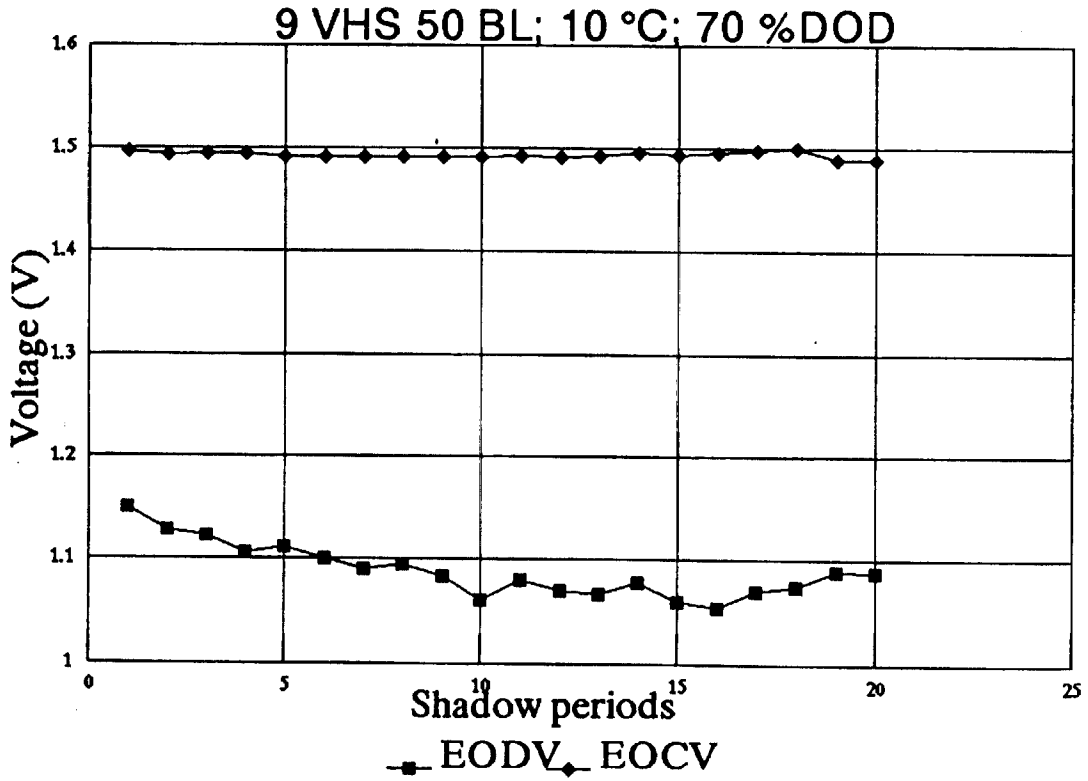

SAFT test N°510
SPACEBUS program
AEROSPATIALE

Shadow periods
1 to 18 at constant
DOD profile and
19 to 20 at real
DOD profile

Discharge:
1 H 12 at 29 A

Charge:
10 H 48 at 3.7 A

No cell removed
Cycling stopped

SAFT

SAFT NICKEL HYDROGEN CELL CYCLING STATUS

3–2 GEO CYCLING (Cont'd)

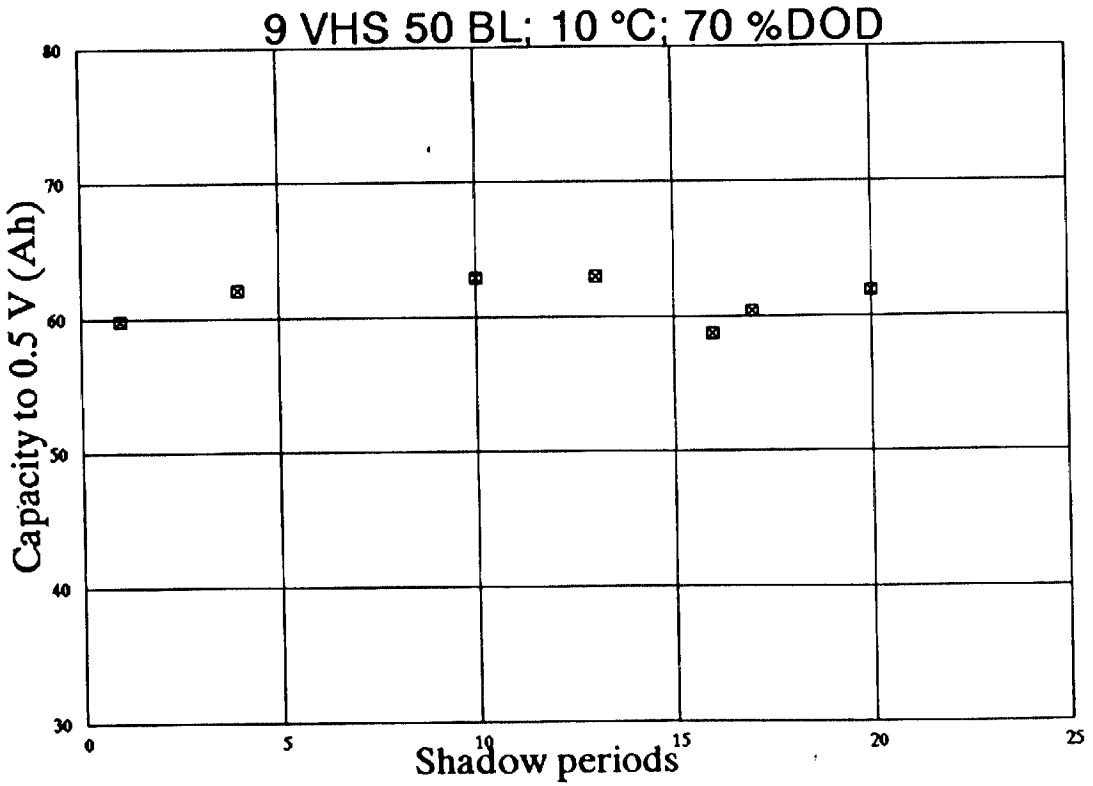

SAFT test N°510

SPACEBUS program
AEROSPATIALE
Capacity check

Charge:
7 H 42 mn at 10 A

Discharge:
25 A first cell
to 0.5V

SAFT

SAFT NICKEL HYDROGEN CELL CYCLING STATUS

4– DPA RESULTS

LEO CYCLING

Cell Type	CYCLING	Saft test reference	Number of Cycles completed	Reason of Removal	DPA Observations
HRN42 n°4	ESA	504	15694	Study of the ageing of electrochemical components	. 9.5 % positive thickness increase . KOH distribution evolution due to the positive expansion
HRN42 n°5	ESA	503	31629	Short circuit	. Short due to too small insulator part compared to the positive swelling : **Old design limitation: no positive expansion accommodation system** . 15.2 % positive thickness increasing . Small loss of positive capacity (9%) . No critical ageing of the separator : only 10 % hydrolysis of polyamid

SAFT
ADVANCED BATTERIES

SAFT NICKEL HYDROGEN CELL CYCLING STATUS

4– DPA RESULTS (Cont'd)

LEO CYCLING

Cell Type	CYCLING	Saft test reference	Number of Cycles completed	Reason of Removal	DPA Observations
VHS50BL n°7	ESA	512	5500	EOD Voltage below 1 V Low EODV since the beginning of cycling	Ageing of electrochemical components: – high internal resistance – high positive swelling – totally modified KOH repartition **due to acceptance test deviation :** **H2 leakage on test equipment**
VHS50BL n°1	CNES at SAFT	509	448	EOD Voltage below 1 V Low EODV since the beginning of cycling as cell n°7	– high internal resistance – FET positive capacity stable – flooding of negative plates and gaz screen **due to acceptance test deviation**

FAILURE LIMITED TO REWORKED CELLS

564,000 HOURS OF LOW EARTH ORBIT CYCLING SIMULATED

SAFT
ADVANCED BATTERIES

SAFT NICKEL HYDROGEN CELL CYCLING STATUS

4– DPA RESULTS (Cont'd)

GEO CYCLING

Cell Type	CYCLING	Saft test reference	Shadow Number	Reason of Removal	DPA Observations
VHS50BL n°11	SAFT	507	28	Short circuit	. Degradation of the rilsan sleeve around the tie rod inducing the short : **Problem of test battery insulation** (at season 27) leading to oxygen evolution by electrolyte electrolysis along the tie rod . Very small ageing of electrochemical components : – 2.1 % positive thickness increasing – FET positive capacity stable – no modification of KOH repartition

NO FAILURE BY POPPING , ELECTRODE SHORTS OR HYDROGEN LEAKAGE

15 YEARS GEO CYCLING : – 6% INCREASING OF INTERNAL RESISTANCE
– 10 % MAXIMUM LOSS OF THE CELL CAPACITY

4.3 MILLION HOURS OF GEOSTATIONNARY ORBIT CYCLING SIMULATED

SAFT
ADVANCED BATTERIES

SAFT NICKEL HYDROGEN CELL CYCLING STATUS

4– CONCLUSION

GEOSTATIONNARY EARTH ORBIT SIMULATED CYCLING PERFORMED ON VHS50BL:

– REACHES 33 SHADOW PERIODS WITH SMALL PERFORMANCES EVOLUTIONS

– VALIDATES THE SUITABILITY OF THE VHS CM FOR GEO MISSIONS

LOW EARTH ORBIT SIMULATED CYCLING:

– REACHES 35,000 CYCLES FOR HRN42

– DEMONSTRATES 10,000 CYCLES ON VHS50BL

– GIVES CONFIDENCE ON THE CYCLE LIFE OF THE DM DESIGN

THE CYCLING AND DPA RESULTS DEMONSTRATE THAT SAFT NiH2 IS CHARACTERISED BY :

– HIGH RELIABILITY

– VERY STABLE PERFORMANCES

Calculation of the Thermoneutral Potential of NiCd and NiH_2 Cells

Albert H. Zimmerman
The Aerospace Corporation
El Segundo, California 90245

The thermoneutral potential of a nickel cadmium or nickel hydrogen cell is the potential at which the cell charge or discharge process puts out zero heat, and thus is the potential corresponding to the enthalpy change of the charge/discharge reaction, ΔH. A relatively straightforward method for obtaining the thermoneutral potential E_{tn}, is based on the measured potential and temperature derivative of the cell reactions, which are related to the free energy change ΔG, and entropy change ΔS, respectively.

$$\Delta H=\Delta G+T\Delta S \tag{1}$$

$$E_{tn}=E-T\left(\frac{\partial E}{\partial T}\right) \tag{2}$$

Where E is the cell potential, and T is the Kelvin temperature.

However, since Eq. (2) is derived for a constant pressure system, it does not fully describe the thermoneutral voltage of NiCd and NiH_2 cells, which are constant volume systems in which the pressure can change significantly. Particularly in the nickel hydrogen cell, the pressure of hydrogen can often vary over an order of magnitude or more during the course of a charge or discharge. In a nickel cadmium cell, although significant changes in oxygen pressure can occur during charge or discharge, since oxygen does not enter into the charge/discharge reaction, these pressure changes are related to the heat generated from oxygen evolution and recombination. However, the entropy changes due to changes in hydrogen pressure relative to the 1 atm standard state must be included in Eq. (1) to apply this method to the nickel hydrogen cell. This gives Eq. (3)., assuming that the variation in reversible potential with temperature is measured at constant pressure.

In Eq. (3) F is the Faraday constant, and P is the hydrogen pressure in the cell in atm.

$$E_{th}=E-T\left(\frac{\partial E}{\partial T}\right)+\frac{RT\ln P}{2F} \tag{3}$$

Nickel Cadmium Cell

The half reactions, and cell reaction in the nickel cadmium cell are given in Eq. (4)-(6).

$$Ni(OH)_2+2OH^- \rightarrow NiOOH+H_2O+e^- \tag{4}$$

$$Cd(OH)_2+2e^- \rightarrow Cd+2OH^- \tag{5}$$

$$2Ni(OH)_2+Cd(OH)_2 \rightarrow 2NiOOH+Cd+2H_2O \tag{6}$$

The standard potential for reaction (6) is 1.299 volts (Ref. 1). The derivative of voltage with respect to temperature at constant pressure is -0.001514, -0.001014, and -0.0005 volts/K for reactions (4)-(6) respectively (Ref. 2). The value for reaction (4) was derived from the values published in Ref. (2) for the NiCd cell and the cadmium electrode, which are more reliably known that that for the nickel electrode. Thus the value used here for the nickel electrode also includes the effect of approximately a 5% cobalt additive level present in the active material of the NiCd cells.

The thermoneutral potential may be derived from Eq. (2), employing Nernstian expressions for the dependence of potential on reagent concentrations, giving Eq. (7).

$$E_{tn}=\Delta E^\circ-T\left(\frac{\partial E^\circ}{\partial T}\right)+\frac{RT^2}{F}\left(\frac{\partial \ln[H_2O][NiOOH]}{\partial T}\right) \tag{7}$$

The last term in Eq. (7) is a second order term that is quite small (approximately 10 μV at 25 deg C). In evaluating the thermoneutral potential of the NiCd cell from Eq. (7), it is found that, to first order, the temperature dependence of the reversible potential cancels out the temperature dependence introduced by the entropic term. Using the reversible potentials and their temperature derivatives for reactions (4)-(6), the thermoneutral potential is found to be 1.448 volts. This voltage is independent of temperature to first

order for the NiCd cell.

Measurements of the thermoneutral potential based on calorimetry have indicated a value of 1.45 volts (Ref. 3). More accurate measurements at different temperatures have indicated 1.454±0.013 volts at 5 deg C, and 1.453±0.004 volts at 20 deg C using data from Ref. 4. All these measurements are in excellent agreement with the value calculated above based on reversible potentials and their temperature coefficients. The temperature derivative of the potential for the nickel electrode reaction may be refined from these data to give -0.001534 volts/K, a value that will be used in the next section for nickel hydrogen cell calculations. These measurements are summarized in Table 1, and are based on measured heat production during discharge over a range of depths-of-discharge, currents, and temperatures. Thermal output was determined by integrating over the charge and discharge cycles, with heat being determined by the difference in temperature between the top and the baseplate of a 50 Ah NiCd battery. The temperature difference was calibrated by holding the battery in steady-state overcharge, where a precisely known thermal output is obtained.

Table 1. Thermal Data for Obtaining Thermoneutral Potentials for NiCd Cells

Test Number	Temp. deg C	DOD	Voltage (volts)	Current (amps)	Power (watts)	Heat (watts)	E_{th} (volts)
1	20	0.167	27.77	14.00	388.85	59.5	1.456
1	20	0.343	27.59	13.77	379.86	59.5	1.450
1	20	0.481	27.53	13.62	374.88	60.0	1.451
2	5	0.302	27.42	20.78	569.76	92.5	1.449
3	20	0.282	27.09	30.76	833.36	154.0	1.459
4	5	0.130	28.36	13.72	389.03	57.0	1.478
4	5	0.270	27.61	13.75	379.72	56.0	1.440
4	5	0.424	27.59	13.59	374.91	58.0	1.448
5	20	0.331	27.26	21.08	574.71	97.5	1.449
6	20	0.357	26.96	30.09	811.15	148.0	1.449
7	20	0.351	27.36	20.83	569.98	99.0	1.460

Table 1A. Average Thermoneutral Potentials for NiCd Cells

	Average E_{th} (volts)	Standard Deviation
5 deg C	1.454	0.013
20 deg C	1.453	0.004
All tests	1.454	0.010

Best Value is 1.454±0.010 volts

Nickel Hydrogen Cell

In the nickel hydrogen cell the reaction at the nickel electrode is nominally the same as that in the NiCd cell, and is given by Eq. (4). The negative electrode reaction and the overall cell reaction are given by Eqs. (8) and (9), respectively.

$$2H_2O+2e^- \rightarrow H_2+2OH^- \tag{8}$$

$$2Ni(OH)_2 \rightarrow 2NiOOH+H_2 \tag{9}$$

As can be seen from reaction (9), there is no net change in water or hydroxide as a result of this reaction. The standard reversible potential of reaction (8) is -0.828 volts, and with a temperature coefficient at constant pressure of -0.000834 V/deg. The standard reversible potential of the cell reaction (9) is 1.318 volts. Based on the value for the temperature coefficient of the reversible potential of the nickel electrode calculated for the nickel electrode, the temperature coefficient of the standard potential of the nickel hydrogen cell, i.e. reaction (9), is -0.000700 volts/deg.

Based on Eq. (3) and the Nernst Equation, the thermoneutral potential of the nickel hydrogen cell may be expressed as

$$E_{tn}=\Delta E^\circ - T\left(\frac{\partial E^\circ}{\partial T}\right) - \frac{RT\ln P}{2F} + \frac{RT}{2F} + \frac{RT^2}{F}\left(\frac{\partial \ln[NiOOH]}{\partial T}\right) \tag{10}$$

The first term in Eq. (10) results from the reversible cell potential and the remaining terms from the change in entropy from the electrochemical process, the entropic decrease from hydrogen compression in the cell volume, and the Nernst Eq. These terms are arranged in decreasing order of significance. At 25 deg C the first term is 1.318 V, the second term is 0.2086 volts, the third term is -0.0295 volts at 10 atm of hydrogen, the fourth term is 0.0128 volts, and the last term is negligable. Thus at 25 deg C the thermoneutral potential of a nickel hydrogen cell is 1.5394-0.01284lnP volts. At 0 deg C it is 1.5384-0.01284lnP volts. These values are approximately 30 mv lower than those in Ref. 5. This difference may in part be due to the use of potentials and temperature derivatives here based on nickel electrodes containing approximately 5% cobalt additive. This additive is known to decrease the reversible potential of the nickel electrode by about 30-40 mV.

Conclusions

The thermoneutral voltage of the nickel hydrogen cell has been semi-empirically evaluated based on the best available thermal data for the nickel cadmium cell, and the known thermodynamics of the cadmium and hydrogen electrodes. The thermoneutral potential thus obtained is dependent on both hydrogen pressure and cell temperature. At room temperature and average cell pressures of about 300 psia, the thermoneutral potential thus obtained is 1.501 volts, which is in reasonable agreement with the value of 1.51 volts commonly employed. In utilizing this voltage for thermal calculations it is necessary to also include heat from self-discharge and oxygen recombination as additional, and independent terms.

References

1. S. U. Falk and A. J. Salkind, in **Alkaline Storage Batteries**, John Wiley and Sons, Inc., New York, 1969, p. 533.

2. A. J. DeBethune and N. A. Swendeman Loud, **Table of Electrode Potentials and Temperature Coefficients**, in *Encyclopedia of Electrochemistry*, C. A. Hampel, editor, Reinhold Publ. Corp., New York, 1964, pp. 414-424.

3. W. R. Scott and D. W. Rusta, in **Sealed-Cell Nickel Cadmium Battery Applications Manual**, NASA Ref. Pub. 1052, NASA NAS5-23514, 1979, p. 104.

4. **NASA 50 A.H. Nickel Cadmium Spacecraft Battery Qualification Report**, TR 70A-127, McDonnell Douglas Astronautics Company, NAS 523844, 1982.

5. D. D. MacDonald and M. L. Challingsworth, **J. Electrochem. Soc., 140** (1993) 606.

Performance Model of a Recirculating Stack Nickel Hydrogen Cell

Albert H. Zimmerman
The Aerospace Corporation
El Segundo, California 90245

A theoretical model of the nickel hydrogen battery cell (Ref. 1) has been utilized to describe the chemical and physical changes during charge and overcharge in a recirculating stack nickel hydrogen cell. In particular, the movement of gas and electrolyte have been examined as a function of the amount of electrolyte put into the cell stack during cell activation, and as a function of flooding in regions of the gas screen in this cell design. Additionally, a two-dimensional variation on this model has been utilized to describe the effects of non-uniform loading in the nickel electrode on the movement of gas and electrolyte within the recirculating stack nickel hydrogen cell. The type of nonuniform loading that has been examined here is that associated with higher than average loading near the surface of the sintered nickel electrode, a condition present to some degree in many nickel electrodes made by electrochemical impregnation methods (Ref. 2). The effects of high surface loading were examined primarily under conditions of overcharge, since the movement of gas and electrolyte in the overcharging condition was typically where the greatest effects of non-uniform loading were found.

The results indicate that significant changes in the capillary forces between cell components occur as the percentage of free volume in the stack filled by electrolyte becomes very high. These changes create large gradients in gas-filled space and oxygen concentrations near the boundary between the separator and the hydrogen electrode when the electrolyte fill is much greater than about 95% of the stack free volume. At lower electrolyte fill levels, these gaseous and electrolyte gradients become less extreme, and shift through the separator towards the nickel electrode. Similarly, flooding of areas in the gas screen cause higher concentrations of oxygen gas to approach the platinum/hydrogen electrode that is opposite the back side of the nickel electrode. These results illustrate the need for appropriate pore size distributions, and the maintenance of both convective electrolyte and gas flow paths through the stack, if the recirculating stack nickel hydrogen cell design is to work properly.

Two models were utilized to examine the role of surface loading. The first of these was like that used in Ref. 3, in which a one-dimensional model allowed a relatively high resolution mapping of cell behavior through the cell stack. The second model was a two-dimensional model that was capable of examining the properties of the cell stack not only across the stack components, but also through the height or width of the individual nickel electrode, separator, or gas screen regions. This second model was applied to cells containing nickel electrodes having surface loading, as well as to cells where the surface loaded nickel electrodes also had surface cracks or localized regions of lower surface loading that could allow a more facile flow of gas or electrolyte. These latter cases allowed the complex interplay of electrode structure, oxygen recombination, and recirculation patterns to be examined in detail, and indicate situations where performance problems specific to a recirculating stack cell could be encountered. The results reported here provide reasonable explanations for many of the popping (i.e. explosive

hydrogen/oxygen recombination) events observed in nickel hydrogen cells. Furthermore, the results suggest some component and stack design changes that would give this design greater margin to tolerate and properly manage oxygen evolution and recombination without damaging the stack components.

DESCRIPTION OF MODELS

The basic architecture of the models applied here have been previously described (Ref. 1), and thus will not be discussed in detail here. The general modelling method builds up the desired cell stack design by combining a number of finite elements in the desired physical arrangement. The elements presently available for this purpose include distinct finite elements for the nickel electrode, hydrogen electrode, separator, wall wick, gas screen, and the gas spaces in the cell. The arrangement of these elements indicated in Fig. 1 was used here as the minimum physically reasonable combination of elements for a one-dimensional model of the recirculating stack cell. The configuration of Fig. 1 provides for recombination and stack recirculation by allowing convective and diffusive movement of oxygen gas through the gas screen (elements 4-13), to recombine at the adjoining hydrogen electrode (element 3). The water produced by this recombination can wick into the separator (element 2), the wall wick (element 1), and back into the separator(elements 24-33) between the active nickel electrode (elements 14-23) and the electroactive hydrogen electrode (element 34). This configuration also allows gas and electrolyte flow in response to capillary, convective, and diffusive forces between the nickel electrode, the separator, and the active hydrogen electrode. Elements 35 and 36 provide the gas space that maintains reasonable variation of hydrogen pressure with state of charge in the cell, and also provide convective and diffusive coupling of gas between the cell gas space and the gas screens at the back sides of the platinum electrodes.

The model described by Fig. 1 consisted of 36 elements. To discern the material gradients through the gas screen, separator, and nickel electrode, each of these components was divided into 10 equally sized finite elements. Thus a scan through elements 2-34 provided at any point

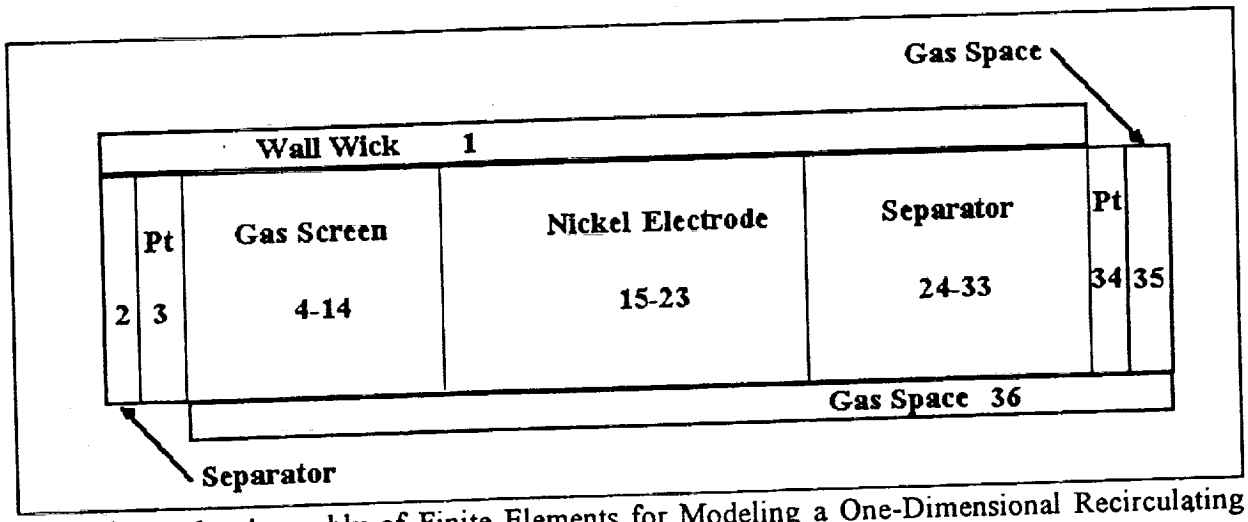

Figure 1. Assembly of Finite Elements for Modeling a One-Dimensional Recirculating Stack Nickel Hydrogen Cell.

in time an indication of how element properties (such as oxygen pressure, hydrogen pressure, state-of-charge, electrolyte concentration, or porosity) varied through the repeating stack unit. The component dimensions employed here were a 1 cm^2 area for all components, coupled with thicknesses of 0.3 mm for the separator, 0.16 mm for the hydrogen electrode, 0.5 mm for the gas screen, 0.8 mm for the nickel electrode, and a 0.1 mm thick wall wick. Appendix A lists the data file used in setting up and running the model, and lists all the physical and electrochemical parameters utilized by the model as well as the geometric arrangement of the elements. For the different cells modeled here, the only parameters that were changed were the electrolyte fill in the stack components (hydrogen and nickel electrodes, separator, and wall wick) and the porosity of the gas screen. Thus, the flooding of the gas screen studied herein applies to the situation where approximately 1 cm^2 of the gas screen is partially or fully flooded. Ref. 1 describes the role of each of the parameters listed in Appendix A in considerably more detail.

The cell described in Fig. 1 contains 55 interfaces across which materials such as gas, electrolyte, or solid-state protons can move. Protons were only allowed to diffuse within the active material of the nickel electrode (elements 14-23). Electrolyte was only allowed to move by capillary, convective, or diffusive forces between the stack and wall wick elements (1-3, 14-34). Gas movement was allowed between all elements by either convective or diffusive forces.

The transport of electrons and the charge exchange processes in the cell were modeled using the component arrangement indicated in Fig. 2. Here the microscopic details within the 5-10 micron layers of active material in the nickel electrode described in Ref. 1 have been replaced with a lumped combination of charge transport processes in each nickel electrode element. This provides an excellent characterization of macroscopic performance of the stack, at the cost of poor fidelity for predicting effects due to microscopic depletion in the nickel electrode. For this reason, the voltage of the nickel hydrogen cell at the start of charge, and near the end of discharge is not expected to agree precisely with real cells. The model illustrated in Fig. 2 contains 52 charge transport and charge transfer components, 10 involving nickel electrode sinter conduction, 10 each involving oxygen evolution and β-β charge transfer processes, 1 each involving structure conduction and hydrogen oxidation/reduction in the hydrogen electrode, and 20 involving ionic conduction in the electrolyte between elements.

For a more detailed picture of how nickel electrode surface loading could affect cell operation, the two-dimensional model illustrated in Fig. 3 was also used. This 2-D model has the cell components stacked in the x-direction. This model includes a second dimension perpendicular to the stack, in the y-direction. The 2-D model sacrifices some of the spatial resolution in the x-direction to obtain a picture of element parameters in both the x and y-

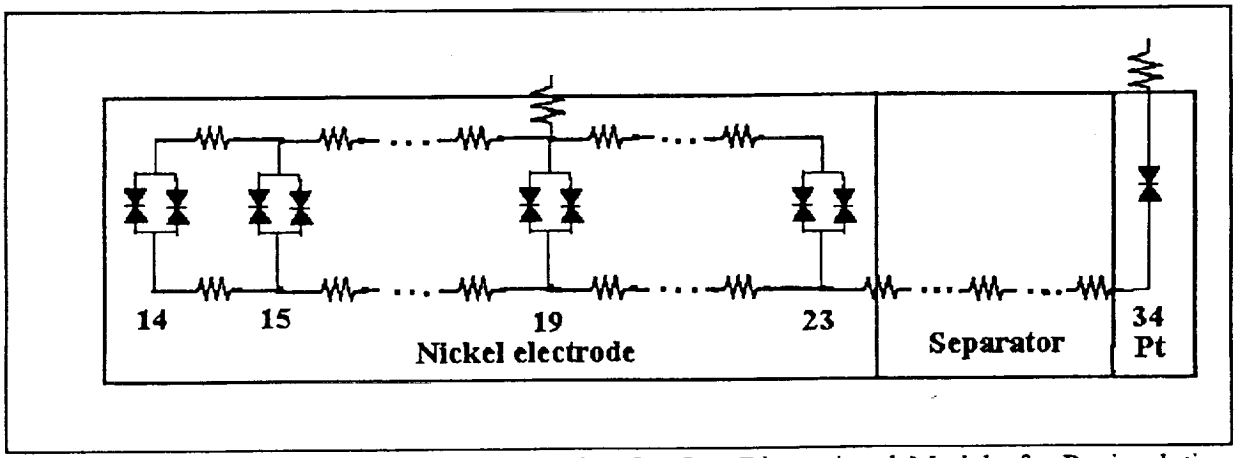

Figure 2. Electrical Component Configuration for One-Dimensional Model of a Recirculating Stack Nickel Hydrogen Cell.

directions. In Fig. 3, which includes 45 total finite elements, the element numbers are indicated in each region of the cell. In Fig. 3, each group of three elements in the gas screen, nickel electrode, and the separator are arranged along the x-direction.

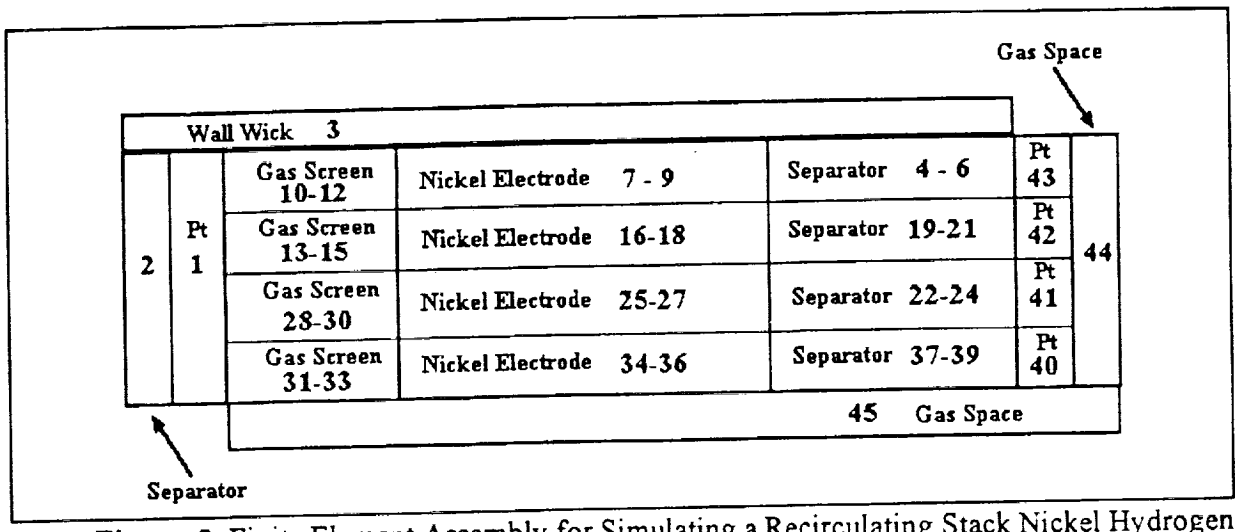

Figure 3. Finite Element Assembly for Simulating a Recirculating Stack Nickel Hydrogen Cell in Two-Dimensions.

The physical size of the system modeled here was 1 cm^2 for all stack components in the one dimensional model . For the 2-D model of Fig. 3, the total surface area of the stack components was also 1 cm^2, however, this area was divided between the different elements in the y-direction according to the details of the system being modeled, as will be discussed later. For example, a crack in the surface of the nickel electrode against the gas screen was simulated by making elements 30-41 0.1 mm high, while elements 4-21, 31-40, and 42-43 were all 3.3 mm high (the crack was actually simulated by giving element 27 a very low loading level). In addition to the 45 finite elements present in the 2-D model, there were 83 interfaces through which gas and/or electrolyte could move, and 95 electrical components describing electronic conduction, ionic conduction, and charge transfer processes. The only charge transfer processes considered here were β-$Ni(OH)_2$ redox, oxygen evolution, and hydrogen redox processes. The detailed parameters describing the these processes and the detailed arrangement of elements, interfaces, and components are given in Appendix B. Ref. 1 describes the role of each of the parameters listed in Appendices A and B in considerably more detail.

Figure 4 indicates the paths for charge transport in the 2-D model, with the 46 electrical nodes being noted. The picture in Fig. 4 can be best thought of as involving a resistive network (highlighted) overlaying a network of ionic conduction, with charge transfer in the nickel and hydrogen electrodes coupling these two networks. The resistive network distributes electrons through the metallic conduction paths of the electrodes, the ionic conduction network describes ionic movement of charge in the electrolyte, with the electrochemical reactions in the nickel and hydrogen electrodes enabling charge conversion between the electronic and ionic charge carriers.

The circles in Figure 4 represent the charge transfer resistances from the Butler-Volmer Eq., with those in the nickel electrode involving the parallel processes of the electrode charge/discharge process and the oxygen evolution process. In the hydrogen electrode, the circles represent the charge transfer resistance of only the hydrogen reaction.

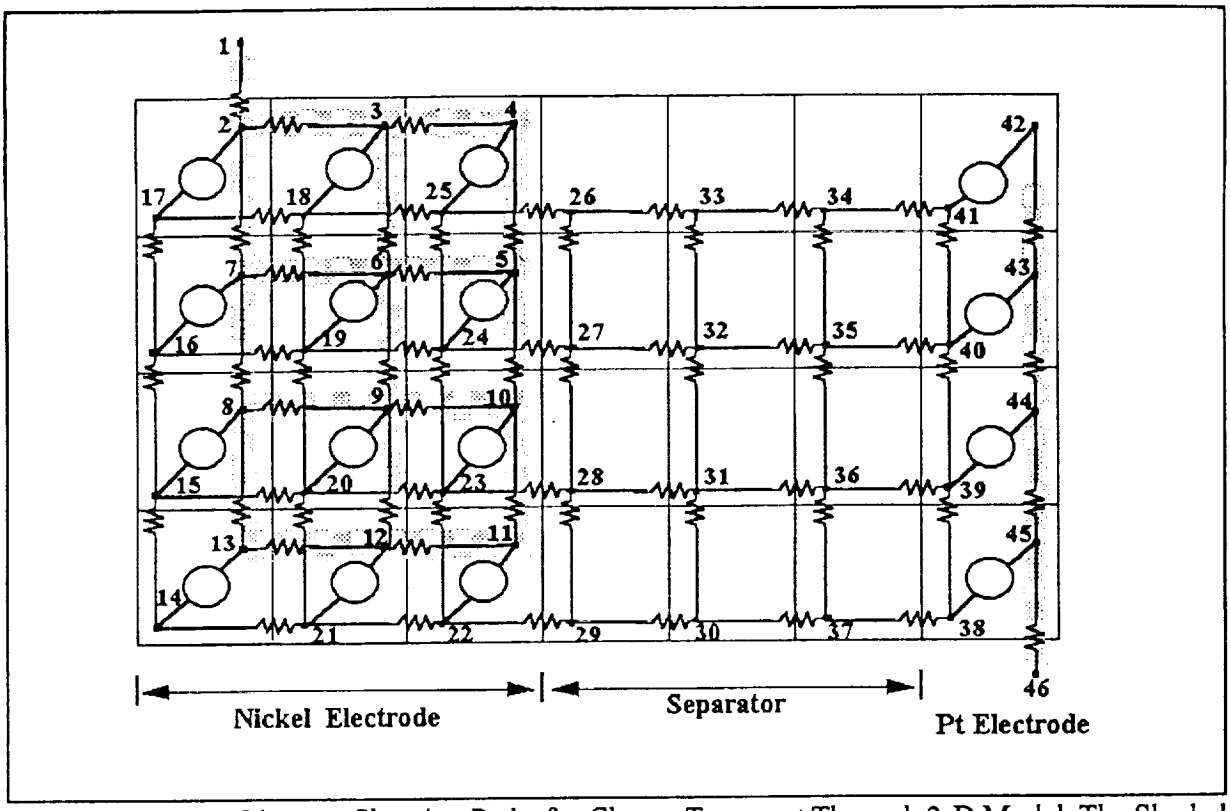

Figure 4. Diagram Showing Paths for Charge Transport Through 2-D Model. The Shaded Paths are Electronic Conduction, Circles are Charge Transfer Processes.

ONE-DIMENSIONAL MODEL RESULTS

EFFECT OF VARYING ELECTROLYTE FILL IN STACK

The percentage of porosity within the stack of components (excluding the gas screen void volume) was varied from 88% to 99%, with the latter fill being very close to a flooded cell. The model was then used to determine where the electrolyte ends up and where gases flow during charge at 2 ma/cm$_2$ (about C/10) for 80,000 sec, which is long enough to bring the cell into oxygen evolution at about 90% of the applied current (i.e. 10% charge efficiency). Figure 5 indicates the typical cell voltage and pressure profiles during charge. Voltage and pressure did not change much as the amount of electrolyte in the stack was varied at these relatively high levels. The lack of a clear transition into overcharge is because the temperature was 20 deg C. At lower temperatures there appears a much clearer distinction between recharge and overcharge, as the oxygen evolution potential increases relative to the recharge potential.

The cell charge was started from an initial state where 0.01 atm of oxygen was artificially present in the gas space, and 2.0 atm of hydrogen gas was initially present in the discharged cell. In some of the data that follows, effects are seen early in the recharge from recombination of this oxygen. After this early equilibration period, the oxygen pressure in the cell was generally low early in the charge period, rising to much higher values at the end of charge. Figures 6 and 7 indicate the variation in oxygen pressure across the stack at 10,000 sec, when the cell is not in

overcharge, and at 80,000 sec, when the cell is in overcharge. These figures clearly show the profile of higher levels of oxygen in the nickel electrode, since this is where the oxygen is being generated. They also show higher levels of oxygen moving into the separator from the nickel electrode as the amount of electrolyte in the stack is increased. At very high levels of electrolyte, this can result in a very steep gradient in oxygen pressure near the surface of the platinum electrode. This is a situation in which it is very possible to form actual bubbles of oxygen gas. It should be noted that this model does not differentiate between gas bubbles and uniformly dispersed gas.

Figure 8 indicates the change in oxygen pressure with time during charge in element 20, which is in the center of the nickel electrode. The oxygen pressure is at its maximum level in this element, since the source of the oxygen is the nickel electrode. Figure 8 shows how the oxygen pressure starts to build up, particularly at the center of the nickel electrode as the cell goes into overcharge at about 36,000 sec. A very similar time dependence for the buildup of oxygen was observed in the other elements of the cell, however because transport of oxygen to the Pt catalyst electrodes was more facile than from element 20, the pressures attained during overcharge were less than in element 20.

Figures 9 and 10 indicate the variation in porosity through the cell stack at 10,000 sec into charge (when very little oxygen evolution occurs), and at 80,000 sec (when most of the charge current is going into oxygen evolution. The porosity, as defined here, refers to the fraction of the element volume available to contain gas, thus is not filled with solid materials or electrolyte. As shown in Fig. 9, when little oxygen is being evolved, there is a large porosity gradient between the hydrophobic Pt catalyst electrode and the separator and nickel electrodes. This is particularly true at high KOH fill levels where both the separator and the nickel electrode are nearly flooded with electrolyte. When there is significant oxygen evolution and recombination (Fig. 10), while the Pt electrode porosity is not changed much, the separator porosity is increased significantly by the movement of oxygen through the separation region. In full overcharge (2 ma/cm^2) at 80,000 sec, most of the oxygen is transported through the gas screen to recombine on the back side of the adjacent Pt electrode. However, at electrolyte fill levels less than 90%, a very significant fraction of the generated oxygen diffuses as gas through the open spaces in the separator material to recombine on the Pt catalyst.

The development of the porosity during the 80,000 sec charge period is indicated in Figs. 11-13, for elements 15, 24, and 34, respectively. In element 15 (nickel electrode) the porosity generally increases through the charge period as the flux of oxygen migrating through the nickel electrode in this region to the gas screen increases. In element 24 (separator), the porosity at high electrolyte fill levels does not change much with oxygen evolution since there is little space for electrolyte to move into. This behavior illustrates that capillary forces essentially disappear at high electrolyte fill levels, since essentially all pores are filled with electrolyte. Most of the free volume tends to end up in the hydrophobic regions of the Pt catalyst electrode. Interestingly, in Fig. 12 with a 98% fill factor or less, a significant upswing in porosity is seen in the separator commencing when oxygen evolution begins, essentially a result of the interplay of increasing capillary forces and the pressure of oxygen evolution and movement from the nickel electrode towards the Pt catalyst. Element 34 (Fig. 13, Pt electrode) indicates that there is a threshold of electrolyte fill at about 95-96%, such that if more electrolyte is present some flooding of the Pt electrode occurs as the Pt electrode recombines oxygen, largely because the other cell components are not able at these high fill levels to wick the electrolyte from the Pt electrode. As the charging continues and gas pressure builds up, more space becomes available in the cell (active

material density increases), and the porosity of the Pt electrode increases. At electrolyte fill levels below 95%, the higher porosity in the Pt electrode is always maintained, because the other cell components are capable of effectively wicking electrolyte at all times.

The concentration of electrolyte varies across the stack in a dynamic way dictated by all reactions in the cell. Fig. 14 indicates the concentration gradient at 10,000 sec into charge, when essentially no oxygen is being evolved. The concentration of KOH is lower in the nickel electrode because water is being generated by the charging reaction, and is higher in the platinum electrode (element 34) because water is being consumed in the generation of hydrogen. These processes maintain about a 2% concentration gradient across the stack modeled here, with little changes being seen in the KOH concentration at the recombination Pt electrode or the wall wick.

However, when oxygen is being evolved (Fig. 15, 80,000 sec into charge) a significant reduction in the KOH concentration in the recombination Pt electrode is seen due to the recombination of oxygen that passes through the gas screen. It should be noted here that this quite low KOH concentration would actually be dispersed across a more extended stack of plate components in a real cell, since an electroactive Pt electrode would cancel out much of the lowered concentration seen here in element 2. The variation in KOH concentration in element 2 also shows that at KOH fill factors above 90-95% the ability of the wall wick to effectively transport electrolyte falls off dramatically. In the remainder of the stack the loss of oxygen to the recirculation process results in a slightly increased concentration profile, all the while maintaining the approximately 2% gradient between the Ni and Pt plates.

Figs. 16-19 focus on the changes in KOH concentration during the full 80,000 sec charge period in elements 2, 15, 24, and 34 respectively. These elements represent the recombination Pt electrode, the nickel electrode, the separator, and the Pt/H_2 electrode. These figures show the KOH concentration dropping in the recombination Pt electrode (element 2) when significant oxygen evolution begins, and at the same time a significant increase in the remainder of the stack (elements 15-34).

It is typically assumed that the nickel electrode charges and discharges uniformly through the thickness of the sintered electrode, simply because the sinter structure is both highly porous and highly conductive. Figures 20 and 21 indicate the gradient in state-of-charge realized across the nickel electrode at 10,000 and 80,000 sec into a 2 ma/cm^2 charge. In Fig. 20 it is clear that the nickel electrode charges more efficiently on the side facing the separator and the Pt/H_2 electrode. This is primarily because of the ionic resistance in the electrolyte through the nickel electrode, with some contribution from the varying oxygen activity and KOH concentration through the nickel electrode. In Fig. 21, this state-of-charge variation through the thickness of the sinter is reduced as the electrode approaches the fully charged state. Fig 21 also shows a cumulative effect of electrolyte fill level on charge efficiency. High fill factors give improved charge efficiency. A number of factors contribute to this effect. First, the greater amount of electrolyte reduces the ionic resistance. Second, the higher oxygen pressure in the nickel electrode slightly improves the charge efficiency by reducing the oxygen evolution rate. Finally, the slightly elevated KOH concentration associated with the higher electrolyte fill factors act to slightly improve charge efficiency.

EFFECTS OF GAS SCREEN FLOODING

The effect of flooding the gas screen in a region of the nickel hydrogen is of interest, because some cell activation procedures may leave excess amounts of electrolyte trapped in the gas screen. Intuitively, it seems clear that this will limit gas transport in and out of the hydrogen electrode, and if enough of the gas screen is flooded, severe impacts on the cell performance will result. The gas screen flooding modeled here was done assuming that only 1 cm^2 of the gas screen is flooded. This is insufficient to significantly affect the electrical performance of the cell much, since there is very little overpotential associated with the hydrogen electrode. However, gas screen flooding will redirect oxygen transport in the flooded regions, giving local areas of higher than normal oxygen pressure. This was modeled here by filling the gas screen region of elements 4-13 with KOH in a 1 cm^2 area. The model was then run with several electrolyte fill levels: 95 and 98%.

Figure 22 indicates the variation in oxygen pressure through the stack when the gas screen is flooded, in comparison with a non-flooded gas screen. Clearly, the flooded gas screen allows high pressures of oxygen gas to approach the Pt electrode through the gas screen. In addition, the increased oxygen flux forced through the nickel electrode and the separator results in considerably higher oxygen pressures through the separator and approaching the active Pt/H_2 electrode. Clearly this situation significantly increases the likelihood of popping, i.e. explosive recombination of oxygen on the Pt surface when the oxygen concentration locally exceeds 4% of the hydrogen (about 1 atm oxygen here).

Figure 23 indicates how gas screen flooding affects the porosity of the cell stack when the cell is in overcharge. The flooding of the gas screen has little effect by itself on the porosity of the components, since this is primarily dictated by the amount of electrolyte in the stack coupled with the pore size distributions of the components. If this model were run in a mode where the electrolyte was not trapped in the gas screen, but could undergo free transport in or out of the stack, greater effects would be seen on the porosity in the stack components.

Figure 24 indicates how gas screen flooding affects the electrolyte concentration gradient through the stack when the cell is in steady-state overcharge (i.e. at 80,000 sec into charge). Again, while gas screen flooding reduces the electrolyte concentration throughout the stack by about 0.3%, there is little change in this concentration profiles for cells of differing KOH fill levels which have flooded gas screens. There is a significant interplay between the KOH fill and gas screen flooding in terms of the wall wick function in the cell. This is because the wall wick loses its capillary function above 95-96% KOH fill, in addition to the change in oxygen recombination as the gas screen floods. Thus, in Fig. 24, at a 95% KOH fill, a cell with a flooded gas screen will tend to wick some electrolyte from the stack, while this essentially is turned off at a 98% KOH fill.

A significant driving force for degradation in nickel hydrogen cells during overcharge, and for developing oxygen bubbles and popping, is the pressure differential developed across the stack components as the cell is charged and discharged. In overcharge it is possible to build up a significant overpressure of oxygen gas if the gas transport is sufficiently inhibited by low component porosity, or the gas evolution rate is sufficiently high. Fig. 25 indicates the pressure differential resulting from the model runs described above at the 80,000 sec point in charge, i.e. when the cell is in overcharge. Fig. 25 plots the maximum pressure differential between the nickel electrode and the separator or gas screen elements adjacent to the Pt electrodes. With the normally functioning gas screen, very little pressure differential is seen until the KOH fill reaches

96-98%. When areas of the gas screen become flooded, the pressure differential is increased 4-5 times. With a flooded gas screen region, electrolyte fill levels above about 90% will likely result in a significant pressure differential across the stack. Clearly , the location of electrolyte in the cell can play a large factor in establishing stress levels during overcharge, and cumulative stress during long term cycling.

RESULTS WITH NON-UNIFORM LOADING

Four differing non-uniform loading profiles in the nickel electrode were examined in comparison with a uniform loading of 1.6 g/cc void. Figure 26 indicates these four loading profiles. Profile A has high loading only on the gas screen side of the nickel electrode. Profile B has high loading only on the separator side, while profiles C and D have high and moderate loading on both surfaces of the nickel electrode. As indicated in Fig. 26, the loading drops linearly to a minimum level in the center of the nickel electrode. The total amount of active material in the nickel electrode is maintained at a constant level in all these simulations. All of these simulations started with 95% of the volume in the components being filled with 31% KOH electrolyte. Other pertinent parameters are indicated in Appendix B. The simulations that were run consisted of charging at 2 ma/cm^2 for 80,000 sec, long enough to charge the cell and to be in overcharge. Typically, the cell was 92% charged by this charge cycle, and the internal hydrogen pressure was 27-28 atm, depending on the quantity of oxygen in the cell when it was in overcharge. The pore size distribution in the nickel electrode was assumed to shift linearly from a generic distribution measured for a relatively uniformly loaded electrode, towards smaller pore sizes according to the remaining free volume in the nickel electrode elements. A density of 3.6 g/cc was used for the nickel electrode active material, thus it was not possible to fill the pores with active material beyond this density.

Figure 27 indicates the effect of non-uniform loading on the buildup of oxygen in the cell components during the charge, showing oxygen partial pressure at the end of the recharge period. The oxygen builds up in the nickel electrode as the cell goes into overcharge, being quite low prior to overcharge. The high surface loading prevents the diffusion of oxygen from the nickel electrode, thus resulting in very high partial pressures of oxygen. Figure 27 indicates the oxygen partial pressure through the stack for loading profiles A-D in Fig. 26, along with the uniformly loaded case. In the case where the high surface loading exists on both surfaces of the nickel electrode, the total pressure in the nickel electrode exceeds that outside the nickel electrode, since even the strong convective flows in the stack are unable to move enough through the nickel electrode surfaces to maintain uniform pressure. This is shown in Fig. 28. These pressure differentials clearly can exert significant stress on the structure of the nickel electrode, possibly contributing to swelling, active material being forced from the pores and into the separator, and blistering.

Fig. 29 compares the electrolyte concentrations for uniformly and non-uniformly loaded nickel electrodes when in overcharge. Local concentration gradients clearly become much more significant when the nickel electrode has local areas of high loading, particularly when the highest loaded areas are adjacent to the separator rather than near the gas screen. These localized areas of high loading tend to support most of the oxygen evolution and charging reactions, thus developing a more strongly graded electrolyte concentration.

TWO-DIMENSIONAL MODEL RESULTS

The two dimensional model described earlier was first run with a uniform loading level in the nickel electrode of 1.6 g/cc void. The results from this simulation are indicated in Figure 30, which shows the percentage of oxygen in the gas phase present within the cell as a function of position within each component. The slightly increased oxygen levels at the top of the cell result from electrolyte recirculation through the wall wick from the Pt electrode on the left, to the separator on the right. This pumps some additional electrolyte into the top of the separator on the right side of the stack in Fig. 30, thus slightly inhibiting oxygen diffusion in this wetter region. As indicated by Fig. 30, the oxygen level only reaches a 4-5% concentration in the middle of the nickel electrode, with levels under 1% existing in the separators and gas screens. Clearly in this case there is facile transport of gas and liquid components through the cell, and there is little risk of popping or other phenomena associated with the buildup of oxygen in the stack. Figure 30 indicates the way the nickel hydrogen cell is supposed to work in terms of gas and electrolyte transport.

Another simulation was run with surface layers 25% of the thickness of the nickel electrode on each side of the electrode. These surface layers were loaded at 3.1 g/cc void. The inner 50% of the electrode thickness was loaded at a level which gave an average loading level of 1.6 g/cc void. It should be noted here that the cell voltage during recharge differed by less than 5 mv between the surface loaded cases and the uniformly loaded cases, with the voltage being slightly higher when the loading was not uniform. Figure 31 indicates contours of oxygen concentration for this case. The oxygen level in the nickel electrode is dramatically increased, with oxygen levels over 80% being obtained in the center of the nickel electrode near the bottom of the stack. Oxygen concentrations as high as 2% penetrate as far as 50% of the way through the separator towards the Pt electrode. Although these oxygen levels are quite high, they are dissipated in a relatively uniform way through the separator and gas screen such that the Pt electrode is not exposed to oxygen concentrations over 1%. This is well below the level of 4% required to initiate a popping event, i.e. a localized hydrogen/oxygen explosion.

The asymmetry between the top and the bottom of the stack in Fig. 31 is again due to the recirculation of electrolyte through the wall wick at the top of the cell. This characteristic recirculation pattern gives higher oxygen levels at the top of the cell. The increased oxygen level at the bottom of the nickel electrode and the adjacent separator is likely to result from gas transport being more facile away from the boundaries of the cell.

Variation in the transport of gas in the y-direction in the cell was modeled by putting a small crack in the position of element 27, which was on the side of the nickel electrode against the gas screen. This crack was a surface region 0.1 mm high and 25% of the electrode thickness, and which was loaded at 0.115 g/cc void. The remaining regions of the nickel electrode were loaded at 0.115 g/ccv if in the center, and 3.1 g/ccv if on the surface. Thus, element 27 provided a channel for gas flow out of the nickel electrode. Clearly, if surface loading exists in nickel electrodes, there will be areas having lower loading and other areas where actual channels exist to allow gas flow out of the electrode. The crack designed into the electrode is meant to simulate these kinds of areas.

Figure 32 indicates the results of this simulation in the form of contours of oxygen concentration throughout the cell stack. As expected, the oxygen preferentially moves out of the nickel electrode and into the gas screen through the crack, giving a small region in the gas screen where a higher concentration of oxygen exists. Because the gas screen allows facile movement

and diffusion of gas, high concentrations of oxygen do not penetrate very far into the gas screen region. Thus, as long as the gas screen is maintained relatively free of entrapped electrolyte, there appears to be little risk of igniting the high oxygen levels in the nickel electrode through the gas screen. Interestingly, a secondary effect of the crack in the nickel electrode in Fig. 32 is that it forces a stronger recirculation pattern by channeling the oxygen through the gas screen. This recirculation pattern is recognized by the curvature of the oxygen contours at the top of the cell stack in Fig. 32. However, the oxygen gradients are still greatest at the surface of the nickel electrode, and oxygen concentrations up to 4% still only penetrate about 50% of the way through the separator.

A final simulation, which was very similar to that of Fig. 32, was done, except that the crack was put on the separator side of the nickel electrode (in the element 25 position). The size and loading associated with this crack were the same as previously described. Fig. 33 shows the contours of oxygen in the cell stack obtained during overcharge. The increased oxygen transport through the crack is seen as a bulge in the contours in the separator on the right side of the cell. As it propagates through the separator, this bulge moves upward, until about 75% of the way to the top of the stack, it touches the Pt electrode at an oxygen concentration of about 4%. It is clearly possible in this situation to ignite the oxygen, and potentially to propagate an ignition front back toward the nickel electrode. Interestingly, if the bulge were to propagate uniformly across the separator, it is unlikely that it would reach the Pt electrode at a 4% oxygen level. The recirculation of electrolyte into the top of the separator makes the dissipation of the oxygen bulge much more difficult near the top of the stack. In addition, some oxygen is being channeled through the wall wick and into the separator on the left side of the stack. These effects from the recirculation process accentuate the increased oxygen concentration in the separator in regions where the wall wick contacts separator. The increased wetness of the top of the separator on the right side of the stack also results in a significantly higher concentration of oxygen within the top of the nickel electrode, where much of the internal volume contains more than 80% oxygen gas.

Clearly, the variation of separator wetness possible in a recirculating design can increase the likelihood of popping if surface loading exists, particularly when compared to a back-to-back design where oxygen is expected to move much more uniformly across the separator. Note that the bottom of the separator on the right side, which is the driest region, is carrying the majority of the oxygen gas, but the 4% oxygen contour reaches only a little more than 50% of the way through the separator.

CONCLUSIONS

The behavior described above for a recirculating stack nickel hydrogen cell is in all cases exactly what would be expected based on the present qualitative physical understanding of the nickel hydrogen cell. The results of this model, however, allow the details of cell performance and operation to be better quantified, and provide some visibility into how the various physical and electrochemical processes operate at a microscopic scale through the component stack. This information can serve as a useful guide for those who design and operate nickel hydrogen cells.

The results of the studies reported here indicate that the transport of gas and electrolyte through the nickel hydrogen cell can have very significant effects on the performance of the cell, depending on the amount and location of electrolyte in the cell. For the recirculating stack

design modeled here, as well as for other cell designs, it is necessary to maintain appropriately designed gas and electrolyte management processes during all periods of cell operation. In the recirculating stack modeled here, it is clear that if the fraction of stack void volume filled with electrolyte exceeds a threshold of 90-95%, significant changes in the internal cell operation occur. Capillary forces become exceedingly weak, wall wicks become much less effective, and the interface between the separator and the Pt electrode can become the site of large gradients in porosity and oxygen pressure.

If the gas screen in the recirculating stack is allowed to flood in localized regions, high oxygen pressures are allowed to approach the Pt electrode through the gas screen. Clearly these results have ramifications both in terms of how the nickel hydrogen cell stack is designed, how individual components are manufactured, and how cells are activated with electrolyte. Further modeling of specific activation processes could be most instructive in indicating techniques to prevent popping and to assure appropriate electrolyte fill levels in the cell. These results clearly show that the major material conversion and transport processes in the nickel hydrogen cell can be usefully modeled, and that the results can provide guidance to cell designers, manufacturers, and users.

The effects of non-uniform nickel electrode loading on the operation of a recirculating stack nickel hydrogen cell were modeled, and it was found that variations in loading levels within the nickel electrode can have a profound effect on local levels of oxygen in the cell, and can also affect local electrolyte concentrations during recharge, and presumably discharge. Loading variations can channel oxygen generated from overcharging the nickel electrode either into the gas screen, or into the separator. Channeling such oxygen into a relatively dry gas screen was found to have no undesirable consequences for a C/10 overcharge rate. Channeling oxygen into the separator was found to couple into the recirculation pattern in the cell such that oxygen concentrations in excess of 4% could contact the Pt electrode. Such contact occurred in regions where separator wetness was maximized by the recirculation process. The coincidence of an area of high wetness due to the cell recirculation path with an area on the nickel electrode surface that channels oxygen into the separator, could lead to very serious popping within the nickel hydrogen cell.

REFERENCES

1. A. H. Zimmerman, *Proc. 183rd Meeting of the Electrochemical Society, Vol. 93-1, The Electrochemical Soc. Inc., Pennington, N. J., 1993, p. 147.*

2. A. H. Zimmerman, *Performance Model of a Nickel Hydrogen Cell, The Aerospace Corporation, to be published.*

3. A. H. Zimmerman, *Performance Model of a Recirculating Stack Nickel Hydrogen Cell, The Aerospace Corporation, to be published.*

ACKNOWLEDGEMENT

This work was supported by the Aerospace Corporation, as part of the ASR Program, and by NASA, Lewis Research Center. Support from both these sources is gratefully acknowledged.

Fig. 5. Recirculating Stack NiH2 Cell
Charge at 2 ma/cm2 from 0.01 SOC, 20 C

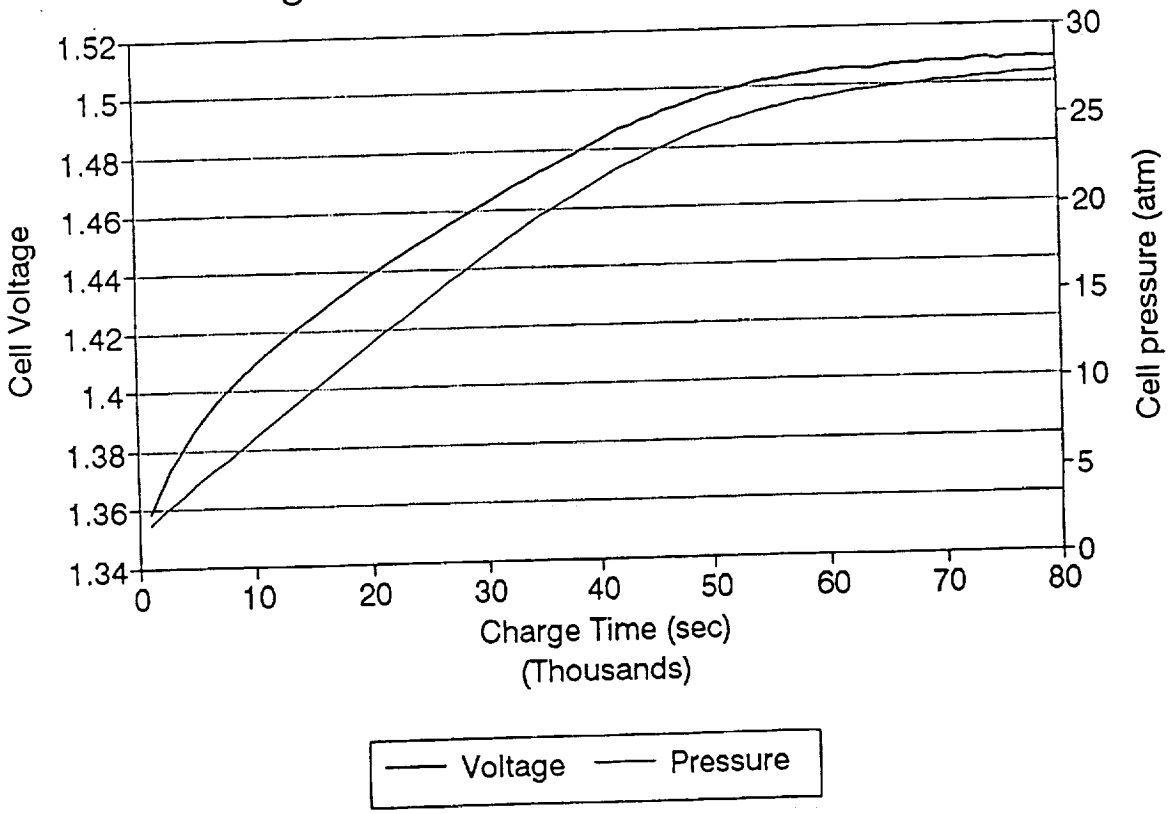

Fig. 6. Recirculating Stack NiH2 Cell
Oxygen Pressure at 10Ks into Charge

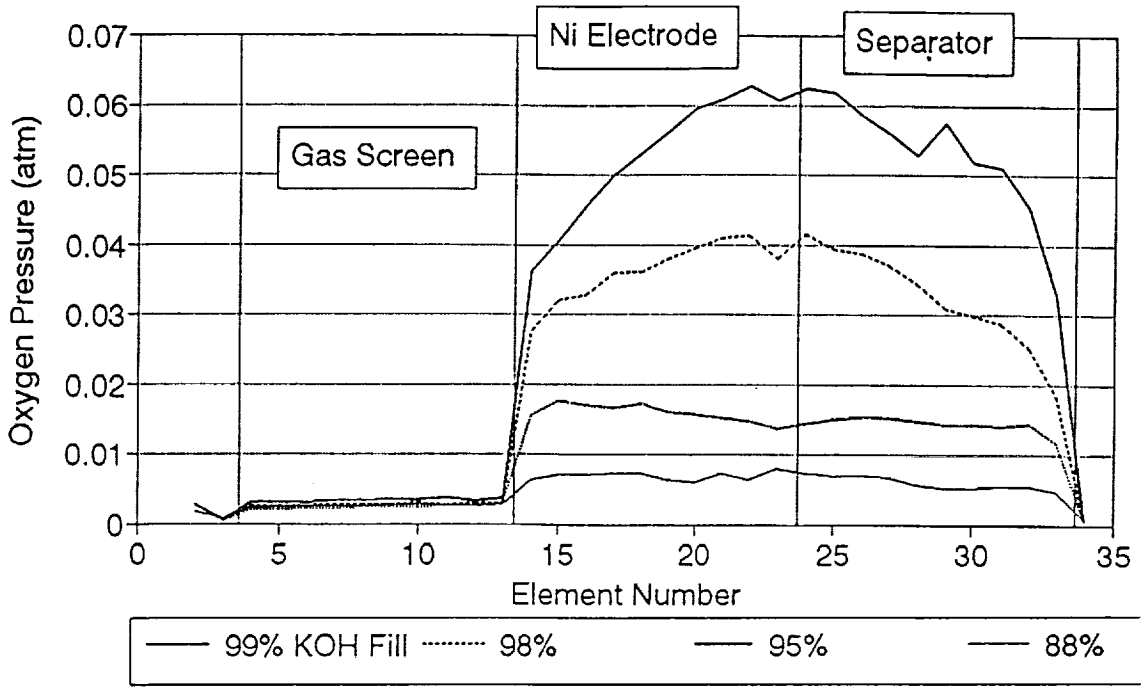

Fig. 7. Recirculating Stack NiH2 Cell
Oxygen Pressure at 80Ks into Charge

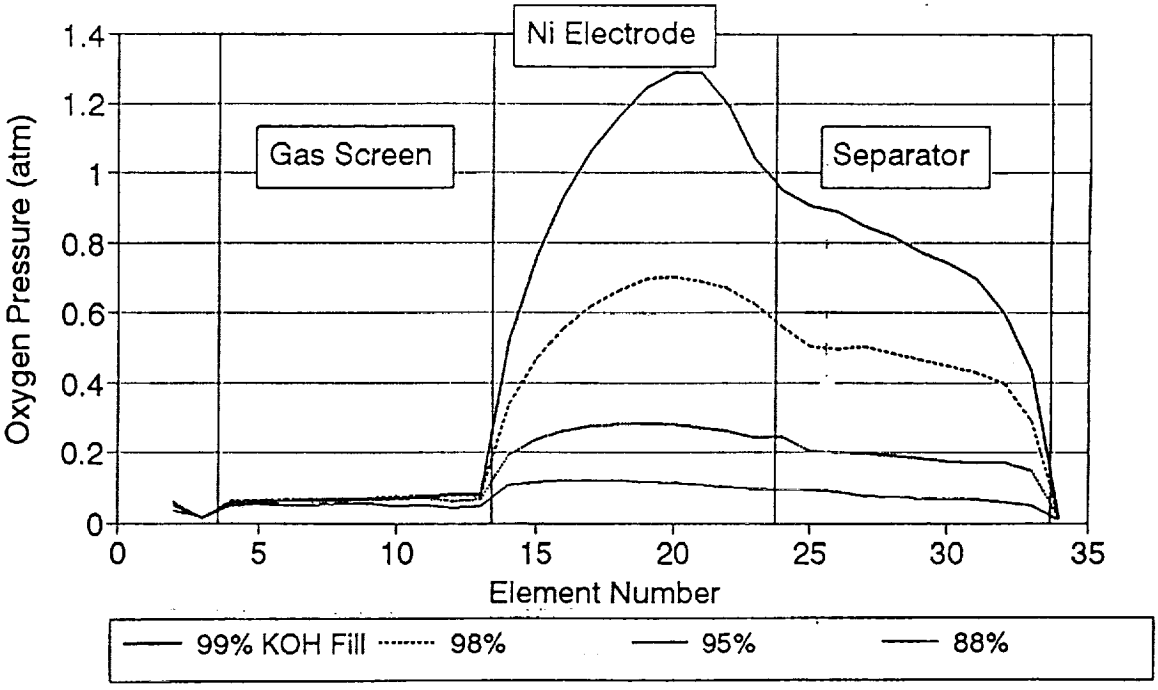

Fig. 8. Recirculating Stack NiH2 Cell
Oxygen Pressure During Charge, Elem 20

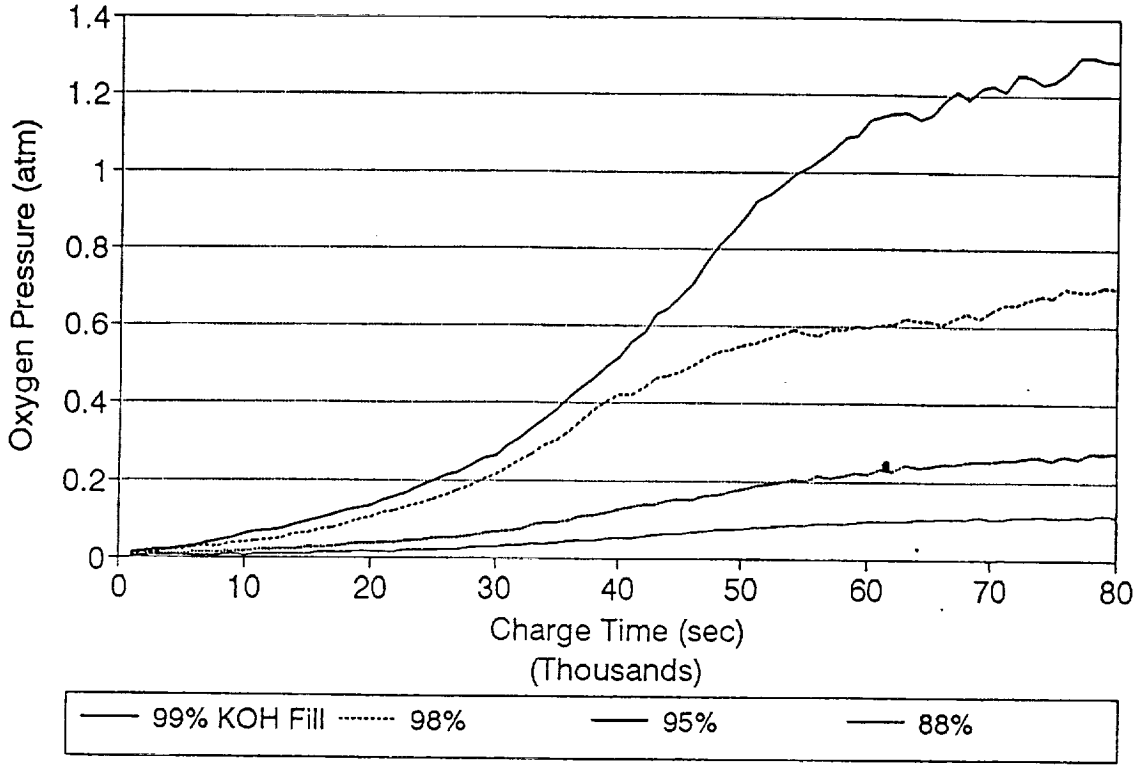

Fig. 9. Recirculating Stack NiH2 Cell
Stack Porosity at 10Ks into Charge

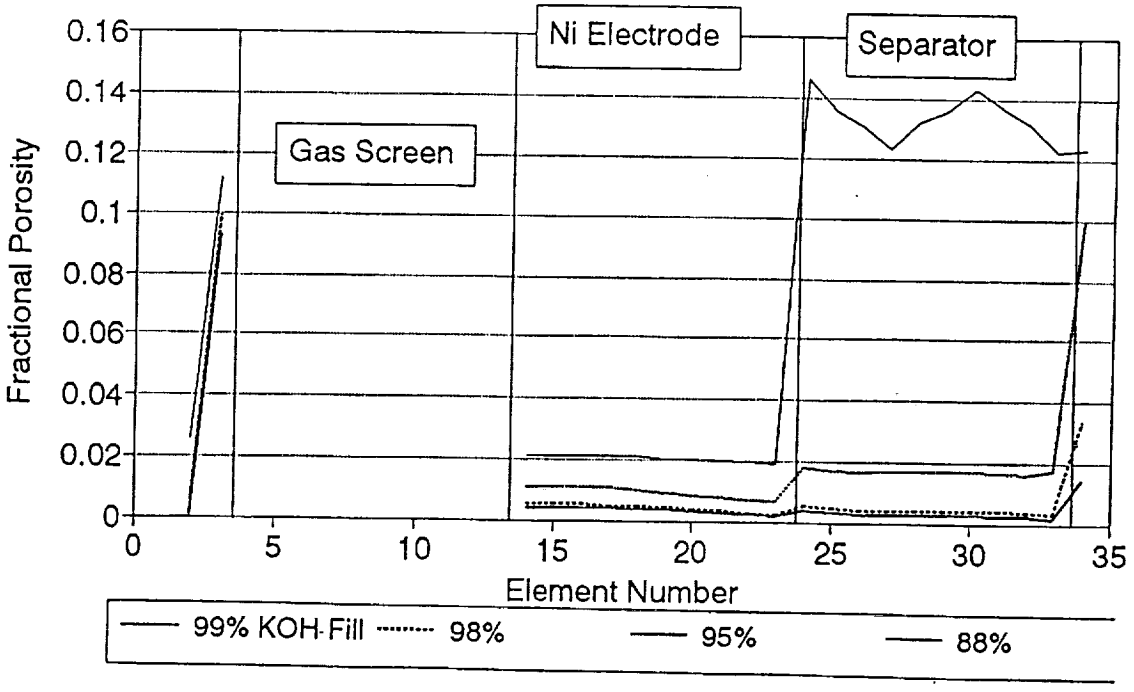

Fig.10. Recirculating Stack NiH2 Cell
Stack Porosity at 80Ks into Charge

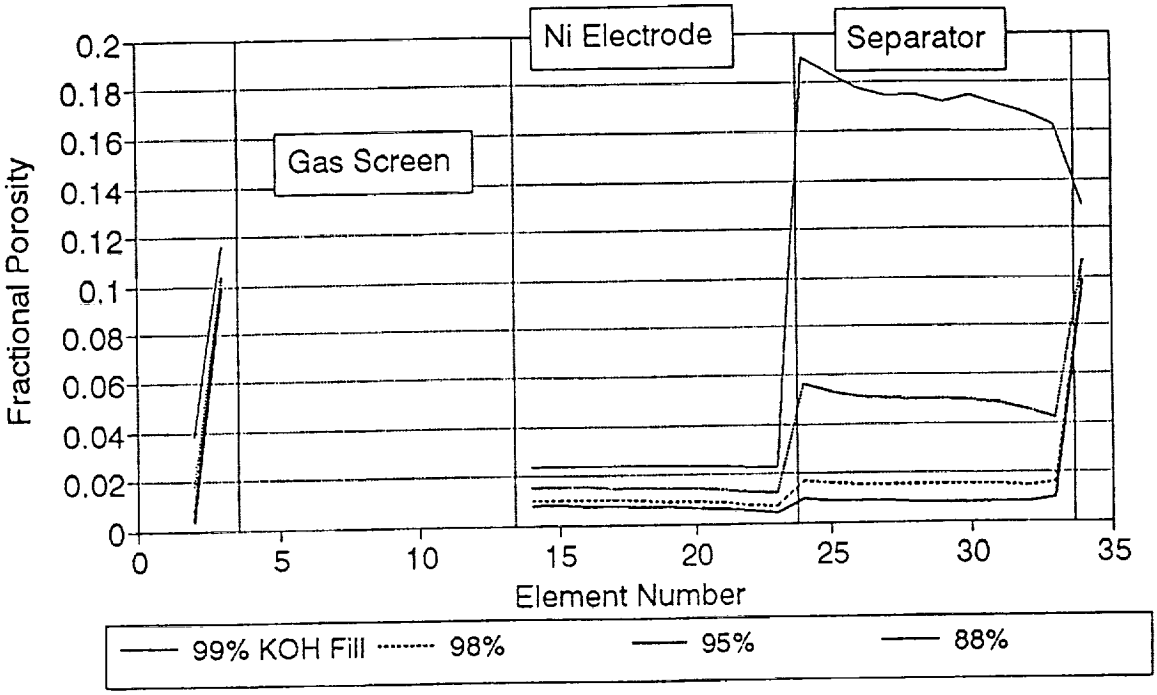

Fig. 11. Recirculating Stack NiH2 Cell
Porosity During Charge, Ni Elem 15

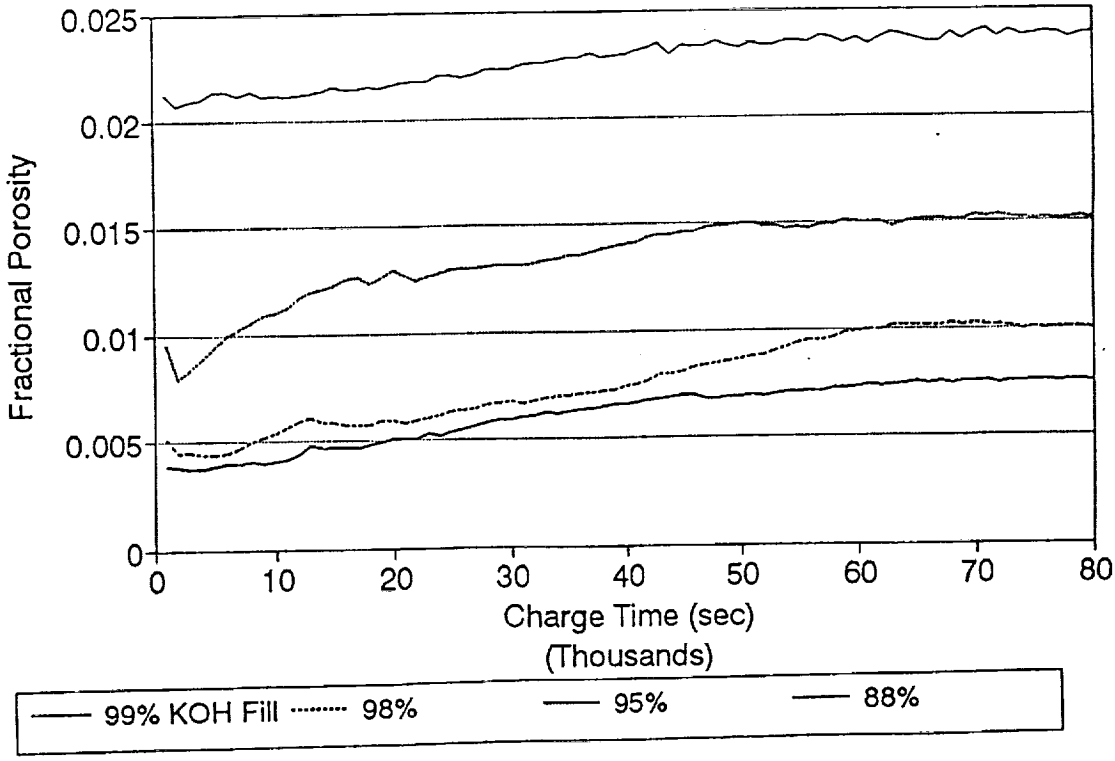

Fig. 12. Recirculating Stack NiH2 Cell

Porosity During Charge, Sep Elem 24

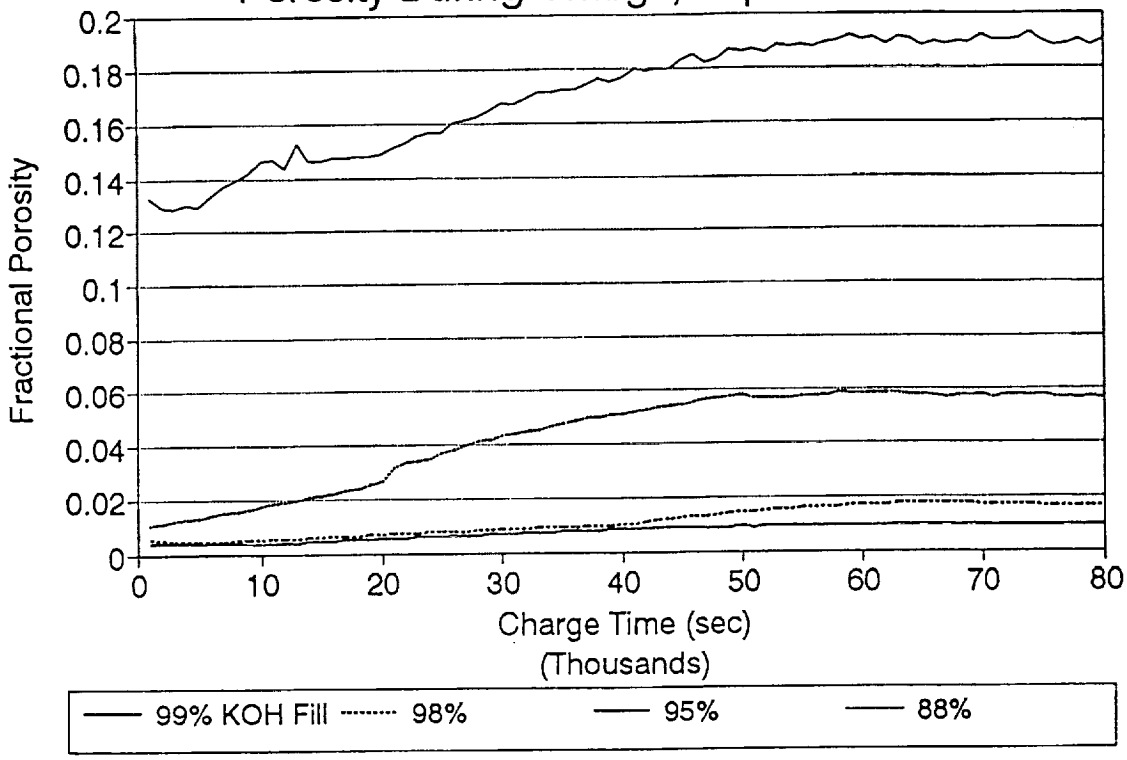

Fig. 13. Recirculating Stack NiH2 Cell

Porosity During Charge, Pt/H2 Elem 34

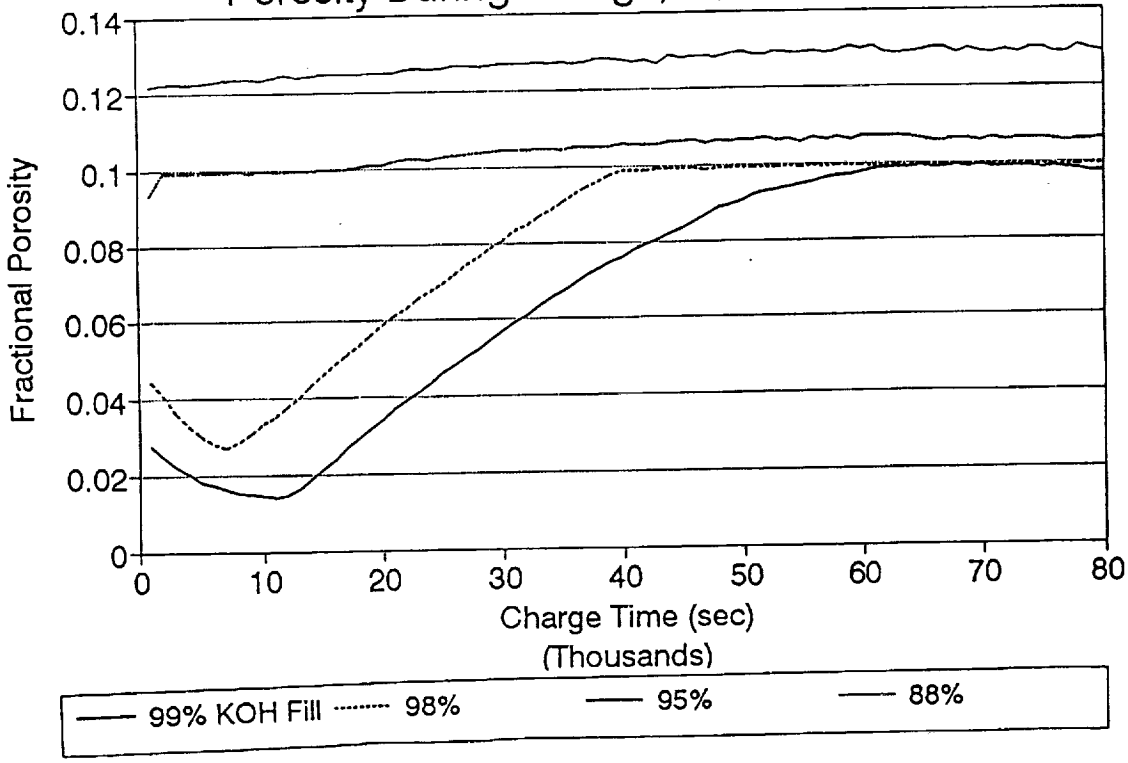

Fig. 14. Recirculating Stack NiH2 Cell
% KOH Concentration at 10Ks into Charge

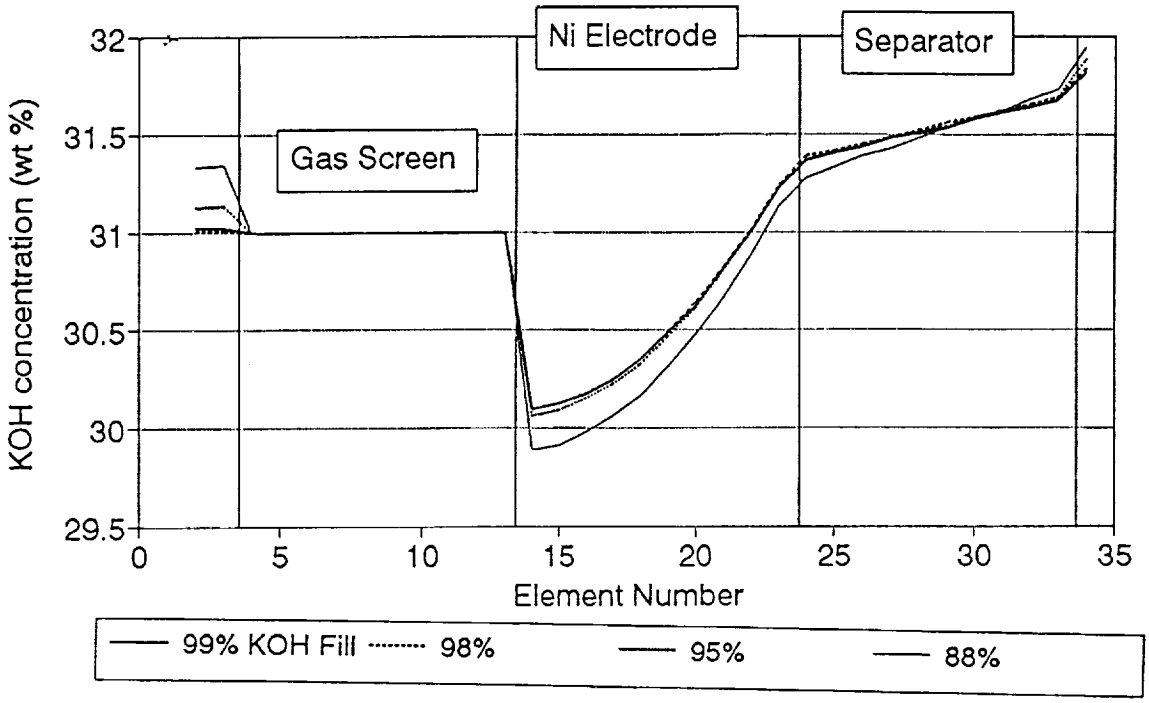

Fig. 15. Recirculating Stack NiH2 Cell
% KOH Concentration at 80Ks into Charge

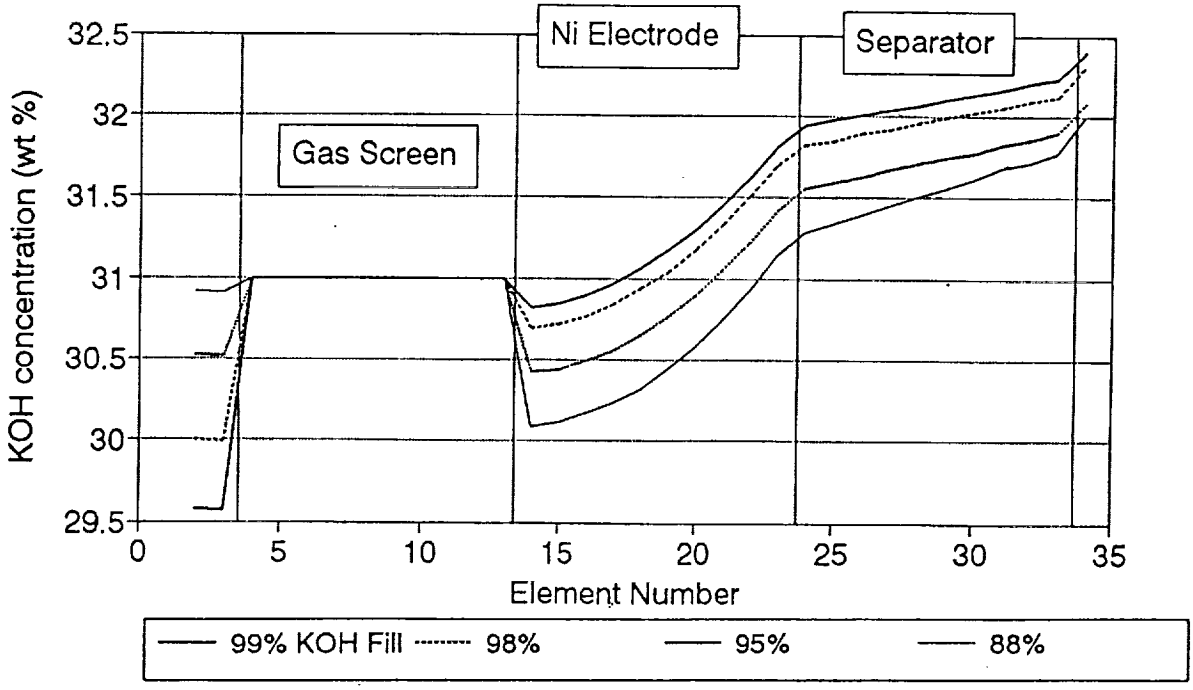

Fig. 16. Recirculating Stack NiH2 Cell
Conc KOH During Charge, Recom Sep Elem 2

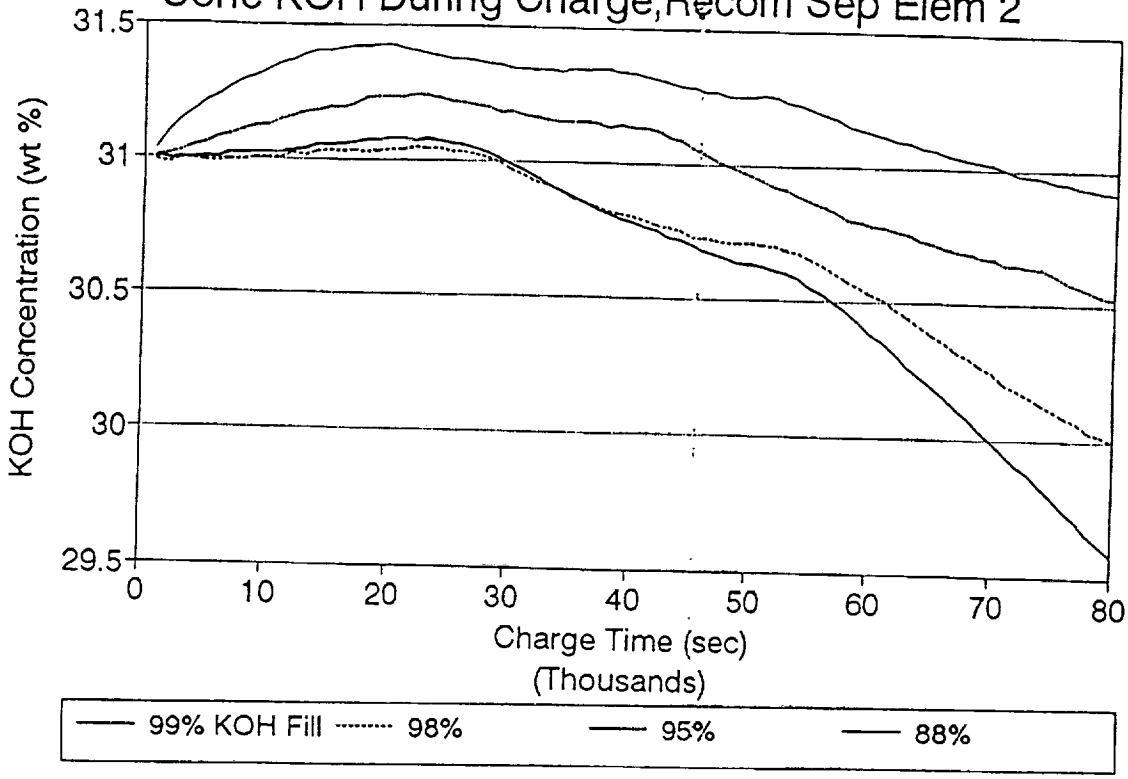

Fig. 17. Recirculating Stack NiH2 Cell
Conc KOH During Chg, Nickel Elem 15

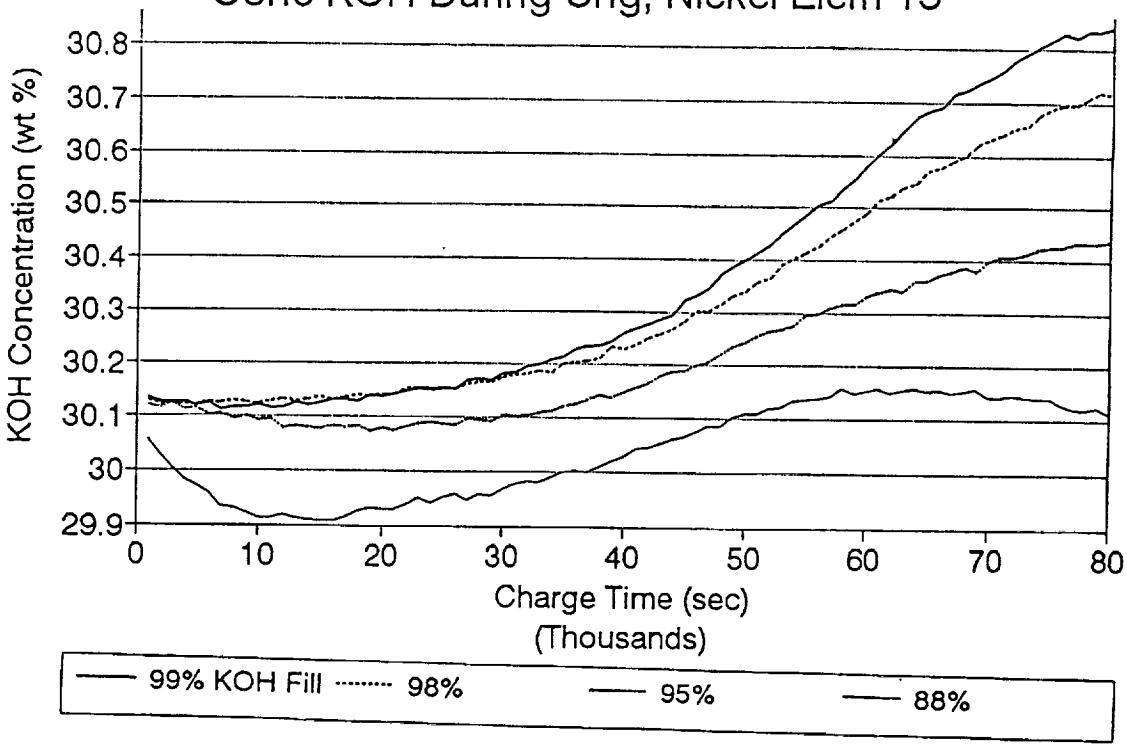

Fig. 18. Recirculating Stack NiH2 Cell
Conc KOH During Chg, Separator Elem 24

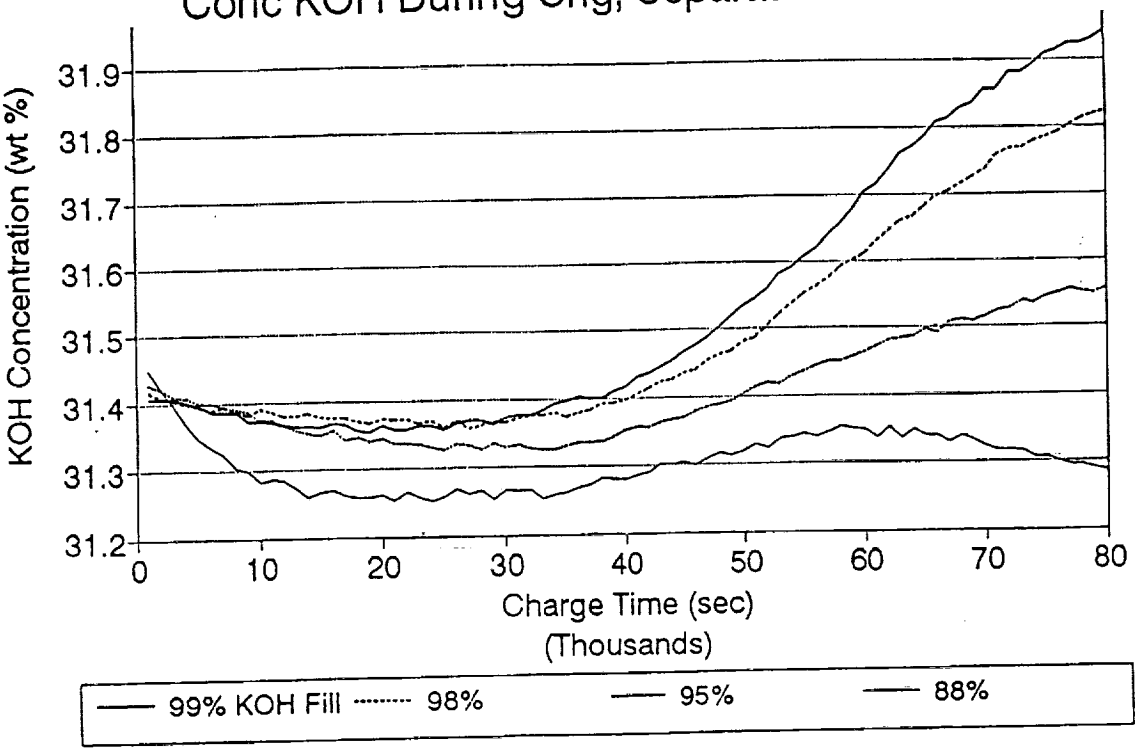

Fig. 19 . Recirculating Stack NiH2 Cell
Conc KOH During Charge, Pt/H2 Elem 34

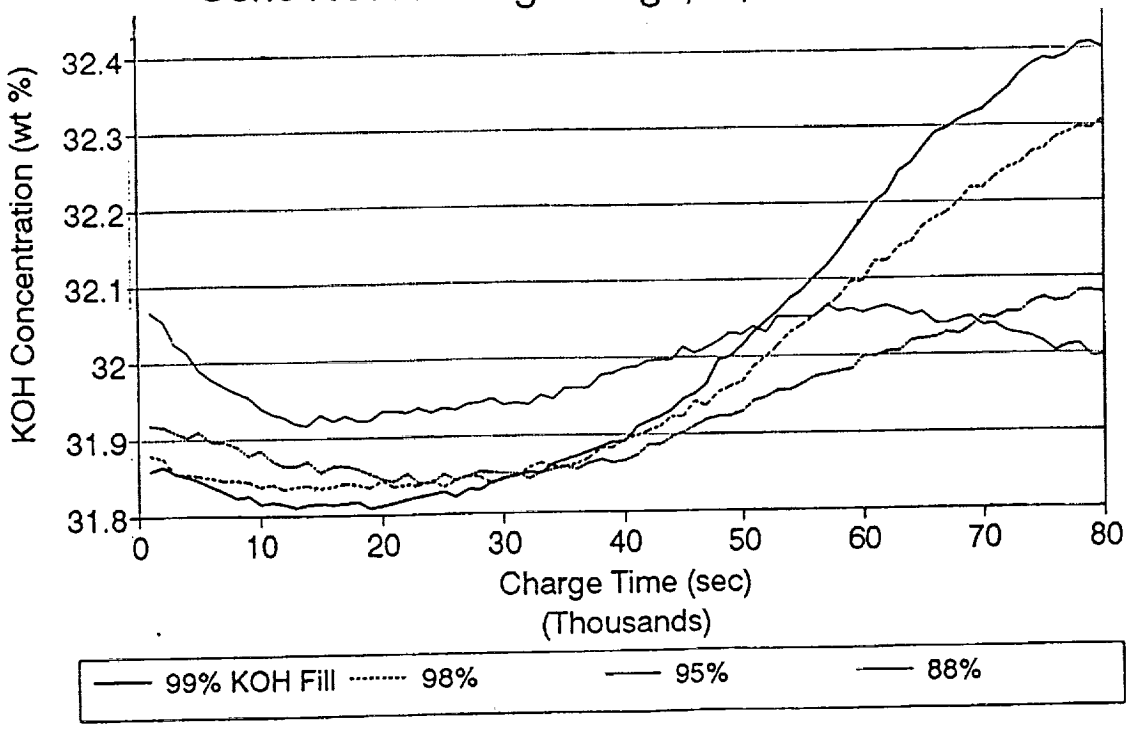

Fig. 20. Recirculating Stack NiH2 Cell
SOC in Ni Electrode at 10 Ks into Chg

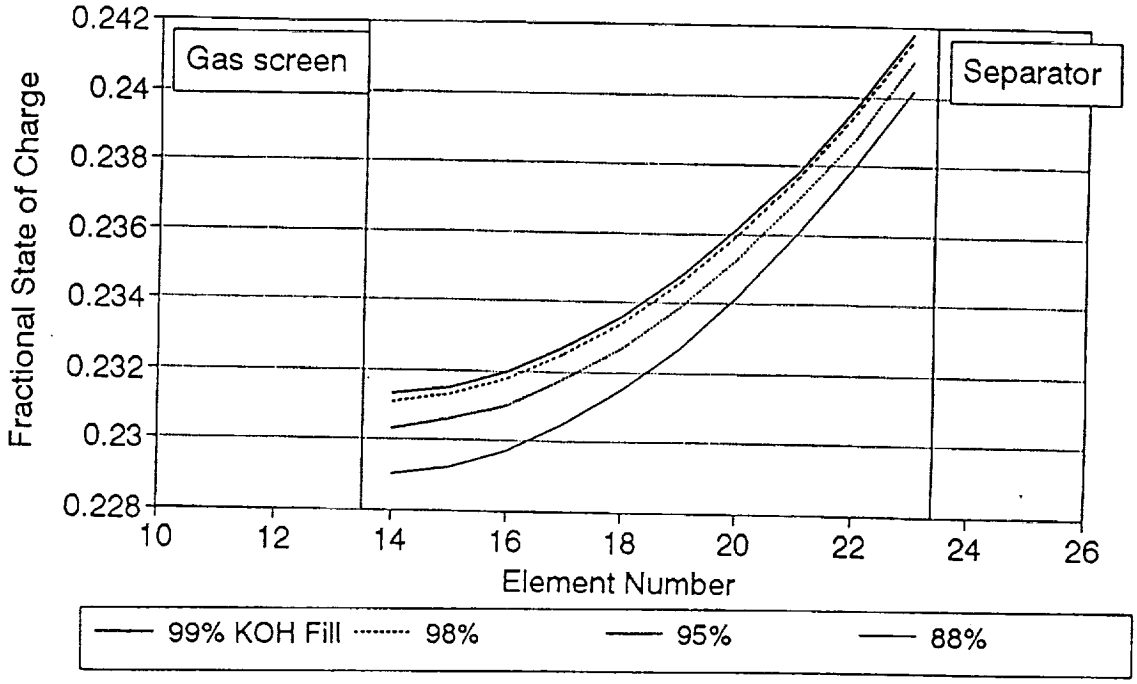

Fig. 21. Recirculating Stack NiH2 Cell
SOC in Ni Electrode at 80 Ks into Chg

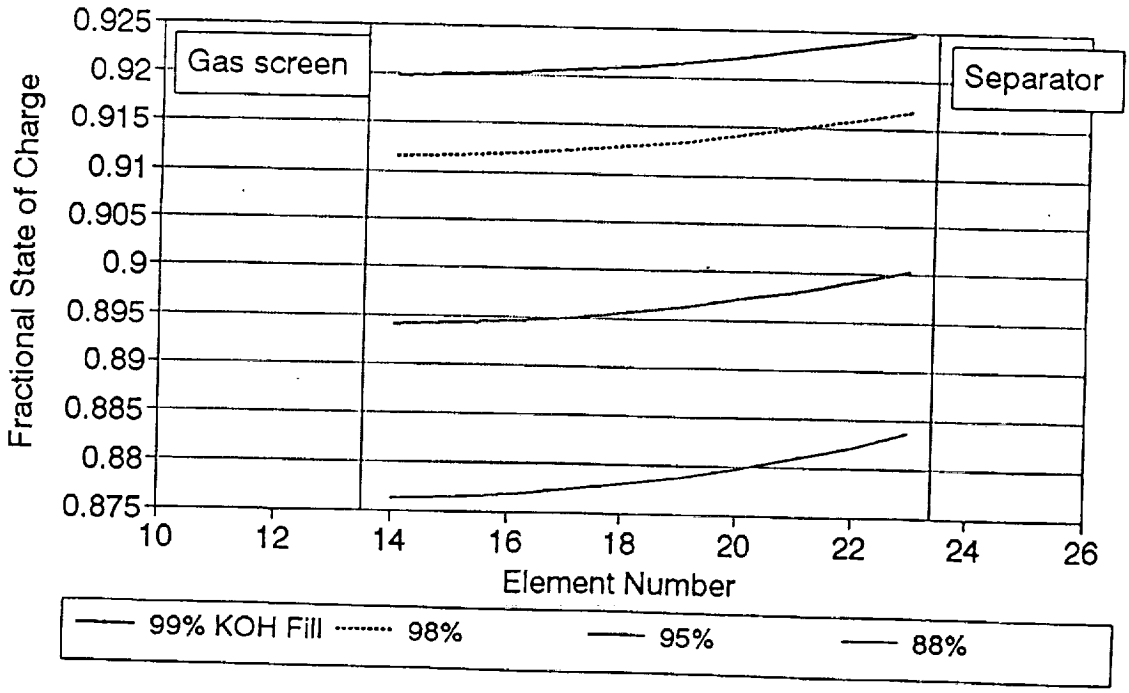

Fig. 22. Recirculating Stack NiH2 Cell
O2 Pressure 80Ks into Charge,Flooded GS

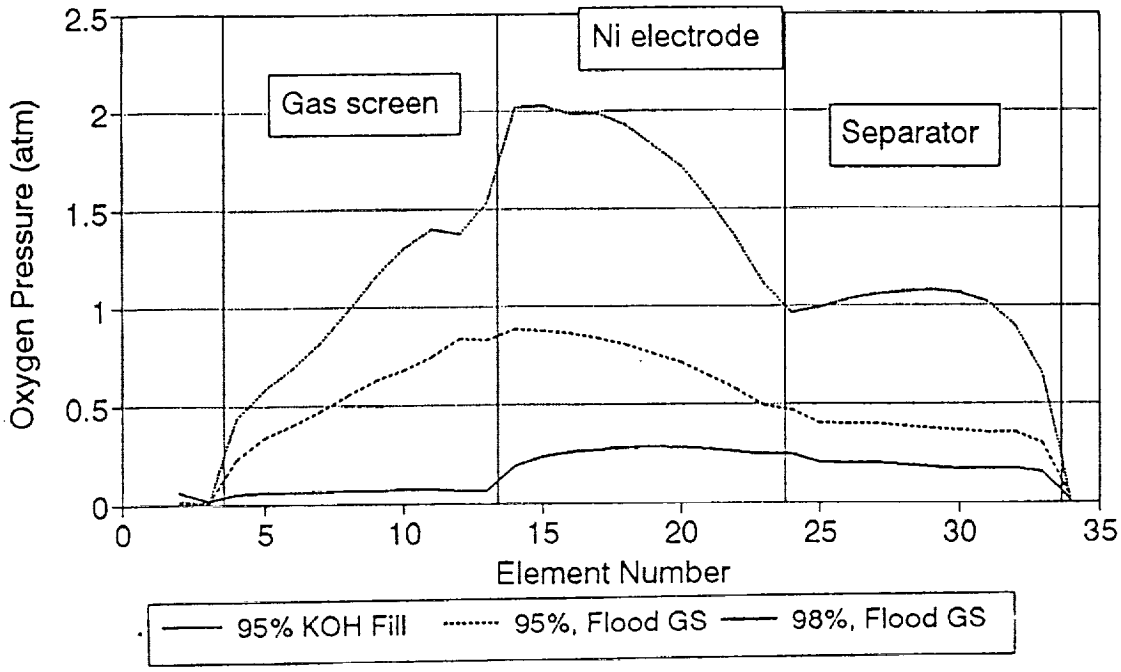

Fig. 23. Recirculating Stack NiH2 Cell
Stack Porosity 80Ks in Chg, Flooded GS

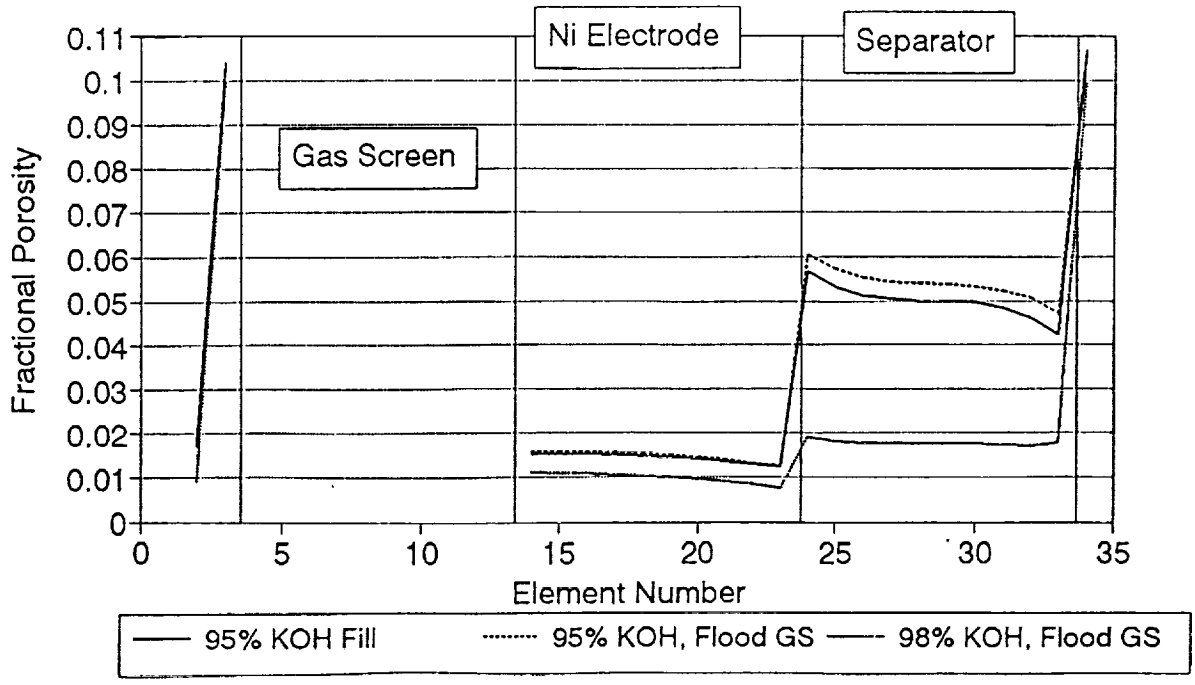

Fig. 24. Recirculating Stack NiH2 Cell
% KOH Conc. 80Ks in Charge, Flooded GS

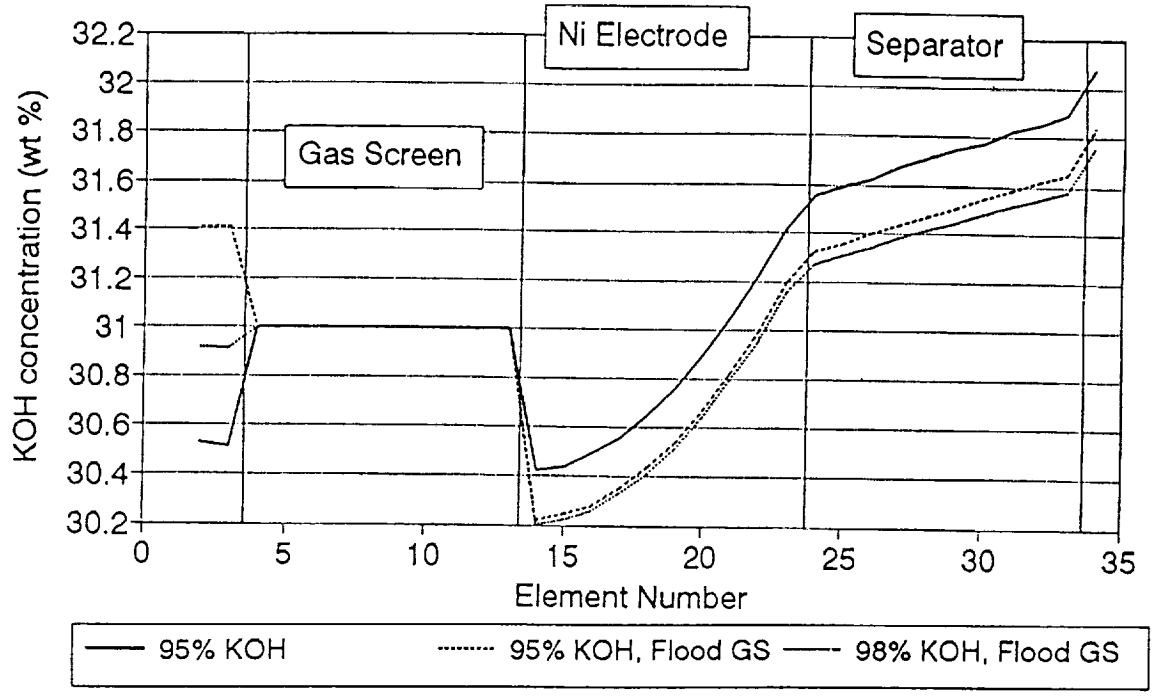

Fig. 25. Max Delta-P Across Stack
In recirc stack NiH2 cell, 80000 s chg

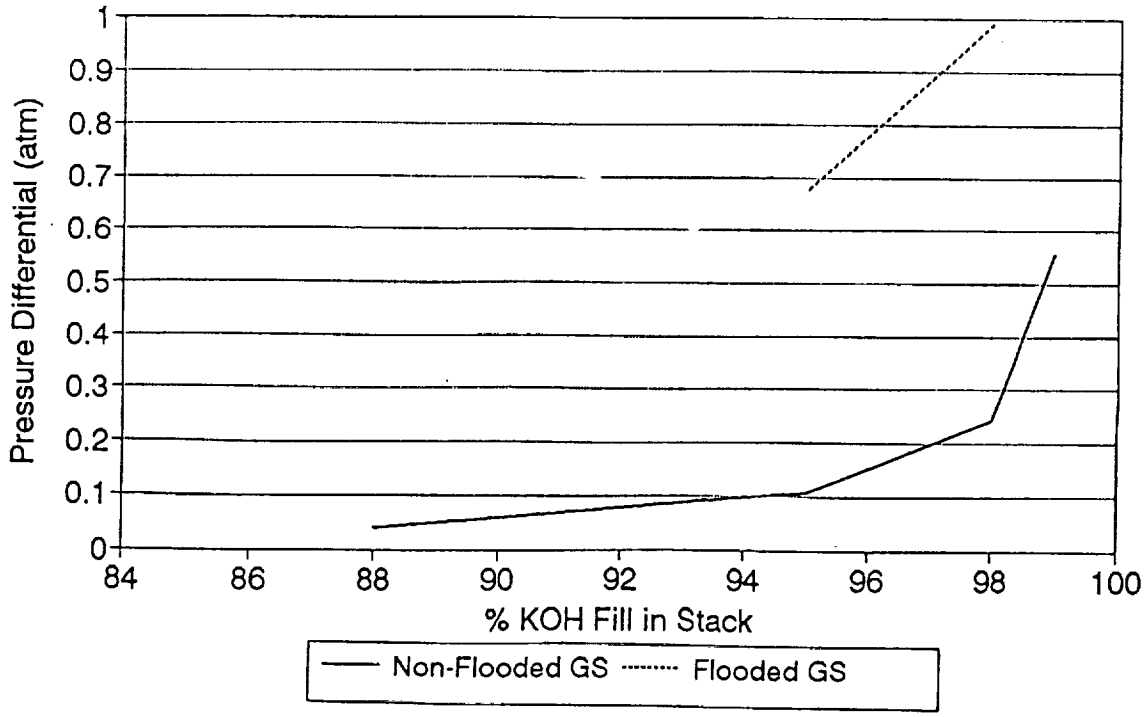

Fig. 26. Loading Profiles for Ni Electrodes
With Various Levels of Surface Loading

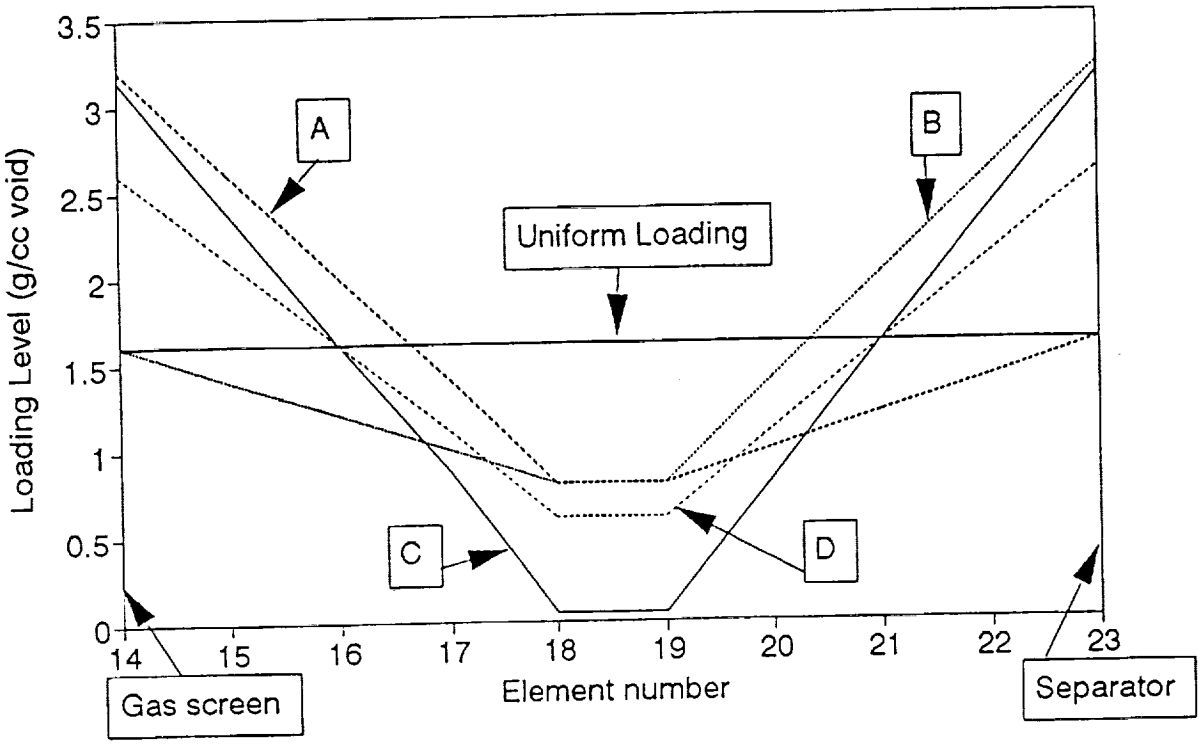

Fig 27. Oxygen Pressure Profile Through
Stack, 80,000 sec into recharge

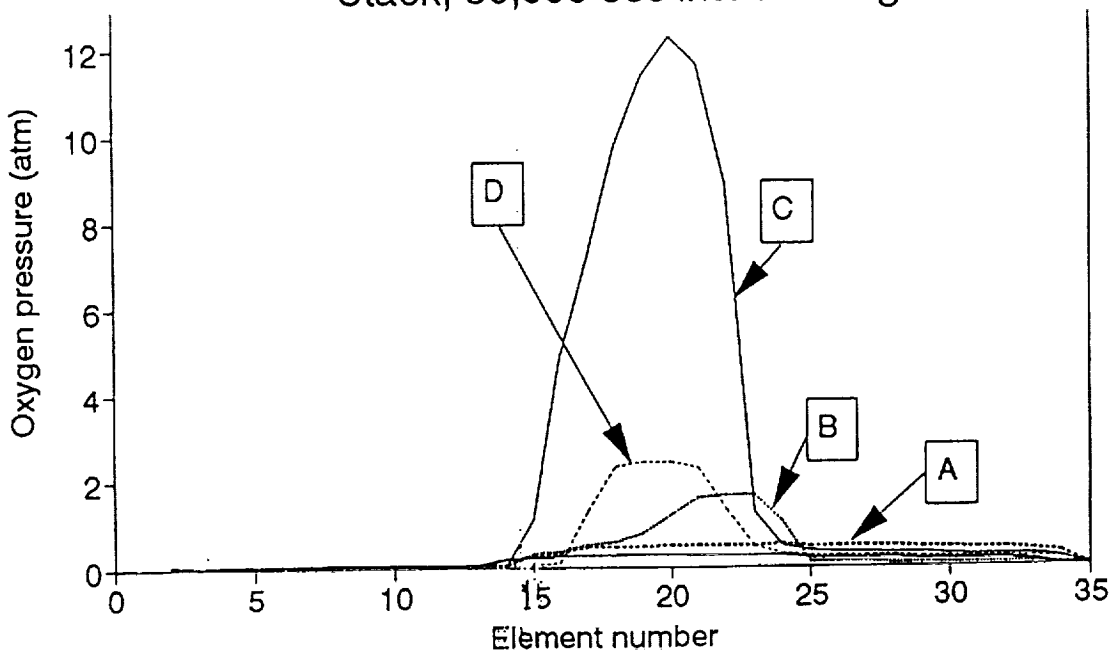

Fig 28. Total Pressure Profile Through Stack, 80,000 sec into recharge

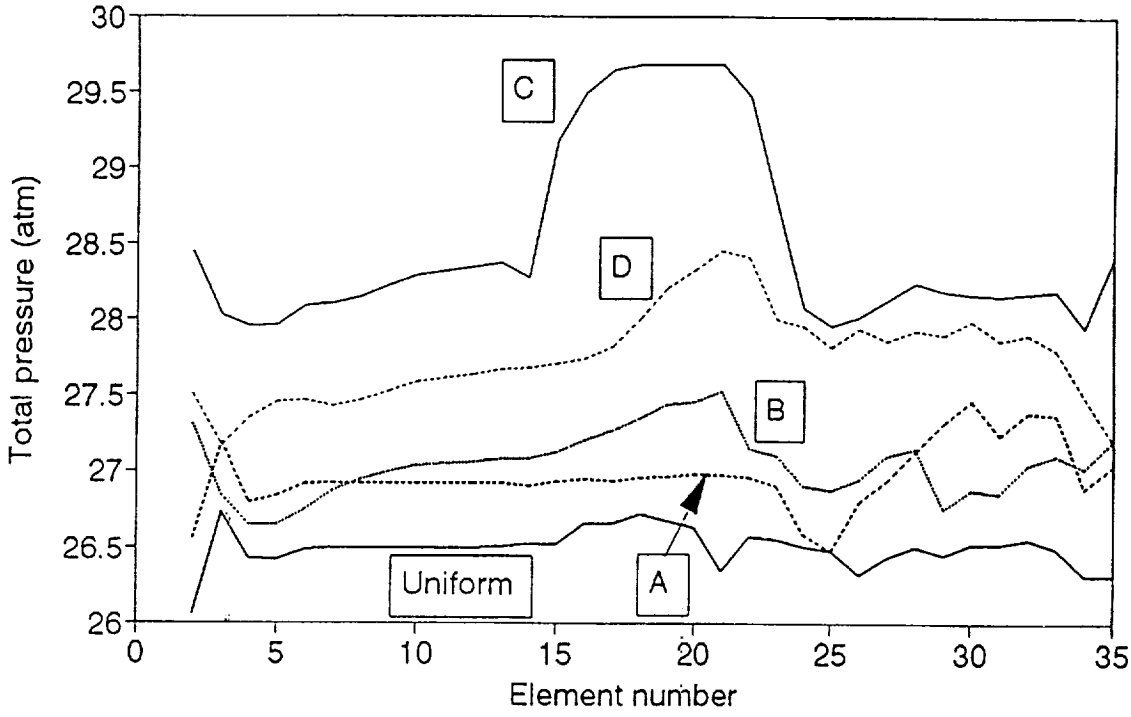

Fig 29. KOH Concentration Profile Through Stack, 80,000 sec into recharge

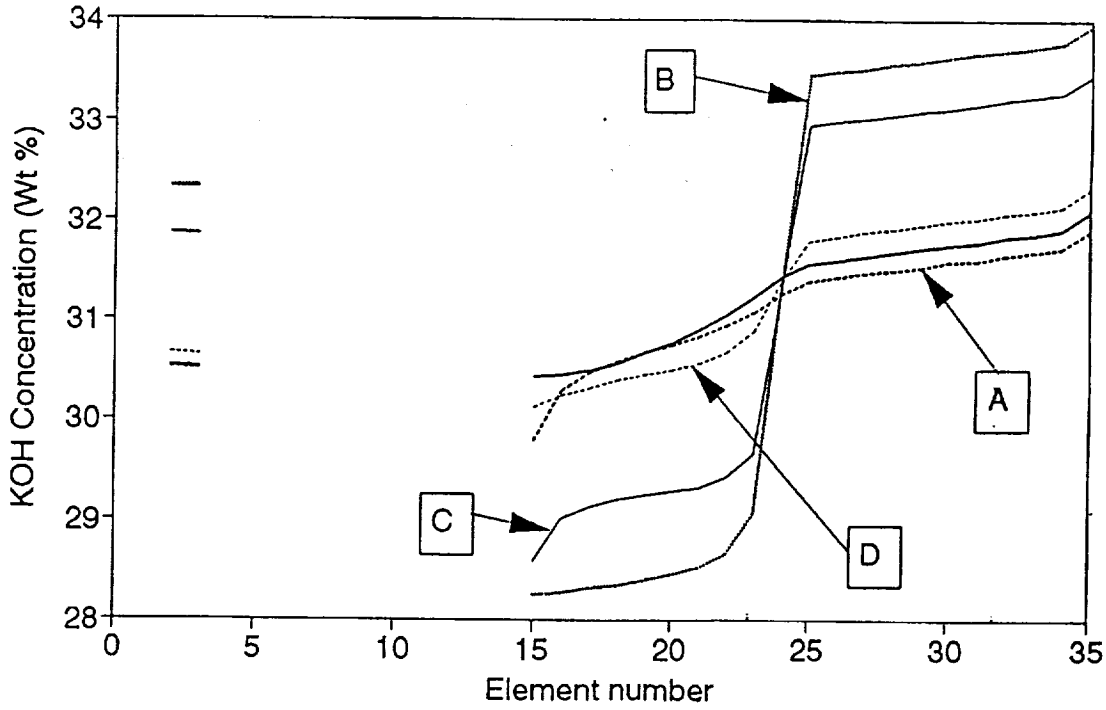

Figure 30. Oxygen Concentration
in Recirculating Stack NiH_2 Cell During Overcharge,
Uniform Loading @ 1.6 g/cc, 95% KOH Fill

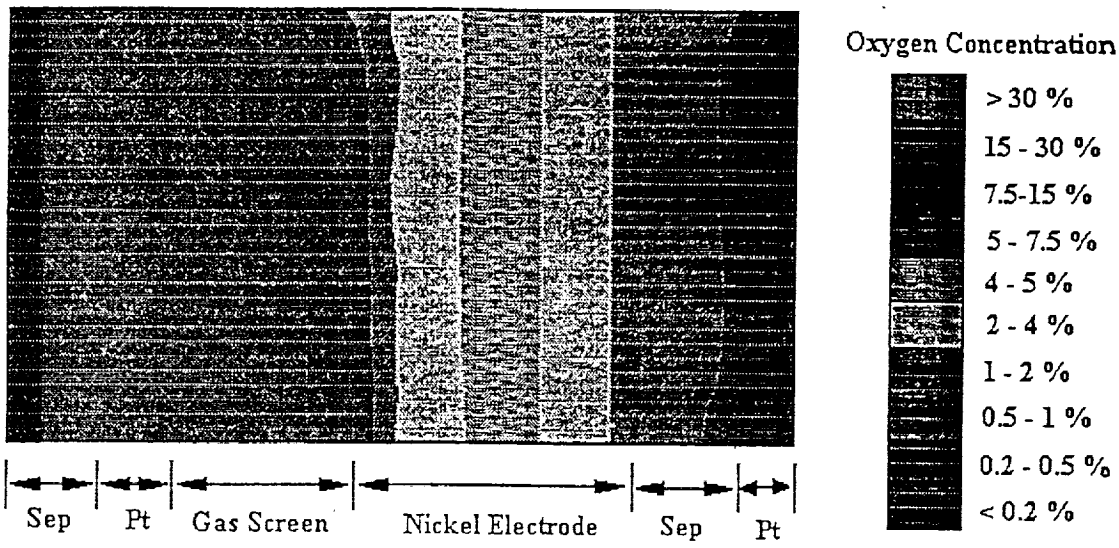

Figure 31. Oxygen Concentration Through a
Recirculating Stack NiH_2 Cell with surface loading
(3.1 g/cc void) in Overcharge

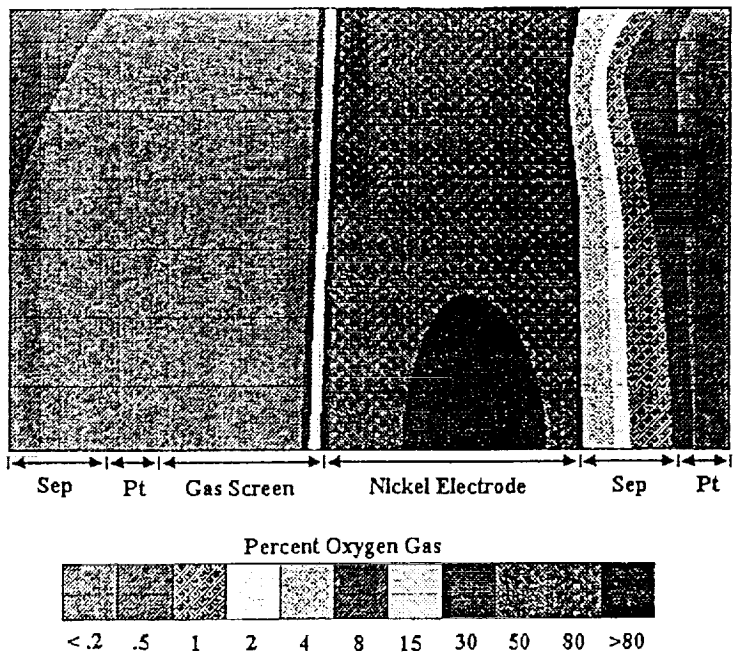

Figure 32. Oxygen Concentration in Recirculating Stack NiH_2 Cell with Surface Loading (3.1 g/ccv), and with surface crack on Gas screen side of Ni electrode

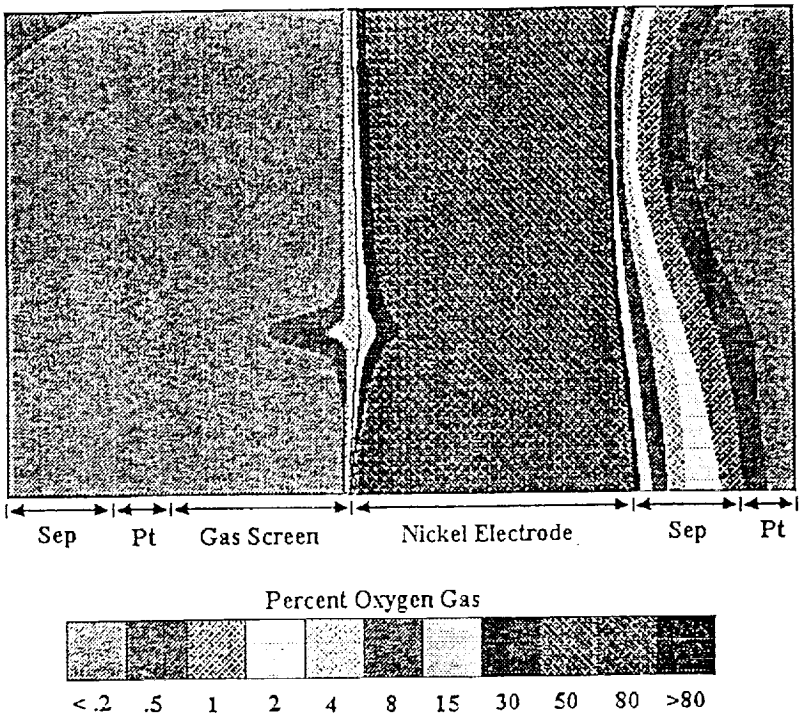

Figure 33. Oxygen Concentration in Recirculating Stack NiH_2 Cell with Surface Loading (3.1 g/ccv), and with surface crack on Separator side of Ni electrode.

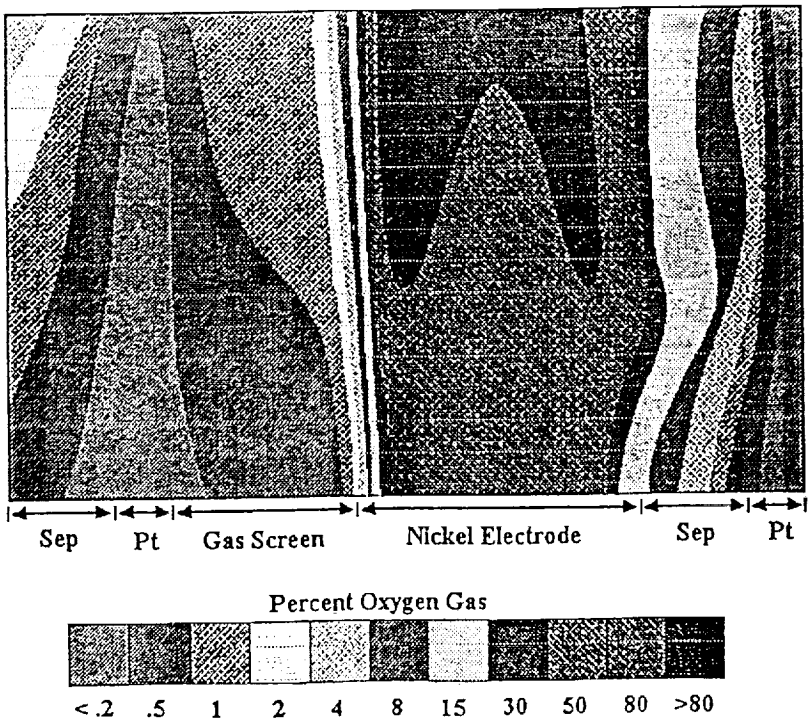

APPENDIX A

FILE FOR NICKEL HYDROGEN CELL MODEL -- RECIRCULATING STACK WITH WALL WICKS

Number of elements is	36	KOH diffusion coeff(xE+5)is	2.13
Number of interfaces is	55	Temperature (deg C) is	20.00
Number of circuit components is	52	Ni Loading level (g/ccv) is	1.60
Number of Electrochemical rxns is	3	Initial KOH percentage is	31.00
Ni electrode plaque porosity is	0.800	Initial Nickel KOH fill is	0.950
Separator solid porosity is	0.500	Initial separator KOH is	0.950
Pt electrode porosity is	0.500	Initial Platinum KOH fill	0.950
Wall wick porosity is	0.500	Initial Wall wick KOH is	0.950
Gas screen porosity is	0.900	Ni flat band potential is	-0.300
Ni electrode tortuosity is	2.00	Shottky I/V slope	10.000
Separator tortuosity is	1.20	Hydrogen diffusion coeff	7.800
Platinum electrode tortuosity	1.60	Total initial pressure(atm)	2.000
Wall wick tortuosity is	1.20	Initial beta-Ni SOC is	0.050

Electrochemical Reaction		Reversible Potential	Charge Rate const	Discharge Rate const	Charge Tafel	Discharge Tafel
Nickel-beta	1	0.490	0.1200	0.0020	77.00	77.00
Oxygen	2	0.400	0.1220	0.1220	52.00	52.00
Hydrogen	3	-0.827	0.0625	0.0625	78.00	78.00

Element Number	Element Type	Center Position (mm) X	Y	Z	mm Center to Edge X	Y	Z
1	5	1.0300	10.0500	0.0	1.03	0.05	5.0
2	2	0.1500	5.0000	0.0	0.15	5.0	5.0000
3	3	0.3800	5.0000	0.0	0.08	5.0	5.0000
4	4	0.4850	5.0000	0.0	0.025	5.0	5.0000
5	4	0.5350	5.0000	0.0	0.025	5.0	5.0000
6	4	0.5850	5.0000	0.0	0.025	5.0	5.0000
7	4	0.6350	5.0000	0.0	0.025	5.0	5.0000
8	4	0.6850	5.0000	0.0	0.025	5.0	5.0000
9	4	0.7350	5.0	0.0	0.025	5.0	5.0
10	4	0.785	5.0	0.0	0.025	5.0	5.0
11	4	0.835	5.0	0.0	0.025	5.0	5.0
12	4	0.885	5.0	0.0	0.025	5.0	5.0
13	4	0.935	5.0	0.0	0.025	5.0	5.0
14	1	1.000	5.0	0.0	0.04	5.0	5.0
15	1	1.08	5.0	0.0	0.04	5.0	5.0
16	1	1.16	5.0	0.0	0.04	5.0	5.0
17	1	1.24	5.0	0.0	0.04	5.0	5.0
18	1	1.32	5.0	0.0	0.04	5.0	5.0
19	1	1.40	5.0	0.0	0.04	5.0	5.0
20	1	1.48	5.0	0.0	0.04	5.0	5.0
21	1	1.56	5.0	0.0	0.04	5.0	5.0
22	1	1.64	5.0	0.0	0.04	5.0	5.0
23	1	1.72	5.0	0.0	0.04	5.0	5.0
24	2	1.775	5.0	0.0	0.015	5.0	5.0
25	2	1.805	5.0	0.0	0.015	5.0	5.0
26	2	1.835	5.0	0.0	0.015	5.0	5.0
27	2	1.865	5.0	0.0	0.015	5.0	5.0
28	2	1.895	5.0	0.0	0.015	5.0	5.0
29	2	1.925	5.0	0.0	0.015	5.0	5.0
30	2	1.955	5.0	0.0	0.015	5.0	5.0
31	2	1.985	5.0	0.0	0.015	5.0	5.0
32	2	2.015	5.0	0.0	0.015	5.0	5.0
33	2	2.045	5.0	0.0	0.015	5.0	5.0
34	3	2.140	5.0	0.0	0.08	5.0	5.0
35	0	4.220	5.0	0.0	2.00	5.0	5.0
36	0	3.340	-0.1	0.0	2.88	0.1	5.0

Interface Number	Interface Type	Element on A Side	Element on B side	First Loop	Second Loop	Third Loop
1	2	1	2	-36	0	0
2	2	2	3	-36	0	0
3	1	3	4	-36	0	0
4	0	4	5	-36	-46	0
5	0	5	6	-36	0	-47
6	0	6	7	-36	-48	0
7	0	7	8	-36	0	-49
8	0	8	9	-36	-50	0
9	0	9	10	-36	0	-51
10	0	10	11	-36	-52	0
11	0	11	12	-36	0	-53
12	0	12	13	-36	-54	0
13	1	13	14	-36	0	-55
14	2	14	15	-36	0	-55
15	2	15	16	-36	0	-55
16	2	16	17	-36	0	-55

17	2	17	18	-36	0	-55
18	2	18	19	-36	0	-55
19	2	19	20	-36	0	-55
20	2	20	21	-36	0	-55
21	2	21	22	-36	0	-55
22	2	22	23	-36	0	-55
23	2	23	24	-36	0	-55
24	2	24	25	0	-37	-55
25	2	25	26	-38	0	-55
26	2	26	27	0	-39	-55
27	2	27	28	-40	0	-55
28	2	28	29	0	-41	-55
29	2	29	30	-42	0	-55
30	2	30	31	0	-43	-55
31	2	31	32	-44	0	-55
32	2	32	33	0	-45	-55
33	2	33	34	0	0	-55
34	1	34	35	0	0	-55
35	0	35	36	0	0	-55
36	2	1	24	36	-37	0
37	2	1	25	-38	37	0
38	2	1	26	38	-39	0
39	2	1	27	-40	39	0
40	2	1	28	40	-41	0
41	2	1	29	-42	41	0
42	2	1	30	42	-43	0
43	2	1	31	-44	43	0
44	2	1	32	44	-45	0
45	2	1	33	0	45	0
46	0	4	36	0	46	0
47	0	5	36	0	-46	47
48	0	6	36	0	48	-47
49	0	7	36	0	-48	49
50	0	8	36	0	50	-49
51	0	9	36	0	-50	51
52	0	10	36	0	52	-51
53	0	11	36	0	-52	53
54	0	12	36	0	54	-53
55	0	13	36	0	-54	55

Entry component interface area is 0.00800 cm2, and distance is 0.50000 cm
Exit component interface area is 0.01200 cm2, and distance is 0.50000 cm

Component Number	Component Type	Inter Face	A-side Elem	B-Side Elem	A-Side Node	B-Side Node	Loop Eqs A	B	C	D
1	7	22	22	23	2	1	0	51	0	0
2	7	21	22	22	3	2	0	49	0	0
3	7	20	20	21	4	3	0	47	0	0
4	7	19	19	20	5	4	0	45	0	0
5	7	18	18	19	7	5	0	43	0	0
6	7	0	0	19	6	5	0	0	0	0
7	7	17	17	18	8	7	0	41	0	0
8	7	16	16	17	9	8	0	39	0	0
9	7	15	15	16	10	9	0	37	0	0
10	7	14	14	15	11	10	0	35	0	0
11	1	-1	14	14	11	12	-34	0	0	0
12	2	14	14	15	12	13	0	-35	0	0
13	2	15	15	16	13	14	0	-37	0	0
14	2	16	16	17	14	15	0	-39	0	0
15	2	17	17	18	15	16	0	-41	0	0
16	2	18	18	19	16	17	0	-43	0	0
17	2	19	19	20	17	18	0	-45	0	0
18	2	20	20	21	18	19	0	-47	0	0
19	2	21	21	22	19	20	0	-49	0	0
20	2	22	22	23	20	21	0	-51	0	0
21	2	23	23	24	21	22	0	0	0	0
22	2	24	24	25	22	23	0	0	0	0
23	2	25	25	26	23	24	0	0	0	0
24	2	26	26	27	24	25	0	0	0	0
25	2	27	27	28	25	26	0	0	0	0
26	2	28	28	29	26	27	0	0	0	0
27	2	29	29	30	27	28	0	0	0	0
28	2	30	30	31	28	29	0	0	0	0
29	2	31	31	32	29	30	0	0	0	0
30	2	32	32	33	30	31	0	0	0	0
31	2	33	33	34	31	32	0	0	0	0
32	3	-1	34	34	32	33	0	0	0	0
33	7	0	34	0	33	34	0	0	0	0
34	4	-1	14	14	11	12	34	-35	0	0
35	1	-1	15	15	10	13	-36	35	0	0
36	4	-1	15	15	10	13	36	-37	0	0

37	1	-1	16	16	9	14	-38	37	0	0
38	4	-1	16	16	9	14	38	-39	0	0
39	1	-1	17	17	8	15	-40	39	0	0
40	4	-1	17	17	8	15	40	-41	0	0
41	1	-1	18	18	7	16	-42	41	0	0
42	4	-1	18	18	7	16	42	-43	0	0
43	1	-1	19	19	5	17	-44	43	0	0
44	4	-1	19	19	5	17	44	-45	0	0
45	1	-1	20	20	4	18	-46	45	0	0
46	4	-1	20	20	4	18	46	-47	0	0
47	1	-1	21	21	3	19	-48	47	0	0
48	4	-1	21	21	3	19	48	-49	0	0
49	1	-1	22	22	2	20	-50	49	0	0
50	4	-1	22	22	2	20	50	-51	0	0
51	1	-1	23	23	1	21	-52	51	0	0
52	4	-1	23	23	1	21	52	0	0	0

The following program contains 1 steps

Program Step	Step Type	Current (ma)	Time(sec)/ V-Limit	Save Time Interval	Calculation Time Interval
1	1	2.0000	80000.0	1000.0	2.000

APPENDIX B.

2 D NiH2 CELL MODEL W/SURFACE CRACK,
RECIRCULATING STACK WITH WALL WICKS

Number of elements is	45	KOH diffusion coeff(xE+5)is	2.13
Number of interfaces is	83	Temperature (deg C) is	20.00
Number of circuit components is	95	Ni Loading level (g/ccv) is	1.60
Number of Electrochemical rxns is	3	Initial KOH percentage is	31.00
Ni electrode plaque porosity is	0.800	Initial Nickel KOH fill is	0.950
Separator solid porosity is	0.500	Initial separator KOH is	0.950
Pt electrode porosity is	0.500	Initial Platinum KOH fill	0.950
Wall wick porosity is	0.500	Initial Wall wick KOH is	0.950
Gas screen porosity is	0.900	Ni flat band potential is	-0.300
Ni electrode tortuosity is	2.00	Shottky I/V slope	10.000
Separator tortuosity is	1.20	Hydrogen diffusion coeff	7.800
Platinum electrode tortuosity	1.60	Total initial pressure(atm)	25.000
Wall wick tortuosity is	1.20	Initial beta-Ni SOC is	0.900

Electrochemical Reaction		Reversible Potential	Charge Rate const	Discharge Rate const	Charge Tafel	Discharge Tafel
Nickel-beta	1	0.490	0.1200	0.0020	77.00	77.00
Oxygen	2	0.400	0.1220	0.1220	52.00	52.00
Hydrogen	3	-0.827	0.0625	0.0625	78.00	78.00

Element Number	Element Type	Center Position (mm) X	Y	Z	mm Center to Edge X	Y	Z
1	3	0.380	5.0	0.0	0.08	5.0	5.0
2	2	0.1500	5.0000	0.0	0.15	5.0	5.0000
3	5	1.0350	10.0500	0.0	1.035	0.05	5.0
4	2	2.0200	8.3500	0.0	0.05	1.65	5.0000
5	2	1.9200	8.3500	0.0	0.05	1.65	5.0000
6	2	1.8200	8.3500	0.0	0.05	1.65	5.0000
7	1	1.6700	8.3500	0.0	0.100	1.65	5.0000
8	1	1.3700	8.3500	0.0	0.200	1.65	5.0000
9	1	1.0700	8.3500	0.0	0.100	1.65	5.0000
10	4	0.8850	8.35	0.0	0.085	1.65	5.0
11	4	0.715	8.35	0.0	0.085	1.65	5.0
12	4	0.545	8.35	0.0	0.085	1.65	5.0
13	4	0.545	5.05	0.0	0.085	1.65	5.0
14	4	0.715	5.05	0.0	0.085	1.65	5.0
15	4	0.885	5.05	0.0	0.085	1.65	5.0
16	1	1.070	5.05	0.0	0.100	1.65	5.0
17	1	1.370	5.05	0.0	0.200	1.65	5.0
18	1	1.670	5.05	0.0	0.100	1.65	5.0
19	2	1.820	5.05	0.0	0.05	1.65	5.0
20	2	1.920	5.05	0.0	0.05	1.65	5.0
21	2	2.020	5.05	0.0	0.05	1.65	5.0
22	2	2.020	3.35	0.0	0.05	0.05	5.0
23	2	1.920	3.35	0.0	0.05	0.05	5.0
24	2	1.820	3.35	0.0	0.05	0.05	5.0
25	1	1.670	3.35	0.0	0.100	0.05	5.0
26	1	1.370	3.35	0.0	0.200	0.05	5.0
27	1	1.070	3.35	0.0	0.100	0.05	5.0
28	4	0.885	3.35	0.0	0.085	0.05	5.0
29	4	0.715	3.35	0.0	0.085	0.05	5.0
30	4	0.545	3.35	0.0	0.085	0.05	5.0
31	4	0.545	1.65	0.0	0.085	1.65	5.0
32	4	0.715	1.65	0.0	0.085	1.65	5.0

33	4	0.885	1.65	0.0	0.085	1.65	5.0
34	1	1.070	1.65	0.0	0.100	1.65	5.0
35	1	1.370	1.65	0.0	0.200	1.65	5.0
36	1	1.670	1.65	0.0	0.100	1.65	5.0
37	2	1.820	1.65	0.0	0.05	1.65	5.0
38	2	1.920	1.65	0.0	0.05	1.65	5.0
39	2	2.020	1.65	0.0	0.05	1.65	5.0
40	3	2.150	1.65	0.0	0.08	1.65	5.0
41	3	2.15	3.35	0.0	0.08	0.05	5.0
42	3	2.15	5.05	0.0	0.08	1.65	5.0
43	3	2.15	8.35	0.0	0.08	1.65	5.0
44	0	4.230	5.00	0.0	2.00	5.0	5.0
45	0	3.345	-0.10	0.0	2.885	0.10	5.0

Interface Number	Interface Type	Element on A Side	Element on B side	First Loop	Second Loop	Third Loop
1	2	2	1	48	0	0
2	2	3	2	48	0	0
3	2	3	4	-46	0	0
4	2	5	4	46	59	0
5	2	6	5	0	47	58
6	2	7	6	48	57	0
7	2	8	7	48	0	56
8	2	9	8	48	55	0
9	1	10	9	48	0	54
10	0	11	10	48	53	0
11	0	12	11	48	0	52
12	0	12	13	0	-49	-52
13	0	13	14	0	-61	-52
14	0	14	15	-62	-53	0
15	1	15	16	0	-63	-54
16	2	16	17	-64	-55	0
17	2	17	18	0	-65	-56
18	2	18	19	-66	-57	0
19	2	19	20	0	-67	-58
20	2	20	21	-68	-59	0
21	2	21	22	-68	-78	0
22	2	23	22	68	76	0
23	2	24	23	75	67	0
24	2	25	24	66	74	0
25	2	26	25	73	65	0
26	2	27	26	64	72	0
27	1	28	27	71	63	0
28	0	29	28	62	70	0
29	0	30	29	0	61	69
30	0	30	31	0	-51	-69
31	0	31	32	0	-45	-69
32	0	32	33	-83	-70	0
33	1	33	34	-71	0	-82
34	2	34	35	0	-72	-82
35	2	35	36	-73	0	-82
36	2	36	37	0	-74	-82
37	2	37	38	-75	0	-82
38	2	38	39	0	-76	-82
39	2	39	40	-77	0	-82
40	2	41	40	77	81	0
41	2	42	41	80	78	0
42	2	43	42	0	79	60
43	1	43	44	0	-79	0
44	0	44	45	0	0	-82
45	0	31	45	0	45	0
46	2	3	5	46	-47	0
47	2	3	6	-48	47	0
48	1	1	12	48	-49	0
49	1	1	13	-50	49	0
50	1	1	30	50	-51	0
51	1	1	31	0	51	0
52	0	11	14	0	-53	52
53	0	10	15	0	53	-54
54	2	9	16	0	-55	54
55	2	8	17	0	55	-56
56	2	7	18	0	-57	56
57	2	6	19	0	57	-58
58	2	5	20	0	-59	58
59	2	4	21	0	59	-60
60	2	4	43	0	0	60
61	0	13	30	-50	61	0
62	0	14	29	62	-61	0
63	0	15	28	-62	63	0
64	2	16	27	64	-63	0

65	2	17	26	-64	65	0
66	2	18	25	66	-65	0
67	2	19	24	-66	67	0
68	2	20	23	68	-67	0
69	0	29	32	0	-70	69
70	0	28	33	-71	70	0
71	2	27	34	71	-72	0
72	2	26	35	-73	72	0
73	2	25	36	73	-74	0
74	2	24	37	-75	74	0
75	2	23	38	75	-76	0
76	2	22	39	-77	76	0
77	2	22	41	77	-78	0
78	2	21	42	0	78	-60
79	1	42	44	-80	79	0
80	1	41	44	80	-81	0
81	1	40	44	0	81	-82
82	0	33	45	-83	0	82
83	0	32	45	83	-45	0

Entry component interface area is 0.04000 cm2, and distance is 0.12500 cm
Exit component interface area is 0.01600 cm2, and distance is 0.12500 cm

Component Number	Component Type	Inter Face	A-side Elem	B-Side Elem	A-Side Node	B-Side Node	Loop Equations A	B	C	D
1	7	0	0	9	1	2	0	0	0	0
2	7	8	9	8	2	3	0	49	-69	0
3	7	7	8	7	3	4	50	-70	0	0
4	7	56	7	18	4	5	0	-70	51	0
5	7	17	17	18	6	5	0	70	72	0
6	7	16	16	17	7	6	71	0	69	0
7	7	64	16	27	7	8	-71	-47	0	0
8	7	26	27	26	8	9	-71	-73	0	0
9	7	25	26	25	9	10	0	0	-72	-74
10	7	73	25	36	10	11	0	53	0	-74
11	7	35	35	36	12	11	-54	0	0	74
12	7	34	34	35	13	12	0	73	0	0
13	1	-1	34	34	13	14	-46	-57	0	0
14	2	71	27	34	15	14	46	77	0	0
15	2	64	16	27	16	15	76	47	0	0
16	2	54	9	16	17	16	48	0	75	0
17	2	8	9	8	17	18	0	-49	-75	0
18	2	55	8	17	18	19	0	-78	-75	0
19	2	65	17	26	19	20	-76	56	-79	0
20	2	72	26	35	20	21	0	-77	55	-80
21	2	35	35	36	21	22	54	0	0	-80
22	2	73	25	36	23	22	83	-53	0	80
23	2	66	18	25	24	23	-52	82	79	0
24	2	56	7	18	25	24	81	78	-51	0
25	2	6	7	6	25	26	-81	0	0	0
26	2	57	6	19	26	27	-81	-84	0	0
27	2	67	19	24	27	28	-85	-82	0	0
28	2	74	24	37	28	29	-83	-86	0	0
29	2	37	37	38	29	30	0	-86	0	0
30	2	75	23	38	31	30	89	86	0	0
31	2	68	20	23	32	31	85	88	0	0
32	2	58	5	20	33	32	87	84	0	0
33	2	4	5	4	33	34	-87	0	0	0
34	2	59	4	21	34	35	-87	-90	0	0
35	2	21	21	22	35	36	-91	-88	0	0
36	2	76	22	39	36	37	-89	-92	0	0
37	2	39	39	40	37	38	0	-92	0	0
38	2	40	41	40	39	38	95	92	0	0
39	2	41	42	41	40	39	91	-94	0	0
40	2	42	43	42	41	40	93	90	0	0
41	3	-1	43	43	41	42	-93	0	0	0
42	7	42	43	42	42	43	-93	0	0	0
43	7	41	42	41	43	44	0	-94	0	0
44	7	40	41	40	44	45	-95	0	0	0
45	7	0	40	0	45	46	0	0	0	0
46	1	-1	27	27	8	15	46	-47	-58	0
47	1	-1	16	16	7	16	-48	47	-59	0
48	1	-1	9	9	2	17	48	-49	-60	0
49	1	-1	8	8	3	18	-50	49	-61	0
50	1	-1	7	7	4	25	50	-62	-51	0
51	1	-1	18	18	5	24	-52	-63	51	0
52	1	-1	25	25	10	23	52	-53	-64	0
53	1	-1	36	36	11	22	-54	53	-65	0
54	1	-1	35	35	12	21	54	-66	-55	0

55	1	-1	26	26	9	20	-67	-56	55	0
56	1	-1	17	17	6	19	-68	56	0	0
57	4	-1	34	34	13	14	0	57	0	0
58	4	-1	27	27	8	15	0	0	58	0
59	4	-1	16	16	7	16	0	0	59	0
60	4	-1	9	9	2	17	0	0	60	0
61	4	-1	8	8	3	18	0	0	61	0
62	4	-1	7	7	4	25	0	62	0	0
63	4	-1	18	18	5	24	0	63	0	0
64	4	-1	25	25	10	23	0	0	64	0
65	4	-1	36	36	11	22	0	0	65	0
66	4	-1	35	35	12	21	0	66	0	0
67	4	-1	26	26	9	20	67	0	0	0
68	4	-1	17	17	6	19	68	0	0	0
69	7	54	9	16	2	7	-48	0	69	0
70	7	55	8	17	3	6	0	70	-69	0
71	7	65	17	26	6	9	71	-56	-72	0
72	7	66	18	25	5	10	52	0	72	0
73	7	71	27	34	8	13	-46	73	0	0
74	7	72	26	35	9	12	0	-73	-55	74
75	2	16	16	17	16	19	-76	0	75	0
76	2	26	27	26	15	20	76	-77	0	0
77	2	34	34	35	14	21	0	77	0	0
78	2	7	8	7	18	25	-50	78	0	0
79	2	17	17	18	19	24	0	-78	79	0
80	2	25	26	25	20	23	0	0	-79	80
81	2	18	18	19	24	27	81	-82	0	0
82	2	24	25	24	23	28	-83	82	0	0
83	2	36	36	37	22	29	83	0	0	0
84	2	5	6	5	26	33	0	84	0	0
85	2	19	19	20	27	32	85	-84	0	0
86	2	23	24	23	28	31	-85	86	0	0
87	2	20	20	21	32	35	87	-88	0	0
88	2	22	23	22	31	36	-89	88	0	0
89	2	38	38	39	30	37	89	0	0	0
90	2	60	4	43	34	41	0	90	0	0
91	2	78	21	42	35	40	91	-90	0	0
92	2	77	22	41	36	39	-91	92	0	0
93	3	-1	42	42	40	43	93	-94	0	0
94	3	-1	41	41	39	44	-95	94	0	0
95	3	-1	40	40	38	45	95	0	0	0

The following program contains 1 steps

Program Step	Step Type	Current (ma)	Time(sec)/ V-Limit	Save Time Interval	Calculation Time Interval
1	1	2.0000	80000.0	1000.0	2.000

THERMAL MODELING OF NIH2 BATTERIES

Agnes PONTHUS (SAFT) and Alain ALEXANDRE (TSR)

1993 NASA AEROSPACE BATTERY WORKSHOP
U'S SPACE AND ROCKET CENTER
HUNTSVILLE AL
NOVEMBER 16–18, 1993

SAFT
ADVANCED BATTERIES

THERMAL MODELING OF NIH2 BATTERIES

TABLE OF CONTENTS

1 – NIH2 BATTERY MISSION AND ENVIRONMENT

2 – NIH2 CELL HEAT DISSIPATION

- 2–1 DISCHARGE
- 2–2 CHARGE – TRICKLE CHARGE

3 – NODAL SOFTWARE

- 3–1 THERMAL ANALYSER ESACAP
- 3–2 INTEGRATING GEAR METHOD

4 – MODEL DEVELOPMENT GENERAL PHILOSOPHY

5 – NIH2 BATTERY MODEL DEVELOPMENT

- 5–1 AT COUPLE LEVEL
- 5–2 AT CELL LEVEL
- 5–3 AT DIODES LEVEL
- 5–4 AT BATTERY BASEPLATE LEVEL
- 5–5 BATTERY COMPLETE MODEL

6 – NIH2 EXPERIMENTAL DEVELOPMENTS

7 – CONCLUSION

SAFT
ADVANCED BATTERIES

THERMAL MODELING OF NIH2 BATTERIES

1 – NIH2 BATTERY MISSION AND ENVIRONMENT

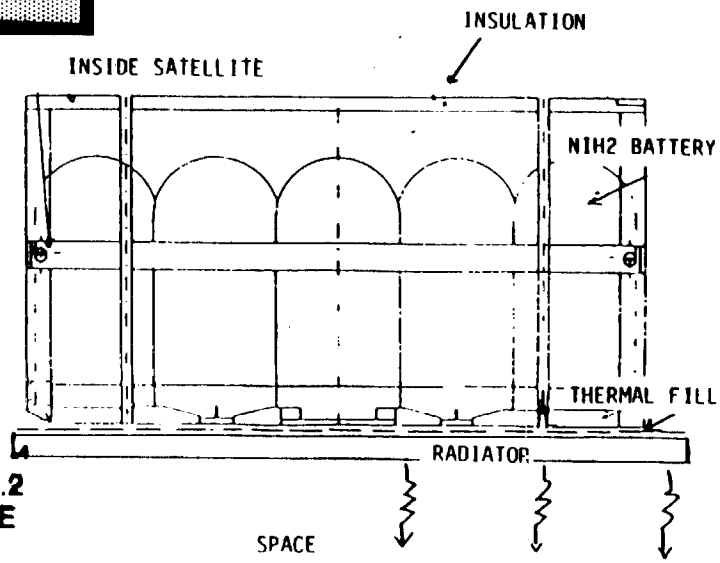

IN GENERAL, GEOSTATIONARY AND LOW ORBIT SATELLITES :

- PRELAUNCH OPERATIONS
- LAUNCH AND TRANSFER ORBIT
- ECLIPSES
- PEAK DISCHARGE DURING SUNLIGHT

FOR THERMAL STUDIES, GEO MAXIMUM ECLIPSE PERIOD WITH :

- C/2 TO C/1.5 DISCHARGE CURRENT DURING 1.2 HOUR
- C/20 TO C/10 CHARGE CURRENT WITH RECHARGE FACTOR OF 1.1 TO 1.2
- C/100 TRICKLE CHARGE CURRENT TO COMPLETE THE 24 HOURS CYCLE

THERMAL OPERATING CONDITIONS :

- TEMPERATURE RANGE : $-5°C < T < +25°C$
- TEMPERATURE DIFFERENCE BETWEEN TWO POINTS OF THE ELECTRODE STACK < 6°C
- TEMPERATURE DIFFERENCE BETWEEN STACK AND CELL WALL < 12°C
- TEMPERATURE DIFFERENCE BETWEEN TWO IDENTICAL POINTS OF TWO CELLS OF THE BATTERY < 9°C

SAFT
ADVANCED BATTERIES

THERMAL MODELING OF NIH2 BATTERIES

2– NIH2 CELL HEAT DISSIPATION

2.1– DISCHARGE

HEAT DISSIPATION FORMULATION :

$PD = ID\ (U0 - UD)$ WITH PD : HEAT DISSIPATION IN DISCHARGE (W)
ID : DISCHARGE CURRENT (A)
UD : DELIVERED CELL VOLTAGE (V)
U0 : THERMO–NEUTRAL POTENTAL (V)

$UD = u - R\ ID^2$ WITH u : VOLTAGE AT COUPLE LEVEL (V)
R : NICKEL TABS AND OUTLET RESISTANCE (mOHM)

$PD = PSTACK + R\ ID^2$ WITH PSTACK = ID (U0 – u) : HEAT DISSIPATION IN THE STACK (W)

THERMO–NEUTRAL POTENTIAL (U0) :

GENERAL ADMITTED VALUE : 1.51 V

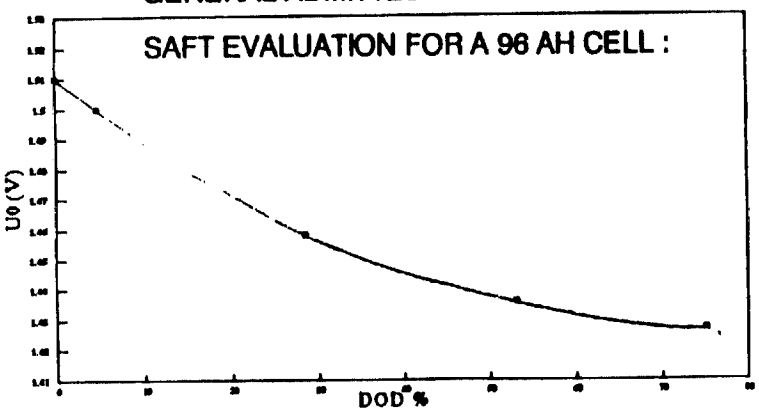

EXAMPLES OF HEAT DISSIPATION (AVERAGE) :

	96 AH	64 AH
PD :	12	10.6
P STACK :	7.7	8.2
R :	1.55	1.7
ID :	52.5	37.7

SAFT
ADVANCED BATTERIES

THERMAL MODELING OF NIH2 BATTERIES

2– NIH2 CELL HEAT DISSIPATION

2.2– CHARGE & TRICKLE

FORMULATION OF HEAT DISSIPATION IN CHARGE :

HEAT DISSIPATION HAPPENS AT END OF CHARGE AND IS LINKED TO EXOTHERMIC REACTIONS IN THE STACK

FORMULATION RESULTS FROM ANALYSIS OF :
- ENERGETIC BALANCE OVER THE CYCLE
- CELL VOLTAGE PROFILE AT END OF CHARGE

ENERGETIC BALANCE :

$QC = Ec - Ed - Qd$ WITH
- Qc : THERMAL ENERGY LOST IN CHARGE (JOULE)
- Ec : ELECTRICAL ENERGY INPUT IN CHARGE (JOULE)
- Ed : ELECTRICAL ENERGY OUTPUT IN DISCHARGE (JOULE)
- Qd : THERMAL ENERGY LOST IN DISCHARGE (JOULE)

CORRELATION HAVE BEEN ESTABLISHED FOR SAFT 96AH CELL AND 64 AH BATTERY, FOR C/10 CHARGE AND K FACTOR OF 1.2 AND 1.1 RESPECTIVELY

FORMULATION OF HEAT DISSIPATION IN TRICKLE CHARGE :

$P = Ut\ It$: ELECTRICAL ENERGY INPUT = HEAT DISSIPATION

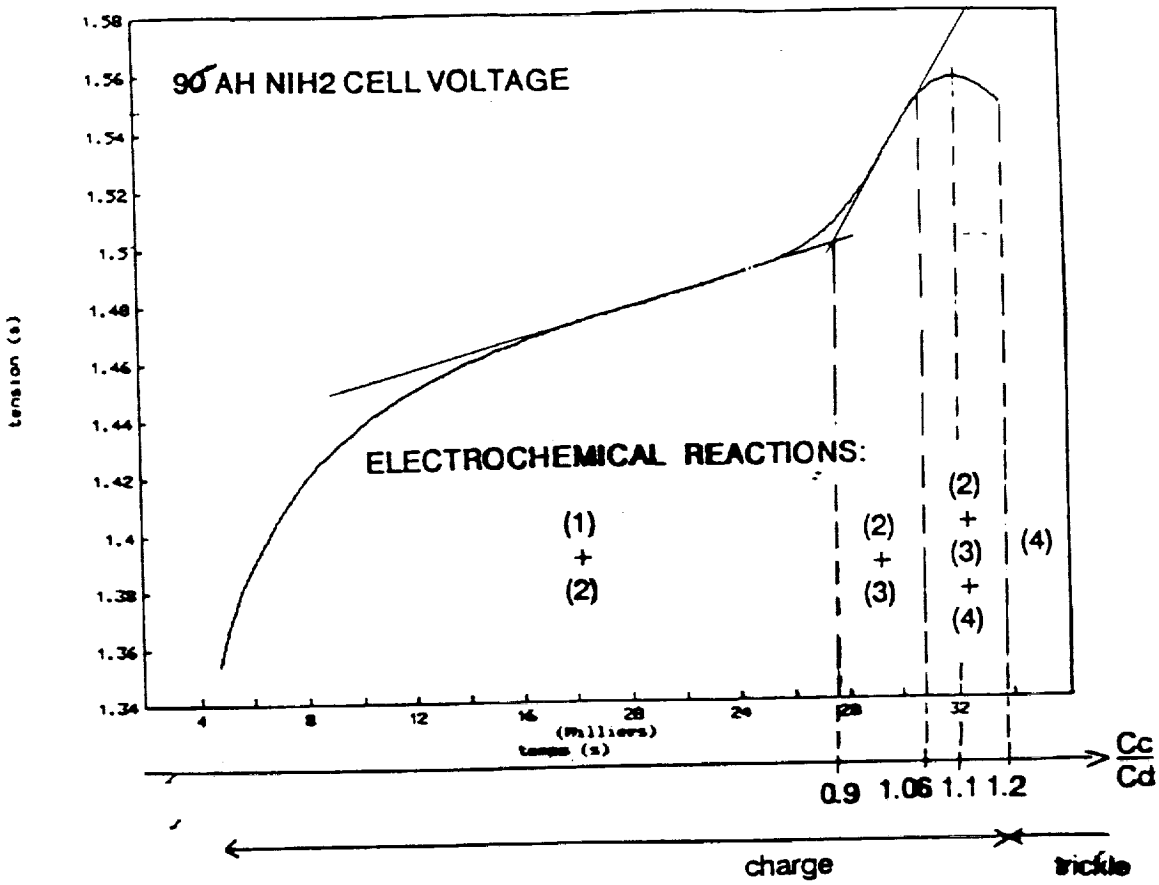

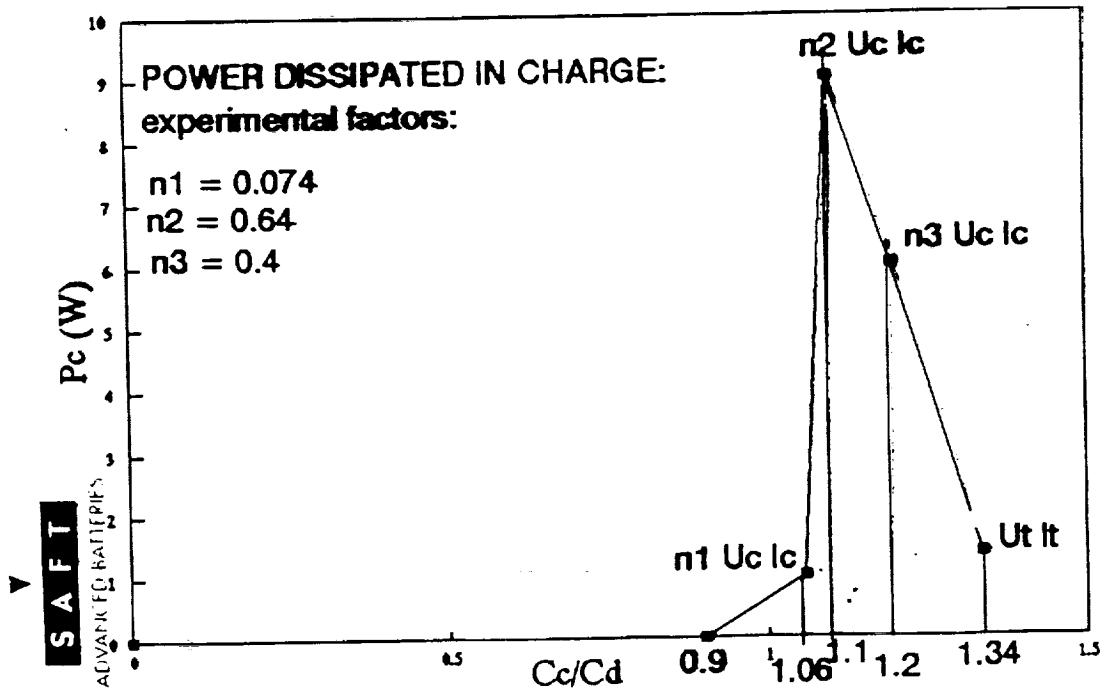

1993 Nasa Aerospace Battery Workshop, November 16–18

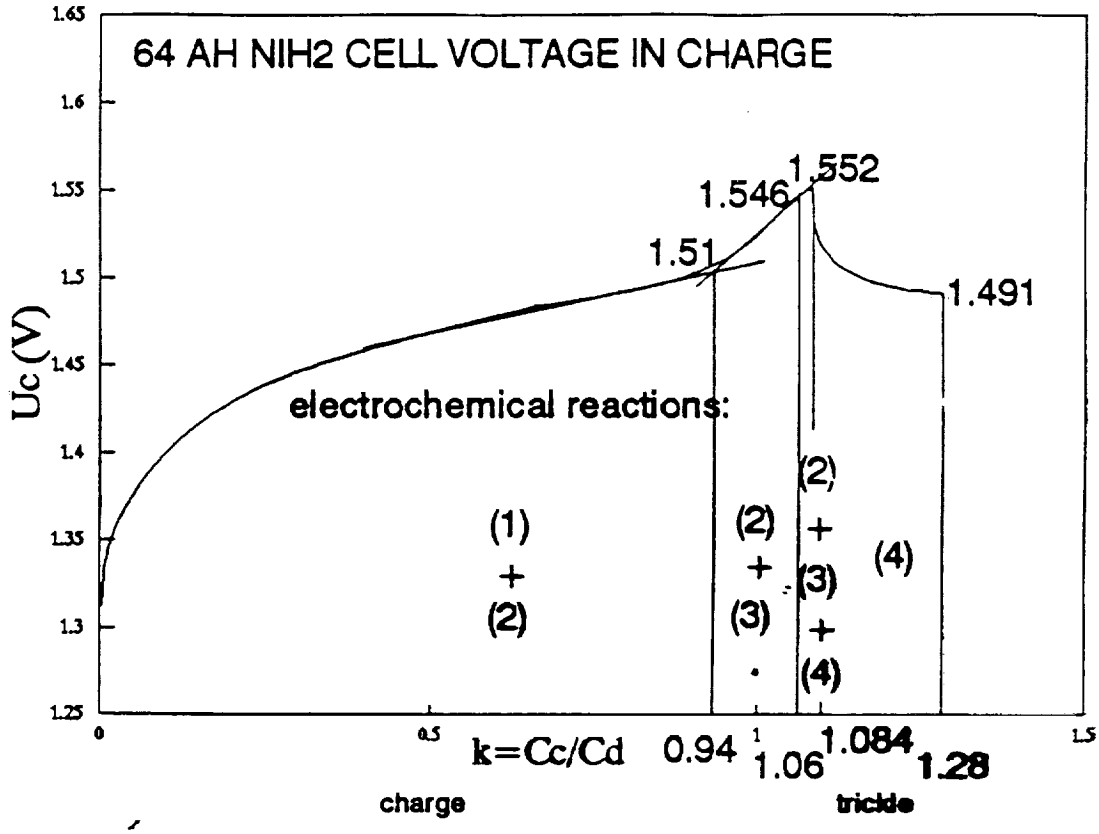

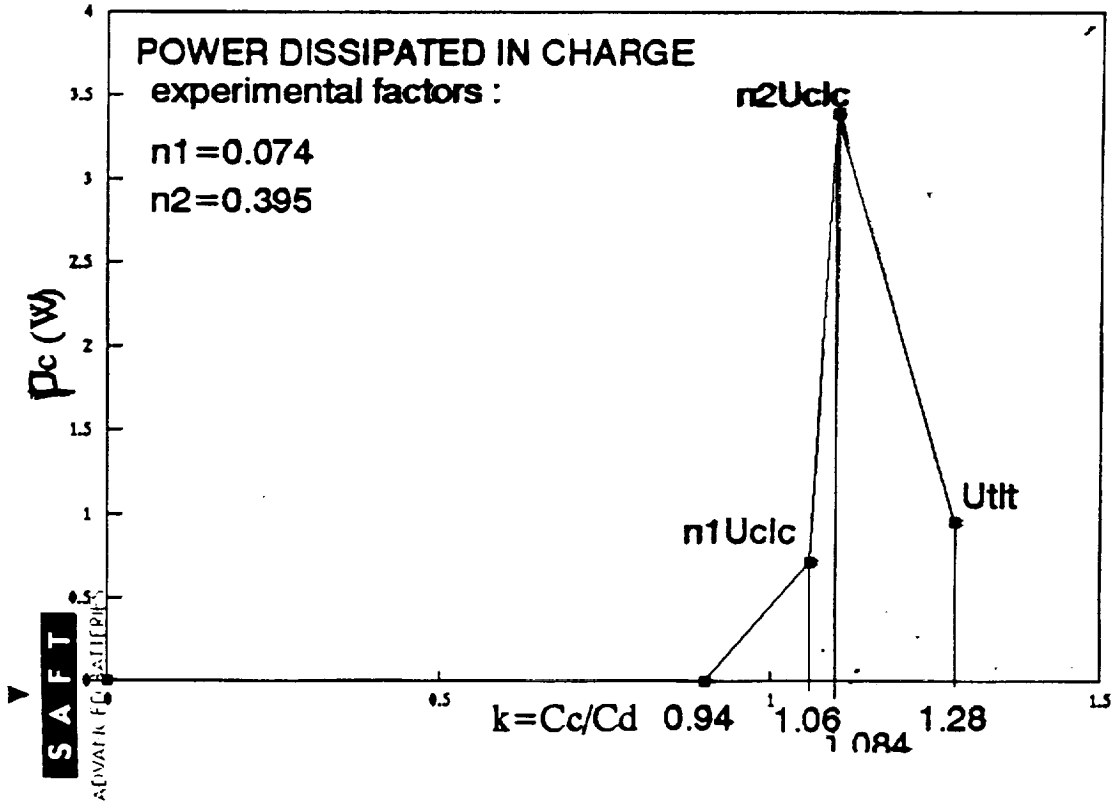

1993 Nasa Aerospace Battery Workshop, November 16–18

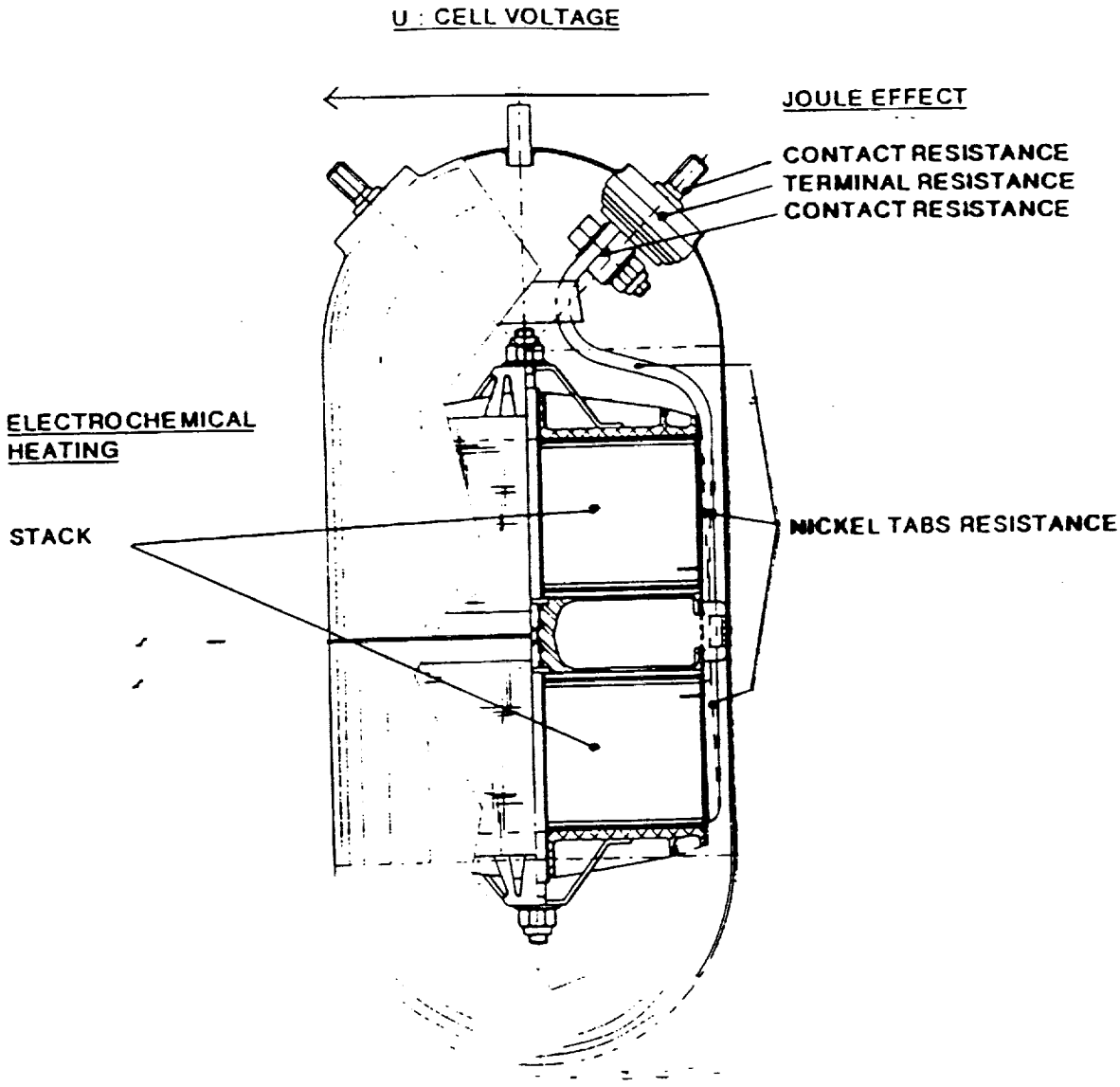

1993 Nasa Aerospace Battery Workshop, November 16–18

SAFT
ADVANCED BATTERIES

THERMAL MODELING OF NIH2 BATTERIES

3– NODAL SOFTWARE

2.1– THERMAL ANALYSER ESACAP

NETWORK ANALYSER FOR THERMAL AND ELECTRONIC PROBLEMS
(PRODUCED BY STANSIM IN DENMARK)

MAIN ADVANTAGES :

- EASY DESCRIPTION BY BASIC COMPONENTS
- EASY DESCRIPTION OF RADIATIVE COMPONENTS
- MODEL APPROACH
- POSSIBILITY TO INTRODUCE NEW COMPONENTS
- LARGE POSSIBILITIES TO INTRODUCE CONTROL
- TREATMENT OF COUPLED PROBLEMS (ELECTRICAL, FLUID FLOW, MECHANIC, TWO PHASE FLOWS)
- LARGE POSSIBILITY TO INTRODUCE PARAMETERS AND PHYSICAL PROPERTIES
- GEAR INTEGRATING METHOD
- SPECIAL METHODS FOR STEADY-STATE ANALYSIS

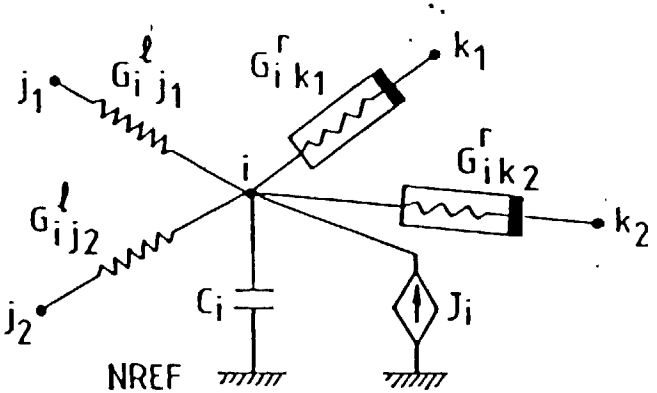

Thermal parameter	Electrical parameter
heat flux	intensity
temperature	potential
capacity	capacity
conductance	conductance
heat source	current generator
impressed temperature	voltage generator
impressed flux	current generator

THERMAL MODELING OF NIH2 BATTERIES

3– NODAL SOFTWARE

2.2– INTEGRATING GEAR METHOD

- A HIGH STABILITY FOR ORDERS K ≤ 6, AND AT THE SAME TIME A HIGH PRECISION,

- THE AUTOMATIC CONTROL OF THE TIME STEP, CONTROL WHICH IS PERFORMED THANKS TO THE EVALUATION OF THE ERROR,

- AN OPTIMUM MODIFICATION OF THE ORDER IN SUCH A WAY THAT THE REQUIRED PRECISION IS OBTAINED,

- BECAUSE THE CONTROL OF THE TIME STEP IS AUTOMATIC, THIS LEADS TO A GAIN OF TIME CALCULATION, WITHOUT INSTABILITY WHICH IS PARTICULARLY IMPORTANT FOR STIFF PROBLEMS.

GEAR PERFORMS THE INTEGRATION IN TWO STEPS :

- PREDICTION WITH AN EXTRAPOLATION BY A NEWTON POLYNOMIAL

- CORRECTION BY SOLVING THE IMPLICIT EQUATION RELATIVE TO THE ENERGY-BALANCE (SUCCESSIVE POINT ITERATION METHOD).

THERMAL MODELING OF NIH2 BATTERIES

4– DEVELOPMENT GENERAL PHILOSOPHY

– TWO FUNDAMENTAL PARTS : CELL AND STRUCTURE , EACH PART CAN BE RUN SEPARATELY

– A CELL HAS TWO FUNDAMENTAL PARTS : ELECTROCHEMICAL HEART AND MECHANICAL STRUCTURE
(CELL WALL, NICKEL TABS, OUTLETS)

IT'S WHY THE THERMAL STUDY IS MANAGED HAS FOLLOW :

– DEVELOPMENT OF A MODEL FOR THE ELECTROCHEMICAL COUPLE WITH THERMOPHYSICAL PARAMETERS AND COMBINATION OF CONDUCTIVITIES, HEAT CAPACITIES, TO TAKE INTO ACCOUNT ALL COMPONENTS (MATTER GRID, SEPARATORS, ...) ======> MODEL OF 100 NODES

– REDUCTION OF NODES NUMBER BUT NOT INITIAL PARAMETERS AND EXTENSION TO A COMPLETE CELL (MORE THAN 100 NODES)

– REDUCTION OF A COMPLETE CELL INTO 10 NODES ALWAYS WITH THE INITIAL PARAMETERS

– DEVELOPMENT OF BATTERY STRUCTURE AND INTRODUCTION, AT EACH PLACE, OF A REDUCED CELL MODEL

– SAME APPROACH FOR SUB–COMPONENTS SUCH AS DIODES FOR EXAMPLE

THERMAL MODELING OF NIH2 BATTERIES

SAFT
ADVANCED BATTERIES

5– NIH2 BATTERY MODEL DEVELOPMENT

5.1 – AT COUPLE LEVEL

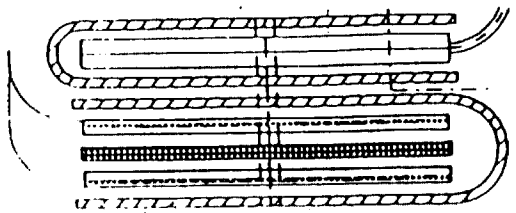

ρC_{EQ} , $\lambda_V \downarrow$, $\lambda_H \rightarrow$

- POSITIVE ELECTRODE
- SEPARATOR
- NEGATIVE ELECTRODE
- NEGATIVE ELECTRODE SEPARATOR
- ELECTROLYTE

FOR EACH COMPONENT :

ρC , λ , THICKNESS (Ep)

EQUIVALENT THERMAL CAPACITY :

ADDITION OF EACH THERMAL CAPACITY OF THE COMPONENTS :

$$\rho C_{EQUIVALENT} = \frac{\Sigma \rho C \text{ Volume}}{\text{Volume couple}}$$

EQUIVALENT THERMAL CONDUCTIVITY :

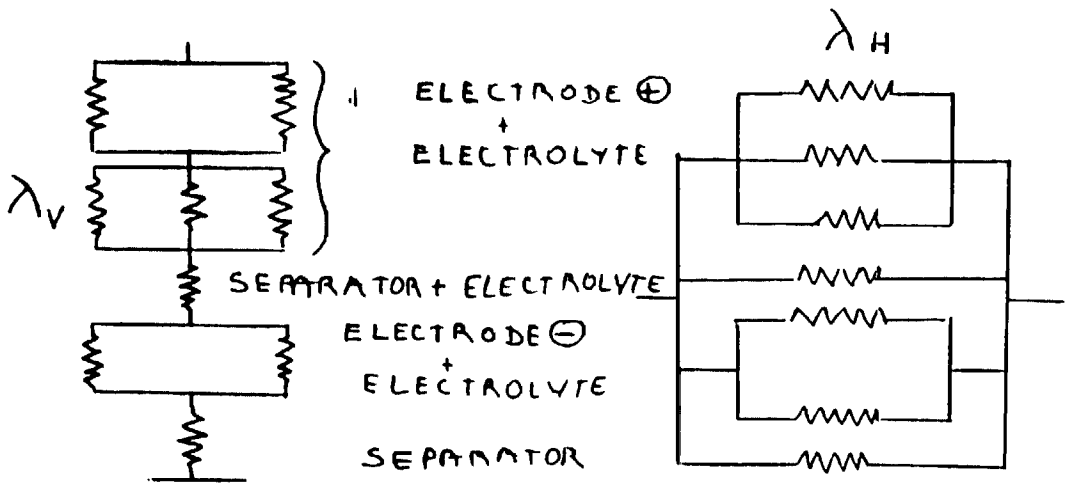

$$\lambda_V = \frac{\Sigma E_p}{\Sigma \lambda / E_p} \qquad \lambda_H = \frac{\Sigma \lambda E_p}{\Sigma E_p}$$

5.2– AT CELL LEVEL (1/4 OF A CELL)

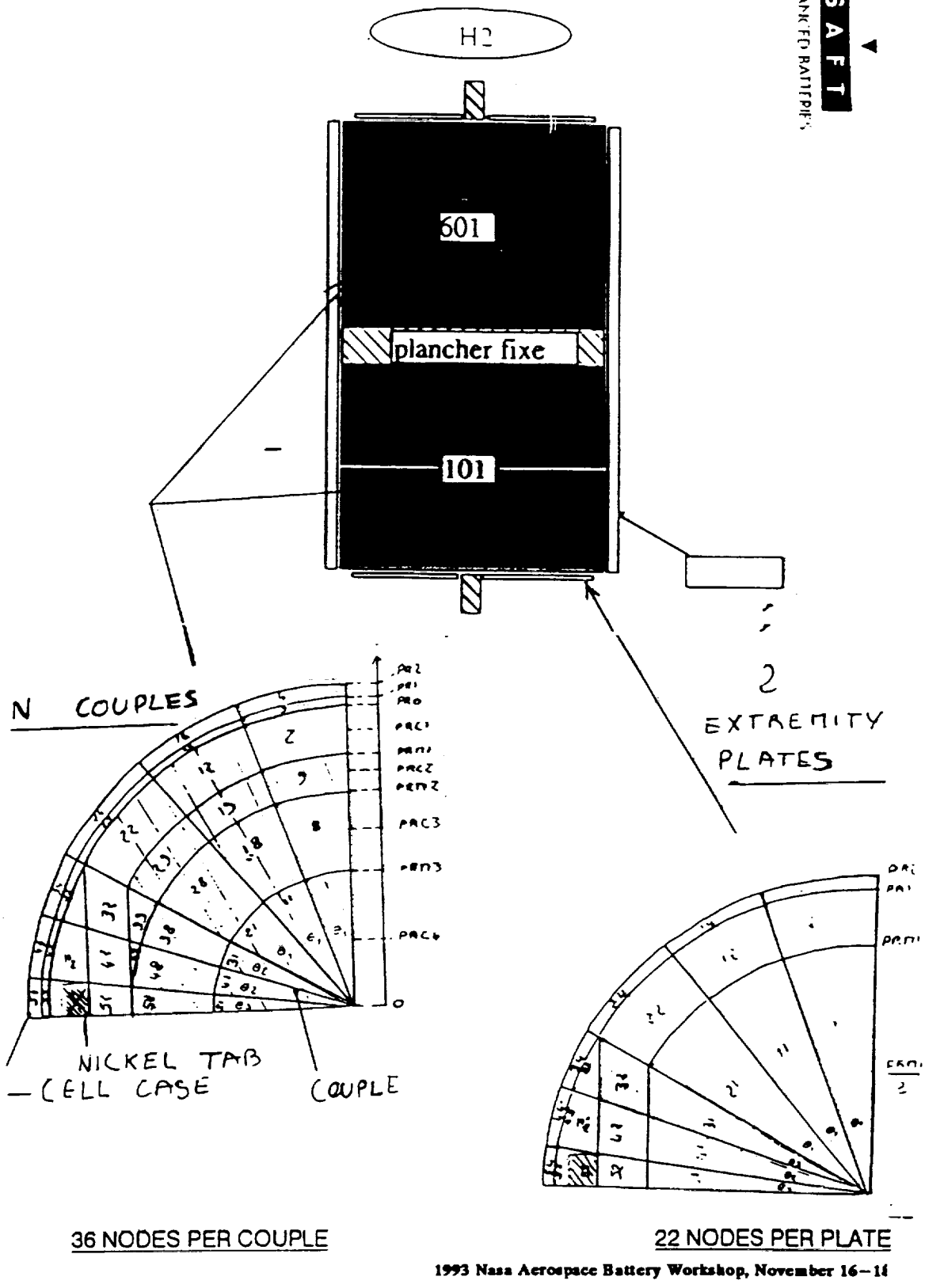

36 NODES PER COUPLE

22 NODES PER PLATE

1993 Nasa Aerospace Battery Workshop, November 16–18

5.2– AT CELL LEVEL (1/4 OF A CELL)

SAFT ADVANCED BATTERIES

INTEGRATION OF BATTERY STRUCTURE AT CELL LEVEL :

MODEL APPROACH :

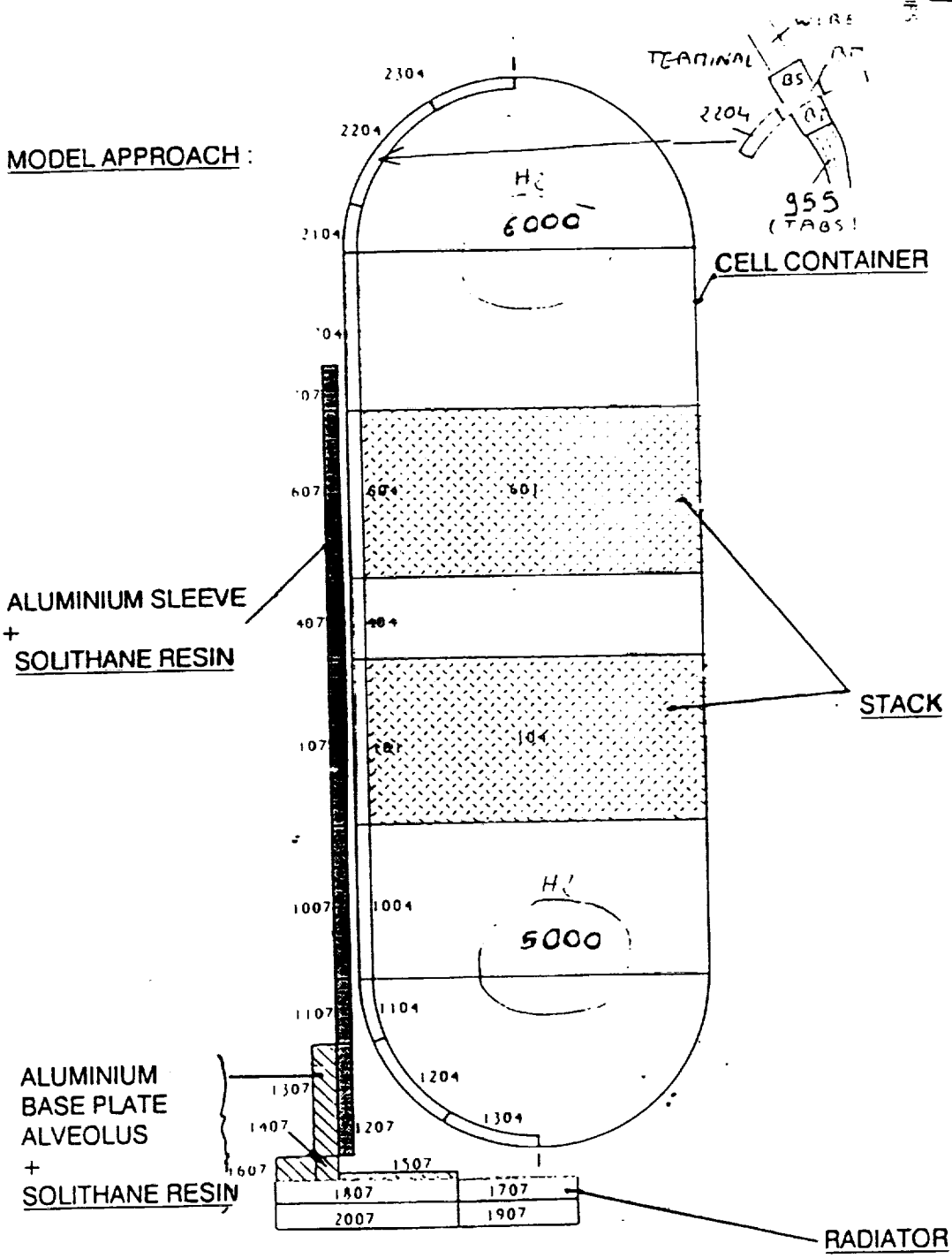

1993 Nasa Aerospace Battery Workshop, November 16–18

SAFT
ADVANCED BATTERIES

THERMAL MODELING OF NIH2 BATTERIES

5.2– AT CELL LEVEL (1/4 OF A CELL)

CELL MODEL REDUCTION : WITH SAME BATTERY STRUCTURE INTERFACE

BASIC INPUTS :

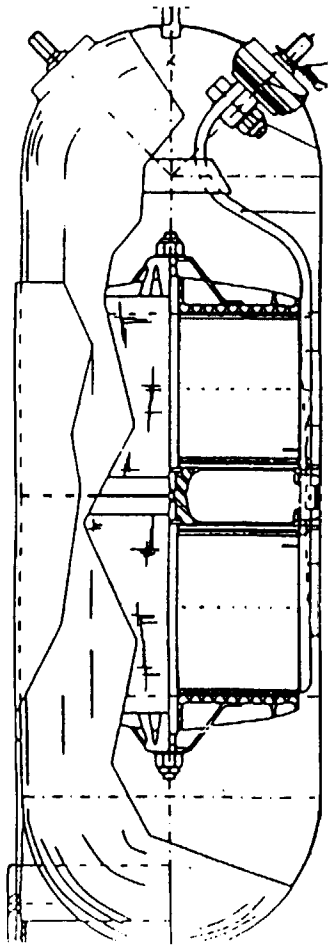

1/4 CELL
DETAILED MODEL :

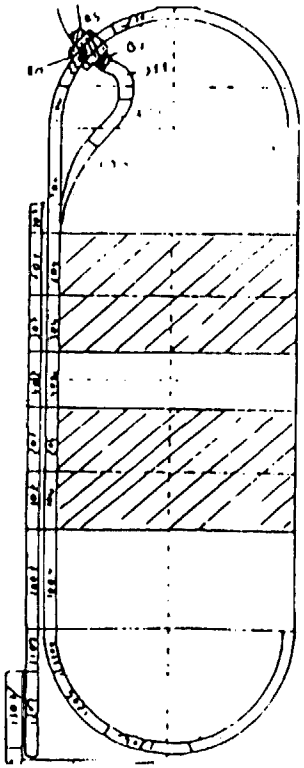

250 NODES

REDUCTION

1 CELL
ROUGH MODEL :

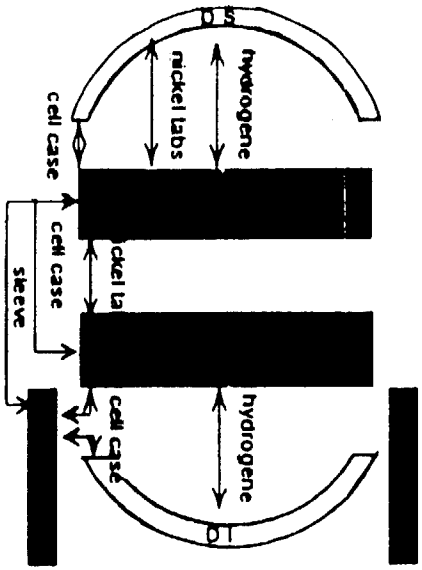

5 NODES

5.1 -

SAFT

EXPERIMENTAL APPROACH :

--> EVALUATION OF THERMAL CAPACITY
(SPECIFIC TEST)

VHS 96 CM
WITH SLEEVE AND ALVEOLUS

--> $\rho C_{calculated}$ = 2333 J/°C

--> $\rho C_{experimental}$ = 2330 J/°C

--> EVALUATION OF HEAT GENERATION
(SPECIFIC TEST)

VHS 96 CM TOTAL AVERAGE HEAT DISSIPATION IN DISCHARGE :

70% DOD : P = 12 W
80% DOD : P = 16.5 W

--> TEMPERATURE DISTRIBUTION ON A VHS 90 CM CELL

CORRELATION WITH MODEL PREDICTIONS

(SEE THERMAL VACCUM TEST ON VHS 96 CM CELL)

SAFT
ADVANCED BATTERIES

THERMAL MODELING OF NIH2 BATTERIES

5.3– AT DIODES LEVEL

EXPERIMENTAL APPROACH :

TWO TESTS HAVE PERMITED TO EVALUATE WITH A GOOD CONFIDENCE :

. HEAT GENERATION WITHIN DISCHARGE AND CHARGE DIODES

. THERMAL CONDUCTION THROUGH THE DIODE ASSEMBLY SYSTEM

. PREDICT DIODES TEMPERATURE AT VARIOUS CURRENT LEVEL.

EXPERIMENTAL RESULTS :

CURRENT	DISCHARGE P	CHARGE P	DISCHARGE MAX T J	CHARGE MAX T J
50 A	30 W	/	95.5 °C	/
37 A	20 W	/	66°C	/
6 A	/	5.5 W	/	52.5 °C

MODEL APPROACH :

- DETAILED MODEL OF DIODES ON THEIR SUPPORT --> 33 NODES
- CORRELATION ACHIEVED WITH TESTS
- ROUGH MODEL --> 8 NODES

THERMAL MODELING OF NIH2 BATTERIES

5.4– AT BATTERY BASEPLATE LEVEL

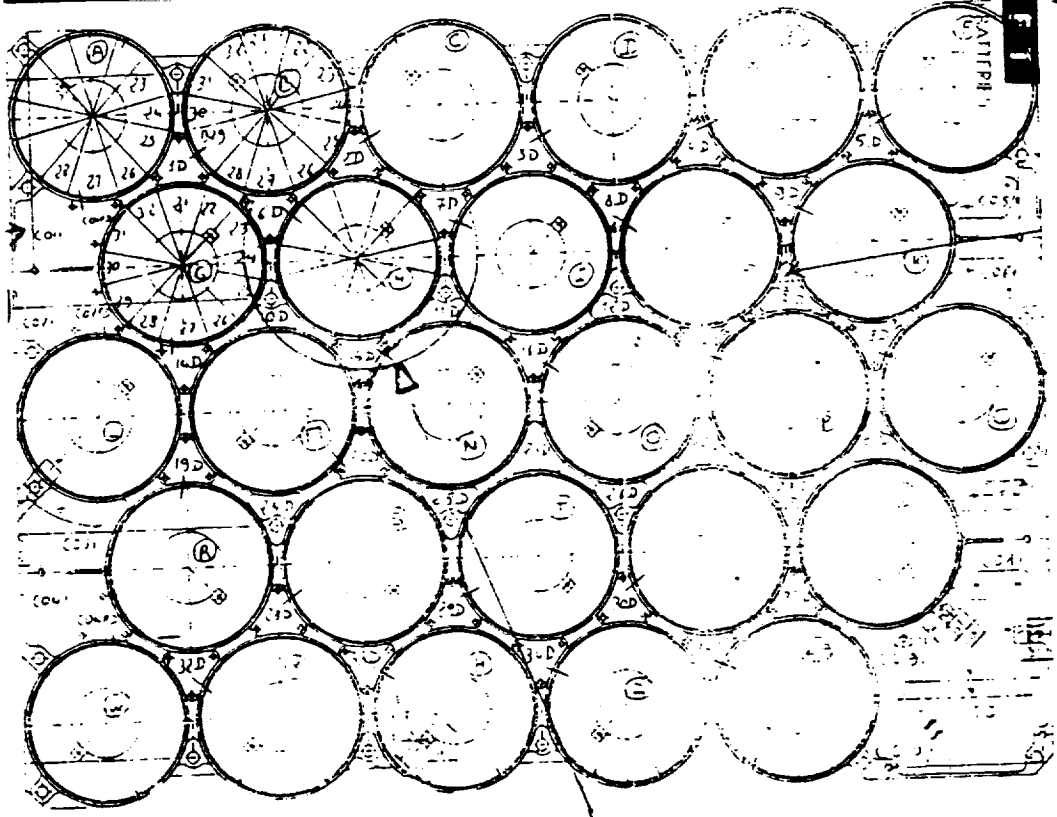

SIDE PLATE (3 NODES)

DIODES PLACE 3 NODES

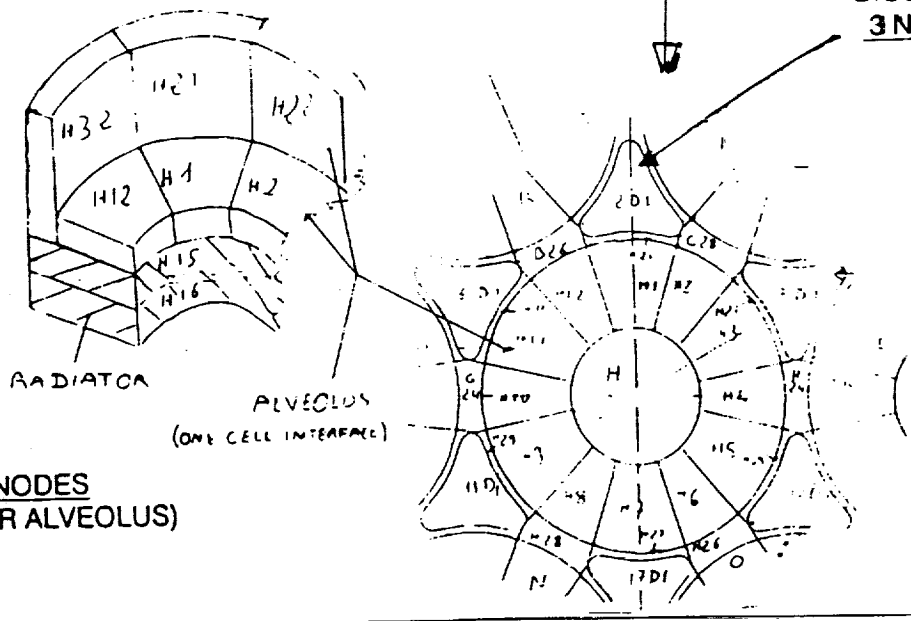

26 NODES (PER ALVEOLUS)

840 NODES FOR THE WHOLE BASEPLATE

5.5– BATTERY COMPLETE MODEL

COMPLETE SYSTEM : 983 NODES

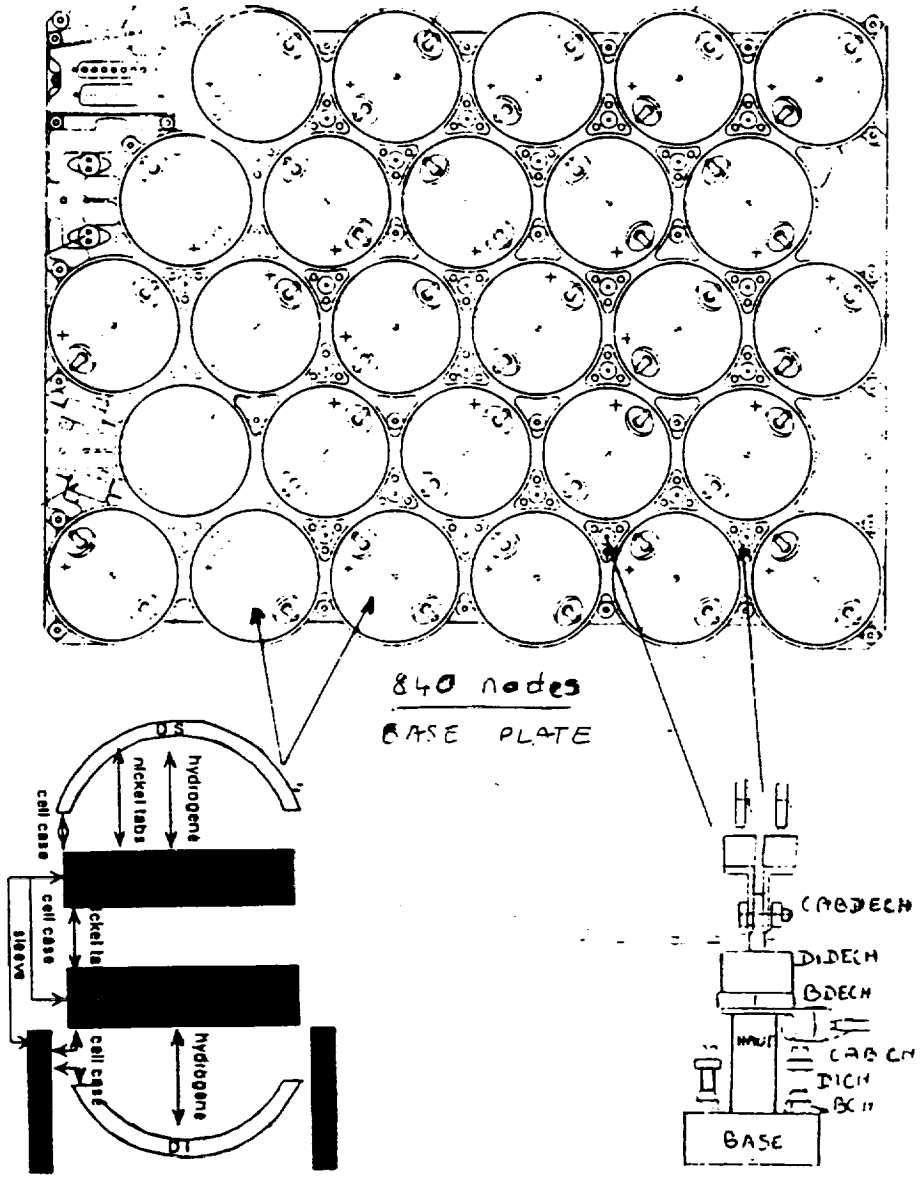

27 CELLS (5 NODES EACH)

DIODES SYSTEM
(8 NODES)

WITH ALL BASIC INPUTS

1993 Nasa Aerospace Battery Workshop, November 16–18

5.1 -

SAFT

WITH THIS APPROACH :

			x 27	
SIMPLIFIED CELL MODEL	:	5 NODES	—>	135 NODES
SIMPLIFIED DIODE MODEL	:	8 NODES	—>	8 NODES
BASEPLATE MODEL	:	840 NODES	—>	840 NODES
COMPLETE SYSTEM :				983 NODES

A COMPLETE DETAILED MODEL :

			x 27	
DETAILED CELL MODEL	:	250 NODES	—>	6750 NODES
DETAILED DIODE MODEL	:	33 NODES	—>	33 NODES
BASEPLATE MODEL	:	840 NODES	—>	840 NODES
COMPLETE SYSTEM :				7623 NODES

FURTHERMORE EXPERIMENTAL STEPS ARE DIRECTLY INCLUDED
IN THE DEVELOPMENT OF THE SYSTEM MODEL
(AT CELL AND DIODE LEVEL)

6– NIH2 EXPERIMENTAL DEVELOPMENT

6.1– CONSIDERATION ON TEST ENVIRONMENT

6.2– THERMAL VACUUM TEST ON A VHS90CM CELL

6.3– QUALIFICATION LIFE TEST ON VHS90CM CELLS

6.4– THERMAL VACUUM QUALIFICATION ON SAFT 27VHS64CM BATTERY

SAFT
ADVANCED BATTERIES

THERMAL MODELING OF NIH2 BATTERIES

6.1 – CONSIDERATION ON TEST ENVIRONMENT

IN ORBIT BATTERY ENVIRONMENT

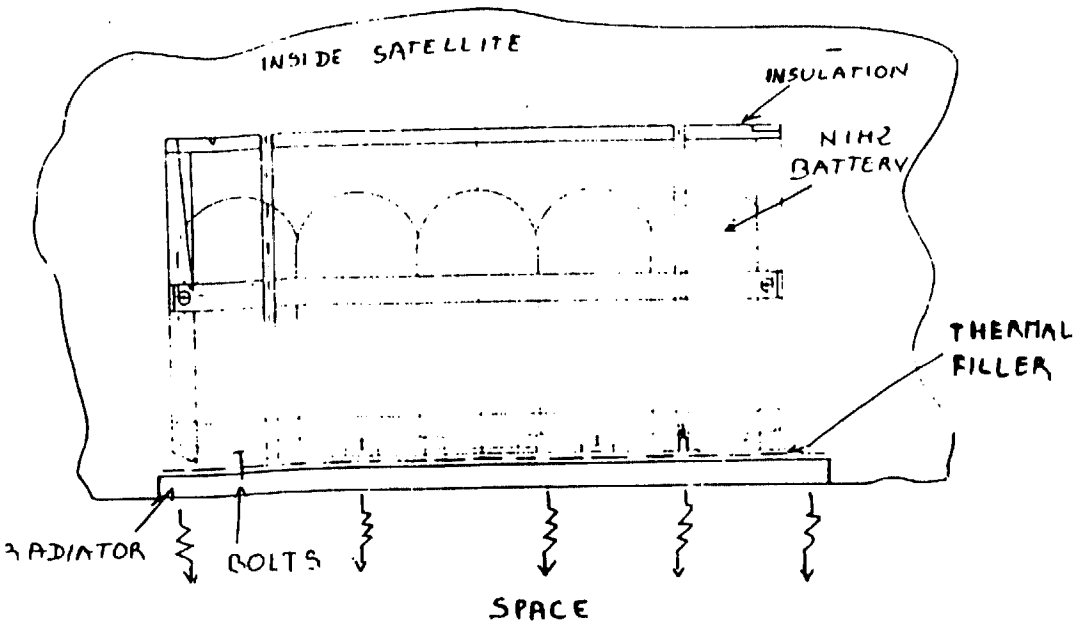

TEST ENVIRONMENT

AMBIANT SIMULATION

- AMBIANT AIR
- THERMAL CHAMBER
- THERMAL VACUUM CHAMBER

RADIATOR SIMULATION

- BATTERY SET ON A PLATE AT CONSTANT TEMPERATURE
- BATTERY SET ON PLATE WITH PILOTED TEMPERATURE PROFILE
- BATTERY FIXED ON A PLATE VIEWING A COLD SOURCE

SAFT
ADVANCED BATTERIES

THERMAL MODELING OF NIH2 BATTERIES

6.2– THERMAL VACUUM TEST ON A VHS90CM CELL

(SAFT POITIERS)

MOUNTING

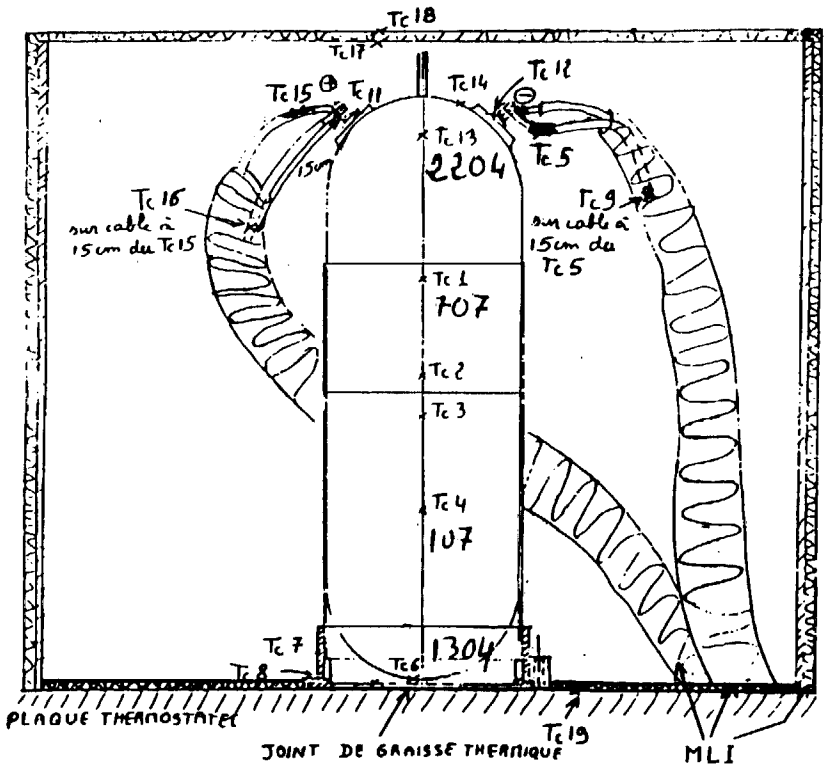

TEST RESULTS COMPARED TO MODEL PREDICTION

	model node	max discrepancy (°C)
upper dome	2204	2.25 (measured : 13.2) end of charge (model : 10.95)
upper stack (on sleeve)	707	1.1 (measured : 26.3) end of discharge (model : 25.2)
lower (on sleeve)	107	1.4 (measured : 17) end of discharge (model : 15.6)
lower dome	1304	0.8 (measured : 2.3) end of trickle (model : 3.1)

SAFT
ADVANCED BATTERIES

THERMAL MODELING OF NIH2 BATTERIES

6.2– THERMAL VACUUM TEST ON A VHS90CM CELL

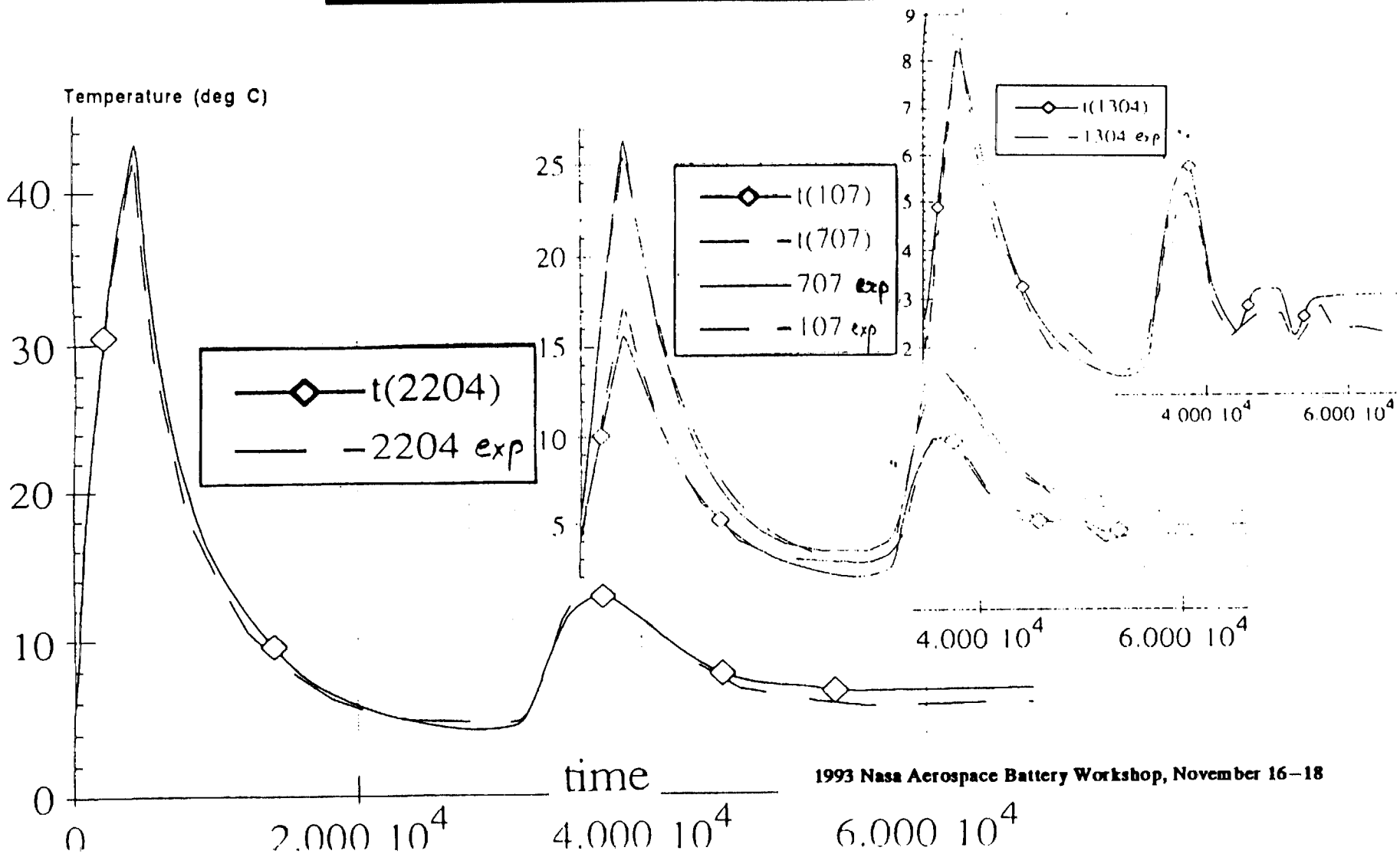

SAFT
ADVANCED BATTERIES

THERMAL MODELING OF NIH2 BATTERIES

6.3– QUALIFICATION LIFE TEST ON VHS90CM CELLS

(ESTEC – NOORDWIJK)

MOUNTING

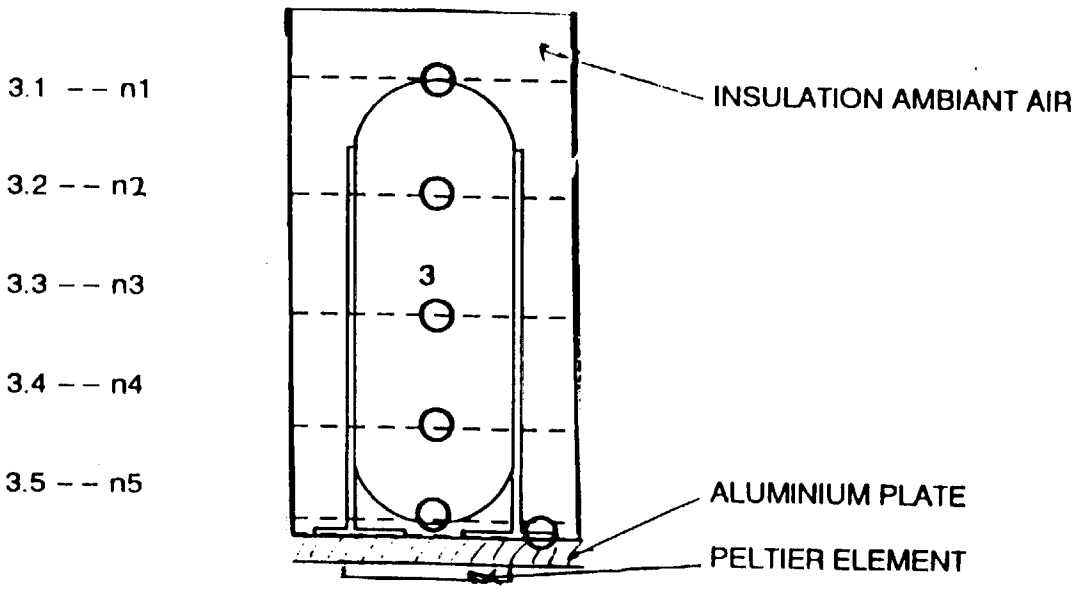

TEMPERATURE PROFILE OF THE PLATE DETERMINED BY THE DETAILED CELL MODEL

TEST RESULTS COMPARED TO MODEL PREDICTIC

Node/Dt level	Temperatures Predicted	Measured	Estimated
3.2 80%	27	29	-
20%	14.4	16.1	-
Upper stack inside (hot)	29	-	31
	-	-	18.3
DT sleeve -dome	8.1	11.6	-
	5.0	7.0	-
DT radial sleeve-stack	2	-	2
	1.2	-	1.2
DT stack-dome	10.1	-	13.6
		-	8.2
DT sleeve	5.38	6.2	-
	2.7	3.5	-
DT stack	5.38	-	6.2
	-	-	3.5

SAFT
ADVANCED BATTERIES

THERMAL MODELING OF NIH2 BATTERIES

6.3– QUALIFICATION LIFE TEST ON VHS90CM CELLS

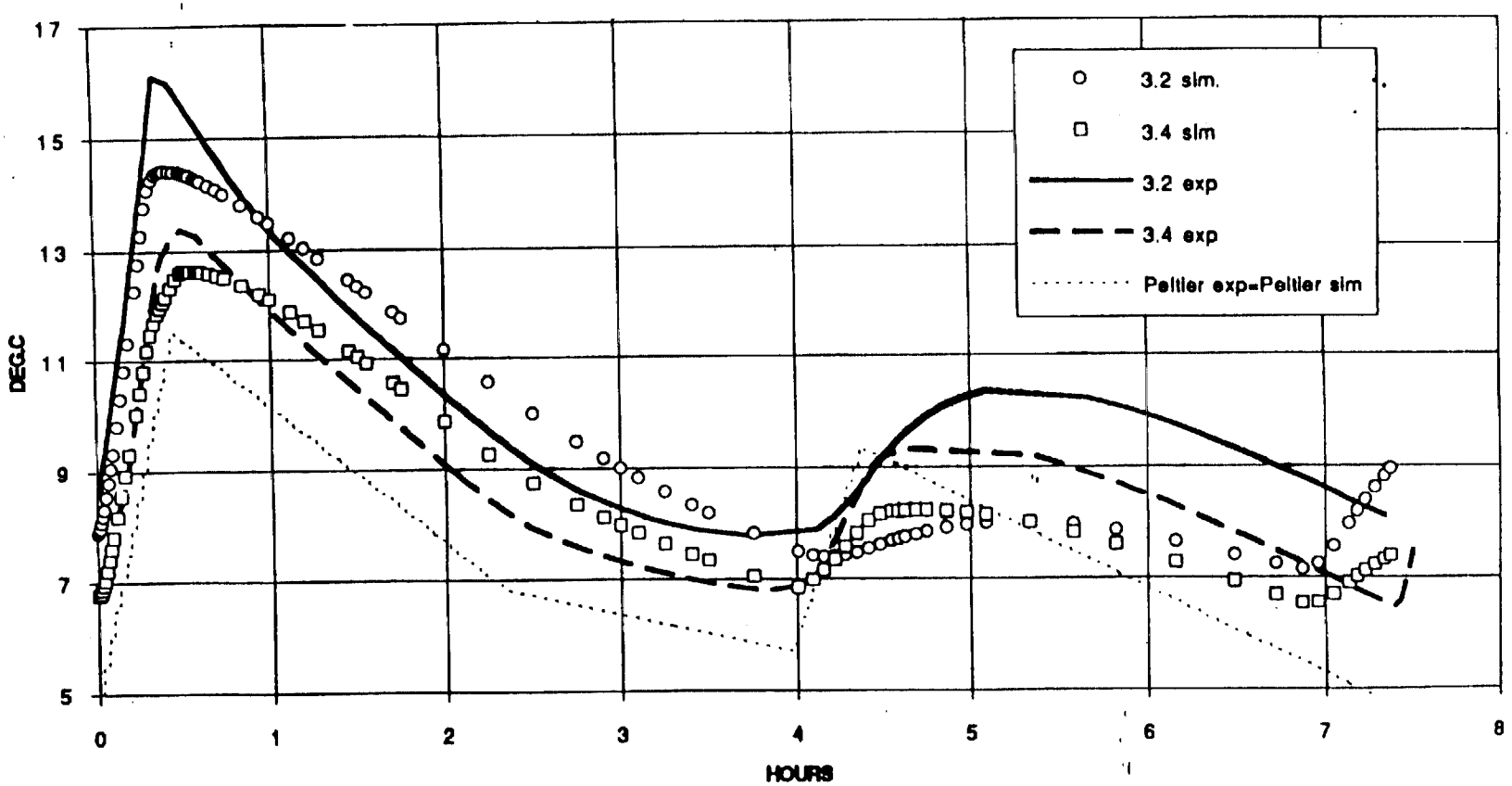

SAFT
ADVANCED BATTERIES

THERMAL MODELING OF NIH2 BATTERIES

6.4– THERMAL VACUUM QUALIF. ON SAFT 27VHS64CM BATTERY

MOUNTING :
- THERMAL VACUUM CHAMBER
- FIXED ON A RADIATIVE PANEL
- SUSPENDED OVER A COLD PLATE AT –170°C

CYCLE :
- 80% DOD DISCHARGE OF 1.2 HOUR
- C/10 CHARGE , K FACTOR OF 1.1
- C/100 TRICKLE CHARGE
- 1.8 W HEATING PER CELL, SWITCH ON WHEN CELL TEMP. IS BETWEEN 2 AND 4 °C

ONE FAILED CELL SIMULATION :
- W CELL IS PUT IN OPEN CIRCUIT AND RELAYED BY DIODES
- DISCHARGE DIODE IS PLACED ON SUPPORT N°32 .
- CHARGE DIODES ARE PLACED ON SUPPORT N°32, 29, 30.

THERMOCOUPLES:
- 81 THERMOCOUPLES WHERE INSTALLED
- 17 ON THE BASEPLATE
- 4 ON THE RADIATIVE PANEL
- 3 CELLS COMPLETELY EQUIPPED (5 thermocouples at least)
- ABOUT 20 CELLS EQUIPPED WITH ONE THERMOCOUPLES PLACED ON THE HOT POINT
- 3 DIODES SUPPORTS COMPLETELY EQUIPPED

SAFT
ADVANCED BATTERIES

THERMAL MODELING OF NIH2 BATTERIES

6.4– THERMAL VACUUM QUALIF. ON SAFT 27VHS64CM BATTERY

RESULTS:

	SPECIFICATION	MODEL	TEST
MAX CELL STACK TEMP.	+35°C	33.7 (X)	34.6 (X)
MIN CELL STACK TEMP.	–5°C	–4 (F)	–3.75 (F)
% HEATING USED	< 80%	70%	73%
MAX STACK GRADIENT	6°C	3.6 (F)	3.6 (F)
MAX STACK TO CELL GRADIENT	12°C	9.7 (F)	9.95 (F)
CELL TO CELL GRADIENT	8°C	7°C (N–F)	8°C (N–F)
MAX DIODE JUNCTION TEMP.	110°C	105	105.6

6.4– THERMAL VACUUM QUALIF. ON SAFT 27VHS64CM BATTERY

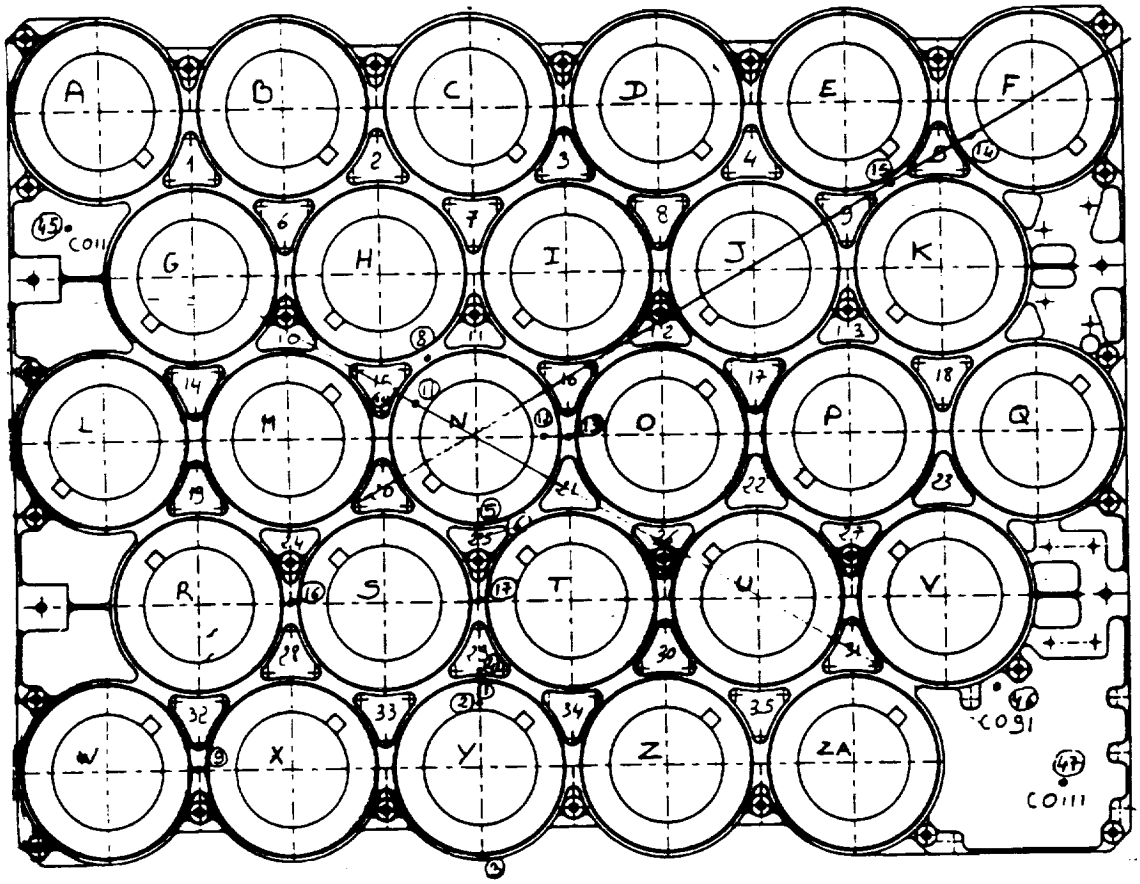

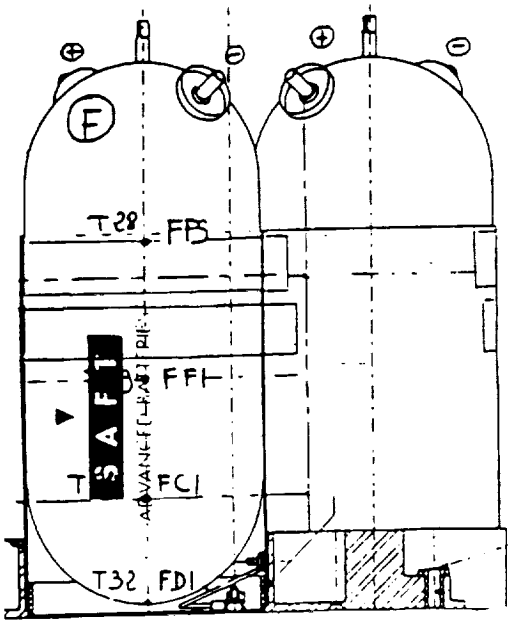

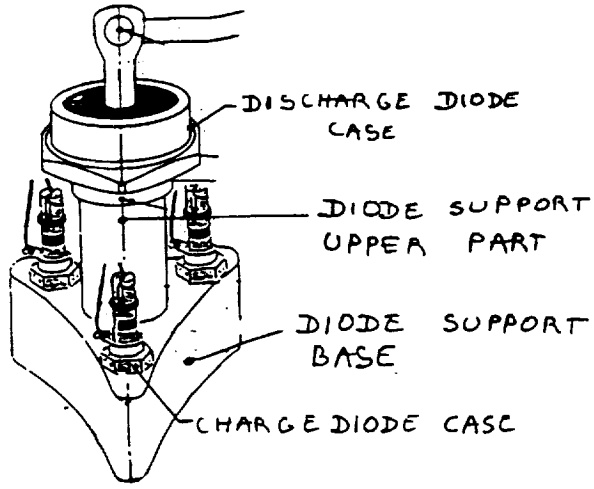

: Nasa Aerospace Battery Workshop, November 16–18

SAFT
ADVANCED BATTERIES

80% DOD GEO ECLIPSE CYCLE

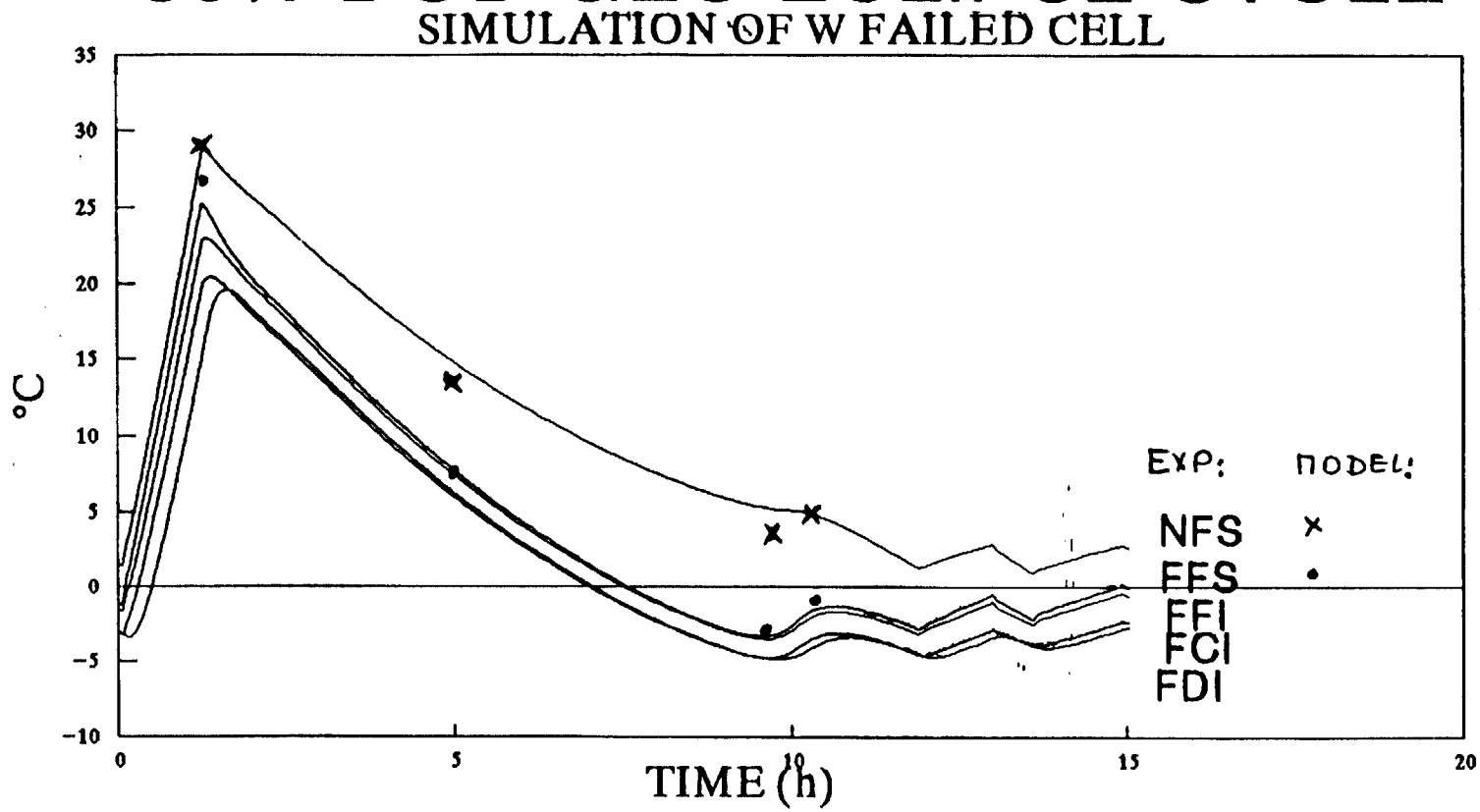

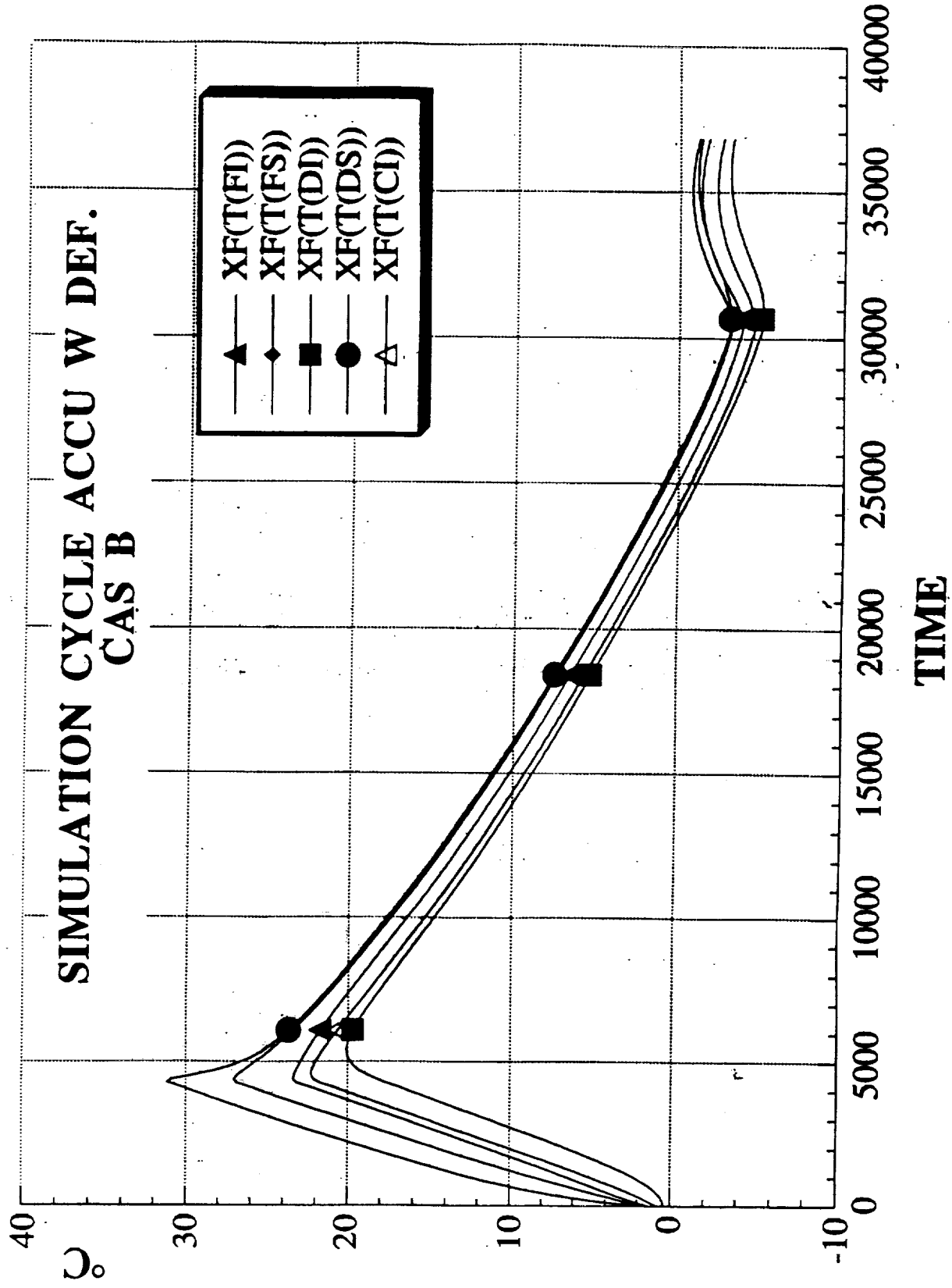
SIMULATION CYCLE ACCU W DEF.
CAS B
XF(T(FI))
XF(T(FS))
XF(T(DI))
XF(T(DS))
XF(T(CI))
40
30
20
10
0
-10
0
5000
10000
15000
20000
25000
30000
35000
40000
TIME

SAFT
ADVANCED BATTERIES

THERMAL MODELING OF NIH2 BATTERIES

7– CONCLUSION

NIH2 BATTERIES ARE CARREFULLY STUDIED FROM A THERMAL POINT OF VIEW

MODEL AT COUPLE LEVEL, CELL LEVEL AND BATTERY LEVEL ARE PERFORMED WITH THE SAME PARAMETERS

THERMAL MODELING IS REALISED WITH AN EASY AND POWERFUL NODAL SOFTWARE : ESACAP

TESTS IN VACUUM CHAMBER OR WITH PELTIER ELEMENTS ARE DEFINED IN ASSOCIATION WITH MODEL

GENERAL THERMAL DEVELOPMENT PROGRAM DELIVER NOW A TOOL ABLE TO ANSWER QUICKLY TO NEW REQUIREMENTS OF FUTURE BATTERIES

NICKEL-HYDROGEN CELL REVERSAL CHARACTERISTICS

C. LURIE
TRW SPACE AND ELECTRONICS GROUP
REDONDO BEACH, CALIFORNIA

THE 1993 NASA AEROSPACE BATTERY WORKSHOP
ALABAMA SPACE AND ROCKET CENTER
NOVEMBER 16 - 18, 1993

NICKEL-HYDROGEN CELL REVERSAL CHARACTERISTICS

NICKEL-HYDROGEN CELL REVERSAL CHARACTERISTICS ARE BEING STUDIED AS PART OF A TRW PROGRAM DIRECTED TOWARDS DEVELOPMENT OF A HIGH CURRENT BATTERY CELL BYPASS SWITCH.

CELL BYPASS SWITCH

- OPEN CIRCUIT FAILURE MODE CONSIDERED CREDIBLE FOR NICKEL-HYDROGEN CELLS
- BYPASS PROTECTION TRADITIONALLY PROVIDED BY DIODES
- DIODE APPROACH IS POWER LIMITED
  - THERMAL DISSIPATION
  - UNAVAILABILITY OF LARGE FLIGHT QUALIFIED DIODES
- BYPASS WITH A SWITCH IS PREFERRED FOR LARGE CELLS
  - LOWER DISSIPATION
  - LIGHTER

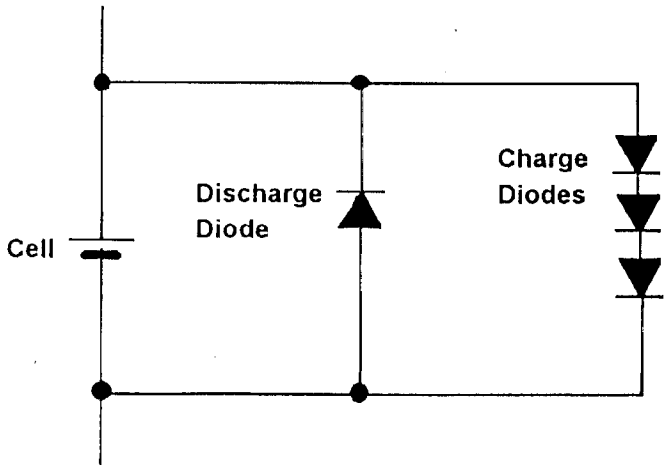

BYPASS SWITCH APPROACH

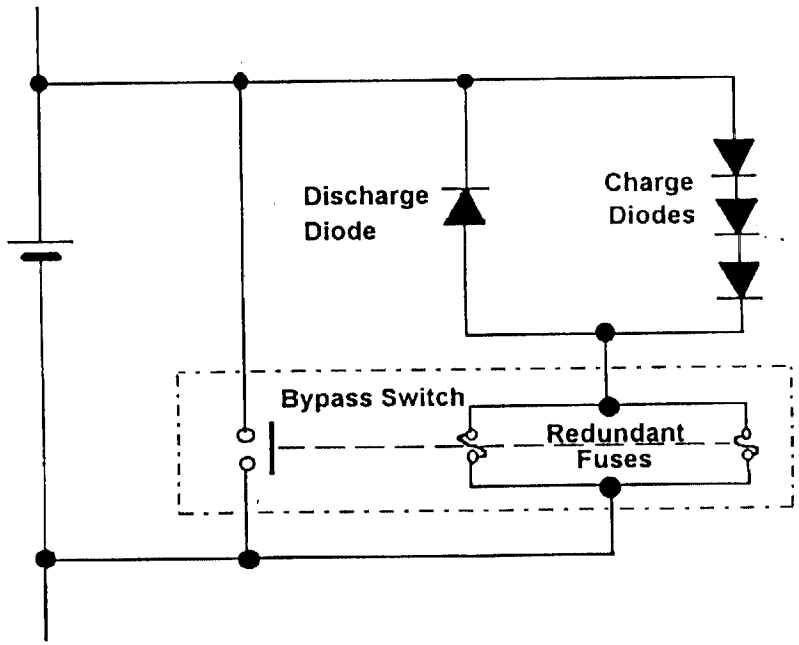

Passive fuse wire actuated bypass switch

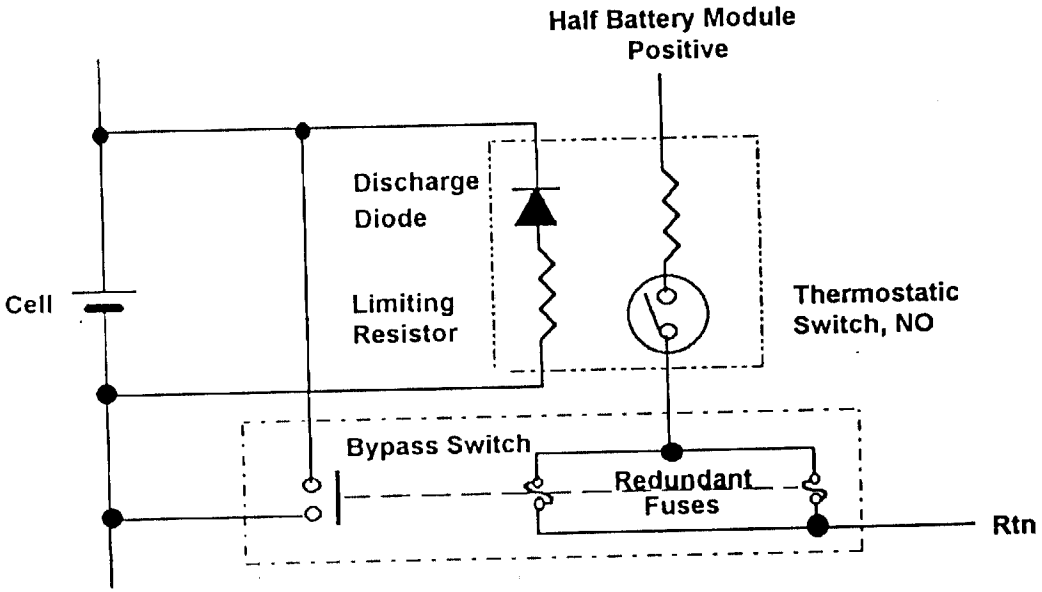

Thermostatically actuated bypass switch

NICKEL-HYDROGEN CELL REVERSAL CHARACTERISTICS

- CHARACTERIZATION OF THE SWITCH INCLUDES UNDERSTANDING
  - HOW LONG IT WILL TAKE TO ACTUATE
  - AT WHAT VOLTAGE IT WILL ACTUATE
- CHARACTERISTICS OF THE FUSE LINKS, DIODE, RESISTOR, AND THERMOSTAT ARE EASILY DETERMINED
- REVERSAL CHARACTERISTICS OF NICKEL HYDROGEN CELLS MUST ALSO BE KNOWN IF THE SWITCH ACTUATION CHARACTERISTICS ARE TO BE DETERMINED

EXPERIMENTAL

- DETERMINE NICKEL HYDROGEN CELL REVERSAL VOLTAGE TRAJECTORIES
  - HYDROGEN AND NICKEL PRECHARGED CELLS
  - NOMINAL AND MINIMUM RATES
  - CELL LEAKING INTO VACUUM (SPACE)
- TEST INSTRUMENTATION

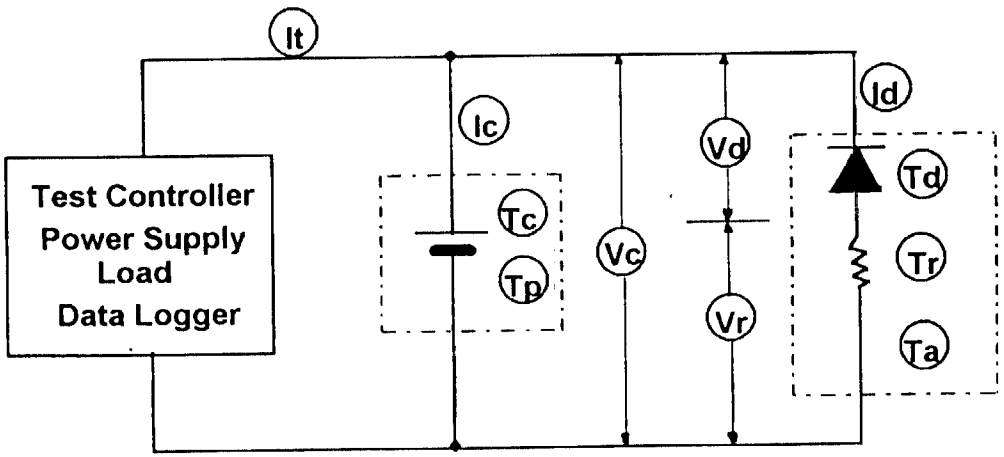

EXPERIMENTAL (CONT'D)

- EP RNH 65-17 CELL, IN THERMAL SLEEVE, ON COLD PLATE AT 5 ± 2 DEG C
  - ZIRCAR SEPARATOR, WALL WICK
  - BACK-TO-BACK STACK CONFIGURATION
- LEAK TO SPACE SIMULATED BY VENTING CELL TO VACUUM

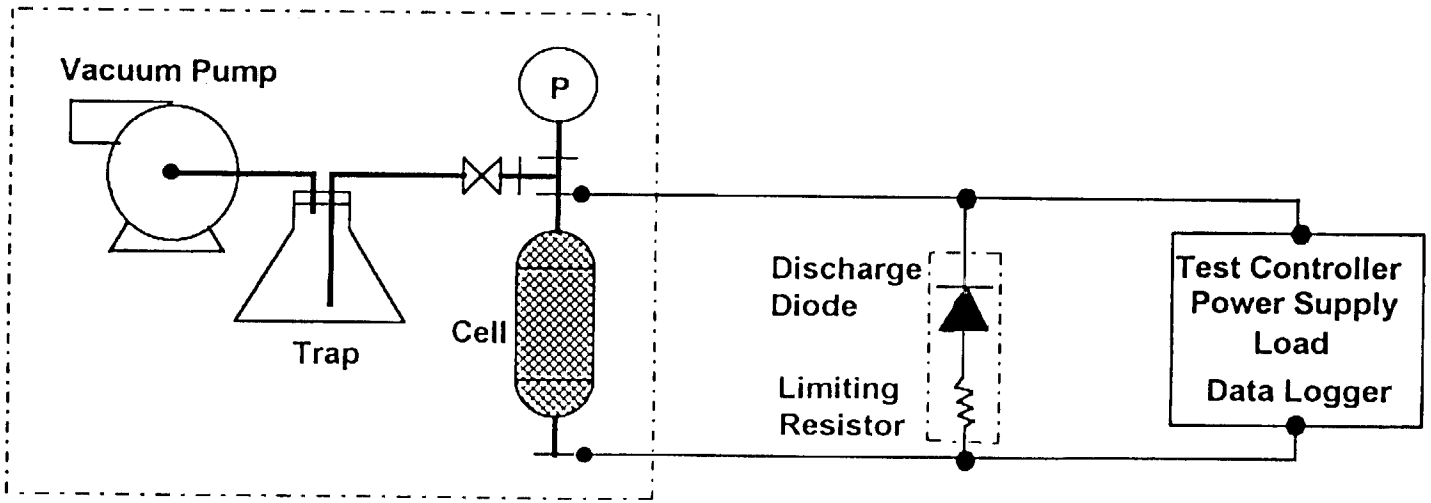

NICKEL-HYDROGEN CELL CHEMISTRY
DISCHARGE/REVERSAL

DISCHARGE

Nickel	$2\ NiOOH + 2\ HOH + 2\ e$	$\rightarrow$	$2\ Ni(OH)_2 + 2\ OH^-$	$E^\circ = +0.5v$
Hydrogen	$H_2 + 2\ OH^- - 2\ e$	$\rightarrow$	$2\ HOH$	$E^\circ = +0.8v$
Total	$2\ NiOOH + H_2$	$\rightarrow$	$Ni(OH)_2$	$E^\circ = +1.3v$

OVERDISCHARGE (REVERSAL) WITH HYDROGEN PRECHARGE

Nickel	$2\ HOH + 2\ e$	$\rightarrow$	$H_2 + 2\ OH^-$	$E^\circ = -0.8v$
Hydrogen	$H_2 + 2\ OH^- - 2\ e$	$\rightarrow$	$2\ HOH$	$E^\circ = +0.8$
	No net reaction; H_2 recombines			

NICKEL-HYDROGEN CELL CHEMISTRY
OVERDISCHARGE (REVERSAL) WITH NICKEL PRECHARGE

ACTIVE NICKEL PRECHARGE PRESENT

Nickel	$2\ NiOOH + 2\ HOH + 2\ e$	$\rightarrow$	$2\ Ni(OH)_2 + 2\ OH^-$	$E^\circ = +0.5v$
Hydrogen	$2\ OH^- - 2\ e$	$\rightarrow$	$1/2\ O_2 + HOH$	$E^\circ = -0.4v$
Total	$2\ NiOOH + HOH$	$\rightarrow$	$2\ Ni(OH)_2 + 1/2\ O_2$	$E^\circ = +0.1v$

ACTIVE NICKEL PRECHARGE EXHAUSTED

Nickel	$2\ HOH + 2\ e$	$\rightarrow$	$2\ OH^- + H_2$	$E^\circ = -0.8v$
Hydrogen	$2\ OH^- - 2\ e$	$\rightarrow$	$1/2\ O_2 + HOH$	$E^\circ = -0.4v$
Total (electrochemical)	HOH	$\rightarrow$	$1/2\ O_2 + H_2$	$E^\circ = -1.2v$
Chemical	$1/2\ O_2 + H_2$	$\rightarrow$	HOH	

DISCHARGE INTO REVERSAL WITH HYDROGEN PRECHARGE (C/2)

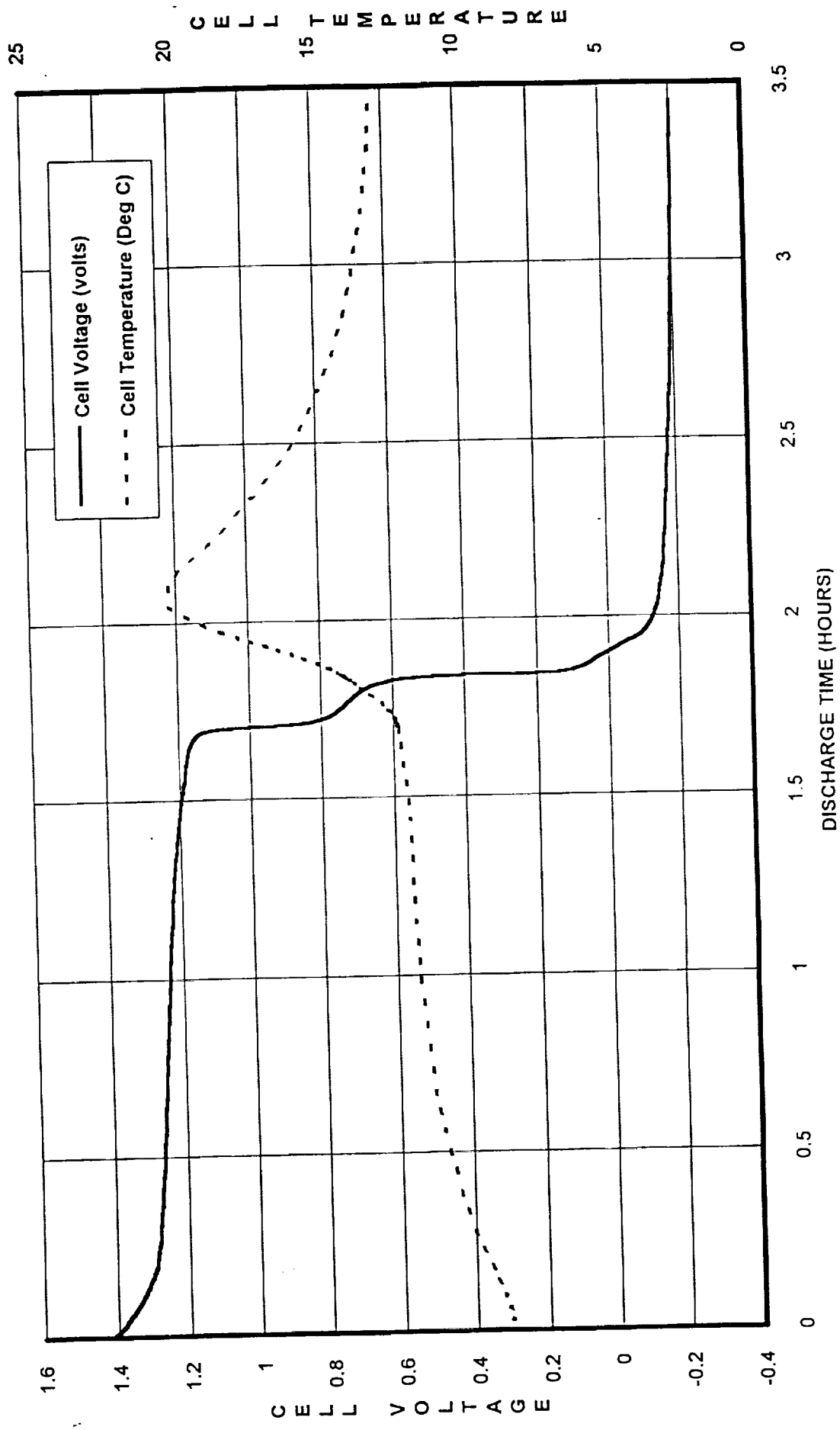

DISCHARGE INTO REVERSAL WITH NICKEL PRECHARGE (C/2)

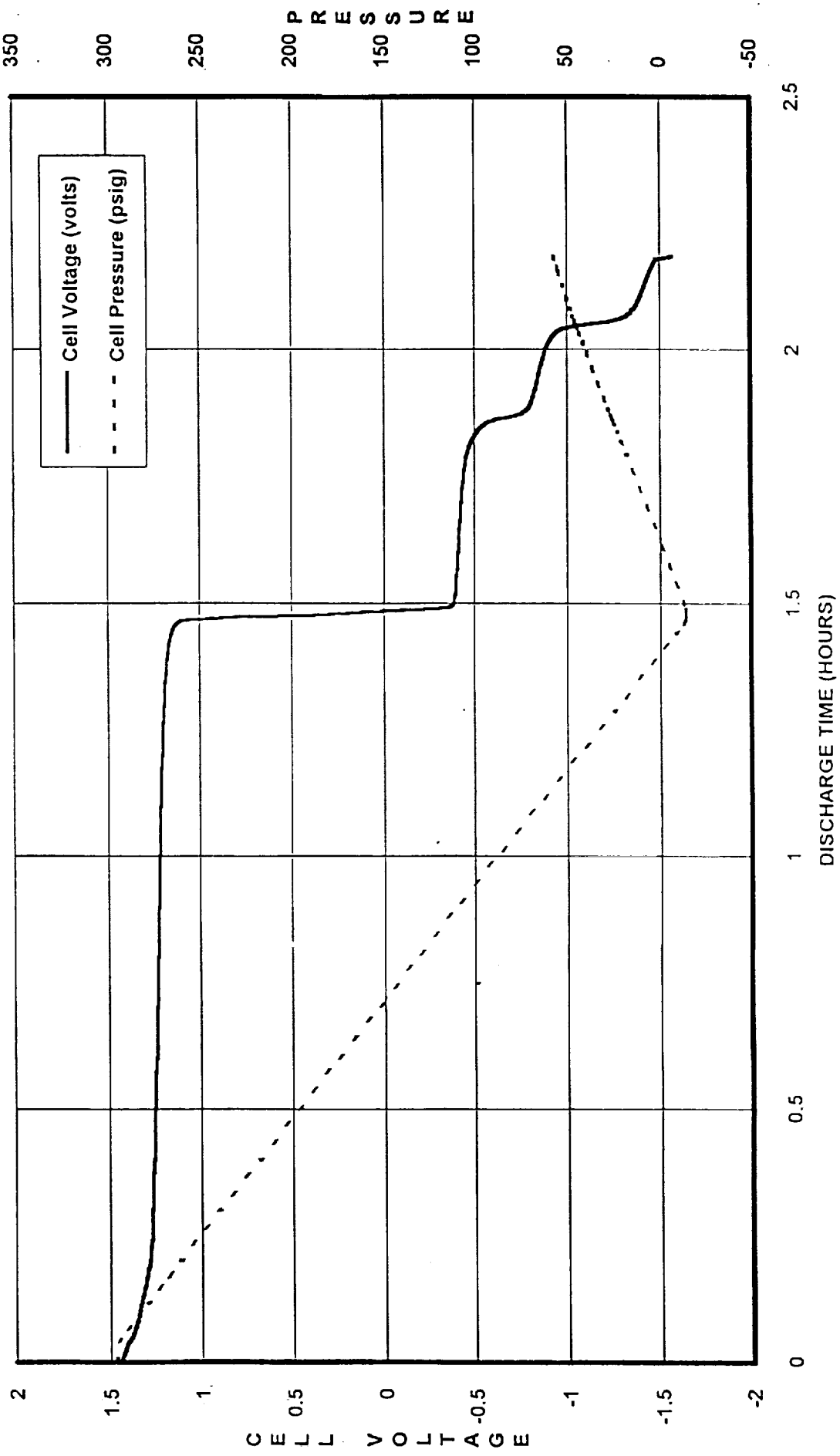

DISCHARGE INTO REVERSAL WITH NICKEL PRECHARGE (C/10)

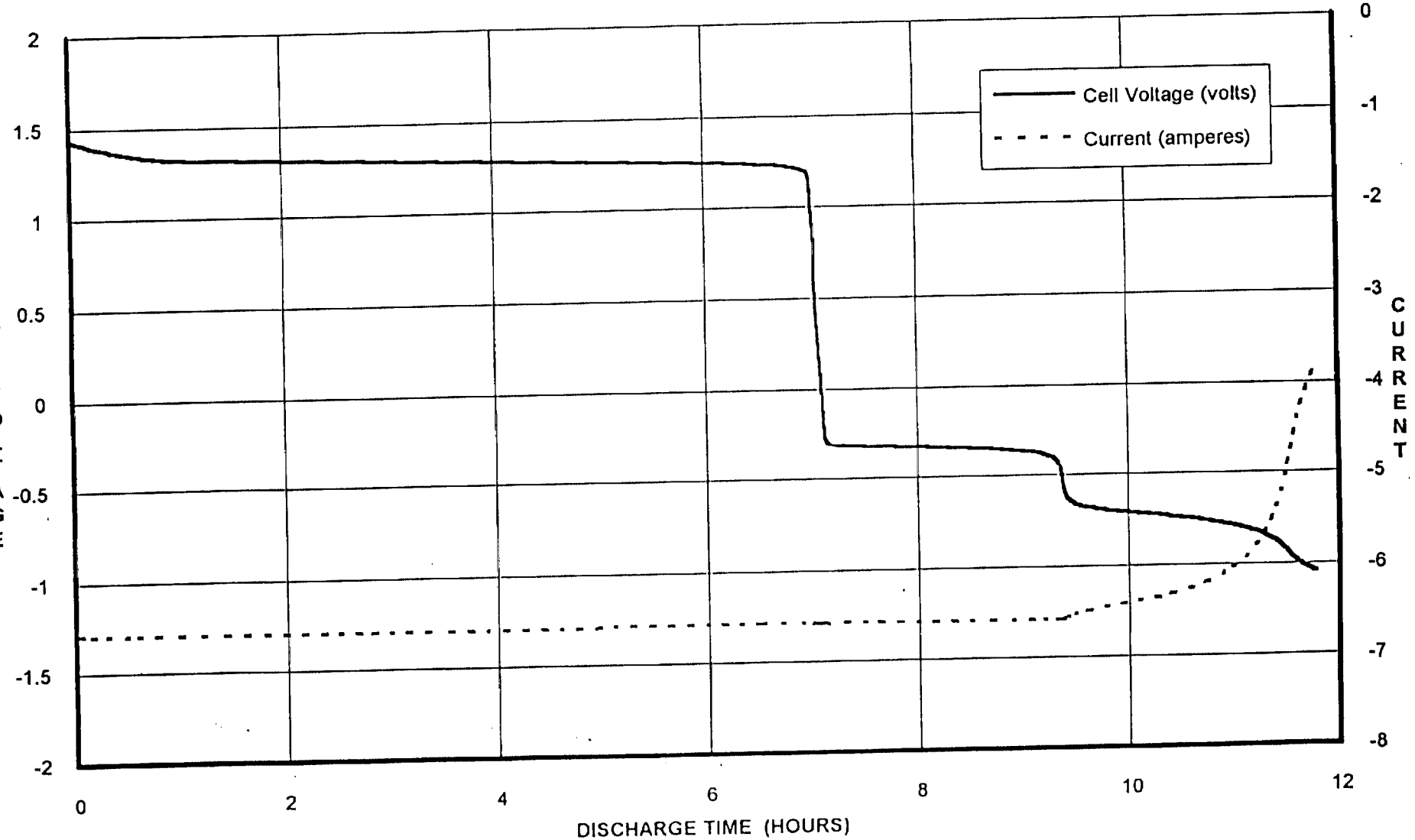

DISCHARGE INTO REVERSAL WITH LEAK-TO-VACUUM

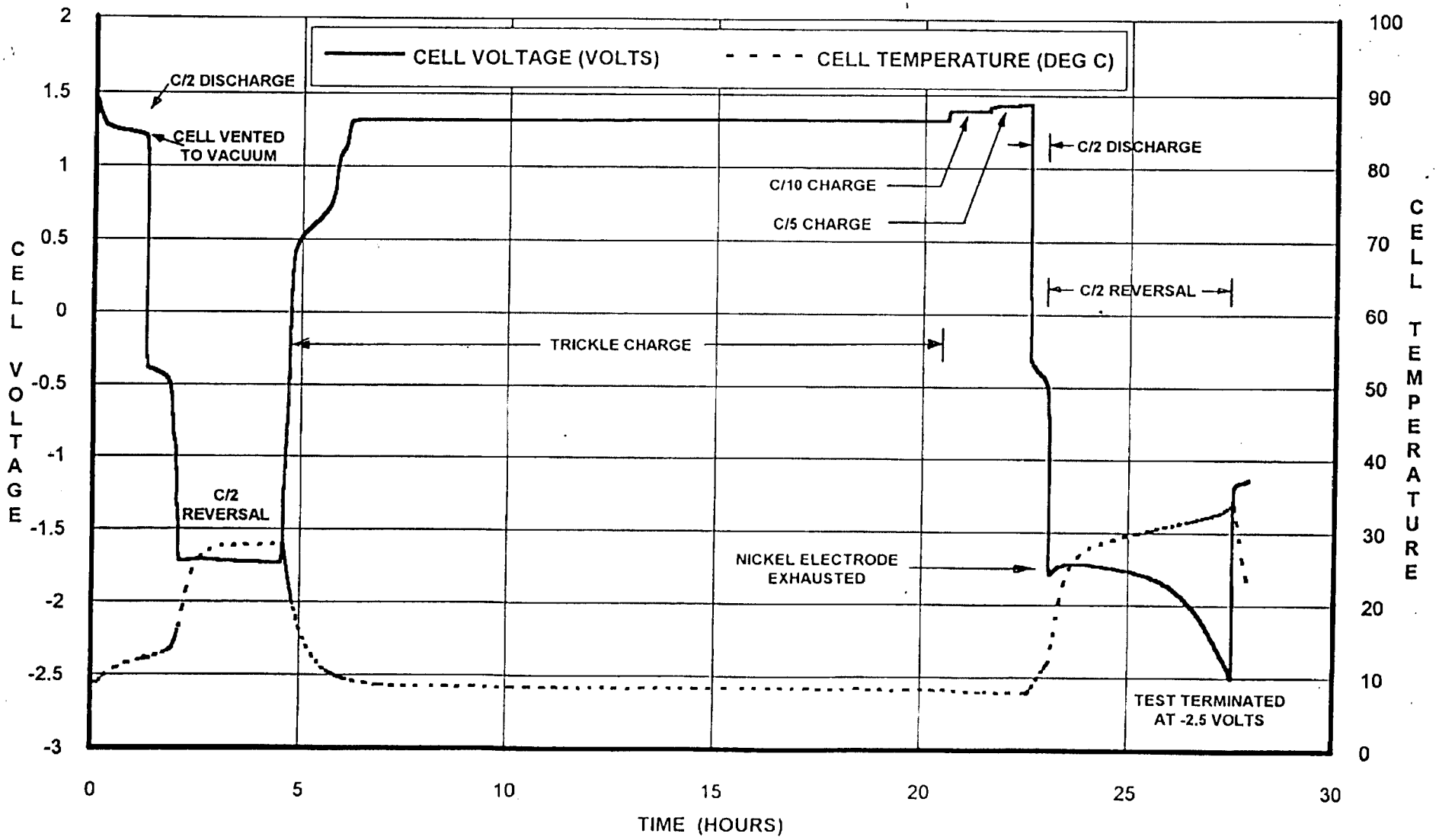

VOLTAGE TRAJECTORY
END OF DISCHARGE AND REVERSAL

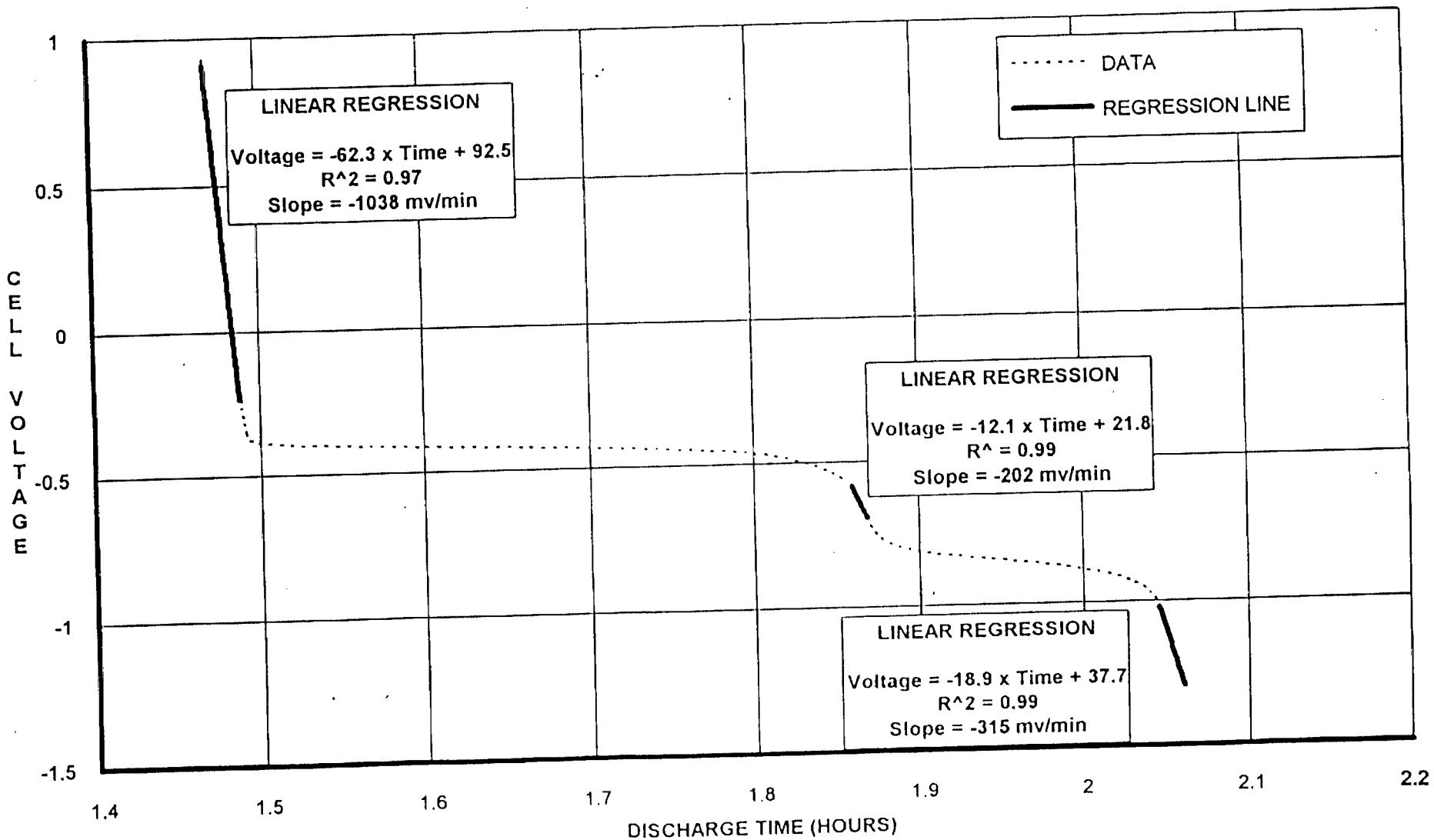

COMPOSITE VOLTAGE TRAJECTORY CURVES

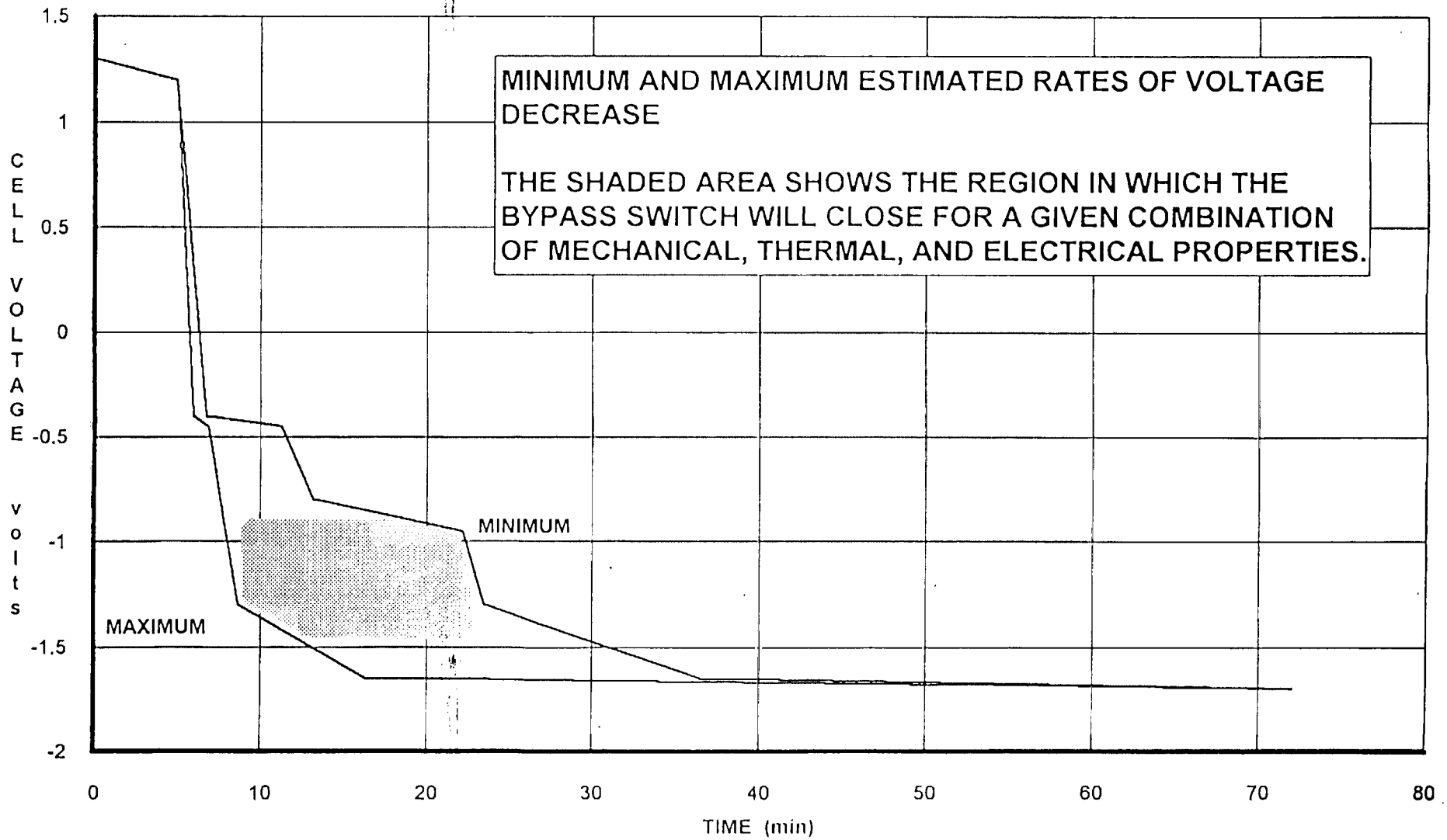

CYCLE LIFE VS DEPTH OF DISCHARGE

UPDATE ON MODELING STUDIES

Lawrence H. Thaller

The Aerospace Corporation

Presented At

1993 NASA Aerospace Battery Workshop
Huntsville, Alabama
November 16-18, 1993

Energy Technology Department
Electronics Technology Center

THE AEROSPACE CORPORATION

PROCESS INVOLVED

- COLLECTED DATA FROM VARIOUS SOURCES
  - MARTIN MARIETTA
  - AIR FORCE/CRANE
  - NASA LeRC
    - JOHN SMITHRICK
    - SPACE STATION
  - IECEC PAPERS
- PLOTTED DATA AGAINST BACKDROP OF SIMPLE WEAROUT MODEL
- MADE SOME GENERAL STATEMENTS BASED ON AVAILABLE DATA
- CONSIDERED OTHER DEGRADATION MECHANISMS
- CONCLUDING REMARKS

The reader is referred to the 1990 NASA Battery Workshop Paper by L. Thaller for background formulas and information on this topic.

CYCLE LIFE VS DEPTH OF DISCHARGE
DATA AS OF THREE YEARS AGO

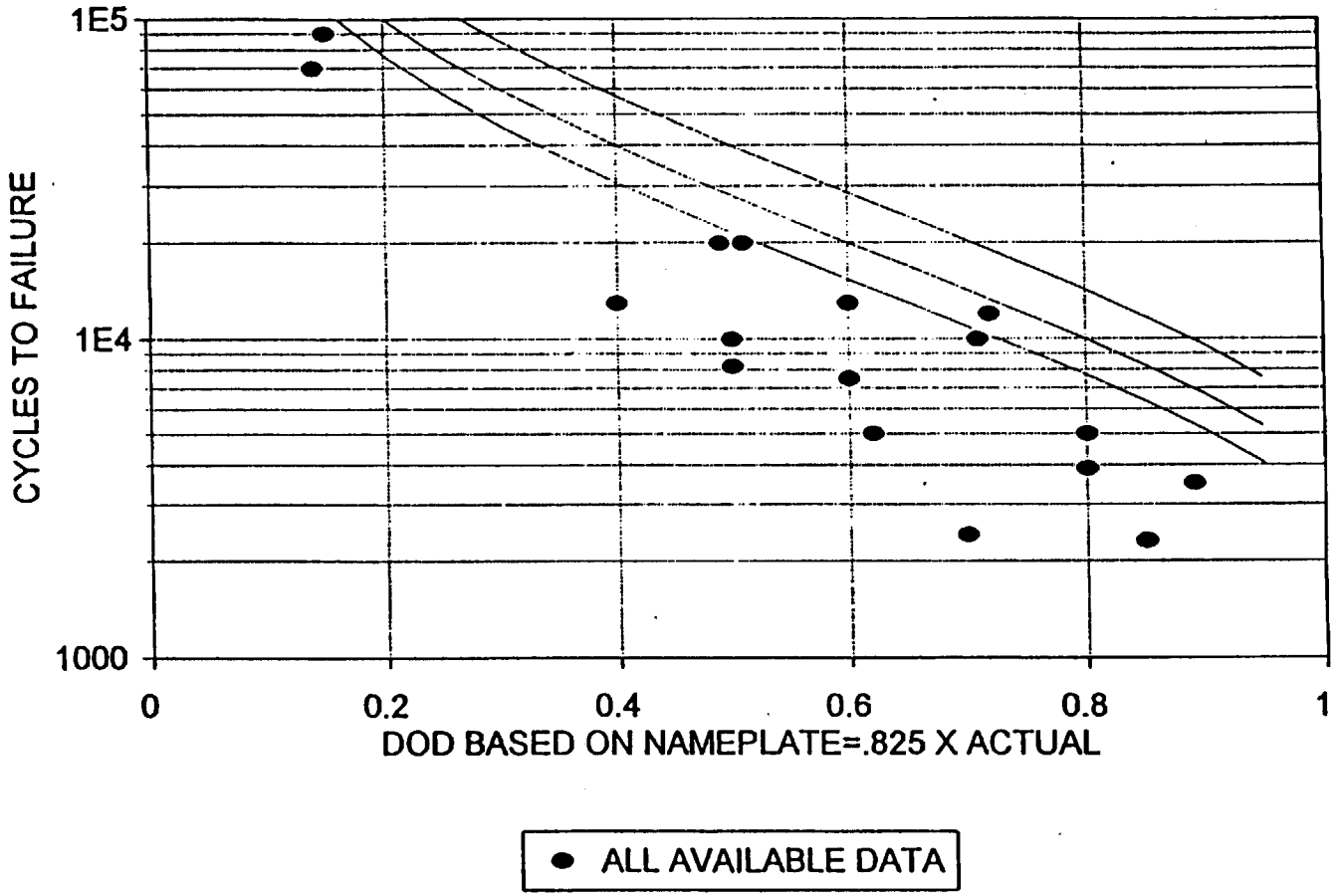

CYCLE LIFE VS DEPTH OF DISCHARGE
AF/CRANE-FUHR-SMITHRICK

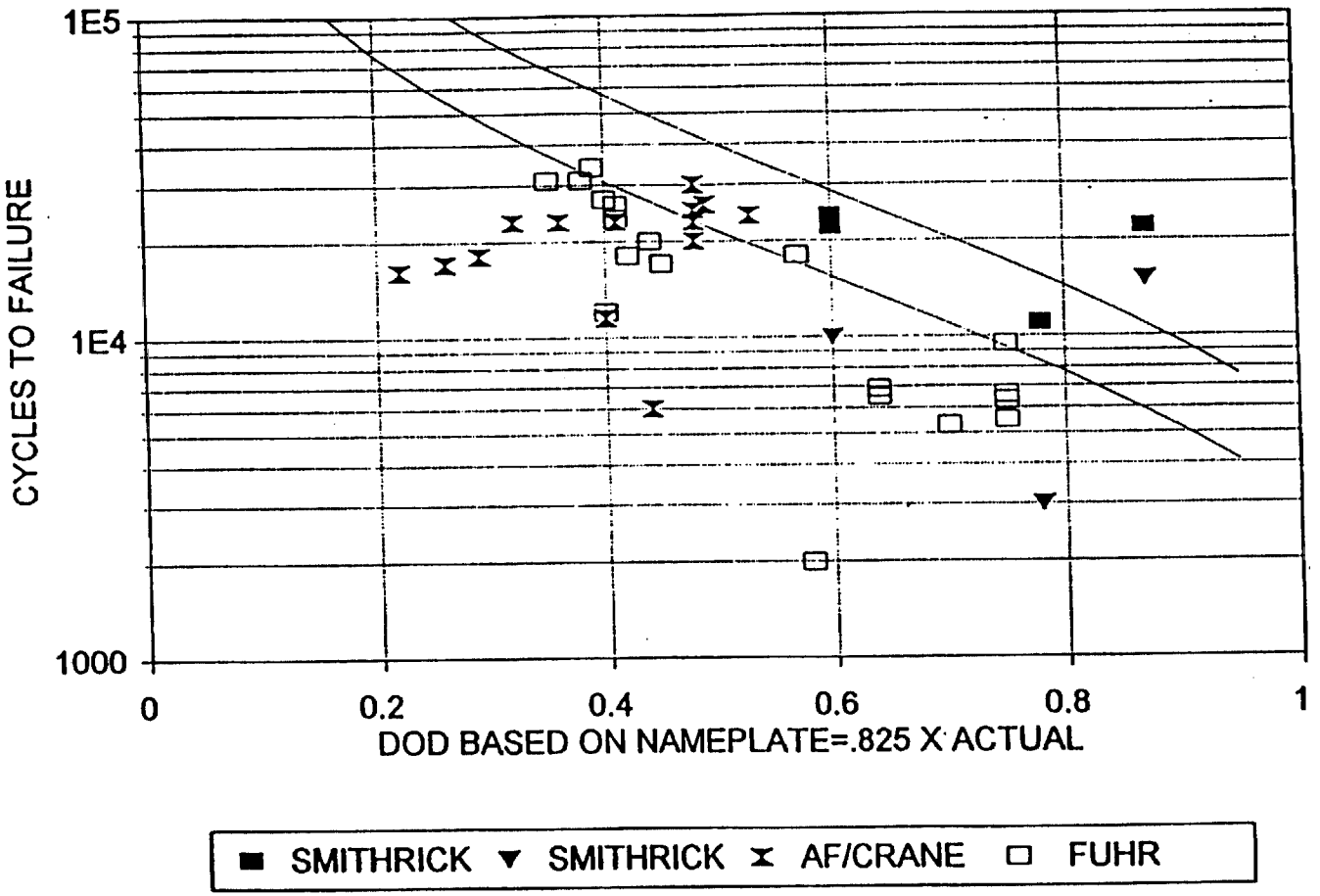

CYCLE LIFE VS DEPTH OF DISCHARGE
KEN FUHR'S DATA

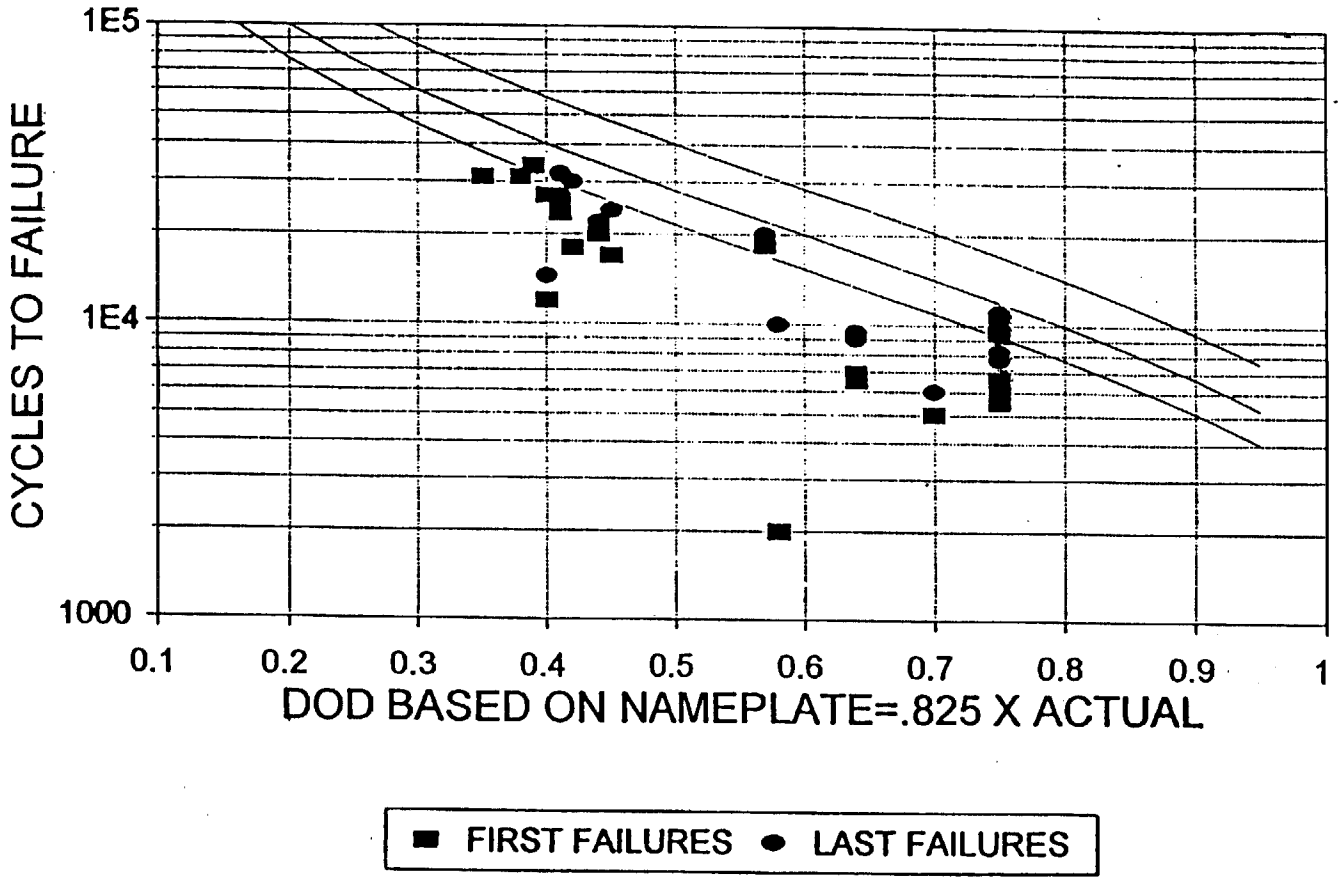

CYCLE LIFE VS DEPTH OF DISCHARGE
AIR FORCE/CRANE DATA

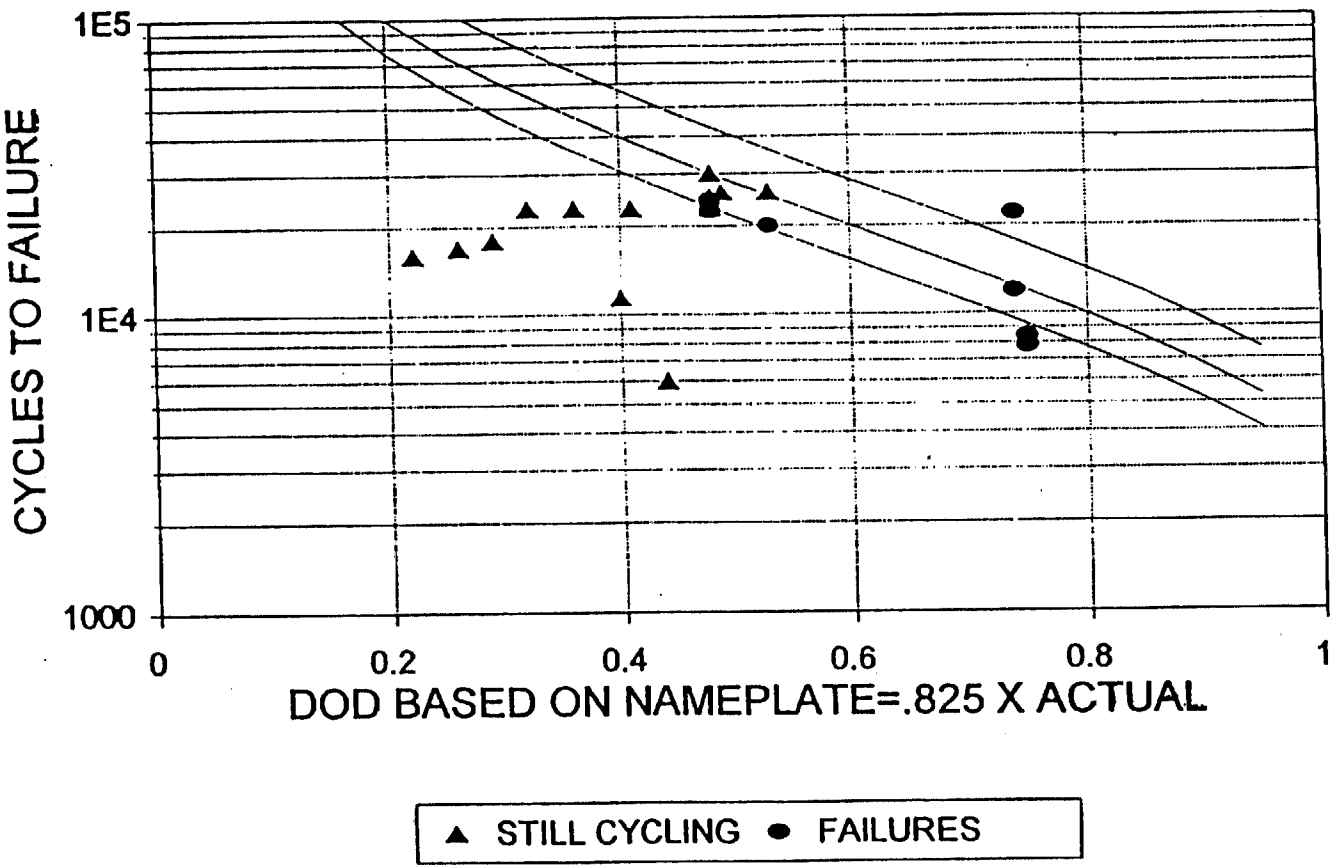

CYCLE LIFE VS DEPTH OF DISCHARGE
EAGLE-PICHER DATA

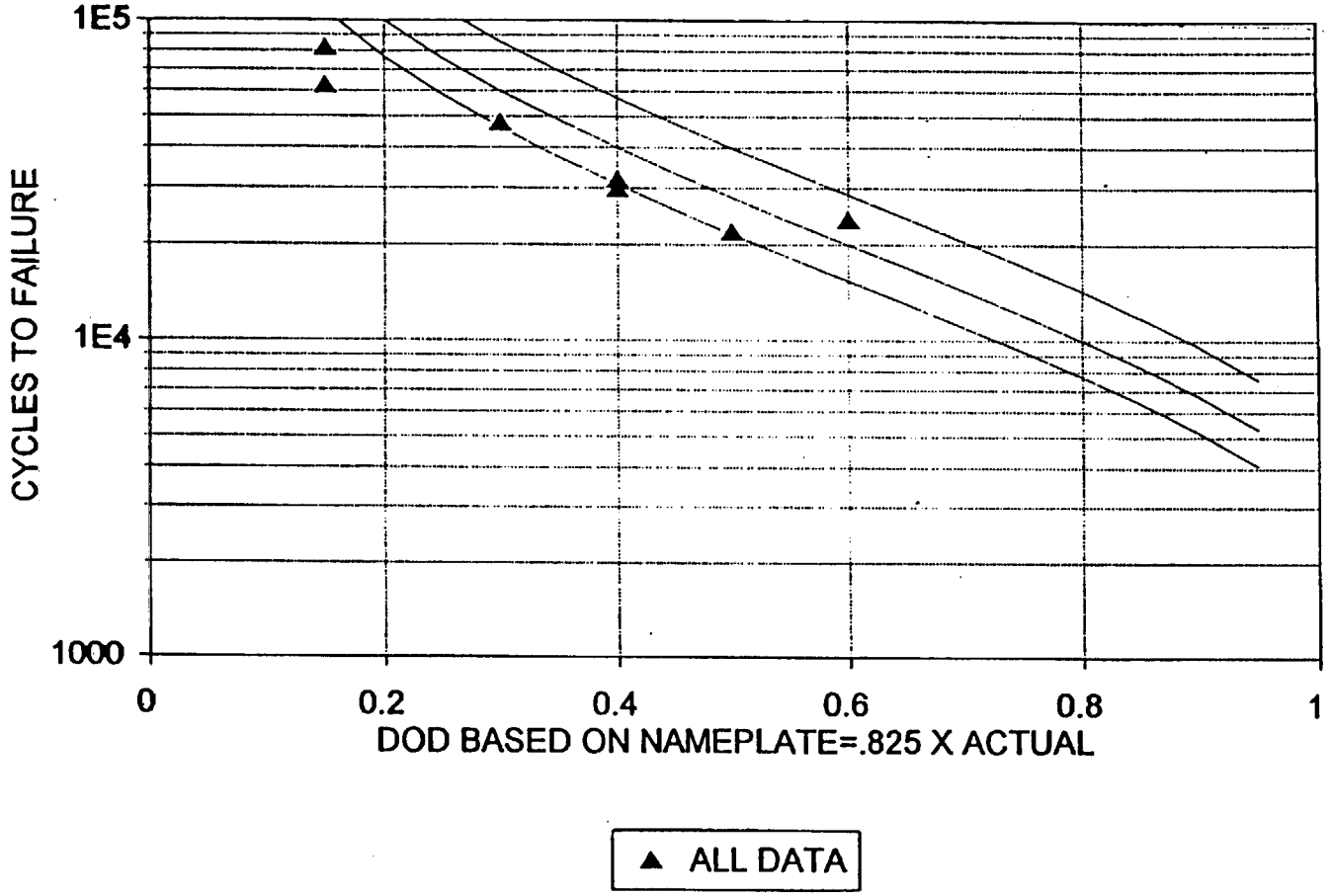

CYCLE LIFE VS DEPTH OF DISCHARGE
STEVE SCHIFFER'S DATA

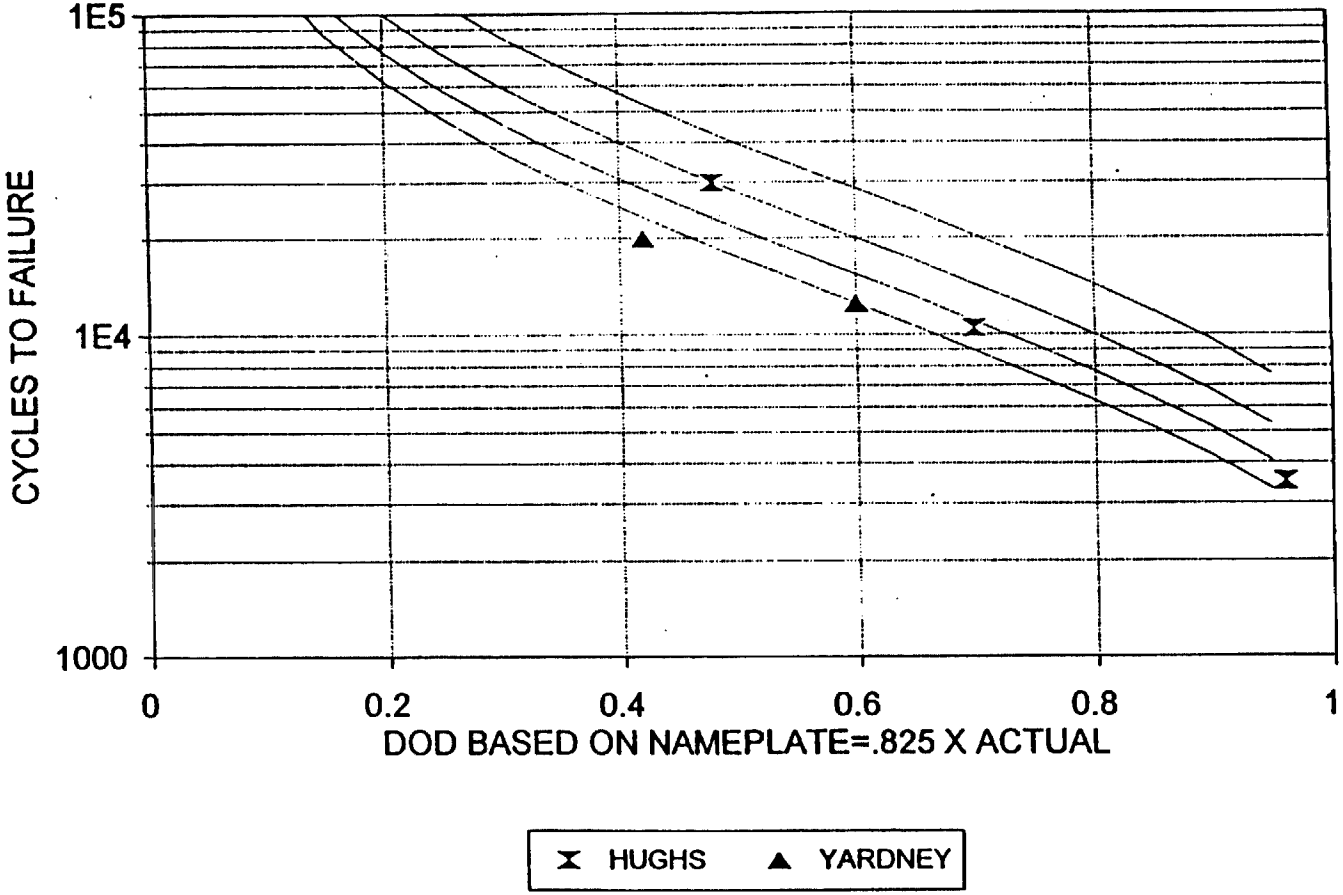

CYCLE LIFE VS DEPTH OF DISCHARGE
JOHN SMITHRICK'S DATA

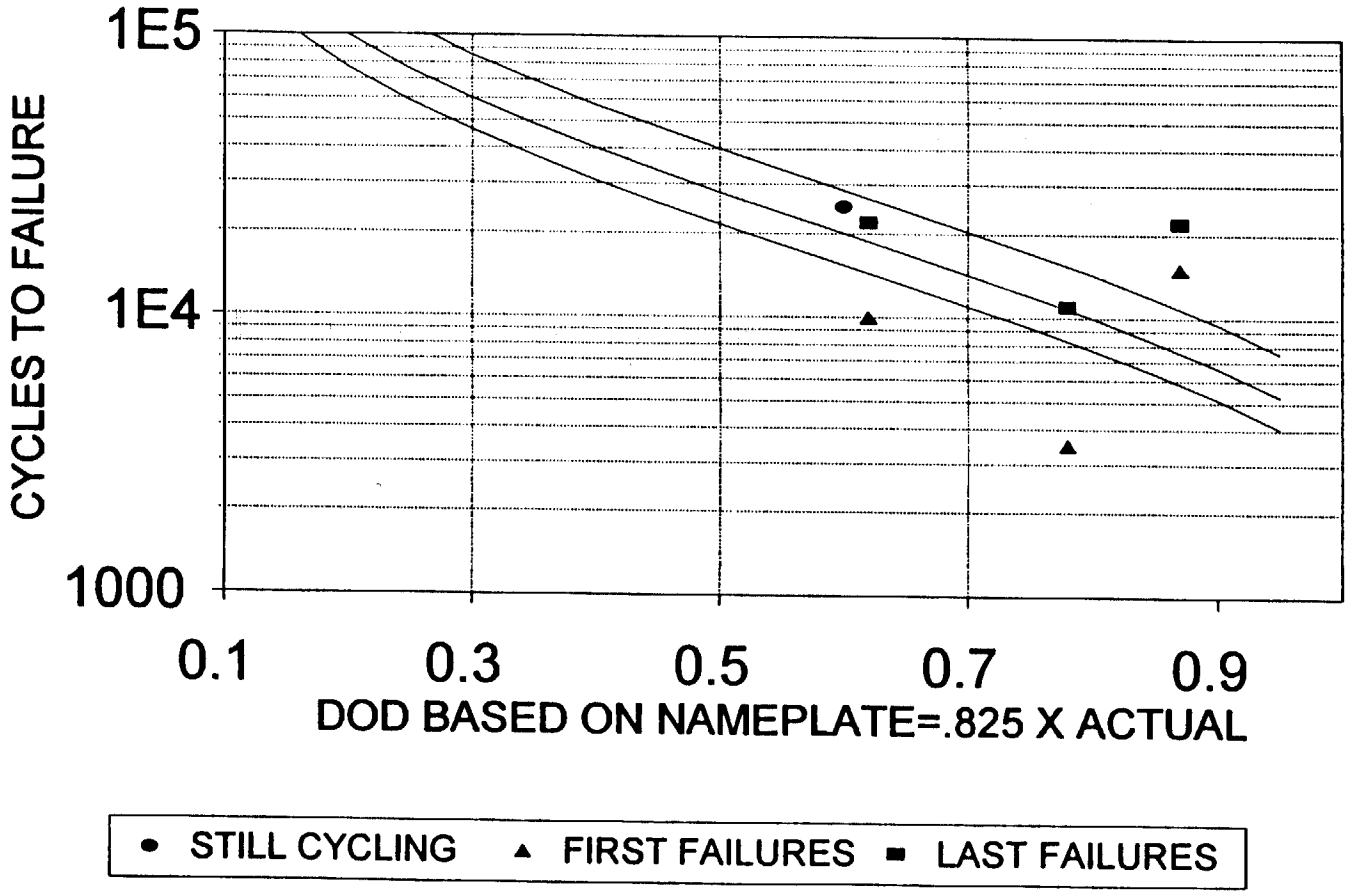

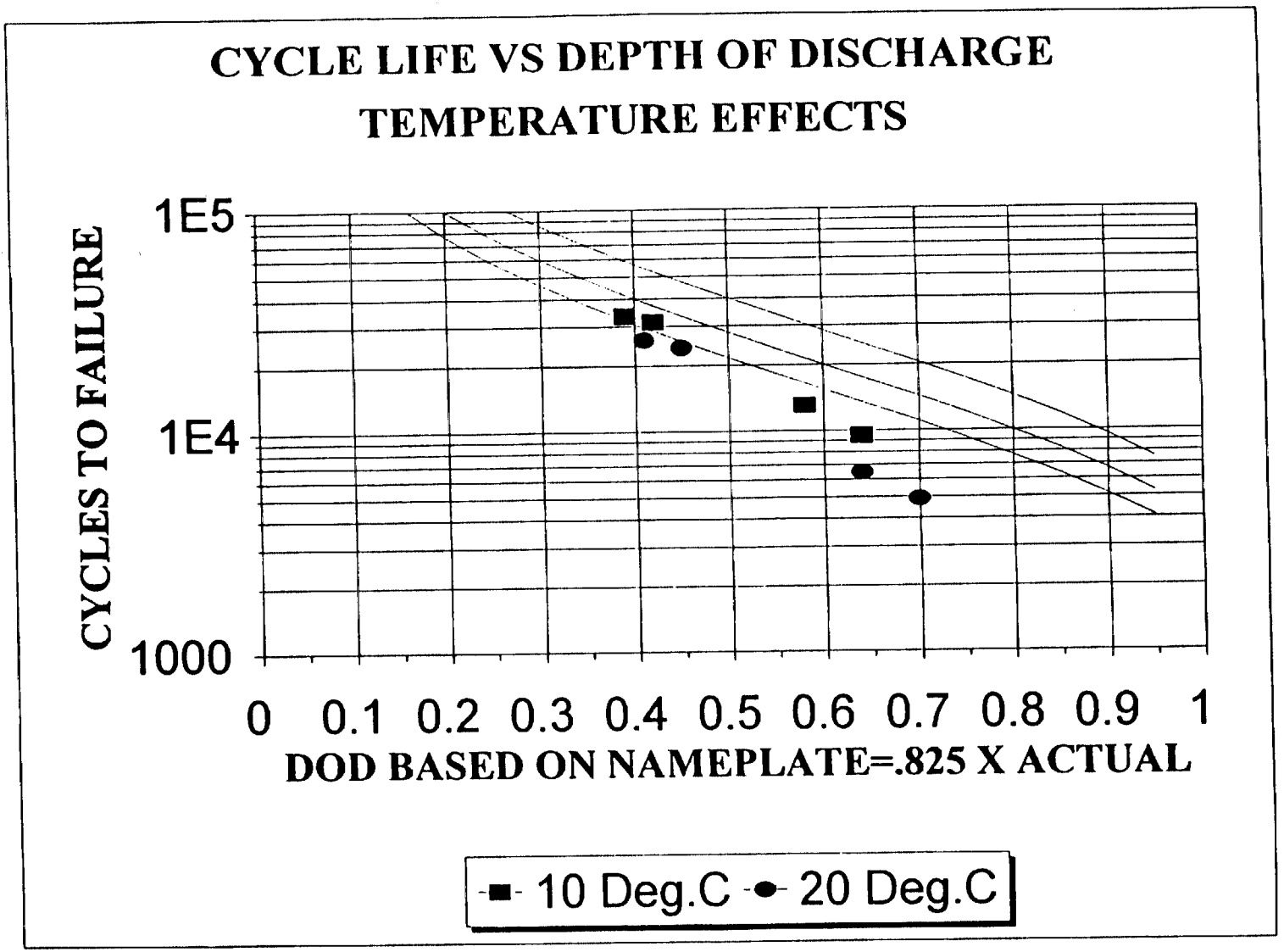
CYCLE LIFE VS DEPTH OF DISCHARGE
TEMPERATURE EFFECTS
CYCLES TO FAILURE
1E5
1E4
1000
0 0.1 0.2 0.3 0.4 0.5 0.6 0.7 0.8 0.9 1
DOD BASED ON NAMEPLATE=.825 X ACTUAL
10 Deg.C
20 Deg.C

CYCLE LIFE VS DEPTH OF DISCHARGE
E-P,YARDNEY, AND HUGHES 26% DATA

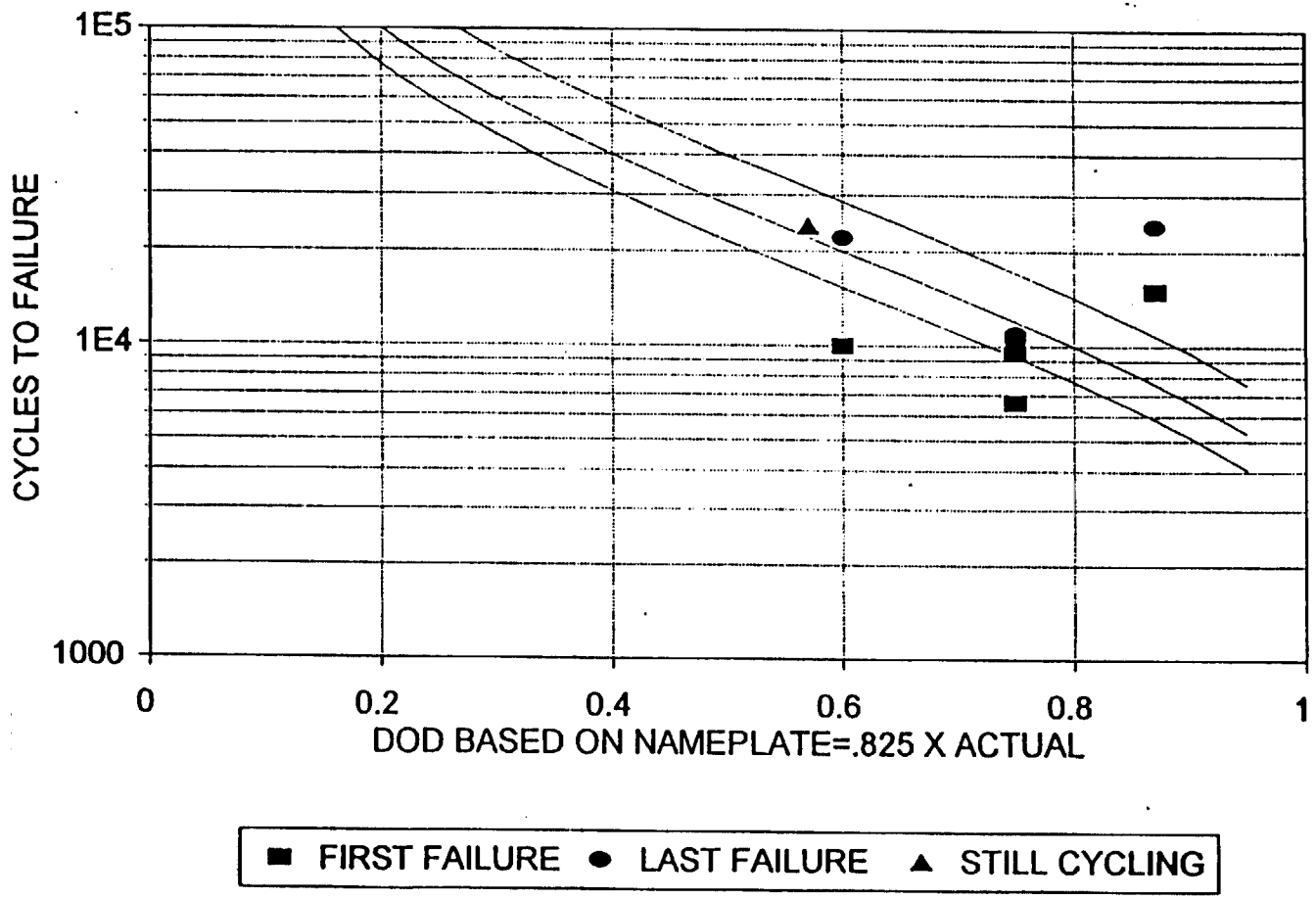

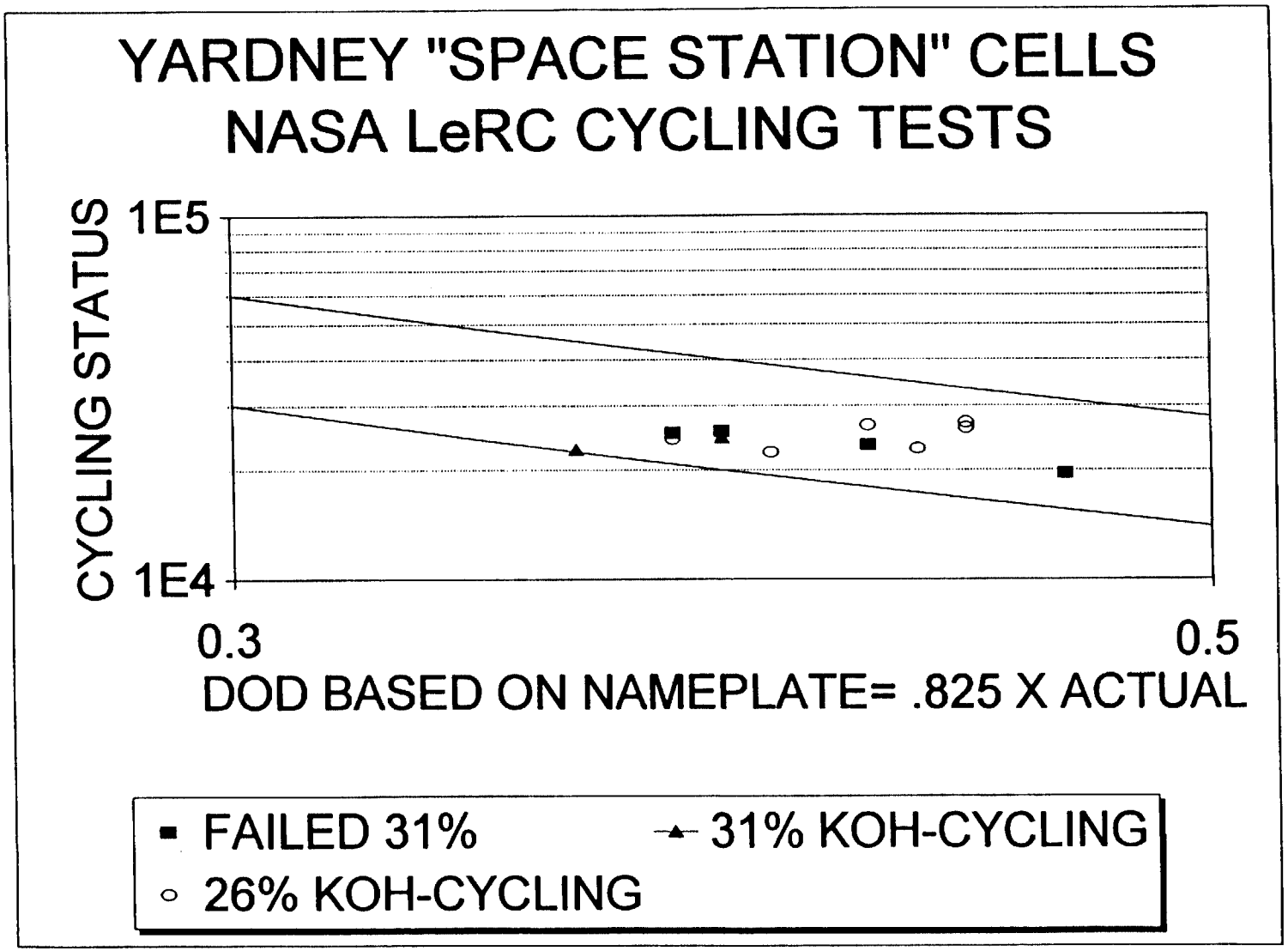
YARDNEY "SPACE STATION" CELLS
NASA LeRC CYCLING TESTS
CYCLING STATUS
1E5
1E4
0.3
0.5
DOD BASED ON NAMEPLATE= .825 X ACTUAL
FAILED 31%
31% KOH-CYCLING
26% KOH-CYCLING

GENERAL STATEMENTS

- o CYCLING DATA STRONGLY SUGGEST THAT:
  - DROPPING TEMPERATURE INCREASES CYCLE LIFE
  - USING 26% KOH VS. 31% KOH INCREASES CYCLE LIFE
  - CYCLE LIVES AMONG "LIKE" CELLS CAN VARY WIDELY (+/- 50%)
  - CELL FAILURES OCCUR FOLLOWING 25 TO 30% LOSS OF CAPACITY
  - CAPACITY CHECKS PROBABLY DO NOT EFFECT CYCLE LIFE

Energy Technology Department
Electronics Technology Center

THE AEROSPACE CORPORATION

GENERAL OBSERVATIONS

- CYCLE LIVES GENERALLY IMPROVING - ESPECIALLY AT DEEP DODs
- NAMEPLATE CAPACITIES SHOULD BE STANDARDIZED
- SOME CELL DESIGNS MAY NO LONGER BE AVAILABLE

GENERAL STATEMENTS

- CYCLING DATA STRONGLY SUGGEST THAT:
  - DROPPING TEMPERATURE INCREASES CYCLE LIFE
  - USING 26% KOH VS. 31% KOH INCREASES CYCLE LIFE
  - CYCLE LIVES AMONG "LIKE" CELLS CAN VARY WIDELY (+/- 50%)
  - CELL FAILURES OCCUR FOLLOWING 25 TO 30% LOSS OF CAPACITY
  - CAPACITY CHECKS PROBABLY DO NOT EFFECT CYCLE LIFE

CYCLE LIFE VS DEPTH OF DISCHARGE TWO DIFFERENT MODELS

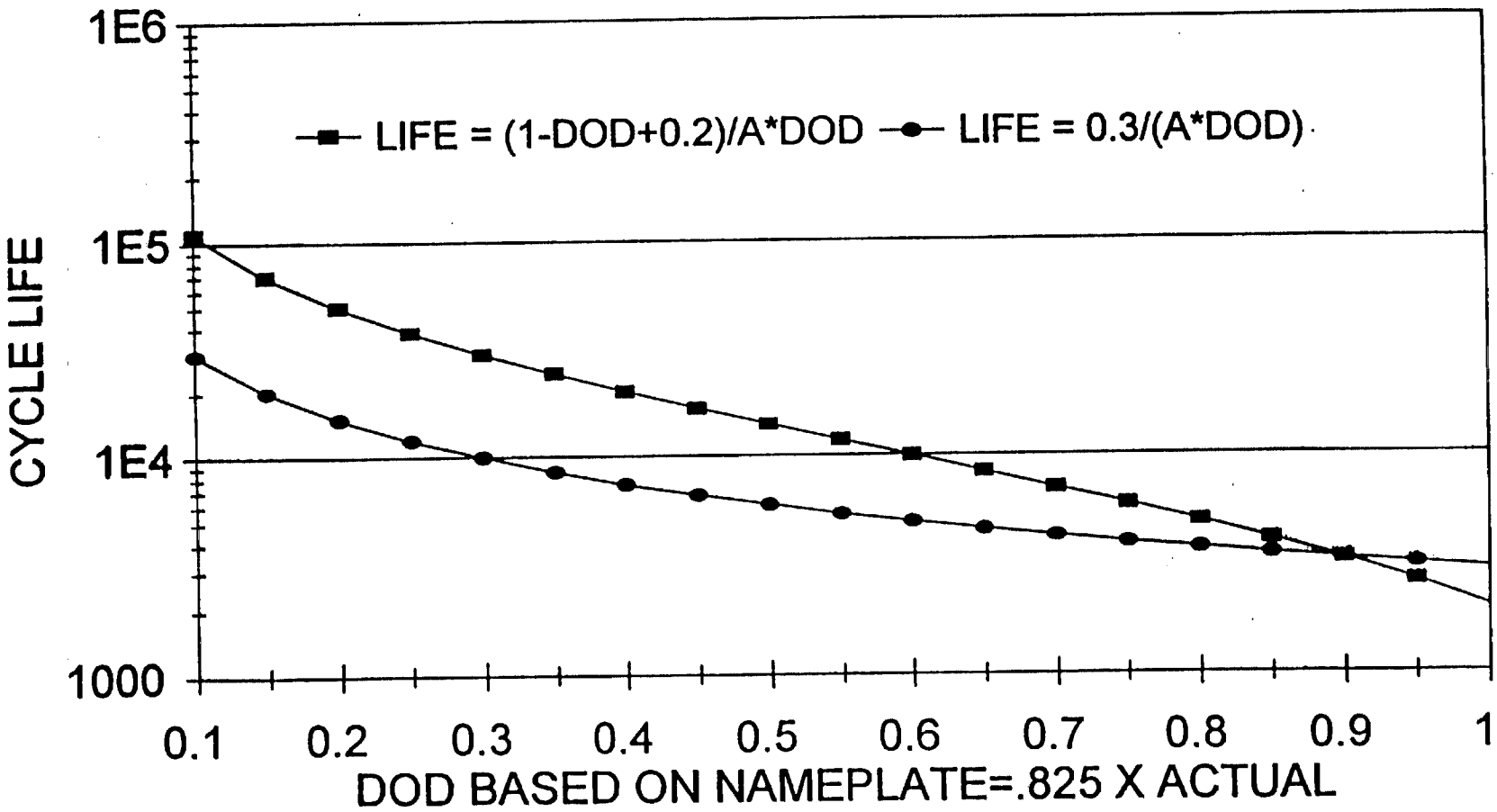

OTHER DEGRADATION MODES

- o EXCESS ELECTROLYTE
- o CONTAMINANTS (NATURAL) IN ASBESTOS
- o HIGH SURFACE LOADING OF ACTIVE MATERIAL
- o COLD FINGERING OF WATER VAPOR
- o INSUFFICIENT PROVISION FOR STACK EXPANSION

SUGGESTED DOs AND DON'Ts

o DO:

- USE CELL DESIGNS THAT OVERCOME KNOWN CELL PROBLEMS
- CONSIDER ELECTROLYTE, THERMAL, AND GAS MANAGEMENT ISSUES

o DON'T:

- USE ASBESTOS THAT HAS NOT BEEN PROPERLY REMANUFACTURED
- USE DESIGNS THAT WERE INTENDED FOR GEO IN LEO

CONCLUDING REMARKS

- CELL DESIGN FACTORS VERY IMPORTANT TO CYCLE LIFE
- CYCLE LIVES AT DEEP DODs GENERALLY IMPROVING
- 40,000 TO 50,000 CYCLES AT 40% DOD NOT AN UNREASONABLE GOAL
- CYCLE LIFE TESTING MUST CONSIDER CYCLING TO 50 TO 70% DOD
- MECHANICAL DESIGN CHANGES CANCEL OUT ESTABLISHED DATA BASES
- SIMPLE EQUATIONS DON'T ACCURATELY FIT OBSERVED FAILURES

AIR FORCE STANDARDS FOR NICKEL HYDROGEN BATTERY

WARREN HWANG AND MARTIN MILDEN
AEROSPACE CORPORATION
16 NOVEMBER 1993

THE AEROSPACE CORPORATION

AF NICKEL HYDROGEN STANDARDIZATION GOALS

- PROMOTE INTERCHANGEABILITY
  - AMONG VENDOR PRODUCTS
  - BETWEEN PROGRAMS
- INCREASE RELIABILITY
  - DESIGN AND PROCESS STABILITY
  - UNIFORM DATA BASE
  - APPROPRIATE HANDLING AND STORAGE
- PERMIT INNOVATIONS AND IMPROVEMENTS
- REDUCE LIFE CYCLE COST

AF NICKEL HYDROGEN STANDARDIZATION PHILOSOPHY

- CONCENTRATE ON STANDARDIZATION AT CELL LEVEL
  - INTERCHANGEABILITY AND RELIABILITY ISSUES ARE MORE IMPORTANT AT THE CELL LEVEL
  - BATTERY DESIGN OFTEN HIGHLY INTEGRATED WITH SPECIFIC POWER SYSTEM AND SPACECRAFT DESIGNS
- CELL LEVEL STANDARDIZATION IS BASICALLY FORM/FIT/FUNCTION TYPE
  - ALLOWS IMPROVEMENT OF INTERNAL DESIGNS
  - INCLUDES STANDARDIZATION OF TESTS, STORAGE, AND HANDLING
- BATTERY LEVEL STANDARDIZATION INCLUDES INTERFACES, TESTS, STORAGE, AND HANDLING

AF NICKEL HYDROGEN STANDARDIZATION PROJECT OUTLINE

- SURVEY AF PROGRAMS TO DETERMINE BATTERY USAGES AND NEEDS
- REVIEW PREVIOUS SPACECRAFT BATTERY STANDARDS
- DEFINE STANDARDIZATION AT CELL LEVEL
- DEFINE STANDARDIZATION AT BATTERY LEVEL
- DISTRIBUTE TO SPACE BATTERY COMMUNITY FOR REVIEW
- INCORPORATE INPUTS INTO STANDARDS

AF NICKEL HYDROGEN STANDARDIZATION
CELL LEVEL STANDARDIZATION

- CAPACITY, SIZE, WEIGHT
- INTERFACES
- PERFORMANCE REQUIREMENTS
- CORE ACCEPTANCE TESTS
- MANUFACTURING PROCESS CONTROL
- GENERIC QUALIFICATION TESTS
- STORAGE AND HANDLING REQUIREMENTS

AF NICKEL HYDROGEN STANDARDIZATION BATTERY LEVEL STANDARDIZATION

- INTERFACES
- CORE ACCEPTANCE TESTS
- GENERIC QUALIFICATION TESTS
- STORAGE AND HANDLING REQUIREMENTS

AF NICKEL HYDROGEN STANDARDIZATION SCHEDULE

COMPLETE INTERNAL DRAFT	FEBRUARY 1994
DISTRIBUTE FOR EXTERNAL REVIEW	MARCH 1994
INPUTS FROM REVIEW	JUNE 1994
COMPLETE FINAL DRAFT	SEPTEMBER 1994

Charge Efficiency of Ni/H_2 Cells During Transfer Orbit of Telstar 4 Satellites

by

W.C. Fang, D.W. Maurer, B. Vyas and M.N. Thomas

INTRODUCTION

The TELSTAR 4 communication satellites being manufactured by Martin Marietta Astro Space (Astro Space) for AT&T are three axis stabilized spacecraft[1] scheduled to be launched on expendable vehicles such as the Atlas or Ariane rockets. Typically, these spacecraft consist of a box that holds the electronics and supports the antenna reflectors and the solar array wings. The wings and reflectors are folded against the sides of the box during launch and the spacecraft is spun for attitude control in that phase; they are then deployed after achieving the final orbit. The launch phase and transfer orbits required to achieve the final geosynchronous orbit typically take 4 to 5 days during which time the power required for command, telemetry, attitude control, heaters, etc., is provided by two 50 AH nickel hydrogen batteries augmented by the exposed outboard solar panels. In the past, this situation has presented no problem since there was a considerable excess of power available from the array.

In the case of large high powered spacecraft such as TELSTAR 4, however, the design power levels in transfer orbit approach the time-averaged power available from the exposed surface area of the solar arrays, resulting in a very tight power margin. To compound the difficulty, the array output of the spinning spacecraft in transfer orbit is shaped like a full wave rectified sine function and provides very low charging rates to the batteries during portions of the rotation (Fig 1). In view of the typically low charging efficiency of alkaline nickel batteries at low rates, it was decided to measure the efficiency during a simulation of the TELSTAR 4 conditions at the expected power levels and temperatures on three nickel hydrogen cells of similar design. The unique feature of nickel hydrogen cells that makes the continuous measurement of efficiency possible is that hydrogen is one of the active materials and thus, cell pressure is a direct measure of the state of charge or available capacity. The pressure is measured with a calibrated strain gage mounted on the outside of the pressurized cell.

[1]The spacecraft is actually spin stabilized in transfer orbit and three axis stabilized (sometimes called body stabilized) on station in the earth centered coordinate system using momentum wheels and magnetic torquers.

SIMULATION PARAMETERS

The array power was calculated in one degree increments of spacecraft rotation and the expected stowed array output. The efficiencies of the charge and discharge converters were in excess of 90%. The resulting battery charge or discharge current is shared by the two batteries for each degree of rotation. These calculations were performed for various spacecraft (S/C) power levels up to 490 W which represents the expected load with active transfer orbit equipment; also covered were lower loads (430W) such as those available after the LAE burns, etc.

Traditionally, both batteries share the charge and discharge currents equally (parallel operation) so that the net time-averaged charging current, with 430 W S/C load, is only C/98. At 490W S/C load the situation would be much worse. A practical solution was to employ "sequential charging" to increase the charging current. In this mode, all the charge current is fed into one battery with the other left on open circuit during the charge phase; after a period of time, e.g. 15 minutes, the batteries are switched. In this case, the charging efficiency increases to well above 90% for the 430W load (Fig.2). Precise measurements of the charge efficiency during sequential charging under simulated transfer orbit cycle power conditions are presented in this study.

EXPERIMENT

The transfer orbit cycle simulation was accomplished by utilizing the output from a programmable arbitrary wave form generator (Wavetek Model 175) into a fast power supply/amplifier (Kepco Model BOP 36-6M; rise time for the current is $5x10^5$ A/sec). The actual current profiles imposed on the cells were measured across a shunt using a storage digital oscilloscope (Nicolet 410). The sampling rate was at 5 msec. Figure 3 shows a typical recorded profile for current. The recorded profiles were then used to calculate the net time-averaged current(I_{ave}). The cells were initially brought to ~50% state of charge (~ 470 psi) by charging or discharging at 5A and then allowed to equilibrate for a minimum of 2 hours before starting the experiment. Two current profiles corresponding to 490 W and 430 W S/C loads were used at a period of 3 sec/cycle (10 RPM on the S/C)[2]. For comparison, the cells were also charged at the equivalent time-averaged constant current of the simulation. The temperatures chosen were 0°C and -15°C corresponding to the most probable and the lowest expected temperatures, including margin, respectively.

[2]This is the baseline S/C spin rate required for attitude control. Other experiments have shown that the spin rate has minimal effect on the charging efficiency.

The cell pressure and voltage were monitored during the run. The strain gage was calibrated at each temperature by charging the cells to various pressures followed by discharging to 1.0V cutoff to get the corresponding available capacity. The charge/discharge rate of 5A was used to have a minimal thermal effect and to correspond to the approximate rate used during the deployment phase. Figure 4 shows the typical results for capacity versus cell pressure. These data can be fit to an equation of the form:

$$Capacity\ (available) = A + BP \qquad (a)$$

where P is the cell pressure and A and B are constants. The charging efficiency, F, by definition is given by:

$$F = \frac{Capacity(available)}{Capacity(input)} \qquad (b)$$

The Capacity(input) is simply the time-averaged current multiplied by the time, i.e., $I_{ave}t$. Therefore the instantaneous charging efficiency, F_t, becomes:

$$F_t = \frac{d}{dt}\left(\frac{A+BP}{I_{ave}t}\right) = \frac{B}{I_{ave}}\left(\frac{dP}{dt}\right) \qquad (c)$$

Thus, the instantaneous charging efficiency is the first derivative of the curve of cell pressure vs. time multiplied by B/I_{ave}.

A typical curve of the change in cell pressure with time is shown in Fig. 5. The curve is rather noisy on a micro scale due to the cyclic nature of the current. Consistent, reliable results were obtained by curve fitting the pressure - time data using TableCurve[3] software with F-statistics as the selection criteria. Figure 6(a) illustrates the typical goodness-of-fit between the equation and the data. The fit is excellent as evidenced by the extremely low values in the percentage residual (<0 2%) as shown in Fig 6(b). Similar fits were obtained for all the data using the equation of the form:

$$P = C + Dt + Et^3 \qquad (d)$$

where C, D and E are constants. Combining equations (c) and (d) the instantaneous charging efficiency, F_t, becomes :

$$F_t = \left(\frac{B}{I_{ave}}\right)(D + 3Et^2) \qquad (e)$$

Fitted curves under various test conditions of S/C power, ambient temperature and

[3]TableCurve, Jandel scientific, Corte Madera, CA.

increasing state of charge are illustrated by the plots in Figs. 7 to 11. For comparison, the charge efficiency under conditions of time-averaged constant charge current at similar S/C power and temperature are also presented.

RESULTS AND DISCUSSION

The AT&T S/C design rules require that the battery must not be discharged more than 70% based on a planning estimate of 58 AH total capacity; this corresponds to 17 AH remaining. It was expected that the batteries would be injected into transfer orbit at 85% state of charge[4] or 49 AH available. The charging efficiency for the 430 W and 490 W S/C loads with sequential charging at 0°C and -15°C are shown in Figs. 7 and 8 respectively for available capacity ranging form 20 to 50 AH. These results indicate that:

- the charging efficiency is greater than 95% in most of the range tested, dropping to 92% at 0°C, 490 W at the 49 AH point expected during planning.
- the charging efficiency decreases with increasing state of charge of the cell and the decrease is more dramatic at 0°C than at -15°C.
- the charging efficiency is higher for 430 W than for 490 W.
- the charging efficiency is higher at lower temperatures due to increased oxygen overpotential as expected.

It must be emphasized that extrapolation of the curves beyond the data range is difficult particularly in the higher state of charge ranges. Note that these cells have nearly 70 AH capacity (c.f. Fig. 4) compared to their 50 AH nameplate capacity as do the TELSTAR 4 cells. Thus, the available capacity levels estimated in planning should be accomplished at reasonable efficiency. However, at the 490 W load, the time- averaged current is so low that it requires a significant amount of time to charge the battery. Thus it will be desirable to operate at lower loads such as 430 W as much as possible, or to utilize several powered down drift orbits to reach a sufficiently high state of charge prior to the deployment phase when no charging is possible.

The comparison of the charging efficiency between the simulations and the equivalent constant current charging is shown in Figs. 9 - 11. (Note that the equivalent constant current for the two cases are close but not identical to the time averaged simulation due to the difficulty in adjusting the programmable power supply. These differences, however, have a negligible effect on the results). In all cases, the constant current charging yields a slightly higher charging efficiency than the simulation. This can

[4]Not 100% due to self discharge on the launch pad and support of the S/C loads during ascent phase

be attributed to the following two factors. First the charging efficiency decreases non-linearly as the charging current is decreased while the time-averaged calculation assumes it to be linear so that the efficiency of the equivalent constant current could be either larger or smaller than that of the time averaged-current depending on whether the deviation of the efficiency from linearity is negative or positive. The other factor is that the simulation consists of both discharge and charge cycles, although the net time-averaged charge current is the same for the simulation as the constant current charging, the net charging efficiency of the simulation is always smaller than the constant current due to the fact that the discharging efficiency is always ~100% while the charging is not. Thus, the difference between the simulation and constant current charging will be determined by the sum of these two factors. The net result, however, is that suitably selected constant current charging can be used to determine the expected performance of the batteries for these conditions in qualification and acceptance testing. An example is given in Figure 12 to illustrate the charging efficiency of constant current charging as a function of both charging current and cell capacity available(state of charge).

SUMMARY

A sequential charging scheme for nickel hydrogen cells during transfer orbit of Telstar4 has been demonstrated to provide >90% charge efficiency necessary for a successful launch of the satellite. As expected, the charge efficiency is higher at lower ambient temperature of -15C and at a lower power load level of 430W. The charge efficiency using simulated conditions is slightly lower than charging at time averaged constant current. However, selected constant current charging can be used to determine the performance of these batteries for qualification and acceptance testing.

ACKNOWLEDGMENT

The authors wish to acknowledge the Martin Marietta Astro Space Telstar 4 Program Office for providing the expeimental cells used in this study and to George Case for numerous helpful discussions. Appreciation is also extended to Linda Palmieri for providing the background data used in the simulation calculations.

LIST OF FIGURES

1. Transfer orbit array current at various rotational angles for a given load current.
2. Comparison of parallel and sequential charging method in terms of charging efficiency
3. Calculated and measured current profile for 490 W, 3 s/cycle, -15 C.
4. Calibration plot of capacity versus cell pressure at zero degree Celsius.
5. Plot of cell pressure variation with time at 490 W, 3 s/cycle simulation, 0 C
6. Plots showing (a) best fit line for the experimental data showing cell pressure change with time and (b) % Residuals for the fitted equation for data from experiment at 490 Watts, 3 s/cycle, 0 C.
7. Charging efficiency versus Capacity at 430 W and 460 W during 3 s/cycle simulation at 0 C.
8. Simulation of Charging efficiency versus Capacity at 430 W and 460 W, 3 s/cycle,0 C
9. Comparison of simulation and constant current charging results at 430 W, 0 C
10. Plot of charging efficiency versus capacity under simulation and constant current conditions at 430 W, -15 C
11. Comparison of simulation and constant current charging at 490 W, -15 C
12. A 3-D presentation of charging efficiency as a function of charging current and cell capacity.

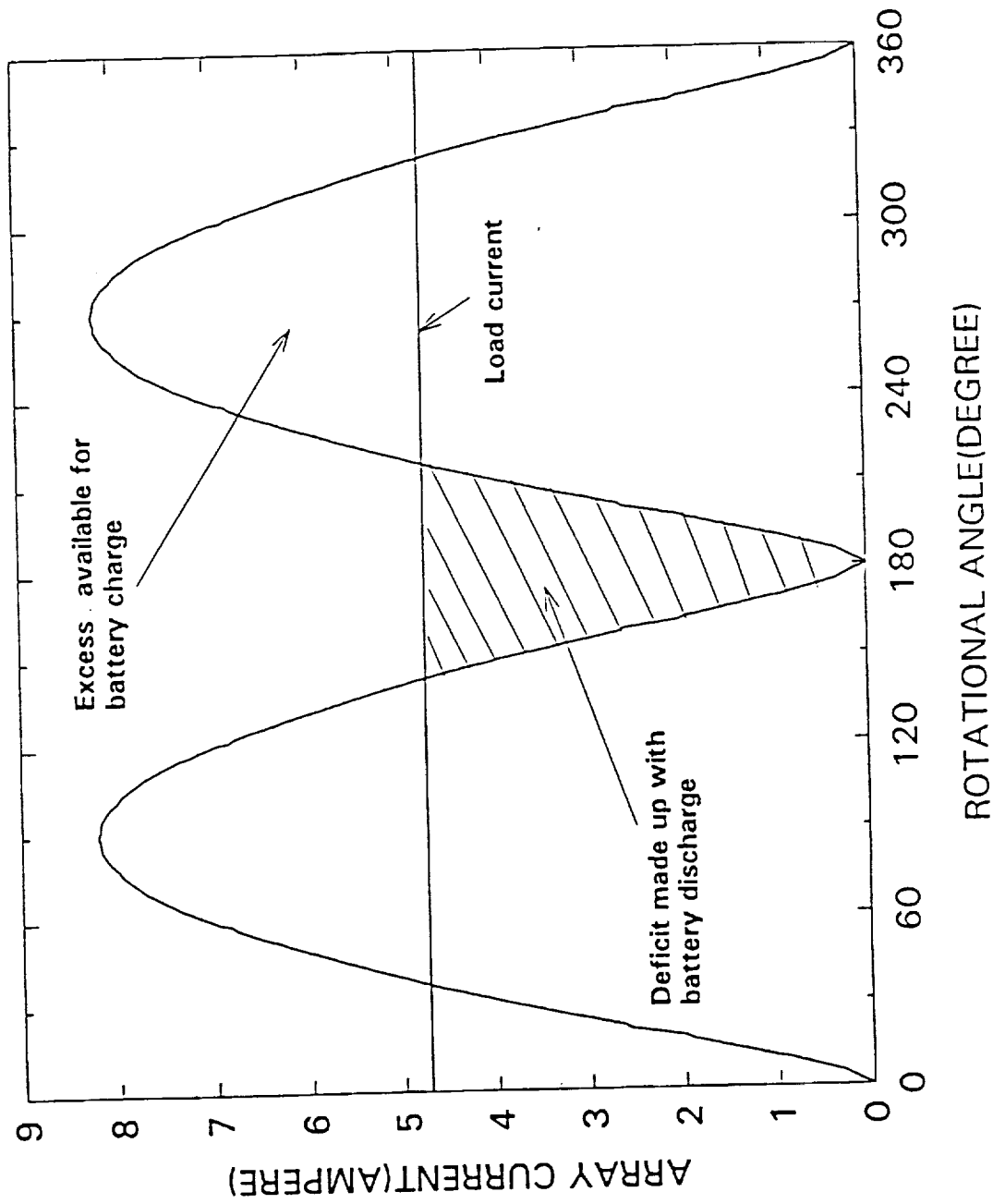

Fig.1 Transfer orbit array current at various rotational angles for a given load current

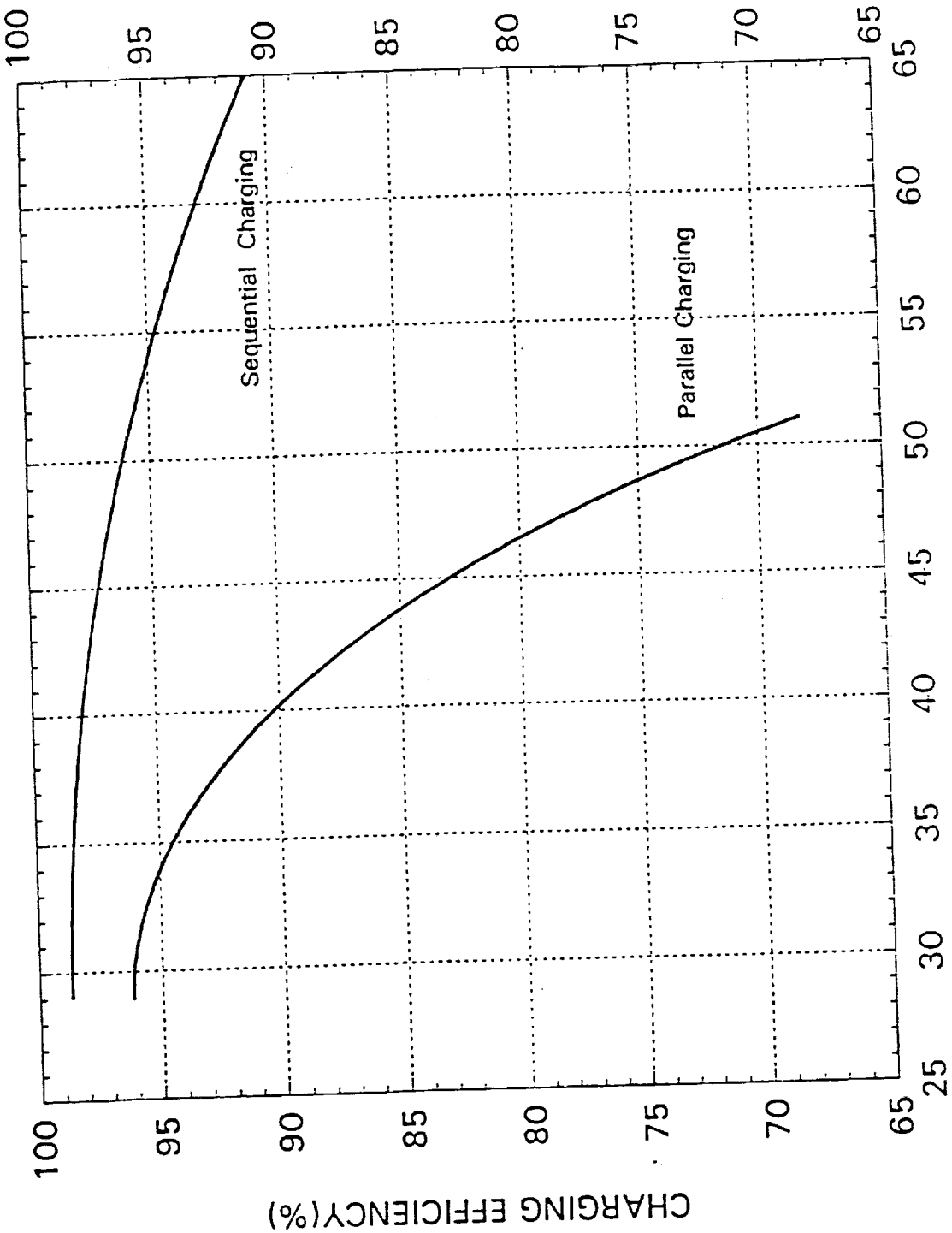

Fig.2 Comparison of parallel and sequential charging method in terms of charging efficiency 430W, 3sec/cycle, 0°C.

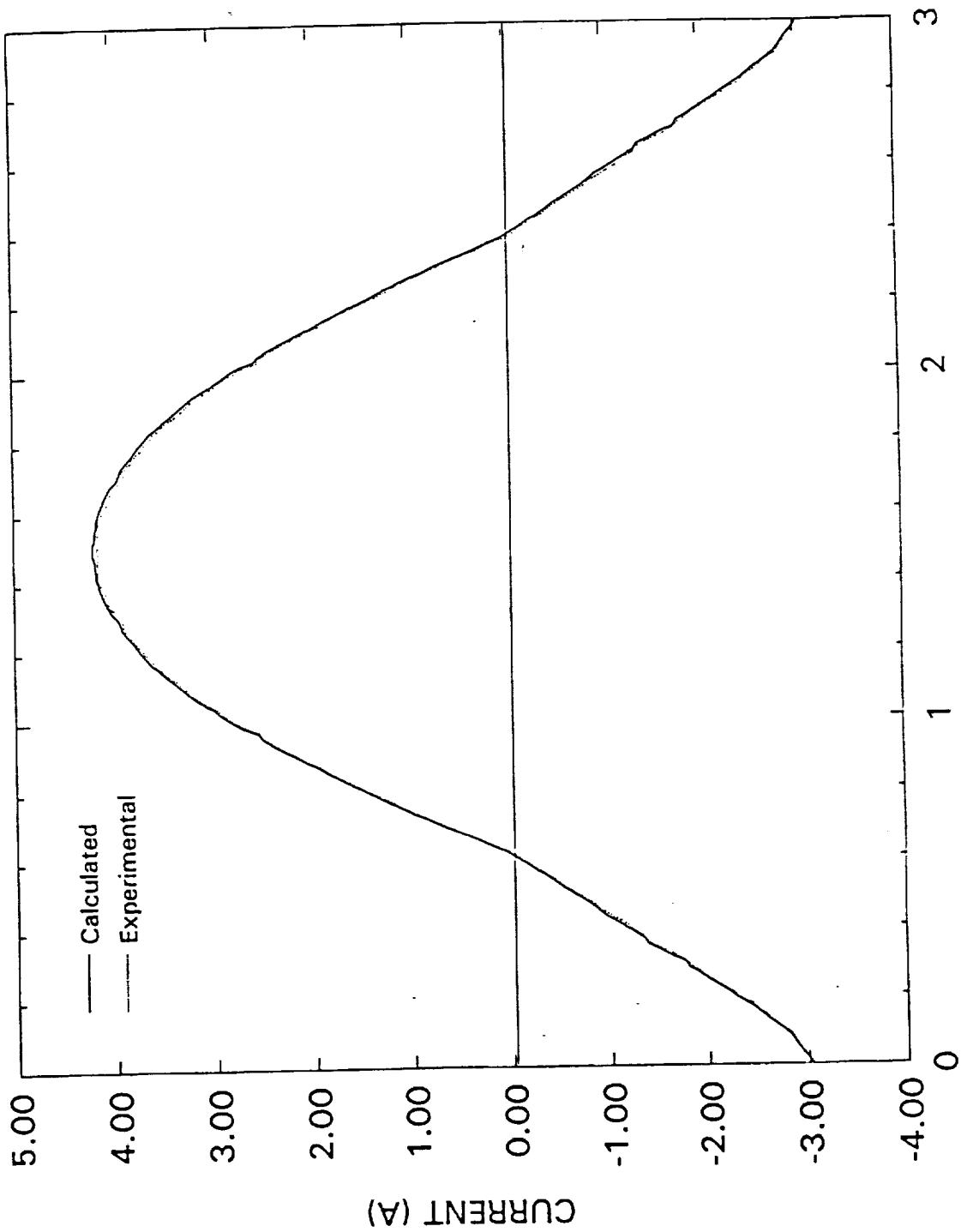

Fig.3. Calculated and measurd current profile for 490 W, 3 sec/cy, -15C.

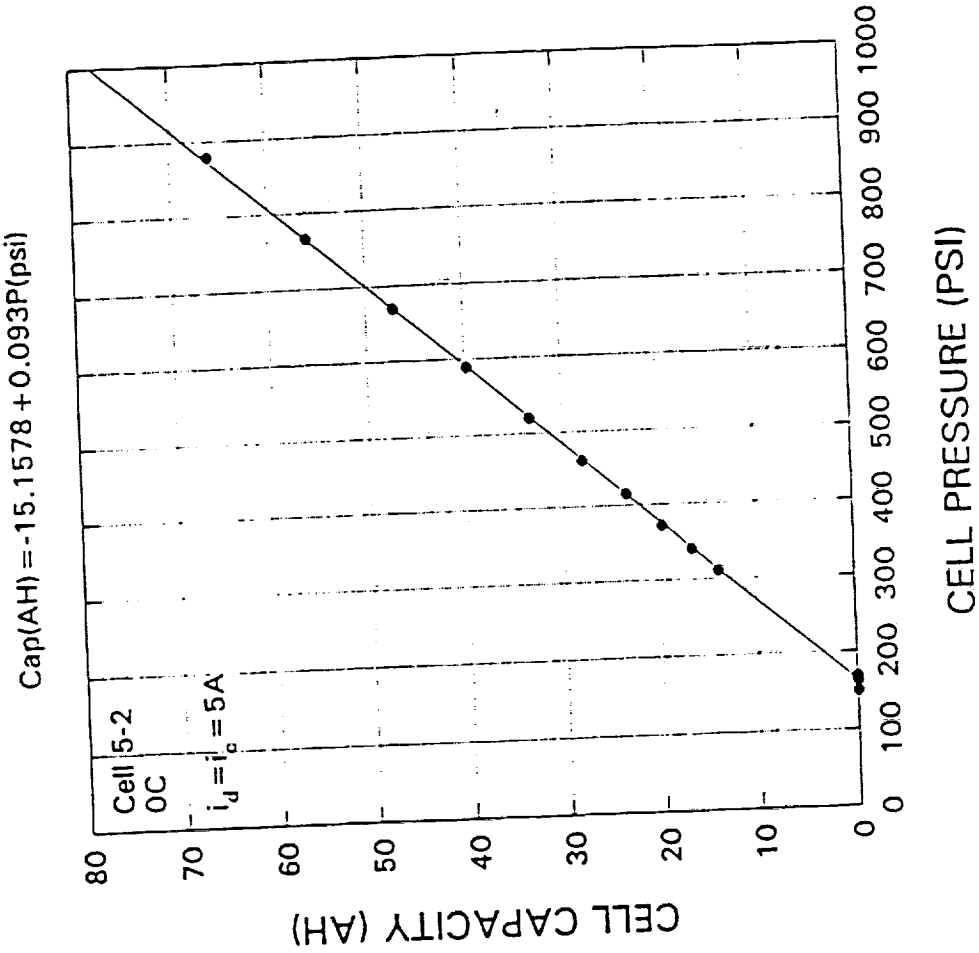

Fig.4 Capacity-pressure calibration curve

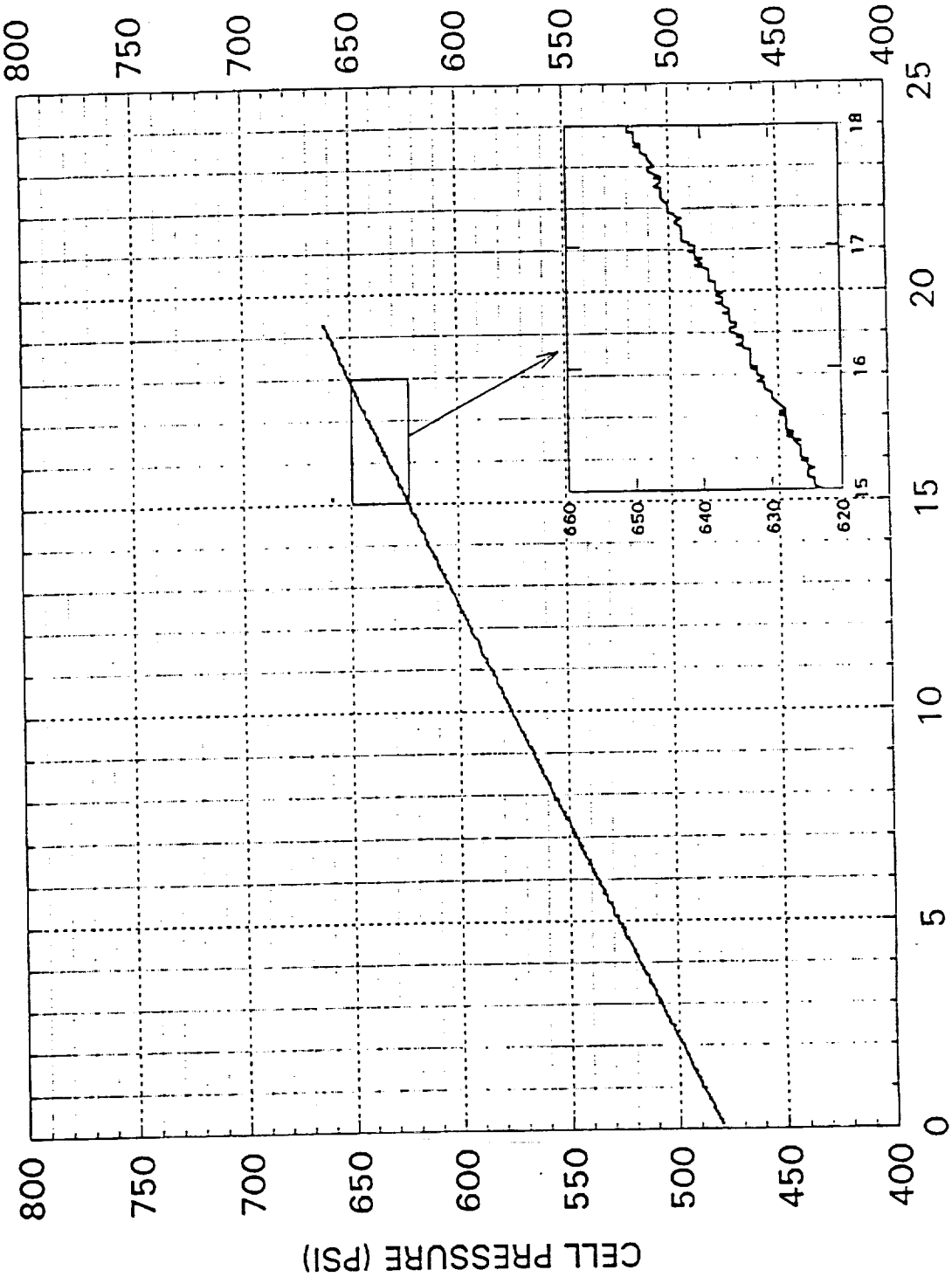

Fig. 5 Cell pressure vs. time plot for 490W load, 3sec/cycle simulation, 0°C

(a)

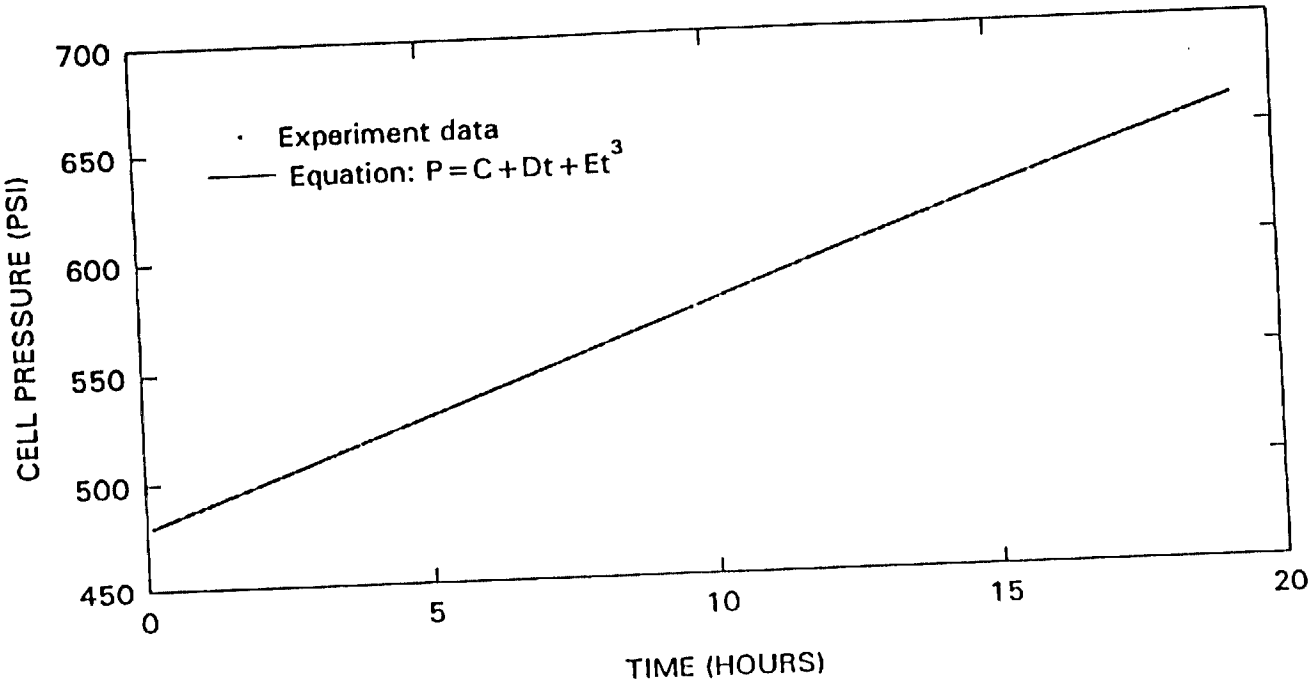

(b)

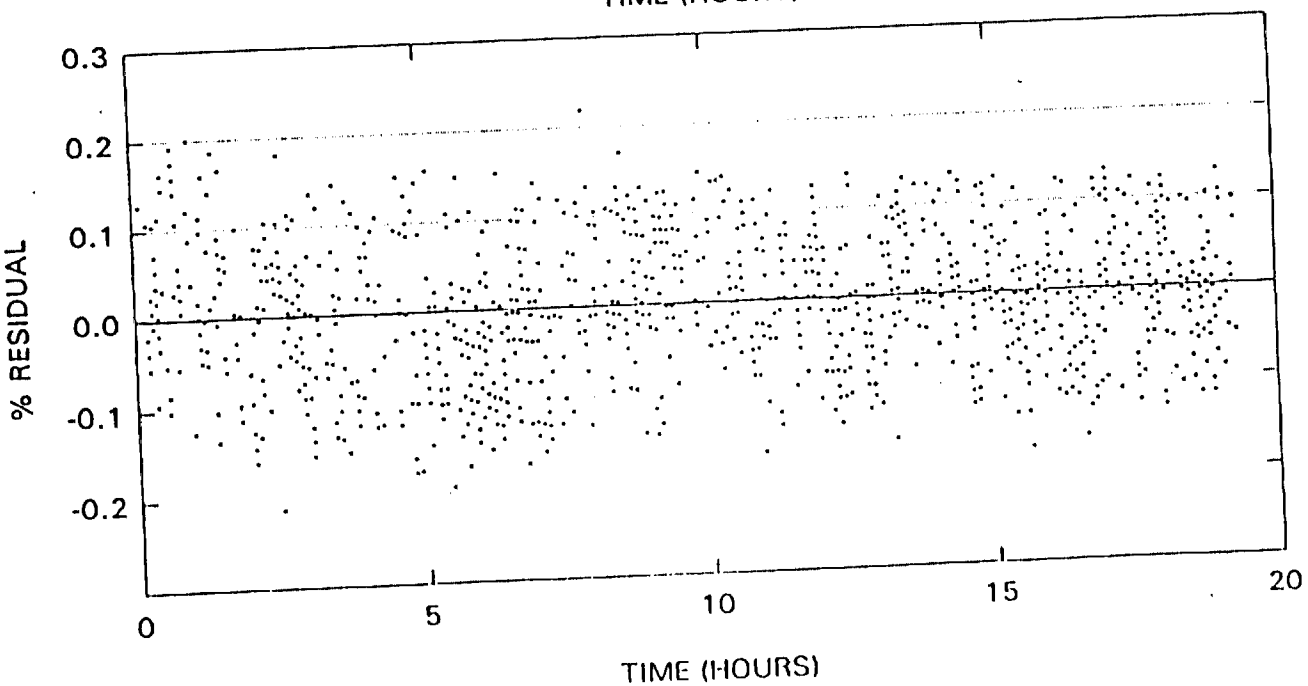

Fig. 6 (a) Experimental data with equation fit (b) % residual of equation fit
490W, 3sec/cy, 0°C

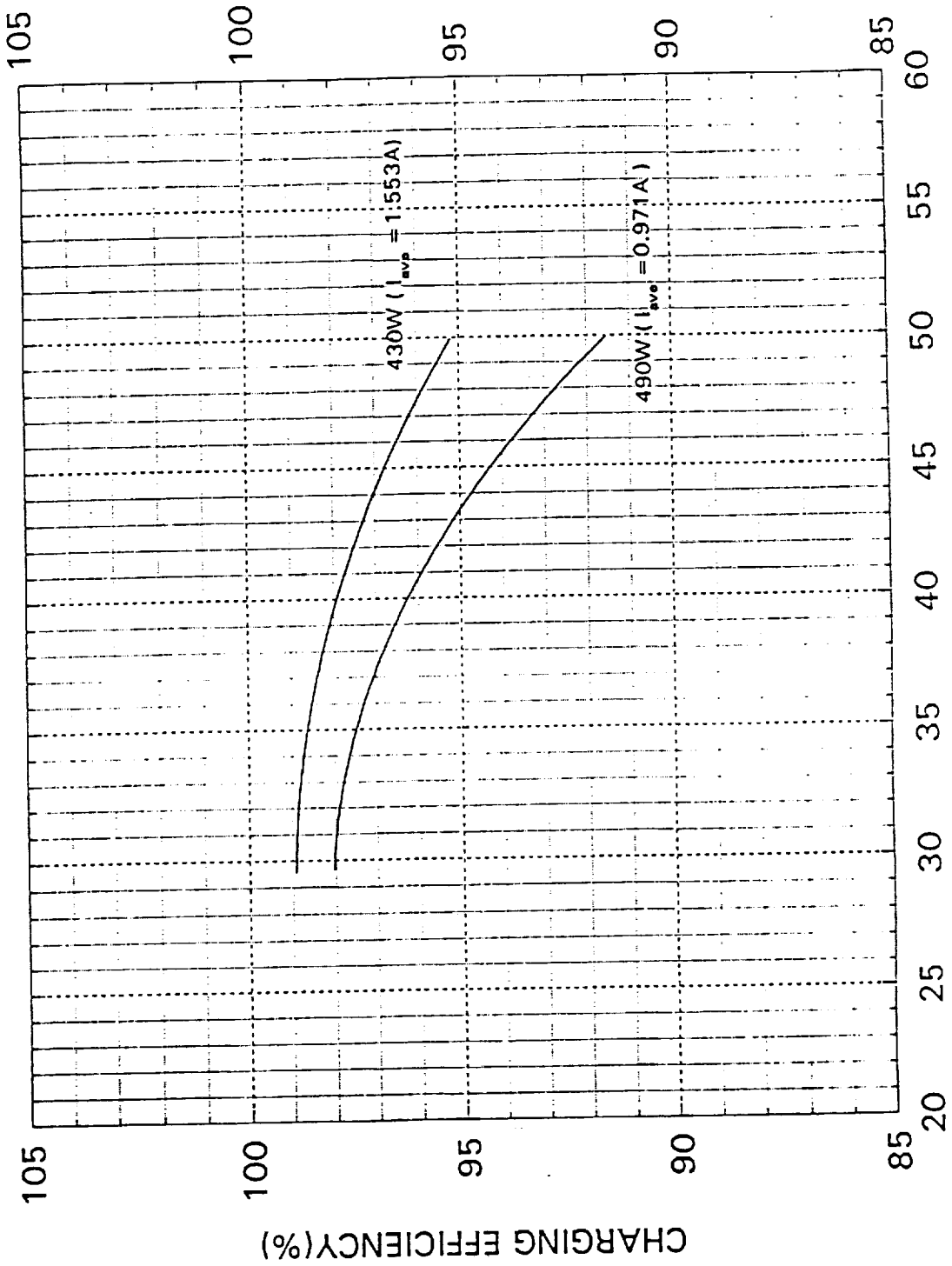

Fig.7 Charging efficiency vs. capacity for 430W and 490W loads. 3sec/cycle simulation, 0°C

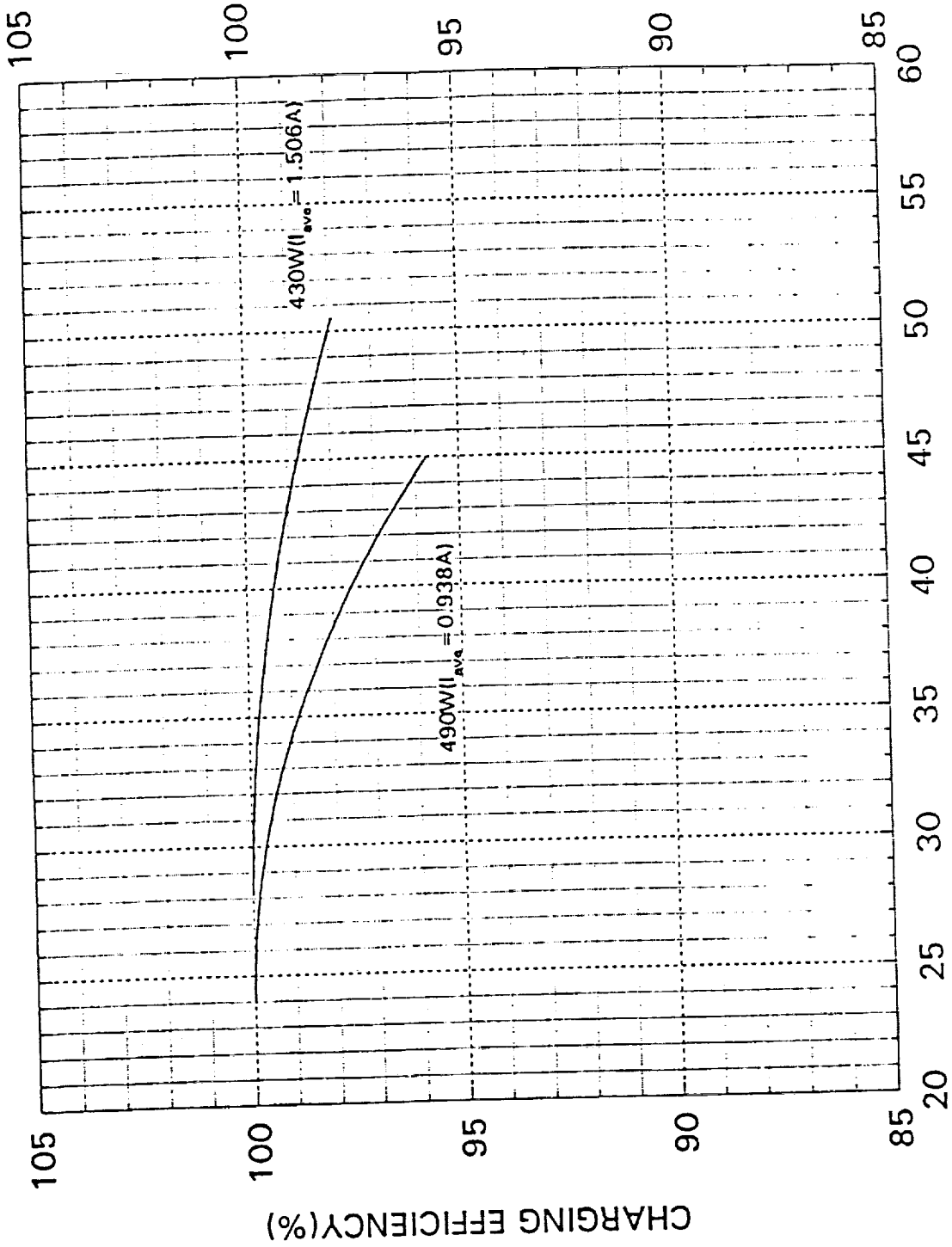

Fig.8 Charging efficiency vs. capacity for 430W and 490w lods. 3sec/cycle simulation, -15°C

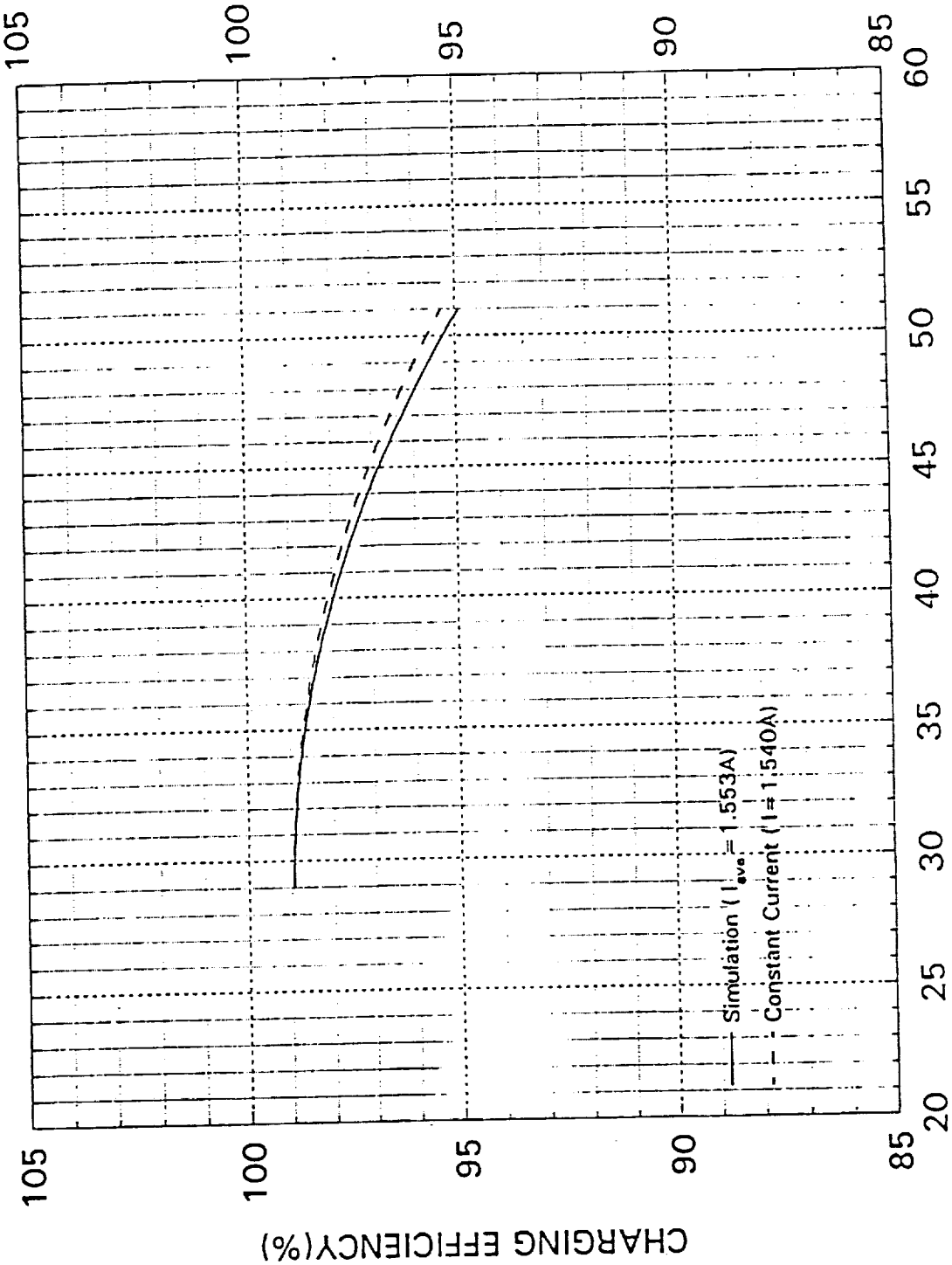

Fig.9 Comparison of simulation and constant current charging. 430W, 0°C

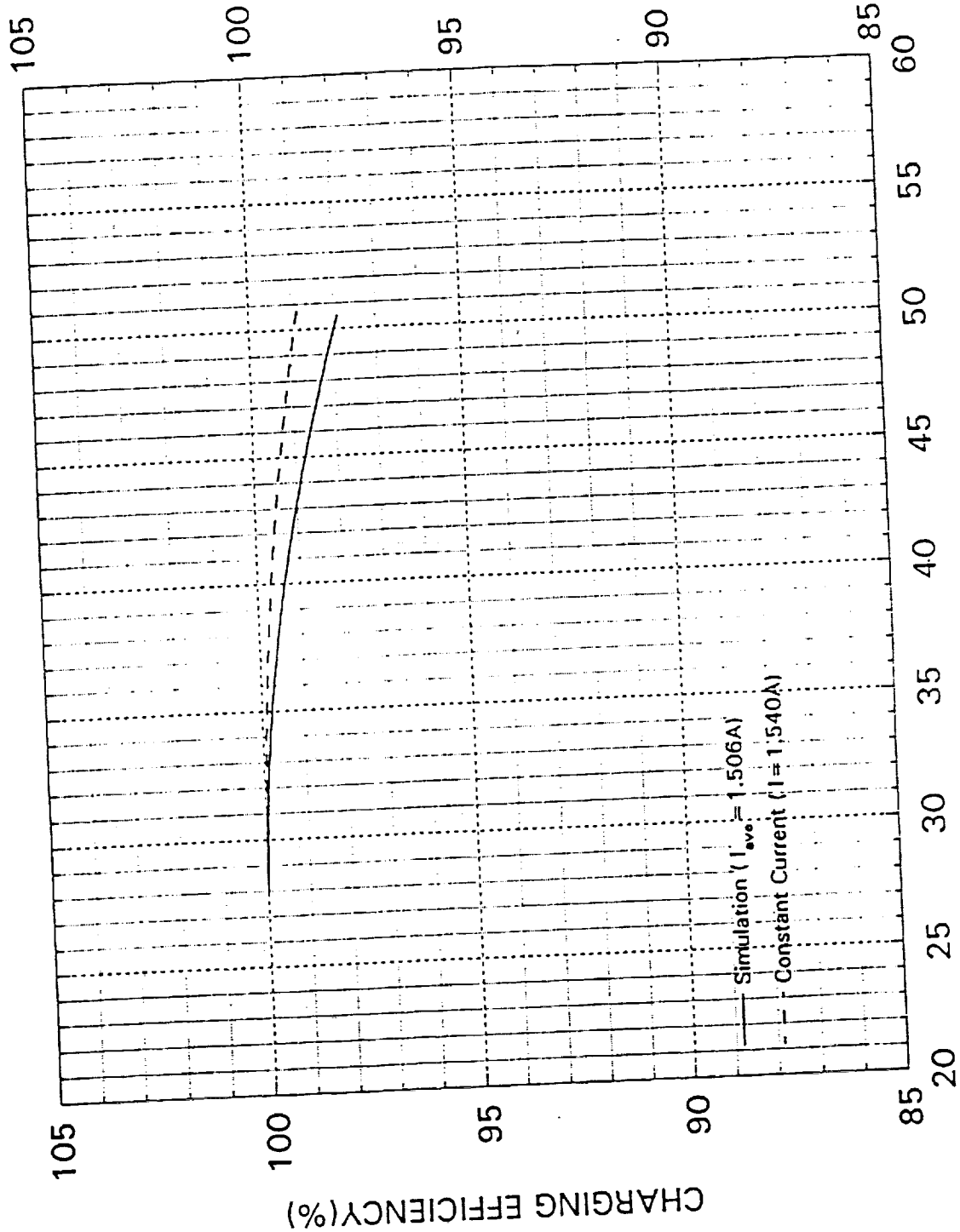

Fig.10. Comparison of simulation and constant current charging. 430W, -15°C

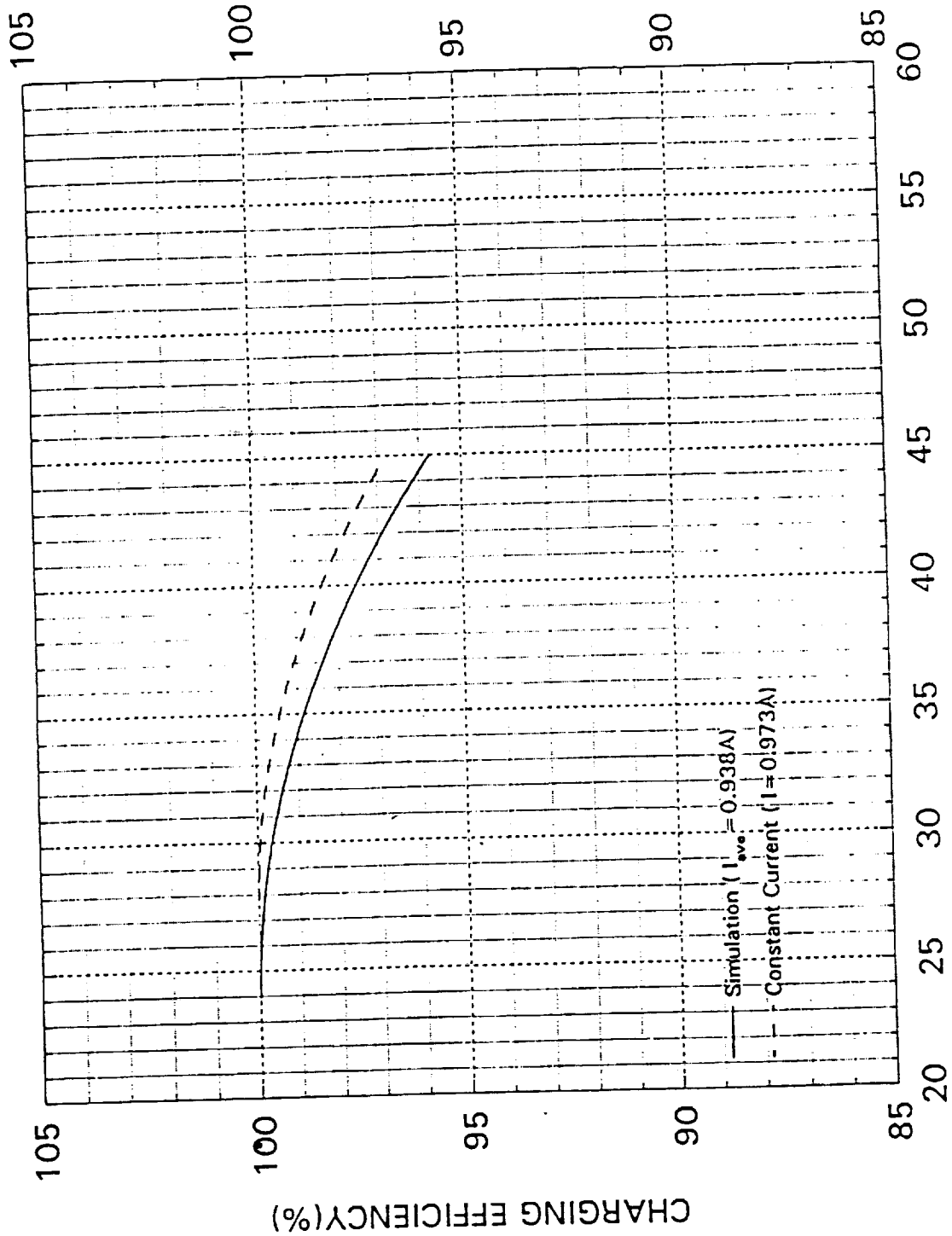

Fig.11. Comparison of simulation and constant current charging. 490W, -15°C

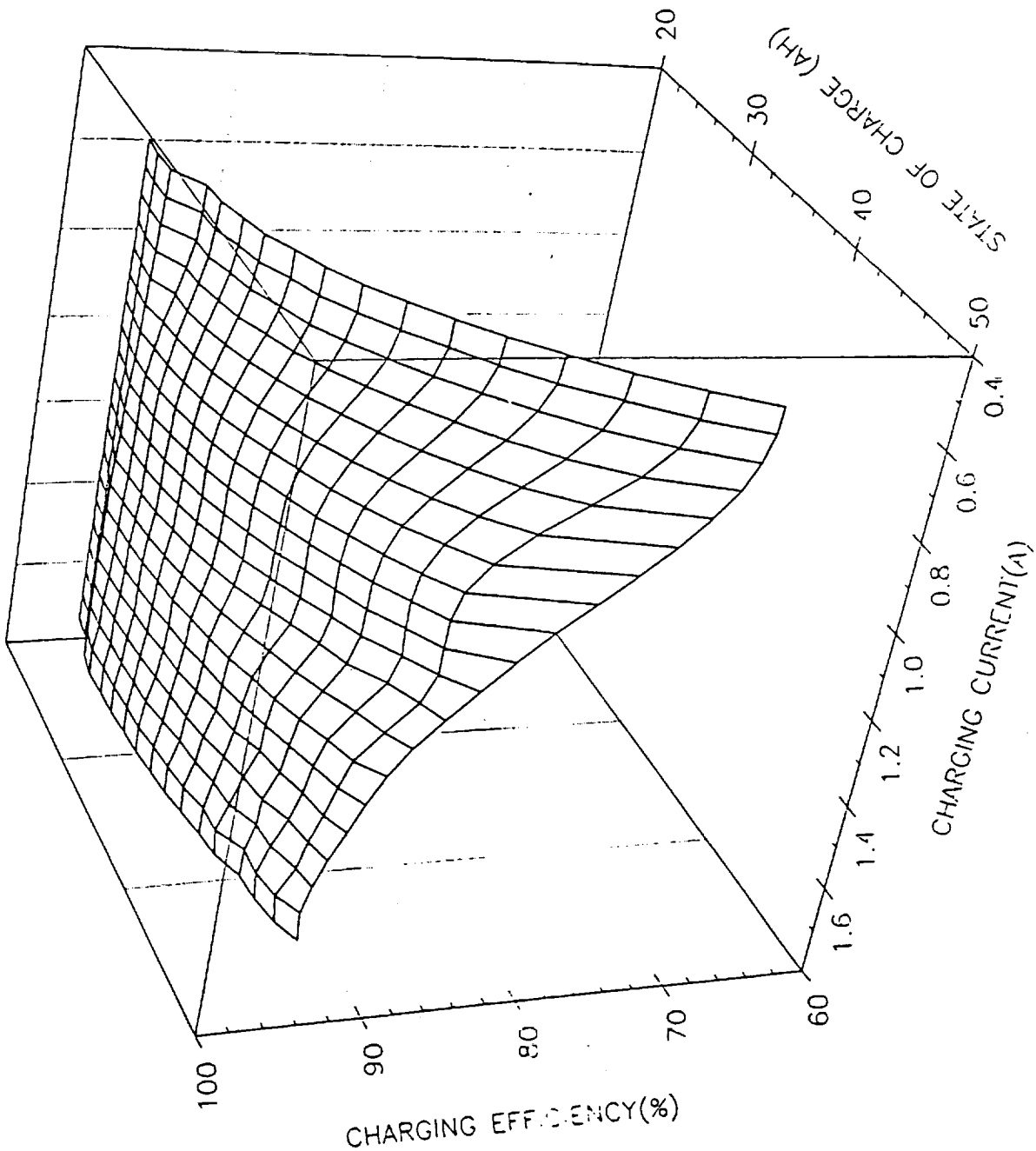

Fig.12 A 3-D presentation of charging efficiency as a function of charging current and cell capacity at 0°

Nickel-Cadmium Technologies Session

Session Organizer: *Patricia O'Donnell*
NASA Lewis Research Center

Orbital Management and Design Considerations for NiCd Satellite Power Systems

Benjamin J. Tausch II

Martin Marietta Astronautics

July 30, 1993

Abstract

Several recently manufactured 50 and 60 ampere hour aerospace NiCd battery cell lots, produced by Gates Aerospace Batteries, are prone to premature on orbit performance degradation. The failure mechanism is cadmium migration, and the consequent development of soft shorts. A Martin Marietta Astronautics satellite program instituted an orbital management strategy for a set of these batteries that reduced the rate of degradation and brought the system to stable operation. This strategy involves: a) minimizing the accumulated battery overcharge, b) regular discharge exercises, and c) periodic battery reconditioning. Because of changes in the NiCd cell manufacturing process the actual performance of subsequent lots of NiCd cells is open to question. Future NiCd based power system designs should therefore allow for fine control of charge parameters, and an on orbit battery reconditioning capability. To minimize risk it is much better to perform a full life test to qualify the cells before launch, rather than in parallel with orbital operations. If there are any changes in the manufacturing process of cells, it is extremely important to maintain very strong cognizance of secondary subcontractors, recognizing that the cell and battery manufacturing discipline is easily atrophied.

Root Cause of Cell Degradation

Investigation into several recent plate lots from Gates Aerospace Batteries [1] led to the conclusion that defects in the negative electrode was the primary cause of the performance degradation. The observations of monitored manufacturing parameters and more esoteric parametric relationships that are not routinely monitored support this. Ground test cells used in the investigation provided data, but correlation to on orbit degradation was the final criteria for comparison. In particular, two NASA missions, Gamma Ray Observatory (GRO), and Upper Atmosphere Research Satellite (UARS), have exhibited severe performance problems early in the mission.

The actual cause of the changes in negative plate parameters is still under investigation. Most are the result of subtle changes and a deterioration in the manufacturing process that accumulated over several years. Over sixty parameters were investigated. Items that showed correlation relate to the negative plate. High N/P ratio, high negative plate utilization, high 0° C capacity, and the ratio of cell 0° C capacity to battery 0° C capacity all correlate very well to bad cell lots. Cells with these characteristics are extremely sensitive to overcharge.

Common Bus Regulated Battery Charging

Batteries require overcharge to maintain state of charge. Constant current charging can lead to thermal runaway. To prevent thermal runaway, a power regulator unit (PRU) with a voltage temperature (V/T) control charging mode was developed.[2] This limits the maximum battery voltage during charge based on battery temperature: the higher the temperature, the lower the terminal voltage. The regulator controls voltage by reducing the charge current into the batteries.

This design is the basis for the McDonnell Douglas Modular Power Subsystem (MPS). The MPS is the power subsystem for NASA Multi-Mission Modular Spacecraft[3] Common bus applications. Parallel charging common bus applications, developed in the late 1960's, have successfully flown straight V/T control for years. Specific examples of this are the early Landsat satellites and the Solar Maximum Mission (SMM).

As the batteries charge, the terminal voltage increases to the V/T limit and the PRU reduces the charge current to the batteries. The current tapers off over the charge cycle. This effect is taper charging. In this mode, altering the V/T level controls the state of charge of the batteries. The higher the V/T level, the higher the current at the end of charge. The higher the current, the more overcharge returned to the batteries. The use of V/T charging eliminated the concern about thermal runaway, and many "old" battery designs accepted overcharge very well. There are many batteries in GEO that have overcharged for years with no problems.

Astronautics Satellite Electrical Power Subsystem (EPS) Configuration

The Astronautics satellite uses an MPS based power system. Figure 1 shows the EPS functional diagram. There are three, 22 cell, 60 ampere hour, Gates 50AB22 lot 13 batteries in the MPS. The PRU uses NASA standard V/T levels 2 through 8. The PRU also has a current mode with three charge rates. The current mode limits the maximum charge current to 0, 5, or 10 amperes, total for all three batteries. There is a ± .25 ampere tolerance in current mode. Current mode is secondary to V/T control. If the battery voltage is greater than the selected V/T level with the 10 ampere current mode selected, V/T control will limit the battery charge current accordingly. The 0 ampere current mode is useful in strict control of battery overcharge and in performing on orbit battery capacity tests.

There are two relays for each battery in the MPS. The batteries connect to the bus in a primary or redundant mode, disconnect from the bus, or are diode isolated from the bus. Off line batteries can connect to reconditioning load banks or a charger external to the MPS. The reconditioning load bank has a high rate discharge at 22 ohms, and a low rate discharge at 66 ohms. The reconditioning battery charger is a constant current charger at a low rate 1.25 or a high rate of 2.5 amps.

The design of the Astronautics MPS allows for on orbit battery capacity tests. During a battery capacity test, called BATMAN, the batteries discharge normally during an eclipse period. Selecting a current mode of 0 amperes, during the eclipse, prevents the batteries from charging

during the next sunlit period of the orbit. The batteries enter the next eclipse period at a higher than normal DOD. These exercises reduce the memory effect and determine operational performance margins. A modified version of a BATMAN, in which loads are turned on and off during the final eclipse, is a BATIFT. This test characterizes performance at high discharge currents. The maximum load seen during nominal operations and BATIFT exercises is 25 amperes per battery.

Electrical Power Subsystem Functional Diagram

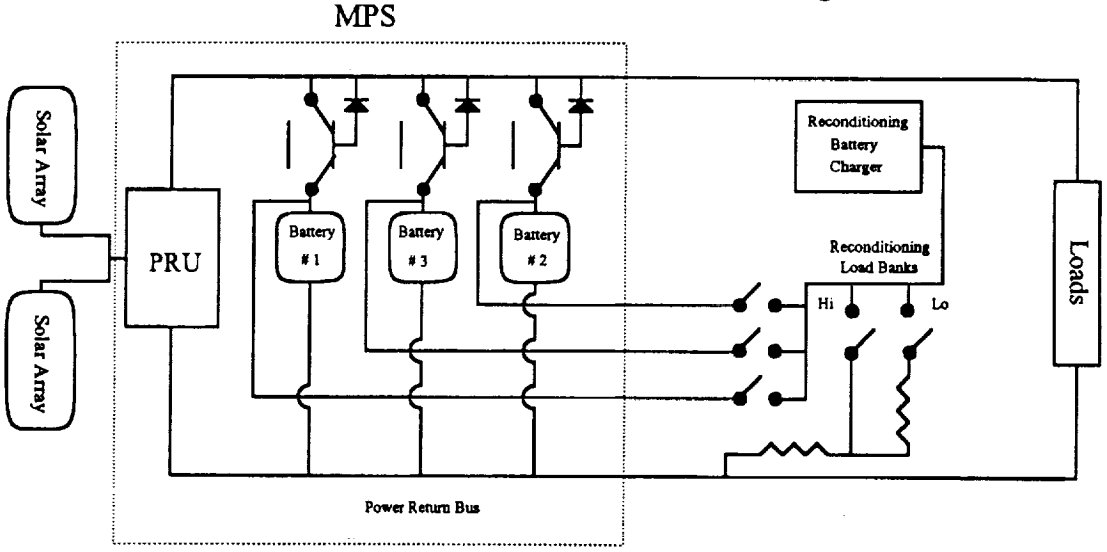

Figure 1.

Circuitry external to the MPS provides orbital reconditioning capability. A full reconditioning starts with high rate discharge using the 22 ohm load bank. High rate discharge continues to 22.44 volts, or approximately 1 volt per cell. The on board computer (OBC) detects the voltage and commands the low rate load bank. The battery continues to discharge into the low rate load bank until it reaches 10 volts and the OBC commands the battery open circuit. The charge cycle begins with one to four hours at a low rate of 1.25 amperes. A high rate charge of 2.5 amperes follows low rate. The amount of time on high rate charge is a function of the ampere hours discharged from the battery, and the thermal response. Reconditioning takes place during short eclipse periods and full sun orbits. Only one battery is reconditioned at a time, and at least two batteries remain on the bus.

On Orbit Symptoms

In the MPS design all three batteries operate in parallel on a common bus. Battery charge current, which is controlled by the PRU, is shared among all three batteries. Parallel charging on a common bus requires similar battery performance to succeed. Flight V/T levels are based on the expected depth of discharge (DOD) and a desired charge to discharge (C/D) ratio. Given a

constant orbital eclipse duration, the natural effect of V/T control is that the lower the DOD, the higher the C/D ratio. On orbit C/D ratio's greater than 1.10 are common, and there are several instances of C/D ratio's at 1.20 and above. The high C/D ratios ensure that the batteries are fully charged every orbit, and end of night discharge voltage will support mission operations. The SMM and Landsat satellites operated successfully this way for years, without reconditioning.

As the recent lots of Gates cells were launched, it became clear that straight V/T charging and high C/D ratio's accelerated battery performance degradation. After a few months of straight V/T control, UARS and GRO started observing divergence in battery performance. Performance divergence occurred in an Astronautics satellite for similar reasons. C/D ratios increased, load sharing became unequal and temperatures diverged. Parallel charging, common bus regulated power systems depend on similar characteristics for each battery. As cells in each battery suffered degradation at different rates, the battery performance suffered. Ultimately, one battery on GRO developed a hard short, and was taken off the bus.

The result of the generation of soft shorts is differences in cell performance within a battery. The differences within a battery when small are invisible, but will manifest themselves on a battery to battery level when deviations are large. On an MPS there are telemetry sensors that monitor battery differential voltage. This is the difference between the sum of the voltages of two sets of 11 cells. The first indication of cell divergence is usually a non zero reading in differential voltage.

V/T level control assumes that each cell voltage is very close to the battery voltage divided by the number of cells. In cases where the battery differential voltage is high, some cells will be at higher voltages than others. Since the battery is a series of cells, all the cells see the same charge and discharge current. The consequence of mismatched cells is that a good cell will have a higher voltage than a bad cell during charge. High charge currents at elevated voltages can cause damage to the cell. Under V/T control with mismatched cells, the system is at a level that will maintain the weak cell, with the potential of damaging good cells.

As the number of cells that are off nominal increases within a battery, the overall performance of the battery becomes affected. All three batteries are on a common bus, and the voltage of each battery is the same. Cell mismatches within each battery cause differences in voltage versus current performance. These differences manifest themselves in battery temperatures and load sharing. What happens on a cell by cell basis within a battery, is now evident on a battery to battery level.

Satellite Anomaly History

The Astronautics satellite is in an inclined low earth orbit. Several times a year, there are full sun periods of more than a week. Figure 2 shows a typical eclipse profile. V/T 5 was the nominal charge level after launch. No overcharge limiting control was in place[4]. The differential voltage divergence began about 9 months after launch, after a full sun period, and the V/T level remained unchanged. The batteries underwent a normal reconditioning during full sun. Four months after the full sun period the differential voltage rose to greater than 200 mv and battery performance

degradation became evident. Figure 3 shows the median value of the differential voltages over time. The long period at V/T 5 during full sun caused soft shorts in the cells. The continued use of V/T 5 caused a runaway soft short situation. As the shorts developed, the battery charge current increased and caused more shorts.

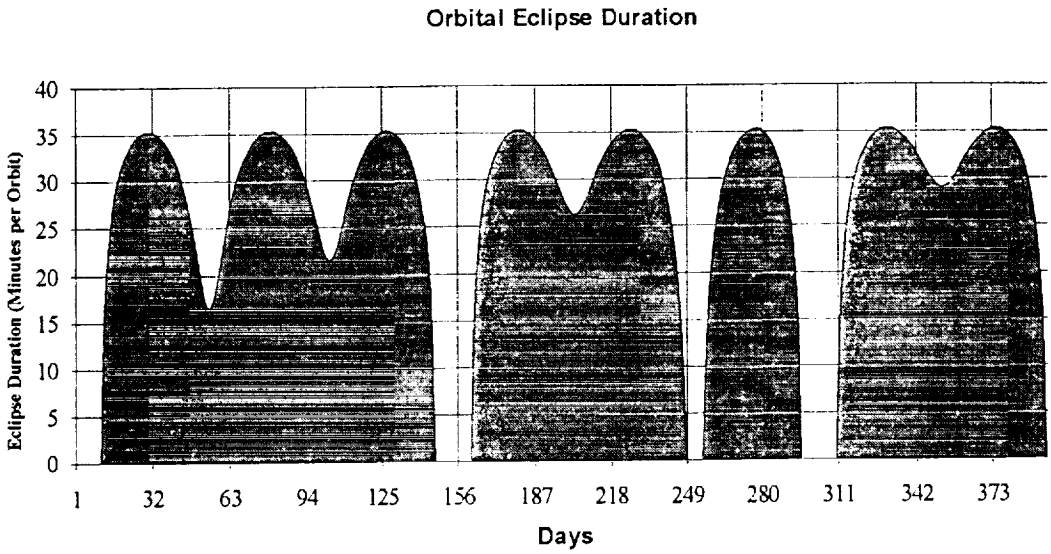

Figure 2.

A change to V/T 4 occurred 12 months into the mission. This was to compensate for the mismatched performance. The C/D ratios reduced slightly but performance continued to degrade. A second reconditioning occurred 14 months after launch. The discharge performance of the batteries on the 22 ohm and 66 ohm load indicated a large discrepancy among cell capacities. Approximately 74 ampere hours discharged out of each battery to approximately 10 volts. Analysis of the data showed that some cells were in reversal for more than 30 ampere hours. There was no concern about pressure in the cell at such a low rate. There was a concern regarding damage to cells because this phenomenon was totally unexpected. The reconditioning demonstrated that straight V/T control did not effectively limit C/D ratios, and was damaging to the batteries.

After the second reconditioning, battery overcharge reduction continued by using the recharge fraction (RCF) method. The use of this charge control method would ultimately lead to a stable operating regime, but the battery degradation had progressed too far to see results in a short time. Performance divergence reached a 5 ampere difference in load sharing at a 70 ampere bus load. There was as much as 3 degrees C difference in battery top of cell temperatures. Differential voltages were very high. The culmination of poor battery performance occurred when a low voltage incident developed during a BATMAN exercise.

The BATMAN exercise spanned three eclipse periods. Load sharing during the first two eclipses was typical of the degraded performance observed before the exercise. During the third eclipse load sharing became poor. Two batteries provided less than 10% of the 30 ampere bus load, and the third battery provided 80%. The consequence of one battery supplying the load at the elevated

DOD of the third eclipse was a steep drop in voltage that resulted in a bus voltage of 24 volts. Minimum voltage allowed without entering safehold mode is 25.12 volts. The low voltage incident prompted changes in the orbital management of the power subsystem.

To minimize overcharge, 0 ampere mode RCF control at V/T 4 to an RCF = 1.08, was instituted. When the ampere hours returned is 108 % of ampere hours removed, the OBC commands the PRU to 0 ampere mode, terminating battery charge. Weekly BATIFT capacity checks to DOD's greater than the nominal mission range were instituted to reduce the memory effect, and to determine operational performance. Future reconditioning would be less stressful.

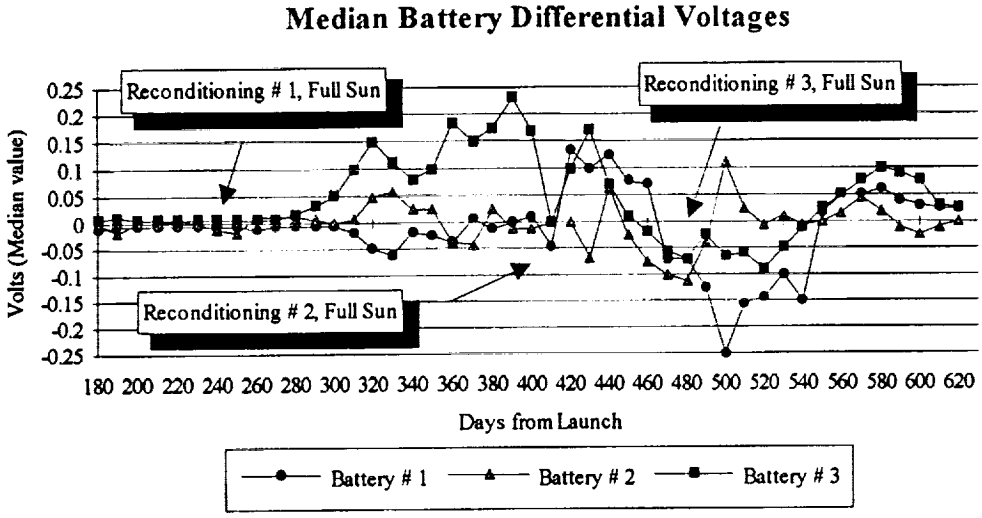

Figure 3.

RCF Control

The Astronautics satellite has OBC software that allows tuning of charge control parameters. RCF, the ratio of ampere hours charged to ampere hours discharged, is the charge control method employed. RCF control limits the percentage of overcharge allowed. To accomplish this, the OBC modifies normal DOD by a predetermined RCF value, and terminates battery charge once the adjusted DOD reaches zero. OBC commanding of the PRU to zero ampere current mode terminates battery charging. The OBC detects battery discharge during the eclipse portion of the orbit and commands the PRU back to a normal V/T 4 charge mode. Specifically, the equation for normal DOD is:

$$DOD(N) = ([\Sigma_{n=0} I_{\text{discharge}}(N)_n \times \Delta t] - [\Sigma_{n=0} I_{\text{charge}}(N)_n \times \Delta t]) \div NAMEPLATE$$

DOD adjusted by an RCF is:

$$DOD(N) = ([\Sigma_{n=0} I_{\text{discharge}}(N)_n \times \Delta t] - [\Sigma_{n=0} \{I_{\text{charge}}(N)_n \times \Delta t\} \div RCF]) \div NAMEPLATE$$

Where :

N = Battery #1, #2, #3
n = Iteration
t = Time
$I_{discharge}$ = Battery Discharge Current
I_{charge} = Battery Charge Current
$NAMEPLATE$ = Rated nameplate capacity of the battery
RCF = Recharge Fraction

The computer performs these calculations every 1.024 seconds. The current sensors used for integration have a resolution of .4 amperes. The granularity of the current sensor data and the integration introduce errors into the calculation, but the relative difference between RCF values remains constant. In other words, an RCF value of 1.06 may be in the actual range of 1.03 to 1.09, but an RCF of 1.07 is greater than 1.06.

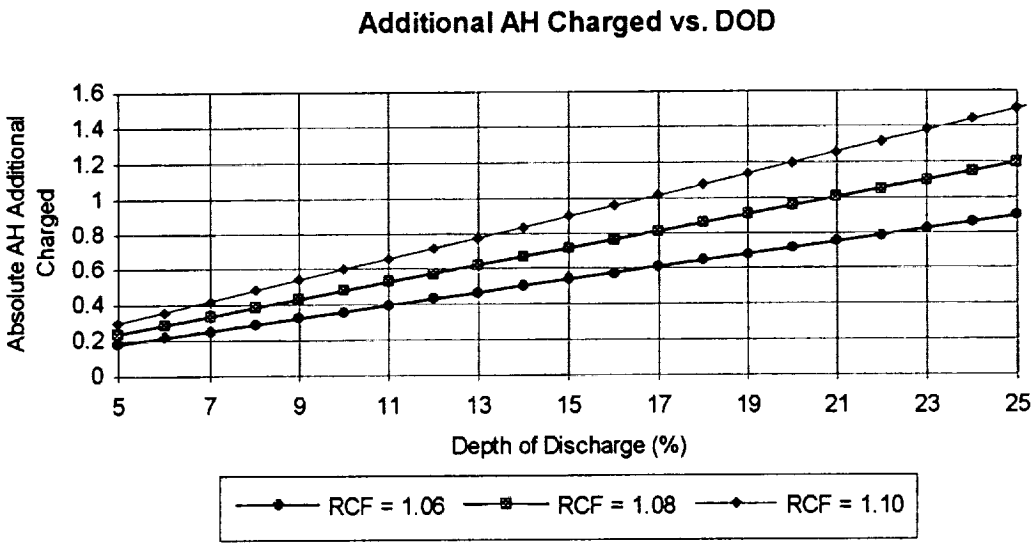

Figure 4.

Closer inspection of the RCF control equation reveals that the ampere hours overcharged during each cycle is a function of DOD and RCF. Figure 4 shows ampere hours overcharged versus DOD and RCF. There are equivalent ampere hours overcharged at an RCF of 1.10 at 10 % DOD and at an RCF of 1.06 at 17 % DOD. Experience has shown that .4 to .5 ampere hours overcharge at 10 % to 15 % DOD provides enough overcharge to adequately maintain voltage, without exacerbating the generation of soft shorts. In short eclipse periods, the overcharge drops to a much smaller number and there is a corresponding drop in the end of night voltage. Generally, the drop in voltage is not enough to cause an impact to the mission.

Orbital Management Corrective Actions

The Astronautics satellite's peak power loads are random and can occur at anytime during the orbit. Maximum DOD's for a nominal mission are 19 % with average DOD's of 12 % to 15 %. Eclipse duration and peak power loads are the main factors that drive orbital DOD. Figure 5 shows nominal mission maximum DOD's and eclipse duration. This data does not include any battery capacity tests that are generally in the 25 % to 35 % DOD range.

Coincident with 0 amp mode RCF control, weekly battery performance exercises and capacity tests, called BATIFT's, started. Performance was extremely poor, and normal operations were very close to putting the satellite into safe hold mode due to low battery voltage. The BATIFT exercises determine the bounds of the performance envelope. The initial exercises started by turning on timed peak power loads during an eclipse period, and assessing performance. This process continued through the eclipse as long as the load sharing and voltage was satisfactory. The combination of the RCF control, the low voltage incident, and the weekly BATIFT exercises, brought the batteries back under control.

Improved performance warranted extending the BATIFT exercises over two eclipses, similar to a BATMAN. The performance during the first eclipse of the exercise determined if extending to two eclipses was warranted.. Good voltage response, load sharing and discharge voltage fulfilled the criteria for continuation. In the subsequent sun period, no charge was applied to the batteries. Using two eclipses allowed DOD excursions beyond the nominal mission DOD. This served two purposes. First, exercise beyond the normal limits helps reduce voltage depression due to the NiCd memory effect. Second, the increase or decrease in performance of the battery is more evident at higher DOD's. BATIFT exercises continued weekly until the next full sun period. During this full sun period reconditioning number three took place.

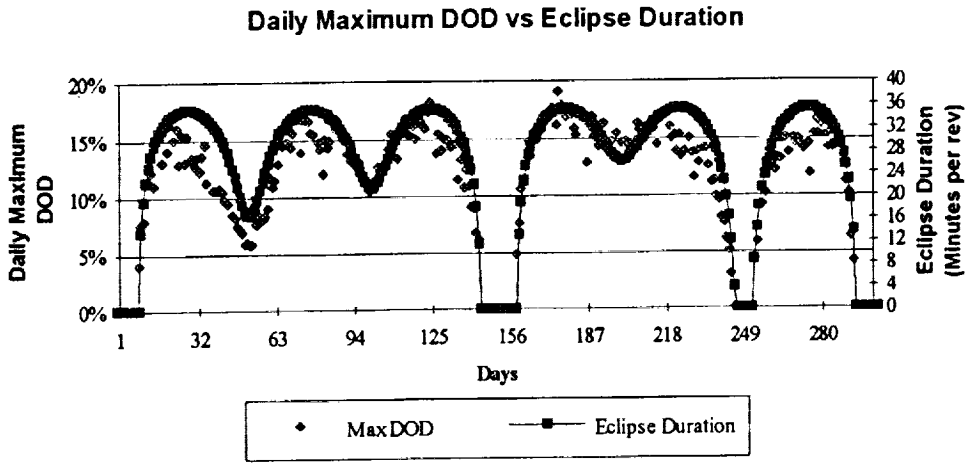

Figure 5.

Normal reconditioning uses the 22 ohm and 66 ohm load banks to discharge each battery individually. Cells were in reversal for extended periods during the second reconditioning. The voltage and differential voltage response to long periods of reversal indicates that this is detrimental to the long term health of the batteries. The batteries that were not on the reconditioning load bank were being trickle charged during full sun at V/T 3. This proved to be extremely damaging to the batteries. Performance after the second reconditioning quickly became worse than before the reconditioning.

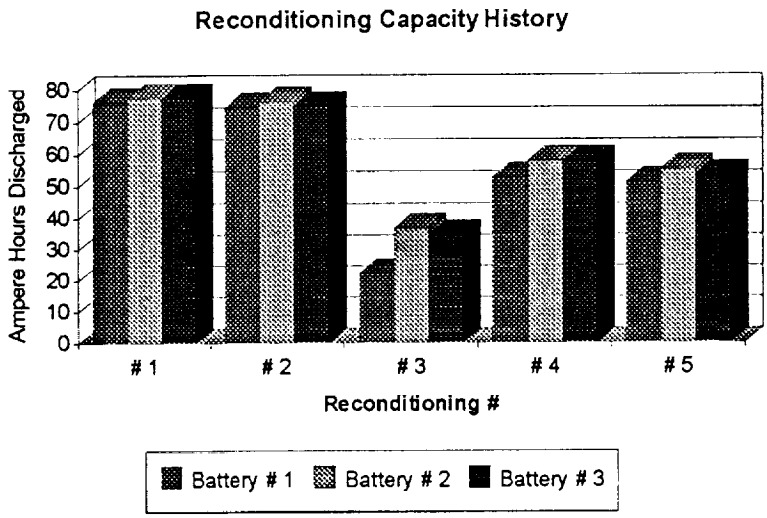

Figure 6.

Reconditioning number three occurred at approximately 16 months of mission life. The approach to reconditioning was to limit the time in reversal, and reduce the overcharge during full sun. To reduce the stress on the weaker cells, the reconditioning discharge terminated at the first cell reversal. The battery voltage, current, differential voltage and ampere hours discharged determine a cell reversal. A spreadsheet assisted in the determination of cell reversal. V/T 2 is selected when full sun is entered to reduce the trickle charge current to an acceptable level. Instead of overcharging after discharge, the battery charged to a specific voltage. In this case the voltage was about 1 1/2 volts above the V/T 2 level bus. The sensitivity of these batteries to overcharge warranted this approach. Also, there is no reason to charge the battery to a higher voltage just to let it discharge when connected to the bus.

Reconditioning to cell reversal proved to be a limited success. The three batteries discharged 22, 37 and 35 ampere hours respectively. The reconditioning sequence completed with several days of full sun left. Selecting the 0 ampere current mode for the remaining days of full sun further reduced overcharge. A design compatibility problem prevents the 0 ampere current mode from being used while any battery is on the reconditioning bus. In the 0 ampere current mode, it became evident that a significant amount of soft shorts remained in the batteries. The bus voltage dropped over a volt per day due to the self discharge effect of the shorts. The differential voltages also increased during this period. A daily V/T 2 short duration charge was used to maintain bus voltage at acceptable levels.

After the third reconditioning, voltage performance improved slightly and battery temperatures came back into line. Differential voltages still were very high, and load sharing was acceptable. Weekly BATIFT exercises resumed after reconditioning. After each BATIFT exercise the load sharing improved, and the differential voltages would tend toward zero. The response of the differential voltage was a byproduct of the BATIFT, and not an objective. Differential voltages provided useful information, but steps taken for remedial treatment of the batteries were not in response to differential voltage signatures. Voltage performance, thermal response and load sharing were the indicators used for state of health assessment. It took several weeks for the batteries to become fairly well matched.

Telemetry analysis became a sizable effort. Determining operational margins at nominal mission DOD's was difficult. The BATIFT performance determined mission margins and limits to the mission. The system performance was good for the next 5 months. The RCF value of 1.08 maintained state of charge, and did not generate more soft shorts.

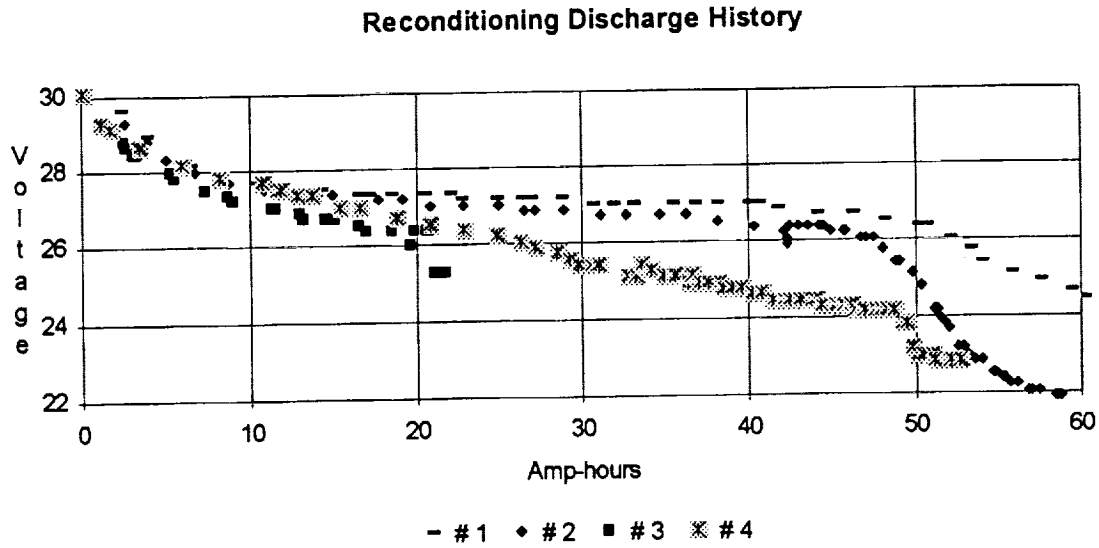

Figure 7.

Reconditioning number four occurred at 19 months into the mission. The rules for this reconditioning were the same as the third one. The performance to cell reversal of this reconditioning improved. Figure 6 shows reconditioning ampere hours discharged for all reconditioning activities. The higher values indicate smaller relative differences among the cells. The I-V curves for reconditioning do not indicate any significant plateau out to 50 ampere hours. This type of reconditioning enhances voltage but it does not recover a long term NiCd plateau. Figure 7 shows voltage versus ampere hours discharged. Reconditioning number one shows a typical I-V curve, and reversals are evident in reconditioning number two. Also shown is the limited reconditioning number three, and the lack of a plateau and downward slope of

reconditioning number four. Reconditioning provides a boost in operational voltage that allows the mission to continue without restrictions.

RCF control at 1.06 started after the fourth reconditioning. Differential voltages increased for about 2 months. Load sharing differences were slightly greater than at an RCF of 1.08. After a period of about 3 months, the batteries became well matched again and performed adequately. The most recent reconditioning took place 26 months into the mission and the results were comparable to the previous reconditioning. The load sharing has improved, and differential voltages are now under 30 millivolts. All mission objectives are being met, and the system has reached stability.

Conclusions

Many future satellites will have to rely on aerospace NiCd battery technology. Changes in the United States aerospace battery manufacturing industry indicate that the future is uncertain at best. Process, personnel and material changes have a large effect on the final product. Isolating the cause of the orbital anomalies to parametric relationships in the manufacturing process was a huge undertaking. The use of the Toft discriminators for 50 ampere hour cells provides early indications into the relative hardiness of a plate lot. This level of effort and scrutiny may not be possible for all future cell builds. Flexibility provided in the design of a satellite power system allows the ability to react to sensitivities of different types of cells.

Variable charge control and orbital reconditioning capability are especially important in parallel charging common bus applications. The MPS is an extremely reliable system. As long as the batteries tolerate overcharge, the system has performed well beyond its intended design life. When cells diverge and batteries become degraded, straight V/T control contributes to further degradation. Hardware and software on the Astronautics satellite provided the tools to mitigate battery degradation through overcharge control. Having a 0 ampere current mode, which is paramount in managing overcharge, was also extremely useful for battery capacity checks

Overcharge is extremely damaging during full sun and short eclipse orbits. Lowering the V/T level or using zero ampere current mode are effective methods to reduce overcharge during the long period of trickle charge. RCF control is effective in limiting overcharge during orbits with long eclipse periods. Eliminating the battery's ability to continue to charge reduces the continued generation of soft shorts, and improves overall battery performance. Daily overcharge limitation is the most important aspect in controlling battery degradation.

The battery capacity checks and reconditioning provided methods for remedial treatment of severe battery degradation. Orbital capacity tests used to determine the performance envelope provided needed exercise for the batteries. Frequent excursions beyond the normal DOD range control the NiCd memory effect. There is little doubt that these controls enabled the mission to continue.

A reconditioning capability in LEO provides a method to recover voltage performance for NiCd based satellite power systems. Overcharge limitation results in batteries operating at a lower state

of charge. Depressed voltage performance is a consequence of operating at a lower state of charge. Reconditioning enhances voltage performance. Reconditioning to different levels has not proven to be a liability. Batteries become matched quickly after reconditioning reacting to the RCF charge control.

Differential voltage monitors provide information about the relative likeness of cells within a battery. The charge control level should not be changed based solely on differential voltage. This could result in a condition of increased overcharge meant to bring the cells closer to one another in performance. Initially the differential voltage will reduce and the change appears to be effective. As the overcharge increases more shorts develop and the differential voltage returns to a high value. Continued overcharge on these types of batteries can lead to a hard short. Differential voltage as an indicator of cell compatibility is useful. The criteria for adequate orbital performance should be voltage, load sharing and thermal response.

Uncertainties in future battery designs indicate that cognizance of battery overcharge should start before launch and continue throughout the mission. Steps to limit overcharge begin immediately after launch. Limiting overcharge early in the mission may prevent the onset of severe degradation. The ability to control overcharge through variable RCF control and zero ampere current mode has proven very effective. Future common bus parallel charge systems should include these capabilities to provide the flexibility to respond to the uncertainties of future battery performance.

[1] Mark R. Toft, "Preliminary Results: Root Cause Investigation of Orbital Anomalies and Failure in NASA Standard 50 Ampere-Hour Nickel-Cadmium Batteries", Proceedings of the 1992 NASA Aerospace Battery Workshop

[2] Robert Gruber, "High Efficiency Solar Cell Array Peak Power Tracker and Battery Charger", IEEE Transactions on Aerospace and Electronic Systems, Power Conditioning Specialists Conference, 1970 Record

[3] Bob Kichack, "Standard Power Regulator for the Multi-Mission Modular Spacecraft," Distributed by McDonnell Douglas Corporation

[4] RCF control is always in effect, although it may not limit overcharge. During the early phases of the mission, RCF control to a current mode of 5 amperes was used. The 5 ampere current mode equates to about 1.7 amperes per battery. When the switch to 5 ampere current mode was commanded by the OBC, the charge current had tapered below 1.7 amperes per battery. V/T control supersedes current mode, so the effective control mode was straight V/T 5. The taper charge under V/T 5 control contributed a substantial amount of current to overcharge the batteries.

TOPEX/POSEIDON BATTERY PERFORMANCE DURING THE FIRST YEAR OF OPERATION

JPL

Frank Deligiannis, Sal DiStefano,
Eric Lopez and Rob Sherwood
Energy Storage Systems Group

1993 NASA Aerospace Battery Workshop
U.S Space and Rocket Center
Huntsville, Alabama
November 16-18, 1993

JPL

OUTLINE

- CELL / BATTERY HISTORY
- OPERATIONAL STRATEGY
- SPACECRAFT DATA

JPL

CELL DESIGN

- GATES MANUFACTURED CELLS
  NASA STANDARD 50 Ah NiCd DESIGN
- GATES CELL LOT DESIGNATION: 42B050AB35 LOT #6
- GATES JOB NUMBER: 1711
- SEPARATOR: GOVERNMENT FURNISHED EP-2505
- ELECTROLYTE QUANTITY: 160 cc
- 3 POSTS NEGATIVE PLATE
- 2 POSTS POSITIVE PLATE
- 113 CELLS

JPL

CELL/BATTERY HISTORY

- PLATE BUYOFF: APRIL 4, 1991
- CELL ACTIVATION: APRIL 25, 1991
- CELL DELIVERY: AUGUST 1, 1991
- BATTERY BUYOFF: 4 BATTERIES FEBRUARY 5, 1992
- COLD STORAGE: FEBRUARY-JULY 1992
- LAUNCH-3 BATTERIES: AUGUST 10, 1992
- JPL RECEIVED SPARE: AUGUST 1992

JPL

OPERATIONAL RECOMMENDATIONS

- LIMIT PEAK CHARGE CURRENT TO 20 A BY OFFSETTING THE SOLAR ARRAY
- LIMIT OVERCHARGE BY CONTROLLING THE RECHARGE FRACTION (C/D) BY OPERATING AT LOWER V/T LEVELS
- AVOID HIGH CHARGE CURRENTS DURING FULL SUN PERIODS BY OPERATING AT LOWER V/T LEVELS
- SWITCH TO LOWER CURRENT SENSOR FOR AMP-HOUR INTEGRATION TO IMPROVE C/D RATIO ACCURACY

BATTERY V/T LEVEL MANAGEMENT

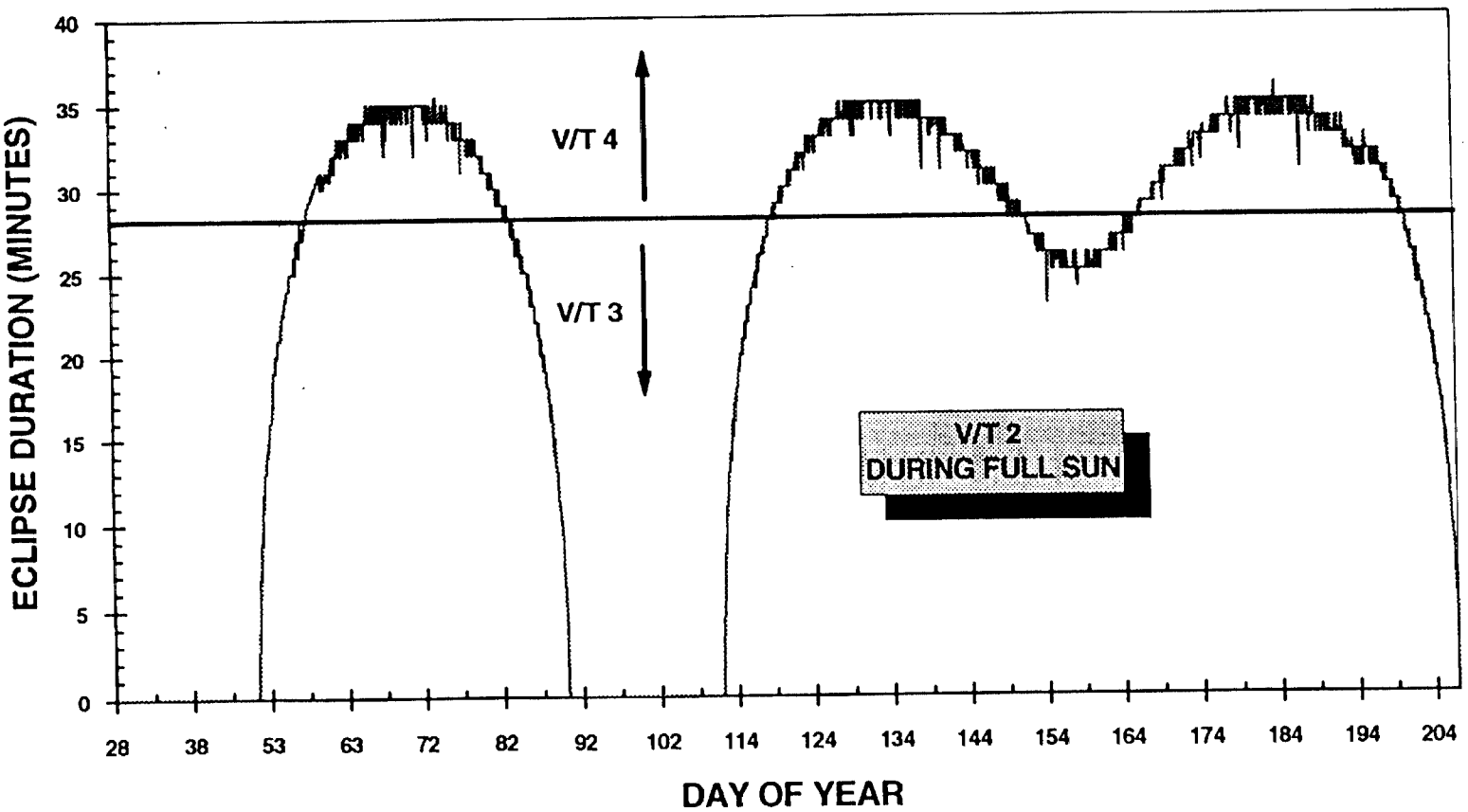

JPL

KEY BATTERY PARAMETERS MONITORED

- **DV - DIFFERENTIAL HALF BATTERY VOLTAGE**
  This parameter historically trended to evaluate battery state of health.

- **C/D - CHARGE/DISCHARGE RATIO**
  Monitors energy balance.

- **NET OVERCHARGE**
  Monitors total excess energy input to the batteries.

- **PEAK CHARGE CURRENT**
  Charge current during peak power mode / initial part of day.

- **TAPER CURRENT**
  Charge current during the taper mode / later part of day.

- **EONV - END OF NIGHT VOLTAGE**
  Battery voltage during the end of night.

- **BATTERY TEMPERATURE**
  Battery temperature monitored on the top of each battery.

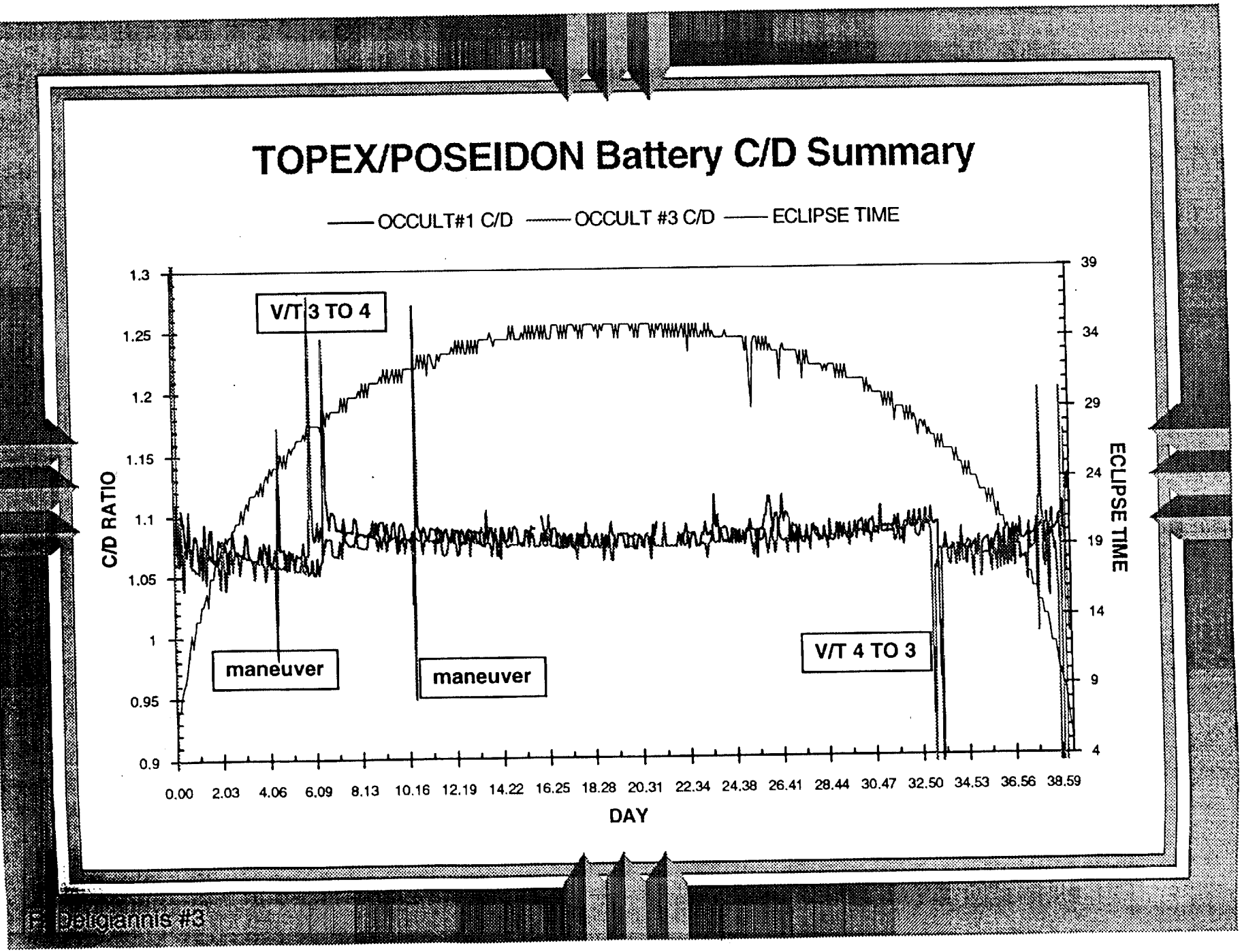
TOPEX/POSEIDON Battery C/D Summary
OCCULT#1 C/D
OCCULT #3 C/D
ECLIPSE TIME
V/T 3 TO 4
maneuver
maneuver
V/T 4 TO 3
C/D RATIO
ECLIPSE TIME
DAY
1.3
1.25
1.2
1.15
1.1
1.05
1
0.95
0.9
39
34
29
24
19
14
9
4
0.00 2.03 4.06 6.09 8.13 10.16 12.19 14.22 16.25 18.28 20.31 22.34 24.38 26.41 28.44 30.47 32.50 34.53 36.56 38.59
F. Deligiannis #3

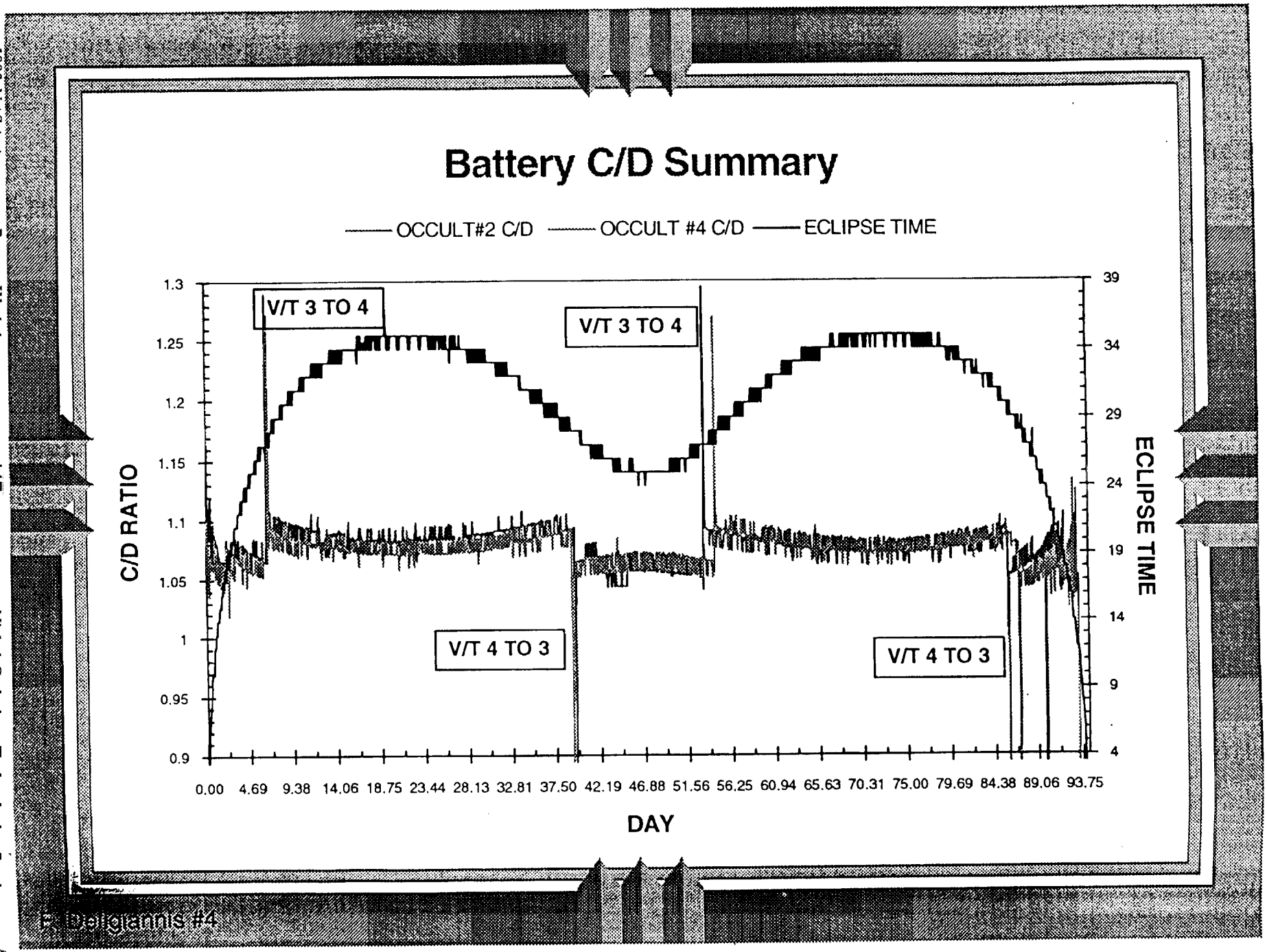
Battery C/D Summary
OCCULT#2 C/D
OCCULT #4 C/D
ECLIPSE TIME
V/T 3 TO 4
V/T 3 TO 4
V/T 4 TO 3
V/T 4 TO 3
C/D RATIO
ECLIPSE TIME
DAY
1.3
1.25
1.2
1.15
1.1
1.05
1
0.95
0.9
39
34
29
24
19
14
9
4
0.00 4.69 9.38 14.06 18.75 23.44 28.13 32.81 37.50 42.19 46.88 51.56 56.25 60.94 65.63 70.31 75.00 79.69 84.38 89.06 93.75

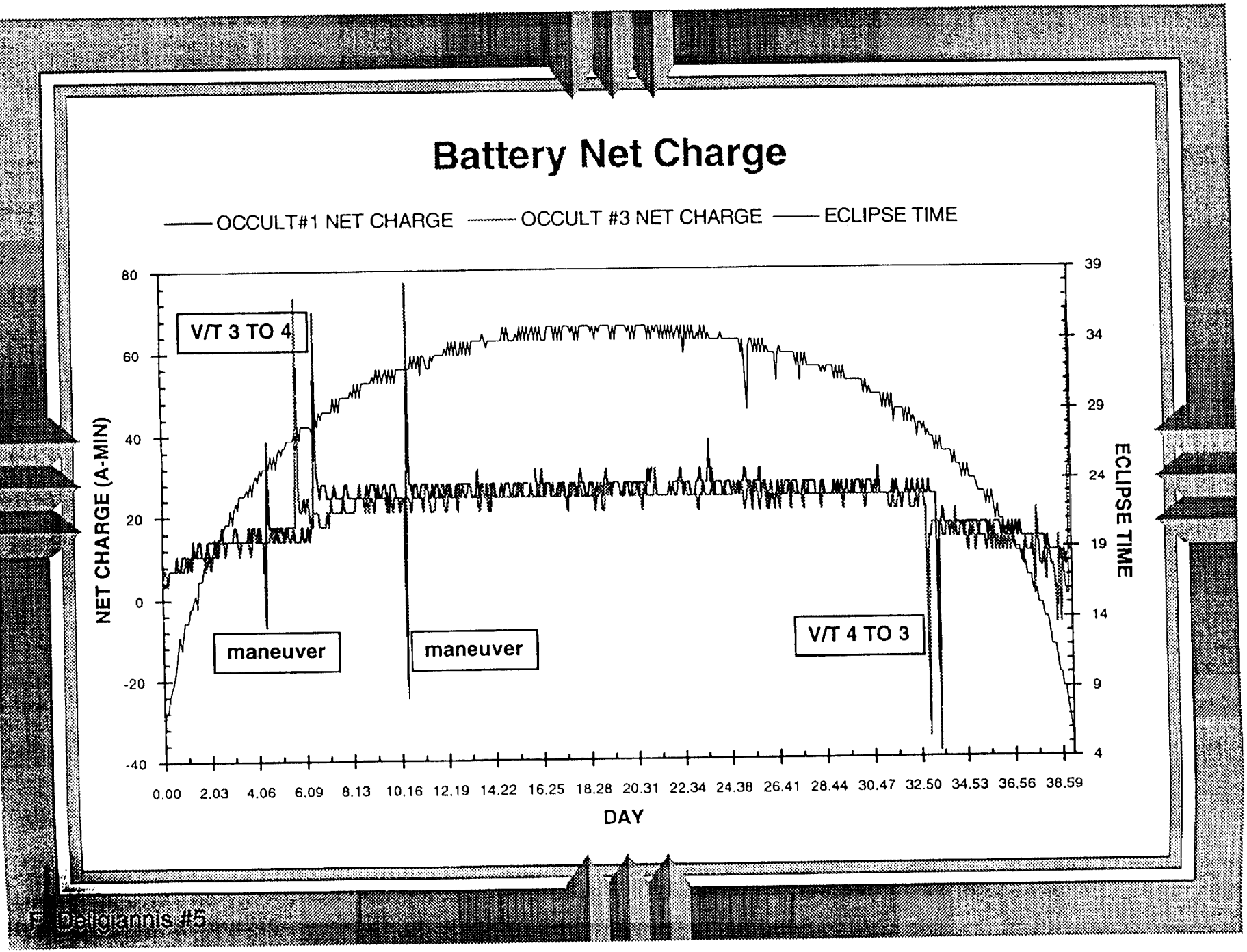

Beiglannis #5

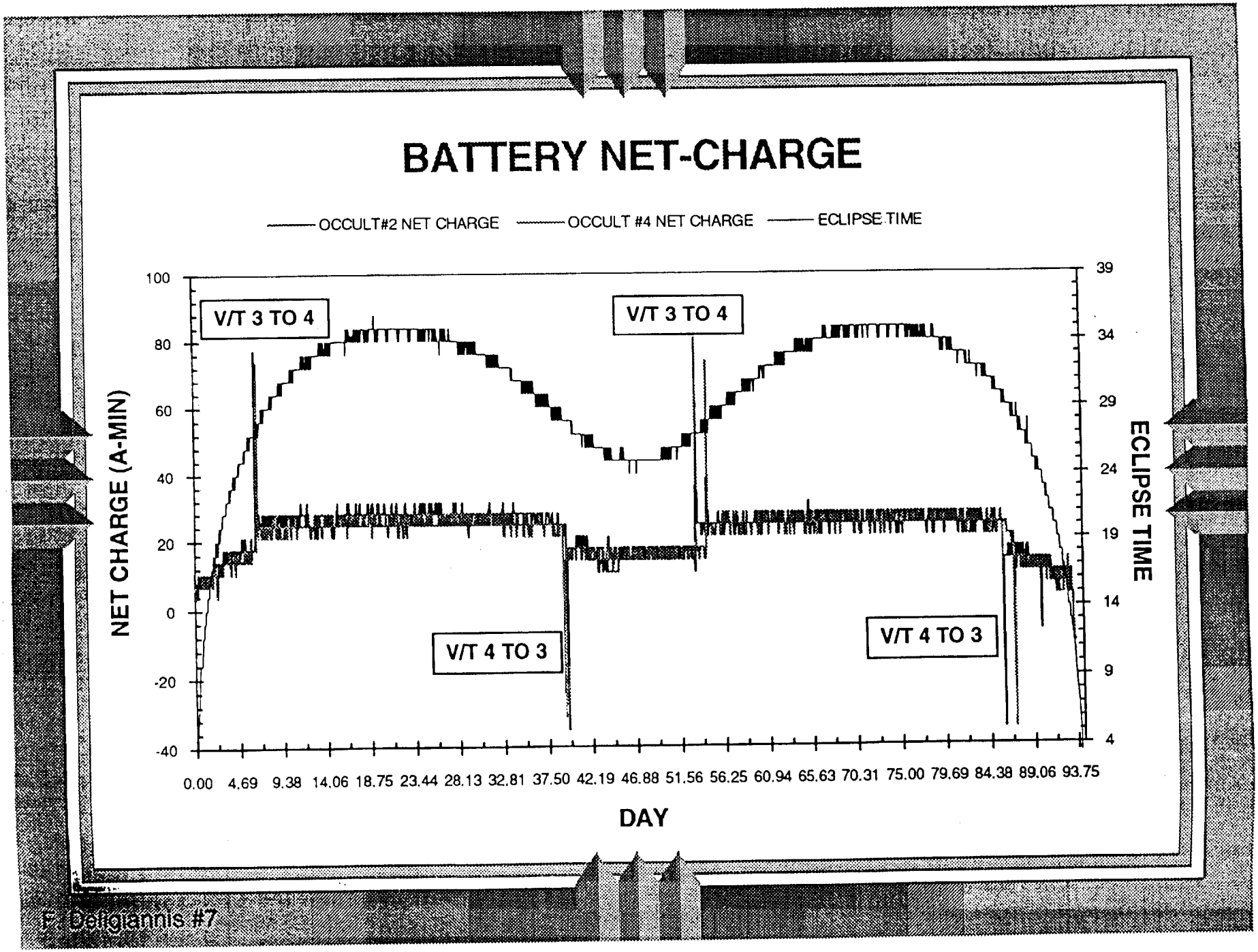
BATTERY NET-CHARGE
OCCULT#2 NET CHARGE
OCCULT #4 NET CHARGE
ECLIPSE TIME
V/T 3 TO 4
V/T 3 TO 4
V/T 4 TO 3
V/T 4 TO 3
NET CHARGE (A-MIN)
ECLIPSE TIME
DAY
100
80
60
40
20
0
-20
-40
39
34
29
24
19
14
9
4
0.00 4.69 9.38 14.06 18.75 23.44 28.13 32.81 37.50 42.19 46.88 51.56 56.25 60.94 65.63 70.31 75.00 79.69 84.38 89.06 93.75
F. Deligiannis #7

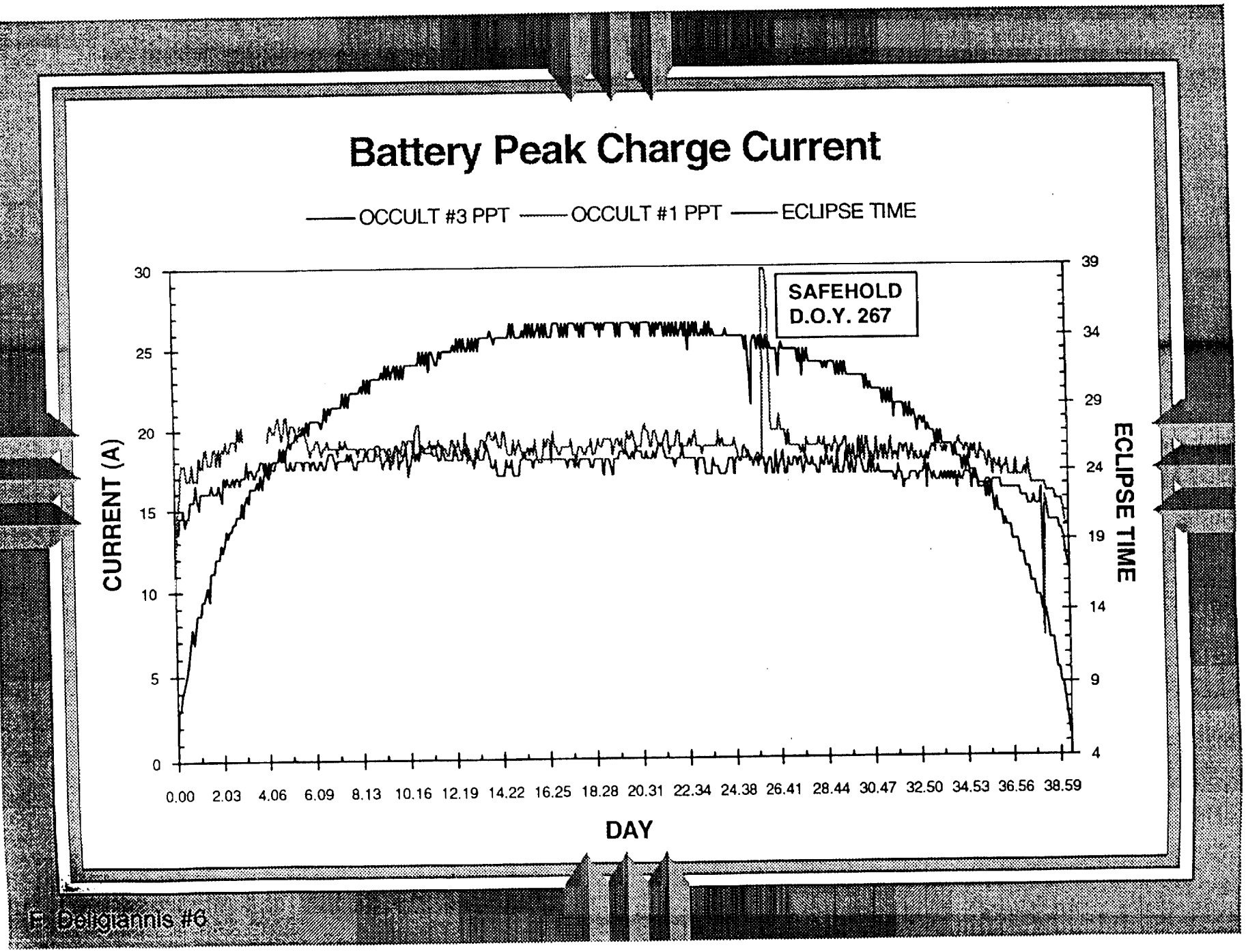
Battery Peak Charge Current
OCCULT #3 PPT
OCCULT #1 PPT
ECLIPSE TIME
SAFEHOLD
D.O.Y. 267
CURRENT (A)
ECLIPSE TIME
DAY
0
5
10
15
20
25
30
4
9
14
19
24
29
34
39
0.00 2.03 4.06 6.09 8.13 10.16 12.19 14.22 16.25 18.28 20.31 22.34 24.38 26.41 28.44 30.47 32.50 34.53 36.56 38.59
F. Deligiannis #6

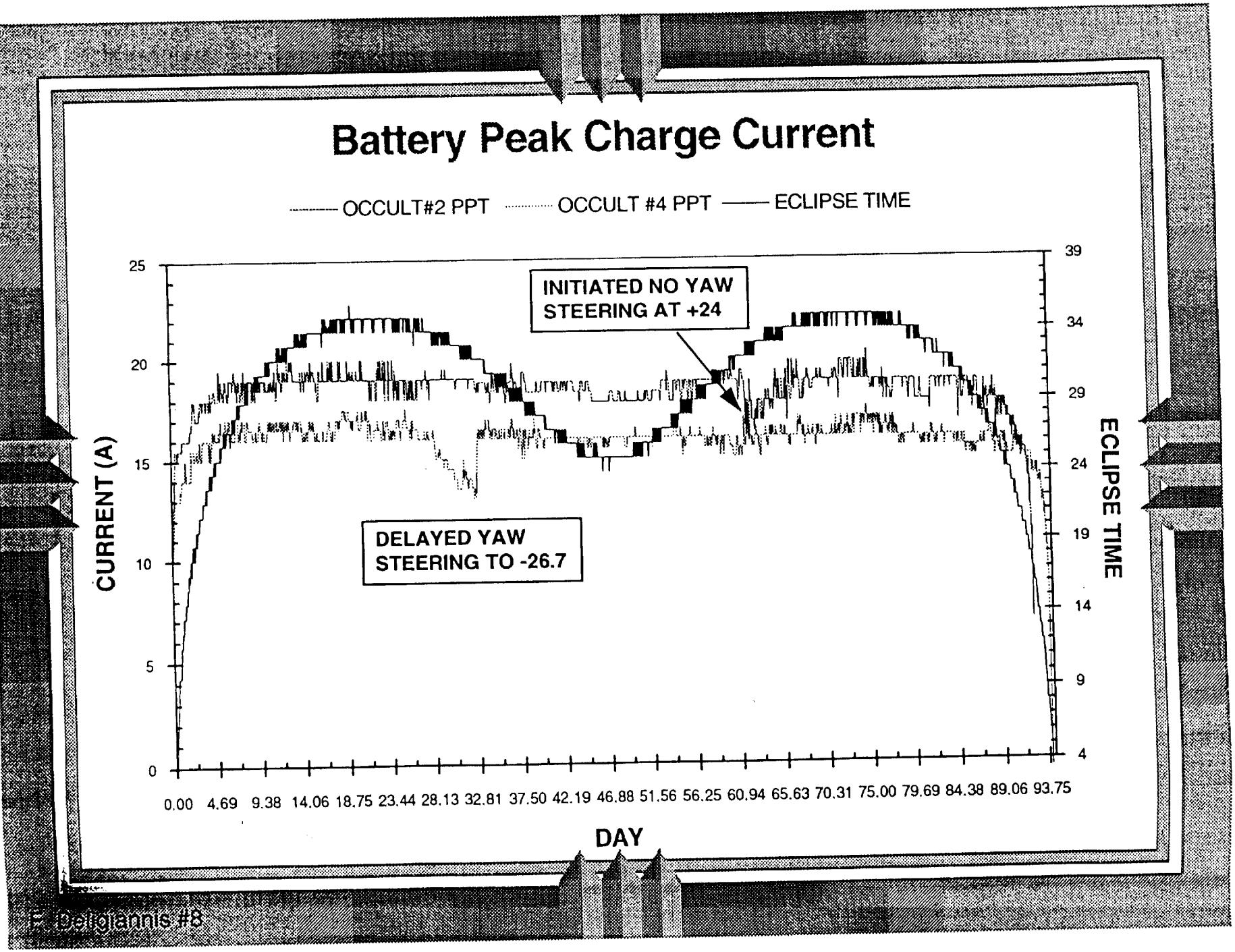
Battery Peak Charge Current
OCCULT#2 PPT
OCCULT #4 PPT
ECLIPSE TIME
INITIATED NO YAW STEERING AT +24
DELAYED YAW STEERING TO -26.7
CURRENT (A)
ECLIPSE TIME
DAY
0
5
10
15
20
25
4
9
14
19
24
29
34
39
0.00 4.69 9.38 14.06 18.75 23.44 28.13 32.81 37.50 42.19 46.88 51.56 56.25 60.94 65.63 70.31 75.00 79.69 84.38 89.06 93.75
F. Deligiannis #8

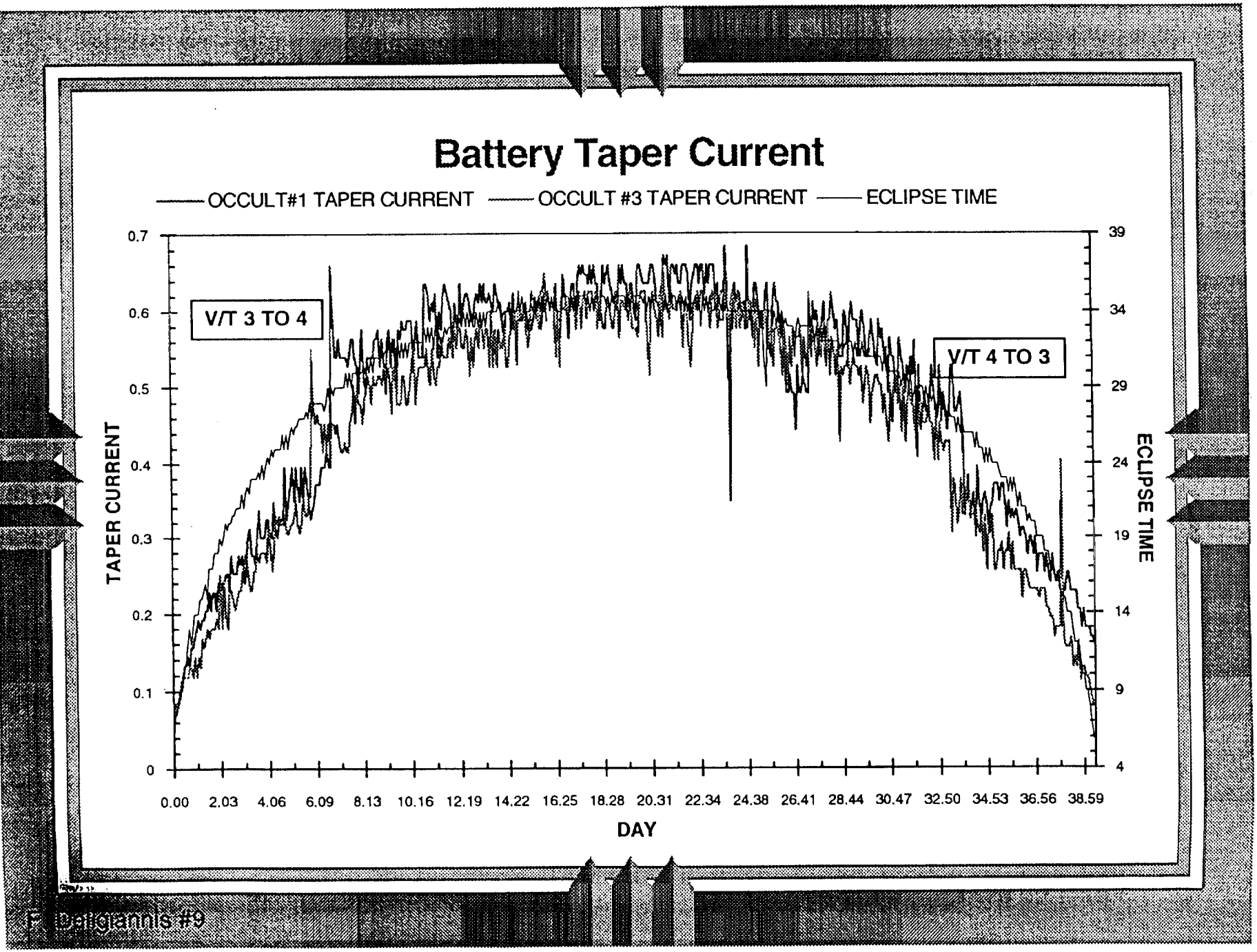
Battery Taper Current
OCCULT#1 TAPER CURRENT
OCCULT #3 TAPER CURRENT
ECLIPSE TIME
V/T 3 TO 4
V/T 4 TO 3
TAPER CURRENT
ECLIPSE TIME
DAY
0.7
0.6
0.5
0.4
0.3
0.2
0.1
0
39
34
29
24
19
14
9
4
0.00 2.03 4.06 6.09 8.13 10.16 12.19 14.22 16.25 18.28 20.31 22.34 24.38 26.41 28.44 30.47 32.50 34.53 36.56 38.59

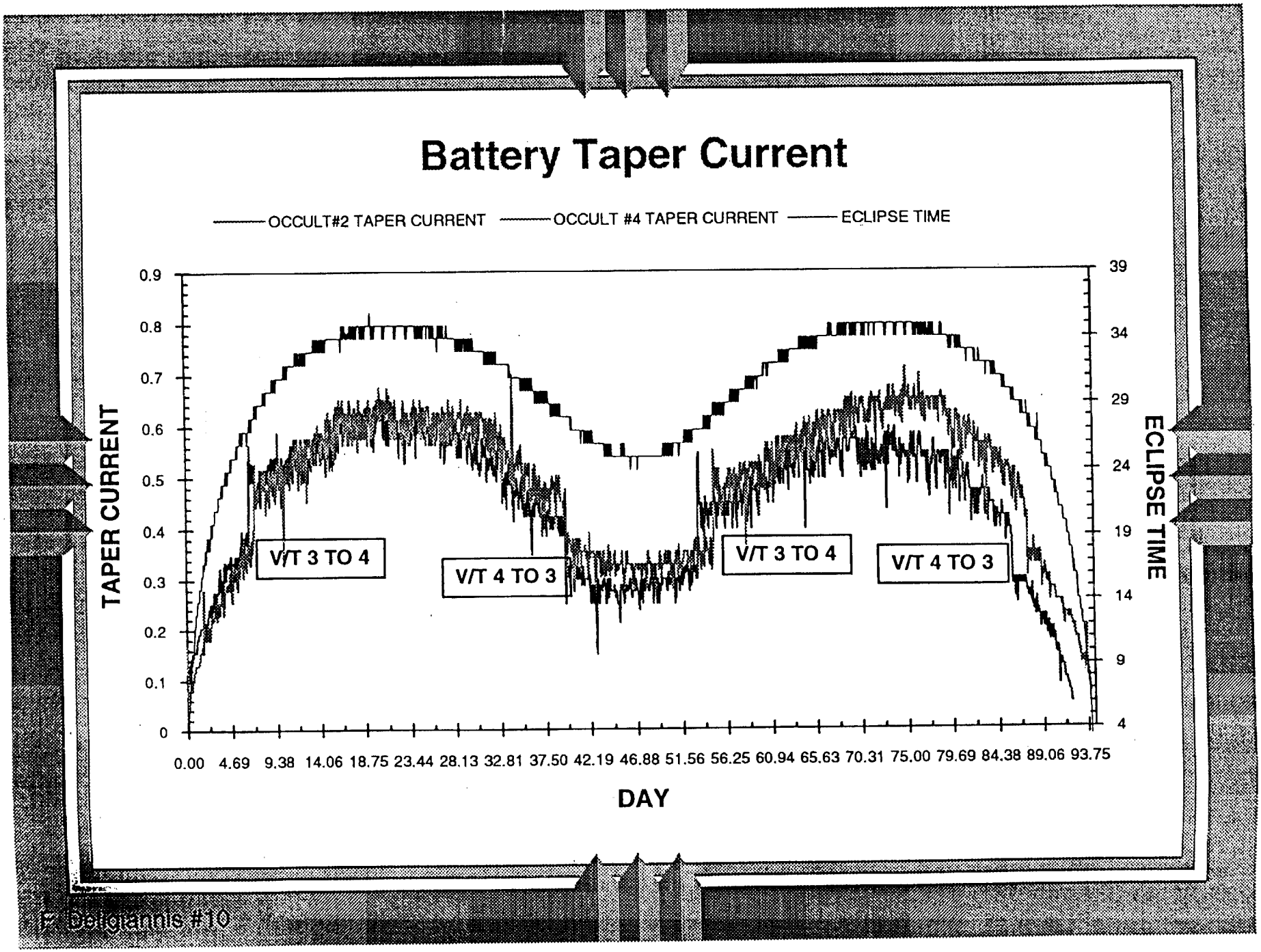
Battery Taper Current
OCCULT#2 TAPER CURRENT
OCCULT #4 TAPER CURRENT
ECLIPSE TIME
TAPER CURRENT
ECLIPSE TIME
0.9
0.8
0.7
0.6
0.5
0.4
0.3
0.2
0.1
0
39
34
29
24
19
14
9
4
V/T 3 TO 4
V/T 4 TO 3
V/T 3 TO 4
V/T 4 TO 3
0.00 4.69 9.38 14.06 18.75 23.44 28.13 32.81 37.50 42.19 46.88 51.56 56.25 60.94 65.63 70.31 75.00 79.69 84.38 89.06 93.75
DAY
F. Deligiannis #10

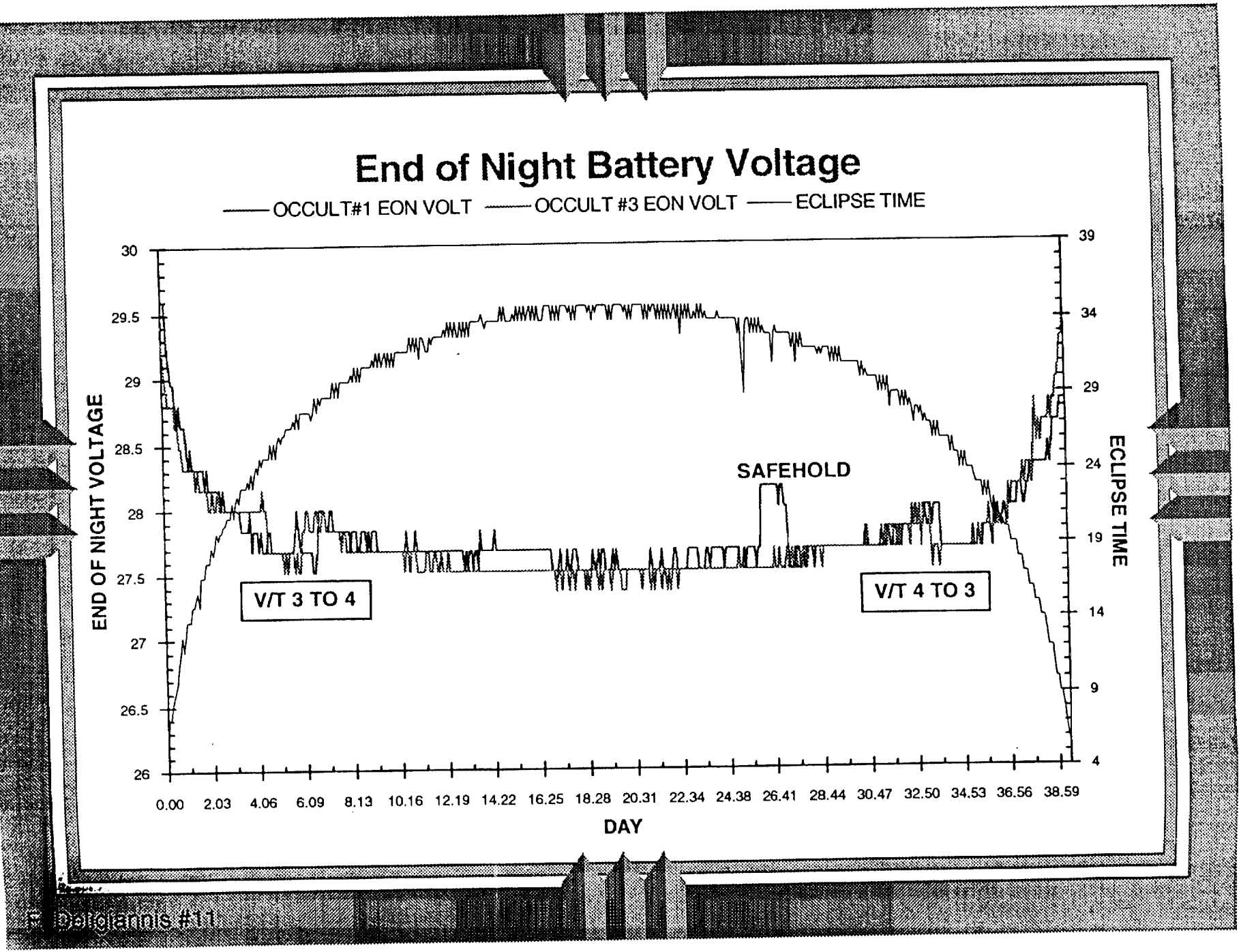
End of Night Battery Voltage
OCCULT#1 EON VOLT
OCCULT #3 EON VOLT
ECLIPSE TIME
END OF NIGHT VOLTAGE
ECLIPSE TIME
DAY
SAFEHOLD
V/T 3 TO 4
V/T 4 TO 3
30
29.5
29
28.5
28
27.5
27
26.5
26
39
34
29
24
19
14
9
4
0.00 2.03 4.06 6.09 8.13 10.16 12.19 14.22 16.25 18.28 20.31 22.34 24.38 26.41 28.44 30.47 32.50 34.53 36.56 38.59
Delgiannis #11

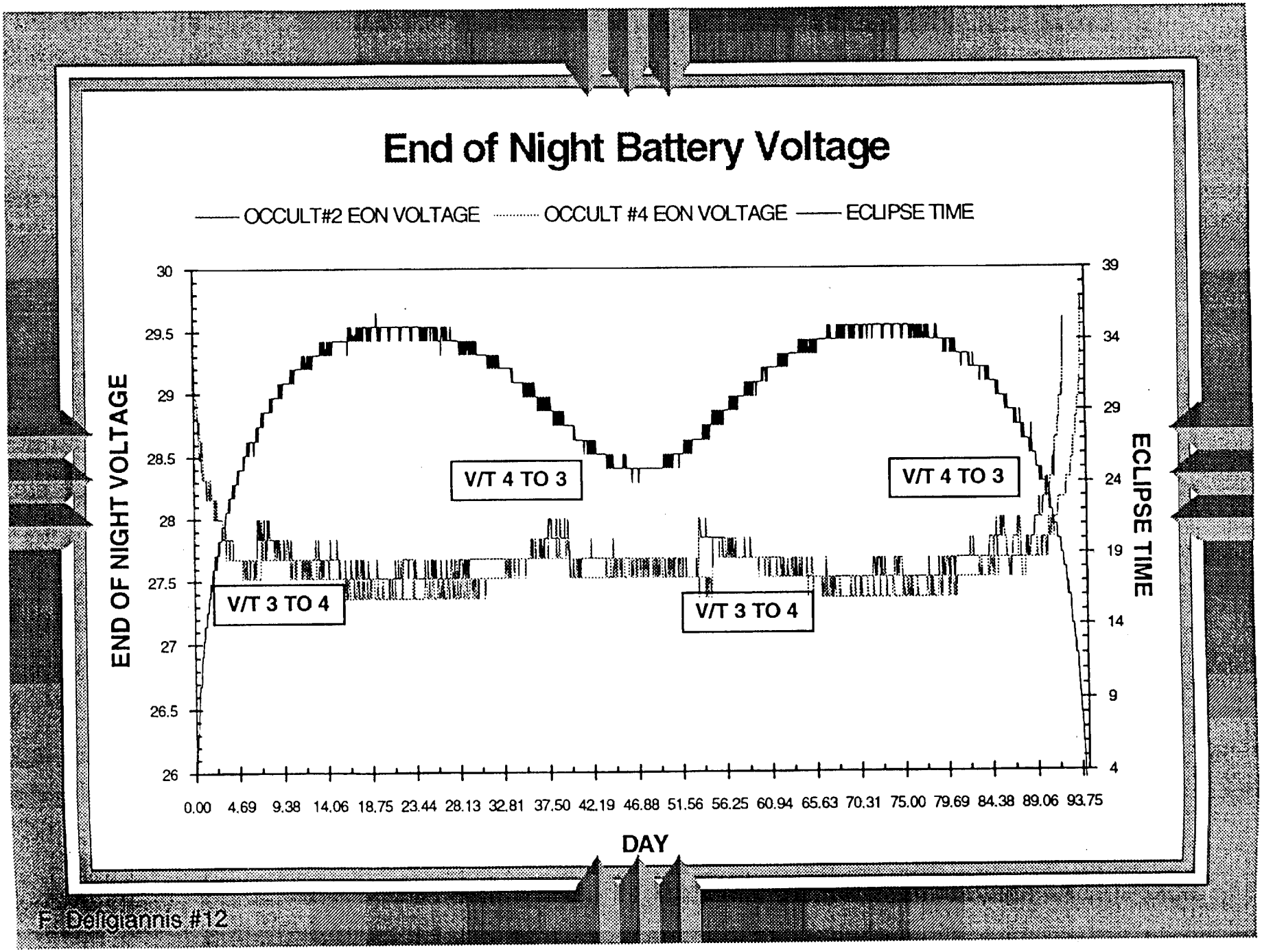
End of Night Battery Voltage
OCCULT#2 EON VOLTAGE
OCCULT #4 EON VOLTAGE
ECLIPSE TIME
END OF NIGHT VOLTAGE
ECLIPSE TIME
DAY
30
29.5
29
28.5
28
27.5
27
26.5
26
39
34
29
24
19
14
9
4
0.00 4.69 9.38 14.06 18.75 23.44 28.13 32.81 37.50 42.19 46.88 51.56 56.25 60.94 65.63 70.31 75.00 79.69 84.38 89.06 93.75
V/T 4 TO 3
V/T 4 TO 3
V/T 3 TO 4
V/T 3 TO 4
F. Deligiannis #12

BATTERY END-OF-NIGHT VOLTAGE AT MAX ECLIPSE DURATION

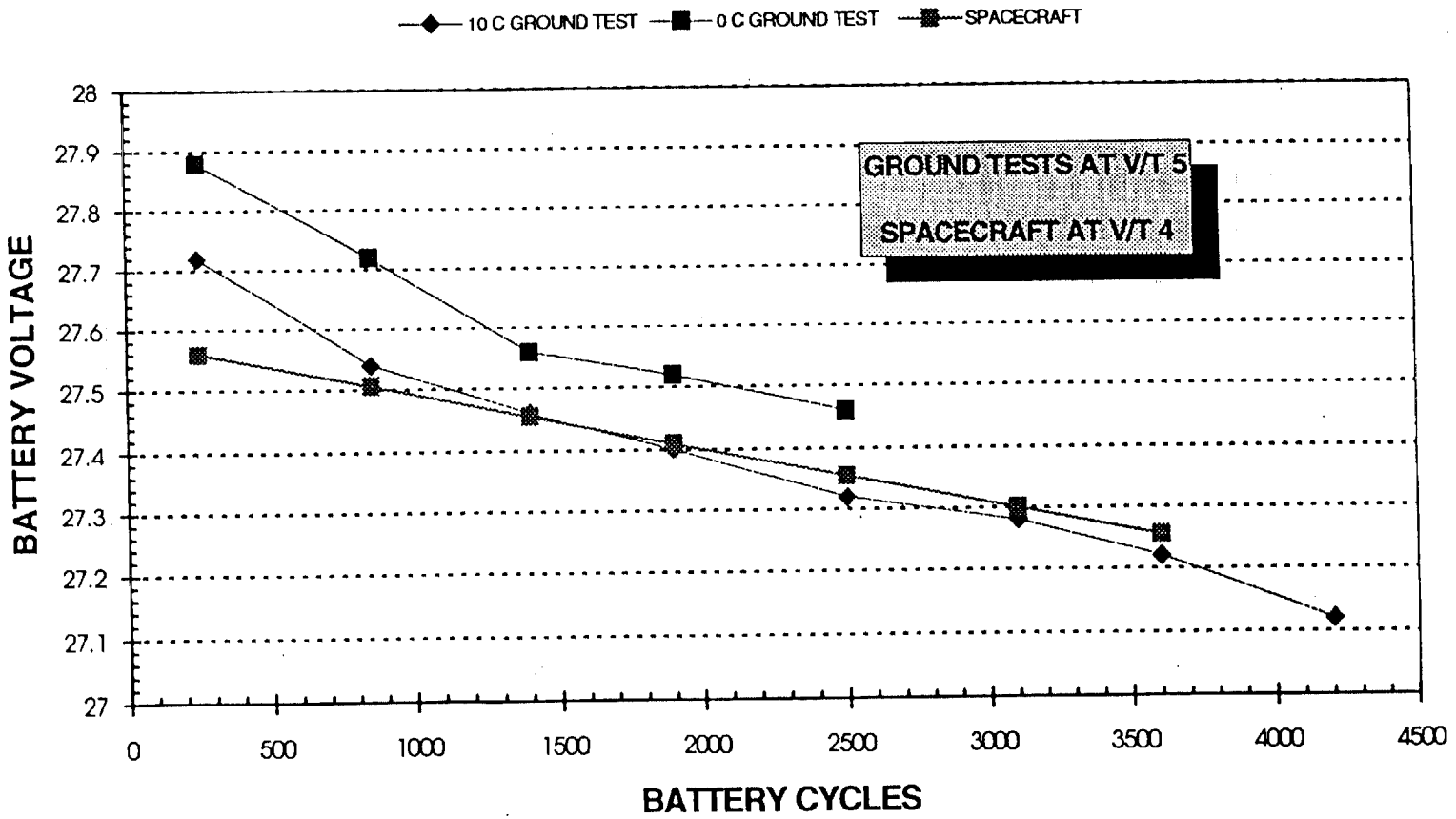

TOPEX BATTERY DIFFERENTIAL VOLTAGE HISTORY DURING PEAK POWER TRACKING MODE

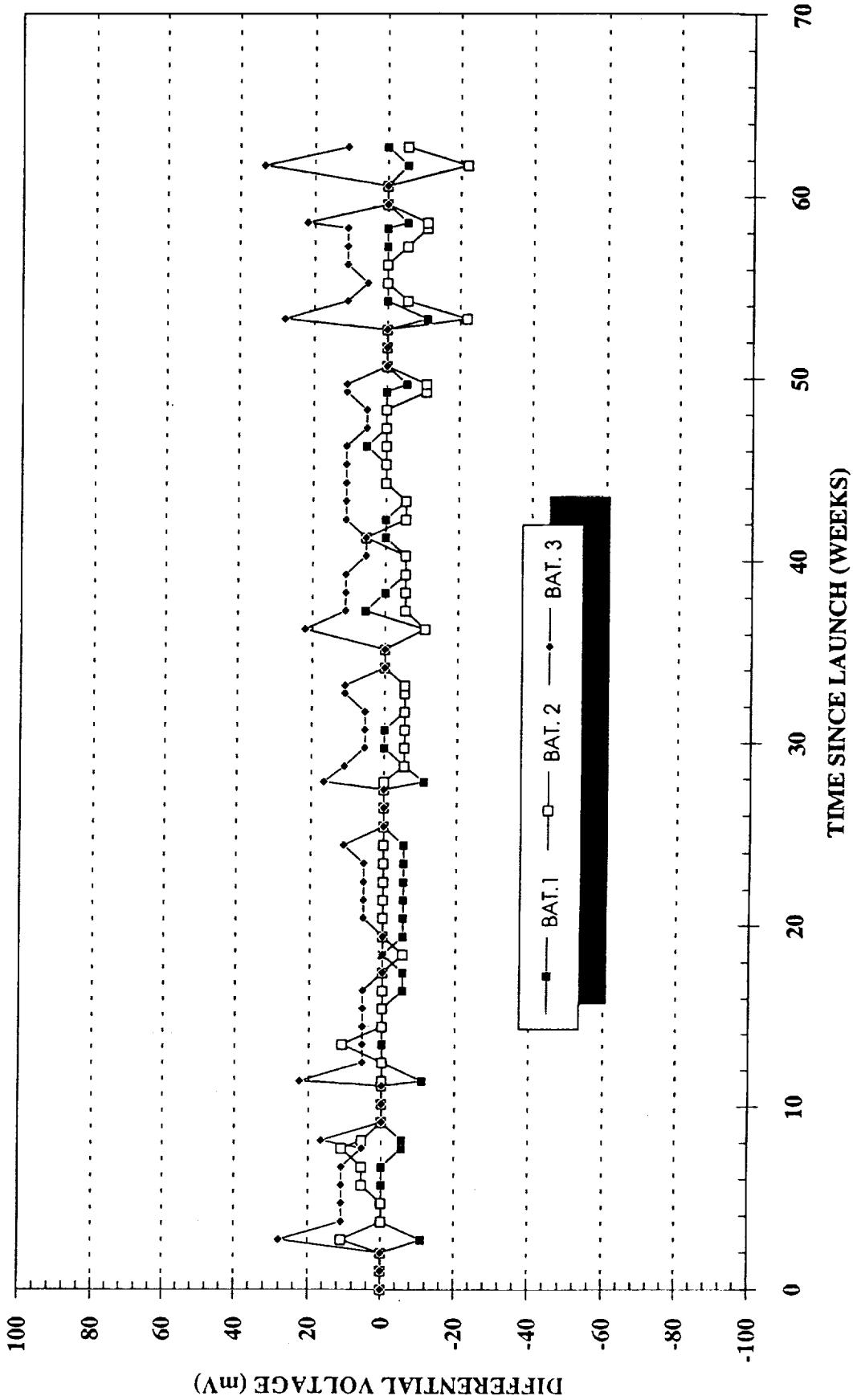

JPL

CONCLUSIONS

- COMPLETED 15 MONTHS OF SUCCESSFUL OPERATION
  - ANOTHER 21 MONTHS OF PRIMARY MISSION REMAINING
  - ADDITIONAL 24 MONTHS OF EXTENDED MISSION
- C/D HAS BEEN MAINTAINED AT APPROXIMATELY 1.07
- PEAK CHARGE CURRENTS WERE SUCCESSFULLY LIMITED TO BELOW 20 A
- END-OF-NIGHT VOLTAGE HAS DROPPED 2 DN COUNTS (0.32 V)
- VOLTAGE DIFFERENTIAL WAS WITHIN A FEW DN COUNTS (16 mV)
- WE ANTICIPATE WITH PROPER BATTERY MANAGEMENT THE BATTERY PERFORMANCE WILL REMAIN AT OPTIMUM LEVELS

N94-28120

Nickel Cadmium Battery Operations On-Orbit: Trials, Tribulations and Success on the Upper Atmosphere Research Satellite

Gopalakrishna M. Rao and Scott D. Miller*

NASA/Goddard Space Flight Center
Greenbelt, Maryland 20771

Abstract

The Upper Atmosphere Research Satellite (UARS), designed, built, integrated, tested and operated by NASA and Martin Marietta is a low-Earth orbiting, Earth-observing spacecraft which was launched via Space Shuttle Discovery on September 12, 1991 and deployed three days later. The Modular Power Subsystem (MPS) on-board the satellite is equipped with three NASA Standard 50 Ampere-hour (Ah) nickel-cadmium (NiCd) batteries. McDonnell Douglas Electronics Systems Company fabricated the MPS, and batteries from Gates Aerospace Batteries cells.

Nominal battery performance was achieved for the first four months of spacecraft operation. First evidence of anomalous battery performance was observed in January 1992, after the first maximum beta angle (low Depth of Discharge) period. Since then, the Flight Operations Team (FOT), under the direction of Goddard Space Flight Center's UARS Project and Space Power Application Branch, has monitored and managed battery performance by adjusting solar array offset angle, conducting periodic deep discharge, and controlling battery recharge ratio. This paper covers a brief overview of the UARS, its MPS, the FOT's operational battery management, and the observed spacecraft battery performance.

---

*Martin Marietta Services Inc. - Goddard Operations, Lanham MD

Introduction

Spacecraft Systems Overview

The Upper Atmosphere Research Satellite (UARS) is NASA's first spacecraft (S/C) in its Mission to Planet Earth. The study of environmental change affecting the entire Earth as a self-contained system via space observations is the mission's goal. Nine instruments (plus one sensor of opportunity) simultaneously and comprehensively study global stratospheric energy input, winds, and chemical composition, in addition to those changes associated with human activities which lead to ozone depletion.

The UARS design is a three axis stabilized spacecraft which combines a Multimission Spacecraft (MMS) bus designed and manufactured by Fairchild Space Company with an Instrument Module (IM) designed, fabricated, integrated and tested by Martin Marietta (formerly General Electric) AstroSpace, East Windsor, New Jersey. This work was completed for NASA/ Goddard Space Flight Center's (GSFC's) Earth Science Mission Operations (ESMO) Project.

UARS achieved orbit through Space Shuttle Discovery launch on September 12, 1991 and was deployed three days later, September 15. Mission Operations have since been carried out by Martin Marietta for NASA's ESMO Project. The mission orbit is a 96 minute, circular orbit inclined 57 degrees to the Equator with a 585 Km height. This allows stratospheric sensors to observe up to 80 degrees in latitude (North and South) and provides near total global coverage. The full range of local times at all geographic locations is viewed every 36 days.

The UARS was designed for a nominal mission life of 18 months covering 2 Northern Hemisphere winters - the design life of the CLAES cryogenic instrument, with a minimum of an additional 18 months planned and a goal of 5 years. The S/C power system was designed for a maximum 1600 Watts (orbital average), 786 Watts of which was reserved for the instrument load. The S/C maximum load has been about 1350 Watts with instrument loads of approximately 450 Watts. S/C weight upon mission orbit insertion was 6800 kg. The FOT utilizes NASA's Space Network and the Tracking and Data Relay Satellite System (TDRSS) to provide routine command uplinks and science and telemetry data downlinks.

The IM is a truss-type torque-box constructed of graphite-epoxy tubes with titanium end fittings and supports all ten instruments. The plus Y side of the S/C, where the limb-looking and cryogenic instruments reside, must be kept in shadow at all times. To satisfy both the shadowing and full globe coverage requirements, a "Yaw-Around" maneuver is performed every 36 to 42 days. This entails turning the S/C around 180 degrees and allows, alternately, Northern (backwards flight) and Southern (forward flight) Hemisphere Limb viewing.

The MMS bus includes the Modular Attitude Control Subsystem (MACS), the Propulsion Module (PM), the Command and Data Handling Subsystem (C&DH) which incorporates the On-Board Computer (OBC), the Earth Sensor Assembly Module, the Signal Conditioning and Control Unit, and the Modular Power Subsystem (MPS) which houses the three NASA Standard 50 Ah NiCd batteries and power control/distribution circuitry.

The UARS Power Subsystem comprises all power control, power distribution and, all other related hardware. It contains the McDonnell Douglas Electronics Systems Company (MDESC) supplied MPS, main and auxilliary Solar Arrays and related equipment. Figure 1 relates how these components are connected and interact.

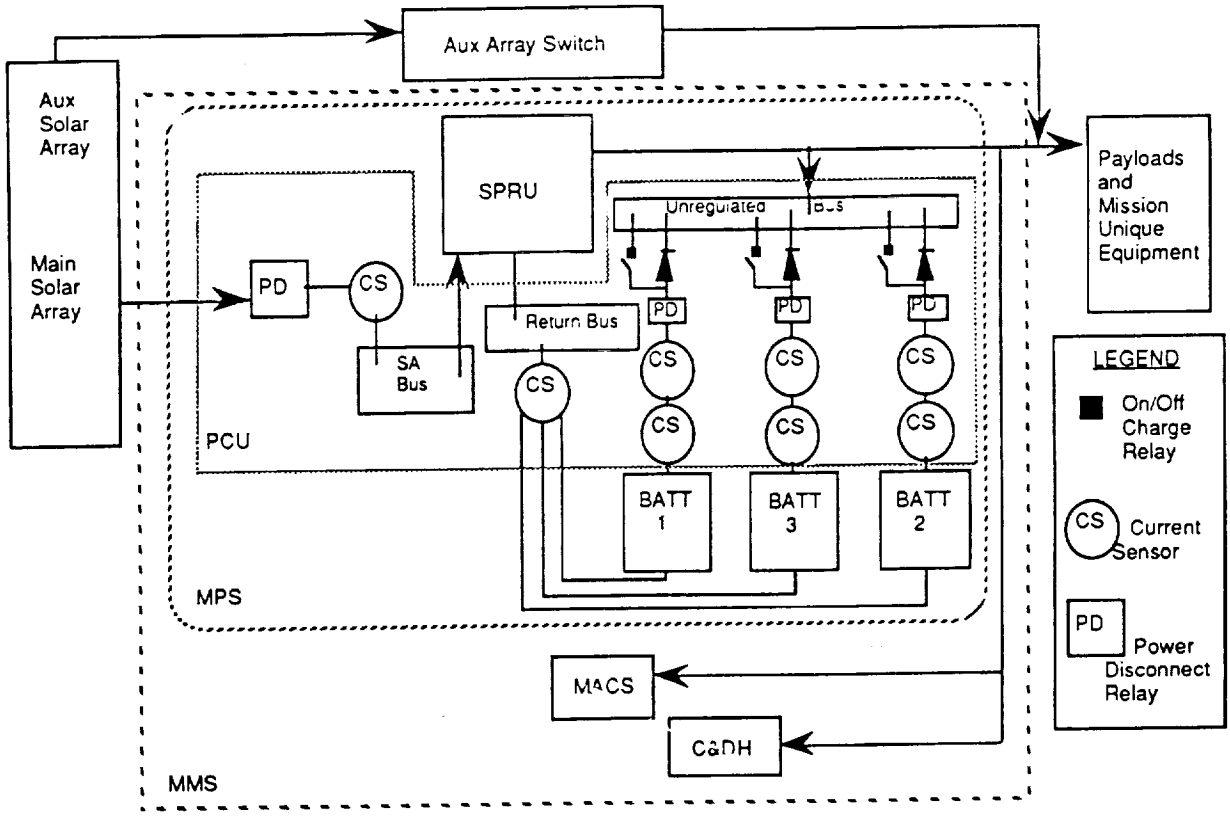

Figure 1. UARS Power Subsystem Block Diagram

Table 1 lists the major Power Subsystem components and their functions.

TABLE 1. UARS Power Subsystem Components and Their Functions

Power Subsystem Component	Function
Standard Power Regulation Unit (SPRU)	Battery charge control.
Signal Conditioning Assembly (SCA)	Command and telemetry conditioning.
Bus Protection Assembly (BPA)	Fusing of internal MPS loads.
50 Ah Batteries	Energy storage.
Power Control Unit (PCU)	Power distribution and system configuration.
Remote Interface Units (RIUs)	C&DH Interfaces.
Main Array	Energy conversion - provides 1200 Watts power for instrument loads and battery charging.
Aux Array	Energy conversion - provides additional 400 Watts power for instrument loads only.
Auxiliary Array Switch	Controls Aux Array power as a function of Instrument load current.
Solar Array Drive and Deployment Electronics (SADDE)	Provides drive and rate control to rotate SA at 1 revolution per orbit, tracking the Sun.
Solar Array Drive (SAD)	Maintains SA Sun-pointing while the S/C is in an Earth-viewing orientation. Can rotate the SA in either direction for both forward and backward S/C flight.

Mission & Power Subsystem Operations

Total S/C operations are provided by Martin Marietta under the direction of the ESMO/UARS Project staff. The power and battery operations are managed in concert with the Space Power Applications Branch.

The Power Subsystem was designed to provide 1600 Watts orbital average by using the MPS in conjunction with an auxilliary Solar Array and auxilliary array switch, since the MPS capability is limited to 1200 Watts. Power is distributed to the MMS and IM modules at 28 +/-7 Volts D.C. The MPS was constructed by MDESC according to the NASA/GSFC Specification for Multimission Modular Spacecraft (MMS) Modular Power Subsystem(1). According to the UARS General Instrument Interface Specification(2), the MPS output voltage range should be between 22 and 35 V.

The MPS receives commands from the OBC for enabling the battery control mode in the SPRU and for setting the operating limits for battery voltage and battery current. The various MPS operation modes are summarized in Table 2.

Table 2. MPS Charge Modes and Their Operations

MPS Battery Charge Mode	Operation
Standby	When no SA power is available and the batteries are supplying the S/C power, the SPRU retains its last commanded state in memory and can receive additional commands.
Peak Power Tracking (PPT)	The SPRU will always operate at the SA maximum power output point in order to transfer all available power to the load and to charge the batteries until the voltage-temperature set point (V/T mode) is reached, or until the battery current reaches the current set point if Constant Current Mode (CCM) is enabled.
Battery Voltage Limited (V/T)	The SPRU will operate on the voltage side of the SA I-V curve in order to control the battery voltage to one of the eight selected voltage-temperature set points, and will allow the battery to charge at a current determined by the battery characteristics.
Constant Current Limited (CCM)	When enabled, the SPRU will operate on voltage side of the SA I-V curve in order to control the battery current to one of three selected levels (0.75, 1.5, 3.0 A), and will allow the batteries to charge at a voltage determined by the battery characteristics up to the selected V/T limit.
Safehold	When an OBC fault is detected, the SPRU will receive a command to disable CCM (if enabled) and to set the V/T set point to a preselected V/T level. This remains in effect until reset by an external command.

MPS telemetry data is reported by the C&DH module and is plotted by the UARS Generalized Plotting Software/Level Zero (UGPL) off-line . Table 3 lists the MPS Telemetry Points that the UARS FOT uses for trend analysis.

Table 3. MPS Telemetry Points

Battery Terminal Voltage (Volts)
Load Bus Voltage (Volts: EOD,EON,Instantaneous)
Battery Current (Amperes: High & Low Sensors)
Total S/C Current (Amperes)
IM Current (Amperes)
Half-Battery Differential Voltage (mV)
Battery Temperatures (C)
MPS Temperatures (C)
Total Discharge (Amp-min)
Net Charge (Amp-min)
C/D Ratios
State Of Charge (%)
Depth Of Discharge (%)
Main SA Power (Watts)
Aux SA Power (Watts)
Solar Array Temperatures (C)
Solar Array Output Power (Watts)

Batteries

The three NASA Standard 50 Ah NiCd Batteries on-board UARS, which were fabricated by MDESC using GAB cells (50AB35, LOT 2), are on a parallel bus and charged to NASA Standard V/T curves using the MPS and NASA Standard Power Regulator Unit (SPRU). The battery cells were constructed according to the NASA/GSFC Specification for the Manufacture of Aerospace Nickel-Cadmium Storage Cells[3 & 4], while the Batteries were manufactured according to NASA/GSFC Specification for the Standard Nickel-Cadmium Spacecraft Batteries[5].

The batteries were specified to a name plate capacity of 50 Ah and to operate in low-Earth orbit up to 20% Depth of Discharge (DOD), and 28+/-7 Volts for a nominal 36-month mission[3 & 4]. Thermal vacuum testing revealed that with a full-up UARS at 24% DOD, the lowest EON Voltage at the beginning of the mission should have been close to 27.0 V[2]. Thermal vacuum testing also revealed nominal performance within specifications on ground tests prior to launch.

Beta Angle

Beta angle is defined as the angle between the orbital plane and the Earth-to-Sun line. Variation of this parameter affects the Solar Array (SA) energy conversion, the S/C loading, and the Battery Charge and Discharge profiles. The cyclical variation of the orbit Beta angle (ß) is caused by the 57 degree orbital inclination and orbital geometry. Figure 2 shows the cyclical Beta angle and Night Length variations since launch. The Beta angle variation changes SA Night periods (in addition to the normal seasonal changes) from a maximum eclipse of 36 minutes at zero degree Beta, to a minimum of zero minutes at Beta angles above 66 degrees. Figure 3 is a plot of the Total S/C Current over the mission to date.

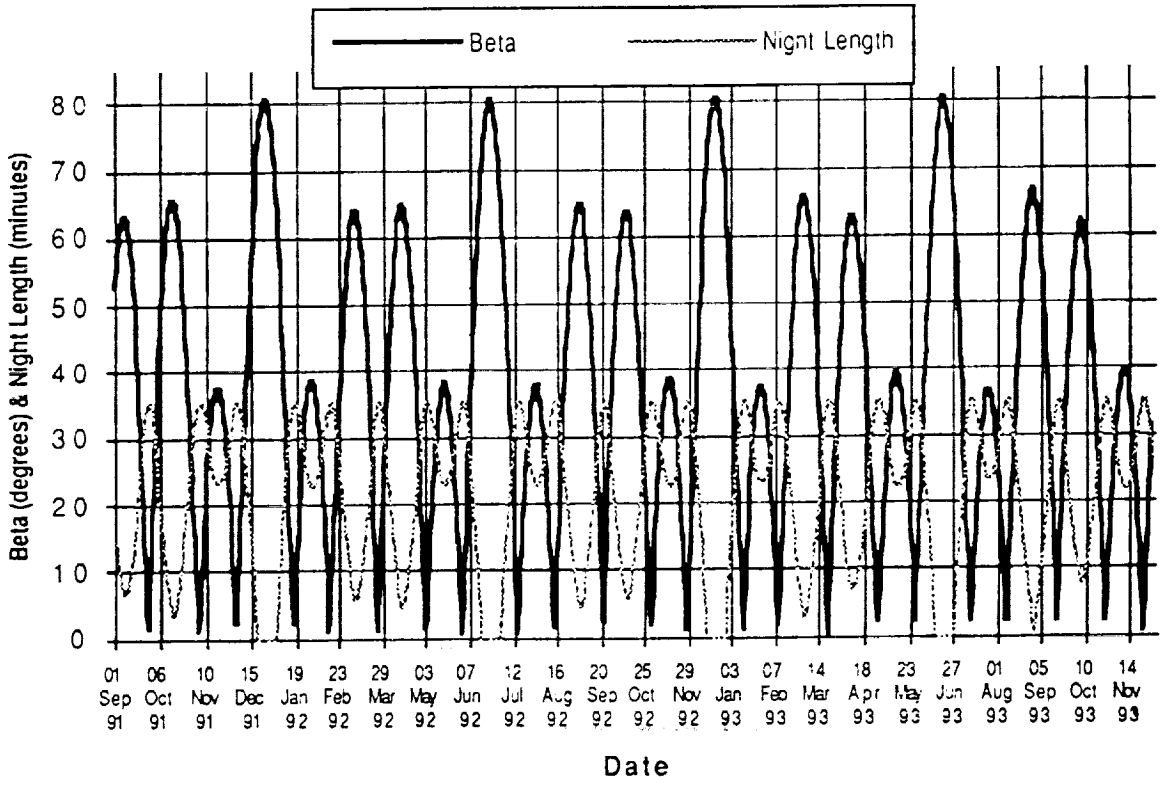

Figure 2. Beta Angle & Night Length vs. Date

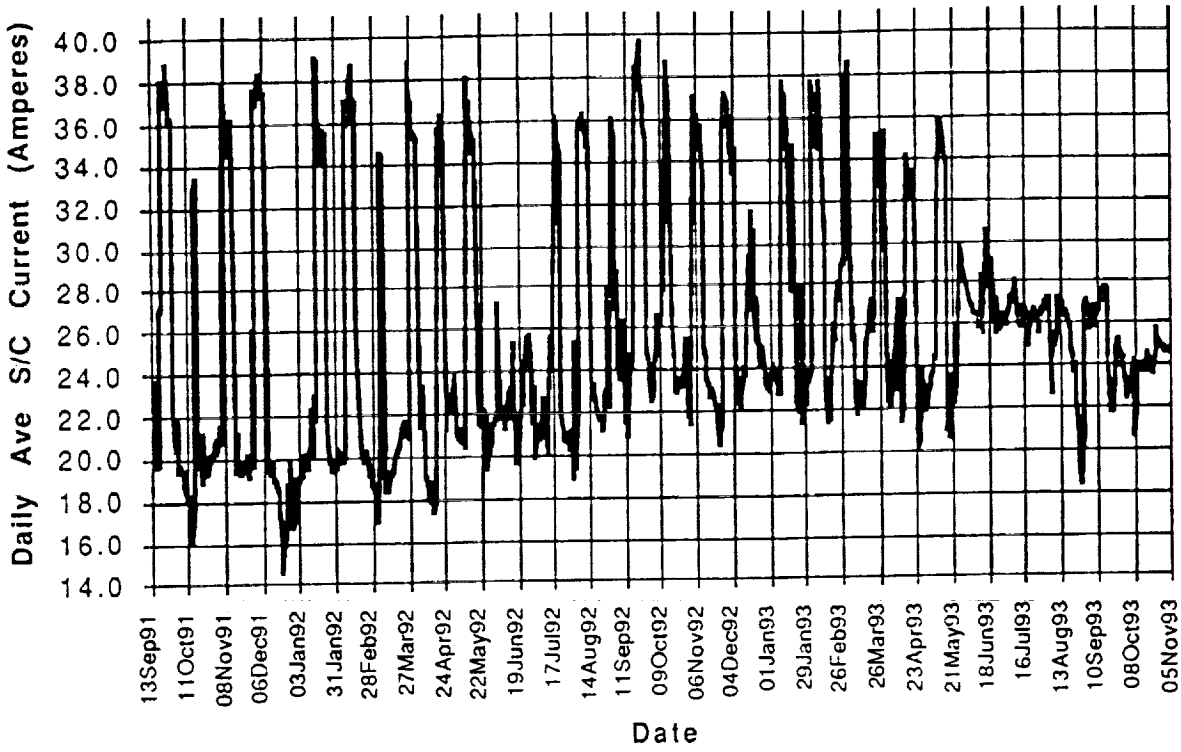

Figure 3. Total S/C Load

Battery/MPS Management

This section highlights UARS MPS and battery management from deployment to 26 October 1993. Table format is used to aid both clarity and brevity. The heading lists the covered periods and orbit beta angles, the battery performance and characteristic parameters are presented in each Table.

The FOT, Project Office and Space Power Applications Branch have managed the MPS and Batteries by monitoring the Half Battery Differential Voltage (Differential Voltage), End Of Night (EON) Voltage, and Battery Charge and Discharge current sharing, and by controlling battery overcharge, recharge ratio, battery temperature, the difference between battery temperature (delta temperature), and DOD. This strategy has continuously been updated and changed to fit the battery performance and characteristics that were of greatest concern at that particular time. The end result is a plan that started with a basic premise that operations would be normal and not intensive.

I. Early Orbit (9/15/91-12/91)

Beta : 27, 0 (Yaw Forward to Backward {F>B}), 65 , 0 (Backward to Forward {B>F}), 37 - 0 (F>B), 80 (Full Sun when Beta >66)

MPS mode(s)	Operations Comments
Switch V/T 6 to V/T 5 by OBC when System C/D = 1.00	Early-orbit/Instrument activation and calibration were priorities. Power Subsystem set-up for 1600 Watt load, actual S/C load ~1350 Watts. No SA offset. High Peak charge current and battery overcharge. NOMINAL PERFORMANCE

II. Post Max Beta #1 (1/92-4/92)

Beta: 80, 0 (B>F), 39, 0(F>B), 63, 0 (B>F),

MPS mode(s)	Operations Comments
V/T 6 to V/T 5 by OBC when System C/D = 1.00	After return to S/C eclipses, onset of Differential Voltage observed, 10-20 mV on all 3 Batteries (Figure 4). Onset of ANOMALOUS PERFORMANCE
Switch to straight V/T charging: V/T6 V/T5, finally V/T4	Began increased battery performance monitoring and investigations. Battery temperature rose and delta temperature increased in V/T6 (Figure 5). Switched to V/T5 until Beta >60 degrees, then switched to V/T4 to decrease both battery temperatures and delta temperature, and reduce overcharge during low DOD period.

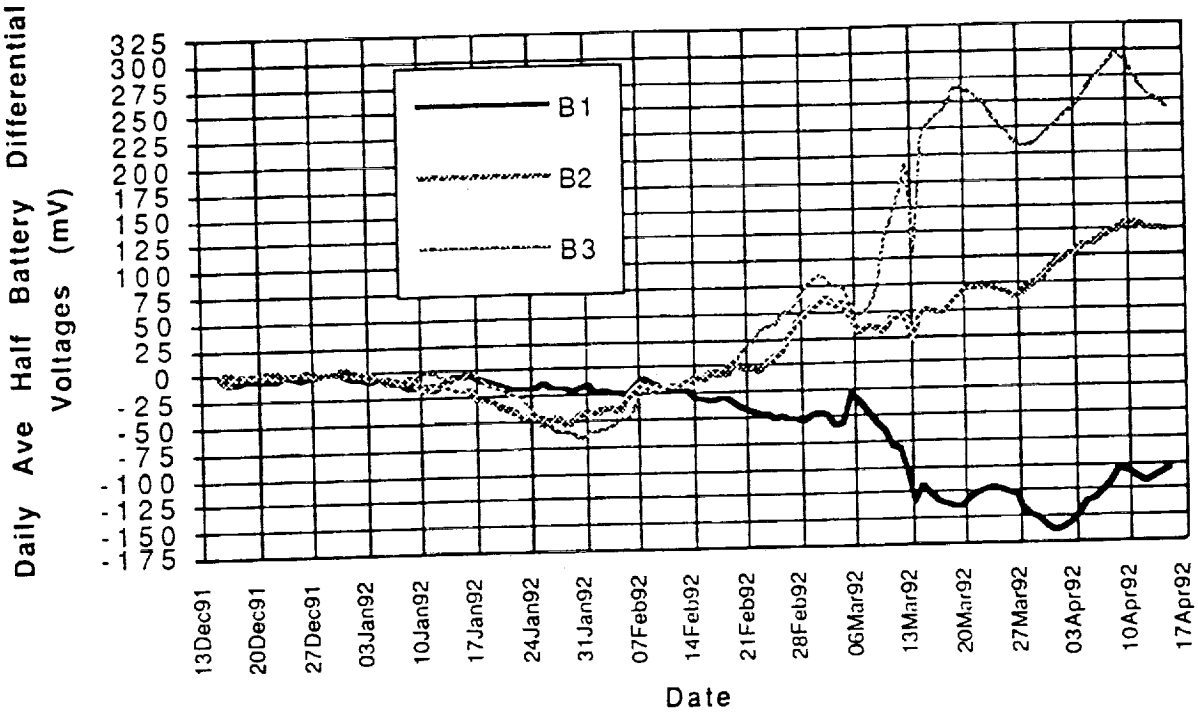

Figure 4. Half Battery Differential Voltage: 15 December 91 - 15 April 92

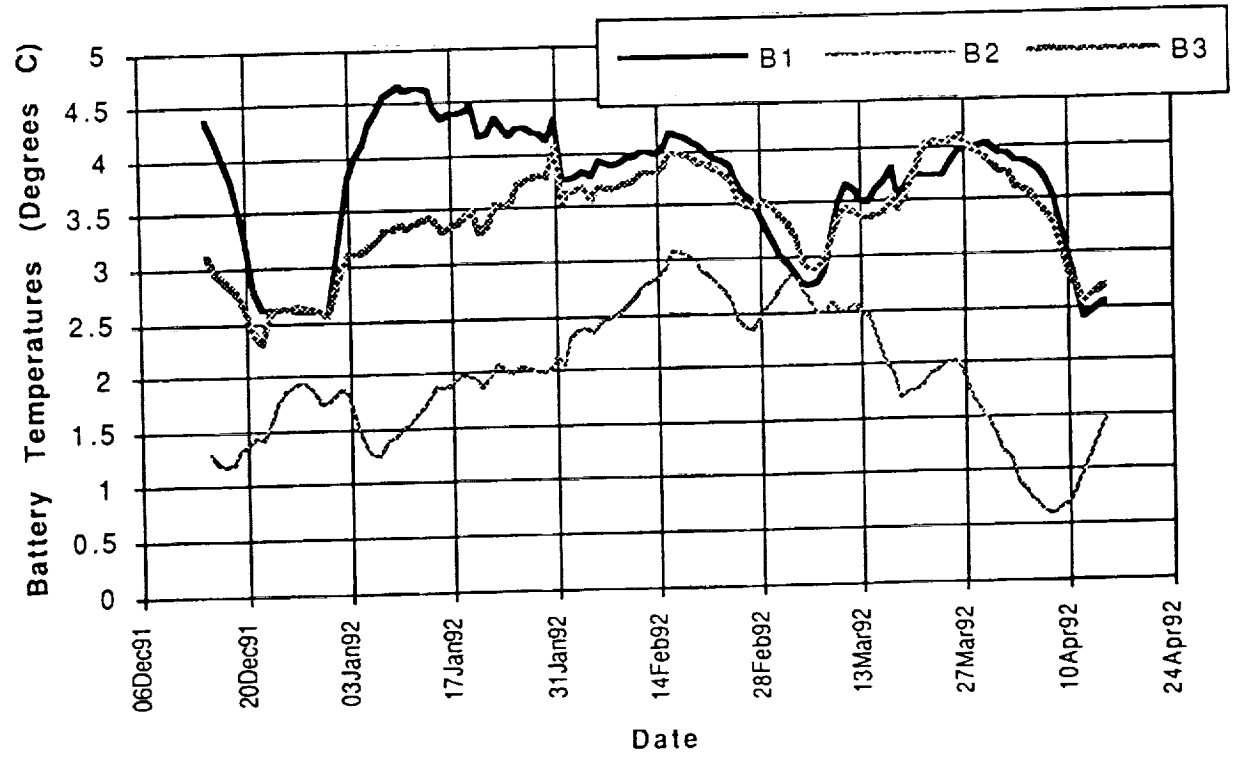

Figure 5. Battery Temperatures :15 December 91 - 15 April 92

III. Through next relative max Beta, low DOD (4/92-5/92)
Beta: , ~65, 0 (F>B), 37,

MPS mode(s)	Operations Comments
V/T4, V/T5, and then back to V/T4	V/T4 at higher Beta angles, switched to V/T5 after increasing the load, but battery temperature rose and delta temperature diverged dramatically, switched back to V/T4 and battery temperature and delta temperature decreased, however still operating with higher delta temperature. Began TMON control of MPS heater thermostat with little to no effect on delta temperature.
V/T4	After next relative max Beta (37 deg), began SA Offset ~35 deg ahead, controlled manually. Reduced peak charge current per battery from 33 A to ~20-25 A. Still no effect on differential voltage, battery temperature or delta temperature.

IV. SA Drive Anomaly (6/92-7/92)
Beta: , 0 (B>F), 80, 0 (F>B),

MPS mode(s)	Operations Comments
V/T4	SA "parked" at S/C Noon. Minimum S/C Load (2 of 10 instruments on) – max DOD 18-20%. S/C nights vary from 54 min to 10 min over Beta cycle with the SA stopped.
V/T4	Reduced charge capability during full sun reduces overcharge during Max Beta. Higher effective load and decreased charge rates. Observed first beneficial battery operations and improved performance during this period. Differential Voltages, delta temperatures and C/Ds decrease.

v. SA Restarted, next Relative max Beta (7/92-8/92)
Beta:, 38, 0 (B>F), 65,

MPS mode(s)	Operations Comments
V/T4	SA rotation restarted with 45 degree offset ahead of Sun. Attempted to maintain improved characteristics. Changed TMON set points for MPS heater activation to maintain low delta temperature. Differential Voltages and delta temperatures increased.

VI. Next Rel Max Beta (9/92-10/92)
Beta:, 0 (F>B), 64, 0 (B>F),

MPS mode(s)	Operations Comments
V/T4	SA offset increased to further limit peak charge current and to decrease heat generation on charge. Decreased time in taper. No effect on delta temperatures. EON Voltage reached new low (26.4V). Consequently, achieved a Power negative condition during relative maximum Beta. Increased DOD, "exercised" batteries during normally low DOD period. Reduced overcharge and delta temperature. As Beta angle decreased and load increased, low EON LBV (<26 V) and increased delta temperature became major concerns. Decreasing SA Offset resulted in poor current sharing. Could not switch to V/T5 due to high delta temperature experienced at V/T5 in 4/92.

VII. EON LBV continues to decrease (11/92)
Beta:, 39, 0 (F>B),

MPS mode(s)	Operations Comments
V/T4	Differential Voltage curves change character, considered a change but not certain if this indicates improvement or further degradation. By Inhibiting the warmest/weakest battery (#1) from controlling the V/T feedback loop, EON voltage was raised. Battery 3 (next warmest battery) controls/delays V/T switch to taper (effective V/T=4.2+), increased charge without increasing peak charge current. Consequently, battery temperatures rose.
V/T4	At maximum S/C loading, could not provide required EON Voltages. Used other than normal MPS configuration to maitain EON LBV above 26.8V when DOD>18%. Load sharing improved slightly with inhibited Battery 1 V/T feedback loop (Figure 6).

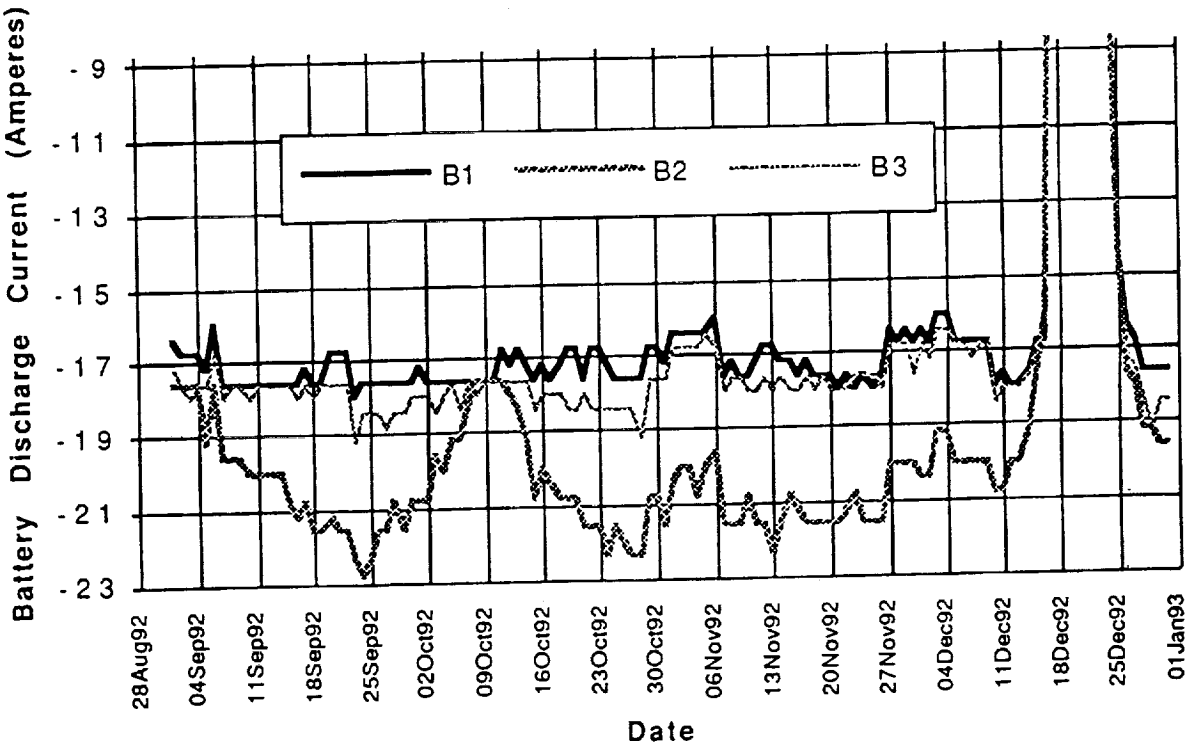

Figure 6. Battery Load Sharing: September - December 92

VIII. Max Beta #3, Deep DOD Conditioning #1 (12/92)
Beta:, 80,

MPS mode(s)	Operations Comments
V/T4, then V/T3 when DOD<10%	Battery 1 differential voltage range surpassed battery 3's. Decreased battery overcharge and increased DOD during low load period.
V/T3/CCM 0.75A	Performed first low earth orbit battery conditioning to boost EON Voltage - Deep DOD (target 35%) conditioning without reconditioning circuitry. Used Full-Sun period 12/12-12/25 when recharge opportunities are the greatest. Increased S/C load to maximum (slow discharge rates ~5-9 Amps), increased SA Offset to achieve a negative energy balance, and took the best performer (battery 2) off the charge bus to force it to discharge through the diode which allowed batteries 1 & 3 to get deeper DODs. Also used Constant Current Mode of 0.75 A to limit charge during Albedo Charge periods.
V/T3	When battery 2 reached 32% DOD; began Peak Power Tracking and decreased SA offset to allow system to be power positive. Put battery 2 back on charge bus when all three battery voltages were approximately the same. Maximum DODs were: Battery 3=34.0%, Battery 1=31.5%, and Battery 2=32%. Voltages increased approximately 1.5 volts per battery (see Figure 7), however, battery discharge sharing remained unchanged (Figure 8).
V/T3	Exercised the batteries when normal DOD<10%. Increased SA Offset to make subsystem power negative and achieve a DOD between 12-18% at least once every other day.
V/T4	When DOD>10%, resumed normal operations. Loaded New PMON Software to autonomously control SA Offset. Three SA Control modes: (1). Select Offset Angle and PMON maintains it, (2). Select Desired Total Peak Charge Current and PMON calculates and commands required SA Offset once per orbit, and (3). Retain Manual Control by rate variation (same as before).

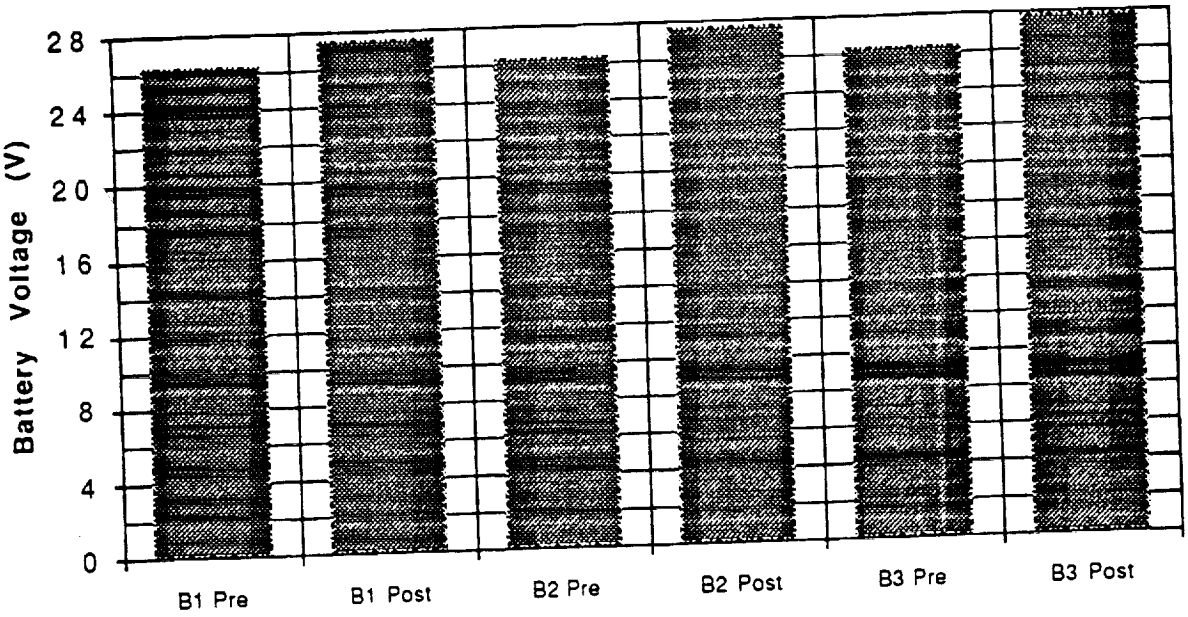

Figure 7. Battery Voltages Pre and Post Conditioning (December 92)

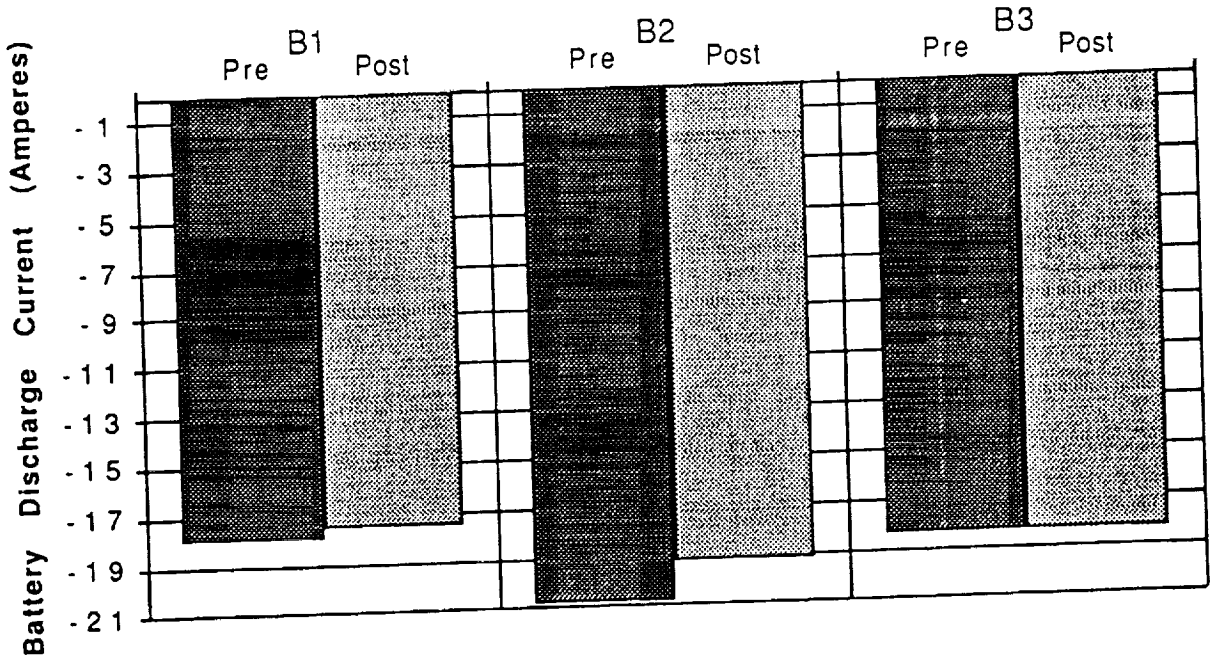

Figure 8. Battery Discharge Currents Pre and Post Conditioning (December 92)

IX. Post Max Beta #3, and next Zero Beta (1/93-2/93)
Beta:, 0 (B>F), 38, 0 (F>B),

MPS mode(s)	Operations Comments
V/T4 & V/T4.2+	Battery delta temperatures and current sharing diverged. Inhibited battery 1 from V/T feedback to increase charge without increasing peak charge currents and boost EON Voltages. Used V/T4 when delta temperatures increase. Also decreased MPS heaters on period with TMONs. Battery temperatures and delta temperature remained unchanged.
V/T4 & V/T4.2+	At Zero Beta (Maximum load) turned off redundant S/C equipment (1 Transponder and 1 Star Tracker) and damaged instruments to reduce load and maintain EON LBV above 24.8V. Further evidence of weak battery performance.

X. Next 2 Relative max Betas (3/93-4/93)
Beta:, 64, 0 (B>F), 64, 0 (F>B),

MPS mode(s)	Operations Comments
V/T4 & V/T4.2+	Battery temperatures and charge/discharge current sharing continued to diverge. MPS battery heaters on at S/C sunrise by stored commands to better control peak charge heating, and also decreased peak charge current and decreased overcharge, but no real effect on temperatures and current sharing.
V/T3	At relative maximum Beta angles, when DOD<10%, cycled SA Offset to achieve 12-18% DOD at least once every other day and exercised batteries. Tested New PMON software allowing a switch from V/T control to CCM based on a selected battery 1 C/D goal. Achieved greater control of battery overcharge. Also utilized SA Offset control to select peak charge current.

XI. Relative Max Beta (5/93)
Beta:, 39, 0 (B>F),

MPS mode(s)	Operations Comments
V/T4	Load decreased due to ISAMS decreased operation, 7 of 10 instruments fully operational. Still observing significant delta temperatures and poor charge/discharge current sharing.
V/T4 to CCM (0.75 A) at selected Battery 1 C/D goal.	Results of decreased overcharge lead to implementation of V/T control to CCM switching upon reaching Battery 1 C/D goal as the operational mode. Continued improvement in charge acceptance, load sharing (Figure 9), and battery delta temperatures (Figure 10).

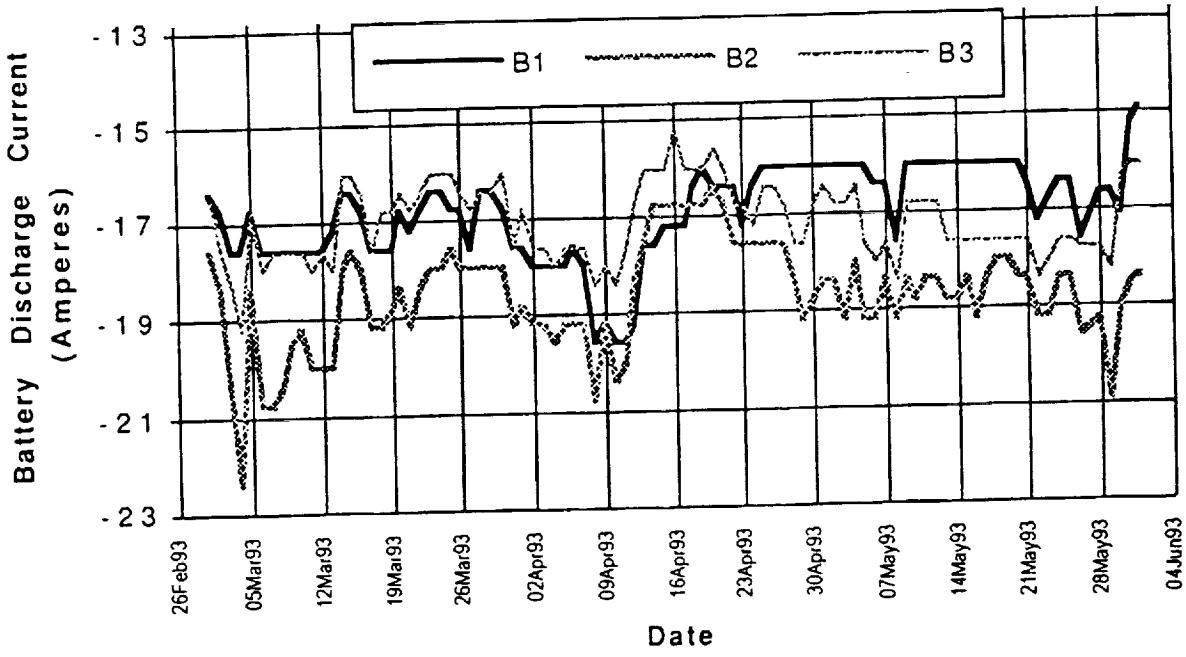

Figure 9. Battery Load Sharing from March - May 93

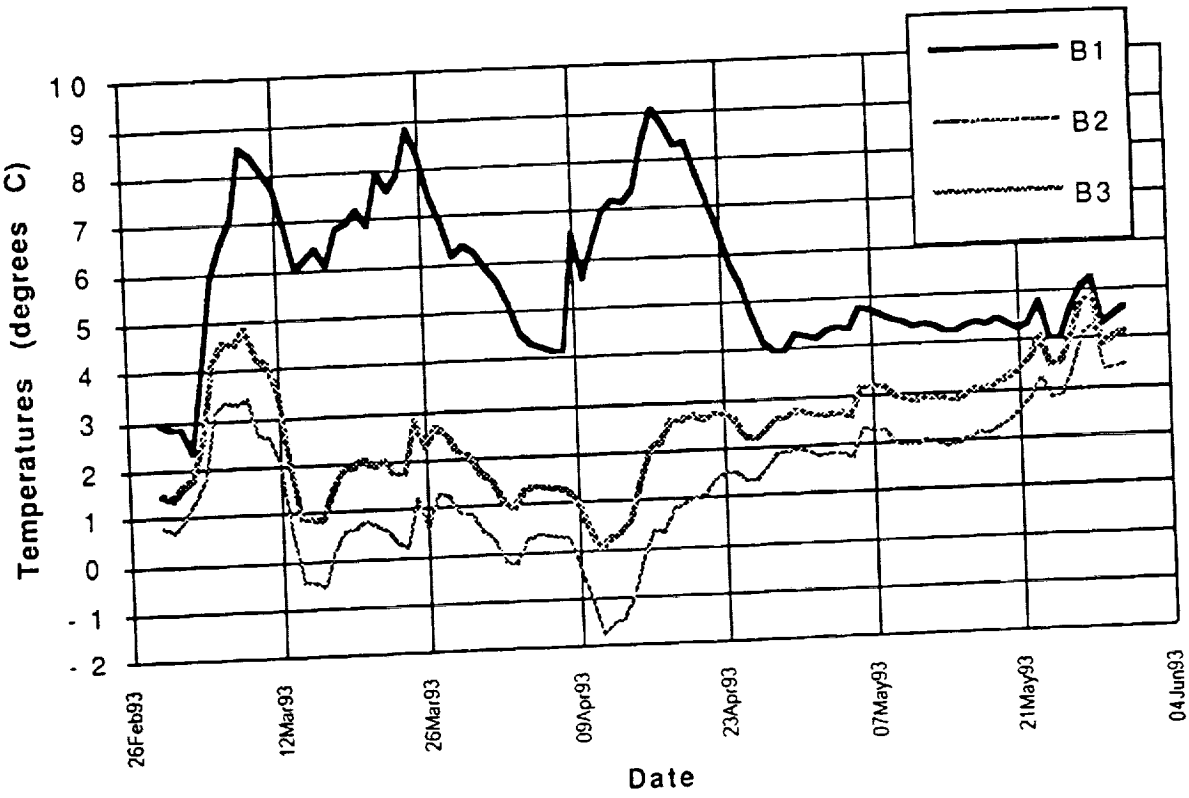

Figure 10. Battery Temperatures from March - May 93

XII. Max Beta #4, Deep, Discharge Conditioning #2 (6/93)
Beta:, 80 (Full Sun, Min DOD, 6/15-6/18),

MPS mode(s)	Operations Comments
V/T3	When DOD<10%, exercised batteries, by cycling SA Offset to achieve 12-18% DOD at least once per day. Decreased overcharge and increased load during low DOD/load period.
V/T3 & CCM 0.75A & V/T1 & CCM 1.5A & V/T3	Deep DOD Conditioning #2: Performed 2 conditioning discharges - one each on consecutive Full-sun days, to achieve the full benefit of the deep discharges based on the ground test results of Zimmerman and Effa(6). **DAY ONE** - Deep Discharge (40% target, discharge rates ~5-9 amps) and Slow Recharge (Increased SA Offset), Battery 2 off the charge bus, and extra heater loads to decrease Albedo charging. When Battery 3=36% DOD (B1=33%, B2=31.5%), decreased SA Offset, Commanded V/T1 at CCM 1.5 A until all 3 battery voltages were same, then put Battery 2 back on the charge bus and switched to straight V/T3 recharge back to 100% SOC. **DAY TWO** - Repeated Day One with all three batteries on charge bus. When Battery 2=40% DOD (B3=38.5%, B1=34.5%) decreased SA Offset, commanded straight V/T3 recharge to 100%. No net EON Voltage gain (Figure 11), however, battery discharge sharing improved (see Figure 12 below).
V/T3 & V/T4	Continued to limit overcharge and to exercise batteries until DOD>10% by cycling SA Offset to achieve 12-18% DOD at least once every other day. Switched to V/T4 when DOD>10%, SA Cycling ceased

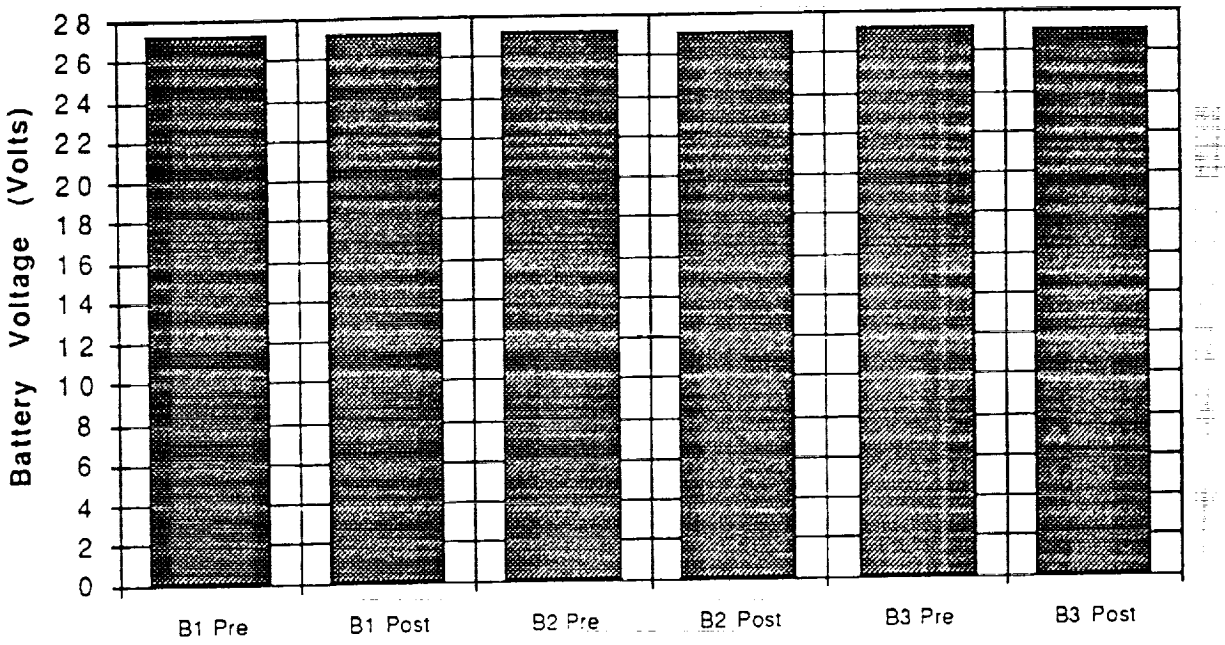

Figure 11. Battery Voltages Pre and Post June 93 Conditioning

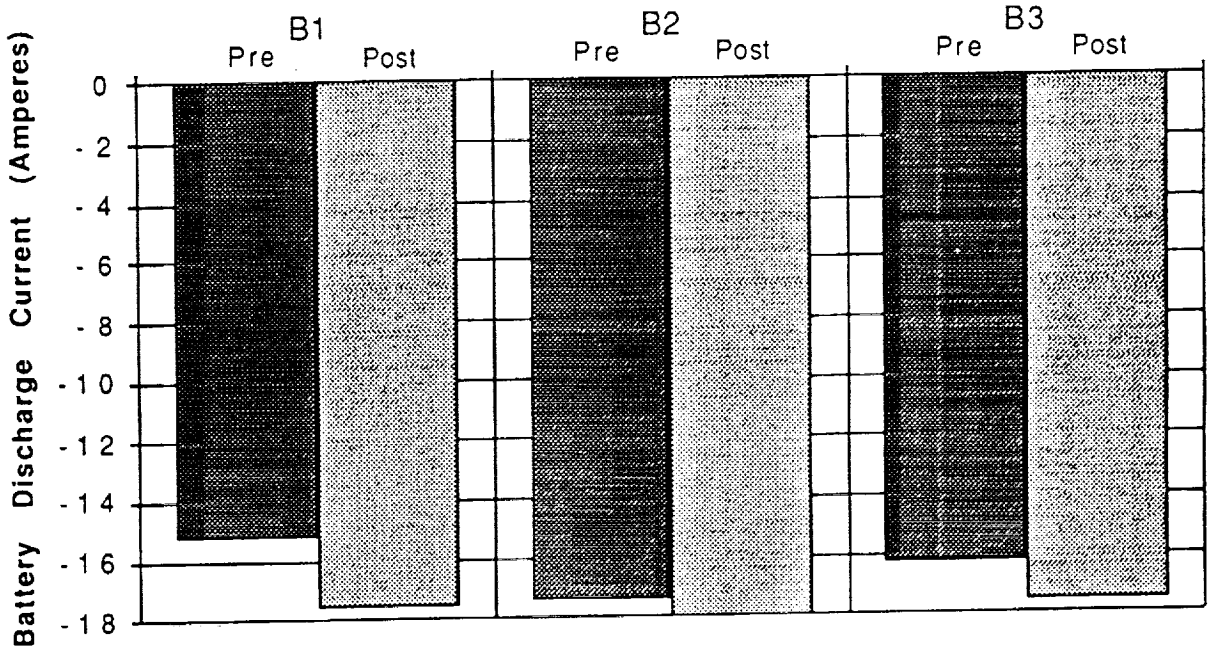

Figure 12. Battery Discharge Current Pre and Post Conditioning June 93

XIII. Post Max Beta #4, Next 2 relative Max Betas (7/93-8/93)
Beta: 0 (F>B), 37, 0 (B>F), 66

MPS mode(s)	Operations Comments
V/T4 and CCM (0.75A)	Battery charge and discharge current sharing continued to improve. Battery delta temperatures decreased. Battery performance improved. Continued to utilize switching from V/T4 to CCM based on selected C/D of battery 1 (maintained Battery 1 C/D between 1.04 and 1.05).
V/T4 and CCM (0.75A)	SA Anomaly - SA parked at S/C Noon from 4 to 8 August led to minimum Instrument Load (2 of 10 on) and a change in battery charge regime due to fixed SA.
V/T4 and CCM (0.75A)	SA restarted with Offset after Yaw around, utilized SA Offset to control peak charge currents. No change in battery performance.

XIV. Next Relative Max Beta: September 93 SA Anomaly to Present (9/93-Present)
Beta: 0 (F>B), 62, 0 (B>F)

MPS mode(s)	Operations Comments
V/T4 and CCM (0.75A)	SA Anomaly - SA parked at S/C noon 9/17-9/21, leads to minimum Instrument Load (4 of 10 on). SA-control TMONS developed and loaded to S/C. SA restarted with SA Offset 9/21. Little change to battery performance.
V/T4 and CCM (0.75A), Straight V/T4, V/T5 & V/T5 and CCM (0.75A)	SA stopped to investigate "jumping ahead" SA motion 10/2-10/25. However, now kept 5 of 10 instruments on with parked SA due to improved battery performance and S/C load management. Switched to V/T5 as load increased and Beta decreased without battery thermal runaway. Differential Voltage pegged (>+728mV) during SA testing (>65 min SA night, EON LBV=24.2V @ 28% DOD).
V/T5 and CCM (0.75A)	SA restarted with Offset after Yaw around. Battery performance continues to improve.

Figure 13 shows the EON LBV from December 1992 (the first deep discharge attempt) though October 26, 1993. It is annotated with significant events effecting the EON LBV and all YAW maneuvers. Yaw maneuvers usually represent the highest DOD for any particular Beta cycle. Figure 14 is a plot of the Minimum EON Voltage for the mission to date. C/D ratios, and Half Battery Differential Voltages over the mission are represented in Figures 15, and 16 respectively. Battery load sharing and Battery Temperatures since launch are presented in Figures 17 and 18.

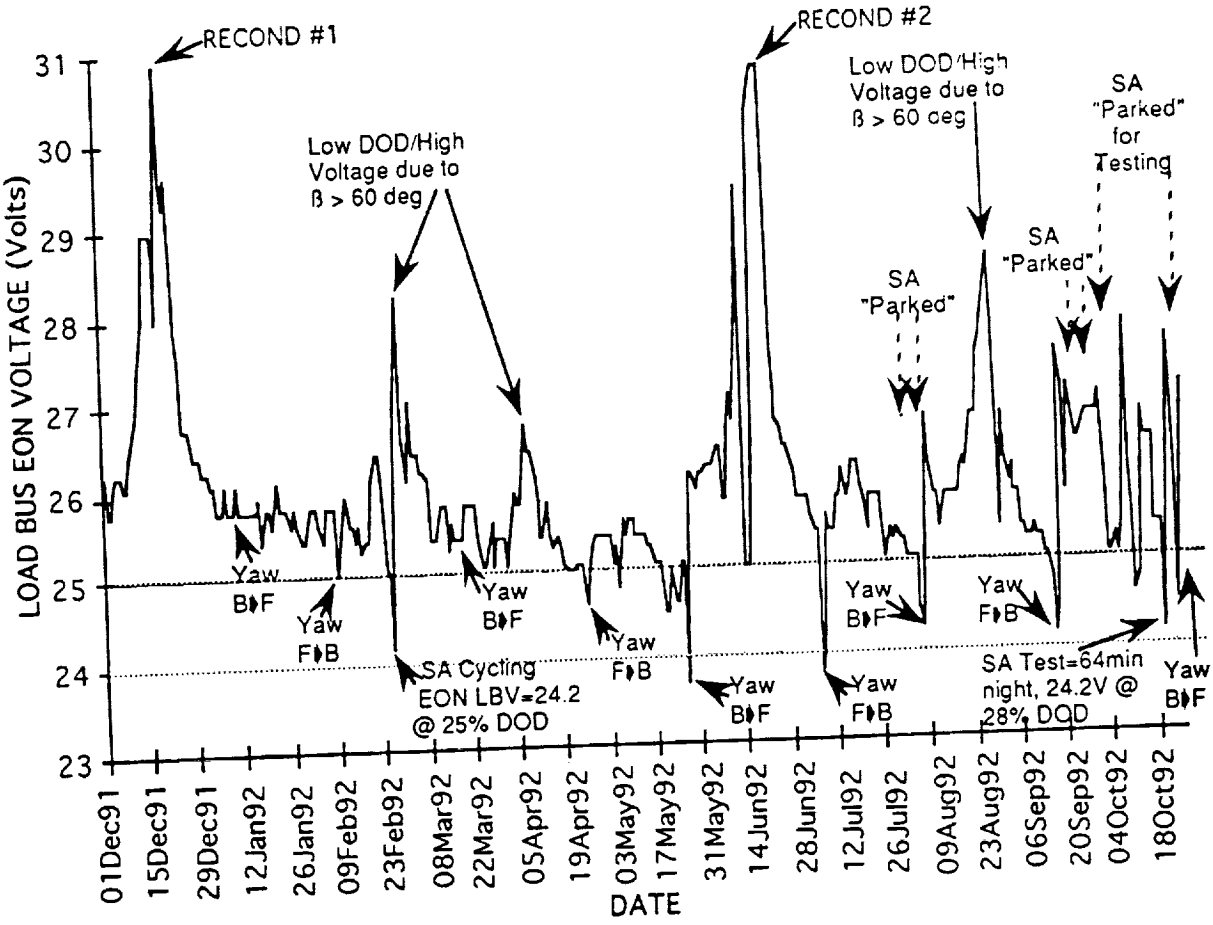

Figure 13. Daily Minimum EON LBV, 1 Dec 92 - 26 Oct 93

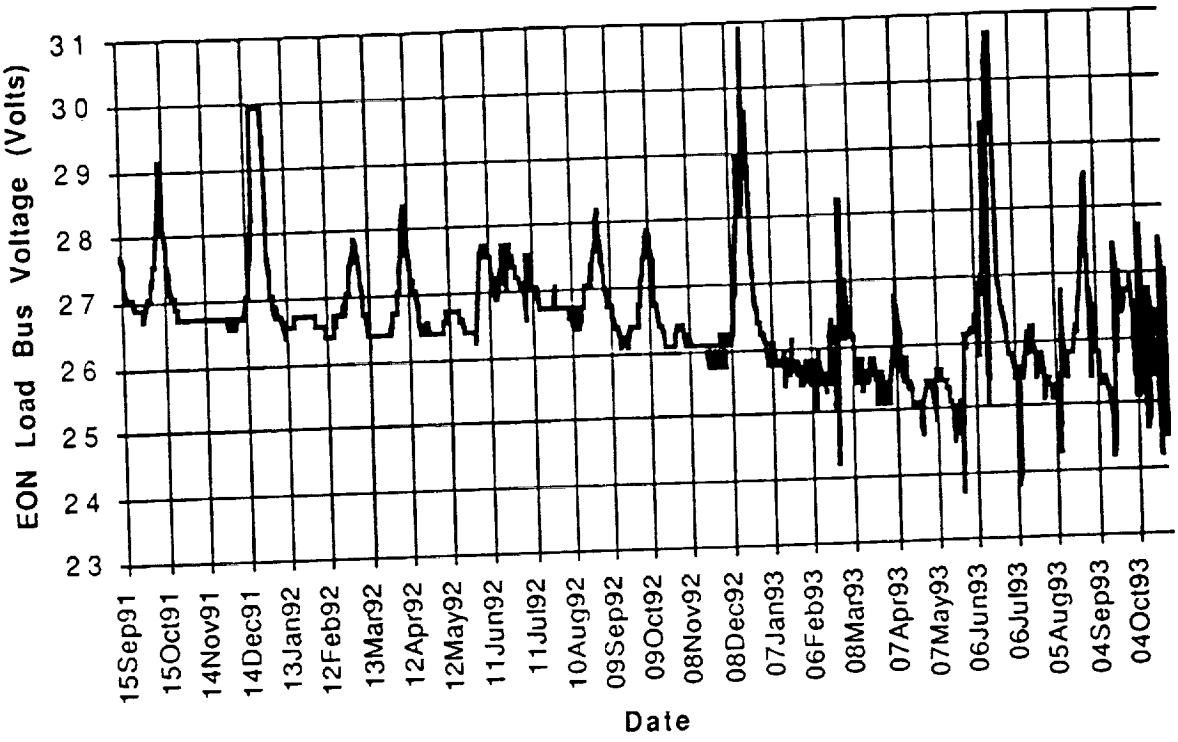

Figure 14. EON Load Bus Voltage

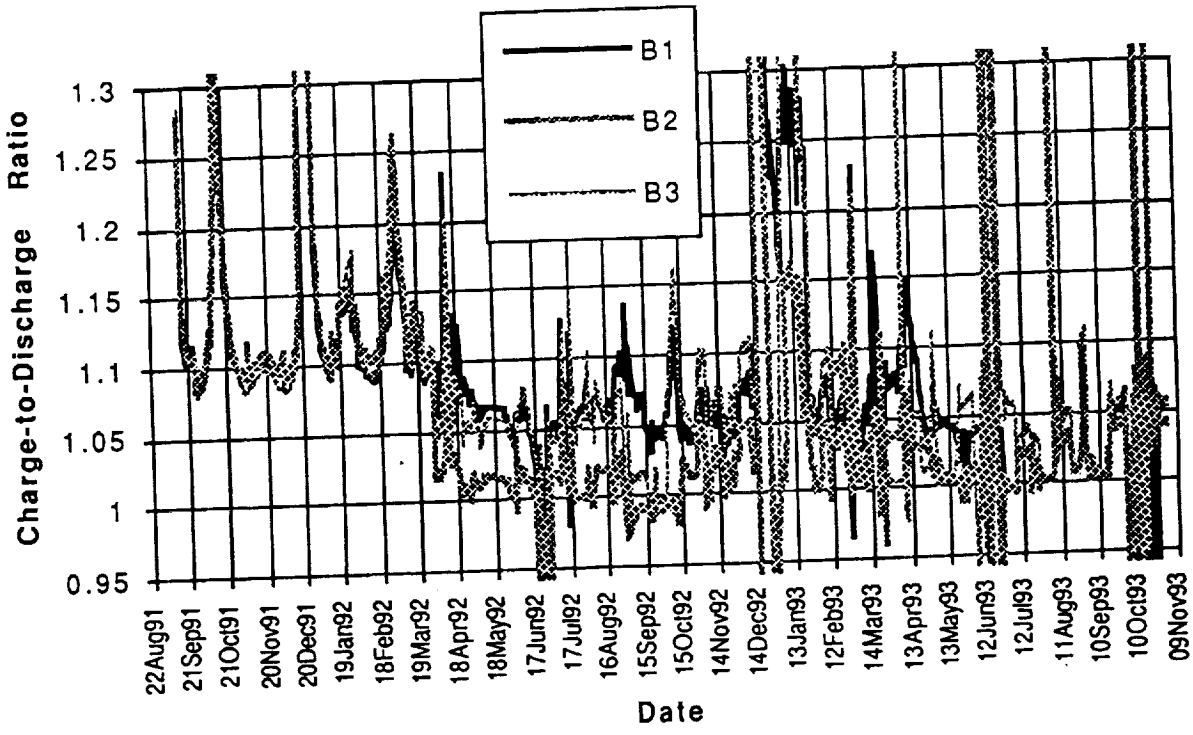

Figure 15. Battery C/D Ratio

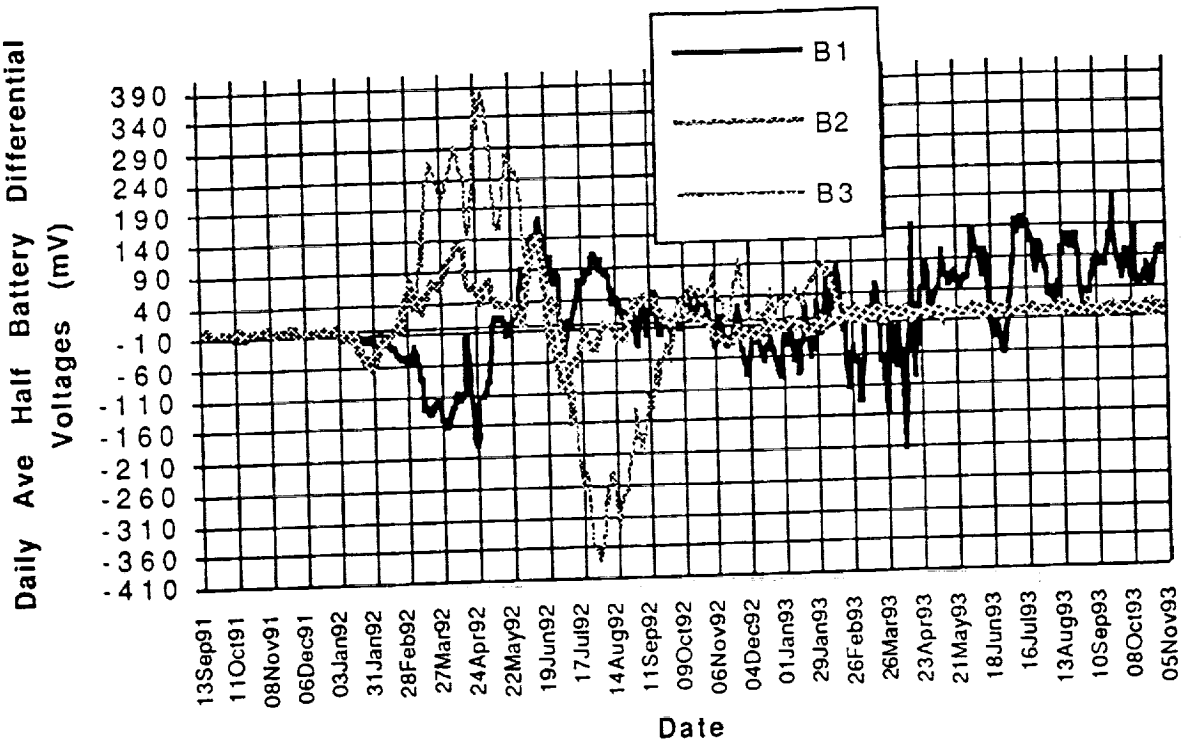

Figure 16. Average Half Battery Differential Voltage

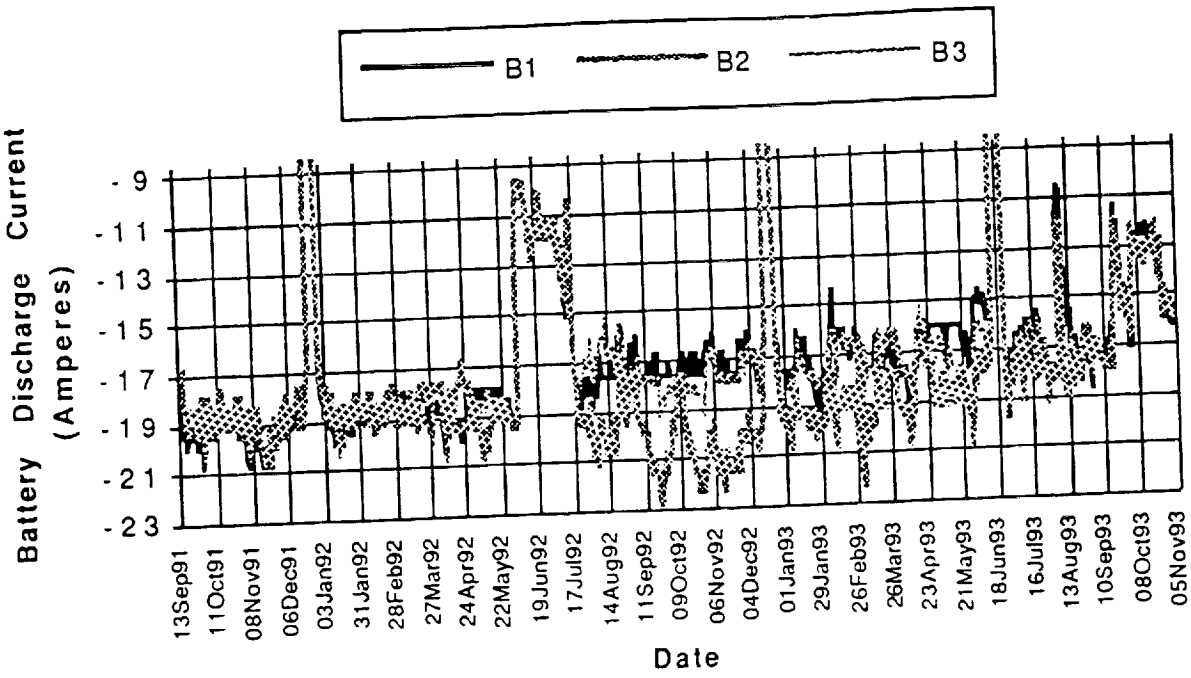

Figure 17. Daily Average Battery Load Sharing

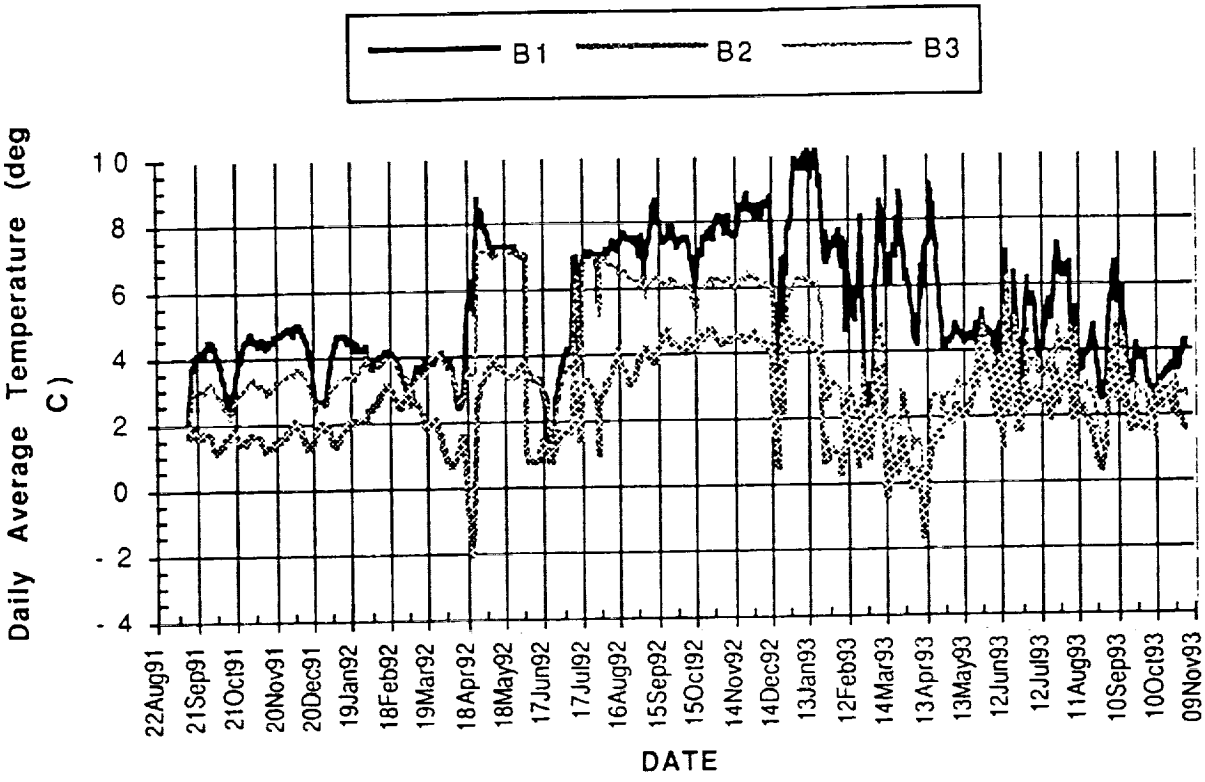

Figure 18. Daily Average Battery Temperatures

Thus, better current sharing; lower recharge ratio, differential voltage, and delta temperature; and fairly stable EON voltage indicate improved battery performance over the past several months. These trends began when overcharge was limited by switching from VT control mode to CCM based on the selected battery 1 C/D ratio.

Conclusions

Anomalous battery performance was first observed in January 1992. During this early mission period, the onset of Half Battery Differential Voltage excursions were considered a problem. However, Half Battery Differential Voltage changes do not tell us whether those changes are an effect of just one or of many cells. As a result, Half Battery Differential Voltages are used as a "first warning" or an indicator of battery degradation. Other battery characteristics and performance parameters must be monitored for additional information. These parameters are used to manage battery performance.

Because the batteries are in parallel in the MPS design (Figure 1), the effective operation of the MPS relies heavily upon having batteries that are well matched. The UARS batteries, although well matched at mission start, have operated with delta temperatures since launch. Temperature differences between batteries along with the battery temperatures have served as good indicators of relative battery performance.

Battery charge and discharge current sharing have both shed light on the battery performance puzzle. Charge and Discharge current sharing go hand-in-hand with battery temperatures in pointing to both the most efficient and the weakest performing batteries. For example, Battery #1 has had the greatest Half Battery Differential Voltage range and the highest temperature. It has also accepted the most charge current while providing the least discharge current, and is hence considered the weakest performer.

In addition, the weakest performer has been the battery receiving the greatest overcharge. Battery and MPS operations during the early part of the mission -- charging at V/T 6 to a system C/D=1.00 and then switching to V/T 5 with taper, probably contributed to battery overcharge.

Aggressive management of overcharge has been the underlying operation leading to improvements and relative stabilization of battery behavior. Battery temperatures, delta temperatures, and current sharing during charge and discharge have all trended back to more nominal behavior.

Battery exercise certainly helps to limit overcharge during low load (high beta angle/minimum S/C night) periods. Cycling the SA Offset to achieve a power negative condition and allowing the batteries to "spiral down" in SOC for several orbits, exercises the batteries during those low load periods when DODs of only 6-10% are expected. The result is a DOD of 12-18% at least once per day over a week when low loads are the norm. In addition, this battery exercise may minimize the so called "memory effects" which are common for NiCd batteries[6].

Deep Discharges have been performed during the bi-annual Full-Sun periods to minimize overcharge and to attempt to improve battery performance. UARS utilizes these very low load (~1-6% DOD) intervals to condition the batteries through low rate, deep discharges up to 40% DOD and followed by low rate recharge. This operation has been added to our operational list in an effort to maintain and possibly boost EON LBV.

Even though these batteries have met the minimum mission requirements, we contend that the amount of "care and feeding" they have required has been considerably greater than was originally anticipated. One of the biggest obstacles the FOT has had to overcome in operating the UARS power subsystem is both the limited number and selection of telemetry points available to trend. Individual cell voltage monitors, more accurately calibrated current sensors, and the addition of battery temperature sensors on and around each battery would indicate early anomalous behavior and overcharge conditions, and would certainly have helped in managing the battery operations as discussed above.

Recognizing that the case for Low-Earth Orbit Battery Reconditioning is still being debated, we have found deep conditioning discharges and periodic battery exercise during low load periods to be beneficial. To aid these operations, it would be useful to have "reconditioning" circuitry available in the S/C Power Subsystem. Deep Discharge is only possible on UARS during the periods of Full-Sun (almost full orbit opportunities to charge batteries) that the S/C experiences bi-annually.

Several additional MPS features that would have been advantageous in conducting the operations outlined above are:

- Independent charge controller for each battery.
- Single commands for each V/T level/MPS charge mode selection.
- Greater thermal control over the MPS.
  - Incorporation of the heat pipe used successfully on other S/C.
  - Additional MPS/Battery heaters and /or heater control.

and

- Incorporation of a charge system based on controlling overcharge.
  - Switching MPS modes at a specific C/D, etc.

NASA is currently implementing some of these features in GSFC's up-coming low-Earth orbiting S/C's Power Subsystem designs.

Finally, the success of the UARS mission and the power subsystem in particular has been directly affected by the successful management of the MPS and the batteries. Anomalous battery performance and its resultant effects have been aggressively attacked through monitoring and managing the following parameters:

Monitor:

- Voltage (EON/EOD/Instantaneous),
- Current Sharing during Charge and Discharge (High and Low currents)
- Half Battery Differential Voltage,
- SOC, and
- Eclipse Time (Beta Angle),

Manage:

- Battery Overcharge,
- Temperature,
- Recharge ratio,
- DOD,
- Time in peak Power Tracking,
- Time in Taper,
- Solar Array Offset (Peak Charge Current),
- V/T control mode, and
- Constant Current Mode.

It is our fervent hope that the Trials, Tribulations, and Successes experienced by the UARS Power Subsystem Operations Group, which includes the UARS GSFC Project Staff, GSFC's Space Power Applications Branch, the UARS FOT, UARS Mission Planning Group/Space Systems Applications Incorporated (SSAI), and MDESC can aid future Power Subsystem Designers and Operators by documenting the problems encountered, solutions stumbled across, and of course the planned, successful operations performed during UARS mission operation to date.

Acknowledgments

The authors wish to sincerely thank all of the extremely professional and expert NASA, Martin Marietta, MDESC, and SSAI employees involved with the UARS MPS and battery operations for their efforts over the design and operational lifetimes of this project. Without their hard work and steadfast dedication, the UARS Project would truly not be what it is today.

Special Thanks to:

NASA/GSFC, Space Power Applications Branch:
Dr. John Day
Marlon Enciso
Jim Jagielski
Dave Jung
Ernie Rodriguez

NASA/GSFC, UARS-Project:
Ken Dolan
John Donley
Sam Osler
Dave Lorenz

Martin Marietta-UARS FOT
Hal Collins
Gene Pearlman
Nick Chilelli
Erik Larson
Rich Calvin
Rich Beck
All On-line Operations Team Members

McDonnell Douglas Electronic Systems Company
Mark Toft
Mo Zollner
Bob Green

Space Systems Applications Incorporated:
Dan Wise
Bob Neff
Barb Holt
Ravi Bahethi
Kim McCarty

References

1. NASA Goddard Space Flight Center Code 408, "Multimission Modular Spacecraft (MMS) Modular Power Subsystem (MPS) Battery Storage And Operating Procedures", Rev B, NASA GSFC, Greenbelt MD, Document # 408-2101-0002, pp. 4-1 to 7-11, February 1980.

2. NASA Goddard Space Flight Center Code 430, "UARS General Instrument Interface Specification (GIIS)", Rev C, NASA GSFC, Greenbelt MD, Document# 430-1601-002, pp. 3-4 to 3-6, February 1985.

3. Toft M., "NASA Standard 50 Ah Nickel Cadmium Battery Cell – Cell Level Performance History", NASA Aerospace Battery Workshop, Huntsville Alabama, NASA Conference Publication # 3140, pp. 343-378, 1991.

4. NASA Goddard Space Flight Center "GSFC Specification of Manufacturing of Aerospace Nickel Cadmium Storage Cells", NASA GSFC, Greenbelt MD, January 1974.

5. NASA Goddard Space Flight Center Code 408, "GSFC Specification For The NASA Standard 20-Ah Spacecraft Battery and the 50 Ah Spacecraft Battery", Rev B, NASA GSFC, Greenbelt MD, Document # S-7111-16, pp. 3-1 through 3-16, September 1980.

6. Zimmerman, A.H. and Effa, P.K., "Nickel-Cadmium Cell Performance Recovery and Reconditioning", Chemistry and Physics Laboratory Operations, The Aerospace Corporation, El Segundo, CA, for Space Division Air Force Systems Command, Los Angeles CA, Report SD-TR-82-63, September 1982.

7. Vasanth, K.L., "Second Plateau Voltage in Nickel Cadmium Cells", NASA/GSFC, Battery Workshop Proceedings, Greenbelt, MD, NASA Conference Publication # 2331, pp. 223-239, 1983.

8. NASA Goddard Space Flight Center Code 430, "GSFC Specification For The Upper Atmosphere Research Satellite (UARS) Observatory", Rev A, NASA GSFC, Greenbelt MD, Document # 430-1101-001, pp 3-14, June 1986.

Performance Test Results Of ETS-VI Ni-Cd Cells

1993 NASA Aerospace Battery Workshop
November 16-18, 1993

K.Nakatani, Y.Yano, S.Kuwajima* and H.Kusawake*
Sanyo Electric Co.,Ltd.
*National Space Development Agency of Japan

SANYO

Background

- Development of 35Ah Ni–Cd cell for ETS–VI was initiated in 1986.
- Cell production of ETS–VI/FM : 1991 to 1992
  - 1st lot : delivered 66 cells to battery manufacturer (MELCO)
  - 2nd lot : delivered 83 cells to battery manufacturer
- ETS–VI uses 4 batteries
  - Each battery consists of 2 packs.
  - 16 series cells per pack
- ETS–VI will be scheduled for launch in 1994.
- ETS–VI/FM Batteries are now storaged at low temperature.
- Same designed cells were delivered to NASA Lewis Research Center for evaluation in this year.

SANYO

Development Schedule

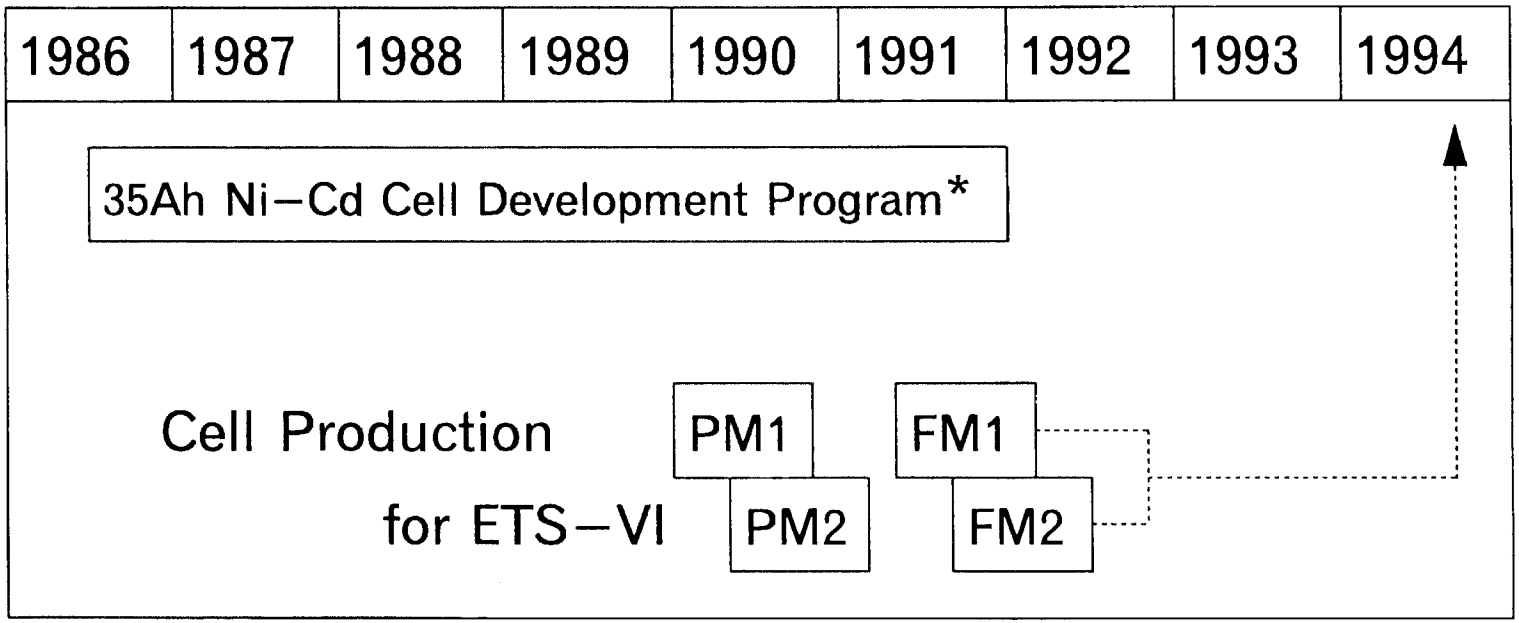

*Life tests are now continued in NASDA.

PM:Prototype Model Cell FM:Flight Model Cell

SANYO

Main Specification

- Model Name : N35S
- Dimension : 107 ^{W} × 25 ^{T} × 127 ^{H} mm
- Weight : max. 1050g
- Nominal Capacity : 35Ah
- Energy Density : 40Wh/kg
- Design Life : 10years in GEO

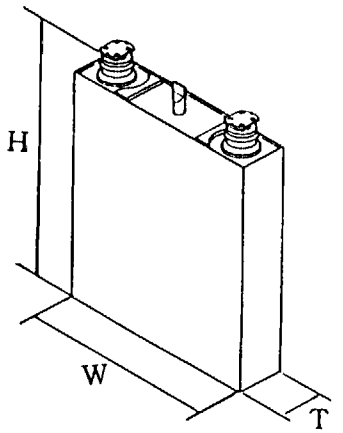

- Electric Performance

Charge Condition	Charge Volt.	Internal Pressure	Capacity *
0.1C x 24hrs. 20 °C	max. 1.50V	max. 3.5kg/cm^2	min. 35.0Ah
0.1C x 24hrs. 35 °C	max. 1.45V	max. 3.5kg/cm^2	min. 32.0Ah
0.05Cx48hrs. −5 °C	max. 1.55V	max. 3.5kg/cm^2	min. 32.0Ah

* Discharge 0.5C

SANYO

Cell Design

	Positive	Negative
Substrate Porosity	Sinter Ni / 85%	Sinter Ni / 86%
Impregnation	Chemical Impreg.	Chemical Impreg.
Additives	Co and Cd	Non
Number of Plate	13	14
Plate Dimension	104 x 100mm	104 x 100mm
Plate Thickness	0.63mm	0.80mm
Loading Level	2.4g/cc−void	3.0g/cc−void
Plate Capacity	42.6Ah	69.7Ah
Capacity Ratio	1.64	
Separator	Nylon Nonwoven Cloth	
Electrolyte	31%KOH 98g	
Design Weight	1040g	
Design Capacity	38.7Ah	

SANYO

Production Flow

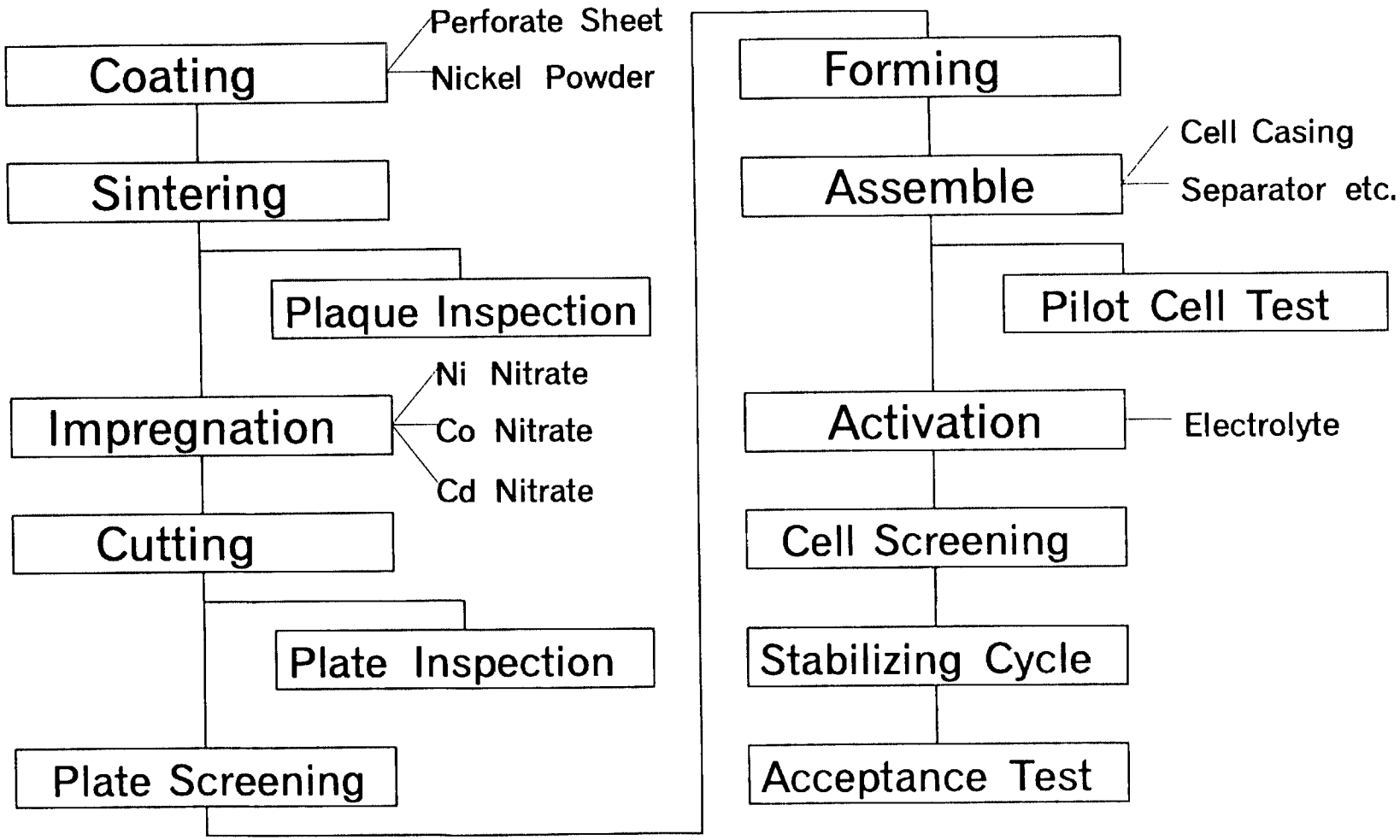

SANYO

Acceptance Test (1)

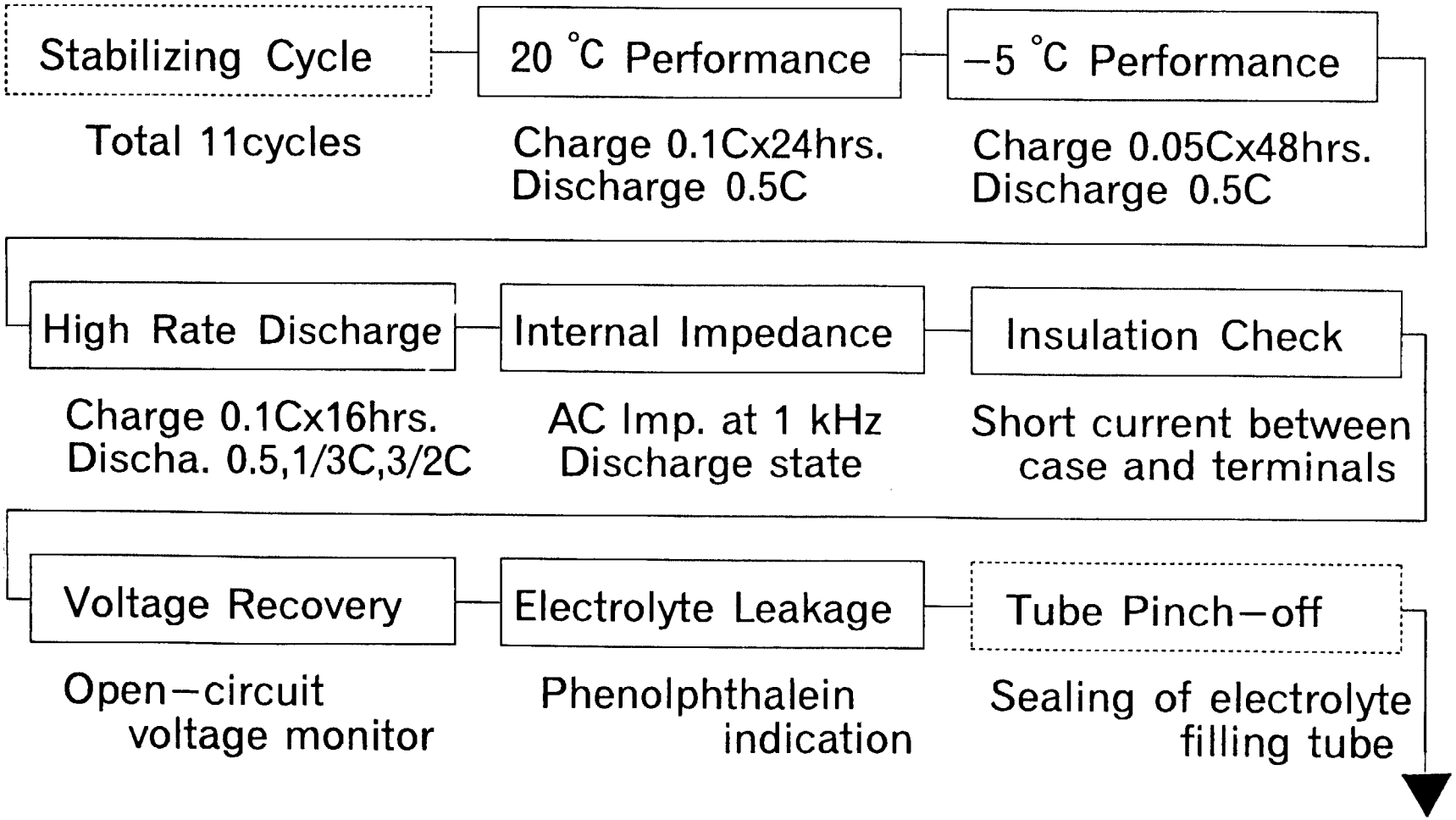

SANYO

Acceptance Test (2)

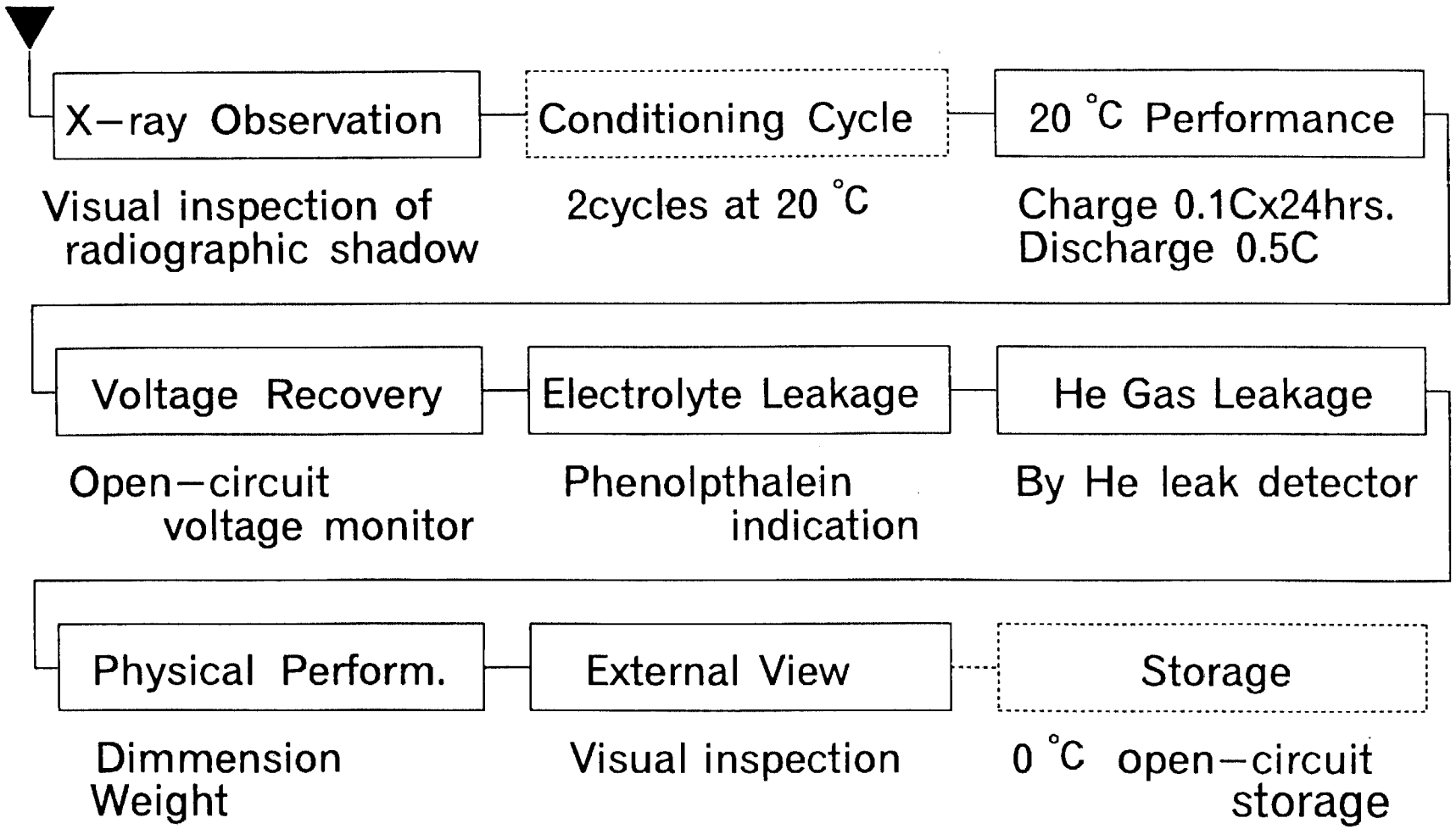

SANYO

Cell Weight

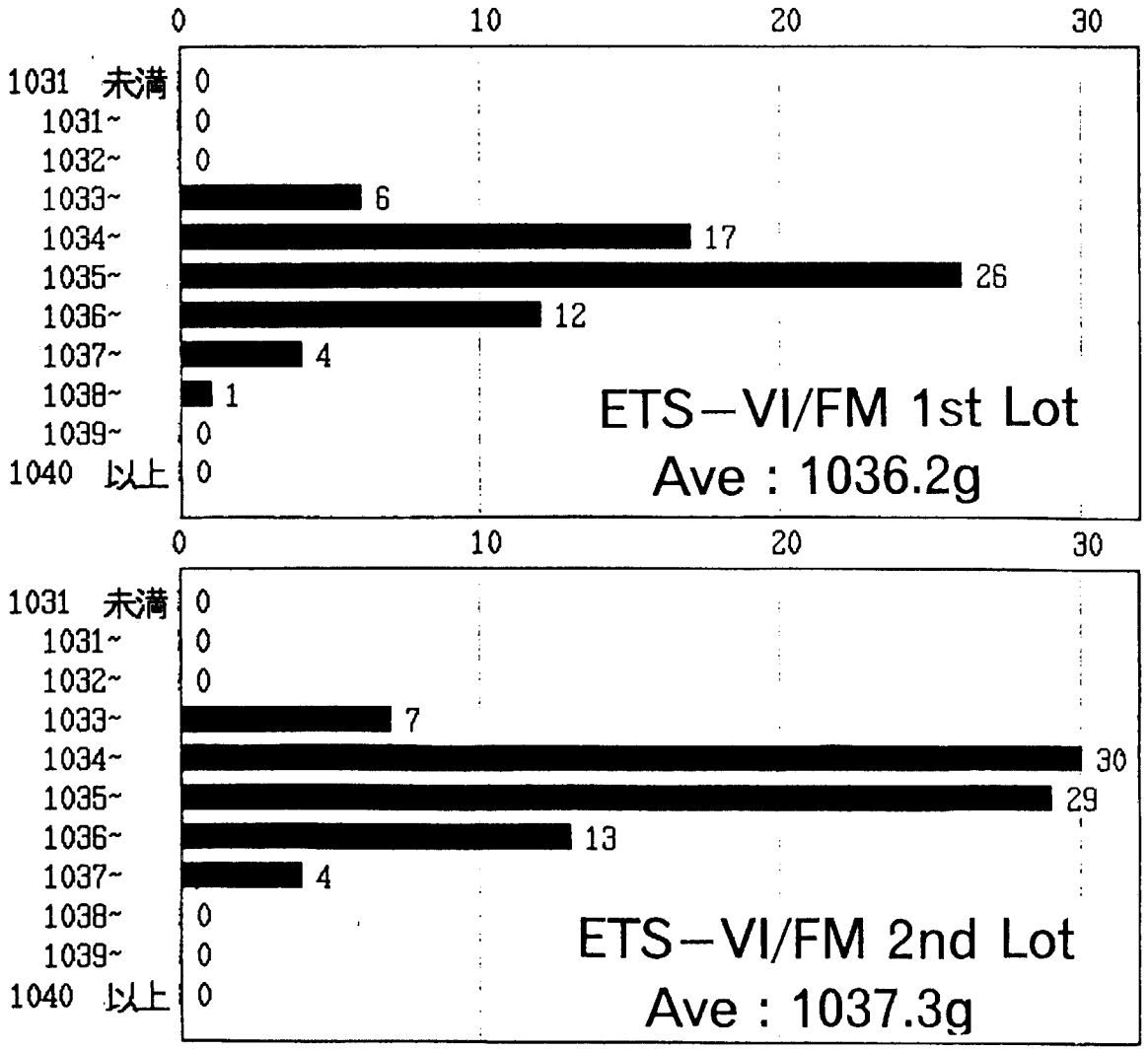

SANYO

20 °C Performance

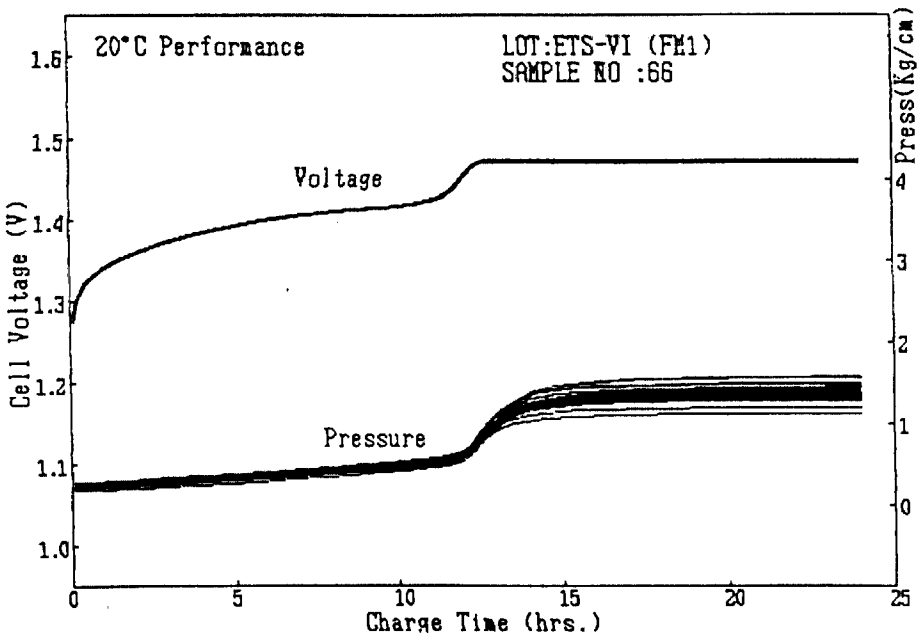

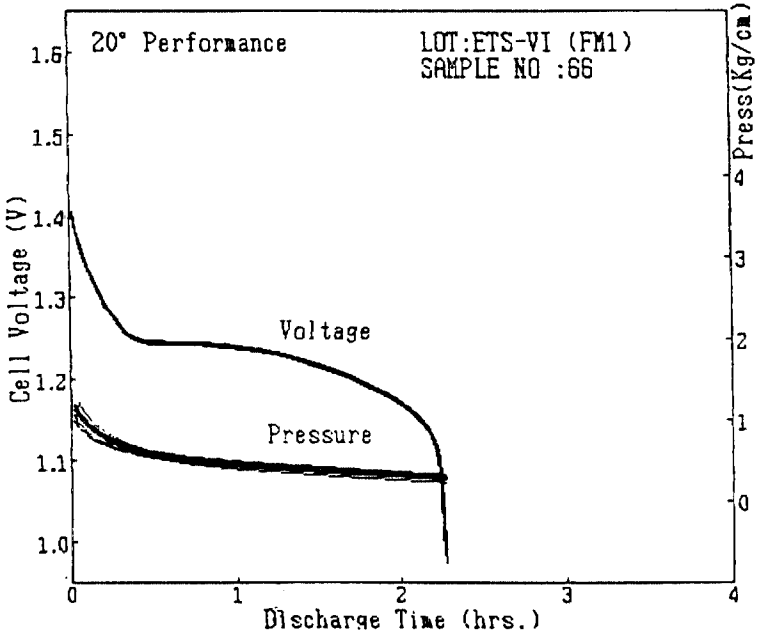

Charge 3.5A x 24hrs. Discharge 17.5A Temp. 20 °C

Overplot of 66 Data of ETS−VI/FM 1st Lot

SANYO

20 ℃ Performance

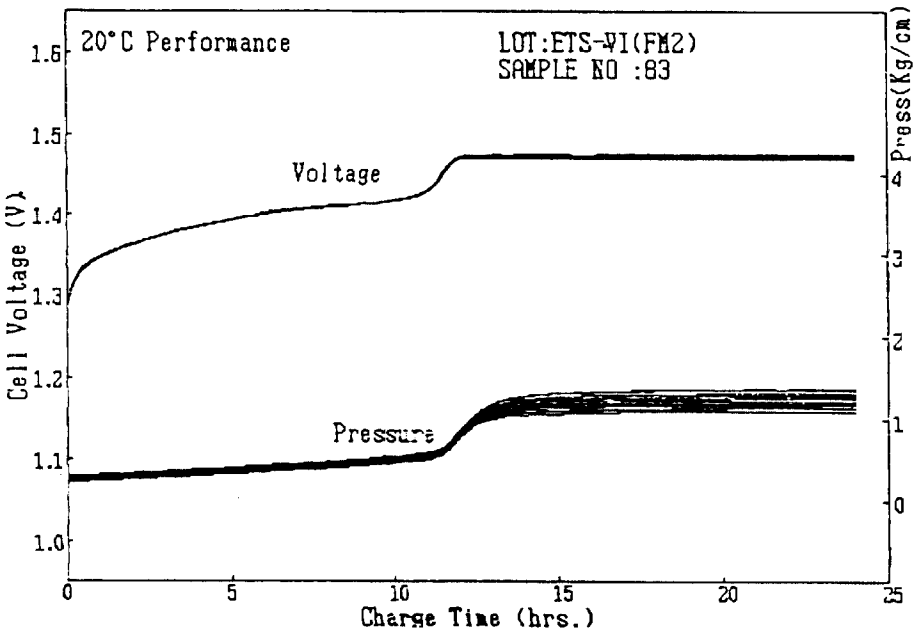

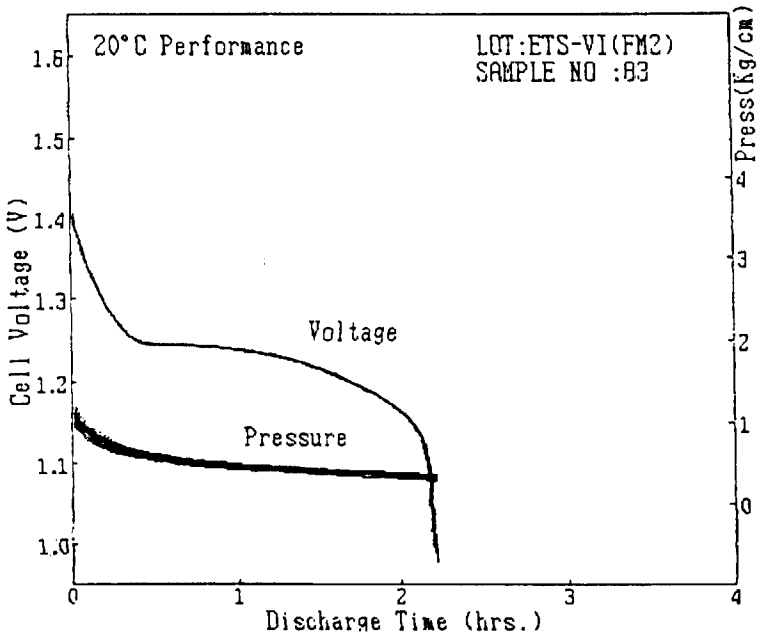

Charge 3.5A x 24hrs. Discharge 17.5A Temp. 20 ℃

Overplot of 83 Data of ETS−VI/FM 2nd Lot

SANYO

Capacity

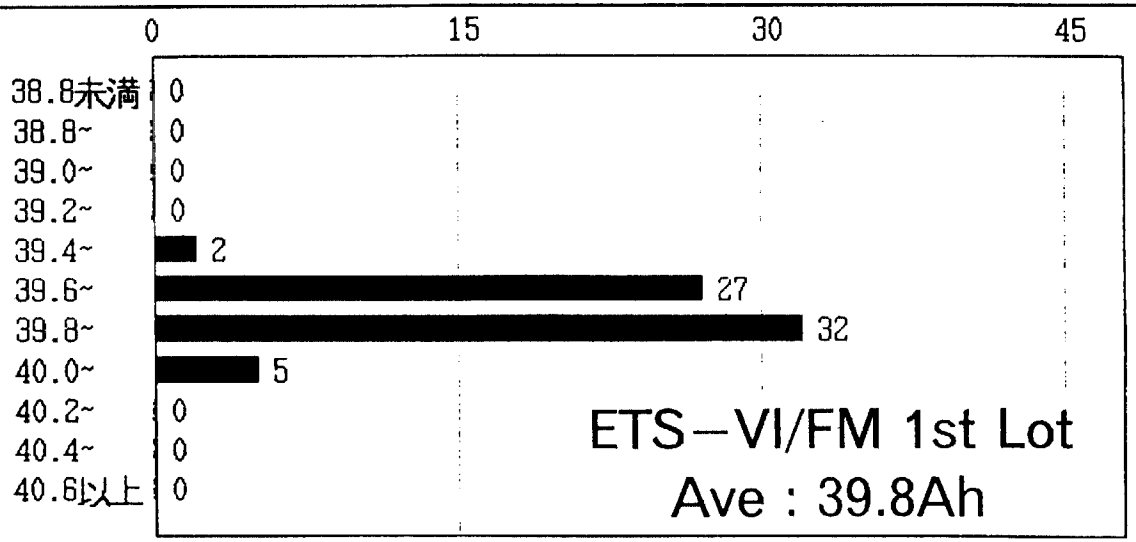

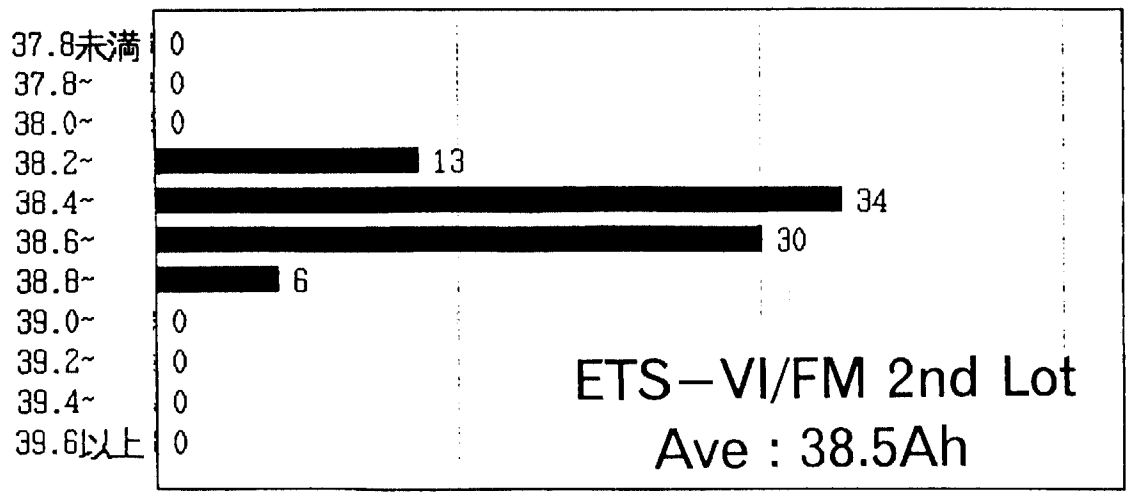

Charge 3.5A x 24hrs. at 20 ℃ Discharge 17.5A

SANYO

Overcharge Pressure

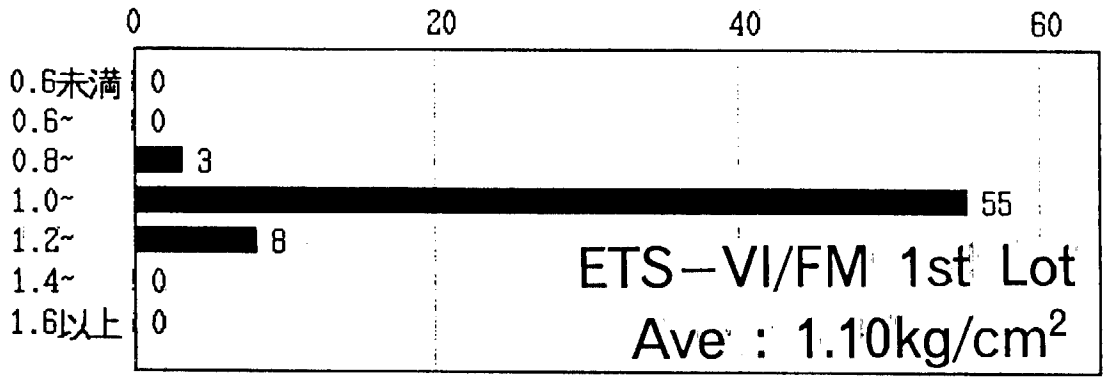

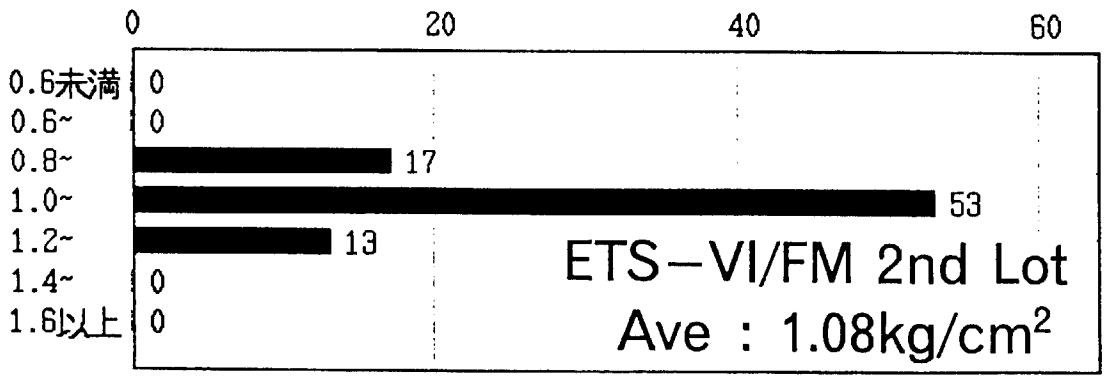

Charge 3.5A x 24hrs. at 20 ℃

SANYO

End of Charge Voltage

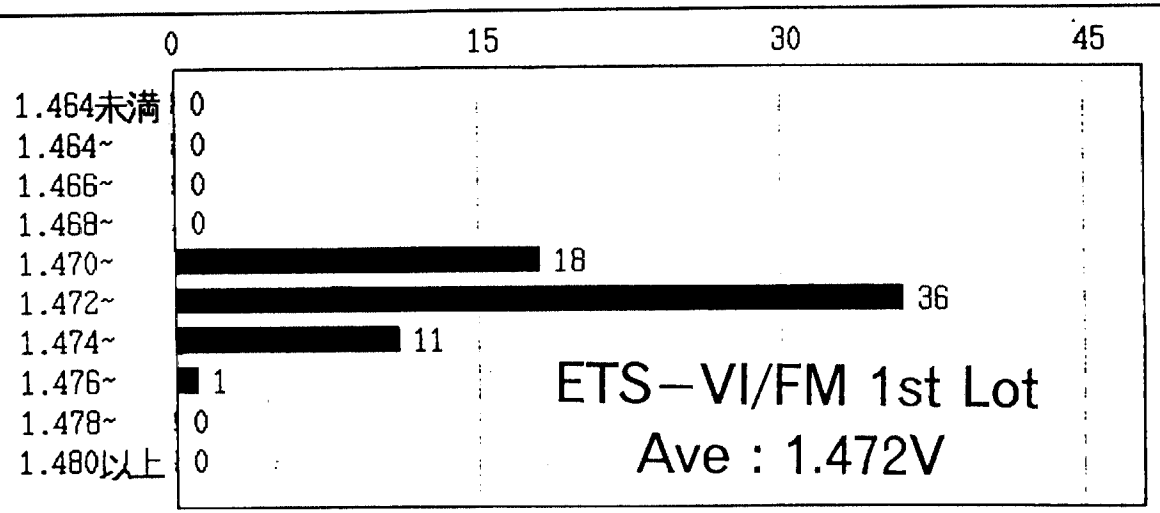

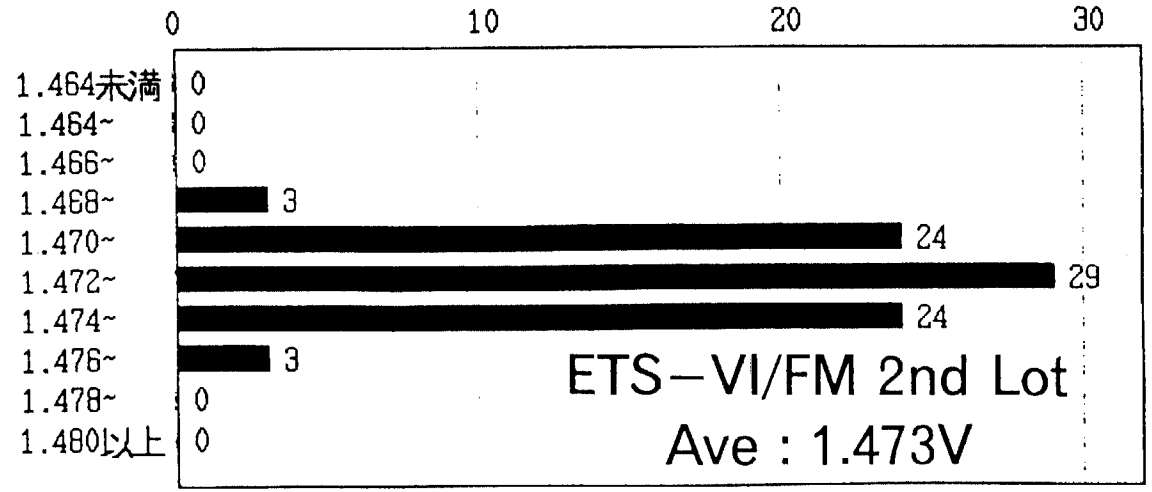

Charge 3.5A x 24hrs. at 20 ℃

SANYO

−5 °C Performance

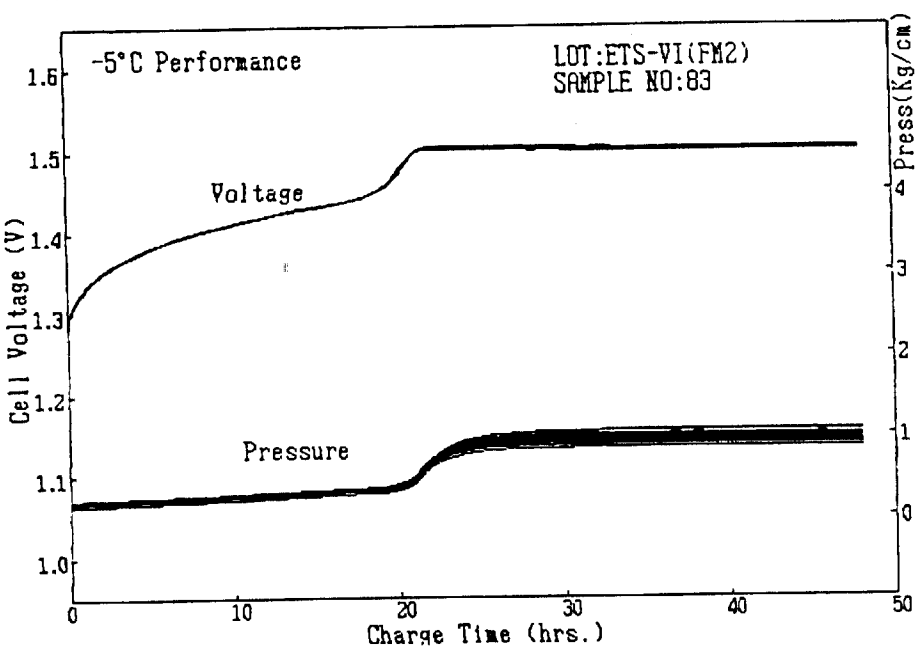

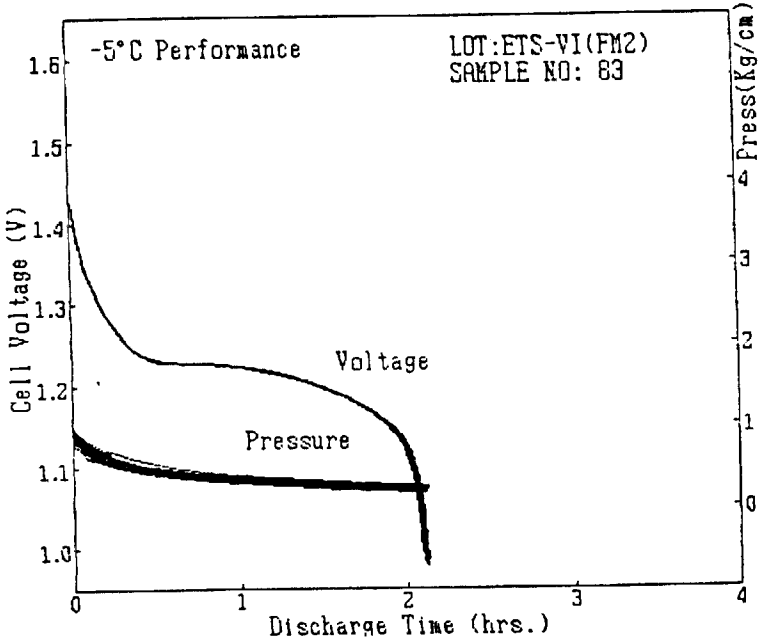

Charge 1.75A x 48hrs. Discharge 17.5A Temp.−5 °C

Overplot of 83 Data of ETS−VI/FM 2nd Lot

SANYO

−5 °C Performance

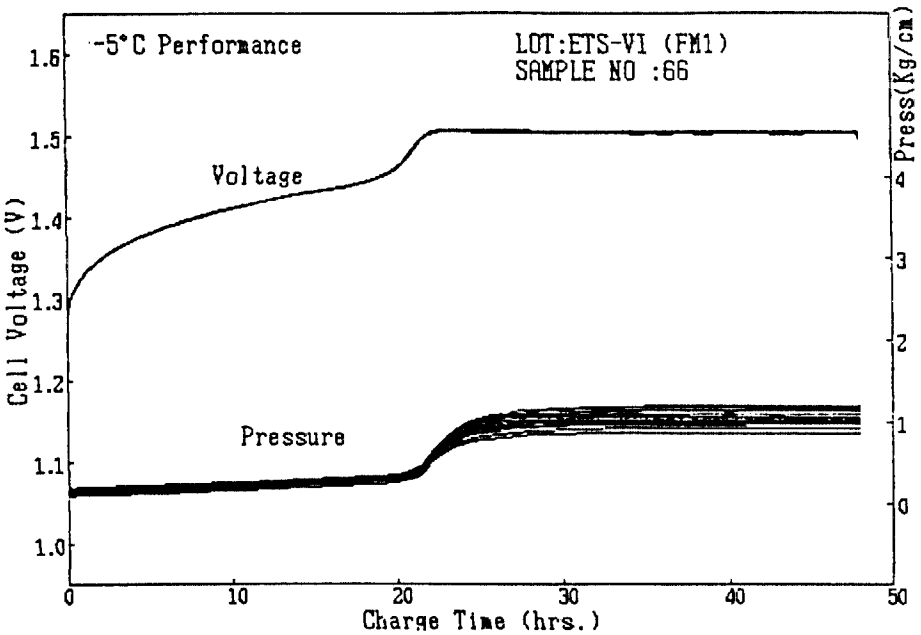

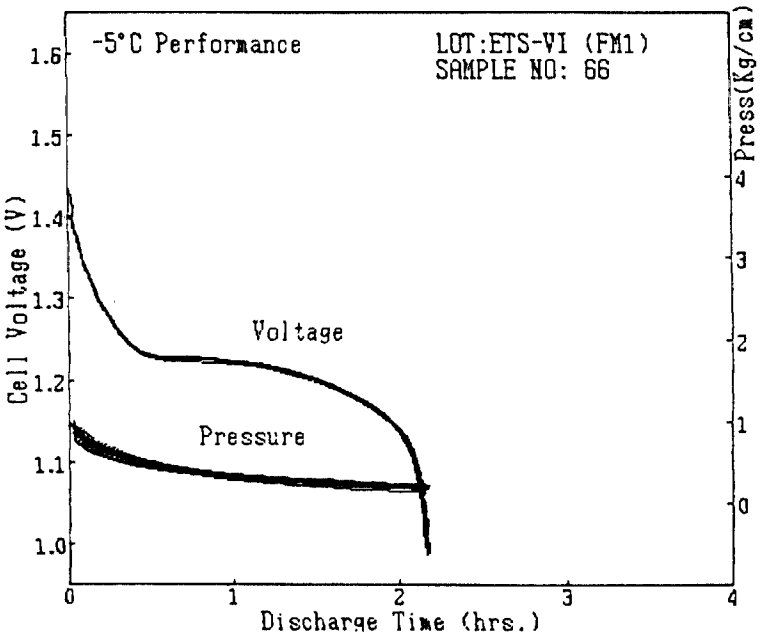

Charge 1.75A x 48hrs. Discharge 17.5A Temp.−5 °C

Overplot of 66 Data of ETS−VI/FM 1st Lot

SANYO

ETS-VI Simulation Cycle Test

Sample :

8cells of PM 2nd lot / electrolyte filling in Nov. 1990

Test fascilities :

in NASDA Tsukuba Space Center

Test Status :

Started in Feb. 1991

Continued in 834cycles of 19th season on Nov.1, 1993

Testing Data Summary :

EOCV about 1.45V/cell

8 cells-sample battery has never reached CV mode.

Reconditioning capacities are about 41AH from 5th to 18th season.

SANYO

ETS-VI Simulation Cycle Test

Test conditions : from 5th season

Repeat 44cycles

- Charge : (CC 1.5A + CV 12.5V/8cells) x 14hrs.
- Trickle Charge : 0.5A x 8.8hrs.*
- Discharge : 14.6A x 1.2hrs. (DOD 50%)
- Temperature : 10 ℃ **

Reconditioning

- Discharge : 0.66A until any cell falls to 1.0V
- Recovery Charge : (CC1.5A+CV12.5V/8cells) x 35hrs.

*Not applied from 4th to 5th season

**Temperature of 20 ℃ was applied from 1st to 4th season.

SANYO

ETS-VI Simulation Cycle Test

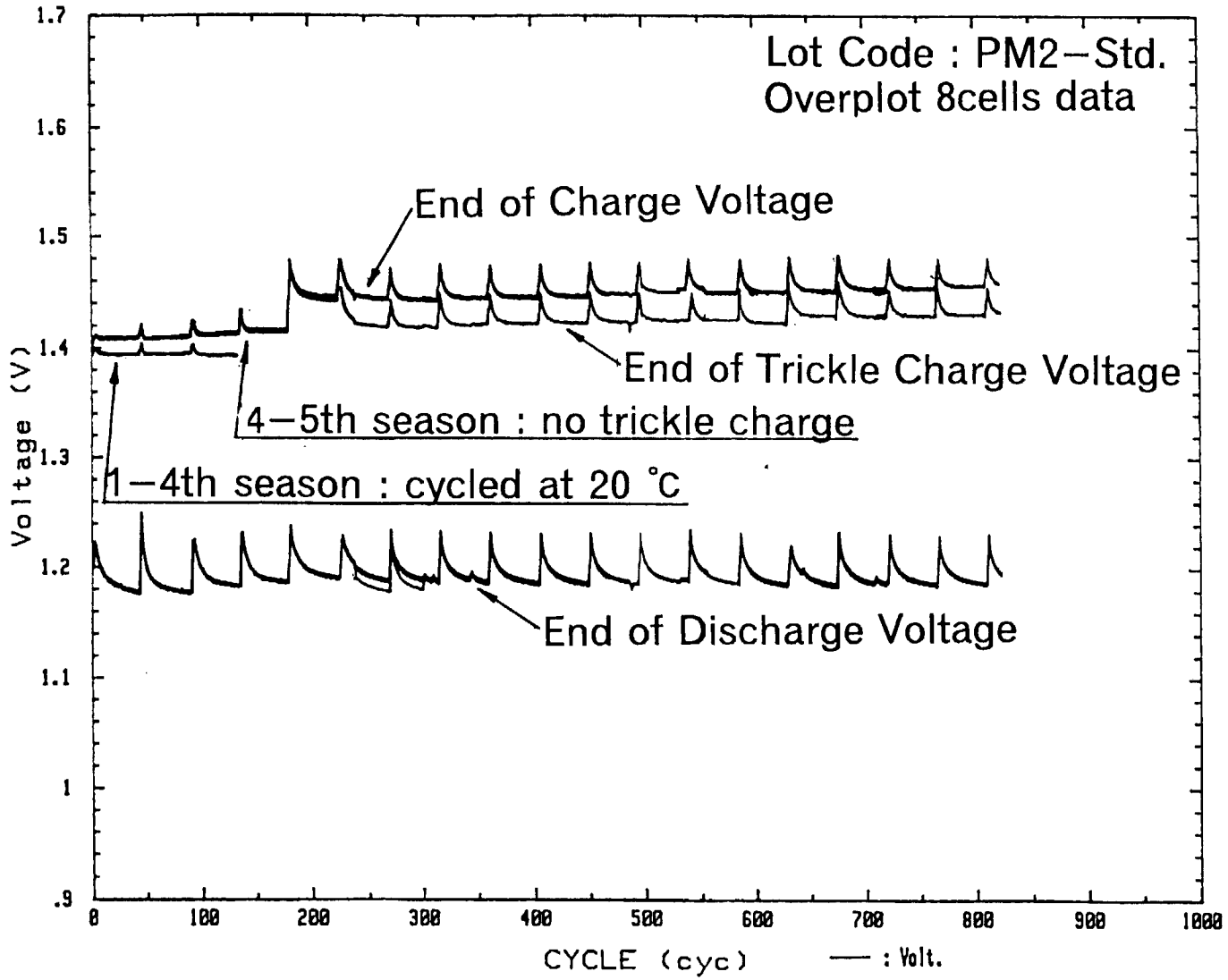

SANYO

Battery Storage

Storage Condition : Below 0 ℃ , Open circuit condition
Short circuit storage causes a small fading of capacity.

6months Storage Test of ETS−VI/PM Cells

N=11	Short / 0 ℃ before → after	Open / 0 ℃ before → after
End of Charge Volt. [V]	1.471 → 1.471	1.471 → 1.472
Max. Press. [kg/sq.cm]	1.27 → 1.33	1.15 → 1.21
Capacity [Ah]	38.9 → 38.1	38.6 → 38.6

SANYO

Conclusion

- 35Ah Ni–Cd cells for ETS–VI/FM showed uniform performance in the initial acceptance test.
- Same designed cells are continuously tested in the simulating cycle mode of ETS–VI in NASDA, and these cells operate in a stable state.
- Our aerospace Ni–Cd cells are surely expected to show good performance in space, and selected by the following succesive program.

  ADEOS to launch in 1996 : now manufacturing FM cells to deliver 176cells

  ETS–VII to be launched in 1998 : will use about 160 cells

N94-28122

AF Ni-Cd Cell Qualification Program

S. Hall and H. Brown NSWC CRANE
G. Collins and W. Hwang Aerospace Corporation

AIR FORCE NI-CD PROGRAM
OVERVIEW OF TEST PROGRAM

BACKGROUND

1976 - QUALIFIED 2505ML SEPARATOR MANUFACTURE DISCONTINUED

1984 - SURPLUS SUPPLY OF 2505ML DEPLETED

1985 - AIR FORCE/NAVY SPONSORED CRANE DIVISION TEST
SEPARATOR QUALIFICATION PROGRAM

1986-1988 - NO GENERIC QUALIFICATION OF REPLACEMENT
PELLON 2536 SEPARATOR

1989 - AIR FORCE SPONSOR CRANE DIVISION TEST NICKEL-CADMIUM
CELL QUQALIFICATION PROGRAM

1990 - SAFT/FRANCE VOS A (up to 40 Ah) DESIGN CELLS
RECOMMENDED FOR GENERIC QUALIFICATION FOR USAF PROGRAMS

AIR FORCE NI-CD PROGRAM
OVERVIEW OF TEST PROGRAM

PURPOSE

GENERIC QUALIFICATION OF AEROSPACE NICKLE-CADMIUM CELLS

MULTIPLE MANUFACTURES
MULTIPLE DESIGNS
INCLUDES CELLS FROM PREVIOUS PROGRAM
HIGH AND LOW ORBIT LIFE CYCLING

CHARACTERIZE BEGINNING OF LIFE PERFORMANCE

AIR FORCE NI-CD PROGRAM
OVERVIEW OF TEST PROGRAM

OUTLINE

ACCEPTANCE TEST - BASED ON MANUFACTURER TEST

CHARACTERIZATION TEST

CHARGE RATE	TEMPERATURE DEGREE C			
	-10	0	10	25
C/2		X	X	X
C/4		X	X	
C/10	X	X	X	X
C/20	X	X		X
C/80		X	X	

NOTE: DISCHARGES AT C/2

STRESS TEST

6351A

TYPE	50 A/H NI-CD, HUGHES
TEMPERATURE	20 DEGREES CENTIGRADE
ORBIT	100 MINUTES
DISCHARGE	36.0 AMPS FOR 34 MINUTES, 40%DOD
CHARGE	25.0 AMPS WITH V/T TAPER AT V/T 7.5 (1.464 V/C)

ANNUAL TRENDPLOT

Pack: 6351A Manf: HUGHES 50.0 AH
Orbit: LEO Temp (C): 20 DOD(%): 40.0
Discharge(Amp/Hrs): 36.0/0.56 Charge(Amp/Hrs): 25.0/1.12

Plot area #1 -- keys:
Left-side:
□ -- High Cell
o -- Average
x -- Low Cell
Right-side:
OFF

Plot area #2 -- keys:
Left-side:
OFF
Right-side:
▽ -- PERCENT REC

Plot area #3 -- keys:
Left-side:
□ -- High Cell
o -- Average
x -- Low Cell
Right-side:
OFF

TEST DATA AS OF OCTOBER 23, 1993

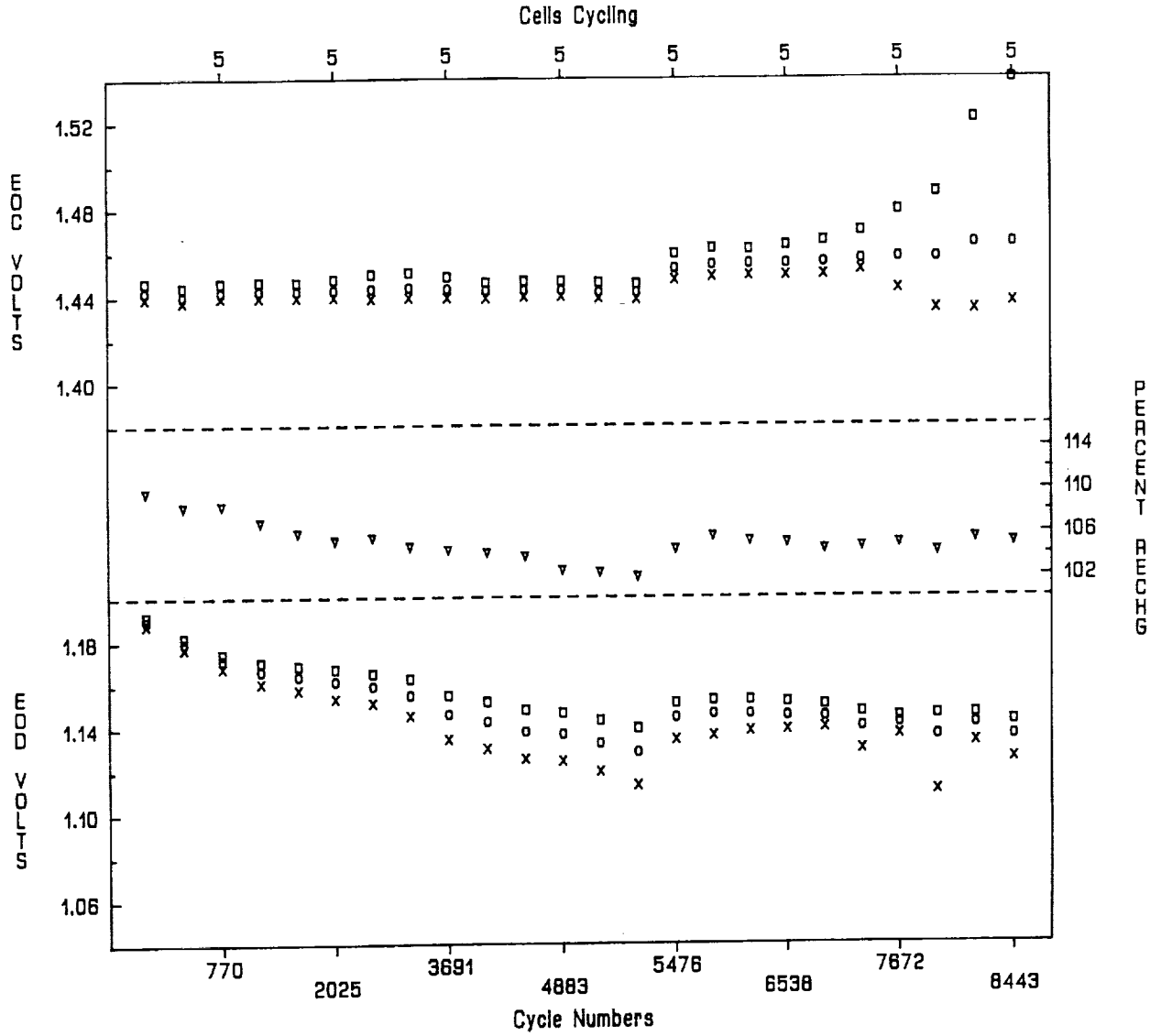

1. CYCLE #18, DECREASED FROM VT 7 (1.454 V/C) TO VT 6.5 (1.444 V/C) DUE TO HIGH PERCENT RECHARGE.
2. CYCLE #5376, INCREASED TO VT 7 (1.454 V/C) DUE TO LOW PERCENT RECHARGE. TEMPERATURE RISE OF .5 DEGREES CENTIGRADE SINCE V/T CHANGE.
3. CYCLE 8257, INCREASED TO VT 7.5 (1.464 V/C) DUE TO LOW EOD'S.

6352A

TYPE	50 A/H NI-CD, HUGHES
TEMPERATURE	5 DEGREES CENTIGRADE
ORBIT	96 MINUTES
DISCHARGE	25.0 AMPS FOR 30 MINUTES, 25%DOD
CHARGE	25. AMPS WITH V/T TAPER AT V/T 5.5 (1.458 V/C)

ANNUAL TRENDPLOT

Pack: 6352A Manf: HUGHES 50.0 AH
Orbit: LEO Temp (C): 5.0 DOD(%): 25.0
Discharge(Amp/Hrs): 25.0/0.50 Charge(Amp/Hrs): 25.0/1.10

Plot area #1 -- keys:
Left-side:
□ -- High Cell
o -- Average
x -- Low Cell
Right-side:
OFF

Plot area #2 -- keys:
Left-side:
OFF
Right-side:
▽ -- PERCENT RECH

Plot area #3 -- keys:
Left-side:
□ -- High Cell
o -- Average
x -- Low Cell
Right-side:
OFF

TEST DATA AS OF OCTOBER 23, 1993

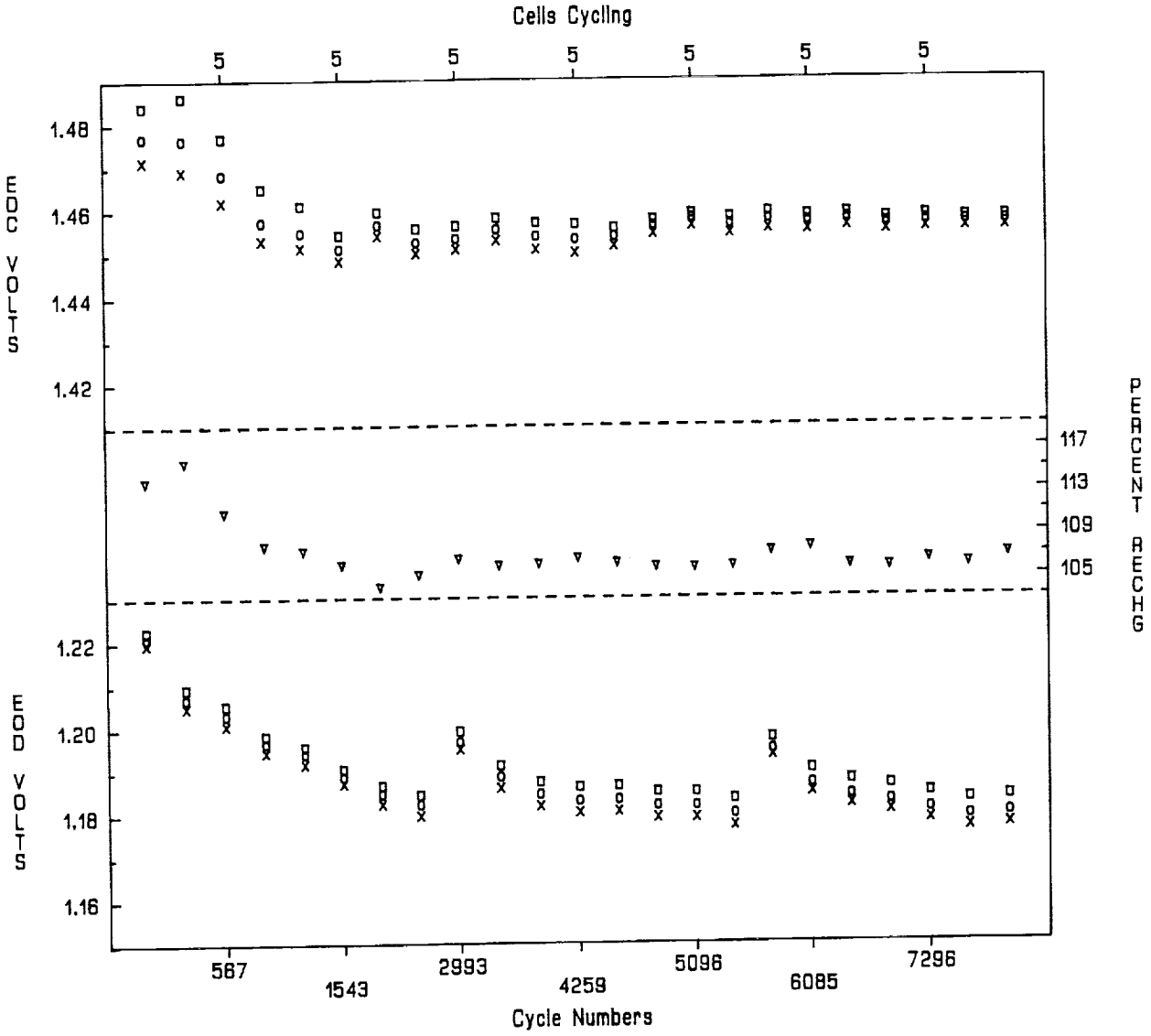

1. CYCLE #47, LOWERED FROM VT 7 (1.488 V/C) TO VT 6.5 (1.478 V/C) DUE TO HIGH PERCENT RECHARGE.
2. CYCLE #529, LOWERED FROM VT 6.5 (1.478 V/C) TO VT 6 (1.468 V/C) DUE TO HIGH PERCENT RECHARGE.
3. CYCLE # 569, LOWERED FROM VT 6 (1.468 V/C) TO VT 5.5(1.458 V/C) DUE TO HIGH PERCENT RECHARGE (111%).
4. CYCLE # 2866, CX @ C/2 TO 1.1 V 1ST CELL, A/HO(36.3)
5. CYCLE # 5628, CX @ C/2 RO 1.1 VOLT FIRST CELL, A/HO (33.8).

RECONDITIONED AT SIX MONTH INTERVALS

6352A

DISCHARGE AT C/2 TO 1.10 VOLT FIRST CELL

MONTHS	A/HO
6	36.3
12	33.8
18	38.0

STRESS TEST

6321H

TYPE	21 A/H NI-CD, HUGHES
TEMPERATURE	20 DEGREES CENTIGRADE
ORBIT	100 MINUTES
DISCHARGE	15.0 AMPS FOR 34 MINUTES, 40%DOD
CHARGE	10.5 AMPS WITH V/T TAPER AT V/T 6.0 (1.434 V/C)

ANNUAL TRENDPLOT

Pack: 6321H Manf: HUGHES 21.0 AH
Orbit: LEO Temp (C): 20 DOD(%): 40.0
Discharge(Amp/Hrs): 15.0/0.56 Charge(Amp/Hrs): 10.5/1.12

Plot area #1 -- keys:
Left-side:
□ -- High Cell
o -- Average
x -- Low Cell
Right-side:
OFF

Plot area #2 -- keys:
Left-side:
OFF
Right-side:
▽ -- PERCENT RECH

Plot area #3 -- keys:
Left-side:
□ -- High Cell
o -- Average
x -- Low Cell
Right-side:
OFF

TEST DATA AS OF OCTOBER 23, 1993

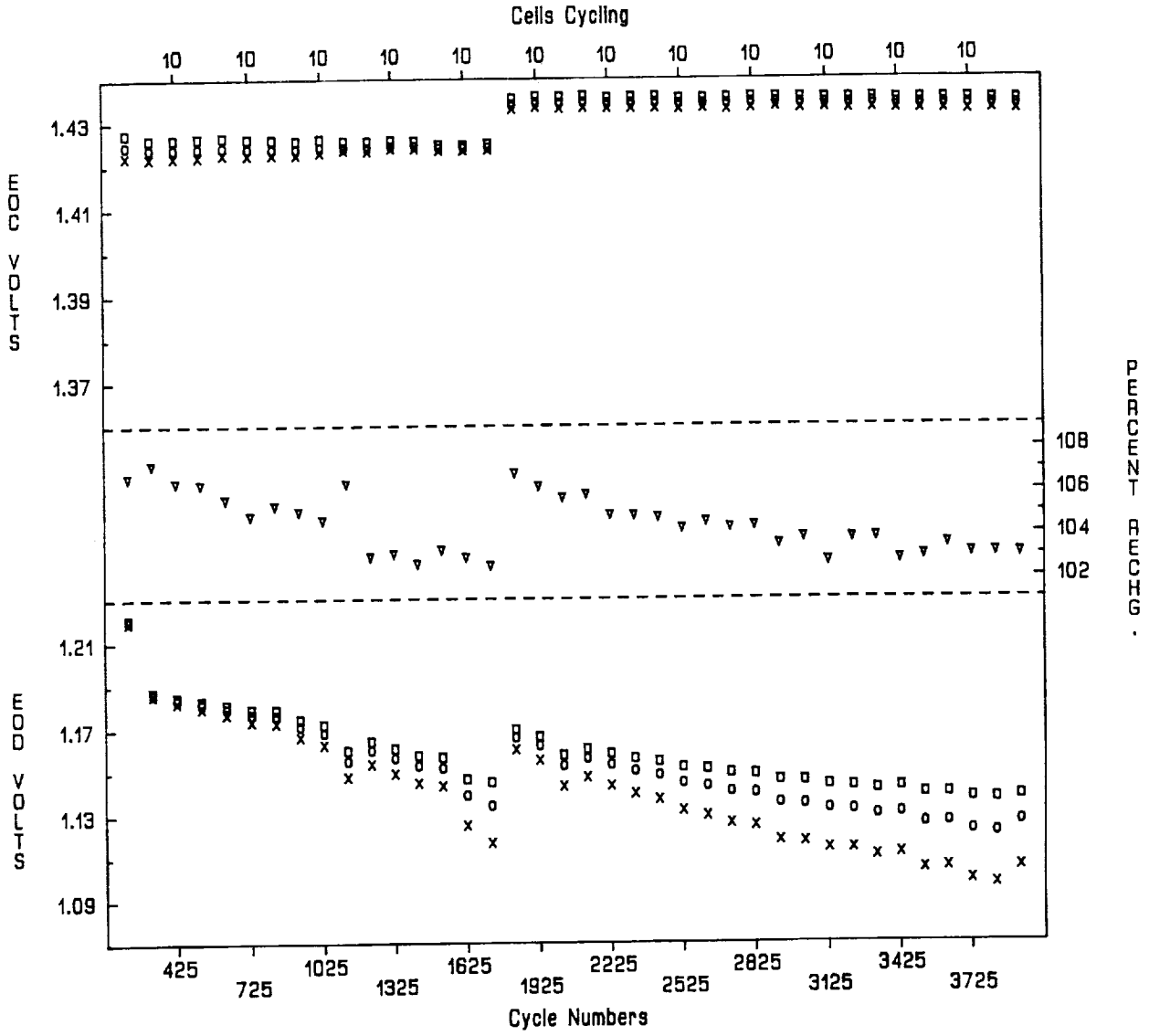

1. START LIFE-CYCLING, V/T 5.5 (1.424 V/C).
2. CYCLE 1851, V/T INCREASED TO 6.0 (1.434 V/C).

RESULTS FOR "SUPER NICD" CELLS

CAPACITY LOSS DUE TO STORAGE/HANDLING PROCEDURES

* 50Ah CELL, 40% DOD & 20 C: EODV > 1.120 AT 8443 CYCLES
INCREASING EOCV DIVERGENCE

* 50Ah CELL, 25% DOD & 0 C: EODV > 1.177 AT 7893 CYCLES

* 21Ah CELL, 40% DOD & 20 C: EODV > 1.093 AT 3882 CYCLES

CONCLUSIONS OF RESULTS FOR "SUPER NICD" CELLS

* THERE IS A STORAGE/HANDLING ISSUE
* 50 Ah, 40% DOD PACK HAS INCREASING EOCV DIVERGENCE
* BEGINNING OF LIFE CAPACITY FADE NOT DETRIMENTAL TO CYCLE LIFE

STRESS TEST

6350S

TYPE	50 A/H NI-CD, SAFT
TEMPERATURE	20 DEGREES CENTIGRADE
ORBIT	100 MINUTES
DISCHARGE	35.3 AMPS FOR 34 MINUTES, 40%DOD
CHARGE	25.0 AMPS WITH V/T TAPER AT V/T 8.5 (1.484 V/C)

ANNUAL TRENDPLOT

Pack: 6350S Manf: SAFT 50.0 AH
Orbit: LEO Temp (C): 20 DOD(%): 40.0
Discharge(Amp/Hrs): 35.3/0.56 Charge(Amp/Hrs): 25.0/1.12

Plot area #1 -- keys:
Left-side:
□ -- High Cell
o -- Average
x -- Low Cell
Right-side:
OFF

Plot area #2 -- keys:
Left-side:
OFF
Right-side:
▽ -- PERCENT RECH

Plot area #3 -- keys:
Left-side:
□ -- High Cell
o -- Average
x -- Low Cell
Right-side:
OFF

TEST DATA AS OF OCTOBER 23, 1993

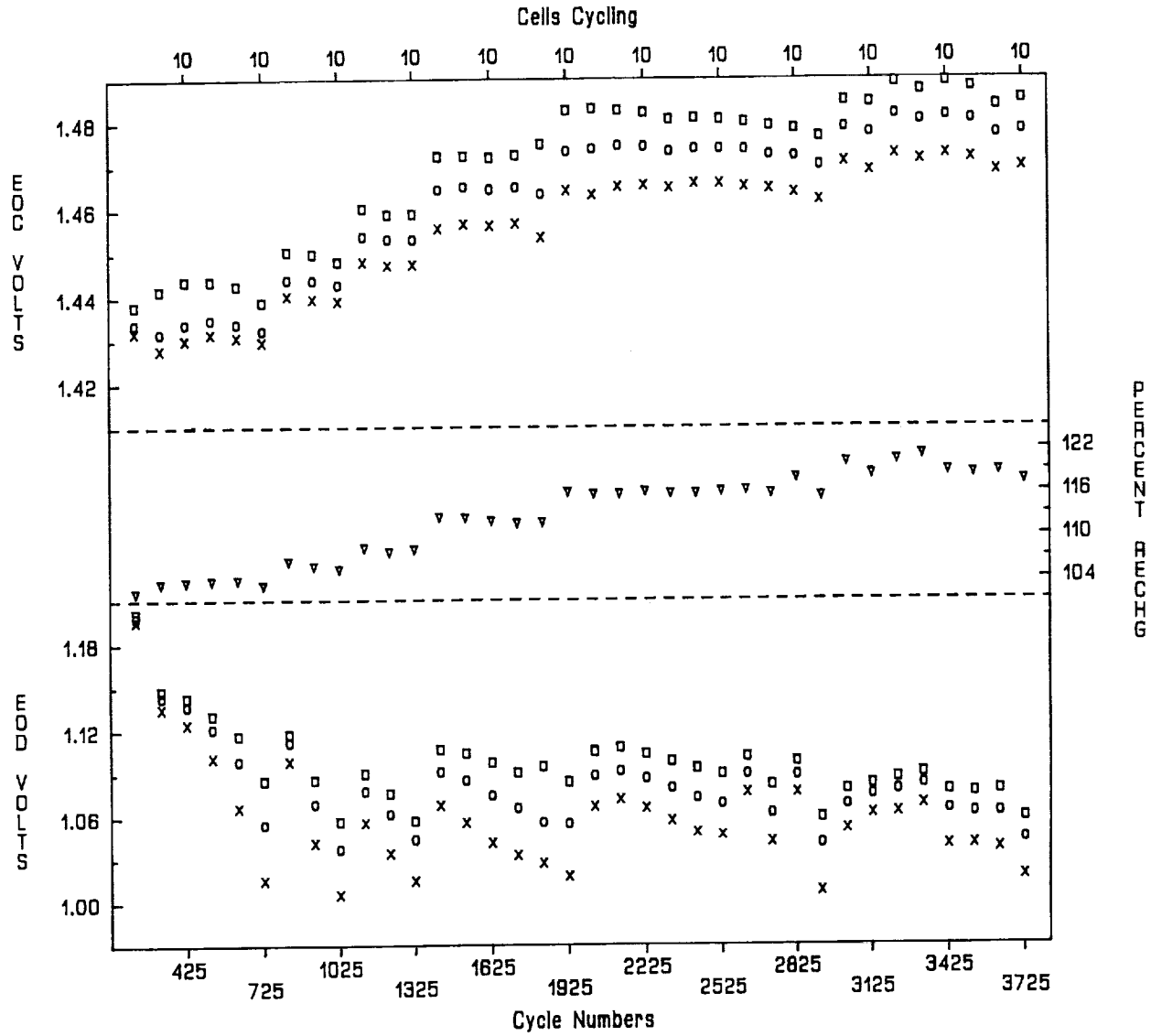

1. START OF LIFE CYCLING, V/T 6.0 (1.434 V/C).
2. CYCLE #775, INCREASED TO V/T 6.5 (1.444 V/C) DUE TO LOW EOD'S.
3. CYCLE #1125, INCREASED TO V/T 7.0 (1.454 V/C) DUE TO LOW EOD'S.
4. CYCLE #1513, INCREASED TO V/T 7.5 (1.464 V/C) DUE TO LOW EOD'S.
5. CYCLE #2020, INCREASED TO V/T 8.0 (1.474 V/C) DUE TO LOW EOD'S.
6. CYCLE #3076, INCREASED TO V/T 8.5 (1.484 V/C) DUE TO LOW EOD'S.

6351S

TYPE	50 A/H NI-CD, SAFT
TEMPERATURE	0 DEGREES CENTIGRADE
ORBIT	96 MINUTES
DISCHARGE	25.0 AMPS FOR 30 MINUTES, 25%DOD
CHARGE	25.0 AMPS WITH V/T TAPER AT V/T 6 (1.480 V/C)

ANNUAL TRENDPLOT

Pack: 6351S Manf: SAFT 50.0 AH
Orbit: LEO Temp (C): 0 DOD(%): 25.0
Discharge(Amp/Hrs): 25.0/0.50 Charge(Amp/Hrs): 25.0/1.10

Plot area #1 -- keys:
Left-side:
□-- High Cell
o-- Average
x-- Low Cell
Right-side:
OFF

Plot area #2 -- keys:
Left-side:
OFF
Right-side:
▽-- PERCENT RECH

Plot area #3 -- keys:
Left-side:
□-- High Cell
o-- Average
x-- Low Cell
Right-side:
OFF

TEST DATA AS OF OCTOBER 23, 1993

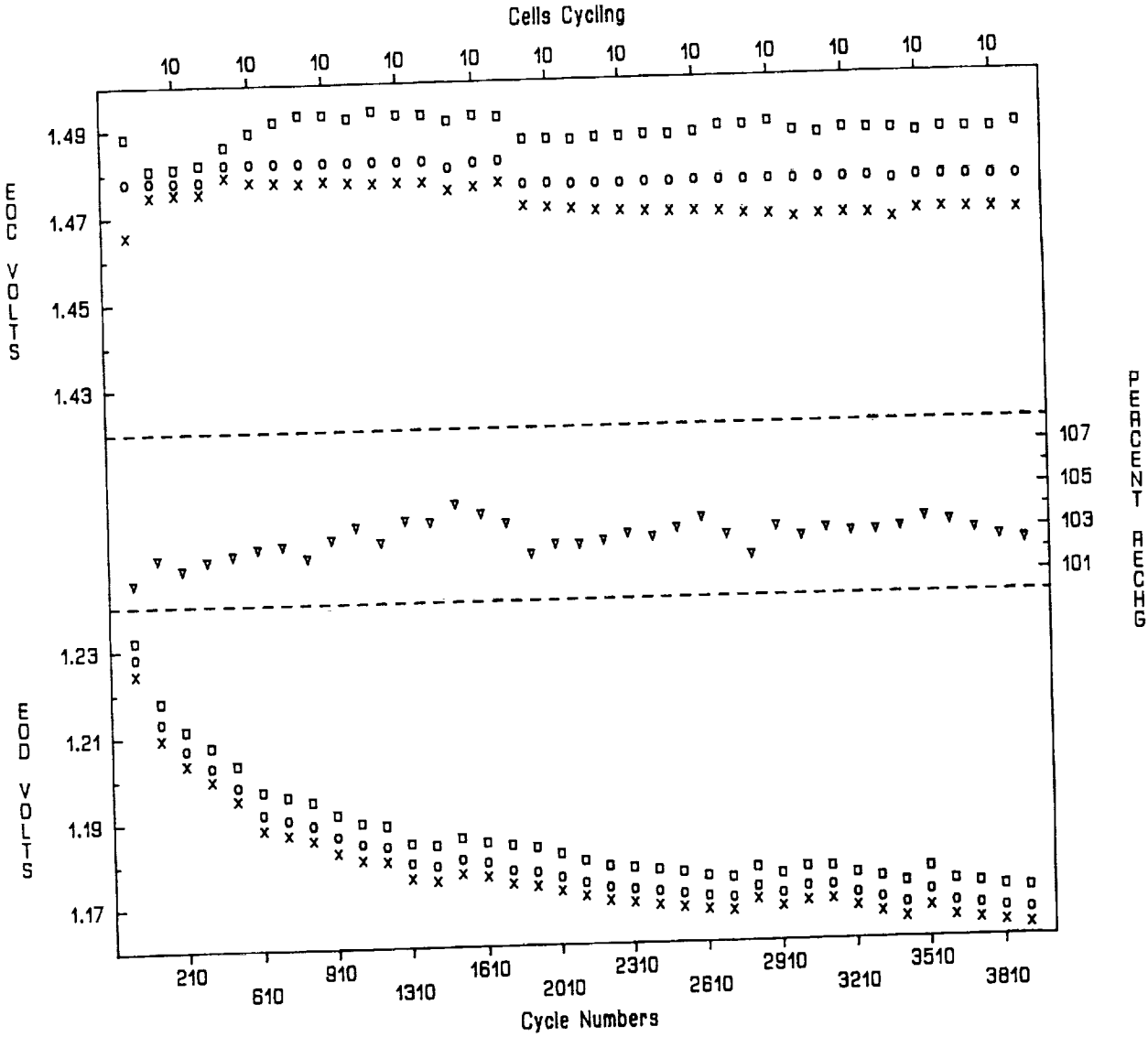

1. STARTED LIFE-CYCLING, V/T 6 (1.480 V/C).

6224S

TYPE	24 A/H NI-CD, SAFT
TEMPERATURE	20 DEGREES CENTIGRADE
ORBIT	24 HOURS
DISCHARGE	16.0 AMPS FOR MAXIMUM OF 80%DOD
CHARGE	2.4 AMPS WITH V/T TAPER AT V/T 5 (1.414 V/C)

GEO AIR FORCE
TREND OF MID SHADOW
Pack: 6224S Manf: SAFT 24.0 AH
Orbit: GEO Temp (C): 20 DOD(%): 80.0

DISCHARGE (16.0 AMPS).
CHARGE (2.4 AMPS) WITH 1.414 V/C

SHADOWS 1 THRU 28

Plot area #1 -- keys:
Left-side:
□ -- High Cell
o -- Average
x -- Low Cell
Right-side:
▽ -- EOC TEMP
△ -- EOC TEMP
▷ -- EOC TEMP
Plot area #2 -- keys:
Left-side:
OFF
Right-side:
▽ -- % RECHG.
Plot area #3 -- keys:
Left-side:
□ -- High Cell
o -- Average
x -- Low Cell
Right-side:
OFF

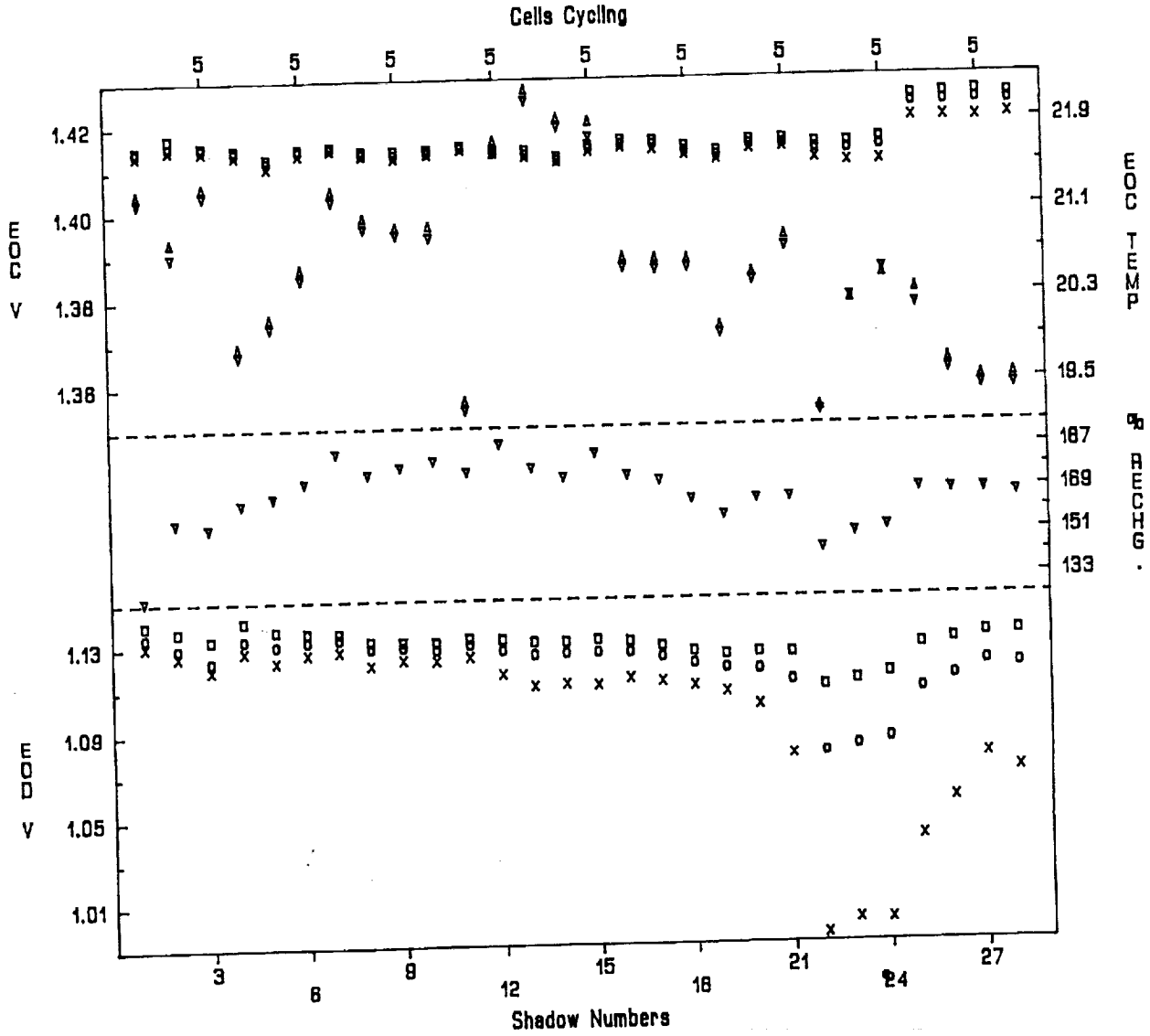

1. Shadow #1, lowered VL to 1.414 v/c, due to high per-cent recharge.
2. Shadow #1, during Cycle # 25, a system problem occured that caused the A/Ho to be read as 21,474 A/H. The pack was then recharged with a V/L for 202 hours.
3. Shadow #3, The DOD was adjusted to 80%.
4. Cycle #218, lowered to VT4 (1.384 v/c) due to cells warming at EOC.
5. Cycle #248, raised to VT4.5 (1.404 v/c) due to low EOD volts.
6. Cycle #307, lowered to VT4 (1.394 v/c) due to warming at EOC.
7. Cycle #338, raised to VT4.5 (1.404 v/c) due to low EOD volts.
8. Cycle #409, started pack using true VT control.
9. Cycle #428, raised to VT5 (1.414 v/c) due to low EOD.
10. Shadow #21, due to chamber problems, the pack remained in OCV 28 days during Shadow Day #36.
11. Cycle #1087, raised to VT5.5 (1.424 v/c) due to low EOD.

6240S

TYPE	40 A/H NI-CD, SAFT
TEMPERATURE	20 DEGREES CENTIGRADE
ORBIT	24 HOURS
DISCHARGE	26.70 AMPS FOR MAXIMUM OF 80%DOD
CHARGE	4.0 AMPS WITH V/T TAPER AT V/T 5 (1.414 V/C)

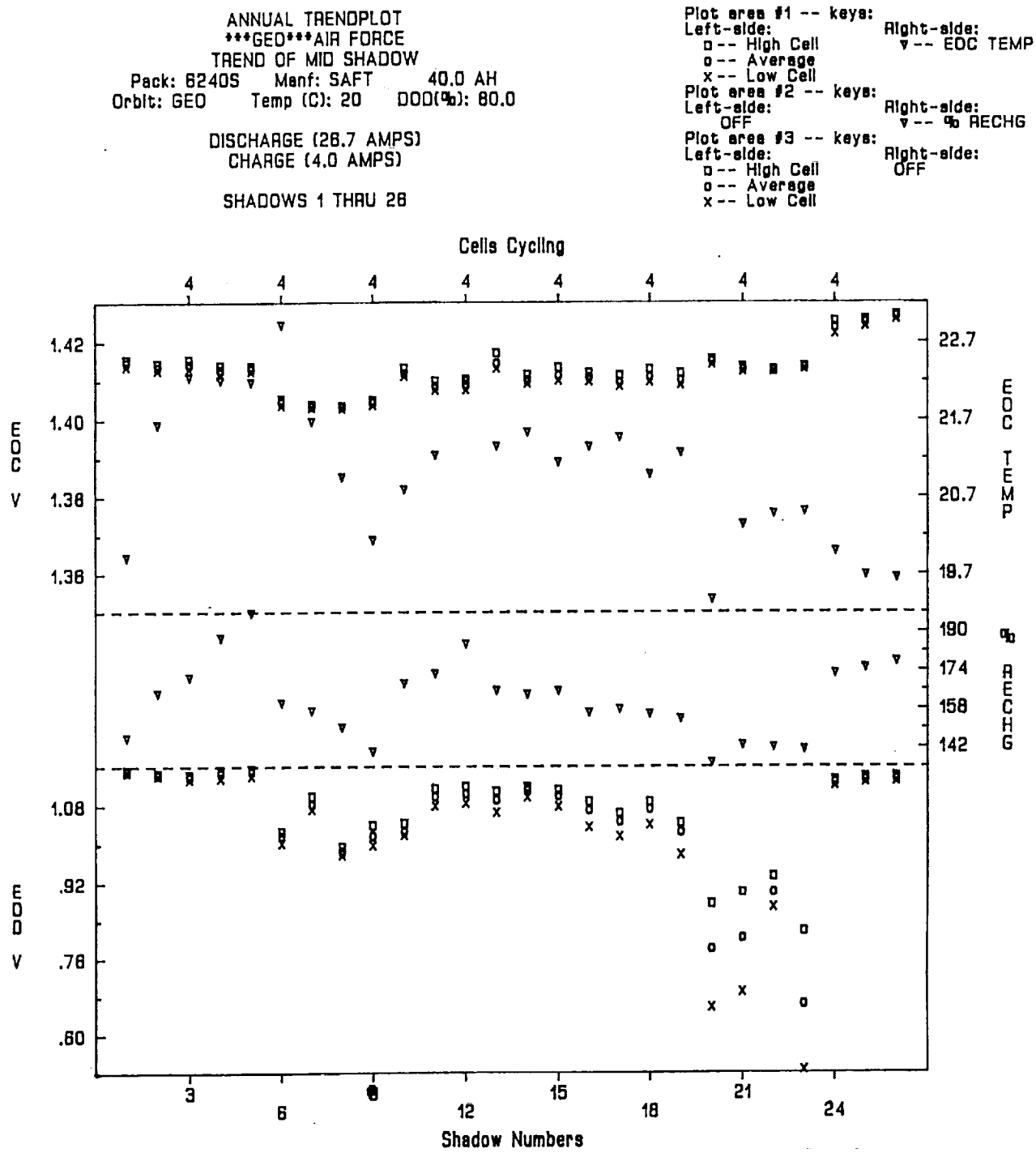

1. Shadow # 1, VT 5 (1.414 V/C).
2. Shadow # 4, DOD changed from 88 to 80 per cent recharge.
3. Shadow # 8, VT 4.5 (1.404 V/C) due to cells warming during charge.
4. During Shadow # 9, the pack was using a 2 step V/T. The first ten days and the last nine days of the shadow period were at VT 4.0 (1.394 V/C). During days 11 thru 33 (mid-shadow) the pack ran at VT 4.5 (1.404 V/C).
5. Shadow # 10, voltage clamp changed to voltage/temperature controlled voltage limit at VT 5 (1.414 V/C).
6. Shadow # 20, due to chamber problems, the pack remained in OCV 28 days during Shadow Day #7.
7. Shadow # 23, increased to VT 5.5 (1.414 V/C), due to low EOD.

RESULTS FOR SAFT CELLS

ADVANCE DESIGN LEO ORBIT

* 50 Ah CELL, 40% DOD & 20 C: EODV > 1.006 AT 3624 CYCLES

* 50 Ah CELL, 25% DOD & 0 C: EODV > 1.163 AT 3795 CYCLES

VOS A DESIGN COMPRESSED GEO ORBIT

* 40 Ah CELL, 80% DOD & 20 C: EODV > 1.129 AT 26 SHADOWS

*24 Ah CELL, 80% DOD & 20 C: EODV > 1.060 AT 27 SHADOWS

CONCLUSIONS OF RESULTS FOR SAFT CELLS

* C/D HIGHER THAN THAT OF PRE-1986 GATES CELLS
* LEO RESULTS VERIFY GENERIC QUALIFICATION OF VOS A (UP TO 40 Ah) CELLS
* RECOMMEND A NEW TERMINAL DESIGN FOR 40Ah CELLS

GPS STRESS TEST

6335A

TYPE	35 A/H NI-CD, GATES
TEMPERATURE	20 DEGREES CENTIGRADE
ORBIT	100 MINUTES
DISCHARGE	25 AMPS FOR 34 MINUTES, 40%DOD
CHARGE	17.5 AMPS WITH V/T TAPER AT V/T 8 (1.474 V/C)

ANNUAL TRENDPLOT

Pack: 6335A Manf: GATES 35.0 AH
Orbit: LEO Temp (C): 20 DOD(%): 40.0
Discharge(Amp/Hrs): 25.0/0.56 Charge(Amp/Hrs): 17.5/1.12

TEST DATA AS OF OCTOBER 23, 1993

Plot area #1 -- keys:
Left-side:
□ -- High Cell
o -- Average
x -- Low Cell
Right-side:
OFF

Plot area #2 -- keys:
Left-side:
OFF
Right-side:
▽ -- PERCENT RECH

Plot area #3 -- keys:
Left-side:
□ -- High Cell
o -- Average
x -- Low Cell
Right-side:
OFF

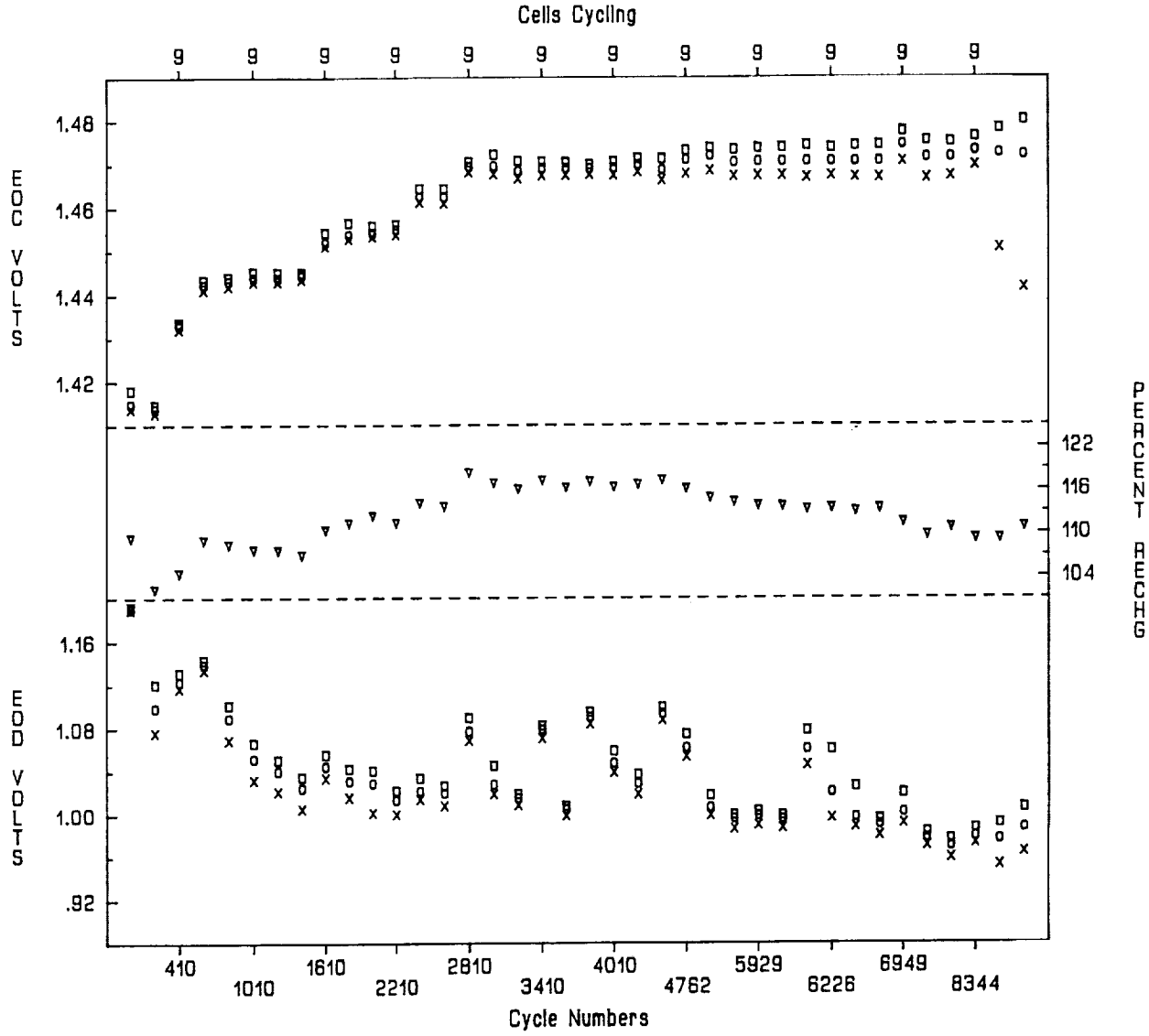

1. LIFE CYCLING STARTED AT VT 4.0 (1.380 V/C).
2. VT'S WERE INCREASED FROM 4.0 TO 8.0 IN 1/2 VT INCREMENTS DUE TO LOW EOD'S AND % RECHARGE.
3. A PERCENT OF RECHARGE INCREASE WAS NOTICED AFTER EXTENDED OPEN CIRCUIT TIMES DURING CHAMBER PROBLEMS.
4. CYCLE #3840, IT WAS NOTICED THAT ALL CELL CASES WERE SWOLLEN DUE TO HIGH PERCENT OF RECHARGE (117%).
5. CYCLE #6073, PACK SLIGHTLY RECONDITIONED WHEN TEST SYSTEM WENT DOWN. VOLTAGE STEADILY INCREASED THE NEXT 25 CYCLES AND THEN DECLLINED.

GPS SIMULATED ORBIT

6335B

TYPE	35 A/H NI-CD, GATES
TEMPERATURE	20 DEGREES CENTIGRADE
ORBIT	10 HOURS, 26 MINUTES
DISCHARGE	16 AMPS FOR 56 MINUTES, 40%DOD
CHARGE	3.5 AMPS WITH V/T TAPER AT V/T 6 (1.434 V/C)

ANNUAL TRENDPLOT

Pack: 6335B Manf: GATES 35.0 AH
Orbit: GPS Temp (C): 20 DOD(%): 41.4
Discharge(Amp/Hrs): 15.8/0.92 Charge(Amp/Hrs): 03.5/9.50

TEST DATA AS OF OCTOBER 23, 1993

Plot area #1 -- keys:
Left-side: Right-side:
□ -- High Cell OFF
o -- Average
x -- Low Cell
Plot area #2 -- keys:
Left-side: Right-side:
OFF ▽ -- PERCENT RECH
Plot area #3 -- keys:
Left-side: Right-side:
□ -- High Cell OFF
o -- Average
x -- Low Cell

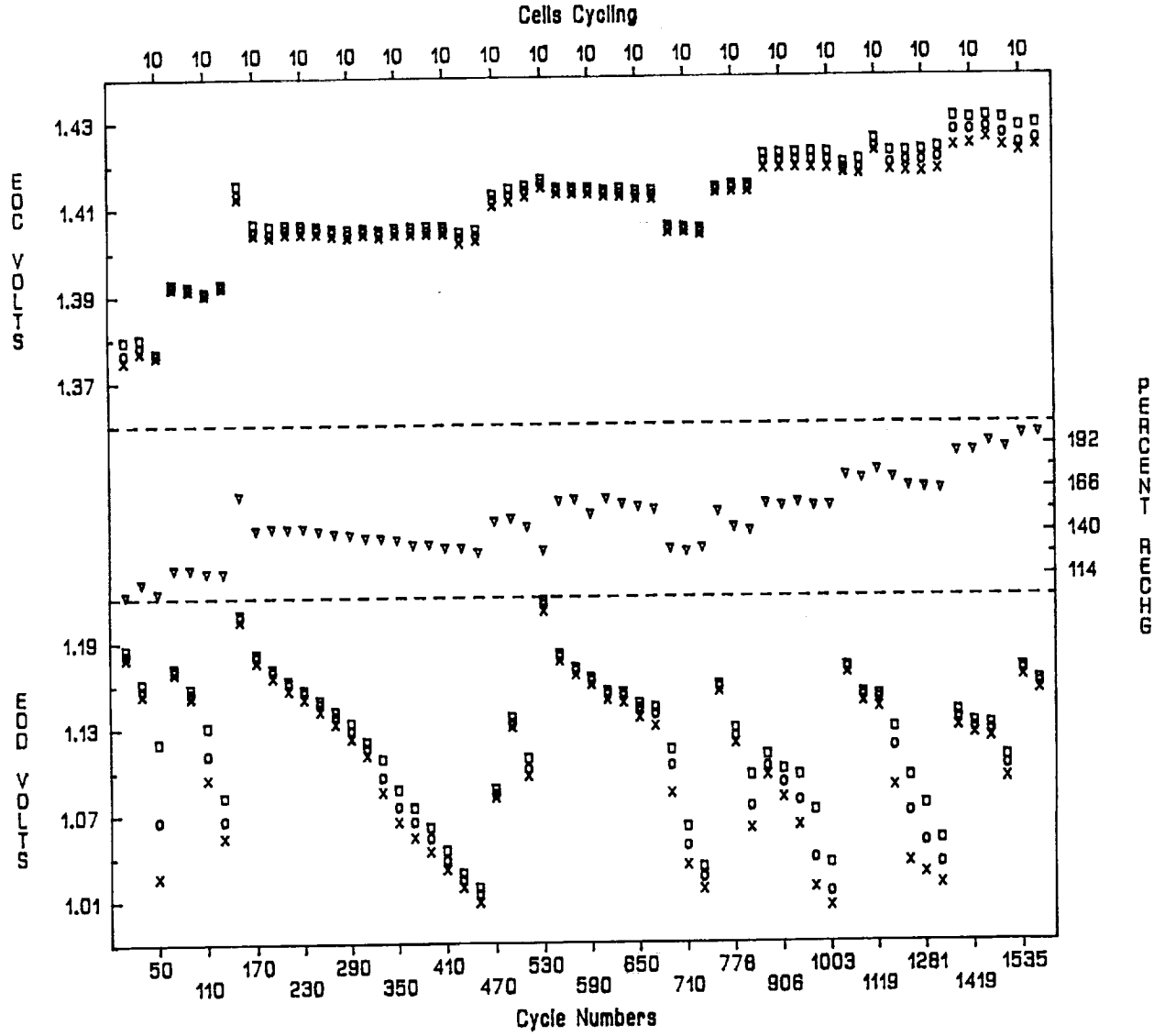

1. STARTED LIFE CYCLING AT V/T 4.0(1.380 V/C).
2. VT'S WERE ADJUSTED FROM 4.0 TO 5.0, IN INCREMENTS OF 1/2 VT, DUE TO LOW EOD'S.
3. CYCLE #528, PACK WAS RECONDITIONED WITH A/HO 20.12.
4. CYCLE #694, DECREASED TO V/T 4.5(1.404 V/C) DUE TO HIGH EOC TEMP.
5. CYCLE #733, INCREASED TO V/T 5.0(1.414 V/C) DUE TO LOW EOD.
6. CYCLE #862, INCREASED TO V/T 5.5(1.424 V/C) DUE TO LOW EOD.
7. CYCLE #1005, PACK WAS RECONDITIONED WITH A/HO 19.0.
8. CYCLE #1374, INCREASED TO V/T 6.0(1.434 V/C) DUE TO LOW EOD.
9. CYCLE #1506, PACK WAS RECONDITIONED WITH A/HO 23.7.

RECONDITIONED AT SIX MONTH INTERVALS

6335B

DISCHARGE AT 15.4 AMPERES TO 0.75 VOLT FIRST CELL

MONTHS	A/HO
6	20.1
12	19.0
18	23.7

STRESS TEST

6353G

TYPE	50 A/H LIGHTWEIGHT NI-CD, GATES
TEMPERATURE	20 DEGREES CENTIGRADE
ORBIT	100 MINUTES
DISCHARGE	35.3 AMPS FOR 34 MINUTES, 40%DOD
CHARGE	25.0 AMPS WITH V/T TAPER AT V/T 6 (1.434 V/C)

Pack: 6353G Manf: GATES 50.0 AH
Orbit: LEO Temp (C): 20 DOD(%): 40.0
Discharge(Amp/Hrs): 35.3/0.56 Charge(Amp/Hrs): 25.0/1.12

Plot area #1 -- keys:
Left-side: Right-side:
□ -- High Cell OFF
o -- Average
x -- Low Cell
Plot area #2 -- keys:
Left-side: Right-side:
OFF ▽ -- PERCENT RECH
Plot area #3 -- keys:
Left-side: Right-side:
□ -- High Cell OFF
o -- Average
x -- Low Cell

TEST DATA AS OF OCTOBER 23, 1993

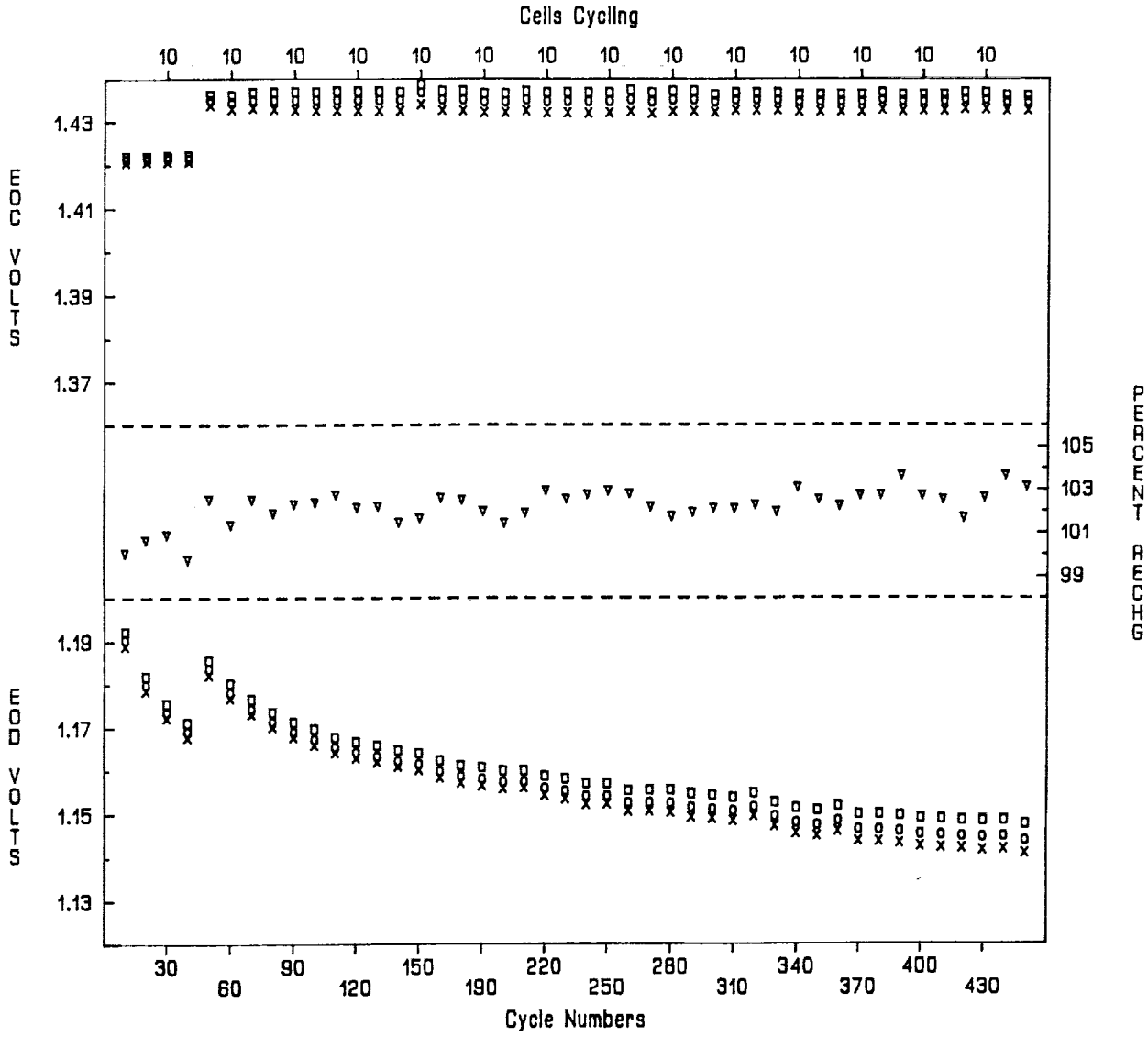

1. STARTED CYCLING @ VT 5.5 (1.424 V/C).
2. CYCLE # 45, INCREASED TO VT 6 (1.434 V/C), DUE TO LOW EOD'S.

RESULTS FOR GATES CELLS

* 35 Ah CELL, 40% DOD & 20 C: EODV > 0.987 AT 9443 CYCLES

* 35 Ah CELL, 41.4% DOD & 20 C: EODV > 1.094 AT 1495 CYCLES
ACCELERATED 10.4 HOUR GPS ORBIT

* 50 Ah CELL, 40% DOD & 20 C: TESTING JUST BEGAN

CONCLUSIONS OF RESULTS FOR GATES CELLS

* EARLY FAILURE OF PRESENT 50-Ah AND 35- Ah CELLS

* NOT ABLE TO GENERICALLY QUALIFY 50-Ah AND 35-Ah CELLS

DISCRIMINATING PERFORMANCE PARAMETERS FOR 50 AMP-HOUR AND 60 AMP-HOUR NICKEL-CADMIUM PLATES AND BATTERY CELLS

PRESENTED: 1993 NASA AEROSPACE BATTERY WORKSHOP
16 - 18 NOVEMBER 1993

BY: MARK R. TOFT
BATTERY ENGINEER
SPACE ELECTRONICS
(314)-925-7692

McDonnell Douglas Aerospace - Defense and Electronic Systems

OVERVIEW

THIS IS A FOLLOW-UP TO STUDIES OF THE NASA STANDARD 50 AMP-HOUR CELL PRESENTED AT THE NASA BATTERY WORKSHOP EACH OF THE LAST TWO YEARS:

1991 - RECOGNITION OF THE DATABASE

1992 - USE OF THE DATABASE TO DETECT ANOMALOUS TRENDS

1993 - DISTILLATION OF DISCRIMINATING PARAMETERS FROM THE DATABASE

THIS IS A DYNAMIC STUDY. DATA TRENDS CONTINUE TO BE DEVELOPED AND ANALYZED FOR THEIR UTILITY IN JUDGING NICD PERFORMANCE.

THE TRENDS AND PARAMETERS PRESENTED HERE MAY BEAR RELEVANCE TO MANY DESIGNS OF CONVENTIONAL NICD BATTERIES, NOT JUST THE 50 AH AND 60 AH SIZES.

McDONNELL DOUGLAS AEROSPACE IS USING THE INSIGHT GAINED FROM THESE TRENDS TO JUDGE THE QUALITY OF PRESENT AND FUTURE CELL LOTS PROCURED FROM GATES AEROSPACE BATTERIES.

OVERVIEW (cont'd)

THE TYPES OF TRENDS AND PARAMETRIC RELATIONSHIPS PRESENTED HERE MAY BE QUITE SUITABLE FOR APPLICATION IN NICKEL-HYDROGEN TECHNOLOGY.

A CONSIDERABLE PERFORMANCE (LIFE-CYCLE) DATABASE FOR NICKEL HYDROGEN IS BEING BUILT.

A DATABASE CHARACTERIZING NICKEL HYDROGEN IS SOMEWHAT LACKING.

THE TYPES OF TRENDS AND PARAMETRIC RELATIONSHIPS PRESENTED HERE MAY BE IDEALLY SUITABLE FOR A FLEDGLING TECHNOLOGY LIKE NICKEL METAL-HYDRIDE.

NICKEL METAL-HYDRIDE MANUFACTURERS SEEK TO CHARACTERIZE THEIR PRODUCT AS WELL AS PROVE ITS PERFORMANCE.

THE TECHNIQUES PRESENTED HERE MAY ALLOW THE END USER TO SUPPLEMENT THOSE MEASURES OF PERFORMANCE THAT ARE LESS READILY ATTAINABLE, SUCH AS COMPLETE LIFE-CYCLE TESTING; OR LESS RELIABLE, SUCH AS CONFIDENCE IN A SUPPLIER OR CONFORMANCE OF THE DELIVERED PRODUCT TO SPECIFICATION.

SCOPE

THIS STUDY BUILDS ON TWO PREVIOUS STUDIES.

THOSE TWO STUDIES HAVE NOW BEEN EXPANDED TO INCLUDE 15 YEARS OF HISTORY ON A 60 AH DESIGN THAT McDONNELL DOUGLAS AEROSPACE HAS BEEN PROCURING OVER THE LAST TEN YEARS.

THROUGHOUT THIS PRESENTATION, THIS "NEW" PRODUCT WILL BE REFERRED TO AS THE "60 AH DESIGN" WHILE NASA CELL LOTS WILL BE REFERRED TO AS THE "NASA STANDARD 50 AH DESIGN".

THE 60 AH DESIGN IS ALMOST IDENTICAL TO THE NASA STANDARD 50 AH DESIGN EXCEPT THAT THE CELL CASE IS TALLER, AND BOTH THE POSITIVE AND NEGATIVE PLATES ARE MORE HEAVILY LOADED.

THE 60 AH DESIGN, LIKE THE NASA STANDARD 50 AH DESIGN, HAS YIELDED SEVERAL CELL LOTS IN THE LAST FIVE YEARS THAT BEGAN TO SHOW PERFORMANCE ANOMALIES EARLY IN CYCLE-LIFE.

ALSO LIKE THE NASA CELLS, THESE 60 AH CELLS CONFORMED TO ALL SPECIFICATIONS (WITH RARE EXCEPTION) DURING ASSEMBLY AND TEST AT THE CELL SUPPLIER.

THE DATABASE

OVER THE LAST 18+ MONTHS, McDONNELL DOUGLAS AEROSPACE HAS BEEN COMPILING A DATABASE OF ALMOST 80 PARAMETERS OR PARAMETRIC RELATIONSHIPS AT THE PLATE, CELL, AND BATTERY LEVEL IN AN EFFORT TO FIND THE ROOT CAUSE OF THE ANOMALOUS PERFORMANCE OF BATTERIES.

OF THESE 80 PARAMETERS, A GROUP OF 16 HAVE BEEN IDENTIFIED, WHICH IF

- TAKEN INDIVIDUALLY, MAY OR MAY NOT IDENTIFY A CAUSE FOR CONCERN ABOUT A PARTICULAR CELL LOT.
- TAKEN TOGETHER, PROVIDE COMPELLING DISCRIMINATION BETWEEN GOOD LOTS AND SUSPICIOUS LOTS.

AT THE SAME TIME, 25 CELL LOTS OF BOTH THE 60 AH AND STANDARD 50 AH DESIGNS WERE IDENTIFIED FROM A DATABASE OF 30 CELL LOTS SPANNING 16 YEARS.

THESE 25 LOTS COULD BE LABELLED "GOOD" OR "SUSPECT" BASED ON THE WEIGHT OF THE EVIDENCE FROM CELL LIFE-CYCLE TESTING, BATTERY LONG-TERM MISSION USAGE, AND/OR LONG-TERM TEST-BATTERY USAGE.

THE DISCRIMINATORS

PLATE LEVEL:

1. MEASURED N/P RATIO
2. RATIO OF POSITIVE LOADING WEIGHT TO TOTAL POSITIVE WEIGHT
3. RATIO OF NEGATIVE LOADING WEIGHT TO TOTAL NEGATIVE WEIGHT
4. NEGATIVE UTILIZATION
5. NEGATIVE ANTI-POLAR MASS
6. NEGATIVE TEFLON LOADING

CELL LEVEL:

7. FORMATION CYCLES: OXYGEN RECOMBINATION CHARACTERISTICS
8. MAXIMUM CAPACITY DURING FORMATION CYCLING

CELL LEVEL:(CONTINUED)

9. OXYGEN RECOMBINED IN PRECHARGE DPA CELLS vs OXYGEN PRECHARGE GOAL
10. OVERCHARGE PROTECTION AS A PERCENT OF TOTAL NEGATIVE CAPACITY
11. MAXIMUM RECORDED VOLTAGE IN THE 0°C CAPACITY TEST
12. 0°C CAPACITY
13. FINAL ELECTROLYTE AMOUNT
14. POSITIVE CAPACITY TO 0.0 VOLTS IN DPA CELLS
15. TRANSFER OF CADMIUM TO THE POSITIVE PLATE UNDER LIMITED CYCLING

BATTERY LEVEL:

16. RATIO OF CELL-LEVEL 0°C CAPACITY TO BATTERY-LEVEL 0°C CAPACITY

THE GOOD LOTS

LOT	JUSTIFICATION
50AB20 LOT 1	QUALIFICATION LOT/BATTERY; LONG LIFE AS TEST BATTERY
50AB20 LOT 2	LONG LIFE AS TEST BATTERIES; CELLS ON LIFE TEST TO 25000 CYCLES AT NSWC-CRANE WITHOUT INCIDENT; CELLS ON STRESS TEST TO 19000+ CYCLES AT NSWC-CRANE
50AB20 LOT 3	LANDSAT 4
50AB20 LOT 4	LANDSAT 5
50AB20 LOT 5	LANDSAT 4
50AB20 LOT 7	LANDSAT 5
50AB20 LOT 12	EARTH RADIATION BUDGET SATELLITE
50AB20 LOT 14	LONG LIFE AS TEST BATTERIES; CELLS ON STRESS TEST TO 15000+ CYCLES AT NSWC-CRANE; CONTAINED DEGRADED NYLON 2505 SEPARATOR
50AB20 LOT 17	COMPTON GAMMA RAY OBSERVATORY (GRO) MPS-2
50AB19 LOT 2	60 AH DESIGN DEVELOPMENT PROGRAM
50AB19 LOT 3	60 AH DESIGN DEVELOPMENT PROGRAM
50AB19 LOT 4	60 AH DESIGN DEVELOPMENT PROGRAM
50AB19 LOT 5	60 AH DESIGN DEVELOPMENT PROGRAM
50AB22 LOT 3	LONG LIFE AS TEST BATTERIES; CELLS ON LIFE TEST TO 15000+ CYCLES
50AB22 LOT 6	CELLS ON LIFE TEST TO 15000+ CYCLES
50AB22 LOT 7	60 AH DESIGN'S MPS-1

THE SUSPECT LOTS

LOT	JUSTIFICATION
50AB22 LOT 2	FIRST ANOMALOUS BATTERIES FOR 60 AH DESIGN; CONTAINED DEGRADED NYLON 2505 SEPARATOR
50AB22 LOT 11	CELLS UNDELIVERABLE: LOW ELECTROLYTE, HIGH VOLTAGE, HIGH PRESSURE
50AB22 LOT 13	60 AH DESIGN'S MPS-2 ANOMALOUS BATTERIES AND ANOMALOUS LIFE-TEST CELLS
50AB36 LOT 2	EARLY ANOMALIES IN LIFE-TEST OF PRE-ACCEPT CELLS
50AB20 LOT 13 / 50AB25 LOT 1	EARLY ANOMALIES IN LIFE-TEST AT NSWC-CRANE; SAME PLATE LOT WITH TWO KINDS OF NYLON SEPARATOR (2505 AND 2536); 50AB20 LOT 13 CELLS CONTAINED DEGRADED NYLON 2505
50AB20 LOT 15 / 50AB25 LOT 2	EARLY ANOMALIES IN LIFE-TEST AT NSWC-CRANE OF PRE-ACCEPT CELLS CONTAINING DEGRADED NYLON 2505 SEPARATOR (50AB20 LOT 15); BULK OF CELL LOT REWORKED TO INSTALL NYLON 2536 SEPARATOR (50AB25 LOT 2)
50AB20 LOT 16	ANOMALOUS* BATTERIES IN EXTREME ULTRAVIOLET EXPLORER (EUVE); EARLY ANOMALIES** IN LIFE-TEST OF PRE-ACCEPT CELLS AT NSWC-CRANE
50AB35 LOT 1	ANOMALOUS BATTERIES IN COMPTON GAMMA RAY OBSERVATORY (GRO) MPS-1; ANOMALIES IN STRESS-TEST OF CELLS AT NSWC-CRANE
50AB35 LOT 2	ANOMALOUS BATTERIES IN UPPER ATMOSPHERE RESEARCH SATELLITE (UARS); EARLY ANOMALIES IN LIFE-TEST OF CELLS AT NSWC-CRANE; EARLY ANOMALIES IN STRESS-TEST OF CELLS AT NSWC-CRANE

* WHILE THE SIGNATURE OF THE EUVE FLIGHT BATTERY ANOMALY IS SIMILAR TO THAT OF THE GRO MPS-1 AND UARS BATTERIES, THE LEVEL OF ITS SEVERITY HAS BEEN MUCH LOWER. THIS DIFFERENCE IN SEVERITY IS DENOTED IN THE ENSUING DATA PLOTS BY THE USE OF A SLIGHTLY DIFFERENT AND SLIGHTLY SMALLER "SUSPECT" SYMBOL FOR THE EUVE PLATE/CELL LOT.

** THESE PRE-ACCEPT CELLS CONTAINED 3 MILLILITERS LESS ELECTROLYTE THAN THE SUBSEQUENTLY-ACTIVATED FLIGHT CELLS. THEIR PERFORMANCE MAY ALSO HAVE BEEN COMPROMISED FROM DAMAGE RECEIVED DURING SHIPMENT TO NSWC-CRANE.

THE FORMAT

CHRONOLOGICALLY FROM LEFT TO RIGHT

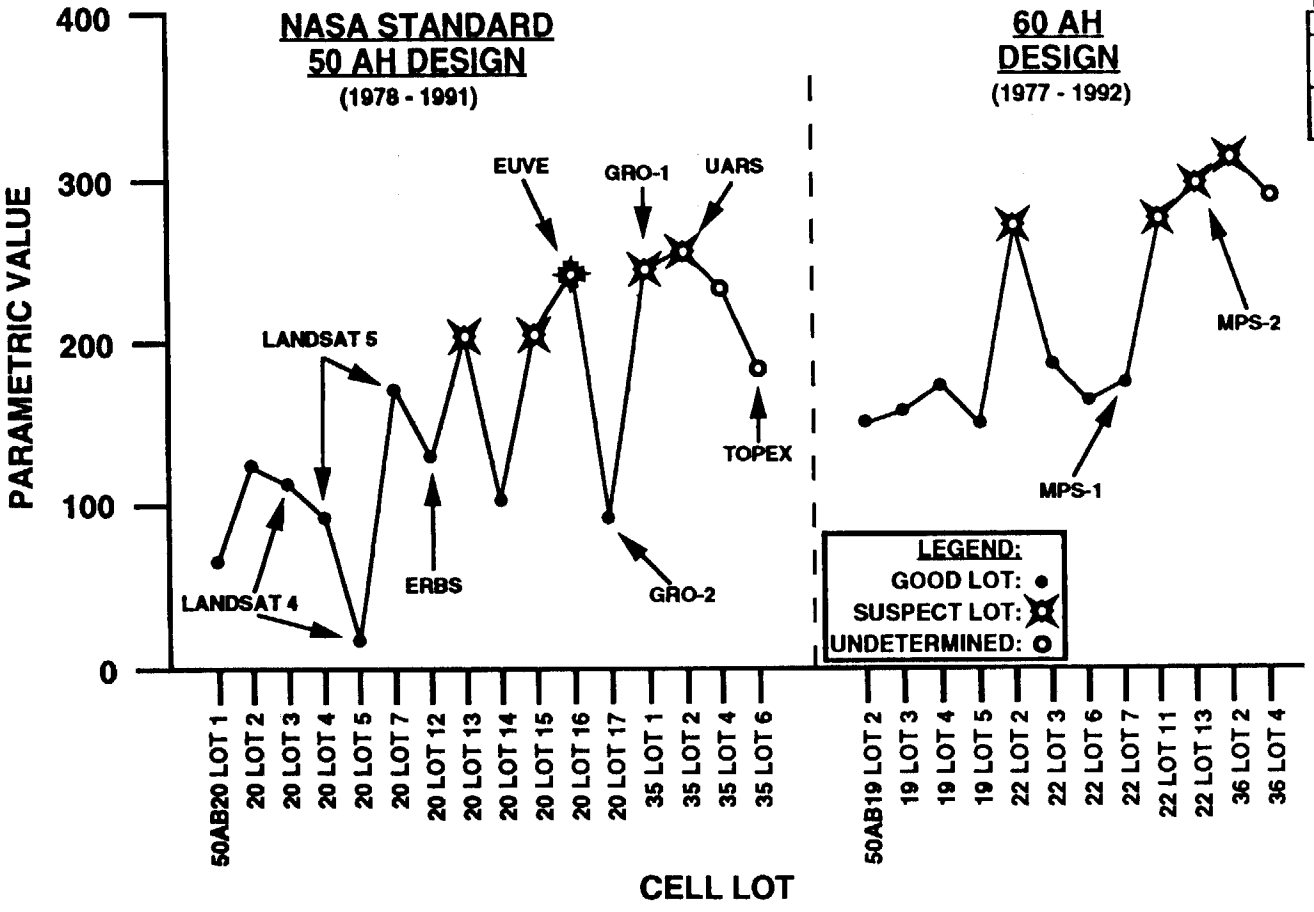

McDonnell Douglas Aerospace - Defense and Electronic Systems

BREAKDOWN OF CELL LOTS:

DISCRIMINATOR	GOOD	SUSPECT
> X.YYY VOLTS	1	7
< X.YYY VOLTS	15	2

NOT ALL CELL LOTS COULD BE EVALUATED vs ALL 16 DISCRIMINATORS DUE TO SLIGHT PROCESSING DIFFERENCES.

SOME CELL LOTS WERE HANDICAPPED WITH DEGRADED SEPARATOR. FOUR SUCH LOTS WERE IDENTIFIED; THREE FAILED PREMATURELY.

THE ERBS CELL LOT HAS BEEN RE-EVALUATED SINCE LAST YEAR'S STUDY. IT IS NOW CONSIDERED A "GOOD" CELL LOT BECAUSE ITS TWO BATTERIES GREATLY EXCEEDED MISSION LIFE REQUIREMENTS. THE BATTERIES DID, HOWEVER, DEVELOP SIGNIFICANT DIFFERENTIAL VOLTAGES AFTER LAUNCH. 4 OF 44 CELLS WERE LOST TO INTERNAL SHORTS BETWEEN 8 AND 9 YEARS AFTER LAUNCH.

ALL LOTS CONTAIN NYLON 2505 EXCEPT 50AB36 LOT 2 WHICH CONTAINS NYLON 2536 SEPARATOR, AND 50AB36 LOT 4 WHICH CONTAINS NYLON 2536.

50AB36 LOT 4 HAS ONE LESS POSITIVE AND ONE LESS NEGATIVE PLATE THAN ALL OTHER LOTS.

1. MEASURED NEGATIVE-TO-POSITIVE RATIO

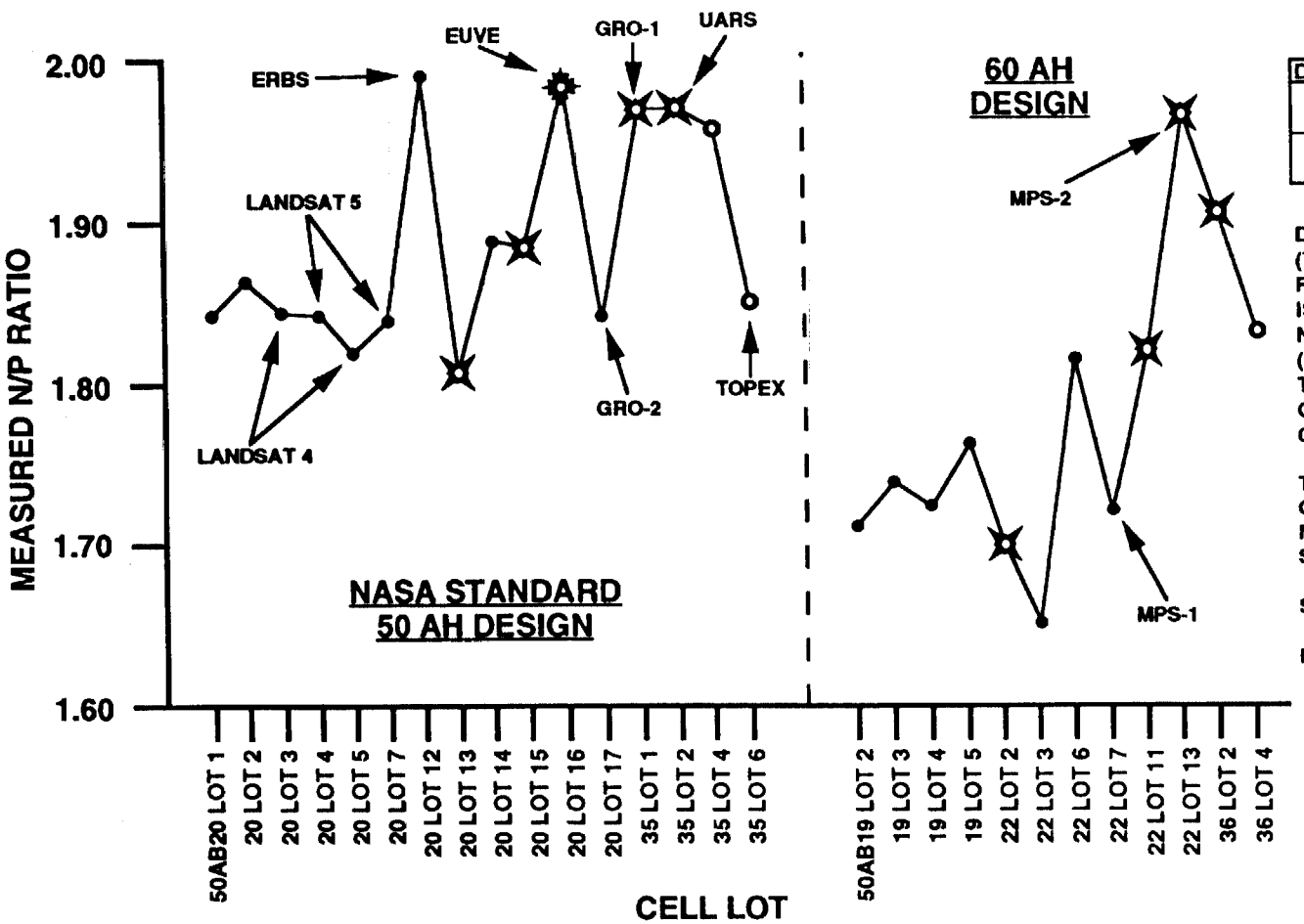

DISCRIMINATOR	GOOD	SUSPECT
> 1.9	1	5
< 1.9	15	4

DATA IS FROM 100% (TEMPORARY) FLOODED-CELL TESTING AND IS THE RATIO OF THE NEGATIVE PLATE CAPACITY (DISCHARGED TO -0.5 VOLTS) TO THE POSITIVE PLATE CAPACITY (DISCHARGED TO 0.7 VOLTS).

TEMPORARY FLOODED CELLS CONTAIN THE SAME NUMBER OF PLATES AS THE SEALED CELL.

SPEC MINIMUM IS 1.5

NO SPEC MAXIMUM.

2. RATIO OF POSITIVE LOADING WEIGHT TO TOTAL POSITIVE WEIGHT

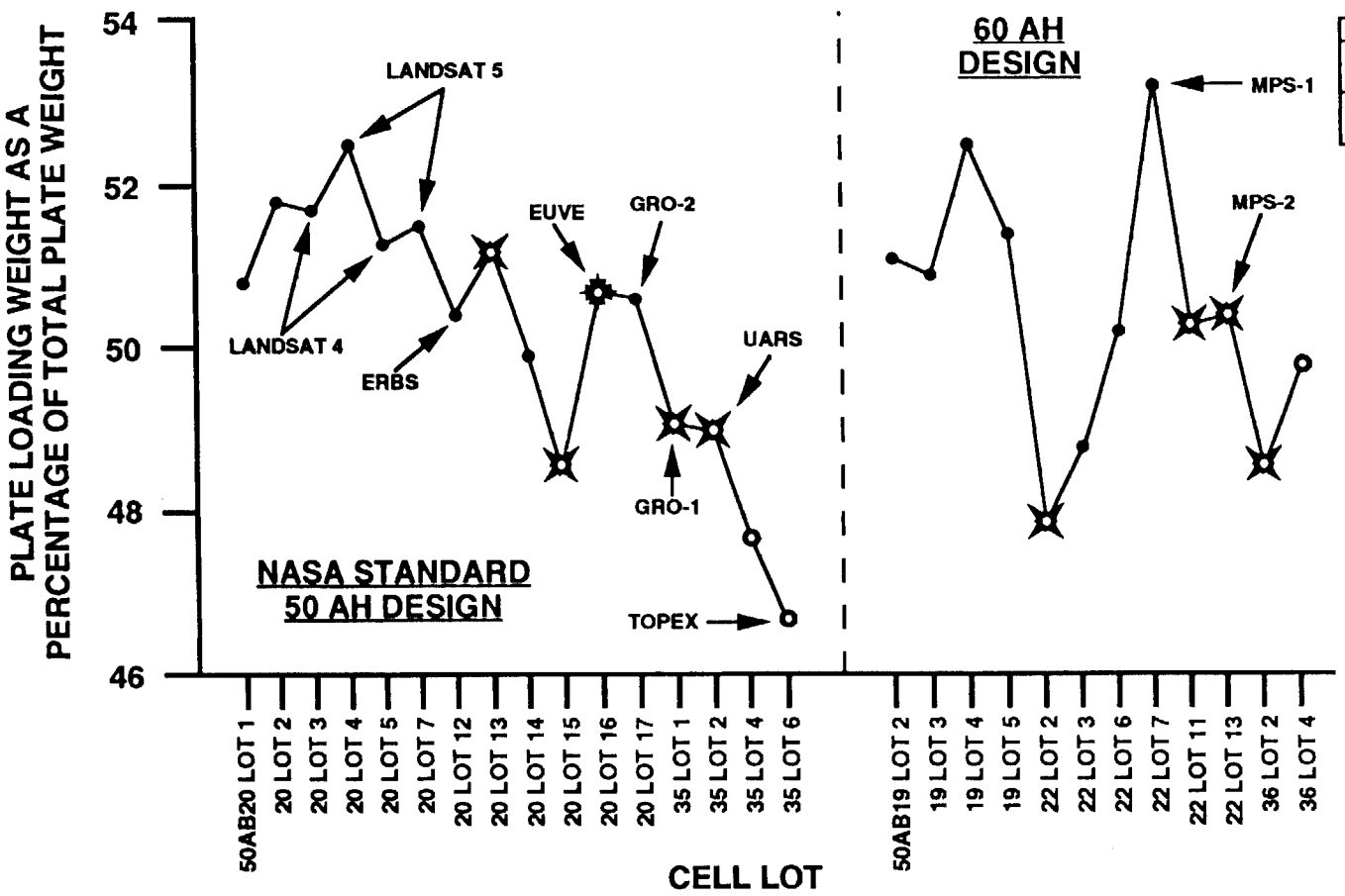

DISCRIMINATOR	GOOD	SUSPECT
< 50.6%	4	7
> 50.6%	12	2

NO SPEC MINIMUM OR MAXIMUM.

RATIO HAS DECREASING IN THE NASA DESIGN.

RATIO IN LATER LOTS IS LOWER THAN EARLY LOTS IN THE 60 AH DESIGN.

CAUSED BY A DECREASE IN CORROSION OF THE NICKEL SINTER (LESS NICKEL ATTACK) COMBINED WITH NO DECREASE IN PLATE LOADING.

NOTE: THIS DISCRIMINATOR IS THE LEAST UNDERSTOOD. IT IS LIKELY CONTRIBUTING TO LOWER ELECTROLYTE LEVELS (MORE PLATE MASS -> LESS CELL FREE VOLUME).

3. RATIO OF NEGATIVE LOADING WEIGHT TO TOTAL NEGATIVE WEIGHT

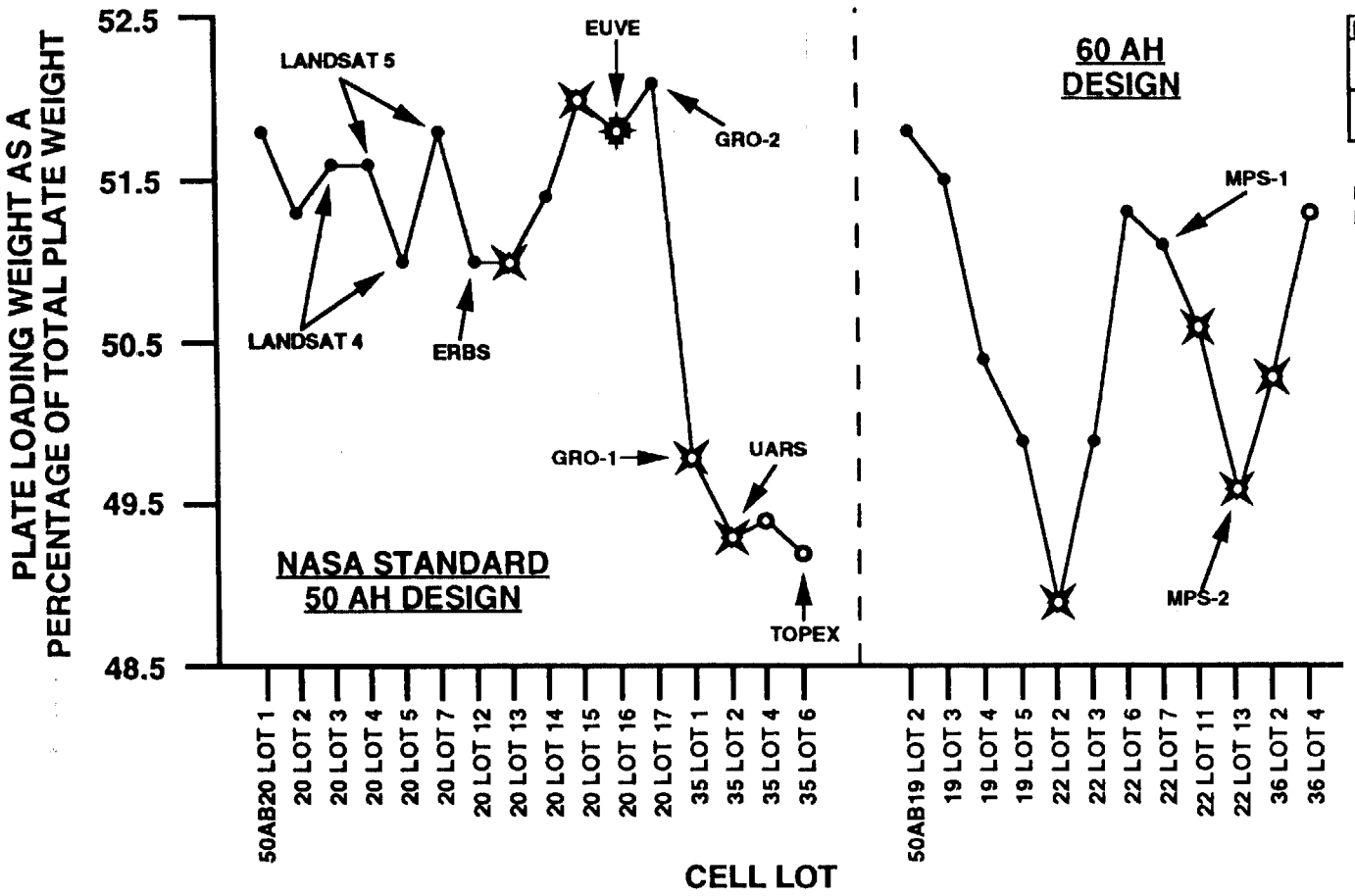

DISCRIMINATOR	GOOD	SUSPECT
≤ 50.6%	3	6
> 50.6%	13	3

NO SPEC MINIMUM OR MAXIMUM.

NASA DESIGN UNDERWENT A DRAMATIC CHANGE AFTER 1985. THE RATIO HAD BEEN DECLINING PARTLY AS A RESULT OF DECREASED (BY SPECIFICATION) LOADING (YET PLATE WEIGHT HAD REMAINED CONSTANT).

THE 60 AH DESIGN HAS VARIED CONSIDERABLY OVER THE LIFE OF ITS DESIGN.

NO KNOWN CHANGES TO THE STEEL SUBSTRATE.

PROBABLE FACTORS IN A DECREASED RATIO:

- HEAVIER SINTER (HEAVIER COATED WEIGHT).
- MORE CONVERSION OF THE SINTER TO NICKEL HYDROXIDE (A.K.A. NEGATIVE ANTI-POLAR MASS -> HEAVIER THAN NICKEL).

McDonnell Douglas Aerospace - Defense and Electronic Systems

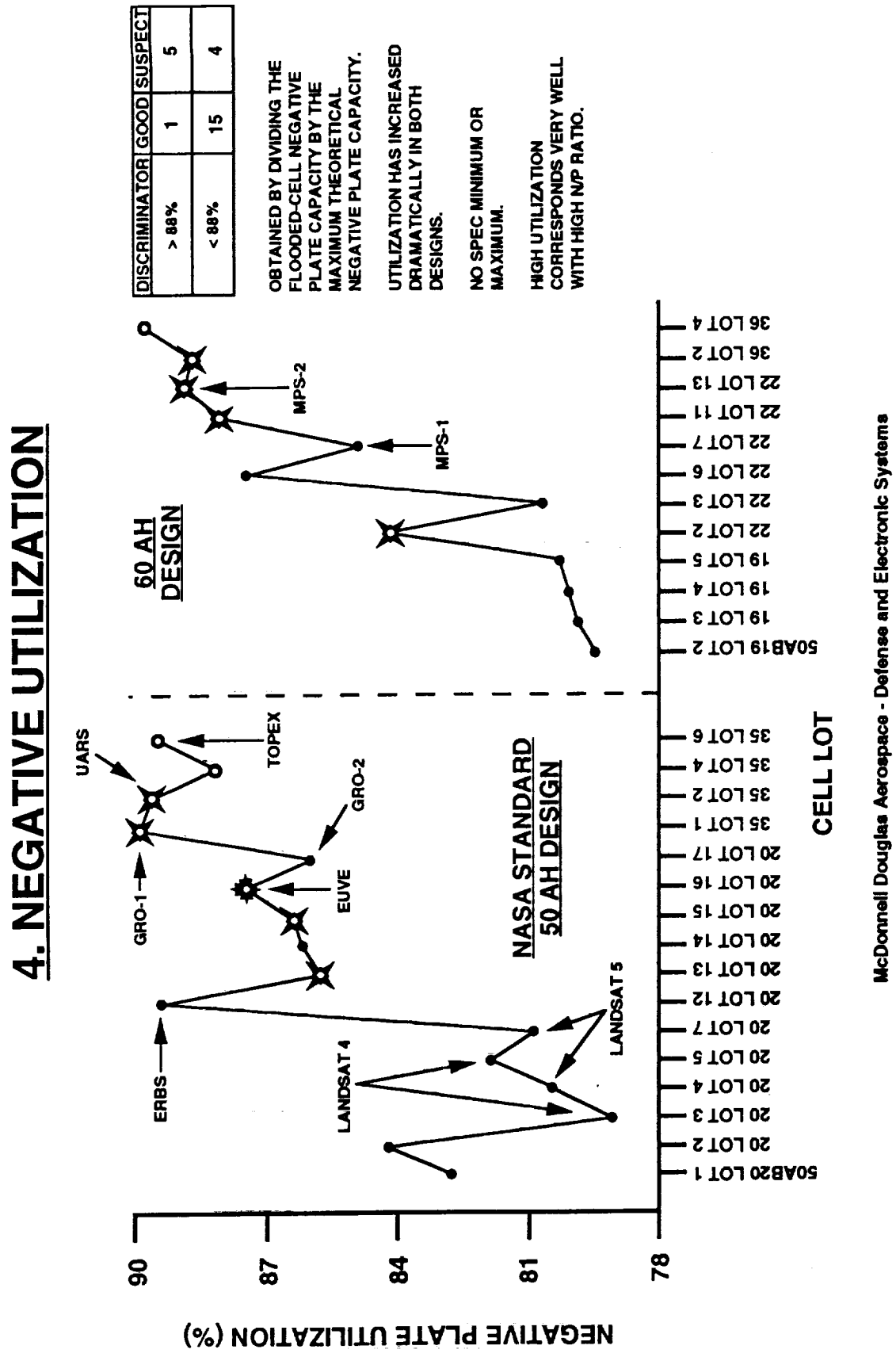
4. NEGATIVE UTILIZATION
DISCRIMINATOR | GOOD | SUSPECT
> 88% | 1 | 5
< 88% | 15 | 4
OBTAINED BY DIVIDING THE FLOODED-CELL NEGATIVE PLATE CAPACITY BY THE MAXIMUM THEORETICAL NEGATIVE PLATE CAPACITY.
UTILIZATION HAS INCREASED DRAMATICALLY IN BOTH DESIGNS.
NO SPEC MINIMUM OR MAXIMUM.
HIGH UTILIZATION CORRESPONDS VERY WELL WITH HIGH N/P RATIO.
60 AH DESIGN
NASA STANDARD 50 AH DESIGN
MPS-2
MPS-1
UARS
GRO-1
TOPEX
GRO-2
EUVE
ERBS
LANDSAT 4
LANDSAT 5
NEGATIVE PLATE UTILIZATION (%)
90
87
84
81
78
CELL LOT
50AB19 LOT 2
19 LOT 3
19 LOT 4
19 LOT 5
22 LOT 2
22 LOT 3
22 LOT 6
22 LOT 7
22 LOT 11
22 LOT 13
36 LOT 2
36 LOT 4
50AB20 LOT 1
20 LOT 2
20 LOT 3
20 LOT 4
20 LOT 5
20 LOT 7
20 LOT 12
20 LOT 13
20 LOT 14
20 LOT 15
20 LOT 16
20 LOT 17
35 LOT 1
35 LOT 2
35 LOT 4
35 LOT 6
McDonnell Douglas Aerospace - Defense and Electronic Systems

5. NEGATIVE ANTI-POLAR MASS (APM)

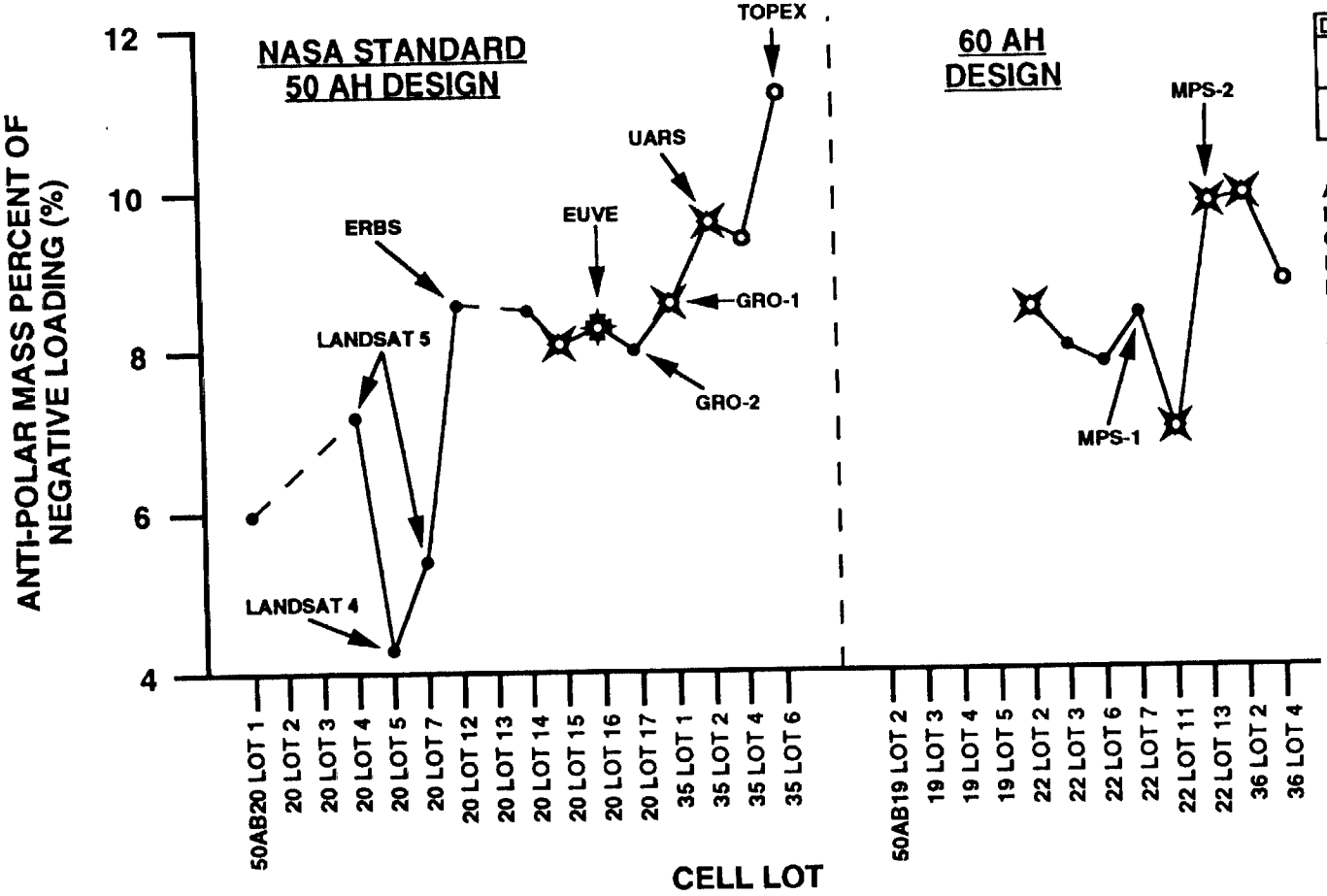

DISCRIMINATOR	GOOD	SUSPECT
> 8.5%	2	5
< 8.5%	8	3

APM IS THE NICKEL HYDROXIDE CREATED BY CORROSION OF THE SINTER IN THE IMPREGNATION PROCESS.

APM IS MUCH HIGHER IN RECENT LOTS OF BOTH DESIGNS.

NO SPEC MINIMUM OR MAXIMUM.

HIGH AMOUNTS OF APM CORRESPOND RATHER WELL WITH HIGH NEGATIVE UTILIZATION.

NO DATA FOR EITHER 50AB19 LOTS 2 THROUGH 5, OR 50AB20 LOTS 2, 3, AND 13.

McDonnell Douglas Aerospace - Defense and Electronic Systems

6. NEGATIVE PLATE TEFLON LOADING

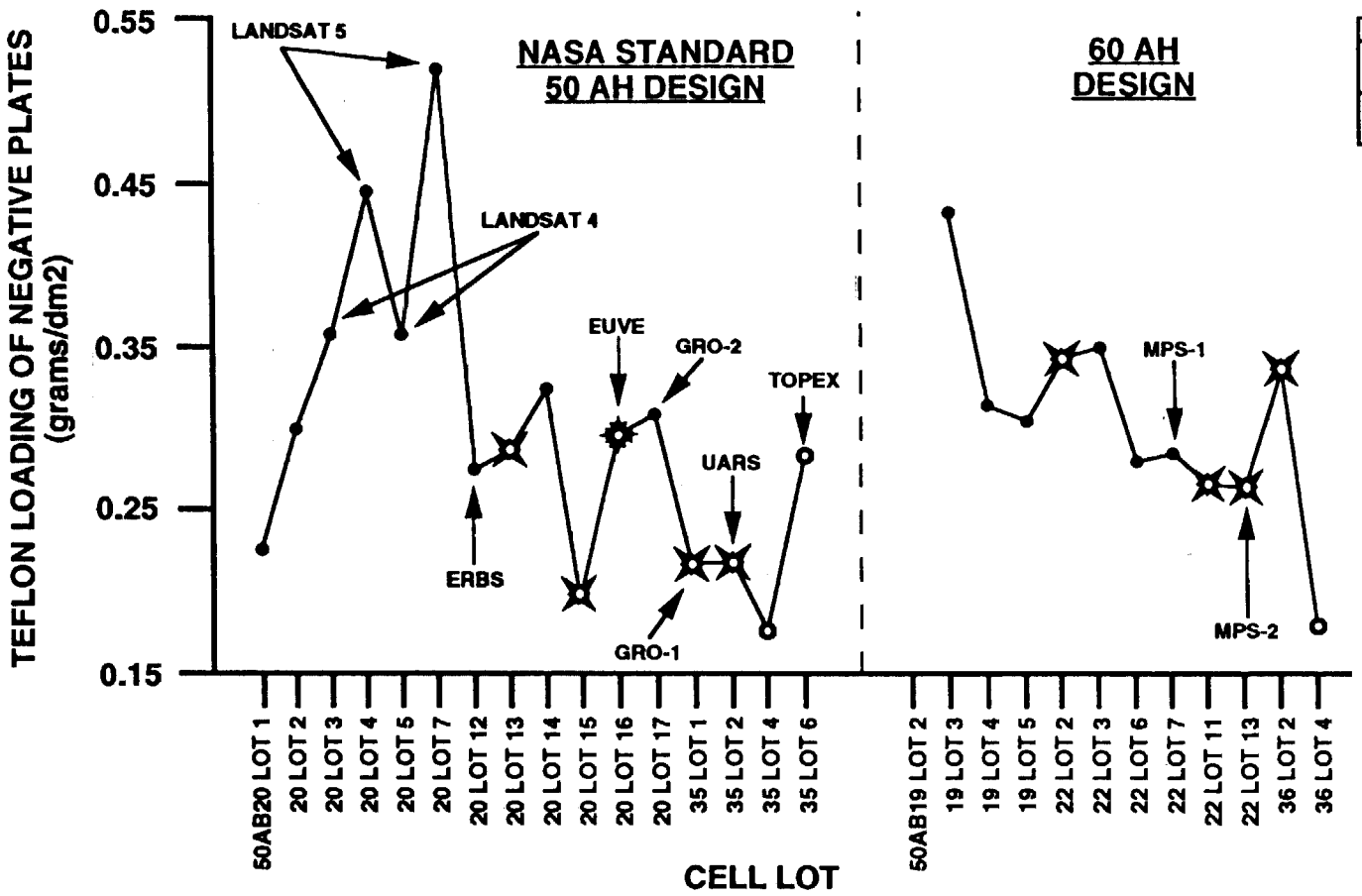

DISCRIMINATOR	GOOD	SUSPECT
< 0.28 gm/dm2	3	5
≥ 0.28 gm/dm2	12	4

NO SPEC MINIMUM OR MAXIMUM.

EARLY LOTS OF BOTH DESIGNS HAD 1.5 - 2.5 TIMES THE LOADING OF RECENT LOTS.

DECREASE MAY BE DUE TO CHANGES IN THE TREATMENT PROCESS AND/OR DUE TO THE CHARACTERISTICS OF THE PLATE UNDERGOING TREATMENT.

DECREASE IS A LIKELY CONTRIBUTOR TO REDUCED ELECTROLYTE AMOUNTS.

LOWER LEVELS OF TEFLON LOADING MAY BE LESS UNIFORM, RENDERING IT INEFFECTIVE AND/OR CREATING NON-UNIFORM DISTRIBUTION OF THE ELECTROLYTE.

NO DATA FOR 50AB19 LOT 2.

McDonnell Douglas Aerospace - Defense and Electronic Systems

FORMATION CYCLE PRESSURE TRENDS

THESE FOUR CYCLES ARE THE FIRST FOUR CHARGES AND DISCHARGES PERFORMED ON ALL NEW CELLS OF THESE TWO DESIGNS.

AT THIS POINT IN THEIR LIFE, CELLS OF THESE TWO DESIGNS SHOULD BE POSITIVE-LIMITED IN A DISCHARGE.

IDEALLY, ANY EXCESS OXYGEN GENERATED ON CHARGE WILL BE RECOMBINED ON THE SUBSEQUENT DISCHARGE. IF NOT, THERE MAY BE A PROBLEM WITH THE NEGATIVE ELECTRODE.

THE PRESENCE OF RESIDUAL UNRECOMBINED OXYGEN IS INDICATED BY A NET INCREASE IN THE BEGINNING OF CHARGE PRESSURE FROM THE 2ND TO THE 4TH FORMATION CYCLE.

THE PRESENCE OF RESIDUAL UNRECOMBINED OXYGEN CAN BE CONFIRMED BY OBSERVING THE FIRST FOUR HOURS OF CHARGING IN THE 4TH FORMATION CYCLE. IF CELL PRESSURE DECREASES IN THIS TIME FRAME, OXYGEN IS BEING CONSUMED BY THE NEWLY-CHARGED CADMIUM IN THE NEGATIVE PLATE.

ACCUMULATION OF LARGE AMOUNTS OF OXYGEN ON CHARGE, IN CONJUNCTION WITH SIGNIFICANT AMOUNTS OF OXYGEN NOT RECOMBINING ON DISCHARGE, HAS SHOWN A STRONG CORRELATION TO SUSPECT LOTS.

FORMATION CYCLE PRESSURE TRENDS (cont'd)

TWO NOTES OF CAUTION HOWEVER:

1.) **HIGH PRESSURES AND POOR RECOMBINATION MAY BE MASKED BY "UNDERFILLING" THE CELLS WITH ELECTROLYTE.**

2.) **CONVERSELY, HIGH PRESSURES AND POOR RECOMBINATION CAN BE ARTIFICIALLY INDUCED BY "OVERFILLING" THE CELLS WITH ELECTROLYTE.**

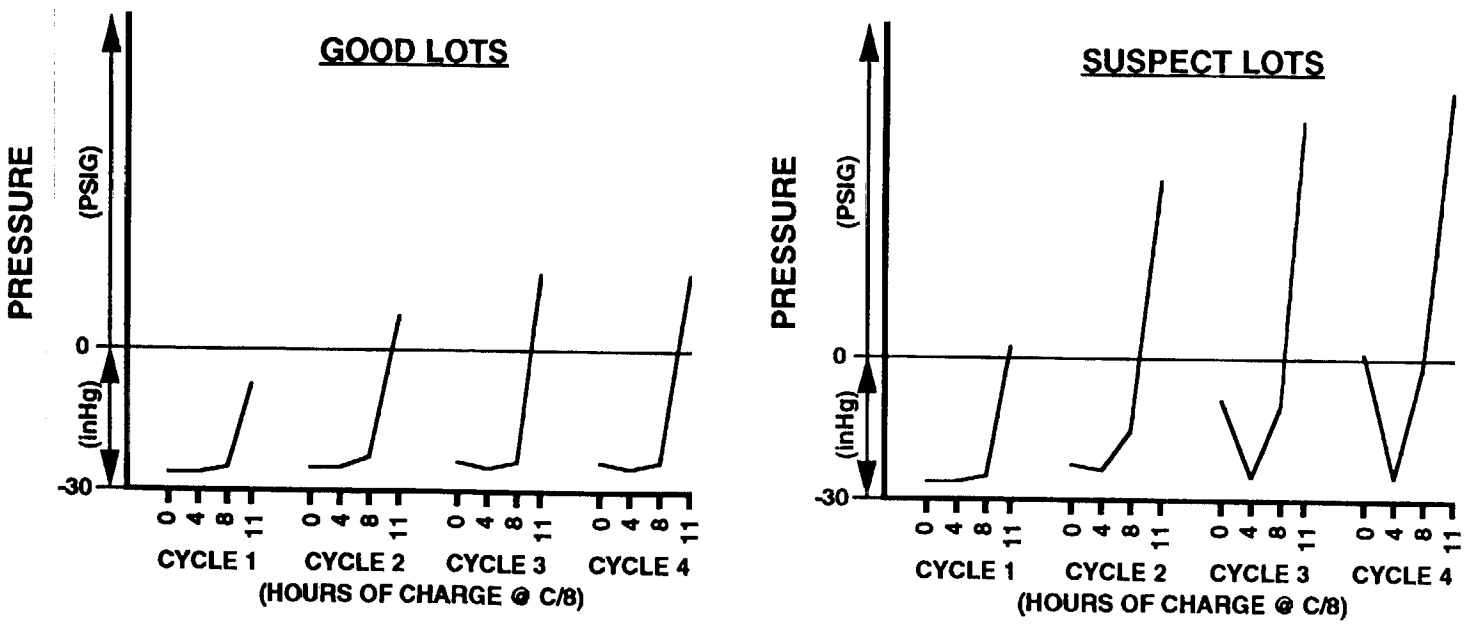

McDonnell Douglas Aerospace - Defense and Electronic Systems

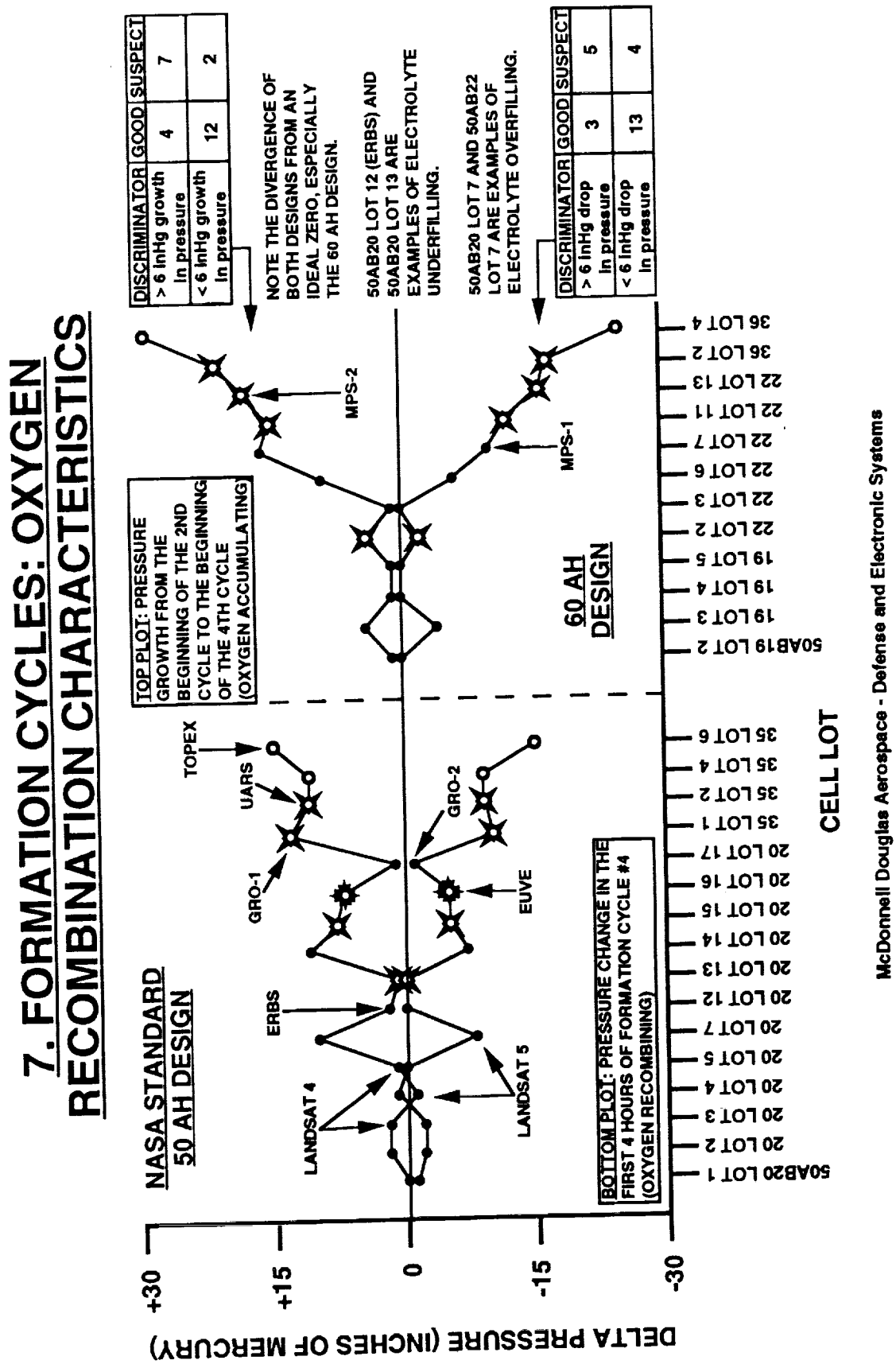
7. FORMATION CYCLES: OXYGEN RECOMBINATION CHARACTERISTICS
NASA STANDARD 50 AH DESIGN
60 AH DESIGN
TOP PLOT: PRESSURE GROWTH FROM THE BEGINNING OF THE 2ND CYCLE TO THE BEGINNING OF THE 4TH CYCLE (OXYGEN ACCUMULATING)
BOTTOM PLOT: PRESSURE CHANGE IN THE FIRST 4 HOURS OF FORMATION CYCLE #4 (OXYGEN RECOMBINING)
DISCRIMINATOR | GOOD | SUSPECT
> 6 inHg growth in pressure | 4 | 7
< 6 inHg growth in pressure | 12 | 2
NOTE THE DIVERGENCE OF BOTH DESIGNS FROM AN IDEAL ZERO, ESPECIALLY THE 60 AH DESIGN.
50AB20 LOT 12 (ERBS) AND 50AB20 LOT 13 ARE EXAMPLES OF ELECTROLYTE UNDERFILLING.
50AB20 LOT 7 AND 50AB22 LOT 7 ARE EXAMPLES OF ELECTROLYTE OVERFILLING.
DISCRIMINATOR | GOOD | SUSPECT
> 6 inHg drop in pressure | 3 | 5
< 6 inHg drop in pressure | 13 | 4
MPS-2
MPS-1
TOPEX
UARS
GRO-1
ERBS
LANDSAT 4
GRO-2
EUVE
LANDSAT 5
+30
+15
0
-15
-30
DELTA PRESSURE (INCHES OF MERCURY)
50AB20 LOT 1
20 LOT 2
20 LOT 3
20 LOT 4
20 LOT 5
20 LOT 7
20 LOT 12
20 LOT 13
20 LOT 14
20 LOT 15
20 LOT 16
20 LOT 17
35 LOT 1
35 LOT 2
35 LOT 4
35 LOT 6
50AB19 LOT 2
19 LOT 3
19 LOT 4
19 LOT 5
22 LOT 2
22 LOT 3
22 LOT 6
22 LOT 7
22 LOT 11
22 LOT 13
36 LOT 2
36 LOT 4
CELL LOT
McDonnell Douglas Aerospace - Defense and Electronic Systems

8. MAXIMUM CAPACITY DURING FORMATION CYCLING

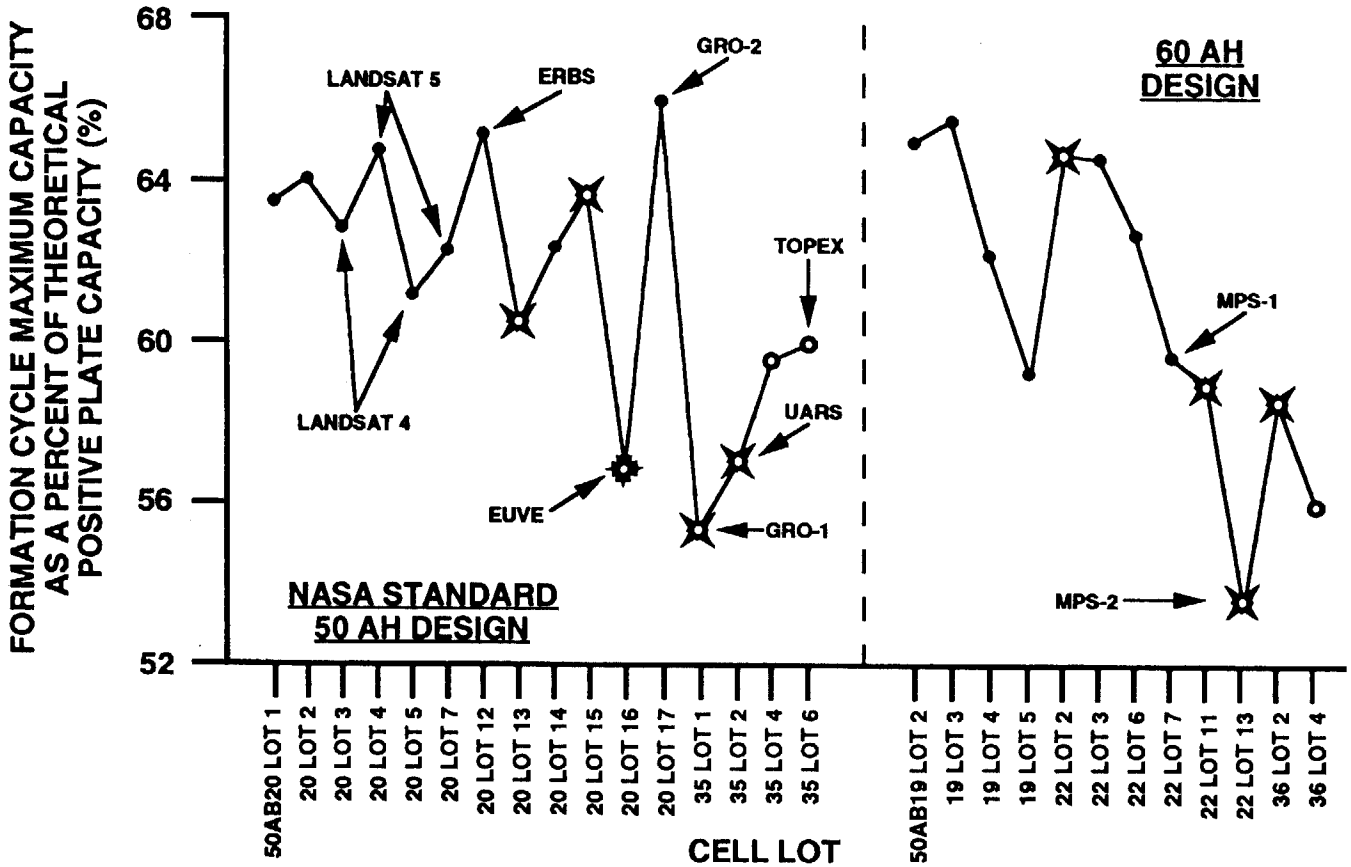

DISCRIMINATOR	GOOD	SUSPECT
≤ 59% OF THEORETICAL	0	6
> 59% OF THEORETICAL	16	3

A MINIMUM OF FOUR CYCLES ARE PERFORMED.

DISCHARGES TO 1.0 VOLT SHOULD BE LIMITED BY THE POSITIVE ELECTRODE.

PRIOR TO 1983, FORMATION CYCLE CHARGE TIME WAS 12 HOURS AND MAXIMUM CAPACITY WAS OBTAINED ON THE FIRST CYCLE.

AFTER 1983, CHARGE TIME WAS REDUCED TO 11 HOURS AND MAXIMUM CAPACITY WAS OBTAINED IN THE SECOND CYCLE.

DATA OBTAINED FROM DIVIDING MAXIMUM FORMATION CYCLE CAPACITY BY MAXIMUM THEORETICAL POSITIVE PLATE CAPACITY.

CAN ALSO BE PLOTTED AS A PERCENT OF THE FLOODED-CELL POSITIVE PLATE CAPACITY:

DISCRIMINATOR	GOOD	SUSPECT
< 77% of flooded cell capacity	1	7
> 77% of flooded cell capacity	15	2

McDonnell Douglas Aerospace - Defense and Electronic Systems

9. OXYGEN RECOMBINED IN PRECHARGE
DPA CELLS VS OXYGEN PRECHARGE GOAL

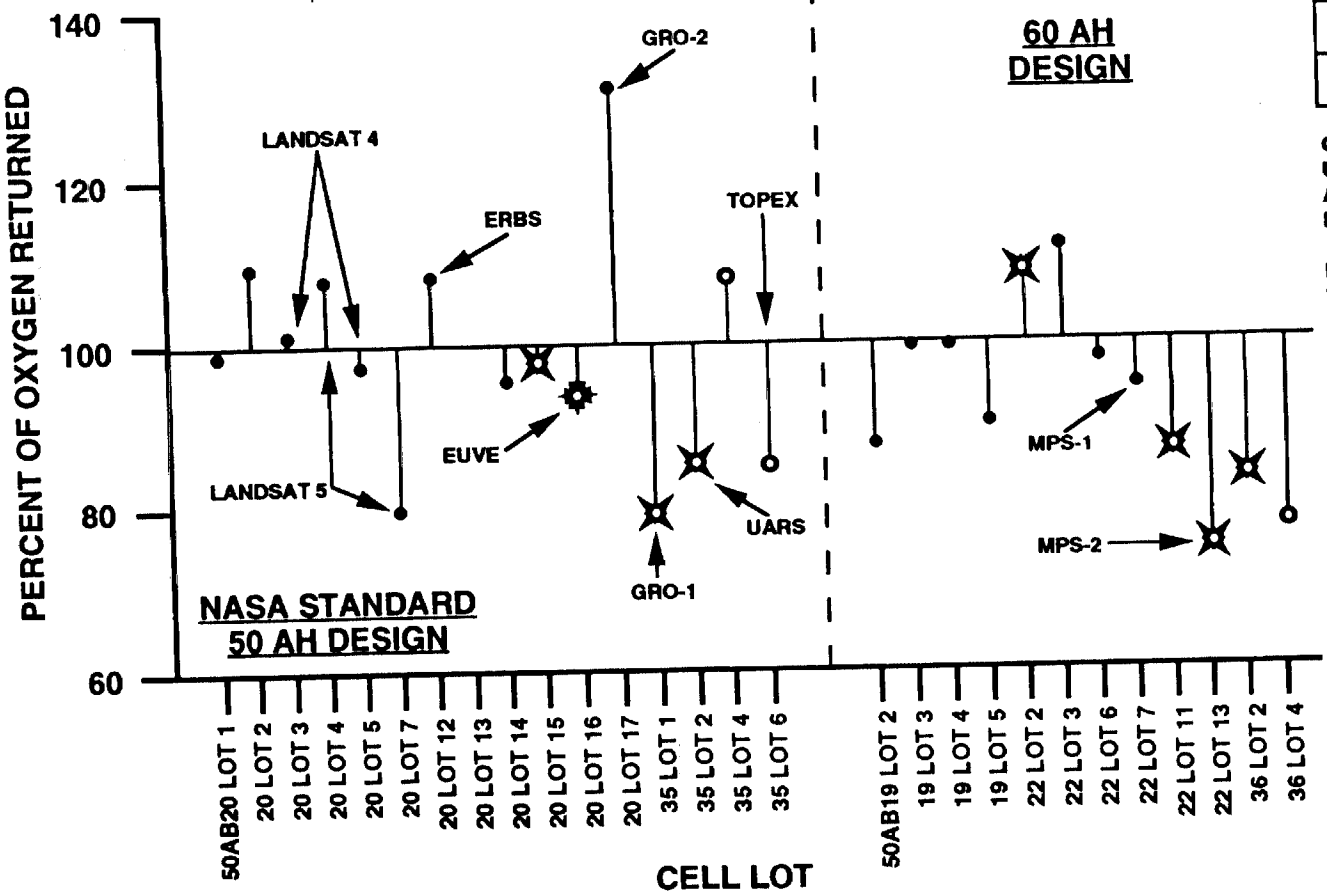

DISCRIMINATOR	GOOD	SUSPECT
< 90%	2	5
> 90%	14	3

ONE CELL FROM EACH LOT UNDERGOES DESTRUCT PHYSICAL ANALYSIS (DPA) TO VERIFY NEGATIVE PRECHARGE.

DPA IS INITIATED BY BACK-FILLING A DISCHARGED CELL WITH OXYGEN UNTIL NO MORE OXYGEN RECOMBINES.

THE OXYGEN ADDED BACK SHOULD BE NEARLY EQUAL TO THE AMOUNT VENTED IN PRECHARGE.

SIGNIFICANT INABILITY TO REACH 100% OXYGEN RETURN MAY SIGNAL A PROBLEM WITH THE NEGATIVE ELECTRODE. [IN SUCH LOTS, CHEMICAL ANALYSIS CONFIRMS THAT THE TOTAL PRECHARGE (RESIDUAL + OXYGEN) WAS CORRECT, BUT THAT THE RESIDUAL IS HIGHER THAN NORMAL.]

SUGGESTS THAT THE MORPHOLOGY OF THE NEGATIVE IS UNDERGOING DRAMATIC CHANGE EVEN AS PRECHARGE IS BEING SET.

NO PRECHARGE DPA CELL FOR 50AB20 LOT 13.

McDonnell Douglas Aerospace - Defense and Electronic Systems

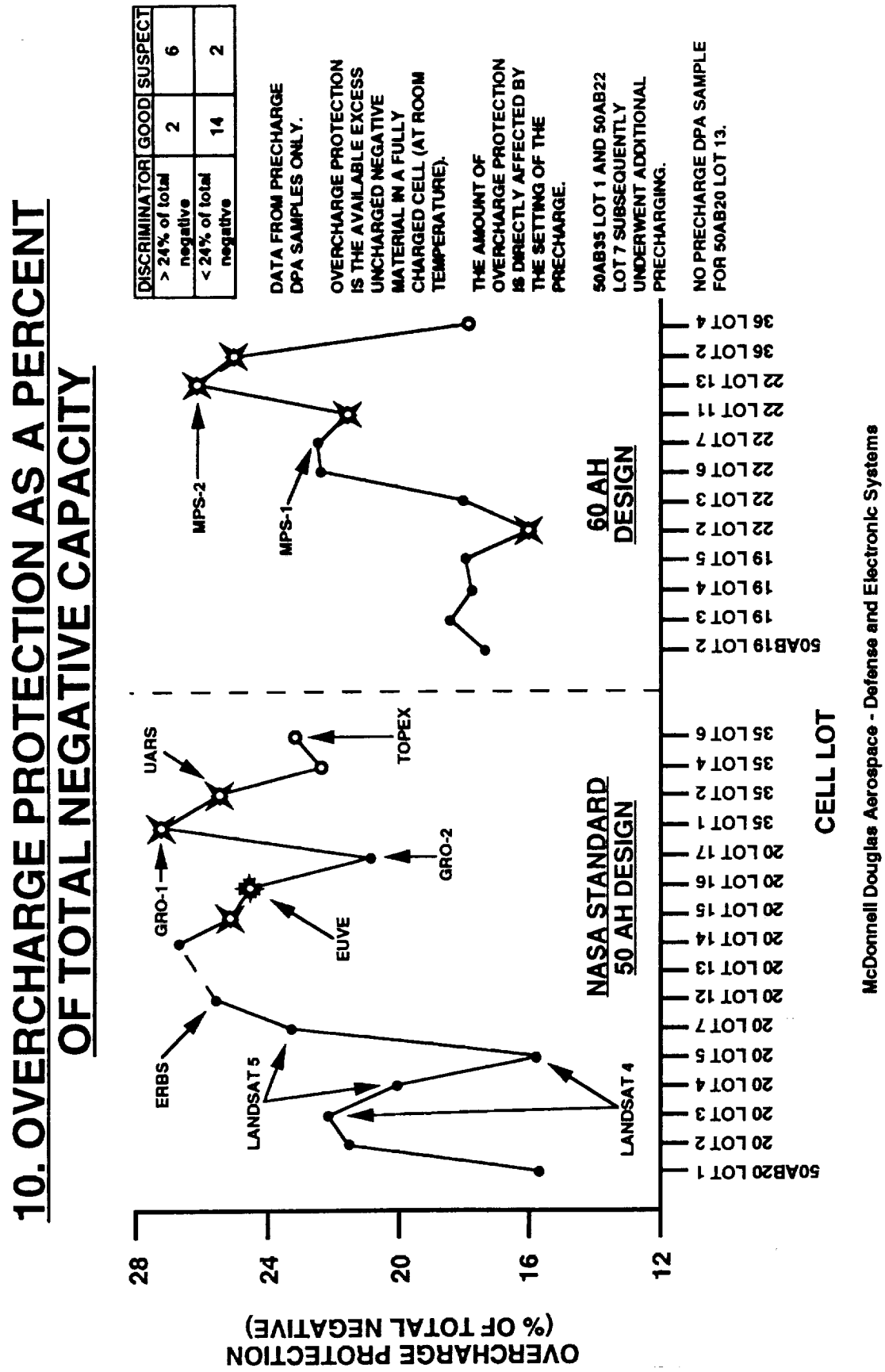
10. OVERCHARGE PROTECTION AS A PERCENT OF TOTAL NEGATIVE CAPACITY
DISCRIMINATOR | GOOD | SUSPECT
> 24% of total negative | 2 | 6
< 24% of total negative | 14 | 2
DATA FROM PRECHARGE DPA SAMPLES ONLY.
OVERCHARGE PROTECTION IS THE AVAILABLE EXCESS UNCHARGED NEGATIVE MATERIAL IN A FULLY CHARGED CELL (AT ROOM TEMPERATURE).
THE AMOUNT OF OVERCHARGE PROTECTION IS DIRECTLY AFFECTED BY THE SETTING OF THE PRECHARGE.
50AB35 LOT 1 AND 50AB22 LOT 7 SUBSEQUENTLY UNDERWENT ADDITIONAL PRECHARGING.
NO PRECHARGE DPA SAMPLE FOR 50AB20 LOT 13.
OVERCHARGE PROTECTION (% OF TOTAL NEGATIVE)
28
24
20
16
12
ERBS
LANDSAT 5
LANDSAT 4
GRO-1
EUVE
GRO-2
UARS
TOPEX
MPS-1
MPS-2
NASA STANDARD 50 AH DESIGN
60 AH DESIGN
CELL LOT
50AB20 LOT 1
20 LOT 2
20 LOT 3
20 LOT 4
20 LOT 5
20 LOT 7
20 LOT 12
20 LOT 13
20 LOT 14
20 LOT 15
20 LOT 16
20 LOT 17
35 LOT 1
35 LOT 2
35 LOT 4
35 LOT 6
50AB19 LOT 2
19 LOT 3
19 LOT 4
19 LOT 5
22 LOT 2
22 LOT 3
22 LOT 6
22 LOT 7
22 LOT 11
22 LOT 13
36 LOT 2
36 LOT 4
McDonnell Douglas Aerospace - Defense and Electronic Systems

11. MAXIMUM RECORDED VOLTAGE IN THE 0°C CAPACITY TEST

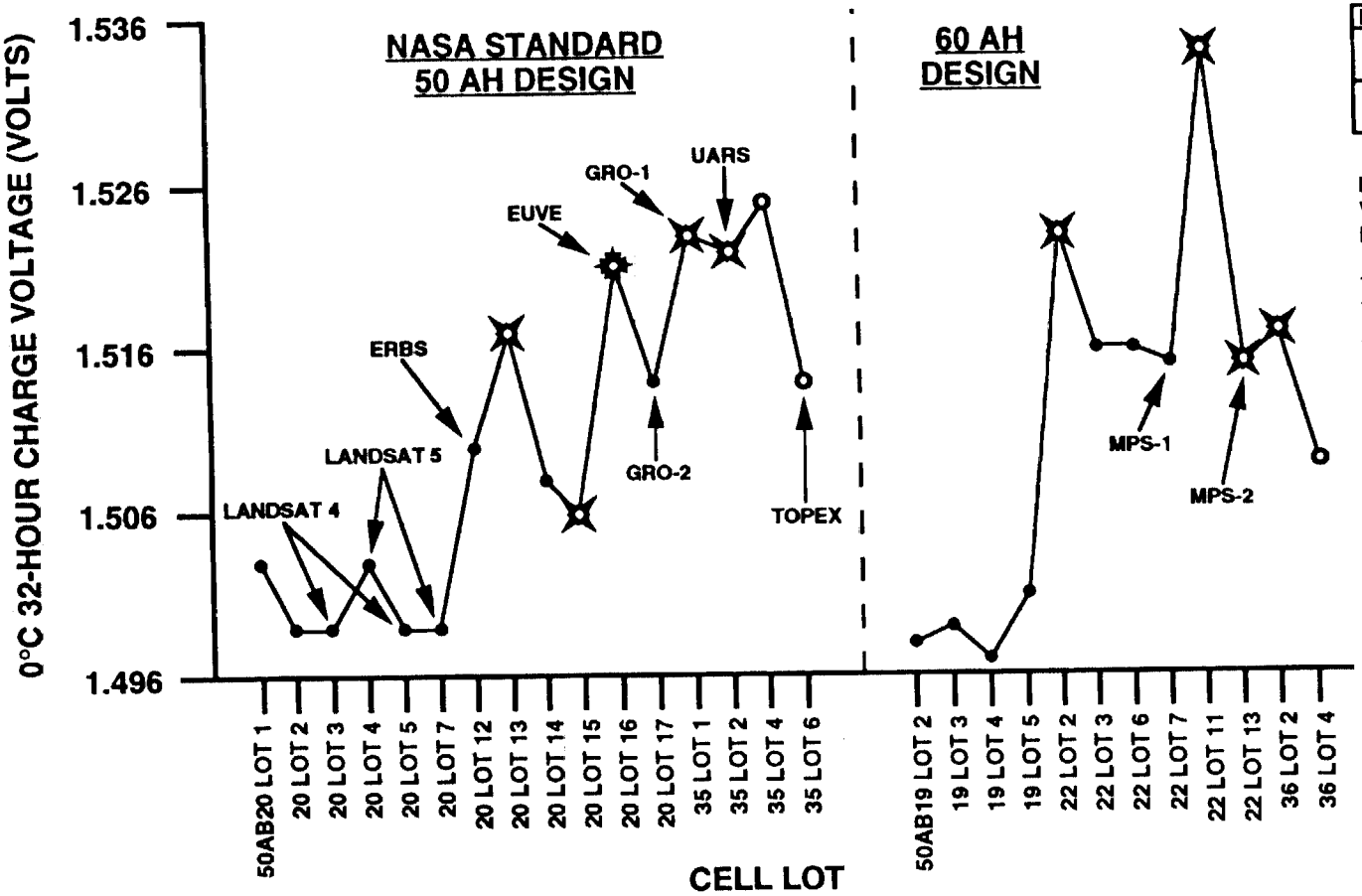

DISCRIMINATOR	GOOD	SUSPECT
> 1.517 VOLTS	0	7
< 1.517 VOLTS	16	2

MAXIMUM RECORDED VOLTAGE OCCURS AT 32 HOURS INTO CHARGE.

THE 32-HOUR CHARGE VOLTAGE IS THE CLOSEST AVAILABLE DATA FOR MAXIMUM (ROLLOVER) VOLTAGE.

BOTH THE MAXIMUM AND END-OF-CHARGE VOLTAGES (NOT SHOWN) HAVE INCREASED SIGNIFICANTLY (20 - 30 MILLIVOLTS) OVER TIME IN BOTH DESIGNS.

THE TREND RAISES THE CONCERN THAT RECENTLY-MADE CELLS MAY NOT BE AS COMPATIBLE WITH THE NASA STANDARD V/T LEVELS.

12. 0°C CAPACITY

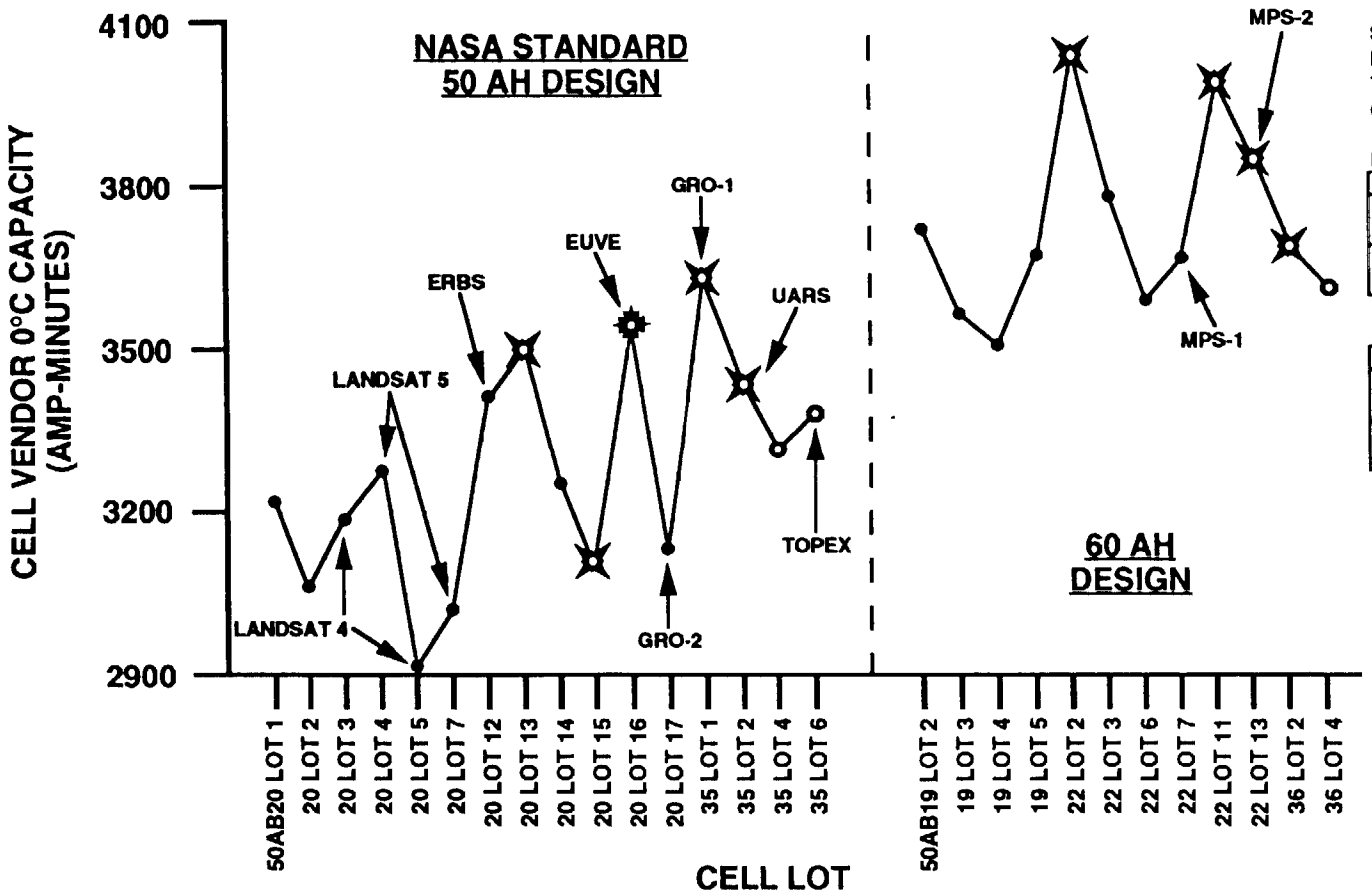

SINCE POSITIVE PLATE LOADING IS A FACTOR, THE TWO DESIGNS SHOULD BE CONSIDERED SEPARATELY:

NASA:

DISCRIMINATOR	GOOD	SUSPECT
> 3400 amp-minutes	1	4
< 3400 amp-minutes	8	1

60 AH DESIGN:

DISCRIMINATOR	GOOD	SUSPECT
> 3800 amp-minutes	0	3
< 3800 amp-minutes	7	1

NO SPEC MAXIMUM.

CAPACITIES IN THE NASA DESIGN HAVE VARIED GREATLY AND HAVE SHOWN A GENERAL INCREASE WITH TIME.

CAPACITIES IN THE 60 AH DESIGN ARE HIGHER THAN NASA, BUT WITHIN THE RANKS OF THE 60 AH DESIGN, CERTAIN LOTS ARE HIGHER THAN OTHERS.

McDonnell Douglas Aerospace - Defense and Electronic Systems

13. FINAL ELECTROLYTE AMOUNT

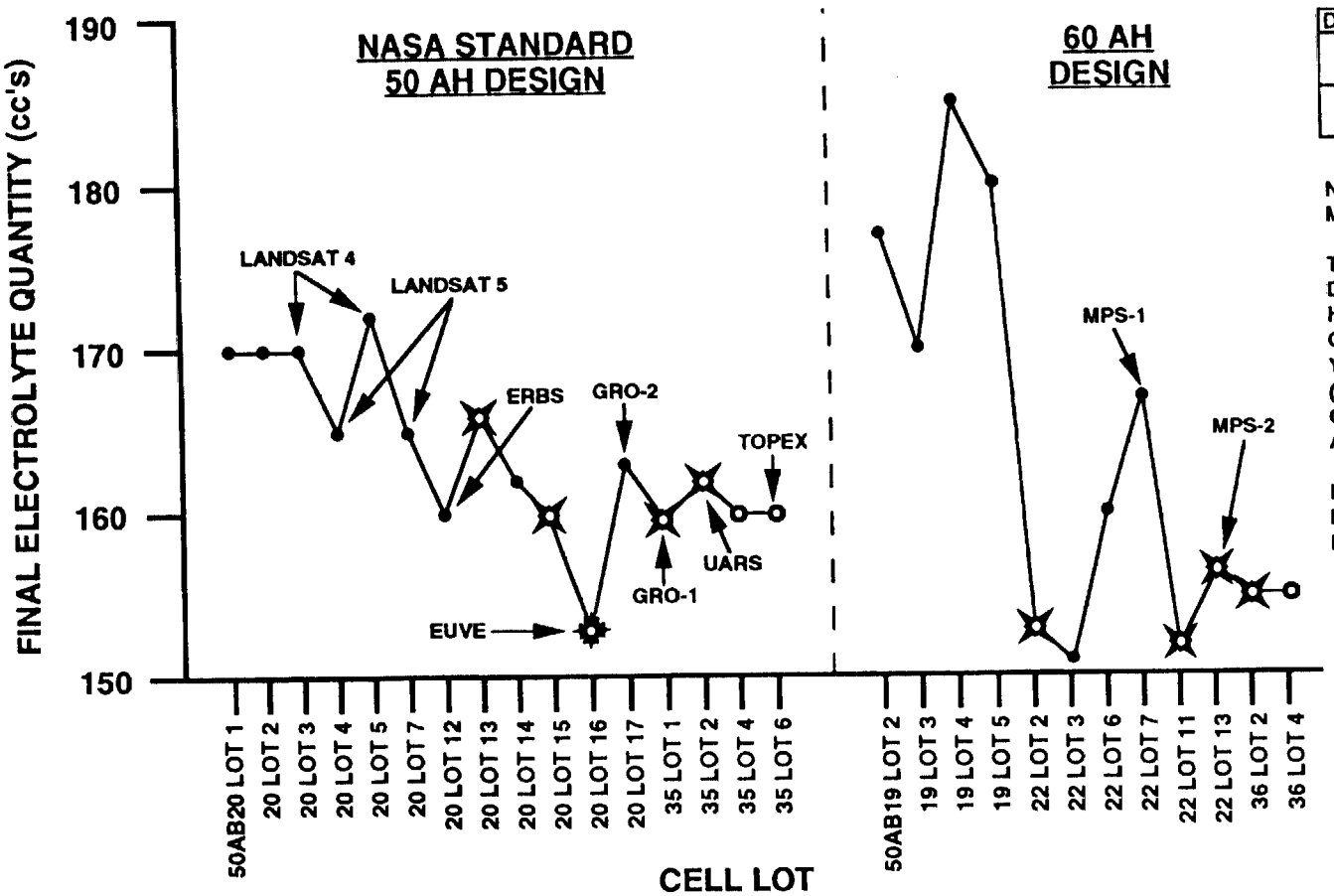

DISCRIMINATOR	GOOD	SUSPECT
< 162 cc's	3	8
≥ 162 cc's	13	1

NO SPEC MINIMUM OR MAXIMUM.

THERE HAS BEEN A DECREASE FROM THE HIGHER AMOUNTS OBSERVED IN THE EARLY YEARS OF BOTH DESIGNS (~6% LESS FOR NASA AND OVER 12% LESS FOR THE 60 AH DESIGN).

BOTH DESIGNS SEEM TO HAVE REACHED A "PLATEAU" FOR ELECTROLYTE AMOUNT.

McDonnell Douglas Aerospace - Defense and Electronic Systems

14. POSITIVE CAPACITY TO 0.0 VOLTS IN DPA CELLS

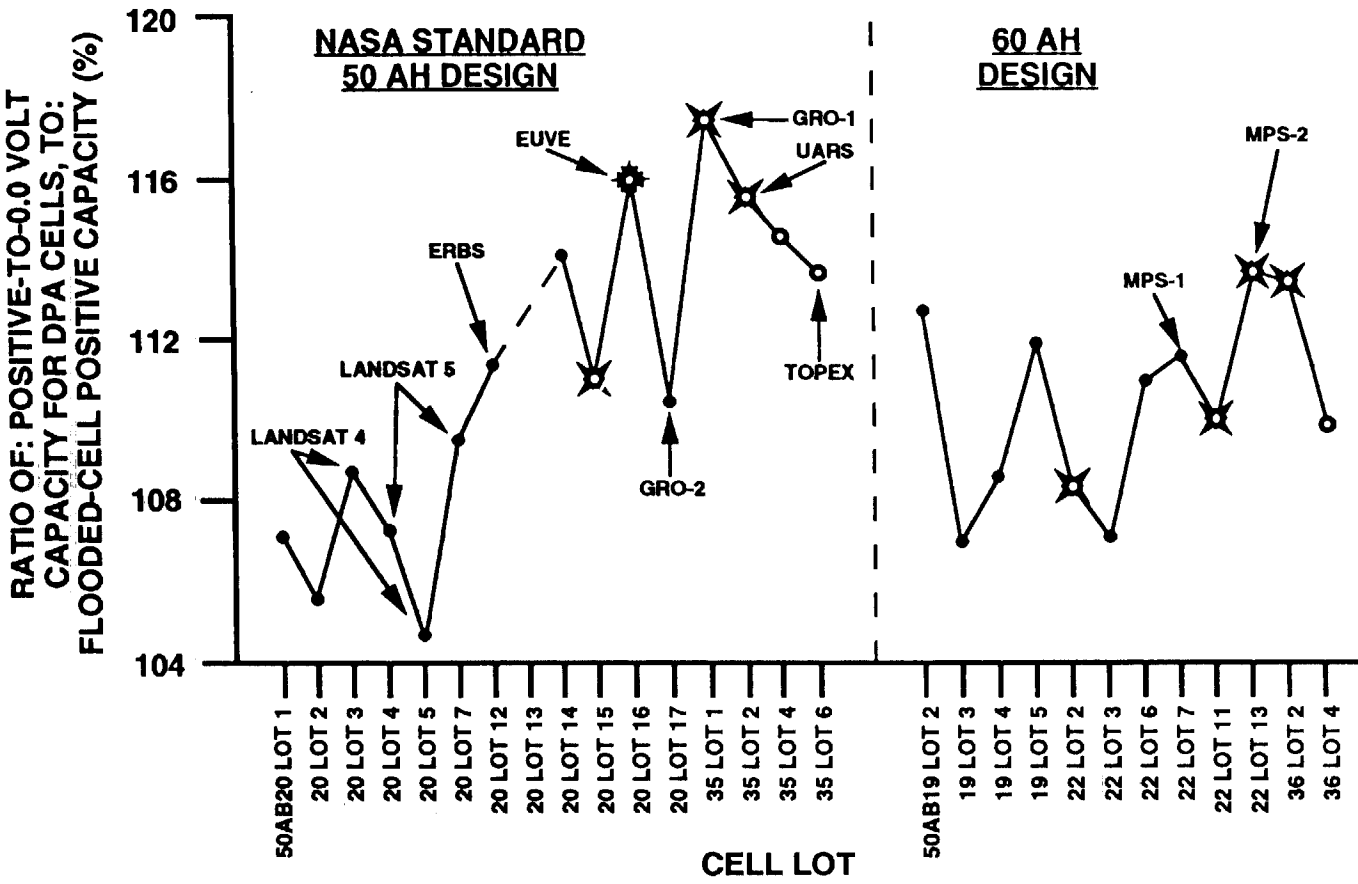

DISCRIMINATOR	GOOD	SUSPECT
> 112%	2	5
< 112%	14	3

BASED ON ALL AVAILABLE STANDARD DPA CELLS:
- PRECHARGE
- POST-ATP
- POST 500-CYCLE

CAPACITY TO 0.0 VOLTS OBTAINED BY A COMBINATION OF A C/2 DISCHARGE FOLLOWED BY RESISTIVE LETDOWN.

AVERAGE CAPACITY TO 0.0 VOLTS OF ALL DPA SAMPLES IS THEN DIVIDED BY THE LOT AVERAGE FLOODED-CELL POSITIVE CAPACITY.

NO SPEC MINIMUM OR MAXIMUM.

COMBINED WITH OTHER ANALYSIS (NOT SHOWN) SUGGESTS THAT A GREAT DEAL OF CAPACITY IS CONTAINED BELOW ONE VOLT IN THE CELLS OF SUSPECT LOTS.

NO STANDARD DPA CELLS FOR 50AB20 LOT 13.

15. TRANSFER OF CADMIUM TO THE POSITIVE PLATE UNDER LIMITED CYCLING

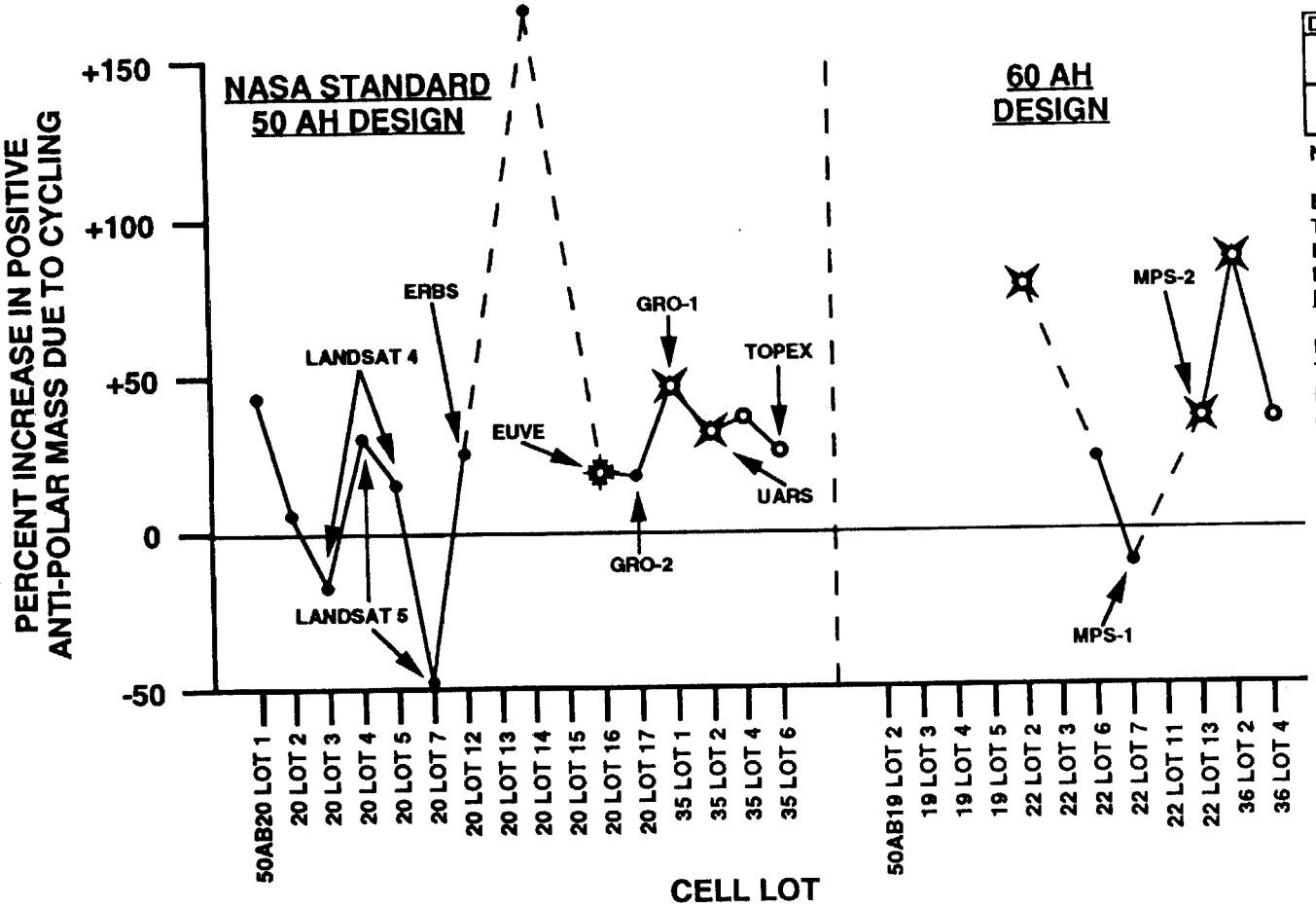

DISCRIMINATOR	GOOD	SUSPECT
> 31%	2	5
< 31%	9	1

NO SPEC MINIMUM OR MAXIMUM.

BOTH DESIGNS HAVE CADMIUM TREATED POSITIVE PLATES (A.K.A. POSITIVE APM), EXCEPT FOR 50AB20 LOT 14 WHICH WAS INADVERTENTLY NOT TREATED.

DATA DERIVED BY CALCULATING THE DELTA IN POSITIVE APM BETWEEN EARLY PLATE SAMPLES (BLANKING, FLOODED-CELL PACKS, DECARB PACKS, PRECHARGE DPA CELLS) AND LATER PLATE SAMPLES (POST 500-CYCLE OR POST-ATP DPA CELLS).

MAY INDICATE THE NEGATIVE PLATE'S PROPENSITY TO LOSE ACTIVE MATERIAL AND/OR THE SEPARATOR'S PROPENSITY TO LET IT PASS.

A TENUOUS DISCRIMINATOR AS IT USUALLY RELIES ON A SINGLE "LATER" SAMPLE .

HAS ALSO BEEN PLOTTED AS DELTA CADMIUM HYDROXIDE:

DISCRIMINATOR	GOOD	SUSPECT
> 0.2 gm/dm2	2	4
< 0.2 gm/dm2	9	2

McDonnell Douglas Aerospace - Defense and Electronic Systems

16. RATIO OF CELL-LEVEL 0°C CAPACITY TO BATTERY-LEVEL 0°C CAPACITY

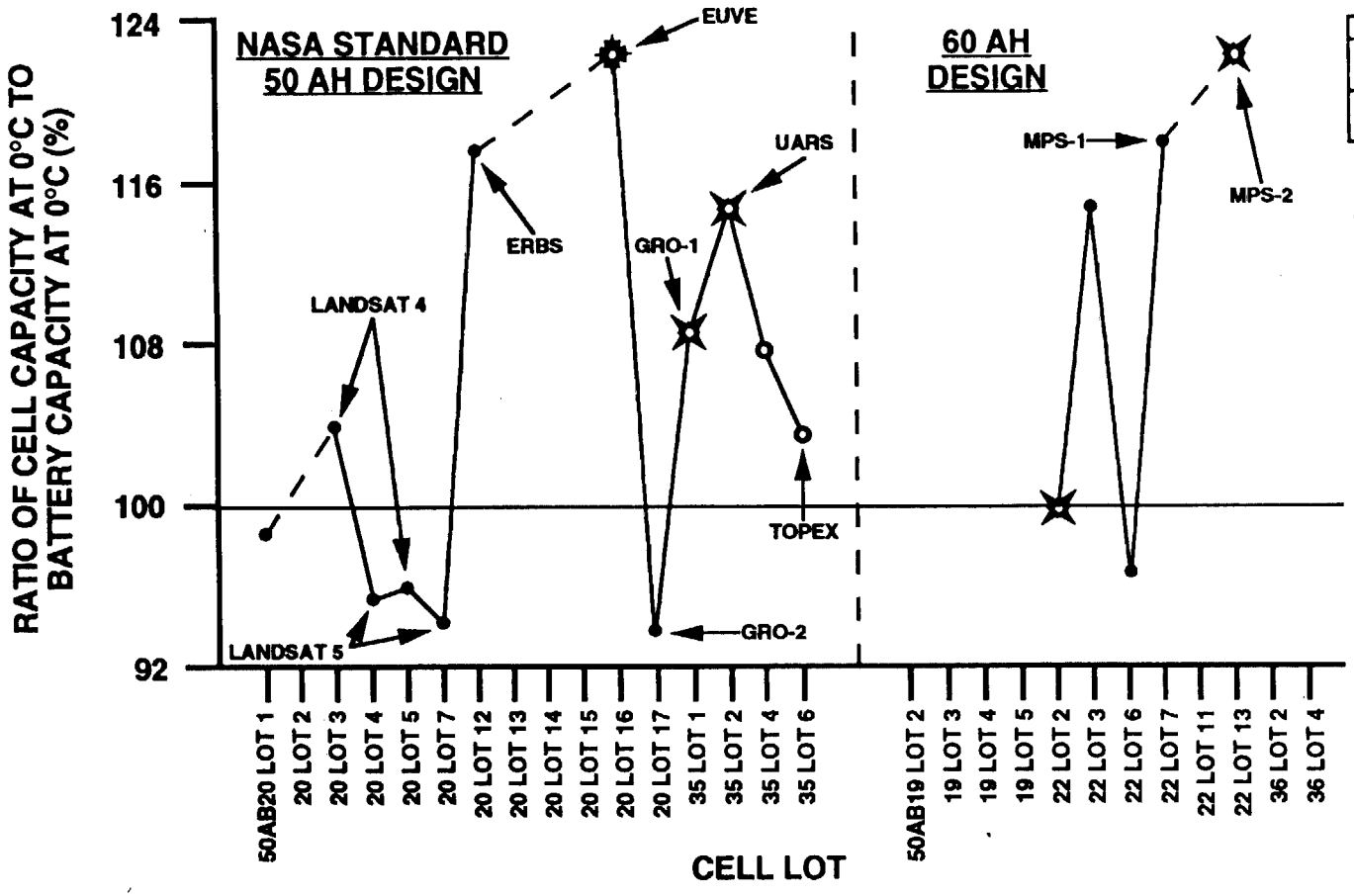

DISCRIMINATOR	GOOD	SUSPECT
> 108%	3	4
< 108%	7	1

NO DIRECT SPEC MINIMUM OR MAXIMUM.

DATA FOR THIS TREND MORE LIMITED AS IT ENCOMPASSES ONLY THOSE LOTS BUILT INTO BATTERIES AND PROCESSED THROUGH A FULL BATTERY ATP.

RATIO INDICATES HOW MUCH MORE CAPACITY A GIVEN LOT HAD AT 0°C AT THE CELL LEVEL VERSUS THE BATTERY LEVEL.

RATIOS GREATER THAN 100% INDICATE CAPACITY LOST BETWEEN CELL VENDOR TESTS AND BATTERY MANUFACTURER TESTS. (INCORRECTLY REPORTED AS CAPACITY GAIN IN LAST YEAR'S STUDY).

THE EFFECT SUGGESTS CONTINUING CHANGES TO THE MORPHOLOGY OF THE NEGATIVE PLATE.

McDonnell Douglas Aerospace - Defense and Electronic Systems

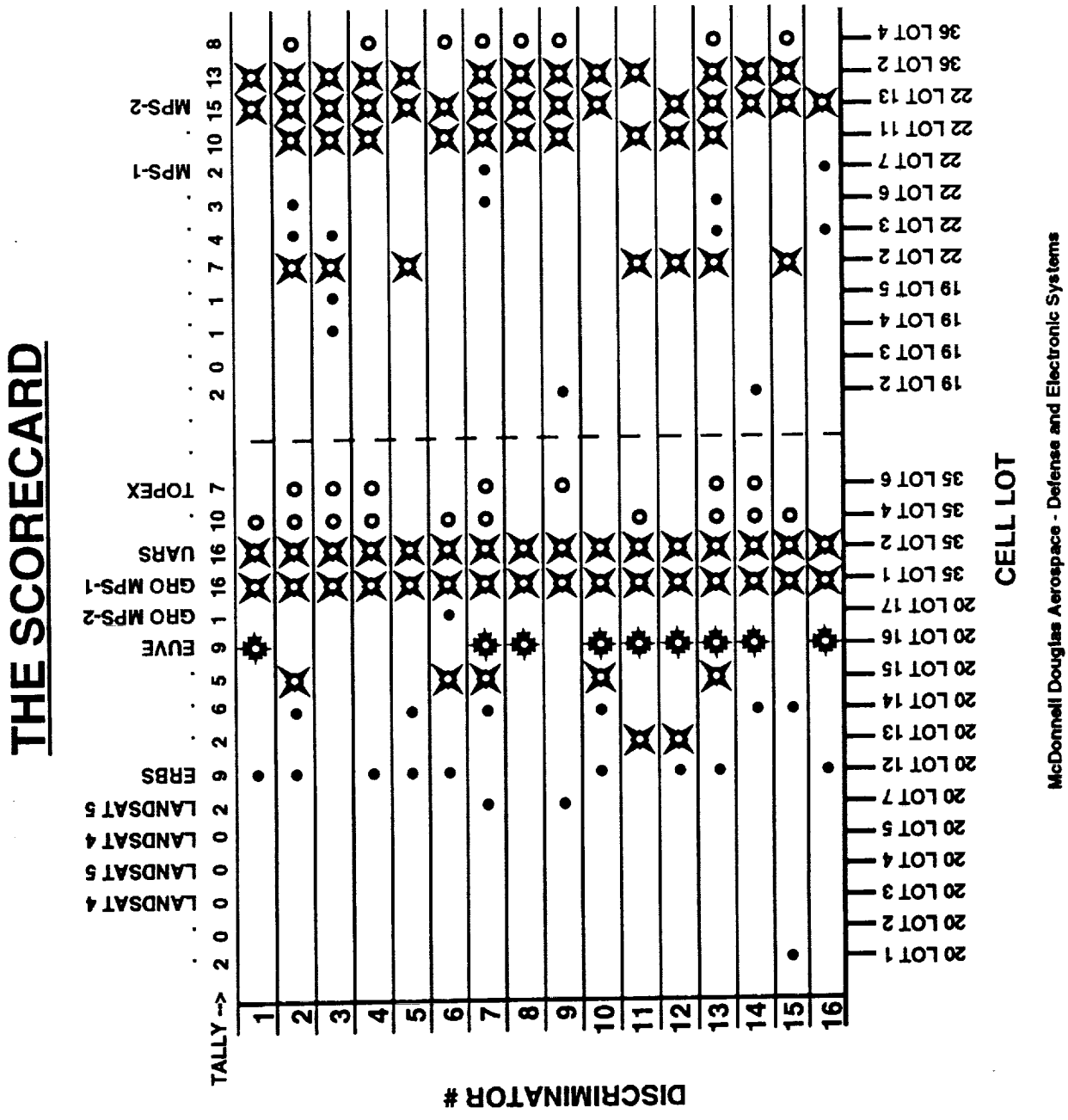
THE SCORECARD
TALLY -->
LANDSAT 4
LANDSAT 5
LANDSAT 4
LANDSAT 5
ERBS
EUVE
GRO MPS-2
GRO MPS-1
UARS
TOPEX
MPS-1
MPS-2
DISCRIMINATOR #
CELL LOT
McDonnell Douglas Aerospace - Defense and Electronic Systems

SUMMARY

1. OVER THE LAST 5 YEARS, McDONNELL DOUGLAS AEROSPACE HAS PROCURED SEVERAL LOTS OF NICD CELLS OF TWO DESIGNS THAT SUBSEQUENTLY DISPLAYED ANOMALOUS PERFORMANCE.

2. RETROSPECTIVE ANALYSIS OF THE CHARACTERISTICS OF THE PLATES AND CELLS FROM THESE SUSPICIOUS LOTS HAS FOUND SEVERAL DISTINGUISHING FEATURES. THEY WERE SO DISTINCTIVE IN FACT, THAT VALUES WERE ESTABLISHED IN 16 DIFFERENT MEASURES OF PERFORMANCE TO DISCRIMINATE BETWEEN GOOD CELL LOTS AND SUSPECT CELL LOTS.

3. THE DATA USED TO GENERATE THESE DISCRIMINATORS IS EITHER OBTAINED DIRECTLY FROM THE CELL SUPPLIER OR IS EASILY DERIVED FROM THE CELL SUPPLIER'S DELIVERABLE DATA. THE RAW DATA IS NEITHER OBSCURE NOR ESOTERIC. THE DERIVED DATA DOES NOT REQUIRE EXTENDED OR CONVOLUTED FORMULAS.

4. MOST OF THE DISCRIMINATORS CONCERN EITHER THE NEGATIVE ELECTRODE ITSELF, OR PERFORMANCE EFFECTS STRONGLY AFFECTED BY THE NEGATIVE ELECTRODE.

5. EVERY SUSPICIOUS CELL LOT NOT ALREADY ASSOCIATED WITH DEGRADED SEPARATOR HAS FAILED A MAJORITY OF THESE 16 DISCRIMINATORS. (TWO NASA LOTS, UARS AND GRO MPS-1, FAILED ALL 16.)

CONCLUSIONS

1. POST-DELIVERY PERFORMANCE OF NICD CELLS AND BATTERIES CAN BE AND SHOULD BE RELATED BACK TO THE PERFORMANCE OBSERVED IN THE PLATES AND CELLS AT THE CELL SUPPLIER.

2. CELL PERFORMANCE AT THE CELL SUPPLIER CAN BE AND SHOULD BE RELATED BACK TO PLATE PERFORMANCE. IN A LIKE MANNER, CELL PERFORMANCE ANOMALIES CAN OFTEN BE TRACED BACK TO THE PLATE COMPONENT LEVEL.

3. PAST PERFORMANCE OF PLATES AND CELLS SHOULD BE USED TO CREATE NEW PERFORMANCE SPECIFICATIONS AS WELL AS UPDATE EXISTING ONES. SOME CELL-LEVEL PERFORMANCE SPECIFICATIONS SHOULD BE DEPENDENT ON PLATE-LEVEL PERFORMANCE.

4. THE PRESENT STRUCTURE OF MOST PERFORMANCE SPECIFICATIONS DOES NOT ADEQUATELY ASSESS THE QUALITY OF THE END-PRODUCT. THE FORMAT IS SUCH THAT INDIVIDUAL SPECIFICATIONS CAN EITHER BE TOO OBJECTIVE OR (MORE LIKELY) NOT OBJECTIVE ENOUGH.

CONCLUSIONS (cont'd)

5. THE EFFORTS TO MAKE A THICKER, MORE POROUS NEGATIVE PLAQUE HAD A PROFOUND EFFECT ON SUBSEQUENT PLATE PROCESSING, AND WAS EVIDENCED BY MARKED CHANGES IN PLATE PHYSICAL CHARACTERISTICS AND NEGATIVE PLATE PERFORMANCE. INCREASED NEGATIVE UTILIZATION, AT LEAST BY THESE MEANS, WAS NOT A PERFORMANCE ENHANCEMENT.

6. THE MOST COST-EFFECTIVE AND SCHEDULE-EFFECTIVE PERFORMANCE DISCRIMINATORS, FOR BOTH CUSTOMER AND SUPPLIER, WOULD BE AT THE PLATE LEVEL. SEVERAL HAVE BEEN IDENTIFIED HERE, BUT IT IS LIKELY THAT A SUFFICIENTLY GREATER NUMBER CAN BE DEVELOPED TO MAKE PLATE "BUY-OFF" A MORE EFFECTIVE SCREENING PROCESS.

ACKNOWLEDGEMENTS

SINCERE THANKS TO THESE PROFESSIONAL MEN AND WOMEN, FOR THEIR CONTRIBUTIONS OF TIME, EFFORT, INSIGHT AND EXPERIENCE:

GATES AEROSPACE BATTERIES

DAN DELL
JUDY ULMER
GUY RAMPEL
ADELL AKRIDGE
WAYNE WILLIAMS
KEN WEBB
GLENN KLEIN

MDC

DON WEBB
TERRY GANLEY
JOANN WANKO
MAURICE ZOLLNER
DON BROWN

NASA - GSFC

MARLON ENCISO
KEN SCHWER
DR. GOPAL RAO
SMITH D. TILLER

NWSC - Crane

STEVE HALL

McDonnell Douglas Aerospace - Defense and Electronic Systems

Charge Control Session

Session Organizer: *Joe Stockel*
Office of Research & Development

INTELSAT BATTERY CHARGE PHILOSOPHY

Andrew Dunnet
INTELSAT
Washington, D.C., U.S.A.

*INTELSAT has 10 rather aged NiCd Batteries and 30 NiH2 batteries of various designs presently in orbit.

*With all of them we try to minimise the overcharge they are exposed to as well as maintaining temperatures in the moderate -5 to +20 deg.C. Preferably keeping the temperature under +10 deg.C.

*INTELSAT uses a current integration on discharge and returns between 105% and 115% depending on the battery and load.

The I-5 NiCd batteries are recharged to 105% or a cell voltage of 1.58V, which ever comes first.

The I-5 NiH2 batteries are recharged to 110% to 115% depending on current load.

The I-K NiH2 batteries are recharged to 112%.

The I-6 NiH2 batteries are recharged to 105%.

The I-7 NiH2 batteries will be recharged to 110%.

*INTELSAT always reconditions their batteries prior to an eclipse season. With the NiH2 the benefit to the batteries is not clear but the twice yearly health check is well worth the effort. Reconditioning is to the first cell to:

1V for the I-5 NiCd batteries.

0.9V for the I-6 NiH2 batteries.

0.5V for all other NiH2 batteries.

*INTELSAT minimises the temperature during solstice by reducing the recharge to just compensate for self discharge.

*In the past INTELSAT has always controlled the recharge by computer generated commands on the ground. Starting with I-7 this function will be controlled by the spacecraft in orbit. All the parameters; recharge ratio, thermal limits and recharge rates, are up-linked from the ground.

PRESSURE-BASED CHARGE CONTROL ON Ni-H_2 CELLS

Dean Maurer, AT&T / Bell Labs

SOME PRESSURE CONTROL CONCERNS

A. ABSOLUTE VALUE

- THERMAL EFFECTS OF OVERCHARGE
- CAPACITY/ TEMPERATURE EFFECTS
- TEMPERATURE/ PRESSURE EFFECTS

B. RATE

- THERMAL EFFECTS

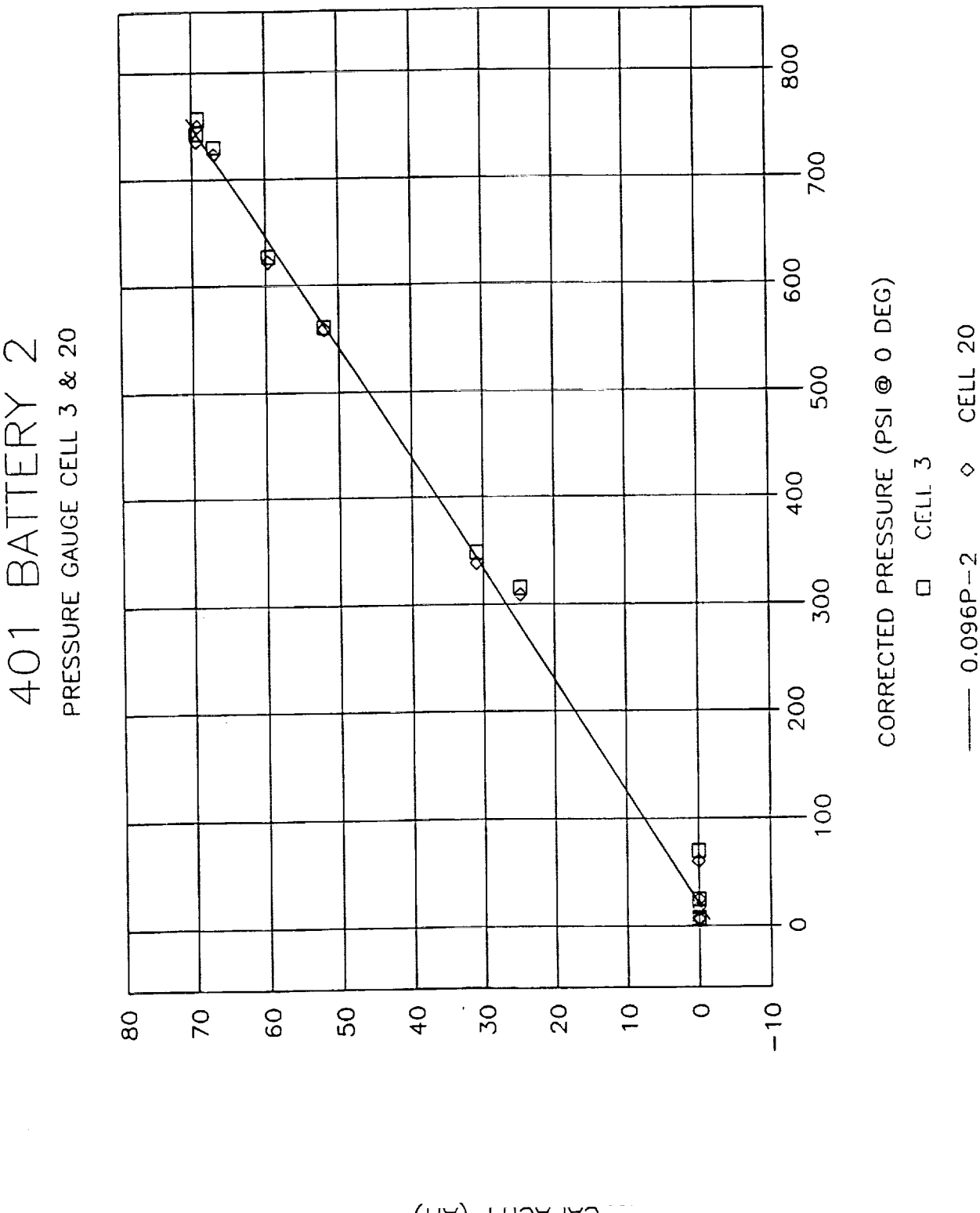
401 BATTERY 2
PRESSURE GAUGE CELL 3 & 20
CAPACITY (AH)
80
70
60
50
40
30
20
10
0
-10
0
100
200
300
400
500
600
700
800
CORRECTED PRESSURE (PSI @ 0 DEG)
□ CELL 3
◇ CELL 20
0.096P-2

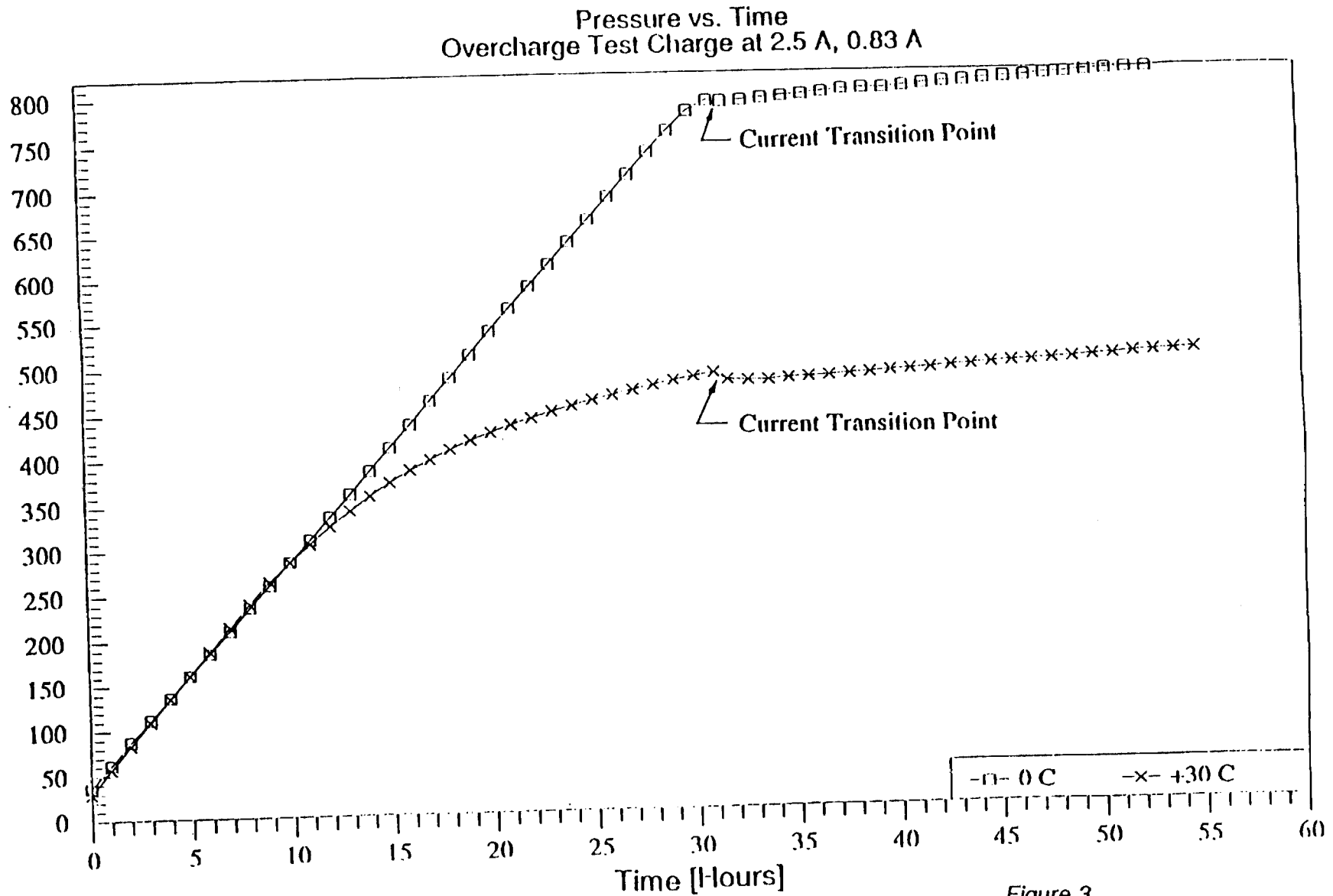
Pressure vs. Time
Overcharge Test Charge at 2.5 A, 0.83 A
Pressure [PSI]
800
750
700
650
600
550
500
450
400
350
300
250
200
150
100
50
0
0
5
10
15
20
25
30
35
40
45
50
55
60
Time [Hours]
Current Transition Point
Current Transition Point
-□- 0 C
-×- +30 C

Figure 3

SOME PRESSURE CONTROL METHODS

A. ABSOLUTE VALUE

- CHARGE TO A $P_f = f(T,R)$, THEN TRICKLE

- CHARGE TO X%P_f THEN ADD (CAP -X) + Y% THEN TRICKLE

B. RATE

- CHARGE TO A $dP/dt = f(R)$ THEN TRICKLE

BATTERY CHARGE CONTROL
WHICH APPROACH IS BEST?

C. LURIE
TRW SPACE AND ELECTRONICS GROUP
REDONDO BEACH, CALIFORNIA

THE 1993 NASA AEROSPACE BATTERY WORKSHOP
ALABAMA SPACE AND ROCKET CENTER
NOVEMBER 16 - 18, 1993

THE "BEST" CHARGE CONTROL APPROACH?
FROM THE BATTERY'S POINT-OF-VIEW

- PERFORMANCE
  - MORE AGGRESSIVE CHARGING CAN RESULT IN HIGHER DISCHARGE VOLTAGE AND CAPACITY (BETTER PERFORMANCE)
  - HOWEVER, AGGRESSIVE CHARGING USUALLY IMPLIES MORE OVERCHARGE AT HIGHER RATES WITH CONCOMITANT HIGHER END OF CHARGE TEMPERATURE (HIGHER STRESS, SHORTER LIFE)

- LIFE
  - BENIGN CHARGING CAN RESULT IN LOWER DISCHARGE VOLTAGE AND CAPACITY (POORER PERFORMANCE)
  - BENIGN, OR LOW STRESS CHARGING, USUALLY IMPLIES LESS OVERCHARGE AT LOWER RATES WITH LOWER END OF CHARGE TEMPERATURE (LOWER STRESS, LONGER LIFE)

THE "BEST" CHARGE CONTROL APPROACH?
FROM THE SPACECRAFT/MISSION POINT-OF-VIEW

- CONSTRAINTS
  - PERFORMANCE
  - LIFE
  - ENVIRONMENT
- IMPACT ON OTHER SYSTEMS
  - POWER SUBSYSTEM ARCHITECTURE
  - SOLAR ARRAY

EXAMPLE

IMPACT OF CHARGE CONTROL APPROACH ON SOLAR ARRAY SIZE IN LEO --- CONSTANT CURRENT *VS* TAPER CHARGE

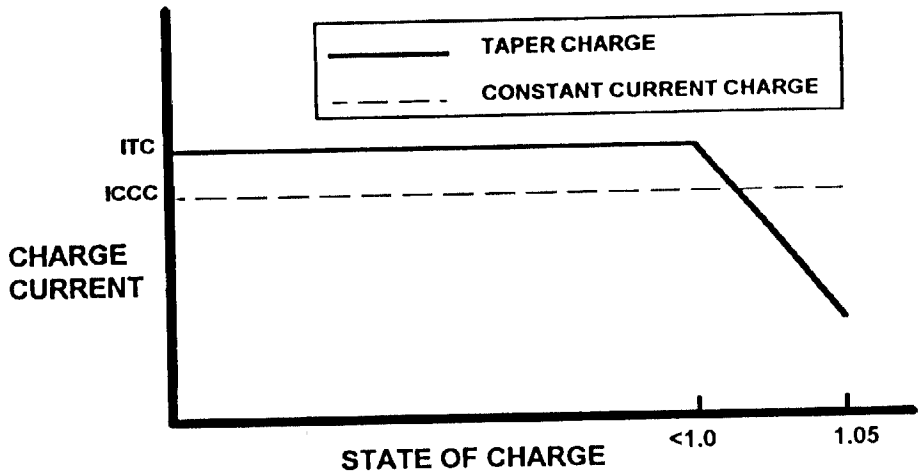

OVERCHARGING AT ICCC IS MORE STRESSFUL THAN OVERCHARGING AT THE TAPER CHARGE CURRENTS WHICH DECREASE DURING OVERCHARGE

- HOWEVER, CHARGE CURRENT DRIVES SOLAR ARRAY SIZE
- ITC > ICCC
- SOLAR ARRAY SIZED FOR ITC > SOLAR ARRAY SIZED FOR ICCC
- SOLAR ARRAY COST >> BATTERY COST

SOME OBSERVATIONS ON BATTERY CHARGE CONTROL

NASA SPACE POWER WORKSHOP

NASA/MARSHALL SPACE FLIGHT CENTER, ALABAMA

11/17/93

G.J. METHLIE

NICAD CHARGE CONTROL -

GSFC TCVL

PROGRAM- SPECIFIC TCVL'S

V/T CHANGES WITH TIME

THINGS THAT CAN BE DONE

DELTA T VS "DIURNAL CYCLE"

- dE/dT

P & DELTA P

INTEGRAL I dt

RECHARGE RATIO CONTROL

1/2 BATTERY VOLTAGE DIVERGENCE

VOLTAGE "OR" DELTA T

GSFC TCVL CONTROL

TRADEOFF BETWEEN STATE-OF-CHARGE AND CELL DAMAGE

EARLY TCVL'S SET MOSTLY TOO HIGH

THERMAL PROBLEMS ABOVE ABOUT 30 CENTIGRADE

POSSIBLE HYDROGEN EVOLUTION AT 0 -10 CENTIGRADE

RECHARGE RATIOS OFTEN 120 - 160%

FLOYD FORD/GSFC & STEVE GASTON - 1972

EXTENSIVE WORK FOR OAO ESTABLISHED 8 TCVL'S

SAFT 20 AHr CELLS

C/2 LEO CYCLING FROM 10 - 30 CENTIGRADE

EARLY MODEL CONFIRMED IN BENCH TESTING AT GULTON

PARAMETER AND E DIVERGENCE CORRELATION LOW

RECHARGE RATIOS EFFECTIVE FROM 100 - 110 %

LESS DAMAGE WITH TIME/TEMPERATURE AND CYCLING

USED TO GENERATE NWSC/CRANE DATA BASE

G.E./NASA (STD) CELLS MOST RELIABLE

WORKED WELL WITH VERY DIFFERENT CELL DESIGNS

PROGRAM-SPECIFIC TCVL'S

CHANGED SLOPE OF E VS T FOR DIFFERENT MISSION T'S

SOME ELIMINATED TRICKLE IN LEO

SOME USED WITH VERY HIGH CHARGE AND DISCHARGE RATES

HENNIGAN - SEQUENTIAL CHARGING NOT ADVANTAGEOUS

WAS HELPFUL FOR VERY HIGH RATE MISSIONS

HIGHER RATE CHARGE - BETTER CAPACITY ON HIGH RATE DISCHARGE - MINIMIZE TRICKLE TIME

"BUILD IN" IR CORRECTION

RECONDITIONING DISCHARGE SHOWED "STAIR STEPS"

NEED REDUNDANT BATTERIES AND CELLS IN THEM

SOFT SHORTS (TEMPORARILY) ERASED

40,000 LEO CYCLES ACHIEVED (LIKE SOLAR MAX)

INTERACTION BETWEEN GS AND VEHICLE EXTENSIVE

EVENTUALLY MAINTENANCE TIME EQUALS OPERATING TIME OR SOMETHING ELSE ENDS MISSION

GSFC TCVL CONTROL (CONT'D)

ALSO EFFECTIVE IN GEO WITH STEP TO C/50-100 TRICKLE

SUPPORTED THE MAJORITY OF LEO & GEO PROGRAMS WELL

"ARRHENIUS" PLOT OF CYCLE LIFE VS DOD BETTER THAN NOW

V/T CHANGES WITH TIME/TEMPERATURE/CYCLING

CELLS DEGRADE

INTERNAL RESISTANCE RISES

HYDROLYSIS OF NYLON *

CORRELATION WITH DPA'S

PROPORTION OF CHARGED NEGATIVE INCREASES

ACTIVITY CHANGE SHIFTS Eo FOR NEGATIVE

HYDROGEN GENERATION & "PRESSURE CYCLING"

[KOH] FALLS FROM 31% TO 19% WITH 10% HYDROLYSIS

NICKEL ELECTRODE Eo SHIFTS WITH pH CHANGE

CAPACITY MEASURED IN R/D'S FALLS AT SAME TCVL'S

*- LIM, H.S., "STUDIES ON THE STABILITY OF NYLON SEPARATOR MATERIAL", 27th Power Sources Symposium, Atlantic City, N.J., 21-24 June, 1976, pp. 83-85.

THINGS THAT CAN BE DONE

WATCH BATTERY VOLTAGE TREND

WATCH BATTERY TEMPERATURES TREND

WATCH LOAD SHARING

APPLY LIM'S RATE CONSTANT TO TIME/TEMPERATURE PROFILE

ESTIMATE EXTENT OF HYDROLYSIS

ESTIMATE Ri BY CURRENT-STEP METHOD

CORRECT FOR Eo and Ri CHANGES

BEST TO CONFIRM WITH CELLS FROM MISSION SIMULATION TEST

REDUCE TASKING AND STAY WITH ORIGINAL TCVL'S

DESIGN FUTURE CELLS WITHOUT NYLON (i.e. "SUPERNICADS")

DELTA T VS "DIURNAL CYCLE"

COMPARE BATTERY TEMPERATURES WITH VEHICLE MODEL

INCREASE OR DECREASE CHARGE LEVELS TO ELIMINATE TREND

-dE/dT

AVOID -ROLLOVER CHARACTERISTICS VARY TOO MUCH

IN ONE TEST, 2/30 CELLS DID NOT EXHIBIT ROLLOVER

TRANSIENT LOADS CAN CAUSE PREMATURE CHARGE TERMINATION

P & DELTA P

CORRELATE WITH DELTA T & SOC

USED AS A "BACKUP" OR CHECK ON NICADS

MAIN APPROACH TO NICKEL/HYDROGEN

CAN BE APPLIED TO EOCP & EODP

PRESSURE GROWTH CORRELATED TO GRID CORROSION

INTEGRAL I dt

DIRECTLY DETERMINES RECHARGE RATIO

HIGHER PARTS COUNT & SEMICONDUCTOR FAILURE SUSCEPTIBILITY

ACCOUNT FOR "SOFT SHORTS:"

1/2 BATTERY VOLTAGE DIVERGENCE

RECENT MISSIONS MANAGED TO KEEP THIS DOWN

ADVERSELY AFFECTED BY "SOFT SHORTS"

DOES THIS "DRIVE" PROBLEMS?

VOLTAGE "OR" DELTA T

USED PRIMARILY TERRESTIALLY

VOLTAGE CUTOFF FIXED AT 1.515 V. +/- 10 mV/CELL

DELTA T AT 3 CENTIGRADE OVER BASEPLATE

SUPPORTED C RATE CYCLING WITH 10 C PEAK LOADS

WORKS FROM 5 - 60 CENTIGRADE

Construction of Temperature Compensated Constant Voltage (VT) Curves for Super NiCd™ Cells

HUGHES
ELECTRON DYNAMICS DIVISION
COMMERCIAL / INDUSTRIAL SECTOR

David A. Baer, David F. Pickett, James M. Pearce
Hughes Industrial Electronics Company
Electron Dynamics Division
Torrance, CA 90509

Gopalakrishna Rao
NASA Goddard Space Flight Center
Space Power Applications Branch
Greenbelt, MD 20771

Abstract

Tests to establish current-voltage characteristics at selected temperatures for 9 ampere-hour Super Nickel-Cadmium™ cells were conducted at Hughes Industrial Electronics Company's Electron Dynamics Division (HIEC/EDD) under sponsorship of NASA Goddard Space Flight Center (NASA/GSFC) through their prime spacecraft contractors Fairchild Space (SMEX/SAMPEX) and TRW (TOMS-EP). Curves were constructed using techniques established by Webster, Ford, et al, at NASA/GSFC in the late 1960 - early 1970 tiime period for conventional nickel cadmium cells used on OAO and OSO spacecraft. The NASA/GSFC techniques were slightly modified by HIEC/EDD to fit the Super Ni-Cd situation.

Construction of Temperature Compensated Constant Voltage (VT) Curves for Super NiCd™ Cells

HUGHES
ELECTRON DYNAMICS DIVISION
COMMERCIAL / INDUSTRIAL SECTOR

AGENDA

I. Introduction
- Purpose of VT Determinations
- Heritage - Use on OAO and OSO and current NASA spacecraft

II. Technique for Generation of VT Curves
- Results from early NASA/GSFC Studies (Webster, Ford)
- Use of Webster and Ford Techniques at HIEC/EDD

III. Results
- Charge/Discharge Ratios
- Characterization Tests
- Plots of Recharge Ratio vs. Charge Voltage Limit
- Voltage/Temperature Characteristics for Multiple Level Nickel-Cadmium Battery Charger

IV. Discussions of Results
- Reasons for Differences in Super NiCd and Conventional NiCd Plots
- Technique for Generation of Curves

V. Conclusions
- Principle the same although curves may be slightly different for Super NiCd.
- One set of curves can be used.

Procedure for Generation of Curves

HUGHES
ELECTRON DYNAMICS DIVISION
COMMERCIAL / INDUSTRIAL SECTOR

- Select % Recharge from Figure 1.
- Select % DOD's (e.g., 25%) characteristic recharge ratio and voltage limit from Figure 2.
- Put % return on curve at appropriate temperature - Drop perpendicular to abcissa for voltage reading.
- To verify plot on cell voltage vs. temperature scale, compare with past curves (Figure 3).
  (Set level 8 at 1.520 $\pm$ .015 at 0°C, 0.020 $\pm$ .002 per level)
- Level 8 limit may not be used.
- Level 7 for max. DOD expected.
  (Curves 1 & 2 allow operation with loss of cell)
- Operate 1 level lower than expected at BOL.
  (Level 3 at 10% DOD, Level 5 at higher DOD)

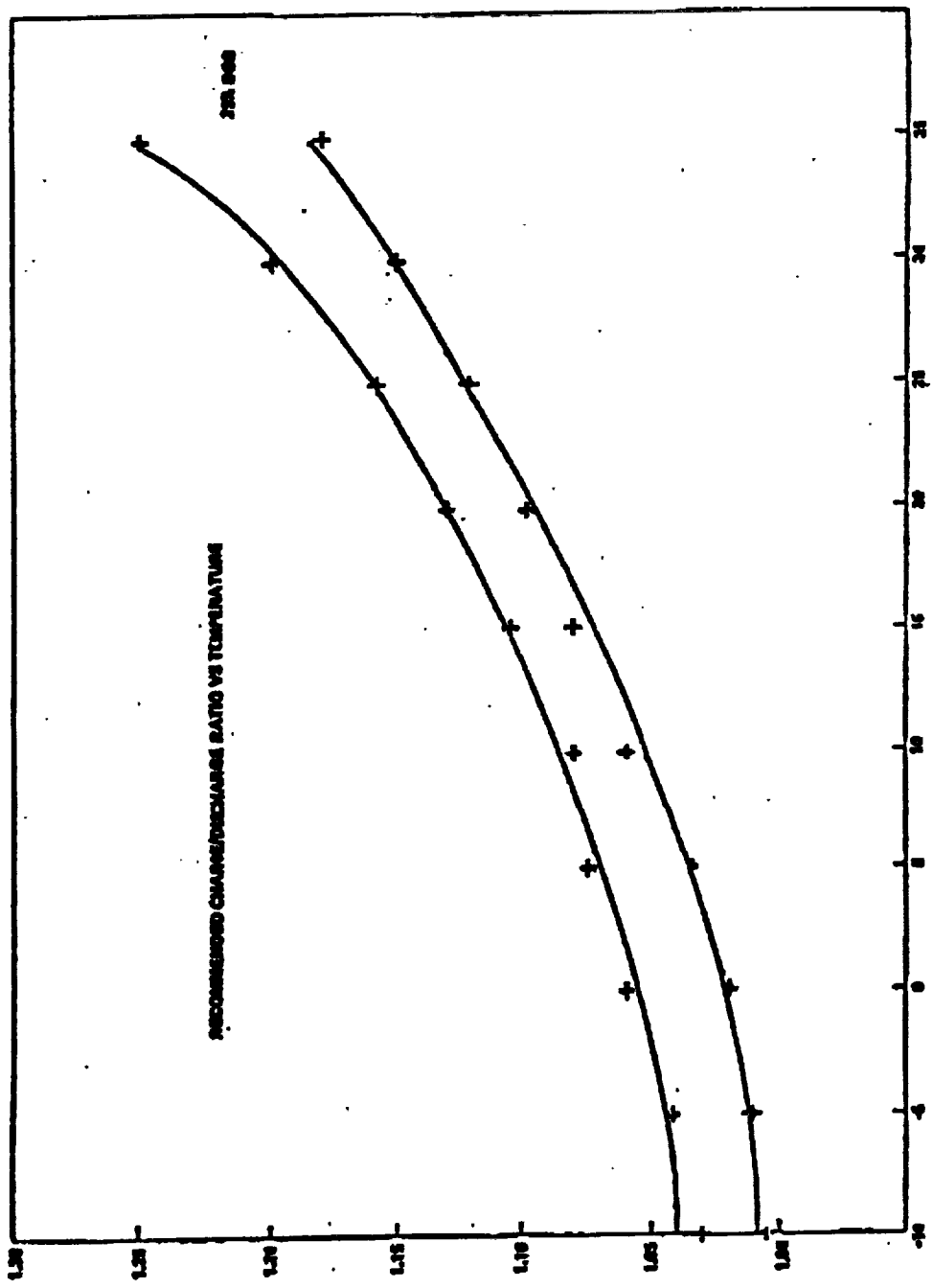

FIGURE 1

Recommended Charge/Discharge Ratio versus Temperature

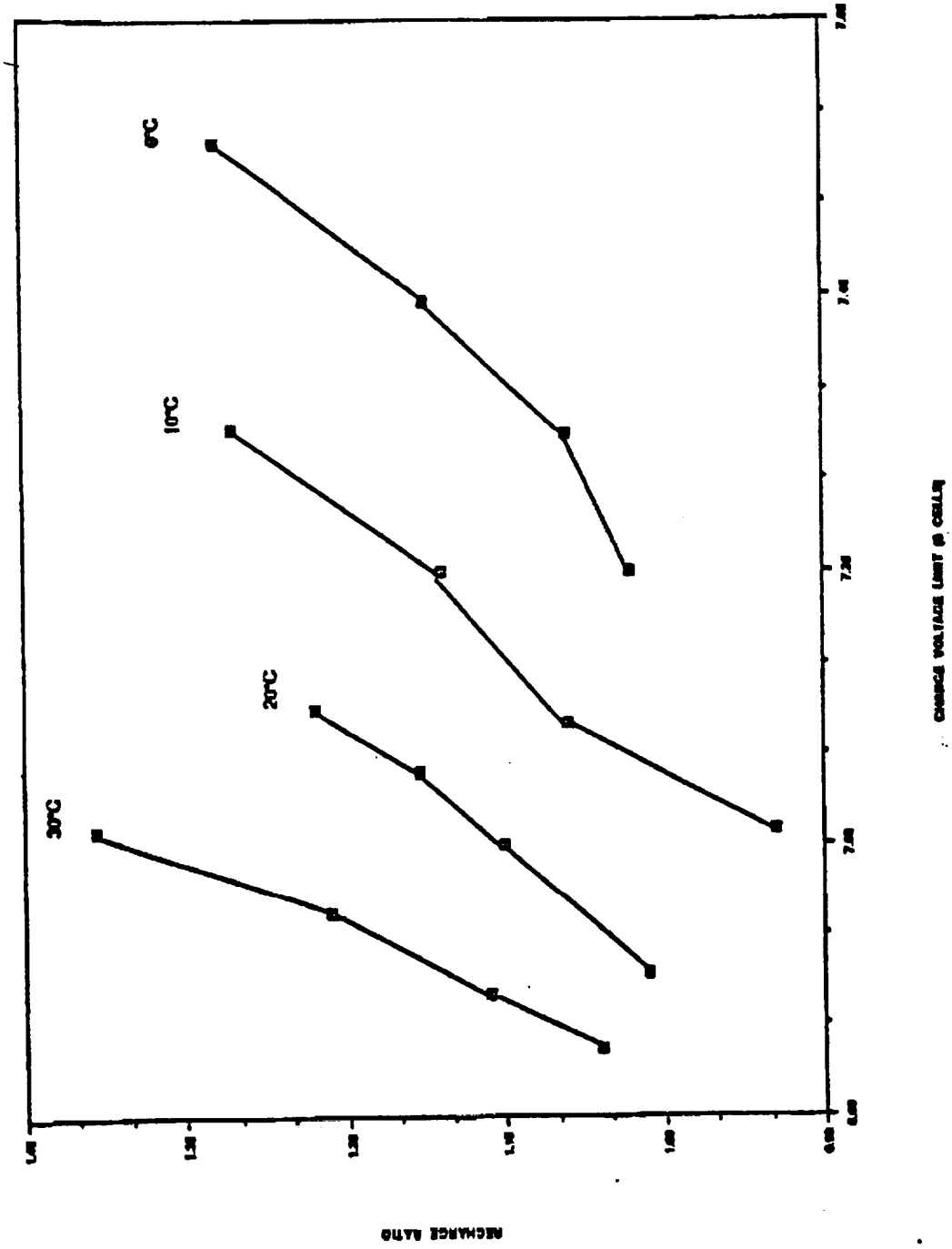

FIGURE 2
25% DOD

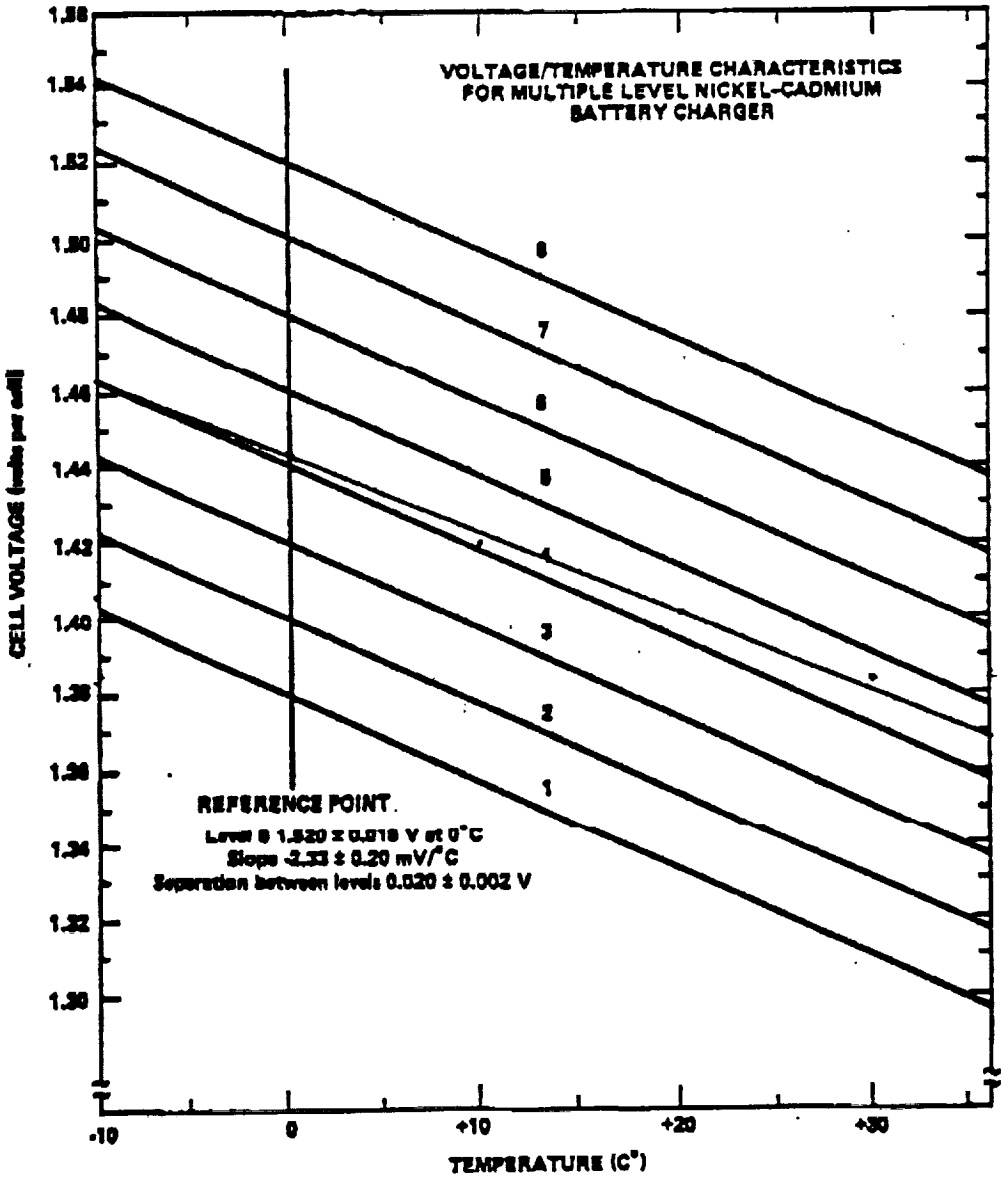

Figure 3 - Cell Voltage Limit versus Temperature

Rev. B

Sept. 1980

TABLE 1
SMEX CHARACTERIZATION TEST

CHARGE/ DISCHARGE RATIOS

EOC VOLTS	0°C DOD			10°C DOD			20°C DOD			30°C DOD		
	10%	25%	40%	10%	25%	40%	10%	25%	40%	10%	25%	40%
6.7												
6.75										1.0806		
6.8							0.9944			1.1744		
6.85										1.3324	1.0391	0.9869
6.9				0.9993			1.1072	1.0101		1.5594	1.1075	
6.95							1.2377				1.2133	1.0637
7.0	0.9895			1.0478	0.9299		1.4024	1.0994	1.0244		1.3558	
7.05								1.1538				1.2169
7.1	1.0063			1.1890	1.0616	0.9397		1.2204	1.1088			
7.15												1.4691
7.2	1.055	1.0168	1.0091	1.4805	1.1403	1.0638			1.1899			
7.25									1.2418			
7.3	1.1764	1.0621	1.0426	1.8630	1.2709	1.1282						
7.35												
7.4		1.1495	1.0934			1.2033						
7.45												
7.5		1.2818	1.1634									

BATTERY CELL CHARACTERIZATION TEST
DATA SUMMARY

			DISCHARGE						CHARGE					
Test Cond	Date 1993	Cycle No.	DoD %	EOD Temp. °C	EOD Curr. A	EOD Volts V	EOD Volts V/Cell	Output Ah	EOC Temp. °C	EOC Curr. A	EOC Volts V	EOC Volts V/Cell	Input Ah	C/D Ratio
1	2-25	6	10	1.1	1.797	23.0580	1.281	0.90	1.0	0.275	25.8980	1.439	1.13	1.256
2	2-25	5	25	2.4	4.490	22.301	1.239	2.25	1.8	0.818	26.4270	1.468	2.60	1.156
3	2-26	15	25	1.4	4.499	22.018	1.223	2.25	1.2	1.291	26.829	1.49	2.97	1.32
4	2-27	8	40	-1.9	7.193	21.687	1.205	3.61	-1.4	0.75	26.434	1.469	3.76	1.042
5	3-4	5	40	3.1	7.200	21.905	1.217	3.61	1.6	2.033	27.158	1.509	4.32	1.197
6	3-5	12	10	10.3	1.799	23.094	1.283	0.91	10.5	0.525	25.853	1.436	1.36	1.495
7	3-6	8	25	10.3	4.500	22.217	1.234	2.25	10.0	0.568	25.636	1.424	2.45	1.089
8	3-6	6	25	11.3	4.455	22.1810	1.232	2.24	11.0	1.24	26.0810	1.449	2.82	1.259
9	3-6	6	25	12.3	4.481	22.1190	1.229	2.25	12.0	1.837	26.2510	1.458	3.15	1.4
10	3-7	5	40	11.3	7.192	21.6880	1.205	3.60	10.9	0.887	25.8550	1.436	4.03	1.119
11	3-7	5	40	12.3	7.194	21.6660	1.204	3.61	12.0	2.282	26.4100	1.467	4.45	1.233
12	3-7	5	40	13.3	7.193	21.6490	1.203	3.60	13.0	3.119	26.5850	1.477	4.84	1.344
13	3-8	5	50	15.3	9.001	21.3930	1.189	4.50	13.3	3.587	26.7210	1.485	5.85	1.300
14	3-8	8	10	20.3	1.811	22.7036	1.261	0.90	19.7	0.199	24.7600	1.376	1.04	1.156
15	3-8	5	25	21.3	4.493	22.062	1.227	2.25	20.2	0.789	25.2015	1.400	2.56	1.138
16	3-9	5	40	22.3	7.194	21.603	1.200	3.61	21.0	1.320	25.4662	1.415	4.16	1.152
17	3-9	5	40	21.3	7.203	21.591	1.199	3.60	20.0	3.313	26.189	1.455	4.93	1.369

A Pressure Based Charge Control System For The DSPSE NiH2 CPV Battery

Presented To The NASA Battery Workshop November 16-18, 1993

C.Garner, W. Barnes & G. Hickman

Naval Research Laboratory Code 8134

Washington D.C.

N94-28127

17 NOVEMBER 1993

CHARGE CONTROL FOR THE DSPSE NiH2 CPV BATTERY

Introduction

- NRL/BMDO Deep Space Probe Science Experiment (DSPSE) To Orbit Moon & Rendevous With Asteroid Geographos
- Launch In January 1994
- DSPSE Spacecraft Will Use NiH2 CPV Battery For Energy Storage
- DSPSE Charge Control System Will Monitor NiH2 CPV Pressure For Switch From High Rate Charge To Trickle Charge

CHARGE CONTROL FOR THE DSPSE NiH2 CPV BATTERY

DSPSE Electrical Power Subsystem

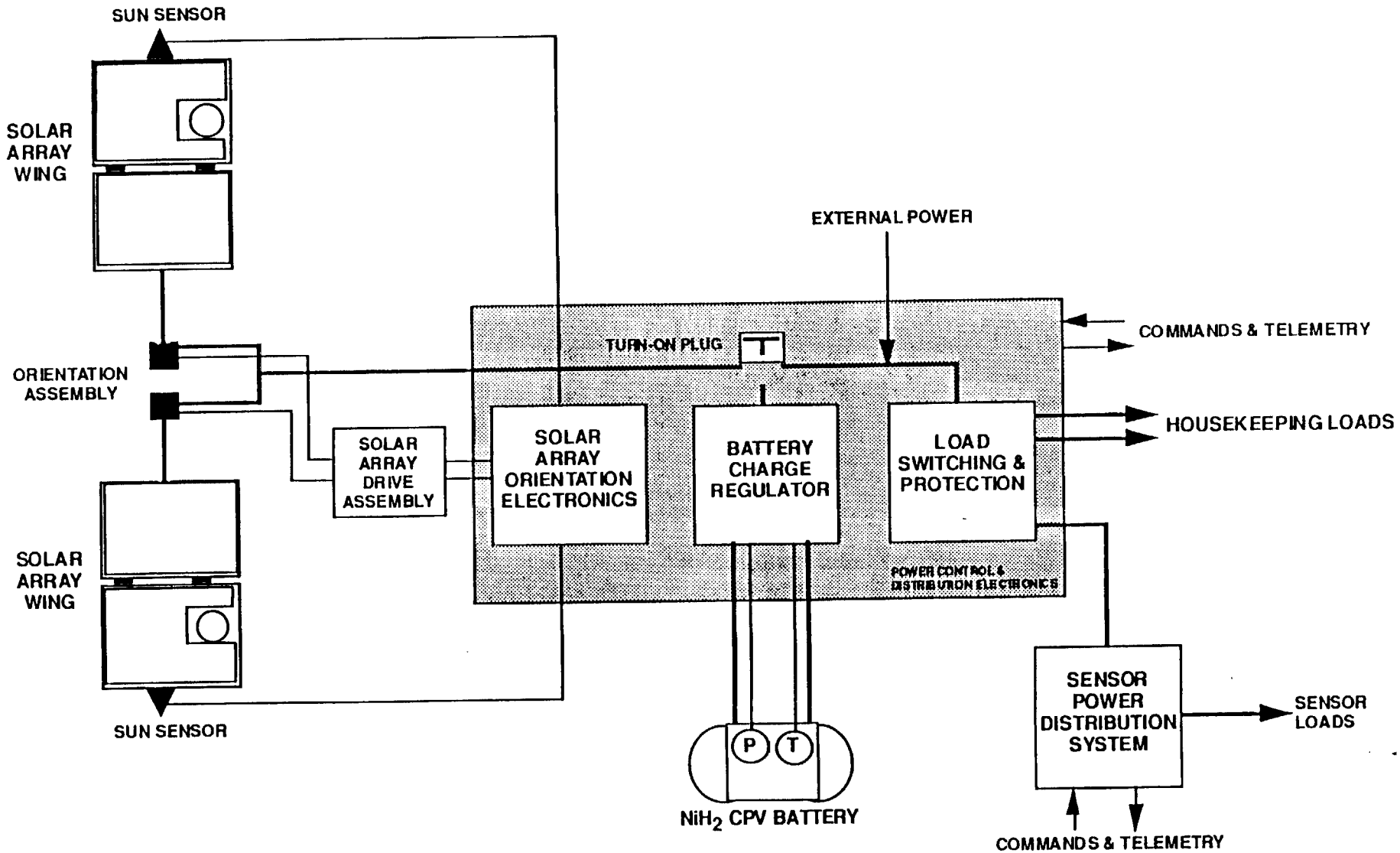

17 NOVEMBER 1993

CHARGE CONTROL FOR THE DSPSE NiH2 CPV BATTERY

DSPSE Eclipse Energy Requirements

Mission Phase	Eclipse Duration (Hrs)	Load (Watts)	AH Out @ 27.5 Volts
Low Earth Orbit	0.60	146	3.19
Lunar	1.17	226	9.62
Trans-Lunar	2.05	121	9.00

LEO Period Is 1.5 Hour

~ 50 LEO Cycles

Lunar Orbit Period Is 5 Hours

`300 Lunar Cycles

3 Trans-Lunar Eclipses Expected

DSPSE NiH2 CPV Battery

- Nickel Hydrogen Common Pressure Vessel Battery
  - Manufacturer — Johnson Controls Inc
  - Part No — 28015SCK
  - Nameplate Capacity — 15.0 Ampere Hour
  - No. Of Cells — Twenty-Two
  - Length — 21.0 inches
  - Diameter — 5.0 inches
  - Weight — 17.60 lbs
  - Pressure Vessel — Inconel 718 0.030 inch thick
  - Separator — Asbestos
  - Electrolyte — Potassium Hydroxide (31%)
- Graphite Epoxy Battery Structure
  - R Cubed Composites
  - Material P120 Thermal & T300 Graphite Fibers In ERL 1939-3 Resin
  - Weight — 2.30 lbs
- Total Battery Weight — 21.20 lbs

CHARGE CONTROL FOR THE DSPSE NiH2 CPV BATTERY

DSPSE NiH2 CPV Battery

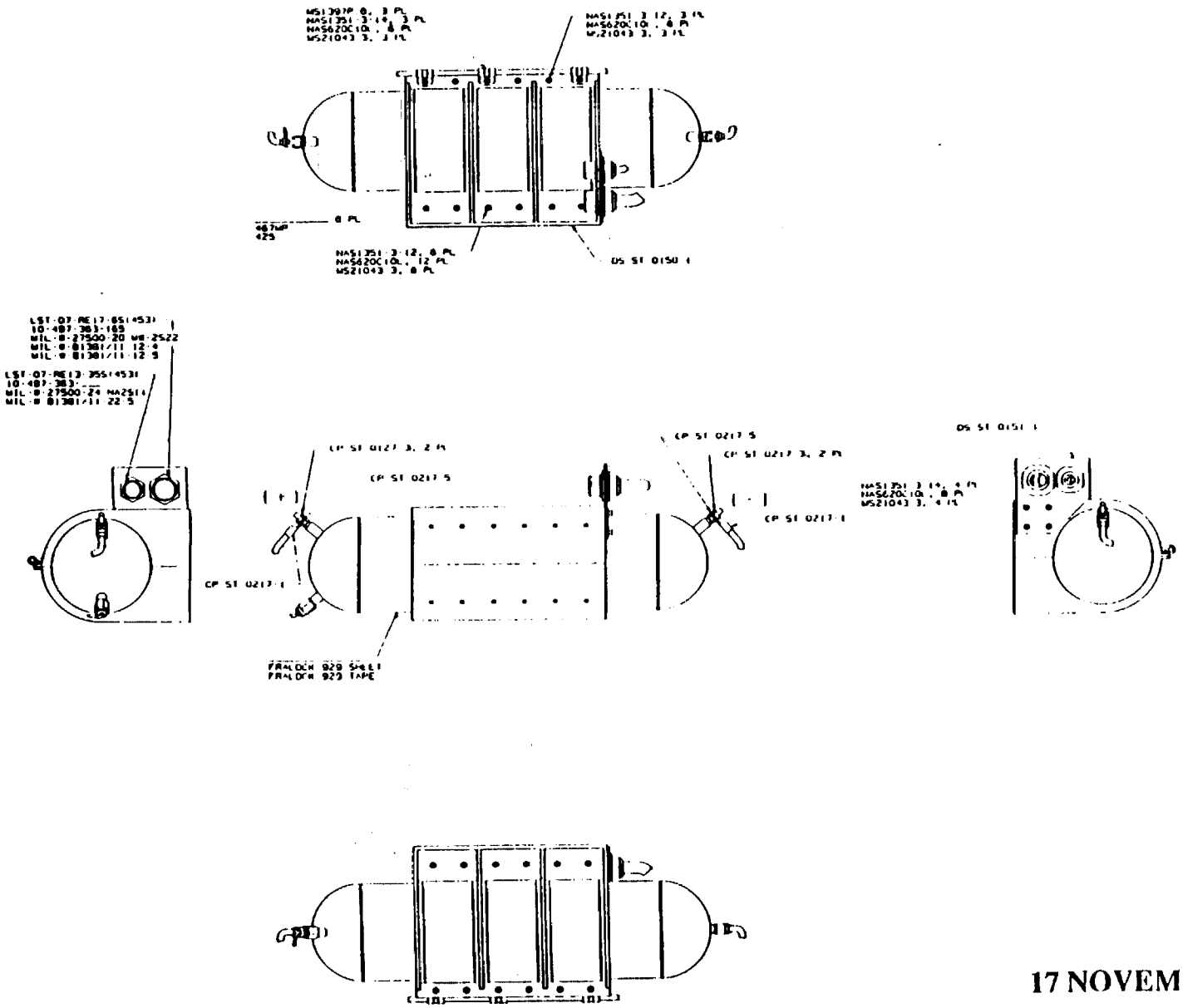

17 NOVEMBER 1993

CHARGE CONTROL FOR THE DSPSE NiH2 CPV BATTERY

DSPSE NiH2 CPV Battery On Spacecraft

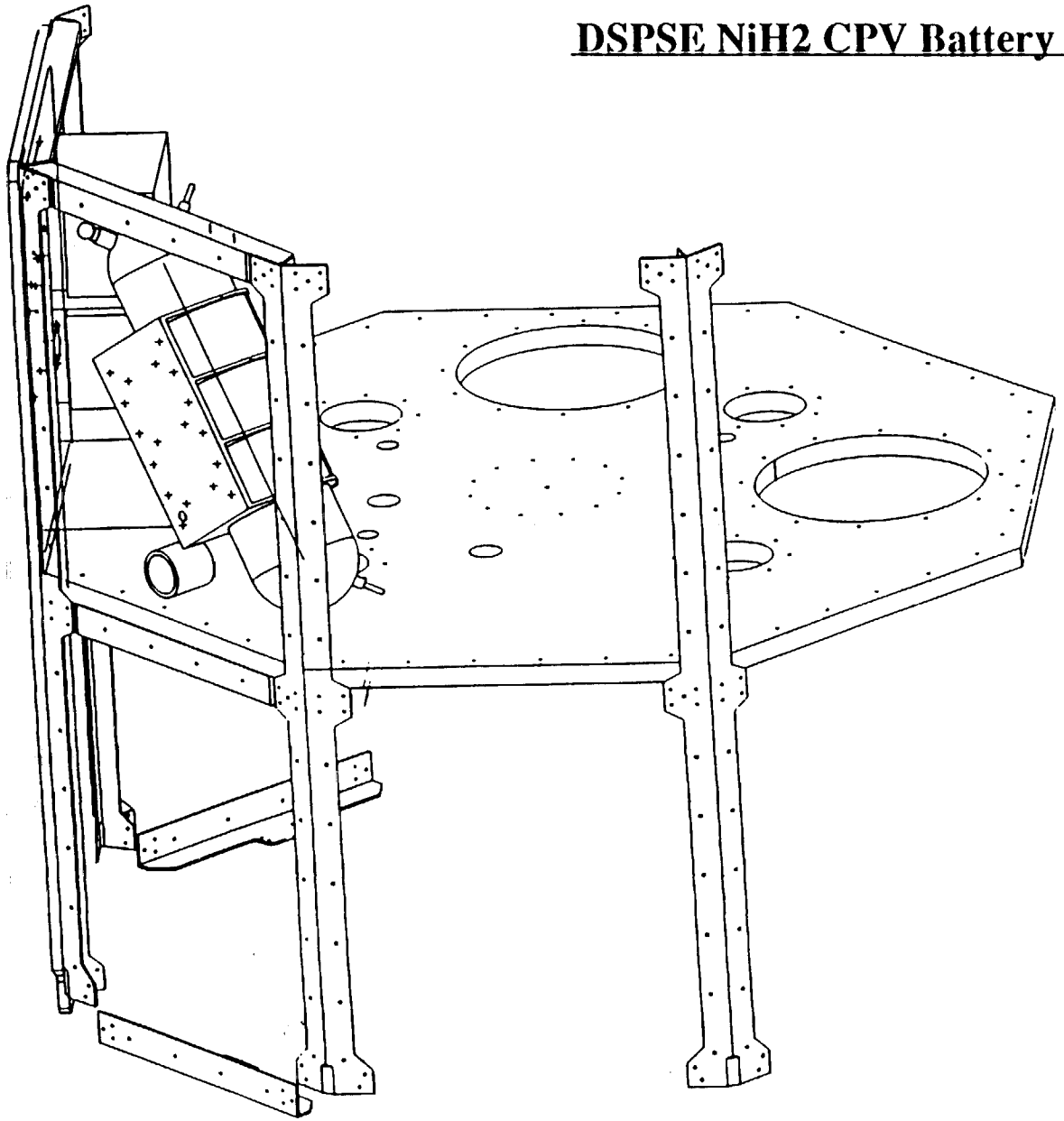

17 NOVEMBER 1993

CHARGE CONTROL FOR THE DSPSE NiH2 CPV BATTERY

Pressure Based Charge Control

- Charge Battery At High Rate (C/5 Amps) To Pressure Switch Point
- Lower Charge Rate To (C/100 Amps) For Remainder Of Orbit
- Characterize All Potential Flight Batteries
  - Establish Temperature (-10,0,10 & 20°C)
  - Charge At High Rate To Voltage Rollover
  - Discharge To 22.0 Volts At C/2 Amps
- Select Two Pressure Set Points For Flight Operation
- Cycle Battery Using P-based Charge Control

CHARGE CONTROL FOR THE DSPSE NiH2 CPV BATTERY

DSPSE Battery Pressure Transducer

- **Manufacturer** Kulite
- **Model No.** ETM - 341-375 -1000A
- **Sensing Principle** Fully Active Four Arm Wheatstone Bridge
- **Pressure Range** 0 - 1000 psia
- **Full Scale Output** 10 Vdc
- **Excitation** +12 Vdc
- **Maximum Current** 25 mA
- **Weight** 35 g (1.23 oz)

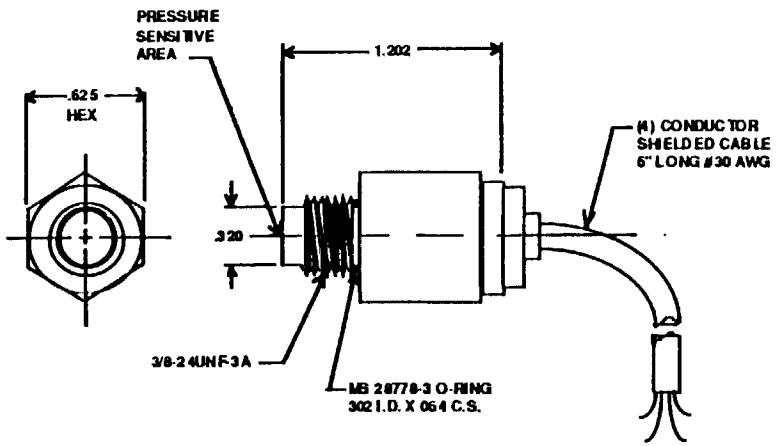

17 NOVEMBER 1993

CHARGE CONTROL FOR THE DSPSE NiH2 CPV BATTERY

3.0 A Charge @-10°C

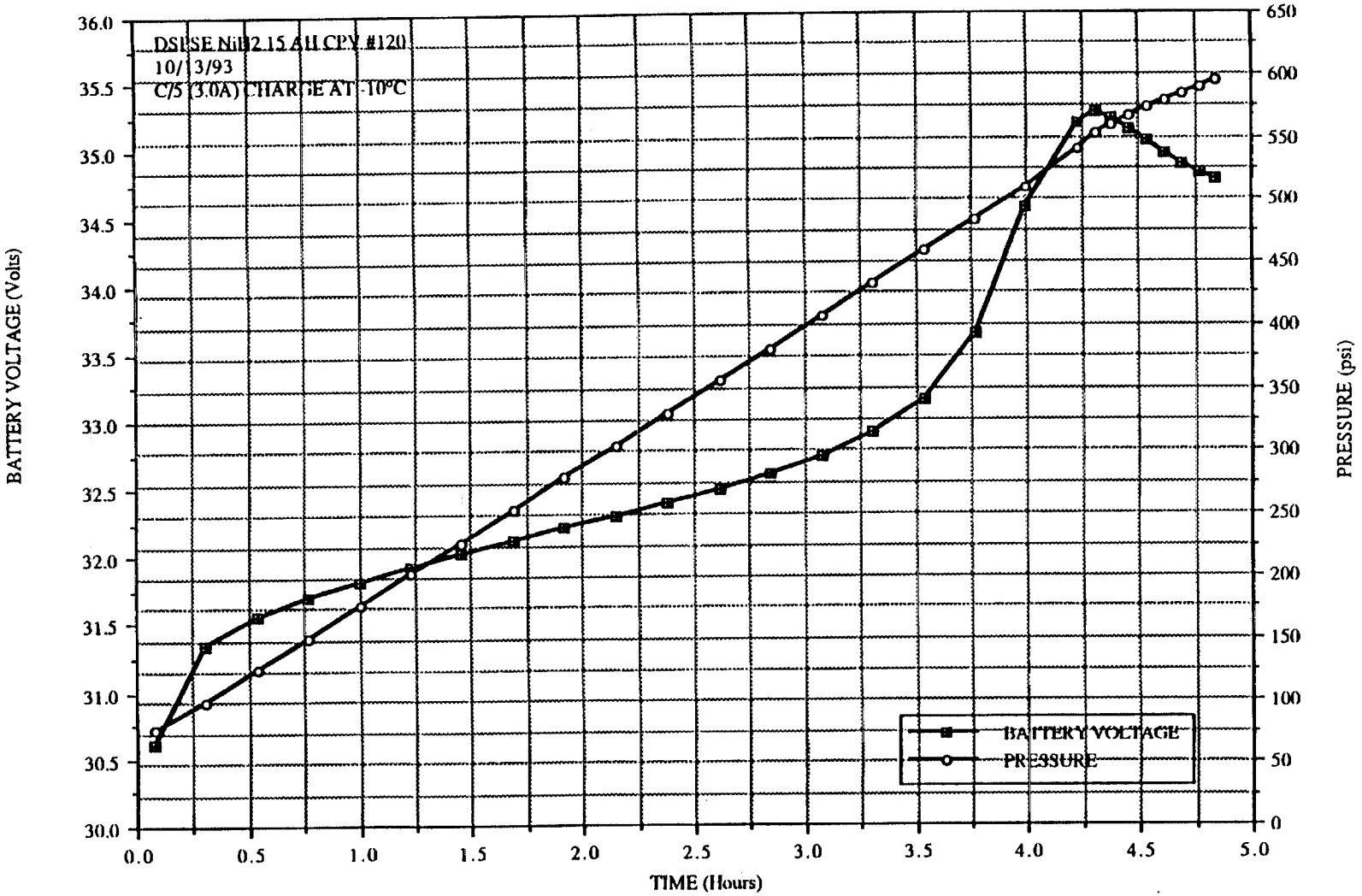

17 NOVEMBER 1993

CHARGE CONTROL FOR THE DSPSE NiH2 CPV BATTERY

3.0 A Charge @ 0°C

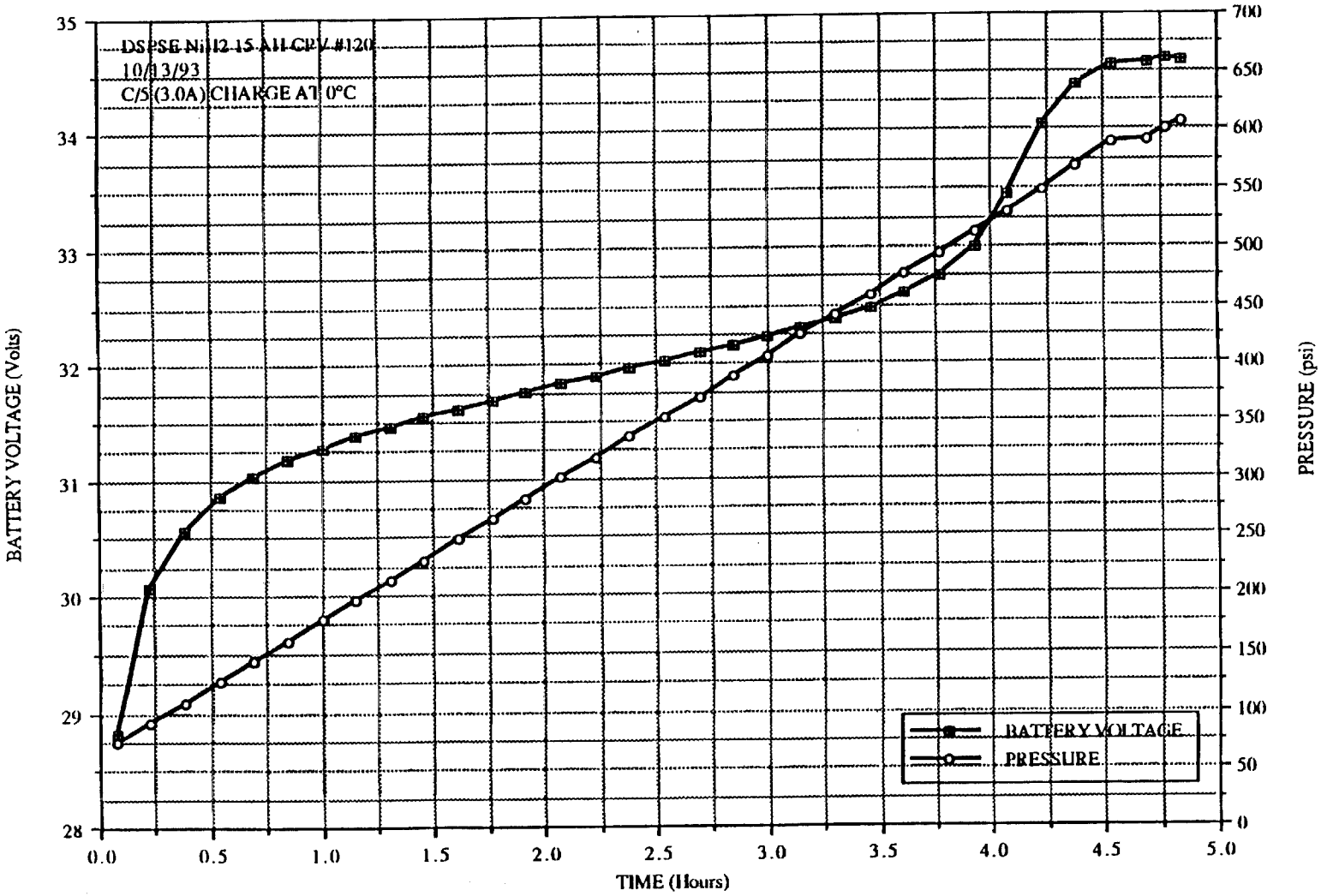

17 NOVEMBER 1993

CHARGE CONTROL FOR THE DSPSE NiH2 CPV BATTERY

3.0 A Charge @ 10°C

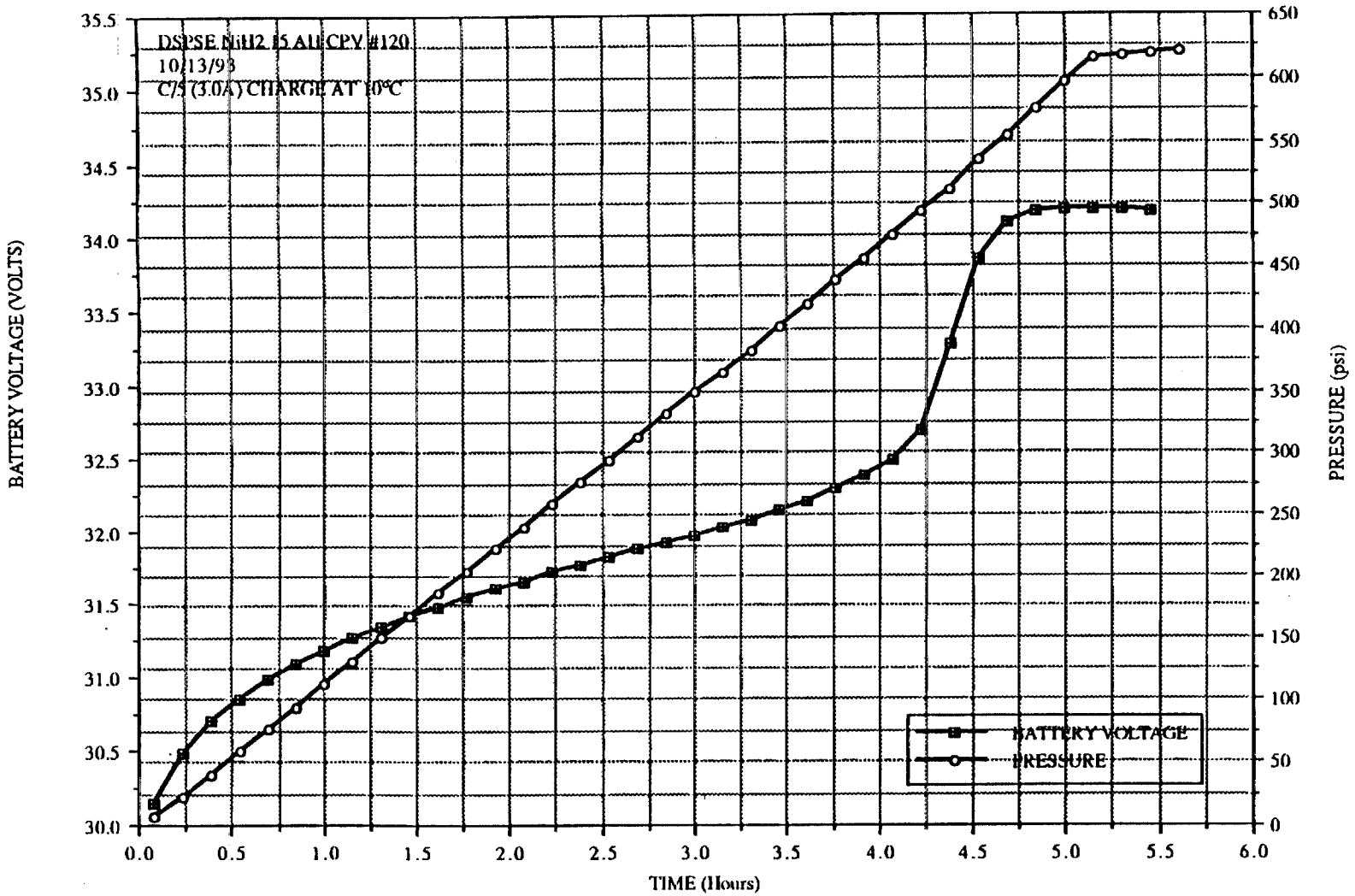

17 NOVEMBER 1993

CHARGE CONTROL FOR THE DSPSE NiH2 CPV BATTERY

3.0 A Charge @ 20°C

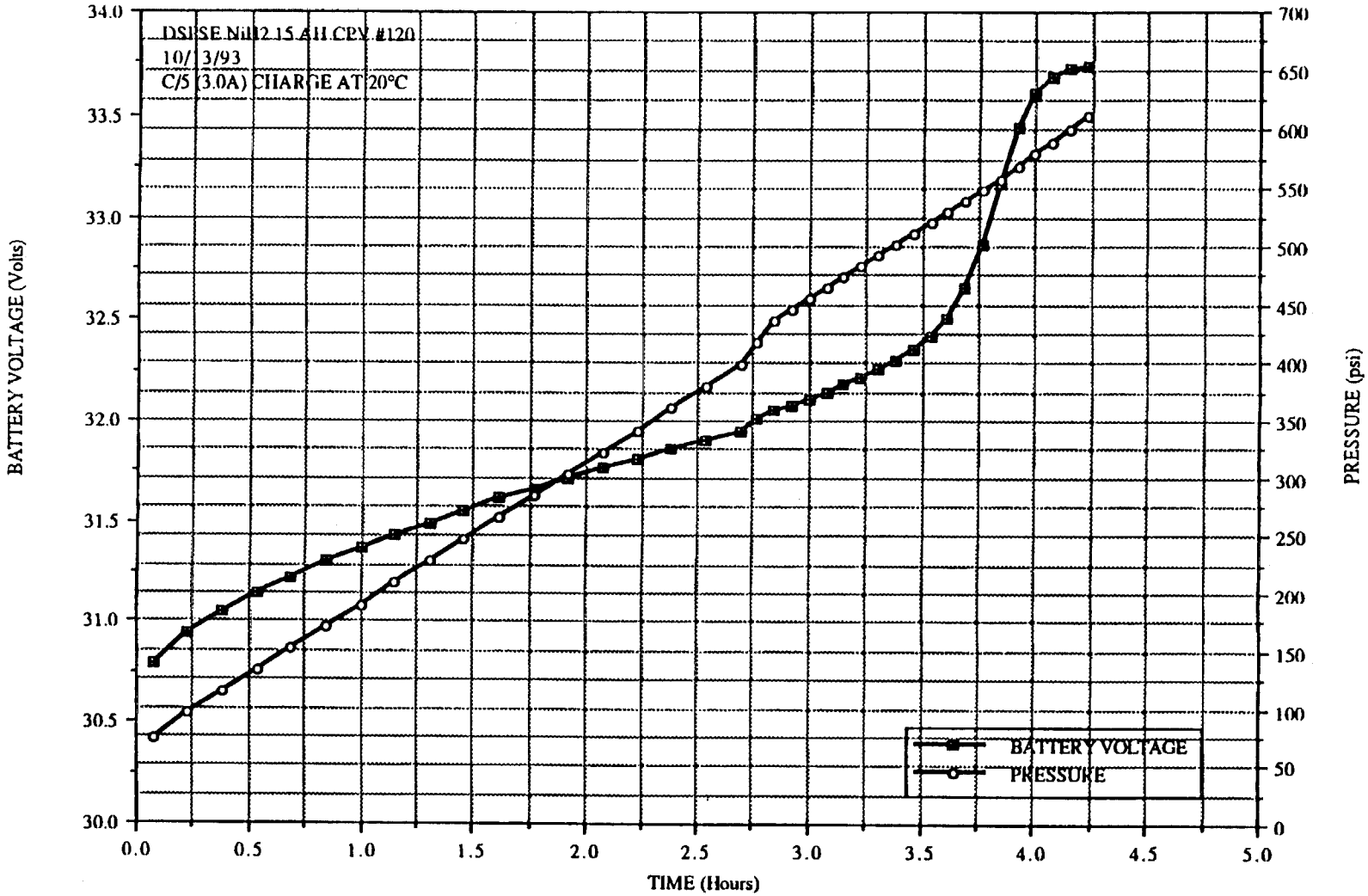

17 NOVEMBER 1993

CHARGE CONTROL FOR THE DSPSE NiH2 CPV BATTERY

3.0 A Charge: Pressure Vs Time

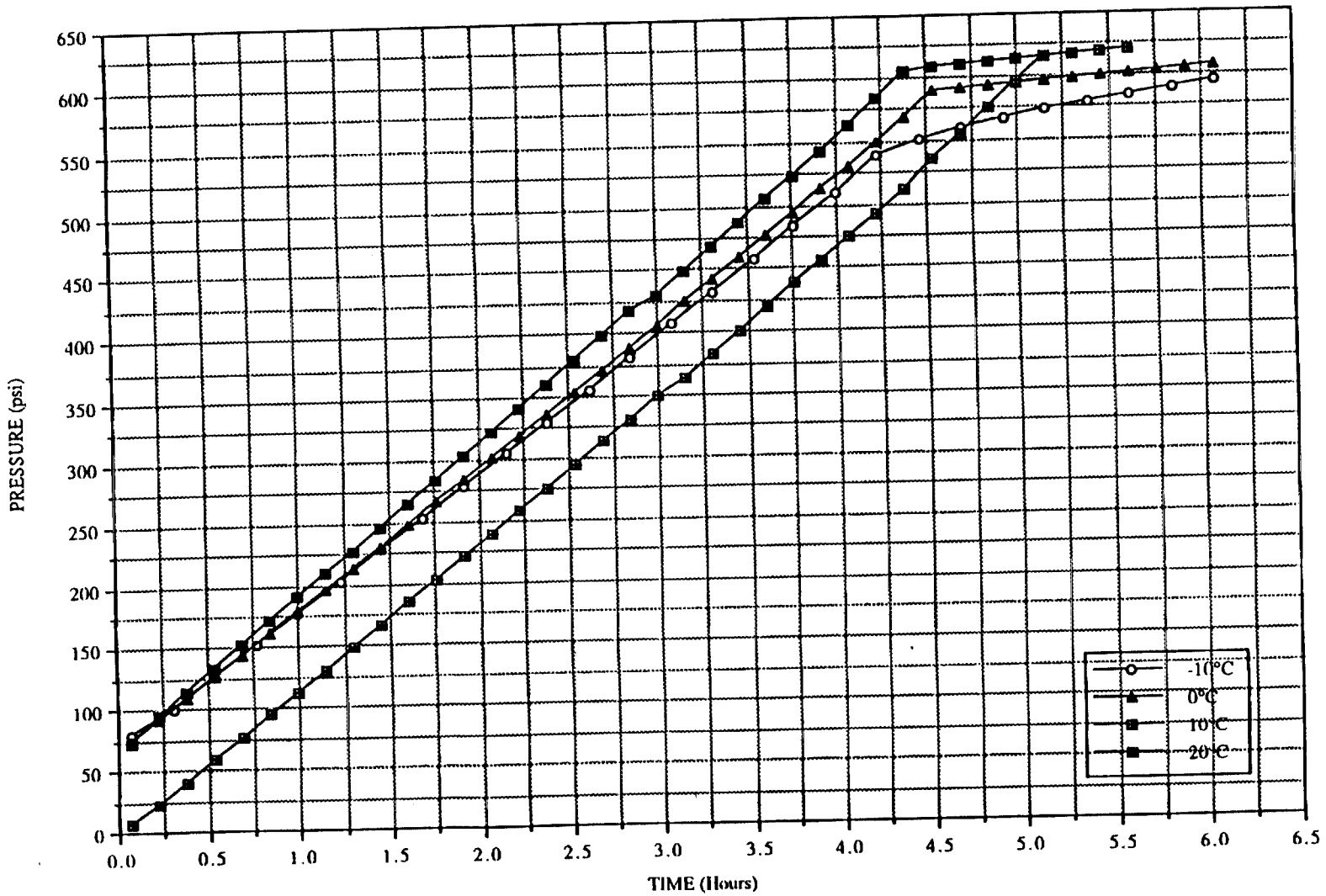

17 NOVEMBER 1993

CHARGE CONTROL FOR THE DSPSE NiH2 CPV BATTERY

-7.5 A Discharge To 22.0 Volts

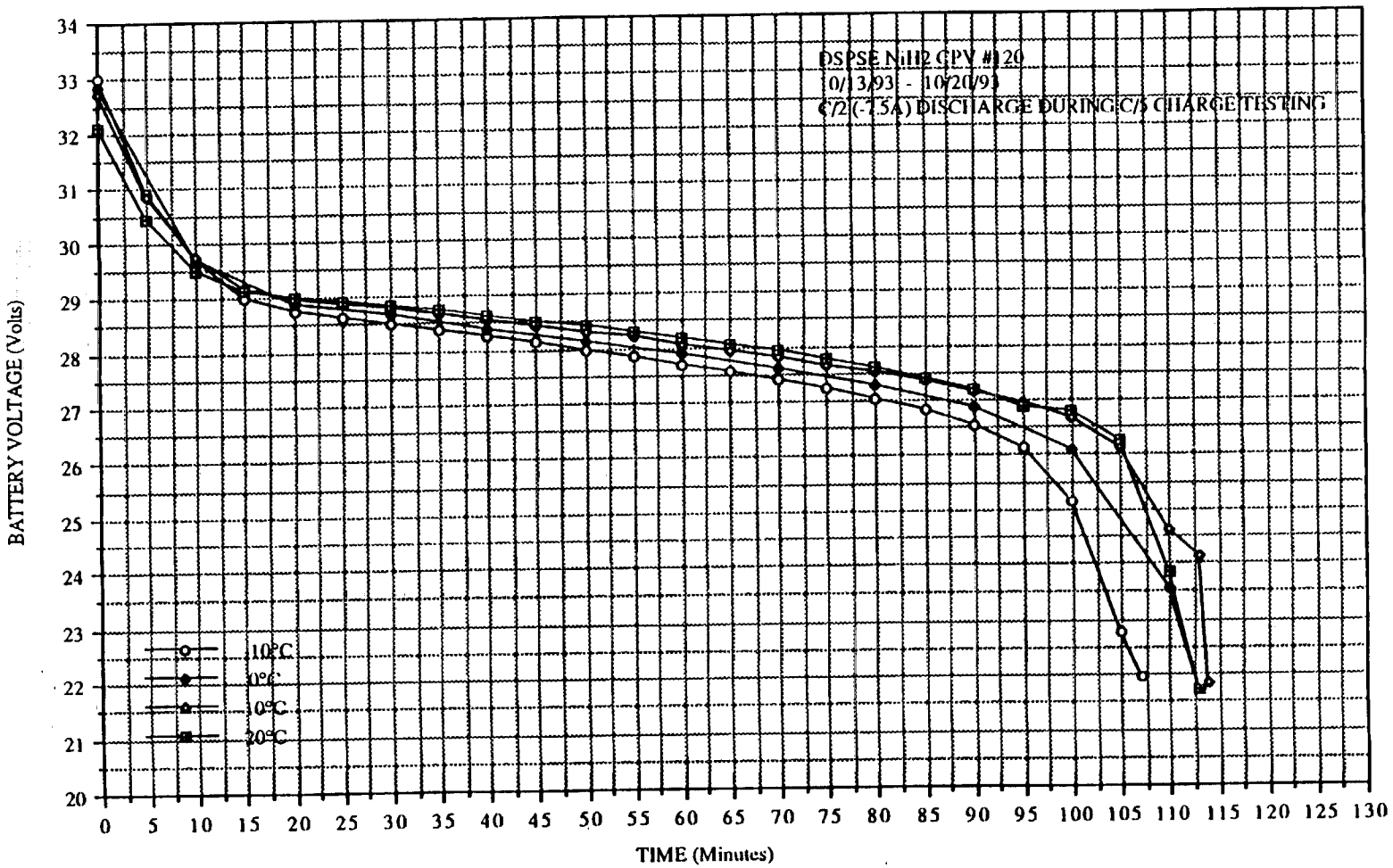

17 NOVEMBER 1993

CHARGE CONTROL FOR THE DSPSE NiH2 CPV BATTERY

S/N 120 vs S/N 124 @ 10°C

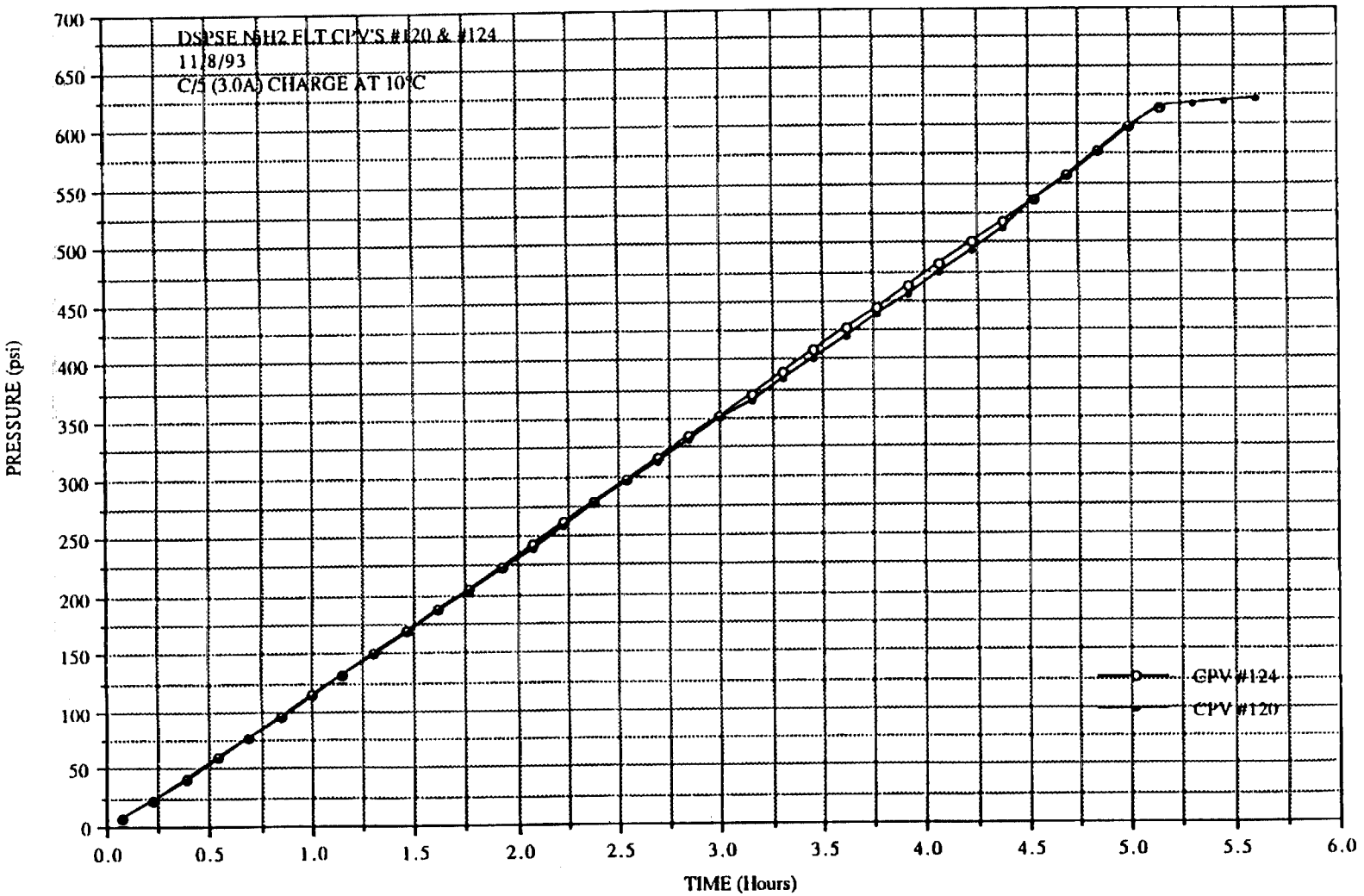

17 NOVEMBER 1993

CHARGE CONTROL FOR THE DSPSE NiH2 CPV BATTERY

S/N 120 vs S/N 124 @ 0°C

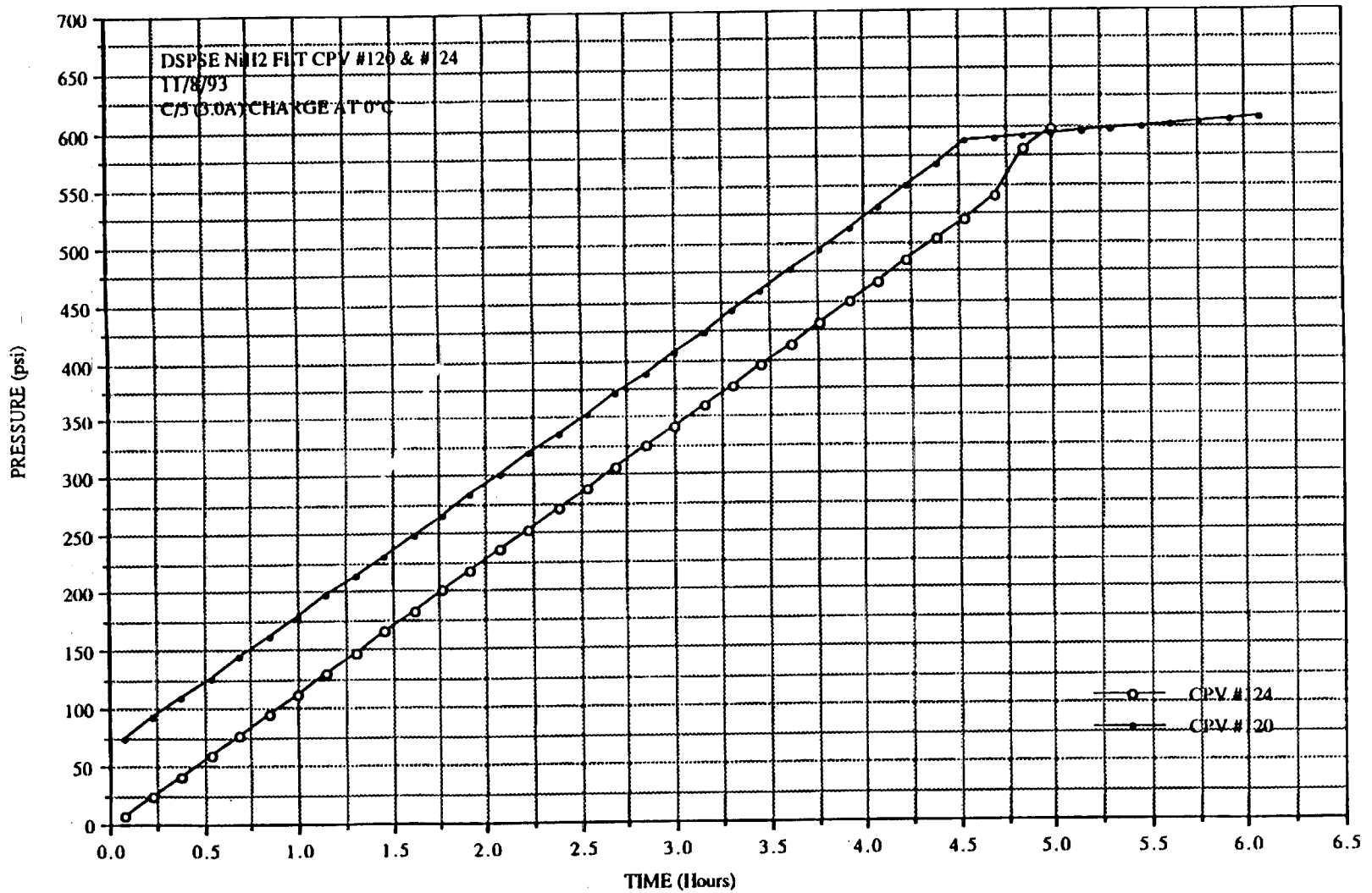

17 NOVEMBER 1993

CHARGE CONTROL FOR THE DSPSE NiH2 CPV BATTERY

S/N 120 LEO Cycling Using P-Based Charge Control

Voltage & Current vs Time

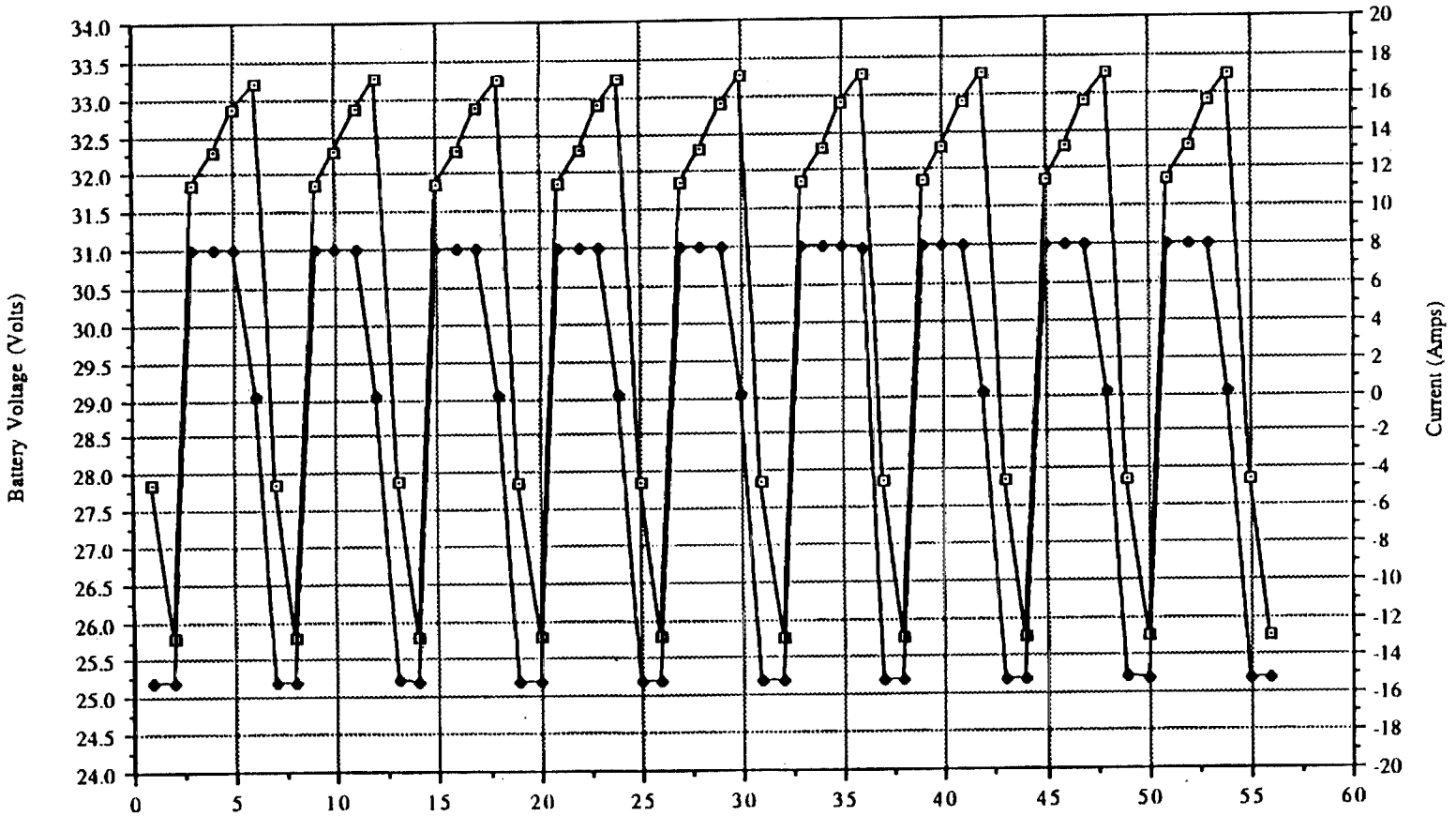

17 NOVEMBER 1993

CHARGE CONTROL FOR THE DSPSE NiH2 CPV BATTERY

S/N 120 LEO Cycling Using P-Based Charge Control

Pressure vs Time

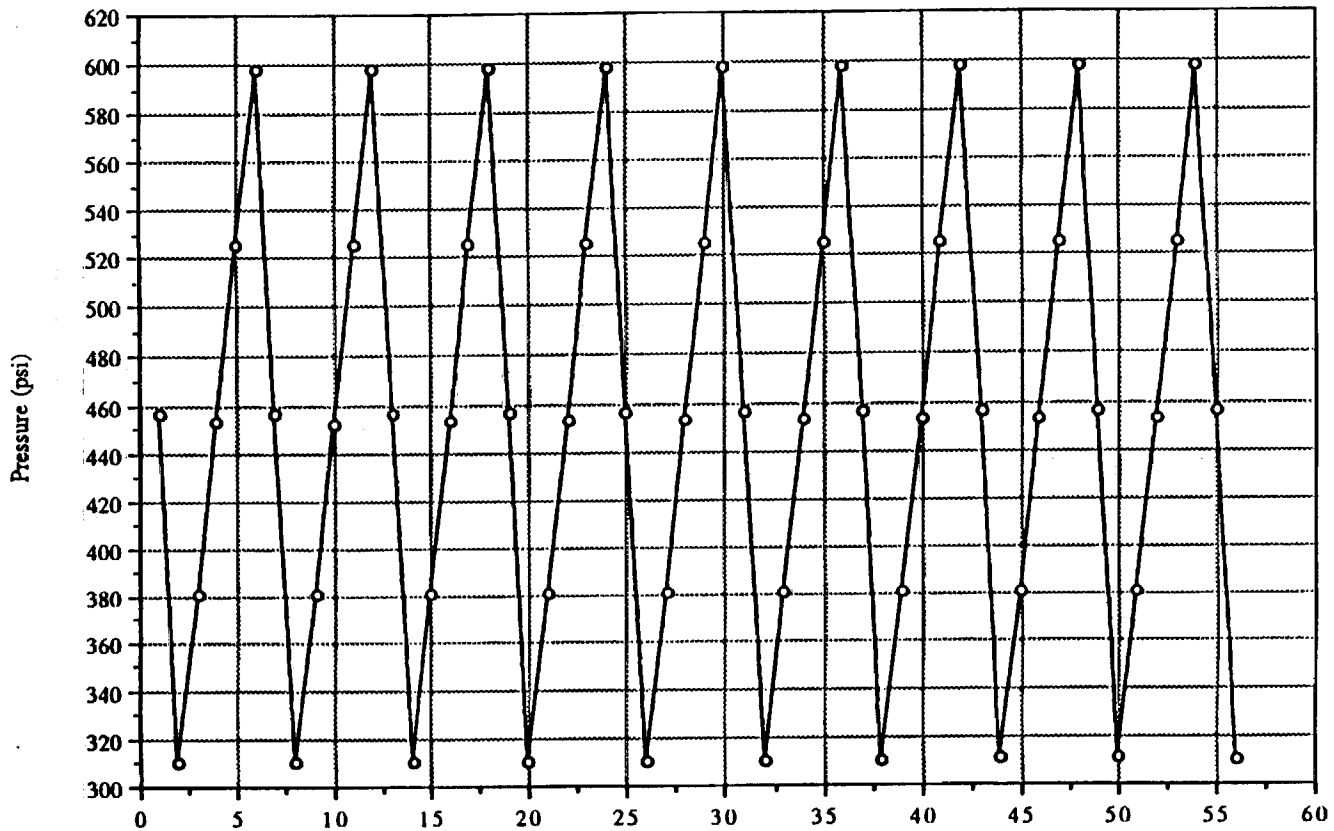

17 NOVEMBER 1993

CHARGE CONTROL FOR THE DSPSE NiH2 CPV BATTERY

Summary

- NRL/BMDO DSPSE Spacecraft To Use NiH2 CPV With Pressure Based Charge Control Method
- Pressure Based Charge Control
  - High Rate (C/5 = 3.0 amps) Pressure Set Point
  - Low Rate (C/100 = 0.150 amps)
- Pressure Set Points Of 600 psi and 650 psi Picked For Flight
- Pressure Characterization Of Batteries Important
- Further Study with Qual/Flight Spare to Investigate Long Term Performance

Use of Calorimetry for End of Charge Determination

Chris J. Johnson
Boeing Defense & Space Group
Seattle, WA

TESTING of AEROSPACE BATTERIES @ BOEING

CHEMISTRY	SYMBOL	APPLICATIONS
Nickel Hydrogen	NiH_2	Future Power Systems
Nickel Cadmium	NiCd	Small Power Subsystems
Nickel Metal Hydride	NiMH	SEDSAT Experiment
Fibrous Nickel Cadmium	F-NiCd	Starter Battery for Boeing 777
Lithium Thionyl Chloride	$Li-SOCl_2$	NASA Space Qual
Lithium Bromine Complex	Li-BCX	NASA - EVA suit
Zinc Silver Oxide	Zn-AgO	Boeing - IUS

Application of Heat Flow Measurements on Batteries

1) ESTABLISH THERMAL NEUTRAL POTENTIAL

PERMITS CALCULATION OF HEAT FLOW FROM VOLTAGE

2) IDENTIFY INEFFICIENT CHARGING

$$\beta\text{-NiOOH} + H_2O + e^- \Leftrightarrow \beta\text{-Ni(OH)}_2 + OH^-$$

$$H_2 + 1/2O_2 \Rightarrow H_2O + Q$$

3) UNDERSTAND SELF DISCHARGE MECHANISMS

$$2\ NiOOH + H_2 \Rightarrow 2\ Ni(OH)_2 \qquad \Delta H = 144.85\ kJ/mole$$

4) PROVIDE ACCURATE VOLTAGE/TEMP. DATA

PARAMETRIC DATA NEEDED FOR VT CONTROL

INDICATORS of INEFFICIENT CHARGING

1) INCREASED HEAT FLOW FROM H_2 + O_2 RECOMBINATION REACTION

2) VOLTAGE "ROLL OVER"

3) LOSS of LINEAR INCREASE IN PRESSURE on NiH_2 CELLS

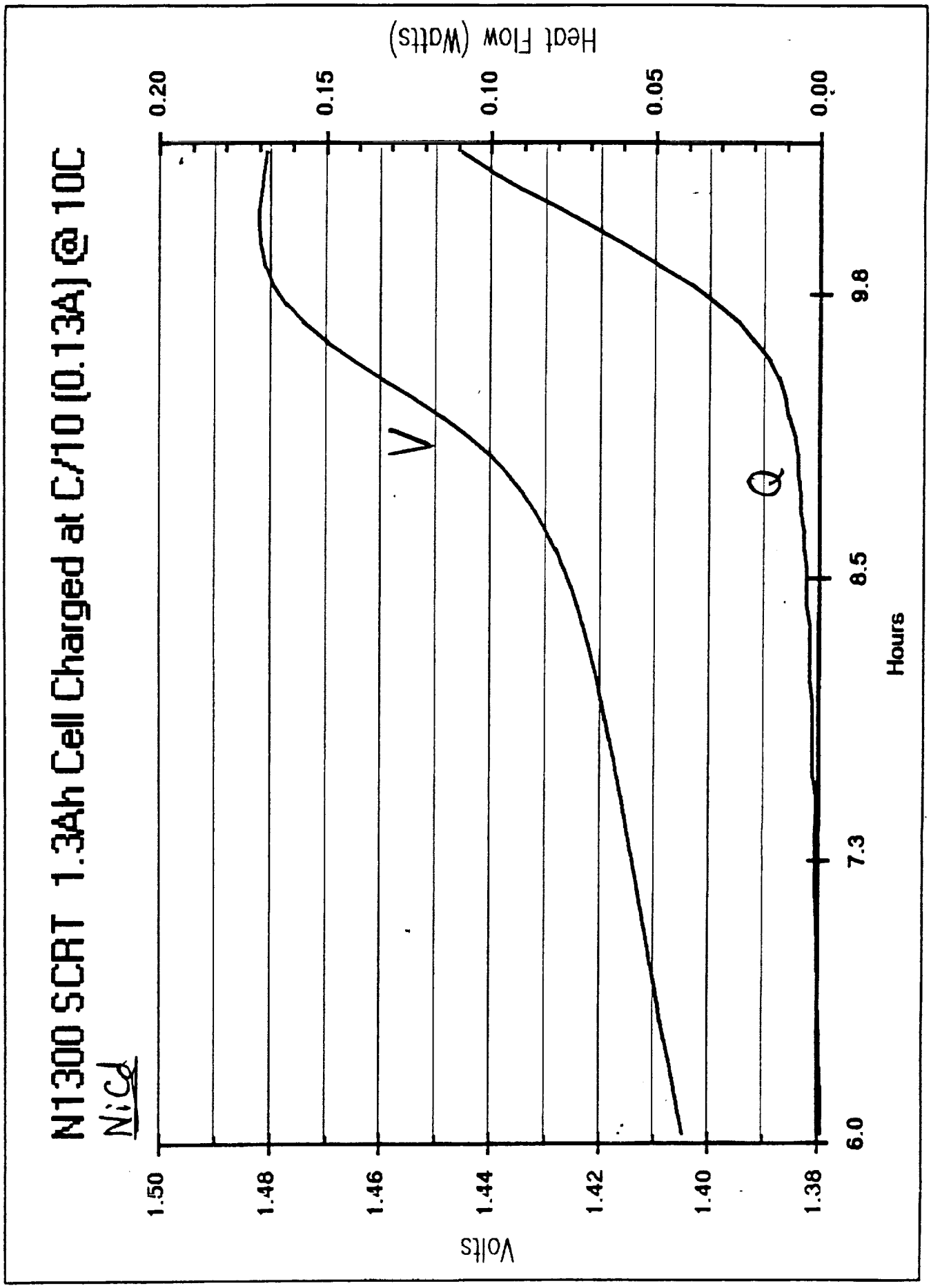
N1300 SCRT 1.3Ah Cell Charged at C/10 (0.13A) @ 10C
NiCd
Heat Flow (Watts)
0.20
0.15
0.10
0.05
0.00
Volts
1.50
1.48
1.46
1.44
1.42
1.40
1.38
V
Q
6.0
7.3
8.5
9.8
Hours

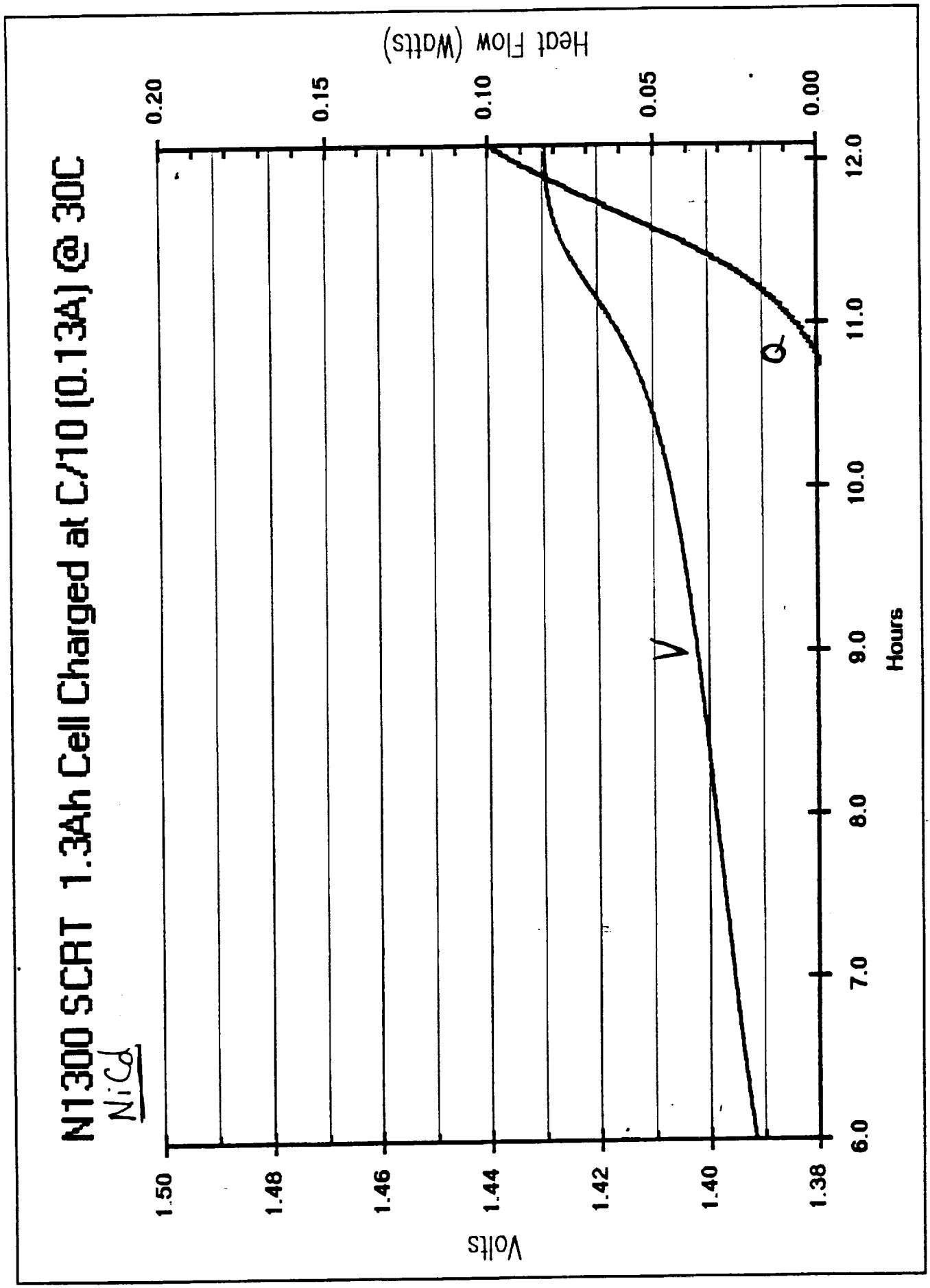
N1300 SCRT 1.34h Cell Charged at C/10 (0.13A) @ 30C
NiCd
Heat Flow (Watts)
0.20
0.15
0.10
0.05
0.00
Volts
1.50
1.48
1.46
1.44
1.42
1.40
1.38
Hours
6.0
7.0
8.0
9.0
10.0
11.0
12.0
Q
V

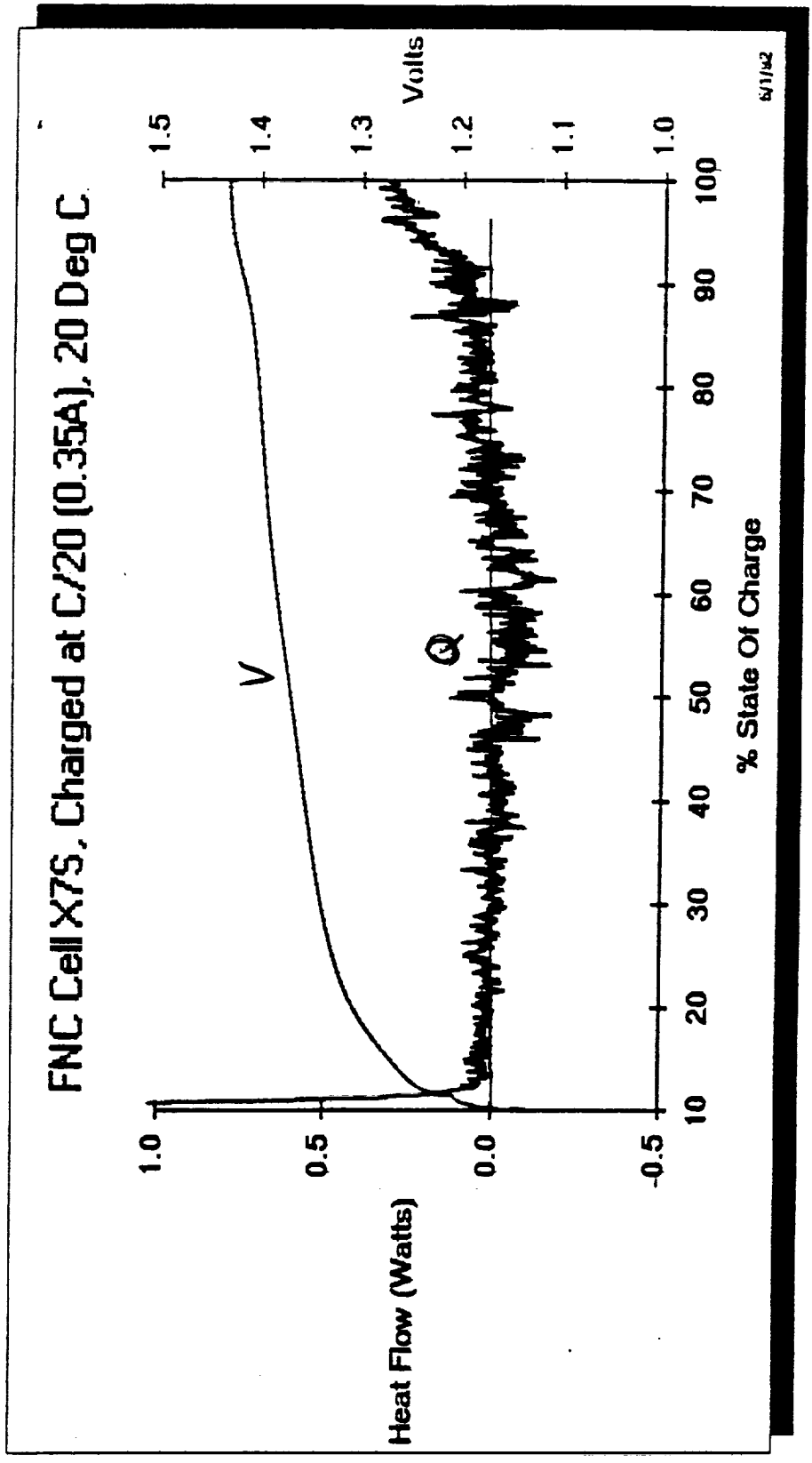
FNC Cell X7S, Charged at C/20 (0.35A), 20 Deg C
6/1/92
Volts
1.5
1.4
1.3
1.2
1.1
1.0
V
Q
% State Of Charge
10
20
30
40
50
60
70
80
90
100
Heat Flow (Watts)
1.0
0.5
0.0
-0.5

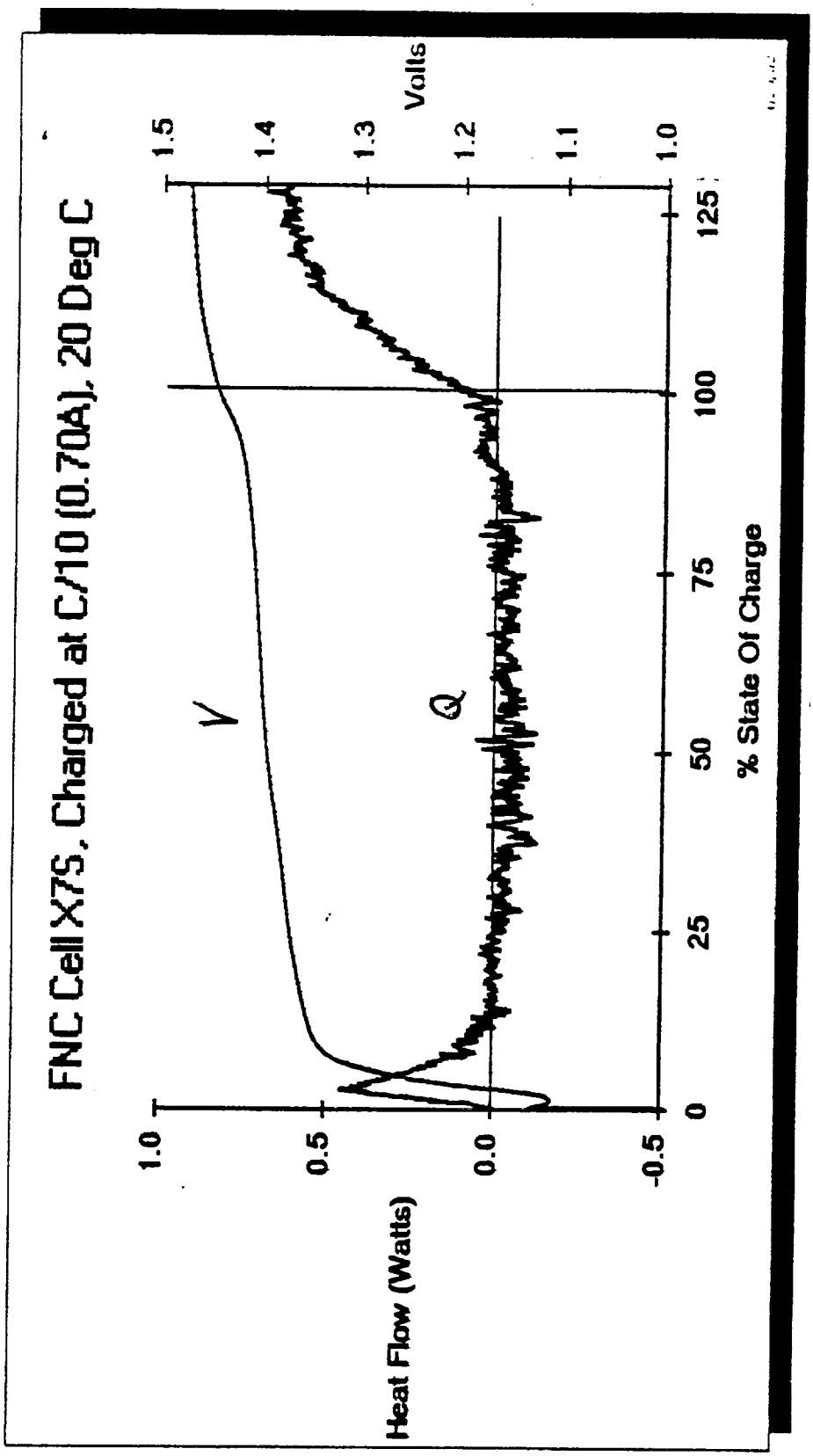
FNC Cell X75, Charged at C/10 (0.70A), 20 Deg C
Volts
1.5
1.4
1.3
1.2
1.1
1.0
V
Q
1.0
0.5
0.0
-0.5
Heat Flow (Watts)
0
25
50
75
100
125
% State Of Charge

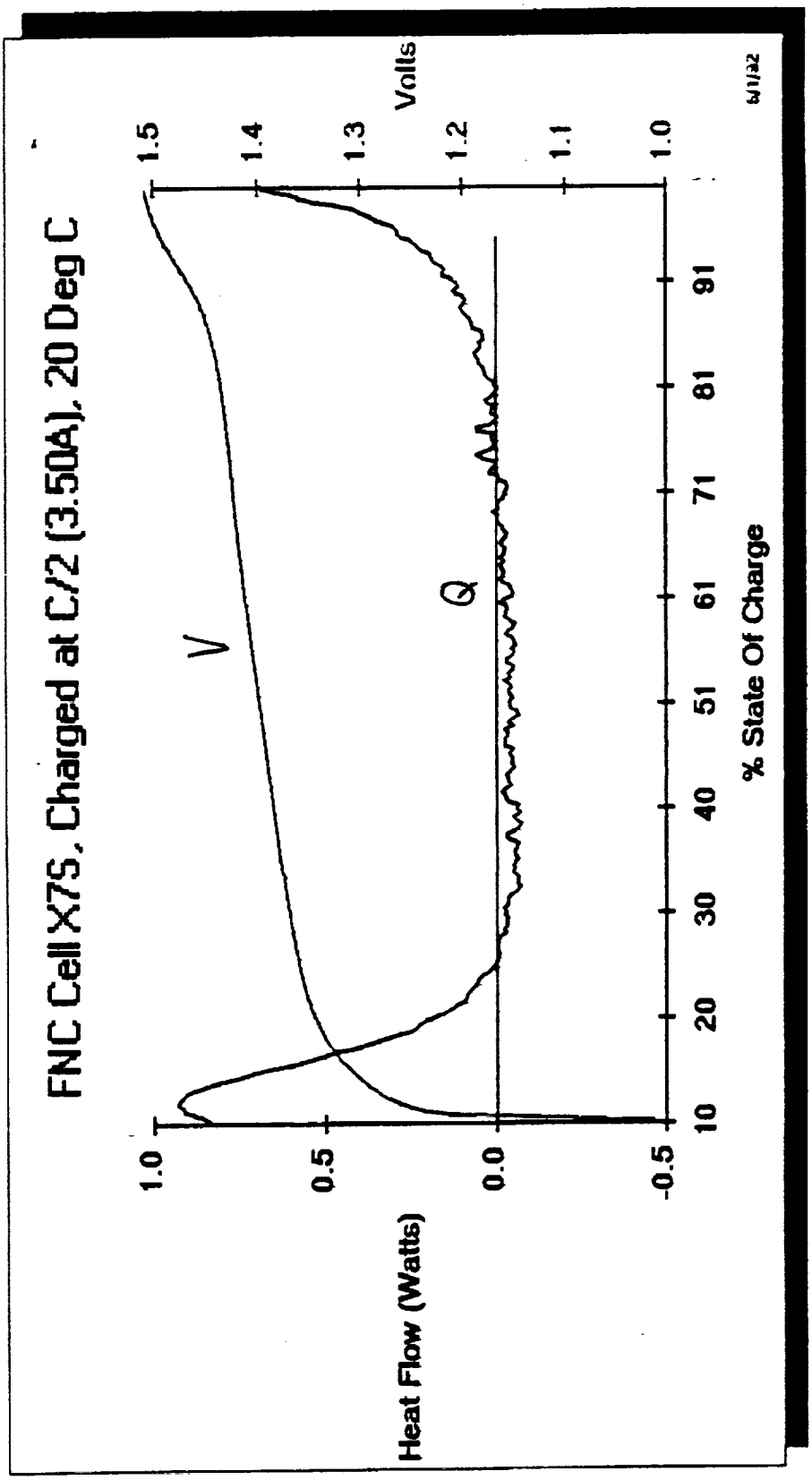
FNC Cell X7S, Charged at C/2 (3.50A), 20 Deg C
Volts
1.5
1.4
1.3
1.2
1.1
1.0
V
Q
1.0
0.5
0.0
-0.5
Heat Flow (Watts)
10
20
30
40
51
61
71
81
91
% State Of Charge

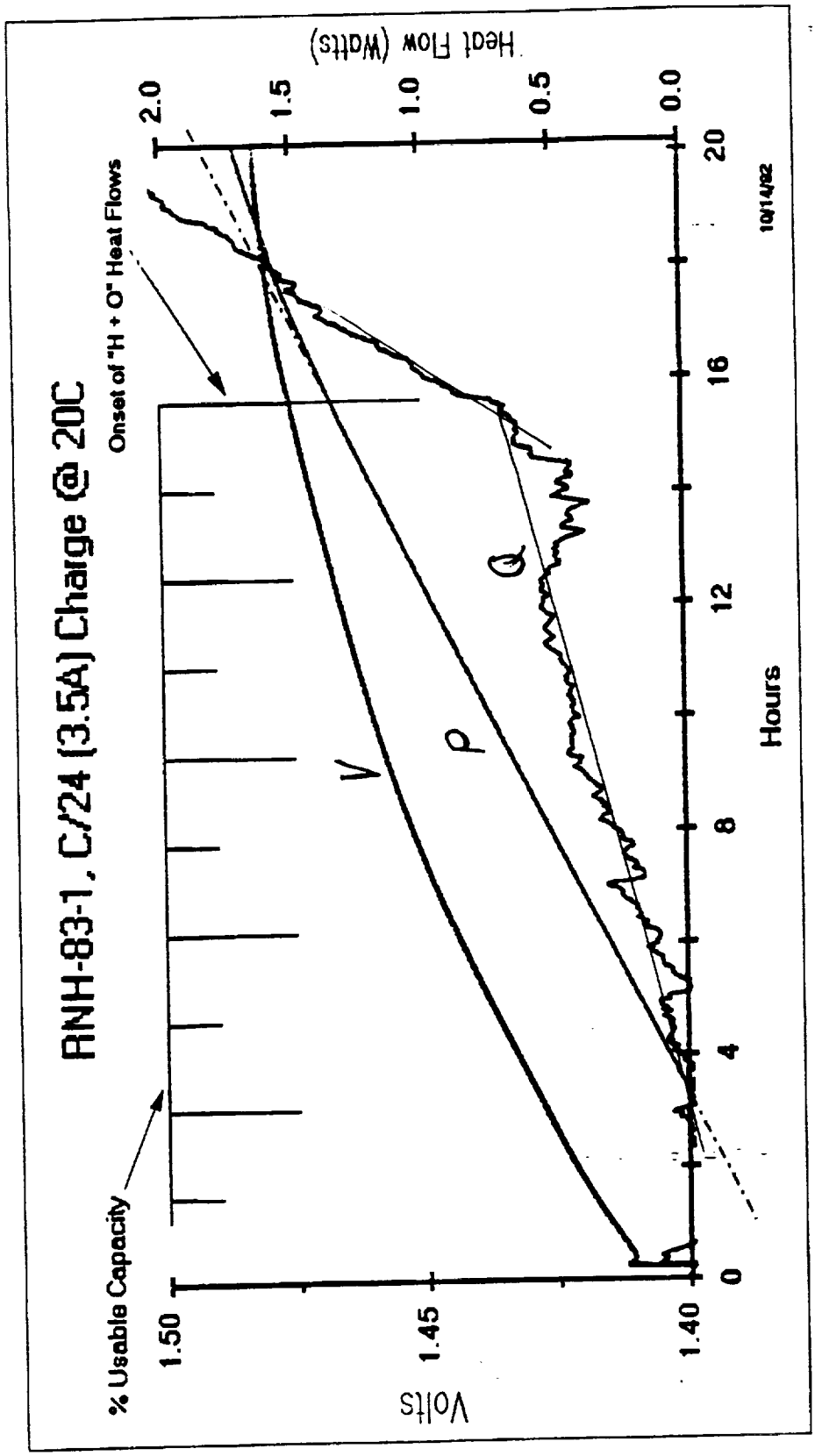
RNH-83-1, C/24 (3.5A) Charge @ 20C
Onset of "H + O" Heat Flows
% Usable Capacity
Heat Flow (Watts)
Volts
Hours
V
P
Q
2.0
1.5
1.0
0.5
0.0
1.50
1.45
1.40
0
4
8
12
16
20
10/14/92

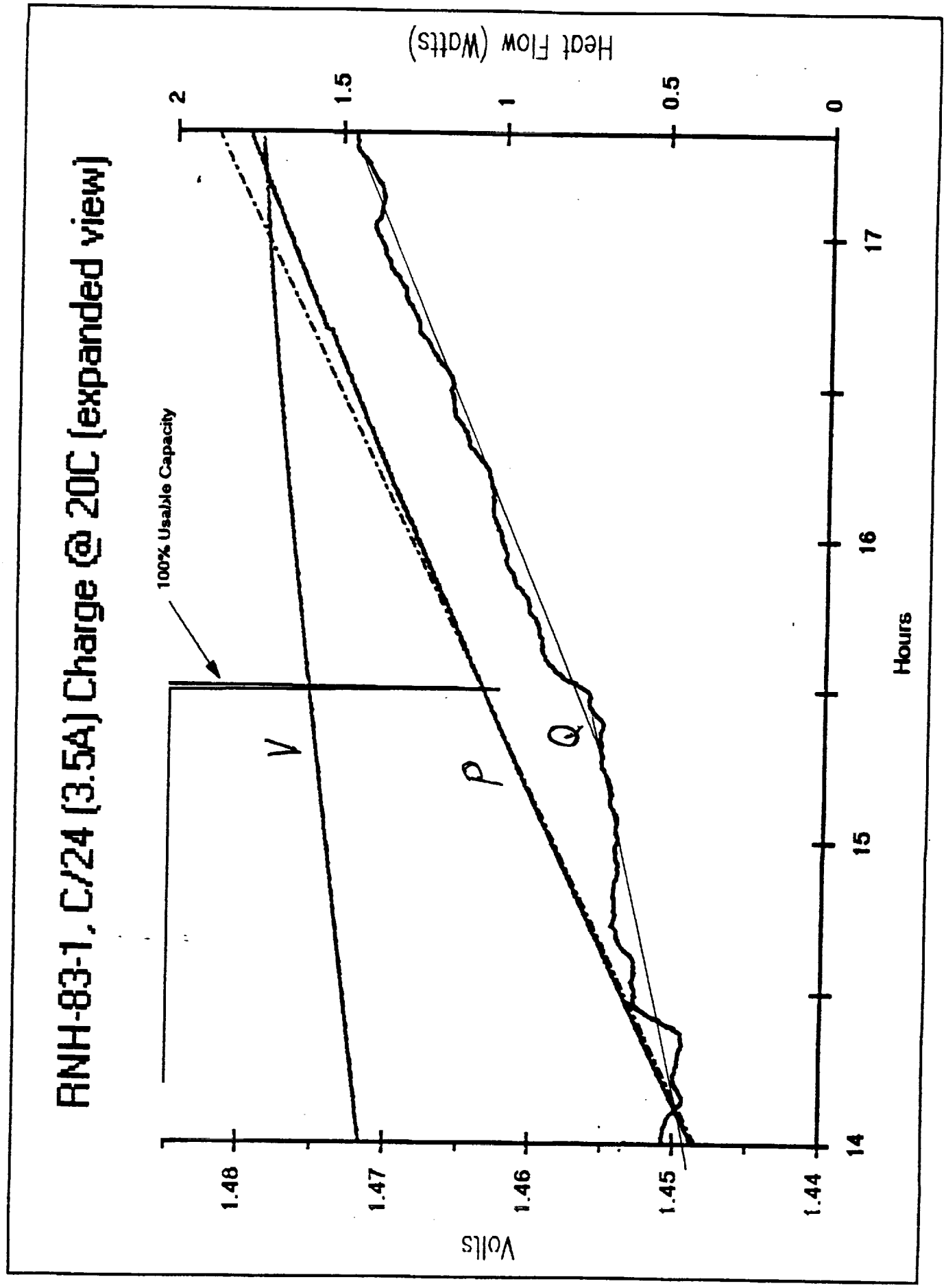
RNH-83-1, C/24 (3.5A) Charge @ 20C (expanded view)
Heat Flow (Watts)
2
1.5
1
0.5
0
100% Usable Capacity
V
P
Q
Volts
1.48
1.47
1.46
1.45
1.44
14
15
16
17
Hours

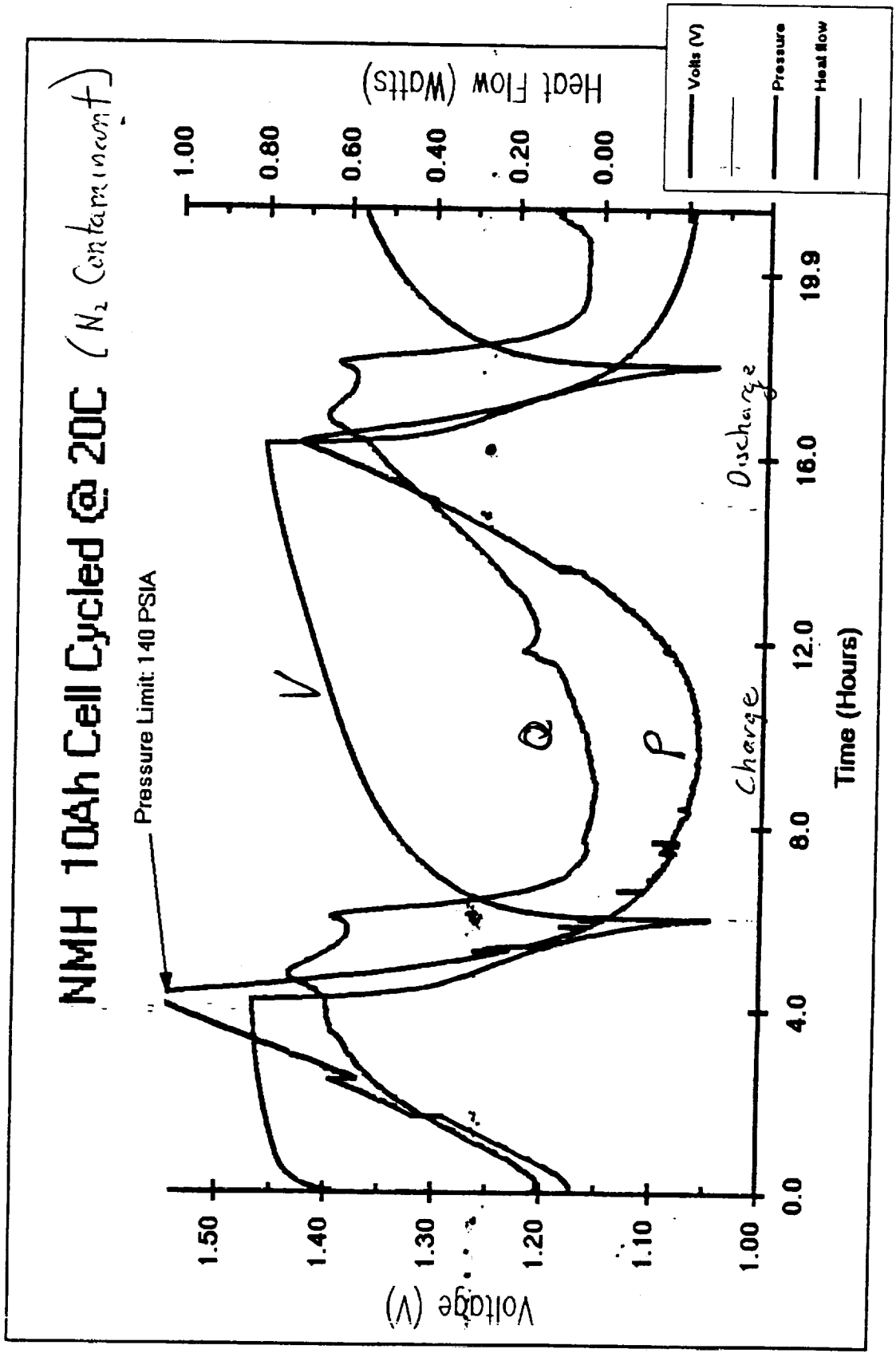
NMH 10Ah Cell Cycled @ 20C (N2 Contaminant)
Pressure Limit: 140 PSIA
V
Q
P
Charge
Discharge
Voltage (V)
Heat Flow (Watts)
Time (Hours)
Volts (V)
Pressure
Heat flow
1.50
1.40
1.30
1.20
1.10
1.00
1.00
0.80
0.60
0.40
0.20
0.00
0.0
4.0
8.0
12.0
16.0
19.9

NIMH Cell Gas Analysis - Preliminary Results Summary

Cell pressure recovers within minutes after sampling

Hydrogen and nitrogen predominant, lesser amounts water, oxygen, others

No evidence for the presence of methane

Significant percentage of oxygen present at 100% charge in one cycle

Oxygen consumed completely during discharge cycle

Explosive mixtures of hydrogen and oxygen are present at some times

Significant gas composition changes occur during storage in a discharged state

SUMMARY

1) All Ni - Based Batteries Studied Indicated Increased Q @ End of Charge

2) NiH_2 Cells Showed Increase in Q related to Charge Inefficiency
   Q Increase & Deviation from Linear Increase in H_2 Pressure synonymous

3) Heat Flow (Q) from NiMH was Complicated by Presence of N_2 Contaminant

Advanced Technologies Session

Session Organizer: *Eric Darcy*
NASA Johnson Space Center

Advanced Nickel-Hydrogen Spacecraft Battery Development

D.K. Coates, C. L. Fox, D. J. Standlee and B. K. Grindstaff
Advanced Systems Operation
Eagle-Picher Industries, Inc.
Joplin, Missouri 64802

N94- 28129

Abstract

Eagle-Picher currently has several advanced nickel-hydrogen (NiH_2) cell component and battery designs under development including common pressure vessel (CPV), single pressure vessel (SPV) and dependent pressure vessel (DPV) designs. A CPV NiH_2 battery, utilizing low-cost 64mm (2.5 in.) cell diameter technology, has been designed and built for multiple smallsat programs, including the TUBSAT B spacecraft which is currently scheduled (24 Nov 93) for launch aboard a Russian Proton rocket. An advanced 90 mm (3.5 in.) NiH_2 cell design is currently being manufactured for the Space Station Freedom program. Prototype 254mm (10 in.) diameter SPV batteries are currently under construction and initial boilerplate testing has shown excellent results. NiH_2 cycle life testing is being continued at Eagle-Picher and IPV cells have currently completed more than 89,000 accelerated LEO cycles at 15% DOD, 49,000 real-time LEO cycles at 30% DOD, 37,800 cycles under a real-time LEO profile, 30 eclipse seasons in accelerated GEO and 6 eclipse seasons in real-time GEO testing at 75% DOD maximum. Nickel-metal hydride battery development is continuing for both aerospace and electric vehicle applications. Eagle-Picher has also developed an extensive range of battery evaluation, test and analysis (BETA) measurement and control equipment and software, based on Hewlett-Packard computerized data acquisition/control hardware.

Introduction/Background

Eagle-Picher Industries, Inc. (EPI) has been supplying the defense and aerospace industry with high quality, high reliability batteries for more than forty years. More than 25 electrochemical systems are represented including nickel-hydrogen, nickel-cadmium, nickel-iron, nickel-metal hydride, nickel-zinc, silver-zinc, silver-metal hydride, sodium-sulfur, lead-acid and a wide variety of thermal and lithium battery systems. EPI batteries have been included in a large number of space and missile systems including the Hubble Space Telescope, Skylab, the Patriot and Cruise missiles, Standard Missile, Sidewinder, Copperhead, AMRAAM, TOW and many others. Eagle-Picher manufactures more than 80% of all batteries used in U. S. missile and weapons systems. Nearly every manned U. S. spaceflight has used EPI batteries including the Mercury, Gemini, Apollo and Space Shuttle missions. Eagle-Picher built the silver-zinc cells which powered the Lunar Rover on the surface of the moon. More than 50 earth-orbital communications and surveillance spacecraft which use EPI nickel-hydrogen batteries have been launched.

EPI batteries have also been used in a number of solar and electric race vehicles in such races as the GM Sunrayce, the Solar 300 and the Australian World Solar Challenge. Eagle-Picher has supplied batteries to more winning electric race vehicles than any other manufacturer. Michigan State University placed first in performance and third overall in a ground-up design vehicle with EPI nickel-metal hydride batteries in the Ford Hybrid Electric Challenge in June, 1993. The University of Michigan solar/electric race vehicle won the 1993 Sunrayce using EPI batteries. Eagle-Picher is currently operating the world's only advanced electric vehicle battery manufacturing plant. This facility is manufacturing nickel-iron batteries for the Chrysler TE electric minivan. In addition, EPI has set multiple land and water speed records for electric vehicles and electric boats and set the world's electric vehicle record for the longest distance driven on a single charge.

Nickel-hydrogen (NiH_2) batteries are the system of choice for both low-earth-orbit (LEO) and geosynchronous-earth-orbit (GEO) communications and surveillance satellites. NiH_2 batteries have almost completely replaced sealed aerospace nickel-cadmium (NiCd) batteries for these applications. The NiH_2 battery system has been in production at EPI for more than fifteen years. The first NiH_2 batteries were launched in 1976 aboard the U. S. Navy NTS-2 satellite and a U. S. Air Force Flight Experiment satellite. There were several additional GEO satellites using EPI NiH_2 batteries launched throughout the 1980's including INTELSAT V, G-Star, AmericanSat, Spacenet and SatCom K1 and K2. Eagle-Picher now has NiH_2 batteries flying aboard more than fifty satellites, including several European spacecraft such as Olympus (British Aerospace), Eutelsat II (Aerospatiale), TVSat II (AEG), Telecom II and HispaSat (Matra). EPI NiH_2 batteries are also being used in demanding LEO applications such as the Hubble Space Telescope (HST). This flight database amounts to more than 97,000,000 operational cell-hours in space.

Nickel-Hydrogen Life Testing

There is also an extensive ground testing database. NiH_2 cells and batteries are being cycle life tested at EPI and other organizations, in both the U. S. and Europe. A full summary of NiH_2 testing at EPI has been recently published (1). EPI currently has more than 100 flight-type NiH_2 cells on life test under several different cycle regimes and depths-of-discharge (DOD). A summary of some of the testing being done is indicated in Figure 1. Cells have accumulated over 89,000 charge/discharge cycles under an accelerated LEO regime at 15% DOD. This test is an accelerated LEO regime in which the cells charge for 23.5 minutes and discharge for 21.5 minutes for a total of 32 cycles per 24 hour day. Testing is done at 5±3 °C. The cells are operating at 15% DOD under the accelerated regime which would be equivalent to 30% DOD under a real-time LEO regime, based on current density. Several 76 Ahr cells are being tested under the same regime and have accumulated more than 69,500 charge/discharge cycles.

Cell	Regime	%DOD	#Cycles*
RNH-30-1	R/T LEO	30	49,000
RNH-50-15	ACC LEO	15	89,000
RNH-76-3	ACC LEO	15	69,500
RNH-76-3	R/T 1	--	21,500
RNH-76-3	R/T 2	--	37,800
RNH-76-3	R/T3	--	37,000
RMH-4	R/T LEO	40	8900
RMH-10	R/T LEO	15	6,700
RNH-65-1-3	ACC GEO	75 MAX	30**
SAR-10017	ACC GEO	75 MAX	16**
SAR-10017	R/T GEO	75 MAX	6**

R/T=Real Time ACC=Accelerated
*As of November, 1993 **Eclipse Seasons

Figure 1 — EPI Life Test Summary

Intelsat V type RNH-30 cells have completed more than 49,000 real-time LEO cycles at 30% DOD. These cells are operating on a standard 55/35 LEO regime for a total of 16 cycles per day. This test has been in continuous operation for more than 9 years. Typical end-of-charge (EOCV) and end-of-discharge voltages (EODV) as a function of the number of cycles are indicated in Figure 2. No performance degradation has been observed to date.

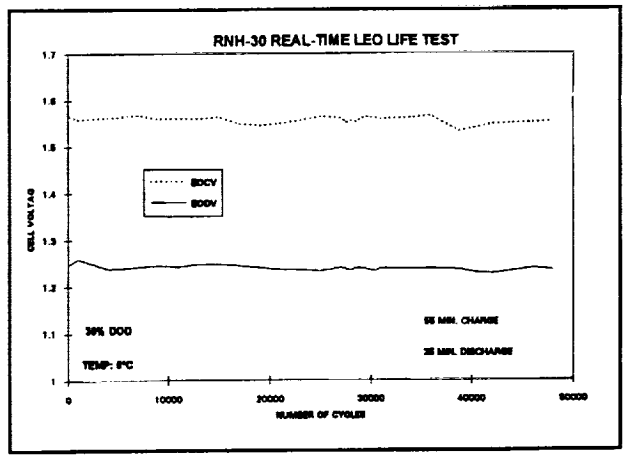

Figure 2 — Real Time LEO Life Test

Cells are also being tested under accelerated and real-time GEO test regimes as indicated in Figure 1. This testing has completed up to 30 eclipse seasons as shown in Figure 3. Each forty-two day eclipse season is performed in real-time. Test acceleration is achieved by eliminating the trickle charge period between seasons. In this

manner, approximately eight eclipse seasons can be performed per calendar year, rather than only two. The test is operating at 75% DOD maximum and the cells are reconditioned every fifth season. Figure 3 shows the EODV for Day 21 for each season. Day 21 is the day on which the maximum DOD occurs and therefore represents the minimum voltage experienced by the cell during the season. Extrapolation of this data indicates that cell failure, defined as an EODV on Day 21 of less than 1.0 volt, would not occur before approximately 42 seasons. Another accelerated GEO test has accumulated 16 seasons and the real-time GEO test is up to 6 seasons. This test includes trickle charging between eclipse seasons. Additional testing indicated in Figure 1 shows 21,500 cycles, 37,000 cycles and 37,800 cycles in three separate real-time test regimes and up to 8900 cycles in nickel-metal hydride cell testing (RMH designation).

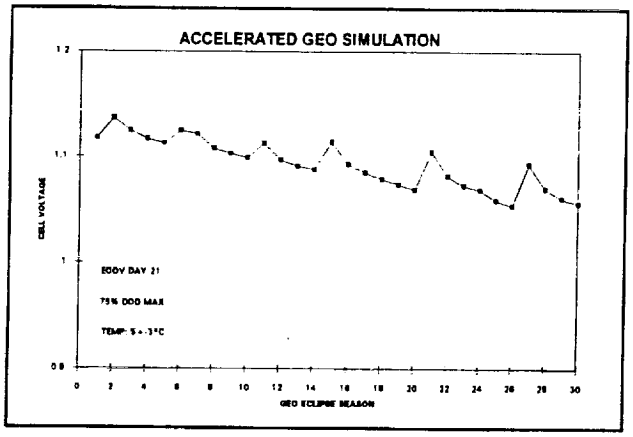

Figure 3 — Accelerated GEO Life Cycle Test

Space Station Freedom Cell Testing

Nickel-hydrogen IPV batteries have been selected as the power supply for the SSF program (2). The batteries will be used to supply power to the station during the eclipse portion of the orbit (LEO). In response to a NASA-Lewis Research Center contract in the fall of 1990, Eagle-Picher delivered 130 NiH_2 cells for life-testing and development work. These cells were designed for service in low-earth-orbit, and specifically for use in evaluating battery requirements for the SSF program. The cells consisted of two basic designs: a "standard" design and an "advanced" design. The standard cell was an Eagle-Picher "Mantech" design using pineapple-slice type electrodes in the back-to-back configuration. The cell uses a zirconium-oxide wall-wick and continuous electrode leads. Terminal seals were of the nylon compression type. All of the cells were nickel precharged (hydrogen limited) in the cell electrolyte activation procedure. The advanced design used a combination of asbestos and Zircar separators, lower cell stack compression, a double spring washer arrangement and a catalyzed wall-wick. The cells were built in two sizes, 65 Ahr and 81 Ahr. Both standard and advanced cells were built in the 65 Ahr size, but only the advanced cell was built in the 81 Ahr size. All cells were equipped with microstrain gages and aluminum thermal sleeves. The sleeve serves to remove heat from the area of the cell adjacent to the dual cell stacks and provides a means of mechanically mounting the cell for testing.

The cells were fully characterized at Eagle-Picher prior to delivery to NASA. Initial acceptance testing at EPI showed excellent electrical performance and uniformity. The cells deliver up to 56 Whr/kg with a very narrow capacity distribution over the production lots. Following delivery of the cells in the fall of 1990, most were placed on cycling tests at the Naval Surface Warfare Center-Crane, as part of the SSF life test program. The standard design 65 Ahr cells were built into 6 cell packs containing 8 cells each. Three cell packs are operating at 35% DOD and the other 3 packs are being tested at 60% DOD. The cells are operating at a charge-return ratio of 1.04 (the ampere-hour ratio of charge to discharge). As of March 1993, these cells had achieved 5200 to 5600 cycles. The advanced 65 Ahr cells were split into four separate tests containing 5 cells each. The four tests have currently completed from 5000 to 10,000 charge/discharge cycles. The advanced 81 Ahr cells are also split into four tests, with each test containing 10 cells. The 81 Ahr cells have completed from 3000 to 8000 cycles. Testing is still underway and is planned to be continued. Three of the advanced 81 Ahr cells were also provided to NASA Goddard Space Flight Center for evaluation as part of the EOS program.

Advanced Hydrogen Electrode Design

Low catalyst loading gas diffusion membrane electrodes have been developed for the aerospace NiH_2 battery system. This has been accomplished through the use of novel catalytic materials, new electrode designs and innovative manufacturing methods. Some of the preliminary data has been published (3). Current state-of-the-art NiH_2 spaceflight battery electrodes use fuel cell grade platinum black at relatively high catalyst loading levels. At this usage level, platinum represents a major cost in the NiH_2 cell. Low-cost NiH_2 cell technology requires lower cost cell components. This is particularly applicable to the emerging "smallsat" market. Novel catalyst supports and alternative catalyst systems have been developed to decrease catalyst loading levels, and therefore reduce cost, without reducing performance or reliability. Electrodes can be produced with platinum loading levels as low as 20% of previous levels, while maintaining current performance levels and retaining the existing aerospace heritage and database. Figure 4 shows representative EOCV and EODV values as a function of cycling for low catalyst loading electrodes which are built into a dual stack CPV cell design. These electrodes exhibit excellent performance and have completed more than 12,000 cycles under a 90-minute LEO test regime operating at 40% DOD.

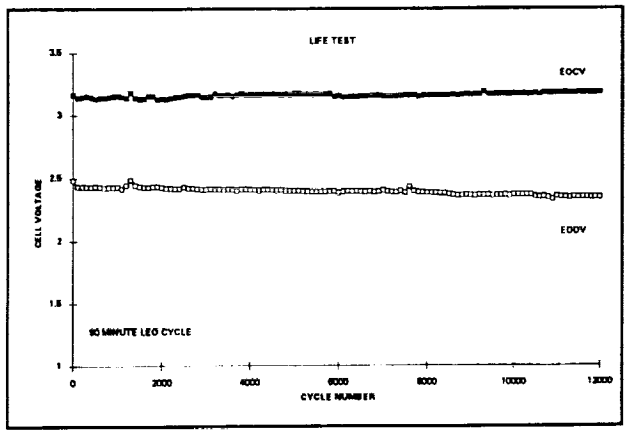

Figure 4 — Reduced Catalyst Loading In CPV

Alternative catalyst systems can further reduce platinum usage to less than 10% of previous levels or completely eliminate the use of platinum with alternate catalyst materials. Materials such as Palladium, Iridium and Ruthenium have been tested at the electrode and cell levels. Novel catalyst support materials have also been evaluated as a method of reducing catalyst loading while maintaining the high surface area necessary for catalytic activity. This advanced electrode technology has currently accumulated more than 13,000 cycles in real-time LEO testing and has been incorporated into several NiH_2 spaceflight programs. Comparative data for several catalyst variables is shown in Figure 5. The chart shows voltage versus time for a full ninety minute LEO cycle, number 12,882. Performance has been excellent for several of the electrode variables with very little degradation being observed as a function of cycling. Palladium is shown in Figure 5 as an example of a material which does not perform well. Testing is being continued. The hydrogen electrode technology developed has been incorporated into several flight programs including a low-cost NiH_2 CPV battery (64mm cell diameter) which was built for the TUBSAT B spacecraft. This satellite, built by the Technical University of Berlin, is scheduled for launch this year aboard a Russian Proton rocket.

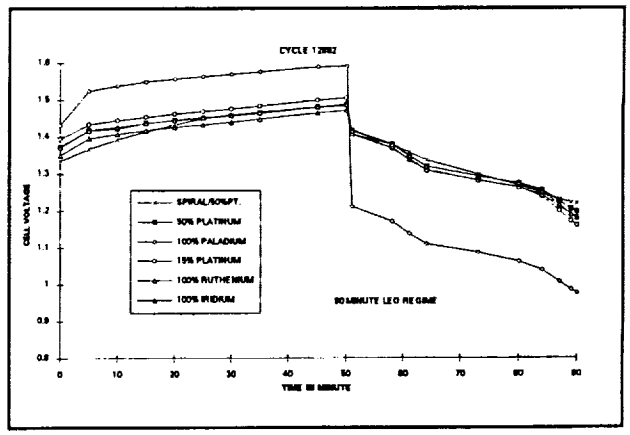

Figure 5 — Alternate Catalyst Test Matrix

Alternative Separator Evaluation Testing

Eagle-Picher currently has over 2,000 NiH_2 cells (equivalent to more than 50 batteries) currently operating in earth-orbital satellites. The vast majority of this flight database is with standard fuel-cell-grade asbestos separator. More recently, zirconium-oxide cloth has become integrated into several cell designs, particularly those which in-

corporate a wall-wick on the inner surface of the pressure vessel. Eagle-Picher has an ongoing program to procure, test and evaluate alternative separator materials. The purpose is to identify and qualify for flight, materials other than the two mentioned above. A large number of candidate materials have been identified from several different manufacturers. These materials are subjected to an initial screening procedure and materials which show promise are then evaluated in actual cell testing. Some of the initial parameters that are considered are material type, chemical compatibility, oxidation resistance, long-term stability, wicking ability, wettability, electrolyte retention, bubble pressure, thickness, availability, cost (near-term and long-term) and other factors. Initial separator evaluation cell testing is typically done at the boilerplate cell level which provides a simple, rapid means of generating comparative data. The most promising samples are built into flight-type NiH_2 cells for performance testing and cycle life evaluation.

Approximately 15 materials have been evaluated for potential applications in the NiH_2 battery system. Additional materials have been evaluated in the NiMH system. The materials range from inorganics to treated polymeric materials. More than 60 flight-type NiH_2 cells have been built specifically for the purpose of separator materials evaluation. Most of the comparative testing is done using the same cell design variables in order to minimize any extraneous effects on the separator being tested. Several separator types have been selected for cycle life testing based on superior performance characteristics in basic material and initial boilerplate cell level testing. This testing has been underway for several years and some materials have accumulated up to 35,000 cycles in accelerated LEO testing. Most of the life testing is being done under accelerated cycle regimes in order to accumulate cycles in the shortest possible time. The effect of DOD and electrolyte concentration on the separator is also being considered. These and other factors may affect the ultimate cycle life obtained. Several versions of polyolefin material are under test along with other types of organic separators. Results are promising to date. Materials continue to be developed in conjunction with separator vendors. Test results and data are fed back to vendors in order to optimize the most promising materials being tested. This cooperative effort will continue as new materials are selected for evaluation and new test results become available.

Common Pressure Vessel (CPV) Technology

Dual stack NiH_2 CPV cells are currently being built in both 64mm and 90mm diameters. The technology is applicable to high power 114mm (4.5 in.) diameter cell designs as well. The 64mm cells are specifically designed for small satellite applications. Cells have been produced for the "APEX", "SeaStar" and "ORBCOMM" programs with Orbital Sciences Corporation and will be flown in the TUBSAT B spacecraft built by the Technical University of Berlin. Several 90mm CPV cells have been built for the "SALT" program with Intraspace and cells were provided to the Naval Research Laboratory (NRL). A typical 64mm CPV battery design is shown in Figure 6.

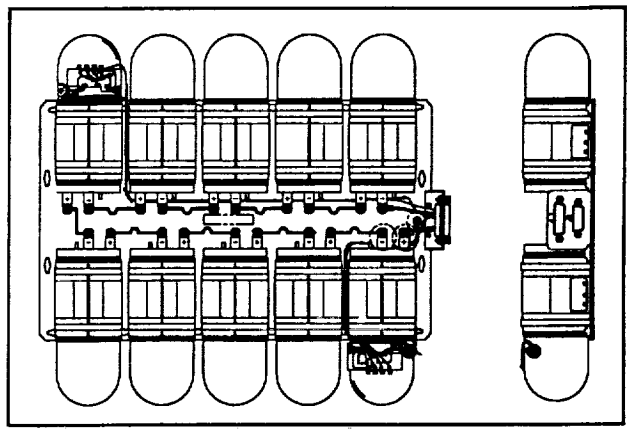

Figure 6 — SAR-10027 Ni-H_2 Battery Outline

The dual stack CPV design provides several important advantages over conventional IPV technology, including a 50% reduction in the mounting footprint of the battery, a 30% reduction in cell volume and a 10% reduction in mass. There are also reduced IR conductor losses due to the shorter internal series connection as compared to wiring two cells together externally. The dual stack approach provides a low technical risk due to mini-

mal deviation from accepted spaceflight qualified designs. The dual stack CPV cell is very similar to the dual stack IPV cell except that the two cell stacks are connected electrically in series instead of in parallel. Therefore, the CPV cell has an output voltage of 2.5 volts, which is the sum of the two series-connected cell stacks. 40 Ahr CPV cells (90mm diameter) have completed over 16,000 cycles at 50% DOD in a real-time LEO test regime. No performance degradation has occurred and testing will be continued.

Single Pressure Vessel (SPV) Technology

SPV technology differs from the previously discussed CPV technology by combining an entire multicell NiH_2 space battery in a single pressure vessel. SPV technology has been developed to simplify the NiH_2 system at the battery level and ultimately to reduce overall battery cost and increase system reliability. The battery mechanical design is shown in Figure 7. The pressure vessel has an outside diameter of 254mm. Internal construction is modular and allows any number of individual cells to be stacked together. Each cell module is designed to deliver the rated capacity of the battery, with the resultant battery voltage being the sum of the series-connected cells. The length of the pressure vessel is determined by the number of cell modules and the desired operating pressure. The system is designed to operate at internal hydrogen pressures up to 1000 psi but the pressure can be reduced by including additional free volume to accommodate the hydrogen gas. Each cell module is sealed to retain the potassium-hydroxide electrolyte. This prevents any potential electrolyte bridging between cells. A microporous plug allows the diffusion of hydrogen gas into and out of each cell module for normal cell operation. The plug is impermeable to the aqueous electrolyte. As the battery is charged, hydrogen gas generated inside each cell module diffuses into the free volume of the pressure vessel. The pressure inside the cell module remains equalized with the internal pressure of the battery. As the individual cell module does not contain any net pressure differential, it can be made of lightweight plastic materials. The SPV battery design is flexible and can be configured for both high voltage, low capacity systems and high capacity, low voltage systems. This design is particularly attractive for large arrays of batteries with multiple series/parallel arrangements for systems such as SSF or other future large space-based systems. The use of SPV batteries would allow increased overall power system flexibility as compared to traditional multicell IPV battery designs.

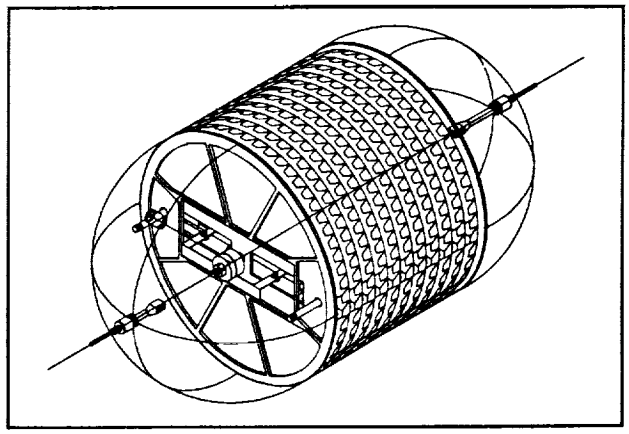

Fig. 7 Single Pressure Vessel Battery

Dependent Pressure Vessel (DPV) Technology

Dependent pressure vessel technology is also a modular approach to NiH_2 space battery design. DPV battery construction offers the potential for substantial improvements in battery specific-energy (weight) and energy-density (volume). The DPV battery offers potential savings in weight and volume of 25 to 30% compared to a conventional IPV battery design. This design was first reported by Eagle-Picher in 1974 (4) and new applications such as large communications satellites and the SSF program have renewed interest in this design. The battery concept is illustrated in Figure 8. As shown in the figure, the geometry of a DPV cell requires some support of the flat surfaces and the cell is partially dependent upon the battery package for gas pressure containment. A major design advantage is that the battery support structure is efficiently required to restrain only the force applied to a portion of the end cell only. As the DPV cells are stacked in series to achieve the desired system voltage, this increment of the total battery weight becomes small.

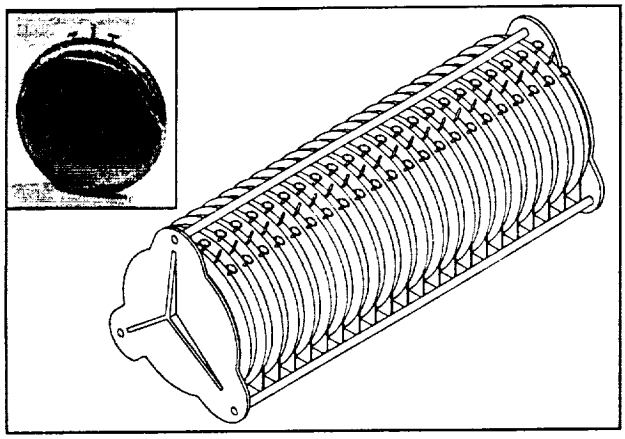

Figure 8 — Ni-H_2 DPV Battery Design

The advantage of the DPV cell design over the SPV design is that the problem of a single point failure in the event of a hydrogen leak is avoided. The DPV provides a lower risk approach to achieving substantial energy density improvement by offering less deviation from accepted flight qualified technology. The geometry of the DPV cell also promotes compact, minimum volume packaging and places all cell terminals in close proximity along the length of the battery. The resulting ability to reduce intercell current conductor size offers additional significant weight savings. Typical internal cell construction is shown in Figure 9. The electrode stack is rectangular within the pressure vessel. A second major advantage, the dramatic improvements in weight and volume are achieved with minimal design risks. The cell's liquid electrolyte is hermetically sealed in a single vessel as are current flight technology cells. And, a maximum, direct electrode stack-to-vessel wall interface is achieved ensuring superior system thermal management. DPV cells of a 50 Ahr design have been built and tested yielding more than 70 Whr/kg. This is the highest specific energy reported for space NiH_2 cells to date.

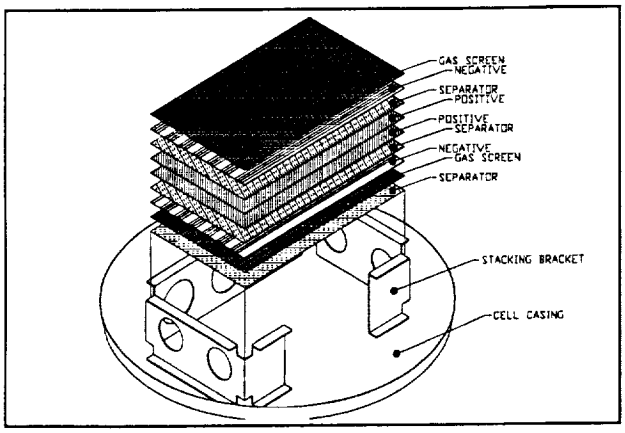

Figure 9 — Internal DPV Cell Stack Construction

Low-Pressure Nickel-Hydrogen Technology

There has been a growing interest recently in several low pressure NiH_2 battery designs, including nickel-metal hydride (NiMH) batteries. The NiMH battery is electrochemically identical with the nickel-hydrogen system except atomic hydrogen is stored as a solid metallic hydride rather than as a molecular gas. Eagle-Picher began working with low pressure NiH_2 battery systems in the early 1970's in connection with space battery R&D programs. Comsat Laboratories also investigated this technology (5). The interest was to increase the volumetric efficiency (energy density) of the NiH_2 battery by lowering the maximum operating pressure (MOP). This would eliminate the need for free volume inside the cell pressure vessel required to accommodate the hydrogen gas at manageable pressures. This would lead to a substantial increase in volumetric energy density and eliminate the need for a cylindrical pressure vessel. The disadvantage is that the linear pressure versus state-of-charge indication of the NiH_2 system is no longer valid. Also, an additional failure mechanism is introduced into the cell in that the hydride material could possibly degrade and fail before the normal cell wear-out mechanism is reached.

Recent advances in hydride materials technology have made possible the use of low pressure NiH_2 batteries for aerospace applications (6). The hydride material can either be used electrochemically as the discharge anode in the cell or can be used as ancillary chemical hydrogen storage for a normal pressure-type nickel-hydrogen cell. In either case the entire system can be hermetically sealed and therefore maintenance-free. Chemical hydrogen storage offers the advantage of potentially much longer cycle life. The problems of hydride material pulverization, performance degradation or oxygen/water/electrolyte poisoning are avoided. Metal hydride cells are

being manufactured and tested in a variety of designs and capacity ranges. These include both nickel and silver cathode cells. Hermetically sealed 10 Ahr aerospace cells have completed more than 2,000 LEO cycles at 45% DOD and 4 Ahr aerospace design cells have completed more than 8,000 cycles at 47% DOD. Low pressure 200 Ahr NiH_2 batteries have been built and tested with excellent results. Low pressure NiH_2 technology offers significant advantages for volume critical applications compared to traditional IPV NiH_2 batteries. The technology is applicable to both aerospace and terrestrial commercial applications. A 300V, 40 Ahr nickel-metal hydride battery was recently supplied to Michigan State University for a ground up design electric vehicle. The vehicle placed first in the performance categories and third overall in the Ford Hybrid Electric Challenge in June, 1993. This is the world's first nickel-metal hydride battery powered vehicle.

Cell and Battery Automated Test Equipment

The Electronics Systems Group, within the Advanced Systems Operation, has developed extensive hardware and software capabilities in the area of cell and battery level automated test equipment (ATE). This capability has been developed and continuously upgraded over a period of several years in tandem with the development of spaceflight qualified battery systems, such as the nickel-hydrogen battery. Current nickel-hydrogen test system capability at Eagle-Picher includes the capacity of simultaneously testing more than 1,000 individual nickel-hydrogen cells and 15 fully integrated spacecraft batteries. This capability is being significantly increased in the near future to keep pace with current and upcoming flight programs. The specialized requirements, extremely tight tolerances and strict system controls dictated by the space industry are not addressed by commercially available test systems. The absence of appropriate computer-based hardware systems and associated software forced Eagle-Picher to develop this capability in-house. As a result, this system level battery test expertise has developed into an independent commercial operation directed at the highly specialized aerospace battery market. Specialized battery test systems are currently being supplied on a custom basis to the industry. These Battery Evaluation, Test and Analysis (BETA) systems can be configured for a variety of specific test requirements.

The core BETA test system is based on Hewlett-Packard computer and data acquisition/control (DAC) hardware. A typical BETA test system is shown in Figure 10. The specific hardware configuration and supporting software is developed in-house to meet the specific requirements of the application. Eagle-Picher is a licensed "Channel Partner" of Hewlett-Packard through the formation of a value-added business partnership. This collaboration allows Eagle-Picher to provide highly specialized advanced battery testing capabilities for military, aerospace, industrial and premium commercial applications. Statistical Process Control (SPC) options can be incorporated into the BETA test system for additional battery test and analysis capabilities. Test systems can be configured for variable levels of operator independence. Some specialized aerospace battery testing requires intensive personnel monitoring for a variety of purposes. In this instance, the BETA system is configured primarily for data acquisition and can be programmed to provide appropriate operator prompts where required. The BETA system can not only prompt specific operator interaction but also monitor and verify that the proper interaction has occurred. Various alarm capability can be included, as well. This minimizes the potential operator-incurred test faults that can

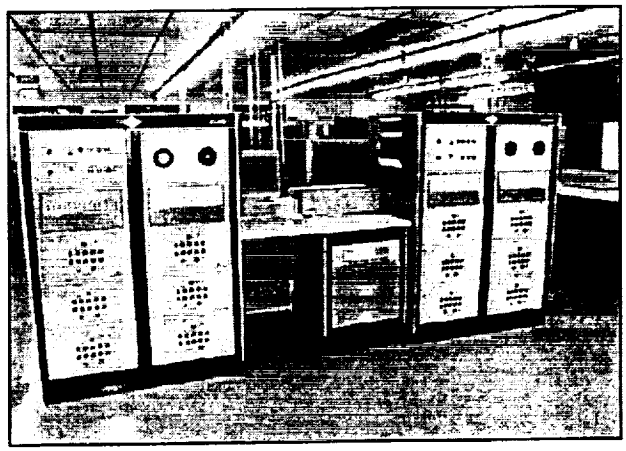

Figure 10 — Typical EPI BETA Test System

occur during 24-hour per day, 7-day per week operation and testing schedules, which are common in the aerospace industry.

Conclusions

Eagle-Picher is currently working in a number of areas to improve and further develop the nickel-hydrogen battery system. These include sub-cell level components, such as nickel and hydrogen electrodes, and cell and battery level design improvements. The technology being developed is applicable to both commercial and aerospace applications. A number of these advanced NiH_2 battery designs are currently in production and under development. The designs are applicable to many aerospace applications including the Space Station Freedom (SSF). New designs such as CPV, SPV and DPV will continue to develop and push forward the state-of-the-art in aerospace battery technology. This evolution in battery design is necessary to keep pace with the rapid advances being made in other aspects of electronics and materials science. NiH_2 battery R&D will be continued in support of future flight programs as varied as SSF and "smallsat" programs. Electrical, mechanical and thermal aspects of battery design will continue to evolve. Battery performance, including useful life and charge/discharge cycle life, must also be maximized. These power systems must provide the high degree of safety and reliability required by manned space programs and large space-based orbital systems. Advanced nickel-hydrogen batteries will continue to fulfill these demanding requirements well into the next century.

References

(1) Coates, D.; et.al. Proc. 35th Intl. Pow. Srcs. Symp. 1992 pp.164-167.

(2) Daman, M.: et.al. Proc. 27th IECEC 1992 pp.483-486.

(3) Grindstaff, B., Coates, D.; Proc. 28th IECEC 1993.

(4) Miller, L. Proc. 26th Intl. Pow. Srcs. Symp. 1974 pp.21-24.

(5) Earl, M., Dunlop, J., Proc. 26th Intl. Pow. Srcs. Symp. 1974 pp.24-27.

(6) Coates, D. Proc. 27th Intersoc. Ener. Con. Eng. Conf. (IECEC) 1992 pp.165-170.

DEVELOPMENT of NICKEL-METAL HYDRIDE CELL An Update

1993 NASA Aerospace Battery Workshop

November 16~18, 1993

S. Kuwajima, H. Kusawake & K. Nakatani, Y. Yano*

National Space Development Agency of Japan

*SANYO Electric Co., Ltd.

NASDA
NATIONAL SPACE DEVELOPMENT AGENCY OF JAPAN

DEVELOPMENT OF NICKEL METAL-HYDRIDE CELL

OVERVIEW

NASDA BATTERY DEVELOPMENT SCHEDULE

EVALUATION OF COMMERCIAL Ni-MH CELLS
- LEO CYCLE TEST
- GEO CYCLE TEST

DEVELOPMENT OF Ni-MH CELL FOR SPACE USE
- CELL DESIGN
- INITIAL CHARACTERISTICS
- TREND OF LEO CYCLE TEST UP TO 3,000 CYCLES

NASDA NATIONAL SPACE DEVELOPMENT AGENCY OF JAPAN

SCHEDULE OF BATTERY DEVELOPMENT IN NASDA

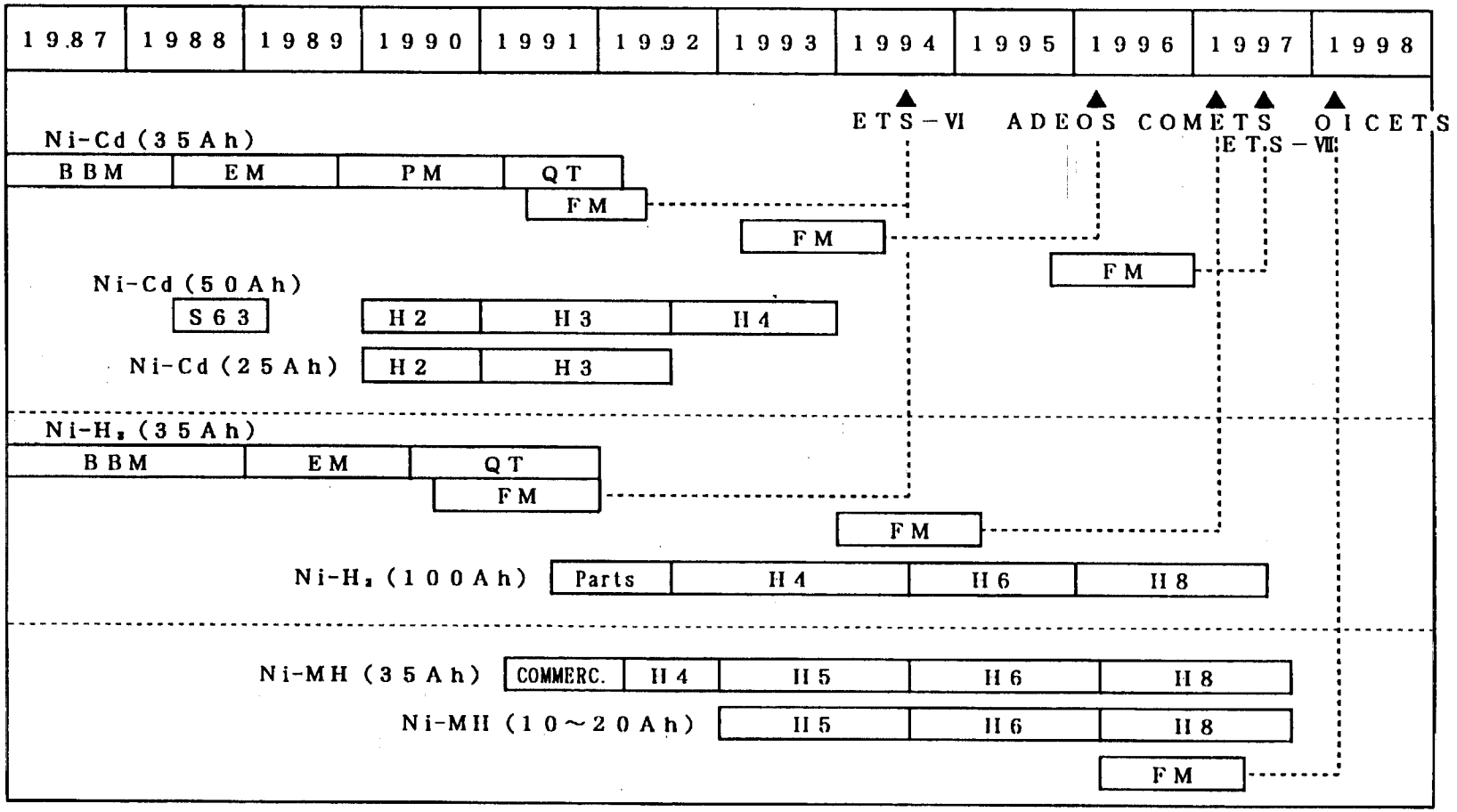

NASDA
NATIONAL SPACE DEVELOPMENT AGENCY OF JAPAN

EVALUATION OF COMMERCIAL Ni-MH CELL

SAMPLE SPECIFICATIONS

	Ni-MH	Ni-Cd
Capacity	2.2Ah	1.8Ah
MODEL No.	HR-4/3A	N-1800CR
Diameter	17 mm	26 mm
Height	67 mm	50 mm
Weight	51 g	80 g

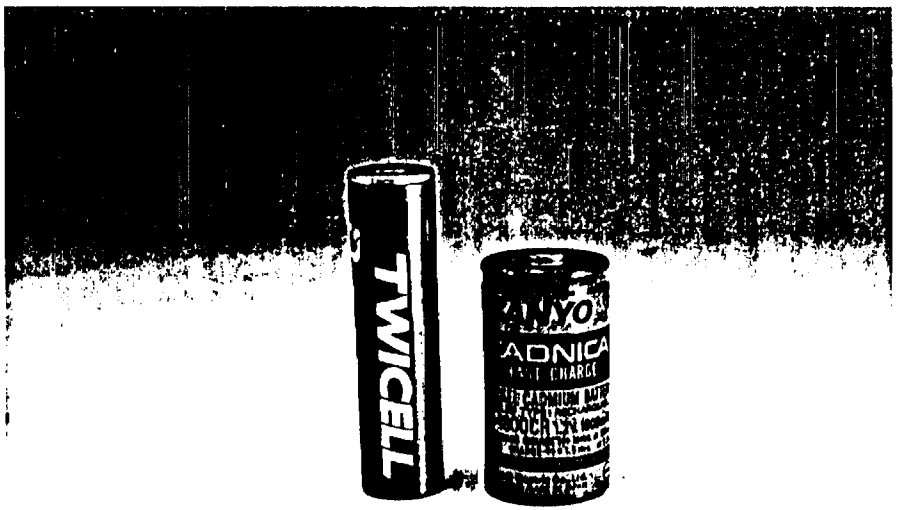

Ni-MH Ni-Cd

EXTERNAL VIEW OF SAMPLES

NASDA NATIONAL SPACE DEVELOPMENT AGENCY OF JAPAN

EVALUATION OF COMMERCIAL Ni-MH CELLS

TEST CONDITIONS OF LIFE TEST

CONDITION \ TEST TYPE	GEO	LEO
CELL	5 Ni-MH + 5 Ni-Cd	5 Ni-MH + 5 Ni-Cd
CHARGE	0.1C、9 hours	0.3C、52.5 min
DISCHARGE	0.5C、1.2hours	0.5C、30 min
DOD	60 %	25 %
CHARGE RETURN	150 %	105 %
TEMPERATURE	20℃ (COOLING PLATE TEMP.)	
CAPACITY CHECK	RECONDITIONING CAPACITY (*1	RESIDUAL CAPACITY (*2
	FULL-CHARGED CAPACITY (*3	FULL-CHARGED CAPACITY (*3
	EVERY 45 CYCLES	ABOUT EVERY 5,000 CYCLES

(C=2.2A)

*1 : Reconditioning Capacity is obtained by 1/80C discharge to 1 Volt after GEO cycling charge.

*2 : Residual Capacity is obtained by 0.5C discharge to 1 Volt after LEO cycling charge.

*3 : Full-charged Capacity is obtained by 0.5C discharge to 1 Volt after full-charging with 0.1C for 16hours.

NASDA NATIONAL SPACE DEVELOPMENT AGENCY OF JAPAN

TREND OF EOCV & EODV ON LEO TEST (COMMERCIAL)

Ni-MH CELLS

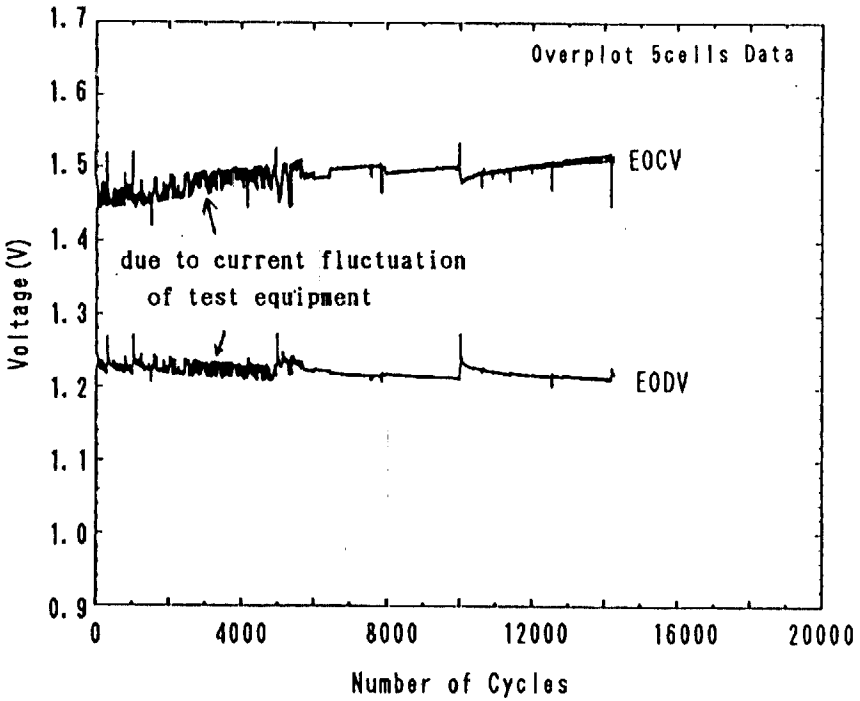

Ni-Cd CELLS

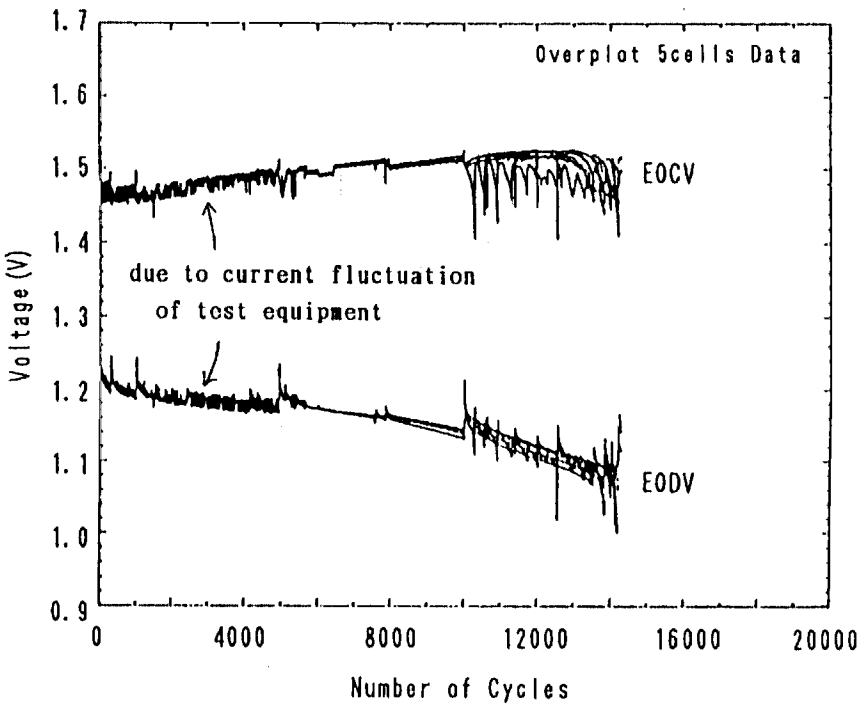

THE COMMERCIAL Ni-MH CELLS HAVE GOOD PERFORMANCE WITH RESPECT TO STABILITY OF EOCV AND EODV

NASDA NATIONAL SPACE DEVELOPMENT AGENCY OF JAPAN

LEO TEST OF COMMERCIAL Ni-MH CELLS

TREND OF CAPACITIES

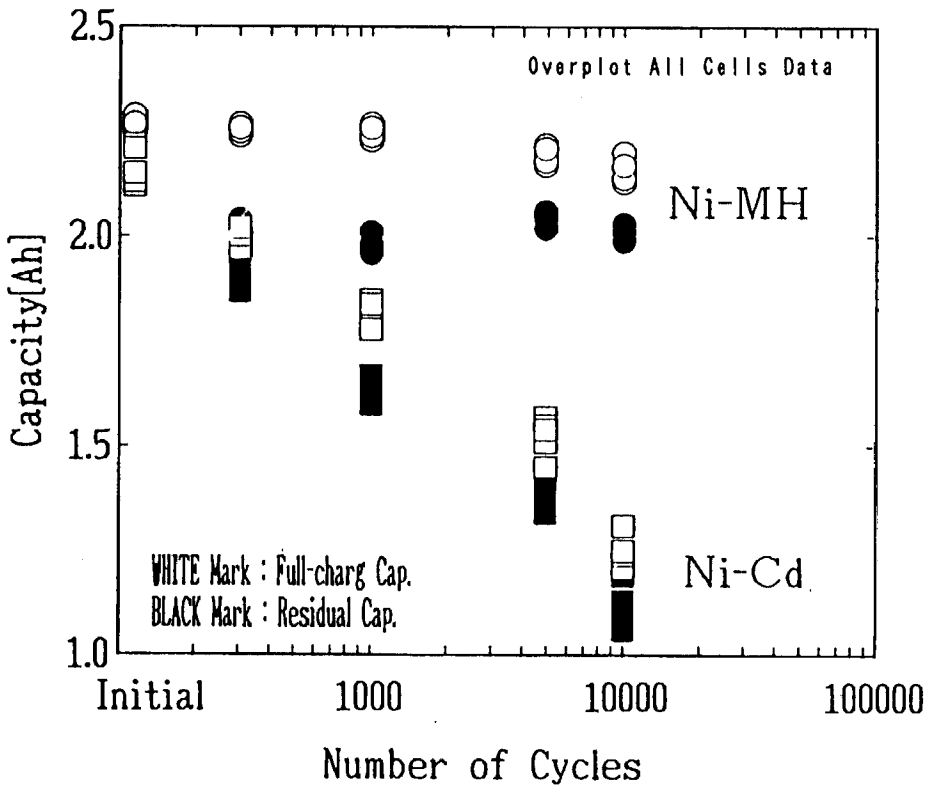

THE COMMERCIAL Ni-MH CELLS HAVE GOOD PERFORMANCE ABOUT CAPACITY REMAINING ESPECIALLY

NASDA NATIONAL SPACE DEVELOPMENT AGENCY OF JAPAN

LEO TEST OF COMMERCIAL Ni-MH CELLS

CHARGE & DISCHARGE CHARACTERISTICS IN CYCLING AT 14020 CYCLES

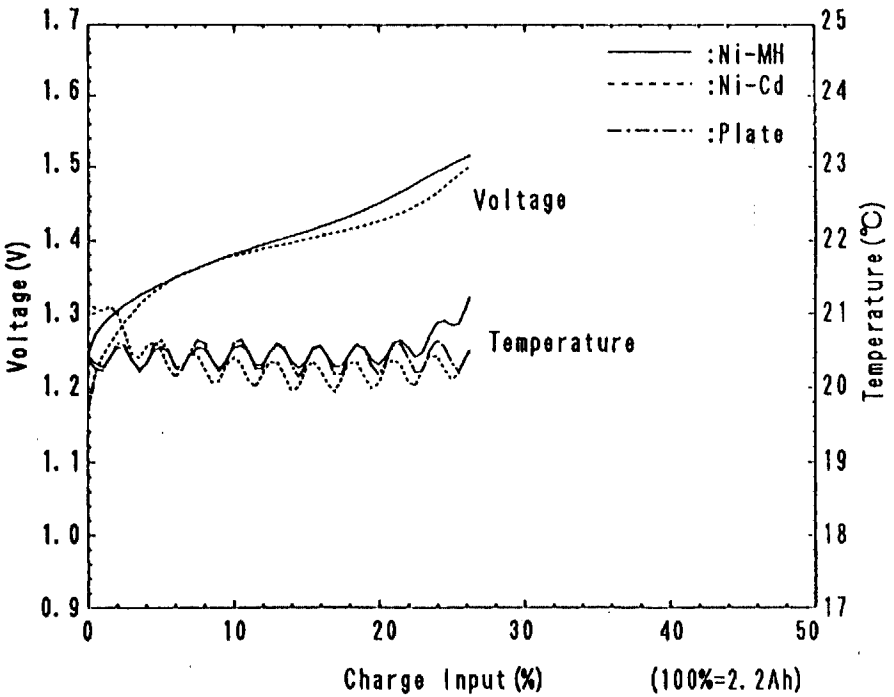

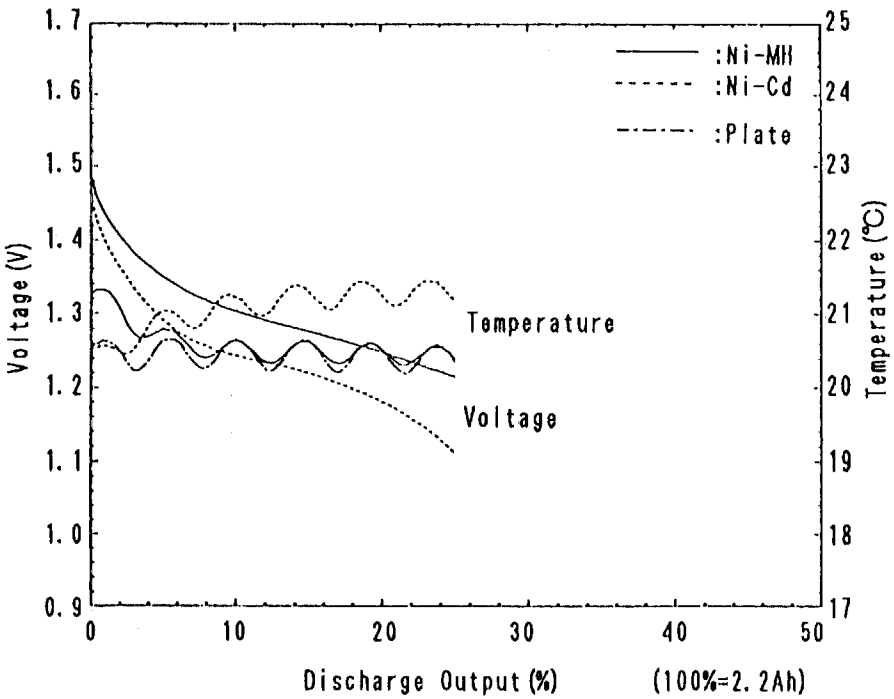

TEST CONDITION/ CHARGE : 0.3C FOR 52.5 MINUTES
DISCHARGE : 0.5C FOR 30 MINUTES (DOD: 25%)
PLATE TEMP: 20℃

NASDA NATIONAL SPACE DEVELOPMENT AGENCY OF JAPAN

TREND OF EOCV & EODV ON GEO TEST (COMMERCIAL)

Ni-MH CELLS

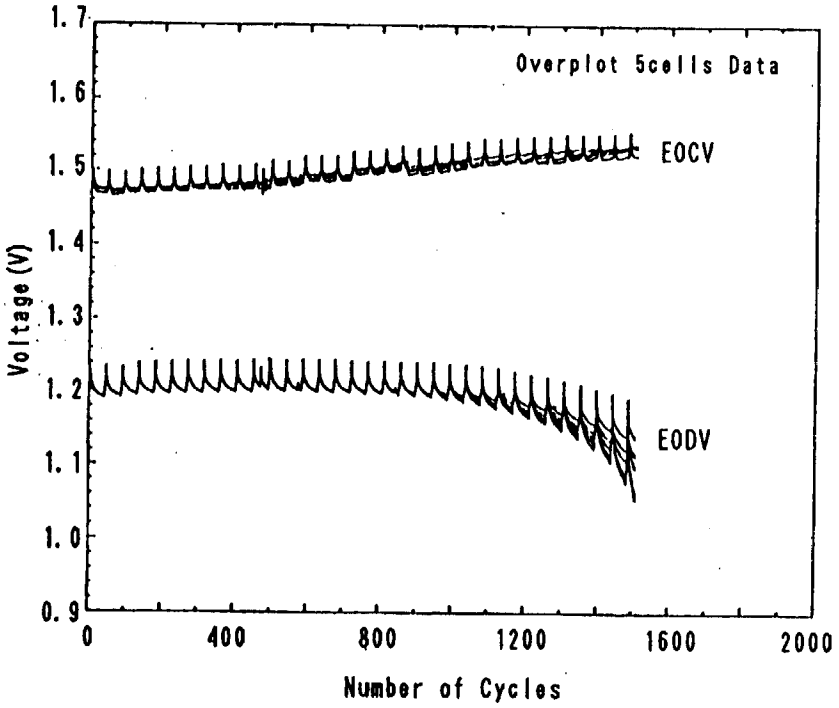

Ni-Cd CELLS

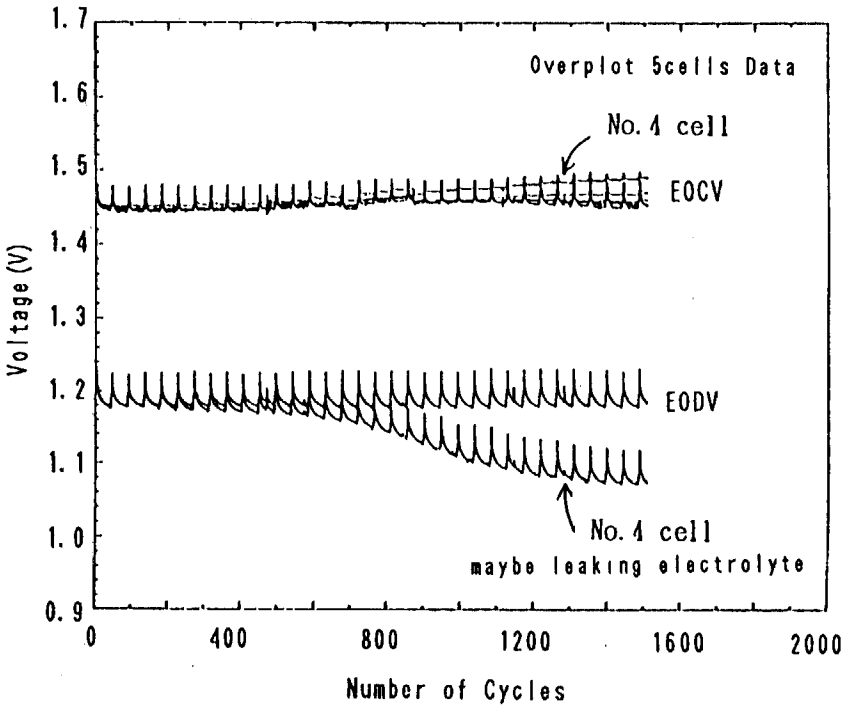

LEAKING OF HYDROGEN GAS WAS ALSO OBSERVED AT EACH EOC FROM AROUND 1,300 CYCLES

NASDA NATIONAL SPACE DEVELOPMENT AGENCY OF JAPAN

DEGRADATION OF COMMERCIAL Ni-MH CELLS ON GEO

OVERCHARGE VOLTAGE INCREASE SO FAR AS HYDROGEN GAS IS EVOLVED AT MH ELECTRODE

↓

INTERNAL PRESSURE EXCEEDS THE LIMIT OF RESEALABLE SAFETY VENT

↓

LEAK OCCURRENCE

↓

THE AMOUNT OF ELECTROLYTE DECREASE

↓

DOWNWARD TREND OF EODV
(INTERNAL IMPEDANCE INCREASE)

NASDA NATIONAL SPACE DEVELOPMENT AGENCY OF JAPAN

GEO TEST OF COMMERCIAL Ni-MH CELLS

TREND OF INTERNAL IMPEDANCE @ 1kHz

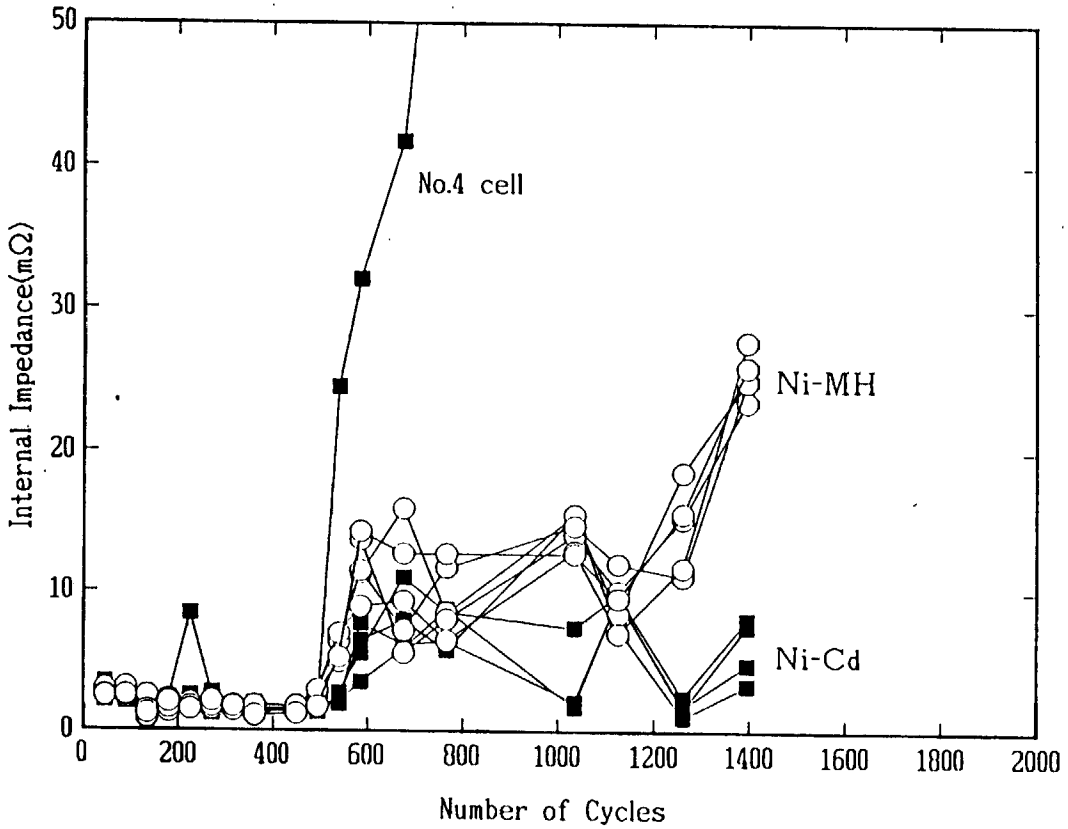

INCREASE OF INTERNAL IMPEDANCE ALSO INDICATES LOSS OF ELECTROLYTE

NASDA NATIONAL SPACE DEVELOPMENT AGENCY OF JAPAN

FAILURE MODE OF COMMERCIAL Ni-MH CELLS ON GEO

DEGRADATION (SUCH AS OXIDATION) OF MH ELECTRODE

↓

LOSS OF HYDROGEN ABSORBING CAPACITY

↓

INCREASE OF OVERCHARGE VOLTAGE

THE RESULTED PHENOMENA ARE SIMILAR TO
LOSS OF OVERCHARGE PROTECTION ON Ni-Cd CELL

- EOCV INCREASE
- EOCP (DUE TO HYDROGEN GAS) INCREASE

NASDA NATIONAL SPACE DEVELOPMENT AGENCY OF JAPAN

EVALUATION OF COMMERCIAL Ni-MH CELLS

SUMMARY

LEO: FEASIBLE & SUITABLE

GEO: NEED THE DURABILITY FOR OVERCHARGE

BECAUSE LONG-TERM CHARGE RETENTION IS REQUIRED

NASDA NATIONAL SPACE DEVELOPMENT AGENCY OF JAPAN

AEROSPACE Ni-MH CELL DESIGN

AEROSPACE Ni-MH CELL DESIGN IS BASED ON AEROSPACE Ni-Cd CELL TECHNOLOGY

Ni-MH CELL DESIGN	(+)	(−)
ACTIVE MATERIAL	$Ni(OH)_2$	$MmNi_5$
PLATE AREA	80.0×104.4 mm	
PLATE THICKNESS	0.60 mm	0.43 mm
SINTER POROSITY	85 %	—
LOADING LEVEL	2.4g/cc-void	—
NUMBER OF PLATES	16	17
ELECTRODES CAPACITY	38.6 Ah	75.2 Ah *
N/P RATIO	1.95	
SEPARATOR	NYLON	
ELECTROLYTE	31%KOH	
CELL DIMENSION (case)	95.0H×106.9W×25.2T mm	
CELL WEIGHT	840 g	
CELL CAPACITY	35.5 Ah	
ENERGY DENSITY (Actual)	50.7 Wh/kg	

REFERENCE (35Ah SPACE Ni-Cd CELL)	
CELL DIMENSION (case)	115.2H×106.9W×25.2T mm
CELL WEIGHT	1040 g
CELL CAPACITY	38.6 Ah
ENERGY DENSITY (Actual)	44.5 Wh/kg

* The capacity of MH electrode is estimated that specific energy of hydrogen storage metal is 290mAh/g.

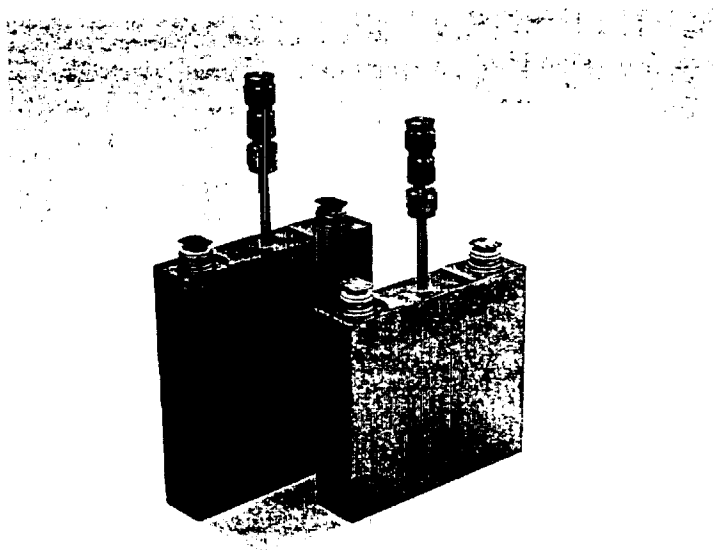

EXTERNAL VIEW OF THE Ni-MH CELL

35Ah CLASS Ni-MH CELL (RIGHT) AND 35Ah Ni-Cd CELL (LEFT)

(A fill-tube is attached to both cells)

NASDA NATIONAL SPACE DEVELOPMENT AGENCY OF JAPAN

ACTIVATION PROCEDURES

AS ACTIVATION IN MANUFACTURE STEP,
TWO PROCEDURES ARE APPLIED
TO EVALUATE THE EFFECT OF ACTIVATIONS
AND RESULTED DIFFERENCE IN THE AMOUNT OF
OVERCHARGE PROTECTION AND PRECHARGE
ON CELL PERFORMANCE

BBM-A (5CELLS) : CAPACITY-STABILIZING CYCLE
AFTER ELECTROLYTE FILLED

BBM-B (5CELLS) : PRECHARGE ARRANGEMENT OF MH ELECTRODE
PRIOR TO STABILIZING CYCLE

Q-8

NASDA NATIONAL SPACE DEVELOPMENT AGENCY OF JAPAN

CAPACITY SCHEMATICS OF Ni-MH CELLS

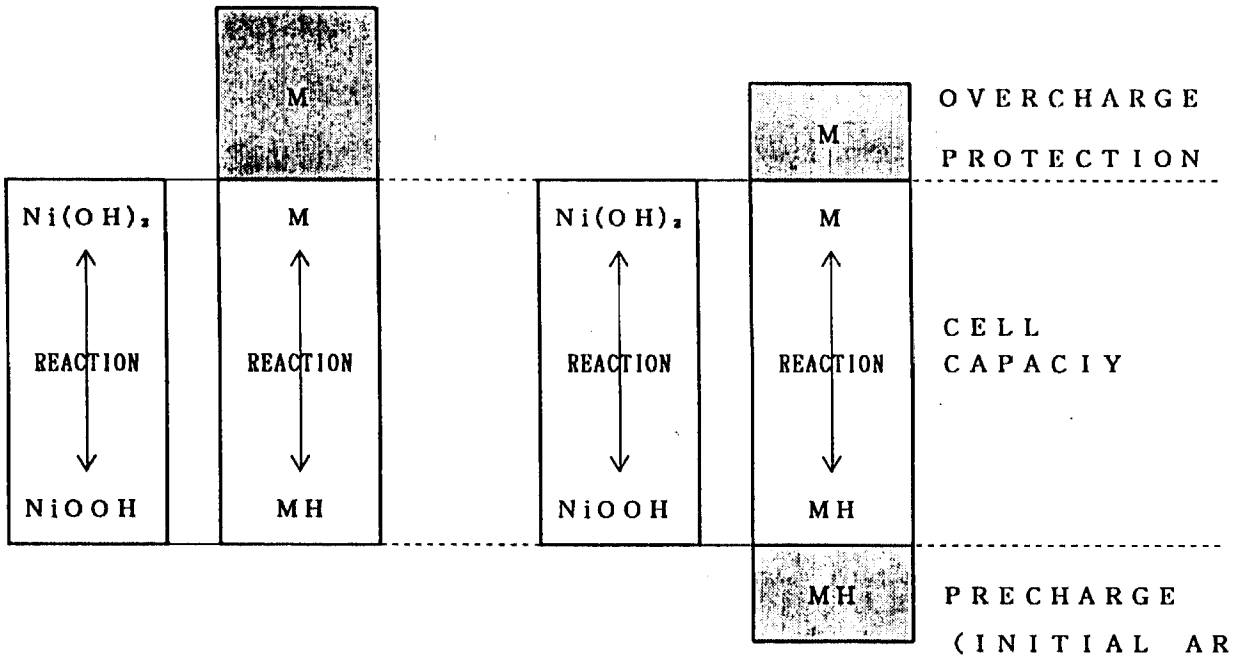

REPRESENTS EXCESS OF HYDROGEN ABSORBING CAPACITY

NASDA NATIONAL SPACE DEVELOPMENT AGENCY OF JAPAN

INITIAL EVALUATION TEST PROCEDURE

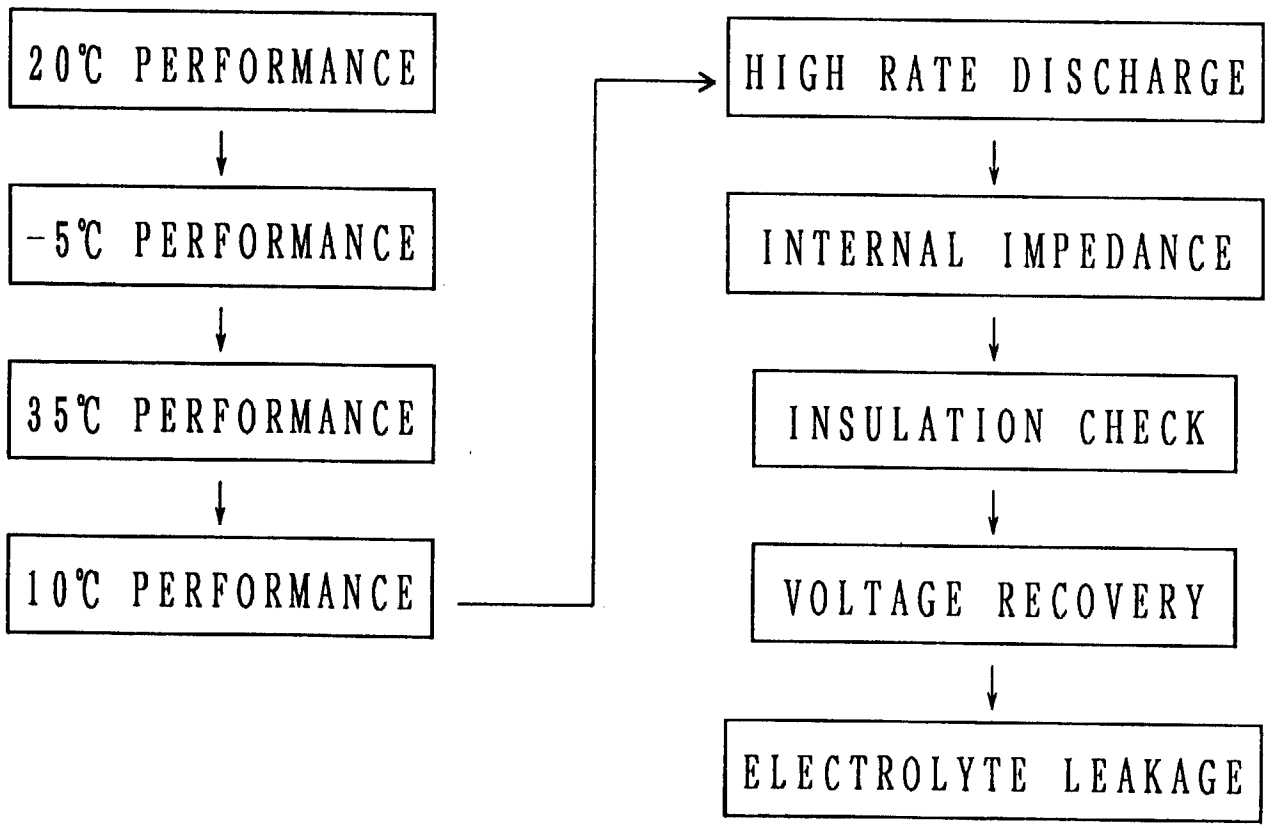

NASDA NATIONAL SPACE DEVELOPMENT AGENCY OF JAPAN

INITIAL CHARACTERISTICS OF THE Ni-MH CELLS AT 20℃

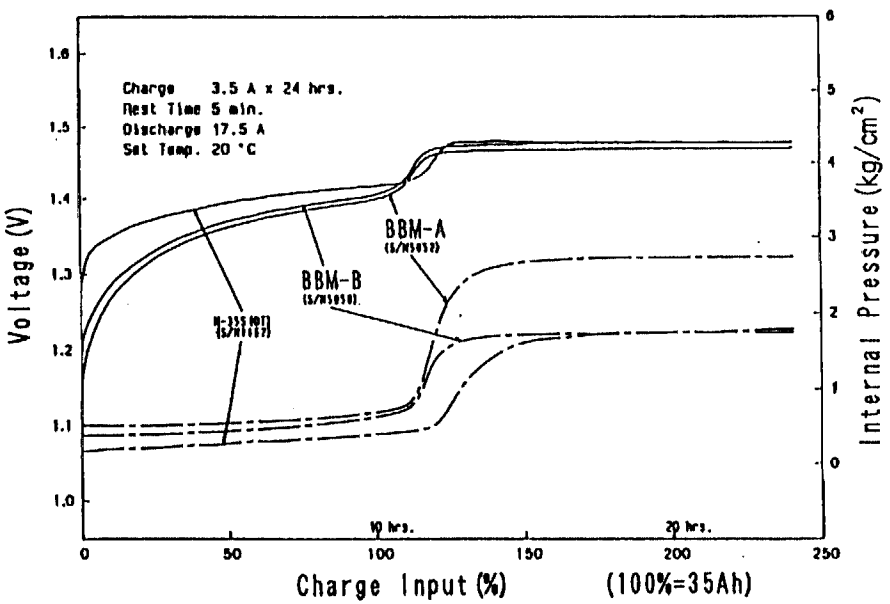

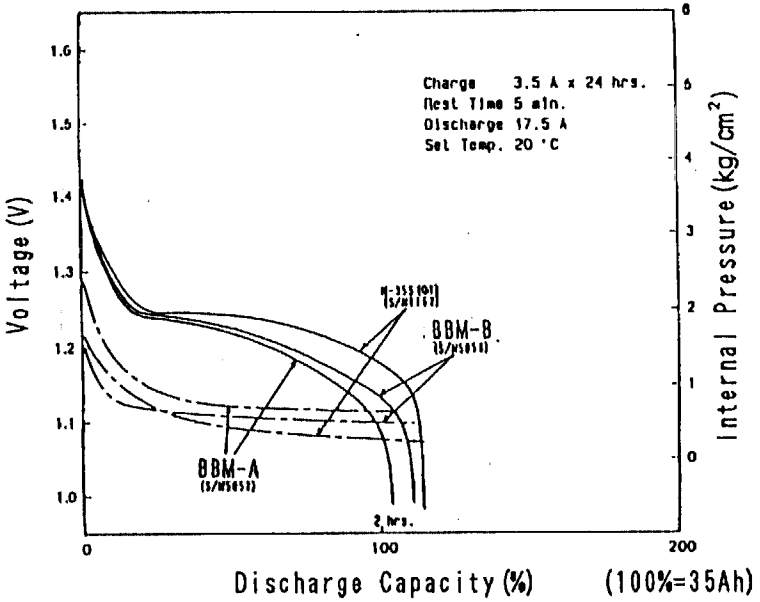

- DISCHARGE CAPACITY IS OVER THE DESIGN CAPACITY 35.5Ah
- EOCP OF BBM-B IS LOWER THAN BBM-A
- DISCHARGE CAPACITY OF BBM-B IS LARGER THAN BBM-A
- THE RATE OF VOLTAGE RISE/DOWN AS CHARGE/DISCHARGE IS LARGE IN Ni-MH CELL

NASDA NATIONAL SPACE DEVELOPMENT AGENCY OF JAPAN

INITIAL CHARACTERISTICS OF THE Ni-MH CELLS AT 35℃

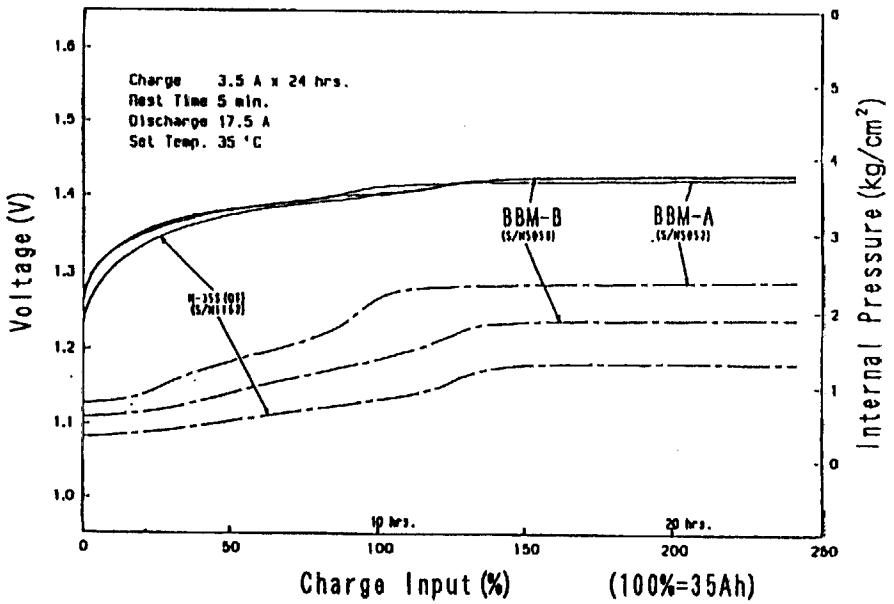

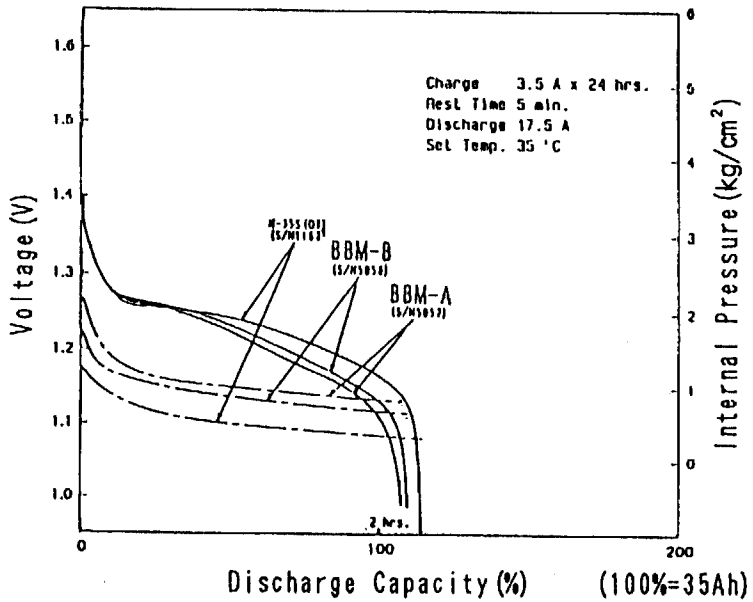

- CHARGE VOLTAGE OF Ni-MH CELL IS SLIGHTLY HIGHER THAN Ni-Cd
- CHARGE EFFICIENCY OF Ni-MH CELL IS LOWER THAN Ni-Cd

NASDA NATIONAL SPACE DEVELOPMENT AGENCY OF JAPAN

INITIAL CHARACTERISTICS OF THE Ni-MH CELLS AT -5℃

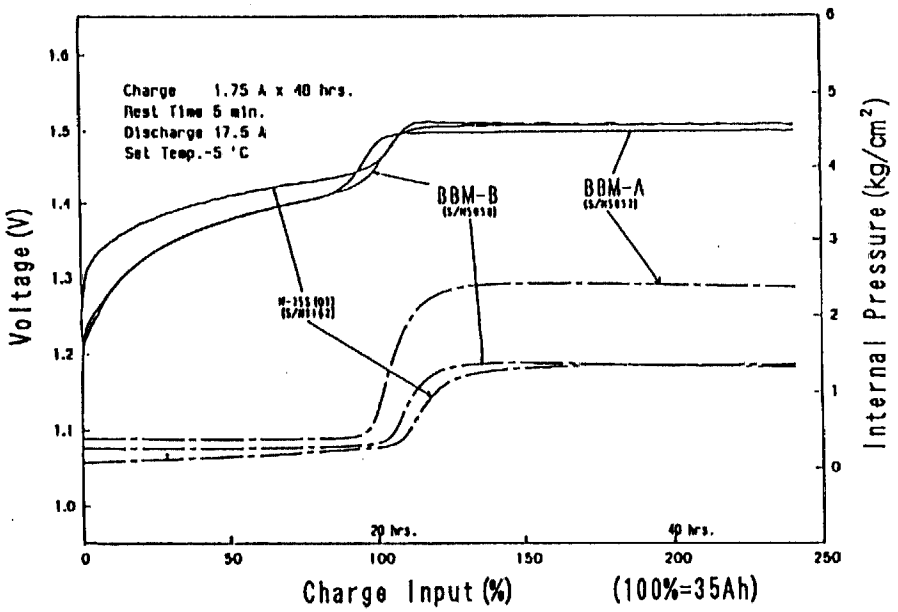

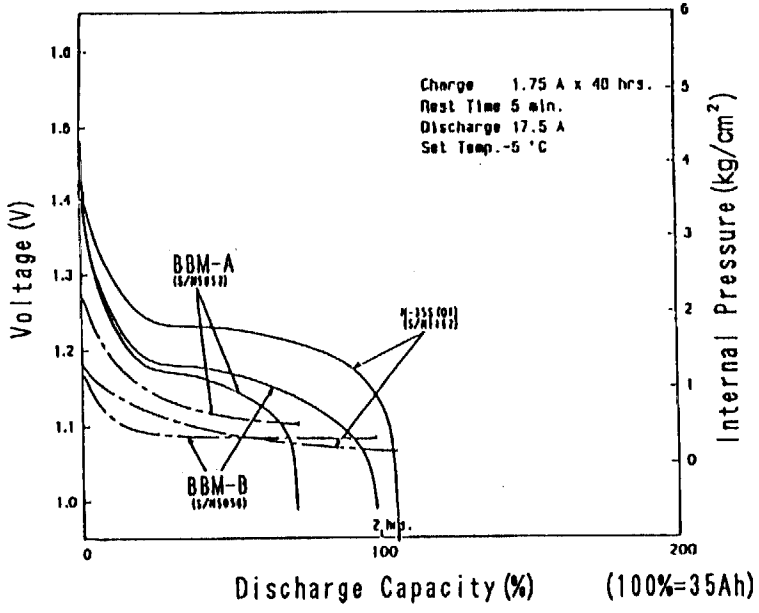

- DISCHARGE VOLTAGE IS ABOUT 50mV LOWER THAN Ni-Cd
- DISCHARGE CAPACITY IS LOWER THAN THE DESIGN CAPACITY 35.5Ah
- THE CAPACITY OF BBM-B IS ABOUT 10Ah LARGER THAN BBM-A

NASDA NATIONAL SPACE DEVELOPMENT AGENCY OF JAPAN

INITIAL CHARACTERISTICS OF THE Ni-MH CELLS AT 10℃

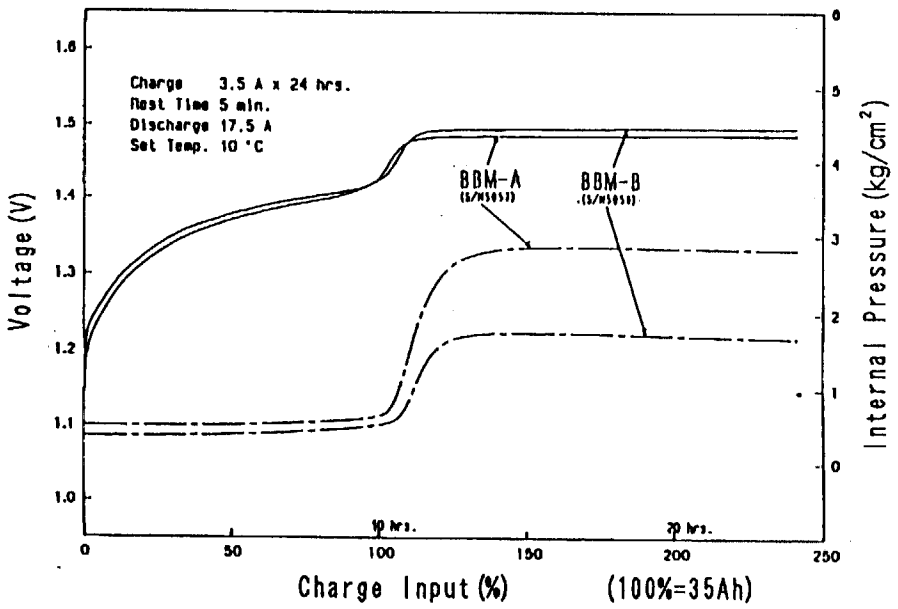

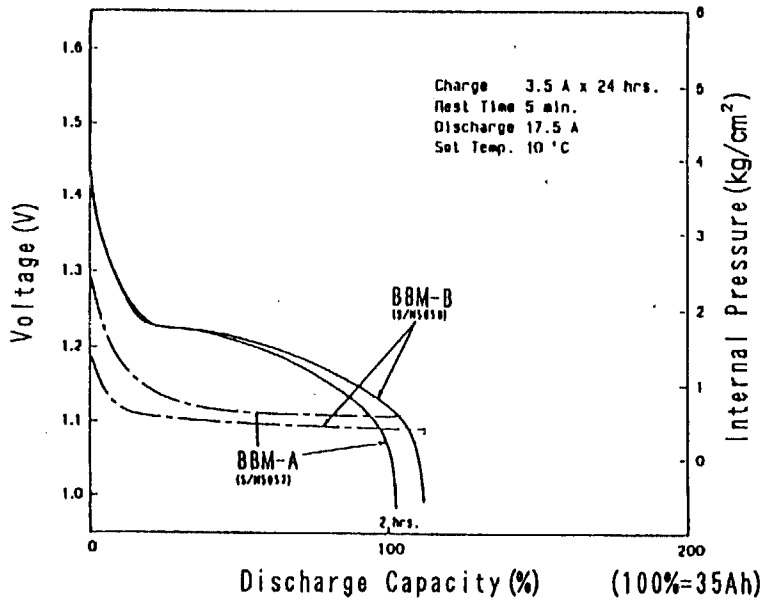

- CHARGE & DISCHARGE CHARACTERISTICS ARE SIMILAR TO THE CHARACTERISTICS AT 20℃

NASDA NATIONAL SPACE DEVELOPMENT AGENCY OF JAPAN

INITIAL CHARACTERISTICS OF THE Ni-MH CELLS

THE DIFFERENCE BETWEEN BBM-A AND BBM-B

INITIAL CHARACTERISTICS		TEMPERATURE
EOCP	BBM-B LOWER THAN BBM-A	ALL TEMP.
CAPACITY	BBM-B SLIGHTLY LARGER THAN BBM-A	10, 20, 35℃
	BBM-B ABOUT 10Ah LARGER THAN BBM-A	-5℃

THE CHARACTERISTICS ARE DERIVED FROM PRECHARGE

NASDA NATIONAL SPACE DEVELOPMENT AGENCY OF JAPAN

INITIAL CHARACTERISTICS OF THE Ni-MH CELLS

THE COMPARISON WITH Ni-Cd CELL

TEMPERATURE	INITIAL CHARACTERISTICS
ALL TEMP.	THE RATE OF VOLTAGE RISE/DOWN AS CHARGE/DISCHARGE IS LARGE
35℃	CHARGE EFFICIENCY IS LOWER THAN Ni-Cd *)
-5℃	DISCHARGE VOLTAGE ABOUT 50mV LOWER THAN Ni-Cd *)

* THE CHARACTERISTICS ARE DERIVED FROM PROPERTY THAT HYDROGEN STORAGE METAL IS ACTIVATED TO RELEASE HYDROGEN AT HIGH TEMPERATURE, AND DEACTIVATED AT LOW TEMPERATURE

NASDA NATIONAL SPACE DEVELOPMENT AGENCY OF JAPAN

LIFE EVALUATION OF 35Ah CLASS Ni-MH CELLS

TEST CONDITIONS OF LIFE TEST

CONDITION \ TEST TYPE	25%DOD-LEO	40%DOD-LEO
CELL	3 BBM-A + 3 BBM-B	2 BBM-A + 2 BBM-B
CHARGE	0.3C、52.5 min	0.48C、52.5min
DISCHARGE	0.5C、30 min	0.8C、30 min
DOD	25 %	40 %
CHARGE RETURN	105 %	
CELL TEMP.	20℃ (MAINTAIND BY CHAMBER)	
CAPACITY CHECK	RESIDUAL CAPACITY *1	
	FULL-CHARGED CAPACITY *2	
	1,000 CYCLES、3,000 CYCLES AND THEN ABOUT EVERY 5,000 CYCLES	

(C=35A)

*1 : Residual Capacity is obtained by 0.5C discharge to 1 Volt after LEO cycling charge.

*2 : Full-charged Capacity is obtained by 0.5C discharge to 1 Volt after full-charging with 0.1C for 16hours.

NASDA NATIONAL SPACE DEVELOPMENT AGENCY OF JAPAN

25%DOD-LEO TEST OF 35Ah CLASS Ni-MH CELLS

CHARGE & DISCHARGE CHARACTERISTICS IN CYCLING AT NEARLY 3000 CYCLES

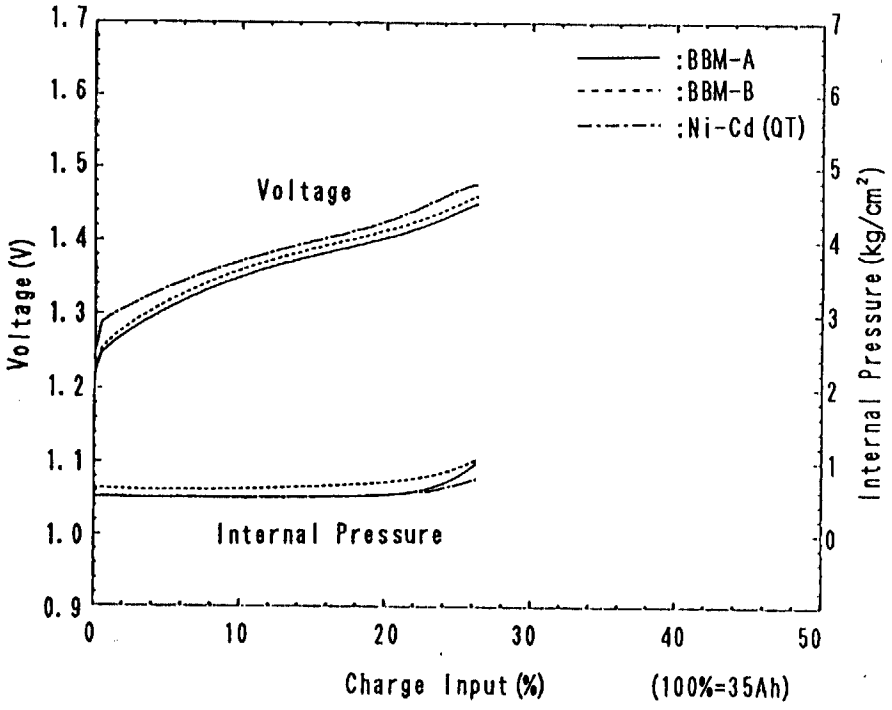

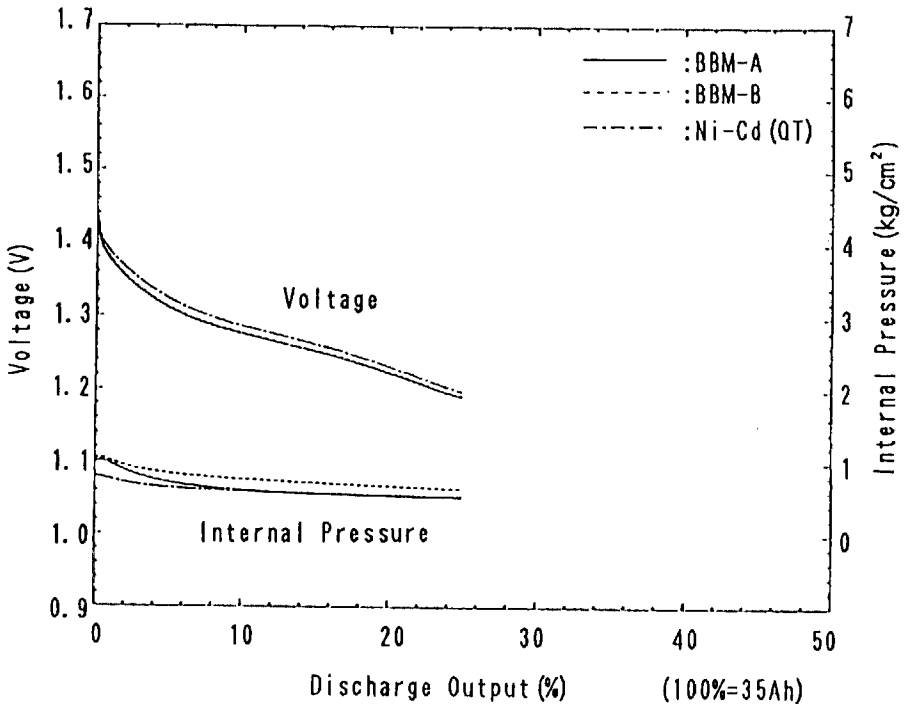

TEST CONDITION/ CHARGE : 0.3C FOR 52.5 MINUTES
DISCHARGE : 0.5C FOR 30 MINUTES (DOD : 25%)
CELL TEMP : 20℃

NASDA NATIONAL SPACE DEVELOPMENT AGENCY OF JAPAN

40%DOD-LEO TEST OF 35Ah CLASS Ni-MH CELLS

CHARGE & DISCHARGE CHARACTERISTICS IN CYCLING AT NEARLY 3000 CYCLES

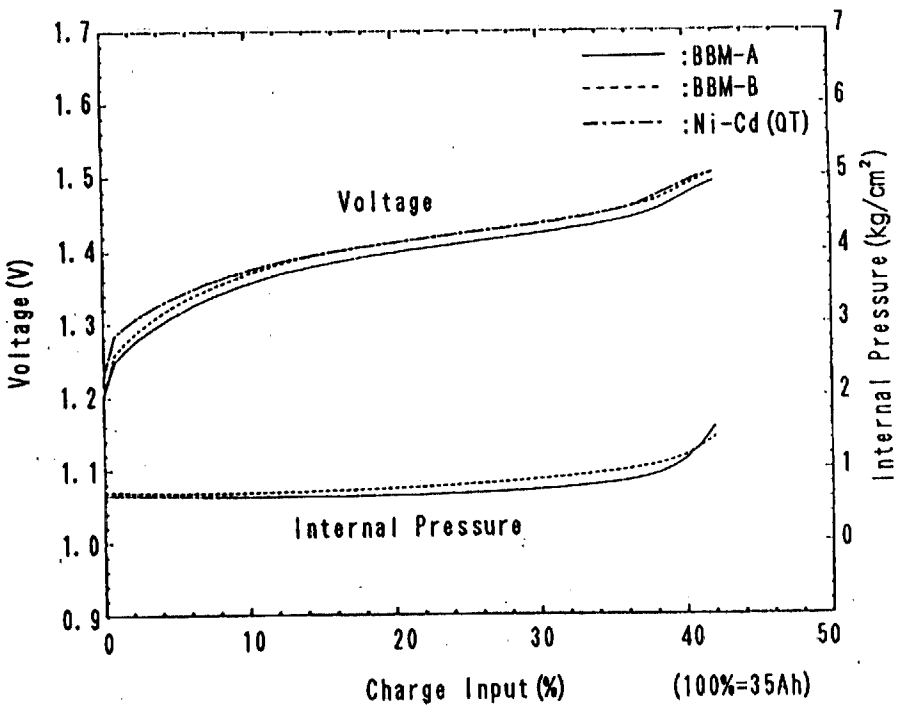

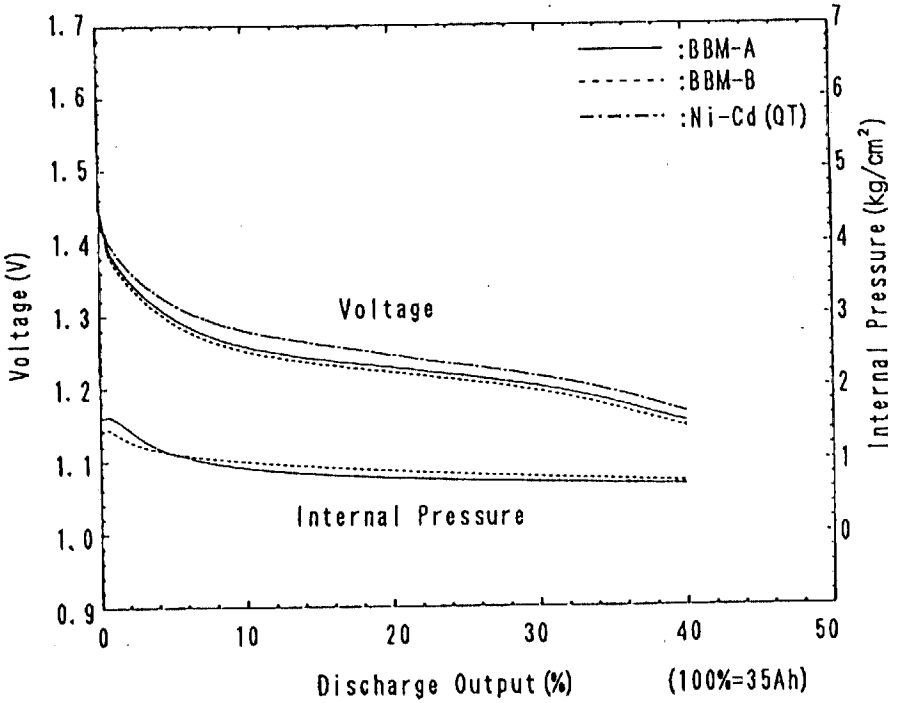

TEST CONDITION/ CHARGE : 0.48C FOR 52.5 MINUTES
DISCHARGE : 0.8C FOR 30 MINUTES (DOD : 25%)
CELL TEMP : 20℃

NASDA NATIONAL SPACE DEVELOPMENT AGENCY OF JAPAN

TREND OF EOCV, EODV, EOCP & EODP ON LEO TEST

25%DOD

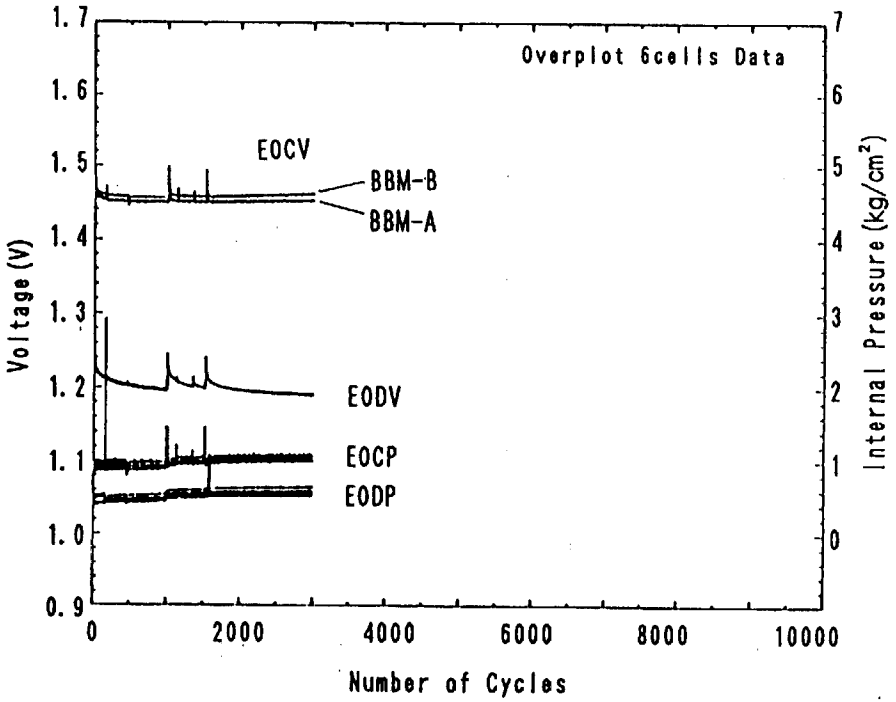

40%DOD

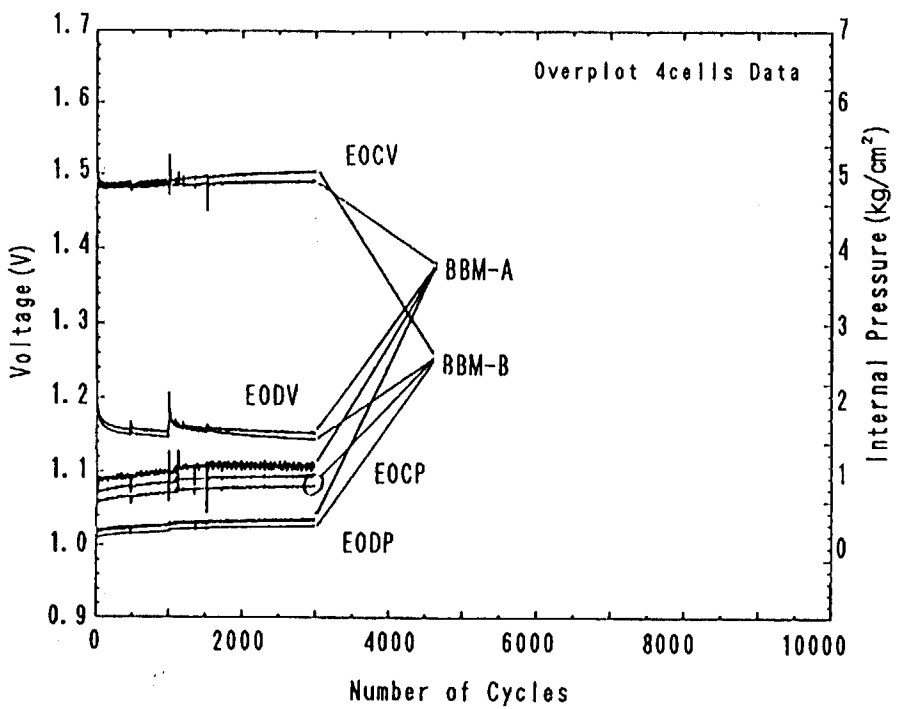

BOTH OF LEO TESTS ARE OVER 3,000 CYCLES SO FAR NO FAILURES
EOCV OF BBM-B ARE GRADUALLY INCREASING ON 40%DOD-LEO CYCLE TEST

NASDA NATIONAL SPACE DEVELOPMENT AGENCY OF JAPAN

TREND OF CAPACITIES ON LEO TEST

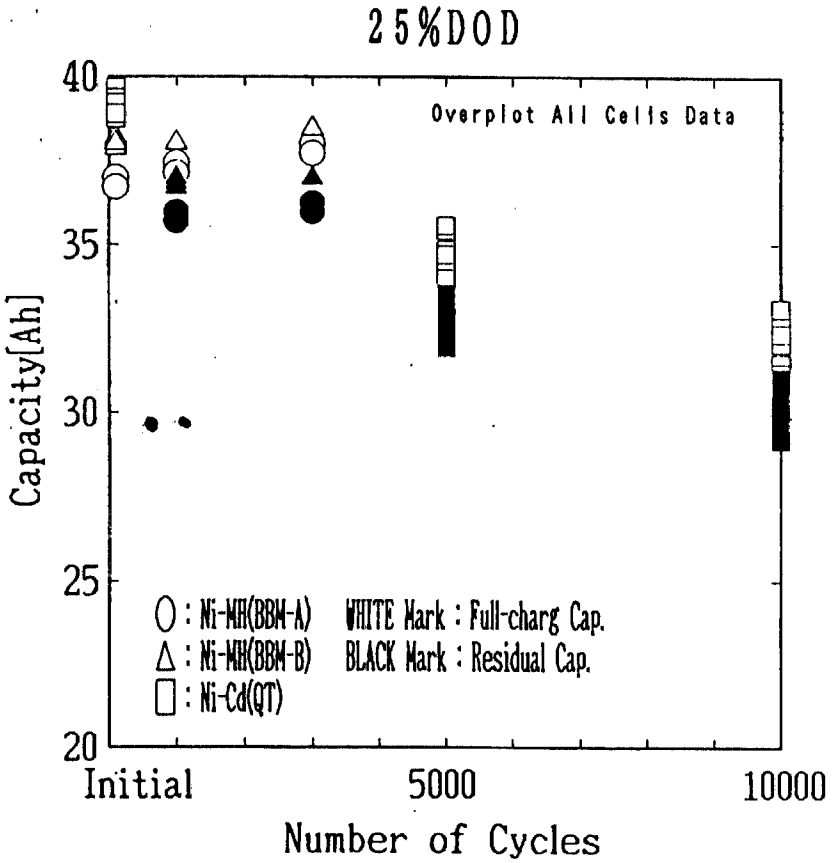

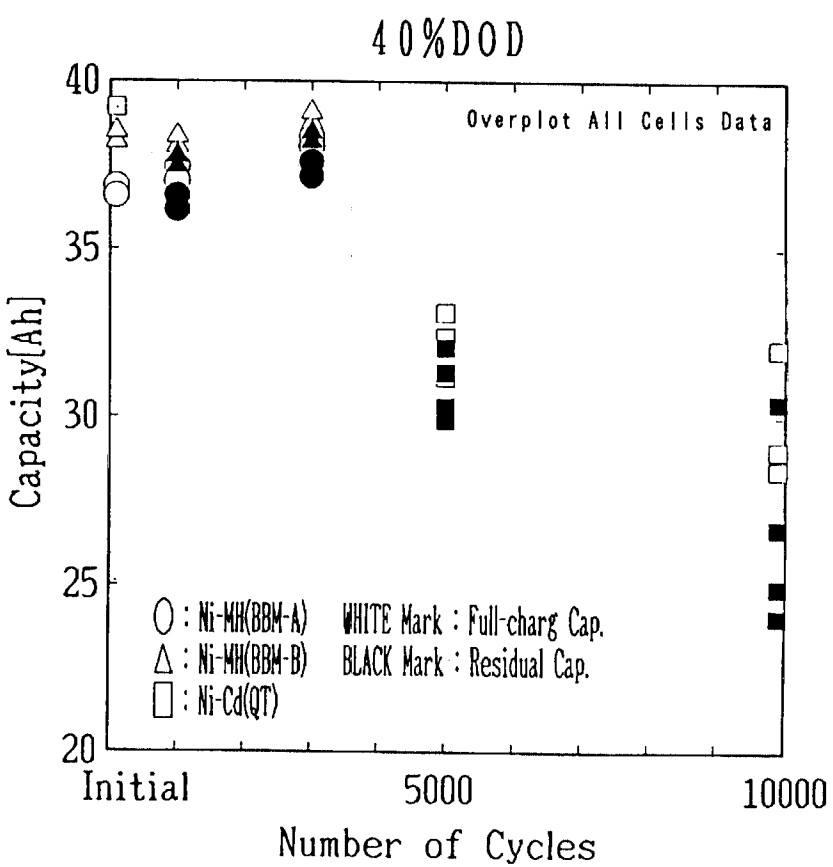

THE Ni-MH CELLS HAVE GOOD PERFORMANCE ABOUT CAPACITY REMAINING ESPECIALLY, AS SIMILAR TO COMMERCIAL Ni-MH CELLS

NASDA NATIONAL SPACE DEVELOPMENT AGENCY OF JAPAN

MEMORY EFFECT OF 35Ah CLASS Ni-MH CELLS

DISCHARGE CHARACTERISTICS IN CAPACITY CHECK ON 25%DOD

Ni-MH (BBM-B) AT 3000 CYCLES

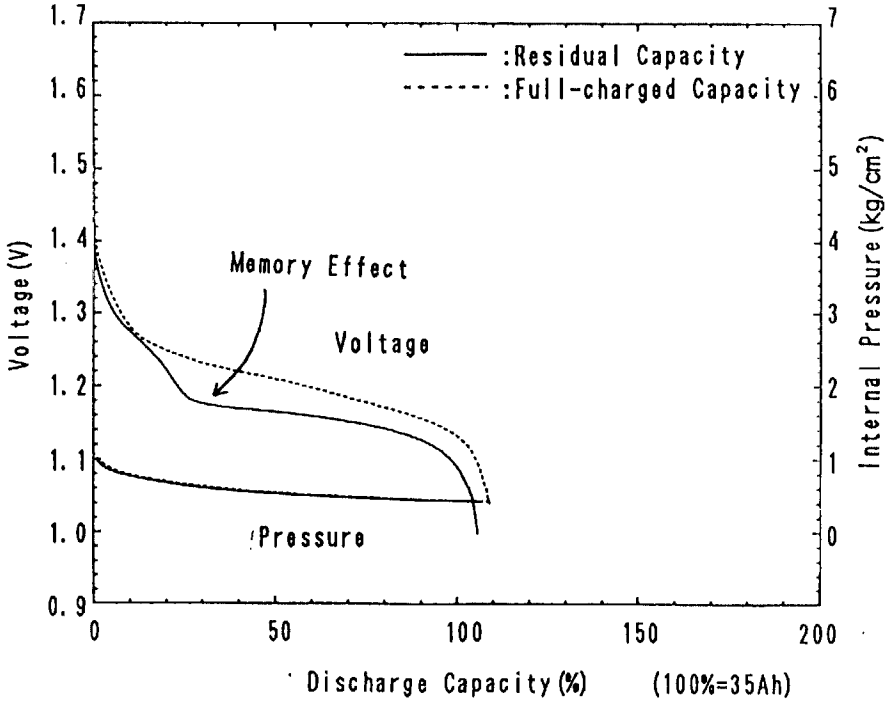

Ni-CD (QT) AT 5000 CYCLES

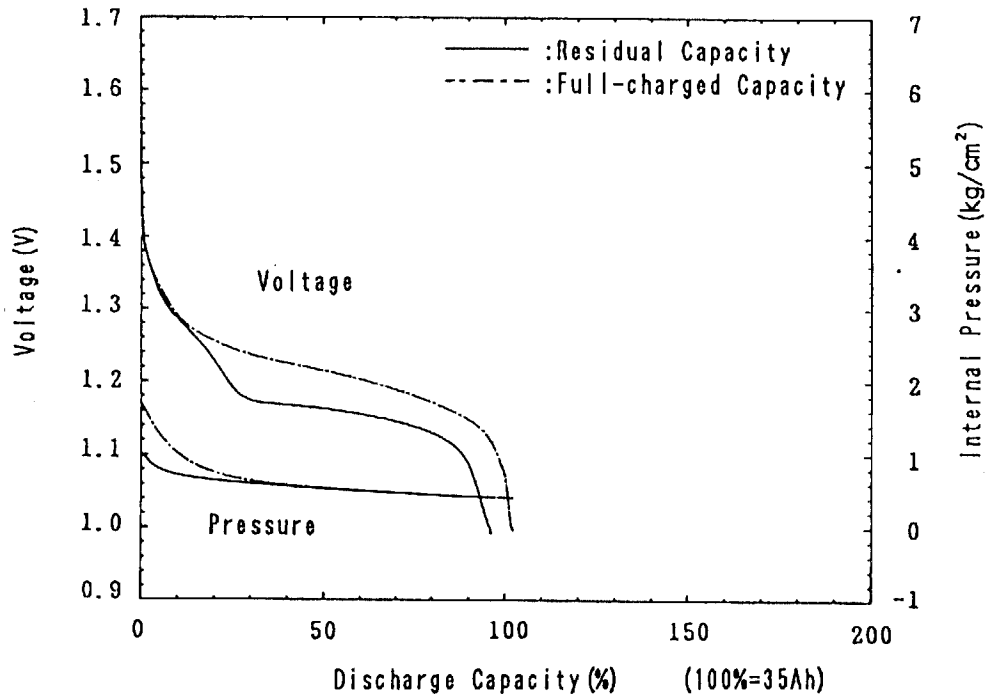

DIFFERENCE OF DISCHARGE VOLTAGE DERIVED FROM THE MEMORY EFFECT IS 50mV THAT IS SIMILAR TO Ni-Cd

NASDA NATIONAL SPACE DEVELOPMENT AGENCY OF JAPAN

LIFE EVALUATION OF 35Ah CLASS Ni-MH CELLS

THE DIFFERENCE BETWEEN BBM-A AND BBM-B

CHARACTERISTICS		DOD
CHARGE VOLTAGE	BBM-A < BBM-B	20, 40%
CHARGE PRESSURE RISE AT OVERCHARGE	BBM-A > BBM-B	20, 40%
INCREASE OF EOCV	BBM-A < BBM-B	40%

NASDA NATIONAL SPACE DEVELOPMENT AGENCY OF JAPAN

DEVELOPMENT OF Ni-MH CELL FOR SPACE USE

SUMMARY

- TWO ACTIVATION PROCEDURES ARE APPLIED TO EVALUATE THE EFFECT OF DIFFERENCE IN THE AMOUNT OF OVERCHARGE PROTECTION & PRECHARGE
- SPECIFIC ENERGY OF THE Ni-MH CELL IS NEARLY ACCOMPLISHED 50Wh/kg
- INITIAL CHARACTERISTICS INDICATE THE EFFECT DERIVED FROM PRECHARGE
- 35Ah CLASS Ni-MH CELLS HAVE GOOD PERFORMANCE FOR LEO CYCLE OF 25% & 40% DOD UP TO 3000 CYCLES AS SIMILAR TO COMMERCIAL CELLS
- THE EFFECT OF THE DIFFERENCE IN THE AMOUNT OF OVERCHARGE PROTECTION WILL APPEAR IN LIFE TEST

NASDA NATIONAL SPACE DEVELOPMENT AGENCY OF JAPAN

CONCLUSION

EVALUATION OF COMMERICAL Ni-MH CELL

- Ni-MH CELL IS SUITABLE TO LEO APPLICATION
- ONE OF THE Ni-MH FAILURE MODE IS DEGRADATION OF MH ELECTRODE SUCH AS OXIDATION, CAUSESING LOSS OF OVERCHARGE PROTECTION

DEVELOPMENT OF Ni-MH CELL FOR SPACE USE

- WE MANUFACTURED 35Ah CLASS FLIGHT-TYPE Ni-MH CELL BASED ON THE COMMERICAL CELL AND AEROSPACE Ni-Cd CELL TECHNOLOGY
- WE CONTINUE TO EVALUATE THE EFFECT OF THE DIFFERENCE IN THE AMOUNT OF OVERCHARGE PROTECTION ON LIFE PERFORMANCE

NASDA NATIONAL SPACE DEVELOPMENT AGENCY OF JAPAN

PLAN OF Ni-MH CELLS FOR SPACE USE

NOW WE ARE DESIGNING OF 10 TO 20Ah FOR SMALL SATELLITE

IT IS PLANNED TO APPLY THE RESULTS OF R&D ON Ni-MH CELLS FOR OPTICAL INTER-SATELLITE COMMUNICATION ENGINEERING TEST SATELLITE(OICETS) TO BE LAUNCHED IN 1998

Gates Energy Products

Gates Aerospace Batteries

NiMH STORAGE TEST

AND CYCLE LIFE TEST

R. Dan Dell
Glenn C. Klein
David F. Schmidt
Gates Aerospace Batteries

Presented at
1993 NASA Aerospace Battery Workshop
Huntsville, Alabama

November 18, 1993

NiMH STORAGE TEST AND CYCLE LIFE TEST

R. Dan Dell, G. C. Klein and D. F. Schmidt
Gates Aerospace Batteries
Gainesville, Florida

Abstract

Gates Aerospace Batteries is conducting two long term test programs to fully characterize the NiMH Cell Technology for aerospace applications. The first program analyzes the effects of long term storage upon cell performance. The second program analyzes cycle life testing and preliminary production lot testing. This paper summarizes these approaches to testing the NiMH couple and culminates with initial storage and testing recommendations.

Long term storage presents challenges to deter the adverse condition of capacity fade in NiMH cells. Elevated but stabilized pressures and elevated but stabilized end-of-charge voltages also appear to be a characteristic phenomenon of long term storage modes. However, the performance degradation is dependent upon specific characteristics of the metal-hydride alloy. To date, there is no objective evidence with which to recommend the proper method for storage and handling of NiMH Cells upon shipment from our facility. This is particularly critical due to limited data points that indicate open circuit storage at Room Temperature for 60 to 90 days will result in irrecoverable capacity loss. Accordingly a test plan was developed to determine what method of mid term to long term storage will prevent irrecoverable capacity loss. The explicit assumption is that trickle charging at some rate above the self-discharge rate will prevent the irreversible chemical changes to the negative electrode that result in the irrecoverable capacity loss. Another premise is that lower storage temperatures, typically 0 °C for aerospace customers, will impede any negative chemical reactions. Three different trickle charge rates are expected to yield a fairly flat response with respect to recoverable capacity versus baseline cells in two different modes of open circuit. Specific attributes monitored include: end-of-charge voltage, end-of-charge pressure, mid-point discharge voltage, capacity, and end-of-discharge pressure.

Cycle life testing and preliminary production lot testing continue to dominate the overall technology development effort at GAB. The Cell Life Test Program reflects continuing improvements in our baseline cell designs. Performance improvements include lower and more stable charge voltages and pressures. The continuing review of Production Lot Testing assures conformance to our design criteria and expectations. This is especially critical during this period of transferring technology from the R & D status to production.

Long Term Storage Test Program

Introduction: NiMH cells with certain alloy negatives are known to experience measurable capacity fade when stored under adverse conditions. However, there was no objective evidence with which Gates Aerospace Batteries could recommend to their customers the proper method for storage and handling of NiMH Cells upon receipt at their facility. This is particularly critical due to limited evidence that indicates that open circuit storage at Room Temperature for 60 to 90 day will result

in irrecoverable capacity loss.

A Test Plan was developed to determine what method of mid term to long term storage would prevent irrecoverable capacity loss. The explicit assumption is that trickle charging at some rate above the self-discharge rate will prevent the irreversible chemical changes to the negative electrode that result in the irrecoverable capacity loss. Another assumption is that lower storage temperatures, typically 0 °C for aerospace customers, will slow down any negative chemical reactions. Finally, the general recommendation to not deplete NiMH cells below 0.5 volts explicitly prevents storage in the shorted condition as is typical with NiCd technology.

Accordingly, a test plan was devised to subject five cells to five different storage methods for a minimum of 90 days. This initial 90 day period was divided into three specific periods of 30 days. Extension of that test plan to a longer period is dependent upon those results in addition to availability of test equipment. Further iterations to that test plan both for test parameters and quantity of cells are dependent upon those results.

Test Cells: The five test cells selected for the test program are residuals from the first production lot of 47B024AM01 cells rated at 24 Amp-Hour. Initial capacity for all cells will be as tested during normal Acceptance Testing. The cells weigh 670 grams with a Specific Energy of 43.77 Whr/Kg.

Test Plan: The overall plan shown in Figure 1 is to subject three cells to three different rates of trickle charge while at 0 °C, this will determine the optimum charge rate should a trickle charge be necessary. Two additional cells to be left in open-circuit and then become the fourth and fifth test cells. The fourth cell will be fully charged, then open-circuited and placed in the same environmental chamber at 0 °C as a first baseline. The fifth cell will be depleted to 0.5 volt, then open-circuited and placed in the same environmental chamber at 0 °C as a second baseline.

The five cells were initially discharged to 0.5 volts at 23 °C upon completion of Acceptance Testing. The cells were then evacuated to a vacuum of 26 to 30 inches Hg, and the gage/valve assembly left on each cell. Cell Nos. 1, 2, and 3 were charged at 2.4 amps for 20 hours @ Room Temp and then stored at trickle charge rates of C/100, C/75 and C/50 based upon actual lot average capacity. Numerical charge rates are 250, 333 and 500 milliamps respectively. Cell No. 4 was charged at 2.4 amps for 20 hours @ Room Temp placed in open circuit and stored in the same environmental chamber at 0 °C. Cell No. 5 was placed in open circuit and stored in the same environmental chamber at 0 °C.

Data Collection: The data collected in this test included response voltage and pressure on a daily basis. Each 30 days the five cells are removed and discharged at 12.0 amps to 0.9 volts. The cells are then subjected to three Room Temperature Verification Capacity Cycles per the standard acceptance testing to determine if capacity loss has occurred. The cells are charged at 2.4 amps for 20 hours before returning to their respective Trickle Charge. It was initially expected that 3 or 4 of these 30 day cycles can be performed with currently available resources.

Expected Results: The three different trickle charge rates are expected to yield a fairly flat response with respect to recoverable capacity. Cell No. 4 stored in fully charged open-circuit is expected to not yield a measurable capacity fade. Cell No. 5 stored in depleted open-circuit is expected to yield a measurable capacity fade, or irrecoverable capacity. These results will be compared with a previous test wherein a single 7 AH cell was stored in open-circuited condition at Room Temperature for 90 days. Specific attributes to be monitored include: end-of-charge voltage

[EOCV], end-of-charge pressure [EOCP], mid-point discharge voltage, capacity, and EODP.

Specific attributes to be analyzed include:

1. Stability of voltages and pressures for the three cells at different trickle charge rates,

2. Stability of voltages and pressures for all cells during the charge portion of the Capacity Verification Cycles following each 30 day storage period; and,

3. Stability of capacities and end-of-discharge pressures for all cells during the discharge portion of the Capacity Verification Cycles following each 30 day storage period.

Test Results: Test Results are summarized in Tables 1 and 2, and are graphically displayed thereafter in Figures 2 to 7. The key to Cell Condition as noted in Tables 1 and 2 is as follows:

0.250A T/C indicates a fully charged cell and trickle charge rate of 0.25 amps during storage;
0.333A T/C indicates a fully charged cell and cell trickle charge rate of 0.25 amps during storage;
0.500A T/C indicates a fully charged cell and cell trickle charge rate of 0.25 amps during storage;
C & O/C indicates a cell that was fully charged and stored in open-circuit; and,
D & O/C indicates a cell that was depleted and stored in open-circuit.

The Ave. Volt. [average pressure] at Day 1 to 3 and at Day 28 to 30 was used to remove any perturbations from a single day. The average pressure was treated similarly. EOCV and EOCP are common abbreviations for end-of-charge voltage and pressure. However, the abbreviation EODP for end-of-discharge pressure has more significance with nickel-metal hydride technology. This is due to residual partial pressures from deterioration of the hydride alloy that may tend to inflate this EODP and thus become a strong indicator of cell deterioration and failure.

Thus, Table 1 becomes the simple summary of performance readings over three periods of thirty days. Table 2 provides the first indication of performance characterization and stability. This data is plotted on Figures 2 to 7 and forms the basis of the following discussion of test results:

End-of-Charge Pressures (see Figure 2) appear consistent for all cells at this point as was expected. These pressures remain fairly constant with increasing number of 30 day cycles. These pressures are somewhat elevated, but otherwise appear unremarkable.

End-of-Charge Voltages (see Figure 3) appear both consistent and constant for all cells with increasing number of 30 day cycles.

End-of-Discharge Pressures (see Figure 4) appear consistent for all cells at this point as was expected. The slight rise and fall with increasing number of 30 day cycles is a test artifact that appears to affect all cells equally.

Capacity (see Figure 5) appears fairly consistent except for Cell Nos. 3 and 5. Certainly, some test artifact appears to have affected those two cells. It is too early to determine from this single indicator whether capacity degradation is occurring on Cell No. 5. Cell No. 3 does appear to be experiencing some continuing capacity growth as confirmed by the mild overcharging indicated in Figure 7.

Voltage Change (see Figure 6) of -360 mV for Cell No. 5 appears to be a test artifact. From Table 1, the cell voltage at the end of the second 30 day period is significantly out-of-family for inexplicable reasons.

Voltage Change over multiple 30 day periods for cells undergoing three different trickle charge rates appears to be independent of their respective charge rates.

Pressure Change (see Figure 7) over multiple 30 day periods appears independent of the initial state-of-charge for those cells in open-circuit.

Pressure Change for multiple 30 day periods appears somewhat inconsistent as regards the trickle charge rate of 0.33 amps in that it would be expected to lie between the response curves for the 0.25 amp and 0.50 amp charge rates. However, Cell No. 2 at 0.33 amp trickle charge rate appears to have a tapering-off of pressure response. Whereas Cell No. 3 at 0.50 amps is still experiencing some mild overcharging during the 30 day period.

LEO Cycle Life Test Program

Cycle life testing under LEO conditions and limited cell production has dominated GAB's in house development program for more than two years. The life test program, involving a host of different cell designs continues to confirm the selection of the first generation cell design earlier this year. This portion of the paper continues to update the battery community of the cycle life performance of the first generation cells, compared to a) early cells put on test 2 years ago, and b) some recent cell designs that show some rather interesting and different performance characteristics.

A first generation cell design was selected out of the many cell designs that have been subjected to a LEO life test cycle of 50% DOD and 23 °C.

Figure 8 shows a tabulation of the (55) cells in the GAB test program of engineering model cells. Twenty-five (25) cells are continuing the life test as of this Battery Workshop.

Additional cells can be added to the program on a periodic basis in order to validate new design parameters as required. Cell test data, predominately LEO life cycle testing, has been reported at various customer meetings, previous NASA Battery Workshops, the AF Space Power Workshop, and in GAB's NiMH Product Information binder. The latter document is presently in the hands of about 150 customers worldwide.

The cells built for the test program have involved a great number of design variables such as positive electrode types and impregnation, AB_2 and AB_5 negative electrodes, electrode processing and treatments, and at least 6 different separators. Each group of cells shown in Figure 8 contains one or two cells built with the same design variable.

Life cycling for all cells in the table was performed in a 90 minute LEO simulation regime of 35 minutes discharge and 55 minutes charge using an integrator controlled cycler. Each cell is monitored using a FLUKE scanning multimeter interfaced to a PC based data collection system. Cell pressures are monitored by direct reading of gauges (Ashcroft A1S1) attached to the cells. Pressure data is manually entered into the correct data file. The specific test conditions are shown on Figure 8.

All cells were cycled at 50% DOD (nameplate) and room temperature, nominally at 23 °C. A 50% DOD level has been shown in previous testing of NiCd and NiH_2 cells to be sufficiently robust to develop meaningful performance data within a reasonable period of time. The conditions of test were held constant throughout the cells development program so that changes in performance could be meaningfully measured.

The data from three cell designs groups are presented graphically in Figure 9. The first cell group , which we will call "early cells" is the 6 Ahr (AP6:1-6) cell design put on test in October 1991. The last cell of this group, #5, was terminated after 6600 cycles in November 1992.

The second set of data represents GAB's First Generation Cell Design. Cells AP7: #8 and #9 are performing well after 7800 cycles. It is estimated that this group of cells will make 10,000 cycles or more before the EODV drops below 1.0 volt, and cell pressure will still be at a tolerable level.

A third cell design designated AP7:#16 is a more recent design that differs in voltage and pressure characteristics from either the Early or First Generation cell designs and is now up to about 3400 cycles. Pressures are much lower, EOCV is lower but rising at a faster rate, and the EODV is dropping rapidly and may stabilize.

Thus far the First Generation Cell Design still remains an excellent choice. Its voltage and pressure characteristics are relatively stable under such a robust test regime and it is continuing on cycle life at this time. With over 7800 cycles, while AP7: #16 provides the lowest pressure, stabilization of the EODV is still uncertain.

The internal design components of the cell designs being discussed are not being disclosed at this time in view of license agreements, competitive pressures, and GAB ownership interests that could have an impact on future sales and profits.

In order to further establish the performance capability of the NiMH chemistry, GAB has committed an additional 10 cells, of the same first generation cell design, to a matrix LEO cell program. Furthermore, some of our customers have also agreed to perform life tests at their facilities on an additional 38 cells. All the cells are based on the same First Generation cell design.

This matrix test program, in time, will further establish the capability of the GAB NiMH design in the Battery Community.

Summary and Conclusions

1. The Long Term Storage Test Program, as originally defined, produced expected results after 3 months. The estimates for the three Trickle Charge rates did show initially to be the probable limits to be used at 0 °C.

2. The true effect of open-circuit storage remains indeterminate during this initial phase of the Long Term Storage Test Program. This is because the state-of-charge is necessarily reset every 30 days by default. Accordingly, since test space is now still available, this test will now be continued uninterrupted for a six month period.

3. GAB has demonstrated LEO life performance to 7800 cycles at 50% DOD and 23 °C. The improvements in cell design have esentially eliminated high pressure as a mode of failure.

Figure 1

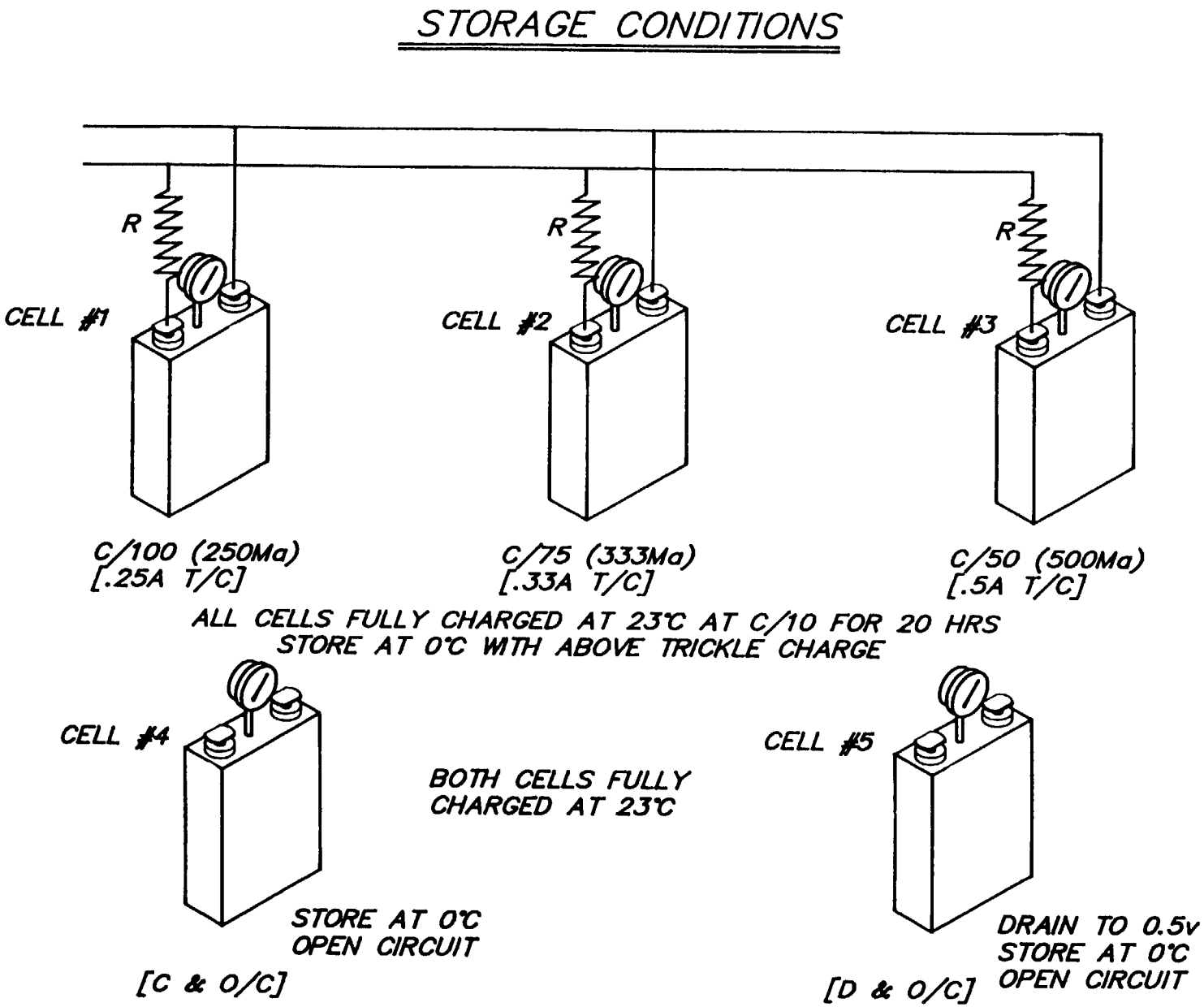
STORAGE CONDITIONS
R
R
R
CELL #1
CELL #2
CELL #3
C/100 (250Ma)
[.25A T/C]
C/75 (333Ma)
[.33A T/C]
C/50 (500Ma)
[.5A T/C]
ALL CELLS FULLY CHARGED AT 23°C AT C/10 FOR 20 HRS
STORE AT 0°C WITH ABOVE TRICKLE CHARGE
CELL #4
STORE AT 0°C
OPEN CIRCUIT
[C & O/C]
BOTH CELLS FULLY
CHARGED AT 23°C
CELL #5
DRAIN TO 0.5v
STORE AT 0°C
OPEN CIRCUIT
[D & O/C]

TABLE 1: Summary of Raw Data

Cell & Condition	30 Day Storage [First Period] Ave. Volt. [day 1-3] (volts)	Ave. Volt. [day 28-30] (volts)	Voltage Change (mV)	Ave. Press. [day 1-3] (PSIA)	Ave. Press. [day 28-30] (PSIA)	Pressure Change (PSIA)	Capacity Verification Cycles [3rd Cycle] Capacity (AH)	EODP (PSIA)	EOCV (volts)	EOCP (PSIA)
1: 0.25A T/C	1.459	1.457	-2	0	2	2	25.95	10	1.460	45
2: 0.33A T/C	1.466	1.465	-1	22	19	-3	25.99	9	1.459	62
3: 0.50A T/C	1.473	1.468	-5	32	22	-10	25.56	8	1.457	64
4: C & O/C	1.303	1.201	-102	12	12	0	25.95	8	1.456	54
5: D & O/C	1.143	1.110	-33	13	13	0	25.30	8	1.459	65

Cell & Condition	30 Day Storage [Second Period] Ave. Volt. [day 1-3] (volts)	Ave. Volt. [day 28-30] (volts)	Voltage Change (mV)	Ave. Press. [day 1-3] (PSIA)	Ave. Press. [day 28-30] (PSIA)	Pressure Change (PSIA)	Capacity Verification Cycles [3rd Cycle] Capacity (AH)	EODP (PSIA)	EOCV (volts)	EOCP (PSIA)
1: 0.25A T/C	1.413	1.454	41	5	3	-2	26.18	7	1.461	60
2: 0.33A T/C	1.428	1.459	31	1	16	15	26.27	6	1.461	61
3: 0.50A T/C	1.441	1.467	26	19	20	1	26.45	8	1.460	51
4: C & O/C	1.272	1.247	-25	8	9	1	26.17	6	1.463	48
5: D & O/C	1.168	0.808	-360	9	9	0	25.87	3	1.466	76

Cell & Condition	30 Day Storage [Third Period] Ave. Volt. [day 1-3] (volts)	Ave. Volt. [day 28-30] (volts)	Voltage Change (mV)	Ave. Press. [day 1-3] (PSIA)	Ave. Press. [day 28-30] (PSIA)	Pressure Change (PSIA)	Capacity Verification Cycles [3rd Cycle] Capacity (AH)	EODP (PSIA)	EOCV (volts)	EOCP (PSIA)
1: 0.25A T/C	1.405	1.447	42	1	1	0	25.85	6	1.459	72
2: 0.33A T/C	1.454	1.448	-6	19	16	-3	25.97	6	1.458	73
3: 0.50A T/C	1.464	1.459	-5	25	20	-5	26.30	6	1.458	62
4: C & O/C	1.272	1.226	-46	8	8	0	25.90	5	1.461	64
5: D & O/C	1.202	1.150	-52	7	7	0	25.15	3	1.465	92

TABLE 2: Performance Characterization and Stability

Performance Characterization

[As a function of multiple 30 day periods]

Cell & Condition	Capacity [AH]			
	ATP	Period 1	Period 2	Period 3
1: 0.25A T/C	25.80	25.95	26.18	25.85
2: 0.33A T/C	25.72	25.99	26.27	25.97
3: 0.50A T/C	25.92	25.56	26.45	26.30
4: C & O/C	25.93	25.95	26.17	25.90
5: D & O/C	25.90	25.30	25.87	25.15

Cell & Condition	End-of-Discharge Pressure [PSIA]			
	ATP	Period 1	Period 2	Period 3
1: 0.25A T/C	3	10	7	6
2: 0.33A T/C	2	9	6	6
3: 0.50A T/C	1	8	8	6
4: C & O/C	4	8	6	5
5: D & O/C	4	8	3	3

Cell & Condition	End-of-Charge Voltage			
	ATP	Period 1	Period 2	Period 3
1: 0.25A T/C	1.457	1.460	1.461	1.459
2: 0.33A T/C	1.457	1.459	1.461	1.458
3: 0.50A T/C	1.458	1.457	1.460	1.458
4: C & O/C	1.454	1.456	1.463	1.461
5: D & O/C	1.458	1.459	1.466	1.465

Cell & Condition	End-of-Charge Pressure [PSIA]			
	ATP	Period 1	Period 2	Period 3
1: 0.25A T/C	78	45	60	72
2: 0.33A T/C	81	62	61	73
3: 0.50A T/C	82	64	51	62
4: C & O/C	57	54	48	64
5: D & O/C	75	65	76	92

Stability of Performance

[During multiple 30 day periods]

Cell & Condition	Voltage Change [mV]		
	Period 1	Period 2	Period 3
1: 0.25A T/C	-2	41	42
2: 0.33A T/C	-1	31	-6
3: 0.50A T/C	-5	26	-5
4: C & O/C	-102	-25	-46
5: D & O/C	-33	-360	-52

Cell & Condition	Pressure Change [PSIA]		
	Period 1	Period 2	Period 3
1: 0.25A T/C	2	-2	-4
2: 0.33A T/C	-3	15	18
3: 0.50A T/C	-10	1	11
4: C & O/C	0	1	1
5: D & O/C	0	0	0

During the 3rd Cycle of Capacity Verification

Figure 2: End-of-Charge Pressure

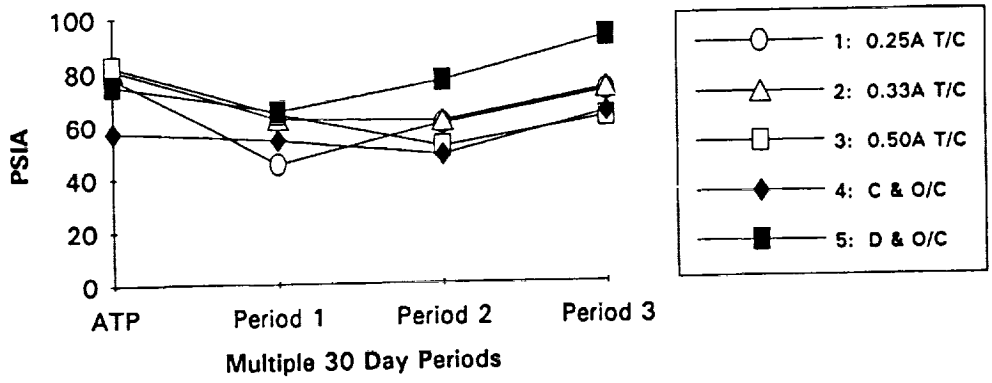

Figure 3: End-of-Charge Voltage

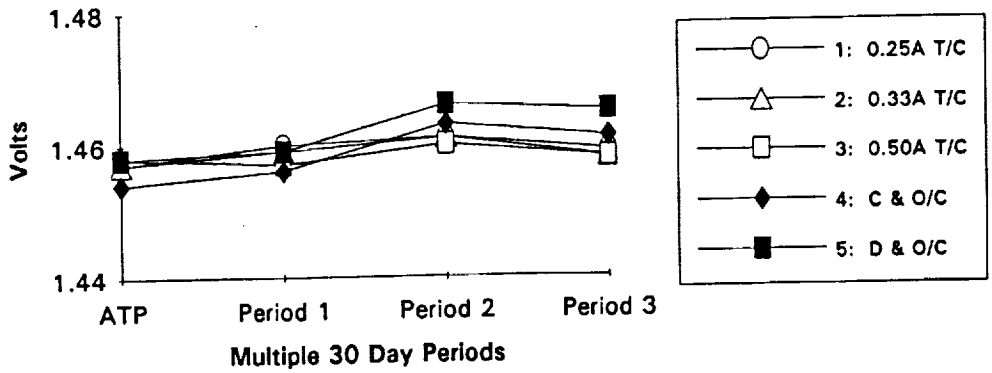

Figure 4: End-of-Discharge Pressure

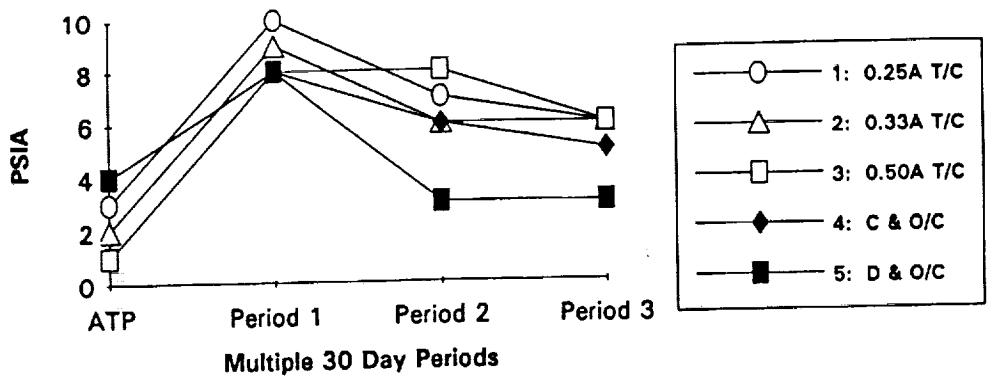

During the 3rd Cycle of Capacity Verification

Figure 5: Capacity

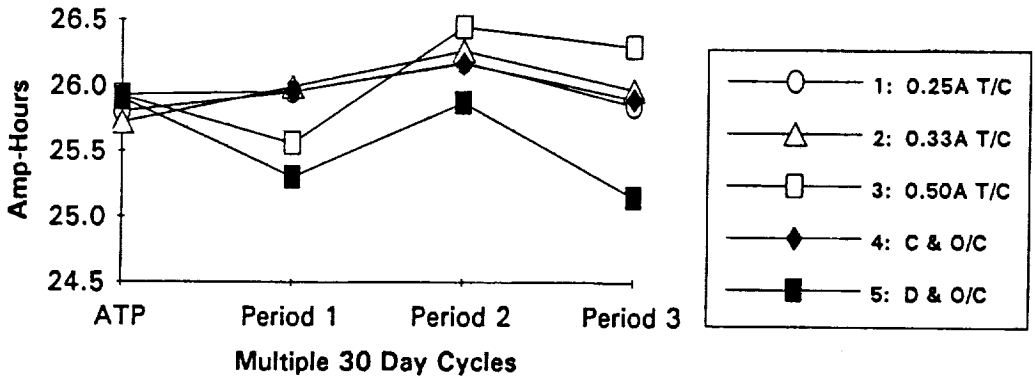

During the 30 Day Storage Periods

Figure 6: Voltage Change

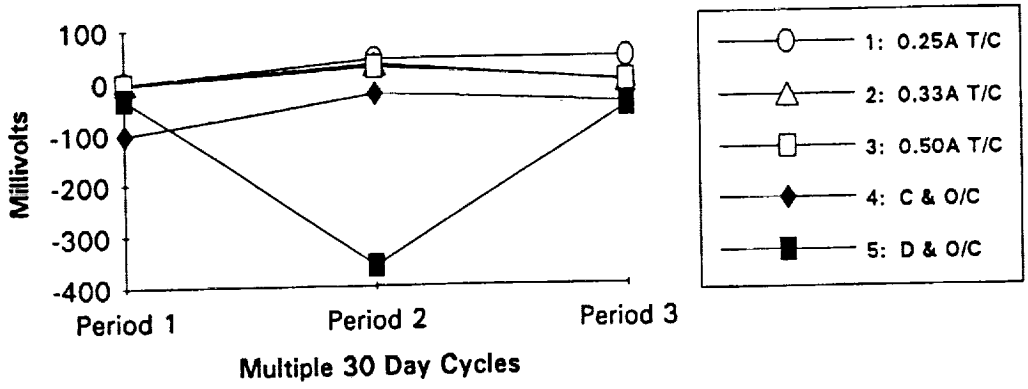

Figure 7: Pressure Change

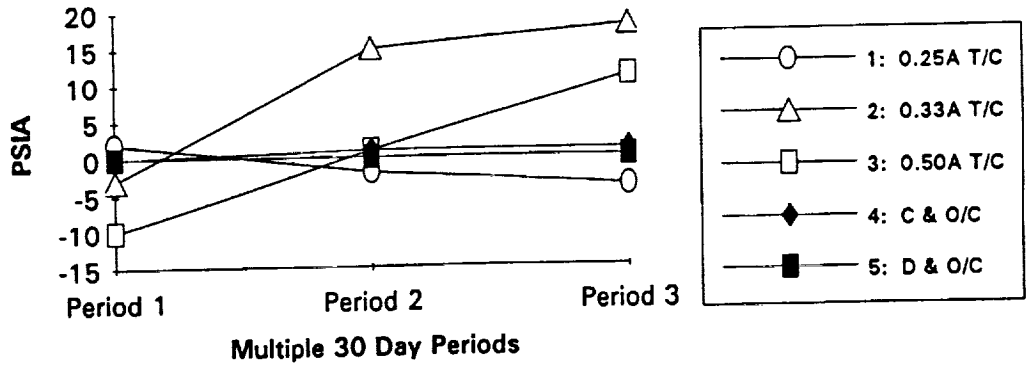

Figure 8

NiMH
CYCLE LIFE PERFORMANCE SUMMARY

(Engineering Model Cells)

Data as of 11/9/93

Cell Rating	Test Group	Temp Deg C	% DOD	# Cells in Test	Maximum Cycles Completed	Cell-cycles	Status
6 Ahr	AP6:1-6	25	50	0(6)	6656	27406	Complete
22 Ahr	AP22:1-2	25	50	0(2)	4236	8472	Complete
22 Ahr	AP22:4	25	50	0(1)	1961	1961	Complete
8 Ahr	AP8:1-12	25	50	0(12)	2206	24600	Complete
7 Ahr	AP7:1-9	25	50	2(9)*	7800	48397	In Test
7 Ahr	AP7:10-21	25	50	9(11)	3400	34600	In Test
7 Ahr	AP7:22-35	25	50	14(14)	2562	35868	In Test
	Total # of Cells			25(55)		181304	

Cells remaining on test.

Original # of cells on test

Total number of Cell-Cycles

Test Conditions:

--Charge at C/2 Rate for 60 Minutes
--Discharge at C Rate for 30 Minutes
--C/D Ratio = 1.05 except in test group AP7:21-35 where some are at 1.03

* 1st Generation cell design represented by #8 and #9 cells still on test.

Cell Design:

--All cells are prismatic construction similiar to NiCd.
--Each cell test group may be composed of several design variations, i.e. separator types, chemical and ED impregnation, processing additives, loadings, alloys, N/P ratio, etc.

Figure 9

COMPARISON OF EARLY TO PRESENT CELLS

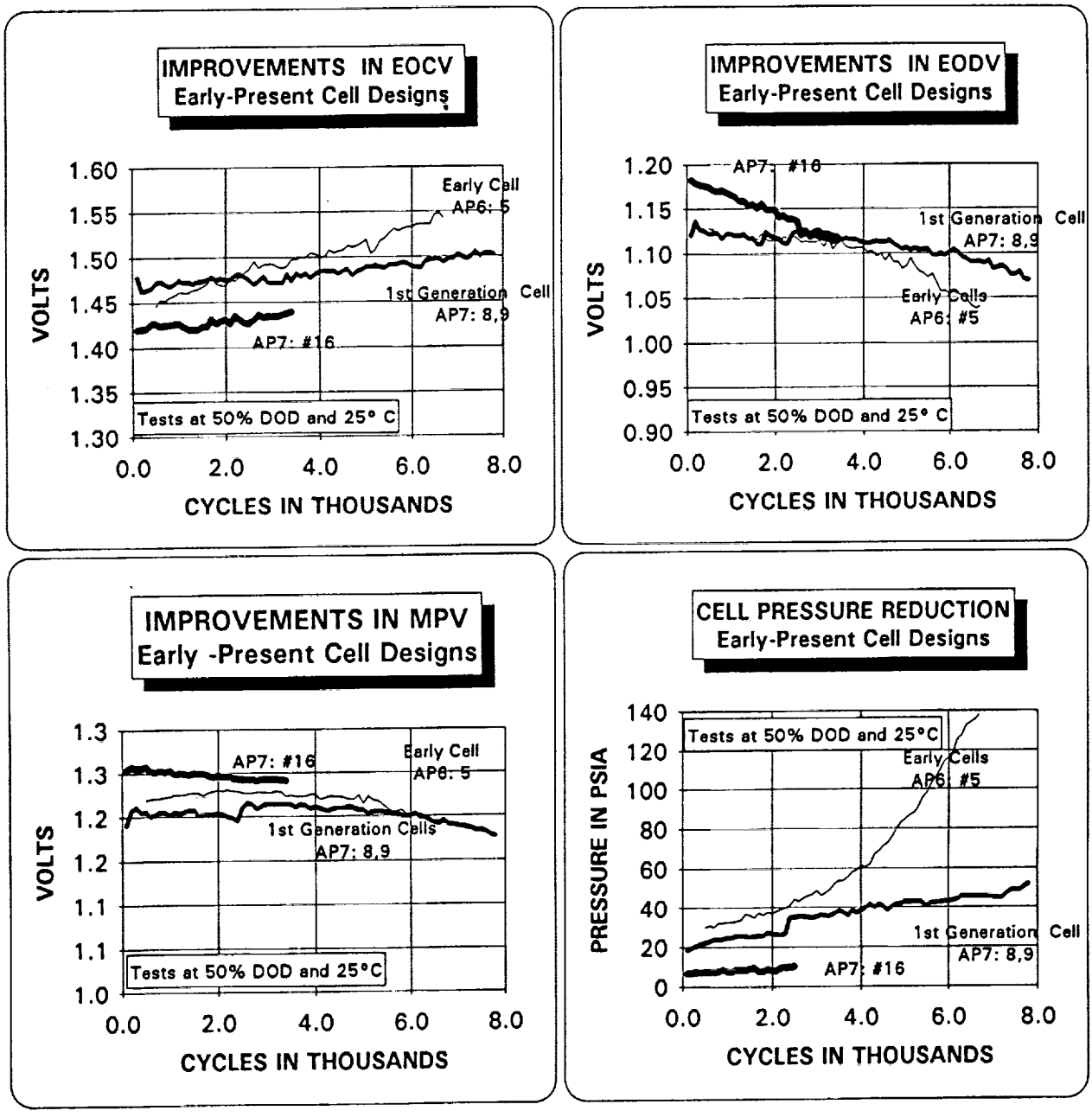

Note: Electrolyte adjustment made at approx. 2400 cycles on 1st Generation Cells.

NASA Johnson Space Center

Engineering Directorate

Propulsion and Power Division

Eric Darcy

1993 NASA Aerospace Battery Workshop

11/18/93

Determination of Thermal Properties of Commercial Ni-MH Cells

Outline

Eric Darcy

11/18/93

- Objectives
- Test plan
- Status and schedule
- Preliminary calorimetric findings
- Summary and future tests

NASA Johnson Space Center | Engineering Directorate

Objectives

Propulsion and Power Division

Eric Darcy | 11/18/93

Test Objectives

- To evaluate the electrical and thermal performance of commercial Ni-MH cells
- To evaluate the effectiveness of commercial charge control circuits
- To assess the abuse tolerance of these cells
- To correlate performance and abuse tolerance to cell design via disassembly

Design Objectives

- To determine which cell designs are most suitable for scale-up
- To guide the design of future Shuttle and Station based battery chargers

NASA Johnson Space Center — Engineering Directorate

Test Plan

Propulsion and Power Division

Eric Darcy — 11/18/93

Cell types

- AB2 - Ovonic C, Harding A and AA
- AB5 - Furikaya prismatic, Gates 4/5A, Sanyo 4/3A, Toshiba 4/5 C

Chargers	Component	Current control	Cut-off method
Benchmarq	DV2003S1	const current	$-\partial V/\partial t$, $\Delta T/\Delta t$
Enstore	ECS-II	4 step current	V inflection
ICS	1700-EB	Reflex current	V inflection
Maxim	MAX712EV	const current	$\partial V/\partial t=0$

1 st Performance Evaluation using L18 Taguchi Matrix

- 3 cell types - Harding A, Sanyo 4/3A, Toshiba 4/5A
- 3 chargers - Benchmarq, Enstore, Maxim
- 3 cyling rates (cycling at 100% DOD)
  - low - C/10 charge, C/7 discharge
  - medium - C/3 charge, C/2 discharge
  - high - 2C charge, 3C discharge
- 2 temperatures - 25 and 5 deg C

Performance criteria

- Discharge capacity vs cycle
- Ah and Wh cycling efficiency

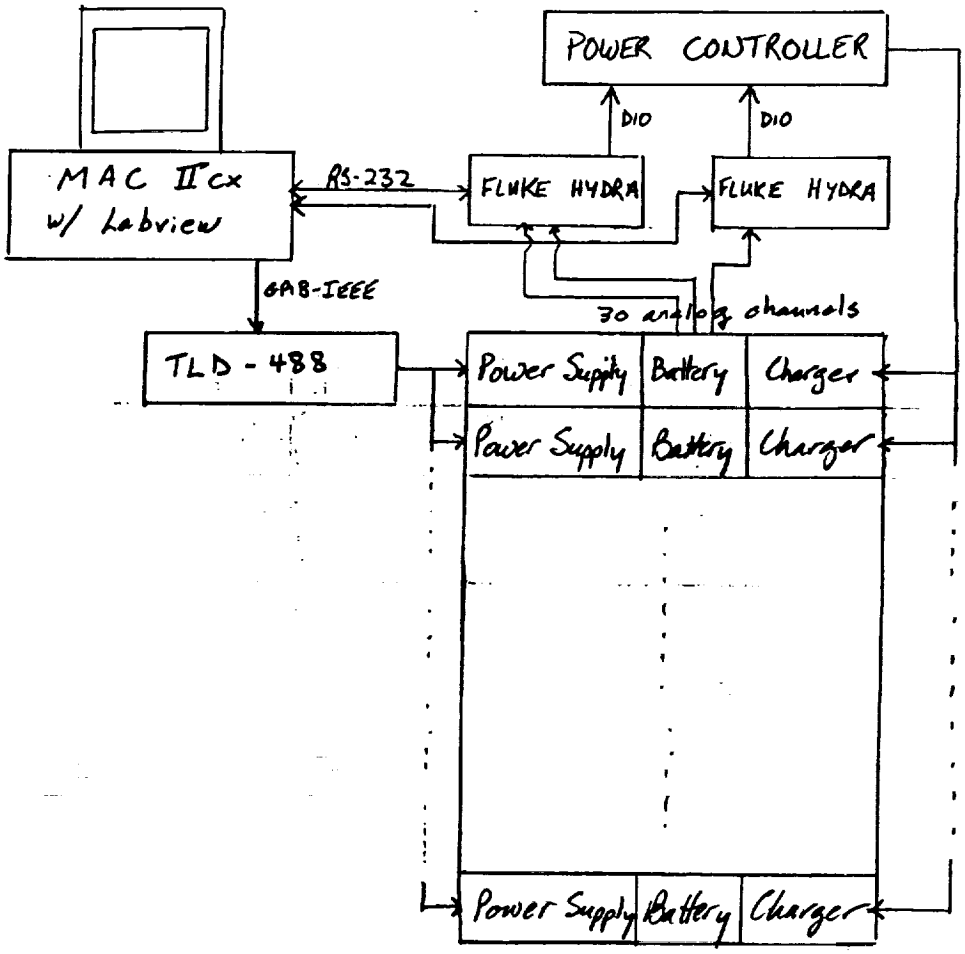

Schematic of

Automated Battery Cycling Test Stand

Test Plan (cont.)

Eric Darcy

11/18/93

- Calorimetric Evaluation
  - Hart Scientific twin cell calorimeter
    - 200 second time constant
    - 100 μW resolution
  - Parameteric Evaluation using L8 Taguchi Matrix
    - 2 cycling rates - medium and high
    - 2 Chargers - Enstore and Maxim
    - 2 Temperatures - 25 and 5 C
    - 2 Cell types - Ovonic C, Sanyo 4/3A
  - Evaluation criteria
    - maximum cycle peak heat, W
    - total cycle heat energy, J

Figure 2 Schematic of Twin Cell Calorimeter
(configured for battery calorimetry)

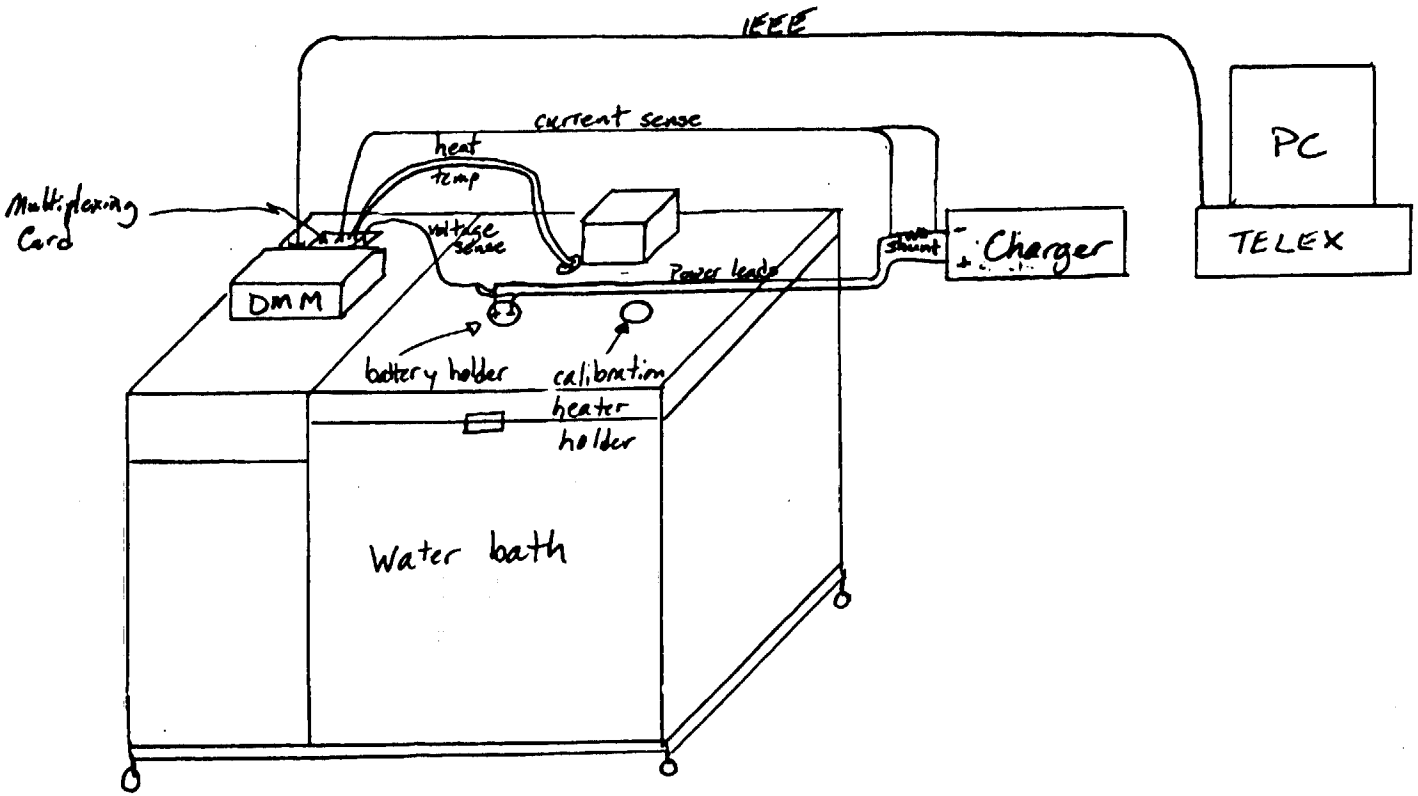

Test Plan (cont.)

Propulsion and Power Division
Eric Darcy
11/18/93

- Abuse Tolerance Assessment on all cell types
  - Overcharge - 2 rates (C/3, 2C), 2 temperatures (25 and 5 C)
  - Overdischarge - 2 rates (C/3, 2C), 2 temperatures (25 and 5 C)
  - Short Circuit - 100 mΩ and 50 mΩ, 2 temperatures (25 and 5 C)
  - Heat-to-Vent

- Destructive Physical Analysis to determine
  - Cell pressure and gas composition
  - Porosity distribution, bulk porosity, total surface area of hydride
  - Electrolyte composition and concentration
  - Reaction distribution across cell cross-section
  - Hydride surface composition (XPS and AES)

NASA Johnson Space Center

Engineering Directorate

Test status and schedule

Propulsion and Power Division

Eric Darcy | **11/18/93**

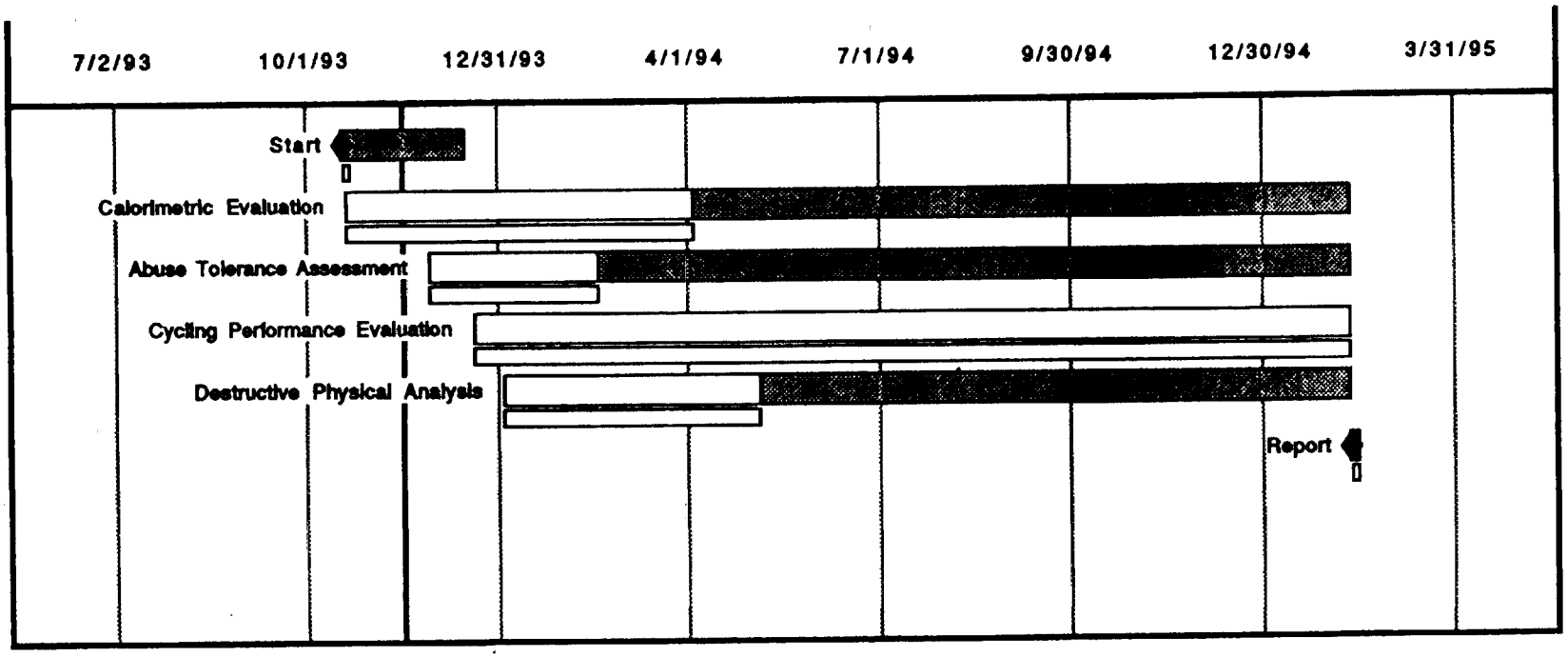

NASA Johnson Space Center | Engineering Directorate

Calorimetric Findings

Propulsion and Power Division	
Eric Darcy	11/18/93

Fig. 1 - Ovonic cells, Enstore charger, low rate (0.5 A charge, 0.5 A discharge)

- Enstore charge fails to terminate at low rate
- 7.5 Ah total charge input with 3.25 Ah discharge output
- Inflection of heat profile occurs at 3.5 Ah (~100% SOC)
- Heat profile levels out to a steady rate of 0.54 W

Fig 2 & 3 - Enstore charger vs Maxim charger at high rates and room temp.

- Enstore's 4 step charge method results in lower heat rise on charge
- Enstore results in less heat energy output for the same Ah input
- Enstore's charge resulted in 35% higher capacity return on discharge

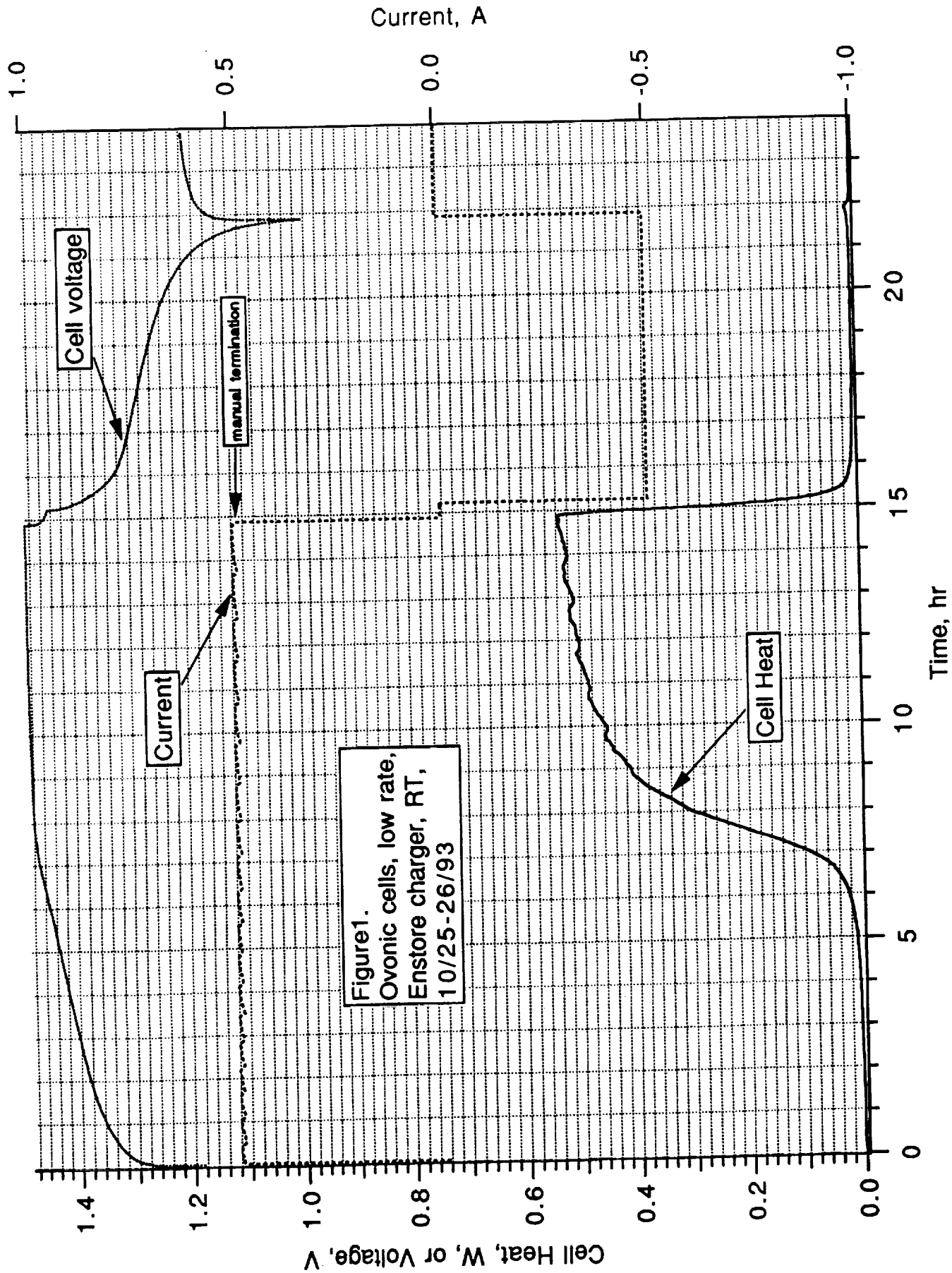
Current, A
1.0
0.5
0.0
-0.5
-1.0
Cell voltage
manual termination
Current
Cell Heat
Figure1.
Ovonic cells, low rate,
Enstore charger, RT,
10/25-26/93
Time, hr
0
5
10
15
20
Cell Heat, W, or Voltage, V
0.0
0.2
0.4
0.6
0.8
1.0
1.2
1.4

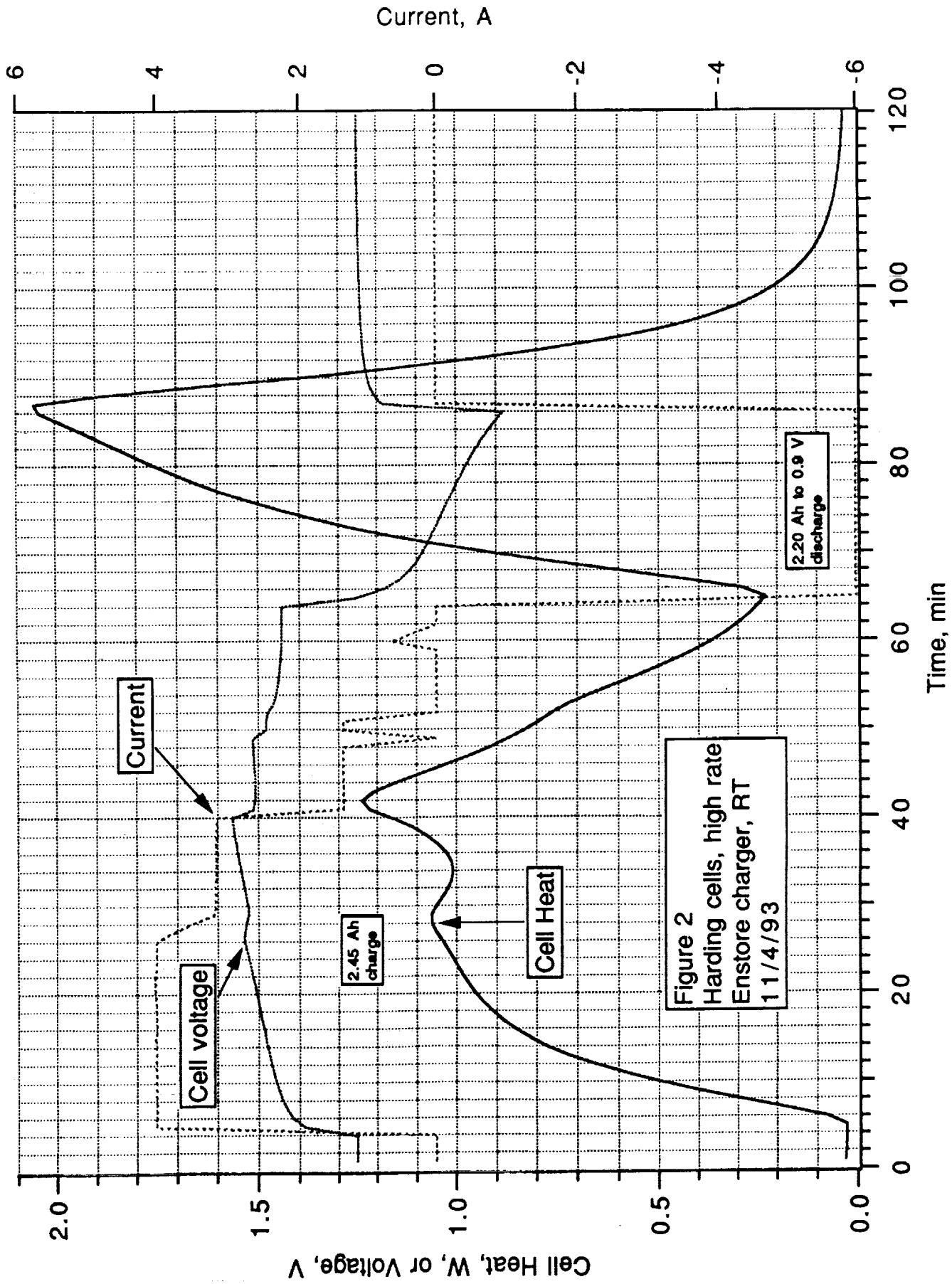
Current, A
6
4
2
0
-2
-4
-6
120
100
80
60
40
20
0
Time, min
2.20 Ah to 0.9 V discharge
Current
Cell voltage
2.45 Ah charge
Cell Heat
Figure 2
Harding cells, high rate
Enstore charger, RT
11/4/93
2.0
1.5
1.0
0.5
0.0
Cell Heat, W, or Voltage, V

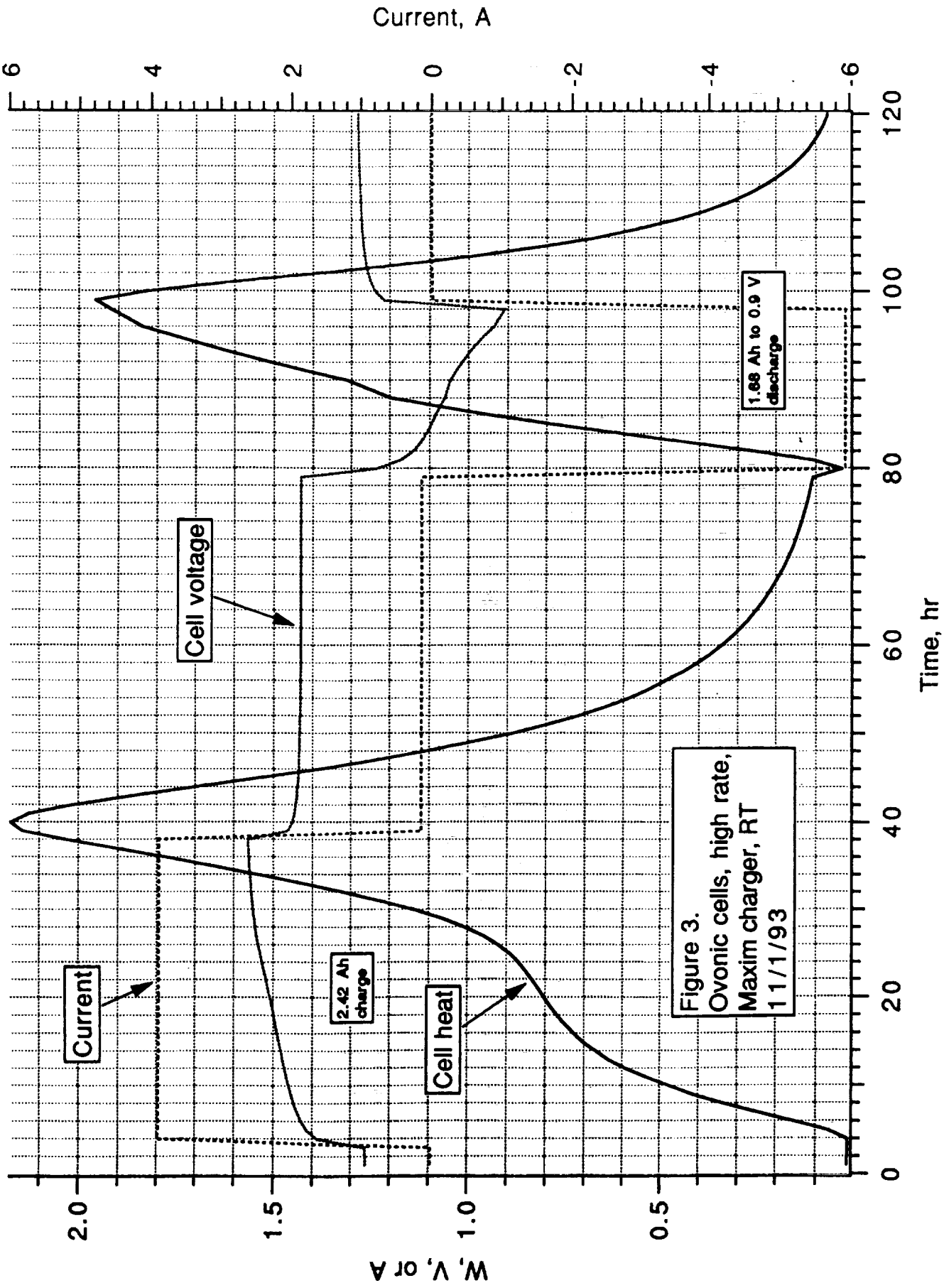
Current, A
6
4
2
0
-2
-4
-6
120
100
80
60
40
20
0
Time, hr
W, V, or A
2.0
1.5
1.0
0.5
1.88 Ah to 0.9 V discharge
Cell voltage
Current
2.42 Ah charge
Cell heat
Figure 3.
Ovonic cells, high rate,
Maxim charger, RT
11/1/93

Findings (cont.)

Eric Darcy | 11/18/93

Fig 4 - Ni/Cd vs Ni/MH C-cells with the Maxim charger

- 1.17 A charge with 1.75 A discharge at RT
- Ni/Cd commercial cell rated at 1.8 Ah from Golden Power, type KR1800C
- Ni/MH charge input is lower, 3.92 vs 4.78 Ah with the $\partial V/\partial t=0$ method
- Ni/Cd charges cooler up to 2.67 Ah
- Ni/Cd generates more heat energy on charge which steadily climbs
- Ni/MH delivered 3.35 Ah vs 1.96 Ah to 1 V
- Ni/MH discharges with much less heat generation

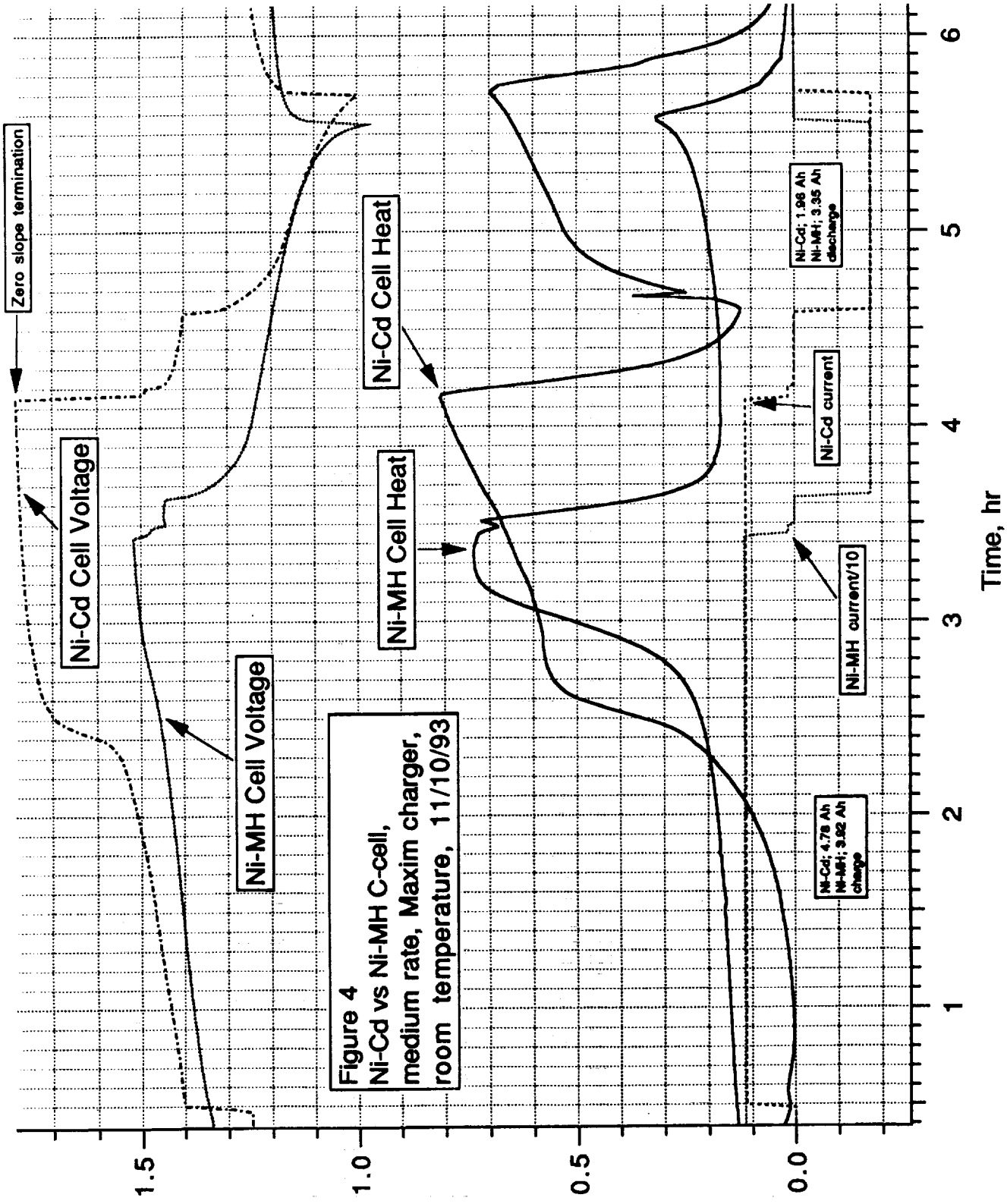

Figure 4
Ni-Cd vs Ni-MH C-cell,
medium rate, Maxim charger,
room temperature, 11/10/93

NASA Johnson Space Center

Engineering Directorate

Summary and future tests

Propulsion and Power Division

Eric Darcy | 11/18/93

- Reflex charging with ICS circuit resulted in premature charge termination
  - Future tests - ICS has promised to provide an upgraded charger (ICS-1702) designed specifically for Ni-MH cells
- Ni-MH cells appear very tolerant to overcharge at low rates
  - Future tests - Validate mechanism with more calorimetry and DPA for O2
- Enstore's method is more electrically and thermally efficient at high rates
  - Future tests
    - compare at medium rate
    - compare at low temperature
- Ni-MH cycles much more efficiently than Ni-Cd with the $\partial V/\partial t=0$ termination
  - Future tests
    - compare using the Enstore charger (inflection method)
    - compare at low temperature

Yardney
TECHNICAL PRODUCTS, INC.

HIGH RATE LITHIUM/THIONYL CHLORIDE BIPOLAR BATTERY DEVELOPMENT

P. G. RUSSELL, F. GOEBEL

YARDNEY TECHNICAL PRODUCTS, INC.
82 Mechanic Street • Pawcatuck, CT 06379

1993 NASA AEROSPACE BATTERY WORKSHOP
November 16 -18, 1993
U.S. Space and Rocket Center
Huntsville, AL

Yardney TECHNICAL PRODUCTS INC

Program Tasks and Accomplishments

- Improved on existing method of manufacturing bipolar plates, Figs. 1A and 1B

- Developed novel method for manufacturing large sheets of carbon cathode material. These cathodes performed better than standard cathodes made by calendering a wetted carbon/TFE mixture in single cell tests during continuous discharge at 25A with 10% duty cycle to 1.0V, Figs 2 and 3

Yardney TECHNICAL PRODUCTS INC

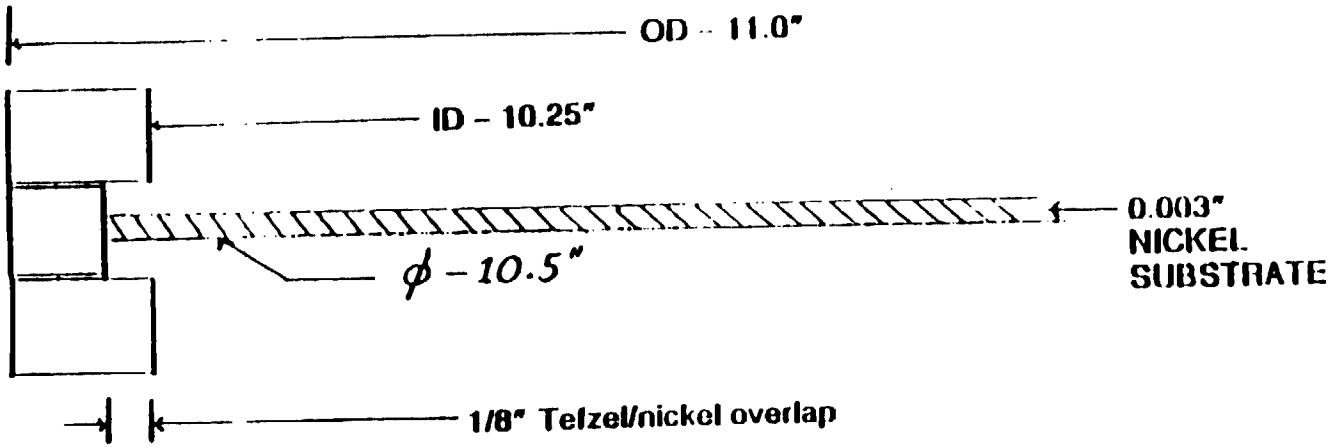

FIG. 1A. TEFZEL/NICKEL SANDWICH PRIOR TO COMPRESSION MOLDING

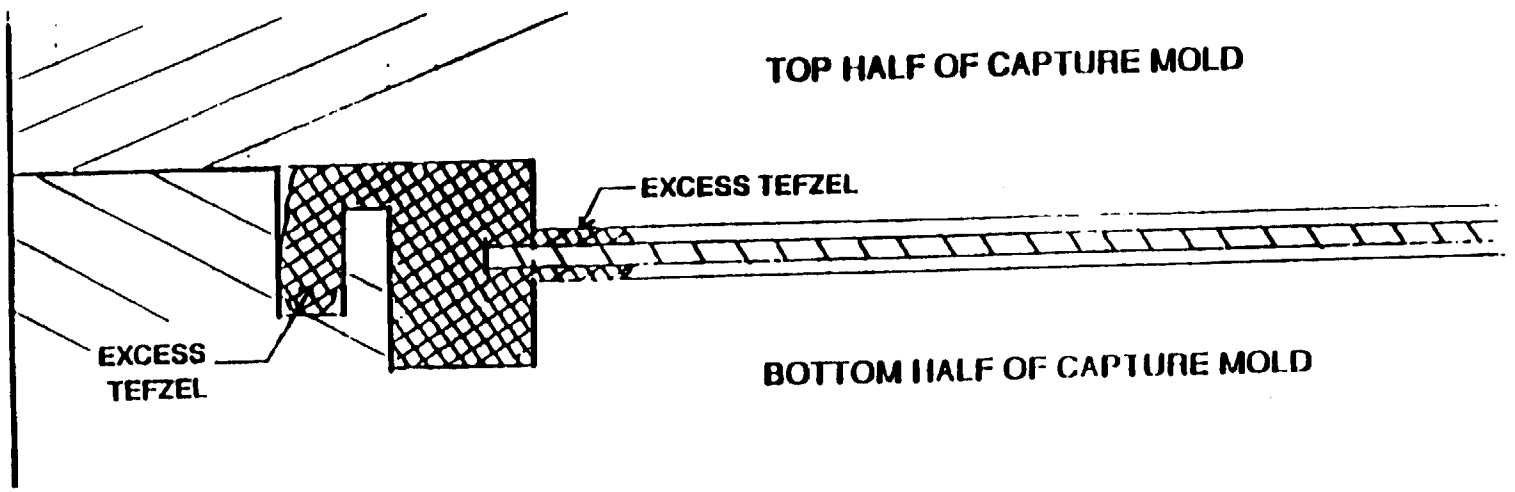

FIG. 1B. TEFZEL/NICKEL SUBSTRATE CONFIGURATION AFTER COMPRESSION MOLDING

Yardney TECHNICAL PRODUCTS INC

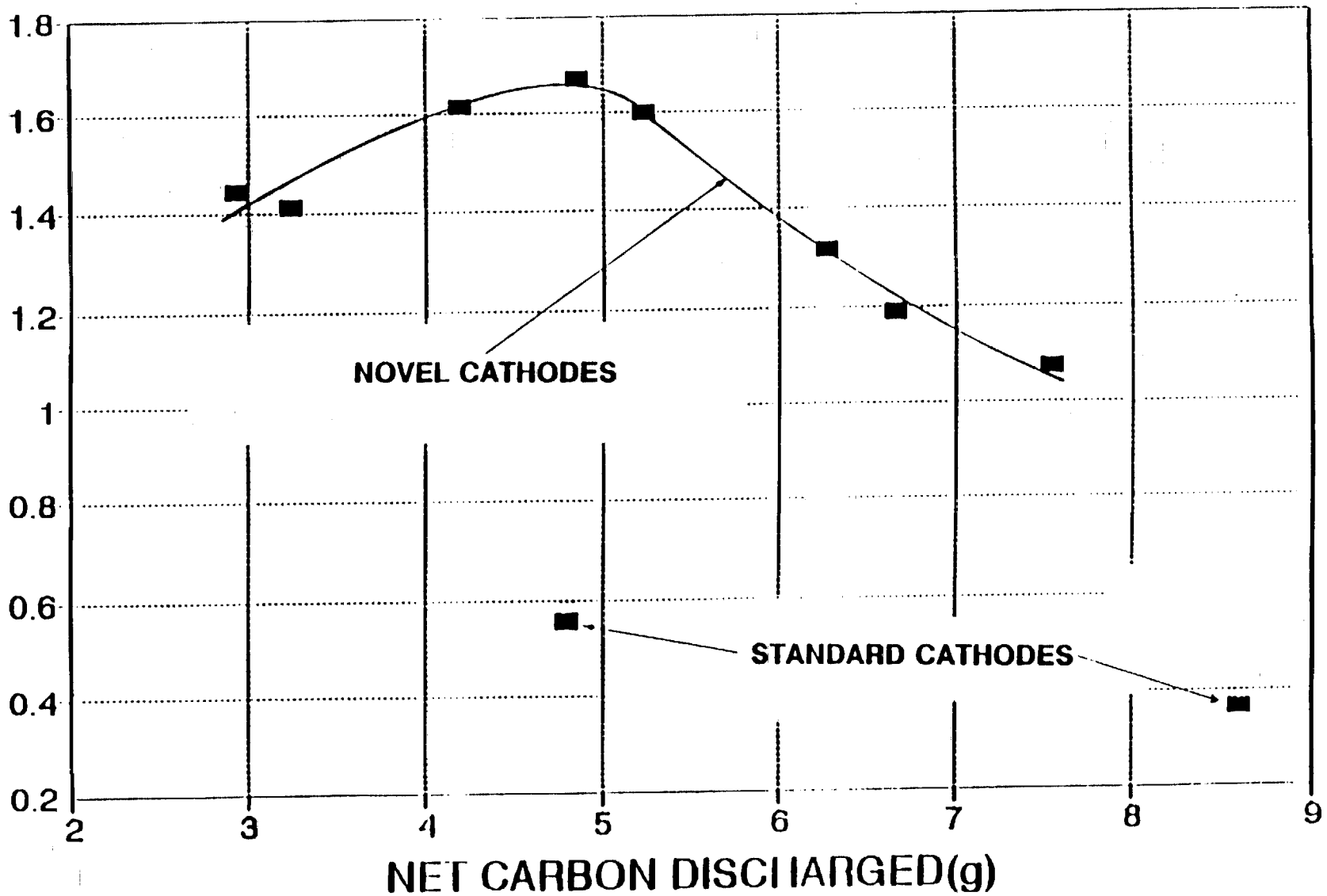

FIG. 2. CATHODE UTILIZATION (Ah/g) VERSUS CATHODE CARBON WEIGHT

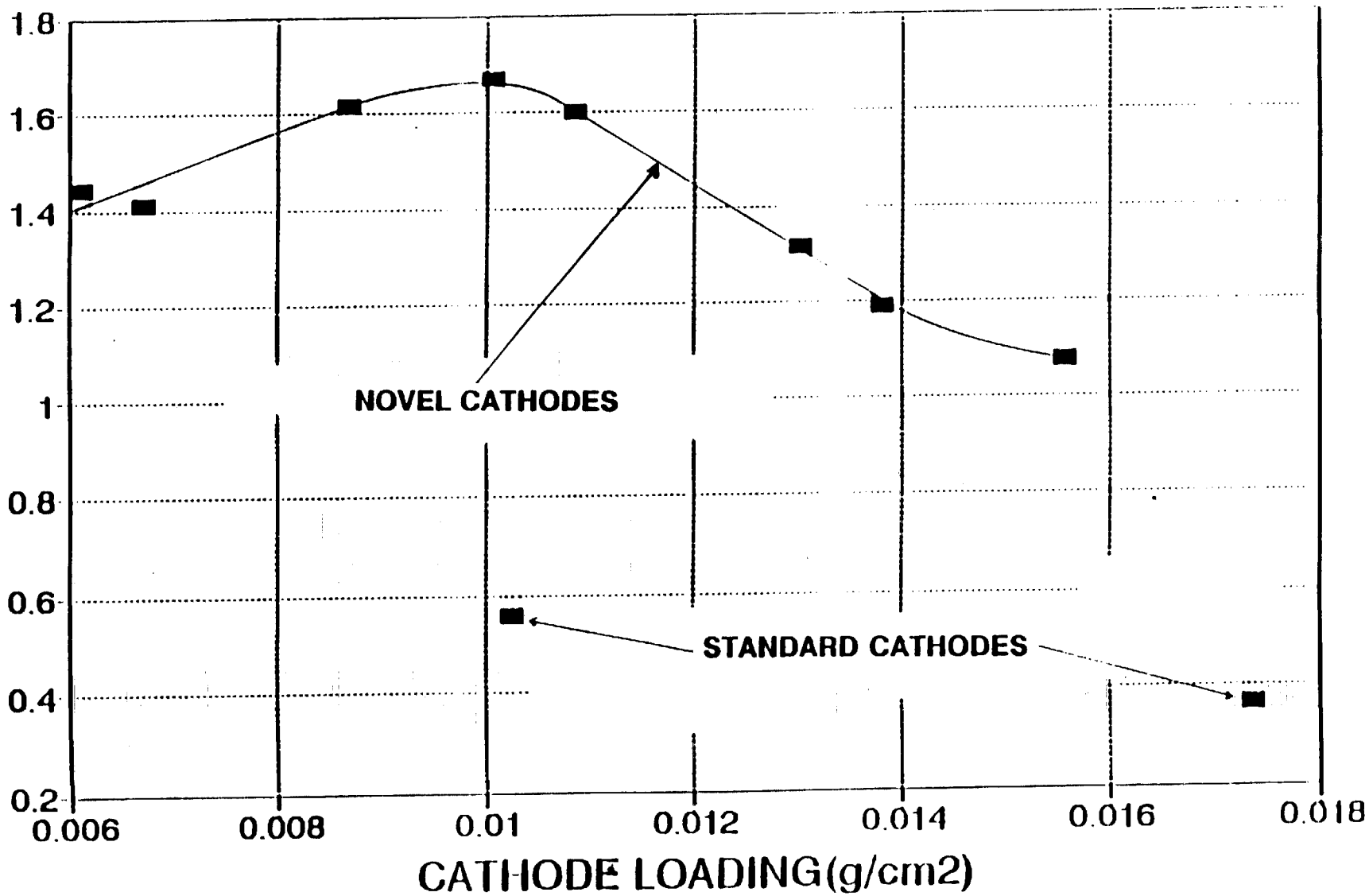

FIG. 3. CATHODE UTILIZATION (Ah/g) VERSUS CATHODE LOADING (g/cm^2)

Yardney TECHNICAL PRODUCTS INC

Program Tasks and Accomplishments(continued)

- A standard 40 wt% low surface area / 60 wt% high surface area carbon composition was selected for cathode evaluation in single cell 20 second pulse discharge tests at 25A and 10% duty cycle, Fig. 4 to 8

- Developed cell design and the procedures for assembly of stacks containing up to 150 cells in bipolar configuration, stack sealing, and the activation of individual cells, Figs. 9A, 9B, and 9C

Yardney TECHNICAL PRODUCTS INC

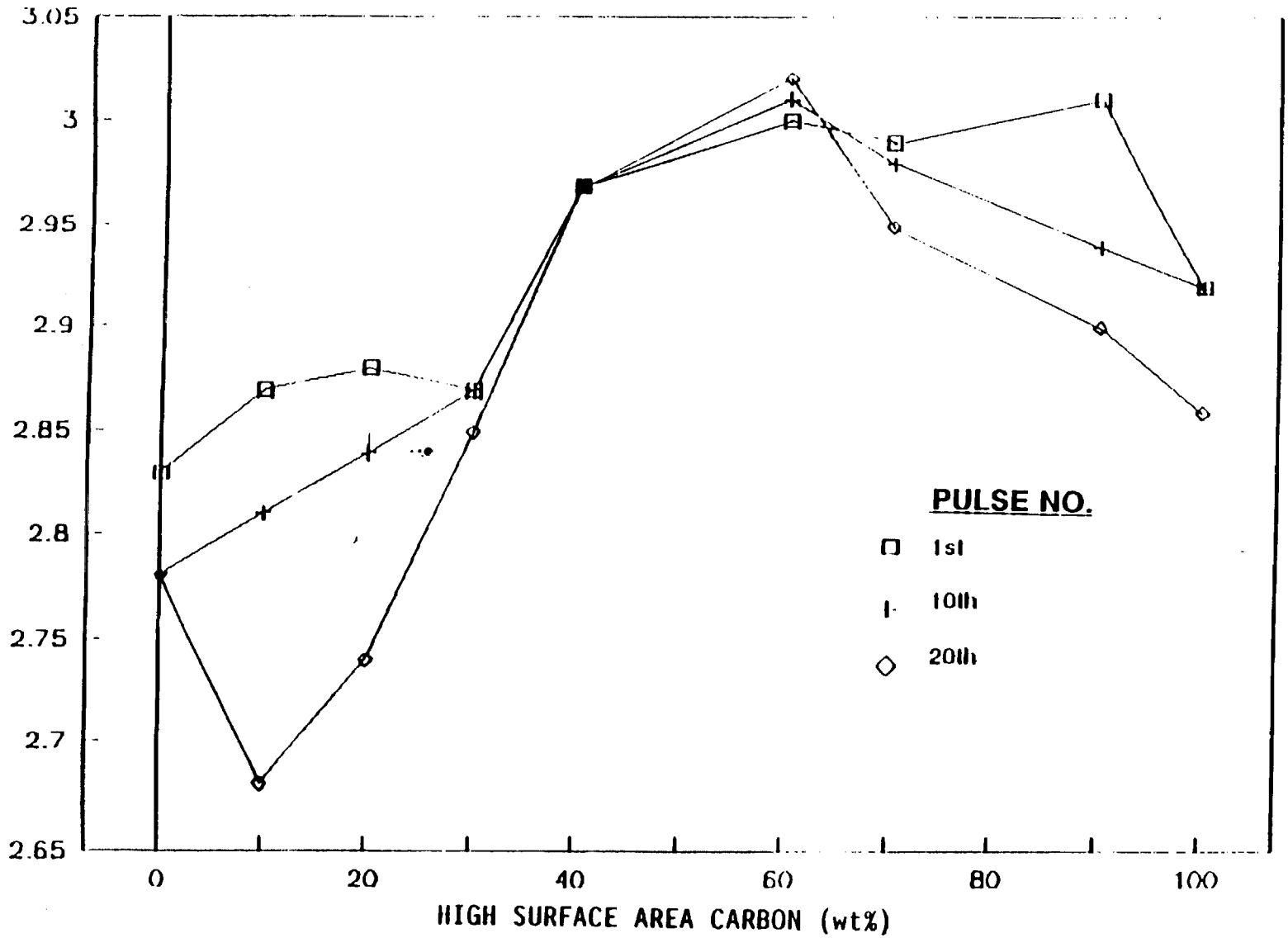

FIG. 4 EOPV VERSUS CARBON COMPOSITION. TWENTY 20-SECOND PULSES

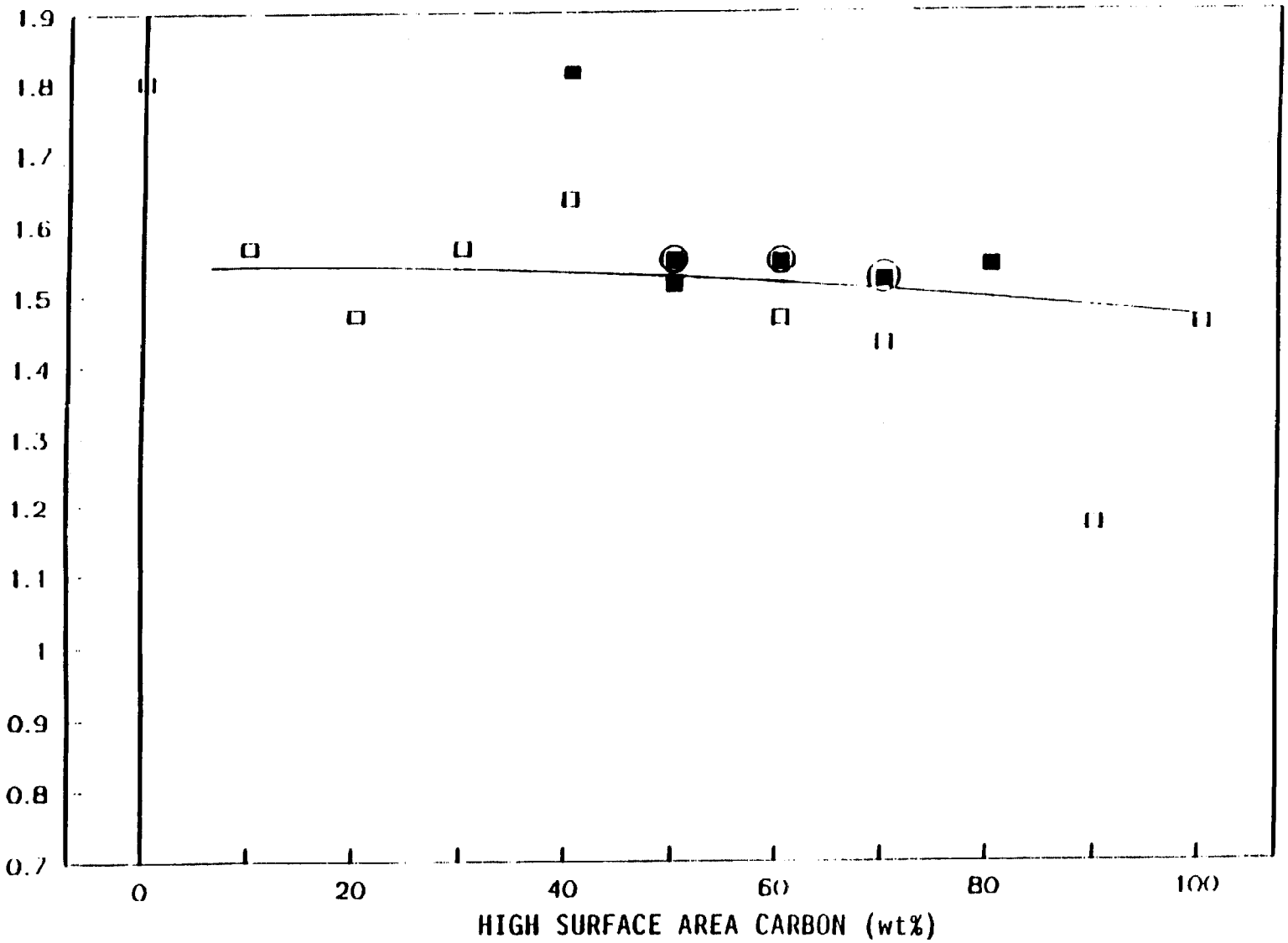

FIG. 5. CATHODE UTILIZATION (Ah/g) VERSUS CARBON COMPOSITION. UTILIZATION INCLUDES CONTINUOUS DISCHARGE TO 1.0V AFTER 400 SECONDS OF PULSE DISCHARGE. OPEN SQUARES-DATA FROM TESTS IN FIG. 4 SOLID SQUARES W/WO CIRCLES-ADDITIONAL TESTS.

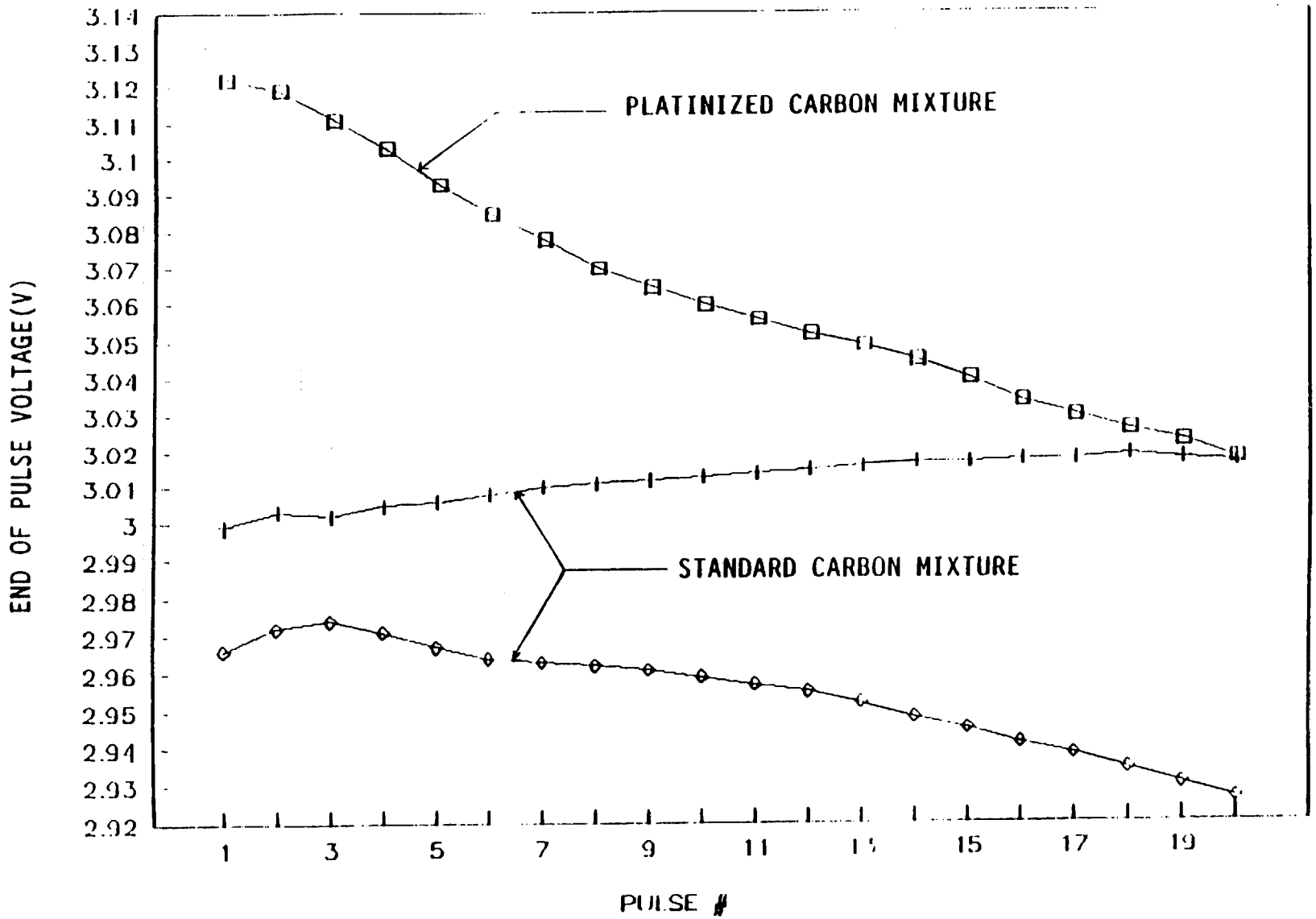

FIG. 6. COMPARISON OF PLATINIZED AND STANDARD 40/60 CARBON CATHODES

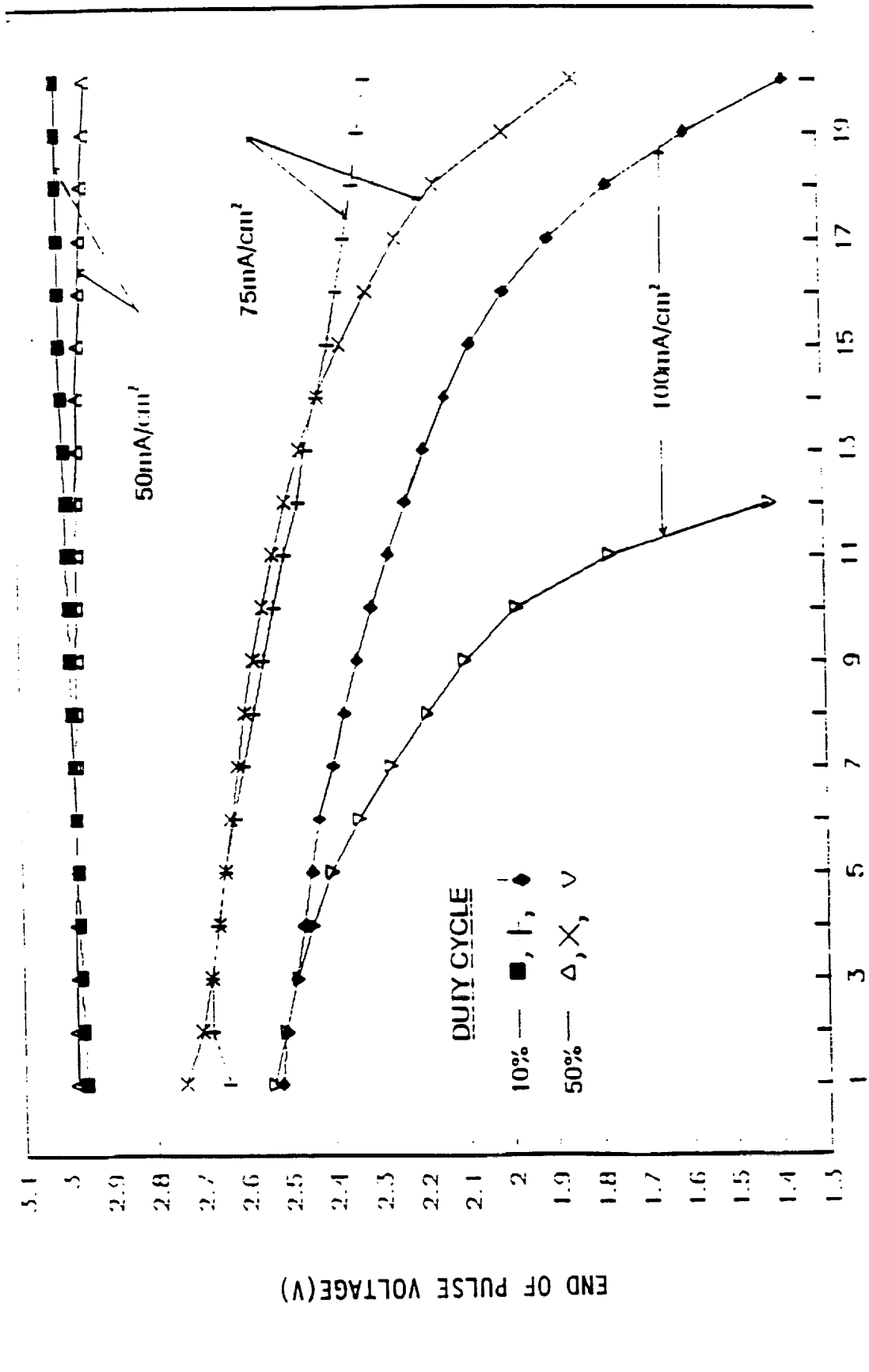

FIG. 7. EFFECTS OF CURRENT DENSITY AND DUTY CYCLE ON END OF PULSE VOLTAGE

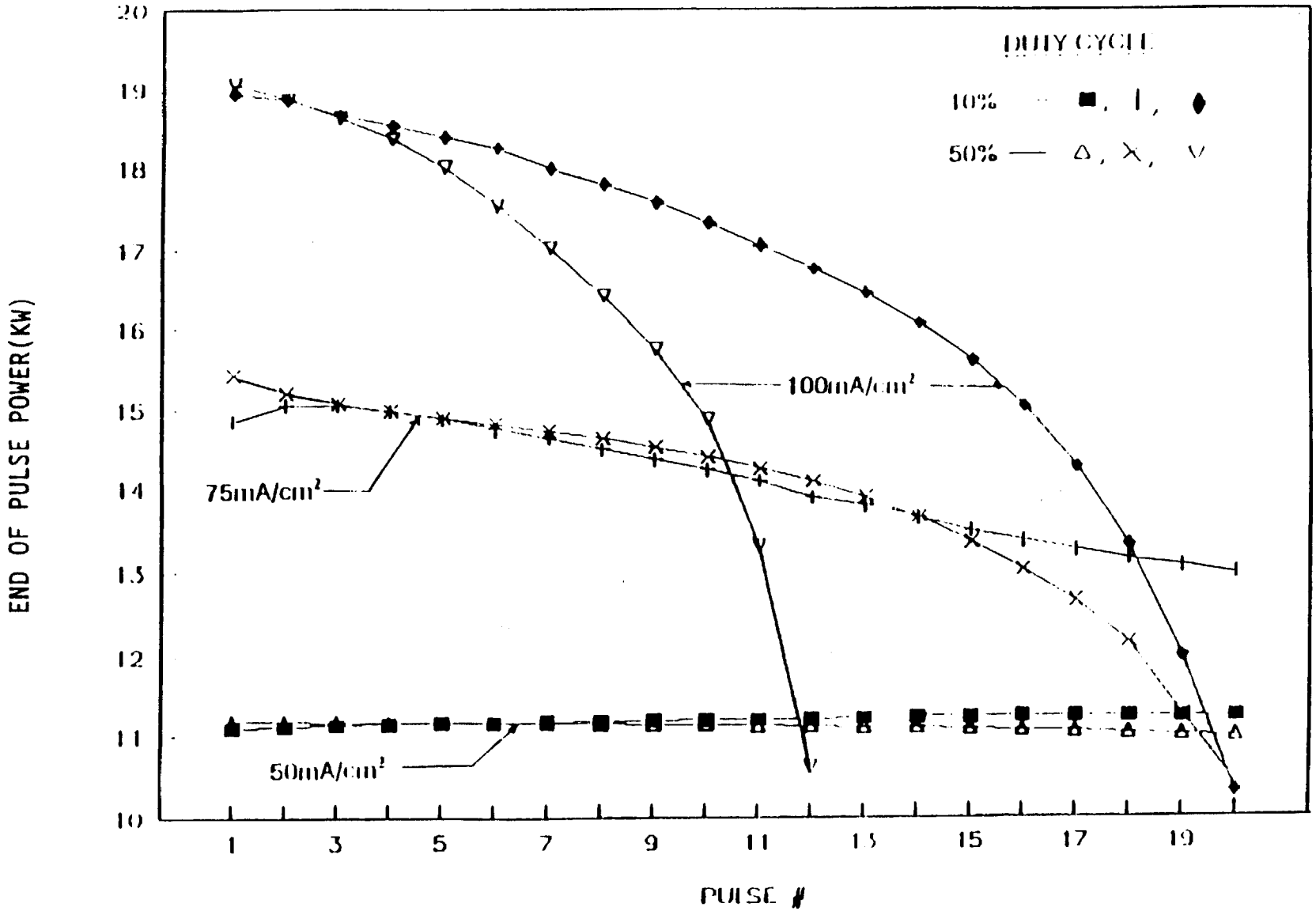

FIG. 8. EFFECTS OF CURRENT DENSITY AND DUTY CYCLE ON EOPP FOR A 150-CELL BIPOLAR STACK

Yardney TECHNICAL PRODUCTS INC

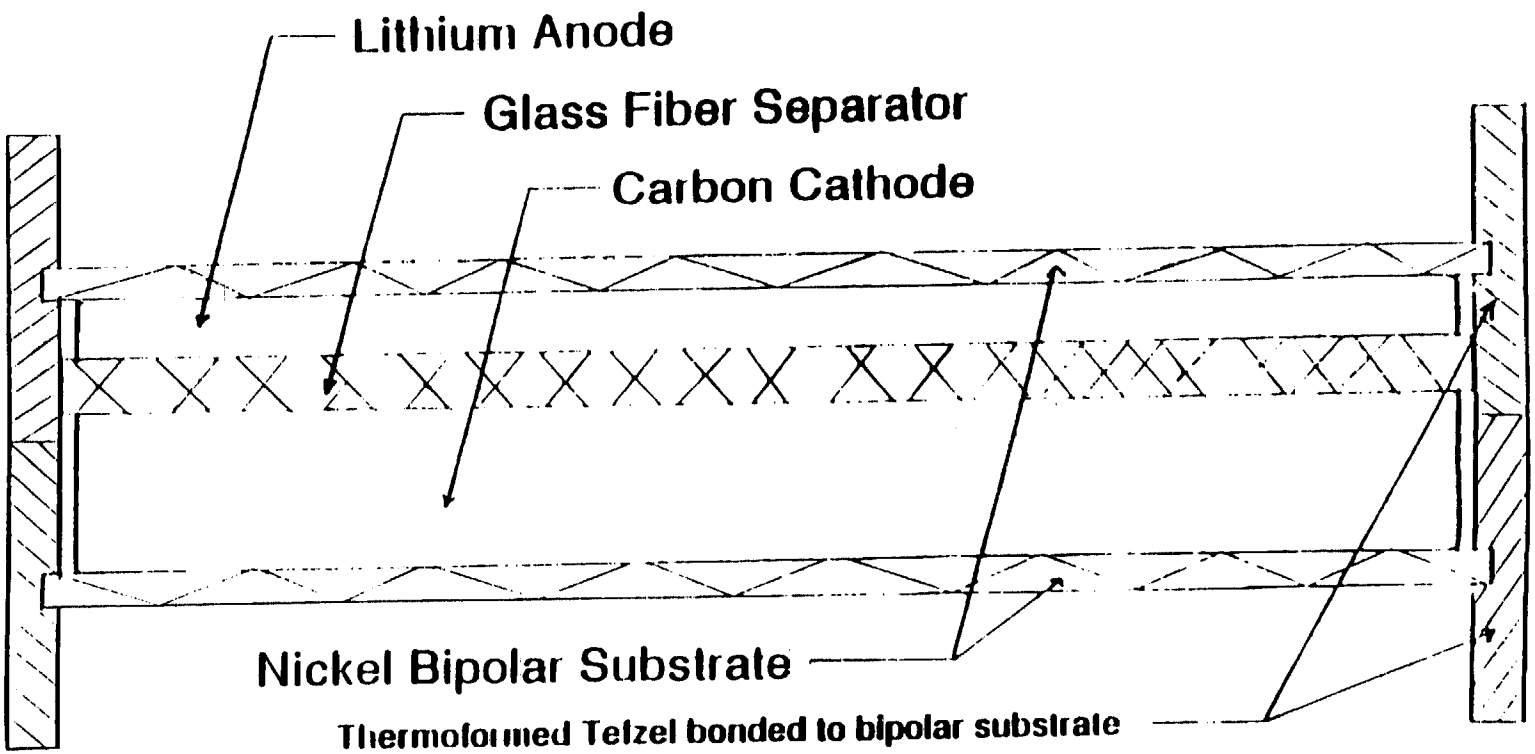

FIG. 9A SINGLE CELL COMPONENTS IN STACK SUBASSEMBLY

Yardney TECHNICAL PRODUCTS INC

Tefzel Sealing

HEAT SOURCES

Heating elements from 330 to 900 Watts

PROCEDURE

- Prepare module surface for sealing
- Increase seal thickness by melting Tefzel surface with heat source
- Add fiberglass/Tefzel composite layer
  - *increases thickness*
  - *improves strength*

FIG. 9B

Yardney TECHNICAL PRODUCTS INC

Multicell Stack Fabrication

- Assemble stack components
- Compress stack to final height
- Three quarter" seal of stacked Tefzel rings
- Electrolyte activation
- Complete Tefzel seal

FIG. 9C

Yardney TECHNICAL PRODUCTS INC

Program Tasks and Accomplishments (continued)

- Evaluated single cells assembled with bipolar stack hardware during constant power Sonobuoy pulse discharge tests (20 second pulse, 10% duty cycle). A 9.25 inch diameter cathode was selected for the torpedo size Sonobuoy battery module, Figs. 10 and 11

- Evaluated 4-cell and 10-cell bipolar stacks and a 50-cell bipolar stack during constant power Sonobuoy pulse discharge tests, Figs. 12 - 15

Yardney TECHNICAL PRODUCTS INC

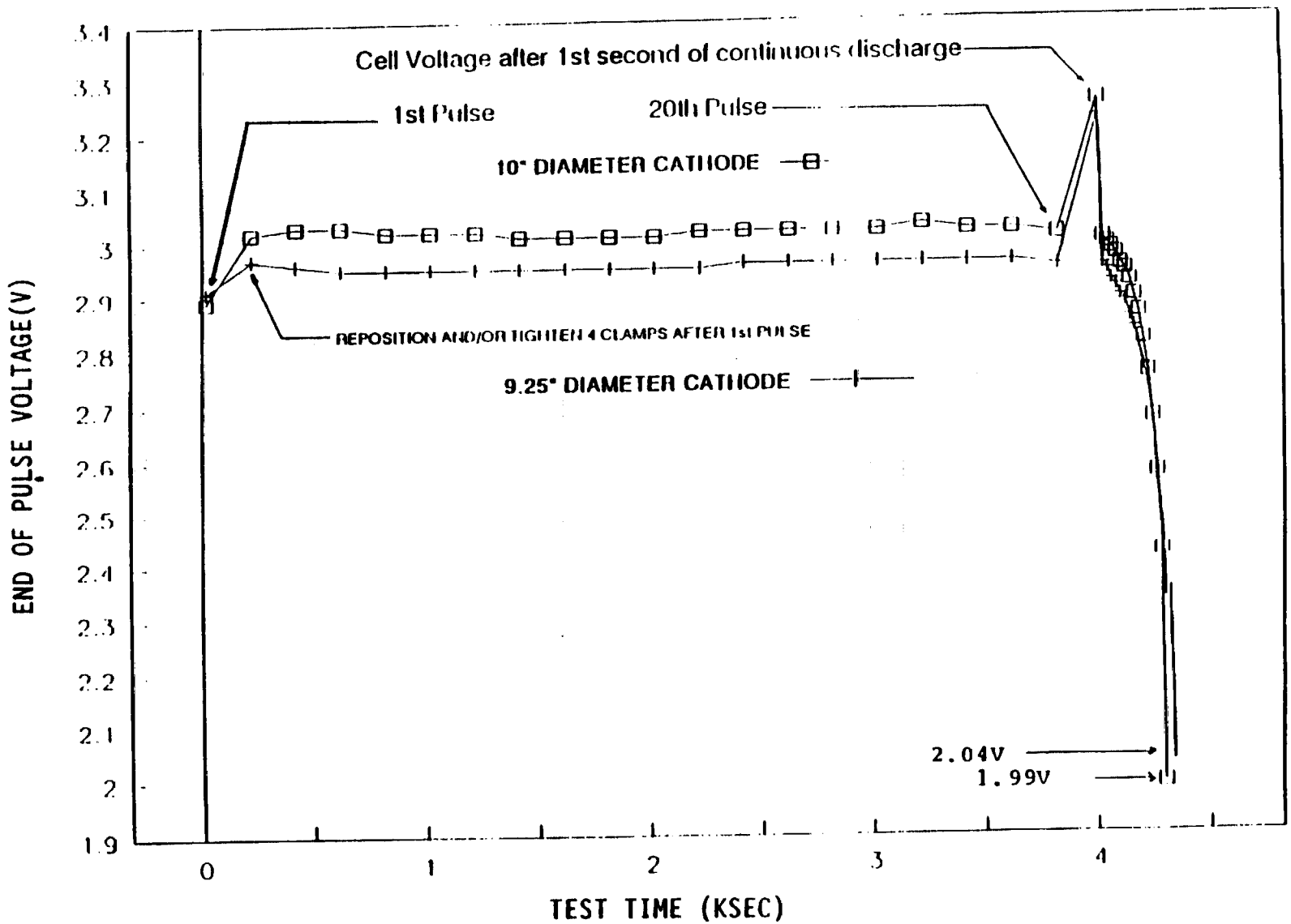

FIG. 10. EFFECT OF CATHODE DIAMETER ON EOPV DURING SINGLE CELL CONSTANT POWER (71.4w) PULSE AND CONTINUOUS DISCHARGE TEST

Yardney TECHNICAL PRODUCTS INC

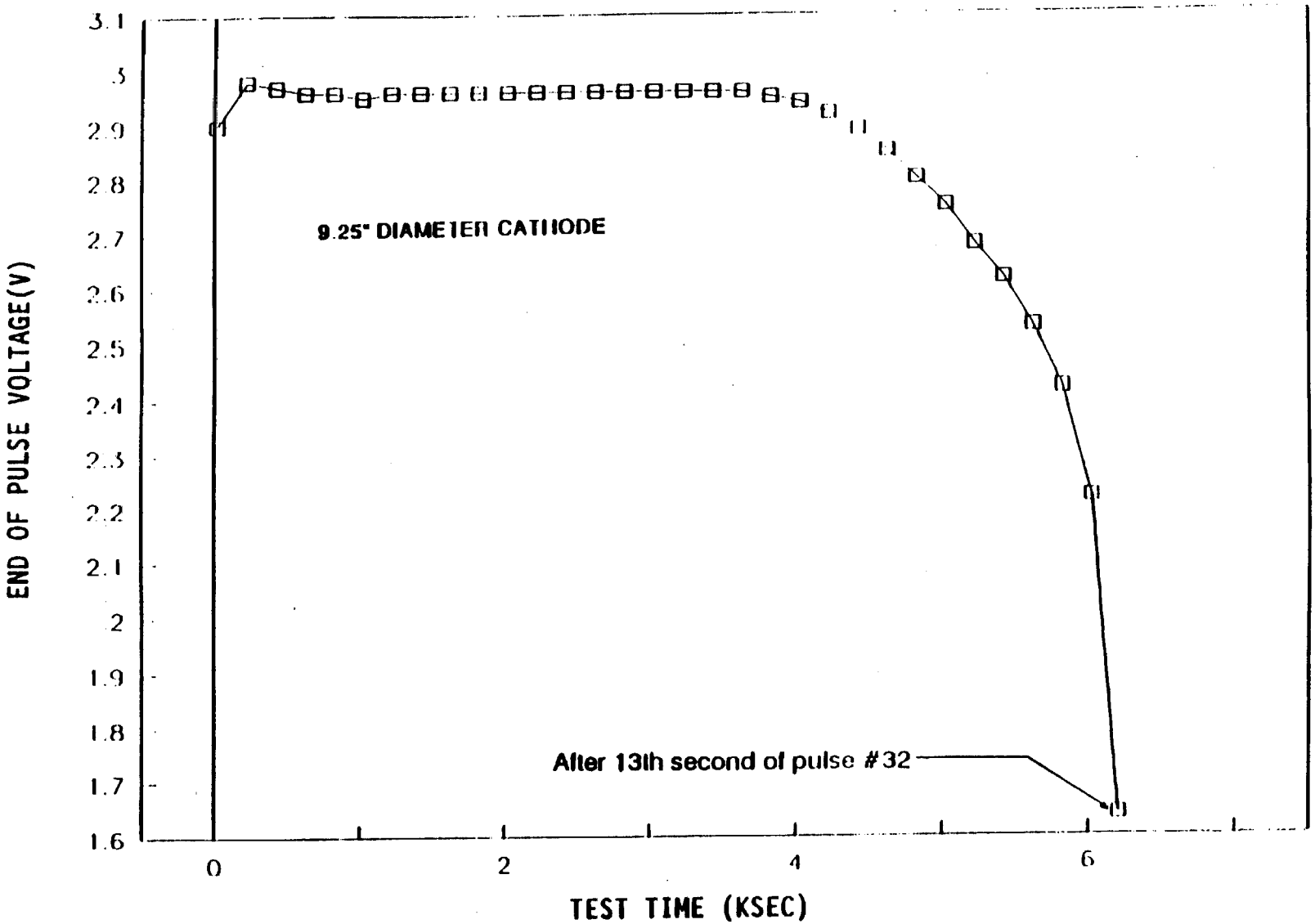

FIG. 11. FIRST SINGLE CELL CONSTANT POWER (71.4W) CONTINUOUS PULSE DISCHARGE EVALUATION OF CATHODE FOR LARGE SIZE SONOBUOY BATTERY

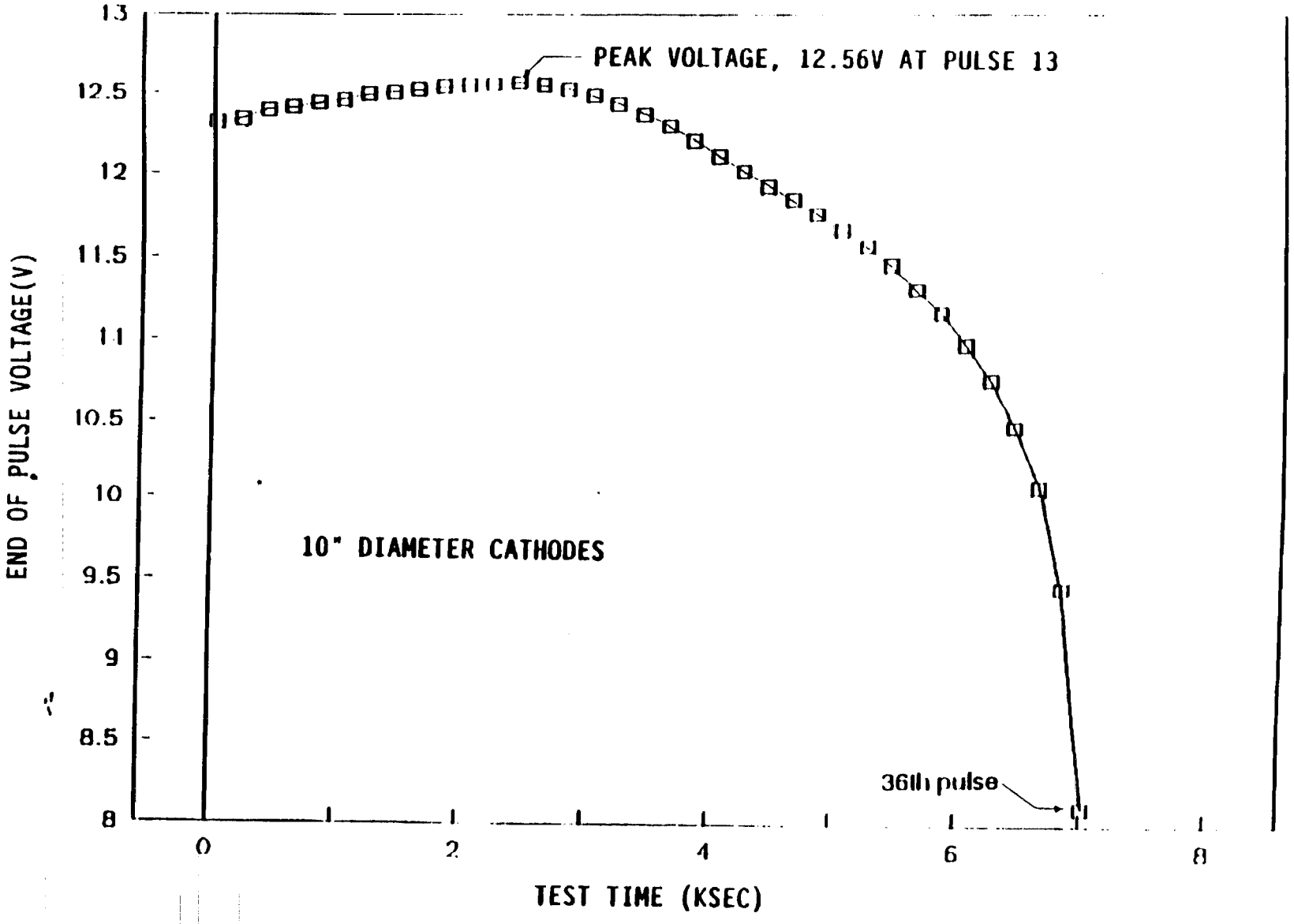

FIG. 12. EOPV FOR 4-CELL STACK DURING CONSTANT POWER (286W) CONTINUOUS PULSE DISCHARGE

Yardney TECHNICAL PRODUCTS INC

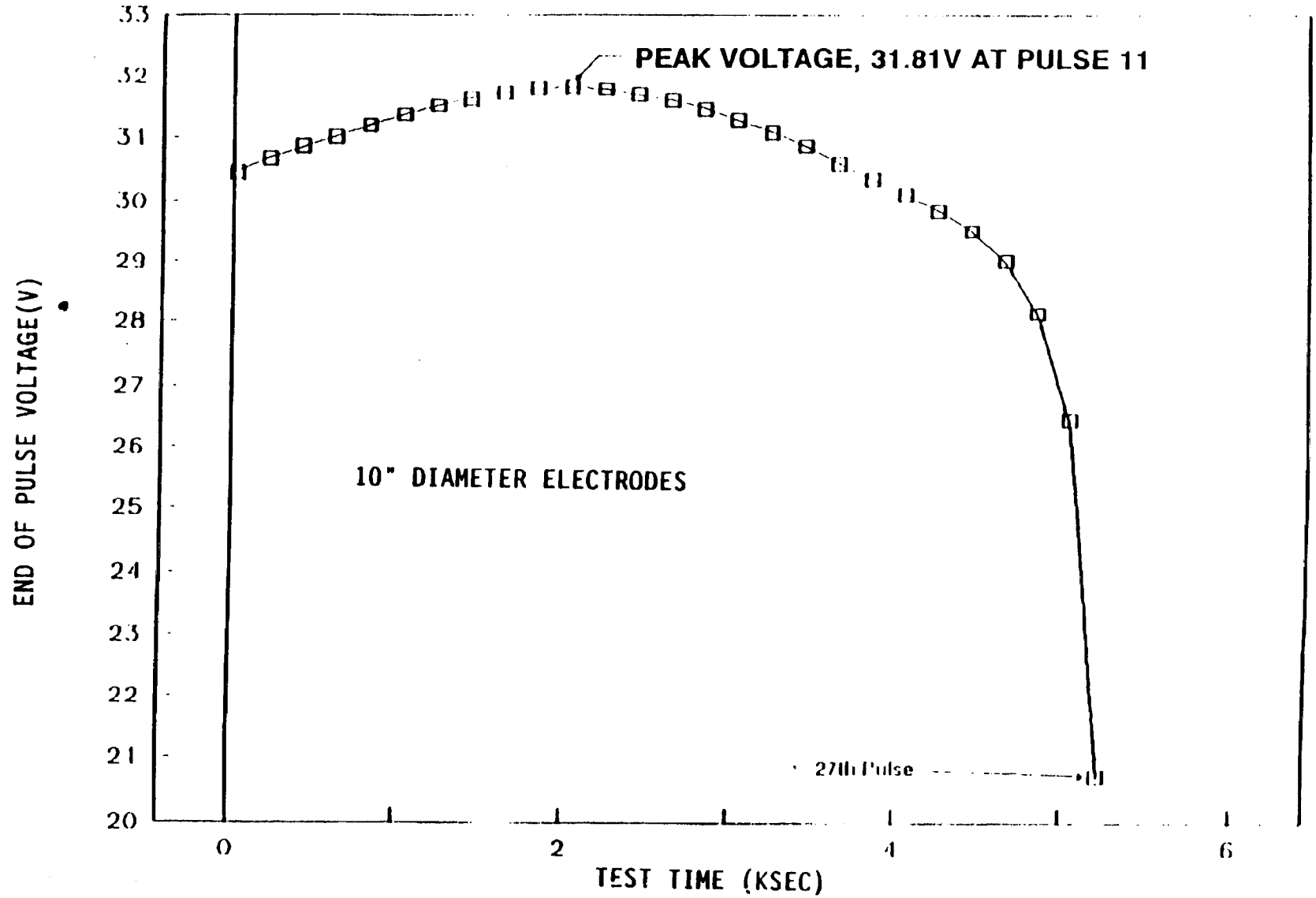

FIG. 13 EOPV FOR FIRST 10-CELL STACK DURING CONSTANT POWER (714W) CONTINUOUS PULSE DISCHARGE

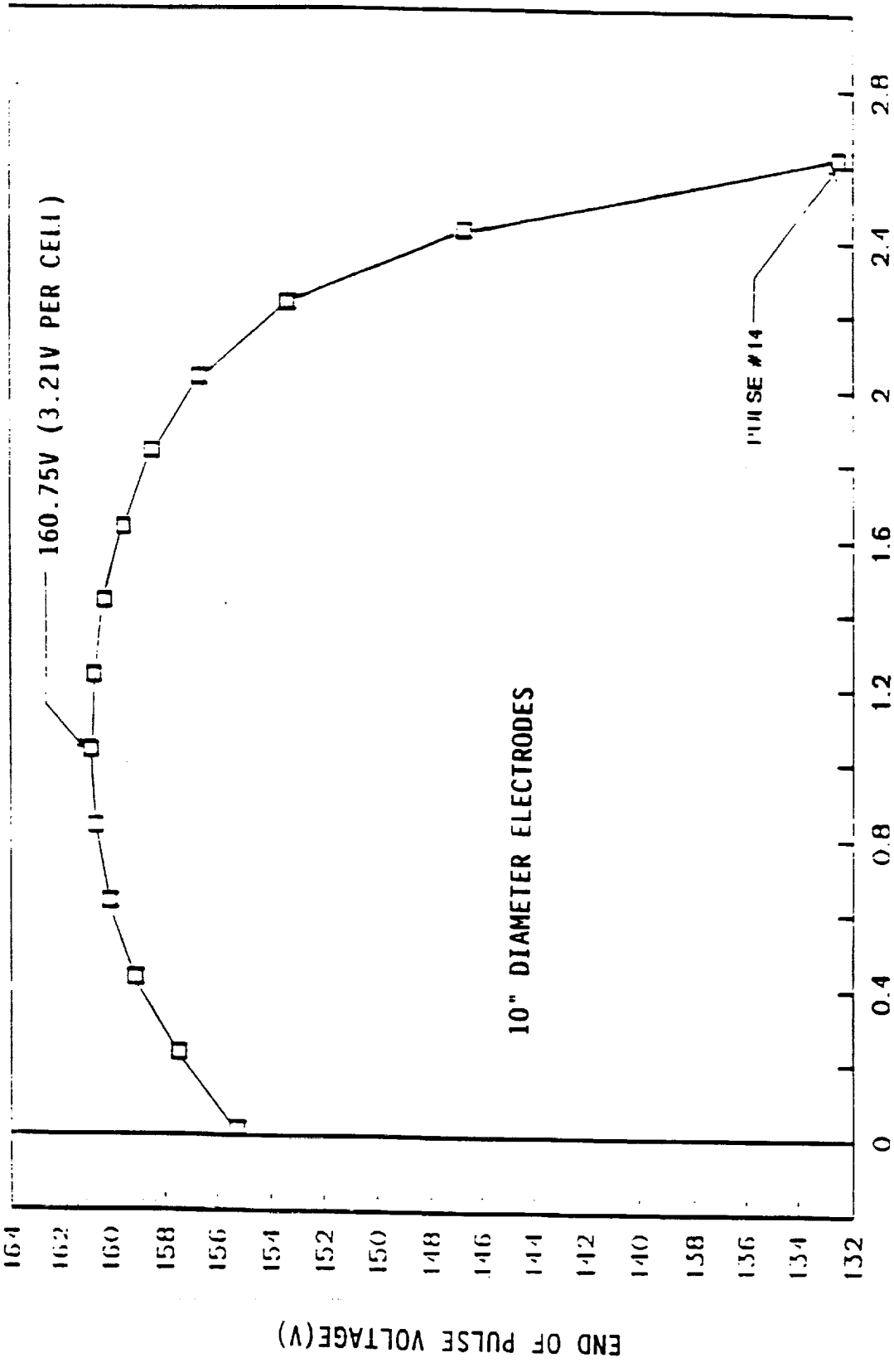

FIG. 14. EOPV FOR FIRST 50-CELL STACK DURING CONSTANT POWER (3570W) PULSE DISCHARGE

Yardney TECHNICAL PRODUCTS INC

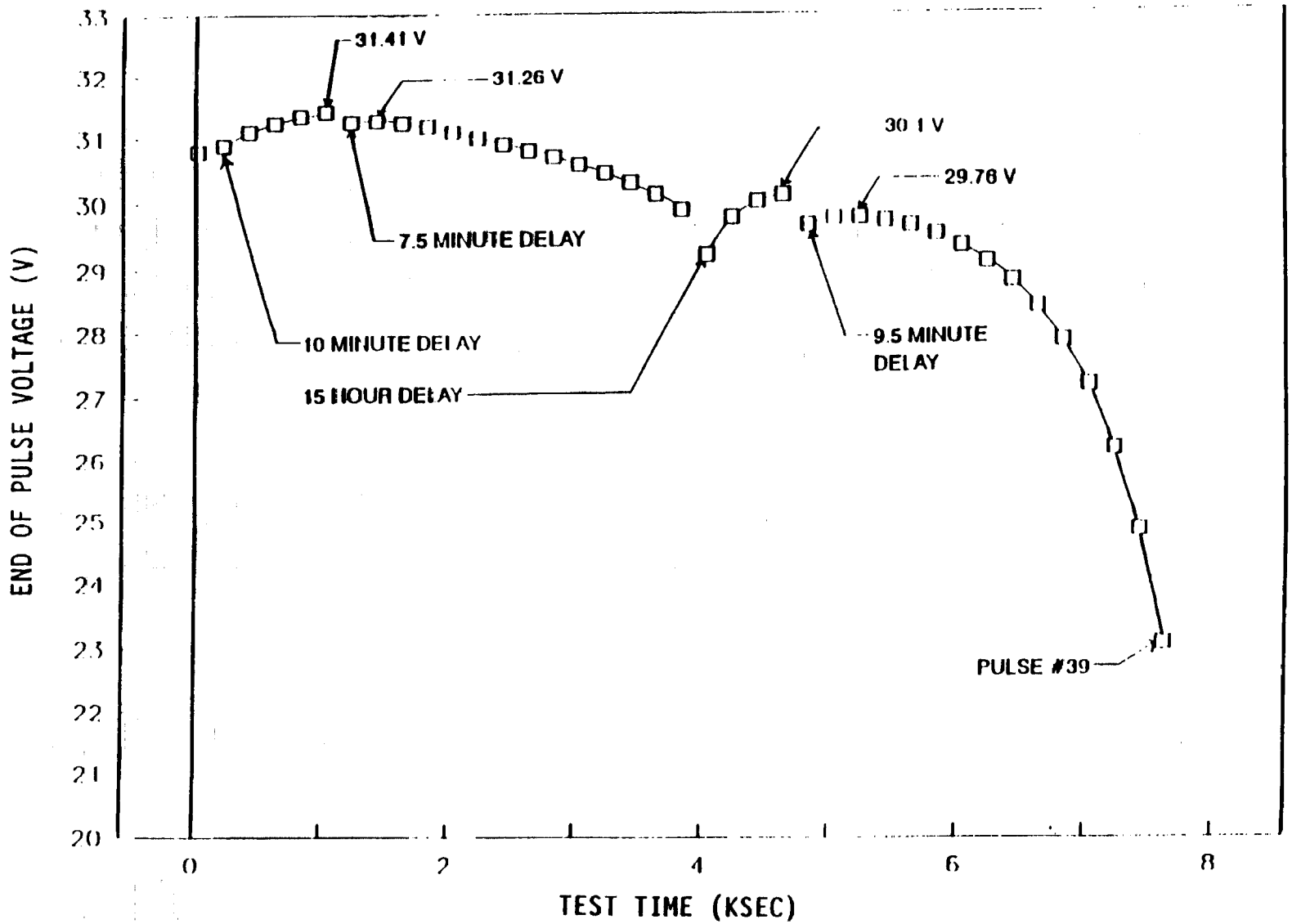

FIG. 15. EOPV FOR THIRD 10-CELL STACK DURING CONSTANT POWER (714W) PULSE DISCHARGE TEST. TEST DELAYS WERE DUE TO AN INSTRUMENTATION/ SOFTWARE PROBLEM

Yardney TECHNICAL PRODUCTS INC

Program Tasks and Accomplishments (continued)

- Conducted first 10.7kW constant power Sonobuoy pulse discharge test, Fig. 16

- Reducing TFE content improved cathode performance. Ten-cell stacks containing high and low TFE cathodes, respectively, were assembled for comparison during a polarization pulse test with current densities in the range of 0.1 to 100 mA/cm^2, Fig. 17

Yardney TECHNICAL PRODUCTS INC

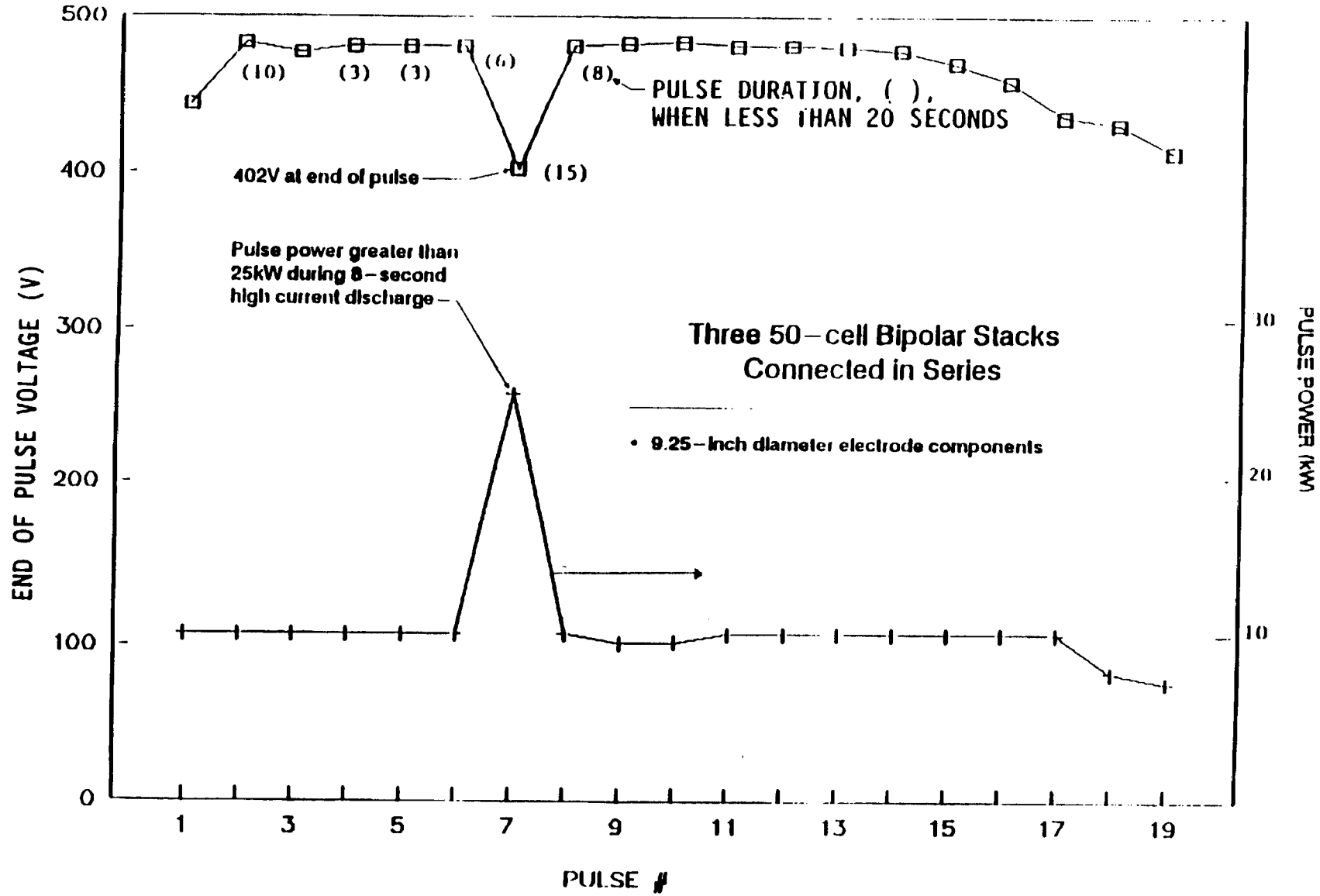

FIG. 16. EOPV FOR FIRST 150-CELL BIPOLAR CONFIGURATION OF THREE 50-CELL STACKS CONNECTED IN SERIES DURING CONSTANT POWER (10.7kW) PULSE DISCHARGE TEST

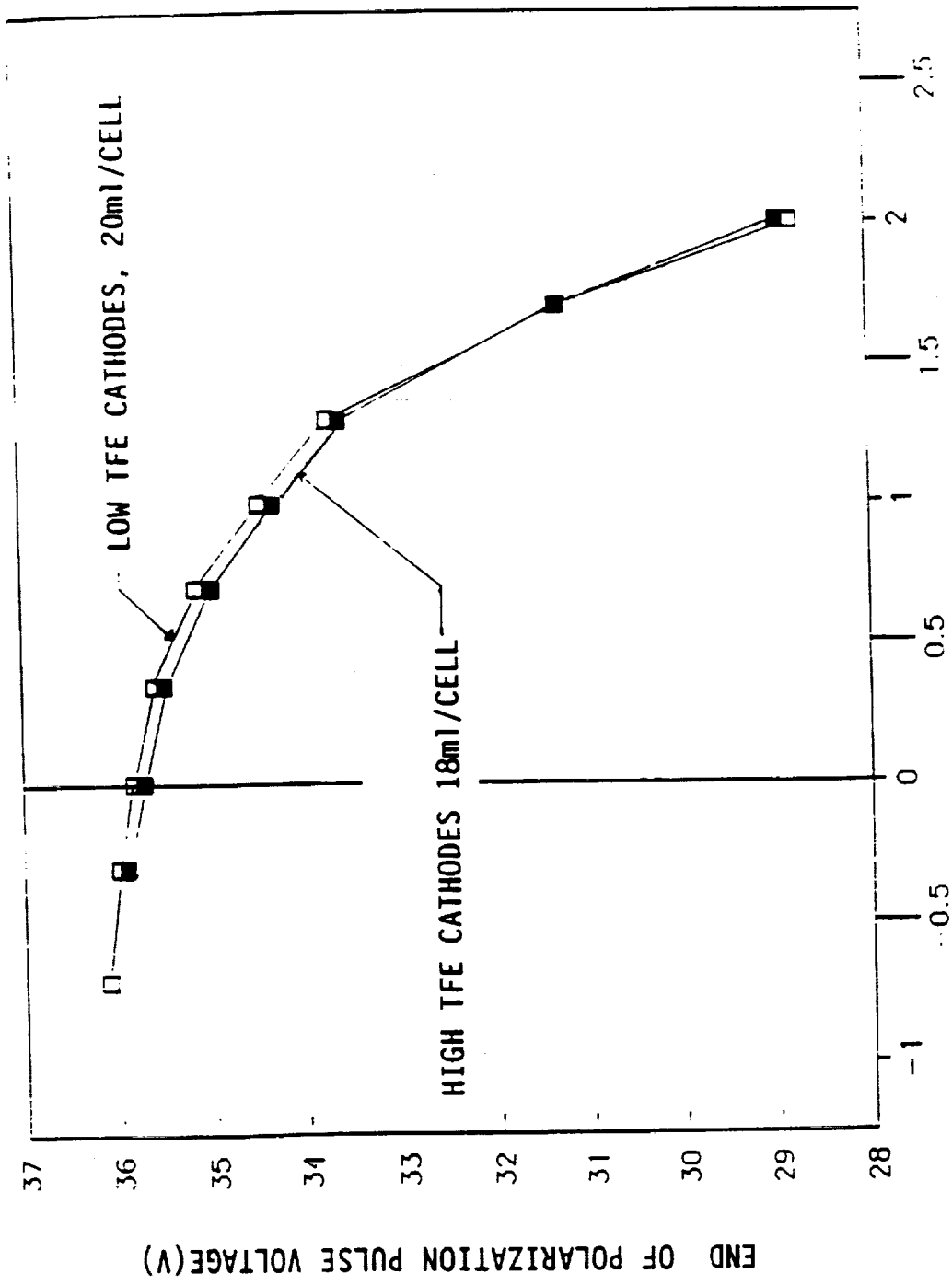

FIG. 17. END OF POLARIZATION PULSE VOLTAGE FOR HIGH AND LOW TFE CATHODES

Yardney TECHNICAL PRODUCTS INC

Yardney TECHNICAL PRODUCTS INC

Program Tasks and Accomplishments (continued)

- Polarization profiles for high and low TFE cathode 10-cell stacks at a pulse current density of 50 mA/cm^2, Figs. 18 and 19

- High and low TFE cathodes were compared during constant power Sonobuoy pulse discharge tests, Fig. 20

- Comparison of polarization pulse test results for the second and third 150-cell 10.7kW bipolar modules, Fig. 21

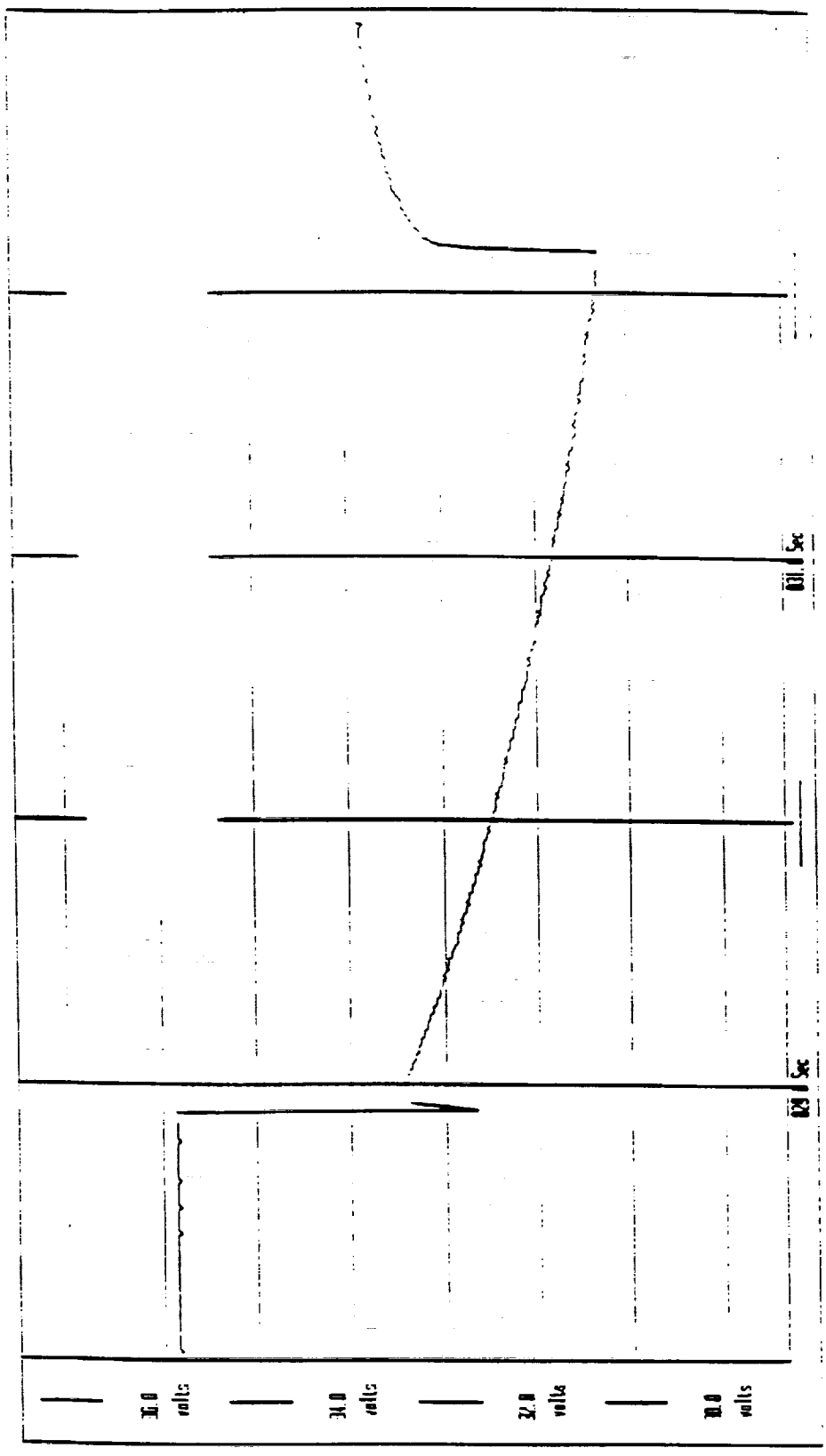

FIG. 18. VOLTAGE PROFILE FOR HIGH TFE CATHODES IN A 10-CELL STACK DURING THE THREE SECOND 20A POLARIZATION CURRENT PULSE.

Yardney TECHNICAL PRODUCTS INC

Yardney TECHNICAL PRODUCTS INC

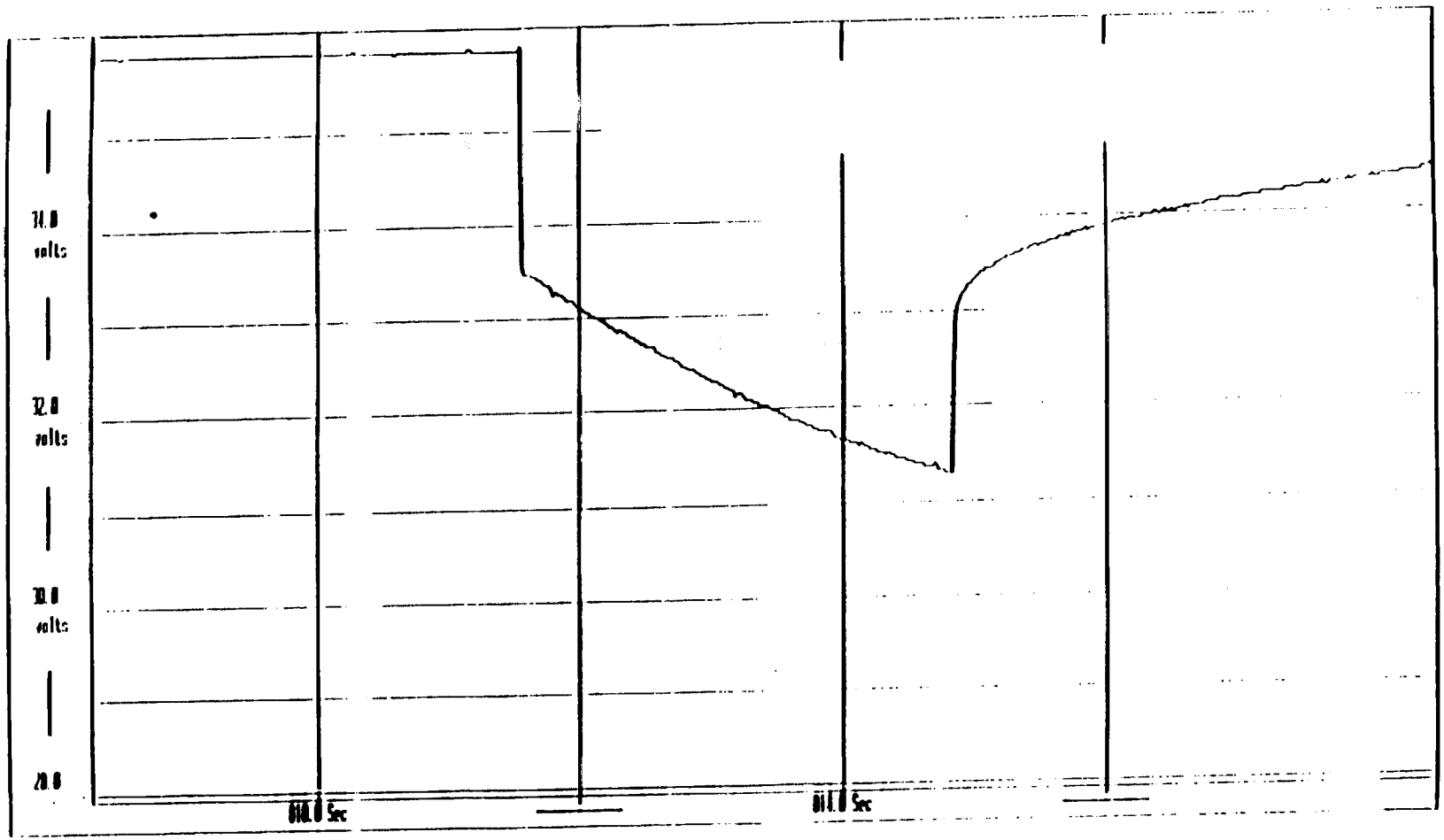

FIG. 19. VOLTAGE PROFILE FOR LOW TFE CATHODES IN THE THIRD 10-CELL STACK DURING THE THREE SECOND 20A POLARIZATION CURRENT PULSE

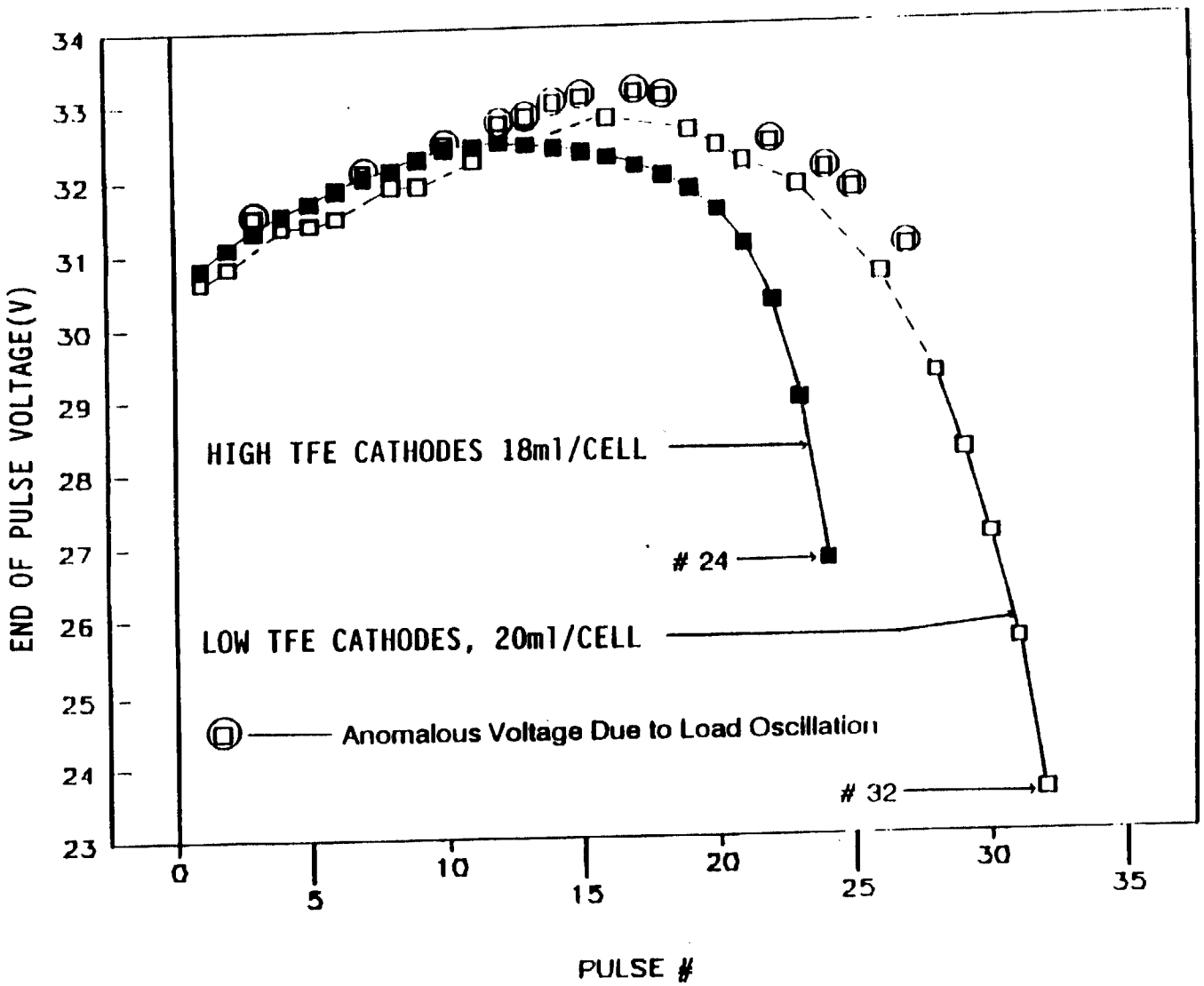

FIG. 20. COMPARISON OF HIGH AND LOW TFE CATHODES DURING 10-CELL STACK PERFORMANCE TESTS.

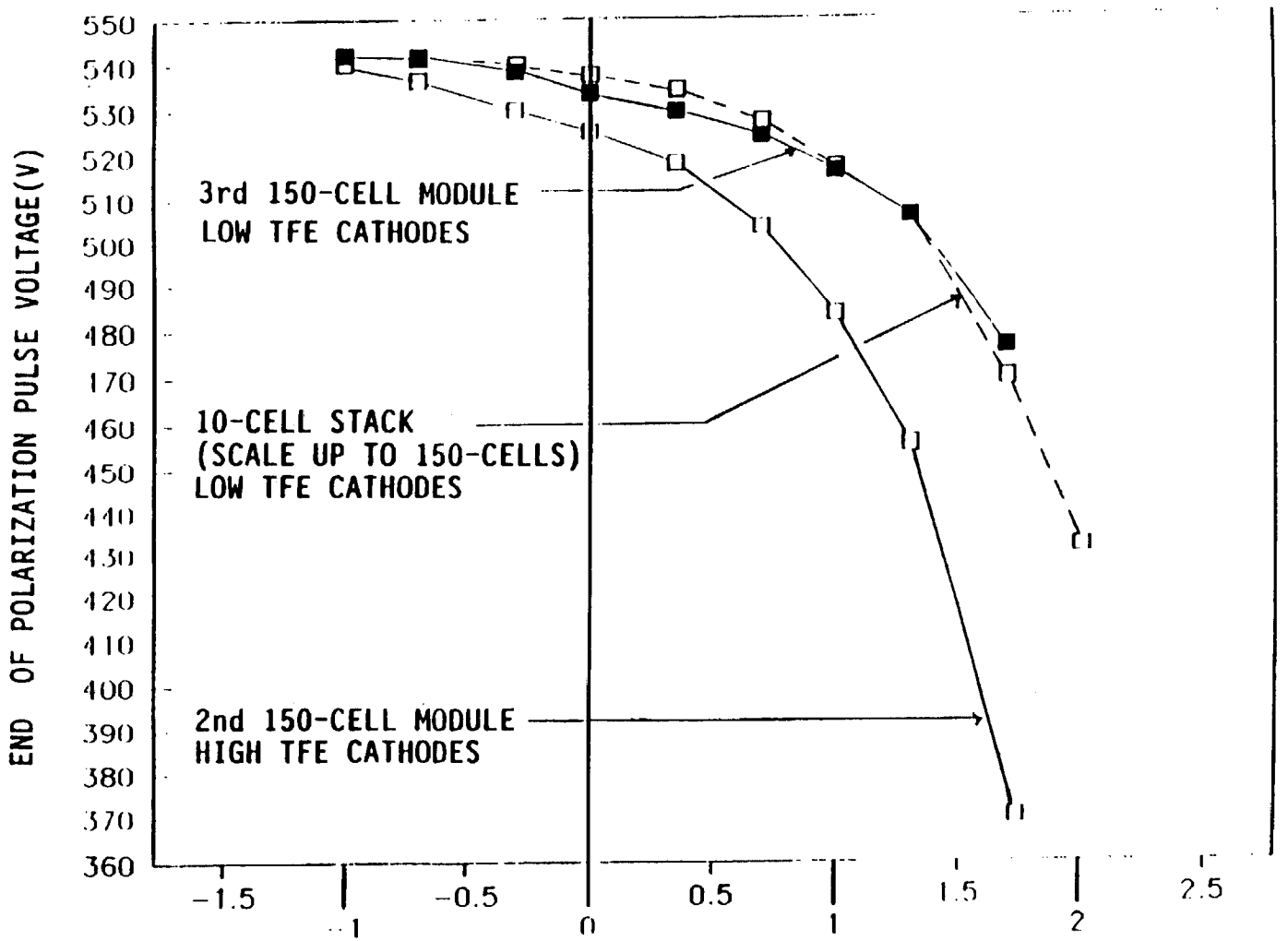

FIG. 21. COMPARISON OF POLARIZATION CURVES FOR 2ND AND 3RD 150-CELL MODULES WITH THE THIRD 10-CELL STACK

Yardney TECHNICAL PRODUCTS INC

Program Tasks and Accomplishments (continued)

- Polarization profile for third 150-cell 10.7kW bipolar module at a pulse current density of 50 mA/cm^2, Fig. 22

- Third 150-cell 10.7kW bipolar module constant power Sonobuoy pulse discharge test, Fig. 23

Yardney
TECHNICAL PRODUCTS INC

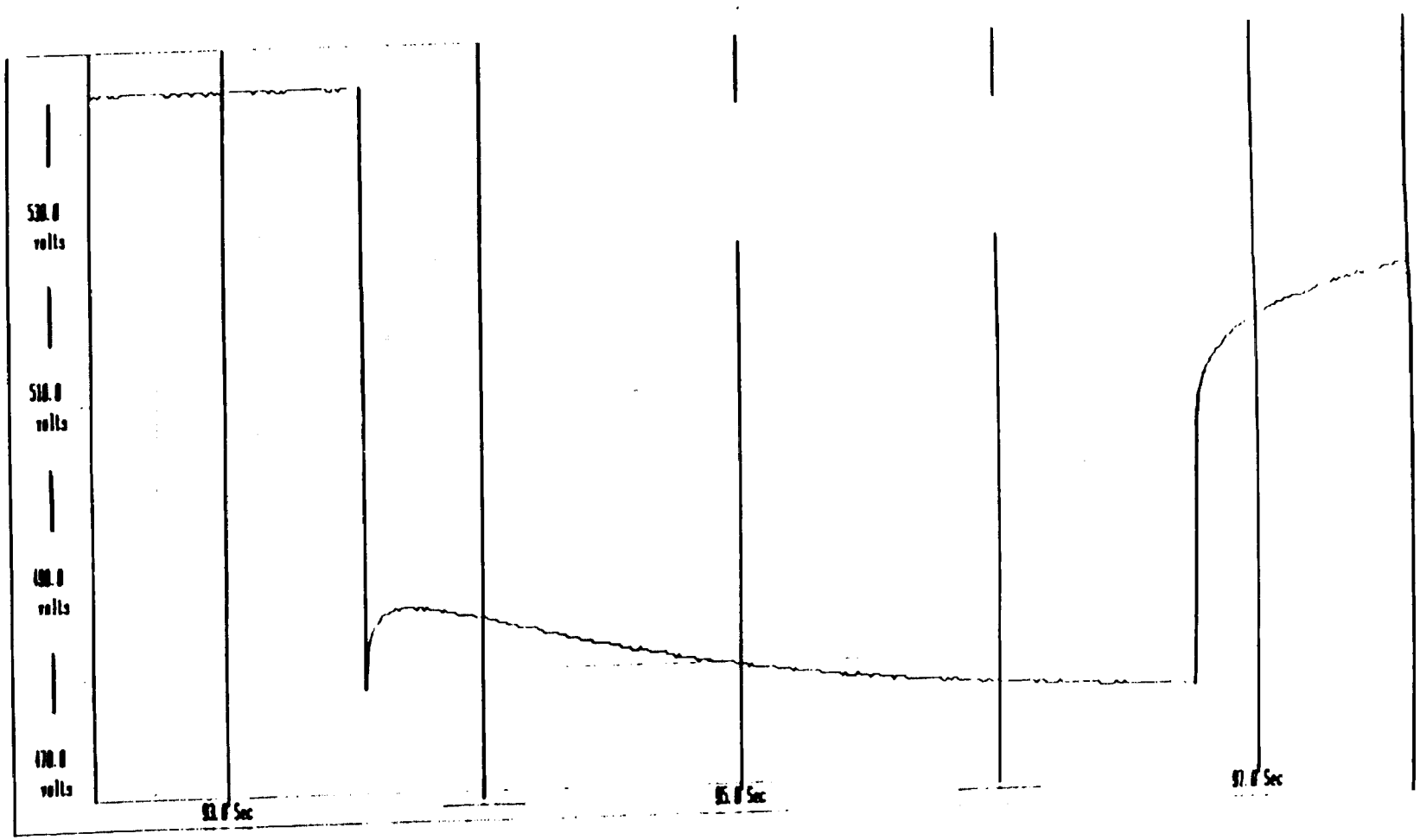

FIG. 22. VOLTAGE PROFILE FOR LOW TFE CATHODES IN 3RD 150-CELL MODULE

Yardney TECHNICAL PRODUCTS INC

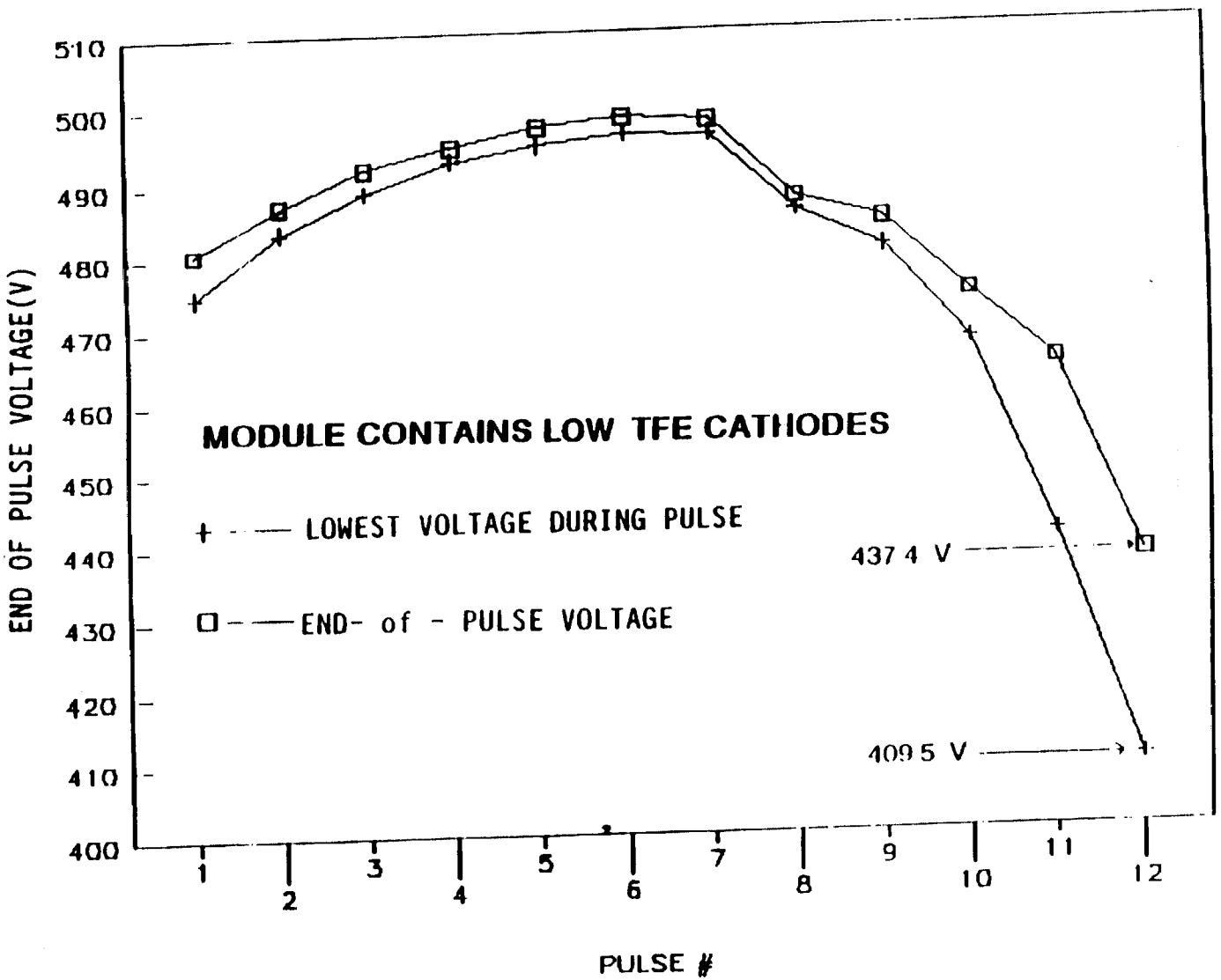

FIG. 23 THE LOWEST VOLTAGE AND EOPV FOR EACH PULSE OF THE THIRD 150-CELL MODULE DURING THE 10.7kW CONSTANT POWER PULSE TEST

Yardney TECHNICAL PRODUCTS INC

PROGRAM SUMMARY

- Developed manufacturing capability for producing large quantities of uniform cathodes and bipolar plates
- Developed assembly, sealing, and activation procedures for fabrication of battery modules containing up to 150 cells in bipolar configuration
- Successful demonstration of a 10.7kW 150-cell module: constant power pulse discharge; 20 second pulse, 10% duty cycle

Yardney TECHNICAL PRODUCTS INC

RECOMMENDATIONS

- Modify capture mold to improve integrity of the bipolar plate at the periphery of the Tefzel insulation
- Improve stack sealing method using "modified" bipolar plates
- Demonstrate improved sealing method and electrolyte activation under full stack compression with large module test

Yardney
TECHNICAL PRODUCTS INC

ACKNOWLEDGEMENTS

Yardney would like to thank the NAVSWC group and ONR for their support of this work, which was performed under Contract N60921-91-C-0124

Project Manager Patricia H. Smith

Contributors
Glenn D. Zoski
Charles W. Fleischmann
Stanley D. James
Timothy C. Murphy
Patrick J. Kelly

ELA NASA BATTERY WORKSHOP PRESENTATION

November 18, 1993

Johnson Controls Battery Group, Incorporated

Douglas C. Pierce

Dr. William O. Gentry

Marshall Space and Flight Center

David Hall

JOHNSON CONTROLS, INCORPORATED

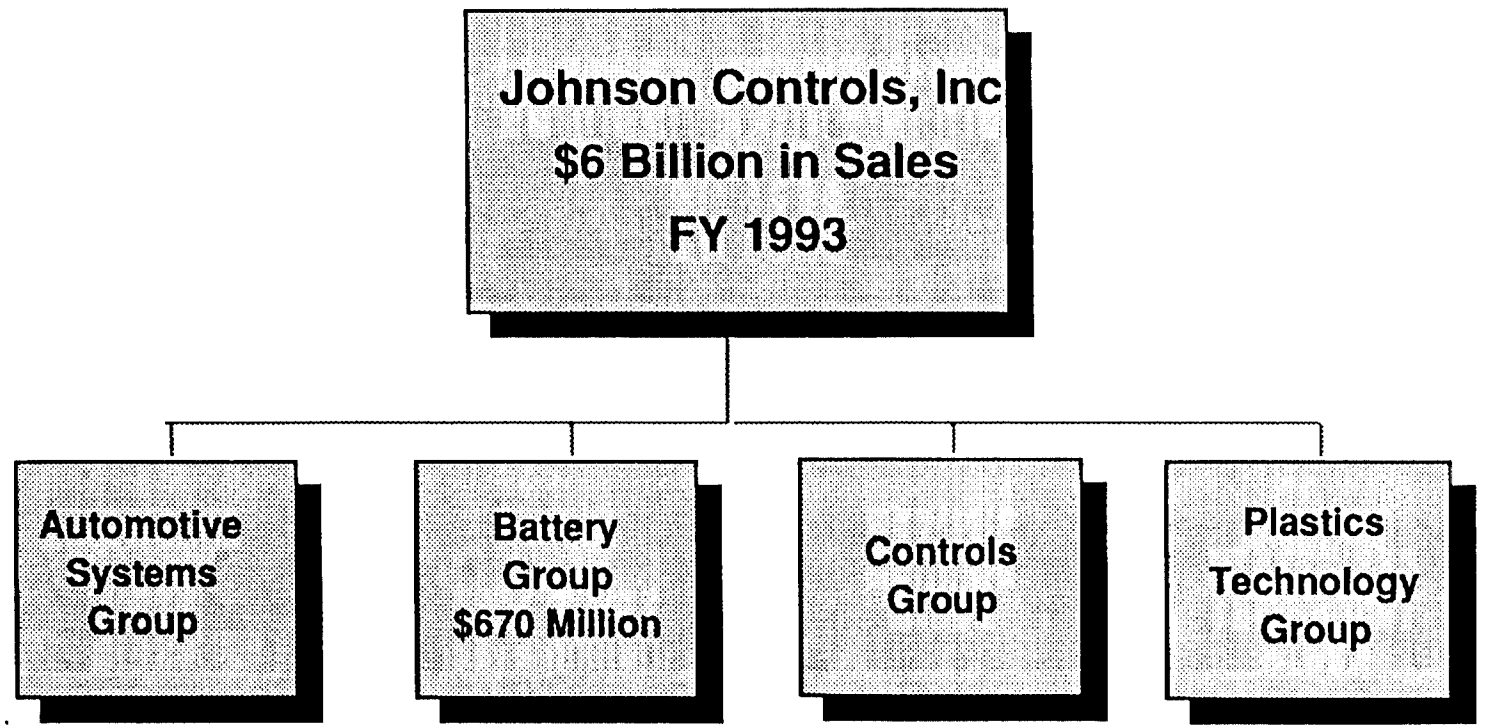

ORGANIZATION STRUCTURE

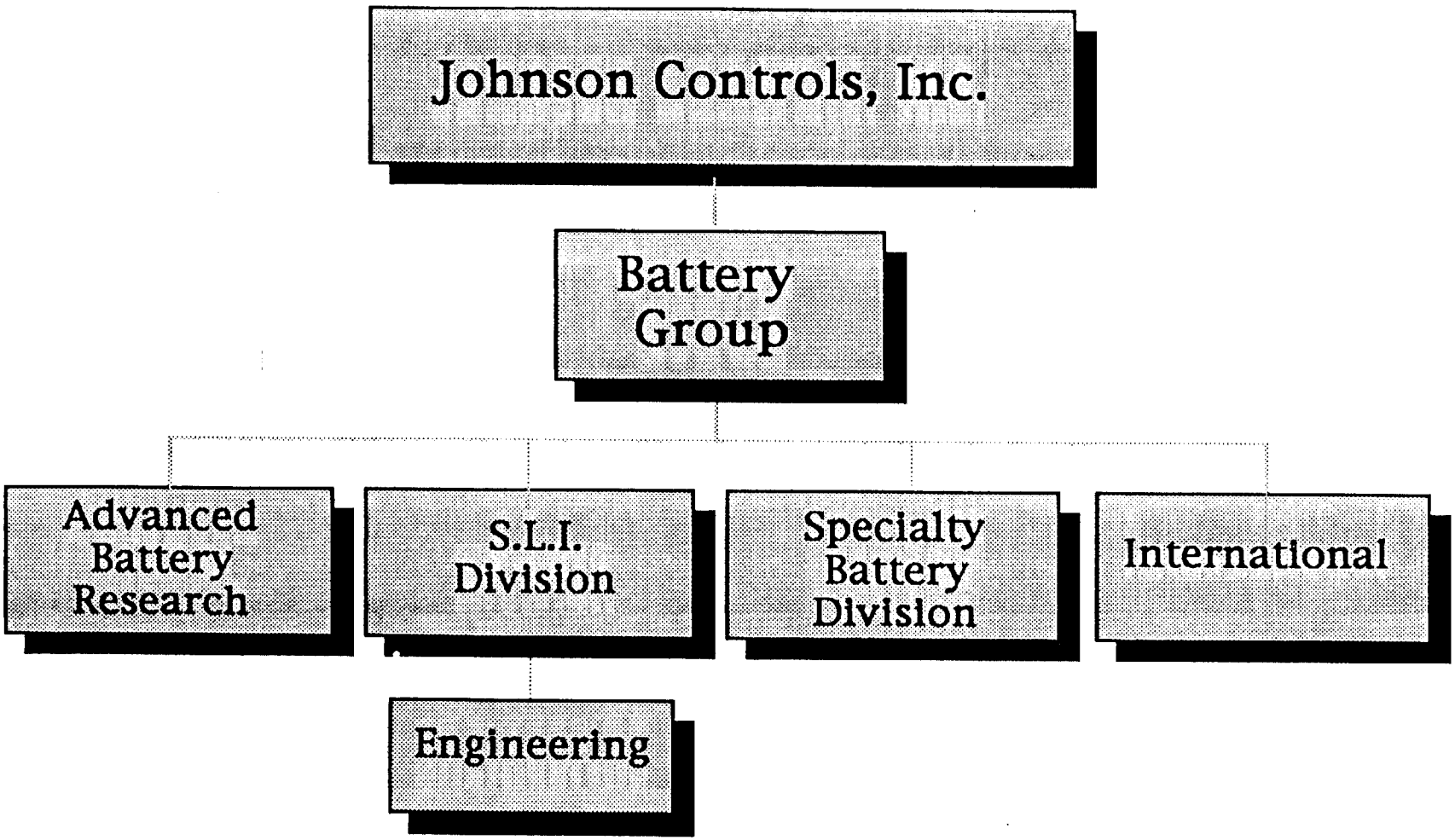

TRUE BIPOLAR BATTERY DEVELOPMENT WPAFB CONTRACT

- GOALS:

  Develop a Composite Bipolar Substrate Material with the Following Characteristics:

Resistivity:	< 2Ω -cm
Thickness:	< 0.064 cm
Weight:	< 150 mg/cm
Area:	> 400 cm2

  The 270 Volt Battery will be Designed to be used in the More Electric Aircraft Program

JOHNSON CONTROLS

TRUE BIPOLAR BATTERY DEVELOPMENT WPAFB CONTRACT

- VALUE:

Contract Total	1,013.4M
Spending To Date	636.4M
Funding For FY'94	377.0M

10% Cost Share to JCBGI

JOHNSON CONTROLS

TRUE BIPOLAR BATTERY DEVELOPMENT WPAFB CONTRACT

- APPROACHES:

  Compound Stable Conductive Filler(s) into Plastic or Thermosets to Produce Non-Porous Highly Conductive, Lightweight Substrate Material

  Use Compounding Additives Which Enhance Conductivity, and Manufacturability While Eliminating Porosity

JOHNSON CONTROLS

TRUE BIPOLAR BATTERY DEVELOPMENT WPAFB CONTRACT

- PROGRESS:

  Conductive Filler Stability Proven

  Conductive Filler Supplier Qualified

  Composition of Substrate Identified

  Project Substrate Thickness of 0.010-0.015"

  Numerous Batteries Tested To Date

JOHNSON CONTROLS

TRUE BIPOLAR BATTERY DEVELOPMENT WPAFB CONTRACT

- NEXT STEPS:

  Improved Containment Design Trial

  Improve Present Manufacturing Techniques - Mass Production

  Produce Lighter, Thinner, More Conductive Substrate

  Test for SLI, EV Applications

JOHNSON CONTROLS

JCBGI LABBM
300 Volt Bipolar Battery System
ELA Program

Battery Parameter	Design Specs	WPAFB Goals
Substrate Thickness	0.015"	0.025"
Substrate Resistivity	2Ω -cm	2Ω -cm
Substrate Weight/Area	150 mg/cm2	150 mg/cm2
Substrate Area	1200 cm2	400 cm2

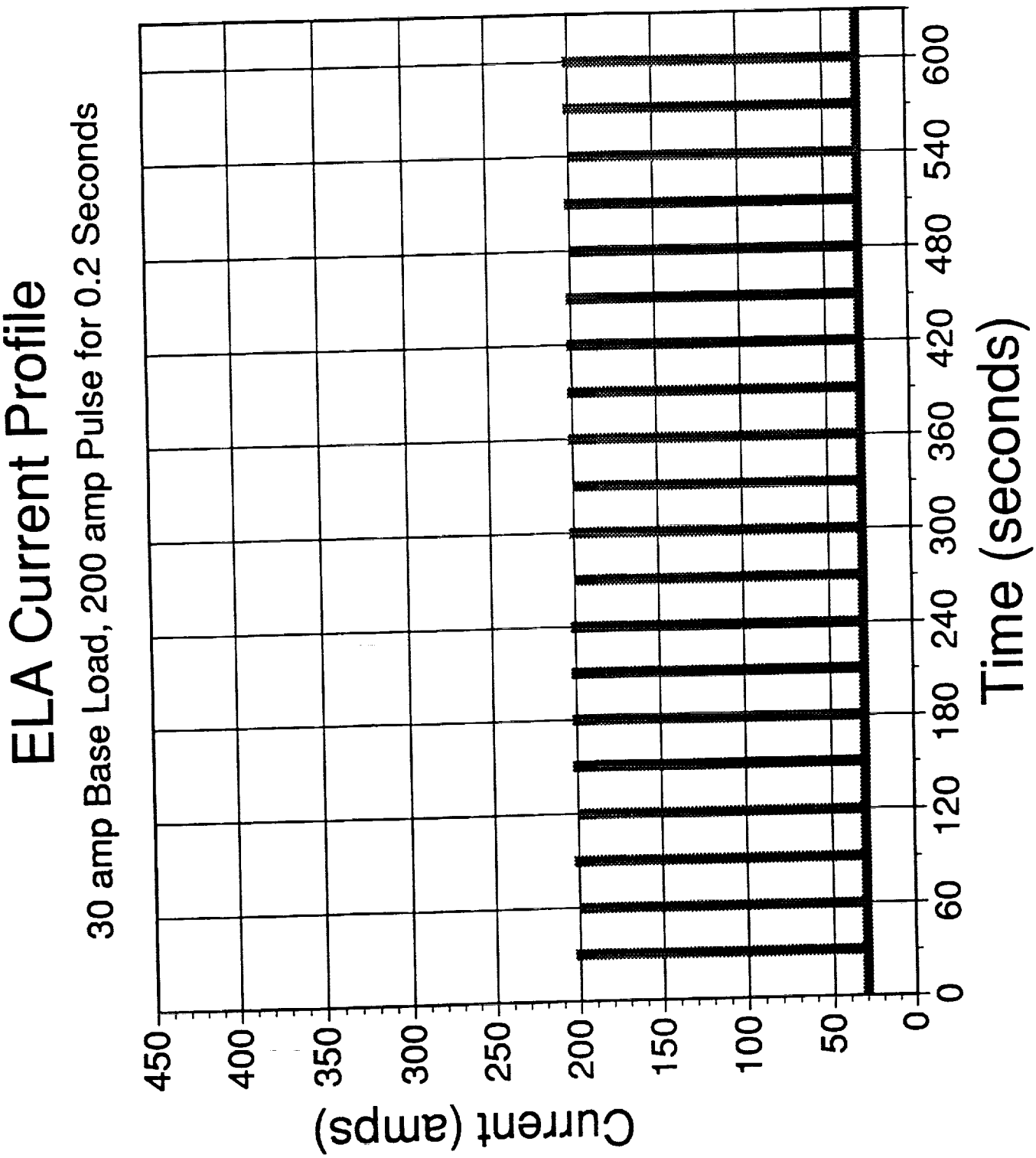
ELA Current Profile
30 amp Base Load, 200 amp Pulse for 0.2 Seconds
Current (amps)
450
400
350
300
250
200
150
100
50
0
Time (seconds)
0
60
120
180
240
300
360
420
480
540
600

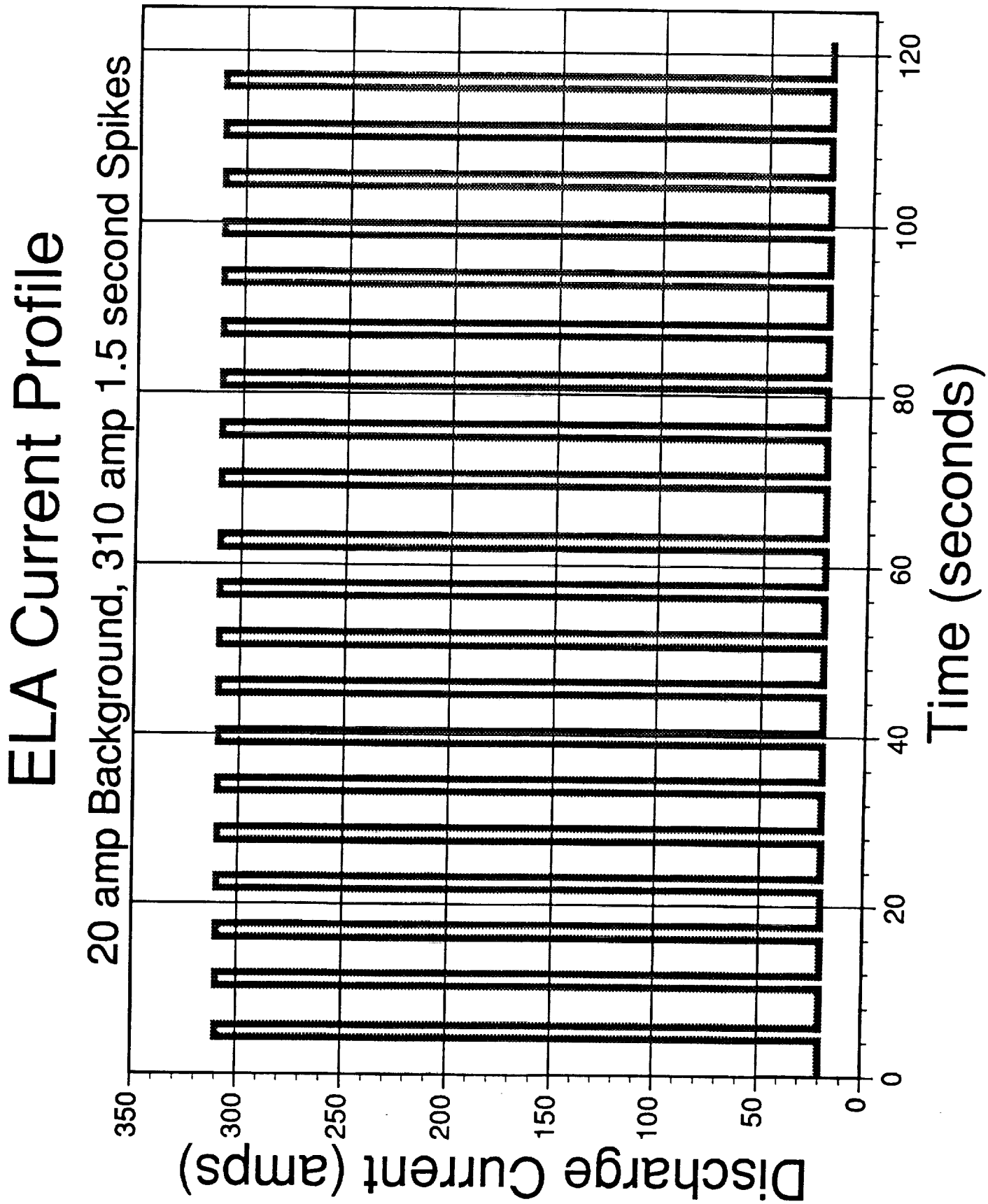
ELA Current Profile
20 amp Background, 310 amp 1.5 second Spikes
Discharge Current (amps)
350
300
250
200
150
100
50
0
Time (seconds)
0
20
40
60
80
100
120

JOHNSON CONTROLS

JCBGI LABBM
300 Volt Bipolar Battery System
ELA Program

Battery System 1 Parameters

Battery Size	15" x 15" x 9"
Weight	228 pounds
Number of Cells	140
OCV	300 Volts
Cell Thickness	0.063"

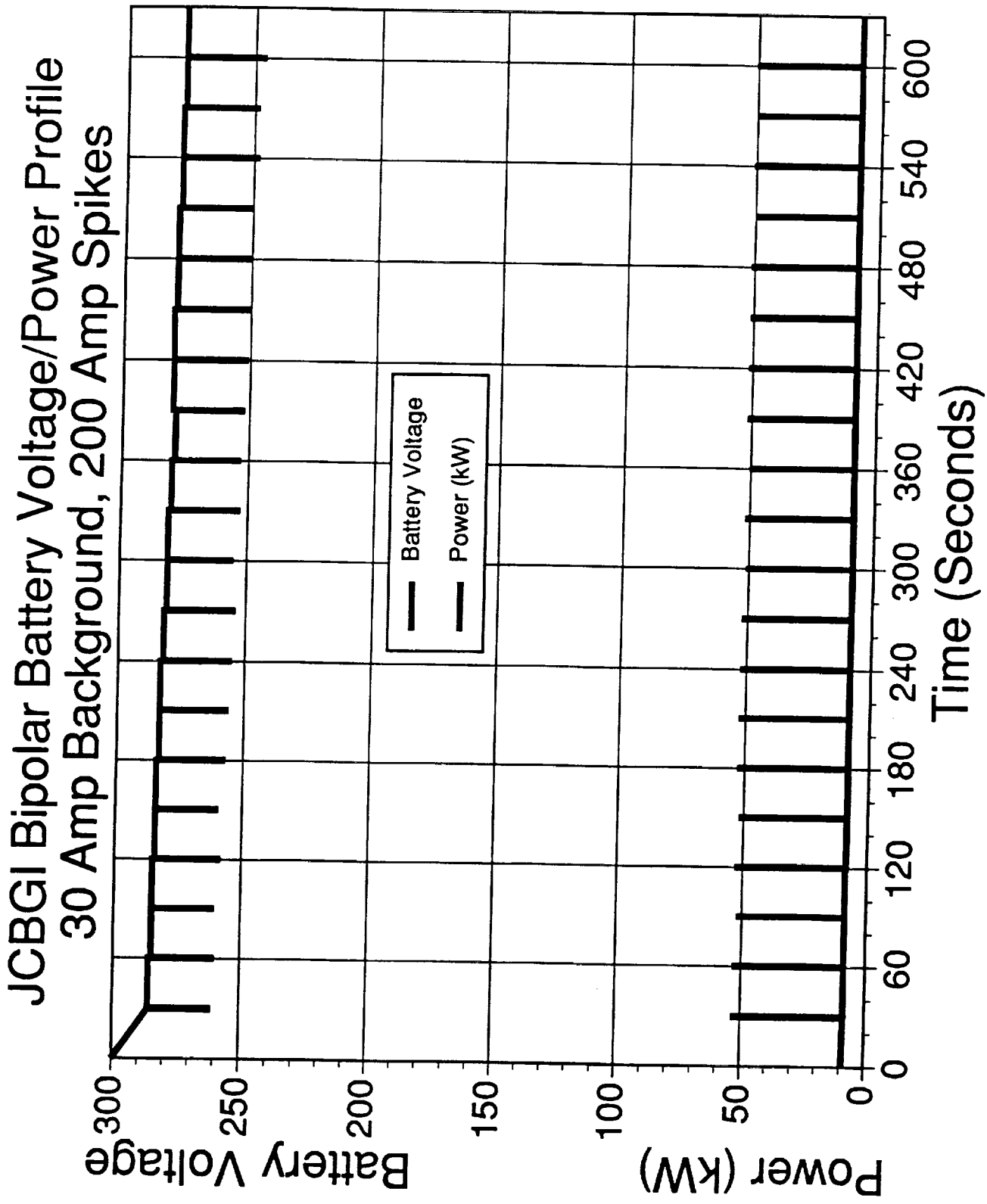
JCBGI Bipolar Battery Voltage/Power Profile
30 Amp Background, 200 Amp Spikes
Battery Voltage
Power (kW)
Time (Seconds)
Battery Voltage
Power (kW)
300
250
200
150
100
50
0
0
60
120
180
240
300
360
420
480
540
600

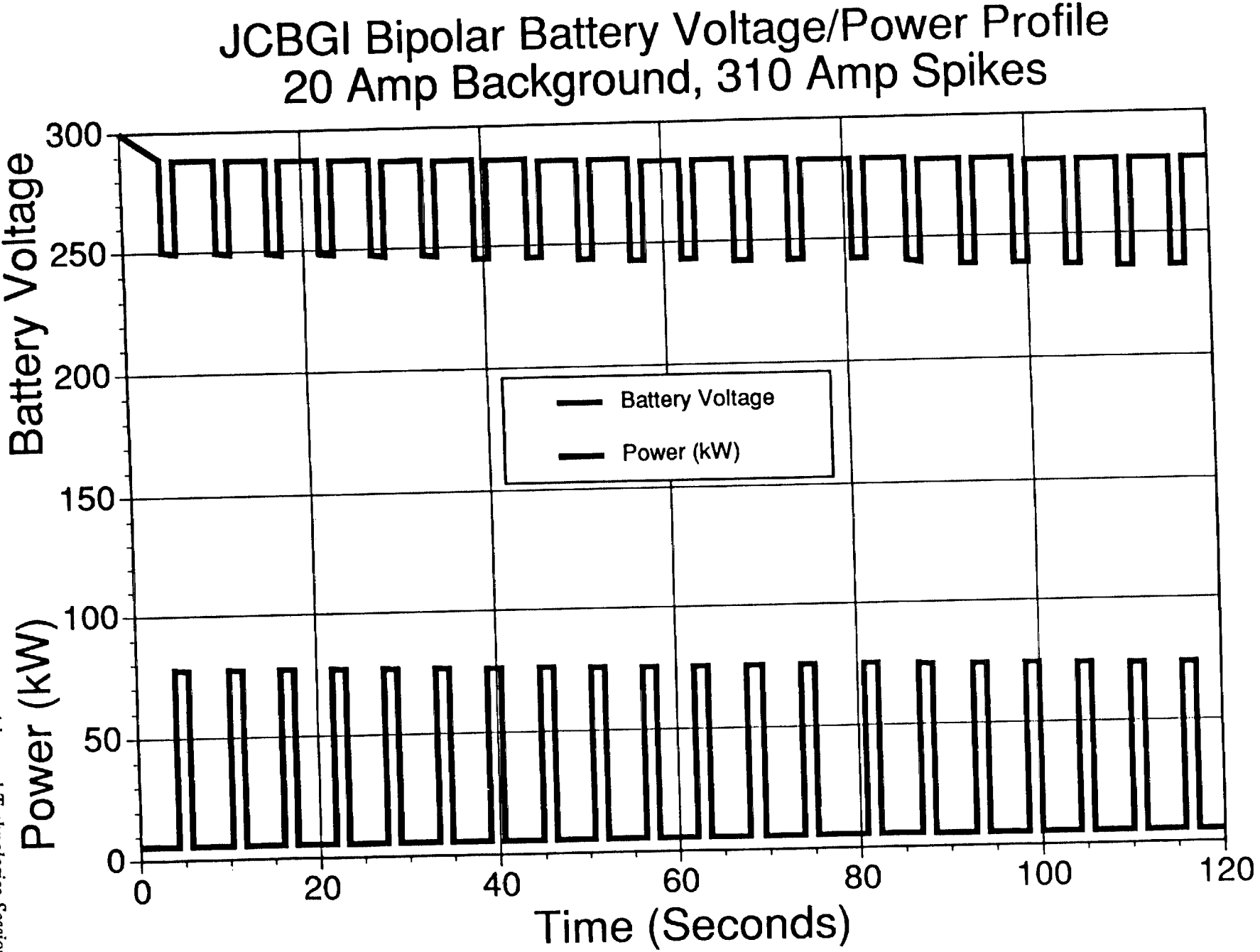
JCBGI Bipolar Battery Voltage/Power Profile
20 Amp Background, 310 Amp Spikes
Battery Voltage
Power (kW)
Time (Seconds)
300
250
200
150
100
50
0
0
20
40
60
80
100
120
Battery Voltage
Power (kW)

JCBGI Bipolar Lead/Acid 300 Volt Battery System 1 ELA Program

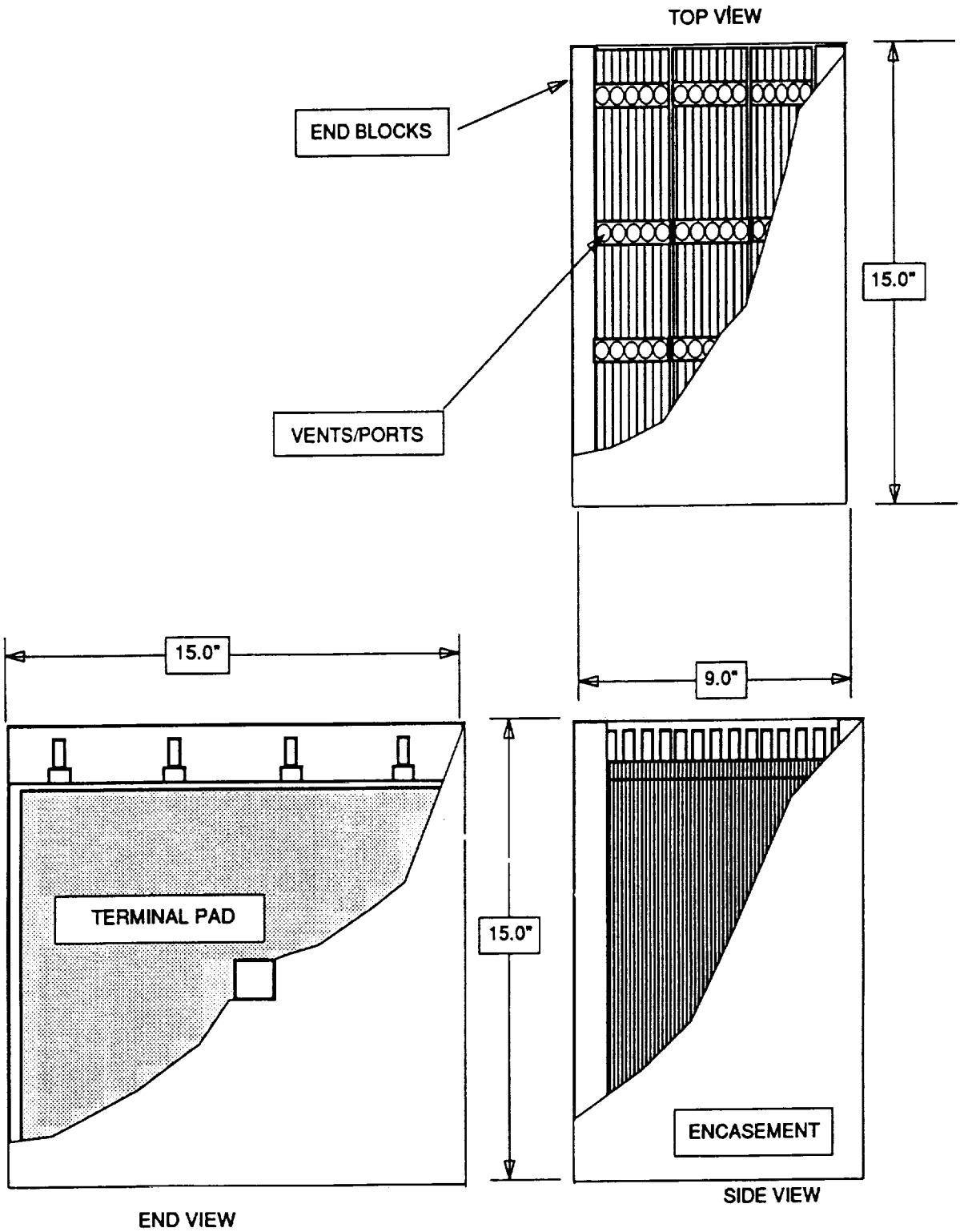

ELA Current Profile

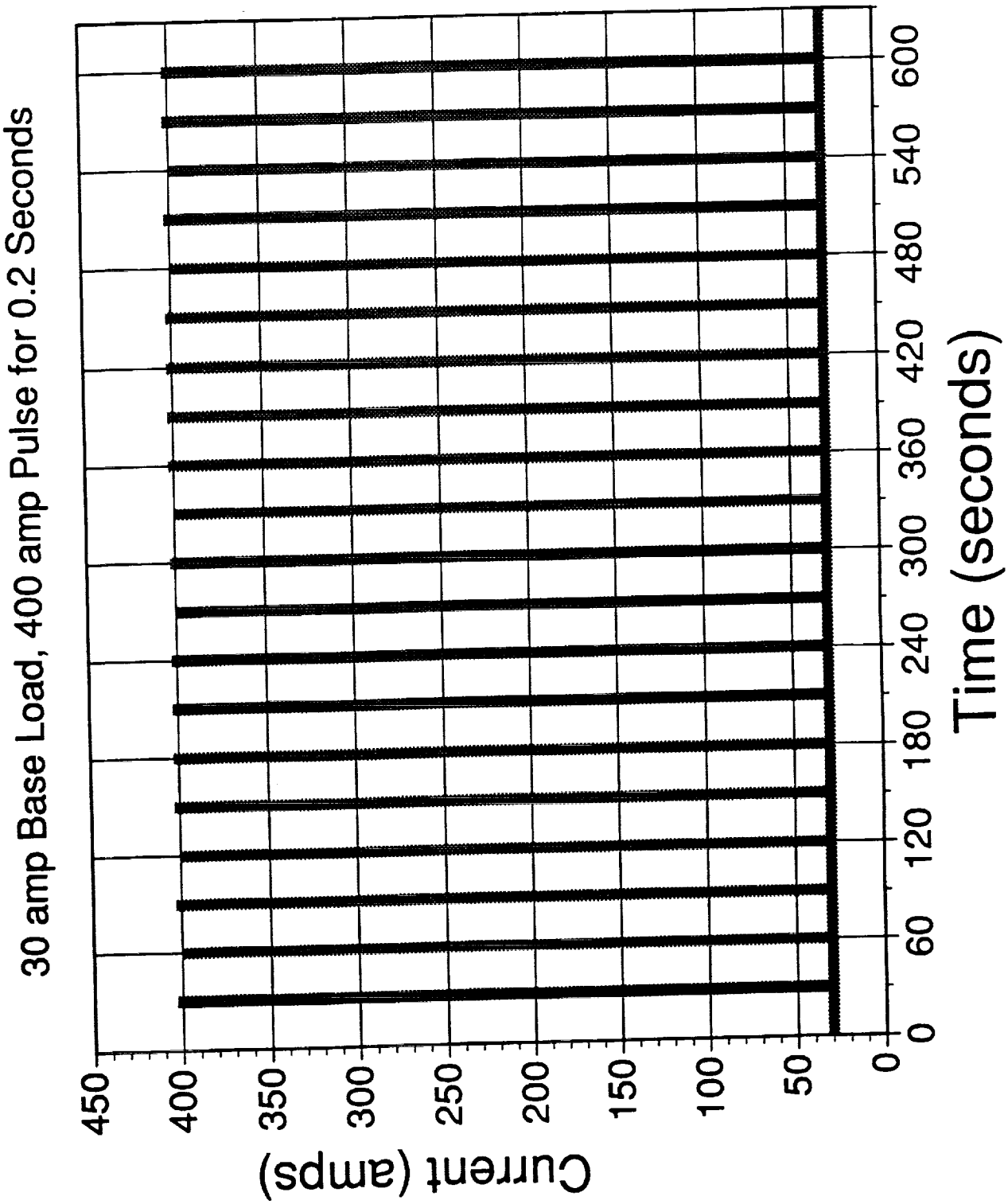

JCBGI LABBM
300 Volt Bipolar Battery System
ELA Program

Battery System 2 Parameters

Battery Size	16.8" x 16.8" x 8.7"
Weight	273 pounds
Number of Cells	140
OCV	300 Volts
Cell Thickness	0.061"

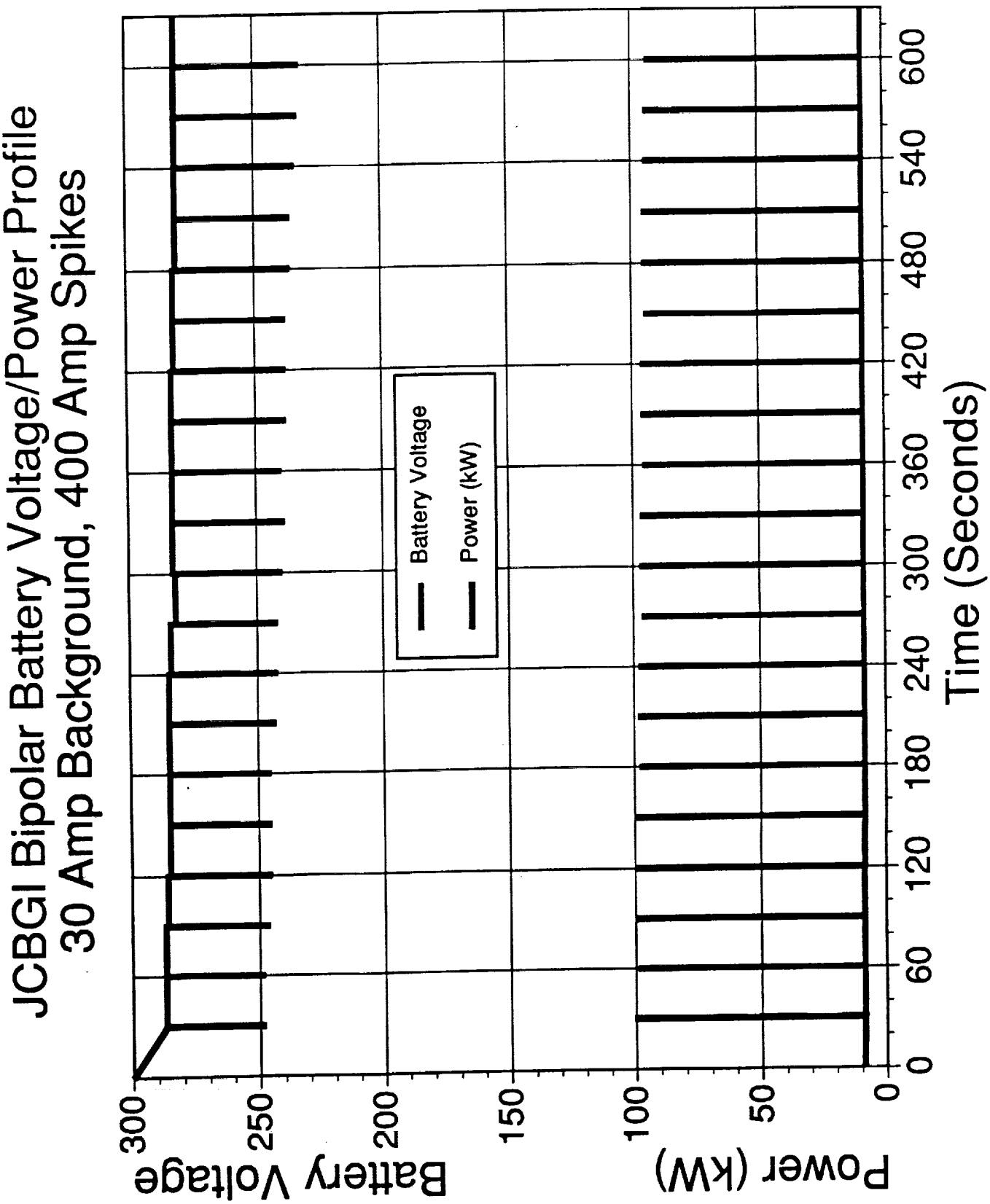
JCBGI Bipolar Battery Voltage/Power Profile
30 Amp Background, 400 Amp Spikes
Battery Voltage
Power (kW)
Time (Seconds)
Battery Voltage
Power (kW)
300
250
200
150
100
50
0
0
60
120
180
240
300
360
420
480
540
600

JCBGI Bipolar Lead/Acid 300 Volt Battery System 2 ELA Program

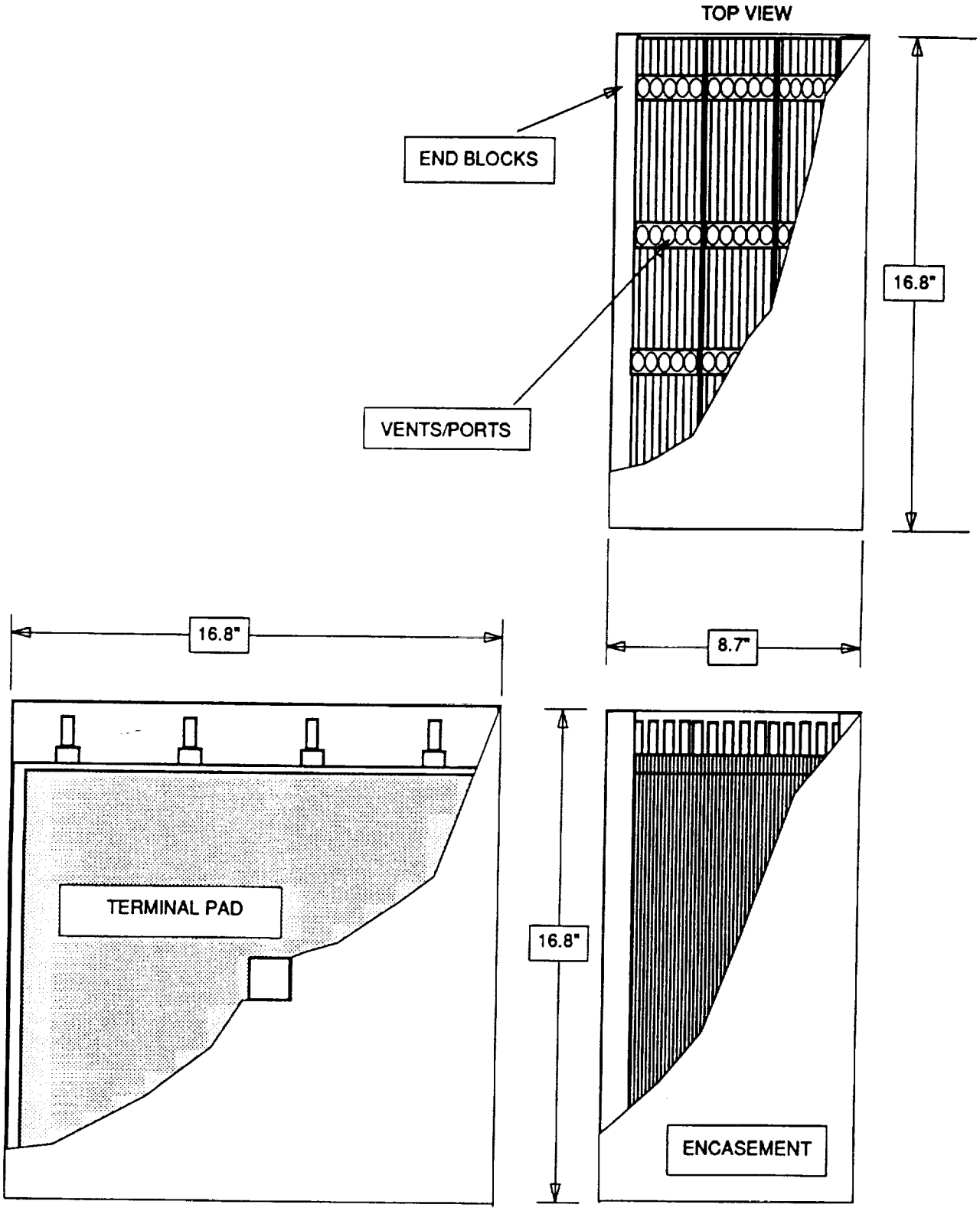

Bi-Polar AgZn Battery

The silver-zinc (AgZn) battery system has been unique in its ability to safely satisfy high power demand applications with low mass and volume. However, a new generation of defense, aerospace and commercial applications will impose even higher power demands. These new power demands can be satisfied by the development of a bi-polar battery design. In this configuration the power consuming, inter-electrode, current conductors are eliminated while the current is then conducted via the large cross-section, electrode substrate. Negative and positive active materials are applied to opposite sides of a solid silver foil substrate.

In addition to reducing the weight and volume required for a specified power level the output voltage performance is also improved as follows.

1.	Reduced Weight:	A.	Elimination of the plastic cell container
		B.	Elimination of plate leads and intercell connector
		C.	Elimination of internal plate current collector
2.	Increase Voltage:	A.	Eliminate resistance of current collector
		B.	Eliminate resistance of plate lead
		C.	Eliminate resistance of intercell connector

EPI worked previously (1974-75) on development of a secondary bipolar silver zinc battery. This development demonstrated the electrical capability of the system and manufacturing techniques. One difficulty with this development was mechanical problems with the seals. However, recent improvements in plastics and adhesives should eliminate the major problem of maintaining a seal around the periphery of the bipolar module. The seal problem is not as significant for a primary battery application or for a requirement for only a few discharge cycles. A second difficulty encountered was with activation (introducing electrolyte into the cell) and with venting gas from the cell without loss of electrolyte.

During previous work, the following projections for energy density were made from test data for a high power system which demonstrated in excess of 50 discharge/charge cycles.

Projected system power = 100 kilowatts
Discharge time = 30 seconds
Discharge current density = 1.75 amps/in^2
System Weight = 86 lbs (9.7 WH/lb)
System Volume = 1071 in^3 (.78 WH/in^3)

EPI is currently working on a development program to produce a bi-polar silver-zinc battery design for NASA. The potential application would be to power electromechanical actuators for space launch vehicles.

Prepared by: L. John Giltner, Project Engineer
Eagle-Picher Ind. Inc., P.O. Box 47
Joplin, MO. 64802 Telephone No. (417)623-8000

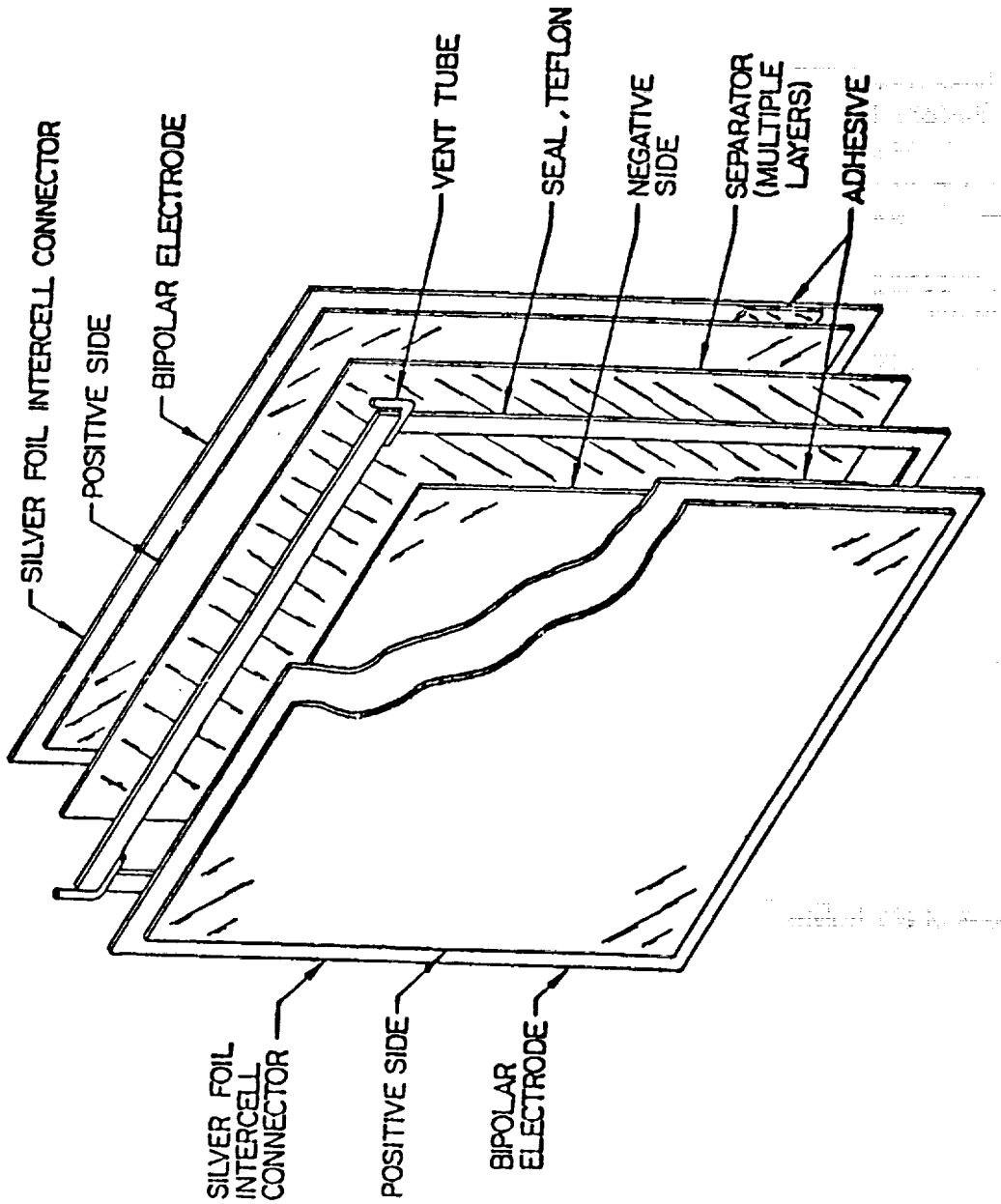

Bi-Polar Silver-Zinc Battery
Relationship of Components

BST SYSTEMS INC.

Advanced Silver Zinc Battery Development for the SRB and ET Range Safety Subsystems

- **Presented by: BST Systems, Plainfield, CT**
- **Presented for: 1993 NASA Aerospace Battery Workshop**
- **November 16-18, 1993**
- **US Space and Rocket Center, Huntsville, Al**

BST SYSTEMS INC.

This work was conducted in support of USBI Purchase Order 44420

BST SYSTEMS INC.

Introduction

- **Design and develop AgZn batteries for the SRB and ET Range Safety Subsystems**
  - AgZn new to the RSS battery--current chemistry is lithium
- **Various engineering techniques were used to meet difficult requirements**
  - » Composite separator systems
  - » New electrode processing techniques
  - » New restrainment techniques

BST SYSTEMS INC.

OFI and RSS Requirements

- **OFI Overall Requirements**
  - Capacity: 50 AH
  - Temperature: 30 F to 105 F
  - Wet Stand: 120 days
  - Weight: 45 lbs max
  - Relief Valve and Pressurizing capability
  - Thermistor circuit
  - Power and monitoring connector harnesses
    - » Monitoring circuit fused

BST SYSTEMS INC.

OFI and RSS Electrical Requirements

- **OFI BATTERY**
  - OCV 40 VDC max
  - Static Loads
    - » 26.00 VDC to 32.00 VDC within 200 ms of application of 0.16 A to 30 A loads
  - Transient Loads
    - » 10.00 VDC to 32.00 VDC during application of pulses up to 30.00 A followed by transition within 100 ms to static load levels

BST SYSTEMS INC.

OFI and RSS Requirements

- **RSS Overall Requirements**
  - Capacity: 14 AH
  - Temperature: 30 F to 118 F
  - Wet Stand: 120 days
  - Weight: 14 lbs max
  - Orientation insensitive--leakproof
  - Relief valve and Pressurizing capability
  - Thermistor circuit
  - Power and monitoring connector harnesses
    - » Monitoring circuit fused

BST SYSTEMS INC.

OFI and RSS Electrical Requirements

- **RSS BATTERY**
  - OCV 44 VDC max
  - Static loads
    - » 30.50 VDC to 35.00 VDC within 100 ms of application of 0.10 A to 1.00 A loads
  - Pulse loads
    - » 27.00 VDC to 35.00 VDC during a 250 ms 3.65 A pulse
  - Transient loads
    - » 10.00 VDC to 35.00 VDC during a 2 ms 8 A pulse followed by transition within 100 ms to static load levels

BST SYSTEMS INC.

Dynamic Environmental Conditions OFI/RSS

- Random vibration levels
  - » Most damaging low frequency levels high throughout flight
- Ordnance shock
- Water impact shock
- Must remain intact following splashdown (RSS)
- Must function after splashdown (OFI)
- Testing conducted up front during development

BST SYSTEMS INC.

Design Considerations

- Rapid voltage transitions at turn on
- Temperature insensitivity (no heater blankets)
- Reliable 120 day wet stand
  - Temperatures up to 118 F
- Capacity retention
- Orientation insensitivity
- Dynamic conditions

BST SYSTEMS INC.

Design Considerations Deperoxidation

- Extensive experimentation conducted to optimize method
- Both thermal and electrical methods considered
- Thermal technique found to provide the best results
- Processing optimized

BST SYSTEMS INC.

Design Considerations

Temperature Insensitivity and 120 day wet stand

- Prototype testing conducted to simulate worst case conditions
- Pack design modified as required
- Incorporated separator system based on data obtained from in-house development testing

BST SYSTEMS INC.

Design Considerations Orientation Insensitivity

- RSS battery oriented connector end up (or down)
- The following techniques were incorporated:
  - Reliable redundant terminal to cover seals
  - Reliable, redundant case to cover seals
  - Electrolyte starvation (RSS only)
  - High pressure cell relief valves
  - Absorbent barriers

BST SYSTEMS INC.

Design Considerations Dynamic Conditions

- Technical approach to engineer unpotted units for both applications
- Advantages to this approach include
  - Ease of manufacturing
  - Improved inspectability
  - Strapping variability
  - Mechanically simple
- Several restraint techniques utilized
  - Internal cell hold down features
  - Spacers and shims to prevent lateral movement
  - Cushioning material on underside of cover to prevent up and down movement

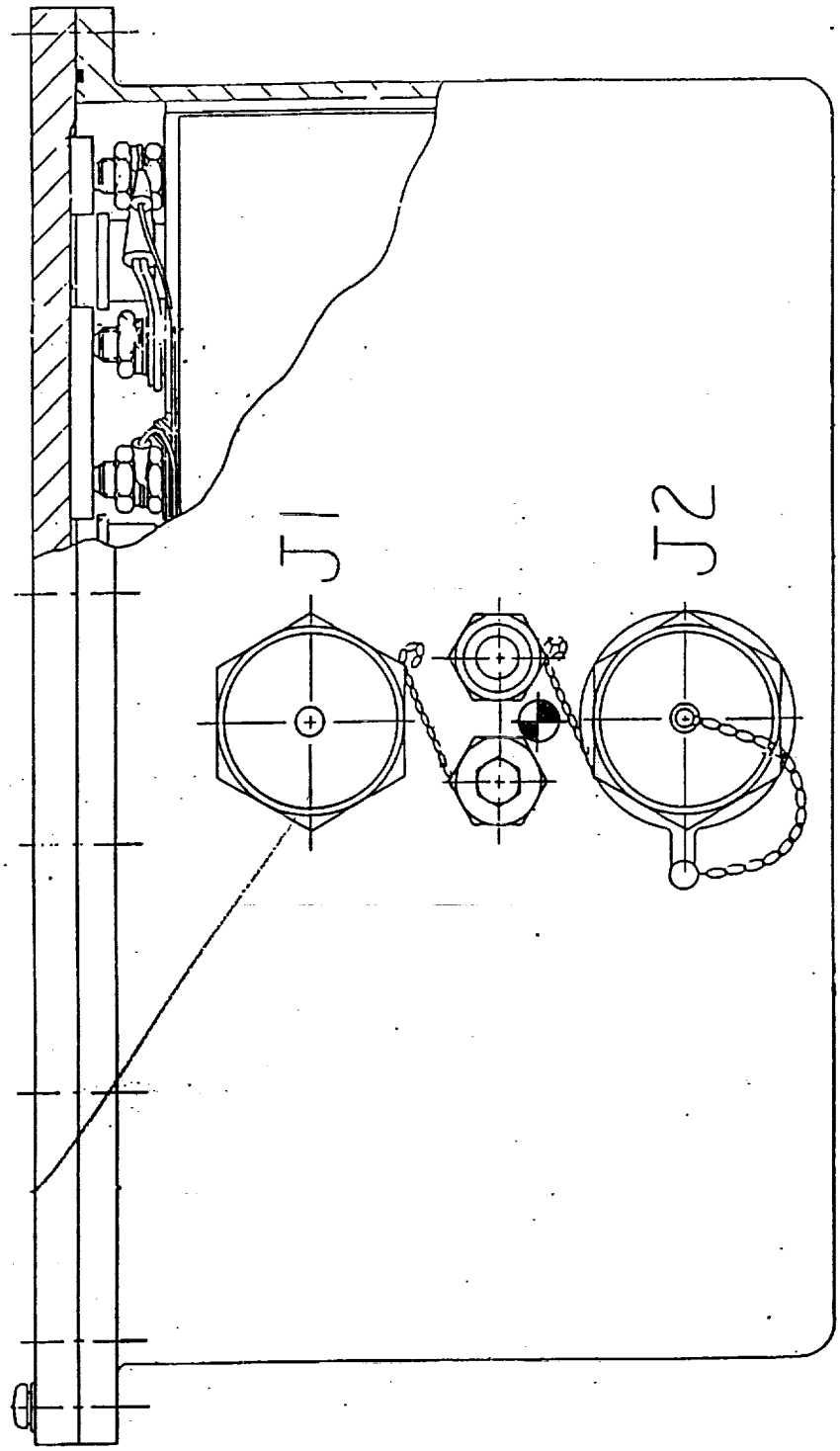

OF H FRONT VIEW

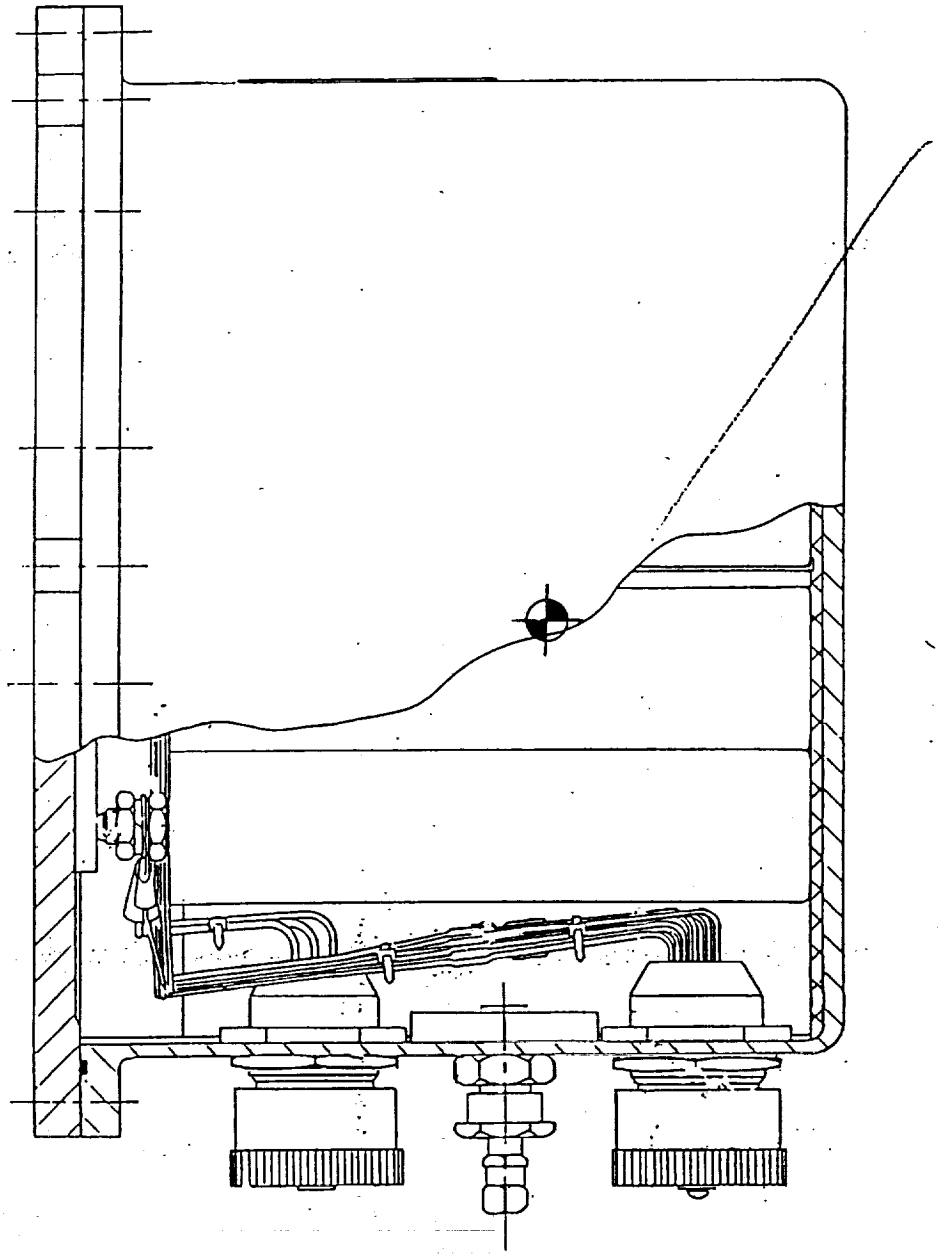

DFI Side View

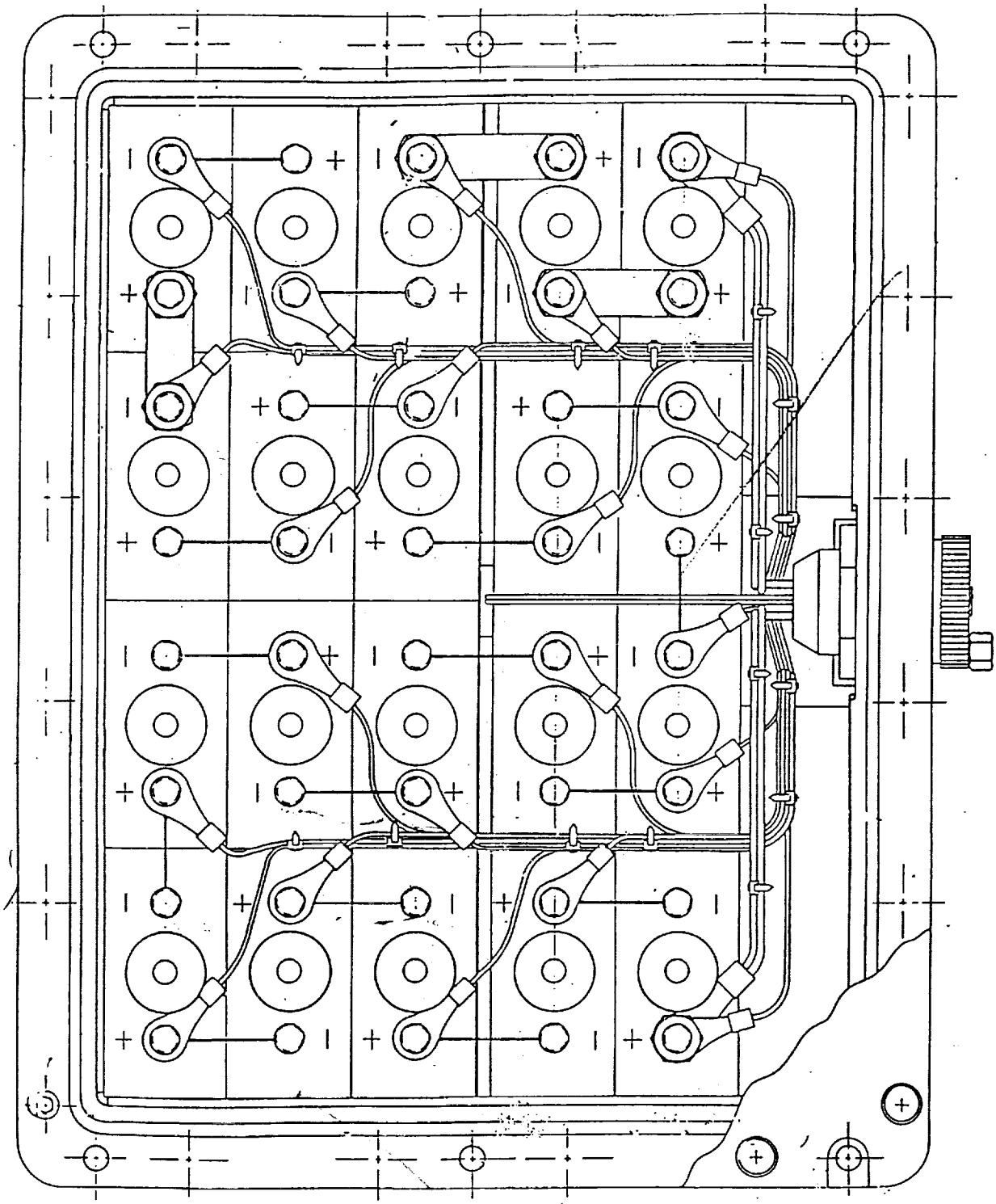

OFI Top View

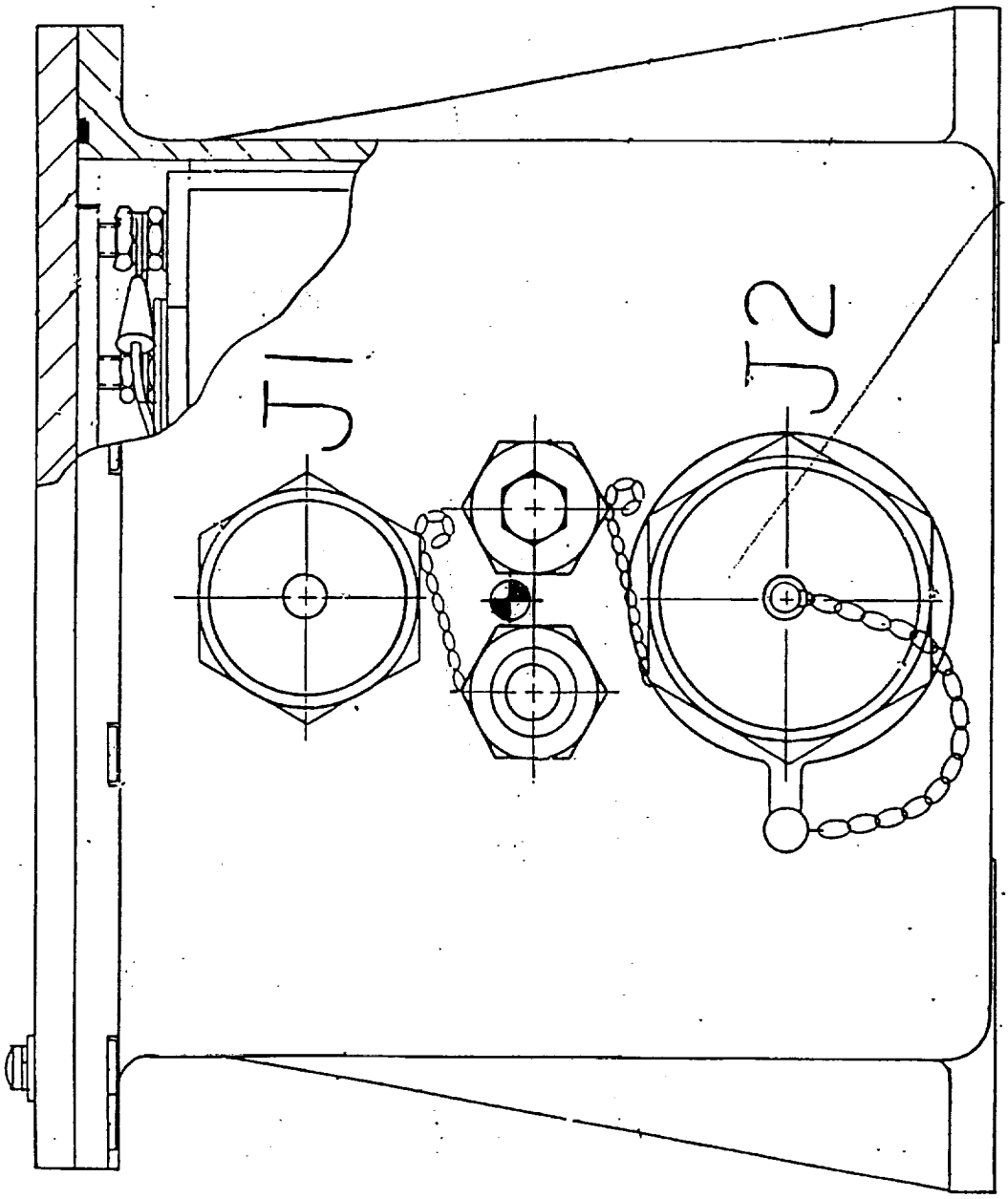

RSS Front View

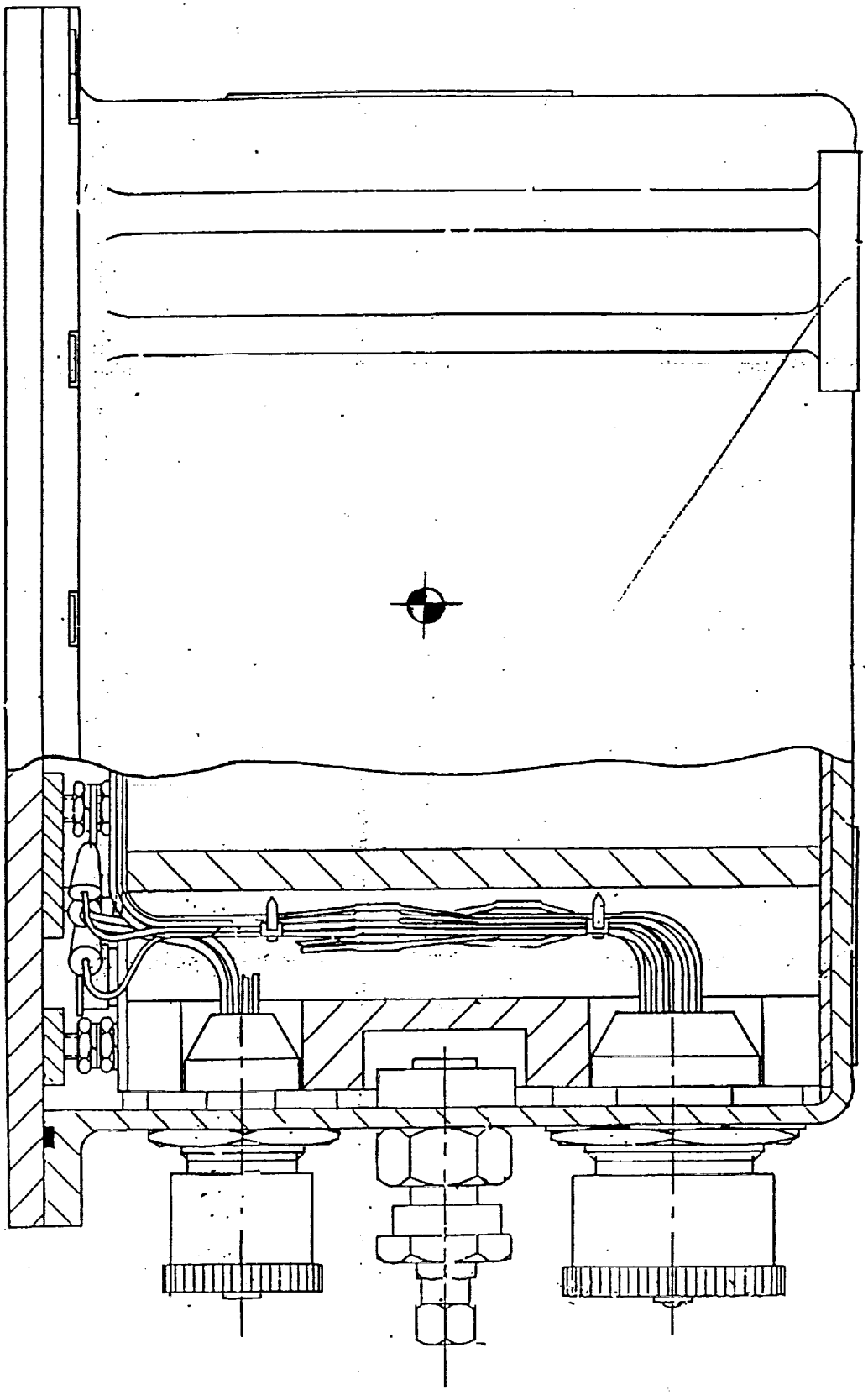

RSS Side View

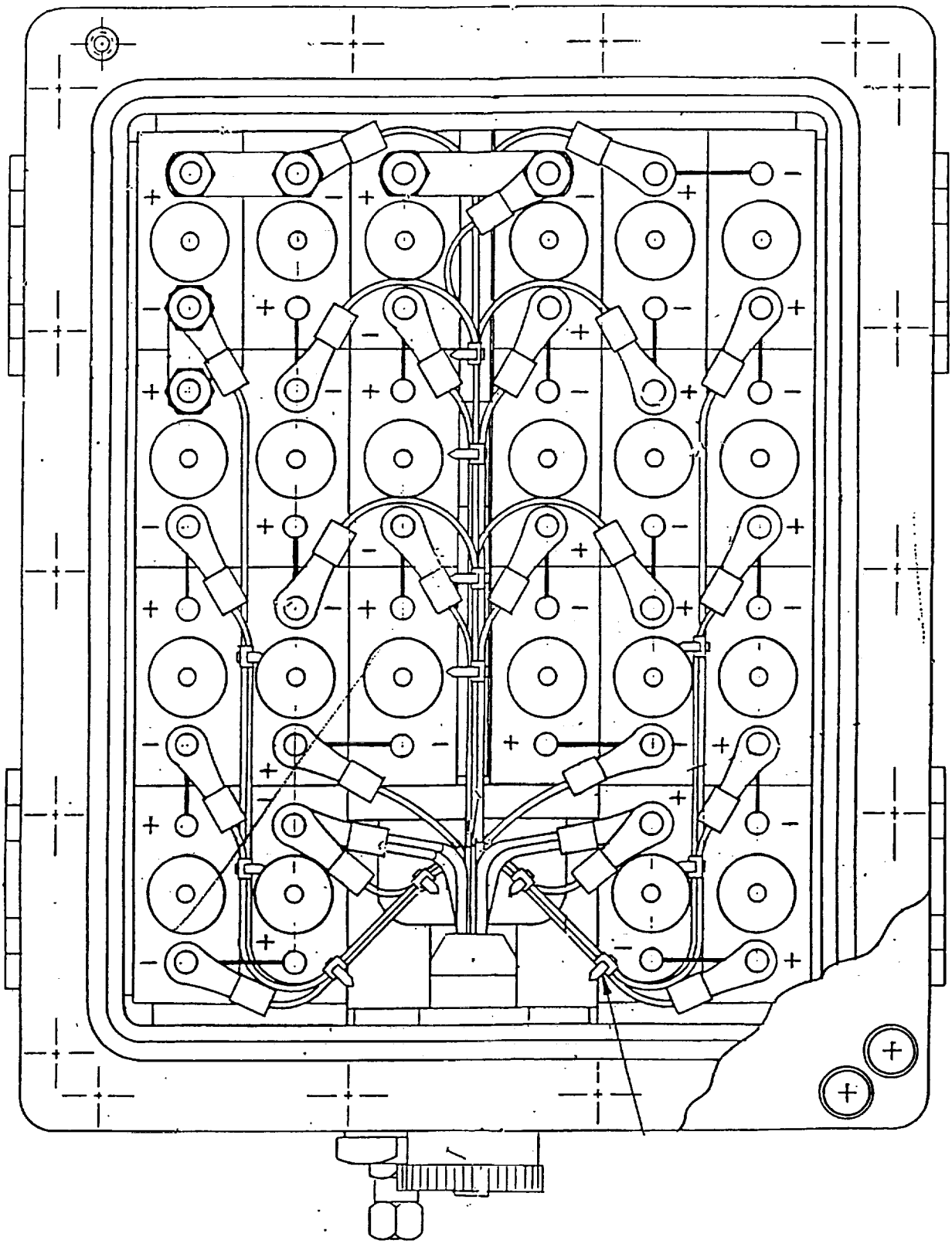

RSS Top View

BST SYSTEMS INC.

Testing Approach

- Conducted on 75 development cells and (at least) 8 batteries of each type to verify design and approach
- Transient load profiles to simulate actual usage
- Samples held at room temperature, hot and cold conditions

OFI Cell Test Matrix

BST SYSTEMS, INC.

OFI Cell Test Matrix (75 Cells)

TEMPERATURE PROFILE	ACTION PERFORMED	GROUP NO.				
		DAY 6	DAY 30	DAY 60	DAY 90	DAY 120
HOT	100% DISCHARGE	1			2	3
	TRANSIENT♦ DISCHARGE	2,3	2,3	2,3	3	
ROOM	100% DISCHARGE	4			5	6
	TRANSIENT DISCHARGE	5,6	5,6	5,6	6	
COLD	100% DISCHARGE	7			8	9
	TRANSIENT' DISCHARGE	8,9	8,9	8,9	9	

Note 1: ♦ means transient discharge will be performed during 105°F section of hot temperature profile.

Note 2: ' means transient discharge will be performed during 30°F section of cold temperature profile.

BST SYSTEMS INC.

OFI Cell Transient Load Profile

III. C. CELL DEVELOPMENT TESTING

TRANSIENT PROFILE

Load	Duration		AH Consumption
0.16A	10	Minutes	0.0267 AH
0.5A	20	Minutes	0.1667 AH
3.5A	250	Milliseconds	0.0002 AH
0.5A	15	Minutes	0.1250 AH
3.5A	250	Milliseconds	0.0002 AH
0.7A	15	Minutes	0.1750 AH
1.0A	5	Minutes	0.0833 AH
2.5A	5	Minutes	0.2083 AH
5.0A	5	Minutes	0.4167 AH
8.0A	2	Millisecond	0.0000 AH
10.0A	3	Minutes	0.5000 AH
15.0A	3	Minutes	0.7500 AH
30.0A	3	Minutes	1.5000 AH
Totals	84	Minutes	3.9521 AH

BST SYSTEMS INC.

OFI Results Capacity, Wet Life & Performance

- All cells met 50 AH capacity requirement after 120 days
- No shorting
- Charge retention good
  - Approx 97% capacity retention at room temperature and cold temperature after 120 days
  - Approx 90% capacity retention at high temperature after 120 days
- Deperoxidation successful
- Load conditions at various temperatures met

BST SYSTEMS INC.

OFI Results Physical

- No case to cover leakage
- No terminal leakage
- No leakage through valve

BST SYSTEMS INC.

RSS Cell Test Matrix

BST SYSTEMS, INC.

RSS Cell Test Matrix

TEMPERATURE PROFILE	ACTION PERFORMED	GROUP NUMBER				
		DAY 6	DAY 30	DAY 60	DAY 90	DAY 120
HOT	100% DISCHARGE	1			2	3
	TRANSIENT♦ DISCHARGE	2,3	2,3	2,3	3	
ROOM	100% DISCHARGE	4			5	6
	TRANSIENT DISCHARGE	5,6	5,6	5,6	6	
COLD	100% DISCHARGE	7			8	9
	TRANSIENT' DISCHARGE	8,9	8,9	8,9	9	

Note 1: ♦ means transient discharge will be performed during 118°F section of hot temperature profile.

Note 2: ' means transient discharge will be performed during 30°F section of cold temperature profile.

BST SYSTEMS INC.

RSS Cell Transient Load Profile

I. C. CELL DEVELOPMENT TESTING

TRANSIENT PROFILE

Load	Duration	AH
0.10A	10 Minutes	0.0166
3.65A	250 Milliseconds	0.0002
0.10A	10 Minutes	0.0166
8.00A	2 Milliseconds	0.0000
0.10A	10 Minutes	0.0166
0.50A	8 Minutes	0.0666
3.65A	250 Milliseconds	0.0002
0.50A	8 Minutes	0.0666
8.00A	2 Milliseconds	0.0000
0.50A	8 Minutes	0.0666
1.00A	5 Minutes	0.0833
3.65A	250 Milliseconds	0.0002
1.00A	5 Minutes	0.0833
8.00A	2 Milliseconds	0.0000
1.00A	5 Minutes	0.0833
	==========	=========
	69 Minutes	0.500 AH

BST SYSTEMS INC.

RSS Results
Capacity and Wet Life

- All cells met the 14 AH capacity requirement
- Charge retention good
  - Approx 90% capacity retention at room temperature and cold temperature after 120 days
  - Approx 84% charge retention at high temperature after 120 days
- No performance variations with respect to orientation
- Deperoxidation successful
- Load conditions at various temperatures met

I. C. RSS CELL DEVELOPMENT TESTING

CAPACITIES vs. TIME

HOT TEMPERATURE CHARGED STAND

DAY OF DISCHARGE	ORIENTATION			
	UPRIGHT	-UP	+UP	AVERAGE
INITIAL	22.9	22.6	22.2	22.6 ± 1.1
DAY 90	18.4	18.7	19.6	
	18.2	14.4*	20.4	
	19.0	17.7	20.0	
	18.5			
AVERAGE	18.5	18.2*	20.0	18.5 ± 4.9
				18.9 ± 2.6*
DAY 120	19.3	18.6	18.4	
	19.0	19.2	18.9	
	18.4	17.6	18.1	
	19.6	18.1	19.6	
	18.5	18.7	19.3	
		18.3	19.3	
Average	19.0	18.4	18.9	18.8 ± 1.7

I. C. RSS CELL DEVELOPMENT TESTING

CAPACITIES vs. TIME

COLD TEMPERATURE CHARGED STAND

DAY OF DISCHARGE	ORIENTATION			
	UPRIGHT	-UP	+POS	
INITIAL	20.8	20.8	21.8	21.2 ± 1.7
DAY 90	19.5	20.9	20.9	
	20.6		21.2	
	20.2	21.0	20.9	
	19.9			
AVERAGE	20.1	20.8	21.0	20.6 ± 1.6
DAY 120	21.0	22.4	20.0	
	21.0	22.0	22.3	
	21.5	22.1	22.3	
	21.5	21.7	22.1	
	22.0	21.9	21.5	
			21.2	
AVERAGE	21.4	22.0	21.6	21.7 ± 1.9

I. C. RSS CELL DEVELOPMENT TESTING

CAPACITIES vs TIME

ROOM TEMPERATURE CHARGED STAND

DAY OF DISCHARGE	ORIENTATION			
	UPRIGHT	-UP	+UP	
INITIAL	23.0	22.3	22.3	22.5 ± 1.2
DAY 90	21.9	22.5	21.4	
	21.4			
AVERAGE	21.7	22.5	21.4	21.8 ± 1.5
DAY 120	19.7	20.0	19.4	
	20.2	19.7	20.1	
		20.5	20.4	
AVERAGE	20.0	20.1	20.0	20.0 ± 1.1

BST SYSTEMS INC.

RSS Results
Physical

- No case to cover leakage
- No leakage through valve

BST SYSTEMS INC.

RSS Battery Testing

- Eight development batteries built and tested
  - Six units to demonstrate wet life and capacity performance
  - Two units to demonstrate performance during shock and vibration
- Batteries oriented on mounting feet or connector end up
- Discharge profile and matrix similar to cell matrices
- The six wet life batteries tested out to 150 days

BST SYSTEMS INC.

RSS Results
Capacity and Wet Life

- All six wet life batteries met the 14.00 AH capacity requirement
- Units were kept on stand from 147 to 161 days at cold, room and high temperatures
- Capacities ranged from 16.95 AH (hot) to 21.0 AH (cold)
- Units were orientation insensitive

BST SYSTEMS INC.

Capacity

Battery #	Temp	Capacity	Days	Orientation
SDB2	Hot	16.96AH	147	Upended
SDB3	Hot	16.95AH	161	Upright
SDB4	Room	19.92AH	152	Upended
SDB5	Room	19.47AH	152	Upright
SDB7	Cold	20.62AH	151	Upended
SDB8	Cold	21.0AH	151	Upright

BST SYSTEMS INC.

RSS Results

- No cell case to cover leakage
- No leakage through valve
- No terminal leakage
- One battery also inverted fully for 48 hours
  - No leakage

BST SYSTEMS INC.

OFI Battery Testing

- **Eight development batteries built and tested**
  - **Six units to demonstrate wet life and capacity performance**
  - **Two units to demonstrate performance during shock and vibration**
- **Discharge profile and matrix similar to cell matrix**

BST SYSTEMS INC.

OFI Results
Capacity and Wet Life

- All six wet life batteries met the 50 AH capacity requirement
- Units were kept on stand from 123 days to 155 days at cold, room and hot temperatures
- Capacities ranged from 61.3 AH (hot) to 74.5 AH (cold)

BST SYSTEMS INC.

Capacity

Battery #	Temp	Capacity	Days
FDB102	Hot	61.60AH	155
FDB103	Hot	61.30AH	133
FDB104	Room	71.40AH	131
FDB105	Room	70.60AH	128
FDB107	Cold	74.50AH	147
FDB108	Cold	74.60AH	121

BST SYSTEMS INC.

OFI Results

- No cell case to cover leakage
- No leakage through valve
- No terminal leakage

BST SYSTEMS INC.

Dynamic Testing

- Testing conducted during development to minimize risk
- One battery of each type tested at SRB levels
  - Reentry vibration
  - Ordnance shock
  - Water impact
- One battery of each type tested at ASRB levels
  - Reentry vibration
  - Ordnance shock
  - Water impact

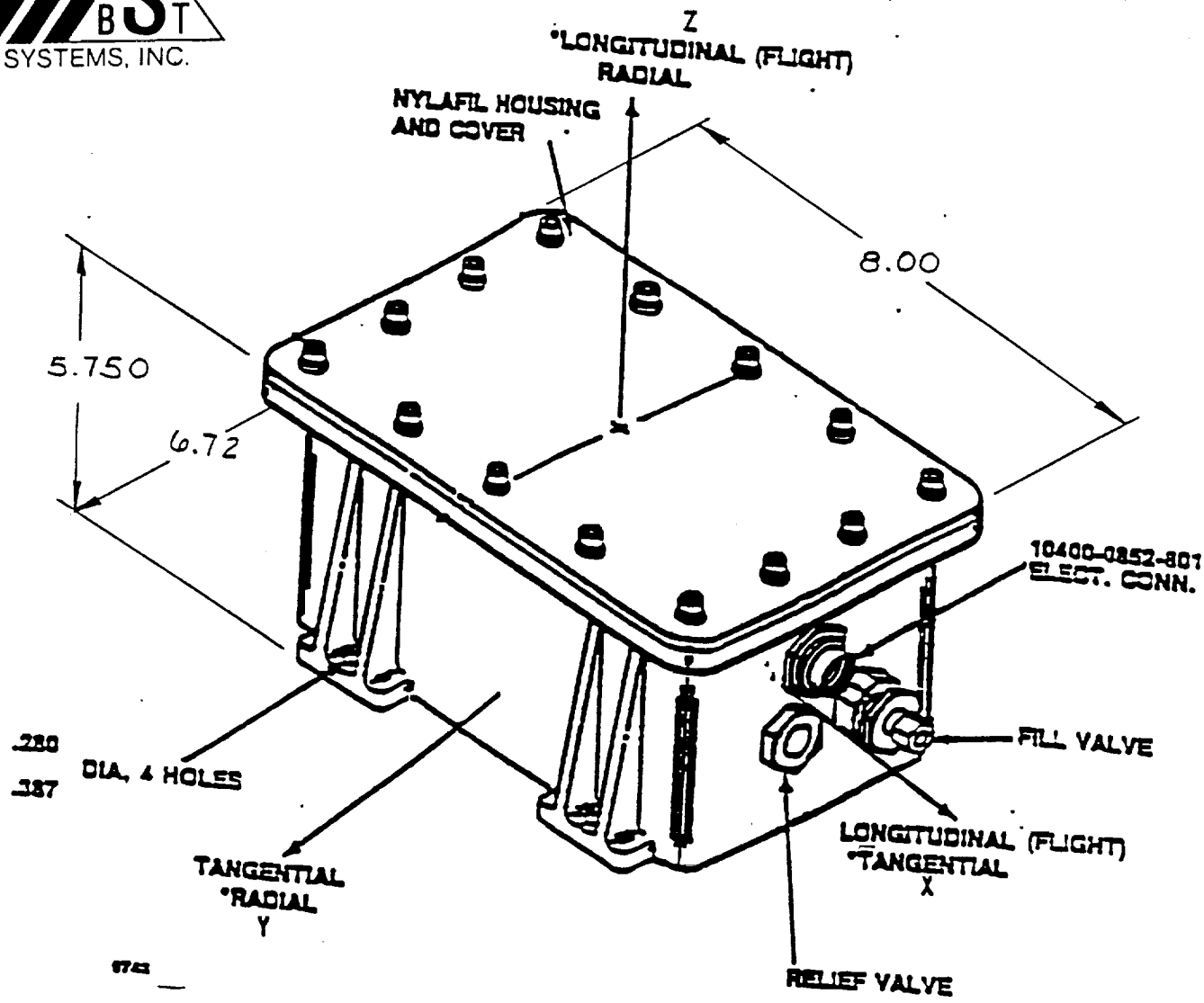

SRB/ET RSS BATTERY ORIENTATION AXIS

NOTE: X, Y, Z Axis orientation is shown for environmental testing.

FIGURE 1

BST SYSTEMS, INC.

RSS VIBRATION

The order of testing shall be Y Axis, then X Axis, followed by the Z Axis.

The Cold Profile is to be vibrated at the following levels:

RANDOM VIBRATION CRITERIA (90 seconds in each axis)

RADIAL AXIS (Y Axis)

20-200 Hz @ 0.02 g^2/Hz
200-250 Hz @ +9.4 dB/oct
250-800 Hz @ 0.04 g^2/Hz
800-2000 Hz @ -7.6 dB/oct
2000 Hz @ 0.004 g^2/Hz

Composite = 6.6 grms

LONG. AND TANG. AXES (Z and X respectively)

20 Hz @ 0.02 g^2/Hz
20-100 Hz @ +5 dB/oct
100-800 Hz @ 0.3 g^2/Hz
800-2000 Hz @ -11 dB/oct
2000 Hz @ 0.01 g^2/Hz

Composite = 17.4 grms

The Hot Profile Unit is to be vibrated at the following levels:

Reentry Random Vibration (90 seconds in each axis)

RADIAL AXIS (Y Axis)

20 - 100 Hz @ 0.05 g^2/Hz
100 - 200 Hz @ +6.0 dB/oct
200 - 500 Hz @ 0.2 g^2/Hz
500 - 2,000 Hz @ -5.0 dB/oct
2,000 Hz @ 0.02 g^2/Hz

Composite = 12.9 g_{rms}

LONG. AND TANG. AXES (Z and X respectively)

20 Hz @ 0.01 g^2/Hz
20 - 100 Hz @ +8.2 dB/oct
100 - 400 Hz @ 0.8 g^2/Hz
400 - 2,000 Hz @ -6.1 dB/oct
2,000 Hz @ 0.03 g^2/Hz

Composite = 22.6 g_{rms}

BST SYSTEMS, INC.

RSS ORDNANCE SHOCK Ref. Doc. 10SPC-0225 Para. 3.2.7.2.2.1

The order of testing shall be X+, X-, Y+, Y-, Z+, Z-.

50 Hz	@	12 G's peak
50-100 Hz	@	+12 dB/oct
100 Hz	@	47 G's peak
100-4000 Hz	@	+6 dB/oct
4000-10000 Hz	@	1,875 G's peak

RSS WATER IMPACT SHOCK Ref. Doc. 10SPC-0225 Para. 3.2.7.2.2.2

The order of testing shall be X+, X-, Y+, Y-, Z+, Z-.

Water Impact (1 shock per axis per mission for all axes)

Longitudinal Axis and Lateral Axes

20 Hz	@	50 G's peak
20-70 Hz	@	+8 dB/oct
70-5000 Hz	@	250 G's peak

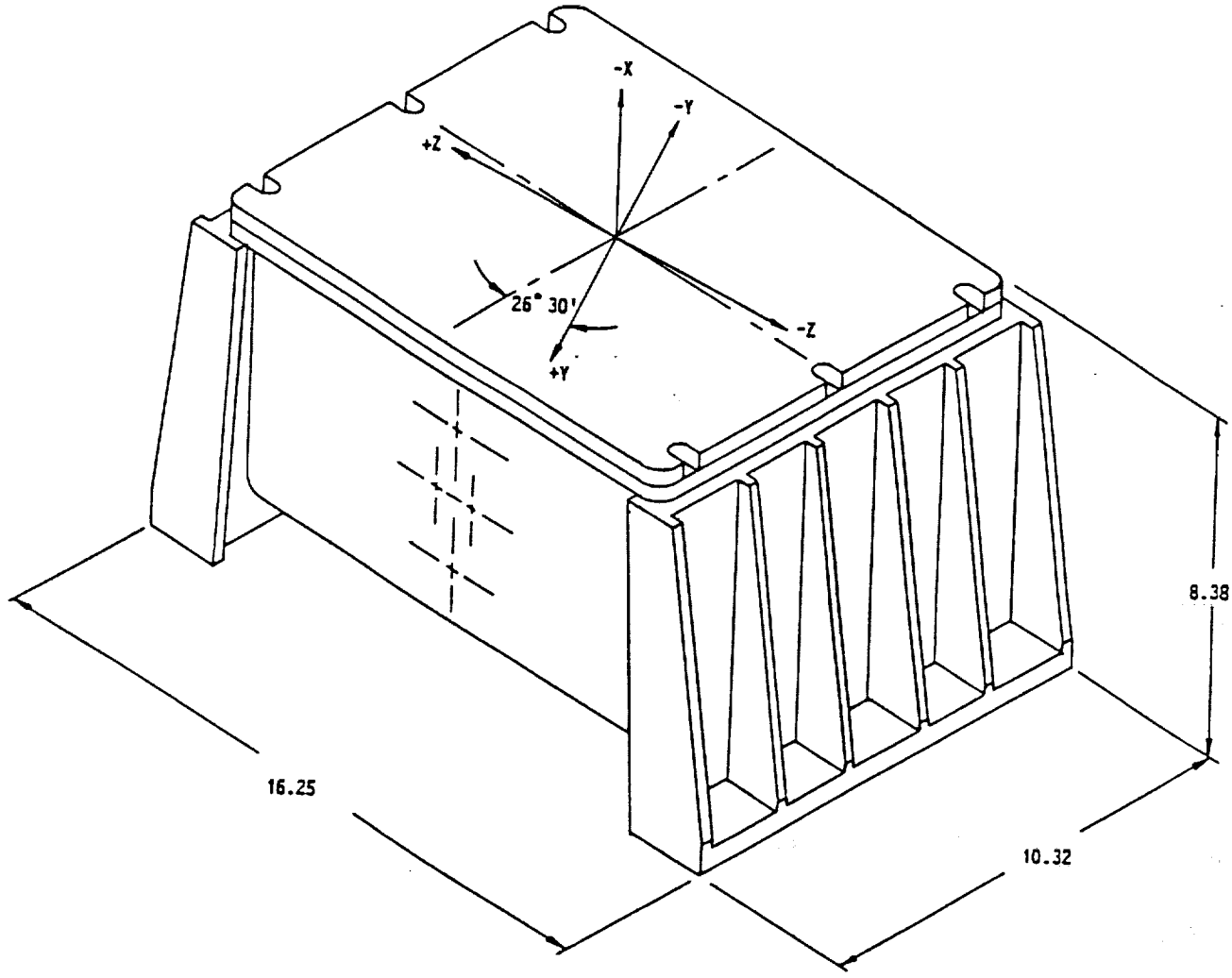

OFI Battery

FIGURE 1

BST SYSTEMS, INC.

OFI VIBRATION

The order of testing shall be Z Axis, then Y Axis, followed by the X Axis.

The Cold Profile Unit is to be vibrated at the following levels:

RANDOM VIBRATION CRITERIA (90 seconds in each axis)

RADIAL AXIS (Z Axis) - 120 seconds

20	Hz @ 0.050 g^2/Hz
20-48	Hz @ +3 dB/oct
48-750	Hz @ 0.12 g^2/Hz
750-2000	Hz @ -9 dB/oct
2000	Hz @ 0.0064 g^2/Hz

Composite = 11.2 grms

LONG. AND TANG. AXES (X and Y respectively) - 90 seconds

20	Hz @ 0.02 g^2/Hz
20-100	Hz @ +5 dB/oct
100-800	Hz @ 0.3 g^2/Hz
800-2000	Hz @ -11 dB/oct
2000	Hz @ 0.01 g^2/Hz

Composite = 17.4 grms

The Hot Profile Unit (Paragraph 4) is to be vibrated at the following levels:

Reentry Random Vibration (90 seconds in each axis)

RADIAL AXIS (Z Axis)

20 - 100	Hz @ 0.05 g^2/Hz
100 - 200	Hz @ +6.0 dB/oct
200 - 500	Hz @ 0.2 g^2/Hz
500 - 2,000	Hz @ -5.0 dB/oct
	2,000 Hz @ 0.02 g^2/Hz

Composite = 12.9 g_{rms}

LONG. AND TANG. AXES (X and Y respectively)

	20 Hz @ 0.01 g^2/Hz
20 - 100	Hz @ +8.2 dB/oct
100 - 400	Hz @ 0.8 g^2/Hz
400 - 2,000	Hz @ -6.1 dB/oct
	2,000 Hz @ 0.03 g^2/Hz

Composite = 22.6 g_{rms}

BST SYSTEMS, INC.

The order of testing shall be Z+, Z-, Y+, Y-, X+, X-.

OFI ORDNANCE SHOCK Ref. Doc. 10SPC-0226 Para. 3.2.7.2.2.1

50 Hz	@	12 G's peak
50-100 Hz	@	+12 dB/oct
100 Hz	@	47 G's peak
100-4000 Hz	@	+6 dB/oct
4000-10000 Hz	@	1,875 G's peak

OFI Water Impact (1 shock per axis per mission for all axes)

20 Hz	@	50 G's peak
20-70 Hz	@	+8 dB/oct
70-5000 Hz	@	250 G's peak

BST SYSTEMS INC.

OFI Dynamic Testing

- Battery tested to SRB levels exhibited no performance anomalies
- Output capacity 77.9 AH
-
- Battery tested to ASRB levels exhibited no performance anomalies
- Output capacity 77.6 AH
- Upon teardown, one cell found to have 1 wire on 1 electrode broken

BST SYSTEMS INC.

RSS Dynamic Testing

- Battery tested to SRB levels exhibited no performance anomalies
- Output capacity 21.8 AH
-
- Battery tested to ASRB levels failed approx 1 minute into vibration
- Upon teardown, all cells found to have sustained some form of wire breakage

BST SYSTEMS INC.

Dynamic Testing Grooming Modification

- Dynamic stress relief incorporated
- Two types proposed
  - Full loops
  - S-turns
- One battery of each type built with cells having both types of loops evenly distributed throughout case

BST SYSTEMS INC.

Dynamic Testing with Stress Relief

- Each battery subjected to full flight levels at SRB conditions
- OFI exhibited no performance anomalies
  - Output capacity 71 AH
- RSS suffered breakage in one cell with S-turn
- Full loops chosen as stress relief method

BST SYSTEMS INC.

Dynamic Testing

- Shims and spacers restrained cells
- Hold down cushions on cover functioned as designed
- Internal cell hold down restrained cell pack

BST SYSTEMS INC.

Summary

- **Requirements were met with silver-zinc as a result of certain engineering approaches:**
  - **Innovative composite separator system**
  - **Carefully controlled deperoxidation resulting in excellent voltage regulation given the wide current range and excellent charge retention**
  - **Unpotted battery restrainment system**
  - **Dynamic stress relief and electrode hold-down structures**

BST SYSTEMS INC.

Acknowledgment

- **BST Systems would like to thank both USBI and MSFC for their technical support and for the use of the dynamic test facilities at MSFC which helped to assist the conclusion of this development program**

List of Attendees

Zoe Adamedes
BST Systems
78 Plainfield Pike Road
Plainfield, CT 06374
(203) 564-4078

Peggy N. Adams
U.S. Army Space & Strategic Defense Command
POB 1500
Attn: CSSD-SD-AM
Huntsville, AL 35807-3801
(205) 955-1599

Menahem Anderman, Ph.D.
ACME-Advanced Energy Systems
528 West 21st Street
Suite 6
Tempe, AZ 85282
(602) 894-6864

David Baer
Hughes Aircraft Company
MS 231/1518
Electron Dynamics Division
POB 2999
Torrance, CA 90509-2999
(310) 517-7604

Bob Bechtel
Marshall Space Flight Center
EB71
Marshall Space Flight Center, AL 35812
(205) 544-3294

Charles W. Bennett
Martin Marietta Astro Space
MS NP-2I
POB 800
Princeton, NJ 08543-0800
(609) 951-7597

Tom Berry
TRW GRO / FOT
Goddard Space Flight Center
Code 519.5, Bldg. 14, Rm. E272
Greenbelt, MD 20770
(301) 286-4184

Sam Bogner
Hughes Aircraft Company
1275 New York Dr.
Altadena, CA 91001

Yannick Borthomieu
SAFT Advanced Batteries
Rue G. Leclanche
BP 1029
86060 Poitiers Cedex
France

(33) 49554014

Jeff Brewer
Marshall Space Flight Center
EB74
Marshall Space Flight Center, AL 35812
(205) 544-3345

Harry Brown
Naval Surface Warfare Center - Crane Div.
Commander
Code 6095 B2949
300 Hwy 301
Crane, IN 47522
(812) 854-1593

David Burns
Marshall Space Flight Center
EB15
Marshall Space Flight Center, AL 35812
(205) 544-4807

Joseph A. Carcone
Sanyo Energy (USA) Corporation
2001 Sanyo Avenue
San Diego, CA 92173
(619) 661-6620

Franco Carnevale
Inmarsat
c/o Martin Marietta Astro Space
MS 115, POB 800
Princeton, NJ 08543
(609) 490-6249

John E. Casey
Lockheed Engineering & Sciences Co.
2400 NASA Rd. 1, EP5
Houston, TX 77058-3799
(713) 483-0446

Guy Chagnon
SAFT R&D Center
107 Beaver Ct.
Cockeysville, MD 21030
(410) 771-3200

Lee Christensen
Freudenberg Nonwovens
20 Industrial Ave.
Chelmsford, MA 01824
(508) 256-6588

Mark Christopher
Physitron, Inc.
3304 Westmill Dr.
Huntsville, AL 35805
(205) 534-4844

Dwaine Coates
Eagle Picher Industries, Inc.
1215 West B St.
Joplin, MO 64802
(417) 623-8000 X403

Anne Conley
Hughes Aircraft
10345 Mary Ave.
Cupertino, CA 95014
(408) 744-1927

Eric C. Darcy
Johnson Space Center
MS EP6
NASA Rd. 1
Houston, TX 77058
(713) 483-9055

PRECEDING PAGE BLANK NOT FILMED

Stephen F. Dawson
Jet Propulsion Laboratory
4800 Oak Grove Dr.
Pasadena, CA 91109
(818) 354-4329

Frank Deligiannis
Jet Propulsion Laboratory
MS 277-104
4800 Oak Grove Dr.
Pasadena, CA 91109
(818) 354-0404

Dan Dell
Gates Aerospace Batteries
POB 147115
Gainesville, FL 32614-7115
(904) 462-6914

Sal DiStefano
Jet Propulsion Laboratory
MS 277-212
4800 Oak Grove Drive
Pasadena, CA 91109
(818) 354-6320

Rajiv Doreswamy
Marshall Space Flight Center
EB73
Marshall Space Flight Center, AL 35812
(205) 544-3366

Orville O. Dunham, Jr.
Ribbon Technology Corp.
POB 30758
Gahanna, OH 43230
(800) 848-0477

Andrew F. Dunnet
INTELSAT
MS 33A
3400 International Dr. NW
Washington, DC 20008
(202) 944-7245

Martin W. Earl
COMSAT Laboratories
22300 Comsat Dr.
Clarksburg, MD 20871
(301) 428-4503

Frank Echols
Teledyne Brown
MS 52
300 Sparkman Dr.
Huntsville, AL 35807

Tim A. Edgar
Eagle Picher Industries, Inc.
3820 South Hancock Expressway
Colorado Springs, CO 80911
(719) 392-4266

Ted Edge
Marshall Space Flight Center
EB11
Marshall Space Flight Center, AL 35812
(205) 544-3381

Robert Edgington
National-Standard
24101 N. Home St.
Mishawaka, IN 46545

Blake A. Emmerich
Zircar Products, Inc
POB 458
110 N. Main St.
Florida, NY 10921-0458
(914) 651-4481 X229

Ted Enomoto
Sanyo Energy (USA) Corporation
2001 Sanyo Avenue
San Diego, CA 92173
(619) 661-6620

Ed Fitzgerald
Teledyne Brown Engineering
MS 16
300 Sparkman Dr. NW
Huntsville, AL 35807
(205) 726-2865

Nicanor A. Flordeliza
GE American Communications
4 Research Way
Princeton, NJ 08540
(609) 987-4453

Chris Fox
Eagle-Picher Industries, Inc.
1215 West B Street
Joplin, MO
(417) 623-8000 X367

Garry Freeman, Jr.
U.S. Army Space & Strategic Defense Command
Route 1, Box 246
Somerville, AL 35670
(205) 955-4576

Chris Garner
Naval Research Laboratory
Code 8134
4555 Overlook Ave. SW
Washington, DC 20375
(202) 767-9075

Dr. William O. Gentry, P.E.
Johnson Controls, Inc.
POB 591
Milwaukee, WI 53201
(414) 228-2228

John Giltner
Eagle-Picher Industries, Inc.
C and Porter Streets
Joplin, MO 64801

Eugena Goggans
Marshall Space Flight Center
EB15
Marshall Space Flight Center, AL 35812
(205) 544-3386

Ray Goins
USBI
29226 Bethel Rd.
Toney, AL 35773
(205) 423-6902

Robert S. Green
Hughes – HITC
1768 Business Ctr. Dr.
Reston, VA 22090
(703) 759-1244

Shahid Habib
NASA Headquarters
Code QW
Washington, DC 20546
(202) 358-0536

Charles Hall
Marshall Space Flight Center
EB74
Marshall Space Flight Center, AL 35812
(205) 544-3330

David Hall
Marshall Space Flight Center
EB72
Marshall Space Flight Center, AL 35812
(205) 544-4215

Steve Hall
Naval Surface Warfare Center - Crane Div.
Code 6095
Crane, IN 47522
(812) 854-1593

Gerald Halpert
Jet Propulsion Laboratory
MS 277-212
4800 Oak Grove Drive
Pasadena, CA 91109
(818) 354-5474

Dr. Alan C. Harkness
Ballard Battery Systems Corporation
1164 West 15th St.
North Vancouver, B.C.
Canada V7P 1M9

(604) 986-4104

James R. Henderson
Westinghouse Electric Corp.
917 Explorer Boulevard
Huntsville, AL 35806
(205) 971-4710

Carole A. Hill
The Aerospace Corporation
MANZ/208
POB 9045
Albuquerque, NM 87119-9045
(505) 846-7063

Albert Himy
Westinghouse Electric Corporation
POB 18249
Pittsburgh, PA 15236
(412) 382-7883

Elmer Hughett
The Enser Corporation
POB 18728
Huntsville, AL 35804-8728

John Iverson
Aero Quality
6101 NW 198 Terr.
Miami, FL 33015
(305) 624-2435

Lorna Jackson
Marshall Space Flight Center
EB72
Marshall Space Flight Center, AL 35812
(205) 544-3318

R. Roy Jackson
The Enser Corporation
POB 18728
Huntsville, AL 35804-8728

Doris Jallice
Goddard Space Flight Center
Code 734.5
Greenbelt, MD 20771

Jason E. Jenkins
Johns Hopkins University / APL
Rm 23-214
Johns Hopkins Rd.
Laurel, MD 20723-6099
(301) 953-5106

Dr. Chris Johnson
Boeing Defense & Space
MS 8C-61
POB 3999
Seattle, WA 98124
(206) 773-9257

Mark Kauchak
Westinghouse
917 Explorer Blvd.
Huntsville, AL 35806
(205) 971-4704

Marcie Kennedy
Marshall Space Flight Center
EB72
Marshall Space Flight Center, AL 35812
(205) 544-3724

Lt. Victoria Kennedy
U.S. Air Force
PL/VTPC
Kirtland AFB, NM 87117-6008
(505) 846-2637

Donald Kleis

110 Wynn Drive
Huntsville, AL

Michael D. Koelling
Hughes Aircraft
MS CHSS
16800 E. CentreTech Parkway
Aurora, CO 80011
(303) 341-3327

Al Kuehl
USASSDC
Active Sensors Division
CSSD-SD-AM
POB 1500
Huntsvile, AL 35807-3801

Hiroaki Kusawake
National Space Development Agency of Japan
Tsukuba Space Center
2-1-1 Sengen, Tsukuba, Ibaraki 305
Japan

81-298-52-2285

Allan Lamb

19672-286 Stuens Creek Blvd.
Cepertino, CA 95014
(408) 282-2040

Roy Lanier
Marshall Space Flight Center
EB71
Marshall Space Flight Center, AL 35812
(205) 544-3301

Ron Lantzy
Martin Marietta
MS S4017
POB 179
Denver, CO 80201
(303) 971-8706

Christine Lehr
Martin Marietta Astro Space
POB 800
Princeton, NJ 08543-0800
(609) 490-3574

Harlan L. Lewis
Naval Surface Warfare Center - Crane Div.

Crane, IN 47522-5060
(812) 854-4104

Herman G. Lewis, Jr.
McDonnell Douglas Aerospace
MS B3-D420/22-2
5301 Bolsa Ave.
Huntington Beach, CA 92647
(714) 896-3137

Karl Liggin
Marshall Space Flight Center
EB15
Marshall Space Flight Center, AL 35812

Eric Lowery
Marshall Space Flight Center
EB74
Marshall Space Flight Center, AL 35812
(205) 544-0080

Steve Luna
Marshall Space Flight Center
EB72
Marshall Space Flight Center, AL 35812
(205) 544-3402

Chuck Lurie
TRW
MS R4/1082
One Space Park
Redondo Beach, CA 90278
(310) 813-4888

Michael Mackowski
McDonnell Douglas
7714 Aragorn Ct.
Hanover, MD 21076
(410) 519-0017

Dr. Tyler X. Mahy
U.S. Government
c/o OTS--2S83, NHB
Washington, DC 20505
(703) 874-0739

Michelle Manzo
Lewis Research Center
MS 309-1
21000 Brookpark Rd.
Cleveland, OH 44135
(216) 433-5261

Nehemiah Margalit
Tracor Battery Technology Center
4294 Mainsail Dr.
Burke, VA 22015
(301) 251-4881

Dean W. Maurer
AT&T / Bell Labs
379 Princeton-Hightstown Rd.
Cranbury, NJ 08512
(609) 448-0687

Louis C. Maus
Marshall Space Flight Center
PD14
Marshall Space Flight Center, AL 35812
(205) 544-0484

Kurt McCall
Marshall Space Flight Center
EB12
Marshall Space Flight Center, AL 35812
(205) 961-4501

Wm. Keith McCoy
Sandia National Labs
POB 5800
MS 0980 Dept. 9231
Albuquerque, NM 87185-0980
(505) 844-7170

David D. McGuire
Martin Marietta
9390 S. Warhawk Rd.
Conifer, CO 80433
(303) 977-8647

Carol McQueary
Hughes Aircraft
Electron Dynamics Division
POB 15999
Torrance, CA 90509

John Metcalfe
CAL Corporation
Engineering and Quality Group
1050 Morrison Drive
Ottawa, Ontario
Canada K2H 8K7

(613) 820-8280

George Methlie

2120 Natahoa Ct.
Falls Church, VA 22043
(202) 965-3420

John Meyer
Johns Hopkins University / APL
Bldg 23/205
Johns Hopkins Rd.
Laurel, MD 20723-6099
(301) 953-5000 X8604

Joseph F. Mibelli
JFM Engineering, Inc.
7880 NW 56th St.
Miami, FL 33166
(305) 592-2272

Ron Miller
Goddard Space Flight Center
Code 405, Bldg. 12, Rm. E-8
Greenbelt, MD 20771
(301) 286-6331

Scott D. Miller
Martin Marietta – UARS FOT
Code 506.9; Bldg. 3, Rm. S-24
Goddard Space Flight Center
Greenbelt, MD 20771
(301) 286-3854

Zane Miller
Sandia National Labs
POB 5800
MS 0980 Dept. 9231
Albuquerque, NM 87185-0980
(505) 844-1426

Arnold Mondrow
Boeing
POB 440272
Aurora, CO 80044-0272
(303) 770-7073

Bruce Moore
Naval surface Warfare Center - Crane Div.
Code 6095
300 Hwy 361
Crane, IN 47522
(812) 854-1593

Kensuke Nakatani
Sanyo Electric Co., Ltd.
221-1 Kaminaizen, Sumoto, Hyogo
Japan

(011-81) 799-23-2851

Suzanne Norris
Martin Marietta
MS S4017
POB 179
Denver, CO 80201
(303) 971-8807

Pat O'Donnell
Lewis Research Center
MS 309-1
21000 Brookpark Rd.
Cleveland, OH 44135
(216) 433-5248

William Todd Owens
Auburn University
231 Leach Science Center
Space Power Institute
Auburn, AL 36849-3501
(205) 844-5141

Craig Partlo
Hughes Aircraft Co.
Colorado Engineering Laboratory
16800 E. CentreTech Parkway
Aurora, CO 80017
(303) 766-9492

Gene Pearlman
Martin Marietta Astro Space
POB 800
Princeton, NJ 08540
(609) 490-3349

Catherine Penafiel
Loral Aerosys
7375 Executive Place
Seabrook, MD 20706
(301) 286-9316

Nguyet H. Phan
The Aerospace Corporation
M/S M2/275
POB 92957
Los Angeles, CA 90009-2957
(310) 336-2295

David F. Pickett
Hughes Aircraft Co.
Electron Dynamics Division
MS 231/1040
POB 2999
Torrance, CA 90509-2999
(310) 517-7601

Agnes-Marie Ponthus
SAFT Advanced Batteries
Rue G. Leclanche
BP 1029
86060 Poitiers Cedex
France

(33) 4955 48 48

Dana L. Potter
Hughes Aircraft
MS CHSS
16800 E. CentreTech Parkway
Aurora, CO 80011
(303) 341-3327

R. Ramesham
Auburn University
Space Power Institute
231 Leach Center
Auburn, AL 36849-3501
(205) 844-5894

Gopal Rao
Goddard Space Flight Center
Code 734.5
Greenbelt, MD 20716
(301) 286-6654

Philip G. Russell
Yardney Technical Products
82 Mechanic St.
Pawcatuck, CT 06379
(203) 599-1100

B. Rutkauskas
MDESC
2840 Upper Hutton
St. Charles, MO 63303

David F. Schmidt
Gates Aerospace Batteries
POB 147115
Gainesville, FL 32614-7115
(904) 462-6947

Jack Schmidt
GE American Communications
95 Edsall Dr.
Sussex, NJ 07461
(609) 987-4356

Todd Schutt
Marshall Space Flight Center
EB12
Marshall Space Flight Center, AL 35812
(205) 544-2027

Darren Scoles
Eagle-Picher Industries, Inc.
3820 South Hancock Expressway
Colorado Springs, CO 80911
(719) 392-4266

Ramakrishnan Sermadevi
Inmarsat
c/o Martin Marietta Astro Space
MS 115, POB 800
Princeton, NJ 08543
(609) 490-6301

James A. Stepro
National Standard Co.
2401 N. Home St.
Mishawaka, IN 46545
(219) 259-8505

Joe Stockel
Office of Research & Development
Ames Building, Rm 762
Washington, DC 20505
(703) 351-2065

Benjamin Tausch
Martin Marietta
MS S4017
POB 179
Denver, CO 80201
(303) 971-8706

Lawrence Thaller
The Aerospace Corporation
MS M2/275
POB 92957
Los Angeles, CA 90009
(310) 336-5180

H. E. Thierfelder

21 Dechert Rd.
Conshohocken, PA 19428
(215) 828-5765

Mark R. Toft
McDonnell Douglas Electronic Systems
MS 500 4174
POB 426
St. Charles, MO 63301
(314) 925-7692

Greta Tracinski
Applied Power International
1236 N Columbus Ave., #41
Glendale, CA 91202-1672
(818) 243-3127

Walter A. Tracinski
Applied Power International
1236 N. Columbus Ave., Suite 41
Glendale, CA 91202-1672
(818) 243-3127

Jean Verniolle
European Space Agency
ESTEC/XPB
POB 299
2200 AG Noordwijk
The Netherlands

31-17198-3868

Harry Wannemacher
McDonnell Douglas
7404 Executive Place
Seabrook, MD 20706-0001
(301) 464-3301

Marvin Warshay
Lewis Research Center
MS 301-5
21000 Brookpark Rd.
Cleveland, OH 44135
(216) 433-5261

William Wells
Vitro Corporation
Suite 825
400 Virginia Ave SW
Washington, DC 20024
(202) 646-6350

James R. Wheeler
Eagle-Picher Industries, Inc.
POB 47
Joplin, MO 64801
(417) 623-8000 X359

Tom Whitt
Marshall Space Flight Center
EB72
Marshall Space Flight Center, AL 35812
(205) 544-3313

Don Williams
Marshall Space Flight Center
PD14
Marshall Space Flight Center, AL 35812

Mona Lisa Williamson
Computer Sciences Corporation
NASA / GSFC
Code 440.9
Greenbelt, MD 20771
(301) 286-2479

Doug Willowby
Marshall Space Flight Center
EB74
Marshall Space Flight Center, AL 35812
(205) 544-3334

Glenn Zeideis
DSTI
600 Blvd. S., Ste. 301
Huntsville, AL
(205) 461-9233

Albert H. Zimmerman
The Aerospace Corporation
MS M2/275
POB 92957
Los Angeles, CA 90009-2957
(310) 336-7415

REPORT DOCUMENTATION PAGE

Form Approved
OMB No. 0704-0188

1. AGENCY USE ONLY (Leave blank)	2. REPORT DATE	3. REPORT TYPE AND DATES COVERED
	February 1994	Conference Publication

4. TITLE AND SUBTITLE
The 1993 NASA Aerospace Battery Workshop

5. FUNDING NUMBERS

6. AUTHOR(S)
Jeffrey C. Brewer, Compiler

7. PERFORMING ORGANIZATION NAME(S) AND ADDRESS(ES)
George C. Marshall Space Flight Center
Marshall Space Flight Center, Alabama

8. PERFORMING ORGANIZATION REPORT NUMBER
M-739

9. SPONSORING / MONITORING AGENCY NAME(S) AND ADDRESS(ES)
National Aeronautics and Space Administration
Washington, DC 20546

10. SPONSORING / MONITORING AGENCY REPORT NUMBER
NASA CP-3254

11. SUPPLEMENTARY NOTES
Proceedings of workshop sponsored by the NASA Aerospace Flight Battery Systems Program, hosted by the Marshall Space Flight Center, and held at the U.S. Space and Rocket Center on November 16-18, 1993.

12a. DISTRIBUTION / AVAILABILITY STATEMENT
Unclassified-Unlimited

Subject Category: 44

12b. DISTRIBUTION CODE

13. ABSTRACT (Maximum 200 words)

This document contains the proceedings of the 26th annual NASA Aerospace Battery Workshop, hosted by the Marshall Space Flight Center on November 16-18, 1993. The workshop was attended by scientists and engineers from various agencies of the U.S. Government, aerospace contractors, and battery manufacturers, as well as international participation in like kind from a number of countries around the world.

The subjects covered included nickel-cadmium, nickel-hydrogen, nickel-metal hydride, and lithium based technologies, as well as advanced technologies including various bipolar designs.

14. SUBJECT TERMS battery, nickel-cadmium, nickel-hydrogen, nickel-metal hydride, lithium, cadmium, battery test, electrode, pressure vessel, charge control

15. NUMBER OF PAGES 851

16. PRICE CODE A99

17. SECURITY CLASSIFICATION OF REPORT	18. SECURITY CLASSIFICATION OF THIS PAGE	19. SECURITY CLASSIFICATION OF ABSTRACT	20. LIMITATION OF ABSTRACT
Unclassified	Unclassified	Unclassified	UL